

SCIENTIFIC ASSESSMENT OF OZONE DEPLETION: 2006

*Pursuant to Article 6 of the Montreal Protocol
on Substances that Deplete the Ozone Layer*

National Oceanic and Atmospheric Administration
National Aeronautics and Space Administration
United Nations Environment Programme
World Meteorological Organization
European Commission

Final Release: February 2007

From *Scientific Assessment of Ozone Depletion: 2006*

**Dedicated to the Memory of
Gérard Mégie
1946-2004**



This report is dedicated to the memory of our friend and colleague, Prof. Gérard Mégie of the Centre National de la Recherche Scientifique of Paris, France.

Gérard worked as a member of the Scientific Assessment Panel of the Montreal Protocol since the very beginning; he was a participant in the Les Diablerets Panel Review Meeting in 1989. Later, he became a Cochair of the Scientific Assessment Panel, cochairing the 1998 and 2002 assessment reports. To that role, he brought his rare combination of scientific excellence and leadership talent, built upon many years as a teacher, researcher, internationally acclaimed scientist, and leader in the atmospheric science community.

One mark of Gérard's insightfulness was his work to guide the Panel toward its increasing emphasis on the connections between the ozone layer and the climate system. The Panel's assessment report for 2006 does contain that emphasis, and indeed it is captured in separate chapters on these issues.

Gérard was dedicated to communicating scientific understanding at many levels, ranging from international decisionmaking to the realm of the general public and schools. This is exemplified by his thoughtful work associated with the Panel's efforts to provide a set of "frequently asked" questions and answers about the ozone layer.

Gérard's many contributions to atmospheric science, as well as his role in forging interactions of the scientific community at its interface with society, have had a lasting impact. He leaves a legacy of scientific leadership that has helped shape the world's actions on the ozone layer. This legacy will endure.

LIST OF INTERNATIONAL AUTHORS, CONTRIBUTORS, AND REVIEWERS

Assessment Cochairs

Ayité-Lô Nohende Ajavon
Daniel L. Albritton
Robert T. Watson

Assessment Scientific Steering Committee

Marie-Lise Chanin
Susana B. Diaz
John A. Pyle
A.R. Ravishankara
Theodore G. Shepherd

Chapters and Lead Authors

I. Source Gases

Chapter 1. Long-Lived Compounds (*Cathy Clerbaux and Derek Cunnold*)
Chapter 2. Halogenated Very Short-Lived Substances (*Katherine S. Law and William T. Sturges*)

II. Ozone Changes

Chapter 3. Global Ozone: Past and Present (*Martyn P. Chipperfield and Vitali E. Fioletov*)
Chapter 4. Polar Ozone: Past and Present (*Paul A. Newman and Markus Rex*)

III. Future Expectations for Ozone, Ozone-Depleting Substances, and UV

Chapter 5. Climate-Ozone Connections (*Mark P. Baldwin and Martin Dameris*)
Chapter 6. The Ozone Layer in the 21st Century (*Greg Bodeker and Darryn W. Waugh*)
Chapter 7. Surface Ultraviolet Radiation: Past, Present, and Future (*Alkiviadis F. Bais and Dan Lubin*)
Chapter 8. Halocarbon Scenarios, Ozone Depletion Potentials, and Global Warming Potentials
(*John S. Daniel and Guus J.M. Velders*)

Twenty Questions and Answers About the Ozone Layer: 2006 Update (*David W. Fahey*)

Coordinating Editor

Christine A. Ennis

Authors, Contributors, and Reviewers

Ayité-Lô Nohende Ajavon	Togo	Elliot Atlas	USA
Hideharu Akiyoshi	Japan	Pieter J. Aucamp	South Africa
Daniel L. Albritton	USA	John Austin	USA
Stephen O. Andersen	USA	Gnon Baba	Togo
John Anderson	USA	Alkiviadis F. Bais	Greece
Gustavo A. Argüello	Argentina	Mark P. Baldwin	USA
Antti Arola	Finland	Leonard A. Barrie	Switzerland
Paul Ashford	UK	David Battisti	USA

AUTHORS, CONTRIBUTORS, AND REVIEWERS

Gufran Beig	India	Tatiana Egorova	Switzerland
Slimane Bekki	France	Andreas Engel	Germany
Peter Bernath	Canada	Christine A. Ennis	USA
Germar Bernhard	USA	Carynelisa Erlick	Israel
Lars Olof Björn	Sweden	David Etheridge	Australia
Donald R. Blake	USA	Wayne Evans	USA
Nicola J. Blake	USA	Veronika Eyring	Germany
Thomas Blumenstock	Germany	David W. Fahey	USA
Mario Blumthaler	Austria	Uwe Feister	Germany
Greg Bodeker	New Zealand	Wuhu Feng	UK
Rumen D. Bojkov	Germany	Vitali E. Fioletov	Canada
Janet F. Bornman	New Zealand	Horst Fischer	Germany
Geir O. Braathen	Switzerland	Lawrence E. Flynn	USA
Peter Braesicke	UK	Ian Folkins	Canada
Bram Bregman	The Netherlands	Piers M.D. Forster	UK
Christoph Brühl	Germany	Paul J. Fraser	Australia
Claus Brüning	Belgium	John Frederick	USA
James B. Burkholder	USA	Katja Frieler	Germany
John P. Burrows	Germany	Stacey Hollandsworth Frith	USA
Neal Butchart	UK	Lucien Froidevaux	USA
James H. Butler	USA	Jan Fuglestvedt	Norway
André Butz	Germany	Rolando R. Garcia	USA
James M. Calm	USA	Marvin A. Geller	USA
Pablo O. Canziani	Argentina	Andrew Gettelman	USA
Daniel Cariolle	France	H. Peter Gies	Australia
Lucy Carpenter	UK	Nathan P. Gillett	UK
Kenneth S. Carslaw	UK	Marco A. Giorgetta	Germany
Marie-Lise Chanin	France	Sophie Godin-Beekmann	France
Martyn P. Chipperfield	UK	David M. Golden	USA
Natalia E. Chubarova	Russia	Marco González	Kenya
Hans Claude	Germany	Florence Goutail	France
Cathy Clerbaux	France	Hans-F. Graf	UK
Pierre-Francois Coheur	Belgium	Claire Granier	USA/France
William J. Collins	UK	Julian Gröbner	Switzerland
Brian J. Connor	New Zealand	Serge Guillas	USA
David B. Considine	USA	Joanna D. Haigh	UK
Eugene Cordero	USA	Neil R.P. Harris	UK
R. Anthony Cox	UK	Dennis Hartmann	USA
John Crowley	Germany	Alain Hauchecorne	France
Paul Crutzen	Germany	Didier A. Hauglustaine	France
Derek M. Cunnold	USA	Sachiko Hayashida	Japan
Martin Dameris	Germany	Peter H. Haynes	UK
John S. Daniel	USA	Jay Herman	USA
Michael Danilin	USA	David J. Hofmann	USA
Philippe Demoulin	Belgium	Lon Hood	USA
Susana B. Diaz	Argentina	Dale Hurst	USA
Marcel Dorf	Germany	Abdelmoneim A.R. Ibrahim	Egypt
Anne R. Douglass	USA	Mohammad Ilyas	Malaysia
Katja Drdla	USA	Takashi Imamura	Japan
Ellsworth G. Dutton	USA	Ivar Isaksen	Norway
Geoffrey S. Dutton	USA	Charles H. Jackman	USA
Kalju Eerme	Estonia	Elena Jimenez	Spain

AUTHORS, CONTRIBUTORS, AND REVIEWERS

Paul Johnston	New Zealand	Rolf Müller	Germany
Roderic L. Jones	UK	Nzioka John Muthama	Kenya
Hiroshi Kanzawa	Japan	Hideaki Nakane	Japan
David Karoly	USA	Eric R. Nash	USA
Jussi Kaurola	Finland	Ray Nassar	Canada
S. Randy Kawa	USA	Michael Newchurch	USA
Jack A. Kaye	USA	Paul A. Newman	USA
M.A.K. Khalil	USA	Ole John Nielsen	Denmark
Douglas E. Kinnison	USA	Simon O'Doherty	UK
Bjørn Knudsen	Denmark	Alan O'Neill	UK
Malcolm K.W. Ko	USA	Samuel Oltmans	USA
Chester Koblinsky	USA	David E. Oram	UK
Peter Koepke	Germany	Yvan J. Orsolini	Norway
Laurie J. Kovalenko	USA	Eduardo Palenque	Bolivia
Karin Kreher	New Zealand	Panos Papagiannakopoulos	Greece
Nickolay A. Krotkov	USA	Steven Pawson	USA
Paul B. Krummel	Australia	Thomas Peter	Switzerland
Janusz W. Krzyściński	Poland	Irina Petropavlovskikh	USA
Lambert Kuijpers	The Netherlands	Klaus Pfeilsticker	Germany
Michael J. Kurylo	USA	Rubén D. Piacentini	Argentina
Esko Kyrö	Finland	Giovanni Pitari	Italy
Shyam Lal	India	John M.C. Plane	UK
Ulrike Langematz	Germany	Ulrich Platt	Germany
Kathleen O. Lantz	USA	Ian Plumb	Australia
Katherine S. Law	France	R. Alan Plumb	USA
Mark G. Lawrence	Germany	David Plummer	Canada
J. Ben Liley	New Zealand	Lorenzo M. Polvani	USA
Zenobia Litynska	Poland	Lamont R. Poole	USA
Nathaniel J. Livesey	USA	Robert W. Portmann	USA
Jennifer Logan	USA	Gilles Poulet	France
Manuel López-Puertas	Spain	Michael Prather	USA
Dan Lubin	USA	Ronald Prinn	USA
Emmanuel Mahieu	Belgium	John A. Pyle	UK
Eva Mancini	Italy	S. Ramachandran	India
Gloria L. Manney	USA	V. Ramaswamy	USA
Alistair Manning	UK	Cora E. Randall	USA
Elisa Manzini	Italy	William Randel	USA
Marion Marchand	France	A.R. Ravishankara	USA
Céline Mari	France	Thomas Reddmann	Germany
Katja Matthes	USA	Claire Reeves	UK
Bernhard Mayer	Germany	Stefan Reimann	Switzerland
Archie McCulloch	UK	Ellis E. Remsberg	USA
Mack McFarland	USA	Markus Rex	Germany
Richard L. McKenzie	New Zealand	Robert Rhew	USA
Richard D. McPeters	USA	Curtis P. Rinsland	USA
Davit Melkonyan	Armenia	Alan Robock	USA
Pauline Midgley	Germany	José M. Rodríguez	USA
Alvin J. Miller	USA	Geert-Jan Roelofs	The Netherlands
John Miller	USA	Bjørn Rognerud	Norway
Kenneth R. Minschwaner	USA	Howard Roscoe	UK
Stephen A. Montzka	USA	Karen Rosenlof	USA
Jens Mühle	USA	Eugene Rozanov	Switzerland

AUTHORS, CONTRIBUTORS, AND REVIEWERS

James M. Russell III	USA	Masaaki Takahashi	Japan
Ross J. Salawitch	USA	David W. Tarasick	Canada
Michelle L. Santee	USA	Yukio Terao	USA
Benjamin D. Santer	USA	Larry W. Thomason	USA
Toru Sasaki	Japan	David W.J. Thompson	USA
Yasuhiro Sasano	Japan	Wenshou Tian	UK
Robert Sausen	Germany	Simone Tilmes	USA
Cornelius Schiller	Germany	Claudisa Timmreck	Germany
Ulrich Schmidt	Germany	Darin Toohey	USA
Robyn Schofield	USA	Cathy Trudinger	Australia
Ulrich Schumann	Germany	Jan C. van der Leun	The Netherlands
John F. Scinocca	Canada	Costas Varotsos	Greece
Robert B. Scott	USA	Guus J.M. Velders	The Netherlands
Gunther Seckmeyer	Germany	Daniel P. Verdonik	USA
Megumi Seki	Kenya	Mario Visca	Italy
Theodore G. Shepherd	Canada	Roland von Glasow	Germany
Kiyotaka Shibata	Japan	Marc von Hobe	Germany
Drew Shindell	USA	John Michael Wallace	USA
Keith P. Shine	UK	Timothy J. Wallington	USA
Emily Shuckburgh	UK	Nicola J. Warwick	UK
Peter Simmonds	UK	Robert T. Watson	USA
Isobel Simpson	USA	Darryn W. Waugh	USA
Howard J. Singer	USA	Elizabeth C. Weatherhead	USA
Cynthia Shaw Singleton	USA	Ann Webb	UK
Björn-Martin Sinnhuber	Germany	Mark Weber	Germany
Miriam Sinnhuber	Germany	Philipp Weihs	Austria
Christopher E. Sioris	USA	Debra K. Weisenstein	USA
Pavla Skrivankova	Czech Republic	Ray F. Weiss	USA
Harry Slaper	The Netherlands	Paul Wennberg	USA
James R. Slusser	USA	Paul Wine	USA
Sergei P. Smyshlyaev	Russia	Stephen Wood	New Zealand
Susan Solomon	USA	Donald J. Wuebbles	USA
Johannes Staehelin	Switzerland	Eun-Su Yang	USA
Knut Stamnes	USA	Margarita Yela	Spain
Wolfgang Steinbrecht	Germany	Shigeo Yoden	Japan
Andrea Stenke	Germany	Yoko Yokouchi	Japan
Richard M. Stimpfle	USA	Vladimir Yushkov	Russia
Richard S. Stolarski	USA	Shari A. Yvon-Lewis	USA
Frode Stordal	Norway	Rudolphe Zander	Belgium
Susan Strahan	USA	Francesco Zaratti	Bolivia
Hamish Struthers	New Zealand	Joseph M. Zawodny	USA
William T. Sturges	UK	Christos S. Zerefos	Greece
Azadeh Tabazadeh	USA	Tong Zhu	China

CONTENTS

SCIENTIFIC ASSESSMENT OF OZONE DEPLETION: 2006

PREFACE xiii

EXECUTIVE SUMMARY xvii

I. SOURCE GASES

CHAPTER 1: LONG-LIVED COMPOUNDS

Lead Authors: Cathy Clerbaux and Derek Cunnold

Scientific Summary	1.1
1.1 Introduction	1.5
1.2 Halogenated Ozone-Depleting Gases in the Atmosphere	1.7
1.3 Emissions Estimated from the Halocarbon Measurements	1.38
1.4 Other Trace Gases	1.46
References	1.52

CHAPTER 2: HALOGENATED VERY SHORT-LIVED SUBSTANCES

Lead Authors: Katherine S. Law and William T. Sturges

Scientific Summary	2.1
2.1 Introduction	2.5
2.2 Sources, Distributions, and Trends of VSLS	2.9
2.3 Atmospheric Chemistry of VSLS	2.19
2.4 Dynamics and Transport in the Tropopause Region and Implications for VSLS	2.24
2.5 Contribution of Halogenated VSLS to Stratospheric Halogen Loading	2.31
2.6 Potential Impact of VSLS on Ozone	2.43
2.7 Potential Future Considerations	2.45
References	2.46

II. OZONE CHANGES

CHAPTER 3: GLOBAL OZONE: PAST AND PRESENT

Lead Authors: Martyn P. Chipperfield and Vitali E. Fioletov

Scientific Summary	3.1
3.1 Introduction	3.5
3.2 Update of Ozone Changes	3.5
3.3 Summary of Other Observations	3.19
3.4 Understanding and Interpretation of Ozone Changes	3.21
References	3.41
Appendix 3A: Description of the Ozone Datasets	3.55

CONTENTS

CHAPTER 4:	POLAR OZONE: PAST AND PRESENT	
	<i>Lead Authors: Paul A. Newman and Markus Rex</i>	
Scientific Summary	4.1
4.0 Introduction	4.3
4.1 Polar Stratospheric Observations Update	4.4
4.2 Progress in Our Understanding of the Physical and Chemical Processes	4.20
4.3 Recent Polar Ozone Changes	4.30
4.4 The Influence of Precipitating Charged Particles on Polar Ozone	4.35
References	4.37
III. FUTURE EXPECTATIONS FOR OZONE, OZONE-DEPLETING SUBSTANCES, AND UV		
CHAPTER 5:	CLIMATE-OZONE CONNECTIONS	
	<i>Lead Authors: Mark P. Baldwin and Martin Dameris</i>	
Scientific Summary	5.1
5.1 Introduction	5.3
5.2 Coupling of the Stratosphere and Troposphere	5.3
5.3 Effects of Anthropogenic Climate Change and of Emissions on Stratospheric Ozone	5.18
References	5.38
Appendix 5A: AOGCMs Used in Chapter 5	5.49
CHAPTER 6:	THE OZONE LAYER IN THE 21ST CENTURY	
	<i>Lead Authors: Greg Bodeker and Darryn W. Waugh</i>	
Scientific Summary	6.1
6.1 Introduction	6.5
6.2 A Framework for Evaluating Changes in Ozone Abundances	6.5
6.3 Factors Affecting the Detection, Attribution, and Timing of Milestones	6.8
6.4 Statistical Methods for Detection of Milestones	6.11
6.5 Attribution of the Recent Behavior of Ozone	6.13
6.6 Projections of the Future Behavior of Ozone	6.20
References	6.37
Appendix 6A: Model Scenarios	6.43
CHAPTER 7:	SURFACE ULTRAVIOLET RADIATION: PAST, PRESENT, AND FUTURE	
	<i>Lead Authors: Alkiviadis F. Bais and Dan Lubin</i>	
Scientific Summary	7.1
7.1 Introduction	7.3
7.2 Factors Affecting UV Radiation: New Findings	7.3
7.3 Resources for Studying Surface UV Radiation	7.13
7.4 UV Climatology	7.21
7.5 Expectations for the Future	7.29
7.6 Remaining Questions and Uncertainties	7.32
References	7.32
Appendix 7A: Spectral Data Available from Databases	7.49
Appendix 7B: Internet Addresses for UV Sites	7.53

CHAPTER 8: HALOCARBON SCENARIOS, OZONE DEPLETION POTENTIALS,
AND GLOBAL WARMING POTENTIALS

Lead Authors: John S. Daniel and Guus J.M. Velders

Scientific Summary	8.1
8.1 Introduction	8.5
8.2 Halocarbon Lifetimes, Ozone Depletion Potentials, and Global Warming Potentials	8.5
8.3 Future Halocarbon Source Gas Concentrations	8.13
8.4 Other Processes Relevant to Future Ozone Evolution	8.34
8.5 Indirect GWPs	8.35
References	8.36

TWENTY QUESTIONS AND ANSWERS ABOUT THE OZONE LAYER: 2006 UPDATE

Lead Author: David W. Fahey

I. Ozone in Our Atmosphere	Q.3
II. The Ozone Depletion Process	Q.9
III. Stratospheric Ozone Depletion	Q.22
IV. Controlling Ozone-Depleting Gases	Q.32
V. Implications of Ozone Depletion	Q.37
VI. Stratospheric Ozone in the Future	Q.43

APPENDICES

A LIST OF INTERNATIONAL AUTHORS, CONTRIBUTORS, AND REVIEWERS	A.1
B MAJOR ACRONYMS AND ABBREVIATIONS	B.1
C MAJOR CHEMICAL FORMULAE AND NOMENCLATURE FROM THIS ASSESSMENT	C.1

PREFACE

The present document will be part of the information upon which the Parties to the United Nations Montreal Protocol will base their future decisions regarding protection of the Earth's stratospheric ozone layer.

The Charge to the Assessment Panels

Specifically, the Montreal Protocol on Substances that Deplete the Ozone Layer states (Article 6): “. . . the Parties shall assess the control measures . . . on the basis of available scientific, environmental, technical, and economic information.” To provide the mechanisms whereby these assessments are conducted, the Protocol further states: “. . . the Parties shall convene appropriate panels of experts” and “the panels will report their conclusions . . . to the Parties.”

To meet this request, the Scientific Assessment Panel, the Environmental Effects Assessment Panel, and the Technology and Economic Assessment Panel have each periodically prepared major assessment reports that updated the state of understanding in their purviews. These reports have been scheduled so as to be available to the Parties in advance of their meetings at which they will consider the need to amend or adjust the Protocol.

The Sequence of Scientific Assessments

The present 2006 report is the latest in a series of ten scientific assessments prepared by the world's leading experts in the atmospheric sciences and under the international auspices of the World Meteorological Organization (WMO) and the United Nations Environment Programme (UNEP). This report is the sixth in the set of major assessments that have been prepared by the Scientific Assessment Panel directly as input to the Montreal Protocol process. The chronology of all the scientific assessments on the understanding of ozone depletion and their relation to the international policy process is summarized as follows:

<u>Year</u>	<u>Policy Process</u>	<u>Scientific Assessment</u>
1981		<i>The Stratosphere 1981: Theory and Measurements.</i> WMO No. 11.
1985	Vienna Convention	<i>Atmospheric Ozone 1985.</i> Three volumes. WMO No. 16.
1987	Montreal Protocol	
1988		<i>International Ozone Trends Panel Report 1988.</i> Two volumes. WMO No. 18.
1989		<i>Scientific Assessment of Stratospheric Ozone: 1989.</i> Two volumes. WMO No. 20.
1990	London Adjustment and Amendment	
1991		<i>Scientific Assessment of Ozone Depletion: 1991.</i> WMO No. 25.
1992		<i>Methyl Bromide: Its Atmospheric Science, Technology, and Economics (Montreal Protocol Assessment Supplement).</i> UNEP (1992).
1992	Copenhagen Adjustment and Amendment	
1994		<i>Scientific Assessment of Ozone Depletion: 1994.</i> WMO No. 37.

PREFACE

1995	Vienna Adjustment	
1997	Montreal Adjustment and Amendment	
1998		<i>Scientific Assessment of Ozone Depletion: 1998.</i> WMO No. 44.
1999	Beijing Adjustment and Amendment	
2002		<i>Scientific Assessment of Ozone Depletion: 2002.</i> WMO No. 47
2006		<i>Scientific Assessment of Ozone Depletion: 2006.</i> WMO No. 50
2007	19 th Meeting of the Parties	

The Current Information Needs of the Parties

The genesis of *Scientific Assessment of Ozone Depletion: 2006* occurred at the 15th Meeting of the Parties to the Montreal Protocol in Nairobi, Kenya, at which the scope of the scientific needs of the Parties was defined in their Decision XV/53 (4), which stated that "...for the 2006 report, the Scientific Assessment Panel should consider issues including:

- (a) Assessment of the state of the ozone layer and its expected recovery;
- (b) Evaluation of specific aspects of recent annual Antarctic ozone holes, in particular the hole that occurred in 2002;
- (c) Evaluation of the trends in the concentration of ozone-depleting substances in the atmosphere and their consistency with reported production and consumption of ozone-depleting substances;
- (d) Assessment of the impacts of climate change on ozone-layer recovery;
- (e) Analysis of atmospheric concentrations of bromine and the likely quantitative implications of the results on the state of the ozone layer;
- (f) Description and interpretation of the observed changes in global and polar ozone and in ultraviolet radiation, as well as set future projections and scenarios for those variables, taking also into account the expected impacts of climate change..."

The Assessment Process

The formal planning of the current assessment was started early in 2005. A Scientific Steering Committee consisting of five scientists from various countries assisted the Scientific Assessment Panel's Cochairs throughout the planning, preparation, review, and finalization of the 2006 assessment. The Cochairs and Scientific Steering Committee considered suggestions from the Parties regarding experts from their countries who could participate in the process. Furthermore, an *ad hoc* international scientific group also suggested participants from the world scientific community. In addition, this group contributed to crafting the outline of the assessment report. As in previous assessments, the participants represented experts from the developed and developing world. In addition to the scientific expertise, the developing country experts bring a special perspective to the process, and their involvement in the process has also contributed to capacity building.

The information of the 2006 assessment is contained in eight chapters associated with ozone-layer topics:

I. SOURCE GASES

Chapter 1. Long-Lived Compounds

Chapter 2. Halogenated Very Short-Lived Substances

II. OZONE CHANGES

Chapter 3. Global Ozone: Past and Present

Chapter 4. Polar Ozone: Past and Present

III. FUTURE EXPECTATIONS FOR OZONE, OZONE-DEPLETING SUBSTANCES, AND UV

Chapter 5. Climate-Ozone Connections

Chapter 6. The Ozone Layer in the 21st Century

Chapter 7. Surface Ultraviolet Radiation: Past, Present, and Future

Chapter 8. Halocarbon Scenarios, Ozone Depletion Potentials, and Global Warming Potentials

A special resource for the Panel's work was the 2005 Special Report of the Intergovernmental Panel on Climate Change (IPCC) and the Technology and Economics Assessment Panel (TEAP) of the Montreal Protocol, *Safeguarding the Ozone Layer and the Global Climate System: Issues Related to Hydrofluorocarbons and Perfluorocarbons*. This report was used as a basis for many scenarios for modeling runs and hypothetical cases that are included here.

The initial plans for the chapters of the 2006 Scientific Assessment Panel's report were examined at a meeting that occurred on 26-27 July 2005 in Paris, France. The Lead Authors, Steering Committee, and Coauthors focused on the content of the draft chapters and on the need for coordination among the chapters.

The first drafts of the chapters were examined at a meeting that occurred on 30 November-2 December 2005 in Herndon, Virginia, United States, at which the Lead Authors, Steering Committee, Coauthors, and a small group of international experts focused on the scientific content of the draft chapters.

The second drafts of the chapters were reviewed by 125 scientists worldwide in a mail peer review. Those comments were considered by the authors. At a Panel Review Meeting in Les Diablerets, Switzerland, held on 19-23 June 2006, the responses to these mail review comments were proposed by the authors and discussed by the 77 participants. Final changes to the chapters were decided upon at this meeting. The Executive Summary contained herein (and posted on the UNEP web site on 18 August 2006) was prepared and completed by the attendees of the Les Diablerets meeting.

The 2006 State-of-Understanding Report

In addition to the scientific chapters and the Executive Summary, the assessment also updates the 2002 assessment report's answers to a set of questions that are frequently asked about the ozone layer. Based upon the scientific understanding represented by the assessments, answers to these frequently asked questions were prepared, with different readerships in mind, e.g., students and the general public. These updated questions and answers are included in this report.

The final result of this two-year endeavor is the present assessment report. As the accompanying list indicates, the *Scientific Assessment of Ozone Depletion: 2006* is the product of 310 scientists from 34 countries who contributed to its preparation and review¹ (205 scientists prepared the report and 183 scientists participated in the peer review process).

What follows is a summary of their current understanding of the stratospheric ozone layer and its relation to humankind.

¹ Participants were from Argentina, Armenia, Australia, Austria, Belgium, Bolivia, Canada, Czech Republic, Denmark, Egypt, Estonia, Finland, France, Germany, Greece, India, Israel, Italy, Japan, Kenya, Malaysia, New Zealand, Norway, Poland, Russia, South Africa, Spain, Sweden, Switzerland, The Netherlands, The People's Republic of China, Togo, United Kingdom, and United States of America.

EXECUTIVE SUMMARY

Contents

INTRODUCTION	xix
Figure 1: Ozone-Depleting Substances, the Ozone Layer, and UV Radiation: Past, Present, and Future . . .	xix
RECENT MAJOR FINDINGS AND CURRENT SCIENTIFIC UNDERSTANDING	xx
Ozone-Depleting Substances	xx
Ozone, Ultraviolet Radiation, and Other Related Changes to Date	xxi
The Future of the Ozone Layer and Surface UV Radiation	xxiv
ADDITIONAL SCIENTIFIC EVIDENCE AND RELATED INFORMATION	xxv
Long-Lived Ozone-Depleting Substances	xxv
Halogenated Very Short-Lived Substances	xxvii
Global Ozone (60°S-60°N)	xxviii
Polar Ozone	xxix
Impact of Climate Change	xxxi
The Ozone Layer in the 21 st Century	xxxii
UV Radiation and Its Changes	xxxiii
Ozone Depletion Potentials and Global Warming Potentials	xxxiv
IMPLICATIONS FOR POLICY FORMULATION	xxxiv

Final Release: February 2007
From *Scientific Assessment of Ozone Depletion: 2006*

EXECUTIVE SUMMARY

The provisions of the 1987 Montreal Protocol on Substances that Deplete the Ozone Layer include the requirement that the Parties to the Protocol base their future decisions on the updated scientific, environmental, technical, and economic information that is assessed through Panels drawn from the worldwide expert communities. To provide that input to the decision-making process, advances in scientific understanding were assessed by the Scientific Assessment Panel in 1989, 1991, 1994, 1998, and 2002. This information helped support discussions among the Parties that led to the subsequent Amendments and Adjustments of the 1987 Protocol. The 2006 Scientific Assessment summarized here is the sixth in that series. The information contained in this Executive Summary is based on the eight detailed chapters of the full report.

The previous Assessment presented evidence that the tropospheric abundances of most ozone-depleting substances, as well as of stratospheric chlorine, were stable or decreasing due to actions taken under the Montreal Protocol (see schematic Figure 1a, b), with the stratospheric abundances showing a time lag due to the time for surface emissions to reach the stratosphere. Based on these facts, it was stated that “The Montreal Protocol is working, and the ozone-layer depletion from the Protocol’s controlled substances is expected to begin to ameliorate within the next decade or so.”

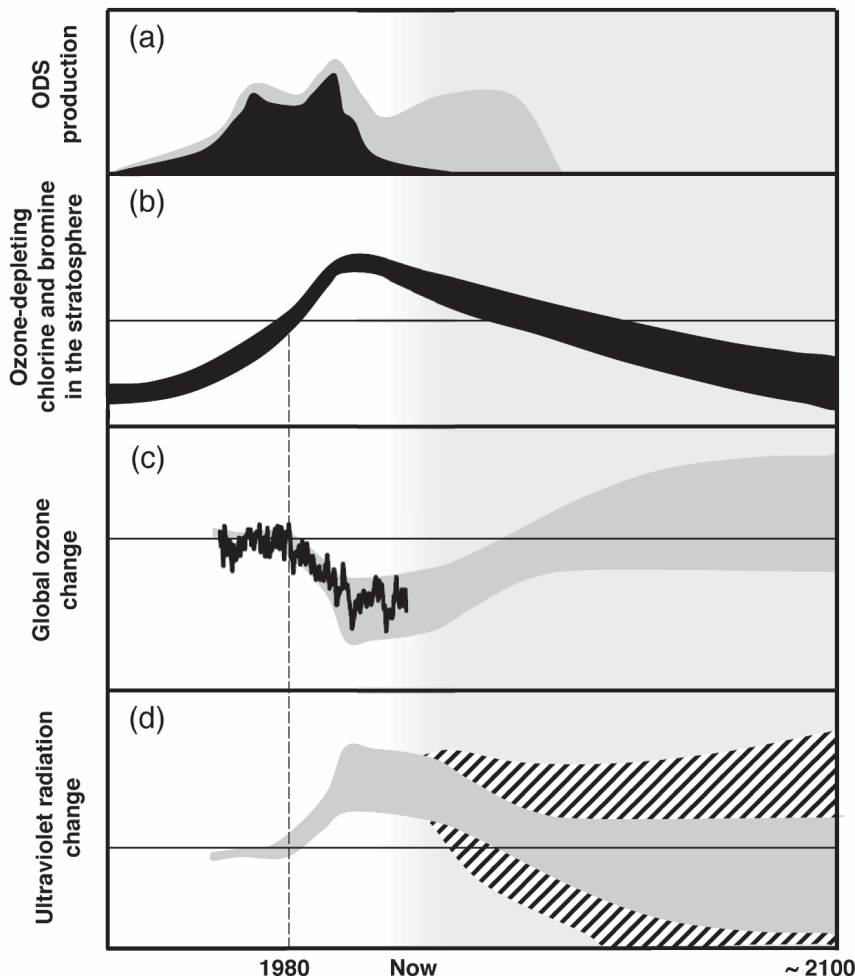


Figure 1. Ozone-Depleting Substances, the Ozone Layer, and UV Radiation: Past, Present, and Future.

(a) Production of ozone-depleting substances (ODSs) before and after the 1987 Montreal Protocol and its Amendments, from baseline scenario A1. Chlorofluorocarbons (CFCs) are shown in black; additional ODSs from hydrochlorofluorocarbons (HCFCs) are in gray. Note: HCFCs, which have been used as CFC replacements under the Protocol, lead to less ozone destruction than CFCs.

(b) Combined effective abundances of ozone-depleting chlorine and bromine in the stratosphere. The range reflects uncertainties due to the lag time between emission at the surface and the stratosphere, as well as different hypothetical ODS emission scenarios.

(c) Total global ozone change (outside of the polar regions; 60°S-60°N). Seasonal, quasi-biennial oscillation (QBO), volcanic, and solar effects have been removed. The black line shows measurements. The gray region broadly represents the evolution of ozone predicted by models that encompass the range of future potential climate conditions. Pre-1980 values, to the left of the vertical dashed line, are often used as a benchmark for ozone and UV recovery.

(d) Estimated change in UV erythemal (“sunburning”) irradiance for high sun. The gray area shows the calculated response to the ozone changes shown in (c). The hatched area shows rough estimates of what might occur due to climate-related changes in clouds and atmospheric fine particles (aerosols).

EXECUTIVE SUMMARY

An important next step is to ask whether stratospheric ozone and surface ultraviolet (UV) radiation are responding as expected to the controls on ozone-depleting substances imposed by the Protocol (see schematic Figure 1c, d). In addressing this question, it is necessary to consider factors other than ozone-depleting substances that also influence ozone and UV radiation. These factors include natural dynamical variability, volcanic eruptions, solar variations, aerosols (airborne fine particles), and climate change.

Pre-1980 values are often used as a benchmark for ozone and UV recovery. However, because of the above-mentioned factors, if and when ozone and UV radiation return to their pre-1980 values would not be associated solely with the return of ozone-depleting substances to their pre-1980 values (see schematic Figure 1c, d).

We address the behavior of ozone-depleting substances, the response of stratospheric ozone and UV radiation to ozone-depleting substances and other factors to date, and the future evolution of ozone and UV radiation. We first present the main findings, then the detailed supporting evidence, and finally the implications for policy formulation.

RECENT MAJOR FINDINGS AND CURRENT SCIENTIFIC UNDERSTANDING

Since the *Scientific Assessment of Ozone Depletion: 2002*, numerous laboratory investigations, atmospheric observations, and theoretical and modeling studies have produced new key findings and have strengthened the overall understanding of the ozone layer and its effect on UV radiation. These advances are highlighted in the following summary of the current understanding of the impact of human activities and natural phenomena on the ozone layer, as well as the coupling between climate change and stratospheric ozone depletion.

Ozone-Depleting Substances

The previous Assessment noted that the tropospheric abundances of ozone-depleting gases were declining, whereas the stratospheric abundances were at or near their peak. Now we ask: Are the tropospheric and stratospheric abundances of ozone-depleting gases showing further changes that can be linked to policy actions, and how are they expected to evolve in the future?

- **The total combined abundances of anthropogenic ozone-depleting gases in the troposphere continue to decline from the peak values reached in the 1992-1994 time period.**
 - The shorter-lived gases (e.g., methyl chloroform and methyl bromide) continue to provide much of the decline in total combined effective abundances of anthropogenic chlorine-containing and bromine-containing ozone-depleting gases in the troposphere. The early removal of the shorter-lived gases means that later decreases in ozone-depleting substances will likely be dominated by the atmospheric removal of the longer-lived gases.
 - By 2005, the total combined abundance of anthropogenic ozone-depleting gases in the troposphere had decreased by 8-9% from the peak value observed in the 1992-1994 time period. The overall magnitude of this decrease is attributable to the estimated changes in emissions and is consistent with the known atmospheric lifetimes and our understanding of transport processes.
 - The tropospheric abundances of hydrochlorofluorocarbons HCFC-22, -141b, and -142b increased much less than projected in the previous Assessment. The implication is that emissions have been lower than anticipated.
 - The sum of bromine from halons and methyl bromide in the troposphere has decreased by 3-5% since 1998 because of decreases in methyl bromide abundance. Methyl bromide abundance has decreased by 14% between 1997 and 2004. This decrease was larger than expected and suggests that when anthropogenic emissions of methyl bromide are reduced, its atmospheric abundance decreases more than previously thought.

- **The combined stratospheric abundances of the ozone-depleting gases show a downward trend from their peak values of the late 1990s, which is consistent with surface observations of these gases and a time lag for transport to the stratosphere.**
 - Measurements of hydrogen chloride give a clear signature in the stratosphere of the decrease in stratospheric ozone-depleting gases since reaching their peak in the late 1990s.
 - Stratospheric bromine has increased in line with its tropospheric trends in preceding years. A decrease in stratospheric bromine has not yet been identified. Bromine continues to play a major role in stratospheric ozone depletion.
- **Our quantitative understanding of how halogenated very short-lived substances contribute to halogen levels in the stratosphere has improved significantly since the 2002 Assessment, with brominated very short-lived substances believed to make a significant contribution to total stratospheric bromine and its effect on stratospheric ozone.**
 - Brominated very short-lived substances (which are mainly of natural origin) contribute ~5 parts per trillion (ppt) of bromine (estimates range from 3 to 8 ppt) to current levels of total stratospheric bromine (which are about 18 to 25 ppt). These values are derived from observations of tropospheric bromine source gases and bromine monoxide in the stratosphere, based on our current understanding of chemical transformations and transport of very short-lived substances to the stratosphere.
 - Chlorinated very short-lived source gases, which are mainly of anthropogenic origin, have now been observed at levels of about 50 ppt in the tropical upper troposphere and currently may be a small source of chlorine to the stratosphere.
 - Evidence suggests that iodine is currently much less important than bromine and chlorine for stratospheric ozone destruction.

Ozone, Ultraviolet Radiation, and Other Related Changes to Date

The previous Assessment noted that stratospheric ozone depletion was expected to begin to reverse within the next decade or so. Now we ask: Are there any signs of this beginning? Have other factors influenced the behavior of ozone during this period? Has surface UV radiation responded as anticipated?

- **Our basic understanding that anthropogenic ozone-depleting substances have been the principal cause of the ozone depletion over the past few decades has been strengthened. During the recent period of near-constant abundances of ozone-depleting gases, variations in meteorology have been particularly important in influencing the behavior of ozone over much of the polar and extrapolar (60°S-60°N) regions.**

POLAR OZONE

- **Springtime polar ozone depletion continues to be severe in cold stratospheric winters. Meteorological variability has played a larger role in the observed variability in ozone, over both poles, in the past few years.**
 - Large Antarctic ozone holes continue to occur. The severity of Antarctic ozone depletion has not continued to increase since the late 1990s and, since 2000, ozone levels have been higher than in some preceding years. These recent changes, seen to different degrees in different diagnostic analyses, result from increased dynamical activity and not from decreases in ozone-depleting substances.

EXECUTIVE SUMMARY

- The Antarctic ozone hole now is not as strongly influenced by moderate decreases in ozone-depleting gases, and the unusually small ozone holes in some recent years (e.g., 2002 and 2004) are attributable to dynamical changes in the Antarctic vortex.
- The anomalous Antarctic ozone hole of 2002 was manifested in a smaller ozone-hole area and much smaller ozone depletion than in the previous decade. This anomaly was due to an unusual major stratospheric sudden warming.
- Arctic ozone depletion exhibits large year-to-year variability, driven by meteorological conditions. Over the past four decades, these conditions became more conducive to severe ozone depletion because of increasingly widespread conditions for the formation of polar stratospheric clouds during the coldest Arctic winters. This change is much larger than can be expected from the direct radiative effect of increasing greenhouse gas concentrations. The reason for the change is unclear, and it could be because of long-term natural variability or an unknown dynamical mechanism. The change in temperature conditions has contributed to large Arctic ozone losses during some winters since the mid-1990s.
- The Arctic winter 2004/2005 was exceptionally cold, and chemical ozone loss was among the largest ever diagnosed. The Arctic remains susceptible to large chemical ozone loss, and a lack of understanding of the long-term changes in the occurrence of polar stratospheric clouds limits our ability to predict the future evolution of Arctic ozone abundance and to detect the early signs of recovery.
- The role of chemical reactions of chlorine and bromine in the polar stratosphere is better quantified. Inclusion of these advances results in improved agreement between theory and observation of the timing of both Arctic and Antarctic polar ozone loss.

GLOBAL OZONE (60°S-60°N)

- **The decline in abundances of extrapolar stratospheric ozone seen in the 1990s has not continued.**
 - Ozone abundances in the extrapolar regions, 60°S-60°N, have not further declined in recent years. The mid-latitude column (i.e., overhead) ozone values for the 2002-2005 period were approximately 3% below pre-1980 values in the Northern Hemisphere and approximately 6% in the Southern Hemisphere, essentially the same as in the 1998-2001 period.
 - The contribution of polar ozone depletion to midlatitude ozone depletion is substantial; the extent of the contribution is estimated to be about one-third in the Northern Hemisphere and one-half in the Southern Hemisphere. The larger contribution in the Southern Hemisphere is to be expected, given the larger polar ozone depletion in the Antarctic relative to the Arctic region, and may explain the differences in magnitude and seasonality of the long-term ozone changes in midlatitudes between the two hemispheres.
 - Changes in tropospheric and stratospheric meteorology are partially responsible for the observed Northern Hemisphere midlatitude winter ozone decline from 1979 to the mid-1990s and the ozone increase thereafter. Quantification of these dynamical effects on long-term trends ranges from ~20% to up to 50%, depending on the study. Most of these dynamically induced ozone changes appear to occur in the lowermost stratosphere.
 - Upper stratospheric ozone declined between 1979 and the mid-1990s, with the largest decrease of about 10-15% near 40 km over midlatitudes, but has been relatively constant during the last decade. Lower stratospheric (20-25 km) ozone over midlatitudes also showed a decrease of up to 10% from 1979 to the mid-1990s and has been relatively constant thereafter.

- Ozone abundances in the Northern Hemisphere midlatitude lowermost stratosphere (12-15 km) show a strong decrease between 1979 and the mid-1990s, followed by an overall increase from 1996 to 2004, giving no net long-term decrease at this level. This lowermost stratosphere ozone change contributed significantly to the column ozone change during the last decade. Southern Hemisphere observations do not show a similar increase in the 12-15 km altitude range since the mid-1990s.
- Total column ozone over the tropics (25°S-25°N) remains essentially unchanged. This finding is consistent with the findings of the previous Assessments.
- **Observations together with model studies suggest that the essentially unchanged column ozone abundances averaged over 60°S-60°N over roughly the past decade are related to the near constancy of stratospheric ozone-depleting gases during this period.**
 - The slowing of the decline and leveling off of midlatitude upper stratospheric (35-45 km) ozone over the past decade have very likely been dominated by the corresponding changes in stratospheric ozone-depleting gases.
 - Over the past decade, changes in stratospheric ozone-depleting gases have likely contributed to the slowing of the midlatitude total column ozone decline and the general leveling off of ozone abundances. Transport has also played an important role in ozone changes, particularly in the lowermost stratosphere, making attribution of column ozone changes to changes in ozone-depleting gases more difficult than in the upper stratosphere.

STRATOSPHERIC TEMPERATURE AND SURFACE UV RADIATION

- **The stratospheric cooling observed during the past two decades has slowed in recent years.**
 - Satellite and radiosonde measurements reveal an overall decrease in the global-mean lower stratospheric temperature of approximately 0.5 K/decade over the 1979-2004 period, with a slowdown in the temperature decline since the late 1990s. The overall temperature decrease is punctuated by transient warmings of the stratosphere associated with the major volcanic eruptions in 1982 and 1991. Model calculations suggest that the observed ozone loss is the predominant cause of the global-mean cooling observed over this period.
 - The lower stratospheric cooling is evident at all latitudes, in particular in both the Arctic and Antarctic winter/spring lower stratosphere, but with considerable interannual variability in those regions.
 - Satellite observations show larger cooling trends in the upper stratosphere, with values of 1 to 2 K/decade, but little additional decline since the middle 1990s. Model calculations suggest that the upper stratosphere trends are due, about equally, to decreases in ozone and increases in well-mixed greenhouse gases.
 - The long-term cooling rate of the Antarctic stratosphere has likewise reduced compared with what was seen by the time of the previous Assessment. There has been large variability in Antarctic temperatures in recent years.
- **Measurements from some stations in unpolluted locations indicate that UV irradiance (radiation levels) has been decreasing since the late 1990s, in accordance with observed ozone increases. However, at some Northern Hemisphere stations UV irradiance is still increasing, as a consequence of long-term changes in other factors that also affect UV radiation.** Outside polar regions, ozone depletion has been relatively small, hence, in many places, increases in UV due to this depletion are difficult to separate from the increases caused by other factors, such as changes in cloud and aerosol. In some unpolluted locations, especially in the Southern Hemisphere, UV irradiance has been decreasing in recent years, as expected from the observed increases in ozone at those sites. Model calculations incorporating only ozone projections show that cloud-free UV irradiance will continue to decrease, although other UV-influencing factors are likely to change at the same time.

EXECUTIVE SUMMARY

- **In polar regions, high UV irradiances lasting for a few days have been observed in association with episodes of low total ozone.** Erythemal (i.e., sunburning) irradiance averaged over several days has been increased by ~70% over sub-Antarctic regions when ozone-depleted air from the polar region passes over. In Antarctica during October, instantaneous enhancements that can exceed a factor of three have been observed. Over northern Europe and Alaska, the observed enhancements were smaller.

The Future of the Ozone Layer and Surface UV Radiation

The previous (2002) Assessment noted that climate change would influence the future of the ozone layer. Now we ask: How has our understanding of this issue progressed? How has our increased understanding led to an improved estimate of the state of the future ozone layer?

Previous Assessments have relied heavily on two-dimensional models for projections of future ozone, and these models are used again here. The 2002 Assessment noted the emerging use of three-dimensional Chemistry-Climate Models; we have now used these models extensively in this current 2006 Assessment.

- **It is unlikely that total ozone averaged over the region 60°S-60°N will decrease significantly below the low values of the 1990s, because the abundances of ozone-depleting substances have peaked and are in decline.** Two-dimensional models and three-dimensional Chemistry-Climate Models suggest that the minimum total column ozone values in this region have already occurred. This conclusion is consistent with the observation that over this region, ozone has not declined further in the 2002-2005 period.
- **The decrease in ozone-depleting substances is the dominant factor in the expected return of ozone levels to pre-1980 values. Changes in climate will influence if, when, and to what extent ozone will return to pre-1980 values in different regions.**
 - The current best estimate is that global (60°S-60°N) ozone will return to pre-1980 levels around the middle of the 21st century, at or before the time when stratospheric abundances of ozone-depleting gases return to pre-1980 levels.
 - Model simulations suggest that changes in climate, specifically the cooling of the stratosphere associated with increases in the abundance of carbon dioxide, may hasten the return of global column ozone to pre-1980 values by up to 15 years, depending on the climate-gas scenario used. However, this would not be considered a “recovery” of stratospheric ozone from ozone-depleting gases, because perceptible depletion due to anthropogenic ozone-depleting substances will still be contributing to the ozone levels.
- **The Antarctic ozone hole is expected to continue for decades. Antarctic ozone abundances are projected to return to pre-1980 levels around 2060-2075, roughly 10-25 years later than estimated in the 2002 Assessment.** The projection of this later return is primarily due to a better representation of the time evolution of ozone-depleting gases in the polar regions. In the next two decades, the Antarctic ozone hole is not expected to improve significantly.
- **Large ozone losses will likely continue to occur in cold Arctic winters during the next 15 years.** The high variability in the volume of polar stratospheric clouds in these cold winters limits our ability to predict their future occurrences. According to Chemistry-Climate Models, Arctic ozone levels are expected, on average, to return to pre-1980 levels before 2050.
- **Climate change will also influence surface UV radiation through changes induced mainly to clouds and the ability of the Earth’s surface to reflect light.** Aerosols and air pollutants are also expected to change in the future. These factors may result in either increases or decreases of surface UV irradiance, through absorption or scattering. As ozone depletion becomes smaller, these factors are likely to dominate future UV radiation levels.

ADDITIONAL SCIENTIFIC EVIDENCE AND RELATED INFORMATION

For the purpose of this report, ozone-depleting substances are considered as being either long-lived (more than 6 months in the atmosphere) or very short-lived (less than 6 months in the atmosphere), and these are considered in the next two sections. The atmospheric lifetime determines the likelihood of halogens emitted in the troposphere reaching the stratosphere, and so being able to deplete stratospheric ozone. The cumulative effective abundance of halogens in the stratosphere is quantified as equivalent effective stratospheric chlorine (EESC).¹

Long-Lived Ozone-Depleting Substances

ATMOSPHERIC TRENDS

- **The decline in the abundance of methyl chloroform and methyl bromide, which are shorter lived than chlorofluorocarbons (CFCs), contributed the most to the decline in effective equivalent tropospheric chlorine levels.** By 2005, the abundances of the total combined anthropogenic ozone-depleting gases in the troposphere had decreased by 8-9% from the peak value observed in the 1992-1994 time period. The total decline was ~120 parts per trillion (ppt) between 2000 and 2004, of which ~60 ppt was due to the decline of methyl chloroform and ~45 ppt due to methyl bromide. The CFCs together accounted for less than 23 ppt of the decline. The contribution of hydrochlorofluorocarbons (HCFCs) was to add 12 ppt.
- **Total tropospheric chlorine-containing chemicals (approximately 3.44 parts per billion (ppb) in 2004) continued to decrease.** Recent decreases (20 ppt/year or 0.59% in 2003-2004) have been at a slightly slower rate than decreases in earlier years (23 ppt/year or 0.64% in 1999-2000) primarily because of the reduced contribution from methyl chloroform. The declines in total chlorine (Cl) during 2000-2004 were slightly faster than projected for these years in the Ab scenario of the previous (2002) ozone assessment report (baseline scenario following the 1999 Beijing Amendments).
 - **Chlorofluorocarbons, consisting primarily of CFC-11, -12, and -113, accounted for 2.13 ppb (~62%) of total Cl in 2004 and accounted for a decline of 9 ppt of Cl from 2003-2004 (or nearly half of the total Cl decline in the troposphere over this period).** Atmospheric mixing ratios of CFC-12, which account for about one-third of the current atmospheric chlorine loading, have been constant within 1% (5 ppt) since 2000, and some in situ and Northern Hemisphere column (i.e., overhead) measurements show that peak values were attained in 2003. CFC-11 mixing ratios are decreasing at approximately 0.8%/year (1.9 ppt/year) and CFC-113 mixing ratios are decreasing at approximately 1%/year (0.8 ppt/year), which is twice as fast as in 1999-2000.
 - **Hydrochlorofluorocarbons (HCFCs), which are substitutes for CFCs, continue to increase in the atmosphere. HCFCs accounted for 214 ppt, or 6%, of total tropospheric chlorine in 2004 versus 180 ppt (5%) of total Cl in 2000.** HCFC-22 is the most abundant of the HCFCs and is currently (2000-2004) increasing at a rate of 4.9 ppt/year (3.2%/year). HCFC-141b and HCFC-142b mixing ratios increased by 1.1 ppt/year (7.6%/year) and 0.6 ppt/year (4.5%/year) over this same period, or at about half the rates found for these two gases in 1996-2000. The rates of increase for all three of these HCFC compounds are significantly slower than projected in the 2002 Ozone Assessment (6.6, 2.6, and 1.6 ppt/year for HCFC-22, HCFC-141b, and HCFC-142b, respectively).

¹ Equivalent effective stratospheric chlorine (EESC), a metric noted in the previous Assessment, has found widespread use. EESC is a gauge of the overall stratospheric burden of ozone-depleting halogen. It is derived from ground-based measurements of ozone-depleting substances, with consideration given to the number of chlorine and bromine atoms in ozone-depleting substances, the rates at which different ozone-depleting substances release their halogen once they reach the stratosphere, and the higher per-atom efficiency for bromine relative to chlorine in destroying ozone.

EXECUTIVE SUMMARY

- **Methyl chloroform has continued to decrease and contributed 13.5 ppt (or more than half) of the overall decline observed for total tropospheric Cl in 2003-2004.** It is currently still the largest contributor to the decline in tropospheric chlorine.
- **The stratospheric chlorine burden derived from ground-based total column and space-based measurements of inorganic chlorine is now in decline.** This is consistent with the decline in tropospheric chlorine from long-lived halocarbons. The burden of total stratospheric chlorine derived from satellite measurements agrees, within ± 0.3 ppb (about 12%), with the amounts expected from surface data when the delay due to transport is considered. The uncertainty in this burden is large relative to the expected chlorine contribution from shorter-lived gases.
- **Total organic tropospheric bromine from halons and methyl bromide peaked in about 1998 at 16.5 to 17 ppt and has since declined by 0.6-0.9 ppt (3-5%).** This observed decrease was solely a result of declines observed for methyl bromide. Bromine from halons continues to increase, but at slower rates in recent years (0.1 ppt Br/year in 2003-2004).
 - **Atmospheric amounts of methyl bromide declined beginning in 1999, when industrial production was reduced.** By mid-2004, mixing ratios had declined 1.3 ppt (14%) from the peak of 9.2 ppt measured before 1999. Reported production of methyl bromide for emissive uses decreased by 50% during this same period.
 - **Both the recently observed decline and the 20th century increase inferred for atmospheric methyl bromide were larger than expected.** Although industrial emissions of methyl bromide were thought to account for 20% (range 10-40%) of atmospheric methyl bromide during 1992-1998 (i.e., before production was reduced), observed concentrations are consistent with this fraction having been 30% (range 20-40%). This suggests that fumigation-related emissions could have a stronger influence on atmospheric methyl bromide mixing ratios than estimated in past Assessments, though uncertainties in the variability of natural emission rates and loss, and in the magnitude of methyl bromide banked in recent years, limit our understanding of this sensitivity.
 - **Mixing ratios calculated from updated emission estimates are in good agreement with the measurements for halon-1211, but they exceed all the halon-1301 measurements since 1980 by more than 10%.** Atmospheric increases in halon-1211 (0.06 ppt/year) in 2000-2004 were about half those in 1996-2000. It is currently unclear whether halon-1301 continues to increase.

EMISSION ESTIMATES

- **Global emissions of CFC-11 (88 Gg/yr, where 1 Gg = 10^9 grams), CFC-12 (114 Gg/yr), and CFC-113 (6 Gg/yr) in 2003 were approximately 25%, 25%, and 3% of their maximum values around 1986.** Emissions of CFC-11, CFC-12, and CFC-113 have all continued to decrease since 2000.
- **Regional emission estimates for CFCs, methyl chloroform, and carbon tetrachloride have been reported for the first time.** Differences between developed and developing regions are indicative of the differing schedules of phase-out. However, the patchiness in the present coverage (especially in developing regions such as Southeast Asia) and the uncertainties in the regional estimates mean that useful comparisons between summed regional emissions and global emissions derived from trends cannot currently be made. Regional emission estimates of methyl chloroform indicate that global emissions after 2000 may have been roughly 22 Gg/year, which is not statistically different from the estimate of 12.9 Gg/year (for 2002) obtained from industry/United Nations Environment Programme data.
- **While emissions of HCFC-22 have remained nearly constant from 2000 to 2004, emissions of HCFC-141b and HCFC-142b decreased by approximately 15% over the same period.**

- **Hydrofluorocarbon-23 (HFC-23) emissions estimated from atmospheric measurements have increased from about 6 Gg/yr in 1990 to about 13 Gg/yr in 2001 (an increase of approximately 120%).** These emissions are a byproduct of HCFC-22 production. HFC-23 mixing ratios (18 ppt in 2004) have continued to increase, at approximately 0.7 ppt/yr (4%/yr), in 2001-2004.

Halogenated Very Short-Lived Substances

- **Observations show that the total inorganic bromine (Br_y) in the stratosphere is more abundant than can be accounted for by the sum of bromine delivered to this region by “long-lived” brominated source gases.** Very short-lived substances (VSLS) are defined as trace gases whose local tropospheric lifetimes are comparable to or shorter than tropospheric transport time scales, such that their tropospheric distributions are non-uniform. Here, VSLS are considered to have atmospheric lifetimes of less than 6 months.
- **Various lines of evidence show that brominated VSLS contribute about 5 ppt (with estimates ranging from 3 to 8 ppt) to total stratospheric Br_y :**
 - The estimate of total stratospheric Br_y abundance existing in the late 1990s is about 18-25 ppt. This value is derived from different observations of bromine monoxide (BrO). This is greater than the 16-17 ppt of bromine delivered to the stratosphere by “long-lived” brominated source gases (i.e., the halons and methyl bromide, CH_3Br) during this period.
 - Measurements of organic brominated very short-lived source gases in the tropical upper troposphere amount to about 3.5 ppt. Compounds resulting from source gas degradation and other sources of tropospheric inorganic bromine may contribute comparable amounts.
- **Levels of total stratospheric bromine continue to show evidence for a trend that is consistent with that of tropospheric total bromine.** Further studies are required to determine if the recent decline in tropospheric bromine will be reflected in stratospheric bromine abundance.
- **It is unlikely that iodine is important for stratospheric ozone loss in the present-day atmosphere.** There is little evidence for measurable iodine in the form of iodine oxide (IO) in the lower stratosphere (i.e., about 0.1 ppt). This difference in behavior compared with bromine may be partly attributed to the short photochemical lifetime and lower abundances of iodine source gases, and aerosol uptake of iodine in the stratosphere.
- **The sum of the chlorine content from very short-lived source gases in the tropical upper troposphere is now estimated to be about 50 ppt.** While 50 ppt of inorganic chlorine (Cl_y) from VSLS would represent only 1-2% of Cl_y from long-lived source gases (~3500 ppt), it would represent a significant contribution to background Cl_y due only to naturally occurring methyl chloride (550 ppt). The value of 100 ppt for Cl_y from short-lived species in the previous Assessment also included a contribution of 50 ppt from phosgene.
- **The majority of known brominated and iodinated very short-lived source gases are predominantly of natural origin and are nearly unchanged in the past few decades,** as indicated by firn air studies. Some have small anthropogenic sources and have increased slightly in the Northern Hemisphere (e.g., certain brominated trihalomethanes) and a few are almost exclusively anthropogenic (notably n-propyl bromide (n-PB)).
- **Chlorinated very short-lived source gases originate largely from anthropogenic emissions,** although natural sources also contribute. There is evidence for significant recent declines in concentrations of some chlorinated very short-lived source gases, notably chloroform, dichloromethane, and tetrachloroethene.

EXECUTIVE SUMMARY

- **The route by which VSLS are most likely to reach the stratosphere is transport out of the boundary layer by deep convection in tropical regions (particularly if co-located with regions of high emissions over tropical oceans) followed by quasi-horizontal transport into the lower stratosphere.** The fraction of source gas and product gas transported into the stratosphere also depends on the local chemical lifetime, where source gases decompose, and the loss of product gases by heterogeneous processes involving aerosols and clouds.

Global Ozone (60°S-60°N)

TOTAL COLUMN OZONE

- **Global mean total column (i.e., overhead) ozone values for 2002-2005 were 3.5% below 1964-1980 average values.** The 2002-2005 values are similar to the 1998-2001 values. This behavior is evident in all available global datasets, although differences of up to 1% between annual averages exist between some individual sets.
- **There are differences between the two hemispheres in the evolution of total column ozone at midlatitudes:**
 - Averaged for the period 2002-2005, total column ozone for the Northern Hemisphere (NH) and Southern Hemisphere (SH) midlatitudes (35°-60°) are about 3% and 5.5%, respectively, below their 1964-1980 average values and are similar to their 1998-2001 values. The NH shows a minimum around 1993 followed by an increase. The SH shows an ongoing decrease through the late 1990s followed by the recent leveling off.
 - There are seasonal differences between the NH and the SH in ozone changes over midlatitudes. Changes since the pre-1980 period over northern midlatitudes (35°N-60°N) are larger in spring, whereas those over southern midlatitudes (35°S-60°S) are nearly the same throughout the year.
- **Total column ozone over the tropics (25°S-25°N) remains essentially unchanged.** These findings are consistent with the findings of the previous Assessments.

VERTICAL OZONE DISTRIBUTION

- **Upper stratospheric ozone declined during 1979-1995, but has been relatively constant during the last decade.** Measurements from Stratospheric Aerosol and Gas Experiment (SAGE I+II) and Solar Backscatter Ultraviolet spectrometer (SBUV(2)) satellite instruments show significant declines through 1995 when averaged over 60°N-60°S and altitudes of 35 to 50 km. The net ozone decrease was ~10-15% over midlatitudes, with smaller, but significant changes over the tropics. Available independent Umkehr, lidar, and microwave ozone measurements confirm these findings.
- **Lower stratospheric ozone declined over the period 1979-1995, but has been relatively constant with significant variability over the last decade.** At midlatitudes of both the Northern and Southern Hemispheres, measurements by the SAGE I+II and SBUV(2) satellite instruments showed declines of up to 10% by 1995 between 20 and 25 km altitude. These decreases did not continue in the last decade.
- **In the lowermost stratosphere of the Northern Hemisphere, between 12 and 15 km, a strong decrease in ozone was observed between 1979 and 1995, followed by an overall increase from 1996 to 2004 leading to no net long-term decrease at this level.** These changes in the lowermost stratosphere have a substantial influence on the column. The Southern Hemisphere midlatitude data do not show similar increases since 1995 at these altitudes.

UNDERSTANDING PAST CHANGES IN GLOBAL OZONE

- **There is good overall agreement between observed long-term changes in extrapolar ozone and model simulations that include the effects of increasing halogens.** The models generally reproduce the observed ozone changes as a function of altitude, latitude, and season, confirming our understanding that halogen changes are the main driver of global ozone changes. This link is supported by the statistical fit of globally averaged ozone observations with equivalent effective stratospheric chlorine (EESC; see footnote at the beginning of this section of the Executive Summary). However, there are discrepancies between the modeled and observed changes. Notably, the models tend to perform less well in simulating changes in the SH compared with the NH.
- **Empirical and model studies have shown that changes in tropospheric and stratospheric dynamics have been partially responsible for the observed NH midlatitude winter ozone decline from 1979 to the mid-1990s and the ozone increase thereafter.** Whether this is due to dynamical variability or results from a long-term trend in stratospheric circulation is not yet clear. Estimates of these dynamical effects on long-term trends range from ~20% up to 50% for the winter period.
- **The inclusion of additional inorganic bromine (Br_y) from very short-lived substances (VSLs) in models yields simulations with larger ozone destruction at midlatitudes and polar regions, compared with studies including only long-lived bromine source gases.** In both regions, the enhanced ozone loss occurs in the lower stratosphere via interactions of this bromine with anthropogenic chlorine. Midlatitude ozone loss is most enhanced during periods of high aerosol loading. Ozone loss through chemical reactions involving bromine and odd-hydrogen (HO_x) is also enhanced at midlatitudes under all conditions. The impact on long-term midlatitude ozone trends (1980-2004), assuming constant VSLs Br_y , is calculated to be small because aerosol loading was low at the start and end of this time period.
- **Several independent modeling studies confirm that dilution of ozone-depleted polar air makes a substantial contribution to midlatitude ozone depletion, especially in the Southern Hemisphere, where polar ozone loss is much larger.** Long-term annually averaged model-based estimates indicate that about one-third of the depletion in the Northern Hemisphere (with large interannual variation), and about one-half in the Southern Hemisphere, results from polar loss. This is supported by the observation that polar ozone depletion in the Antarctic spring is strongly correlated with southern summer midlatitude ozone depletion.
- **Identification of the solar cycle signal in observed ozone has been improved because of the absence of major volcanic eruptions over the past 15 years.** The deduced solar cycle variation in column ozone has a mean amplitude of 2-3% (from minimum to maximum) in low to midlatitudes from the extended data series.

Polar Ozone

ARCTIC

- **Arctic spring total ozone values over the last decade are lower than values observed in the 1980s, but somewhat larger than those in the 1990s; they are highly variable depending on dynamical conditions.** For current halogen levels, anthropogenic chemical loss and variability in ozone transport are about equally important for year-to-year Arctic ozone variability. Lower-than-average Arctic vortex temperatures result in larger halogen-driven chemical ozone losses.
- **For the “coldest” Arctic winters, the volume of air with temperatures low enough to support polar stratospheric clouds (called “ V_{PSC} ”) has increased significantly since the late 1960s.** This change is much larger than expected from the direct radiative effect of increasing greenhouse gas concentrations. The reason for the change is not clear, and it could be due to long-term natural variability or an unknown dynamical mechanism.

EXECUTIVE SUMMARY

- **Column ozone chemical loss in the 2004/2005 Arctic winter was among the largest ever diagnosed.** The 2004/2005 Arctic stratosphere was exceptionally cold, particularly at altitudes below 18 km, leading to a value of V_{PSC} 25% larger than the previous record value. Various independent studies and methods suggest that the chemical column ozone loss in 2004/2005 was among the largest ever observed.
- **The chemical loss of column ozone for Arctic winters exhibits a near-linear relation with V_{PSC} during each winter.** A similar relation between ozone loss and V_{PSC} is now seen for two independent analyses of chemical ozone loss, increasing our confidence in the robustness of this relation. Observations of the large Arctic ozone loss in 2004/2005 are in line with the relationship established for prior winters.

ANTARCTIC

- **Large Antarctic ozone holes continue to occur. The severity of Antarctic ozone depletion has not continued to increase since the late 1990s and, since 2000, ozone levels have been higher in some years.** These recent changes, evident to different degrees in different diagnostic measures, result from increased dynamical wave activity and not from decreases in ozone-depleting substances.
- **In September 2002, the first-ever observed major stratospheric sudden warming occurred in the Southern Hemisphere. This early spring warming caused a drastic reduction of the ozone hole area and resulted in a less severe ozone hole.** This warming resulted from anomalously strong dynamical wave activity in the Southern Hemisphere. The Antarctic winter of 2004 was also dynamically very active and had higher ozone levels than in previous years.

GENERAL

- **Large interannual variability in polar stratospheric temperatures complicates the interpretation of temperature trends.** Previously reported estimates of temperature trends in polar regions have differed from assessment to assessment. In retrospect, it is evident that temperature trends derived over time scales of 1-2 decades, though they may appear statistically significant, are not robust because of large interannual and decadal variability in observed temperatures. Therefore, changes in reported temperature trends do not necessarily indicate systematic changes in physical or chemical processes.
- **Calculated chemical loss rates of polar ozone substantially increase in models that assume: 1) more efficient ozone destruction by reactions involving two chlorine monoxide (ClO) molecules (referred to as the ClO dimer cycle) and 2) higher concentrations of bromine.** The higher concentrations of bromine are assumed because of new evidence that natural bromocarbons play a considerable role in the stratospheric bromine budget. More efficient ozone destruction by the ClO dimer cycle is supported by analyses of the first stratospheric observations of the ClO dimer. These two changes to models improve the comparison between measured and modeled Arctic ozone loss rates that was noted in the past Assessment. These changes also improve comparison between theory and observation of the timing of ozone loss over Antarctica.
- **For the first time, measurements show unambiguously that nitric acid trihydrate (NAT) polar stratospheric cloud (PSC) particles can nucleate above the ice frost point, and there is additional evidence of their widespread occurrence.** Widespread, low-number-density NAT clouds can lead to denitrification and enhanced ozone loss. Incorporating NAT nucleation above the ice frost point into chemical transport models has improved denitrification simulations, but discrepancies in interannual variability remain, probably because the NAT nucleation mechanisms are not fully understood.

Impact of Climate Change

- **The stratospheric cooling observed during the past two decades has slowed in recent years.**
 - Satellite and radiosonde measurements reveal an overall decrease in the global-mean lower stratospheric temperature of approximately 0.5 K/decade over the 1979-2004 period, with a slowdown in the temperature decline since the late 1990s. The overall temperature decrease is punctuated by transient warmings of the stratosphere associated with the major volcanic eruptions in 1982 and 1991. Consistent with the previous Assessment, model calculations indicate that the observed ozone loss is the predominant cause of the global-mean lower stratospheric cooling observed over this period.
 - The cooling of the lower stratosphere is evident at all latitudes. The annual-mean temperature in the Arctic lower stratosphere has decreased by approximately 1 K over the 1979-2004 period. There continues to be a large interannual variability in the winter and springtime, which makes it difficult to determine reliable trends in the Arctic lower stratosphere.
 - A considerable interannual variability in the temperature of the Antarctic lower stratosphere has become evident in recent years; this has reduced the estimate of the decadal-scale cooling trend in that region from that in the previous Assessment.
 - Satellite observations show large global-mean cooling trends in the upper stratosphere (1 to 2 K/decade over 1979-2004), but there is little additional decline since the middle 1990s. The conclusion of the previous Assessment, that the observed upper stratosphere trends are due to approximately similar contributions from decreases in ozone and increases in well-mixed greenhouse gases, is reaffirmed.
- **Future increases of greenhouse gas concentrations will contribute to the average cooling in the stratosphere.** Estimates derived from climate models (AOGCMs, coupled ocean-atmosphere general circulation models) and Chemistry-Climate Models (CCMs) with interactive ozone consistently predict continued cooling of the global average stratosphere. The predicted cooling rate within the next two decades is dependent on the prescribed scenario and the type of model used for the Assessment. At 50 hPa (an altitude of about 20 km), an average of all AOGCMs gives approximately 0.1 K/decade, while CCMs predict a larger cooling of about 0.25 K/decade caused by the interactive consideration of ozone changes. All models calculate a stronger cooling at 10 hPa (about 30 km), averaging approximately 0.5 K/decade. Simulations of polar temperatures in the future are less certain than global mean temperatures because of greater interannual variability.
- **Chemical reaction rates in the atmosphere are dependent on temperature, and thus the concentration of ozone is sensitive to temperature changes.** Decreases in upper stratospheric temperature slow the rate of photochemical ozone destruction in this region. Hence the concentration of upper stratospheric ozone increases in response to cooling. Cooling of the polar lower stratosphere would lead to more efficient chlorine activation on aerosols and polar stratospheric clouds, and enhanced ozone destruction. Therefore, the concentration of ozone in the springtime polar lower stratosphere would decrease in response to cooling.

INTERACTIONS BETWEEN STRATOSPHERE AND TROPOSPHERE

- **Changes to the temperature and circulation of the stratosphere affect climate and weather in the troposphere.** Consistent evidence for this coupling comes from both observational analyses and models, but the mechanisms responsible are not well understood. The dominant tropospheric response comprises changes in the strength of the midlatitude westerlies (the prevailing winds from the west). Observations and models suggest that Antarctic ozone depletion, through its effects on the lower stratospheric vortex, has contributed to the observed strengthening of tropospheric winds and Antarctic surface cooling during December-February.

EXECUTIVE SUMMARY

- **Updated datasets of stratospheric water vapor concentrations now show differences in long-term behavior.** Recent trend analyses, which are based on only two available multiyear datasets, cast doubt on the positive stratospheric water vapor trend that was noted in the previous Assessment. Balloonborne water vapor measurements at Boulder, Colorado, for the period 1980-2005 show a significant increase of 5-10% per decade over altitudes of 15-28 km. Global water vapor measurements from the Halogen Occultation Experiment (HALOE) satellite instrument for 1991-2005 do not show a corresponding positive lower stratospheric trend. Interannual water vapor changes derived from HALOE data exhibit quantitative agreement with temperature variations near the tropical tropopause. In contrast, the long-term increases inferred from the Boulder data are larger than can be explained by observed tropopause temperature changes or past increases in tropospheric methane.

The Ozone Layer in the 21st Century

- **The slowing of the decline and leveling off of midlatitude upper stratospheric (35-45 km) ozone over the past 10 years has very likely been dominated by changes in equivalent effective stratospheric chlorine (EESC).** Gas-phase chemistry, modulated by changes in temperature and other gases such as methane, directly controls ozone in this region, and observed ozone increases are similar to those modeled from EESC decreases.
- **Over the past 10 years, changes in EESC have likely contributed to the slowing of midlatitude total column ozone decline and the leveling off of column ozone.** Transport also has played an important role, particularly in the lowermost stratosphere, making attribution of ozone changes to solely EESC difficult. For northern midlatitudes, increases in ozone have been greater than expected from EESC decreases alone; whereas over southern midlatitudes, ozone changes are more consistent with the range expected from EESC decreases.
- **The decline in EESC has not caused the large annual variations observed in Arctic ozone depletion.** Indeed, the onset of ozone recovery in the Arctic has not been detected. The large interannual variations driven by changes in meteorology are likely to preclude the detection of the first stage of recovery.

MODEL PROJECTIONS

Two-dimensional models and three-dimensional coupled Chemistry-Climate Models (CCMs), both of which incorporate many of the factors that affect ozone as well as their feedbacks, have been used in this Assessment to make projections of the evolution of ozone throughout the 21st century. The model projections guiding the conclusions below were based on the surface time series of halocarbons from the “Ab” scenario (baseline scenario following the Beijing Amendments) from the 2002 ozone assessment, as well as the well-mixed greenhouse gas concentrations from the Third Assessment Report of the Intergovernmental Panel on Climate Change, *Climate Change 2001: The Scientific Basis*. To focus on long-term changes, the projected ozone anomalies have been decadal smoothed.

- **The CCMs used to project future ozone abundances have been critically evaluated and more emphasis has been given to those models that best represent the processes known to strongly affect column ozone abundances.** The CCMs vary in their skill in representing different processes and characteristics of the atmosphere. However, there is sufficient agreement between the majority of the CCMs and the observations, so that some confidence can be placed in their projections.
- **Averaged over 60°S to 60°N, total column ozone is projected to increase by 1% to 2.5% between 2000 and 2020, reaching 1980 values at the same time or before EESC in that region declines to 1980 values (2040-2050). By 2100, ozone should be up to 5% above 1980 values.** Both two-dimensional models and CCMs suggest that minimum total column ozone values have already occurred in this region. Ozone exceeds pre-1980 values at the time EESC returns to 1980 values in nearly all models that include coupling between well-mixed greenhouse gases and temperature (interactive two-dimensional models and the CCMs). Similarly the elevated ozone levels in 2100 are observed in all interactive two-dimensional models and in the one CCM that extended to 2100.

- **Antarctic springtime ozone is projected to increase by 5% to 10% between 2000 and 2020, reaching 1980 values close to when Antarctic EESC decreases to 1980 values (2060-2075), and changing little thereafter.** Different diagnostic indicators of ozone depletion show different sensitivities to EESC. The most rapid change (decrease) occurs in the ozone mass deficit and the slowest change (increase) occurs in ozone minimum values and October ozone anomalies. Minimum ozone values remain roughly constant between 2000 and 2010 in many models. The projected onset of decreases in the ozone mass deficit occurs between 2000 and 2005, whereas the projected onset of increases in minimum Antarctic ozone does not occur until after 2010 in many models.
- **Arctic springtime ozone is projected to increase by 0% to 10% between 2000 and 2020, reaching 1980 values much earlier than when Arctic EESC decreases to 1980 values (2060-2070). By 2100, Arctic ozone is projected to be substantially above 1980 values.** While the large interannual variability in projected Arctic ozone obscures the date when the ozone turnaround due to decreasing EESC occurs, this is projected to occur before 2020. The increase in Arctic ozone does not follow EESC as closely as in the Antarctic, and in the majority of CCMs, Arctic ozone exceeds 1980 values before the Antarctic. There is no indication of future large decreases in Arctic column ozone in any of the model simulations. There is large uncertainty in predictions of Arctic ozone because of the smaller ozone depletion and the larger interannual variability in the Arctic stratosphere.
- **The projected ozone in 2100 is sensitive to future levels of the well-mixed greenhouse gases.** For example, expected future increases in nitrous oxide (N_2O) will increase stratospheric nitrogen oxides (NO_x), which may exacerbate ozone depletion. However, the expected stratospheric cooling induced by increasing concentrations of greenhouse gases, primarily carbon dioxide (CO_2), is expected to slow gas-phase ozone depletion reactions and, thereby, increase ozone. The net effect on ozone amounts will depend on future levels of the different well-mixed greenhouse gases. The importance of this temperature feedback is demonstrated by the non-interactive two-dimensional models, which predict that extrapolar column ozone will be less than or near 1980 values through the latter half of the century.
- **Human activities are expected to affect stratospheric ozone through changes in tropospheric emissions of trace gases.** Enhanced methane (CH_4) emission (from wetter and warmer soils) is expected to enhance ozone production in the lower stratosphere, whereas an increase in nitrous oxide emission (from extended use of artificial fertilizer) is expected to reduce ozone in the middle and high stratosphere. Also, changes in non-methane hydrocarbons and NO_x emissions are expected to affect the tropospheric concentrations of hydroxyl radical (OH) and, hence, impact the lifetimes and concentrations of stratospheric trace gases such as CH_4 and organic halogen species.
- **Future changes of stratospheric water vapor concentrations are uncertain.** If water vapor concentrations increase in the future, there will be both a radiative and a chemical effect. Modeling studies suggest increased water vapor concentrations will enhance odd hydrogen (HO_x) in the stratosphere and subsequently influence ozone depletion. Increases in water vapor in the polar regions would raise the temperature threshold for the formation of polar stratospheric clouds, potentially increasing springtime ozone depletion.

UV Radiation and Its Changes

- **Some unpolluted sites show that UV radiation has been decreasing since the late 1990s. However, at some midlatitude stations in the Northern Hemisphere, surface UV irradiance continued to increase at rates of a few percent per decade.** The observed increases and their significance depend on location, wavelength range, and the period of measurements. These increases cannot be explained solely by ozone depletion and could be attributed to a decreasing tendency in aerosol optical extinction and air pollution since the beginning of the 1990s and partly to decreasing cloudiness, as estimated from satellites.

EXECUTIVE SUMMARY

- **Tropospheric aerosols are responsible for the overestimation of UV irradiance from satellite instruments (e.g., TOMS, the Total Ozone Mapping Spectrometer) that use solar backscattered ultraviolet radiation to derive surface UV irradiance.** At clean sites the agreement with ground-based measurements is good. However, over more polluted locations the bias can be as large as 40%, because the lowermost atmosphere containing the absorbing aerosols is not adequately probed by the measurements. The presence of clouds and snow or ice cover can also lead to significant biases. New algorithms have been developed to improve the parameterization of aerosol, snow, and ice effects on satellite-derived surface UV irradiance, as well as of cloud effects using Advanced Very High Resolution Radiometer (AVHRR) and Meteosat images, showing on average good agreement with ground-based UV observations. Although the TOMS instrument is no longer available, the continuity of satellite-derived global UV data is maintained with the new Ozone Monitoring Instrument (OMI) onboard the Aura satellite.
- **Clouds are the major factor limiting the detectability of long-term changes in UV radiation due to ozone changes or other factors.** Even if ozone trends were linear, at least 10-15 years of measurements would be needed for detecting a trend in UV radiation. At most extrapolar locations, the effects on UV-B radiation from ozone depletion are relatively small, and the influence of clouds is dominant.
- **Air pollutants may counterbalance the UV radiation increases resulting from ozone depletion.** Observations confirm that UV-absorbing air pollutants in the lower troposphere, such as ozone, nitrogen dioxide (NO₂) and sulfur dioxide (SO₂), attenuate surface UV irradiance by up to ~20%. This effect is observed at locations near the emission sources. Air pollution exerts stronger attenuation in UV compared with attenuation in total solar irradiance.

Ozone Depletion Potentials and Global Warming Potentials

- **The effectiveness of bromine compared with chlorine for global ozone depletion (on a per-atom basis), typically referred to as α , has been re-evaluated upward from 45 to a value of 60.** The calculated values from three independent two-dimensional models range between 57 and 73, depending on the model used and depending on the assumed amount of additional bromine added to the stratosphere by very short-lived substances.
- **Ozone Depletion Potentials (ODPs) have been re-evaluated, with the most significant change being a 33% increase for bromocarbons due to the update in the estimate for the value of α .** A calculation error in the previous ozone assessment leading to a 13% overestimate for the ODP of halon-1211 has been corrected.
- **Direct and indirect Global Warming Potentials (GWPs) have been updated. The direct GWPs were revised for changes in radiative efficiencies of HFC-134a, carbon tetrafluoride (CF₄), HFC-23, HFC-32, HFC-227ea, and nitrogen trifluoride (NF₃), as well as changes in the lifetimes of trifluoromethylsulfurpentafluoride (SF₅CF₃) and methyl chloride (CH₃Cl).** In addition, the direct GWPs for all compounds are affected by slight decreases in the CO₂ absolute Global Warming Potentials for various time horizons. Indirect GWPs have been updated primarily to reflect the later return of ozone-depleting substances to 1980 levels estimated in this Assessment compared with the earlier Assessment and to account for the increased bromine efficiency factor.

IMPLICATIONS FOR POLICY FORMULATION

The results from over three decades of research have provided a progressively better understanding of the interaction of human activity and the ozone layer. New policy-relevant insights into the roles of ozone-depleting gases have been conveyed to decisionmakers through a series of international state-of-understanding assessment reports. The research findings in the *Scientific Assessment of Ozone Depletion: 2006* that are given above and are summarized here provide direct current scientific input to governmental, industrial, and other policy decisions associated with protection of the ozone layer:

- **Our basic understanding that anthropogenic ozone-depleting substances have been the principal cause of the ozone depletion over the past decades has been strengthened.**
- **The Montreal Protocol is working: There is clear evidence of a decrease in the atmospheric burden of ozone-depleting substances and some early signs of stratospheric ozone recovery. As noted earlier in this Executive Summary:**
 - Abundances of ozone-depleting substances, taken together, are clearly decreasing in the lower atmosphere. Nearly all the abundances of individual ozone-depleting substances are also decreasing.
 - There are clear indications that the equivalent effective stratospheric chlorine (which is a standardized measure of ozone-depleting capacity of bromine and chlorine in the stratosphere; see footnote in the previous section of this Executive Summary) has also started to decrease.
 - In the last decade, the depletion of the global ozone layer has not worsened.
 - Measurements from some unpolluted locations show that UV radiation has decreased since the late 1990s, in accordance with observed ozone increases at those sites.
- **The unusually small 2002 Antarctic ozone hole was characterized by a smaller area and higher ozone levels than observed during the past decade.** This was due to an unusually strong meteorological event (a “major stratospheric sudden warming”) and was not due to changes in ozone-depleting gases. The 2003 and 2005 ozone holes exhibited severe depletions as observed since the early 1990s. Severe Antarctic ozone losses will very likely continue to be observed for at least the next 10-20 years because of the expected slow decline of the long-lived ozone-depleting gases.
- **Bromine is now estimated to be approximately 60 times as effective as chlorine in global ozone depletion, on a per-atom basis.** This value is larger than the effectiveness of 45 used in the 2002 Assessment. This increase in the effectiveness of bromine increases the Ozone Depletion Potential of bromine-containing compounds, evaluated using the semi-empirical method that has been used in previous Assessments.
- **Long-term recovery of the ozone layer from the effects of ozone-depleting substances is expected to span much of the 21st century and is estimated to occur later than projected in the previous Assessment (2002).** An important milestone in the recovery process is the time when combined chlorine and bromine amounts (equivalent effective stratospheric chlorine, EESC) decline to pre-1980 values.
 - The date when equivalent effective stratospheric chlorine at midlatitudes returns to pre-1980 levels is now calculated to be 2049, for the case of global compliance with the Montreal Protocol with no significant exceptions (Scenario A1). This date is about 5 years later than projected in the previous (2002) Assessment. This projected later date primarily results from (i) an increase in CFC-11 and CFC-12 emissions due to the larger recent estimates of amounts currently contained in equipment and products (banks) and (ii) an increase in HCFC-22 emissions due to larger estimated future production, as reported in the 2005 Intergovernmental Panel on Climate Change/Technology and Economic Assessment Panel (IPCC/TEAP) Special Report on *Safeguarding the Ozone Layer and the Global Climate System: Issues Related to Hydrofluorocarbons and Perfluorocarbons*.
 - The return to pre-1980 conditions of equivalent effective stratospheric chlorine for the Antarctic vortex is projected to occur around 2065, more than 15 years later than the return of midlatitude equivalent effective stratospheric chlorine to pre-1980 levels. This projected later recovery is because, unlike in previous Assessments, we now recognize that the age of air is greater in the Antarctic lower stratosphere, which affects the amount of ozone-depleting gases available for ozone depletion. The equivalent effective stratospheric chlorine evaluation for the Antarctic vortex has not been presented in previous Ozone Assessments.

EXECUTIVE SUMMARY

- Potential options for accelerating the recovery of the ozone layer have been evaluated.** The table provided below shows hypothetical estimates of the *upper limits* of improvements that could be achieved if global anthropogenic *production* of ozone-depleting substances were to stop after 2006, if emissions were eliminated from existing banks at the end of 2006, or if global anthropogenic *emissions* of ozone-depleting substances were to stop after 2006. Some options show greater effectiveness for accelerating recovery of the ozone layer than in previous Assessments, for reasons noted below.

Table 1. Percentage reductions in integrated equivalent effective stratospheric chlorine relative to the baseline (A1) scenario that can be achieved in the hypothetical cases. ¹

Compound or Compound Group	Column A: All Emissions Eliminated from Production after 2006	Column B: All Emissions Eliminated from Existing Banks at End of 2006	Column C: All Emissions Eliminated after 2006
Chlorofluorocarbons (CFCs)	0.3	11	11
Halons	0.5	14	14
Carbon tetrachloride (CCl ₄)	3	(a)	3
Methyl chloroform (CH ₃ CCl ₃)	0.2	(a)	0.2
Hydrochlorofluorocarbons (HCFCs)	12	4	16
Methyl bromide (CH ₃ Br) (anthropogenic)	5	(a)	5

¹ Column A corresponds to a hypothetical elimination of all emissions from production after 2006. Column B corresponds to a hypothetical elimination of all emissions from banks existing at the end of 2006 (for example, capture and destruction). Column C corresponds to a hypothetical elimination of all emissions after 2006 and is approximately equal to the sum of columns A and B.

(a) For these compounds, banks are uncertain and therefore emissions are equated to production in these calculations.

- The percentage cumulative (integrated) reductions in equivalent effective stratospheric chlorine for halons and CFCs, integrated from 2007 until the 1980 level is reattained (shown in Column B), are larger than previously reported. This is because recent bank estimates from the 2005 Intergovernmental Panel on Climate Change/Technology and Economic Assessment Panel (IPCC/TEAP) Special Report on *Safeguarding the Ozone Layer and the Global Climate System: Issues Related to Hydrofluorocarbons and Perfluorocarbons* are significantly larger and likely more reliable than values presented in previous Assessments for CFC-11, CFC-12, and halon-1211.
- The percentage reduction in integrated equivalent effective stratospheric chlorine for HCFCs shown in Column A is larger than previously reported. This is because of significantly larger estimates of future HCFC-22 production in Article-5 countries.
- The percentage reduction in integrated equivalent effective stratospheric chlorine for methyl bromide in Column A is larger than previously reported. This is because of the upward revision of the fraction of anthropogenic emissions relative to total methyl bromide emissions, as well as being due to the upward revision in the ozone-depletion effectiveness of bromine atoms compared with chlorine atoms mentioned earlier.
- In addition to the percentage reductions in integrated equivalent effective stratospheric chlorine, these scenarios can reduce the time for equivalent effective stratospheric chlorine to drop below 1980 values. A hypothetical elimination of all emissions of ozone-depleting substances after 2006 (Column C) would advance this time by about 15 years, from 2049 to 2034. A hypothetical elimination of all emissions from production of ozone-depleting substances after 2006 (Column A) would advance it by about 6 years, to 2043.

- A methyl bromide phase-out has been in effect since 2005 in developed countries, with critical-use exemptions granted in 2005 and 2006 at levels that are 30-40% of the 2003-2004 production levels. Two additional hypothetical cases of critical and quarantine and pre-shipment (QPS) exempted uses of methyl bromide were considered. In the analysis of both cases, equivalent effective stratospheric chlorine is integrated above the 1980 level from 2007 until it returns to the 1980 level. The size of the critical use exemptions is similar to the estimated use of methyl bromide for QPS use.
 - > If critical-use methyl bromide exemptions continue indefinitely at the 2006 level compared to a cessation of these exemptions in 2010 or 2015, midlatitude integrated equivalent effective stratospheric chlorine would increase by 4.7% or 4.0%, respectively.
 - > If production of methyl bromide for QPS use were to continue at present levels and cease in 2015, midlatitude integrated equivalent effective stratospheric chlorine would decrease by 3.2% compared with the case of continued production at present levels.
- **Failure to comply with the Montreal Protocol would delay, or could even prevent, recovery of the ozone layer.** Emissions associated with continued or expanded exemptions, QPS, process agents, and feedstocks may also delay recovery.
- **The role of very short-lived halogenated substances in stratospheric ozone depletion is now believed to be of greater importance than previously assessed.** This suggests that significant anthropogenic production of such substances could enhance ozone depletion. Current understanding of the Ozone Depletion Potentials of these classes of substances is:
 - The Ozone Depletion Potentials of n-propyl bromide are 0.1 for tropical emissions and 0.02-0.03 for emissions restricted to northern midlatitudes. These are unchanged from the previous Assessment.
 - New analyses suggest upper-limit Ozone Depletion Potentials for CF₃I of 0.018 for tropical emissions and 0.011 for midlatitude emissions. The previous Assessment had an upper limit of 0.008.
 - Any chlorinated very short-lived source gas with a lifetime of ~25 days, one chlorine atom, and a similar molecular weight to CFC-11, has an Ozone Depletion Potential of about 0.003.
- **Understanding the interconnections between ozone depletion and climate change is crucial for projections of future ozone abundances.** The ozone-depleting substances and many of their substitutes are also greenhouse gases; changes in ozone affect climate; and changes in climate affect ozone. These issues were recently the subject of the IPCC/TEAP 2005 Special Report on *Safeguarding the Ozone Layer and the Global Climate System: Issues Related to Hydrofluorocarbons and Perfluorocarbons*, and some aspects of the coupling between ozone depletion and climate change have been considered in this 2006 Ozone Assessment. An important development has been the emerging use of three-dimensional models that incorporate the interaction between chemistry and climate.

World Meteorological Organization

7 bis, avenue de la Paix
Case postale No. 2300
CH-1211, Geneva 2
Switzerland

United Nations Environment Programme

Ozone Secretariat
P.O. Box 30552
Nairobi 00100
Kenya

U.S. Department of Commerce National Oceanic and Atmospheric Administration

14th Street and Constitution Avenue NW
Herbert C. Hoover Building, Room 5128
Washington, DC 20230
USA

National Aeronautics and Space Administration Earth Science Division

NASA Headquarters
300 E Street SW
Washington, DC 20546-0001
USA

European Commission Directorate-General for Research

B-1049 Bruxelles
Belgium

Published in March 2007

ISBN: 978-92-807-2756-2

OZO/0872/NA

Copies of this report are available from:

WORLD METEOROLOGICAL ORGANIZATION

7 bis, avenue de la Paix
Case postale No. 2300
CH-1211, Geneva 2
Switzerland

*Photo of Gérard Mégie courtesy of the Centre
National de la Recherche Scientifique library.*

This report can be viewed on the World Wide Web at the following locations:

<http://www.wmo.ch/web/arep/ozone.html>

http://ozone.unep.org/Assessment_Panels/SAP/Scientific_Assessment_2006/index.asp

<http://esrl.noaa.gov/csd/assessments>

Citation for the whole report:

WMO (World Meteorological Organization), *Scientific Assessment of Ozone Depletion: 2006*, Global Ozone Research and Monitoring Project—Report No. 50, 572 pp., Geneva, Switzerland, 2007.

Example chapter citation:

Daniel, J.S., and G.J.M. Velders (Lead Authors), A.R. Douglass, P.M.D. Forster, D.A. Hauglustaine, I.S.A. Isaksen, L.J.M. Kuijpers, A. McCulloch, and T.J. Wallington, Halocarbon scenarios, ozone depletion potentials, and global warming potentials, Chapter 8 in *Scientific Assessment of Ozone Depletion: 2006*, Global Ozone Research and Monitoring Project—Report No. 50, 572 pp., World Meteorological Organization, Geneva, Switzerland, 2007.

CHAPTER 1

Long-Lived Compounds

Lead Authors:

C. Clerbaux
D.M. Cunnold

Coauthors:

J. Anderson
A. Engel
P.J. Fraser
E. Mahieu
A. Manning
J. Miller
S.A. Montzka
R. Nassar
R. Prinn
S. Reimann
C.P. Rinsland
P. Simmonds
D. Verdonik
R. Weiss
D. Wuebbles
Y. Yokouchi

Contributors:

P. Bernath
D. Blake
T. Blumenstock
J. Butler
P.-F. Coheur
G. Dutton
D. Etheridge
L. Froidevaux
P. Krummel
J. Mühle
S. O'Doherty
D. Oram
E. Remsberg
R. Rhew
J.M. Russell III
C. Trudinger
D. Waugh
R. Zander

CHAPTER 1

LONG-LIVED COMPOUNDS

Contents

SCIENTIFIC SUMMARY	1.1
1.1 INTRODUCTION	1.5
1.2 HALOGENATED OZONE-DEPLETING GASES IN THE ATMOSPHERE	1.7
1.2.1 Updated Atmospheric Observations of Ozone-Depleting Gases	1.7
1.2.1.1 Chlorofluorocarbons (CFCs)	1.7
1.2.1.2 Hydrochlorofluorocarbons (HCFCs)	1.10
1.2.1.3 Halons	1.12
1.2.1.4 Carbon Tetrachloride (CCl ₄)	1.14
1.2.1.5 Methyl Chloroform (CH ₃ CCl ₃)	1.14
1.2.1.6 Methyl Chloride (CH ₃ Cl)	1.15
1.2.1.7 Methyl Bromide (CH ₃ Br)	1.18
1.2.2 Lifetimes	1.22
1.2.2.1 Halocarbon Lifetime Updates and Variability	1.22
1.2.2.2 Uncertainties in Ozone-Destroying Halocarbon Lifetimes	1.22
1.2.3 Total Atmospheric Chlorine and Bromine	1.27
1.2.3.1 Total Organic Chlorine in the Troposphere	1.27
1.2.3.2 Total Chlorine in the Stratosphere and Hydrogen Chloride (HCl)	1.27
1.2.3.3 Organic Bromine in the Troposphere from Methyl Bromide and Halons	1.32
1.2.4 Effective Equivalent Chlorine and Equivalent Effective Stratospheric Chlorine	1.33
1.2.5 Fluorine in the Stratosphere	1.35
1.2.5.1 Total Stratospheric Fluorine and Hydrogen Fluoride (HF) at 55 km	1.35
1.2.5.2 Total and Stratospheric Column Inorganic Fluorine	1.36
1.3 EMISSIONS ESTIMATED FROM THE HALOCARBON MEASUREMENTS	1.38
1.3.1 Regional Emissions and Inverse Modeling	1.38
1.3.2 Global Emissions	1.41
1.3.2.1 CFCs	1.41
1.3.2.2 HCFCs	1.44
1.3.2.3 Halons	1.44
1.3.2.4 Carbon Tetrachloride	1.45
1.3.2.5 Methyl Chloroform	1.45
1.4 OTHER TRACE GASES	1.46
1.4.1 Carbon Dioxide (CO ₂)	1.46
1.4.2 Methane (CH ₄), Including Isotopic Data	1.47
1.4.3 Nitrous Oxide (N ₂ O)	1.47
1.4.4 Hydrofluorocarbons (HFCs)	1.48
1.4.4.1 HFC-134a	1.48
1.4.4.2 HFC-23	1.48
1.4.4.3 HFC-143a, HFC-125, and HFC-152a	1.49
1.4.5 Perfluorocarbons, Sulfur Hexafluoride (SF ₆), and SF ₅ CF ₃	1.49
1.4.5.1 CF ₄ and CF ₃ CF ₃	1.49
1.4.5.2 CF ₃ CF ₂ CF ₃ and c-C ₄ F ₈	1.50
1.4.5.3 SF ₆	1.51
1.4.5.4 SF ₅ CF ₃	1.51
REFERENCES	1.52

SCIENTIFIC SUMMARY

- **The fully amended and revised Montreal Protocol is continuing to be very successful in reducing the emissions and atmospheric abundances of most ozone-destroying gases. By 2005, the total combined abundance of anthropogenic ozone-depleting gases in the troposphere had decreased by 8-9% from the peak value observed in the 1992-1994 time period.**

Tropospheric Chlorine

- **Total tropospheric chlorine-containing chemicals (approximately 3.44 parts per billion (ppb) in 2004) continued to decrease.** Recent decreases (–20 parts per trillion per year (ppt/yr) or –0.59% in 2003-2004) have been at a slightly slower rate than in earlier years (–23 ppt/yr or –0.64% in 1999-2000) primarily because of the reduced contribution from methyl chloroform. The declines in total chlorine (Cl) during 2000-2004 were slightly faster than projected for these years in the Ab (most likely, or baseline) scenario of the previous (2002) Assessment (WMO, 2003).
- **Chlorofluorocarbons (CFCs), consisting primarily of CFC-11, -12, and -113, accounted for 2.13 ppb (~62%) of total Cl in 2004 and accounted for a decline of 9 ppt Cl from 2003-2004 (or nearly half of the total Cl decline in the troposphere over this period).** Atmospheric mixing ratios of CFC-12, which account for about one-third of the current atmospheric chlorine loading, have been constant within 1% (5 ppt) since 2000, and some in situ and Northern Hemisphere column measurements show that peak values were attained in 2003. CFC-11 mixing ratios are decreasing at approximately 0.8%/yr (1.9 ppt/yr) and CFC-113 mixing ratios are decreasing by approximately 1%/yr (0.8 ppt/yr), which is twice as fast as in 1999-2000.
- **Hydrochlorofluorocarbons (HCFCs), which are substitutes for CFCs, continue to increase in the atmosphere. HCFCs accounted for 214 ppt or 6% of total tropospheric chlorine in 2004 versus 180 ppt of Cl (5% of total Cl) in 2000.** HCFC-22 is the most abundant of the HCFCs and is currently (2000-2004) increasing at a rate of 4.9 ppt/yr (3.2%/yr). HCFC-141b and HCFC-142b mixing ratios increased by 1.1 ppt/yr (7.6%/yr) and 0.6 ppt/yr (4.5%/yr) over this same period or at about half the rates found for these two gases in 1996-2000. The rates of increase for all three of these HCFC compounds are significantly slower than projected in the previous Assessment (6.6, 2.6, and 1.6 ppt/yr for HCFC-22, HCFC-141b, and HCFC-142b, respectively) (WMO, 2003). HCFC-123 and -124 are currently measured, but contribute less than 1% to total chlorine from HCFCs.
- **Methyl chloroform (CH₃CCl₃) has continued to decrease and contributed 13.5 ppt (or more than half) of the overall decline observed for total tropospheric Cl in 2003-2004. It is currently still the largest contributor to the decline in tropospheric chlorine.** Globally averaged surface mixing ratios were 22.6 ppt in 2004 versus 46.4 ppt in 2000.
- **An imbalance exists between the emissions inferred from the atmospheric measurements and the emissions needed to account for the stratospheric and ocean sinks and the more recently discovered soil sink of CCl₄.** CCl₄ continues to decline at an approximately steady rate of 1 ppt/yr (about 1%/yr).
- **The globally averaged abundance of methyl chloride of 550 ± 30 ppt is the same as that given in the previous Assessment, and there has been no consistent trend in the atmospheric values in recent years.** Mixing ratios at midlatitudes of the two hemispheres are 5-10% lower than the high values measured in 1997-1998 (which were probably related to large-scale effects of forest fires). Firm air measurements show an increase of approximately 50 ppt (10%) from 1940 to 1990.

Stratospheric Chlorine and Fluorine

- **The stratospheric chlorine burden derived by the ground-based total column and space-based measurements of inorganic chlorine is now in decline. This is consistent with the decline in tropospheric chlorine from long-lived halocarbons (CFCs, carbon tetrachloride, methyl chloroform, HCFCs, methyl chloride, and halon-1211).** The burden of total stratospheric chlorine derived from satellite measurements agrees, within ±0.3 ppb (about 12%), with the amounts expected from surface data when the delay due to transport is considered. The uncertainty in this burden is large relative to the expected chlorine contribution from shorter-lived gases (0.05 to 0.1 ppb, see Chapter 2).

LONG-LIVED COMPOUNDS

- **Column and satellite measurements of hydrogen fluoride continued to show the reduction in the upward trend that began in the late 1990s.** This reduction is consistent with the change in tropospheric fluorine burden derived from CFCs, HCFCs, and hydrofluorocarbons (HFCs).

Total Tropospheric Bromine

- **Total organic bromine from halons and methyl bromide (CH₃Br) peaked in about 1998 at 16.5 to 17 ppt and has since declined by 0.6 to 0.9 ppt (3 to 5%).** This observed decrease was solely a result of declines observed for methyl bromide. Bromine (Br) from halons continues to increase, but at slower rates in recent years (+0.1 ppt Br/yr in 2003-2004).
- **Atmospheric amounts of methyl bromide declined beginning in 1999, when industrial production was reduced.** By mid-2004, mixing ratios had declined 1.3 ppt (14%) from the peak of 9.2 ppt measured before 1999. Reported production of methyl bromide for emissive uses decreased by 50% during this same period.
- **Both the recently observed decline and the 20th-century increase inferred for atmospheric methyl bromide were larger than expected.** Although industrial emissions of methyl bromide were thought to account for 20 (10-40)% of atmospheric methyl bromide during 1992-1998 (i.e., before production was reduced), the observations are consistent with this fraction having been 30 (20-40)%. This suggests that fumigation-related emissions could have a stronger influence on atmospheric methyl bromide mixing ratios than estimated in past Assessments, though uncertainties in the variability of natural emission rates and loss, and in the magnitude of methyl bromide banked in recent years, influence our understanding of this sensitivity.
- **Mixing ratios calculated from updated emission estimates are in good agreement with the measurements for halon-1211 but they exceed all the halon-1301 measurements since 1980 by more than 10%.** Atmospheric increases in halon-1211 (0.06 ppt/yr or 1%/yr) in 2000-2004 were about half those in 1996-2000. It is currently unclear whether atmospheric mixing ratios of halon-1301 continue to increase.

Equivalent Effective Stratospheric Chlorine (EESC) and Effective Equivalent Chlorine (EECI)

- **The decrease in EECI over the past 10 years has been 20% of what would be needed to return EECI values to those in 1980 (i.e., before the Antarctic stratospheric ozone hole).** EECI has decreased at a mean rate of 29 ppt EECI per year from 1994 to 2004 in the lower atmosphere. This amounts to a total decline of 277 ppt or 8-9% for EECI over this period. The reduction in stratospheric EESC is somewhat less because it takes a few years for near-surface trends to be reflected in the stratosphere. These declines are slightly larger than projected in the previous Assessment primarily because of the decline in methyl bromide.
- **The decline in the short-lived methyl chloroform and methyl bromide contributed the most to the decline in the effective equivalent chlorine in the atmosphere.** The total decline was about 120 ppt between 2000 and 2004, of which about 60 ppt was due to the decline of methyl chloroform and about 45 ppt due to methyl bromide. The CFCs together accounted for less than 23 ppt of this decline. The contribution of HCFCs was 12 ppt in the other direction, i.e., an increase.

Emission Estimates

- **Global emissions of CFC-11 (88 Gg/yr), CFC-12 (114 Gg/yr), and CFC-113 (6 Gg/yr) in 2003 were approximately 25%, 25%, and 3% of their maximum values around 1986.** Emissions of CFC-11, CFC-12 and CFC-113 have all continued to decrease since 2000.
- **Reported regional emission estimates for CFCs, methyl chloroform, and CCl₄ have been summed for the first time.** Differences between developed and developing regions are indicative of the differing schedules of phase-out. However, the patchiness in the present coverage (especially in developing regions such as Southeast Asia) and the uncertainties in the regional estimates, mean that useful comparisons between summed regional emissions and global emissions derived from trends cannot currently be made. Regional emission estimates of methyl chloroform indicate that global emissions after 2000 may have been roughly 22 Gg/yr, which is not statistically different from the estimate of 12.9 Gg/yr (for 2002) obtained from industry/United Nations Environment Programme data.

- **While emissions of HCFC-22 have remained nearly constant from 2000 to 2004, emissions of HCFC-141b and HCFC-142b decreased by approximately 15% over the same period.**
- **HFC-23 emissions estimated from atmospheric measurements have increased from about 6 Gg/yr in 1990 to about 13 Gg/yr in 2001 (an increase of approximately 120%).** These emissions are a byproduct of HCFC-22 production.

Hydrofluorocarbons (HFCs)

- **The atmospheric abundances of all measured HFCs are increasing due to their rapid introduction as CFC and HCFC replacements.** HFC-134a concentrations reached 30 ppt in 2004 and are increasing at 3.9 ppt/yr (13%/yr). Globally averaged concentrations of HFC-125 and HFC-152a were both approximately 3.1 ppt in 2004, increasing by about 23%/yr and 17%/yr, respectively. HFC-23 mixing ratios in the Southern Hemisphere were 18 ppt in 2004, having increased at a mean rate of 0.7 ppt/yr (4%/yr) in 2001-2004.

Sulfur Hexafluoride (SF₆)

- **Measurements of SF₆ suggest its global average concentration in 2003 was 5.2 ppt and it was growing by 0.23 ppt/yr (4%/yr).** Similar percentage rates of increase have been estimated from column measurements over Switzerland. Temporal extrapolation of the past 20 years of measurements results in significantly smaller atmospheric concentrations in the future than those produced in the most likely emission scenario from the previous Assessment.

1.1 INTRODUCTION

Ozone depletion observed in the stratosphere over the past three decades has resulted from the accumulation of trace gases in the atmosphere. This was due to industrial activities and to a much-reduced extent to agricultural practices, which led to increases in the concentrations of chlorine, bromine, nitrogen, and hydrogen radicals in the stratosphere. These radicals are produced from long-lived source gases that, because their atmospheric lifetimes are long compared with the transport time to reach the stratosphere, are able to be transported intact into the stratosphere. The Montreal Protocol and its Amendments and Adjustments have, however, led to reductions in the tropospheric abundances of the chlorine- and bromine-containing source gases as a result of reductions in the production and consumption of manufactured halogenated source gases.

Direct observations of most chemical species that cause stratospheric ozone depletion began in the late 1970s or later. The ground-based in situ and flask measurements have provided the most complete picture of the evolution of these species because of the regularity of the measurements. The complete 20th century and earlier pictures of the accumulation of ozone-depleting chemicals in the atmosphere also rely on calculations based on historic emission estimates, and analysis of air trapped in polar firn and ice or measurements of air archives. Ground-based remote sensing techniques, in particular numerous Network for the Detection of Atmospheric Composition Change (NDACC, formerly Network for the Detection of Stratospheric Change or NDSC) sites equipped with Fourier transform infrared (FTIR) instruments, have also provided multidecadal information of relevance to this chapter. Satellite observations have also provided information on the most abundant ozone-depleting substances since the mid-1980s. Although the long-term trends are difficult to measure with space-based techniques due to the generally short lifetime of the space missions, they can be inferred by combining data from multiple instruments operating in different years. This method was applied by Harries et al. (2001), using data from the Infrared Radiation Interferometer Spectrometer (IRIS) sensor in 1970 and the Interferometric Monitor for Greenhouse Gases (IMG) sensor in 1997, to identify the long-term changes in the Earth's outgoing longwave radiation, notably due to the rise of the chlorofluorocarbons (CFCs) in that time period. More recently, Rinsland et al. (2005) have compared data from the Atmospheric Trace Molecule

Spectroscopy (ATMOS) missions in 1985 and 1994 and the Atmospheric Chemistry Experiment - Fourier Transform Spectrometer (ACE-FTS) data in 2004 to determine lower-stratospheric trends of several target species during the last two decades.

The atmospheric history of ozone-depleting substances in years before regular measurements began have been examined using Antarctic firn air samples (Butler et al., 1999; Sturges et al., 2001; Sturrock et al., 2002; Trudinger et al., 2004; Reeves et al., 2005). These analyses have revealed that atmospheric mixing ratios of the various CFCs and halons underwent large increases beginning in the 1950s to 1970s. As a result of international production and consumption restrictions, all of these gases now exhibit substantially reduced rates of atmospheric growth, and, for many of them, mixing ratio declines. The hydrochlorofluorocarbons (HCFCs) first appeared in the atmosphere in the 1960s to the 1980s and their mixing ratios continued to increase through 2004. Firn air results also indicate that nearly all of the CFCs, halons, methyl chloroform, and carbon tetrachloride (CCl₄) present in today's atmosphere are the result of anthropogenic production, though the existence of small natural sources or some anthropogenic production and use in years predating the oldest firn air samples cannot be ruled out.

This chapter provides a scientific update to various sections of Chapter 1 of the previous World Meteorological Organization Assessment Report (WMO, 2003; hereafter referred to as *WMO 2002*). It reports the measurements of long-lived compounds obtained from many typical observation means (Table 1-1), including firn air analysis, ground-based in situ and remote sensing stations, and satellite observations, for ozone-depleting substances and for other climate-related gases through 2004. The latter gases, which include the hydrofluorocarbons, are also discussed in Section 1.4, because they can contribute indirectly to ozone change and ozone recovery through their effects on the radiative forcing of the atmosphere. Trace gases with lifetimes shorter than 0.5 years (in particular nitrogen and hydrogen radicals) are reported in Chapter 2. The observations provide important constraints on past emissions and thereby on future emissions. Chapter 1 compares the current observed trends with the expectations based on standard emission scenarios. Further results on EEC1 (effective equivalent chlorine) and EESC (equivalent effective stratospheric chlorine) calculations from assumed future emission scenarios and for calculations of the remaining banks may be found in Chapter 8. The reader is referred to Table 1-4 for the chemical formulae of the gases discussed.

LONG-LIVED COMPOUNDS

Table 1-1. Measurements of long-lived compounds.*

<i>Name</i> Location	Technique
Firn air	
<i>Law Dome</i> Antarctica	Firn ice
On-Site Sampling — Ground-Based	
<i>AGAGE – Advanced Global Atmospheric Gases Experiment</i>	
Cape Grim, Tasmania (41°S, 145°E)	In situ GC measurements
Cape Matatula, Samoa (14°S, 171°E)	
Ragged Point, Barbados (13°N, 59°W)	
Mace Head, Ireland (53°N, 10°W)	
Trinidad Head, United States (41°N, 124°W)	
<i>SOGE – System for Observation of Halogenated Greenhouse Gases in Europe</i>	
Jungfrauoch, Swiss Alps (46.5°N, 8.0°E)	In situ GC measurements
Ny Ålesund, Norway (78°N, 11.5°E)	
Monte Cimone, Italy (44° N, 10.5°E)	
<i>NOAA/ESRL – National Oceanic and Atmospheric Administration/Earth System Research Laboratory</i>	
South Pole, Antarctica ^{1,2,3,4}	Flasks-GC, and in situ-GC
Palmer Station, Antarctica ⁴	Flasks-GC
Cape Grim, Tasmania ^{2,3,4}	Flasks-GC
Cape Matatula, Samoa ^{1,2,3,4}	Flasks-GC, and in situ-GC
Mauna Loa, United States ^{1,2,3,4}	Flasks-GC, and in situ-GC
Cape Kumukahi, United States ^{2,3,4}	Flasks-GC
Niwot Ridge, United States ^{1,2,3}	Flasks-GC, and in situ-GC
Wisconsin, United States ^{2,4}	Flasks-GC
Harvard Forest, United States ⁴	Flasks-GC
Barrow, United States ^{1,2,3,4}	Flasks-GC, and in situ-GC
Alert, Canada ^{2,3,4}	Flasks-GC
<i>UCI – University of California at Irvine</i>	
40-45 Pacific sites from 71°N to 47°S sampled approximately twice per season. www.physsci.uci.edu/~rowlandblake/ samplinglocationsmap.html	Flasks-GC
<i>UEA – University of East Anglia</i>	
Cape Grim, Tasmania	Flasks-GC, Archived air
Remote Sensing — Ground-Based	
Kiruna, Sweden (67.8°N, 20.4°E)	Ground-based infrared FTS
Jungfrauoch, Swiss Alps (46.5°N, 8.0°E)	Total column measurements
Kitt Peak, Arizona (32.0°N, 111.6°W)	
Izaña, Tenerife (28.3°N, 16.5°W)	
Remote Sensing — Satellite	
<i>HALOE - Halogen Occultation Experiment</i>	
U.S. experiment (1991-2005)	Infrared gas filter correlation and broadband filter radiometry (solar occultation)
Latitudinal coverage from 80°S to 80°N/1 year	Stratospheric-mesospheric profiles
<i>IMG - Interferometric Monitor for Greenhouse Gases</i>	
Japanese experiment (1996-1997)	Spaceborne infrared FTS (nadir)
Global coverage	Tropospheric columns

Table 1-1, continued.

<i>MIPAS - Michelson Interferometer for Passive Atmospheric Sounding</i>	
European experiment (launched in 2002)	Spaceborne infrared FTS (limb)
Global coverage	Strato-mesospheric profiles
<i>ACE/FTS - Atmospheric Chemistry Experiment</i>	
Canadian experiment (launched in 2003)	Spaceborne infrared FTS (solar occultation)
Latitudinal coverage from about 80°S to 80°N/1 year	Upper troposphere to the lower thermosphere
<i>MLS - Microwave Limb Sounder</i>	
U.S. experiment (launched in 2004)	Microwave sounder (limb)
Latitudinal coverage from 82°N to 82°S daily	Upper troposphere to the lower thermosphere

* The list provided here is restricted to the measurements reported in this chapter. GC = gas chromatographic.

¹ Data from in situ instruments at these stations are used by NOAA to derive global tropospheric means for CFCs and CCl₄.

² Data from flasks collected at these stations are used by NOAA to derive global tropospheric means for CH₃CCl₃.

³ Data from flasks collected at these stations are used by NOAA to derive global tropospheric means for HCFCs and halons.

⁴ Data from flasks collected at these stations are used by NOAA to derive global tropospheric means for CH₃Br.

1.2 HALOGENATED OZONE-DEPLETING GASES IN THE ATMOSPHERE

1.2.1 Updated Atmospheric Observations of Ozone-Depleting Gases

In this section, measurements of halogenated gases by the ground-based networks are summarized. As indicated in Table 1-1, these network measurements include those by the Advanced Global Atmospheric Gases Experiment (AGAGE), the System for Observation of Halogenated Greenhouse Gases in Europe (SOGE, although the measurements used here were from Jungfraujoch and Ny Ålesund only), the National Oceanic and Atmospheric Administration / Earth System Research Laboratory (NOAA/ESRL, formerly NOAA/CMDL) and the University of California at Irvine (UCI). In a number of cases this also includes measurements of air samples collected at Cape Grim, Australia since 1978 that have been archived (Langenfelds et al., 1996). The section extends the time series described in *WMO 2002* (Montzka and Fraser et al., 2003) beyond 2000 and emphasizes the measurements from 2001 to the end of 2004. The time series for these gases shown in the Figures and Tables throughout this Chapter are from monthly means of data from individual sites that have been combined to produce monthly hemispheric and global means. Annual means of these are also used in some Figures and Tables.

Table 1-2 shows annual means of the measured ozone-depleting halocarbons. The precisions and accuracies of the measurements may mostly be judged by the differences between the reported values. Only for CFC-12, HCFC-22, and halon-1301 are the differences in the trends

observed by the various groups statistically significant. All uncertainties are one sigma unless otherwise specified. Terms used to describe measured values throughout Chapter 1 are mixing ratios (for example parts per trillion, ppt, pmol/mol), mole fractions, and concentrations. These terms have been used interchangeably and, as used here, they are all considered to be equivalent.

Methyl chloride and methyl bromide have substantial natural sources and the emissions of these gases are also discussed in their subsections. The emissions of the other halocarbons are discussed in Section 1.3.

1.2.1.1 CHLOROFLUOROCARBONS (CFCs)

CFC-11 (CCl₃F), CFC-12 (CCl₂F₂), and CFC-113 (CCl₂FCClF₂) are routinely measured by the three ground-based gas-sampling networks (see Table 1-1) using gas sampling techniques. Results from these independent laboratories generally agree to within 2% (Figure 1-1). CFC-11 and CFC-12 are also measured using ground-based infrared solar absorption spectroscopy, such as at the Jungfraujoch station. From space, CFCs have been measured by a variety of shuttle- or satellite-based instruments operating in the infrared spectral region. Most of these data concern CFC-11 and CFC-12. They were obtained from thermal infrared nadir sounders (Harries et al., 2001; Coheur et al., 2003; Dufour et al., 2005), limb instruments (Bacmeister et al., 1999; Hoffmann et al., 2005), or solar occultation sounders (Khosrawi et al., 2004; Rinsland et al., 2005).

Recent measurements from the gas sampling networks indicate that the CFC-12 global trend is now approximately zero, and two of the three networks plus the remote sensing measurements at Jungfraujoch indi-

LONG-LIVED COMPOUNDS

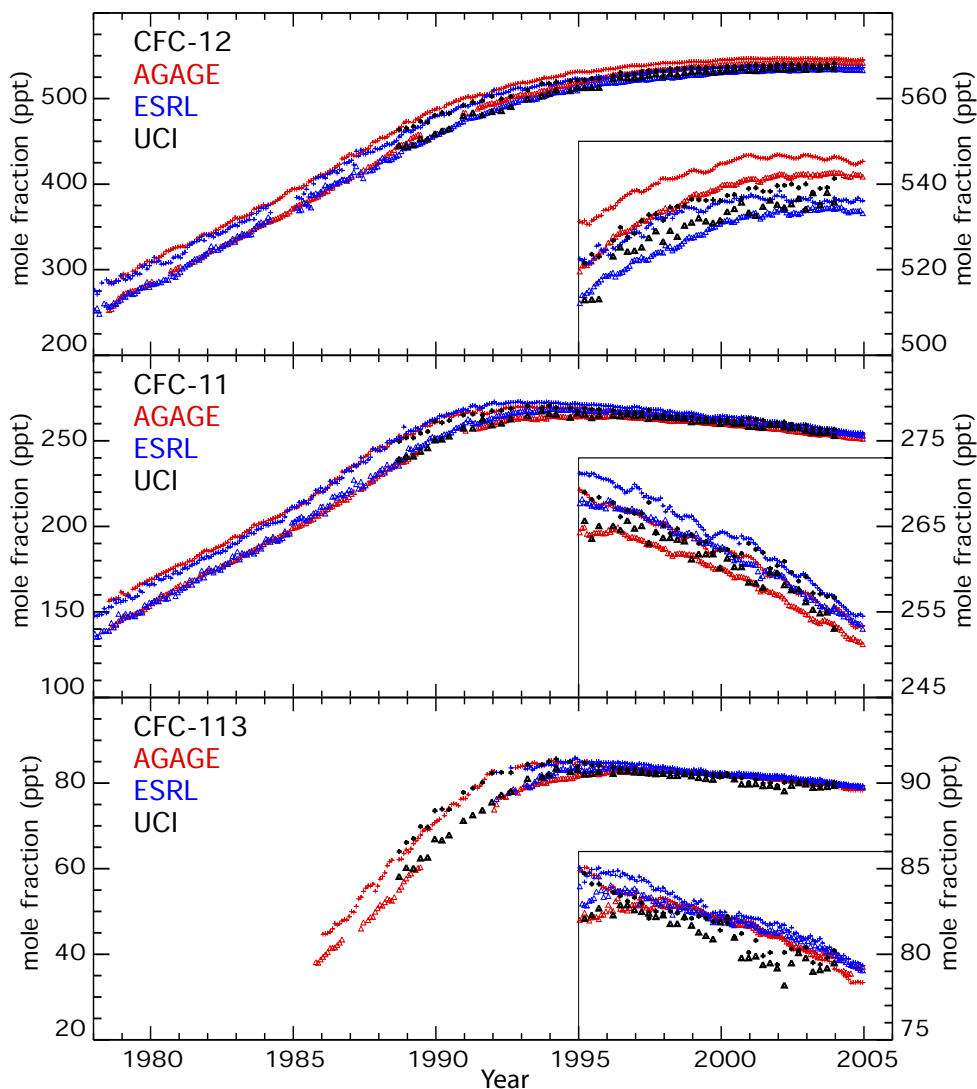


Figure 1-1. Hemispheric monthly means of the major chlorofluorocarbons CFC-12, CFC-11, and CFC-113 (crosses for Northern Hemisphere and triangles for Southern Hemisphere). Measurements from the AGAGE network (Prinn et al., 2000 updated), the NOAA/ESRL network (Montzka et al., 1999 updated; Thompson et al., 2004), and UCI (D.R. Blake et al., 1996; N.J. Blake et al., 2001) are shown. To increase visibility, recent measurements are depicted on a larger scale in the inserts (the scales are on the right-hand sides of the panels).

cate that Northern Hemispheric mole fractions are now decreasing. These observations are consistent with the analyses of Rinsland et al. (2005) using ATMOS and ACE satellite data. The measured annual column change above Jungfraujoch in 2003-2004 is -0.11×10^{14} molec cm^{-2} ($-0.16\%/yr$) (Zander et al., 2005) compared with 0.50×10^{14} molec cm^{-2} ($+0.71\%/yr$) in 1998 (*WMO 2002*) and 0.27×10^{14} molec cm^{-2} ($+0.39\%/yr$) in 1999-2000. Trends from column measurements in $\%/yr$ should be almost directly comparable with trends for similar periods derived from the sampling networks, because of the long lifetimes of the species being discussed. Averaged over

Kiruna (68°N) and Izaña (28°N), the column trend from 2000 to 2005 is $-0.09 \pm 0.10\%/yr$ (update from Kopp et al., 2003, and Schneider et al., 2005). Since the CFC-12 lifetime is approximately 100 years, the measured rate of change indicates that there are still significant emissions of CFC-12. Differences between measured Northern Hemisphere and Southern Hemisphere mole fractions have been decreasing since approximately the end of the 1980s (Figure 1-1). The hemispheric difference in 2004 was still approximately 3 ppt (0.6%), indicating that the remaining emissions are still occurring predominantly in the Northern Hemisphere.

Table 1-2. Mole fractions and growth rates of ozone-depleting gases.

Chemical Formula	Common or Industrial Name	Annual Mean Mole Fraction (ppt)			Growth (2003-2004)		Laboratory, Method
		2000	2003	2004	(ppt yr)	(% yr)	
CFCs							
CCl ₂ F ₂	CFC-12	543.0	544.2	543.8	-0.6	-0.1	AGAGE, in situ
		534.1	535.2	535.0	-0.2	0.0	NOAA*
		535.6	537.9	539.7	1.8	0.3	UCI
CCl ₃ F	CFC-11	260.6	254.9	253.1	-1.8	-0.7	AGAGE, in situ
		262.5	256.6	254.7	-1.9	-0.7	NOAA*
		261.2	256.1	253.7	-2.4	-0.9	UCI
		263.9	257.3	254.7	-2.7	-1.0	SOGE, in situ (Europe)
CCl ₂ FCClF ₂	CFC-113	81.8	79.6	78.7	-0.9	-1.1	AGAGE, in situ
		82.1	80.5	79.5	-0.9	-1.2	NOAA*
		81.1	79.5	79.1	-0.4	-0.5	UCI
CClF ₂ CClF ₂	CFC-114 including -114a	17.21	17.24	17.31	0.07	0.4	AGAGE, in situ (Cape Grim only)
			14.90	14.72	-0.18	-1.2	UCI
CClF ₂ CF ₃	CFC-115	8.10	8.26	8.34	0.08	1.0	AGAGE, in situ
		8.19	8.18	8.29	0.11	1.3	SOGE, in situ (Europe)
HCFCs							
CHClF ₂	HCFC-22	142.8	159.0	163.9	4.9	3.0	AGAGE, in situ
		141.7	157.9	162.1	4.2	2.6	NOAA, flasks
			161.9	169.1	7.2	4.4	UCI
CH ₃ CCl ₂ F	HCFC-141b	12.82	16.70	17.42	0.72	4.2	AGAGE, in situ
		12.66	16.58	17.18	0.60	3.6	NOAA, flasks
		15.05	18.57	19.20	0.60	3.2	SOGE, in situ (Europe)
CH ₃ CClF ₂	HCFC-142b	12.46	14.74	15.38	0.64	4.2	AGAGE, in situ
		11.72	13.99	14.53	0.54	3.8	NOAA, flasks
CHCl ₂ CF ₃	HCFC-123	0.050	0.060	0.064	0.004	6.5	AGAGE, in situ (Cape Grim only)
CHClFCF ₃	HCFC-124	1.40	1.63	1.64	0.01	0.1	AGAGE, in situ
		1.46	1.71	1.72	0.01	0.1	SOGE, in situ (Europe)
Halons							
CBr ₂ F ₂	halon-1202	0.044	0.040	0.038	-0.002	-5.1	UEA, flasks (Cape Grim only)
CBrClF ₂	halon-1211	4.12	4.28	4.33	0.05	1.2	AGAGE, in situ
		3.98	4.13	4.15	0.02	0.0	NOAA, flasks
		4.43	4.68	4.77	0.09	1.9	UEA, flasks (Cape Grim only)
		4.32	4.52	4.62	0.08	1.8	SOGE, in situ (Europe)
CBrF ₃	halon-1301	2.95	3.04	3.14	0.10	3.2	AGAGE, in situ
		2.57	2.61	2.60	-0.01	0.0	NOAA, flasks
		2.26	2.38	2.45	0.07	2.9	UEA, flasks (Cape Grim only)
		3.04	3.06	3.16	0.10	3.2	SOGE, in situ (Europe)
CBrF ₂ CBrF ₂	halon-2402	0.425	0.427	0.427	0.0	0.0	UEA, flasks (Cape Grim only)
		0.48**	--	0.48			NOAA, flasks

LONG-LIVED COMPOUNDS

Table 1-2, continued.

Chemical Formula	Common or Industrial Name	Annual Mean Mole Fraction (ppt)			Growth (2003-2004)		Laboratory, Method
		2000	2003	2004	(ppt yr)	(% yr)	
Chlorocarbons							
CH ₃ Cl	Methyl chloride	532.1	523.4	527.8	4.4	0.8	AGAGE, in situ (Ireland/Cape Grim average)
CCl ₄	Carbon tetrachloride	529.5	523.0	526.0	3.0	0.6	SOGE, in situ (Europe)
		96.4	93.5	92.6	-0.8	-1.0	AGAGE, in situ
		100.2	97.2	96.1	-1.1	-1.1	NOAA*
		99.2	96.3	95.1	-1.2	-1.2	UCI
CH ₃ CCl ₃	Methyl chloroform	45.6	26.5	22.0	-4.5	-18.6	AGAGE, in situ
		45.8	26.5	22.0	-4.5	-18.7	NOAA, flasks
		47.7	28.3	23.9	-4.4	-16.8	UCI
		44.3	26.7	22.2	-4.5	-18.5	SOGE, in situ (Europe)
Bromocarbons							
CH ₃ Br	Methyl bromide	10.3	8.8	9.1	0.3	3.3	AGAGE, in situ (Ireland only)
		8.7	8.1	7.9	-0.2	-2.4	NOAA, flasks

All values are estimates for the global troposphere unless specified otherwise.

* These NOAA values consist of a combination of flask and in situ measurements.

** Earlier halon-2402 data from NOAA are for 1996, not 2000.

The sampling networks indicate that global mole fractions of CFC-11 decreased by approximately 2.0 ± 0.1 ppt/yr (0.8%/yr) from 2000 to 2004 (Table 1-2). This rate of decrease is larger than that reported in *WMO 2002* (Montzka and Fraser et al., 2003), 1.4 ppt/yr (0.5%/yr), for 1996 to 2000. Zander et al. (2005) indicate that the CFC-11 column change and the corresponding annual trend have remained constant since the late 1990s over the Jungfraujoch, amounting to -1.85×10^{13} molec cm⁻² (-0.59%/yr in 2004). A slightly smaller downtrend is to be expected in the CFC-11 column than in the surface measurements, by approximately 0.1%/yr, because the proportion of CFC-11 that is in the stratosphere is predicted to have been continuing to increase slowly. The decline in the tropospheric CFC-11 mole fractions from 2000 to 2004 is approximately 20% less than that projected in the Ab (baseline, most likely) scenario of *WMO 2002* (Table 1-14, Chapter 1, WMO (2003)). The measured hemispheric difference for CFC-11 has been decreasing (Figure 1-1), but it was still approximately 2 ppt (0.8%) in 2004. This and the 45-year lifetime of CFC-11 indicate that significant Northern Hemispheric emissions are still occurring.

CFC-113 has decreased by approximately 1% (0.8 ppt) from 2003 to 2004. This is larger than the rate of decrease of 0.5%/yr reported for 1999-2000 in *WMO 2002*

(Montzka and Fraser et al., 2003). Since the lifetime is estimated to be 85 years, the recent decrease indicates that global emissions of CFC-113 are now small. Consistent with this, the hemispheric gradient is less than 1 ppt (Figure 1-1). A global decrease of CFC-113 of 1%/yr provides an upper limit to its atmospheric lifetime of 100 years.

CFC-114 (CClF₂CClF₂) and CFC-115 (CClF₂CF₃) have been measured in Cape Grim (41°S) air samples since 1978. As noted by Sturrock et al. (2001), and by Mangani et al. (2000) for Antarctica, the mixing ratio of CFC-114 was not changing in the atmosphere in mid-2000. Recent measurements indicate that there have only been small but insignificant changes of CFC-114/-114a (Table 1-2). In contrast, CFC-115, which is used with HCFC-22 (CHClF₂) in refrigeration blends, has continued to increase at about 1%/yr (0.08 ppt/yr), which is only half of the growth rate reported in *WMO 2002* (Montzka and Fraser et al., 2003).

1.2.1.2 HYDROCHLOROFLUOROCARBONS (HCFCs)

Measurements of HCFCs from the gas sampling networks have been updated through 2004 (O'Doherty et al., 2004; Krummel et al., 2004). Furthermore, recent remote measurements of HCFC-22 (Rinsland et al., 2005) and HCFC-142b (Dufour et al., 2005), which show gen-

eral consistency with the AGAGE and the NOAA/ESRL values, have recently become available from the ACE satellite mission.

Global mixing ratios of the three most abundant HCFCs have all increased due to sustained emissions (resulting from their being substitutes for CFCs and other ozone-depleting substances (ODSs) (Figure 1-2). The annual global mole fraction of HCFC-22 (CHClF_2) was

approximately 165 ppt in 2004, with an averaged annual growth rate of about 4.9 ± 0.5 ppt/yr ($3.2 \pm 0.3\%$ /yr) (2000-2004, with more weight being given to the more precise trend estimates from AGAGE and NOAA/ESRL).

Combined vertical column abundances of HCFC-22 above Kiruna (68°N) and Izaña (28°N) yield a trend of $3.5 \pm 0.3\%$ /yr (1.1×10^{14} molec cm^{-2} yr^{-1}) for 2000-2004 (updated from Kopp et al., 2003; Schneider et al., 2005).

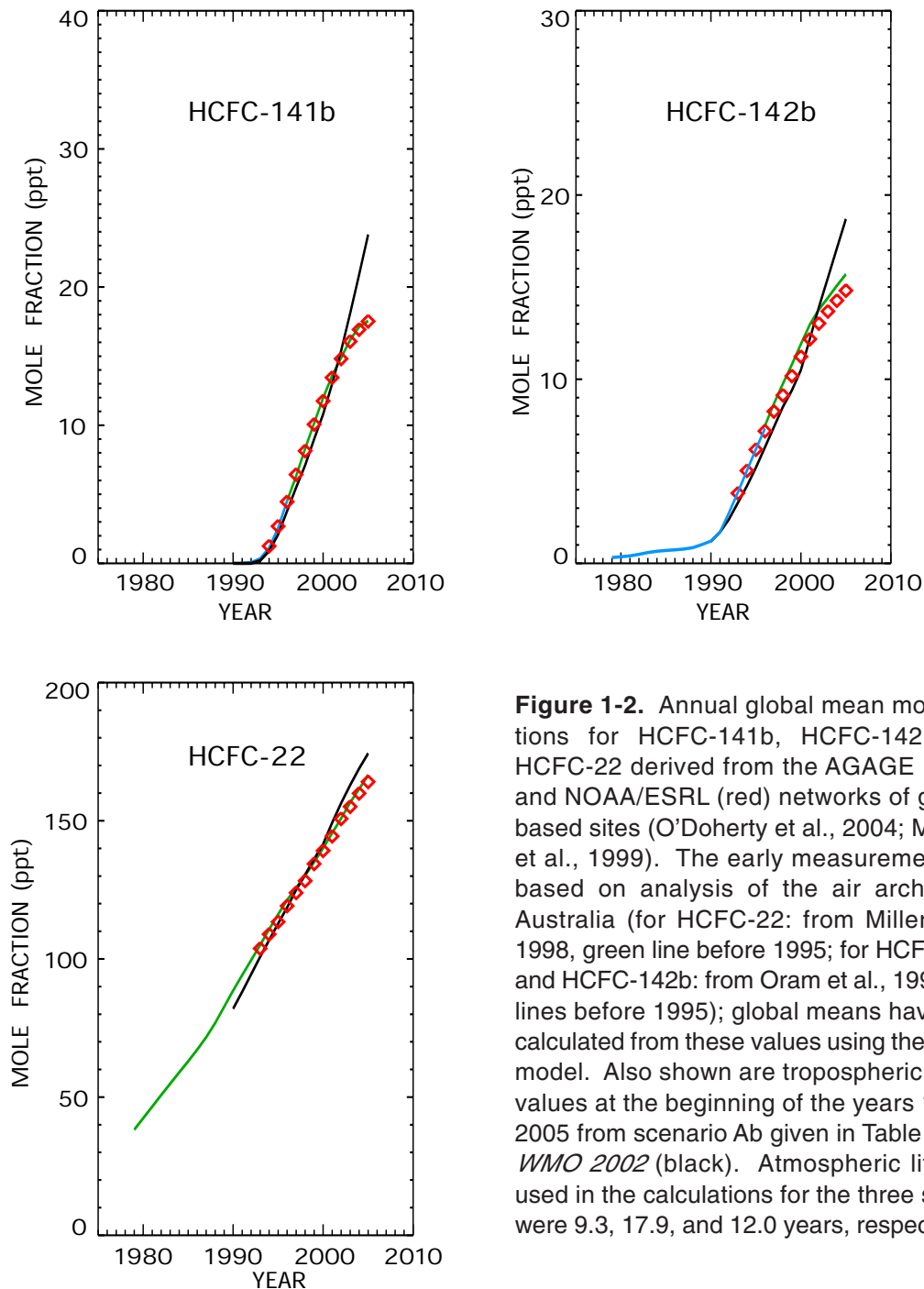


Figure 1-2. Annual global mean mole fractions for HCFC-141b, HCFC-142b, and HCFC-22 derived from the AGAGE (green) and NOAA/ESRL (red) networks of ground-based sites (O'Doherty et al., 2004; Montzka et al., 1999). The early measurements are based on analysis of the air archived in Australia (for HCFC-22: from Miller et al., 1998, green line before 1995; for HCFC-141b and HCFC-142b: from Oram et al., 1995, blue lines before 1995); global means have been calculated from these values using the 12-box model. Also shown are tropospheric annual values at the beginning of the years 1990 to 2005 from scenario Ab given in Table 1-14 of *WMO 2002* (black). Atmospheric lifetimes used in the calculations for the three species were 9.3, 17.9, and 12.0 years, respectively.

LONG-LIVED COMPOUNDS

Column abundances above the Jungfraujoch station (last reported for 1986 to 2001 in Figure 1-2 of *WMO 2002*) have been measured since 1986. The column abundances found at the extremes of the Jungfraujoch observational time base are 0.90×10^{15} molec cm^{-2} in January 1986 and 2.42×10^{15} molec cm^{-2} in December 2004. This corresponds to an increase of a factor of nearly 2.7 over this 19-year period (Zander et al., 2005). This factor is only a few percent larger than (i.e., not significantly different from) that determined from the Australian archived air (Langenfelds et al., 1996), AGAGE, and NOAA measurements.

There has been a substantial slowdown in the rates of accumulation of HCFC-141b ($\text{CH}_3\text{CCl}_2\text{F}$) and HCFC-142b (CH_3CClF_2), particularly in the last two years. The global mean mixing ratio of HCFC-142b has increased to about 15 ppt in mid-2004, compared with about 12 ppt in mid-2000, with an annual average growth rate of 0.6 ± 0.1 ppt/yr (4%/yr, 2003-2004). This is approximately half of the previously reported growth rate of 1.1 ppt/yr averaged from 1999-2002, based on data from both AGAGE and NOAA/ESRL measurements (O'Doherty et al., 2004). The growth rate of HCFC-141b has also slowed from an annual average rate of about 1.6 ppt/yr in 1999-2000 to 0.6 ± 0.1 ppt/yr (4%/yr) in 2003-2004, resulting in a global mean surface mole fraction of 17.3 ± 0.2 ppt in mid-2004. Northern Hemisphere mean mole fractions were approximately 2.5 ppt and 1.4 ppt higher than in the Southern Hemisphere, for HCFC-141b and 142b respectively, in mid-2004.

Figure 1-2 shows that the slowdown in the growth rates of all three gases in the atmosphere was not anticipated in the projections made in the Ab scenario in *WMO 2002*. The observed growth rates for 2000-2004 were 4.9, 1.1, and 0.6 ppt/yr for HCFC-22, HCFC-141b, and HCFC-142b, respectively, versus projected growth rates of 6.6, 2.6, and 1.6 ppt/yr.

Figure 1-3 shows monthly mean baseline mixing ratios (and occasional pollution events) for HCFC-123 (CHCl_2CF_3) measured at Cape Grim from 1998 through 2004 (Krummel et al., 2004). Its mixing ratio in 2004 is 0.064 ppt. A strong annual cycle is evident because of the annual cycle in hydroxyl and the short atmospheric lifetime (1.3 years) of HCFC-123. Overall the atmospheric mixing ratios have been increasing over the seven-year period at approximately $6 \pm 1\%$ /yr. These are the only reported measurements of HCFC-123 since a value of 0.03 ppt for 1996 by Oram (1999). Despite its small mixing ratio, there is considerable interest in this gas because as a refrigerant it is operated at sub-ambient temperatures and leakage is therefore exceptionally small. Moreover what does get into the atmosphere is rapidly destroyed. Equally important it has a very low Ozone Depletion Potential (ODP).

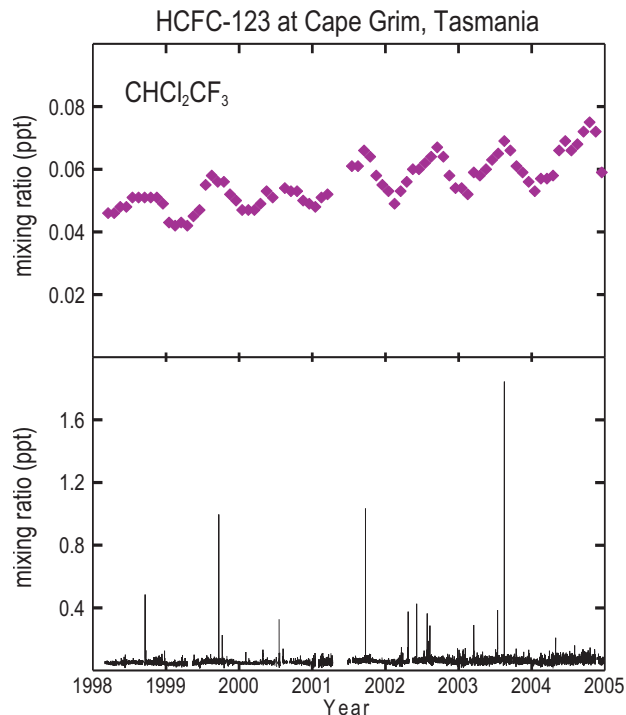


Figure 1-3. Monthly mean baseline mixing ratios (ppt) of HCFC-123 measured at Cape Grim, Tasmania (upper panel) (Krummel et al., 2004). The lower panel shows the continuous series of the measurements with the pollution events included.

Measurements of HCFC-124 (CHClF_2), which were first reported in *WMO 2002* (Montzka and Fraser et al., 2003), have been updated from AGAGE measurements at the two AGAGE stations at Mace Head, Ireland, and Cape Grim, Tasmania (Prinn et al., 2000). Trends and annual global means are reported in Table 1-2. The increase of HCFC-124 has been slowing rapidly since 1998 (see also *WMO 2002*). No new measurements of HCFC-21 (CHCl_2F) have been reported since *WMO 2002*. The atmospheric histories of several HCFCs have been reconstructed from analyses of air trapped in firn, and show that concentrations at the start of the 20th century were less than 2% of current mixing ratios (Sturrock et al., 2002).

1.2.1.3 HALONS

From the introduction of halons in the early 1960s, halon use grew steadily worldwide until the Montreal Protocol required an end to their consumption in developed countries by the end of 2003; however, production in developed countries was allowed for essential uses and to supply the needs of developing countries. Global production of halon-1211 (CBrClF_2) and halon-1301 (CBrF_3) peaked in 1988 at 43 Gg/yr and 13 Gg/yr, respectively

(UNEP, 2003). In developing countries, halon-1211 production began in the 1980s and showed a growth curve similar to that in developed countries until Multilateral Fund projects began to reverse that trend in the 1990s (UNEP, 2003). A third halon, halon-2402 ($\text{CBrF}_2\text{CBrF}_2$), was used predominantly in the former Soviet Union. No information on the production of halon-2402 before 1986 has been found. Fraser et al. (1999) developed emission projections for halon-2402 based on atmospheric measurements. They reported that the emissions grew steadily in the 1970s and 1980s, peaking in the 1988-1991 time frame at 1.7 Gg/yr. They found these results to be qualitatively consistent with the peak production of 28,000 ODP tonnes reported by the Russian Federation under Article VII of the Montreal Protocol (or assuming all production was halon-2402 and an ODP of 6, a peak production of approximately 4.650 Gg/yr).

Figure 1-4 shows the comparisons of the global mean mole fractions for halon-1211 and halon-1301 from the twelve times per day measurements by AGAGE (green lines) and the multiple samples per month analyzed by NOAA/ESRL (red lines). Also shown are the values derived from measurements of the air that has been archived several times per year in Australia and analyzed at the University of East Anglia (UEA) (blue lines; Oram et al., 1995; Fraser et al., 1999).

Observations from NOAA/ESRL, AGAGE, and UEA since 2000 suggest that the rate of increase of halon-1211 has continued to slow down, although halon-1211 mixing ratios continue to increase in the global atmosphere. The ground-based sampling network measurements of halon-1211 show that the global tropospheric mixing ratio of halon-1211 in 2004 was approximately 4.4 ppt, with a calibration uncertainty of approximately 0.3 ppt (Table 1-2). The mean rate of increase from 2000 to 2004 was 0.06 ± 0.01 ppt/yr (1.4%/yr). This is significantly lower than the rate of increase in 1999-2000, which was 0.12 ppt/yr (*WMO 2002*, Montzka and Fraser et al., 2003).

For halon-1301, the AGAGE, UEA, and NOAA/ESRL measurements show a large disparity in mixing ratio and rate of change during 2000-2004. The NOAA data show a negligible change (0.01 ± 0.01 ppt/yr), whereas AGAGE and UEA show an average rate of increase of 0.05 ± 0.01 ppt/yr (1.8%/yr). This discrepancy was not present in the pre-2000 measurements, perhaps because AGAGE measurements only began in 1998. Thus it is currently unclear whether there has been a significant slowdown in the growth rate compared with that reported in *WMO 2002* of 0.06 ppt/yr for 1999-2000 (Montzka and Fraser et al., 2003). Because of this, the observations do not provide as strong a constraint on the emissions as they do for the CFCs, HCFCs, and halon-1211.

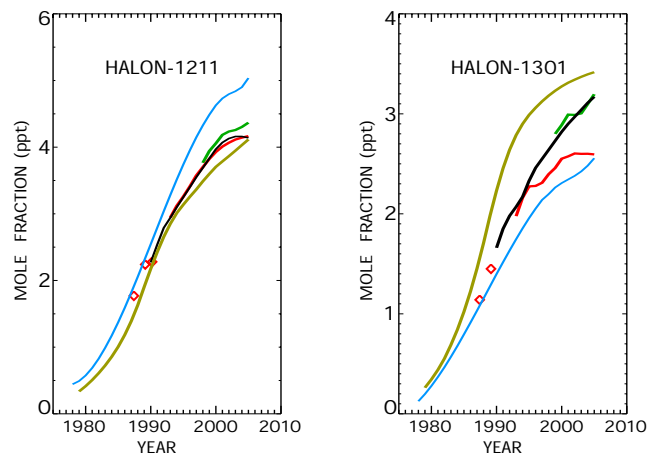


Figure 1-4. Annual global mean mole fractions for halon-1211 and halon-1301 derived from measurements at multiple sites in the AGAGE (green lines) and NOAA/ESRL (red diamonds, an update to Butler et al., 1998; red lines, from Montzka et al., 1999) networks. Also shown are annual global means calculated from measurements of archived air sampled at Cape Grim, Australia (blue lines, updated from Fraser et al., 1999) using the 12-box model. These measurements are compared against tropospheric annual means for the beginning of the years 1990 to 2005 given in Table 1-14 (scenario Ab) of *WMO 2002* (black lines). The greenish gold lines for halon-1211 and halon-1301 have been calculated from the UNEP Halons Technical Options Committee emission scenarios (UNEP, 2003) (modified for halon-1211, see text) using a 12-box model.

The measurements of the Australian air archive by UEA indicate that halon-2402 has remained approximately constant over the 2000-2004 period, and a fourth halon, 1202 (CBr_2F_2), which is not controlled under the Montreal Protocol, has declined by approximately 14%. The projections for this period given in *WMO 2002* were that halon-2402 would have declined slowly and halon-1202 would have declined by about 40%. Because the atmospheric lifetime of halon-1202 is approximately three years (Fraser et al., 1999), some residual production of halon-1202 is indicated, perhaps from over-bromination during the small remaining production of halon-1211.

All four halons have been measured in firn air from Dome C (75°S, Antarctica), Devon Island (75°N, Canada), and Greenland (75°N) (Reeves et al., 2005). At the base of the firn, the halon concentrations are below detection (<0.001 ppt), confirming that these species are entirely anthropogenic. The global halon mole fractions derived from these firn air samples are consistent with those

LONG-LIVED COMPOUNDS

obtained from an analysis of the Cape Grim air archive (Fraser et al., 1999; Reeves et al., 2005).

By 2000, total tropospheric bromine from halons was about 8 ppt, having approximately doubled over the previous 10 years (Figure 1-5). The measurements show clear signs that the atmospheric accumulation of total halon bromine is slowing. However the Ab scenario in *WMO 2002* (Montzka and Fraser et al., 2003) projected that it should stop growing by approximately 2006, because of reductions in halon-1211 starting in 2003 (the black line in Figure 1-4). The *WMO 2002* Ab scenario provides a reasonable fit to the halon-1211 observations (Figure 1-4) but there is little evidence that halon-1211 stopped increasing in the 2000-2004 period. Therefore it seems likely that the total halon bromine maximum will be delayed by a year or two.

1.2.1.4 CARBON TETRACHLORIDE (CCl₄)

The major use for CCl₄ during the 1980s was believed to be as a feedstock for the production of the CFCs (Simmonds et al., 1988). Therefore as production of the CFCs was substantially reduced during the 1990s because of the Montreal Protocol, atmospheric mixing ratios of CCl₄ decreased (Figure 1-6). Global surface mixing ratios of CCl₄ are shown to have reached a maximum of about 106 ± 1 ppt in late 1990 and they have declined subsequently at a steady rate of 1.0 ± 0.1 ppt/yr (about 1%/yr) as a result of reduced emissions (Figure 1-6). Calibration differences between the different reporting groups since 1995 are 3-4%. The annual global mean in 2004 was 92-96 ppt (group average is 94.6 ppt) depending on which group made the measurements. For this gas in particular, a comparison of the measurements at the common measurement site in Samoa confirms that the NOAA/AGAGE difference is due to calibration and not due to the effects of differing site locations used to produce global means. Significant emissions of CCl₄ are still occurring and these sustain the interhemispheric difference of 1.4 ± 0.3 ppt, which has been relatively constant since 1995.

In *WMO 2002* (Montzka and Fraser et al., 2003), the estimated atmospheric lifetime of carbon tetrachloride was reduced to 26 years because of ocean losses (Yvon-Lewis and Butler, 2002). More recently, soil losses measured in North America have led to an estimated lifetime contribution from soil losses globally of 90 years, with an uncertainty range of 50 to 418 years (Happell and Roche, 2003; see also Borch et al., 2003). Combining this lifetime contribution with those due to ocean losses (94 years, with a range of 82 to 191 years) and an atmospheric lifetime from the 1998 WMO Assessment (35 years, with a

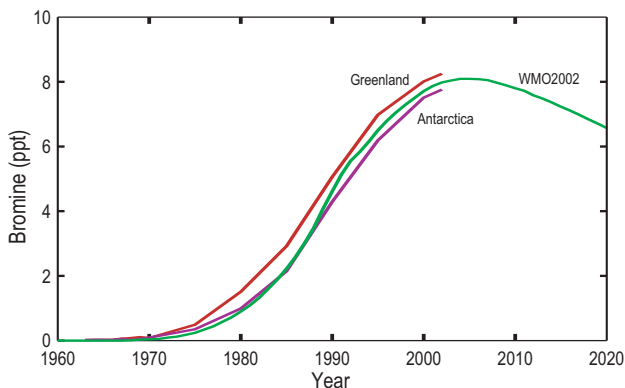


Figure 1-5. Tropospheric bromine from four halons (1211, 1301, 2402, 1202) at high northern (red) and high southern (purple) latitudes, based on model-derived emissions that best-fit the firm air data from Greenland and Antarctica and the air archive data from Cape Grim, Tasmania (Reeves et al., 2005). Those estimates are compared with model estimates (green) for the Southern Hemisphere (Fraser et al., 1999), using the Ab halon emission scenario prepared for *WMO 2002* (Montzka and Fraser et al., 2003).

range of 21 to 43 years; WMO, 1999) led Happell and Roche (2003) to infer an overall lifetime for carbon tetrachloride of 20 years. However, based on the discussion in the emissions section (Section 1.3.2.4), it was decided not to change the recommended overall lifetime from the *WMO 2002* value of 26 years at this time.

1.2.1.5 METHYL CHLOROFORM (CH₃CCl₃)

Because of Montreal Protocol restrictions, there has been a steady decline from an all-time high in methyl chloroform concentrations of more than 130 ppt in 1992 (Figure 1-6). The decline was due to a rapid decline in the emissions during the 1990s (McCulloch and Midgley, 2001) that resulted from the combination of an efficient replacement of methyl chloroform as an industrial solvent and its relatively short atmospheric lifetime of 5 years. The global mean surface mixing ratio of methyl chloroform has steadily decreased to 22.6 ± 1.0 ppt averaged over 2004 from 46.4 ppt in 2000 (averages of the AGAGE, NOAA, and UCI values given in Table 1-2). The decline since 1998 (Montzka et al., 2000) has occurred at an approximately exponential rate consistent with relatively small emissions. Furthermore, elevated concentrations have practically ceased to exist during pollution events at background sites such as Mace Head (Ireland), although

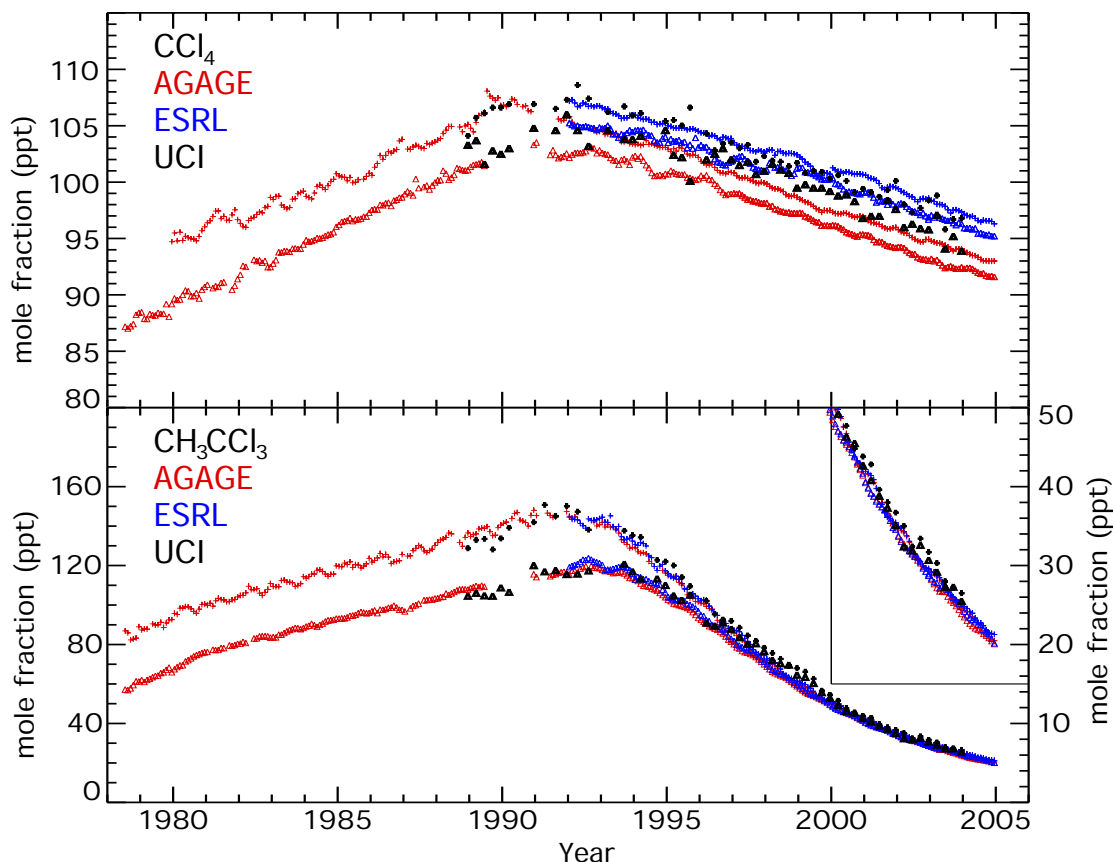


Figure 1-6. Hemispheric monthly mean of CH_3CCl_3 and CCl_4 (crosses for Northern Hemisphere and triangles for Southern Hemisphere) from the AGAGE stations (Prinn et al., 2000, 2005), the NOAA/ESRL network (Thompson et al., 2004; Montzka et al., 1999 updated), and UCI (D.R. Blake et al., 1996; N.J. Blake et al., 2001). Recent measurements for methyl chloroform are depicted in magnified form in the insert, using the scale on the right-hand side of the panel.

other European remote sites have reported distinct methyl chloroform excursions (Gros et al., 2003).

Background concentrations of CH_3CCl_3 from both hemispheres have been converging steadily from an inter-hemispheric gradient of more than 10% to an essentially constant annual mean difference of $2.1 \pm 0.4\%$ (corresponding to an uncertainty of ± 0.1 ppt) since 1999. In fact, during the warm season, Northern Hemispheric background concentrations can even be lower than in the Southern Hemisphere at the same time, due to the different hemispheric hydroxyl radical (OH) abundances. Calibration scales between the networks of NOAA/ESRL and AGAGE used to differ by several percent (*WMO 2002*, Montzka and Fraser et al., 2003), but since the newest scale updates by AGAGE (SIO-98) and NOAA (Hall et al., 2002) came into force, an excellent agreement exists. At stations with concurrent measurements from both net-

works, only small mean offsets of $0.4 \pm 1.8\%$ (1 sigma) are observed (AGAGE-NOAA) between 2000 and 2005.

1.2.1.6 METHYL CHLORIDE (CH_3Cl)

Methyl chloride (CH_3Cl) is the most abundant chlorine-containing compound in the atmosphere, with globally averaged concentrations of about 550 ppt. Before *WMO 2002*, there had been an imbalanced budget and large missing source, but in *WMO 2002* tropical and subtropical plants were proposed as potential sources to fill the gap. Recently, abiotic release of CH_3Cl by senescent or dead leaves has been proposed as a new significant source in the tropics and subtropics. The short- and long-term trends of atmospheric CH_3Cl , and source/sink estimates for biomass burning, oceans, rice paddies, OH reaction, and loss to polar oceans have been updated.

LONG-LIVED COMPOUNDS

Atmospheric Distribution and Trends

Observations from NOAA/ESRL (since 1995) and AGAGE (since 1998) are consistent with the global average concentration ($\sim 550 \pm 30$ ppt) and the latitudinal variation (higher concentrations at the lower latitudes) reported in *WMO 2002* (Simmonds et al., 2004; Yoshida et al., 2004). These observations also suggest interannual variability for CH_3Cl , with significant enhanced concentrations during 1998 and a subsequent steady decrease until 2001, a trend that may be explained by large-scale forest fires in Indonesia and Canada during 1997-1998 (Simmonds et al., 2004; see also Table 1-2).

Aydin et al. (2004) and Trudinger et al. (2004) independently produced atmospheric histories of CH_3Cl for the 20th century based on Antarctic firn air measurements. These two studies both revealed an increase of about 10% in the 50 years prior to 1990 for atmospheric CH_3Cl mixing ratios over Antarctica, with a rather steady level after 1980 (~ 480 -530 ppt). These tendencies are similar to the finding of Butler et al. (1999) in *WMO 2002*. The firn reconstruction of Kaspers et al. (2004), however, showed higher concentrations and a decreasing trend of 1.2 ppt/yr between 1975 and 2001; the difference from the results of the above studies remains unexplained. The ice core measurements during the past 300 years reported by Aydin et al. (2004) suggested a cyclic natural variability on the order of 110 years, which is in phase with the 20th-century rise inferred from firn air measurements.

Sources

Table 1-3 lists the revised estimates of source and sink strengths for atmospheric methyl chloride. Tropical forests remain a major source in the global atmospheric budget. High concentrations of atmospheric CH_3Cl have been observed in the tropical rainforests in Southeast Asia (up to 1500 ppt; Yokouchi et al., 2000) and above the canopy of tropical rainforests in South America (up to 809 ppt; Moore et al., 2005), supporting the significance of tropical forests as a potentially large CH_3Cl source. However, this source's strength and geographical distribution are still highly uncertain, mostly due to the large diversity of tropical vegetation.

Hamilton et al. (2003) reported abiotic release of CH_3Cl by senescent or dead plant material, both foliar and woody, and that these emissions rose dramatically when temperature increased. They estimated the global annual CH_3Cl emission from the weathering of leaf litter, between 30°N and 30°S , to be 30-2500 Gg/yr, possibly exceeding the source from live tropical vegetation.

For biomass burning, Andreae and Merlet (2001) provided a revised inventory (650 ± 325 Gg/yr) based

on evaluation and integration of the available biomass-burning emission data. The value is closer to the lower limit of the estimate range (655-1125 Gg/yr) reported in *WMO 2002*, suggesting that biomass burning emissions may have been overestimated in *WMO 2002*. Three-dimensional (3-D) model studies (Lee-Taylor et al., 2001; Yoshida et al., 2004) have also shown that a smaller burning source is more consistent with observations.

The oceanic source estimate, which once had been understood as the major CH_3Cl source, has been revised downward again. On the basis of measurements of the solubility of CH_3Cl in seawater, Moore (2000) reported a global annual flux from warm waters ranging from 465 to 495 Gg/yr. Recalculation of the oceanic CH_3Cl flux with the empirical relationship between saturation and SST by Yoshida et al. (2004) gave a net flux of 350 Gg/yr, which requires an oceanic emission of 380-500 Gg/yr to compensate for the oceanic uptake of 30-150 Gg/yr (discussed below). These values are at the lower end of the *WMO 2002* estimate range (325-1300 Gg/yr).

Large CH_3Cl emission from some salt marshes has been attributed to the plants growing in these regions (Rhew et al., 2002; but see also Cox et al., 2004), and the emissions are probably influenced by the high concentrations of available chloride ions (Cl^-). In addition to white-rot fungal sources, ectomycorrhizal fungi recently have been found to emit CH_3Cl (0.003 - $65 \mu\text{g g dry}^{-1}\text{d}^{-1}$; Redeker et al., 2004), but this source's global emission strength has not been estimated. Moore et al. (2005) suggested the possibility that some of the emission from woodrot fungi might compete with microbial uptake in the soil (see below). Thus, uncertainties for the fungal emissions of CH_3Cl have been added. Finally, the emissions from rice paddies have been revised downward from 5.0 to 2.4-4.9 Gg/yr using a new emission algorithm (Lee-Taylor and Redeker, 2005).

Sinks

The largest sink of CH_3Cl from the atmosphere is the reaction with the OH radical. The rate constant of the $\text{CH}_3\text{Cl} + \text{OH}$ reaction was re-evaluated to be $2.4 \times 10^{-12} e^{1250/T}$ or $3.6 \times 10^{-14} \text{ cm}^3 \text{ molec}^{-1} \text{ s}^{-1}$ at 298 K (Sander et al., 2003). The annual loss of CH_3Cl due to reaction with OH, calculated with detailed OH distributions, was 3800-4100 Gg/yr (Lee-Taylor et al., 2001; Yoshida et al., 2004), which exceeds the best estimate from *WMO 2002* of 3180 Gg/yr.

Soils are another important sink for CH_3Cl (Khalil and Rasmussen, 2000), and several bacterial strains capable of growth on CH_3Cl have been isolated recently from a variety of soils (McDonald et al., 2002; Miller et al., 2004). In addition to the ubiquitous bacteria capable of growing

Table 1-3. Estimated source and sink strengths for atmospheric methyl chloride from observations and three-dimensional model studies.

Source or Sink Type	Source or Sink Estimate ^a (Gg/yr)	3-D Model Studies	
		Lee-Taylor et al. (2001) ^b	Yoshida et al. (2004) ^c
Sources			
Tropical and subtropical plants	820-8200 ^d		
Tropical senescent or dead leaves	30-2500 ^e	2380	2900
Biomass burning	325-1125 ^{d,f}	733	611
Oceans	380-500 ^{g,h}	477 ⁱ	508
Salt marshes	65-440 ^d	170	170
Fungi	43-470 ^d	128	-
Wetlands	48 ^j	48	48
Rice paddies	2.4-4.9 ^k	-	-
Fossil fuel burning	5-205 ^d		
Waste incineration	15-75 ^d	162	162
Industrial processes	10 ^c		
<i>Subtotal</i>	<i>(1743-13,578)</i>	<i>(4098)</i>	<i>(4399)</i>
Sinks			
OH ⁻ reaction	3800-4100 ^{h,k}		3994
Loss to stratosphere	100-300 ^d	3850	-
Cl reaction	180-550 ^d	-	-
Soil	100-1600 ^d	256	256
Loss to cold waters (polar oceans)	93-145 ^g	-	149
<i>Subtotal</i>	<i>(4273-6695)</i>	<i>(4106)</i>	<i>(4399)</i>

^a Best estimates that appeared in the 2002 WMO Assessment table (WMO, 2003) are not given here, due to the difficulty of reasonable selection.

^b Mean value of their best estimates is given.

^c Model mean is given.

^d WMO, 2003.

^e Hamilton et al., 2003.

^f Andreae and Merlet, 2001.

^g Moore, 2000.

^h Yoshida et al., 2004.

ⁱ Net ocean flux is given.

^j Varner et al., 1999; no range was given.

^k Lee-Taylor and Redeker, 2005.

aerobically on CH₃Cl, the potential importance of anoxic biodegradation as a CH₃Cl sink was shown by Freedman et al. (2004), but its global strength has not been quantified.

The oceanic uptake to cold waters (i.e., polar oceans) was re-examined using the measured solubility of CH₃Cl (Moore, 2000), and the estimate has been revised upward from 37-113 Gg/yr in *WMO 2002* to 93-145 Gg/yr. Studies by Tokarczyk et al. (2003a, b) using a stable-isotope incubation technique indicated that microbial activity plays an important role in CH₃Cl degradation in coastal seawater (Bedford Basin, Nova Scotia) as well as in the Southern Ocean. Thus, CH₃Cl-degrading bacteria are found in both terrestrial and marine environments. A common set of genes and proteins is found in certain ter-

restrial and marine methyl halide-oxidizing bacteria (Schafer et al., 2005). McDonald et al. (2002) suggested that these bacteria may play an important role in mitigating ozone depletion resulting from CH₃Cl.

There is no update for the other sinks, such as the reaction with Cl⁻ and loss to the stratosphere.

Atmospheric Budget

With high CH₃Cl emission from plants and dead leaves in the tropics and subtropics, global sinks of 4300-6700 Gg/yr could be balanced by known sources (Table 1-3), although uncertainties in emissions are so large that the possibility of missing sources or sinks cannot be denied.

LONG-LIVED COMPOUNDS

By adding tropical terrestrial biogenic sources of 2400-2900 Gg/yr, model simulations of atmospheric CH₃Cl showed general agreement with the observations (Lee-Taylor et al., 2001; Yoshida et al., 2004).

An isotopic study (Gola et al., 2005) shows that the atmospheric isotopic ratio of CH₃Cl is not well explained by known sources and sinks unless the flux from senescent and dead leaves is quite large (1800-2500 Gg/yr). The values have large uncertainties, however, due to high variability of the stable carbon isotope ratios of biomass burning emission and tropical plants, as well as limited information on the isotope ratio of the oceanic source. In addition, no measurements of CH₃Cl emission from senescent and dead leaves have been made in the field.

Our understanding of the budget of CH₃Cl has been revised based upon the considerations discussed above, but it is still difficult to assess how atmospheric CH₃Cl levels might be affected by changes in global climate and land-use patterns, mostly due to large uncertainties in the strengths and geographical distribution of tropical terrestrial sources.

1.2.1.7 METHYL BROMIDE (CH₃Br)

Methyl bromide is the most abundant brominated gas regulated by the Montreal Protocol. Additional observational and modeling studies of methyl bromide have been published since 2002 Assessment (WMO, 2003). Recent atmospheric measurements have become available, as have additional results from the analysis of firn air. Methyl bromide also was measured in ice core air bubbles for the first time. New techniques have become available for the analysis and quantification of sources and sinks, and progress has been made in refining estimates of methyl bromide fluxes from the natural environment.

Recent Atmospheric Trends

Since the previous Assessment (WMO, 2003), three different groups have published multiyear observational records for CH₃Br at different surface sites (Yokouchi et al., 2002; Montzka et al., 2003; Simmonds et al., 2004). The updated studies indicate a global mean mixing ratio for CH₃Br of 9.2 ppt in the three years before 1999, which was the first year industrial production declined as a result of the Montreal Protocol. The observations also show that the tropospheric mixing ratio of CH₃Br started declining in 1999, with the largest decline observed in the Northern Hemisphere (Figure 1-7). By mid-2004, the global tropospheric mixing ratio of CH₃Br had declined by approximately 1.3 ppt (14%) from the amount observed in the

years before anthropogenic production began decreasing (9.2 ppt in 1996-1997). Reported industrial production of methyl bromide for emissive uses decreased by 50% during this same period (UNEP, 2002a, updated). Methyl bromide is unique among ODS regulated by the Montreal Protocol because it is emitted in substantial quantities from natural processes. As a result, attributing the observed declines to reduced industrial production is less straightforward than for other ODS. The coincidence of the observed decline with reduced anthropogenic production (as a result of Montreal Protocol), and the observation that the largest declines were observed in the NH argue that the atmospheric decline is primarily the result of reduced anthropogenic emissions. The decline observed through 2004 was somewhat larger than projected by scenario Ab (see black curve in Figure 1-4) from *WMO 2002* (Montzka and Fraser et al., 2003).

The enhanced decline observed for CH₃Br from the mid-1990s to mid-2004 could imply that its atmospheric abundance is more sensitive to changes in anthropogenic production than suggested in the best-estimate budget in *WMO 2002* (Montzka and Fraser et al., 2003), or that non-anthropogenic sources or sinks of CH₃Br changed systematically and simultaneously. For example, declines in CH₃Br mixing ratios from 1998 to 2001 may have been accelerated as the atmosphere recovered from high biomass burning levels in 1998 (Simmonds et al., 2004), although the influence of burning on CH₃Br trends over longer periods (1996-2004) is not well defined.

Interlaboratory differences for the absolute calibration of methyl bromide in the atmosphere are smaller than they were in *WMO 2002*. The range of results from the three laboratories reporting recent atmospheric data is ±2%.

Preindustrial Mixing Ratios

Methyl bromide was measured in air trapped in ice cores for the first time (Saltzman et al., 2004). The results from Siple Dome (81°S, 149°W) suggest that ambient air mixing ratios of CH₃Br over Antarctica during 1700-1900 were 5-6 ppt, or substantially lower than the 8 ppt observed during the 1990s (Figure 1-8). Independent measurements of CH₃Br in firn air at Law Dome suggest mixing ratios over Antarctica of 5.5 ppt in the 1930s (Trudinger et al., 2004). These firn air results are consistent with those obtained previously from numerous sites across Antarctica: South Pole, Siple Dome, Dome Concordia, and Dronning Maud Land (Butler et al., 1999; Sturges et al., 2001). Despite the variations in snow temperature, humidity, marine influence, and snow accumulation rates at these different Antarctic sites, similar atmospheric his-

LONG-LIVED COMPOUNDS

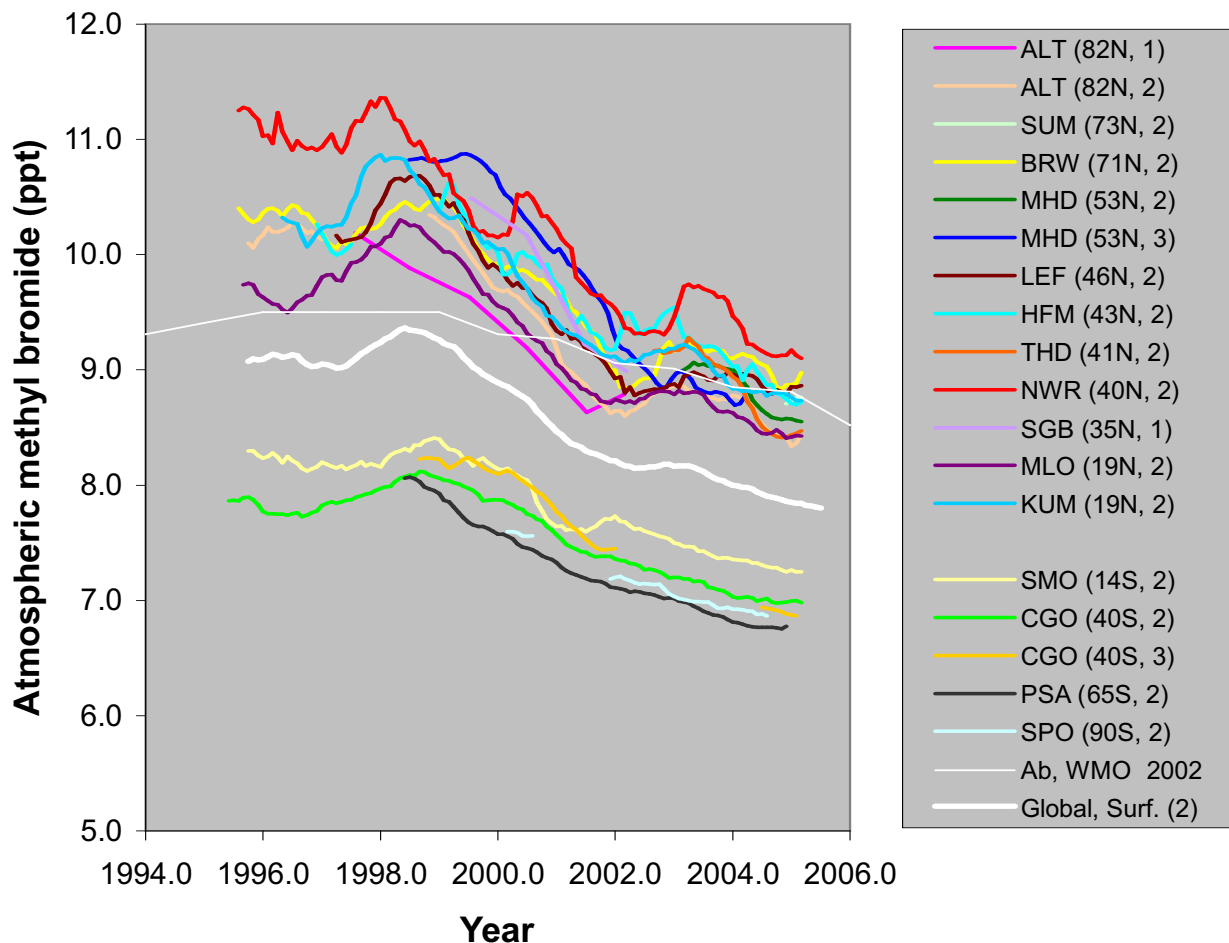


Figure 1-7. Measured mixing ratios of methyl bromide at different surface sites in the Northern and Southern Hemispheres. Most results are displayed as 12-month running means to highlight the observed long-term mixing ratio changes (larger seasonal variations that are observed at some sites are minimized here as a result). Results from the National Institute for Environmental Studies (NIES) are displayed as annual means connected by lines. Sampling latitudes and the data source are indicated in parentheses next to the site acronym: from NIES (1; Yokouchi et al., 2002), NOAA/ESRL (2; Montzka et al., 2003), and AGAGE (3; Simmonds et al., 2004). Sites are listed in the legend with the highest NH latitudes first: ALT (Alert, 82.5°N); SUM (Summit, 72.6°N), BRW (Barrow, 71.3°N), MHD (Mace Head, 53.3°N), LEF (Wisconsin, 45.9°N), HFM (Harvard Forest, 42.5°N), THD (Trinidad Head, 41.0°N), NWR (Niwt Ridge, 40.0°N), SGB (Sagami Bay, 35.0°N), MLO (Mauna Loa, 19.5°N), KUM (Kumukahi, 19.5°N), SMO (American Samoa, 14.2°S), CGO (Cape Grim, 40.4°S), PSA, (Palmer, 64.9°S), and SPO (South Pole, 90.0°S). A global mean derived from most of the NOAA/ESRL (2) data is shown as the thick white line; the thin white line is the global surface mixing ratio of CH₃Br from scenario Ab of *WMO 2002* (Montzka and Fraser et al., 2003).

ories have been derived for CH₃Br from firn and ice-core results from samples at all these locations. This consistency argues against processes that significantly influence CH₃Br mixing ratios during extended periods in contact with Antarctic snow and ice. In the Northern Hemisphere, however, this is not true; firn air results from different sites in Greenland show unusual variations that can be explained only by invoking in situ production of CH₃Br (Butler et al., 1999; Sturges et al., 2001).

Although consistent histories have been inferred from firn air samples collected at South Pole and Law Dome, the nature of the firn at Law Dome allows the derivation of a history with finer time resolution. For example, the results from Law Dome imply that the 20th-century mixing ratio increases for CH₃Br in the high-latitude Southern Hemisphere occurred mostly from 1950 to 1980 (Trudinger et al., 2004), not gradually over the entire century (Butler et al., 1999).

LONG-LIVED COMPOUNDS

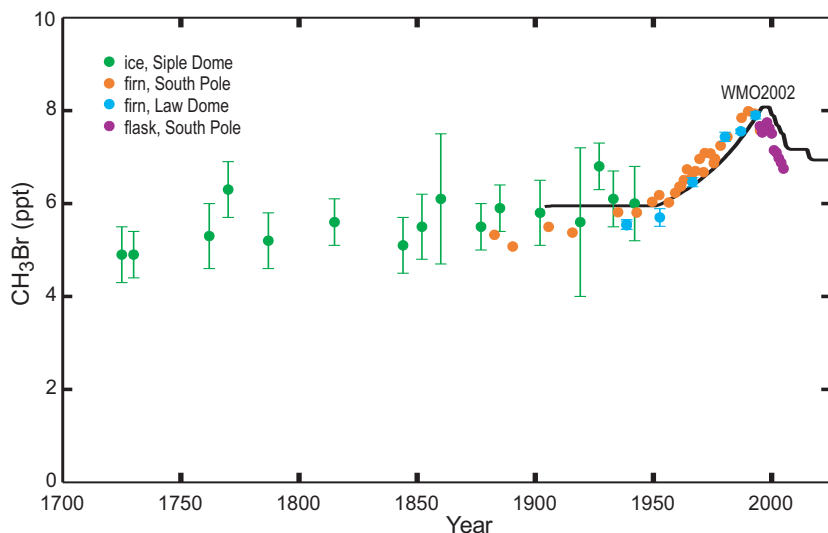


Figure 1-8. The history of methyl bromide abundance in the southern polar atmosphere, as measured in air samples from Antarctic ice and firn and from flasks collected at the South Pole (orange symbols, Butler et al. (1999) profiles dated with the Trudinger et al. (2004) firn diffusion model; blue symbols, Trudinger et al., 2004; green symbols, Saltzman et al., 2004; purple symbols, Montzka et al., 2003; <http://www.cmdl.noaa.gov/noah/>) compared with calculated Southern Hemisphere CH_3Br levels based on the Ab emission scenario in *WMO 2002* (black line) (Montzka and Fraser et al., 2003).

Updated Information on Nonindustrial Sources and Sinks

Work has continued since *WMO 2002* on identifying and quantifying the contribution of non-industrial fluxes of methyl bromide to and from the atmosphere. While progress has been made in improving our understanding of these fluxes, best estimates of their magnitudes remain essentially unchanged from Table 1-9 in the previous Assessment (Montzka and Fraser et al., 2003).

Regarding the oceans, previously it was learned that aqueous concentrations and saturations of methyl bromide in the temperate open ocean depend upon sea surface temperature (Groszko and Moore, 1998; King et al., 2000). Additional studies have attempted to refine this relationship (King et al., 2002), though it is clear that in some waters, additional unidentified factors influence methyl bromide saturation levels (Sturrock et al., 2003; Tokarczyk and Moore, 2006). These studies have confirmed that the ocean on average is a net sink of atmospheric methyl bromide. The role of biology in driving seasonal changes in flux through both production and degradation of methyl bromide has been further confirmed and quantified in temperate (Yvon-Lewis et al., 2002), polar (Tokarczyk et al., 2003b; Yvon-Lewis et al., 2004), and coastal (Sturrock et al., 2003) waters. The findings support the conclusions of *WMO 2002* regarding the lifetime of methyl bromide with respect to oceanic losses (1.9 (1.1-3.9) years).

The global contribution of plant emissions to the atmospheric burden of methyl bromide remains poorly quantified, given the plethora of species not yet studied. Improvements in quantifying this source may be possible

with the identification of a gene that encodes an enzyme capable of producing methyl halides from aqueous chloride, bromide, and iodide ions (Rhew et al., 2003a). This finding may allow a genetic basis for understanding and predicting methyl halide production by plants. Other studies relating to plants have led to a slightly reduced estimate of emissions from rice paddies (Lee-Taylor and Redeker, 2005).

Uptake by soils has been studied further since the previous Ozone Assessment (WMO, 2003). A laboratory study of methyl bromide uptake by boreal soils found uptake rates similar to those measured in the past (Rhew et al., 2003b). This work was the first to allow the quantification of both uptake and emission fluxes through use of isotopically labeled methyl halides. Field measurements continue to show that terrestrial ecosystems can act both as a source and sink of CH_3Br . While net emission has been observed in coastal grasslands and wetlands in Tasmania, Australia, net uptake was observed at similar sites with exposed soil or leaf litter (Cox et al., 2004). A study of CH_3Br losses to a temperate forest soil over the 1999 growing season revealed a loss that was apparently an order of magnitude less than previous uptake estimates for this soil type (Varner et al., 2003). Also, a multiyear study in freshwater peatlands showed a close balance between emissions and uptake (White et al., 2005), in contrast with earlier studies that suggested large net sources from these ecosystems. Discrepancies between these recent studies and prior estimates may be caused by competing production and consumption mechanisms at individual field sites. Emissions from fungi, for example, may affect the net CH_3Br flux measured at different sites

(Varner et al., 2003; Redeker et al., 2004). Such discrepancies underscore the potential for isotopic studies to provide improved estimates of gross CH_3Br fluxes.

Ambient air measurements in a coastal region confirm previous findings from smaller-scale experiments that methyl bromide can be emitted from coastal areas (Sturrock et al., 2003; Cox et al., 2005). Enhanced mixing ratios were also observed at multiple sites on the west coast of California, though these measurements may have been influenced by agricultural activities in the region (Low et al., 2003). Unusual enhancements of CH_3Br have been observed during spring in the Arctic, however, that do not appear to be explained by surface-based emissions or other known sources (Wingenter et al., 2003). The authors proposed a photochemical mechanism by which CH_3Br may be produced in the background atmosphere in substantial amounts, though analogous reactions have been shown to be quite slow and unlikely.

Estimates of global carbon monoxide (CO) emissions from fires and their interannual variability have been derived based upon satellite data (Duncan et al., 2003). These estimates are similar in magnitude to those described in Andreae and Merlet (2001), who applied burning-specific emission factors to all major pyrogenic processes (grassland and forest fires, the burning of bio-fuels and agricultural residues, and the making and burning of charcoal) to derive a global emission for methyl bromide of 29 Gg $\text{CH}_3\text{Br}/\text{yr}$. Though this newer source estimate is slightly larger than the 20 (10-40) Gg $\text{CH}_3\text{Br}/\text{yr}$ quoted in the previous Assessment for biomass burning (Montzka and Fraser et al., 2003), it falls well within the uncertainties of the older estimate.

On the Imbalance of CH_3Br Sources and Sinks and the Contribution of Industrially Derived CH_3Br

Despite the recent work on identifying and quantifying sources and sinks, best estimates of the magnitudes of sources cannot sustain measured mixing ratios during the past 25 years given the best estimates of loss (WMO, 2003). The firn air and ice bubble air data imply that this discrepancy existed before CH_3Br was produced industrially (Reeves, 2003; Saltzman et al., 2004). Though observational evidence for a significant CH_3Br source in the tropics is currently lacking, modeling studies have suggested that such a source could diminish the discrepancy in a way that is reasonably consistent with observations (Lee-Taylor et al., 1998; Warwick et al., 2006). Others (Reeves, 2003) have noted that the discrepancy could also be reduced if the CH_3Br lifetime were longer than 0.7 year (0.5-0.9 year) (WMO, 1999; WMO, 2003).

The firn air and ice bubble air results also suggest an atmospheric increase in the Southern Hemisphere

during the 20th century that is larger than expected from increases in emissions of anthropogenically produced CH_3Br alone (Reeves, 2003; Saltzman et al., 2004). The increase can be explained if emissions from anthropogenic activities accounted for a larger fraction of the total flux than presumed in the “best-estimate” budget (1992 fumigation emissions of 41 Gg/yr in 1992 relative to a total flux of 204 Gg/yr; Montzka and Fraser et al., 2003), or if other emissions had also increased over this time, such as biomass burning. The large uncertainties in CH_3Br fluxes from biomass burning over time prevent deriving tight constraints on the CH_3Br fluxes from industrially derived production from the 20th century firn air and ice bubble results (Saltzman et al., 2004).

Previous Assessments have suggested that anthropogenic CH_3Br emissions in 1992 of 41 Gg/yr derived from industrial production accounted for 20 (10-40)% of the total annual flux at that time (this range encompasses a total flux estimated by total sources or sinks; WMO, 2003). Alone, the 20th-century increase in atmospheric CH_3Br inferred from firn air and ice bubble air, or the large decline observed in ambient air since 1999, do not tightly constrain this fraction additionally. Both the recent observed decline and the 20th-century increase inferred for atmospheric methyl bromide were larger than expected, however, given our understanding of the CH_3Br budget and declines in reported production (UNEP, 2002a; Yokouchi et al., 2002; Montzka et al., 2003; Reeves, 2003; Saltzman et al., 2004; Trudinger et al., 2004). Because CH_3Br emitted from fumigation changed more than any other known flux during both periods, the results suggest a contribution from fumigation-related emissions in the middle to upper half of the range quoted in the past, or 30 (20-40)%. This suggests that fumigation-related emissions could have a stronger influence on atmospheric methyl bromide mixing ratios than estimated in past Assessments, though uncertainties in the variability of natural emission rates and loss, and in the magnitude of methyl bromide banked in recent years, influence our understanding of this sensitivity.

The higher contribution of anthropogenic CH_3Br to the total flux may be explained in part by a mean release fraction of CH_3Br after application to soils for agriculture fumigation purposes that is greater than 50%. In past WMO Ozone Assessments, a mean release fraction of 50% had been suggested for this application; the Methyl Bromide Technical Options Committee (MBTOC), however, suggests a mean release fraction of 70% (40-87%; UNEP, 2002a). Such a larger fraction would imply emissions from all types of fumigation of 51 Gg instead of 41 Gg in 1992; this additional emission would partially reduce the imbalance between known sources and sinks. A rela-

LONG-LIVED COMPOUNDS

tively larger contribution of fumigation-related emissions could also be explained if the total atmospheric lifetime of CH_3Br were longer than 0.7 year (Yokouchi et al., 2002; Reeves, 2003).

1.2.2 Lifetimes

1.2.2.1 HALOCARBON LIFETIME UPDATES AND VARIABILITY

After being emitted, most environmentally important trace gases, including methane and other organic compounds, carbon monoxide, nitrogen oxides, and sulfur gases, are removed from the atmosphere by oxidation. The strengths of the tropospheric sinks are essentially determined by the concentrations of oxidants, in particular the highly reactive hydroxyl radical (OH) that dominates the removal of many gases, including methane (CH_4), other hydrocarbons, CO, and natural and anthropogenic hydrohalocarbons. For that reason, global OH levels are often taken as a proxy for the oxidizing efficiency of the atmosphere. Through the OH feedback, even changes in the tropospheric emissions of gases that are too short lived to reach the stratosphere can affect the stratosphere when they influence tropospheric OH. The most important such gases are CO and nitrogen oxides. Lifetimes of many ozone-depleting substances are also determined by photolysis rates in the stratosphere. Hence, lifetimes of these gases can depend on the intensity of the Brewer-Dobson circulation as well. Changes in the oxidizing power of the atmosphere could have large impacts on air pollution, aerosol formation, greenhouse radiative forcing, and stratospheric ozone depletion. The quantification of possible recent changes in tropospheric OH continues to be an active and controversial area of research. The evidence for such changes is based primarily on inverse models of CH_3CCl_3 emissions and tropospheric observations that have deduced OH variations on the order of $\pm 10\%$ in recent decades but no systematic long-term trends (Bousquet et al., 2005; Prinn et al., 2005). In the future, the Intergovernmental Panel on Climate Change/Technology and Economic Assessment Panel (IPCC/TEAP Chapter 2; Velders and Madronich et al., 2005) concludes that tropospheric OH in the 21st century may change by -18% to $+5\%$, depending on the choices of emission scenarios.

The atmospheric lifetimes for the vast majority of the gases listed in Table 1-4 are unchanged from *WMO 2002*. The list of gases and lifetimes in this Table is not limited only to gases with atmospheric lifetimes longer than 6 months, because it was decided to put all the lifetimes needed for Chapters 1 and 2 of this Assessment in

a single table. This section describes the basis for changes that were made either due to new laboratory experiments or due to including additional gases. The best estimate lifetime for methyl chloride (CH_3Cl) was reduced due to the discovery of additional sinks. Analysis by Tokarczyk et al. (2003a, b) of the partial atmospheric lifetime with respect to ocean removal for CH_3Cl (4.1 years) reduces the total lifetime to 1.0 years.

The atmospheric lifetime for methyl chloroform has been left at 5.0 years, the same as in *WMO 2002* (Montzka and Fraser et al., 2003), because the suggestion by Prinn et al. (2005) for a lifetime of 4.9 years and a tropospheric lifetime due to reaction with OH of 6.0 years (6.1 years used in this Assessment) was not deemed to represent a significant change.

Although the atmospheric lifetime of the hydrofluoroether CHF_2OCF_3 (HFE-125) is unchanged at 136 years, the much longer atmospheric lifetime (1800 years) implied by the theoretical analysis of Wu et al. (2004) suggests that further study is needed for this compound.

The atmospheric lifetime of trifluoromethylsulfurpentafluoride (SF_5CF_3) was modified to a range of 650-950 years to better account for the findings in Takahashi et al. (2002). It did not seem warranted to use a single lifetime of 800 years. However, it should be noted that laboratory data by Chim et al. (2003) and Limão-Vieira et al. (2004) both imply an atmospheric lifetime closer to 1000 years for SF_5CF_3 .

A number of additional gases have been included in Table 1-4 based on new laboratory data for their reaction rates with OH. These include: $\text{CFH}_2\text{CH}_2\text{OH}$, $\text{CHF}_2\text{CF}_2\text{OCHF}_2$, $\text{CF}_3\text{CHF}_2\text{CF}_2\text{OCH}_2\text{CF}_2\text{CF}_3$, $\text{CF}_3\text{OC(O)H}$, $\text{C}_2\text{F}_5\text{OC(O)H}$, $\text{CF}_3\text{CHFCF}_2\text{CH}_2\text{OH}$, $\text{C}_2\text{F}_5\text{C(O)CF(CF}_3)_2$, and $n\text{-C}_3\text{F}_7\text{OC(O)H}$. Some other compounds were not included because only room temperature reaction data were available.

Also included are several compounds that were otherwise included in the Global Warming Potential (GWP) analysis in *WMO 2002*: $c\text{-C}_3\text{F}_6$ ($\tau = 1000$ years), NF_3 (740 years), $(\text{CF}_3)_2\text{CHOCHF}_2$ (3.1 years), and $(\text{CF}_2)_4\text{CH(OH)}$ (0.85 year).

1.2.2.2 UNCERTAINTIES IN OZONE-DESTROYING HALOCARBON LIFETIMES

In order to estimate the remaining banks (and their uncertainties) of CFCs and other ozone destroying halocarbons, it is useful to have the best possible estimates of the uncertainties in their lifetimes. For this purpose, the model-based stratospheric lifetime estimates from the 1998 Assessment (Table 1-4 in WMO, 1999) are combined with values derived from stratospheric measurements

Table 1-4. Trace gas lifetimes for selected halocarbons and perfluorinated gases. For completeness, estimates for local lifetimes for some very short-lived (lifetime (τ) < 0.5 year) species are included (in italics). As discussed in Chapter 2, the atmospheric lifetimes for these species (defined as the ratio of burden to emission) (Prather and Ehhalt et al., 2001; Montzka et al., 2003) depend on the location and time of emission. Thus, these local lifetimes should not be used in semi-empirical ODP, GWP, or EESC calculations for these gases.

Industrial Designation or Common Name	Chemical Formula	Lifetime (years)	Notes
Halogen-substituted methanes			
HFC-41	CH ₃ F	2.4	1
HFC-32	CH ₂ F ₂	4.9	1
HFC-23	CHF ₃	270	1
FC-14 (Carbon tetrafluoride)	CF ₄	50 000	2
Methyl chloride	CH ₃ Cl	1.0	1, 3
Dichloromethane	CH ₂ Cl ₂	<i>0.38</i>	15, 16
Chloroform	CHCl ₃	<i>0.41</i>	15, 16
Carbon tetrachloride	CCl ₄	26	5
HCFC-31	CH ₂ ClF	1.3	4
HCFC-22	CHClF ₂	12.0	1, 6
HCFC-21	CHCl ₂ F	1.7	1, 6
CFC-13	CClF ₃	640	2
CFC-12	CCl ₂ F ₂	100	2, 7
CFC-11	CCl ₃ F	45	2, 7
Methyl bromide	CH ₃ Br	0.7	3
Dibromomethane	CH ₂ Br ₂	<i>0.33</i>	8, 15, 16
Bromoform	CHBr ₃	<i>0.07</i>	8, 15, 16, 19
Bromodifluoromethane	CHBrF ₂	5.8	4
Bromochloromethane	CH ₂ BrCl	<i>0.41</i>	8, 15, 16
Bromodichloromethane	CHBrCl ₂	<i>0.19</i>	7, 15, 16
Dibromochloromethane	CHBr ₂ Cl	<i>0.21</i>	7, 15, 16
Halon-1301	CBrF ₃	65	2, 7
Halon-1211	CBrClF ₂	16	9
Halon-1202	CBr ₂ F ₂	2.9	17
Methyl iodide	CH ₃ I	<i>0.02</i>	7, 15, 16, 20
Diiodomethane	CH ₂ I ₂	<i>Minutes</i>	7, 15, 16
Chloroiodomethane	CH ₂ ClI	<i>Hours</i>	7, 15, 16
Trifluoroiodomethane	CF ₃ I	<i>0.01</i>	2, 15
Halogen-substituted ethenes			
Trichloroethene	C ₂ HCl ₃	<i>0.01</i>	15
Perchloroethene	C ₂ Cl ₄	<i>0.27</i>	15
Halogen-substituted ethanes			
HFC-161	CH ₃ CH ₂ F	<i>0.21</i>	2, 15
HFC-152	CH ₂ FCH ₂ F	0.60	2, 15
HFC-152a	CH ₃ CHF ₂	1.4	1, 6
HFC-143	CH ₂ FCHF ₂	3.5	1

LONG-LIVED COMPOUNDS

Table 1-4, continued.

Industrial Designation or Common Name	Chemical Formula	Lifetime (years)	Notes
HFC-143a	CH ₃ CF ₃	52	1
HFC-134	CHF ₂ CHF ₂	9.6	1
HFC-134a	CH ₂ FCF ₃	14.0	1, 6
HFC-125	CHF ₂ CF ₃	29	1, 6
FC-116 (Perfluoroethane)	CF ₃ CF ₃	10 000	2
Chloroethane	CH ₃ CH ₂ Cl	0.08	15
1,2 Dichloroethane	CH ₂ ClCH ₂ Cl	0.19	10, 15
Methyl chloroform	CH ₃ CCl ₃	5.0	9
HCFC-142b	CH ₃ CClF ₂	17.9	1, 6
HCFC-141b	CH ₃ CCl ₂ F	9.3	1, 6
HCFC-123	CHCl ₂ CF ₃	1.3	6, 11
HCFC-124	CHClF ₂ CF ₃	5.8	6, 11
CFC-113	CCl ₂ FCClF ₂	85	2
CFC-113a	CCl ₃ CF ₃	NA	NA
CFC-114	CClF ₂ CClF ₂	300	2
CFC-115	CClF ₂ CF ₃	1700	2
Halon-2402	CBrF ₂ CBrF ₂	20	17
Iodoethane	C ₂ H ₅ I	0.01	7, 15, 16, 20
Halogen-substituted propanes			
HFC-281ea	CH ₃ CHFCH ₃	0.06	15
HFC-263fb	CH ₃ CH ₂ CF ₃	1.6	2
HFC-245ca	CH ₂ FCF ₂ CHF ₂	6.2	1
HFC-245ea	CHF ₂ CHFCHF ₂	4.0	2
HFC-245eb	CH ₂ FCHFCF ₃	4.0	12
HFC-245fa	CHF ₂ CH ₂ CF ₃	7.6	1
HFC-236cb	CH ₂ FCF ₂ CF ₃	13.6	1
HFC-236ea	CHF ₂ CHFCF ₃	10.7	1
HFC-236fa	CF ₃ CH ₂ CF ₃	240	1
HFC-227ea	CF ₃ CHF ₂ CF ₃	34.2	1
FC-218 (Perfluoropropane)	CF ₃ CF ₂ CF ₃	2600	2
n-Propyl chloride	CH ₃ CH ₂ CH ₂ Cl	0.06	13, 15
HCFC-243cc	CH ₃ CF ₂ CCl ₂ F	26.4	4
HCFC-225ca	CHCl ₂ CF ₂ CF ₃	1.9	11
HCFC-225cb	CHClF ₂ CF ₂ CClF ₂	5.8	11
n-Propyl bromide (n-PB)	CH ₃ CH ₂ CH ₂ Br	0.03	15, 16
n-Propyl iodide	CH ₃ CH ₂ CH ₂ I	0.001	7, 15, 16, 20
Isopropyl iodide	CH ₃ CHICH ₃	0.003	7, 15, 20
Halogen-substituted higher alkanes			
HFC-365mfc	CH ₃ CF ₂ CH ₂ CF ₃	8.6	1, 14
HFC-356mcf	CH ₂ FCH ₂ CF ₂ CF ₃	1.2	1, 14
HFC-356mff	CF ₃ CH ₂ CH ₂ CF ₃	8.1	1, 14
HFC-338pcc	CHF ₂ CF ₂ CF ₂ CHF ₂	12.3	1, 14

Table 1-4, continued.

Industrial Designation or Common Name	Chemical Formula	Lifetime (years)	Notes
FC-C318 (Perfluorocyclobutane)	c-C ₄ F ₈	3200	1
FC-31-10 (Perfluorobutane)	C ₄ F ₁₀	2600	2
HFC-43-10mee	CF ₃ CHFCHFCF ₂ CF ₃	15.9	1
HFC-458mfcf	CF ₃ CH ₂ CF ₂ CH ₂ CF ₃	23.2	1
FC-41-12 (Perfluoropentane)	C ₅ F ₁₂	4100	2
Perfluorodecalin	C ₁₀ F ₁₈	2000	29
HFC-55-10mcff	CF ₃ CF ₂ CH ₂ CH ₂ CF ₂ CF ₃	7.7	2
FC-51-14 (Perfluorohexane)	C ₆ F ₁₄	3200	2
Perfluorocyclopropane	c-C ₃ F ₆	>1000	2
Fluorinated alcohols and ketones			
	CF ₃ CH ₂ OH	0.41	15
	CF ₃ CF ₂ CH ₂ OH	0.39	15, 23
	(CF ₃) ₂ CHOH	2.0	4
	CF ₃ (CF ₂) ₃ CH ₂ OH	0.45	23
	CFH ₂ CH ₂ OH	0.04	27
	CF ₃ CHFCH ₂ CH ₂ OH	0.34	22
	C ₂ F ₅ C(O)CF(CF ₃) ₂	0.04	21
Fluorinated ethers			
HFE-152a	CH ₃ OCHF ₂	1.6	1
HFE-143a	CH ₃ OCF ₃	4.3	1
HFE-134	CHF ₂ OCHF ₂	26	1
HFE-125	CHF ₂ OCF ₃	136	1
HFE-227ea	CF ₃ OCHFCH ₂ CF ₃	11	2
HCFE-235da2	CHF ₂ OCHClCF ₃	2.6	2
HFE-236ea2	CHF ₂ OCHFCH ₂ CF ₃	5.8	2
HFE-236fa	CF ₃ OCH ₂ CF ₃	3.7	2
HFE-245fa1	CHF ₂ CH ₂ OCF ₃	2.2	2
HFE-245fa2	CHF ₂ OCH ₂ CF ₃	4.9	1
HFE-245cb2	CH ₃ OCF ₂ CF ₃	5.1	4
HFE-254cb2	CH ₃ OCF ₂ CHF ₂	2.6	4
HFE-263fb2	CH ₃ OCH ₂ CF ₃	0.1	2
HFE-329mcc2	CF ₃ CF ₂ OCF ₂ CHF ₂	6.8	2
HFE-338mcf2	CF ₃ CF ₂ OCH ₂ CF ₃	4.3	2
HFE-347mcc3	CH ₃ OCF ₂ CF ₂ CF ₃	5.2	4
HFE-347mcf2	CF ₃ CF ₂ OCH ₂ CHF ₂	2.8	2
HFE-347pf3	CHF ₂ OCH ₂ CF ₂ CF ₃	5.9	4
HFE-347sy2	CF ₃ CF(OCH ₃)CF ₃	3.7	4
HFE-356mec3	CH ₃ OCF ₂ CHFCH ₂ CF ₃	0.94	2
HFE-356mff2	CF ₃ CH ₂ OCH ₂ CF ₃	0.4	15
HFE-356pcc3	CH ₃ OCF ₂ CF ₂ CHF ₂	0.93	2
HFE-356pcf3	CHF ₂ OCH ₂ CF ₂ CHF ₂	3.6	4
HFE-356pcf2	CHF ₂ CH ₂ OCF ₂ CHF ₂	2.0	2
HFE-365mcf3	CH ₃ OCH ₂ CF ₂ CF ₃	0.11	2, 15

LONG-LIVED COMPOUNDS

Table 1-4, continued.

Industrial Designation or Common Name	Chemical Formula	Lifetime (years)	Notes
HFE-374pc2 ^a	CH ₃ CH ₂ OCF ₂ CHF ₂	5.0	2
	CHF ₂ CF ₂ OCHF ₂	26.5	24
	CF ₃ CHF ₂ OCF ₂ CH ₂ CF ₂ CF ₃	9.1	24
	(CF ₃) ₂ CHOCHF ₂	3.1	2
	CF ₃ CH(OCF ₃)CHF ₂	3.1	2
	(CF ₃) ₂ CFOCH ₃	3.4	2
	CF ₃ OC(O)H	3.6	25
	C ₂ F ₅ OC(O)H	3.6	26
	n-C ₃ F ₇ OC(O)H	2.6	26
	HFE-7100 (HFE-44-9)	CH ₃ OC ₄ F ₉	5.0
HFE-7200 (HFE-56-9)	C ₂ H ₅ OC ₄ F ₉	0.77	2
HFE-43-10pccc124 ^b	CHF ₂ OCF ₂ OCF ₂ CF ₂ OCHF ₂	6.3	2
HFE-236ca12 (HG-10)	CHF ₂ OCF ₂ OCHF ₂	12.1	2
HFE-338pcc13 (HG-01)	CHF ₂ OCF ₂ CF ₂ OCHF ₂	6.2	2
Other fluorinated species			
Trifluoromethylsulfur-pentafluoride	SF ₅ CF ₃	650-950	18
Sulfur hexafluoride	SF ₆	3200	2
Nitrogen trifluoride	NF ₃	740	2

Notes:

- Global lifetime estimated from a process lifetime with respect to tropospheric OH calculated relative to 6.1 years for CH₃CCl₃, assuming an average temperature of 272 K (Spivakovsky et al., 2000; Prather and Ehhalt et al., 2001); OH rate constants from Sander et al. (2006); and stratospheric loss lifetimes inferred from IPCC (2001).
- Prather and Ehhalt et al. (2001) and Ramaswamy et al. (2001).
- See Section 1.2.1.6 for further discussion related to methyl halide global lifetimes. Includes estimate of ocean sink from Tokarczyk et al. (2003a, b).
- Lifetime calculated as in Note 1 except that no estimate of a stratospheric loss lifetime was available to include in the lifetime estimate listed. Hence this is an upper bound to the global lifetime estimate.
- Based on *WMO 2002*, including oceanic loss term with 94-year partial lifetime observed in saturation data and ascribed to an unidentified process (Yvon-Lewis and Butler, 2002) but also accounting for soils sink with 90-year partial lifetime (Happell and Roche, 2003). However, see Section 1.3.2.4 for additional considerations based on atmospheric measurements.
- Including oceanic loss term from Yvon-Lewis and Butler (2002). The contribution of oceanic loss to the lifetime of HCFC-21, HCFC-22, HCFC-123, HCFC-124, HCFC-141b, HFC-125, and HFC-152a is small; for HFC-134a and HCFC-142b it is negligibly small at the reported precision.
- WMO (1999).
- Lifetimes listed include local tropospheric photolysis lifetimes from Table 2-9 in Kurylo and Rodríguez et al. (1999). Consideration of only tropospheric OH loss results in local lifetimes of 0.34 years for CH₂Br₂, 0.21 years for CHBr₃, and 0.37 years for CH₂BrCl.
- See Section 1.4 text for discussion.
- OH rate constant from Qiu et al. (1992).
- Lifetime calculated as in Note 1, but with stratospheric loss from Naik et al. (2000).
- Lifetime calculated as in Note 1, but with OH rate constant and stratospheric loss from Naik et al. (2000).
- Markert and Nielsen (1992).
- OH rate constant from DeMore and Bayes (1999).
- The values estimated correspond to local lifetimes in the free troposphere from Chapter 2 (this Assessment). For species that react with OH, the process lifetime due to OH reaction is calculated using the rate constant at 275 K (for lifetimes greater than 10 days) or 300 K (for lifetimes less than 10 days) and OH concentration of 1 × 10⁶ molec cm⁻³. These should not be used in estimating ODP, GWP, or EESC because the atmospheric burden for these short-lived gases (τ < 0.5 year) depends on the location and time of emissions.
- See Chapter 2.
- From the 2-D model calculation in Fraser et al. (1999).
- Takahashi et al. (2002), Chim et al. (2003), and Limão-Vieira et al. (2004). Range in lifetime depends on whether solar proton events reduce the lifetime.
- Bayes et al. (2003).

Table 1-4, continued.

20. Cotter et al. (2003).
21. Taniguchi et al. (2003).
22. Chen et al. (2003).
23. Hurley et al. (2004) estimate the lifetimes of $F(CF_2)_nCH_2OH$, for $n = 1-4$, to be 0.45 year.
24. Chen et al. (2005).
25. Chen et al. (2004a).
26. Chen et al. (2004b).
27. Rajakumar et al. (2005).
28. Li et al. (2006).
29. Shine et al. (2005).

^a Referred to as HFE-374pcf2 in past Assessments.

^b Referred to as H-Galden 1040x in past Assessments.

by Volk et al. (1997, Table 5). This provides lifetime uncertainties that are almost entirely independent of the estimates that can be produced by using the atmospheric measurements from the ground-based networks combined with emissions estimated from industrial production figures. The uncertainties are obtained by taking the root mean square sum of the variances from the model-based estimates and the variances given by Volk et al. The results are lifetime uncertainty ranges of 35-57 years for CFC-11, 79-113 years for CFC-12, and 66-114 years for CFC-113. However, it was indicated in Section 1.2.1.1 that CFC-113 is decreasing in the atmosphere at a rate of 1%/yr, which implies a maximum lifetime of approximately 100 years. A range of 66-100 years is then derived for CFC-113. The stratospheric lifetime uncertainty range for CCl_4 calculated in the same way is 28-46 years. It may be noted that the recommended lifetimes in the previous section do not lie exactly in the middle of these uncertainty ranges. That is because, except where new measurements had been made, there was no justification for changing the values used in *WMO 2002*.

For the major HCFCs, the lifetime uncertainty ranges are obtained by combining the uncertainty in the hydroxyl value of 14% given by Prinn et al. (2001) with the uncertainties in the reaction rates between the HCFCs and hydroxyl from Sander et al. (2006). This gives lifetime uncertainties of $\pm 17\%$ for HCFC-22, $\pm 20\%$ for HCFC-141b, and $\pm 24\%$ for HCFC-142b.

1.2.3 Total Atmospheric Chlorine and Bromine

1.2.3.1 TOTAL ORGANIC CHLORINE IN THE TROPOSPHERE

Total organic chlorine (CCl_y) from long-lived source gases continued to slowly decrease in the troposphere during 2001-2004 (Montzka et al., 2003;

O'Doherty et al., 2004) (Figure 1-9 and Table 1-5). In mid-2004 tropospheric CCl_y was approximately 3.44 parts per billion (ppb), or about 0.25 ppb Cl (nearly 7%), below the peak observed in 1992-1994. The rate of decline in CCl_y from 2003 to 2004 (-20 ppt Cl/yr or $-0.59\%/yr$) was slightly less than in previous years (-23 ppt Cl/yr or $-0.64\%/yr$), owing to the reduced influence of methyl chloroform. In 2004, mixing ratio changes for methyl chloroform still contributed substantially to the decrease in CCl_y (-13.5 ppt Cl/yr), though this contribution was nearly matched by the decline observed in the aggregate of CFCs plus CCl_4 (-12.7 ppt Cl/yr). In 2004, the CFCs accounted for 62% of CCl_y in long-lived gases in the lower atmosphere; this fraction has increased slightly over the past decade as Cl from shorter-lived gases has diminished more rapidly than Cl from CFCs.

Increases in CCl_y from HCFCs slowed during 2000-2004. CCl_y from the three major HCFCs increased at a rate of nearly 6 ppt Cl/yr during 2004, or almost half the rate of annual increase measured in 1996 (Table 1-5). HCFCs accounted for 214 ppt of CCl_y in mid-2004, or about 6%.

1.2.3.2 TOTAL CHLORINE IN THE STRATOSPHERE AND HYDROGEN CHLORIDE (HCl)

Stratospheric chlorine time series are different from tropospheric time series in many respects. Stratospheric chlorine levels lag tropospheric levels, due to the time it takes for the trends to propagate. During the propagation of tropospheric trends into the stratosphere, mixing leads to a distribution of transit times in any air parcel in the stratosphere, which is described by the concept of "age of the air." This mixing will inevitably make long-term trends in stratospheric time series less sharp, if they are driven by tropospheric trends (see, e.g., Waugh et al., 2001, and Engel et al., 2002). The peak in the tropospheric chlorine is thus expected to occur later in the stratosphere and be broader and have somewhat lower mixing ratios in its

LONG-LIVED COMPOUNDS

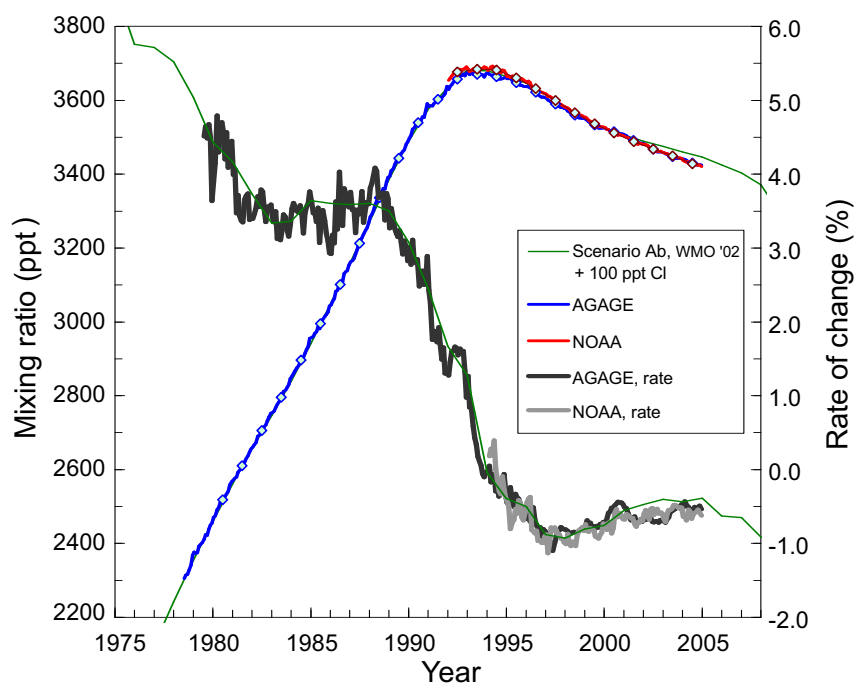


Figure 1-9. The tropospheric abundance of organic chlorine (CCl_f) from the NOAA/ESRL and AGAGE global measurement networks (updates of Montzka et al., 1999, and O'Doherty et al., 2004) and its rate of change over time. Quantities are based upon independently measured mixing ratios of CFC-11, CFC-12, CFC-113, HCFC-22, HCFC-141b, HCFC-142b, methyl chloroform, and carbon tetrachloride. Results for CFC-114 and CFC-115 from Prinn et al. (2000) are used in both compilations. An additional constant 550 ppt was added for CH_3Cl and 100 ppt was added for short-lived gases such as CH_2Cl_2 , CHCl_3 , C_2Cl_4 , and COCl_2 . Rates of change are determined from 12-month differences and are plotted with respect to the right-hand axis. Observations are compared with the projections from *WMO 2002* (green line).

Table 1-5. Contributions of halocarbons to total chlorine (Cl) in the troposphere. An average of AGAGE and NOAA/ESRL global means was used to derive these mid-year mixing ratios. Rates of change were calculated as the difference between the indicated year and the previous year. Uncertainties in rates of change (1 standard deviation) are estimated from the difference in rates derived from observations by the different global networks, NOAA/ESRL and AGAGE. The uncertainty in total Cl is approximately 25 ppt Cl (1 standard deviation) throughout the period 1996-2004 (based on the sum of differences in global tropospheric means derived for individual gases between the AGAGE and NOAA/ESRL networks).

	Total Cl (ppt Cl)			Contribution to Total Cl (%)			Rate of Change in Total Cl (ppt Cl/yr)		
	1996	2000	2004	1996	2000	2004	1996	2000	2004
Aggregated CFCs	2160	2156	2126	59%	61%	62%	5.8 (3.4)	-1.4 (2.0)	-8.9 (0.4)
CH_3Cl ^a	550	550	550	15%	16%	16%	0.0 ^b	0.0 ^b	0.0 ^b
CCl_4	407	393	378	11%	11%	11%	-4.2 (0.6)	-3.6 (0.3)	-3.8 (0.7)
Aggregated HCFCs	141	180	214	4%	5%	6%	10.3 (0.5)	9.2 (0.8)	5.9 (1.0)
CH_3CCl_3	274	137	66	8%	4%	2%	-39.7 (0.2)	-26.8 (1.0)	-13.5 (0.4)
CH_2Cl_2 , CHCl_3 , etc. ^c	100	100	100	3%	3%	3%	0.0 ^b	0.0 ^b	0.0 ^b
Halon-1211	3.5	4.0	4.2	0%	0%	0%	0.2	0.1	0.0
Total Cl	3636	3521	3437				-28 (3.5)	-23 (2.4)	-20 (1.4)
							-0.76%	-0.64%	-0.59%

^a CH_3Cl assumed to be 550, consistent with the previous Assessment (Montzka and Fraser et al., 2003).

^b Growth rate assumed to be zero here, though some very short-lived gases have been declining over the past decade (see Chapter 2).

^c CH_2Cl_2 , CHCl_3 , etc., also includes the very short-lived gases C_2Cl_4 , C_2HCl_3 , and $\text{CH}_2\text{ClCH}_2\text{Cl}$, and an additional 50 ppt to account for Cl from COCl_2 (see Chapter 2 for additional discussion of the contribution of short-lived gases to total Cl).

maximum (about 150 ppt lower; see Engel et al., 2002). Figure 1-10 shows an update of stratospheric chlorine trends for midlatitudes (44°N) calculated by Engel et al. (2002), based on tropospheric observations by NOAA/ESRL up to the year 2005, mean profiles of mean age, and a parameterization of the width of the age spectrum. Based on these calculations, the maximum chlorine levels were expected in the lower stratosphere around 1995 and were expected to have reached altitudes above 30 km by about 2000. It is expected that total chlorine is now decreasing at all altitudes.

Total chlorine in the stratosphere could either be in the form of organic chlorine or inorganic chlorine. Figure 1-11 is constructed based on the profiles of organic and inorganic species derived from observations and modeling results (see figure caption for details). Nassar et al. (2006a) derived the total chlorine budget for 30°N-60°N, based mainly on observations by the ACE-FTS, yielding 3.65 ppb chlorine (with an estimated accuracy of ± 0.13 ppb) in 2004. This value is slightly larger than the value of 3.54 ppb (with a precision of ± 0.10 ppb) derived by Zander et al. (1996) for 1994 from ATMOS experiment

observations, when stratospheric chlorine levels were still increasing.

At high altitudes (above 50 km) the total chlorine budget is dominated by hydrogen chloride (HCl), which at this altitude may serve as a good proxy for total inorganic chlorine (Cl_y) and even total chlorine. The longest continuous time series of HCl from satellite observations is that of the Halogen Occultation Experiment (HALOE) (Russell et al., 1993; Anderson et al., 2000). For about 55 km altitude, Figure 1-12 compares the HCl measurements with model values of HCl that are derived from a total chlorine time series that has been convoluted with spectra of various widths, each having a mean age of 5.5 years. The total chlorine values are based on the NOAA/ESRL and AGAGE measurements including a 100 ppt contribution from very short-lived (VSL) source gases (full lines), whereas the dashed curve (from scenario Ab in *WMO 2002*) excludes a contribution from VSL compounds. These Cl_y time series have been reduced by a factor of 0.96, which represents model estimates of the HCl/ Cl_y ratio at 55 km, in order to arrive at the model curves for HCl shown in Figure 1-12.

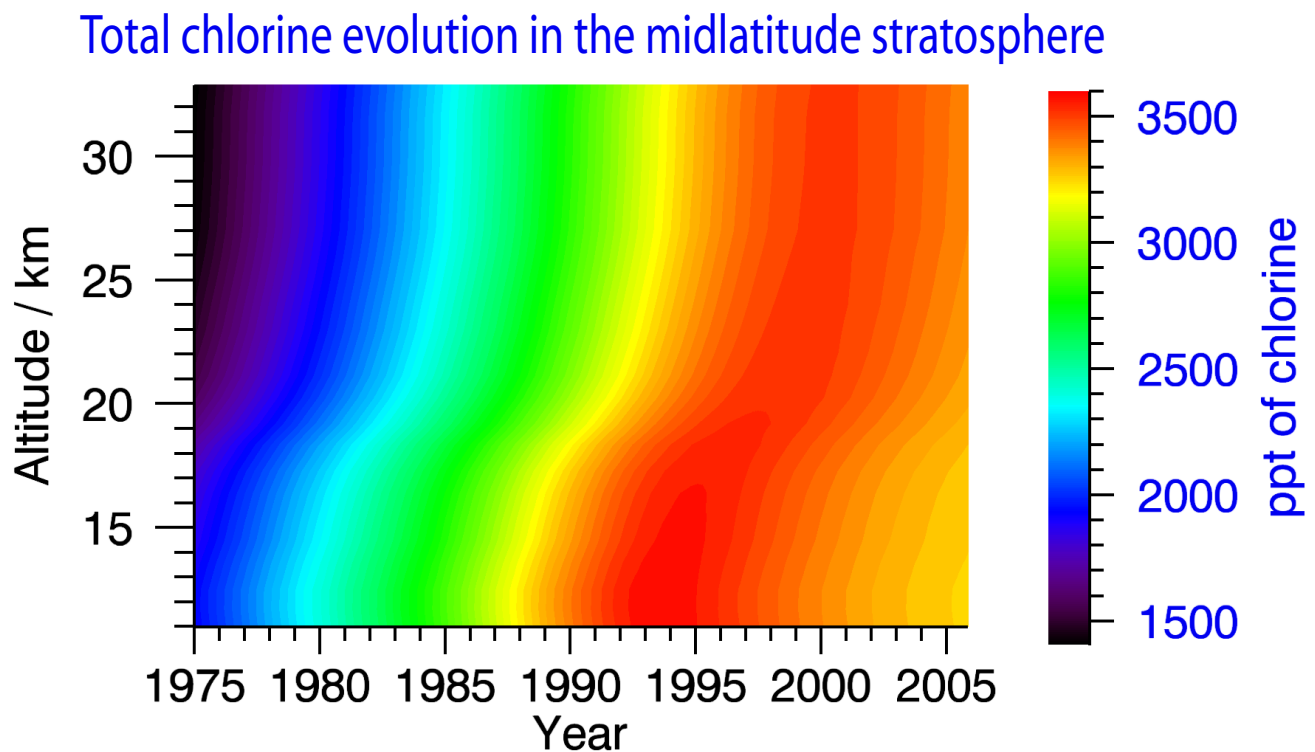


Figure 1-10. Total chlorine calculated based on the vertical distribution of mean age (derived from observations of the age tracers sulfur hexafluoride (SF_6) and carbon dioxide (CO_2)) and assumptions on the width of the age spectrum. Tropospheric data by NOAA/ESRL are used as the basis of the calculation (updated from Engel et al., 2002). No chlorine contribution from very short-lived (VSL) species is included in this calculation.

LONG-LIVED COMPOUNDS

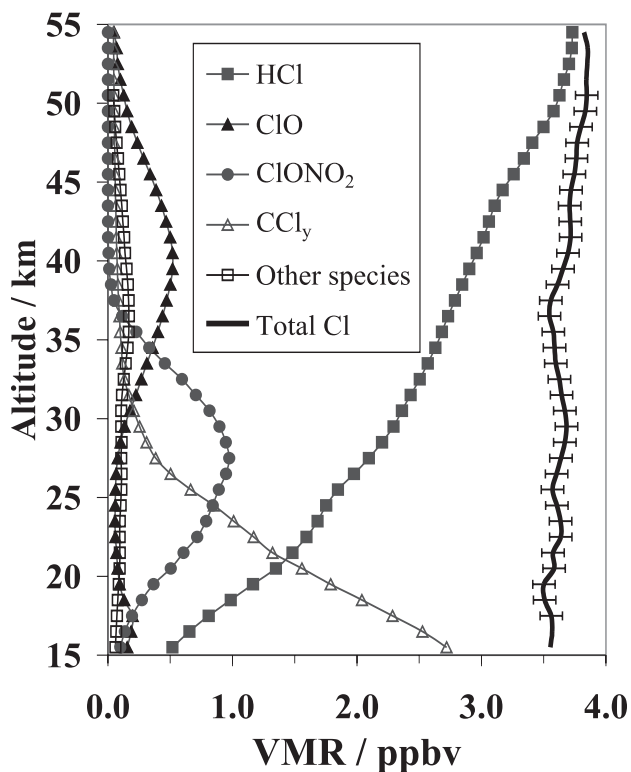


Figure 1-11. The northern midlatitude (30°N-60°N) stratospheric chlorine budget for 2004 expressed in volume mixing ratio (VMR) (Nassar et al., 2006a). It includes ACE-FTS measurements of HCl, chlorine nitrate (ClONO_2), chlorofluorocarbonyl (COClF), CH_3Cl , CCl_4 , CFC-11, CFC-12, CFC-113, HCFC-22, and HCFC-142b, which are complemented by chlorine monoxide (ClO) observations from the Sub-Millimeter Receiver (SMR) on the Odin satellite (Berthet et al., 2005), hypochlorous acid (HOCl) measurements by the Michelson Interferometer for Passive Atmospheric Sounding (MIPAS) (von Clarmann et al., 2006), and phosgene (carbonyl chloride, COCl_2) observations from the balloon-borne MkIV (Toon et al., 2001). ACE-FTS measurements of HCFC-22 were extended above 25 km based on values from the Stratospheric Chemistry Transport Model-1 (Rummukainen, 1996; Coheur et al., 2003). CH_3CCl_3 and the minor contributors CFC-114, CFC-114a, CFC-115, HCFC-141b, and halon-1211 were based on SAGE III Ozone Loss and Validation Experiment (SOLVE) measured profiles (Schaufler et al., 2003) scaled to 2004. The sum of the chlorine contributions from these species gives the total chlorine profile, with error bars indicating the 1-sigma precision.

The linear trend in HALOE values from January 1999 to November 2005 is -26 ± 12 ppt/yr (one sigma), which is larger than, but not significantly different from, the trend in the total chlorine based on the organic record. The time of the peak in HCl is somewhat ill defined in the HALOE data. Rinsland et al. (2005) showed that the HCl change observed between ATMOS observations in 1985 and 1994 and ACE observations in 2004 are broadly consistent with the expectations due to the changes in total stratospheric chlorine (Figure 1-12). Overall, the time series of the lower mesospheric HCl (Cl_y) are qualitatively consistent with expectations from ground-based measurements after considering lag times (~ 5 -6 years) (Waugh et al., 2001; Waugh and Hall, 2002) associated with transport of tropospheric air to the lower mesosphere, although the fine-scale structure observed between 1997 and 2002 in the HALOE data remains unexplained.

There are considerable differences in the amount of upper stratospheric HCl measured by the four instruments. The systematic difference in HCl observations between MLS and HALOE is about 0.2-0.4 ppb (about 7-15%, HALOE lower), while ACE and MLS show better agreement (Froidevaux et al., 2006). Measurements of HCl by MLS and ACE both show values between 3.4 and 3.6 ppb in 2006 (Figure 1-12), which would imply a peak value for total chlorine of ~ 3.5 to 3.8 ppb, larger than can be supplied by the 12 long-lived source gases. The HALOE measurements of HCl are consistent with supply of chlorine from only long-lived source gases. The differences between the instruments are not currently understood, but it should be noted that the different measurements do agree within the stated accuracies, indicated by the error bars (± 2 sigma) in Figure 1-12. Due to these differences in absolute values of these observations, it is at present not possible to state whether upper stratospheric inorganic chlorine is consistent with supply from only the 12 long-lived source gases, or it is large enough to allow for a chlorine contribution from short-lived gases of 0.05 to 0.1 ppb. This issue is discussed further in Section 2.5.2 of Chapter 2, which focuses on possible contributions from the very short-lived substances.

As is evident from Figure 1-11, column observations of HCl and chlorine nitrate (ClONO_2) can also be used to gain insight regarding the total inorganic chlorine in the stratosphere. Recent high spectral resolution infrared ground-based observations have also provided evidence that the total loading of stratospheric chlorine has reached its maximum, with tentative evidence, at the 1-sigma level, of the onset of a long-term decline. For example, observations from the Network for the Detection of Atmospheric Composition Change (NDACC) from the 3 stations with measurements spanning up to 24 years have

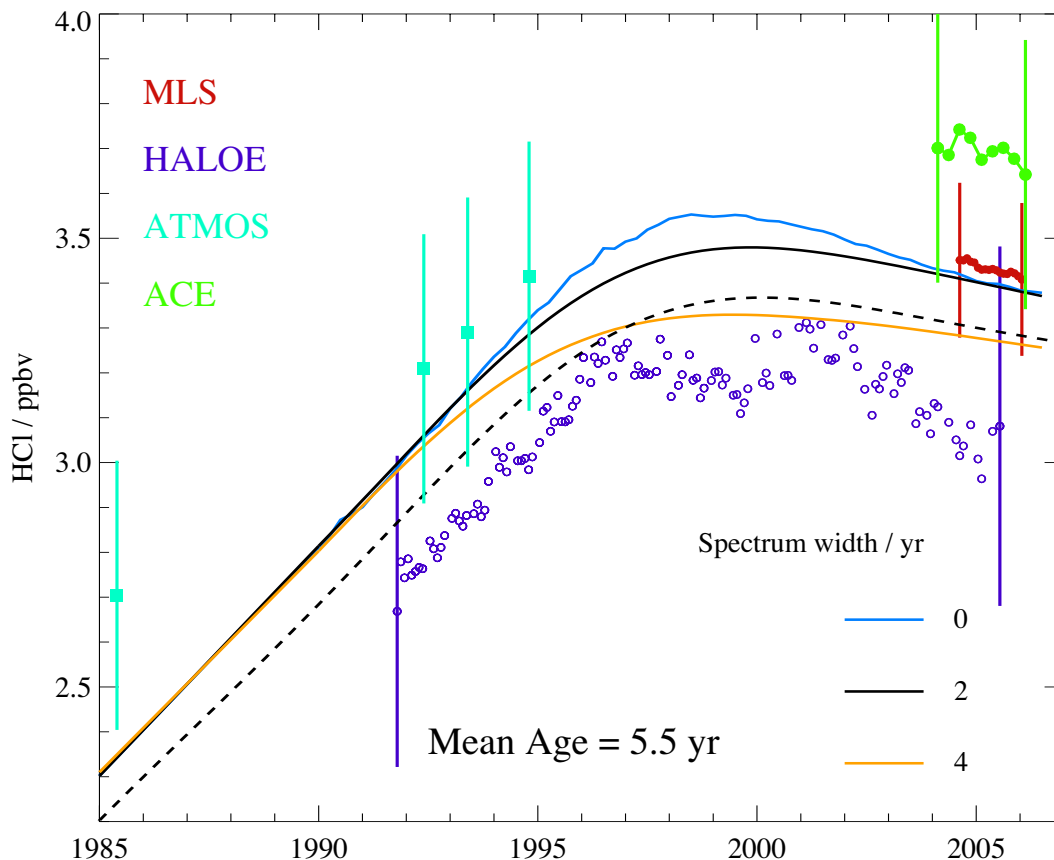


Figure 1-12. HCl monthly averages for 60°S-60°N at 0.46 hPa from MLS (red dots; Froidevaux et al., 2006 updated) and HALOE (purple circles; Anderson et al., 2000 updated), along with quarterly averages from ACE (in green; Nassar et al., 2006a updated) and ATMOS version 3 data averages (cyan squares; Irion et al., 2002; Rinsland et al., 2005) for 50-60 km; error bars are 2-sigma estimates of accuracy. Solid curves use total chlorine time series from tropospheric data (including 100 ppt from very short-lived (VSL) chlorinated substances) and a mean age assumption of 5.5 years, with various age spectrum widths, as indicated; a factor of 0.96 is applied to get HCl. The dashed black curve shows expected HCl based on the *WMO 2002* scenario Ab (no contributions from VSL compounds) and a mean age of 5.5 years, with a spectrum width of 2 years.

provided evidence for stabilization in total chlorine loading, with a broad peak starting at the end of the 1990s, following a rapid buildup during the 1980s (Rinsland et al., 2003). Figure 1-13 provides an update to the NDACC time series from the Jungfraujoch station measurements extending through 2004 from monthly mean time series. It indicates that the total stratospheric inorganic chlorine loading (Cl_y) has decreased slowly ($-0.7 \pm 0.3\%/yr$, 1σ) since it peaked in late 1996, at the limit of being statistically significant at the 2σ level (an update of Mahieu et al., 2004). Multiplying this percentage by a stratospheric Cl_y burden of 3.6 ppb suggests a trend in Cl_y of -25 ± 11 ppt/yr. The column measurements are in good agreement with model calculations by a two-dimensional (2-D) model

run at the University of Leeds (orange trace in Figure 1-13, described in Rinsland et al., 2003).

Solomon et al. (2006) have reported a steeper downtrend for stratospheric chlorine monoxide (ClO) from 1996 to 2005 of $-1.5 \pm 0.2\%/yr$, based on remotely sensed millimeter wave measurements. They calculate however that this downtrend contains an enhancement of about $-0.5\%/yr$, relative to Cl_y trends, because of increases in upper stratospheric methane that have been measured by HALOE. Their observations, which extend from 1984 to present, are broadly consistent with the rise in total chlorine due to human activities and recent declines due to the Montreal Protocol.

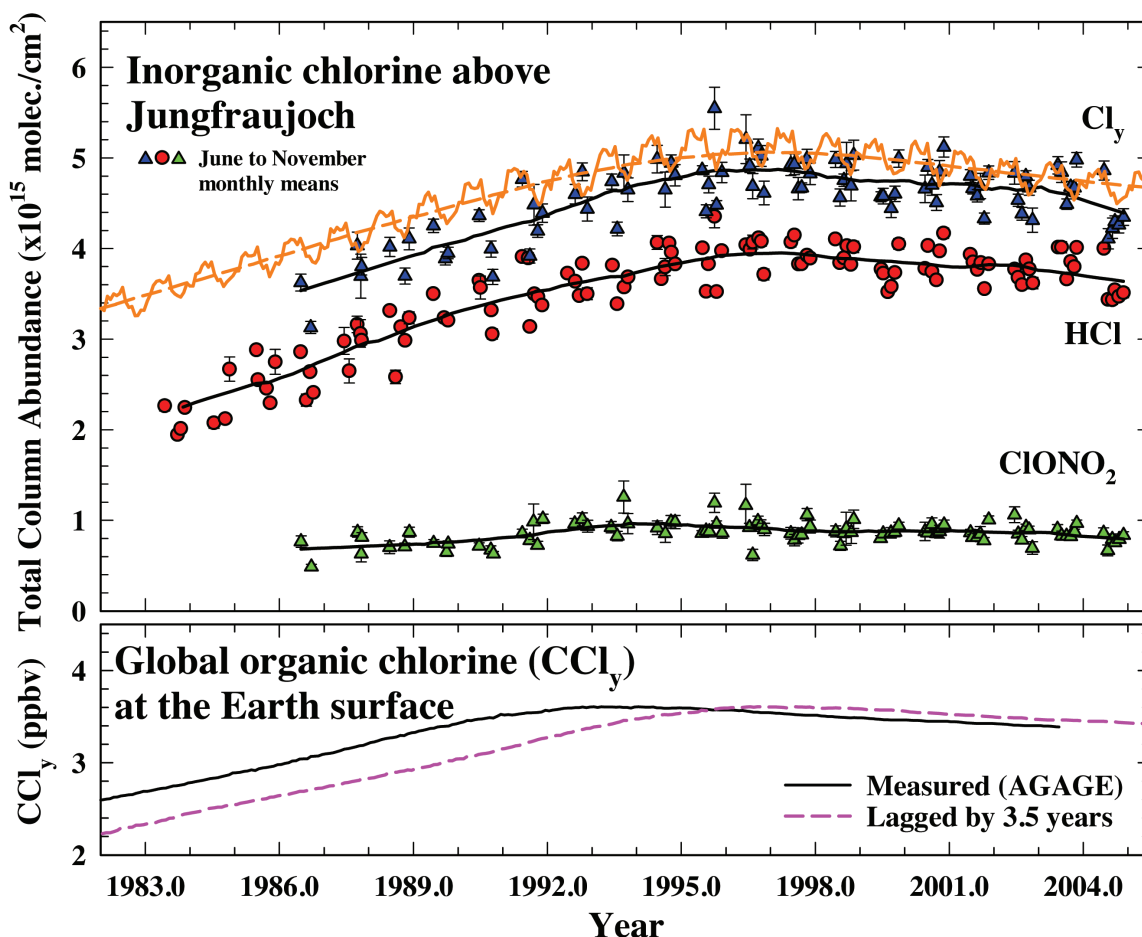


Figure 1-13. Top: Time series of monthly mean total column HCl (red circles) and ClONO_2 (green triangles), as derived from the Jungfraujoch (46.5°N) observational database; Cl_y (blue triangles) results from the summation of the corresponding HCl and ClONO_2 data points. To avoid the influence of the significant variability affecting measurements in winter- and springtime, these time series have been limited to the June to November months. Nonparametric least-square fits to these datasets are reproduced as thick black curves; they help to appraise the two-decade mean evolution of HCl, ClONO_2 , and Cl_y . Also shown is the sum of the HCl and ClONO_2 columns calculated by the University of Leeds 2-D model (top orange curve). Bottom: Evolution of total surface organic chlorine derived from measurements performed by the AGAGE network. For better comparison with the Jungfraujoch data, the tropospheric chlorine trend is also shown with a 3.5-year time shift (magenta line). Updated from Mahieu et al. (2004).

1.2.3.3 ORGANIC BROMINE IN THE TROPOSPHERE FROM METHYL BROMIDE AND HALONS

Because bromine is an efficient catalyst for depleting stratospheric ozone, the Montreal Protocol set limits on anthropogenic production and consumption of the most abundant and long-lived brominated gases in the atmosphere: methyl bromide and the halons. Increased anthropogenic production and use of these gases led to increasing amounts of bromine (Br) in the atmosphere during the second half of the 20th century. Enhanced human-related emissions of methyl bromide and halons likely dominated

changes in atmospheric bromine concentrations over the past 50 years. By the late 1990s, about half of the Br in the stratosphere was derived from anthropogenic activities (Montzka and Fraser et al., 2003).

Natural processes deliver bromine to the stratosphere in the form of methyl bromide and short-lived bromocarbons or oxidation products of these gases. Long-term changes in atmospheric Br arising from natural processes likely were smaller than the changes in anthropogenically-derived Br during the 20th century. The background level of stratospheric Br accounted for by short-lived bromocarbons is an area of active research (Chapter 2).

New measurements of methyl bromide have been reported (see Section 1.2.1.7) since the previous Ozone Assessment (WMO, 2003) and they allow trends in total bromine from regulated gases to be assessed. The results (Figure 1-14) indicate that the global tropospheric burden of Br from the sum of methyl bromide and halons peaked in 1998 and has declined since (Montzka et al., 2003). By mid-2004, tropospheric Br was 0.6 to 0.9 ppt below the peak; the mean decline from 1998 to 2004 was between -0.1 and -0.15 ppt Br/yr (a range is given here to reflect differences in recent trends for halon data from different networks and the possibility that mean tropospheric CH_3Br mixing ratios trends are 7% less than observed at Earth's surface). The decline is solely the result of a decrease in global mixing ratios of methyl bromide, which declined at a mean rate of -0.24 ppt/yr from 1999 to 2004, or somewhat faster than expected. Mixing ratios of halon-1301 and halon-1211 still increased slowly from 1999 to 2004; the mean increase in Br from these gases over this period was between 0.08 and 0.12 ppt/yr. Continued increases in the halons are consistent with the existence of substantial banks of halons that are released at a slow rate to the atmosphere.

The decline observed for bromine from regulated gases is significant relative to changes in chlorine, considering that the efficiency for Br to deplete stratospheric ozone is 60 times greater than Cl on a per-atom basis (see Chapter 2 and Chapter 8 for an updated discussion of this efficiency factor, α). A decline of -0.1 to -0.15 ppt Br/yr, multiplied by 60, corresponds to a rate of -6 to -9 ppt Cl equivalents/yr, or more than one-third of the rate of decline in atmospheric chlorine over this same period (-20 ppt Cl/yr; Table 1-5).

As was the case for Cl, initial declines in atmospheric Br have been achieved through reduced production and emission of a short-lived gas even while the long-lived gases continued to slowly increase.

1.2.4 Effective Equivalent Chlorine and Equivalent Effective Stratospheric Chlorine

Effective equivalent chlorine (EECl) and equivalent effective stratospheric chlorine (EESC) provide a rough means of gauging the influence of measured changes in both chlorinated and brominated halocarbons on the ozone-depleting halogen abundance in the future stratosphere (see

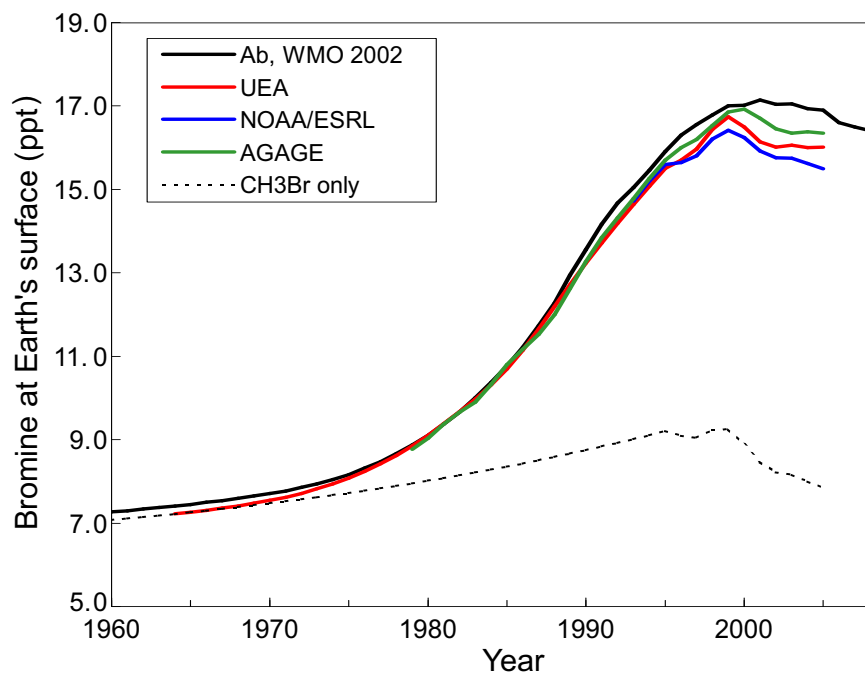


Figure 1-14. Trends in the abundance of Br from brominated gases regulated by the Montreal Protocol on Substances that Deplete the Ozone Layer (halon-1211, halon-1301, halon-2402 and methyl bromide) as projected in the *WMO 2002 Ab* scenario (black line) and as measured by different stations (red, green, and blue lines). Although independent global surface means are derived for halon-1211 and halon-1301 by different laboratories, the same is not true for methyl bromide and halon-2402. For these gases, the source of data included in the compilation of total Br for all labs was solely NOAA/ESRL (methyl bromide) and UEA (halon-2402). The global surface estimates are made with samples collected from single sites (AGAGE prior to the mid-1990s and UEA) or multiple sites (AGAGE after the mid-1990s and NOAA/ESRL).

LONG-LIVED COMPOUNDS

descriptive box on EECl and EESC in Chapter 8). EECl and EESC are derived from ground-based observations of trace gas mixing ratios. As currently formulated, EECl and EESC do not include contributions from very short-lived halogen source gases. Weighting factors are applied to measured mixing ratios to account for the variable rates at which these gases undergo degradation in the stratosphere and liberate halogen atoms for interaction with ozone. Mixing ratios of bromine are multiplied by a factor α , which reflects the enhanced per-atom efficiency for bromine to catalyze the destruction of stratospheric ozone, relative to chlorine (60 is used here). Finally, a lag time is applied in estimating EESC to account for the time it takes air to be transported from the surface to regions in the stratosphere. A lag of 3 years is used to approximate transport

times and halogen burdens in the midlatitude lower stratosphere (Daniel et al., 1995); longer lag times are more appropriate for the polar stratosphere and the upper stratosphere (Andrews et al., 2001; Newman et al., 2006). No time lag is applied when deriving EECl, so that dates quoted for EECl correspond to sampling dates. Further details on uncertainties and limitations of these quantities are discussed in Chapter 8 of this Assessment, as well as in Chapter 1 of the previous Assessment (WMO, 2003).

Decreases in EECl and EESC continued during 2000-2004, owing to continued declines in tropospheric mixing ratios of most regulated ozone-depleting source gases (Figure 1-15). By 2005, EECl was 277 ppt, or 8-9% below the peak observed in the 1992-1994 time period. This decline represents about 20% of the decline

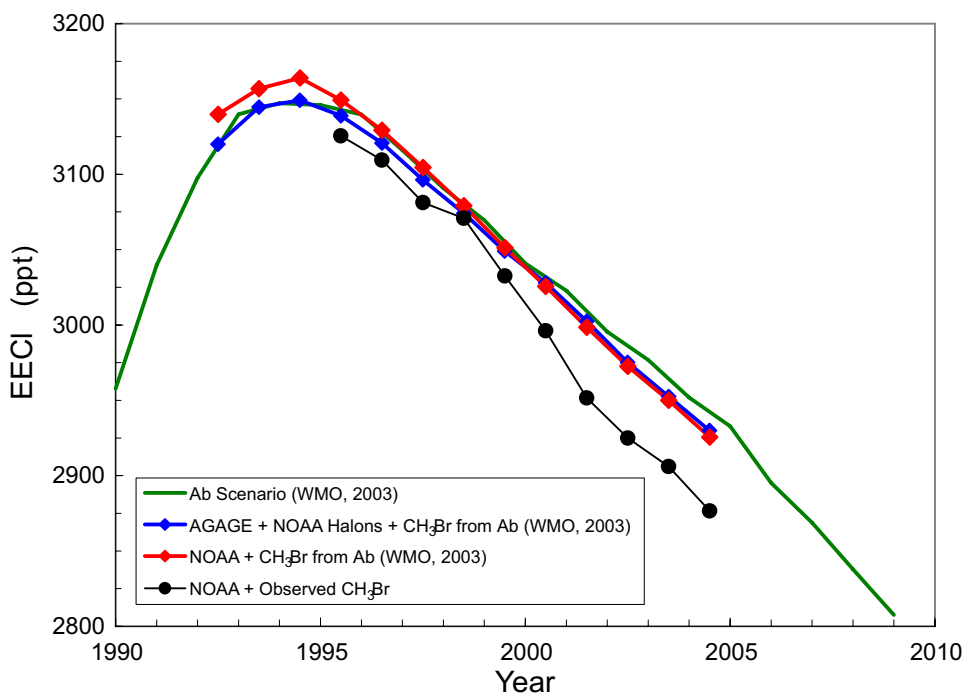


Figure 1-15. EECl calculated from observations of the most abundant long-lived chlorinated gases (CFC-11, -12, -113, CH₃CCl₃, CCl₄, HCFC-22, -141b, and -142b) and the longest-lived brominated gases (halon-1211 and halon-1301). Results for CH₃Br are also included either as projected in the *WMO 2002* Ab scenario (WMO, 2003) (in data represented by blue, red, and green symbols and lines) or as observed in the NOAA/ESRL network along with observational data for all other gases (black points and line). Results from global measurements programs AGAGE (blue diamonds and line; O'Doherty et al., 2004) and NOAA/ESRL (red diamonds and line; Montzka et al., 2003) are compared with scenario Ab from the 2002 WMO Assessment report (Montzka and Fraser et al., 2003) (green line). In the calculations presented here, all bromine atoms are multiplied by a factor of 60, owing to evidence suggesting that Br atoms are 60 times more effective at destroying stratospheric ozone (see discussion in Chapter 8). Fractional release factors used here are taken from Table 8-1, and all release factors have been normalized to 0.8 for CFC-11, despite reports that absolute release factors may be substantially smaller for the middle stratosphere (Schauffler et al., 2003). Using a smaller absolute release factor would affect all absolute mixing ratios and growth rates reported here, but would not affect relative quantities or integrated EESC calculated for future scenarios in Chapter 8.

needed for atmospheric EESC to return to 1980 levels (Figure 1-16). The mean rate of decline during 2000-2004 was similar to that observed during 1996-2000 but was faster than projected in scenario Ab of *WMO 2002* (Montzka and Fraser et al., 2003). This discrepancy arises primarily from a more rapid decline in CH_3Br , though slower-than-projected increases in measured mixing ratios of HCFCs and halon-1301, and a more rapid decline than projected for CH_3CCl_3 , also contributed (Figure 1-15). Note that discussions related to trends in observationally derived EECl and EESC did not include CH_3Br in the recent WMO 1998 and 2002 reports, because of a lack of CH_3Br measurements for recent years that have since become available. Declines in shorter-lived gases (CH_3Br and CH_3CCl_3) continue to be the largest contributors to declining EECl. The early removal of shorter-lived gases means that later decreases in EECl and EESC will likely be dominated by the atmospheric decay of the longer-lived gases. Despite diminished mixing ratios of CH_3CCl_3 , this gas remained the single largest contributor to decreasing EECl during 2000-2004 (-61 ppt EECl out of a decline from all gases

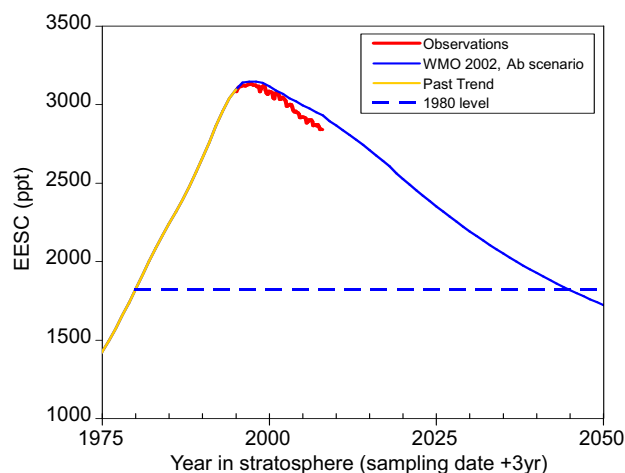


Figure 1-16. Observed and projected changes in EESC relative to the 1980 level. The 1980 level is chosen to represent the atmospheric EESC burden before the ozone hole was observed. Here, EESC is derived from observations of all gases included in the *WMO 2002* Ab scenario (Montzka and Fraser et al., 2003). The observed decline in EESC of 277 ppt EESC from its peak in the 1990s is 20% of the difference between the peak and 1980 EESC levels. Dates are meant to be relevant for the midlatitude stratosphere and are derived by adding 3 years to the date at which samples were collected at the surface (to account for the time it takes for air at Earth's surface to reach the midlatitude stratosphere).

of -120 ppt EECl over this period). Declines in CH_3Br accounted for about one-third of the overall decline (-44 ppt EECl); the CFCs together accounted for less of the overall decline (-23 ppt EECl) as did CCl_4 (-13 ppt EECl). These decreases were offset somewhat by continued increases from HCFCs (+12 ppt EECl) and halons (+11 ppt EECl).

Calculations of EECl discussed here include the assumption that mixing ratios measured at the Earth's surface provide an accurate estimate of the amount of Cl and Br from halocarbons entering the stratosphere. For source gases whose tropospheric loss rates are similar to rates of vertical mixing within the troposphere, surface-based observations may overestimate the amount and trend of Cl and Br reaching the stratosphere. Such influences may affect CH_3Br more than other gases considered in the calculation of EECl here, because it has the shortest lifetime with respect to atmospheric photochemical loss in the troposphere (~1.7 years). Vertical gradients on the order of 0-15% have been observed for CH_3Br between the lower and upper troposphere (Schauffler et al., 1999).

1.2.5 Fluorine in the Stratosphere

1.2.5.1 TOTAL STRATOSPHERIC FLUORINE AND HYDROGEN FLUORIDE (HF) AT 55 KM

The majority of the fluorine in today's atmosphere is derived from anthropogenic activities, as there are no known significant natural fluorine sources (Zander et al., 1994). Stratospheric fluorine is unimportant for stratospheric ozone depletion in comparison to chlorine and bromine, but, because it is mainly due to CFCs, HCFCs, and HFCs, it provides an important consistency check on the anthropogenic chlorine input. An inventory of total fluorine (F_{TOT}) in the stratosphere, including both organic and inorganic species, from 82°N to 82°S over the period of February 2004-January 2005 inclusive has been reported by Nassar et al. (2006b), based primarily on ACE-FTS measurements. Stratospheric F_{TOT} values were 2.50-2.59 ppb at all latitudes with a precision of ± 0.04 -0.07 ppb. The highest value of mean F_{TOT} occurred in the tropics, which is qualitatively consistent with increasing stratospheric fluorine and the mean stratospheric circulation pattern. Figure 1-17 shows the stratospheric F_{TOT} budget for 30°N-60°N in 2004.

The main source of stratospheric HF is photodissociation of chlorofluorocarbons (CFCs), and it is therefore an effective tracer of fluorine input to the stratosphere. As altitude increases, the organic fluorine compounds decom-

LONG-LIVED COMPOUNDS

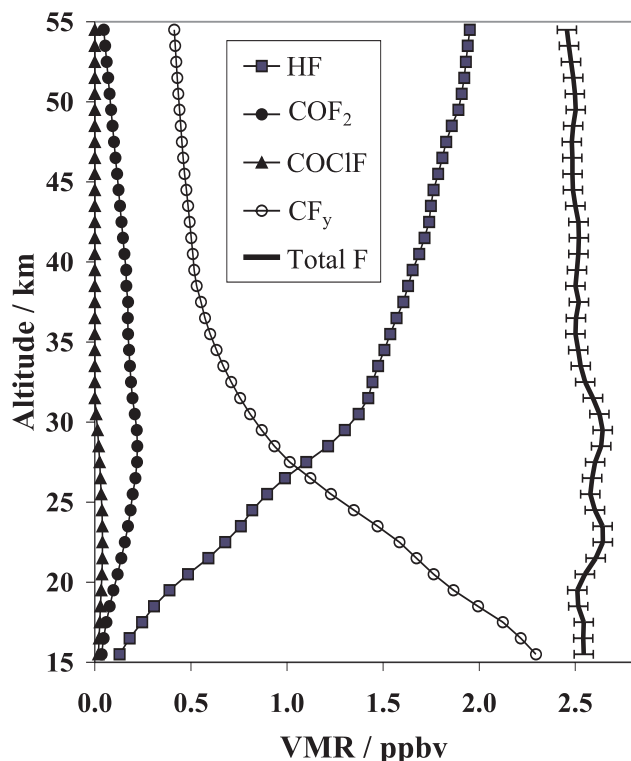


Figure 1-17. The northern midlatitude (30°N-60°N) stratospheric fluorine budget for 2004 expressed in volume mixing ratio (VMR) (Nassar et al., 2006b), which includes hydrogen fluoride (HF), carbonyl fluoride (COF₂), chlorofluorocarbonyl (COCIF), carbon tetrafluoride (CF₄), CFC-11, CFC-12, CFC-113, HCFC-22, and HCFC-142b measured by the ACE-FTS, along with estimates of 15 minor organic fluorine species (including CFCs, HCFCs, hydrofluorocarbons (HFCs), fluorocarbons (FCs), and halons) based on predicted values in the previous WMO Assessment (WMO, 2003). ACE-FTS measurements of COF₂ were extended above 40 km based on the model of Kaye et al. (1991). SF₆ is not shown, but its contribution has been accounted for. The sum of the fluorine contributions from these species gives the total fluorine profile, with error bars indicating the 1-sigma precision of 0.05 ppb.

pose due to photolysis and chemistry, forming inorganic compounds. At 55 km altitude, HF comprises ~93% of the total inorganic fluorine (F_y) at high latitudes and ~86% near the equator, based on National Center for Atmospheric Research (NCAR) two-dimensional model results (Brosseur et al., 1990). The HALOE instrument has provided temporal and spatial information on the near-global distribution of HF since October 1991. The accuracy for a single HF profile at 55 km is ~14% and the precision is

better than 0.05 ppb (Russell et al., 1996). Figure 1-18 shows the time series of HALOE-observed near-global HF, HALOE-derived F_y using latitude-dependent HF/F_y ratios between 86 and 93%, (updated from Anderson et al., 2000), and the WMO 2002 scenario Ab convolved with an age spectrum with a mean age of six years and a width of three years (Waugh et al., 2001). The HALOE-derived F_y at 55 km was increasing at an approximately constant rate until about 1996, and at a slower rate thereafter. Overall, these changes in the F_y record are strongly consistent with expectations from ground-based measurements after considering lag times (~6 years) associated with transport of tropospheric air to the lower mesosphere (Waugh et al., 2001; Waugh and Hall, 2002). This lag time is also consistent with the lag time derived for Cl_y in Section 1.2.4.

1.2.5.2 TOTAL AND STRATOSPHERIC COLUMN INORGANIC FLUORINE

Of the three species relevant for column inorganic chlorine measurements (HF, COF₂, and COCIF), COCIF cannot be monitored by FTIR measurements from the ground but F_y* = HF + 2COF₂ is an excellent surrogate of the total F_y burden in the stratosphere (Zander et al., 1994). Monthly mean total column time series of HF, COF₂, and

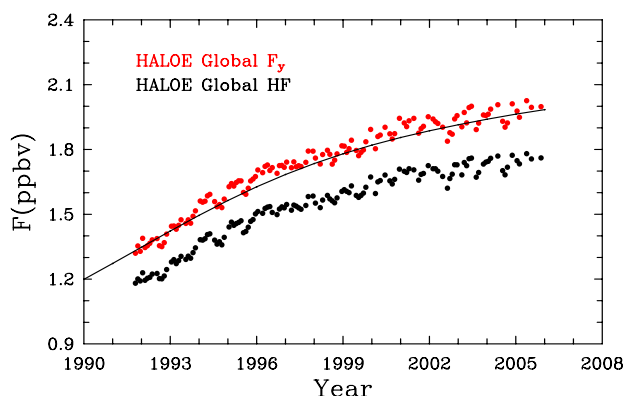


Figure 1-18. Time series of HALOE-observed near-global HF (black dots) and HALOE-derived total inorganic fluorine (F_y) at 55 km (red dots). The total F_y was derived from HALOE by applying 86-93% HF/F_y ratios to the observed HF. The estimated precision (±1 sigma) of the near-global HF and F_y averages is on the order of the size of the data points. The black solid line through the F_y data points is the WMO 2002 baseline scenario (Ab) convolved with a spectrum with mean of 6 years and width 3 years. Updated from Anderson et al. (2000).

F_y^* derived from the Jungfraujoch observational database are shown in Figure 1-19. The F_y^* curve indicates a temporal slowing in 1999, mainly resulting from the COF_2 behavior. Overall, there has been a slowing down of the F_y^* accumulation, with a mean rate of increase of $(1.3 \pm 1.2)\%/yr$ (1 sigma) determined over the 2000-2004 time period. This has essentially resulted from the phasing out of important fluorine-containing source gases (CCl_2F_2 (CFC-12), CCl_3F (CFC-11), and $\text{CCl}_2\text{FCClF}_2$ (CFC-114)), which at present has only been partially compensated for by increases in substitute products such as CHClF_2 (HCFC-22) and CH_2FCF_3 (HFC-134a) (Anderson et al., 2000; Anderson and Russell, 2004). The sum of the HF and 2 times COF_2 contributions as deduced from 2-D model runs for 47°N (Chipperfield et al., 1997) are also reproduced on Figure 1-19 (upper trace). These calculations account for the evolution of the relevant source gas concentrations characterized by past measurements and by the Ab baseline scenario (WMO, 2003). However, it is

important to mention that, so far, the Chipperfield et al. 2-D model runs have not properly reproduced the partitioning among the two main fluorine reservoirs (with an overestimation of the COF_2 contribution to F_y^*). A possible cause for the latter discrepancy would be a new pathway for destroying COF_2 .

A 27-year time series record of daily mean stratospheric HF columns has also been derived by Rinsland et al. (2002) from analysis of infrared solar spectra recorded from the U.S. National Solar Observatory on Kitt Peak (31.9°N , 111.6°W , 2.09 km altitude). The long-term HF evolution is modeled by assuming a seasonal cycle combined with a polynomial expression that solves for coefficients to determine linear and quadratic coefficients for the 14-50 km column as a function of time. The measurements show a continued buildup of the stratospheric HF column, with a spring maximum and an autumn minimum superimposed on significant short-term variability. The latter variations are presumably due to latitudinal trans-

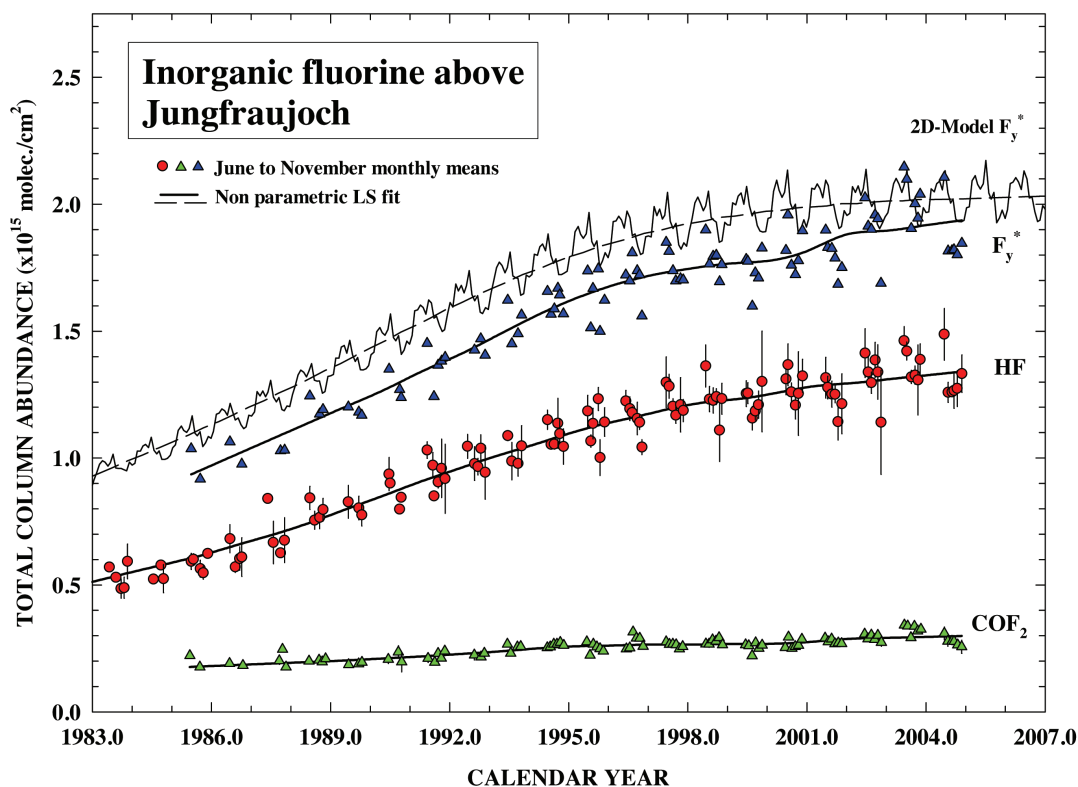


Figure 1-19. Time series of monthly mean total column HF (red circles) and COF_2 (green triangles), as derived from the Jungfraujoch (46.5°N) observational database; F_y^* (blue triangles) results from the summation of the corresponding HF and 2 times COF_2 data points. To avoid the influence of the significant variability affecting measurements in winter- and springtime, these time series have been limited to the June to November months. Nonparametric least-square fits to these datasets are reproduced as thick black solid and dashed curves; they help to appraise the two-decade mean evolution of HF, COF_2 , and F_y^* . Also shown is column F_y^* above the Jungfraujoch station calculated with a two-dimensional model (top black curve) (Chipperfield et al., 1997).

LONG-LIVED COMPOUNDS

port of lower stratospheric air above the Kitt Peak station. The updated results also indicate a rapid buildup in fluorine loading in the middle atmosphere, and that the rate of increase has slowed during recent years.

1.3 EMISSIONS ESTIMATED FROM THE HALO-CARBON MEASUREMENTS

1.3.1 Regional Emissions and Inverse Modeling

In the last few years, inverse modeling of ground-based measurements has been increasingly used to assess emissions of trace gases on regional to continental scales. This approach provides a tool for the validation of emissions and a real-world check for compliance with international agreements. For the Montreal Protocol, in particular, these regional studies have a potential to be used as a tool to test the consistency of different phase-out schemes within the developed and the developing regions of the world. In this section, an assessment of regional emissions, which are estimated by inverse modeling, will be given, together with an attempt to account for uncertainties due to systematic and random errors. A global integration is then attempted to check for compliance with worldwide emissions derived from trends, although the significance of this analysis is limited by large uncertainties in the summed regional emissions.

For the estimation of regional emissions by inverse modeling of ground-based measurements, the same basic principles are generally followed. Observations at one or more locations within the region of interest are separated by statistical or meteorological methods into periods that are influenced by emissions and those that are representative of background conditions. Afterwards the regional emissions are estimated by two principal approaches. In the first method, emissions are calculated by comparing concentrations of the gas with unknown sources with concurrent data on a gas for which a regional emission inventory is available (tracer-ratio method). In the second method, the recent travel histories of the air masses arriving at the observation site are combined with the measured concentrations. The recent history of the air can be deduced using a range of methods including single or multiple back trajectories, or Lagrangian particle dispersion models (LPDM). Results of such inverse modeling-derived emission estimates for ozone-depleting trace gases for different regions of the globe are summarized in Table 1-6.

For Europe, emissions of CFCs have been estimated for the period of 1995-2000 by a combination of measurements from Mace Head (Ireland) and calculations using a

sophisticated LPDM model (Numerical Atmospheric Dispersion Modeling Environment, NAME) (Manning et al., 2003). Resulting European emissions in this period were 8.5-9.6 Gg/yr and 13.5-15.2 Gg/yr for CFC-11 and CFC-12, respectively. Interestingly, consumption-based emissions (UNEP, 2002b) show considerably higher values for CFC-11 (18.5-23.0 Gg/yr), whereas values for CFC-12 (9.6-25.0 Gg/yr) were in the same range. Recent European HCFC emissions were estimated to be highest for HCFC-22 (38-41 Gg/yr) and approximately 10 Gg/yr or less for HCFCs 141b and 142b (O'Doherty et al., 2004).

For CH_3CCl_3 , a combined analysis of 4 years of data from Jungfraujoch (Switzerland) and Mace Head (Ireland) provided estimates of European emissions in the years 2000-2003 between 0.3 and 3.4 Gg/yr (Reimann et al., 2005), which contrasts with estimated European emissions of over 20 Gg/yr in 2000 from a short-term aircraft campaign over Germany (Krol et al., 2003). On the basis of the much larger time period covered by the study of Reimann et al. (2005), it is assumed that average emissions in Europe after 2000 were in the range of a few Gg/yr and that the higher results of more than 20 Gg/yr were probably due to short-term emissions not being representative for longer time periods.

In contrast to these observations, consumption-based emission estimates for CH_3CCl_3 in Europe were declared to be smaller than 0.1 Gg/yr after 1997. The observed ongoing emissions could have been caused, in part, by consumers banking CH_3CCl_3 in anticipation of the restrictions of the Montreal Protocol. This hypothesis is supported by the drastic decline in consumption-based estimates between 1995 and 1996 (McCulloch and Midgley, 2001), which is not represented by observation-based estimates. Additional sources of CH_3CCl_3 not covered by industry or Montreal Protocol consumption data could include hazardous waste sites, illegal imports, and small releases during HCFC production. Although these ongoing emissions are not significant for stratospheric ozone depletion, they point to the possibility of noncompliance with the Montreal Protocol (see Section 1.3.2.5 for further discussion). For Eastern and South Eastern Europe (Ukraine, Bulgaria, Romania, Turkey, and Greece), indications exist that emissions of CH_3CCl_3 and CFC-113 were still occurring at a non-negligible level in August 2001 (Gros et al., 2003).

In the United States, several studies have been performed in the last decade. Between 1996 and 2003, ongoing emissions have been detected for CFC-11 and CFC-12. Whereas sources of CFC-11 have not changed much over the period, estimated emissions of CFC-12 have declined unambiguously (Barnes et al., 2003; Hurst et al., 2006; Li et al., 2005; Millet and Goldstein, 2004). This

Table 1-6. Annual emissions derived from regional models and from networks (Gg/yr).

	Europe (EU-15)	United States	Australia	Japan	Asia (including Japan)	Russia	Global Total from Regional Models	Global Total Emissions (Section 1.3.2)
CFC-11	8.5-9.6 ¹	6.6 ⁷ 7.3 ⁴	0.2 ⁸	1.4 ⁹	30.1 ¹⁰	1.2 ¹¹	49	90
CFC-12	13.5-15.2 ¹	13.4 ⁷ 16.4 ⁴	0.5 ⁸	2.2 ⁹	39.4 ¹⁰	64 ¹¹	135	122
CFC-113	NA	0.6 ⁴ 1.4 ⁶	ND	NA	NA	0.8 ¹¹	(1.8)	10
CCl ₄	NA	<0.6 ⁴	ND	1.2 ⁹	21.5 ¹⁰	0.6 ¹¹	(22)	70
CH ₃ CCl ₃	0.3-3.4 ² 24 ³	2.2 ⁵ 3.6 ⁷ 4.4 ⁶	ND	2.0 ⁹	14.2 ¹⁰	0.4 ¹¹	22-46	See Section 1.3.2.5

NA: not available; ND: not detected; values in parenthesis: data coverage is too weak to derive a global figure. Global emission estimates are an average from 2001-2003.

¹ 1995-2000 (Manning et al., 2003).

² 2000-2003 (Reimann et al., 2005).

³ 2000 (Krol et al., 2003).

⁴ 1999-2002 (Li et al., 2005); for the total emissions from the U.S., combined emissions from (Li et al., 2005) and (Barnes et al., 2003) were used, except for CCl₄, where emissions from California alone were extrapolated to the U.S. using a population figure of 273 million.

⁵ 2001-2002 (Li et al., 2005).

⁶ 2001-2002 (Millet and Goldstein, 2004).

⁷ 2003 (Hurst et al., 2006) (only estimating U.S. emissions, related to 273 million inhabitants).

⁸ 1998-2000 (Dunse et al., 2005).

⁹ 2002 (Yokouchi et al., 2005).

¹⁰ 2001 (Palmer et al., 2003).

¹¹ 2001 (Hurst et al., 2004).

behavior can be rationalized by different emission functions for these substances in the U.S. Whereas CFC-11 emissions are primarily originating from in-use foams with small but continuing emissions from a large reservoir, CFC-12 emissions from its use in refrigeration and air conditioning occur over a shorter time span and CFC-12 is being replaced by non-ozone depleting substances. United States emissions of CFC-113 between 1996 and 2002 were small and those of CCl₄ have essentially been no longer detectable in the regional studies. On the other hand, CH₃CCl₃ emissions were estimated to be between 2.2-4.4 Gg/yr, which is comparable to values in Europe on an emissions per capita basis.

In Australia and Japan, emissions of the most important ozone-depleting substances were estimated to be of the order of a few Gg/yr in the last few years (Dunse et al., 2005; Yokouchi et al., 2005). Noteworthy is that CH₃CCl₃ emissions were no longer detectable in Australia after 1998, but continuing emissions of 1.7 Gg/yr were estimated in Japan in 2000-2003. For the developing coun-

tries in Asia available emission inventories are of limited quality. This is unfortunate because production and usage was still allowed within the Montreal Protocol in many of these countries (e.g., China and India). An aircraft campaign studying the outflow of the Asian subcontinent (Transport and Chemical Evolution over the Pacific, TRACE-P) resulted in estimates of the emissions of several countries within the region in 2001 (Blake et al., 2003; Palmer et al., 2003). For East Asia (China, Japan, and Korea), emissions of 21.5 Gg/yr for CCl₄, 14.2 Gg/yr for CH₃CCl₃ (with a considerable share from sources around Shanghai), 30.1 Gg/yr for CFC-11, and 39.4 Gg/yr for CFC-12 were found. In addition, halon-1211 emissions were 0.2 Gg/yr from Southeast Asia and 2.3 Gg/yr from South China, primarily originating from the Shanghai region.

Emission estimates for Russia are also based on insufficient coverage. This is an important issue because of large uncertainties in the production and banks of ozone-depleting substances for this country. A campaign along

LONG-LIVED COMPOUNDS

the Trans-Siberian railway (Trans-Siberian Observations Into the Chemistry of the Atmosphere, TROICA-7) indicated only very small emissions of 1.2 Gg/yr for CFC-11, which contrasted with high estimates of 64 Gg/yr for CFC-12 (Hurst et al., 2004). The latter possibly originated from releases due to leakage from excessively large banks or from unaccounted production. On the other hand, emissions of CCl_4 and CH_3CCl_3 were small, in accordance with expectations.

Summation of the regional emission estimates for CFCs, CH_3CCl_3 , and CCl_4 (Table 1-6) provides a consistency check on the global emissions that have been calculated from the combination of the background trends in their concentrations and their atmospheric lifetimes (Section 1.3.2). This comparison is however hampered by several likely sources of random and systematic errors. The largest source of potential error is the result of the substantial gaps in the spatial and temporal coverage in the existing regional studies. Whereas in Europe, the U.S., and Australia continuous measurements are being routinely exploited for deriving regional emissions, capabilities for doing this in regions with a substantial potential for large uncounted emissions (e.g., Southeast Asia) are still to be developed. Furthermore, the emission estimates described contain uncertainties resulting from the meteorological information or from the emission inventories that are often used as a priori information. In addition, errors can arise from inadequate calibration or sampling (e.g., contamination) as well as insufficient measurement precision. The quantification of these errors is far from straightforward.

A comparison between several of the reported regional emission estimates provides a possible range of uncertainty for an individual estimate. For methyl chloroform three independent studies were performed in the United States within the period of 2001-2003 and ranging from the East Coast to the West Coast (Hurst et al., 2006; Li et al., 2005; Millet and Goldstein, 2004). The three emission estimates for the U.S. ranged from 2.2-4.4 Gg/yr, giving a standard deviation around the mean of 33%. Larger uncertainties were found in a study on European methyl chloroform emissions (Reimann et al., 2005), which was based on two measurement sites and three techniques of analysis. The spread of the emission estimates for Western Europe ranged from 0.33 to 3 times the geometric annual means. The larger uncertainties for Europe than for the U.S. possibly originate from traditional differences in industrial activities between the European countries.

The substantial range of uncertainty in the regional emissions indicated by the European estimates for CH_3CCl_3

may have been significantly affected by the generally small remaining emissions detected in these recent observations. In fact a substantially smaller spread in the estimates from the Mace Head observations for 1995-2000 is reported in Reimann et al. (2005). Moreover Simmonds et al. (2006), using continuous observations at Mace Head, report a spread in the annual estimates of Western European emissions of dichloromethane, trichloroethene, and tetrachloroethene, for all of which the current emissions are more than ten times those of CH_3CCl_3 , of a factor of three in the worst case. Therefore when pollution events may be easily separated from baseline observations, a factor of three in the inferred regional emission uncertainty is probably to be expected. This factor is likely to increase significantly when the pollution events are small. In addition, for some large areas of the world (e.g., Asia), where estimates are dependent on only a few short-term campaigns, the uncertainties are also likely to be considerably larger.

A first indicative comparison between global and the summed regional emission estimates is attempted (Table 1-6). For CFC-11, only about 54% of the estimated global emissions are found in the summed regional emissions, with the partitioning between CFC-11 and CFC-12 from Russia especially appearing to be suspect. For CFC-12 a good consistency is obtained, with the principal contributions coming from Russia and China. For CFC-113 regional emissions are consistently low, with most studies not being able to identify detectable emissions. For CCl_4 the only detectable current emissions were from China, but the amount was only a relatively small fraction (31%) of the inferred global emissions for a 26-year lifetime. Unfortunately only limited data are available from regions such as Korea and India, which might be responsible for significant emissions. There are indications that India in particular is still a source of CCl_4 emitted from solvent use and from process agent applications. For example, air from India observed at a background site in the Indian Ocean has been found to contain elevated concentrations of CCl_4 (Lobert and Harris, 2002). Furthermore, a study in Mumbai (India) found concentrations of CCl_4 that were noticeably above the background (Srivastava et al., 2006). For CH_3CCl_3 , indications of Indian emissions have also been found during campaigns, although their extent could not be quantified (Lobert and Harris, 2002; Srivastava et al., 2006).

In summary, however, the present spatial and temporal coverage, especially in developing regions (e.g., Southeast Asia), is still too inhomogeneous to provide quantifiably useful comparisons of the summed regional emissions with the global emissions derived from trends in observed concentrations.

1.3.2 Global Emissions

This section describes time series of global emissions inferred from the measurements by the ground-based sampling networks (see Section 1.2.1). For the AGAGE measurements, the estimates are based on an inverse procedure using the AGAGE two-dimensional model (12 boxes: 4 in the lower troposphere, 4 in the upper troposphere, and 4 in the stratosphere), with transport parameters tuned to simulate the observed latitudinal gradients for the CFCs (Cunnold et al., 1994; 1997). There are five AGAGE sites with long time series of measurements (e.g., for the CFCs) using electron capture detectors, but there are only two AGAGE sites (Mace Head, Ireland, and Cape Grim, Tasmania) employing mass spectrometer detectors that have provided shorter time series of measurements of gases such as the HCFCs and the HFCs.

For the derivation of global emission rates from the NOAA/ESRL measurements, the estimation procedure starts from their reported tropospheric mean mole fractions. Those tropospheric means are derived from weighting (usually by latitude) high-frequency results at 5 sites, or low-frequency flask measurements at 8-10 remote sites (Montzka et al., 1999). The stratospheric contents are derived from the tropospheric means by ratioing the values to the AGAGE tropospheric means and multiplying by the stratospheric contents calculated in the 12-box model that was tuned to the AGAGE measurements.

Measurements of the halocarbons in the Australian archived air samples have been used to extend the time series back to 1978 for a number of the gases (e.g., Langenfelds et al., 1996; Fraser et al., 1996). In this case, the 12-box model, and other two-dimensional models (Oram et al., 1995; Fraser et al., 1999), have been used to infer global means and global emission rates from measurements at this one location.

For most of these long-lived gases, the largest sources of uncertainty in the emission estimates are the species lifetimes. Smaller uncertainties arise from absolute calibration uncertainties (except for halon-1301, for which the calibration uncertainties are quite large) and from inadequacies in simulating atmospheric transport. The effects of measurement errors are substantially reduced by reporting emissions averaged over three-year periods. The effects of these errors may be seen in Figures 1-20 and 1-21 in differences, if any, between the emission estimates derived from the AGAGE and the NOAA/ESRL measurements. The upper and lower envelopes of the error bars in these two figures for the AGAGE-based estimates, corresponding to the shortest and the longest lifetimes respectively, were calculated using the 12-box model using those lifetimes. Note that the trends in the emission esti-

mates in %/yr are not very sensitive to the lifetime uncertainties. Errors in the representativeness of the measurement sites for deriving global means also adds uncertainty to derived emissions, but during periods when emissions and atmospheric gradients are small (CFCs and CH_3CCl_3 currently), these uncertainties are dramatically reduced.

1.3.2.1 CFCs

Figure 1-20 illustrates the global emission estimates derived from the combination of AGAGE and NOAA/ESRL measurements for three different years for the CFCs. It shows that, as suggested by the latitudinal gradient information in Section 1.2.1.1, emissions of CFC-11 and CFC-12 are continuing but at lower levels than in 2000 (Table 1-7). Moreover, the emissions are about 25% of those (in 1986) before the Montreal Protocol was enacted. On the basis of the regional emission estimates summarized in Section 1.3.1, it would appear that most of the remaining emissions are coming from Asia and Russia. It should be noted that the estimates for CFC-11 emissions in 2003 are very sensitive to its lifetime. Emissions of CFC-113 have now almost ceased (now 3% of 1986 values) and the regional emission estimates, at the few sites where measurements have been made, support the current, low global emissions. Except for CFC-11, the decays of the CFC emissions from 2000 to 2003 derived from global observations are not significantly different from those predicted by the Ab (most likely) scenario from *WMO 2002*. For CFC-11, a significantly faster decline in the emissions was projected in that scenario relative to those given in Figure 1-20. The emissions from the Ab scenario are not shown in Figure 1-20 because those emissions were calculated from the Ab scenario mixing ratios using a one-box model, whereas the emissions in Figure 1-20 were calculated using a 12-box model. The differences between emissions calculated by the 12-box model and the 1-box model are illustrated in Figure 8-1 of Chapter 8. It can therefore be misleading to compare emissions calculated by the two different models. The faster decline in the CFC-11 emissions in 2000-2004 than projected in *WMO 2002* is therefore inferred from the more rapid decline in the observed mixing ratios (see Section 1.2.1.1) versus those projected in the Ab scenario.

An important objective of this report is to estimate the remaining banks, which will be responsible for the emissions of ozone-destroying halocarbons over the next few years. Total emissions up to the present time can be estimated from the ground-based measurements. These are shown in Table 1-7. An assumption about how these emissions were distributed in time prior to the start of observations in 1978 is needed. However, because the

LONG-LIVED COMPOUNDS

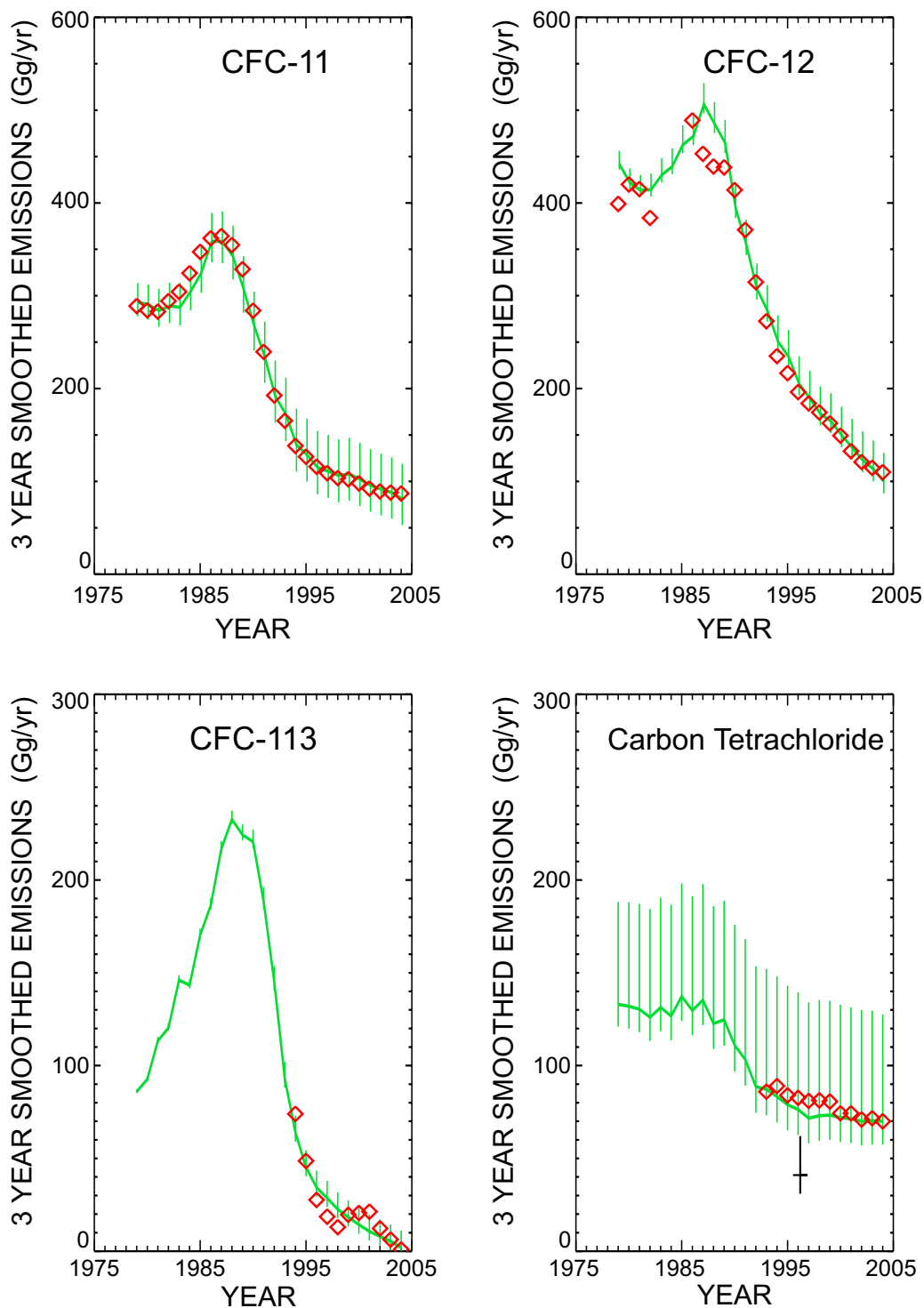


Figure 1-20. Annual global emissions for CFC-11, CFC-12, CFC-113, and carbon tetrachloride, smoothed over three-year intervals, calculated by inverting measurements, using the 12-box model, from the AGAGE (green lines) and NOAA/ESRL (red diamonds) ground-based networks (as in Cunnold et al., 1997). The calculations used equilibrium lifetimes of 45, 100, 85, and 26 years for CFC-11, CFC-12, CFC-113, and carbon tetrachloride, respectively. The green error bars indicate the uncertainties in the estimates due to the uncertainties in the species lifetimes (see Table 1-7). The TEAP (UNEP, 1998) estimate of the CCl_4 emissions in 1996 is indicated in black.

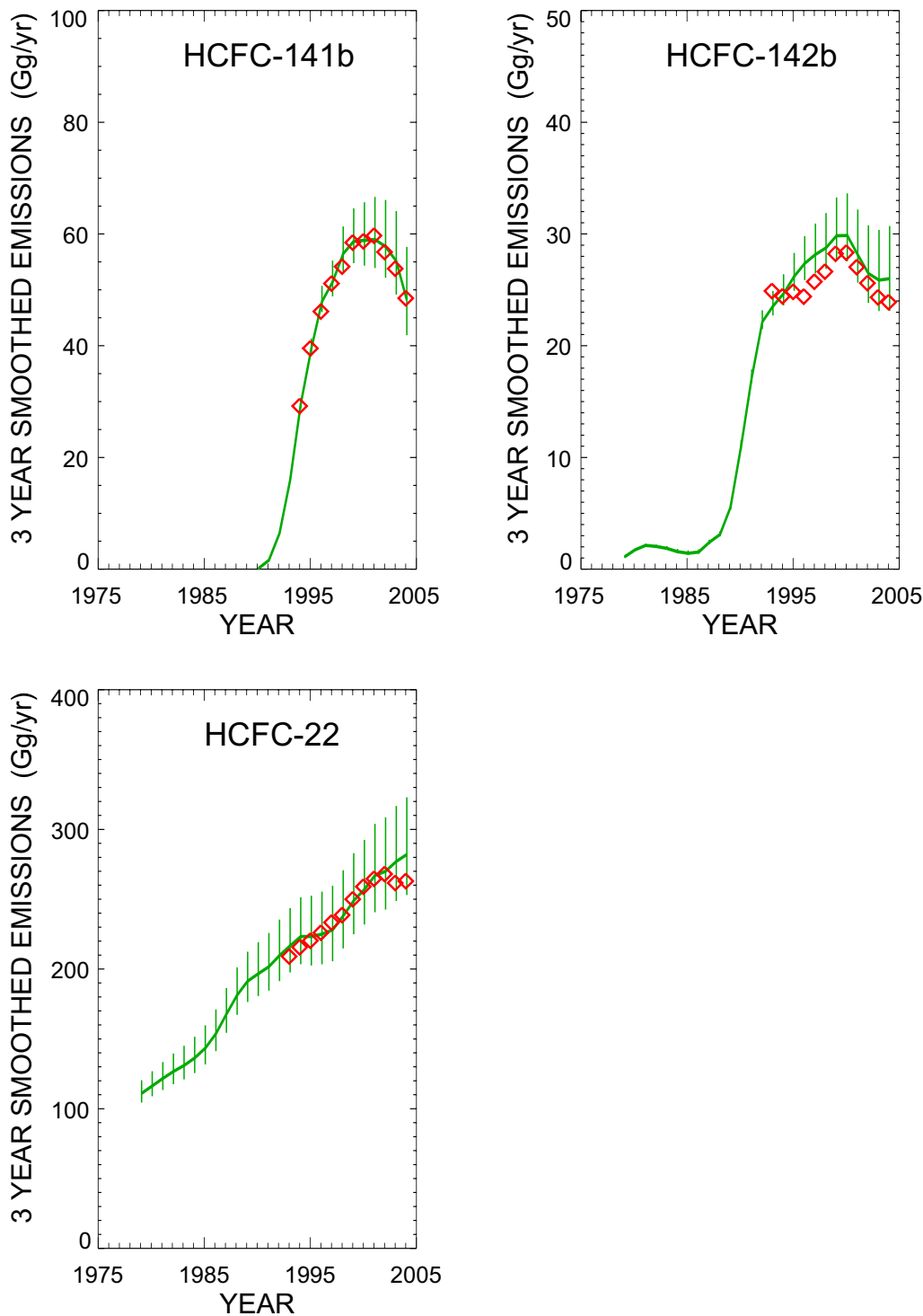


Figure 1-21. Annual global emissions for HCFC-141b, HCFC-142b, and HCFC-22, smoothed over three-year intervals, calculated by inverting the measurements (see Figure 1-2) from the AGAGE (green lines starting from 1995) and NOAA/ESRL (red diamonds) ground-based networks and measurements of the air archived in Australia (green lines before 1995) with a 12-box model (as in, and updated from, O’Doherty et al., 2004). The calculations were based on equilibrium lifetimes of 9.3, 17.9, and 12.0 years for HCFC-141b, HCFC-142b, and HCFC-22, respectively. The green error bars indicate the effects of uncertainties in the lifetimes listed in Table 1-7.

LONG-LIVED COMPOUNDS

Table 1-7. Global emission estimates. Emissions are in Gg/yr, smoothed over 3-year intervals and given to 3 significant figures, and are derived using a 12-box model from a combination of AGAGE and NOAA/ESRL measurements. The total emissions are based solely on AGAGE measurements and they include emission estimates for 2004. The lifetimes and their uncertainties are from Sections 1.2.2.1 and 1.2.2.2. Uncertainty ranges, instead of standard deviations, are given because the central values typically do not lie in the centers of the uncertainty ranges, primarily because the estimated emissions are typically proportional to the inverses of the lifetimes.

Species	Release Estimates (Gg/yr)			Rate of Change (2000-2003) (%/yr)	Total Emissions (1920-2004) (Gg)	Lifetime Used (yr)	Lifetime Uncertainty Range (yr)	2003 Emission Estimate Range	Total Emissions Uncertainty Range	
	1986	2000	2003						Gg	%
CFC-11	360	100	88	-4.3	9,450	45	57-35	60-126	8,700-10,460	18
CFC-12	472	150	114	-9.1	14,300	100	113-79	101-144	14,000-15,000	7.5
CFC-113	186	18	6	-33.3	3,170	85	100-66	1-15	3,080-3,340	8.4
CCl ₄	130	73	71	-0.9	6,620	26	30-16	58-131	6,060-8,590	34
HCFC-22	154	258	270	+1.5	6,040	12	14.0-10.0	242-310	5,530-6,760	20
HCFC-141b	0	58.8	54.4	-2.6	589	9.3	11.2-7.4	48.4-63.5	548-651	17
HCFC-142b	1.5	29.1	25.1	-4.9	407	17.9	22.2-13.6	22.3-29.6	380-450	17
HFC-134a	0	76	104	+10.4	721	14	16.4-11.6	99-111	696-757	8.4

largest emissions occurred after 1979, and they have been in the atmosphere for a shorter time, this introduces uncertainties that are small compared with the effects of atmospheric lifetime uncertainties that are shown in Table 1-7. The remaining banks may be estimated by subtracting the accumulated production from the numbers in Table 1-7. Chapter 8 provides both those numbers and estimates of the banks. The effects of using the 12-box model used here to estimate the emissions that have already occurred may be compared against the one-box model results given in Chapter 8.

Table 1-7 also provides estimates of the total emissions integrated from the beginning of production to 2004. It may be noted that these total emission estimates and their one sigma uncertainty limits, when combined with total production numbers that are known fairly accurately (e.g., from UNEP 2005), can be used to constrain the expectations of future emissions (e.g., the current global banks of unreleased gases).

1.3.2.2 HCFCs

Figure 1-21 shows HCFC emission estimates derived from applying the 12-box model to the AGAGE and NOAA/ESRL ground-based network measurements. The two sets of estimates differ because of absolute calibration differences (e.g., 4-5% for HCFC-142b, less for HCFC-141b and HCFC-22) and some other minor differences in the most recent measurements. The emissions of

HCFC-141b (54.4 Gg/yr in 2003) and HCFC-142b (25.1 Gg/yr in 2003) are calculated to have decreased from 2000 to 2004 by approximately 15% (10 and 4 Gg/yr for HCFC-141b and HCFC-142b, respectively) and this is seen by both networks. These emission estimates correspond to a recent decrease in the rates of growth in the atmospheric mole fractions compared with the growth rates reported in *WMO 2002* (Figure 1-2, Montzka and Fraser et al., 2003). HCFC-22 emissions have been increasing fairly slowly or not at all from 2000 to 2004 (e.g., at less than 2%/yr for AGAGE and less than 1%/yr for NOAA/ESRL). This is down from increases of approximately 3%/yr from 1994 to 2000. Note that the ranges of uncertainty, in percent, on the 2003 emissions of the HCFCs and HFC-134a (Table 1-7) are less than for those other gases in Table 1-7 that have much longer emission histories.

The recent decreases in the emissions of HCFC-141b and HCFC-142b, and the fact that the measured mole fractions in 2000-2004 are less than projected (see Section 1.2.1.2) in the best-guess scenario in *WMO 2002*, may mean that emissions are occurring more slowly than expected and the future emissions from the banks will be larger and occur over a longer time than originally anticipated.

1.3.2.3 HALONS

Difficulties in reconciling the halon measurements with emission estimates derived from production and the

remaining banks of halon-containing fire extinguishing equipment (e.g., the estimates shown on page 75 of IPCC/TEAP 2005) were previously pointed out by Fraser et al. (1999). Currently the remaining very small worldwide production of these halons is insignificant in relation to the size of the global halon bank. For halon-1301, the estimates are from the United Nations Environment Programme/Halons Technical Options Committee (UNEP, 2003) emission scenario. Those emissions have been run through the 12-box model to yield the gold curve in the halon-1301 panel of Figure 1-4 (which is similar to that in Figure 1-17 of *WMO 2002*). A smaller emission rate for halon-1301 has recently been suggested by the work of Verdonik and Robin (2004).

For halon-1211, there is less spread in the measurements and the mole fractions estimated from the emission banks do not differ as much as they do for halon-1301. The emission scenario used is that of TEAP (an update to the UNEP (1999) model, see *WMO 2002*, Section 1.6.1.5), which is similar to the UNEP (1999) model. It should be noted that this scenario contains lower emissions than those shown in IPCC/TEAP (2005, page 75), which were from UNEP (2003). An error in that model was recently discovered in accounting for the production by Article 5(1) countries in 1987-1993. The *WMO 2002* Ab scenario also provides a reasonable fit to the observations except that, although the observations indicate a slowing of the increases, there is little evidence that halon-1211 stopped increasing in the 2000-2004 period as the Ab model predicted.

1.3.2.4 CARBON TETRACHLORIDE

Table 1-7 and Figure 1-20 show the estimated emissions of carbon tetrachloride, for a lifetime of 26 years, determined from the measurements by the ground-based sampling networks combined with AGAGE 12-box model calculations. The emission uncertainty error bars are based on the combined uncertainties in the contributions of stratospheric, oceanic, and soil losses. A lifetime of 20 years increases the calculated emissions by approximately 26 Gg/yr, from 71 Gg/yr in 2003 to 97 Gg/yr. Simmonds et al. (1988 and 1998) argued that most of the CCl₄ emissions in the past were fugitive emissions from the carbon tetrachloride used in the manufacture of CFCs. For a lifetime of 20 years, not only would the CCl₄ emissions have to have been equivalent to approximately 16% of CFC production prior to 1994, versus approximately 9% based on International Trade Commission figures on CCl₄ production in the U.S. in 1979-1985 (Simmonds et al., 1988), but the proportion would have had to have increased to almost 60% after 1995 as a result of the substantial reduc-

tion in CFC manufacture (cf. *WMO 2002*, Montzka and Fraser et al., 2003, Figure 1-15). TEAP (UNEP, 1998) indicated that approximately 23 Gg/yr of carbon tetrachloride emissions could arise from uses other than in CFC manufacture; that report also estimated total emissions from industry data of 31 to 62 Gg in 1996, with a most likely value of 41 Gg (see Figure 1-20). Therefore it is difficult to reconcile the atmospheric observations with an atmospheric lifetime for CCl₄ of 20 years.

In addition, recent high-frequency atmospheric measurements (see Section 1.3.1) at a number of global locations have only detected approximately 22 Gg/yr in 2001, which came almost entirely from Eastern Asia. Therefore, even though emissions from India are unknown, it is difficult to account for the approximately 97 Gg/yr in 2003 (99 Gg/yr in 2001) required for consistency with a 20-year lifetime (or even the 71 Gg/yr in 2003 required for a lifetime of 26 years). Simmonds et al. (1998) showed that the observed latitudinal gradient from the AGAGE observations was reasonably well simulated by a lifetime of 42 years. Updated calculations suggest a gradient-based lifetime of approximately 35 years, unless a substantial fraction of the emissions are coming from the Southern Hemisphere.

Overall the budget of carbon tetrachloride remains poorly understood. Because the currently observed regional emissions, the TEAP emission estimate, and the measured interhemispheric gradient seem inconsistent with an overall lifetime of 20 years and because the uncertainty ranges for both the ocean and soil sinks allow for the possibility of only very small sinks, no change from the lifetime of 26 years given in *WMO 2002* is recommended at this time.

1.3.2.5 METHYL CHLOROFORM

Global production and sales of methyl chloroform from 1970 to 1995 were tabulated in a database from annually provided figures from the producing companies. According to McCulloch and Midgley (2001), the uncertainties were 2.1% on production and 4.2% on emissions. These uncertainties are smaller than for most other ozone-destroying gases because of the smaller number of companies that produced methyl chloroform and because of the generally short time (less than a year) between production and emission into the atmosphere. After 1995, emissions were derived from figures on production and consumption reported to the United Nations Environment Programme (UNEP, 2002b). Global emissions have been calculated to be 19.7 ± 2.3 Gg in 2000 and 12.9 Gg in 2002. This may be compared against maximum emissions of 718 Gg, which occurred in 1990 (McCulloch and Midgley, 2001).

LONG-LIVED COMPOUNDS

McCulloch and Midgley also pointed out that there are discrepancies in the databases for 1994-1996. In particular, there is a production versus consumption discrepancy in the UNEP figures in 1995-1996. It was noted in Section 1.3.1 that regional emission estimates suggested an anomalous large disagreement for methyl chloroform emissions versus global emissions in 1996. Furthermore Prinn et al. (2005) suggested that, based on summing the recent regional emission estimates, the global emissions in the past ten years might be somewhat low. They pointed out that the regional emissions could be approximately accommodated (within the uncertainties of the measurements) by placing 5% of the global emissions in a slower release category, with emissions being divided equally over a 10-year interval. This would not have affected the production numbers. The slower releases would have increased the emissions in 2002 by 3.6 Gg to 16.5 Gg and from 93.5 Gg to 112.3 Gg in 1996. The revised global totals would not, however, account for the European emissions estimate of over 20 Gg in 2000 by Krol et al. (2003), which Prinn et al. (2005) did not include because of the much lower estimates from the European ground stations (see also Section 1.3.1). This discrepancy, and hence the global emissions since 2000, are not understood. These ongoing emissions are not, however, significant for stratospheric ozone depletion.

Historically, accurate methyl chloroform emissions data have been useful in the estimation of global OH abundance. Prinn et al. (2005) used the emission estimates just described to calculate the annual atmospheric loss rates for methyl chloroform that produce the best fit to the AGAGE observations. This resulted in a time series of annual globally averaged tropospheric OH concentrations from 1979 to 2003 and particularly low OH values (by 10%) in 1997/1998. Monte Carlo estimates of the uncertainties in the recent emissions of methyl chloroform produce uncertainties of only a few percent in these OH estimates. Wennberg et al. (2004) pointed out that the methyl chloroform that had entered the ocean could have been trapped in the polar region and, because of the very steep decline in the atmospheric concentrations in recent years, much of it could now be returning to the atmosphere. Prinn et al. (2005) estimated that these ocean fluxes could make annual contributions to the methyl chloroform budget that varied between 4 and 7 Gg/yr between 1995 and 2003. This increased the OH estimates by approximately 5% after 2000.

In order to derive methyl chloroform emissions using the ground-based networks' measurements, independent estimates of OH are required. Calculations of OH in chemical models yield a methyl chloroform lifetime approximately 10% less (Spivakovsky et al., 2000) than

the Prinn et al. value of 4.9 years, and other models produce larger differences (*WMO 2002*, Montzka and Fraser et al., 2003). Therefore because of the relatively small uncertainties in the emissions given by McCulloch and Midgley (2001), it is not generally very productive to estimate emissions from the measurements.

1.4 OTHER TRACE GASES

1.4.1 Carbon Dioxide (CO₂)

Carbon dioxide is the primary agent of anthropogenic climate change, accounting for 60% of the increase in direct radiative forcing since preindustrial times (IPCC, 2001). Climate change can affect the ozone budget, for example due to temperature changes in the polar vortices, and due to changes in atmospheric transport. Such changes may delay ozone recovery. In 2004, global annual average (surface) CO₂ was 377 ± 0.2 parts per million by volume (ppmv), as determined through the NOAA/ESRL global network.

The atmospheric growth rate of CO₂ has averaged about 0.5% per year over the nearly 50 years of in situ measurements (Keeling and Whorf, 2005). The observed atmospheric growth rate is explained by about one-half of CO₂ emissions from fossil fuel combustion and land use change being absorbed at the surface of the Earth. CO₂ can be taken up by either the ocean or terrestrial biosphere; there is considerable year-to-year variability in the uptake that, at the global scale, is closely related to the impact of El Niño on both ocean and land. Two tracers complementary to CO₂ are molecular oxygen (O₂) and ¹³CO₂. Both tracers allow for partitioning of total uptake into terrestrial and oceanic components, and both indicate that the majority of interannual variability is driven by terrestrial processes (Battle et al., 2000). Over the long term (> 500 years), however, it is likely that the oceans, as the largest carbon reservoir, will exert the strongest control on atmospheric CO₂.

Future levels of atmospheric CO₂ will be strongly determined by future fossil fuel emissions. Additionally, there are no guarantees that the current uptake rate of 50% will be maintained, because both the terrestrial and oceanic carbon cycles may change as a result of changing climate. Furthermore, the mechanisms by which carbon is absorbed at the surface, especially by the terrestrial biosphere, are not fully understood. Simulations in which simple models of the carbon cycle are coupled to climate models have shown positive feedbacks between temperature and CO₂ emissions in the 21st century, which can reduce or even eliminate net CO₂ uptake of anthropogenic emissions. In

one study (Cox et al., 2000), coupling resulted in an additional 1.5 K global temperature increase by 2100, compared with the uncoupled case. Although the magnitude of the feedbacks is uncertain, the direction is likely to be positive, and it is clear that the carbon cycle is a first-order uncertainty in prediction of future climate.

1.4.2 Methane (CH₄), Including Isotopic Data

Methane is important for its impact on climate both through its radiative properties and chemically as a major source of water vapor to the stratosphere and as a sink for Cl. In the troposphere, its oxidation products are controlling the chemistry. The global average CH₄ mixing ratio for 2004 at the surface was 1777 ± 0.6 ppb, determined from marine boundary layer sites in the NOAA/ESRL and other surface monitoring networks (GLOBALVIEW-CH₄, 2005). This compares with glacial values of about 400 ppb (Spahni et al., 2005) and 700 ppb in 1800 AD (MacFarling-Meure, 2004). The precise reasons for interglacial/glacial CH₄ variability as well as variability during the Holocene (Flückiger et al., 2002; Ruddiman, 2003) are not well known but may relate to large-scale moisture and temperature changes affecting wetland emissions. The rise to present-day values has resulted from increases in emissions related to fossil fuel extraction, biomass combustion, and agriculture, and current atmospheric mixing ratios are unprecedented in at least the last 650,000 years (Spahni et al., 2005). The global growth rate of methane has varied from about 14 ppb/yr in 1985 to near zero in 2000 but with significant interannual variability. Since 2000, the growth rate has averaged to 0 ± 4 ppb/yr. The decline in growth rate has been explained as an approach to steady state, with a constant total of global sources and constant sink strength (Dlugokencky et al., 1998). However, despite evidence for only small variations in the global total, individual sources like biomass burning (van der Werf et al., 2004) and emissions from the former Soviet Union (Dlugokencky et al., 2003) have seen substantial changes during this period (Simpson et al., 2002). Changes in the dominant CH₄ sink, the hydroxyl radical (OH), also affect atmospheric interannual variability and trends (Bousquet et al., 2005; Krol et al., 1998; Prinn et al., 2001).

The source budget of atmospheric methane is very diverse, with no dominant source (IPCC, 2001), making determination of the causes of atmospheric changes difficult. Major sources include boreal and tropical wetlands, leakage during coal and natural gas extraction, enteric fermentation, fires, and rice agriculture. Recent laboratory measurements (Keppler et al., 2004) have also shown

living plants to be a source, but their global impact is currently unknown. “Bottom-up” inventories rely on spatial and temporal extrapolation of small-scale field measurements, leading to significant uncertainties in the total. On the other hand, “top-down” approaches inverting atmospheric data can accurately determine continental-scale totals, but cannot independently identify the different sources in a given region. Prediction of future atmospheric levels of CH₄ would require, at a minimum, a much better understanding of how different sources and sink variations have changed the atmospheric burden.

Measurements of the carbon (¹³C) (Lowe et al., 1994; Quay et al., 1999; Miller et al., 2002) and hydrogen (²H or “D”) (Quay et al., 1999; Rice et al., 2001) isotopic ratio of atmospheric methane ($\delta^{13}\text{C}$ or δD) can be used to help quantify the contribution of different sources to the atmospheric growth rate. For $\delta^{13}\text{C}$, sources can be divided into microbial, biomass burning, and fossil fuel sources, which have distinct isotopic signatures. Isotopic and mixing ratio mass balances can be used to constrain the source distribution of these broad categories. One consistent result of carbon isotopic data is to infer a significantly stronger global biomass burning source than bottom-up estimates both in the modern (Quay et al., 1999; Miller et al., 2002) and paleo atmospheres, where recent results have shown much larger than expected combustion sources between 0 and 1200 AD (Ferretti et al., 2005), possibly due to human activity. Though there are currently only a few δD measurements, they, along with ¹⁴CH₄ measurements (which help constrain the fossil-fuel related source), will likely allow for better determination of atmospheric growth rate variations. New measurements of CH₄ from space (Frankenberg et al., 2005), with unprecedented spatial coverage, also afford an opportunity to improve our understanding of the CH₄ source distribution.

The broad range of CH₄ sources (roughly half anthropogenic, half non-anthropogenic) and the fact the source mixture has likely changed over the last century, imply great difficulty in prediction of future mixing ratios. Predictions range from 1575 to 3730 ppb, depending on emission scenario (IPCC, 2001). However, these predictions do not include the possibility of large source changes like destabilization of vast quantities of CH₄ hydrates in Arctic permafrost, which adds further uncertainty to predicted methane abundances at the end of the 21st century.

1.4.3 Nitrous Oxide (N₂O)

Nitrous oxide is the major source of nitrogen oxides (NO_x) in the stratosphere, with the latter contributing significantly to ozone depletion. In addition,

LONG-LIVED COMPOUNDS

N_2O , which has a lifetime of about 120 years, is an important greenhouse gas targeted by the Kyoto Protocol. Its actual global concentration is close to 320 ppb. This constituent is emitted at the Earth surface by a large number of sources; major natural contributions are from the oceans and tropical forests, while most important anthropogenic emissions are from cultivated soils, cattle, and biomass burning (IPCC, 2001).

Several studies have dealt with the historical evolution of the N_2O atmospheric concentration. Nitrous oxide levels started to decrease in the early Holocene and reached minimum levels (less than 260 ppb) around 8,000 B.C., before exhibiting a slow increase to the preindustrial value of about 265 ppb. MacFarling-Meure (2004) has produced a 2,000-year record of atmospheric N_2O variations from measurements on air in ice from Law Dome, Antarctica. Notable features in the N_2O record are a preindustrial level of 260-275 ppb, a slowing of growth in the 1940s and 1950s, a 5 ppb lowering during the Little Ice Age (LIA: 1300-1850 A.D.), and a 10 ppb increase between 670 and 810 A.D. The origin of this latter increase is unknown and was not reflected in corresponding CH_4 or CO_2 changes.

N_2O isotopic composition studies of air from Greenland ice and Antarctic (South Pole) firn (1785-1990) show a decline in $\delta^{15}N$ (1.9 per mil) since preindustrial times, consistent with a 30% increase in total N_2O emissions that are primarily related to agricultural activities (Sowers et al., 2002). A similar decrease in $\delta^{15}N$ (1.8 per mil) since preindustrial times has been reported from analyses of Antarctic (Maud Dronning Land and Dome C) firn air (Röckmann et al., 2003). The corresponding latter data have been interpreted as due to an increasing soil source of N_2O with a time-dependent isotopic signature. A larger trend in $\delta^{15}N$ (2.8 per mil) of N_2O since preindustrial times has been reported in firn and ice air from Greenland and Antarctica (Berkner Island). The data are consistent with an increase in the use of fertilizers in agriculture (Bernard et al., 2006).

Since the 2002 WMO Assessment, measurements performed by the AGAGE and NOAA/ESRL networks have confirmed the steady increase of the N_2O atmospheric concentration observed over the last two decades: globally averaged surface mixing ratio amounted to 318-319 ppb in January 2005 (updated from Prinn et al., 2000; Conway et al., 2004). On the basis of flask samples collected regularly at 11 worldwide sites from 1981 to 1996 (Khalil et al., 2002), concentrations are higher on average by 0.7 ± 0.04 ppb in the Northern Hemisphere, and differences of concentrations over land and oceans indicate large land-based emissions. Annual rates of change of the N_2O concentrations have been monotonic but quite vari-

able, with a mean annual increase of 0.69 ± 0.02 ppb/yr (0.22%/yr) for 1985-1996 (Khalil et al., 2002) and 0.74 ± 0.02 ppb/yr (0.24%/yr) for 1986-2005 (updated from Prinn et al., 2000).

Remote Fourier transform infrared (FTIR) measurements performed at the NDACC site of Jungfraujoch have also shown a regular buildup of the N_2O atmospheric burden, with a linear fit to the monthly mean total column dataset indicating an annual increase of 1.06×10^{16} molec/cm², which corresponds to 0.26%/yr in 2003-2004 (Zander et al., 2005).

1.4.4 Hydrofluorocarbons (HFCs)

HFCs have rapidly replaced CFCs in refrigeration, foam blowing, and aerosol applications. For example, mobile air conditioning accounted for 60% of CFC-12 in 1990 and by 1994 had been replaced by HFC-134a in all but a few countries. HFC-134a (CH_2FCF_3) and HFC-23 (CHF_3) are the two most abundant hydrofluorocarbons in the atmosphere, and they are continuing to grow rapidly (Prinn et al., 2000; Sturrock et al., 2001; O'Doherty et al., 2004). Recently Culbertson et al. (2004) have also reported measurements of these two principal HFCs from the analyses of flask samples collected at Cape Meares, Oregon; Point Barrow, Alaska; and Palmer Station, Antarctica. Updated measurements of HFC-125 (CHF_2CF_3) and HFC-152a (CH_3CHF_2), which were first reported in the previous Assessment (WMO, 2003), also exist.

1.4.4.1 HFC-134a

HFC-134a has rapidly mostly replaced CFC-12 in several refrigeration and air-conditioning applications. As a consequence of increased emissions, the annual global mean concentration in mid-2004 was about 30 ppt, increasing at an annual average rate of approximately 3.9 ppt/yr (2000-2004) (O'Doherty et al., 2004; updates to Montzka et al., 1996) (Figure 1-22 (a)). Annual emissions have been increasing at approximately 10 Gg/yr from 2000 to 2004 (Figure 1-22 (b)). Because so little of the HFC-134a has yet been destroyed in the atmosphere, the error bars on the annual emission estimates in 2003 are just ± 6 Gg/yr.

1.4.4.2 HFC-23

HFC-23 is primarily emitted as a byproduct of HCFC-22 production, with smaller amounts released from semiconductor etching and refrigeration and fire extinguisher losses (Oram et al., 1998). HFC-23 has been measured since 1978 in flask samples from Cape Grim (Oram

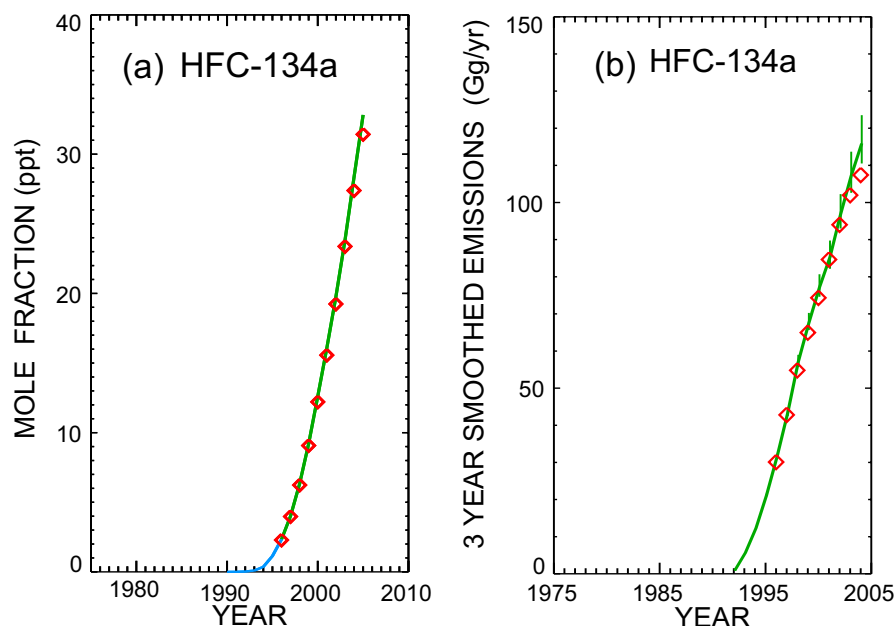


Figure 1-22. (a) Annual global mean mole fractions for HFC-134a derived from the AGAGE (green line) and NOAA/ESRL (red diamonds) networks of ground-based sites (O'Doherty et al., 2004; Montzka et al., 1996). The early measurements (before 1995, in blue) are based on analysis of the air archived in Australia (Oram et al., 1996). (b) Annual global emissions of HFC-134a smoothed over three-year intervals, calculated by inverting the measurements in (a) using the 12-box model. A lifetime of 14.0 years was used. The green error bars, which are very small, indicate the effect of a $\pm 17\%$ uncertainty in the lifetime.

et al., 1998) and, until 1997, approximately 10% larger values from Oregon (Culbertson et al., 2004). The mixing ratio at Cape Grim in 2004 was approximately 18 ppt and the average growth rate in 2001-2004 was approximately 0.7 ppt/yr (Figure 1-23). This rate of growth is significantly less than that (approximately 0.9 ppt/yr) in 1994-2001. The IPCC/TEAP report (Velders and Madronich et al., 2005, Figure 2.4) shows estimated emissions, on the basis of the Cape Grim measurements, of 13 Gg/yr in 2001 versus 6.4 Gg/yr in 1990.

1.4.4.3 HFC-143a, HFC-125, AND HFC-152a

Measurements of HFC-143a (CH_3CF_3) have been reported by Culbertson et al. (2004) for flask samples collected at Cape Meares, Oregon; Point Barrow, Alaska; and Palmer Station, Antarctica. Tropospheric mixing ratios in the Oregon samples increased from about 0.2 ppt in 1978 to about 2 ppt in 1997. Average annual concentrations during 1997 at Alaska and Antarctica were 1.7 and 1.3 ppt, respectively.

HFC-125 is mainly used in refrigeration, while the primary uses of HFC-152a are in foam-blowing and aerosol propellants. Measurements from Cape Grim (updated from Sturrock et al., 2001) and at Mace Head are shown in Figure 1-23. In 2000-2004, mixing ratios have been increasing approximately exponentially at 23%/yr (HFC-125) and 17%/yr (HFC-152a). In mid-2004, globally averaged values derived from these measurements were 3.1 ppt for both gases.

1.4.5 Perfluorocarbons, Sulfur Hexafluoride (SF_6), and SF_5CF_3

Perfluorocarbons (PFCs) and SF_6 are very powerful and long-lived greenhouse gases whose emissions contribute to national inventories of greenhouse gas emissions that are regulated under the Kyoto Protocol. Trifluoromethylsulfurpentafluoride (SF_5CF_3) is a similar chemical species whose source is very uncertain and that is not included in the Kyoto Protocol.

1.4.5.1 CF_4 AND CF_3CF_3

Aoki and Makide (2004) have measured CF_4 (FC-14) levels of 80-81 ppt in Tokyo during August 2003. Long-term trend data (1978-1997) have been reported for CF_4 and CF_3CF_3 (FC-116) in the Cape Meares, Oregon, air archive, and in flask data from Point Barrow, Alaska, and Palmer Station, Antarctica (Khalil et al., 2003). The observed mixing ratios of CF_4 and CF_3CF_3 in 1997 at Cape Meares were 74 ppt and 2.9 ppt, respectively. These mixing ratios are consistent with the values given in *WMO 2002* (Montzka and Fraser et al., 2003). CF_4 increases have been determined from infrared high spectral resolution solar occultation Fourier transform spectrometer measurements between 3 and 50 hPa (~ 20 to 40 km altitude) and latitudes from 50°N to 50°S during 1985, 1992, 1993, 1994, and 2004. These space-based measurements show that the slowdown in the rate of CF_4 accumulation previously reported from surface measurements through

LONG-LIVED COMPOUNDS

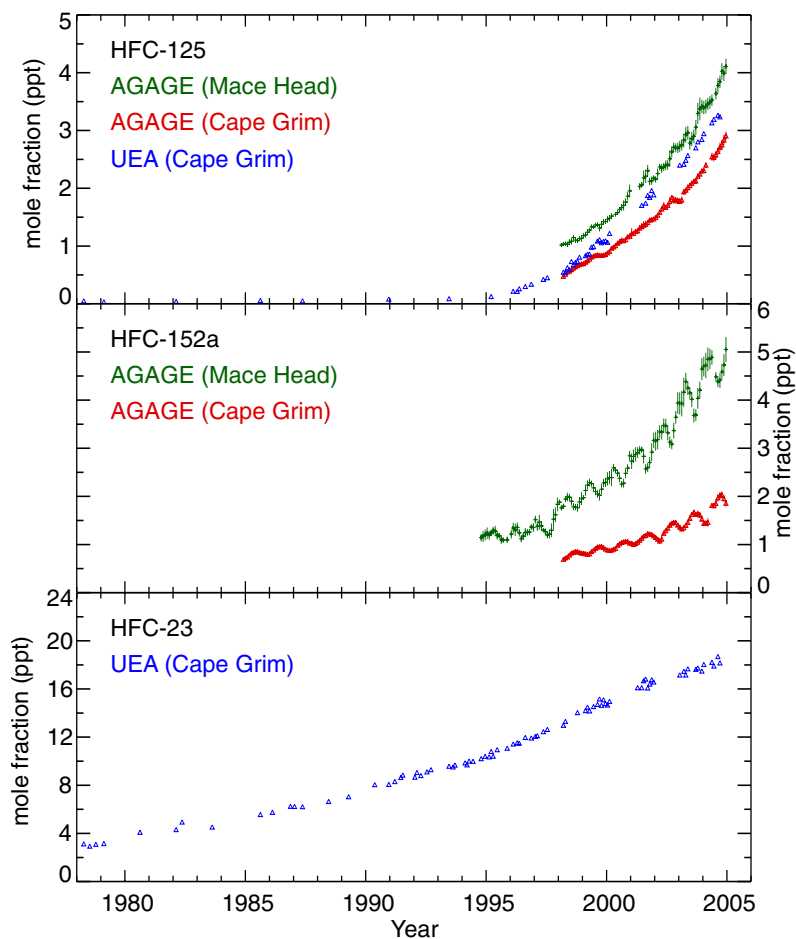


Figure 1-23. Monthly means (ppt) and standard deviations of the AGAGE measurements of HFC-125, HFC-152a, and HFC-23 at Mace Head, Ireland (green) and Cape Grim, Tasmania (red). Individual measurements of the Australian air archive for Cape Grim analyzed by Oram (1999) are shown in blue.

1997 has propagated to the stratosphere and is continuing (Rinsland et al., 2006).

Using historical estimated emissions rates of CF_4 for the aluminum industry and the semiconductor industry, Khalil et al. (2003) estimated that the aluminum industry and the semiconductor industry contributed 33 ppt and 1 ppt, respectively, to the 74 ppt observed in 1997. CF_3CF_3 is also emitted in aluminum processing. By assuming that the CF_3CF_3 and CF_4 emissions in 1997 associated with the aluminum industry maintained a constant ratio through the years, Khalil et al. concluded that the aluminum industry emissions are responsible for 2.4 ppt of the observed CF_3CF_3 concentration, with the balance assumed to be from the semiconductor industry.

Harnisch and Höhne (2002) have compared the estimates of global emissions of CF_4 and CF_3CF_3 from atmospheric observations (top-down) with a summation of emissions in national inventories (bottom-up). For CF_4 , atmospheric measurements indicate global emissions of 16 Gg/yr (late 1980s) decreasing to 12 Gg/yr (late 1990s), compared with a decrease from 11 to 8 Gg/yr over the same period based on a summation of national inventories. Khalil et al. (2003) estimated a decrease from 16 to 10

Gg/yr, respectively, based on global aluminum production (using an industry-based, varying emission factor) together with a small (of order 10%) contribution from the semiconductor industry. Atmospheric measurements of CF_3CF_3 indicating constant global emissions of about 2 Gg/yr (late 1980s to late 1990s) compare well with 1.4-2.2 Gg/yr over the same period based on a summation of national inventories. An estimate of the annual emissions of CF_3CF_3 from Japan (0.19 Gg/yr, 2003) has been made, based on interspecies ratios (with HCFC-22) observed in aircraft profiles near Tokyo (Yokouchi et al., 2005).

1.4.5.2 $\text{CF}_3\text{CF}_2\text{CF}_3$ AND $\text{C-C}_4\text{F}_8$

Long-term trend data (1978-1997) have been reported for perfluoropropane ($\text{CF}_3\text{CF}_2\text{CF}_3$) in the Cape Meares, Oregon, air archive, and in flask data from Point Barrow, Alaska, and Palmer Station, Antarctica (Khalil et al., 2003; Culbertson et al., 2004). $\text{CF}_3\text{CF}_2\text{CF}_3$ mixing ratios at Cape Meares were <0.1 ppt in 1978, growing to >0.2 ppt in 1997, corresponding to global emissions of 0.04 Gg/yr in 1977-1982, rising to 0.48 Gg/yr in 1992-1997. An estimate of the annual emissions of $\text{CF}_3\text{CF}_2\text{CF}_3$

and perfluorocyclobutane ($c\text{-C}_4\text{F}_8$) from Japan (0.06 and 0.02 Gg/yr, respectively, 2003) has been made, based on interspecies ratios (with HCFC-22) observed in aircraft profiles near Tokyo (Yokouchi et al., 2005).

1.4.5.3 SF₆

Sulfur hexafluoride (SF₆), which is mostly used as an insulating fluid in transformers, has been measured by a number of laboratories at Cape Grim, Tasmania, since 1978 via a combination of in situ and flask measurements, including measurements on the Cape Grim air archive (Fraser et al., 2004) (Figure 1-24). The long-term growth rate of SF₆ as observed at Cape Grim has increased from 0.1 ppt/yr in the late 1970s to 0.24 ppt/yr in the mid-1990s. Since then the growth rate has remained relatively constant at 0.23 ± 0.02 ppt/yr, indicating relatively constant global emissions ($\pm 10\%$) since 1995. The 2003 annual mean SF₆ concentration at Cape Grim was 5.0 ± 0.1 ppt (Fraser et al., 2004). The global average SF₆ mixing ratio in 2003 was 5.2 ppt, growing at 0.2 ppt/yr (Thompson et al., 2004).

The burden of SF₆ above the Jungfraujoch (Switzerland) has continued to accumulate during the past few years by 3.4×10^{12} molec cm²/yr, which corresponds to an increase of 4.1%/yr in 2003-2004 (Zander et al., 2005). Corroboration of the regular accumulation of atmospheric SF₆ at other sites, namely, Kitt Peak (32°N) and Ny Ålesund (79°N), has been reported by Krieg et al. (2005). These authors have also shown that the temporal extrapolation of the best fit to the two decades-long Jungfraujoch database of SF₆ results in atmospheric SF₆ loadings in 2050 and 2100 that are significantly lower than

those predicted by the most realistic emission scenarios (see Figure 1-21 in *WMO 2002*, Montzka and Fraser et al., 2003). Satellite observations of SF₆ show a globally-averaged upper tropospheric mixing ratio of 4.3 ppt and stratospheric value of 3.5 ppt in September 2002 (Burgess et al., 2004).

Harnisch and Höhne (2002) have compared the estimates of global emissions of SF₆ from atmospheric observations (top-down) with a summation of emissions in national inventories (bottom-up). The bottom-up estimates of emissions, which are critically dependent on the accuracy of assumed leak rates from electrical transformers, are $60 \pm 10\%$ of the top-down estimates. An estimate of the annual emissions of SF₆ from Japan (0.15 Gg/yr, 2003) has been made, based on interspecies ratios (with HCFC-22) observed in aircraft profiles near Tokyo, which compare favorably to the national emissions for 2001 (0.20 Gg/yr) (Yokouchi et al., 2005).

1.4.5.4 SF₅CF₃

Trifluoromethylsulfurpentafluoride (SF₅CF₃) has an exceptionally large radiative forcing efficiency and was reported to have an atmospheric mixing ratio of about 0.12 ppt in 1999 (Sturges et al., 2000). A potential source of this gas has recently been identified (Huang et al., 2005). Under spark discharge conditions, SF₆ does not react with PFCs, but does so with HFC-23 (CHF₃) and HFC-32 (CH₂F₂), which may be emitted from the surface of fluoropolymers in high-voltage equipment. The only other potential source that has been identified is a byproduct during the manufacture of certain fluorochemicals (Santoro, 2000).

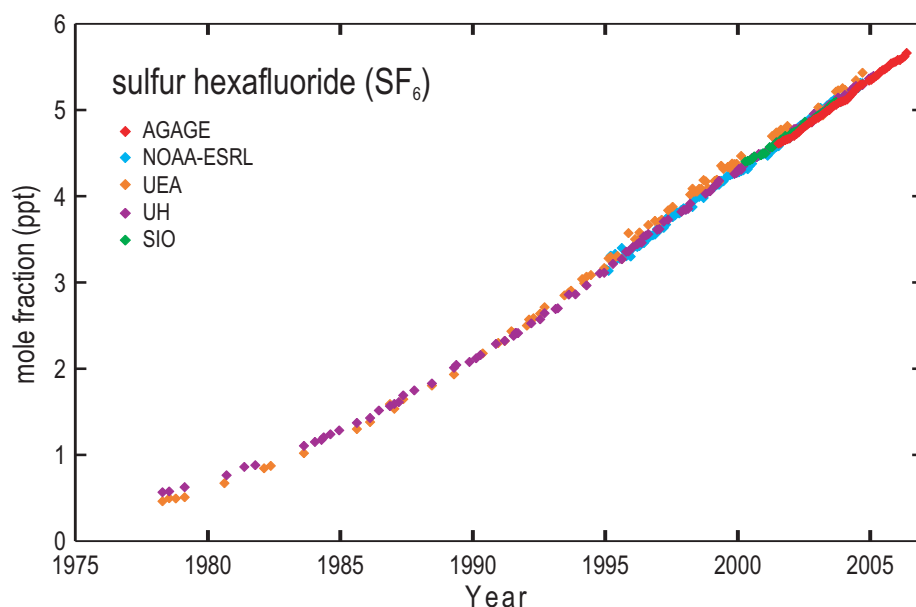


Figure 1-24. Ground-based measurements of sulfur hexafluoride at Cape Grim, Tasmania. The data are updates of the following time series: continuous AGAGE measurements (red; Fraser et al., 2004); NOAA/ESRL flask measurements (blue; Thompson et al., 2004); individual measurements of the Cape Grim air archive analyzed by Oram (orange; UEA, 1999) and by Maiss and Brenninkmeijer (purple, University of Heidelberg-UH, 1998); and Scripps Institution of Oceanography flask measurements by Vollmer and Weiss (green; SIO, 2002).

LONG-LIVED COMPOUNDS

REFERENCES

- Anderson, J., and J.M. Russell III, Long term changes of HCl and HF as observed by HALOE, in *Ozone Vol. I, Proceedings of the XX Quadrennial Ozone Symposium*, 1-8 June 2004, Kos, Greece, edited by C.S. Zerefos, 223-224, Int. Ozone Comm., Athens, Greece, 2004.
- Anderson, J., J.M. Russell, S. Solomon, and L.E. Deaver, Halogen occultation experiment confirmation of stratospheric chlorine decreases in accordance with the Montreal protocol, *J. Geophys. Res.*, *105* (D4), 4483-4490, 2000.
- Andreae, M.O., and P. Merlet, Emission of trace gases and aerosols from biomass burning, *Global Biogeochem. Cycles*, *15* (4), 955-966, 2001.
- Andrews, A.E., K.A. Boering, B.C. Daube, S.C. Wofsy, M. Loewenstein, H. Jost, J.R. Podolske, C.R. Webster, R.L. Herman, D.C. Scott, G.J. Flesch, E.J. Moyer, J.W. Elkins, G.S. Dutton, D.F. Hurst, F.L. Moore, E.A. Ray, P.A. Romashkin, and S.E. Strahan, Mean ages of stratospheric air derived from in situ observations of CO₂, CH₄, and N₂O, *J. Geophys. Res.*, *106* (D23), 32295-32314, 2001.
- Aoki, N., and Y. Makide, Precise determination of the atmospheric CF₄ concentration by using natural Kr in the atmosphere as an internal reference in the pre-concentration/GC/MS analysis, *Chem. Lett.*, *33* (12), 1634-1635, 2004.
- Aydin, M., E.S. Saltzman, W.J. De Bruyn, S.A. Montzka, J.H. Butler, and M. Battle, Atmospheric variability of methyl chloride during the last 300 years from an Antarctic ice core and firn air, *Geophys. Res. Lett.*, *31*, L02109, doi: 10.1029/2003GL018750, 2004.
- Bacmeister, J.T., V. Kuell, D. Offermann, M. Riese, and J.W. Elkins, Intercomparison of satellite and aircraft observations of ozone, CFC-11, and NO_y using trajectory mapping, *J. Geophys. Res.*, *104* (D13), 16379-16390, 1999.
- Barnes, D.H., S.C. Wofsy, B.P. Fehla, E.W. Gottlieb, J.W. Elkins, G.S. Dutton, and S.A. Montzka, Urban/industrial pollution for the New York City - Washington, DC, corridor, 1996-1998: 2. A study of the efficacy of the Montreal Protocol and other regulatory measures, *J. Geophys. Res.*, *108* (D6), 4186, doi: 10.1029/2001JD001117, 2003.
- Battle, M., M.L. Bender, P.P. Tans, J.W.C. White, J.T. Ellis, T. Conway, and R.J. Francey, Global carbon sinks and their variability inferred from atmospheric O₂ and delta ¹³C, *Science*, *287* (5462), 2467-2470, 2000.
- Bayes, K.D., D.W. Toohey, R.R. Friedl, and S.P. Sander, Measurements of quantum yields of bromine atoms in the photolysis of bromoform from 266 to 324 nm, *J. Geophys. Res.*, *108* (D3), 4095, doi: 10.1029/2002JD002877, 2003.
- Bernard, S., T.R. Röckmann, J. Kaiser, J.-M. Barnola, H. Fischer, T. Blunier, and J. Chappellaz, Constraints on N₂O budget changes since pre-industrial time from new firn air and ice core isotope measurements, *Atmos. Chem. Phys.*, *6*, 493-503, 2006.
- Berthet, G., P. Ricaud, F. Lefèvre, E. Le Flochmoën, J. Urban, B. Barret, N. Lautié, E. Dupuy, J. De La Noë, and D. Murtagh, Nighttime chlorine monoxide observations by the Odin satellite and implications for the ClO/Cl₂O₂ equilibrium, *Geophys. Res. Lett.*, *32*, L11812, doi: 10.1029/2006GL022649, 2005.
- Blake, D.R., T.-Y. Chen, T.W. Smith Jr., C.J.-L. Wang, O.W. Wingenter, N.J. Blake, F.S. Rowland, and E.W. Mayer, Three-dimensional distribution of non-methane hydrocarbons and halocarbons over the northwestern Pacific during the 1991 Pacific Exploratory Mission (PEM-West A), *J. Geophys. Res.*, *101* (D1), 1763-1778, 1996.
- Blake, N.J., D.R. Blake, I.J. Simpson, J.P. Lopez, N.A.C. Johnston, A.L. Swanson, A.S. Katzenstein, S. Meinardi, B.C. Sive, J.J. Colman, E. Atlas, F. Flocke, S.A. Vay, M.A. Avery, and F.S. Rowland, Large-scale latitudinal and vertical distributions of NMHCs and selected halocarbons in the troposphere over the Pacific Ocean during the March-April 1999 Pacific Exploratory Mission (PEM-Tropics B), *J. Geophys. Res.*, *106* (D23), 32627-32644, 2001.
- Blake, N.J., D.R. Blake, I.J. Simpson, S. Meinardi, A.L. Swanson, J.P. Lopez, A.S. Katzenstein, B. Barletta, T. Shirai, E. Atlas, G. Sachse, M. Avery, S. Vay, H.E. Fuelberg, C.M. Kiley, K. Kita, and F.S. Rowland, NMHCs and halocarbons in Asian continental outflow during the Transport and Chemical Evolution over the Pacific (TRACE-P) Field Campaign: Comparison with PEM-West B, *J. Geophys. Res.*, *108* (D20), 8806, doi: 10.1029/2002JD003367, 2003.
- Borch, T., P. Ambus, F. Laturus, B. Svensmark, and C. Gron, Biodegradation of chlorinated solvents in a water unsaturated topsoil, *Chemosphere*, *51* (2), 143-152, 2003.
- Bousquet, P., D.A. Hauglustaine, P. Peylin, C. Carouge, and P. Ciais, Two decades of OH variability as inferred by an inversion of atmospheric transport and chemistry of methyl chloroform, *Atmos. Chem. Phys.*, *5*, 2635-2656, 2005.

- Brasseur, G., M.H. Hitchman, S. Walters, M. Dymek, E. Falise, and M. Pirre, An interactive chemical dynamic radiative two-dimensional model of the middle atmosphere, *J. Geophys. Res.*, *95* (D5), 5639-5655, 1990.
- Burgess, A.B., R.G. Grainger, A. Dudhia, V.H. Payne, and V.L. Jay, MIPAS measurement of sulphur hexafluoride (SF₆), *Geophys. Res. Lett.*, *31* (5), L05112, doi: 10.1029/2003GL019143, 2004.
- Butler, J.H., S.A. Montzka, A.D. Clarke, J.M. Lobert, and J.W. Elkins, Growth and distribution of halons in the atmosphere, *J. Geophys. Res.*, *103* (D1), 1503-1511, 1998.
- Butler, J.H., M. Battle, M.L. Bender, S.A. Montzka, A.D. Clarke, E.S. Saltzman, C.M. Sucher, J.P. Severinghaus, and J.W. Elkins, A record of atmospheric halocarbons during the twentieth century from polar firn air, *Nature*, *399* (6738), 749-755, 1999.
- Chen, L., K. Tokuhashi, S. Kutsuna, A. Sekiya, Y. Yonei, and A. Yamamoto, Kinetic study of the gas-phase reaction of CF₃CHFCF₂CH₂OH with OH radicals at 230-430 K, *Chem. Phys. Lett.*, *382* (3-4), 277-282, 2003.
- Chen, L., S. Kutsuna, K. Tokuhashi, and A. Sekiya, Kinetics of the gas-phase reactions of CF₃OC(O)H with OH radicals at 253-328 K, *Int. J. Chem. Kinet.*, *36* (6), 337-344, 2004a.
- Chen, L., S. Kutsuna, K. Tokuhashi, and A. Sekiya, Kinetic study of the gas-phase reactions of C₂F₅OC(O)H and n-C₃F₇OC(O)H with OH radicals at 253-328 K, *Chem. Phys. Lett.*, *400* (4-6), 563-568, 2004b.
- Chen, L., S. Kutsuna, K. Tokuhashi, and A. Sekiya, Kinetic study of the gas-phase reactions of CHF₂CF₂OCHF₂ and CF₃CHFCF₂OCH₂CF₂CF₃ with OH radicals at 253-328 K, *Chem. Phys. Lett.*, *403* (1-3), 180-184, 2005.
- Chim, R.Y.L., R.A. Kennedy, and R.P. Tuckett, The vacuum-UV absorption spectrum of SF₅CF₃; implications for its lifetime in the earth's atmosphere, *Chem. Phys. Lett.*, *367* (5-6), 697-703, 2003.
- Chipperfield, M.P., M. Burton, W. Bell, C.P. Walsh, T. Blumenstock, M.T. Coffey, J.W. Hannigan, W.G. Mankin, B. Galle, J. Mellqvist, E. Mahieu, R. Zander, J. Notholt, B. Sen, and G.C. Toon, On the use of HF as a reference for the comparison of stratospheric observations and models, *J. Geophys. Res.*, *102* (D11), 12901-12919, 1997.
- Coheur, P.F., C. Clerbaux, and R. Colin, Spectroscopic measurements of halocarbons and hydrohalocarbons by satellite-borne remote sensors, *J. Geophys. Res.*, *108* (D4), 4130, doi: 10.1029/2002JD002649, 2003.
- Conway, T.J. (Ed.), A.E. Andrews, L. Bruhwiler, A. Crotwell, E.J. Dlugokencky, M.P. Hahn, A.I. Hirsch, D.R. Kitzis, P.M. Lang, K.A. Masarie, A.M. Michalak, J.B. Miller, P.C. Novelli, W. Peters, P.P. Tans, K.W. Thoning, B.H. Vaughn, and C. Zhao, Carbon Cycle Greenhouse Gases, in *Climate Monitoring and Diagnostics Laboratory: Summary Report No. 27, 2002-2003*, edited by R.C. Schnell, A.-M. Buggle, and R.M. Rosson, 32-57, NOAA/Climate Monitoring and Diagnostics Laboratory, Boulder, Colo., 2004.
- Cotter, E.S.N., C.E. Canosa-Mas, C.R. Manners, R.P. Wayne, and D.E. Shallcross, Kinetic study of the reactions of OH with the simple alkyl iodides: CH₃I, C₂H₅I, 1-C₃H₇I and 2-C₃H₇I, *Atmos. Environ.*, *37* (8), 1125-1133, 2003.
- Cox, M.L., P.J. Fraser, G.A. Sturrock, S.T. Siems, and L.W. Porter, Terrestrial sources and sinks of halo-methanes near Cape Grim, Tasmania, *Atmos. Environ.*, *38* (23), 3839-3852, 2004.
- Cox, M.L., G.A. Sturrock, P.J. Fraser, S.T. Siems, and P.B. Krummel, Identification of regional sources of methyl bromide and methyl iodide from AGAGE observations at Cape Grim, Tasmania, *J. Atmos. Chem.*, *50* (1), 59-77, 2005.
- Cox, P.M., R.A. Betts, C.D. Jones, S.A. Spall, and I.J. Totterdell, Acceleration of global warming due to carbon-cycle feedbacks in a coupled climate model, *Nature*, *408* (6809), 184-187, 2000.
- Culbertson, J.A., J.M. Prins, E.P. Grimsrud, R.A. Rasmussen, M.A.K. Khalil, and M.J. Shearer, Observed trends for CF₃-containing compounds in background air at Cape Meares, Oregon, Point Barrow, Alaska, and Palmer Station, Antarctica, *Chemosphere*, *55* (8), 1109-1119, 2004.
- Cunnold, D.M., P.J. Fraser, R.F. Weiss, R.G. Prinn, P.G. Simmonds, B.R. Miller, F.N. Alyea, and A.J. Crawford, Global trends and annual releases of CCl₃F and CCl₂F₂ estimated from ALE/GAGE and other measurements from July 1978 to June 1991, *J. Geophys. Res.*, *99* (D1), 1107-1126, 1994.
- Cunnold, D.M., R.F. Weiss, R.G. Prinn, D. Hartley, P.G. Simmonds, P.J. Fraser, B. Miller, F.N. Alyea, and L. Porter, GAGE/AGAGE measurements indicating reductions in global emissions of CCl₃F and CCl₂F₂ in 1992-1994, *J. Geophys. Res.*, *102* (D1), 1259-1269, 1997.
- Daniel, J.S., S. Solomon, and D.L. Albritton, On the evaluation of halocarbon radiative forcing and global warming potentials, *J. Geophys. Res.*, *100* (D1),

LONG-LIVED COMPOUNDS

- 1271-1285, 1995.
- DeMore, W.B., and K.D. Bayes, Rate constants for the reactions of hydroxyl radical with several alkanes, cycloalkanes, and dimethyl ether, *J. Phys. Chem. A*, *103* (15), 2649-2654, 1999.
- Dlugokencky, E.J., K.A. Masarie, P.M. Lang, and P.P. Tans, Continuing decline in the growth rate of the atmospheric methane burden, *Nature*, *393* (6684), 447-450, 1998.
- Dlugokencky, E.J., S. Houweling, L. Bruhwiler, K.A. Masarie, P.M. Lang, J.B. Miller, and P.P. Tans, Atmospheric methane levels off: Temporary pause or a new steady-state?, *Geophys. Res. Lett.*, *30* (19), 1992, doi: 10.1029/2003GL018126, 2003.
- Dufour, G., C.D. Boone, and P.F. Bernath, First measurements of CFC-113 and HCFC-142b from space using ACE-FTS infrared spectra, *Geophys. Res. Lett.*, *32*, L15S09, doi: 10.1029/2005GL022422, 2005.
- Duncan, B.N., R.V. Martin, A.C. Staudt, R. Yevich, and J.A. Logan, Interannual and seasonal variability of biomass burning emissions constrained by satellite observations, *J. Geophys. Res.*, *108* (D2), 4100, doi: 10.1029/2002JD002378, 2003.
- Dunse, B.L., L.P. Steele, S.R. Wilson, P.J. Fraser, and P.B. Krummel, Trace gas emissions from Melbourne, Australia, based on AGAGE observations at Cape Grim, Tasmania, 1995-2000, *Atmos. Environ.*, *39* (34), 6334-6344, 2005.
- Engel, A., M. Strunk, M. Muller, H.P. Haase, C. Poss, I. Levin, and U. Schmidt, Temporal development of total chlorine in the high-latitude stratosphere based on reference distributions of mean age derived from CO₂ and SF₆, *J. Geophys. Res.*, *107* (D12), 4136, doi: 10.1029/2001JD000584, 2002.
- Ferretti, D.F., J.B. Miller, J.W.C. White, D.M. Etheridge, K.R. Lassey, D.C. Lowe, C.M.M. Meure, M.F. Dreier, C.M. Trudinger, T.D. van Ommen, and R.L. Langenfelds, Unexpected changes to the global methane budget over the past 2000 years, *Science*, *309* (5741), 1714-1717, 2005.
- Flückiger, J., E. Monnin, B. Stauffer, J. Schwander, T.F. Stocker, J. Chappellaz, D. Raynaud, and J.-M. Barnola, High-resolution Holocene N₂O ice core record and its relationship with CH₄ and CO₂, *Global Biogeochem. Cycles*, *16* (1), 1010, doi: 10.1029/2001GB001417, 2002.
- Frankenberg, C., J.F. Meirink, M. van Weele, U. Platt, and T. Wagner, Assessing methane emissions from global space-borne observations, *Science*, *308* (5724), 1010-1014, 2005.
- Fraser, P., D. Cunnold, F. Alyea, R. Weiss, R. Prinn, P. Simmonds, B. Miller, and R. Langenfelds, Lifetime and emission estimates of 1,1,2-trichlorotrifluoroethane (CFC-113) from daily global background observations June 1982 - June 1994, *J. Geophys. Res.*, *101* (D7), 12585-12599, 1996.
- Fraser, P.J., D.E. Oram, C.E. Reeves, S.A. Penkett, and A. McCulloch, Southern Hemispheric halon trends (1978-1998) and global halon emissions, *J. Geophys. Res.*, *104* (D13), 15985-15999, 1999.
- Fraser, P.J., L.W. Porter, S.B. Baly, P.B. Krummel, B.L. Dunse, L.P. Steele, N. Derek, R.L. Langenfelds, I. Levin, D.E. Oram, J.W. Elkins, M.K. Vollmer, and R.F. Weiss, Sulfur hexafluoride at Cape Grim: long term trends and regional emissions, in *Baseline Atmospheric Program (Australia) 2001-2002*, edited by J.M. Cainey, N. Derek, and P.B. Krummel, 18-23, Bureau of Meteorology and CSIRO Division of Atmospheric Research, Melbourne, Australia, 2004.
- Freedman, D.L., M. Swamy, N.C. Bell, and M.F. Verce, Biodegradation of chloromethane by *Pseudomonas aeruginosa* strain NB1 under nitrate-reducing and aerobic conditions, *Appl. Environ. Microbiol.*, *70* (8), 4629-4634, 2004.
- Froidevaux, L., N.J. Livesey, W.G. Read, Y.B.B. Jiang, C. Jimenez, M.J. Filipiak, M.J. Schwartz, M.L. Santee, H.C. Pumphrey, J.H. Jiang, D.L. Wu, G.L. Manney, B.J. Drouin, J.W. Waters, E.J. Fetzer, P.F. Bernath, C.D. Boone, K.A. Walker, K.W. Jucks, G.C. Toon, J.J. Margitan, B. Sen, C.R. Webster, L.E. Christensen, J.W. Elkins, E. Atlas, R.A. Lueb, and R. Hendershot, Early validation analyses of atmospheric profiles from EOS MLS on the Aura satellite, *IEEE Trans. Geosci. Remote Sens.*, *44* (5), 1106-1121, 2006.
- GLOBALVIEW-CH₄, Cooperative Atmospheric Data Integration Project - Methane. CD-ROM, NOAA CMDL, Boulder, Colo., 2005. Available via anonymous FTP to ftp.cmdl.noaa.gov, Path: ccg/ch4/GLOBALVIEW.
- Gola, A.A., B. D'Anna, K.L. Feilberg, S.R. Sellevag, L. Bache-Andreassen, and C.J. Nielsen, Kinetic isotope effects in the gas phase reactions of OH and Cl with CH₃Cl, CD₃Cl, and ¹³CH₃Cl, *Atmos. Chem. Phys.*, *5*, 2395-2402, 2005.
- Gros, V., J. Williams, J.A. van Aardenne, G. Salisbury, R. Hofmann, M.G. Lawrence, R. von Kuhlmann, J. Lelieveld, M. Krol, H. Berresheim, J.M. Lobert, and E. Atlas, Origin of anthropogenic hydrocarbons and halocarbons measured in the summertime european outflow (on Crete in 2001), *Atmos. Chem. Phys.*, *3*, 1223-1235, 2003.

- Groszko, W., and R.M. Moore, Ocean-atmosphere exchange of methyl bromide: NW Atlantic and Pacific Ocean studies, *J. Geophys. Res.*, *103* (D13), 16737-16741, 1998.
- Hall, B.D. (Ed.), J.H. Butler, A.D. Clarke, G.S. Dutton, J.W. Elkins, D.F. Hurst, D.B. King, E.S. Kline, J. Lind, L.T. Lock, D. Mondeel, S.A. Montzka, F.L. Moore, J.D. Nance, E.A. Ray, P.A. Romashkin, and T.M. Thompson, Halocarbons and other atmospheric trace species, in *Climate Monitoring and Diagnostics Laboratory: Summary Report No. 26, 2000-2001*, edited by D.B. King, R.C. Schnell, and R.M. Rosson, 106-135, NOAA/Climate Monitoring and Diagnostics Laboratory, Boulder, Colo., 2002.
- Hamilton, J.T.G., W.C. McRoberts, F. Keppler, R.M. Kalin, and D.B. Harper, Chloride methylation by plant pectin: An efficient environmentally significant process, *Science*, *301* (5630), 206-209, 2003.
- Happell, J.D., and M.P. Roche, Soils: A global sink of atmospheric carbon tetrachloride, *Geophys. Res. Lett.*, *30* (2), 1088, doi: 10.1029/2002GL015957, 2003.
- Harnisch, J., and N. Höhne, Comparison of emissions estimates derived from atmospheric measurements with national estimates of HFCs, PFCs and SF₆, *Environ. Sci. Pollut. Res.*, *9* (5), 315-320, 2002.
- Harries, J.E., H.E. Brindley, P.J. Sagoo, and R.J. Bantges, Increase in greenhouse forcing inferred from the outgoing longwave radiation spectra of the Earth in 1970 and 1997, *Nature*, *410*, 355-357 and 1124 (erratum), 2001.
- Hoffmann, L., R. Spang, M. Kaufman, and M. Riese, Retrieval of CFC-11 and CFC-12 from Envisat MIPAS observations by means of rapid radiative transfer calculations, *Adv. Space Res.*, *36* (5), 915-921, 2005.
- Huang, L., L.L. Zhu, X.X. Pan, J.L. Zhang, O.Y. Bin, and H.Q. Hou, One potential source of the potent greenhouse gas SF₅CF₃: the reaction of SF₆ with fluorocarbon under discharge, *Atmos. Environ.*, *39* (9), 1641-1653, 2005.
- Hurley, M.D., T.J. Wallington, M.P.S. Anderson, D.A. Ellis, J.W. Martin, and S.A. Mabury, Atmospheric chemistry of fluorinated alcohols: Reaction with Cl atoms and OH radicals and atmospheric lifetimes, *J. Phys. Chem. A*, *108* (11), 1973-1979, 2004.
- Hurst, D.F., P.A. Romashkin, J.W. Elkins, E.A. Oberlander, N.F. Elansky, I.B. Belikov, I.G. Granberg, G.S. Golitsyn, A.M. Grisenko, C.A.M. Brenninkmeijer, and P.J. Crutzen, Emissions of ozone-depleting substances in Russia during 2001, *J. Geophys. Res.*, *109*, D14303, doi: 10.1029/2004JD004633, 2004.
- Hurst, D.F., J.C. Lin, P.A. Romashkin, B.C. Daube, C. Gerbig, D.M. Matross, S.C. Wofsy, B.D. Hall, and J.W. Elkins, Continuing global significance of emissions of Montreal Protocol-restricted halocarbons in the United States and Canada, *J. Geophys. Res.*, *111*, D15302, doi: 10.1029/2005JD006785, 2006.
- IPCC (Intergovernmental Panel on Climate Change), *Climate Change 2001: The Scientific Basis: Contribution of Working Group I to the Third Assessment Report of the Intergovernmental Panel on Climate Change*, edited by J.T. Houghton, Y. Ding, D.J. Griggs, M. Noguer, P.J. van der Linden, X. Dai, K. Maskell, and C.A. Johnson, 881 pp., Cambridge University Press, Cambridge, U.K., 2001.
- IPCC/TEAP (Intergovernmental Panel on Climate Change/Technology and Economic Assessment Panel), *IPCC/TEAP Special Report on Safeguarding the Ozone Layer and the Global Climate System: Issues Related to Hydrofluorocarbons and Perfluorocarbons*. Prepared by Working Groups I and III of the Intergovernmental Panel on Climate Change, and the Technical and Economic Assessment Panel, Cambridge University Press, Cambridge, U.K. and New York, N.Y., 2005.
- Irion, F.W., M.R. Gunson, G.C. Toon, A.Y. Chang, A. Eldering, E. Mahieu, G.L. Manney, H.A. Michelsen, E.J. Moyer, M.J. Newchurch, G.B. Osterman, C.P. Rinsland, R.J. Salawitch, B. Sen, Y.L. Yung, and R. Zander, Atmospheric Trace Molecule Spectroscopy (ATMOS) Experiment Version 3 data retrievals, *Appl. Opt.*, *41* (33), 6968-6979, 2002.
- Kaspers, K.A., R.S.W. van de Wal, J.A. de Gouw, C.M. Hofstede, M.R. van den Broeke, C. van der Veen, R.E.M. Neubert, H.A.J. Meijer, C.A.M. Brenninkmeijer, L. Karlof, and J.G. Winther, Analyses of firn gas samples from Dronning Maud Land, Antarctica: Study of nonmethane hydrocarbons and methyl chloride, *J. Geophys. Res.*, *109*, D02307, doi: 10.1029/2003JD003950, 2004.
- Kaye, J.A., A.R. Douglass, C.H. Jackman, R.S. Stolarski, R. Zander, and G. Roland, Two-dimensional model calculation of fluorine-containing reservoir species in the stratosphere, *J. Geophys. Res.*, *96* (D7), 12865-12881, 1991.
- Keeling, C.D., and T.P. Whorf, Atmospheric CO₂ records from sites in the SIO air sampling network, in *Trends: A Compendium of Data on Global Change*, Carbon Dioxide Information Analysis Center, Oak

LONG-LIVED COMPOUNDS

- Ridge National Laboratory, U.S. Department of Energy, Oak Ridge, Tenn., U.S.A., 2005.
- Keppeler, F., R.M. Kalin, D.B. Harper, W.C. McRoberts, and J.T.G. Hamilton, Carbon isotope anomaly in the major plant C-1 pool and its global biogeochemical implications, *Biogeosciences*, 1 (2), 123-131, 2004.
- Khalil, M.A.K., and R.A. Rasmussen, Soil-atmosphere exchange of radiatively and chemically active gases, *Environ. Sci. Pollut. Res.*, 7 (2), 79-82, 2000.
- Khalil, M.A.K., R.A. Rasmussen, and M.J. Shearer, Atmospheric nitrous oxide: patterns of global change during recent decades and centuries, *Chemosphere*, 47 (8), 807-821, 2002.
- Khalil, M.A.K., R.A. Rasmussen, J.A. Culbertson, J.M. Prins, E.P. Grimsrud, and M.J. Shearer, Atmospheric perfluorocarbons, *Environ. Sci. Technol.*, 37 (19), 4358-4361, 2003.
- Khosrawi, F., R. Muller, H. Irie, A. Engel, G.C. Toon, B. Sen, S. Aoki, T. Nakazawa, W.A. Traub, K.W. Jucks, D.G. Johnson, H. Oelhaf, G. Wetzel, T. Sugita, H. Kanzawa, T. Yokota, H. Nakajima, and Y. Sasano, Validation of CFC-12 measurements from the Improved Limb Atmospheric Spectrometer (ILAS) with the version 6.0 retrieval algorithm, *J. Geophys. Res.*, 109, D06311, doi: 10.1029/2003JD004325, 2004.
- King, D.B., J.H. Butler, S.A. Montzka, S.A. Yvon-Lewis, and J.W. Elkins, Implications of methyl bromide supersaturations in the temperate North Atlantic Ocean, *J. Geophys. Res.*, 105 (D15), 19763-19769, 2000.
- King, D.B., J.H. Butler, S.A. Yvon-Lewis, and S.A. Cotton, Predicting oceanic methyl bromide saturation from SST, *Geophys. Res. Lett.*, 29 (24), 2199, doi: 10.1029/2002GL016091, 2002.
- Kopp, G., H. Berg, T. Blumenstock, H. Fischer, F. Hase, G. Hochschild, M. Höpfner, W. Kouker, T. Reddmann, R. Ruhnke, U. Raffalski, and Y. Kondo, Evolution of ozone and ozone-related species over Kiruna during the SOLVE/THESEO 2000 campaign retrieved from ground-based millimeter-wave and infrared observations, *J. Geophys. Res.*, 108 (D5), 8308, doi: 10.1029/2001JD001064, 2003.
- Krieg, J., J. Nothholt, E. Mahieu, C.P. Rinsland, and R. Zander, Sulphur hexafluoride (SF₆): comparison of FTIR-measurements at three sites and determination of its trend in the northern hemisphere, *J. Quant. Spectrosc. Radiat. Transfer*, 92 (3), 383-392, 2005.
- Krol, M., P.J. van Leeuwen, and J. Lelieveld, Global OH trend inferred from methylchloroform measurements, *J. Geophys. Res.*, 103 (D9), 10697-10711, 1998.
- Krol, M.C., J. Lelieveld, D.E. Oram, G.A. Sturrock, S.A. Penkett, C.A.M. Brenninkmeijer, V. Gros, J. Williams, and H.A. Scheeren, Continuing emissions of methyl chloroform from Europe, *Nature*, 421 (6919), 131-135, 2003.
- Krummel, P.B., L.W. Porter, P.J. Fraser, S.B. Daly, B.L. Dunse, and N. Derek, HCFCs, HFCs, halons, minor CFCs, PCE and halomethanes: The AGAGE in situ GC-MS Program at Cape Grim, 1998-2002, in *Baseline Atmospheric Program (Australia) 2001-2002*, edited by J.M. Caaney, N. Derek, and P.B. Krummel, 57-63, Bureau of Meteorology and CSIRO Division of Atmospheric Research, Melbourne, Australia, 2004.
- Kurylo, M.J., and J.M. Rodríguez (Lead Authors), M. Andreae, E. Atlas, D. Blake, J. Butler, S. Lal, P. Midgley, S. Montzka, P. Novelli, C. Reeves, P. Simmonds, P. Steele, W.T. Sturges, R. Weiss, and Y. Yokouchi, Short-lived ozone-related compounds, Chapter 2 in *Scientific Assessment of Ozone Depletion: 1998, Global Ozone Research and Monitoring Project-Report No. 44*, World Meteorological Organization, Geneva, Switzerland, 1999.
- Langenfelds, R.L., P.J. Fraser, R.J. Francey, L.P. Steele, L.W. Porter, and C.E. Allison, The Cape Grim Air Archive: The first seventeen years, 1978-1995, in *Baseline Atmospheric Program (Australia) 1994-95*, edited by R.J. Francey, A.L. Dick, and N. Derek, 53-70, Bureau of Meteorology and CSIRO Division of Atmospheric Research, Melbourne, Australia, 1996.
- Lee-Taylor, J.M., and K.R. Redeker, Reevaluation of global emissions from rice paddies of methyl iodide and other species, *Geophys. Res. Lett.*, 32, L15801, doi: 10.1029/2005GL022918, 2005.
- Lee-Taylor, J.M., S.C. Doney, G.P. Brasseur, and J.-F. Muller, A global three-dimensional atmosphere-ocean model of methyl bromide distributions, *J. Geophys. Res.*, 103 (D13), 16039-16057, 1998.
- Lee-Taylor, J.M., G.P. Brasseur, and Y. Yokouchi, A preliminary three-dimensional global model study of atmospheric methyl chloride distributions, *J. Geophys. Res.*, 106 (D24), 34221-34233, 2001.
- Li, J.L., D.M. Cunnold, H.-J. Wang, R.F. Weiss, B.R. Miller, C. Harth, P. Salameh, and J.M. Harris, Halocarbon emissions estimated from Advanced Global Atmospheric Gases Experiment measured pollution events at Trinidad Head, California, *J. Geophys. Res.*, 110 (D14308), doi: 10.1029/2004

- JD005739, 2005.
- Li, Y., K.O. Patten, D.J. Wuebbles, and D. Youn, Potential impacts of CF₃I on ozone as a replacement for CF₃Br in aircraft applications, *Atmos. Chem. Phys. Discuss.*, 6 (3), 5163-5195, 2006.
- Limão-Vieira, P., S. Eden, P.A. Kendall, N.J. Mason, A. Giuliani, J. Heinesch, M.-J. Hubin-Franskin, J. Delwiche, and S.V. Hoffmann, An experimental study of SF₅CF₃ by electron energy loss spectroscopy, VUV photo-absorption and photoelectron spectroscopy, *Int. J. Mass Spectrom.*, 233 (1-3), 335-341, 2004.
- Lober, J., and J.M. Harris, Trace gases and air mass origin at Kaashidhoo, Indian Ocean, *J. Geophys. Res.*, 107 (D19), 8013, doi: 10.1029/2001JD000731, 2002.
- Low, J.C., N.Y. Wang, J. Williams, and R.J. Cicerone, Measurements of ambient atmospheric C₂H₅Cl and other ethyl and methyl halides at coastal California sites and over the Pacific Ocean, *J. Geophys. Res.*, 108 (D19), 4608, doi: 10.1029/2003JD003620, 2003.
- Lowe, D.C., C.A.M. Brenninkmeijer, G.W. Brailsford, K.R. Lassey, A.J. Gomez, and E.G. Nisbet, Concentration and ¹³C records of atmospheric methane in New Zealand and Antarctica: Evidence for changes in methane sources, *J. Geophys. Res.*, 99 (D8), 16913-16925, 1994.
- MacFarling-Meure, C., The variation of atmospheric carbon dioxide, methane and nitrous oxide during the Holocene from ice core analysis, Ph.D. thesis, University of Melbourne, Australia, 2004.
- Mahieu, E., P. Duchatelet, R. Zander, P. Demoulin, C. Servais, C.P. Rinsland, M.P. Chipperfield, and M. De Mazière, The evolution of inorganic chlorine above the Jungfraujoch station: An update, in *Ozone Vol. II, Proceedings of the XX Quadrennial Ozone Symposium*, 1-8 June 2004, Kos, Greece, edited by C.S. Zerefos, 997-998, Int. Ozone Comm., Athens, Greece, 2004.
- Maiss, M., and C.A.M. Brenninkmeijer, Atmospheric SF₆: Trends, sources and prospects, *Environ. Sci. Technol.*, 32 (20), 3077-3086, 1998.
- Mangani, F., M. Maione, L. Lattanzi, and J. Arduini, A gas chromatographic-mass spectrometric method for trace analysis of chlorofluorocarbons and their replacement compounds in atmospheric samples, *Chromatographia*, 51 (5-6), 325-330, 2000.
- Manning, A.J., D.B. Ryall, R.G. Derwent, P.G. Simmonds, and S. O'Doherty, Estimating European emissions of ozone-depleting and greenhouse gases using observations and a modeling back-attribution technique, *J. Geophys. Res.*, 108 (D14), 4405, doi: 10.1029/2002JD002312, 2003.
- Markert, F., and O.J. Nielsen, The reactions of OH radicals with chloroalkanes in the temperature range 295-360 K, *Chem. Phys. Lett.*, 194 (1-2), 123-127, 1992.
- McCulloch, A., and P.M. Midgley, The history of methyl chloroform emissions: 1951-2000, *Atmos. Environ.*, 35 (31), 5311-5319, 2001.
- McDonald, I.R., K.L. Warner, C. McAnulla, C.A. Woodall, R.S. Oremland, and J.C. Murrell, A review of bacterial methyl halide degradation: Biochemistry, genetics and molecular ecology, *Environ. Microbiol.*, 4 (4), 193-203, 2002.
- Miller, B.R., J. Huang, R.F. Weiss, R.G. Prinn, and P.J. Fraser, Atmospheric trend and lifetime of chlorodifluoromethane (HCFC-22) and the global tropospheric OH concentration, *J. Geophys. Res.*, 103 (D11), 13237-13248, 1998.
- Miller, J.B., K.A. Mack, R. Dissly, J.W.C. White, E.J. Dlugokencky, and P.P. Tans, Development of analytical methods and measurements of ¹³C/¹²C in atmospheric CH₄ from the NOAA/Climate Monitoring and Diagnostics Laboratory global air sampling network, *J. Geophys. Res.*, 107 (D13), 4178, doi: 10.1029/2001JD000630, 2002.
- Miller, L.G., K.L. Warner, S.M. Baesman, R.S. Oremland, I.R. McDonald, S. Radajewski, and J.C. Murrell, Degradation of methyl bromide and methyl chloride in soil microcosms: Use of stable C isotope fractionation and stable isotope probing to identify reactions and the responsible microorganisms, *Geochim. Cosmochim. Acta*, 68 (15), 3271-3283, 2004.
- Millet, D.B., and A.H. Goldstein, Evidence of continuing methyl chloroform emissions from the United States, *Geophys. Res. Lett.*, 31, L17101, doi: 10.1029/2004GL020166, 2004.
- Montzka, S.A., and P.J. Fraser (Lead Authors), J.H. Butler, D. Cunnold, J. Daniel, D. Derwent, P. Connell, S. Lal, A. McCulloch, D. Oram, C. Reeves, E. Sanhueza, P. Steele, G.J.M. Velders, R.F. Weiss, and R. Zander, Controlled substances and other source gases, Chapter 1 in *Scientific Assessment of Ozone Depletion: 2002, Global Ozone Research and Monitoring Project-Report No. 47*, World Meteorological Organization, Geneva, Switzerland, 2003.
- Montzka, S.A., R.C. Myers, J.H. Butler, J.W. Elkins, L.T. Lock, A.D. Clarke, and A.H. Goldstein, Observations of HFC-134a in the remote troposphere, *Geophys. Res. Lett.*, 23 (2), 169-172, 1996.
- Montzka, S.A., J.H. Butler, J.W. Elkins, T.M. Thompson, A.D. Clarke, and L.T. Lock, Present and future

LONG-LIVED COMPOUNDS

- trends in the atmospheric burden of ozone-depleting halogens, *Nature*, 398 (6729), 690-694, 1999.
- Montzka, S.A., C.M. Spivakovsky, J.H. Butler, J.W. Elkins, L.T. Lock, and D.J. Mondeel, New observational constraints for atmospheric hydroxyl on global and hemispheric scales, *Science*, 288 (5465), 500-503, 2000.
- Montzka, S.A., J.H. Butler, B.D. Hall, D.J. Mondeel, and J.W. Elkins, A decline in tropospheric organic bromine, *Geophys. Res. Lett.*, 30 (15), 1826, doi: 10.1029/2003GL017745, 2003.
- Moore, R.M., The solubility of a suite of low molecular weight organochlorine compounds in seawater and implications for estimating the marine source of methyl chloride to the atmosphere, *Chemosphere: Global Change Sci.*, 2 (1), 95-99, 2000.
- Moore, R.M., A. Gut, and M.O. Andreae, A pilot study of methyl chloride emissions from tropical woodrot fungi, *Chemosphere*, 58 (2), 221-225, 2005.
- Naik, V., A.K. Jain, K.O. Patten, and D.J. Wuebbles, Consistent sets of atmospheric lifetimes and radiative forcings on climate for CFC replacements: HCFCs and HFCs, *J. Geophys. Res.*, 105 (D5), 6903-6914, 2000.
- Nassar, R., P.F. Bernath, C.D. Boone, C. Clerbaux, P.F. Coheur, G. Dufour, L. Froidevaux, E. Mahieu, J.C. McConnell, S.D. McLeod, D.P. Murtagh, C.P. Rinsland, K. Semeniuk, R. Skelton, K.A. Walker, and R. Zander, A global inventory of stratospheric chlorine in 2004, *J. Geophys. Res.*, 111, D22312, doi: 10.1029/2006JD007073, 2006a.
- Nassar, R., P.F. Bernath, C.D. Boone, S.D. McLeod, R. Skelton, K.A. Walker, C.P. Rinsland, and P. Duchatelet, A global inventory of stratospheric fluorine in 2004 based on Atmospheric Chemistry Experiment Fourier transform spectrometer (ACE-FTS) measurements, *J. Geophys. Res.*, 111, D22313, doi: 10.1029/2006JD007395, 2006b.
- Newman, P.A., E.R. Nash, S.R. Kawa, S.A. Montzka, and S.M. Schauffler, When will the Antarctic ozone hole recover?, *Geophys. Res. Lett.*, 33, L12814, doi: 10.1029/2005GL025232, 2006.
- O'Doherty, S., D.M. Cunnold, A. Manning, B.R. Miller, R.H.J. Wang, P.B. Krummel, P.J. Fraser, P.G. Simmonds, A. McCulloch, R.F. Weiss, P. Salameh, L.W. Porter, R.G. Prinn, J. Huang, G. Sturrock, D. Ryall, R.G. Derwent, and S.A. Montzka, Rapid growth of hydrofluorocarbon 134a, and hydrochlorofluorocarbons 141b, 142b and 22 from Advanced Global Atmospheric Gases Experiment (AGAGE) observations at Cape Grim, Tasmania, and Mace Head, Ireland, *J. Geophys. Res.*, 109, D06310, doi: 10.1029/2003JD004277, 2004.
- Oram, D.E., Trends of long-lived anthropogenic halocarbons in the Southern Hemisphere and model calculations of global emissions, Ph.D. thesis, University of East Anglia, Norwich, U.K., 1999.
- Oram, D.E., C.E. Reeves, S.A. Penkett, and P.J. Fraser, Measurements of HCFC-142b and HCFC-141b in the Cape Grim air archive: 1978-1993, *Geophys. Res. Lett.*, 22 (20), 2741-2744, 1995.
- Oram, D.E., C.E. Reeves, W.T. Sturges, S.A. Penkett, P.J. Fraser, and R.L. Langenfelds, Recent tropospheric growth rate and distribution of HFC-134a (CF₃CH₂F), *Geophys. Res. Lett.*, 23 (15), 1949-1952, 1996.
- Oram, D.E., W.T. Sturges, S.A. Penkett, A. McCulloch, and P.J. Fraser, Growth of fluoroform (CHF₃, HFC-23) in the background atmosphere, *Geophys. Res. Lett.*, 25 (1), 35-38, 1998.
- Palmer, P.I., D.J. Jacob, L.J. Mickley, D.R. Blake, G.W. Sachse, H.E. Fuelberg, and C.M. Kiley, Eastern Asian emissions of anthropogenic halocarbons deduced from aircraft concentration data, *J. Geophys. Res.*, 108 (D24), 4753, doi: 10.1029/2003JD003591, 2003.
- Prather, M., and D. Ehhalt (Co-ordinating Lead Authors), F. Dentener, R. Derwent, E. Dlugokencky, E. Holland, I. Isaksen, J. Katima, V. Kirchhoff, P. Matson, P. Midgley, and M. Wang (Lead Authors), Atmospheric chemistry and greenhouse gases, Chapter 4 in *Climate Change 2001: The Scientific Basis Contribution of Working Group I to the Third Assessment Report of the Intergovernmental Panel on Climate Change*, edited by J.T. Houghton, Y. Ding, D.J. Griggs, M. Noguer, P.J. van der Linden, X. Dai, K. Maskell, and C.A. Johnson, 881 pp., Cambridge University Press, Cambridge, U.K., 2001.
- Prinn, R.G., R.F. Weiss, P.J. Fraser, P.G. Simmonds, D.M. Cunnold, F.N. Alyea, S. O'Doherty, P. Salameh, B.R. Miller, J. Huang, R.H.J. Wang, D.E. Hartley, C. Harth, L.P. Steele, G. Sturrock, P.M. Midgley, and A. McCulloch, A history of chemically and radiatively important gases in air deduced from ALE/GAGE/AGAGE, *J. Geophys. Res.*, 105 (D14), 17751-17792, 2000.
- Prinn, R.G., J. Huang, R.F. Weiss, D.M. Cunnold, P.J. Fraser, P.G. Simmonds, A. McCulloch, C. Harth, P. Salameh, S. O'Doherty, R.H.J. Wang, L. Porter, and B.R. Miller, Evidence for substantial variations of atmospheric hydroxyl radicals in the past two decades, *Science*, 292 (5523), 1882-1888, 2001.
- Prinn, R.G., J. Huang, R.F. Weiss, D.M. Cunnold, P.J.

- Fraser, P.G. Simmonds, A. McCulloch, C. Harth, S. Reimann, P. Salameh, S. O'Doherty, R.-H.J. Wang, L.W. Porter, B.R. Miller, and P.B. Krummel, Evidence for variability of atmospheric hydroxyl radicals over the past quarter century, *Geophys. Res. Lett.*, *32*, L07809, doi: 10.1029/2004GL022228, 2005.
- Qiu, L.X., S.H. Shi, S.B. Xing, and X.G. Chen, Rate constants for the reactions of OH with five halogen-substituted ethanes from 292 to 366 K, *J. Phys. Chem.*, *96* (2), 685-689, 1992.
- Quay, P., J. Stutsman, D. Wilbur, A. Snover, E. Dlugokencky, and T. Brown, The isotopic composition of atmospheric methane, *Global Biogeochem. Cycles*, *13* (2), 445-461, 1999.
- Rajakumar, B., J.B. Burkholder, R.W. Portmann, and A.R. Ravishankara, Rate coefficients for the OH + CFH₂CH₂OH reaction between 238 and 355 K, *Phys. Chem. Chem. Phys.*, *7* (12), 2498-2505, 2005.
- Ramaswamy, V. (Co-ordinating Lead Author), O. Boucher, J. Haigh, D. Hauglustaine, J. Haywood, G. Myhre, T. Nakajima, G.Y. Shi, and S. Solomon (Lead Authors), Radiative forcing of climate change, Chapter 6 in *Climate Change 2001: The Scientific Basis, Contribution of Working Group I to the Third Assessment Report of the Intergovernmental Panel on Climate Change*, edited by J.T. Houghton, Y. Ding, D.J. Griggs, M. Noguer, P.J. van der Linden, X. Dai, K. Maskell, and C.A. Johnson, 881 pp., Cambridge University Press, Cambridge, U.K., 2001.
- Redeker, K.R., K.K. Treseder, and M.F. Allen, Ectomycorrhizal fungi: A new source of atmospheric methyl halides?, *Global Change Biol.*, *10* (6), 1009-1016, 2004.
- Reeves, C.E., Atmospheric budget implications of the temporal and spatial trends in methyl bromide concentration, *J. Geophys. Res.*, *108* (D11), 4343, doi: 10.1029/2002JD002943, 2003.
- Reeves, C.E., W.T. Sturges, G.A. Sturrock, K. Preston, D.E. Oram, J. Schwander, R. Mulvaney, J.-M. Barnola, and J. Chappellaz, Trends of halon gases in polar firn air: implications for their emission distributions, *Atmos. Chem. Phys.*, *5*, 2055-2064, 2005.
- Reimann, S., A.J. Manning, P.G. Simmonds, D.M. Cunnold, R.H.J. Wang, J.L. Li, A. McCulloch, R.G. Prinn, J. Huang, R.F. Weiss, P.J. Fraser, S. O'Doherty, B.R. Grealley, K. Stemmler, M. Hill, and D. Folini, Low European methyl chloroform emissions inferred from long-term atmospheric measurements, *Nature*, *433* (7025), 506-508, 2005.
- Rhew, R.C., B.R. Miller, M. Bill, A.H. Goldstein, and R.F. Weiss, Environmental and biological controls on methyl halide emissions from southern California coastal salt marshes, *Biogeochemistry*, *60* (2), 141-161, 2002.
- Rhew, R.C., L. Ostergaard, E.S. Saltzman, and M.F. Yanofsky, Genetic control of methyl halide production in Arabidopsis, *Curr. Biol.*, *13* (20), 1809-1813, 2003a.
- Rhew, R.C., M. Aydin, and E.S. Saltzman, Measuring terrestrial fluxes of methyl chloride and methyl bromide using a stable isotope tracer technique, *Geophys. Res. Lett.*, *30* (21), doi: 10.1029/2003GL018160, 2003b.
- Rice, A.L., A.A. Gotoh, H.O. Ajie, and S.C. Tyler, High-precision continuous-flow measurement of delta ¹³C and delta D of atmospheric CH₄, *Anal. Chem.*, *73* (17), 4104-4110, 2001.
- Rinsland, C.P., R. Zander, E. Mahieu, L.S. Chiou, A. Goldman, and N.B. Jones, Stratospheric HF column abundances above Kitt Peak (31.9 degrees N latitude): trends from 1977-2001 and correlations with stratospheric HCl columns, *J. Quant. Spectrosc. Radiat. Transfer*, *74* (2), 205-216, 2002.
- Rinsland, C.P., E. Mahieu, R. Zander, N.B. Jones, M.P. Chipperfield, A. Goldman, J. Anderson, J.M. Russell III, P. Demoulin, J. Notholt, G.C. Toon, J.-F. Blavier, B. Sen, R. Sussmann, S.W. Wood, A. Meier, D.W.T. Griffith, L.S. Chiou, F.J. Murcray, T.M. Stephen, F. Hase, S. Mikuteit, A. Schulz, and T. Blumenstock, Long-term trends of inorganic chlorine from ground-based infrared solar spectra: Past increases and evidence for stabilization, *J. Geophys. Res.*, *108* (D8), 4252, doi: 10.1029/2002JD003001, 2003.
- Rinsland, C.P., C. Boone, R. Nassar, K. Walker, P. Bernath, E. Mahieu, R. Zander, J.C. McConnell, and L. Chiou, Trends of HF, HCl, CCl₂F₂, CCl₃F, CHClF₂ (HCFC-22) and SF₆ in the lower stratosphere from Atmospheric Chemistry Experiment (ACE) and Atmospheric Trace Molecule Spectroscopy (ATMOS) measurement near 30°N latitude, *Geophys. Res. Lett.*, *32* (16), L16S03, doi: 10.1029/2005GL022415, 2005.
- Rinsland, C.P., E. Mahieu, R. Zander, R. Nassar, P. Bernath, C. Boone, and L.S. Chiou, Long-term stratospheric carbon tetrafluoride (CF₄) increase inferred from 1985-2004 infrared space-based solar occultation measurements, *Geophys. Res. Lett.*, *33* (2), L02808, doi: 10.1029/2005GL024709, 2006.
- Röckmann, T., J. Kaiser, and C.A.M. Brenninkmeijer, The isotopic fingerprint of the pre-industrial and the

LONG-LIVED COMPOUNDS

- anthropogenic N₂O source, *Atmos. Chem. Phys.*, **3**, 315-323, 2003.
- Ruddiman, W.F., Orbital insolation, ice volume, and greenhouse gases. *Quart. Sci. Rev.*, **22** (15-17), 1597-1629, 2003.
- Rummukainen, M., Modeling stratospheric chemistry in a global three-dimensional chemical transport model, SCTM-1: Model development, *Finn. Meteorol. Inst. Contrib.*, **19**, 206 pp., 1996.
- Russell, J.M. III, L.L. Gordley, J.H. Park, S.R. Drayson, W.D. Hesketh, R.J. Cicerone, A.F. Tuck, J.E. Frederick, J.E. Harries, and P.J. Crutzen, The Halogen Occultation Experiment, *J. Geophys. Res.*, **98** (D6), 10777-10797, 1993.
- Russell, J.M. III, L.E. Deaver, M.Z. Luo, R.J. Cicerone, J.H. Park, L.L. Gordley, G.C. Toon, M.R. Gunson, W.A. Traub, D.G. Johnson, K.W. Jucks, R. Zander, and I.G. Nolt, Validation of hydrogen fluoride measurements made by the Halogen Occultation Experiment from the UARS platform, *J. Geophys. Res.*, **101** (D6), 10163-10174, 1996.
- Saltzman, E.S., M. Aydin, W.J. De Bruyn, D.B. King, and S.A. Yvon-Lewis, Methyl bromide in preindustrial air: Measurements from an Antarctic ice core, *J. Geophys. Res.*, **109**, D05301, doi: 10.1029/2003JD004157, 2004.
- Sander, S.P., R.R. Friedl, D.M. Golden, M.J. Kurylo, R.E. Huie, V.L. Orkin, G.K. Moortgat, A.R. Ravishankara, C.E. Kolb, M.J. Molina, and B.J. Finlayson-Pitts, *Chemical Kinetics and Photochemical Data for Use in Atmospheric Studies: Evaluation No. 14*, JPL Publication 02-25, Jet Propulsion Laboratory, Pasadena, Calif., 2003.
- Sander, S.P., R.R. Friedl, D.M. Golden, M.J. Kurylo, G.K. Moortgat, H. Keller-Rudek, P.H. Wine, A.R. Ravishankara, C.E. Kolb, M.J. Molina, B.J. Finlayson-Pitts, R.E. Huie, and V.L. Orkin, *Chemical Kinetics and Photochemical Data for Use in Atmospheric Studies: Evaluation No. 15*, JPL Publication 06-2, Jet Propulsion Laboratory, Pasadena, Calif., 2006.
- Santoro, M.A., Clarifying the SF₅CF₃ record, *Science*, **290** (5493), 935-935, 2000.
- Schafer, H., I.R. McDonald, P.D. Nightingale, and J.C. Murrell, Evidence for the presence of a CmuA methyltransferase pathway in novel marine methyl halide-oxidizing bacteria, *Environ. Microbiol.*, **7** (6), 839-852, 2005.
- Schauffler, S.M., E.L. Atlas, D.R. Blake, F. Flocke, R.A. Lueb, J.M. Lee-Taylor, V. Stroud, and W. Travnicek, Distributions of brominated organic compounds in the troposphere and lower stratosphere, *J. Geophys. Res.*, **104** (D17), 21513-21535, 1999.
- Schauffler, S.M., E.L. Atlas, S.G. Donnelly, A. Andrews, S.A. Montzka, J.W. Elkins, D.F. Hurst, P.A. Romashkin, G.S. Dutton, and V. Stroud, Chlorine budget and partitioning during the Stratospheric Aerosol and Gas Experiment (SAGE) III Ozone Loss and Validation Experiment (SOLVE), *J. Geophys. Res.*, **108** (D5), 4173, doi: 10.1029/2001JD002040, 2003.
- Schneider, M., T. Blumenstock, M.P. Chipperfield, F. Hase, W. Kouker, T. Reddman, R. Ruhnke, E. Cuevas, and H. Fischer, Subtropical trace gas profiles determined by ground-based FTIR spectroscopy at Izaña (28°N, 16°W): Five-year record, error analysis, and comparison with 3-D CTMs, *Atmos. Chem. Phys.*, **5**, 153-167, 2005.
- Shine, K.P., L.K. Gohar, M.D. Hurley, G. Marston, D. Martin, P.G. Simmonds, T.J. Wallington, and M. Watkins, Perfluorodecalin: Global warming potential and first detection in the atmosphere, *Atmos. Environ.*, **39** (9), 1759-1763, 2005.
- Simmonds, P.G., D.M. Cunnold, F.N. Alyea, C.A. Cardelino, A.J. Crawford, R.G. Prinn, P.J. Fraser, R.A. Rasmussen, and R.D. Rosen, Carbon-tetrachloride lifetimes and emissions determined from daily global measurements during 1978-1985, *J. Atmos. Chem.*, **7** (1), 35-58, 1988.
- Simmonds, P.G., D.M. Cunnold, R.F. Weiss, R.G. Prinn, P.J. Fraser, A. McCulloch, F.N. Alyea, and S. O'Doherty, Global trends and emission estimates of carbon tetrachloride (CCl₄) from in-situ background observations from July 1978 to June 1996, *J. Geophys. Res.*, **103** (D13), 16017-16027, 1998.
- Simmonds, P.G., R.G. Derwent, A.J. Manning, P.J. Fraser, P.B. Krummel, S. O'Doherty, R.G. Prinn, D.M. Cunnold, B.R. Miller, H.J. Wang, D.B. Ryall, L.W. Porter, R.F. Weiss, and P.K. Salameh, AGAGE observations of methyl bromide and methyl chloride at Mace Head, Ireland, and Cape Grim, Tasmania, 1998-2001, *J. Atmos. Chem.*, **47** (3), 243-269, 2004.
- Simmonds, P.G., A.J. Manning, D.M. Cunnold, A. McCulloch, S. O'Doherty, R.G. Derwent, P.B. Krummel, P.J. Fraser, B. Dunse, L.W. Porter, R.H.J. Wang, B.R. Grealley, B.R. Miller, P. Salameh, R.F. Weiss, and R.G. Prinn, Global trends, seasonal cycles, and European emissions of dichloromethane, trichloroethene, and tetrachloroethene from the AGAGE observations at Mace Head, Ireland, and Cape Grim, Tasmania, *J. Geophys. Res.*, **111**, D18304, doi: 10.1029/2006JD007082, 2006.
- Simpson, I.J., T.-Y. Chen, D.R. Blake, and F.S. Rowland,

- Implications of the recent fluctuations in the growth rate of tropospheric methane, *Geophys. Res. Lett.*, **29** (10), 1479, doi: 10.1029/2001GL014521, 2002.
- Solomon, P., J. Barrett, T. Mooney, B. Connor, A. Parrish, and D.E. Siskind, Rise and decline of active chlorine in the stratosphere, *Geophys. Res. Lett.*, **33**, L18807, doi: 10.1029/2006GL027029, 2006.
- Sowers, T., A. Rodebaugh, N. Yoshida, and S. Toyoda, Extending records of the isotopic composition of atmospheric N₂O back to 1800 A.D. from air trapped in snow at the South Pole and the Greenland Ice Sheet Project II ice core, *Global Biogeochem. Cycles*, **16** (4), 1129, doi: 10.1029/2002GB001911, 2002.
- Spahni, R., J. Chappellaz, T.F. Stocker, L. Louergue, G. Hausammann, K. Kawamura, J. Flückiger, J. Schwander, D. Raynaud, V. Masson-Delmotte, and J. Jouzel, Atmospheric methane and nitrous oxide of the late Pleistocene from Antarctic ice cores, *Science*, **310** (5752), 1317-1321, 2005.
- Spivakovsky, C.M., J.A. Logan, S.A. Montzka, Y.J. Balkanski, M. Foreman-Fowler, D.B.A. Jones, L.W. Horowitz, A.C. Fusco, C.A.M. Brenninkmeijer, M.J. Prather, S.C. Wofsy, and M.B. McElroy, Three-dimensional climatological distribution of tropospheric OH: Update and evaluation, *J. Geophys. Res.*, **105** (D7), 8931-8980, 2000.
- Srivastava, A., A.E. Joseph, and S. Devotta, Volatile organic compounds in ambient air of Mumbai - India, *Atmos. Environ.*, **40** (5), 892-903, 2006.
- Sturges, W.T., T.J. Wallington, M.D. Hurley, K.P. Shine, K. Sihra, A. Engel, D.E. Oram, S.A. Penkett, R. Mulvaney, and C.A.M. Brenninkmeijer, A potent greenhouse gas identified in the atmosphere: SF₅CF₃, *Science*, **289** (5479), 611-613, 2000.
- Sturges, W.T., H.P. McIntyre, S.A. Penkett, J. Chappellaz, J.-M. Barnola, R. Mulvaney, E. Atlas, and V. Stroud, Methyl bromide, other brominated methanes, and methyl iodide in polar firn air, *J. Geophys. Res.*, **106** (D2), 1595-1606, 2001.
- Sturrock, G.A., L.W. Porter, P.J. Fraser, N. Derek, and P.B. Krummel, HCFCs, HFCs, halons, minor CFCs and halomethanes—the AGAGE in situ GC-MS program, 1997-1998, and related measurements on flask air samples collected at Cape Grim, in *Baseline Atmospheric Program (Australia) 1997-98*, edited by N.W. Tindale, R.J. Francey, and N. Derek, 97-100, Bureau of Meteorology, CSIRO Division of Atmospheric Research, Melbourne, Australia, 2001.
- Sturrock, G.A., D.M. Etheridge, C.M. Trudinger, P.J. Fraser, and A.M. Smith, Atmospheric histories of halocarbons from analysis of Antarctic firn air: Major Montreal Protocol species, *J. Geophys. Res.*, **107** (D24), 4765, doi: 10.1029/2002JD002548, 2002.
- Sturrock, G.A., C.E. Reeves, G.P. Mills, S.A. Penkett, C.R. Parr, A. McMinn, G. Corno, N.W. Tindale, and P.J. Fraser, Saturation levels of methyl bromide in the coastal waters off Tasmania, *Global Biogeochem. Cycles*, **17** (4), 1101, doi: 10.1029/2002GB002024, 2003.
- Takahashi, K., T. Nakayama, Y. Matsumi, S. Solomon, T. Gejo, E. Shigemasa, and T.J. Wallington, Atmospheric lifetime of SF₅CF₃, *Geophys. Res. Lett.*, **29** (15), 1712, doi: 10.1029/2002GL015356, 2002.
- Taniguchi, N., T.J. Wallington, M.D. Hurley, A.G. Guschin, L.T. Molina, and M.J. Molina, Atmospheric chemistry of C₂F₅C(O)CF(CF₃)₂: Photolysis and reaction with Cl atoms, OH radicals, and ozone, *J. Phys. Chem. A*, **107** (15), 2674-2679, 2003.
- Thompson, T.M. (Ed.), J.H. Butler, B.C. Daube, G.S. Dutton, J.W. Elkins, B.D. Hall, D.F. Hurst, D.B. King, E.S. Kline, B.G. LaFleur, J. Lind, S. Lovitz, D.J. Mondeel, S.A. Montzka, F.L. Moore, J.D. Nance, J.L. Neu, P.A. Romashkin, A. Scheffer, and W.J. Snible, Halocarbons and other atmospheric trace species, Section 5 in *Climate Monitoring and Diagnostics Laboratory: Summary Report No. 27, 2002-2003*, edited by R. Schnell, A.-M. Buggle, and R. Rosson, 115-135, NOAA/Climate Monitoring and Diagnostics Laboratory, Boulder, Colo., 2004.
- Tokarczyk, R., E.S. Saltzman, R.M. Moore, and S.A. Yvon-Lewis, Biological degradation of methyl chloride in coastal seawater, *Global Biogeochem. Cycles*, **17** (2), 1057, doi: 10.1029/2002GB001949, 2003a.
- Tokarczyk, R., K.D. Goodwin, and E.S. Saltzman, Methyl chloride and methyl bromide degradation in the Southern Ocean, *Geophys. Res. Lett.*, **30** (15), 1808, doi: 10.1029/2003GL017459, 2003b.
- Tokarczyk, R., and R.M. Moore, A seasonal study of methyl bromide concentrations in the North Atlantic (35°-60°N), *J. Geophys. Res.*, **111**, D08304, doi: 10.1029/2005JD006487, 2006.
- Toon, G.C., J.-F. Blavier, B. Sen, and B.J. Drouin, Atmospheric COCl₂ measured by solar occultation spectrometry, *Geophys. Res. Lett.*, **28** (14), 2835-2838, 2001.
- Trudinger, C.M., D.M. Etheridge, G.A. Sturrock, P.J. Fraser, P.B. Krummel, and A. McCulloch, Atmospheric histories of halocarbons from analysis of Antarctic firn air: Methyl bromide, methyl chloride, chloroform, and dichloromethane, *J. Geophys. Res.*,

LONG-LIVED COMPOUNDS

- 109, D22310, doi: 10.1029/2004JD004932, 2004.
- UNEP (United Nations Environment Programme), 1998 *Report of the Technology and Economic Assessment Panel (TEAP)*, 286 pp., Nairobi, Kenya, 1998.
- UNEP (United Nations Environment Programme), 1998 *Assessment Report of the Halons Technical Options Committee (HTOC)*, 209 pp., Nairobi, Kenya, 1999.
- UNEP (United Nations Environment Programme), 2002 *Report of the Methyl Bromide Technical Options Committee 2002 Assessment (MBTOC)*, 437 pp., Nairobi, 2002a.
- UNEP (United Nations Environment Programme), *Production and Consumption of Ozone Depleting Substances under the Montreal Protocol 1986-2000*, Ozone Secretariat, Nairobi, Kenya, Available: <http://ozone.unep.org>, 2002b.
- UNEP (United Nations Environment Programme), *Assessment Report of the Halons Technical Options Committee (HTOC)*, 69 pp., Nairobi, Kenya, 2003.
- UNEP (United Nations Environment Programme), Information provided by the Parties in accordance with Article 7 of the Montreal Protocol on Substances that Deplete the Ozone Layer, Nairobi, Kenya, 2005.
- van der Werf, G.R., J.T. Randerson, G.J. Collatz, L. Giglio, P.S. Kasibhatla, A.F. Arellano Jr., S.C. Olsen, and E.S. Kasischke, Continental-scale partitioning of fire emissions during the 1997 to 2001 El Niño/La Niña period, *Science*, 303 (5654), 73-76, 2004.
- Varner, R.K., P.M. Crill, and R.W. Talbot, Wetlands: a potentially significant source of atmospheric methyl bromide and methyl chloride, *Geophys. Res. Lett.*, 26 (16), 2433-2435, 1999.
- Varner, R.K., M.L. White, C.H. Mosedale, and P.M. Crill, Production of methyl bromide in a temperate forest soil, *Geophys. Res. Lett.*, 30 (10), 1521, doi: 10.1029/2002GL016592, 2003.
- Velders, G.J.M., and S. Madronich, (Co-ordinating Lead Authors), C. Clerbaux, R.G. Derwent, M. Grutter, D.A. Hauglustaine, S. Incecik, M.K.W. Ko, J.-M. Libre, O.J. Nielsen, F. Stordal, and T. Zhu (Lead Authors), Chemical and radiative effects of halocarbons and their replacement compounds, Chapter 2 in *IPCC/TEAP Special Report on Safeguarding the Ozone Layer and the Global Climate System*, edited by B. Metz, L. Kuijpers, S. Solomon, S.O. Andersen, O. Davidson, J. Pons, D. de Jager, T. Kestin, M. Manning, and L.A. Meyer, 478 pp., Cambridge University Press, Cambridge, U.K., 2005.
- Verdonik, D.P., and M.L. Robin, Analysis of emission data, estimates, and modeling of fire protection agents, *Proceedings of the Earth Technology Forum*, Washington, D.C., 11 pp., 2004.
- Volk, C.M., J.W. Elkins, D.W. Fahey, G.S. Sutton, J.M. Gilligan, M. Loewenstein, J.R. Podolske, K.R. Chan, and M.R. Gunson, Evaluation of source gas lifetimes from stratospheric observations, *J. Geophys. Res.*, 102 (D21), 25543-25564, 1997.
- Vollmer, M.K., and R.F. Weiss, Simultaneous determination of sulfur hexafluoride and three chlorofluorocarbons in water and air, *Mar. Chem.*, 78 (2-3), 137-148, 2002.
- von Clarmann, T., N. Glatthor, U. Grabowski, M. Höpfner, S. Kellmann, A. Linden, G.M. Tsidu, M. Milz, T. Steck, G.P. Stiller, H. Fischer, and B. Funke, Global stratospheric HOCl distributions retrieved from infrared limb emission spectra recorded by the Michelson Interferometer for Passive Atmospheric Sounding (MIPAS), *J. Geophys. Res.*, 111, D05311, doi: 10.1029/2005JD005939, 2006.
- Warwick, N.J., J.A. Pyle, and D.E. Shallcross, Global modelling of the atmospheric methyl bromide budget, *J. Atmos. Chem.*, 54 (2), 133-159, 2006.
- Waugh, D.W., and T.M. Hall, Age of stratospheric air: Theory, observations, and models, *Rev. Geophys.*, 40 (4), 1010, doi: 10.1029/2000RG000101, 2002.
- Waugh, D.W., D.B. Considine, and E.L. Fleming, Is upper stratospheric chlorine decreasing as expected?, *Geophys. Res. Lett.*, 28 (7), 1187-1190, 2001.
- Wennberg, P.O., S. Peacock, J.T. Randerson, and R. Bleck, Recent changes in the air-sea gas exchange of methyl chloroform, *Geophys. Res. Lett.*, 31, L16112, doi: 10.1029/2004GL020476, 2004.
- White, M.L., R.K. Varner, P.M. Crill, and C.H. Mosedale, Controls on the seasonal exchange of CH₃Br in temperate peatlands, *Global Biogeochem. Cycles*, 19, GB4009, doi: 10.1029/2004GB002343, 2005.
- Wingenter, O.W., B.C. Sive, D.R. Blake, F.S. Rowland, and B.A. Ridley, Unexplained enhancements of CH₃Br in the Arctic and sub-Arctic lower troposphere during TOPSE spring 2000, *Geophys. Res. Lett.*, 30 (22), 2160, doi: 10.1029/2003GL018159, 2003.
- WMO (World Meteorological Organization), *Scientific Assessment of Ozone Depletion: 1998, Global Ozone Research and Monitoring Project-Report No. 44*, Geneva, Switzerland, 1999.
- WMO (World Meteorological Organization), *Scientific Assessment of Ozone Depletion: 2002, Global Ozone Research and Monitoring Project-Report No. 47*, Geneva, Switzerland, 2003. [referred to as *WMO 2002* in this chapter]
- Wu, J.-Y., J.-Y. Liu, Z.-S. Li, and C.-C. Sun, Theoretical study of the reactions of CF₃OCHF₂ with the

- hydroxyl radical and the chlorine atom, *ChemPhysChem*, 5 (9), 1336-1344, 2004.
- Yokouchi, Y., Y. Noijiri, L.A. Barrie, D. Toom-Sauntry, T. Machida, Y. Inuzuka, H. Akimoto, H.J. Li, Y. Fujinuma, and S. Aoki, A strong source of methyl chloride to the atmosphere from tropical coastal land, *Nature*, 403 (6767), 295-298, 2000.
- Yokouchi, Y., D. Toom-Sauntry, K. Yazawa, T. Inagaki, and T. Tamaru, Recent decline of methyl bromide in the troposphere, *Atmos. Environ.*, 36 (32), 4985-4989, 2002.
- Yokouchi, Y., T. Inagaki, K. Yazawa, T. Tamaru, T. Enomoto, and K. Izumi, Estimates of ratios of anthropogenic halocarbon emissions from Japan based on aircraft monitoring over Sagami Bay, Japan, *J. Geophys. Res.*, 110, D06301, doi: 10.1029/2004JD005320, 2005.
- Yoshida, Y., Y.H. Wang, T. Zeng, and R. Yantosca, A three-dimensional global model study of atmospheric methyl chloride budget and distributions, *J. Geophys. Res.*, 109, D24309, doi: 10.1029/2004JD004951, 2004.
- Yvon-Lewis, S.A., and J.H. Butler, Effect of oceanic uptake on atmospheric lifetimes of selected trace gases, *J. Geophys. Res.*, 107 (D20), 4414, doi: 10.1029/2001JD001267, 2002.
- Yvon-Lewis, S.A., J.H. Butler, E.S. Saltzman, P.A. Matrai, D.B. King, R. Tokarczyk, R.M. Moore, and J.Z. Zhang, Methyl bromide cycling in a warm-core eddy of the North Atlantic Ocean, *Global Biogeochem. Cycles*, 16 (4), 1141, doi: 10.1029/2002GB001898, 2002.
- Yvon-Lewis, S.A., D.B. King, R. Tokarczyk, K.D. Goodwin, E.S. Saltzman, and J.H. Butler, Methyl bromide and methyl chloride in the Southern Ocean, *J. Geophys. Res.*, 109, C02008, doi: 10.1029/2003JC001809, 2004.
- Zander, R., C.P. Rinsland, E. Mahieu, M.R. Gunson, C.B. Farmer, M.C. Abrams, and M.K.W. Ko, Increase of carbonyl fluoride (COF₂) in the stratosphere and its contribution to the 1992 budget of inorganic fluorine in the upper stratosphere, *J. Geophys. Res.*, 99 (D8), 16737-16743, 1994.
- Zander, R., E. Mahieu, M.R. Gunson, M.C. Abrams, A.Y. Chang, M. Abbas, C. Aellig, A. Engel, A. Goldman, F.W. Irion, N. Kämpfer, H.A. Michelsen, M.J. Newchurch, C.P. Rinsland, R.J. Salawitch, G.P. Stiller, and G.C. Toon, The 1994 northern midlatitude budget of stratospheric chlorine derived from ATMOS/ATLAS-3 observations, *Geophys. Res. Lett.*, 23 (17), 2357-2360, 1996.
- Zander, R., E. Mahieu, P. Demoulin, P. Duchatelet, C. Servais, G. Roland, L. DelBouille, M. De Mazière, and C.P. Rinsland, Evolution of a dozen non-CO₂ greenhouse gases above central Europe since the mid-1980s, *Environ. Sci.*, 2 (2-3), 295-303, 2005.

CHAPTER 2

Halogenated Very Short-Lived Substances

Lead Authors:

K.S. Law
W.T. Sturges

Coauthors:

D.R. Blake
N.J. Blake
J.B. Burkholder
J.H. Butler
R.A. Cox
P.H. Haynes
M.K.W. Ko
K. Kreher
C. Mari
K. Pfeilsticker
J.M.C. Plane
R.J. Salawitch
C. Schiller
B.-M. Sinnhuber
R. von Glasow
N.J. Warwick
D.J. Wuebbles
S.A. Yvon-Lewis

Contributors:

A. Butz
D.B. Considine
M. Dorf
L. Froidevaux
L.J. Kovalenko
N.J. Livesey
R. Nassar
C.E. Sioris
D.K. Weisenstein

CHAPTER 2

HALOGENATED VERY SHORT-LIVED SUBSTANCES

Contents

SCIENTIFIC SUMMARY	2.1
2.1 INTRODUCTION	2.5
2.2 SOURCES, DISTRIBUTIONS, AND TRENDS OF VSLS	2.9
2.2.1 New Observations of the Distributions and Abundances of VSL Source Gases	2.9
2.2.1.1 Bromine and Iodine	2.12
2.2.1.2 Chlorine	2.13
2.2.2 Terrestrial Emissions	2.13
2.2.3 Oceanic Emissions	2.15
2.2.3.1 Bromine	2.15
2.2.3.2 Iodine	2.17
2.2.3.3 Chlorine	2.17
2.2.4 Industrial and Other Anthropogenic Emissions	2.17
2.2.4.1 Bromine	2.17
2.2.4.2 Chlorine	2.18
2.2.4.3 New VSL Gases	2.18
2.2.5 Sources and Distributions of Inorganic Halogens of Marine Origin	2.18
2.3 ATMOSPHERIC CHEMISTRY OF VSLS	2.19
2.3.1 Removal of Halogen Source Gases	2.19
2.3.2 Tropospheric Lifetimes of Halocarbons	2.20
2.3.3 Production and Gas-Phase Removal of VSL Organic Product Gases	2.21
2.3.4 Multiphase Processes Involving Inorganic Bromine and Iodine Compounds	2.21
2.3.4.1 Wet Deposition Processes	2.21
2.3.4.2 Heterogeneous Halogen Activation	2.23
2.3.5 Iodine Chemistry	2.23
2.4 DYNAMICS AND TRANSPORT IN THE TROPOPAUSE REGION AND IMPLICATIONS FOR VSLS	2.24
2.4.1 Tropical Convection, the TTL, and Tropical Troposphere-to-Stratosphere Transport	2.25
2.4.2 Stratosphere-Troposphere Exchange in the Extratropics	2.28
2.4.3 Predictive Modeling of the Tropopause Region	2.30
2.5 CONTRIBUTION OF HALOGENATED VSLS TO STRATOSPHERIC HALOGEN LOADING	2.31
2.5.1 Source Gas Injection (SGI) and Product Gas Injection (PGI)	2.31
2.5.1.1 Observational Evidence for SGI	2.31
2.5.1.2 Observational Evidence for PGI	2.32
2.5.1.3 Model Estimates of SGI and PGI	2.34
2.5.2 Estimates of VSLS Contributions to Stratospheric Halogens Based on Measurements of Inorganic Species	2.35
2.5.2.1 Bromine	2.36
2.5.2.2 Chlorine	2.41
2.5.2.3 Iodine	2.42
2.6 POTENTIAL IMPACT OF VSLS ON OZONE	2.43
2.6.1 Effects of Halogenated VSLS on Column Ozone	2.43
2.6.2 ODPs for Halogenated VSLS	2.45

2.7 POTENTIAL FUTURE CONSIDERATIONS2.45
REFERENCES2.46

SCIENTIFIC SUMMARY

Definition of Halogenated Very Short-Lived Substances (VSLS)

- Very short-lived substances (VSLS) are defined as trace gases whose local tropospheric lifetimes are comparable to, or shorter than, tropospheric transport time scales, such that their tropospheric distributions are non-uniform. In practice, VSLS are considered to have atmospheric lifetimes of less than 6 months. We consider only halogenated VSLS, i.e., those that contain bromine, chlorine, or iodine. We consider VSLS to include very short-lived (VSL) source gases (SGs), halogenated organic and inorganic product gases (PGs) arising from SG degradation, and other sources of tropospheric inorganic halogens.

Importance of VSLS for Stratospheric Halogen and Ozone Trends

BROMINE

- **Our quantitative understanding of how halogenated very short-lived substances contribute to halogen levels in the stratosphere has improved significantly since the last Assessment (WMO, 2003), with brominated VSLS believed to make a significant contribution to total stratospheric bromine and its effect on stratospheric ozone. Various lines of evidence show that brominated VSLS contribute about 5 ppt (with estimates ranging from 3 to 8 ppt) to total stratospheric inorganic bromine (Br_y):**
 - Estimates of total stratospheric Br_y derived from different observations of bromine monoxide (BrO) relevant to the late 1990s are about 18 to 25 parts per trillion (ppt). This is greater than the 16 to 17 ppt of bromine delivered to the stratosphere by “long-lived” brominated source gases (i.e., the halons and methyl bromide, CH_3Br) during this period.
 - Measurements of organic brominated very short-lived source gases (VSL SGs) in the tropical upper troposphere amount to about 3.5 ppt. Product gases (from SG degradation) and other sources of tropospheric inorganic bromine may also contribute comparable amounts.
- **The inclusion of additional stratospheric Br_y from VSLS in models leads to larger ozone destruction at mid-latitudes and polar regions compared with studies including only long-lived bromine source gases.** In both regions, the enhanced ozone loss occurs in the lower stratosphere via interactions of this bromine with anthropogenic chlorine. Midlatitude ozone loss is most enhanced during periods of high aerosol loading. Ozone loss through cycles involving bromine and odd-hydrogen (HO_x) is also enhanced at midlatitudes under all conditions, becoming comparable with ozone loss by HO_x cycles alone. This additional amount of stratospheric bromine has not, to date, been routinely included in model calculations of midlatitude ozone depletion.
- **Levels of stratospheric Br_y continue to show evidence for a trend that is consistent with that of tropospheric total bromine.** Further studies are required to determine if the recent decline in tropospheric bromine is reflected in stratospheric bromine abundance.

IODINE

- **It is unlikely that iodine is important for stratospheric ozone loss in the present-day atmosphere.** There is little evidence for inorganic iodine, in the form of iodine monoxide (IO), in the lower stratosphere at concentrations above about 0.1 ppt. This difference in behavior compared with bromine may be partly attributed to the short photochemical lifetime of iodine SGs, their lower abundance, and aerosol uptake of iodine oxides.

CHLORINE

- **The sum of the chlorine content from VSL SGs in the tropical upper troposphere is currently estimated to be about 50 ppt, on the basis of available observations.** While a 50 ppt contribution to total inorganic stratospheric chlorine (Cl_y) from VSLS represents only 1 to 2% of Cl_y from long-lived source gases (~3500 ppt), it would represent a significant contribution compared with the background Cl_y from methyl chloride of about 550 ppt (Chapter 1).

VERY SHORT-LIVED SUBSTANCES

- **Phosgene (COCl₂), which can be produced from chlorinated VSL SGs as well as long-lived chlorine gases, has been observed at levels of around 20 to 25 ppt in the tropical upper troposphere.** The contribution of this gas to stratospheric Cl_y (up to about 40 to 50 ppt) is not currently included in most models.
- **Analyses of upper stratospheric hydrogen chloride (HCl) measurements from satellite instruments are generally consistent with a possible contribution of VSLS to stratospheric Cl_y.** Further improvements in HCl measurement accuracy are required to quantify this contribution.

Sources and Trends of Halogenated Very Short-Lived Source Gases

BROMINE

- **The majority of known brominated VSL SGs are of natural origin. A few brominated VSLS have almost exclusively anthropogenic sources, notably n-propyl bromide (n-PB).** Some have small contributions from anthropogenic sources, e.g., certain brominated trihalomethanes.
- **Most brominated VSL SGs are emitted from the ocean, with higher emissions in tropical coastal regions.** Sea surface supersaturations of some gases, due to production by marine microorganisms, have been found to be elevated in the tropical open ocean. High concentrations in air have been observed near coasts over tropical and temperate waters.
- **Inorganic tropospheric sources of bromine, such as sea salt and volcanoes, may also contribute to inorganic bromine in the free troposphere.** Some fraction of this contribution could be subsequently transported to the stratosphere.
- **There is no evidence for a trend in the sum of brominated VSL SGs during the latter half of the 20th century.** This is according to trend reconstructions from firm air studies, and reflects their predominantly natural origins. The exceptions are some trihalomethane species, which have increased slightly in the Northern Hemisphere, possibly due to small anthropogenic sources.

IODINE

- **Iodinated VSLS are exclusively of natural origin in the present-day atmosphere, although the possibility of deliberate future anthropogenic use of new SGs exists.** A notable example is the proposed use of trifluoroiodomethane (CF₃I).
- **Iodinated VSL SGs are emitted from the ocean, with higher emissions in tropical ocean regions.** Emissions in the marine boundary layer are dominated by iodomethanes such as methyl iodide (CH₃I) and chloriodomethane (CH₂ClI), which are produced both by marine organisms and by abiotic photochemical processes in surface waters. There is some evidence for enhanced marine emissions of iodinated VSL SGs in the tropics and subtropics, and also in regions of high productivity in coastal zones.

CHLORINE

- **Chlorinated VSL SGs originate largely from anthropogenic emissions, although natural sources also contribute.** Their principal emissions are, therefore, more likely to be located at northern midlatitudes.
- **There is evidence for significant recent declines in concentrations of some chlorinated VSL SGs, notably chloroform, dichloromethane, and tetrachloroethene.**

Transport, Lifetimes, and Sinks of Halogenated VSLS

- **The predominant pathways for VSLS transport into the upper troposphere are likely to be in tropical convection regions, co-located with high emissions of VSLS over tropical oceans.** The fraction of a halogenated VSL SG that reaches the stratosphere via the source gas injection (SGI) pathway depends on its local chemical lifetime relative

to local transport time scales. Local SG lifetimes depend strongly on distributions of photochemical sinks and emission patterns and, as such, this limits the value of using a single “global” lifetime, as has often been used previously.

- **The amount of VSL PGs entering the stratosphere depends on the locations of their tropospheric production and loss processes.** The fraction of halogenated organic and inorganic PGs (produced from the decomposition of VSL SGs) that enters the stratosphere via the product gas injection (PGI) pathway depends on the location in the troposphere where the “parent” SG decomposes, and on subsequent loss processes such as (possibly irreversible) uptake of the PG on to aerosol/cirrus, or uptake of soluble species in precipitating clouds.
- **Many more data have become available on Henry’s Law constants, uptake coefficients, and heterogeneous reactivity for a number of relevant surfaces and for a wide range of PGs.** Many uncertainties, however, still remain. Furthermore, incorporation of this knowledge into large-scale models is often lacking, thus limiting assessment of the location-dependent lifetimes and distributions of VSL PGs.
- **The impact of halogens from VSL SGs on column ozone is likely to be greatest in the extratropics. The dominant transport pathway is likely to be via quasi-horizontal transport from the tropical upper troposphere into the extratropical lowermost stratosphere.** While transport time scales via this pathway, and back to the troposphere, are relatively short (a few months), the short chemical lifetime of VSL SGs means that they will be fully degraded into inorganic halogen before they can be transported back into the troposphere. Quasi-horizontal transport from the tropical upper troposphere is highly seasonal, being much larger in the summer than winter.
- **Recent model simulations continue to suggest that, depending on lifetime and location of emissions, less than 1% of the VSL SG flux emitted at the surface enters the stratosphere via the SGI pathway, and a larger amount (up to a few percent) enters via the PGI pathway.** Studies are limited, however, by the ability of current global models to accurately simulate deep convection and transport into the lower stratosphere.

Ozone Depletion Potentials (ODPs) of Halogenated VSL SGs

- **There are no new evaluations for the ODP of n-propyl bromide (0.1 for tropical emissions, and 0.02-0.03 for emissions restricted to northern midlatitudes).**
- **New analyses suggest ODPs for CF₃I ranging from 0.011 to 0.018 for surface emissions at midlatitudes and in the tropics, respectively, which are higher than found previously (<0.008).** The model studies do not include uptake of iodine on aerosols, the inclusion of which could result in lower calculated values. If CF₃I were to be used for fire fighting/inhibition on aircraft, then it could be emitted at higher altitudes and the corresponding ODP would be larger.
- **New analyses confirm previous estimates that the ODP of a chlorinated VSL SG with a lifetime of ~25 days, one chlorine atom, and similar molecular weight to CFC-11, is about 0.003.**

Future Considerations for Halogenated VSLS

- **Possible future changes in anthropogenic VSLS.** If anthropogenic emissions increased, or if presently unused halogenated VSL SGs were to come into widespread commercial use, then halogenated VSLS would become of increased importance in affecting the future behavior of stratospheric ozone.
- **Delivery of VSLS to the stratosphere may change in the future in response to circulation changes.** The impact of natural halogenated VSLS might also be influenced by changes in the atmospheric circulation, which could, for example, increase the rate of delivery of VSL SGs and PGs into the stratosphere.
- **Natural VSLS emissions may respond to future changes in climate processes.** Natural sources could respond to changes in, for example, carbon dioxide (CO₂), land use, wind speed, and temperature. Our knowledge about these potential effects, and many other relevant feedbacks, is very limited at present.

2.1 INTRODUCTION

An important goal of previous Assessments was to quantify the impact of halogen-containing source gases on stratospheric ozone (e.g., WMO, 2003, 1999). In the last Assessment (WMO, 2003), the possible contribution of very short-lived substances (VSLS) was examined in detail in Chapter 2 (Ko and Poulet et al., 2003) and an approach for determining their Ozone Depletion Potentials (ODPs) was presented. VSLS are defined as substances that have atmospheric lifetimes comparable to, or less than, average tropospheric transport time scales of about 6 months. We consider halogenated very short-lived (VSL) organic source gases (SGs), and the halogenated organic and inorganic product gases (PGs) arising from the atmospheric degradation of VSL SGs, and also inorganic tropospheric halogen sources such as sea salt. Note that, in contrast to WMO (2003), sulfur-containing VSLS (e.g., dimethyl sulfide (DMS), and sulfur dioxide (SO₂)) are dealt with in Chapter 5 of this Assessment. Halogen atoms bound in SGs and intermediate degradation products are referred to as organic halogen, and the final products are referred to as inorganic halogen (containing no carbon

(e.g., hydrogen chloride (HCl), hydrogen bromide (HBr), chlorine monoxide (ClO), bromine monoxide (BrO), and iodine monoxide (IO)). Some important acronyms used in this chapter are defined in Box 2-1 below.

This chapter assesses the contribution of halogenated VSLS to the halogen loading in the stratosphere, as well as their possible contribution to past, present, and future stratospheric ozone loss, and considers the ODPs of substances that are, or might be, released as a result of human activities. Table 2-1 provides a list of the VSL SGs discussed in this chapter, together with an estimation of their local photochemical lifetimes and an indication of whether these gases have predominantly natural or anthropogenic origins and/or are proposed for new commercial applications. The majority of currently observable VSL SGs are thought to be partly or wholly of natural origin. A few halogenated VSLS have predominantly anthropogenic origins (e.g., n-propyl bromide (n-C₃H₇Br), 1,2-dibromoethane (CH₂BrCH₂Br), dichloromethane (CH₂Cl₂), tetrachloroethene (C₂Cl₄), and, to a lesser extent, chloroform (CHCl₃)). Currently, among the compounds listed in Table 2-1, only bromochloromethane (CH₂BrCl) is considered by the Montreal Protocol. In the light of observed

Box 2-1. Definition of Acronyms in Chapter 2

VSLS	Very Short-Lived Substances – organic and inorganic gases with lifetimes of less than 0.5 years
VSL	Very Short-Lived
SG/SGI	Source Gas / Source Gas Injection – refers to a halogenated organic source gas and its injection into the stratosphere
PG/PGI	Product Gas / Product Gas Injection – refers to the sum of the halogenated organic and inorganic degradation products for a particular source gas and their injection into the stratosphere
CFC	Chlorofluorocarbon
HCFC	Hydrochlorofluorocarbon
Br _x	Inorganic bromine oxides and radicals (e.g., BrO, atomic bromine (Br), bromine nitrate (BrONO ₂))
Br _y	Total inorganic bromine (e.g., HBr, Br _x) resulting from degradation of bromine-containing organic-source gases (halons, methyl bromide, VSLS), and natural inorganic bromine sources (e.g., volcanoes, sea salt, and other aerosols)
Br _y ^{VSLS}	The component of stratospheric Br _y from the degradation of brominated organic VSL SGs and tropospheric inorganic bromine sources (also called “additional” stratospheric Br _y)
Br _y ^{CH₃Br+Halons}	The component of stratospheric Br _y from the degradation of methyl bromide (CH ₃ Br) and halons
Cl _y	Total inorganic stratospheric chlorine (e.g., HCl, ClO) resulting from degradation of chlorine-containing source gases (CFCs, HCFCs, VSLS), and natural inorganic chlorine sources (e.g., sea salt and other aerosols)
Cl _y ^{VSLS}	The component of stratospheric Cl _y from the degradation of chlorinated organic VSL SGs and tropospheric inorganic chlorine sources
I _y	Total inorganic stratospheric iodine (e.g., IO, iodine dioxide (OIO), hypoiodous acid (HOI)) resulting from degradation of iodine-containing source gases (VSLS), and natural inorganic sources (e.g., sea salt and other aerosols)
ODP	Ozone Depletion Potential
EESC	Equivalent Effective Stratospheric Chlorine

VERY SHORT-LIVED SUBSTANCES

Table 2-1. Halogenated VSL source gases considered in this Assessment. New additions since WMO (2003) are shown in boldface; other compounds were assessed in WMO (2003).

Source Gas	Formula	Local Lifetime ^a (days)	Atmospheric Source ^b
Bromochloromethane	CH ₂ BrCl	150	N
Dibromomethane	CH ₂ Br ₂	120	N
Bromodichloromethane	CHBrCl ₂	78	N(A)
Dibromochloromethane	CHBr ₂ Cl	69	N(A)
1,2-Dibromoethane (ethylene dibromide, EDB)	CH ₂ BrCH ₂ Br	55	A
Bromoethane (ethyl bromide)	C ₂ H ₅ Br	34	A
Tribromomethane (bromoform)	CHBr ₃	26	N(A)
1-Bromopropane (n-propyl bromide)	n-C ₃ H ₇ Br	13	A
Phosphorous tribromide (“PhostrEx”)	PBr ₃	<0.01	A ^c
Iodomethane (methyl iodide)	CH ₃ I	7	N
Trifluoroiodomethane	CF ₃ I	4	A ^c
Iodoethane (ethyl iodide)	C ₂ H ₅ I	4	N
2-Iodopropane (isopropyl iodide)	i-C ₃ H ₇ I	1.2	N
1-Iodopropane (n-propyl iodide)	n-C ₃ H ₇ I	0.5	N
Chloriodomethane	CH ₂ ClI	0.1	N
Bromiodomethane	CH ₂ BrI	0.04	N
Diiodomethane	CH ₂ I ₂	0.003	N
Trichloromethane (chloroform)	CHCl ₃	150	AN
Dichloromethane (methylene chloride)	CH ₂ Cl ₂	140	A(N)
Tetrachloroethene (perchloroethylene, PCE)	C ₂ Cl ₄	99	A
1,2-Dichloroethane	CH ₂ ClCH ₂ Cl	70	A
Chloroethane (ethyl chloride)	C ₂ H ₅ Cl	30	AN
Trichloroethene (trichloroethylene; TCE)	C ₂ HCl ₃	4.6	A

^a Local lifetimes are calculated as $(\tau_{\text{local}})^{-1} = (\tau_{\text{OH}})^{-1} + (\tau_{\text{I}})^{-1}$, with $[\text{OH}] = 1 \times 10^6 \text{ molec cm}^{-3}$, $T = 275 \text{ K}$, and a globally and seasonally averaged solar flux for 5 km altitude. See Section 2.3.2.

^b N = entirely natural atmospheric sources; A = entirely anthropogenic atmospheric sources; AN = combination of natural and anthropogenic atmospheric sources (a minor component shown in parentheses).

^c Proposed application.

and predicted decreases in anthropogenic chlorofluorocarbons (CFCs), halons, etc., it is important to quantify the contribution of these VSLS to the natural background halogen loading in the stratosphere. Possible changes in the emissions of naturally occurring compounds, for example as a result of changing climatic factors, also need to be assessed.

In order to quantify the contribution of halogenated VSLS to halogen loading and ozone loss in the stratosphere, it is necessary to quantify the amount of VSLS entering the stratosphere directly via the SG injection (SGI) pathway, the degradation of SGs in the troposphere, transport of organic and inorganic PGs into the stratosphere via the PG injection (PGI) pathway, and also injection of inorganic tropospheric halogen. The contribution

to, for example, total inorganic bromine (Br_y) in the stratosphere, which derives from the sum of VSL SGs (via the SGI and PGI pathways) and tropospheric inorganic halogen, is denoted $\text{Br}_y^{\text{VSLS}}$. The impact of such VSLS-derived inorganic halogen on stratospheric ozone loss will depend on the abundance of different halogen radicals and their efficiency at destroying ozone. Note that one atom of iodine is much more efficient at removing ozone than bromine, which in turn is more efficient than chlorine, as expressed by so-called α -factors (see Chapter 8 and Section 2.6.1 for further discussion).

Figure 2-1 shows a schematic of the processes influencing the transport, degradation, and loss of VSL SGs and PGs in the troposphere and stratosphere. It is an updated version of Figure 2-2 in Chapter 2, WMO (2003).

Chemical and Dynamical Processes Affecting VSLS

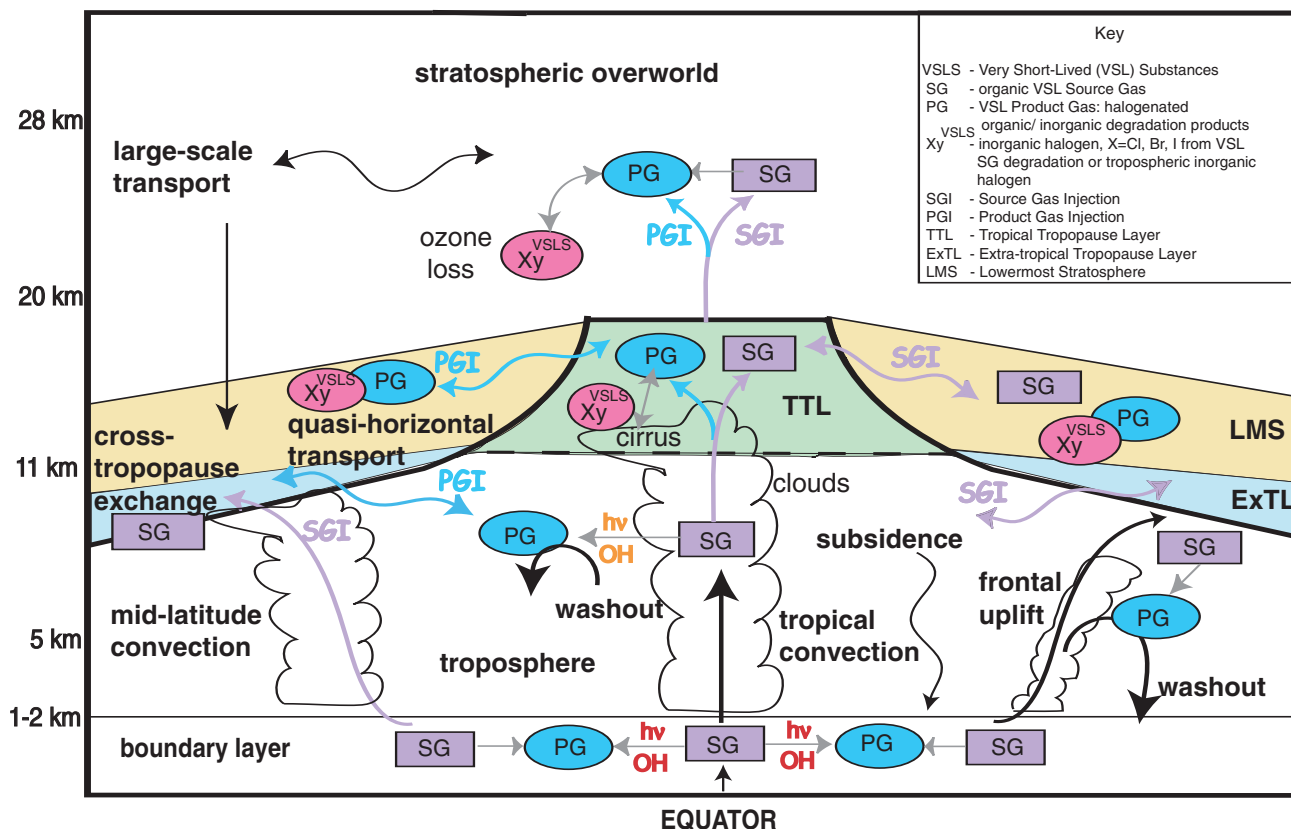


Figure 2-1. Schematic showing principal chemical and dynamical pathways transporting VSL source gases (SG) and organic/inorganic product gases (PG). Stratospheric halogen loading is maintained by transport of source gases followed by their degradation in the stratosphere (the SGI pathway), and transport of intermediate products and inorganic halogens produced in the troposphere (the PGI pathway). Tropospheric inorganic halogens can derive from degradation of VSL SGs, or from inorganic halogen sources. This figure is an update to Figure 2-2 in WMO (2003); courtesy of K.S. Law (Service d’Aéronomie/CNRS, France) and P.H. Haynes and R.A. Cox (University of Cambridge, U.K.).

In terms of chemical processes affecting VSLS, it is the degradation and loss of intermediate products, and inorganic multiphase heterogeneous chemistry, that remain the largest uncertainties in our knowledge about the fate of VSLS. The most efficient transport pathway is in the tropics, where there is rapid transport of air from the surface to the tropical tropopause layer (TTL) by deep convection, followed by transport of a small fraction into the stratosphere. Quasi-horizontal transport of air from the TTL into the lowermost stratosphere (LMS), as well as direct transport of air from the surface at midlatitudes either by frontal processes or deep convection, also need to be considered.

Given that VSL SGs and PGs have, by definition, shorter photochemical lifetimes than the large-scale transport time constant in the troposphere of roughly 6 months,

mixing ratios (molar fractions) of both SGs and PGs (unless the latter are long-lived) are not uniform in the troposphere, and significant vertical as well as horizontal gradients can exist. Therefore, the amount of halogen entering the stratosphere may be sensitive to, among other factors, the location and timing of emission of VSL SGs, chemical degradation to produce organic and inorganic PGs, tropospheric transport processes, and location/altitude of removal of inorganic degradation products by wet deposition or other heterogeneous processes. Measured ratios of boundary layer (BL) to upper tropospheric (UT) mixing ratios of VSL SGs can provide an indication of the fraction available to be transported into the stratosphere. It has been noted previously that brominated and iodinated VSL SGs have been observed at mixing ratios of a few parts per trillion (ppt or pmol mol⁻¹) at the surface (WMO,

VERY SHORT-LIVED SUBSTANCES

2003). An estimate was also given for the tropospheric abundance of chlorinated VSL SGs ranging from 50 to 100 ppt. This value also included phosgene (carbonyl dichloride, COCl_2), produced from the degradation of VSL SGs and long-lived chlorine gases. Apart from phosgene, very few measurements of organic VSL PGs are available in the free troposphere or stratosphere. Measurements of inorganic halogen are available and represent the final

degradation products of halogen-containing sources gases (e.g., CFCs, halons, VSLS) as well as direct emission of inorganic halogens (e.g., sea salt, volcanoes).

The different radical families that are important for ozone loss in the midlatitude stratosphere are shown in Figure 2-2. At the levels of total inorganic iodine used in these model calculations ($I_y = 0.1$ ppt), which are representative of upper limits based on rather limited observa-

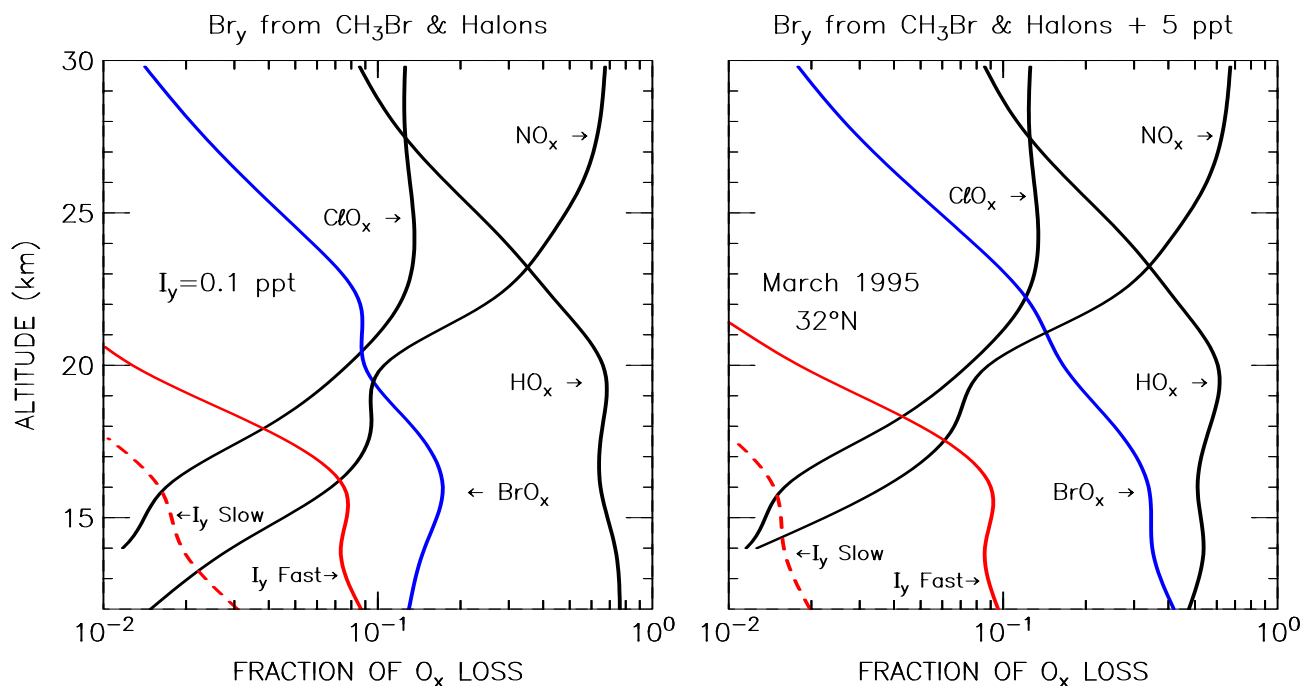


Figure 2-2. Calculated fractional contribution to odd oxygen (O_x) loss by catalytic cycles involving nitrogen (NO_x), hydrogen (HO_x), chlorine (ClO_x), bromine (BrO_x), and iodine (I_y Fast and Slow; see below) radicals for March 1995, 32°N . Jet Propulsion Laboratory (JPL) kinetics (Sander et al., 2006) were used, except for the rate constant of $\text{IO} + \text{HO}_2$, for which the expression given by Knight and Crowley (2001) representing all available data, $1.4 \times 10^{-11} \exp(554/T)$, was used (this is the same rate constant as given by the February 2006 International Union of Pure and Applied Chemistry (IUPAC) evaluation, posted at <http://www.iupac-kinetic.ch.cam.ac.uk/>). Total inorganic stratospheric iodine was set equal to 0.1 ppt, the upper limit reported by Bösch et al. (2003) and Butz (2006). For the left-hand panel, other model inputs are the same as given in Table 4 of Wennberg et al. (1997), which assumed stratospheric Br_y derived only from the breakdown of CH_3Br and halons. For the right-hand panel, 5 ppt has been added to Br_y at all altitudes, representing $\text{Br}_y^{\text{VSLs}}$ (see text and Section 2.5). The ClO_x curve represents loss from the $\text{ClO} + \text{O}$ and $\text{ClO} + \text{HO}_2$ cycles, plus other minor cycles that involve ClO , but not BrO or IO . The BrO_x curve represents loss from the $\text{BrO} + \text{ClO}$ and $\text{BrO} + \text{HO}_2$ cycles, plus other minor cycles that involve BrO , but not IO . Two model curves are given to represent loss by all cycles that involve IO in the rate-limiting step. The “ I_y Fast” curve uses the rate constant for $\text{IO} + \text{BrO}$ given by Rowley et al. (2001) and assumes all products of this reaction lead to catalytic loss of ozone. The “ I_y Slow” curve uses the JPL rate constant for $\text{IO} + \text{BrO}$ and assumes that production of OIO results in a null cycle. These two curves are shown to illustrate the sensitivity of iodine-induced ozone loss to the rate constant of $\text{IO} + \text{BrO}$ and to the fate of OIO (e.g., photolysis of OIO to $\text{O} + \text{IO}$ leads to a null cycle, whereas photolysis to $\text{I} + \text{O}_2$ leads to O_3 loss). If the temperature-independent rate constant for $\text{IO} + \text{HO}_2$ given by JPL is used, the fractional contribution to ozone loss by iodine in the LMS is about a factor of two less than illustrated. Adapted from Wennberg et al. (1997); see also the extensive discussion of iodine kinetics in Bösch et al. (2003).

tions in the stratosphere (Bösch et al., 2003; Butz, 2006), loss of ozone by iodine is unlikely to be a driving factor for present-day midlatitude ozone loss. Note that the efficiency of ozone loss by iodine is sensitive to unresolved details of the photochemical mechanism, regarding the rate constant of the IO + BrO reaction and different decomposition products resulting from iodine dioxide (OIO) photolysis (“I_y Fast” versus “I_y Slow” in Figure 2-2; see caption). The likely relatively small contribution of iodine to stratospheric ozone loss is in contrast to bromine, which has been observed regularly in the stratosphere at levels significantly higher than can be supplied solely by the longer lived brominated gases (CH₃Br and halons) and at sufficient concentrations in the lower stratosphere to make a difference to present-day ozone.

A key question for this chapter, then, is to what extent brominated VSLS contribute to stratospheric Br_y. The contributions of chlorinated and iodinated VSLS to stratospheric Cl_y and I_y budgets are also considered. Figure 2-3, which is an updated version of Figure 1-8, Chapter 1, WMO (2003), shows Br_y estimated from balloonborne BrO observations adjusted to the time when the measured air masses were last in the troposphere (see Figure 2-3 caption for further details). In the late 1990s, this amounted to about 18 to 25 ppt of Br_y. Also shown are observed trends in surface mixing ratios of bromine-containing halons and methyl bromide (CH₃Br) since 1980 (see Chapter 1 for details). Note that the trends of CH₃Br have not been corrected to account for vertical gradients in the troposphere, so that this contribution to stratospheric Br_y may be overestimated, and therefore Br_y^{VLSL} underestimated. It can be seen that there is an apparent discrepancy between Br_y from halons plus CH₃Br, and Br_y inferred from BrO data. In WMO (2003), this discrepancy, denoted “additional” stratospheric bromine, was attributed to either direct injection into the stratosphere of inorganic bromine from the troposphere as well as from degradation of organic VSLS, or to possible calibration errors in the measurement of either BrO or the organic source gases. Since the last Assessment, there have been many studies focused on quantification of this “additional” bromine (Br_y^{VLSL}). Figure 2-3 shows possible contributions of Br_y^{VLSL} varying between 3, 5, and 7 ppt, as indicated by the thin blue lines. If 5 ppt of Br_y^{VLSL} is incorporated into a photochemical model, then ozone loss in the lower stratosphere from reactions involving BrO occurs at a rate approaching that due to the traditionally considered hydrogen oxide cycles alone (see Figure 2-2).

The structure of this chapter is as follows. Section 2.2 discusses the emissions, observations, and trends of VSL SGs, including vertical distributions at different locations, and their likely mixing ratios in the upper tropo-

sphere. Section 2.3 provides an update to our knowledge about the atmospheric chemistry of halogenated VSL SGs and PGs (organic and inorganic), wet removal of PGs, and a discussion about the geographical variability of chemical lifetimes. The role of heterogeneous chemistry in the inorganic halogen budget is also discussed. Section 2.4 revisits our understanding of transport processes that are important for the transport of VSL SGs and PGs to the stratosphere via the SGI and PGI pathways in both the tropics and extratropics. The ability of current models to simulate the distributions of short-lived gases is also examined, since these are the tools used to estimate the impact of VSLS on stratospheric halogen loading, ozone loss, and their ODPs. Section 2.5 presents an assessment of the contribution of VSL SGs and PGs to stratospheric halogen budgets. Model estimates of the SGI and PGI fraction entering the stratosphere are also discussed. The possible contribution of VSLS (bromine) to stratospheric ozone loss, and an update of ODPs for VSLS, are discussed in Section 2.6. Finally Section 2.7 summarizes recent evidence for, and speculates on, possible future changes in halogenated VSLS that could affect future stratospheric halogen loadings and ozone loss.

2.2 SOURCES, DISTRIBUTIONS, AND TRENDS OF VSLS

2.2.1 New Observations of the Distributions and Abundances of VSL Source Gases

Since the last Assessment (WMO, 2003), a number of shipboard, atmospheric, firn air, and coastal observations have provided new information that either adds to or constrains earlier estimates of atmospheric mixing ratios of VSL SGs, which are known to exhibit significant geographical variation. Table 2-2 provides updated information since the last Assessment on VSL SG mixing ratios in the atmosphere and, in particular, it assesses the subset of relevant observations required to arrive at an estimated range of mixing ratios in the tropical marine boundary layer and tropical upper troposphere for each source gas. It suggests mean tropical boundary layer mixing ratios of 8.4, 1.2, and 81 ppt for total bromine, iodine, and chlorine, respectively, in VSL SGs; and corresponding mixing ratios in the tropical upper troposphere of 3.5, 0.08, and 55 ppt. It is clear from these observations that many of the chlorinated and brominated compounds are delivered efficiently from the boundary layer to the upper troposphere. Bromoform (CHBr₃) and dibromomethane (CH₂Br₂) contribute the most VSL organic bromine

VERY SHORT-LIVED SUBSTANCES

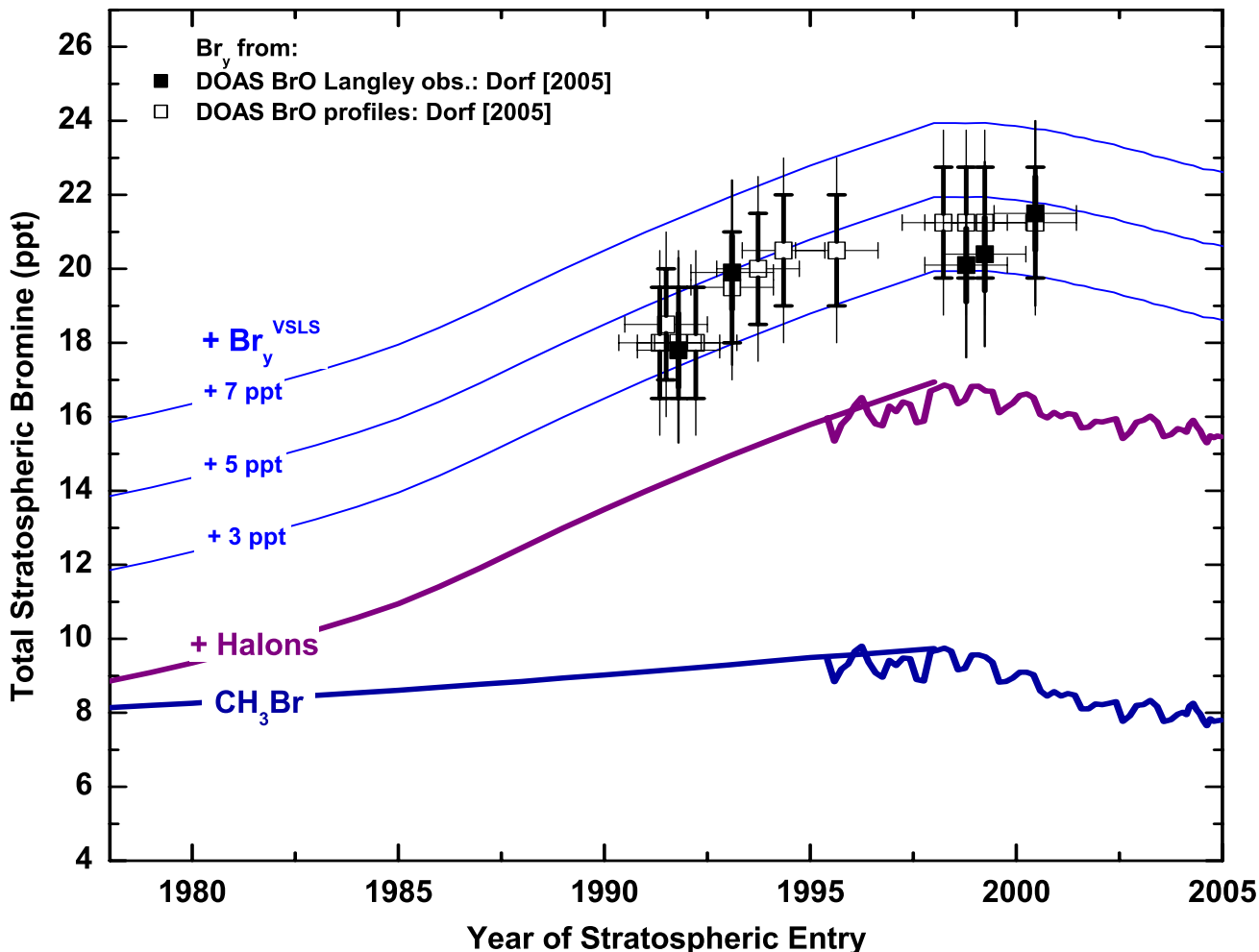


Figure 2-3. Trends (solid lines) of expected total inorganic stratospheric bromine (Br_y) due to measured tropospheric abundances of bromine from methyl bromide (CH_3Br ; thick blue lines), the sum of CH_3Br plus halons (thick purple lines), and this sum together with assumed additional bromine (3, 5, and 7 ppt) derived from VLSL and/or inorganic tropospheric bromine sources (thin blue lines). This figure is an update of Figure 1-8 from the last Assessment (WMO, 2003). The smooth thick blue and purple lines prior to 1995 are based on a combination of Antarctic firn air reconstructions and ambient air measurements from a number of studies, adjusted to represent mean global abundances (references in WMO, 2003), and updated here with mean ambient air measurements (non-smooth blue and purple lines post-1995) from NOAA global monitoring stations (Montzka et al., 2003; updated). There may be small calibration differences between the different studies (see, for example, Fraser et al., 1999). The points (open and filled squares) are total inorganic bromine derived from stratospheric balloon measurements of BrO and photochemical modeling to account for BrO/ Br_y partitioning. The filled black squares are from the slopes of Langley plot BrO observations above balloon float altitude, while the open squares are lowermost stratospheric BrO measurements (Dorf, 2005, and Dorf et al., 2006a, and references therein; together with more recent data as described in Section 2.5.2.1). Bold/faint error bars correspond to the precision/accuracy of the estimates, respectively (Dorf, 2005). For stratospheric data, the date corresponds to the time when that air was last in the troposphere, i.e., sampling date minus mean age of air in the stratosphere. No correction has been made for gradients of CH_3Br in the troposphere (see text for discussion). Preindustrial levels of CH_3Br of 5.8 and 5.5 ppt have been inferred by Saltzman et al. (2004) from Antarctic ice cores and by Trudinger et al. (2004) from Antarctic firn air, respectively, whereas preindustrial levels of the halons have been reported to all be below detection limits in Arctic and Antarctic firn air by Reeves et al. (2005). Adapted from Dorf (2005); see also Dorf et al. (2006b).

Table 2-2. Reported mixing ratios of VSL source gases in the troposphere (global and hemispheric values), at 10 km in the tropics, and best estimates from this Assessment of median mixing ratios in the tropical marine boundary layer [MBL] (<1 km), and tropical upper troposphere [UT]. All mixing ratio values are in parts per trillion (ppt). New information since WMO (2003) is indicated in boldface.

Species	Reported Tropospheric Mixing Ratio ^a	Reported 10-km Tropical Mixing Ratio ^a	Estimated Tropical [MBL] Mixing Ratio and Range	Estimated Tropical [UT] Mixing Ratio and Range	Estimated Ratio of [UT]/[MBL]
CH₂BrCl			0.47 (0.38-0.59)^c	0.32 (0.26-0.35)^c	0.7
CH ₂ Br ₂	0.8-3.4	0.6-0.9	1.1 (0.7-1.5)^{b,c,f}	0.9 (0.7-1.0)^{b,c,e}	0.8
CHBr ₂ Cl	0.1-0.5	0.04-0.11	0.30 (0.06-0.76)^{b,g,i}	0.08 (0.03-0.12)^{b,c}	0.3
CHBrCl ₂	0.12-0.6	0.04-0.11	0.33 (0.14-0.91)^{b,c,g,j}	0.12 (0.05-0.15)^{b,c}	0.4
CHBr ₃	0.6-3.0	0.4-0.6	1.6 (0.5-2.4)^{b,c,f,g}	0.37 (0.13-0.7)^{b,c,e}	0.2
CH ₃ I	0.1-2.0	0.05-0.2	0.8 (0.3-1.9)^{b,c,f}	0.08 (0.02-0.18)^{b,c}	0.1
CH₂ClI			0.35^g		
CH ₂ Cl ₂			17.5 (9-39)^{b,c,f}	13.2 (9-19)^{b,c,e}	0.75
CHCl ₃	NH, 10-15 12.4 (9.8-14.5)^k SH, 5-7 8.0 (6.5-9.1)^k	3.1 ±0.7	7.8 (5.2-13.3)^{b,c,f,k}	6.0 (4.8-7.5)^{b,c,e}	0.78
C ₂ HCl ₃	NH, 1-5 SH, 0.01-0.1	0-0.1	0.5 (0.05-2)^{b,c,d}	0.14 (0.02-0.3)^{b,c,d,e}	0.3
C ₂ Cl ₄	NH, 5-15 5.3 (3.3-7.3)^k SH, 0.7-1.5 1.5 (1.1-1.6)^k	1-3	1.8 (1.2-3.8)^{b,c,f,k}	1.3 (0.9-1.6)^{b,c,e}	0.7
C ₂ H ₅ Cl	NH, 2.6^l SH, 1.6^l		5.0 (2.7-5.9)^d	1.5 (1.0-1.8)^d	0.3
CH ₂ CICH ₂ Cl	NH, 20-40 SH, 5-7	14.9 ±1.1	3.7 (0.7-14.5)^{b,c,h}	1.8 (0.7-3.3)^{b,c,e,h}	0.5
COCl ₂				22.5 (20-25)^m	
Total Cl			81 (75-99)ⁿ	55 (52-60)^{n,o}	
Total Br			8.4 (6.9-9.6)ⁿ	3.5 (3.1-4.0)ⁿ	
Total I			1.2 (0.7-2.3)ⁿ	0.08 (0.02-0.18)ⁿ	

NH = Northern Hemisphere, SH = Southern Hemisphere.

^a Kurylo and Rodríguez et al. (1999), except as noted.

^b Transport and Chemical Evolution Over the Pacific (TRACE-P), Pacific Exploratory Missions (PEM) “Tropics A”/“Tropics B,” Tropospheric Ozone Production about the Spring Equinox (TOPSE); Blake et al. (1999a,b, 2001, 2003a,b).

^c 10-14 km tropical upper troposphere data from the Biomass Burning and Lightning Experiment-B (BIBLE-B) (Choi et al., 2003; Kondo et al., 2002).

^d TRACE-P data only.

^e 10-17.5 km non-stratospheric data from the Preliminary Aura Validation Experiment (preAVE; ozone < 75 ppt) (ftp://espoarchive.nasa.gov/archive/pre_ave/data/wb57).

^f Cruise data (Butler et al., 2006).

^g Chuck et al. (2005).

^h TRACE-P and PEM-Tropics A only (see above).

ⁱ High value from Chuck et al. (2005) increased mean from 0.15 to 0.30.

^j High value from Chuck et al. (2005) increased mean from 0.19 to 0.33.

^k 2002-2004 surface (Simpson et al., 2004; Blake, 2005).

^l Low et al. (2003).

^m Toon et al. (2001).

ⁿ Sum of medians and the root mean square (rms) range determined from data for individual compounds shown in the table.

^o COCl₂ is not included in Total Cl, as part of it may be derived from long-lived species (see text).

VERY SHORT-LIVED SUBSTANCES

(>80%) to both the marine boundary layer and the upper troposphere. Similarly chloroform (CHCl_3) and dichloromethane (CH_2Cl_2) contribute most of the VSL organic chlorine (~80%) to the marine boundary layer and the upper troposphere. There are few observations of measurable iodine source gases in the upper troposphere or lower stratosphere.

As discussed later in this chapter, many of the compounds listed in Table 2-2 are converted to inorganic forms, but few of these have been measured in the upper troposphere. A notable exception is phosgene (COCl_2) which may account for an additional c. 45 ppt of chlorine (Cl) in the tropical upper troposphere although, as discussed in Section 2.3.3, part of the phosgene might be associated with the decomposition of long-lived source gases in either the troposphere or stratosphere.

The abundances, distributions, and sources of these short-lived, potentially ozone-depleting gases are considered in more detail below.

2.2.1.1 BROMINE AND IODINE

Atmospheric mixing ratios of many brominated and iodinated VSLS are typically higher where marine influence is significant. They tend to be highest near coastal areas, oceanic fronts, and in the tropics or subtropics (e.g., Quack and Wallace, 2003; Carpenter, 2003; Chuck et al., 2005; Yokouchi et al., 2005b; Butler et al., 2006). The tropics, including coastal areas, are significant in that they comprise the main region where deep convection occurs, and are therefore the most likely location for transport of gases emitted at the surface to be carried to the upper troposphere and lower stratosphere.

Carpenter et al. (2003) compared atmospheric measurements of a range of reactive organic halogens at Mace Head, Ireland (September, 1998) and Cape Grim, Tasmania (January-February, 1999). Mixing ratios of methyl iodide (CH_3I), chloriodomethane (CH_2ClI), dibromochloromethane (CHBr_2Cl), CHBr_3 , and CH_2Br_2 at Cape Grim were on average only 25-50% of those at Mace Head, Ireland, which is more strongly influenced by emissions from local macroalgae (seaweeds). Average total VSL bromine abundances at Cape Grim and Mace Head during these campaigns were 18 ppt and 39 ppt as bromine (Br), respectively. These amounts are much higher than the global averages of 2.4-3.5 ppt reported in the last Assessment, and reflect the intense emissions from coastal waters. Bromoform contributed 45% and 54% of the total VSL bromine at these two sites, respectively, and accounted for most of the variability. Peters et al. (2005) noted extremely high values of CH_3I , CHBr_3 , and other VSLS over seaweed beds in northern Europe. These

values, as high as 1830 ppt for CH_3I and 393 ppt for CHBr_3 , have not been reported by any other investigations, the closest being 40 ppt of CHBr_3 reported by Yokouchi et al. (2005b). Other iodinated VSLS have been observed in such coastal environments, including diiodomethane (CH_2I_2), bromiodomethane (CH_2BrI), iodoethane ($\text{C}_2\text{H}_5\text{I}$), and 1-iodopropane ($n\text{-C}_3\text{H}_7\text{I}$), but at smaller concentrations (Carpenter et al., 2003; Peters et al., 2005).

Quack and Wallace (2003), summarizing global air and seawater mixing ratios of CHBr_3 by oceanic region, showed that background mixing ratios of CHBr_3 in marine boundary layer air are generally in the range 0.5-1.5 ppt. This is consistent with data in Butler et al. (2006), but it is about half of the range of 1.3-3.9 ppt reported by Chuck et al. (2005) for the open ocean. This difference may have resulted from natural temporal and spatial variability, but it may also be due to differences in calibration scales, which underscores the need for intercalibration of these gases among laboratories. Quack and Wallace (2003) and Butler et al. (2006) showed high and variable coastal marine boundary layer CHBr_3 mixing ratios ranging between 1 and 8.3 ppt, and levels in the open ocean ranging between 0.4 and 2.5 ppt. These levels are consistent with the previous Assessment (WMO, 2003). Yokouchi et al. (2005b) recently reported over 40 ppt of CHBr_3 (i.e., >120 ppt as Br) in the first study of air over tropical coastal waters, suggesting that such areas may be particularly important in delivering halogenated VSLS to the stratosphere.

Seasonality in mixing ratios of VSLS is evident over most of the ocean (Butler et al., 2006) and is particularly marked in coastal areas. Cohan et al. (2003) and Cox et al. (2005) reported high frequency, in situ observations at Cape Grim. Average background levels of CH_3I for 1998-2001 were 1.4 ppt (Cox et al., 2005). Mixing ratios peaked during the summer (amplitude 0.47 ppt) despite faster photolytic loss, suggesting that the local oceanic emissions were a significant source of this gas (Cohan et al., 2003). Carpenter et al. (2005) found a strong, broad seasonal range of CHBr_3 (1.8-5.3 ppt) at Mace Head, noting higher values in the summer, and identifying both terrestrial and marine sources.

Although organic VSL source gases predominate in the marine boundary layer, it is possible that small amounts of inorganic bromine or iodine in the boundary layer could also be rapidly convected to the lower stratosphere. Recent observations suggest that bromine monoxide (BrO) in the marine boundary layer, whether from organic or inorganic sources, is on the order of 0-2 ppt (Leser et al., 2003; Saiz-Lopez et al., 2004a), with higher values observed locally. High amounts of iodine monoxide (IO) are routinely observed in the marine

boundary layer near macroalgae, with values as high as 7-8 ppt having been reported along the coasts of Ireland and France (Saiz-Lopez and Plane, 2004; Saiz-Lopez et al., 2004b; Peters et al., 2005). Saiz-Lopez and Plane (2004) suggest that emission of molecular iodine (I_2) from macroalgae may be the dominant source of IO. Although VSLs produced at midlatitudes are not as likely to be convected into the upper troposphere as are VSLs produced in tropical regions, this still underscores the potential contribution of VSLs from coastal regions.

2.2.1.2 CHLORINE

Cox et al. (2005) reported background mixing ratios of 6.3 ppt for $CHCl_3$ at Cape Grim (1998-2000), and Simmonds et al. (2006) reported 8.7 ppt for CH_2Cl_2 also at Cape Grim (1998-2004). Observed elevated levels of $CHCl_3$ (55 ppt) were attributed to local natural sources, while elevated levels of CH_2Cl_2 (up to 70 ppt above background) were attributed to anthropogenic sources. Data referenced in Butler et al. (2006) show higher tropical marine air mixing ratios of CH_2Cl_2 (18.8 ppt), but similar tropical mixing ratios of $CHCl_3$ (7.4 ppt) to those observed at Cape Grim. Numerous studies (e.g., Prinn et al., 2000; Thompson et al., 2004; Simmonds et al., 2006) show higher Northern Hemispheric mixing ratios of both of these gases, which suggest greater emissions in the Northern Hemisphere and are consistent with a large anthropogenic source.

Low et al. (2003) reported the first calibrated measurements of atmospheric chloroethane (C_2H_5Cl). The median mixing ratios observed at a clean California coastal site were 3.3 and 0.3 ppt for C_2H_5Cl and C_2H_5Br , respectively. No significant correlation was found between the atmospheric concentrations of the methyl halides and the ethyl halides, suggesting different source-sink relationships. These results, combined with data from the Transport and Chemical Evolution over the Pacific experiment (TRACE-P), suggest an average global mixing ratio for C_2H_5Cl of 2.6 ppt. Using these data with an average hydroxyl radical (OH) lifetime of ~1 month, the global burden and required annual source of C_2H_5Cl to the atmosphere are 25 Gg ($1 \text{ Gg} = 10^9 \text{ g}$), and 300 Gg yr^{-1} , respectively (Redeker et al., 2003).

2.2.2 Terrestrial Emissions

Terrestrial emissions of brominated or iodinated VSLs are generally thought to be smaller than from the ocean (Table 2-3). Emissions from many terrestrial sources, such as rice cultivation, fires, and wastewater effluents, are anthropogenically influenced. Several eval-

uations of fluxes from rice paddies, using both new data and modeling techniques, indicate that rice paddies remain a significant source of CH_3I to the atmosphere. Lee-Taylor and Redeker (2005) re-evaluated the global fluxes of CH_3I from rice cultivation, including the effects of temperature, seasonality, and soil moisture. Their best estimate was 16 to 29 Gg yr^{-1} of CH_3I . This range is similar to the previous estimate of Muramatsu and Yoshida (1995), but is considerably lower than the earlier estimates of Redeker et al. (2000) and Redeker and Cicerone (2004). Redeker and Cicerone (2004) did note that CH_3I emissions from paddies were positively correlated with temperature, essentially doubling with an increase of 10 degrees (25-35°C).

The first measurements of emissions of C_2H_5Cl , $CHBr_3$, and bromodichloromethane ($CHBrCl_2$) from rice paddies, or any other terrestrial ecosystem, were reported by Redeker et al. (2003). Integrated seasonal emissions of C_2H_5Cl were 0.60 ± 0.50 milligrams ($1 \text{ mg} = 10^{-3} \text{ g}$) per meter squared ($mg \text{ m}^{-2}$), about 25 micrograms ($1 \mu\text{g} = 10^{-6} \text{ g}$) m^{-2} for $CHBr_3$, and $2.9 \mu\text{g} \text{ m}^{-2}$ for $CHBrCl_2$. Redeker et al. (2003) extrapolated their findings to the global coverage of rice and calculated an annual emission of about 1 Gg of C_2H_5Cl , which is insignificant compared with annual global emissions of c. 300 Gg yr^{-1} .

Evidence for direct terrestrial input of inorganic and organic halogens into the lower troposphere comes from studies of volcanoes and salt flats. Bureau et al. (2000) estimated the bromine yield of recent volcanic eruptions based on laboratory examination of ejected gases, and Bobrowski et al. (2003) measured enhanced BrO in a volcanic plume. Both authors suggest that these emissions could contribute to stratospheric bromine. Bobrowski et al. (2003) further estimated that volcanoes might emit c. 30 Gg BrO yr^{-1} into the lower atmosphere. Afe et al. (2004), however, showed that space-based measurements of column BrO are not correlated with enhancements of column sulfur dioxide in volcanic plumes, casting some doubt on the latter hypothesis. Volcanic perturbation to stratospheric bromine is not commonly considered in ozone assessment simulations.

Stutz et al. (2002) recorded elevated levels of BrO (6 ± 0.4 ppt) and ClO (15 ± 2 ppt) associated with mobilization of halogens from salt near the Great Salt Lake in the U.S. However, no flux estimates were provided, and it is not clear how widespread this phenomenon may be. Similarly, Zingler and Platt (2005) reported IO abundances of 0.3-2 ppt, and occasionally more than 10 ppt, over Dead Sea salt flats, apparently from inorganic sources. It is unlikely, however, that these emissions could contribute significantly to stratospheric halogen loading.

VERY SHORT-LIVED SUBSTANCES

Table 2-3. Estimated local lifetimes, burdens, removal rates, and sources for some halogenated VSLs.
New information since WMO (2003) is indicated in boldface.

Compound	Local Lifetime (days)	Estimated Burden (Gg)	Estimated Removal Rate (Gg yr ⁻¹)	Estimated Source from Inventory or Estimate of Biogeochemical Cycle (Gg yr ⁻¹)
CH ₂ BrCl	150 ^a	1.2 (Br), 0.5 (Cl) ¹	2.9 (Br), 1.3 (Cl) ^c	
CH ₂ Br ₂	120 ^a	18-22 (Br) ^b 19 (Br) ¹	55-67 (Br) ^c 58 (Br) ^c	
CHBrCl ₂	78 ^a	1.3-1.5 (Br) ^b 1.2-1.3 (Cl) 1.2 (Br), 1.1 (Cl) ¹	6.1-7.0 (Br) ^c 5.4-6.2 (Cl) 5.5 (Br), 4.9 (Cl) ^c	17 (Cl) open ocean ^{15,h} 19 (Br) open ocean ^{15,h}
CHBr ₂ Cl	69 ^a	0.8-2.2 (Br), 0.2-0.5 (Cl) ^b 2.3 (Br), 0.5 (Cl) ¹	4.2-12 (Br), 0.9-2.7 (Cl) ^c 12 (Br), 2.7 (Cl) ^c	5 (Cl) open ocean ^{15,h} 23 (Br) open ocean ^{15,h}
CHBr ₃	26 ^a	11-18 (Br) ^b 14 (Br) ¹	150-250 (Br) ^c 200 (Br) ^c 285 ^{2, d}	209 (47-370) (Br) ³ 800 (240-1760) (Br) ⁹ 28 (20-112) (Br) industry ⁹
CH ₃ I	5 ^c 6 ^f	1.7-2.2 (I) ^b 4.8 (I) ^f	120-160 (I) ^c 214 (I) ^f	90-450 (I) ⁴ 272 (I) total ¹⁰ 191 (I) net ocean (incl. 66 anthropogenic) ¹⁰ 180 (I) open ocean ^{15,h}
C ₂ H ₅ I CH₂CI	4 ^a 0.1^a	0.5 (I)	46 (I) ^c	95 (I) open ocean ^{15,h} 27 (Cl) open ocean ^{15,h}
CH ₂ Cl ₂	140 ^a 180 ^{6, c}	83-250 (Cl) ^b 250 (Cl) ⁶	220-650 (Cl) ^c 650 (Cl) ^c 500 (Cl) ^{6,d}	487 (Cl) industrial ⁵ 160 (Cl) ocean 49 (Cl) biomass burning ^{16,i}
CHCl ₃	150 ^a 183 ^{7,c}	66-130 (Cl) ^b 210 (Cl) ⁷	160-320 (Cl) ^c 511 (Cl) ^c 470 (350-600) ^{7,c} 412 (Cl) ^{6,d}	564 (Cl) ⁶ 588 (392-784) (Cl) ¹¹ 320 (240-400) (Cl) seawater ¹¹ 196 (107-285) (Cl) soil ¹¹
C ₂ HCl ₃	4.6 ^a 5.5 ^{6,c}	3.1 (Cl) ^b 5.30 (Cl) ⁶	260 (Cl) ^c 440 (Cl) ^c 350 (Cl) ^{6,e}	95 (Cl) industry ⁵ 20 (Cl) ocean ⁶ 3 (Cl) fossil fuel ⁶
C ₂ Cl ₄	99 ^a 133 ^{6,c}	17-85 (Cl) ^b 160 (Cl) ⁶	63-310 (Cl) ^c 590 (Cl) ^c 440 (Cl) ^{6,e}	313 (Cl) industry ⁵ 16 (Cl) ocean ⁶ 2 (Cl) fossil fuel ⁶ 222 (210-235) (Cl) ^{12,g}
C₂H₅Cl	~ 30 ¹³ ~ 24 ¹⁴	14 (Cl) ¹³ 4.6-7.3 (Cl) ¹⁴	165 (Cl) ^c 70-110 (Cl) ^c	
CH ₂ ClCH ₂ Cl	70 ^a	5-26 (Cl) ^b	26-130 (Cl) ^c	700 ⁸

References: ¹Kurylo and Rodríguez et al. (1999); ²Dvortsov et al. (1999); ³Carpenter and Liss (2000); ⁴Singh et al. (1983), Liss and Slater (1974), Moore and Groszko (1999); ⁵McCulloch et al. (1999); ⁶Keene et al. (1999); ⁷Khalil and Rasmussen (1999); ⁸Khalil (1999); ⁹Quack and Wallace (2003); ¹⁰Bell et al. (2002); ¹¹McCulloch (2003); ¹²Simpson et al. (2003); ¹³Redeker et al. (2003); ¹⁴Low et al. (2003); ¹⁵Chuck et al. (2005); ¹⁶Lobert et al., (1999).

^a From Table 2-4 of Ko and Poulet et al. (2003).

^b Burden estimated using Equation 2.3 and the median BL mixing ratios from Table 2-7 in Ko and Poulet et al. (2003), and the estimated scale height from Table 2-10 in Ko and Poulet et al. (2003).

^c From estimated lifetime and estimated burden, i.e., (column 3)/(column 2). The range reflects the range in the estimated burden.

^d From two-dimensional (2-D) model.

Table 2-3, continued.

- ^e Burden estimated from information given in Ko and Poulet et al. (2003): Equation 2.3, Table 2-7 (median BL mixing ratios), Table 2-10 (estimated scale heights).
- ^f From three-dimensional (3-D) model simulation of Bell et al. (2002).
- ^g Estimate for 2002.
- ^h Estimated using data from Chuck et al. (2005). The surface ocean during the Chuck et al. study was generally a sink for CHBr_3 .
- ⁱ May be a less significant and more uncertain source than estimated here, although no new global emission estimates are available (Simmonds et al., 2006; Scheeren et al., 2002).

2.2.3 Oceanic Emissions

Numerous studies evaluating the oceanic production, degradation, and emission of VSLS suggest high spatial and temporal variability, with emissions generally high in the tropics and near ocean fronts, and highest in coastal regions (Figure 2-4). These studies continue to suggest that oceanic emissions constitute by far the largest source of brominated and iodinated VSLS to the atmosphere, making up 90-95% of the total global flux of these gases. The potential for spatially and seasonally dependent variability is shown clearly in the work of Cohan et al. (2003), where model results indicate that the mean oceanic flux of CH_3I from the Southern Ocean into the marine boundary layer at 40°S - 50°S is 3.1 (1.9 - 5.2) $\mu\text{g m}^{-2} \text{day}^{-1}$ during the summer. For comparison, the global annual oceanic flux estimate reported by Moore and Groszko (1999) corresponds to 1.0 to 2.7 $\mu\text{g m}^{-2} \text{day}^{-1}$, and the open ocean range given in Butler et al. (2006) is 0.6 to 5.7 $\mu\text{g m}^{-2} \text{day}^{-1}$.

2.2.3.1 BROMINE

Both Butler et al. (2006) and Quack et al. (2004) show the highest open ocean fluxes of CHBr_3 in areas of upwelling, such as near the equator and at ocean fronts, and their combined data suggest that tropical fluxes are highest in the Pacific, where equatorial upwelling is most intense. Quack and Wallace (2003) noted that subtropical coastal and shelf oceans of both hemispheres contribute significantly to global emissions, with 180 (72 - 270) $\text{Gg Br} (\text{CHBr}_3) \text{yr}^{-1}$ emitted from their “shore” regime and 380 (240 - 940) $\text{Gg Br} (\text{CHBr}_3) \text{yr}^{-1}$ emitted from their “shelf” regime, representing 23 and 48% of the entire oceanic CHBr_3 flux, respectively. Extrapolating Atlantic open ocean fluxes to the global ocean yielded 240 (32 - 800) $\text{Gg Br} (\text{CHBr}_3) \text{yr}^{-1}$, representing about one-third of the global oceanic CHBr_3 emission of ~ 800 (240 - 1800) $\text{Gg Br} (\text{CHBr}_3) \text{yr}^{-1}$. These estimates are similar to the 160 and 890 Gg Br yr^{-1} reported by Butler et al. (2006) for open ocean and global sources respectively. Quack and Wallace (2003) attribute much

of the source to CHBr_3 production by phytoplankton, which they calculated to be ~ 240 Gg Br yr^{-1} .

The large differences between estimated open ocean fluxes and global fluxes underscore the importance of coastal waters as a substantial source of CHBr_3 . High fluxes of many polyhalogenated VSLS are attributed mainly to attached macroalgae (e.g., Laturnus et al., 1996; Carpenter et al., 2000), and numerous investigators have reported very high mixing ratios in and above coastal waters (e.g., Carpenter and Liss, 2000). There have been, however, no systematic investigations of these gases in tropical coastal regions until recently, when Yokouchi et al. (2005b) measured atmospheric concentrations of CHBr_3 , CH_2Br_2 , and CHBr_2Cl over several areas, including both Arctic and tropical coastal waters, and the open ocean, finding by far the highest amounts of these gases in association with tropical coasts. Their global estimate of the oceanic CHBr_3 source was 820 (± 310) Gg Br yr^{-1} , which is consistent with the independent estimates of Quack and Wallace (2003) and Butler et al. (2006).

Although coastal macroalgae are undoubtedly an important global source, Quack et al. (2004) and Butler et al. (2006) also provide evidence that the sources of CHBr_3 and CH_2Br_2 throughout the tropical open ocean are associated with the deep chlorophyll maximum near the thermocline. Transport of these gases to the ocean surface in association with upwelling and mixing is consistent with the higher concentrations and fluxes observed at the equator and near ocean fronts (Chuck et al., 2005; Butler et al., 2006). This may be significant because equatorial upwelling, which carries these gases to the surface where they are emitted, is influenced by wind speed and direction, which in turn are affected by climate, weather, and El Niño-Southern Oscillation (ENSO) events. This suggests a link between climate, wind-driven upwelling, and the supply of bromine to the tropical upper troposphere, where it can be transported to the lower stratosphere (see Section 2.4).

Several studies indicate that CHBr_3 sources contribute more organic and reactive bromine to the lower atmosphere than other organobromines. Carpenter et al.

VERY SHORT-LIVED SUBSTANCES

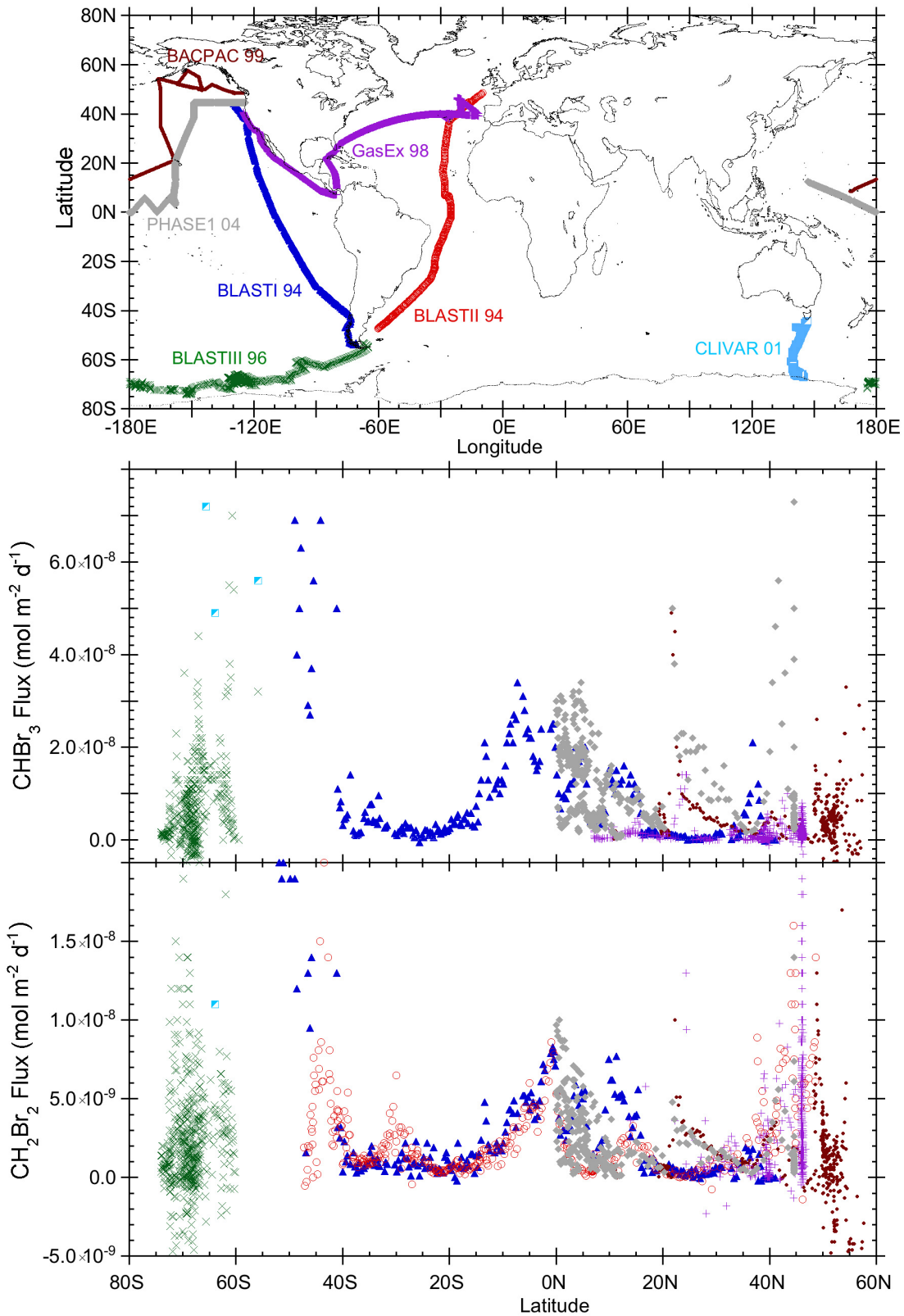


Figure 2-4. Plots of the oceanic fluxes of CHBr₃ and CH₂Br₂ into the marine boundary layer based upon data from seven research cruises between 1994 and 2004 (Butler et al., 2006). Cruise data are color-coded to match those in the map. All measurements are on the same calibration scale.

(2003) extrapolated their data to estimate molar source strengths of CHBr_2Cl and CH_2Br_2 , suggesting that the flux of CHBr_2Cl is about 3-6% of that of CHBr_3 , and that CH_2Br_2 emissions would be about 15-25% of the global CHBr_3 flux. Yokouchi et al. (2005b) suggest somewhat similar molar emission ratios, with CHBr_2Cl amounting to ~7% and CH_2Br_2 to ~11% of the flux in coastal waters. Butler et al. (2006) noted that CH_2Br_2 fluxes were about 25-35% of CHBr_3 fluxes for data collected mostly in the open ocean. These values all fall within ranges estimated independently from concentration and lifetime data.

2.2.3.2 IODINE

Fluxes of iodinated VSLs are driven in part through photochemistry in the surface waters. Results of a study of the production of CH_3I in the tropical Atlantic Ocean support prior inferences that CH_3I is produced in the open ocean by a light-dependent production pathway that is not directly dependent on biological activity (Richter and Wallace, 2004). This assertion is supported by data from Smythe-Wright et al. (2005) and Chuck et al. (2005). Also, photo- or biodegradation of some polyhalogenated methanes can lead to the production of others. For example, Martino et al. (2005) carried out laboratory studies of aqueous degradation kinetics of the photolabile compounds CH_2I_2 , CH_2BrI , and CH_2ClI in different types of natural and artificial seawater. Photolysis of CH_2I_2 in artificial and natural seawater generated CH_2ClI with a yield of 25-30%, suggesting that this reaction is an important source of marine CH_2ClI . Dark-incubations indicated that photolysis is the main abiotic degradation mechanism of CH_2I_2 in seawater and that CH_2I_2 originating at depth and transported to the surface would be photolyzed before escaping into the atmosphere. The longer aquatic photolytic lifetime of CH_2ClI allows this compound to vent to the atmosphere and indeed, although CH_2ClI has been detected at very low levels in the remote marine boundary layer, its sea-air fluxes appear to be of the same order as those of CH_3I (Carpenter et al., 2003; Chuck et al., 2005).

2.2.3.3 CHLORINE

Although previous studies (e.g., Khalil et al., 1999) led Keene et al. (1999) to conclude that oceanic emissions of dichloromethane (CH_2Cl_2) could account for about 25% of the total emissions to the atmosphere, recent work by Moore (2004) suggests that the apparent supersaturation of this gas in higher latitude waters is an artifact of circulation and mixing. Moore (2004) interpreted the measurements of CH_2Cl_2 in waters of the North Atlantic and Labrador Sea to show that the compound at depth in the

ocean is imprinted with an older atmospheric source, and appears to persist for years to decades in deeper waters. In this sense, the observed surface supersaturation of the gas would likely have resulted from the recent decline of this gas in the atmosphere (e.g., Simmonds et al., 2006; Thompson et al., 2004) with the ocean gradually re-equilibrating, and not necessarily the result of production in the ocean. Thus, the ocean "source" of 200 Gg Cl yr^{-1} would likewise be a matter of re-equilibration, not production.

2.2.4 Industrial and Other Anthropogenic Emissions

2.2.4.1 BROMINE

Except for the chlorinated VSLs, anthropogenic emissions of most halogenated VSLs are presently dwarfed by natural emissions (Table 2-3). Emissions of CHBr_3 through water treatment, however, can be locally significant. Quack and Wallace (2003) reassessed the anthropogenic CHBr_3 source from water chlorination, including reactions on saltwater effluents, and suggested that it would amount to about 28 Gg Br yr^{-1} (0.20-110 Gg Br yr^{-1}), which is minor compared with natural sources (<5% of biogenic CHBr_3 emissions). Zhou et al. (2005) reported contributions from effluents from the chlorination of drinking, waste, and recreational waters of ~1-10% of the CHBr_3 emitted from the Great Bay area of New England, U.S. In the same region, they determined that the contribution from coastal power plant cooling effluents amounted to 15-50% of the CHBr_3 measured in the Great Bay, constituting most, if not all, of the anthropogenic source to the bay.

Because polar firn air provides a natural archive of "old" (typically from early 20th century) air, long-term trends of various gaseous species can, with some caveats, be reasonably reconstructed. Significant 20th century trends are often indicative of increasing anthropogenic emissions. For example, Worton et al. (2006) reported firn air measurements of the brominated trihalomethanes (THMs: CHBr_3 , CHCl_2Br , CHClBr_2) and dihalomethanes (DHMs: CH_2Br_2 and CH_2ClBr) in Greenland. The brominated DHMs showed no annual trend over time, suggesting that their sources are almost entirely natural. The THMs, however, appeared to increase by 20% from 1950-1990. This translates to increases of 16 ± 9 , 0.7 ± 0.4 , and 0.8 ± 0.3 Gg Br yr^{-1} for CHBr_3 , CHBr_2Cl , and CHBrCl_2 , respectively. Worton et al. (2006) noted that similarities in the trends in the deepest sections of the firn (oldest air) indicate that the three THMs may have similar sources. The authors further suggested that

VERY SHORT-LIVED SUBSTANCES

chlorination of seawater for cooling coastal power plants may be the largest anthropogenic source of the brominated THMs. Emissions of THMs from water chlorination could potentially increase in the future in response to increasing demand for water treatment (potable and waste water) and power generation.

2.2.4.2 CHLORINE

Antarctic firn air measurements from Trudinger et al. (2004) show CHCl_3 and CH_2Cl_2 increasing in atmospheric mixing ratios from 3.9 ppt to 6.35 ppt and 1.4 ppt to 8.9 ppt, respectively, between 1940 and 1990. They noted that records of anthropogenic emissions of CH_2Cl_2 were consistent with their results. Northern Hemisphere firn air measurements from Worton et al. (2006) also support an anthropogenic contribution to CHCl_3 . Their model calculations suggest anthropogenic emissions were ~14-20% of total CHCl_3 emissions (270-335 Gg Cl yr^{-1}) in 1950, and increased to 41-50% of the total (417-506 Gg Cl yr^{-1}) at the peak in global mixing ratio in about 1990. Anthropogenic emissions subsequently decreased to ~19% of total emissions (310 Gg Cl yr^{-1}) in 2001. This anthropogenic component was attributed mostly to paper and pulp manufacture, and the declining emissions since ~1990 to changes in working practices in this industry.

Recent ambient atmospheric data also suggest that emissions of these two gases are declining. Prinn et al. (2000) report data for CHCl_3 from 1983-1998 with a trend ranging from -0.1 to -0.4 ppt yr^{-1} . Simmonds et al. (2006) noted that measurements from Mace Head, Ireland, and from the National Oceanic and Atmospheric Administration (NOAA) U.S. global monitoring sites (Thompson et al., 2004) show a decrease in CH_2Cl_2 mixing ratios from 1995-2004 with trends of -0.7 ppt yr^{-1} (1995-2004) and -0.3 ppt yr^{-1} (1998-2004), while an increase of 0.05 ppt yr^{-1} was observed at Cape Grim, Australia.

Emissions of some chlorinated gases such as tetrachloroethene (C_2Cl_4) have been targeted for reduction owing to public health concerns. Levels of tropospheric C_2Cl_4 , for which sources were estimated in WMO (2003) to be 95% anthropogenic, declined substantially between 1989 and 2002 (Simpson et al., 2004). During this period, annual mean C_2Cl_4 mixing ratios for the extratropical Northern Hemisphere dropped from 13.9 ± 0.5 ppt to less than half this value (6.5 ± 0.2 ppt), and global averages declined from 6.3 ± 0.6 ppt to 3.5 ± 0.2 ppt (Simpson et al., 2004). These values suggest that the global C_2Cl_4 burden decreased by roughly 820 Gg Cl between 1989-2002, and is consistent with decreasing anthropogenic Northern Hemispheric emissions. Simmonds et al. (2006)

showed continued declines in C_2Cl_4 from 2000-2004. They report means (trends in parentheses) for Mace Head, Ireland, and Cape Grim, Australia, of 4.9 ppt (-0.18 ppt yr^{-1}) and 0.75 ppt (-0.01 ppt yr^{-1}), respectively.

High regional variability in emissions of anthropogenic VSLS is underscored by the study of Barnes et al. (2003) who, in contrast to the above, found no uniform trend of C_2Cl_4 between 1996 and 1999 at Harvard Forest, Massachusetts, U.S., but suggested that urban and industrial emissions of C_2Cl_4 for the New York City-Washington, D.C. corridor were increasing. Similarly, estimates from an aircraft study over Sagami Bay, Japan, suggest high emission rates of CH_2Cl_2 (61.8 Gg Cl yr^{-1}) and C_2Cl_4 (28.0 Gg Cl yr^{-1}) (Yokouchi et al., 2005a). These estimates, as well as those for CHCl_3 (6.2 Gg Cl yr^{-1}) and trichloroethene C_2HCl_3 (39.8 Gg Cl yr^{-1}), are consistent with the Japanese Pollutant Release and Transfer Register for 2002 (PRTR, 2004).

2.2.4.3 NEW VSL GASES

Future emissions of VSLS in the upper troposphere are potentially problematic. Trifluoriodomethane (CF_3I) is being considered as a direct replacement for halon use in aircraft, and as a replacement for the potent greenhouse gas, hexafluoroethane (C_2F_6), currently used in the plasma etching industry. No information on its emission is currently available, although its use on aircraft could potentially lead to emission at altitude. This species is rapidly photolyzed (Table 2-1), but emission at altitude could provide a pathway for future injection of iodine to the stratosphere (Li et al., 2006). A new product, "PhostrEx" (PBr_3), has recently won approval from the U.S. Environmental Protection Agency for in-flight aircraft engine fire protection, and has passed all Federal Aviation Administration certification fire testing; future widespread use is possible. Although this compound is highly soluble and consequently has a very short lifetime (<0.1 s at 50% humidity), its release during flight in the upper troposphere could be of concern because of the low humidity and hence slower removal rates of the gas and its degradation products at these altitudes.

2.2.5 Sources and Distributions of Inorganic Halogens of Marine Origin

Any substance present in the upper troposphere can potentially be exported to the stratosphere; therefore inorganic halogens in the upper troposphere have to be considered to quantify the total import of halogens into the stratosphere. In the tropics, rapid convective transport means that VSLS may also be transported from the

boundary layer into the tropical upper troposphere (see Section 2.4.1).

BrO has been observed directly in the midlatitude marine boundary layer (Leser et al., 2003; Saiz-Lopez et al., 2004a). The presence of inorganic bromine generally in the marine boundary layer has also been inferred from the routinely observed large bromide deficit in sea salt aerosol (e.g., Sander et al., 2003). These occurrences are almost certainly due to halogen activation from sea salt by heterogeneous reaction chemistry.

Combinations of space-, ground-, and balloon-based measurements indicate that BrO is widely present in the free troposphere, with mixing ratios of 0.2-2 ppt (Harder et al., 1998; Wagner and Platt, 1998; Pundt et al., 2000; McElroy et al., 1999; Fitzenberger et al., 2000; Wagner et al., 2001; Van Roozendaal et al., 2002; Richter et al., 2002; Schofield et al., 2004). The study by Yang et al. (2005), incorporating a detailed bromine chemistry scheme of gas-phase and heterogeneous reactions, showed that monthly mean mixing ratios of 0.1-1.0 ppt of BrO in the free troposphere can be explained by a combination of bromine release from sea salt aerosol and the breakdown of bromomethanes. Other bromine sources were not considered in this study, but might contribute (e.g., volcanic BrO, as noted above, and tropospheric decomposition of other organic bromine gases). They suggest that sea salt might contribute as much as 10% of the total Br in the upper troposphere.

In contrast to bromine, there is limited evidence for the presence of inorganic chlorine radicals in the free troposphere.

McFiggans et al. (2004) and Saiz-Lopez et al. (2006) reported direct coastal boundary layer observations of molecular iodine, ultrafine particle production, and iodocarbons. They demonstrated for the first time that ultrafine iodine-containing particles are produced by intertidal macroalgae exposed to ambient levels of ozone. However, the lifetime of inorganic iodine species released in the boundary layer is short, and they are generally unlikely to be transported to the stratosphere.

2.3 ATMOSPHERIC CHEMISTRY OF VSLS

The halogenated source compounds considered here are listed in Table 2-1. The Table gives the estimated local lifetimes (τ_{local}) for these compounds, defined as $(\tau_{\text{local}})^{-1} = (\tau_{\text{OH}})^{-1} + (\tau_{\text{J}})^{-1}$ where (τ_{OH}) is the lifetime due to reactions with hydroxyl radical (OH), and (τ_{J}) is the lifetime due to ultraviolet (UV) photolysis. It is worth noting that even within these halogenated VSLS there is a wide range of local lifetimes, with values ranging from a few minutes to 150 days. The atmospheric loss processes for

the source gases (organic halogens) occurs primarily in the gas phase via reaction with OH and UV photolysis. Multiphase processing of source gases is not a significant loss process and is not considered in this chapter.

The removal of inorganic halogenated reservoir species (e.g., hydrogen chloride, HCl) by wet and dry deposition is the main atmospheric loss process for inorganic halogens. Heterogeneous processes that recycle inorganic bromine and (most probably) iodine to insoluble reactive forms, may significantly increase the effective lifetime of Br_x and I_x (see boxed text in Section 2.1 for definition of Br_x; I_x is analogously defined) in the troposphere and the lower stratosphere and, as a result, enhance the efficiency of halogen transport via the PG pathway into the lower stratosphere, as discussed in Section 2.5.

Processing of both organic and inorganic halogenated degradation products on atmospheric aerosol and cloud particles is currently not well represented in atmospheric models, although the knowledge of these processes continues to improve. For example, a clearer picture is evolving regarding the partitioning of trace gases onto ice surfaces in cirrus clouds (Abbatt, 2003), and the mechanisms of halogen reactions on ice surfaces under tropospheric conditions (Fernandez et al., 2005). In this section, we assess the data needed to represent the atmospheric processing in both the gas and condensed phases of halogenated VSLS in atmospheric models.

2.3.1 Removal of Halogen Source Gases

The halogenated VSL SGs listed in Table 2-1, with the exception of CF₃I, C₂H₅Br, 1,2-dibromoethane (CH₂BrCH₂Br), and PBr₃ were evaluated in WMO (2003). The kinetic and photochemical parameters for the previously assessed VSL source gases have been updated in the recent evaluations of the International Union of Pure and Applied Chemistry (IUPAC, Atkinson et al., 2005; <http://www.iupac-kinetic.ch.cam.ac.uk>), and the National Aeronautics and Space Administration (NASA) Jet Propulsion Laboratory (JPL), U.S. (Sander et al., 2006; <http://jpldataeval.jpl.nasa.gov>), with only minor revisions.

The atmospheric loss of the VSL SGs can be summarized as follows: chlorinated VSL compounds have long photolysis lifetimes and are predominantly removed in the troposphere through reaction with OH; the brominated VSLS are removed by a combination of UV photolysis and OH reaction depending on the degree of halogen substitution (for example, increased importance of photolysis with higher bromine substitution); and iodine-containing VSLS are removed almost exclusively by photolysis. Bayes et al. (2003) reported bromine atom quantum yields for the photolysis of CHBr₃ at several wavelengths be-

VERY SHORT-LIVED SUBSTANCES

Table 2-4. OH rate coefficient and photochemical parameters for bromoethanes added since the WMO (2003) Assessment. Temperatures (T) in Kelvin.

Compound	$k(\text{OH})$ ($\text{cm}^3 \text{ molec}^{-1} \text{ s}^{-1}$)	$k_{300}(\text{OH})$ ($\text{cm}^3 \text{ molec}^{-1} \text{ s}^{-1}$)	Photolysis Rate Constant, J^a (s^{-1})	References
Bromoethane ($\text{C}_2\text{H}_5\text{Br}$)	$2.9 \times 10^{-12} \exp(-640/T)$	3.43×10^{-13}	$<1 \times 10^{-9}$	Sander et al. (2006)
1,2-dibromoethane ($\text{CH}_2\text{BrCH}_2\text{Br}$)	$1.44 \times 10^{-11} \exp(-1270/T)$	2.1×10^{-13}	$<1 \times 10^{-9}$	Qiu et al. (1992); Sander et al. (2006)

^a Atmospheric photolysis rate constants are globally and seasonally averaged estimates for 5 km altitude (because different models were used, the values should be considered approximate).

tween 303 and 324 nanometers (nm). Their results imply that the UV absorption cross section data currently recommended for use in the determination of the atmospheric photolysis rate of CHBr_3 may be systematically high by as much as 20% over this wavelength region.

The OH rate coefficients and atmospheric photolysis rates for $\text{C}_2\text{H}_5\text{Br}$ and $\text{CH}_2\text{BrCH}_2\text{Br}$ are given in Table 2-4. The photolysis lifetimes are significantly longer than their respective OH reaction lifetimes, and therefore photolysis is not an important atmospheric loss process for these compounds.

2.3.2 Tropospheric Lifetimes of Halocarbons

The lifetimes given in Tables 2-1 and 2-3 provide only an approximate estimate of the global mean lifetimes, because of significant regional variations in the OH radical concentration, solar flux, and the spatial and seasonal distributions of the halogen source gases. The geographic distribution of VSL SG surface fluxes with respect to these regional variations in the corresponding sinks is an important factor in determining the global mean atmospheric lifetimes of the VSL SGs. Warwick et al. (2006) have provided an estimate of the importance of the geographic flux distribution on the atmospheric lifetime of CHBr_3 by using a global atmospheric three-dimensional (3-D) model to calculate the CHBr_3 global atmospheric lifetime for a set of prescribed oceanic CHBr_3 emission data. In their calculations, the CHBr_3 atmospheric lifetime, defined as the global burden divided by the annual global loss, varied from 37 days in a scenario containing emissions distributed over the entire open ocean, to 15 days in a scenario in which CHBr_3 was emitted from tropical coastline regions only (see Table 2-5). The shorter lifetime in the tropical emission scenario is due to higher OH concentrations and UV levels in this region. This represents an uncertainty of approximately $\pm 40\%$ in the CHBr_3 atmospheric lifetime

that is solely due to changes in the emission distribution. For halogen source gases with longer atmospheric lifetimes and better constrained flux distributions, this uncertainty will be reduced.

The different CHBr_3 emission scenarios in the Warwick et al. (2006) study also showed a significant variation in the amount of CHBr_3 reaching the tropical upper troposphere. A scenario based on a uniform ocean emission distribution of $210 \text{ Gg CHBr}_3 \text{ yr}^{-1}$ (Kurylo and Rodríguez et al., 1999; Carpenter and Liss, 2000) showed CHBr_3 peak mixing ratios of 0.2 ppt at 110 hPa, whereas a scenario with larger emissions ($587 \text{ Gg CHBr}_3 \text{ yr}^{-1}$) predominantly situated in the oceanic tropics, which showed better agreement to tropospheric observations, contained peak CHBr_3 mixing ratios of ~ 1 ppt at the same altitude.

Table 2-5. Bromoform emission scenarios used by Warwick et al. (2006).

Global Flux (Gg CHBr_3 yr^{-1})	Geographic Distribution of Emissions	Modeled Atmospheric Lifetime (days)
210	uniform ocean ^a	30
235	open ocean ^b	37
587	global coastlines ^b	26
400	tropical ocean ^c	21
587	tropical coastlines ^c	15
595	tropical ocean and tropical coastlines ^c	18

^a Kurylo and Rodríguez et al. (1999).

^b Quack and Wallace (2003).

^c Warwick et al. (2006).

2.3.3 Production and Gas-Phase Removal of VSL Organic Product Gases

The first generation of stable reaction products formed following the gas-phase degradation of the halogenated VSL SGs was reviewed in WMO (2003). In general, the stable products consist of a variety of organic carbonyl (RC(O)R') and peroxide (ROOR') compounds, and inorganic halogen species. Since the last Assessment, little new evidence for the atmospheric reactivity and photolysis of these compounds has been reported. The recent IUPAC and JPL evaluations include the updates for these compounds where available. Detailed degradation mechanisms for halomethanes in general, and n-propyl bromide (n-C₃H₇Br) specifically, were given in WMO (2003). A major uncertainty in the evaluation of the impact of the degradation products is a lack of experimental data for their reactivity and photolysis.

The atmospheric degradation mechanisms for the VSL SGs are reasonably well understood, although quantification of the various possible reaction channels and degradation products is lacking in some cases. In general, the atmospheric degradation of the halogenated VSL source gases leads to the formation of compounds with atmospheric lifetimes shorter than the lifetime of the source gas. A notable exception is the formation of phosgene, COCl₂, which is a product formed in the degradation of the VSLS chloroform (CHCl₃) and tetrachloroethene (C₂Cl₄). Phosgene is also formed in the degradation of longer lived chlorinated compounds such as carbon tetrachloride (CCl₄) and methyl chloroform (CH₃CCl₃). In the stratosphere, COCl₂ is removed mainly by photolysis, since the rate constant for reaction with OH is relatively small (<5 × 10⁻¹⁵ centimeters cubed per molecule per second). On the basis of recently published cross sections (Atkinson et al., 2005; Sander et al., 2006), the local photolysis lifetime of COCl₂ is estimated to be similar to that of CFC-11 (trichlorofluoromethane; CCl₃F), and about twice that of CCl₄, at altitudes above 18 km at 30°N; thus significant stratospheric loss of COCl₂ is to be expected. Kindler et al. (1995), using a one-dimensional (1-D) model, reported a stratospheric lifetime for COCl₂ of ~2 years (for COCl₂ produced in the stratosphere); less than lifetimes calculated for long-lived SGs such as CCl₄. Kindler et al. calculated a much longer stratospheric lifetime (>8 years) for COCl₂ produced in the troposphere, which they explain as being due to the requirement for COCl₂ produced in the troposphere to be transported to higher stratospheric altitudes, where photolysis rates are greater. In the troposphere, removal of COCl₂ is dominated by aerosol washout (total wet removal lifetime of ~60 days from Kindler et al. (1995) and ~70 days from

WMO, 2003). Therefore, wet removal of COCl₂ may further reduce the contribution of chlorinated source gases (both long-lived and VSLS) to stratospheric chlorine (see Section 2.3.4.1).

When loss of CHBr₃ is initiated by reaction with OH, the final organic decomposition product is likely to be carbonyl dibromide (COBr₂). When loss is initiated by photolysis, then formyl bromide (COHBr) is thought to be produced (Ko and Poulet et al., 2003). Present kinetics (Sander et al., 2006) indicate about two-thirds of the loss of CHBr₃ occurs by photolysis. There are few kinetic studies of COBr₂ and COHBr and no atmospheric observations of these species. Measurements of the UV cross sections (Libuda, 1992) indicate, however, that these compounds have a shorter lifetime due to photolysis loss than does CHBr₃. Many other organic intermediates are involved with the decomposition of other VSL SGs (e.g., Ko and Poulet et al., 2003).

2.3.4 Multiphase Processes Involving Inorganic Bromine and Iodine Compounds

Models used to predict tropospheric amounts of halocarbons and their degradation products currently use very simplified algorithms for heterogeneous processes and physical removal. Although the multiphase chemistry for inorganic bromine, and especially iodine compounds, is still poorly known, there are significant new data and understanding since the last Assessment, which are summarized below. This opens the possibility for a more realistic treatment of multiphase chemistry and more quantitative representation of the heterogeneous recycling of reactive halogens, the potential importance of which was highlighted in WMO (2003). In future model studies, the partitioning of gases on ice should be described using the suggested Langmuir description. Uptake on aqueous particles should, especially for very soluble species (see Yin et al., 2001), be calculated kinetically, i.e., not assuming instant equilibrium between gas and aqueous phase. The relevant Henry's law coefficients are provided in this section.

2.3.4.1 WET DEPOSITION PROCESSES

The parameters needed to evaluate the rates of the processes leading to wet deposition are the partition coefficients for gas-phase degradation products into liquid water (the effective Henry's constants, H_{eff}), and on to ice surfaces (the Langmuir equilibrium constants, K_{eq}). Henry's constants were given for HOX and XONO₂ (X = Br and I) in the last Assessment. Subsequently, an exten-

VERY SHORT-LIVED SUBSTANCES

sive database that covers these and other compounds including HCl, HBr, HI, ClONO₂, HOCl, BrCl, Br₂, I₂, ICl, and IBr is available from the National Institute of Standards and Technology (NIST) webbook (<http://webbook.nist.gov/chemistry/>). H_{eff} values for these species and for the organic chlorine reservoir COCl₂ are given in Table 2-6. The tropospheric removal of this and similar halogenated carbonyls was considered in depth in WMO (1995), and the conclusion that these compounds are relatively rapidly removed by precipitation remains valid.

A substantial amount of new data for trace gas-ice interaction at temperatures of the upper troposphere/lower stratosphere (UTLS; 200-230 K) has been reported from laboratory and field studies (Abbatt, 2003; Popp et al., 2004). Partitioning of HX (X = Cl or nitrate, NO₃) to the ice phase occurs by Langmuir-type adsorption, in which the amount of material adsorbed is normally limited to sub-monolayer surface coverage, depending on the partial pressure of the gas and the Langmuir equilibrium constant, K_{eq} ($= k_{\text{adsorption}}/k_{\text{desorption}}$). The surface coverage, θ (mole cm⁻²), is given in terms of N_s (the maximum coverage in

Table 2-6. Henry's Law constants (H , in units of moles per liter per atmosphere) and uptake coefficients (γ_{het}) for heterogeneous processing of inorganic halogens.

	H_{298} (M atm ⁻¹)	γ_{het}				
		H ₂ O _(l)	H ₂ O ice	H ₂ O ice HCl/HBr doped	Sulfuric acid, H ₂ SO ₄ (aq)	H ₂ SO ₄ (aq) HCl/HBr doped (X = Cl, Br)
HOCl	260	–	$\gamma_0 > 0.2$ saturates ^a	0.3	time dependent	0.02-0.2 ^a dependent on H_{HOX} and H_{HX}
HOBr	93-1900	>0.01	0.3	0.004-0.3	>0.01 ^b	0.1-1
HOI	>45	–	–	0.05	0.015-0.07 ^b	>0.02
ClONO ₂	hydrolysis	0.024 ^c	–	0.3-0.6	dependent on [H ₂ SO ₄], H , and T	dependent on H_{HX} ^a
BrONO ₂	hydrolysis	0.06 ^c	>0.3	>0.2 ^b	>0.2 ^c	0.9 (H ₂ SO _{4(s)})
IONO ₂	hydrolysis	>0.1 ^c	–	>0.05 ^b	>0.3 ^c	–
Cl ₂	0.093	–	>0.2 (+HBr _(g))	–	–	–
Br ₂	0.76	–	–	–	–	–
I ₂	3.3	5×10^{-4}	–	0.02 (HI doped)	–	–
BrCl	0.94	<0.03	–	–	–	–
ICl	110	–	0.02	0.3	–	–
IBr	24	–	0.03	0.3	–	–
HCl	$1.1^*(K_a = 10^7)^d$	physical uptake only				
HBr	$0.71^*(K_a = 10^9)^d$	physical uptake only				
HI	$2.5^*c(K_a = 3.2 \times 10^9)^d$	physical uptake only				
COCl ₂	0.07^f					

* $H_{\text{eff}} = H_{298} \times \exp(-\Delta H_s/R \times (1/T - 1/298)) \times (1 + K_a/[H^+])$ (K_a = acidity constant)

^a <http://www.iupac-kinetic.ch.cam.ac.uk/>

^b Protonation followed by reaction to form dihalogens.

^c Reaction leading to hydrolysis to form HOX, where X = Br, I.

^d The dissociation constants are from Arnaud (1966), or see Schweitzer et al. (2000).

^e The physical constant is from Marsh and McElroy (1985).

^f Slow hydrolysis occurs; see WMO (1995).

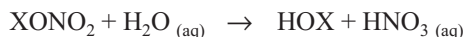
molec cm⁻² at saturation), K_{eq} , and the gas partial pressure of the gas (P_{HX}):

$$\theta = N_s \frac{K_{eq} P_{HX}}{1 + K_{eq} P_{HX}}$$

For uptake on ice, the value of N_s is approximately 3×10^{14} molec cm⁻² (Abbatt, 2003). At UTLS temperatures, nitric acid (HNO₃) and HX (X = Cl, Br, I) are strongly adsorbed and the process is important. Weak acids and organic species are generally weakly adsorbed and do not partition efficiently to ice. When formation of long-lived compounds (e.g., nitric acid trihydrate: NAT) is thermodynamically favored, there is a greater capacity for partitioning, since adsorption is not confined to the surface layer.

2.3.4.2 HETEROGENEOUS HALOGEN ACTIVATION

Conversion of stable inorganic halogen reservoirs, which are removed by deposition, into reactive halogen radicals potentially lengthens the lifetime of inorganic halogen because the reactive products remain in the gaseous phase. The key heterogeneous reactions (where X and Y are atoms of Br, Cl, or I) leading to release of reactive halogens are:



These reactions can occur in aqueous aerosols (water, sulfuric acid, sea salt) or on ice or solid aerosol, and XY is partitioned into the gas phase where it is photolyzed.

Heterogeneous reaction kinetics are expressed in terms of dimensionless reactive uptake coefficients, γ_{het} , which allow the rate to be evaluated on a per-collision basis for a prescribed surface area of the condensed phase. Table 2-6 provides a summary, extended since the last Assessment, of representative γ_{het} values for surfaces relevant for the troposphere and the stratosphere. These are based on the updated IUPAC and JPL evaluations, and other recent literature sources.

The large uptake coefficients of halogen nitrates (XONO₂, where X = Cl or Br) into aqueous droplets (Deiber et al., 2004) means that uptake in liquid water clouds will be efficient, and since concentrations of bromide and iodide in precipitating clouds are likely to be very small, wet deposition will predominate over activation. Evaporating cloud droplets, however, will lead to

reactive halogen recycling. Model calculations have suggested that uptake into cloud droplets can extend reactive halogen lifetime and lead to a vertical redistribution of inorganic bromine compounds (von Glasow et al., 2002). In their global model runs, von Glasow et al. (2004) showed that heterogeneous reactions can extend the lifetime of Br_y from about 6-9 days to about 9-15 days below 500 hPa, with smaller changes in the free troposphere. A laboratory study showed the release of labile dibromine monoxide (Br₂O) and molecular bromine (Br₂) from sulfuric acid solutions following exposure to the soluble species hypobromous acid (HOBr) and hydrogen bromide (HBr) (Iraci et al., 2005). These observations suggest that the PGI of Br_y species should be evaluated for various aerosol and cloud washout lifetimes.

Activation of halogens can also occur on ice surfaces, such as those in cirrus clouds. Laboratory studies have shown that Cl and Br activation by reaction of chlorine nitrate (ClONO₂) and HOBr with hydrogen chloride (HCl) on ice surfaces at UTLS temperatures scale linearly with the surface coverage of HCl (Mössinger et al., 2002; Fernandez et al., 2005). At typical tropospheric HCl concentrations, the rate of activation of bromine on ice clouds is probably fast, but chlorine activation is less efficient. Nevertheless recent field observations (Thornton et al., 2003) suggest that Cl activation is occurring on cirrus clouds, leading to the local production of ClO.

2.3.5 Iodine Chemistry

All iodine source gases with significant emissions fall into the category of halogenated VSLs. However, ozone destruction in the lower stratosphere due to catalytic cycles involving iodine remains poorly understood. New information on the chemistry of iodine species relevant for the atmosphere has been obtained since the WMO (2003) Assessment. The new chemical kinetics information may have significance for the efficiency of transport of iodine species to the UTLS and the ozone destruction efficiency factor for stratospheric I_y. Relevant multiphase iodine chemistry is presented in Section 2.3.4 above.

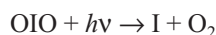
The IUPAC and JPL kinetics evaluations have critically reviewed all but the most recent kinetic and photochemical studies. Rate coefficients for the reactions of atomic iodine (I), IO, and nitric oxide (NO) with OIO (Joseph et al., 2005; Plane et al., 2006), and IO with methyl peroxy radicals (CH₃O₂) (Bale et al., 2005) have since been reported (in units of cm³ molec⁻¹ s⁻¹) to be 1.1×10^{-10} , 1.2×10^{-10} , $7.6 \times 10^{-13} \exp(607/T)$, and 6.0×10^{-11} , respectively (rates are for room temperature only, except where noted). New photolysis quantum yield studies for OIO have also been reported (Joseph et al., 2005; Tucceri et al.,

VERY SHORT-LIVED SUBSTANCES

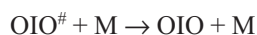
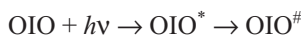
2006). The OIO quantum yield (Φ) measurements indicate $\Phi(\text{O}(^3\text{P})) < 0.007$ at 532 nm and between 558 and 578 nm, and $\Phi(\text{I}) < 0.24$ at 532 nm and < 0.05 between 560 and 580 nm. Photolysis quantum yields at longer wavelengths have not yet been reported.

Reactions between halogen monoxide radicals have several product channels. The efficiency of ozone (O_3) loss depends on the halogen species and the product yields. For example, the IO self-reaction produces OIO (~40%) and iodine oxide dimer IOIO (~55%) at 1000 hPa (Bloss et al., 2001). The IOIO product is unstable (Misra and Marshall, 1998) and most likely rapidly thermally decomposes to yield OIO. Therefore, the effective OIO yield from the IO self-reaction is high. The efficiency of O_3 loss is reduced by photolysis of the halogen dioxides formed in the IO + IO and IO + BrO reactions, if an oxygen atom is produced.

OIO has a series of strong diffuse absorption bands in the region between 470 and 610 nm, but only the I atom-producing channel is energetically possible:



The alternate channel producing IO + O leading to no net O_3 loss requires wavelengths < 470 nm. Recent laboratory studies (Joseph et al., 2005) show that OIO absorption at 562 nm leads to internal conversion from the excited state (OIO^*) to the vibrationally excited ground state ($\text{OIO}^\#$), rather than dissociation:



Nevertheless, a small probability of photolysis, integrated over the entire OIO absorption band, could still lead to significant photochemical conversion of OIO to I and consequent ozone loss.

Studies have shown that higher iodine oxides can nucleate to form new particles (Hoffmann et al., 2001; O'Dowd and Hoffmann, 2005). The formation of OIO in the gas phase appears to initiate this process. In the atmosphere, the oxidation of OIO by reaction with IO or OIO may lead to the formation of higher oxides (e.g., I_2O_3 and I_2O_4) that are of low volatility and may condense on pre-existing particles, providing a sink for reactive iodine. This is different from the oxidation mechanisms of chlorine and bromine oxides that do not lead to the formation of unreactive low-volatility oxides. This mechanism provides a possible explanation for the absence of detectable IO concentrations in the UTLS from degradation of iodocarbons, while the BrO radical derived from the oxi-

lation of bromine source gases is clearly present in this region (see Sections 2.2.5 and 2.5).

2.4 DYNAMICS AND TRANSPORT IN THE TROPOPAUSE REGION AND IMPLICATIONS FOR VSLS

The distribution of VSLS is governed by the distribution of surface sources, and by competition between vertical transport (boundary layer to free troposphere to stratosphere) and chemical destruction or removal via washout. The implication for VSLS-related stratospheric ozone loss therefore depends crucially on the strength and spatial distribution of transport processes, and of the chemical, microphysical, or moist processes that remove the degradation product gases (PGs). Note in particular (see following sections) that rapid vertical transport, which potentially takes VSL SGs and PGs from the boundary layer to the tropopause region, is usually associated with moist processes (warm conveyor belts, convective clouds) that can potentially remove soluble PGs through washout. Nevertheless, such processes are potentially effective in the vertical transport of total bromine (or other halogens), since the time scale for such transport in an individual convection event (hours) is short compared with the time scale for chemical breakdown of the VSLS.

Given that VSL SGs and PGs reach the upper troposphere through potentially rapid transport mechanisms, it is important to establish how rapidly they are subsequently transported into the stratosphere via the SGI and PGI pathways. A schematic depiction of transport processes in the upper troposphere and lower stratosphere relevant to VSLS is shown in Figure 2-1. There is net transport across the tropopause from troposphere to stratosphere in the tropics and net transport across the tropopause from stratosphere to troposphere in the extratropics, with this net transport controlled by global-scale processes as part of the Brewer-Dobson circulation (Holton et al., 1995). However, when considering VSLS, it is particularly important to note first, that transport across the tropopause is in fact two-way, especially at mid-latitudes, with both troposphere-to-stratosphere transport (TST) and stratosphere-to-troposphere transport (STT), and second, that the transition from tropospheric chemical characteristics to stratospheric chemical characteristics takes place not in a sharp jump across a uniquely defined tropopause, but across a finite tropopause transition layer, most notably in the tropics. In the tropics, it is now conventional to describe the transition layer as the "tropical tropopause layer" (TTL). It is now clear that in the extratropics there is a corresponding "extratropical tropopause

layer” (ExTL). In both the tropics and the extratropics, large-scale and small-scale processes together play important roles in determining the structure of the tropopause layers. Representing these processes correctly poses particular difficulties for global chemical models. In the following, the tropics, including the tropical tropopause layer, and both vertical and quasi-horizontal exchange to the stratosphere, are discussed in Section 2.4.1. The extratropics and the extratropical tropopause layer are discussed in Section 2.4.2, and the representation of relevant processes in global models is discussed in Section 2.4.3.

2.4.1 Tropical Convection, the TTL, and Tropical Troposphere-to-Stratosphere Transport

The lower part of the tropical troposphere is dominated by ascent in convective clouds. The outflow from these clouds is concentrated in two distinct layers, a lower layer from about 2 to 5 km (800-550 hPa), and an upper layer from about 10 to 15 km (300-150 hPa). The compensating descent in the regions surrounding the clouds is associated with evaporative cooling in the lower layer, and radiative cooling in the upper layer (e.g., Folkins and Martin, 2005). In the lower part of the troposphere, moist convection can efficiently transport chemical species vertically via strong convective updrafts, but at the same time, the scavenging associated with convective precipitation can efficiently remove the soluble species (Crutzen and Lawrence, 2000; Mari et al., 2000; Barth et al., 2001). Studies using explicit modeling of convection have shown that scavenging in warm clouds should be considered as a kinetic rather than an equilibrium process (Yin et al., 2001; Barth et al., 2001). Such treatment is not included in the vast majority of global chemical models.

So far, the observational data on soluble species in the entrainment and detrainment zones of isolated or organized convective systems in the tropics that might better constrain these model results are still very limited. In cold clouds, as liquid water freezes and riming occurs around ice, chemical species are also absorbed into ice crystals by various processes, such as bubble inclusions within crystals. A limited number of field laboratory and theoretical studies have proposed trapping coefficients of chemicals in ice (e.g., Stuart and Jacobson, 2003; Krämer et al., 2006; see also Section 2.3.4.1). The current experimental data are apparently inconsistent, poorly understood, and only available for a limited set of chemical species (e.g., HCl, HBr). Parameterization of scavenging by ice crystals is only now being implemented in global models (Kärcher and Basko, 2004). For example, it has been found that if the gas retention coefficient (the frac-

tion of dissolved gas that is retained as a liquid droplet freezes) of a highly soluble gas is allowed to vary in a relatively narrow range (0.5-1.0), the corresponding bulk gas transport within the cloud varies, for maritime clouds, by as much as a factor of 4 (Yin et al., 2002). See also Section 2.3 for a discussion of washout and solubilities of VSL SGs and PGs. In addition, the microphysical structure of convective clouds and ice clouds is highly sensitive to the boundary layer aerosol concentration and shows variations between, for example, maritime and continental clouds (Yin et al., 2002; Kärcher and Lohmann, 2003; Nöber et al., 2003; Ekman et al., 2004). This has implications for the concentration of trace gases inside anvil ice crystals.

The part of the tropical atmosphere above the level of maximum convective outflow (at about 12 km altitude, 345K potential temperature), and below the cold point tropopause (at about 17 km altitude, 380K potential temperature), is now commonly described as the TTL (see, for example, WMO, 2003; Gettelman and Forster, 2002). This definition of the TTL, equivalent to the “sub-stratosphere” of Thuburn and Craig (2002), has it as the region of the troposphere in which there is a transition between radiative-convective domination and radiative domination of the thermal balance. The TTL acts as a source region both for the stratospheric overworld and for the extratropical lowermost stratosphere (see Figure 2-1). Net exchange from the TTL to the stratospheric overworld in the tropics, say across the 100 hPa level as an approximation to the cold point tropopause, is regarded as dominated by large-scale ascent in the Brewer-Dobson circulation, with the strength of this circulation controlled by large-scale dynamical processes (e.g., Holton et al., 1995).

The overall picture of TTL processes is somewhat updated from WMO (2003), though estimates of transport time scales between the boundary layer and the lower part of the TTL are largely unchanged. A useful recent description of the relevant processes is given, for example, in Folkins and Martin (2005). In the “lower TTL” (12-15 km, 345-360K), convective penetration is sufficiently frequent so that most of the air detraining from convection descends to the lower troposphere. The upward mass flux in convective clouds, the magnitude of the radiative cooling outside the clouds, and hence the magnitude of the implied descent decays with height. Küpper et al. (2004) give estimates of the upward cumulus mass flux as a function of height from various modeling and data studies, but note that there are significant difficulties in estimating this flux. At a level z_0 (the level of zero radiative heating) of about 15 km or 360K, there is a transition from clear-sky radiative cooling to clear-sky radiative

VERY SHORT-LIVED SUBSTANCES

heating. Only above z_0 in the “upper TTL” (15-17 km, 360-380K), where the upward cumulus mass flux is comparable to or less than the large-scale upward mass flux in the Brewer-Dobson circulation, does most air detraining from clouds ascend into the stratosphere.

Note at this stage that the TTL has been defined by some authors (e.g., Folkins et al., 1999; Sherwood and Dessler, 2001; Füglistaler et al., 2004; Sinnhuber and Folkins, 2006) to be only this “upper TTL,” i.e., only as the region above z_0 . This definition is based on sound reasoning, but for consistency with WMO (2003) it is not adopted here, and the terms “lower TTL” and “upper TTL” are used as introduced previously.

Gottelman et al. (2004) noted that clouds reach the typical level z_0 (in their case identified by cloud brightness temperature <200K) only in relatively localized geographical regions, implying that air that is likely to ascend into the stratosphere is drawn from the surface in similarly localized regions. An equivalent statement is that the transport time scale from the surface to the upper TTL is likely to be significantly less in these localized regions than on average over the tropics. Such regions include the Western Equatorial Pacific during October to March (with a continuing but lesser role in other months) and the Bay of Bengal, Southeast Asia, and Panama regions during April to September (e.g., see Gottelman et al., 2004; Figure 9).

Somewhat similar conclusions to the above follow from recent trajectory calculations based on European Centre for Medium-Range Weather Forecasts (ECMWF) three-dimensional wind fields. In particular, the trajectory calculations of Füglistaler et al. (2004) show that air that ultimately ascends into the tropical lower stratosphere crosses the lower boundary of the TTL preferentially in the West Pacific region in Northern Hemisphere winter and in a region centered on southeast Asia, but extending toward India and into the West Pacific, in Northern Hemisphere summer. The longitudinal variation of transport across the lower boundary of the TTL, according to the Füglistaler et al. (2004) calculations, is shown in Figure 2-5. It should be noted that the wind datasets on which such trajectory calculations are based do not resolve individual convective cells and, therefore, that any results need cautious interpretation. Nonetheless, the overall behavior of the calculated trajectories is broadly as expected from the schematic picture of the TTL outlined previously. For example, the probability of ascent of forward trajectories into the stratosphere rapidly increases with the height of trajectory initialization.

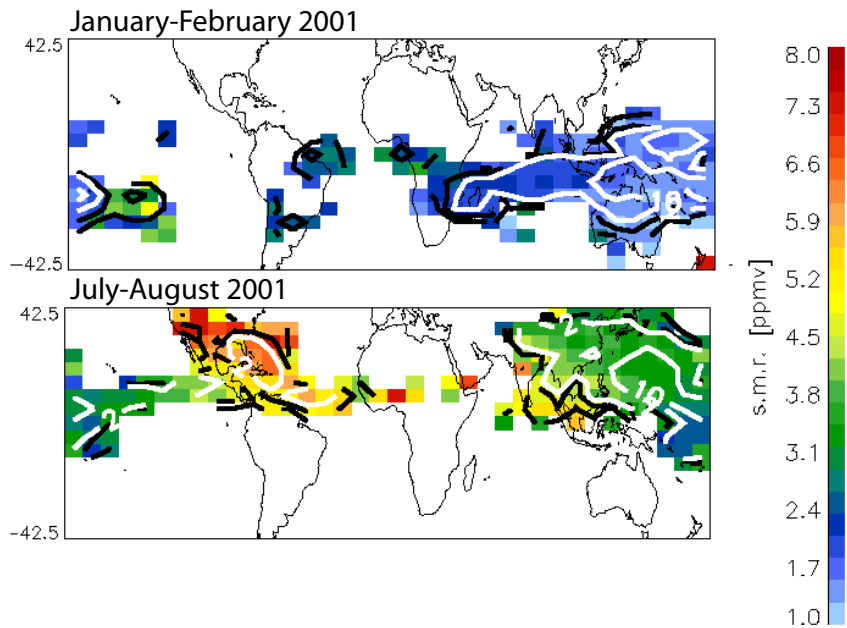
The Füglistaler et al. (2004) trajectory calculations predict a residence time (the time for forward trajectories to move up or down by 10K in terms of potential temperature) that is maximum (about 12 days) for trajectories

starting at 360K (corresponding to z_0) and decreases to about 9 days for a layer centered at 370K. This implies a residence time for the 360K-380K layer of about 20 days. This is expected to be an underestimate, since it is expected that such transport calculations, through their use of vertical winds from meteorological datasets, overestimate vertical transport rates (both net transport and dispersion). On the other hand, the time scale of about 80 days to cross the 360-380K layer that has been inferred from a one-dimensional tropical-mean model (Folkins and Martin, 2005) is almost certainly an overestimate, since it neglects the dispersive effects of geographical variation in vertical velocity. On the evidence currently available, therefore, the residence time for air parcels in the 360K-380K layer is likely to be somewhat greater than 20 days. New calculations based on improved meteorological datasets, or using radiative transfer codes to calculate vertical velocities, are likely to refine this estimate of residence time in the near future. Transport time scales for the upper TTL (20 to 80 days on the basis of the Füglistaler et al. (2004) and Folkins and Martin (2005) results mentioned above) are expected to be significantly longer than those for the lower TTL, i.e., about 10 days on the basis of typical cumulus mass fluxes estimated by Küpper et al. (2004). It is therefore inappropriate to assign a single transport time scale to the whole TTL extending from the maximum in convective outflow to the cold point. This point was noted in WMO (2003), but was confused by also giving estimates for a single turnover or replacement time of 10 to 13 days for the 250 hPa-100 hPa layer (i.e., the whole TTL by the more common definition).

The consequence of the longer timescale in the upper TTL for injection of VSLS is not yet clear; there might be more time for conversion from SG to PG, but the net effect of this on total halogen entering the stratosphere is likely to be small. A more important issue is whether there is significant scavenging of PGs in the upper TTL associated with uptake on cirrus clouds (see Section 2.3.4), thus limiting the transport of halogen into the stratosphere via the PGI pathway.

As noted previously, upward transport out of the TTL into the stratosphere is understood to be primarily controlled by large-scale dynamical processes, and there has been no reason to revise significantly net flux estimates over those given previously (e.g., Rosenlof, 1995). However, there have been recent changes in temperatures of the tropical lower stratosphere (e.g., Randel et al., 2004), with a significant reduction in temperatures more recently, i.e., 2000-2004 appears to be 1K cooler than the period 1995-1999. Implications for stratospheric water vapor are discussed in Chapter 5 of this Assessment. Simple dynamical arguments imply that this may be

Figure 2-5. Results of 2-month backward trajectory calculations, using three-dimensional winds from ECMWF operational analysis data, reported by Füglistaler et al. (2004). The backward trajectories were to points distributed evenly over the 400K surface in the tropics. The contour lines indicate the density of intersections of the backward trajectories with the 340K surface (corresponding roughly to the lower boundary of the TTL), relative to the density of such intersections if spread uniformly over the globe. The upper and lower panels show the density calculated from trajectories followed over the periods January-February 2001 (Northern Hemisphere (NH) winter) and July-August 2001 (NH summer), respectively. The conclusion is that air parcels reaching the tropical lower stratosphere are in NH winter drawn preferentially from the lower troposphere in the Western Pacific and, to a lesser extent, the Indian Ocean region. In the NH summer, the corresponding regions include the West Pacific, but extending significantly over Southeast Asia. (The color scale indicates the average mixing ratio of water vapor determined by the minimum saturation mixing ratio along each trajectory and assigned to the point of intersection of that trajectory with the 340K surface. See Chapter 5, Sections 5.2.5 and 5.3.5 for further discussion of water vapor and its implications for ozone.)



explained by a 10% increase in the upward mass flux out of the TTL, and that this is driven by changes in large-scale dynamical processes (Randel et al., 2006). It is, however, impossible to predict how long the current anomalously large upward mass flux will persist.

Exchange between the TTL and the extratropical lowermost stratosphere is achieved through quasi-horizontal transport associated with synoptic-scale eddies. This has been apparent for some time on the basis of observations of subtropical filaments in midlatitudes (e.g., Vaughan and Timmis, 1998; O'Connor et al., 1999), water vapor observations (e.g., Dessler et al., 1995) and, more recently, chemical observations in the extratropics (see Section 2.4.2). Trajectory and similar transport calculations based on meteorological data also show the possibility of such transport, particularly above the level of the subtropical jet (Chen, 1995; Haynes and Shuckburgh, 2000). Both direct observations of the chemical composition of the extratropical lowermost stratosphere (e.g., Randel et al., 2001; Prados et al., 2003) and transport calculations imply that transport from the TTL to the lowermost stratosphere is, at least in the Northern Hemisphere, highly seasonal, with much greater transport in summer

than in winter. The air in the extratropical lowermost stratosphere may be regarded as a mixture of air that has been transported from the TTL, and air that has descended from the stratospheric overworld. The fraction of air from the TTL has been estimated by Hoor et al. (2005), on the basis of observed concentrations of carbon monoxide (CO) and of the carbon dioxide (CO₂) seasonal cycle, to be about one-third in winter, perhaps increasing to about one-half in summer. Similar conclusions have been obtained from other datasets.

Recent trajectory calculations of Levine et al. (2006) for Northern Hemisphere winter show that more than 75% of the air that enters the TTL, and subsequently reaches the stratosphere, does so through quasi-horizontal transport into the extratropical stratosphere. It is likely that this fraction will be larger in summer than in winter. It is interesting that, according to the Levine et al. (2006) calculations, the distribution of the entry locations of such air through the base of the TTL is spread relatively uniformly in longitude, in contrast to the corresponding contribution for air that subsequently reaches the tropical lower stratosphere. Note also that while the strength of this quasi-horizontal exchange with the extratropics is not

VERY SHORT-LIVED SUBSTANCES

uniform with height, there is little reason to believe that convective penetration to the level z_0 has the same significance for such exchange as it does for exchange with the stratospheric overworld, since the quasi-horizontal exchange transport is not strongly affected by the direction of slow vertical motion.

A final issue concerns the spatial structure of chemical fields within the TTL. There is no reason to expect chemical fields to be homogeneous. Recent in situ observations have shown complex spatial structure in this region in chemical species with a whole range of lifetimes (e.g., Tuck et al., 2004) apparently resulting from several different mechanisms including different surface source regions, and transport out of the extratropical stratosphere. The spatial structure of VSL SGs and PGs are expected to be correspondingly variable.

2.4.2 Stratosphere-Troposphere Exchange in the Extratropics

Transport from the tropical upper troposphere to the extratropical lower stratosphere has been discussed in the previous section. There is also significant transport directly from the extratropical troposphere to the extratropical lower stratosphere, particularly in summer (e.g., Hintsä et al., 1998; Pan et al., 1997). However, the high static stability in the lower stratosphere, and the fact that the average circulation is downward, limit the vertical penetration of tropospheric air. The result is a finite transition layer (the ExTL) in which chemical characteristics vary continuously between the extratropical upper troposphere and lower stratosphere (see Figure 2-1). In principle, this transition layer is a region in which concentrations of VSL SGs and PGs may be relatively high, and in which substantial in situ ozone loss due to VSLS may take place. However, typical ozone mixing ratios in the ExTL are 300 parts per billion (ppb) or less, which limits the possible impacts on the ozone column.

Chemical measurements in the ExTL have increased significantly since WMO (2003). The location of the ExTL can be deduced, for example, from ozone, carbon monoxide (CO), total reactive nitrogen (NO_y), and water vapor (H_2O) data collected as part of the Stratosphere-Troposphere Experiments by Aircraft Measurements (STREAM) and the German Spurenstofftransport in der Tropopausenregion (SPURT) programs (Hoor et al., 2002; Fischer et al., 2000; Hoor et al., 2004; Krebsbach et al., 2006; Engel et al., 2006), which also show that the layer is deeper in summer, with a stronger tropospheric influence, than in winter. Note that CO has a short chemical lifetime of 2 to 3 months, making it a useful proxy for VSLS transport into the lower stratosphere. The

upper limit of the ExTL has been estimated from enhanced CO and H_2O mixing ratios to be about 25K in potential temperature above the local tropopause defined by the 2 PVU (potential vorticity unit) surface, corresponding to about 2 km in height. Pan et al. (2004) identified the transition layer using aircraft data and characterized it as centered on the thermal tropopause, and about 2-3 km thick. Note that the thermal tropopause is usually above the tropopause defined by the 2 PVU surface.

Alongside the new observations of chemical species in the extratropical tropopause region, many recent studies have used trajectory calculations based on winds from large-scale meteorological datasets to investigate vertical transport processes, such as in the large body of work coordinated in the STACCATO (Influence of Stratosphere-Troposphere Exchange in a Changing Climate on Atmospheric Transport and Oxidation Capacity) project as summarized in Stohl et al. (2003). An important conclusion relevant to VSLS has been that warm conveyor belts associated with synoptic-scale baroclinic eddies, and associated frontal zones, play an important role in rapid transport from the boundary layer to the tropopause region. One consequence is that rapid upward transport tends to originate from the boundary layer in preferential longitudinal regions, such as the midlatitude storm track regions east of Japan and east of the U.S. (e.g., Sprenger and Wernli, 2003; see Figure 2-6 for further details). Surface emissions (e.g., anthropogenic or coastal VSLS) in these regions may therefore be more likely to contribute to the chemical composition of the extratropical tropopause region. The importance of warm conveyor belt transport, and the usefulness of trajectory calculations for studying such transport, have been confirmed in various case studies. For example, Nedelec et al. (2005) showed very high CO concentrations arising from Siberian fires observed by MOZAIC (Measurement of Ozone, Water Vapor, Carbon Monoxide and Nitrogen Oxides by In-service Airbus Aircraft) aircraft in the lower stratosphere.

Trajectory studies have confirmed that many air parcels moving from the boundary layer to the tropopause region remain in that region for several days (e.g., Wernli and Bourqui, 2002; Sprenger and Wernli, 2003), thus implying that VSL SGs or PGs transported into the very low stratosphere could have an impact on ozone loss. Since stretching rates of material surfaces in the extratropical tropopause region (which give an indication of the rate at which an anomalous air mass is stirred with, and eventually mixed with, its environment) are of the order of a few days (e.g., Stohl, 2001), it seems very unlikely that air masses arriving in the tropopause region

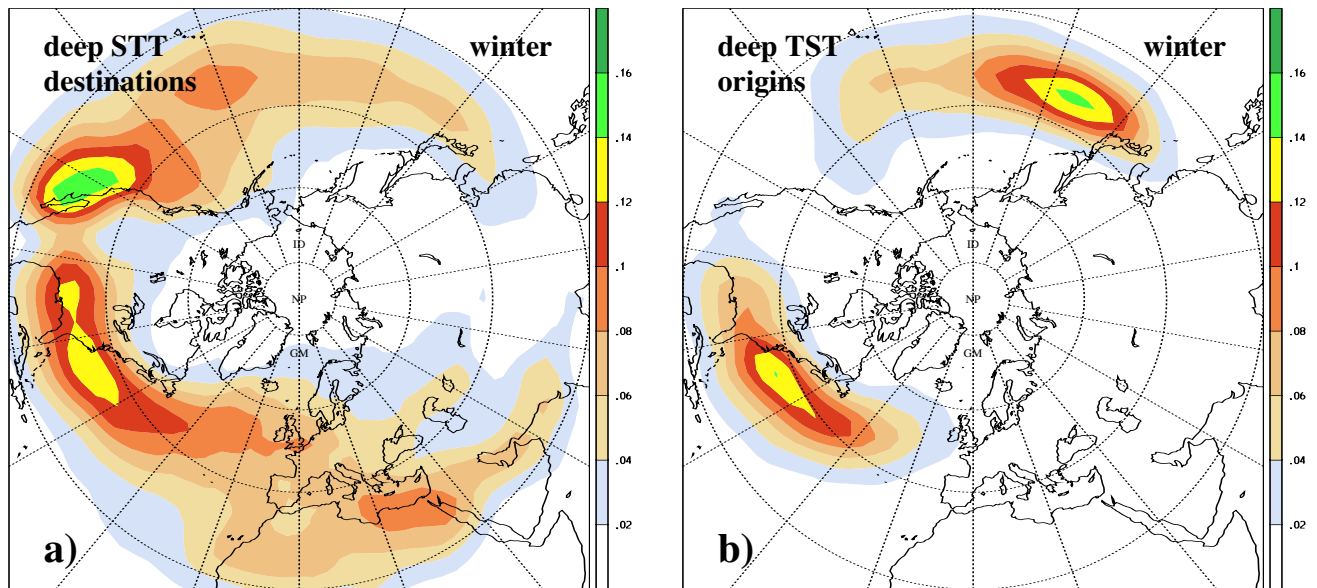


Figure 2-6. Geographical distribution of the (a) low tropospheric “destinations” of deep STT and (b) low tropospheric “origins” of deep TST events during winter. Values are in % and correspond to the probability that a low tropospheric air parcel (pressure > 700 hPa) was transported downward from the lowermost stratosphere during the previous four days (deep STT) or will be transported upwards into the lowermost stratosphere during the next four days (deep TST). The implication of (b) is that the probability of rapid transport from the surface to the tropopause region is strongly dependent on geographical location (at the surface). From Sprenger and Wernli (2003).

are predisposed to descend rapidly, but instead are likely to mix into the background.

Trajectory studies for the SPURT dataset (Hoor et al., 2004) imply that the composition of the ExTL is influenced by recent transport from the troposphere on time scales of days to a few weeks. While trajectory studies might be expected to capture the effects of warm conveyor belts, they almost certainly miss the effect of smaller-scale processes such as deep convection or convection embedded in frontal systems. The quantitative effect of deep convective injection of tropospheric chemical species into the extratropical lower stratosphere remains relatively uncertain. There are some in situ chemical measurements that point very clearly to such injection (e.g., Poulida et al., 1996; Fischer et al., 2003), while other measurements have given no direct evidence of penetration of extratropical convection into the stratosphere (Ridley et al., 2004). There are also studies that combine chemical measurements with meteorological or trajectory studies that argue for such penetration (e.g., Hegglin et al., 2004). Dessler and Sherwood (2004) argue that convective penetration to the 380K surface in midlatitudes, while much less frequent than in the tropics, is frequent enough to have a significant effect on water vapor at these altitudes, though not on ozone since the relative difference in ozone

concentrations between troposphere and stratosphere is much smaller than the relative difference in water vapor concentrations.

Convection might contribute to troposphere to stratosphere transport (TST) directly by overshooting the tropopause at the anvil outflow (Mullendore et al., 2005), or indirectly by exciting gravity waves that break significantly above the convective clouds (Wang, 2003). Further, recent evidence for convective transport of low-altitude air into the lowermost stratosphere in the extratropics is provided by in situ observations in the stratosphere that show clear evidence of biomass burning products such as CO and aerosols, apparently arising from forest fires over Canada (e.g., Ray et al., 2004). Fromm and Servranckx (2003) have suggested that enhanced convective cells associated with the fires themselves may be very likely to penetrate the lower stratosphere; terms such as “pyro-convection” or “pyro-cumulonimbus” are becoming widely used to describe this phenomenon (e.g., Fromm et al., 2005). While the occasional penetration of pyro-convection events into the lower stratosphere has been observed, it is not clear at present that the pyro-convection has a significant effect on the overall chemical balance of the extratropical lowermost stratosphere.

VERY SHORT-LIVED SUBSTANCES

2.4.3 Predictive Modeling of the Tropopause Region

Predictive modeling of the impact of VSLS on ozone depends on model representation of the processes discussed in Sections 2.4.1 and 2.4.2. In the tropics, the greatest challenge for models is representing convective processes, although in the TTL the subtle interplay between different processes, and the fact that significant changes in dynamical and chemical characteristics take place over 2-3 km, also present a challenge. In the extratropics, the transport characteristics of synoptic-scale eddies, and their interplay with smaller-scale processes, must be captured. These smaller-scale processes include gravity wave breaking, turbulence in the vicinity of jet streams, and radiative processes associated with upper level clouds. From the chemistry point of view, the representation of soluble species, as well as aerosols and microphysical processes, is still poor in global models. Scaling up the heterogeneous reactions on ice and aerosols to realistic parameterizations is still a major challenge for prediction of the tropopause region. Uncertainties in surface and lightning emissions may cause significant biases in simulating the chemical composition of the upper troposphere.

The parameterization of tropical convective processes in global-scale models remains a conceptual challenge, with different theoretical approaches possible. Basic thermodynamics are not well characterized, while transport and scavenging processes are even less well understood. One widely used method for parameterizing convective transport processes is based on the mass-flux formulation (Arakawa and Schubert, 1974), in which transport processes are represented by an ensemble of vertical mass fluxes at subgrid scales. This formulation however was originally developed for representing the subgrid-scale thermodynamic effects (phase changes and fluxes of heat and moisture) of convection, and its generalization to chemical transport processes is not straightforward (Donner et al., 2001). Lawrence and Rasch (2005) have shown that, for a single convection parameterization, differences in the implementation of detrainment and entrainment fluxes can result in significant differences in the upper tropospheric mixing ratios of short-lived tracers (lifetimes of a few days or less). In particular, the bulk formulation of convection, widely used in global models, in which entrainment and detrainment are each assumed to occur at a single level, may lead to underestimation of up to 30% in zonal and monthly mean concentrations of such tracers, relative to, for example, a more sophisticated formulation in which a distribution of entrainment and

detrainment levels is assumed. One implication of the above is that VSLS could play an even more important role in the upper troposphere than previously thought.

Detailed evaluation of cumulus parameterizations, in comparison with observations and cloud resolving models, have recently taken place both with respect to thermodynamics (Yano et al., 2004) and with respect to tracers (Bell et al., 2002; Collins et al., 2002). More accurate estimates of mass fluxes, based on high-resolution data from either observations or modeling, could lead to improved parameterizations of these convective transports. Evaluation of the mass flux formulation against high-resolution spatial data obtained from explicit numerical models reveals that, in its standard form, it substantially underestimates vertical transport of heat, moisture, and momentum by deep convection (Yano et al., 2004), with improvement possible through nonlinear averaging of the large-scale variables. Similar issues will almost certainly arise in the convective transport of chemical tracers.

Notwithstanding these recent results on convective transport and scavenging effects (see Section 2.4.1), current global models necessarily make significant simplifications in their representation of convective transport and scavenging processes. In some models the two are linked (e.g., Considine et al., 2005), whereas in others the two are completely separate. Lack of relevant observations and model simulations means that there has been no systematic validation of model representation of convective processes acting on halogenated VSLS against observations. Historically, model representations of such processes have been validated against observations of radon and lead mixing ratios. Lead-210 (^{210}Pb) is produced in the atmosphere by radioactive decay of radon-222 (^{222}Rn), which has a radioactive half-life of 3.8 days. Lead-210, which has a radioactive half-life of about 22 years and can therefore be considered radioactively stable for this purpose, is removed by attachment to aerosols and washout. Most recently, building on the large amount of previous work on this subject, Considine et al. (2005) have presented an inter-comparison of ^{222}Rn and ^{210}Pb calculated by the NASA Goddard GMI (Global Modeling Initiative) model using meteorological fields from three different general circulation models (GCMs)/data assimilation systems, and comparison with observations. The three different simulations show some common discrepancies relative to observations and the authors deduce, in particular, that midlatitude convective transport may represent detrainment at too great an altitude, and that cloud scavenging frequency in midlatitudes may be too great. Convective transport is confirmed to play a very important role in setting upper troposphere and lower stratosphere concentrations that are in good agreement with observations, though part of this role may

be indirect, for example, in bringing species from the boundary layer to the upper troposphere, from which they can be transported effectively by the larger-scale circulations. These findings are all potentially relevant to model simulations of halogenated VSLs, though it is difficult to extrapolate results directly to model skill for predicting VSLs, since the chemical properties and the location and time of emissions of the VSLs will be different from these radioactive tracers.

In the extratropics, the role of convection is not as great as in the tropics, and the fact that many of the relevant processes are relatively large scale might seem to make this region more accessible to global chemical transport models and global chemistry-climate models. The success of trajectory studies based on meteorological wind fields in reproducing chemical distributions observed in field experiments is encouraging in this regard. However, “operational” resolutions used for global chemical models are still relatively coarse. Comparison between global models and chemical data (e.g., Brunner et al., 2003) has revealed the limitations of such models that, for example, overestimate the two-way transport in the tropopause region, resulting in excessive ozone in the upper troposphere and excessive CO in the lower stratosphere. This is an indication that, for current models, useful quantitative prediction of the effect of halogens from VSLs penetrating the lower stratosphere in the extratropics remains difficult.

2.5 CONTRIBUTION OF HALOGENATED VSLs TO STRATOSPHERIC HALOGEN LOADING

2.5.1 Source Gas Injection (SGI) and Product Gas Injection (PGI)

The concept of source gas injection (SGI) and product gas injection (PGI) into the stratosphere was described in Chapter 2 of the last Assessment (Ko and Poulet et al., 2003) as well as the introduction to this chapter. For SGI, the VSL source gas (SG) is transported to the stratosphere and then reacts to release halogen atoms. Supply to the stratosphere depends on emission location and time, as well as details of the tropospheric transport (e.g., convection) and troposphere-to-stratosphere exchange. For PGI, either intermediate (i.e., organic) products or final (i.e., inorganic) products are produced in the troposphere, and these species are transported to the stratosphere. The details of PGI depend on the same factors as SGI, plus factors such as the photochemistry of the source species, intermediate products, and final products. The gas-phase partitioning between

radical and longer lived inorganic reservoirs, as well as the solubility and heterogeneous reactivity of all species, are critical for assessing the efficiency of PGI (see Section 2.3). Indeed, differences in the efficiency of stratospheric supply of chlorine, bromine, and iodine from VSL organics might be due to differences in the photochemical properties of the respective inorganic products. Another important consequence of PGI is that measurements of the organic VSL SGs alone are not sufficient to determine the efficiency of stratospheric injection.

Injection of tropospheric particles into the stratosphere is another mechanism for cross-tropopause transport of halogens, depending on the chemical composition of the particles. The substantial organic content of many aerosol particles just above the tropopause suggests injection of tropospheric particles into the stratosphere, and the presence of Br on these particles suggests that cross-tropopause transport of bromine, in both directions, can occur by aerosols (Murphy et al., 1998; Murphy and Thomson, 2000). However, observations of this process are limited and, as a consequence, quantification of cross-tropopause halogen transport by aerosols is a considerable gap in our present state of knowledge. Most model simulations do not include cross-tropopause transport of halogens by aerosols in their estimates of PGI.

2.5.1.1 OBSERVATIONAL EVIDENCE FOR SGI

Bromine

Bromoform (CHBr_3) is thought to be the most abundant bromine-bearing VSL compound near the surface (Table 2-2). As noted previously in this chapter, CHBr_3 levels can reach or exceed 40 ppt near sea level (Yokouchi et al., 2005b). Observations reveal between ~0.2 ppt (Schauffler et al., 1998) and 1 ppt (Sturges et al., 2000) of CHBr_3 in the tropical free troposphere (see also Table 2-2). Measurements in the upper troposphere and tropopause region by Sturges et al. (2000) indicated CHBr_3 abundances of 0.5 ± 0.2 ppt for data collected during three flights (June and August 1998 and March 1999). Schauffler et al. (1998) measured 0.1 ppt of CHBr_3 at the tropical tropopause during February 1996. However, CHBr_3 was only detected at the tropical tropopause for one of three flight series that sampled this region. Bromoform exhibits similar variability near the midlatitude tropopause, ranging from near zero to a maximum abundance of ~0.7 ppt (Schauffler et al., 1999). The cross-tropopause transport of CHBr_3 is difficult to quantify from observations because of atmospheric variability and limited sampling. However, there are indications that, on

VERY SHORT-LIVED SUBSTANCES

occasions, values of CHBr_3 are high enough near the tropical tropopause for SGI of CHBr_3 to be important for the bromine budget of the lowermost stratosphere. Specifically, if the approximately 0.5 ppt of CHBr_3 measured near the tropical tropopause by Sturges et al. (2000) turns out to be representative of the average mixing ratio in the TTL, it would provide an SGI flux that could maintain an additional 1.5 ppt of Br_y .

The VSL species CH_2Br_2 and CH_2BrCl are less abundant near the surface than CHBr_3 , but are longer lived and therefore more likely to enter the stratosphere via SGI (Tables 2-1 and 2-3). Wamsley et al. (1998) showed that CH_2Br_2 and CH_2BrCl cross the tropopause, supplying ~2.3 ppt of Br_y by the SGI pathway. The total bromine content of the VSL species CH_2Br_2 , CH_2ClBr , CHCl_2Br , CHClBr_2 , and CHBr_3 was measured to be 2.2 ppt at the tropical tropopause during February 1996 (Schauffler et al., 1998) (see also the compilation in Table 2-2, which concludes a higher value of 3.5 ppt of bromine from these species). Plots of CH_2BrCl versus CFC-11, and CH_2Br_2 versus CFC-11, in the Wamsley study show that bromine from these compounds is released in the lowermost stratosphere (LMS), prior to the release of the majority of bromine from CH_3Br and halons. Bromine release in the LMS has important consequences for the photochemistry of this region. Significant supply of inorganic bromine (Br_y) leads to much faster ozone loss by two catalytic cycles represented by the rate-limiting steps defined by the BrO plus ClO , and BrO plus hydroperoxy radical (HO_2) reactions, compared with calculations that consider supply of bromine only from CH_3Br plus halons (Salawitch et al., 2005). A significant role for SGI injection of CH_2BrCl and CH_2Br_2 at all times, and lack thereof for CHBr_3 under some conditions, is consistent with their lifetimes for photochemical removal in the troposphere of 150, 120, and 26 days, respectively (Table 2-1).

Chlorine

Contributions to stratospheric inorganic chlorine (Cl_y) from VSL SGs are dominated by the species CHCl_3 , $\text{CH}_2\text{ClCH}_2\text{Cl}$, CH_2Cl_2 , $\text{C}_2\text{H}_5\text{Cl}$, and C_2Cl_4 and can potentially supply about 55 ppt of chlorine to the stratosphere (Table 2-2). These gases have natural and anthropogenic sources, as described in Section 2.2. The tropospheric lifetimes of these gases (30 to 150 days) are comparable to those for some of the brominated VSL SGs (see Table 2-1), so if SGI is important for bromine, it may also play a role for chlorine. Although the overall perturbation of Cl_y by VSLS is small (because the chlorine content of longer lived gases is much larger than that of the VSLS), this perturbation could be significant for the LMS, where the VSL

SGs are more likely to release their chlorine content. This could lead to significantly higher levels of ClO in the LMS than would be present in models that only consider supply of Cl_y from long-lived gases.

Iodine

The supply of stratospheric iodine presently appears to be dominated by methyl iodide (CH_3I) (e.g., Davis et al., 1996; Table 2-2). Abundances of CH_3I range from ~0.8 ppt in the marine boundary layer to ~0.08 ppt in the tropical upper troposphere (Table 2-2). Higher values of CH_3I , occasionally reaching ~1.0 ppt, were reported in the subtropical upper troposphere (Davis et al., 1996). The much shorter lifetimes of iodinated VSLS compared with most brominated VSLS (Table 2-1) suggests, in general, less efficient SGI of iodine to the stratosphere.

2.5.1.2 OBSERVATIONAL EVIDENCE FOR PGI

Bromine

PGI refers to cross-tropopause transport of degradation products of VSL source gases, as well as final inorganic products. For bromine, the discussion of observational evidence for PGI begins with the suggestion of a global, ubiquitous background abundance of 1 to 2 ppt of bromine monoxide (BrO) distributed throughout the troposphere (Harder et al., 1998; Müller et al., 2002; Richter et al., 2002; Van Roozendaal et al., 2002). Model simulations indicate that Br_y levels of 4 to 8 ppt are needed in the middle troposphere to sustain this much BrO (Yang et al., 2005). If 4 to 8 ppt of Br_y is present in the global troposphere, then cross-tropopause transport of these species could dominate the bromine budget of the LMS (Ko et al., 1997; Pfeilsticker et al., 2000). As explained below, it is unclear whether BrO is present at this level in the whole troposphere. There is no evidence of enough inorganic chlorine or iodine in the global troposphere to perturb stratospheric Cl_y or I_y in a manner comparable to the potential perturbation to stratospheric Br_y by tropospheric, inorganic bromine.

The presence of 1 to 2 ppt of BrO in the troposphere was first suggested based on comparison of total column BrO from the Global Ozone Monitoring Experiment (GOME) to stratospheric columns inferred from balloon measurements of BrO profiles (Harder et al., 1998). Observations of the solar zenith angle (SZA) variation of differential slant column density of GOME BrO also indicated that much of the column measured by GOME lies below the tropopause, perhaps due to the presence of 2 to 3 ppt of BrO between the tropopause and the surface

(Müller et al., 2002; Van Roozendaal et al., 2002). Measurements of BrO and O₄ (the O₂-dimer) columns over the Pacific suggest 0.5 to 2.0 ppt of BrO uniformly distributed throughout the troposphere (Richter et al., 2002). A global, ubiquitous distribution of 2 to 3 ppt of BrO would account nearly completely for the “additional” stratospheric bromine reported by GOME (Van Roozendaal et al., 2002; Salawitch et al., 2005). The fact that excess BrO is seen year round by GOME, at all latitudes (e.g., Chance, 1998; Hegels et al., 1998), argues against the springtime release of bromine from sea-ice and frost flowers (the so-called bromine explosion; see, for example McElroy et al., 1999) being the primary source of tropospheric background BrO.

Other observations, however, contradict the notion of a global, background level of BrO at an abundance of 2 to 3 ppt. Ground-based observations of direct and scattered sunlight reveal mean abundances of BrO in the troposphere over Lauder, New Zealand (45°S), of ~0.2 ppt and an upper limit of 0.9 ppt over this site (Schofield et al., 2004). Low values of tropospheric BrO are also observed over Arrival Heights, Antarctica (78°S), except for bromine explosion events (Schofield et al., 2006). Balloon profiles of tropospheric BrO indicate levels that peak at ~2.3 ppt, but more commonly lie between ~0.4 and 0.6 ppt (Fitzenberger et al., 2000). If BrO levels in the global free troposphere are less than 1 ppt, then the GOME observations of total BrO columns imply larger stratospheric BrO columns than can be accounted for by that supplied by CH₃Br and halons (Salawitch et al., 2005).

The role of VSLS in maintaining the global tropospheric background levels of BrO and total Br_y is a subject of active research. Von Glasow et al. (2004) showed that the stratosphere-to-troposphere flux of inorganic bromine combined with the tropospheric decomposition of CH₃Br was insufficient to maintain tropospheric levels of BrO approaching ~2 ppt. They examined the sensitivity of tropospheric BrO to various latitudinal distributions of surface emissions of VSL SGs. Although the resulting distributions of BrO and Br_y differed, the available data were too sparse and uncertain to place strong constraints on the geographic distribution of surface emissions. Yang et al. (2005) presented model results indicating that sea salt sources dominate the supply of bromine to the lower troposphere, and that VSL SGs are responsible for the majority of bromine in the upper troposphere. Warwick et al. (2006) suggested, based on a comparison of modeled and measured CHBr₃, that a large portion of CHBr₃ emissions occurs in the tropics. They also showed that emissions of VSL SGs (i.e., CHBr₃, CH₂Br₂, CH₂BrCl, CHBrCl₂), together with CH₃Br, could maintain ~2 ppt of Br_y in the tropical free troposphere, and between 0 and 2

ppt of Br_y in the rest of the troposphere. Levels of Br_y were lower in the rest of the troposphere in this simulation, which involved only VSL SGs, because of aerosol washout of product gas and the co-location of surface emissions and convection in the tropics.

There have been no atmospheric observations of organic degradation products of VSL SG decomposition to date, such as COBr₂ and COHBr from decomposition of CHBr₃ (Section 2.3). Most modeling studies have assumed direct conversion to inorganic bromine upon the decomposition of CHBr₃ and other VSL SGs. Field observations to assess the accuracy of this assumption represent another gap in our present knowledge.

Chlorine

In contrast to the situation for bromine and iodine, the tropospheric abundance of Cl_y is likely dominated by hydrogen chloride (HCl). The reason for the different behavior of the halogen families is that production of HCl from Cl plus methane (CH₄) is exothermic, while production of hydrogen bromide and hydrogen iodide (HBr and HI) by reactions involving CH₄ is endothermic. As a result, PGI for chlorine should be defined by the troposphere-to-stratosphere transport of HCl. Efficient scavenging of HCl by clouds and aerosols is generally considered to lead to negligible PGI of inorganic chlorine species. Measurements of HCl in the subtropical upper troposphere reveal abundances between 0 and 80 ppt, but simultaneous observations of other species indicate these levels of HCl are maintained by stratosphere-to-troposphere transport of Cl_y, rather than tropospheric degradation of VSL SGs (Marcy et al., 2004).

There are many organic decomposition products of chlorinated VSLS, most of which have not been measured in the atmosphere to date. An important exception is phosgene (COCl₂), produced by the decomposition of chlorinated organic gases (see Section 2.3.3). COCl₂ has a significant abundance in the upper tropical troposphere (on average 22.5 ppt, or 45 ppt as chlorine, Table 2-2), and a longer photochemical lifetime than some of its VSLS parent compounds (Section 2.3.3). There are no known surface sources of COCl₂. If COCl₂ were present in the TTL, where its removal processes are inefficient, it could potentially play a role in the PGI of chlorinated VSLS.

In this Assessment we have not, however, included phosgene in our evaluation of the contribution of VSLS to stratospheric Cl_y. One reason for COCl₂ not being included is that tropospheric COCl₂ is evidently produced by the decomposition of both long-lived and VSL source gases (Section 2.3.3). In the case of degradation of long-

VERY SHORT-LIVED SUBSTANCES

lived gases that decompose primarily in the stratosphere, the majority of the tropospheric COCl_2 contribution is transported from the stratosphere (Kindler et al., 1995). Consequently, upper tropospheric measurements of COCl_2 do not necessarily define the contribution from degradation of VSL source gases alone to its abundance. The possibility exists for some degree of “double-counting” of Cl_y if COCl_2 is included in a summation of chlorine derived from the tropospheric abundances of all source gases. In addition, Kindler et al. (1995), based on a 1-D model, stated that only about 0.4% of COCl_2 produced in the troposphere is transported to, and decomposes in, the stratosphere. Measured stratospheric profiles of COCl_2 presented by Toon et al. (2001), however, appear to contradict this conclusion, since they show a much larger decline in mixing ratio with altitude than the model profiles of Kindler et al. (1995), and are instead consistent with the expected stratospheric loss of this compound discussed in Section 2.3.3. More detailed modeling and measurement studies of COCl_2 are needed to quantify whether or not it represents a significant route for PGI of stratospheric chlorine from VSL source gases. For the present we conclude that the contribution of COCl_2 to “additional” stratospheric Cl_y may range from a negligible amount (based on Kindler et al., 1995) to an upper limit of 40-50 ppt based on observed upper tropospheric abundances (Table 2-2 and Section 2.2.1).

Iodine

Both I_2 and IO have been observed in the marine boundary layer (Section 2.2.1). The tropospheric photochemical lifetimes of I_2 and IO are very short (Saiz-Lopez and Plane, 2004), and iodine oxides may self-nucleate, leading to efficient atmospheric removal by aerosols (Hoffmann et al., 2001). As a result, ozone depletion models do not typically consider transfer of inorganic iodine species across the tropopause, even though these species are abundant in parts of the boundary layer.

Product gas injection of decomposition products of CH_3I could be important, particularly if rapid convection lofted air parcels containing CH_3I into the TTL, where aerosol and cloud washout may be inefficient. In the future, decomposition products of CF_3I may also have to be considered (Section 2.2.4.3). However, no field observations of CH_3I and CF_3I decomposition products are available. The present state of knowledge for iodine is focused on defining stratospheric levels of I_y , rather than quantification of PGI sources.

2.5.1.3 MODEL ESTIMATES OF SGI AND PGI

The SGI and PGI fluxes can be calculated from global model simulations of a single source gas and their products by tagging and keeping separate the degradation products produced in the stratosphere from those produced in the troposphere. The lack of atmospheric observations of the organic intermediate species, combined with limited knowledge of the kinetics of these intermediates and the recycling of inorganic halogen compounds, means estimates of PGI injection presently rely on parameterizations of these processes that are untested against observations. The studies described below, updating progress since the last Assessment, consider SGI and PGI of bromine.

Prior to this Assessment, calculations involving two-dimensional (2-D) (Dvortsov et al., 1999) and 3-D (Nielsen and Douglass, 2001) models showed that oceanic release of CHBr_3 could maintain about 1 ppt of bromine to the stratosphere. These calculations assumed a 10-day lifetime due to “washout” by aerosols and clouds for the inorganic products produced following the decomposition of CHBr_3 .

Sinnhuber and Folkins (2006) used a one-dimensional mechanistic model of the tropical troposphere to quantify stratospheric supply of Br_y from CHBr_3 as a function of aerosol and cloud washout lifetime. In the model, Br_y reaching the stratosphere is determined by the detrainment from convection of CHBr_3 above the level of zero radiative heating (z_0 , see Section 2.4.1). Convective mass fluxes are constrained by observed temperature and humidity. Rapid washout of Br_y in the convective cloud was assumed, resulting in no detrainment of Br_y (i.e., product gas). Product gas is therefore formed from degradation of source gas following detrainment. A first order, uniform washout lifetime for Br_y in the clear-sky atmosphere below 17 km was treated as an adjustable parameter. By assuming rapid washout for Br_y in a particular simulation, they showed that injection of Br_y from the SGI pathway maintains about 0.5 ppt of Br_y per ppt of surface CHBr_3 , generally consistent with the results of Dvortsov et al. (1999) and Nielsen and Douglass (2001). They also examined the sensitivity of PGI to washout lifetime. The PGI of Br_y was 0.3 ppt, 0.8 ppt, and 1.6 ppt, per ppt of surface CHBr_3 , for lifetimes of 10, 30, and 100 days, respectively (Figure 2-7). They discussed how the washout of soluble species from the TTL depends on details of ice microphysics and could, in principle, be inefficient if air detraining from deep convection is dry.

The delivery of total Br_y via both SGI and PGI routes varied from 0.8 to 2.1 ppt, per ppt of surface CHBr_3 , as the washout lifetime increased from 10 to 100 days.

It is also useful to use model results to diagnose the SGI and PGI flux as a percentage of the flux of VLSL emitted at the surface, as opposed to relating it to mixing ratios as in the above study. Warwick et al. (2006) conducted a 3-D model simulation considering surface fluxes of CHBr_3 and other VSL SGs. Convection in this model was parameterized using the mass flux scheme of Tiedtke (1989) and included convective updrafts and large-scale subsidence associated with deep and shallow convection. An average tropospheric lifetime of 10 days relative to rainout was assumed for inorganic bromine. Among the scenarios were two cases where the CHBr_3 emission flux was either uniform in the open ocean or was limited to the tropical coastlines. As discussed in Section 2.3.2, the calculated lifetimes for the open ocean case are 30-37 days, compared with 15 days for the tropical coastline case. The SGI fluxes in the two simulations were practically the same at about 0.7% of the total surface emission flux. The PGI fluxes were 4% and 5% respectively. The Warwick et al. study also showed that CHBr_3 , together with the VLSL CH_2Br_2 , CH_2BrCl , CHBr_2Cl , and CHBrCl_2 , could together maintain 3 to 4 ppt Br_y in the tropical lower stratosphere.

The Atmospheric and Environmental Research, Inc. (AER) 2-D model (Rinsland et al., 2003) was also used to simulate CHBr_3 . The model used the convection parameterization from Dvortsov et al. (1998). Washout in the model was parameterized by a first-order removal rate that was constant in time. For a fixed uniform surface mixing ratio boundary condition, the SGI flux was 0.3% of the surface emission flux and the residence time of SGI Br_y in the stratosphere was 1.4 years. Assuming the same residence time, the PGI flux was 0.6%, about twice the SGI value. Note that in the Dvortsov et al. (1999) and the Nielsen and Douglass (2001) studies, the PGI flux was three times and twice the SGI flux, respectively. These studies confirm the suggestion that the sum of the two (PGI + SGI fluxes) could be as large as a few percent of surface emissions. As discussed in Section 2.4.3, the calculated mixing ratio of the product gas in the stratosphere is related to the SGI and PGI fluxes through the residence time in the model stratosphere. It is important to note that the larger fluxes calculated in Warwick et al. (2006) (a few percent versus less than 1%) were accompanied by smaller residence times for the stratosphere (0.2 years versus about 1.4 years). This may be related to whether diagnosed fluxes represent the net fluxes across the tropopause.

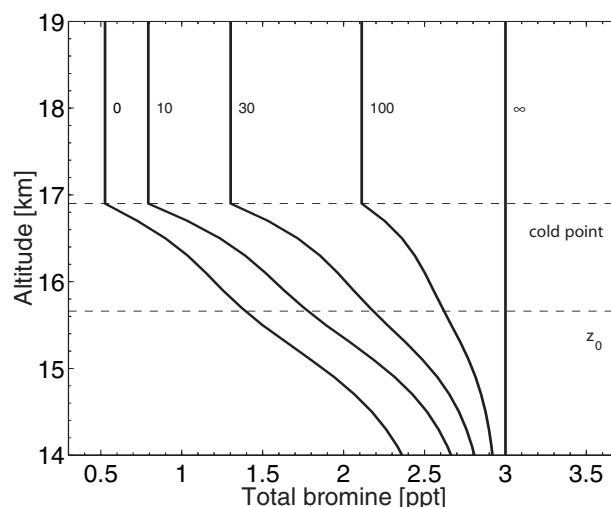


Figure 2-7. Calculated profile of total bromine from bromoform present as both product gas (Br_y) and source gas (CHBr_3), defined as $\text{Br}_y + 3 \times \text{CHBr}_3$, for different values of the lifetime of Br_y in days (numbers given in graph), based on a one-dimensional model of the tropical atmosphere. The calculations assume 1 ppt of CHBr_3 in the boundary layer and that no Br_y is detrained from convection (i.e., model assumes efficient uptake and removal of Br_y in clouds). Locations of the level of zero radiative heating and the cold point tropopause in the model are indicated. From Sinnhuber and Folkins (2006).

Finally it should be noted that the aforementioned model studies do not include possible heterogeneous reactions (Platt and Hönninger, 2003) that liberate inorganic bromine back to the gas phase (Section 2.3.4), which might result in more efficient PGI of Br_y from CHBr_3 than was considered in past Assessments.

2.5.2 Estimates of VLSL Contributions to Stratospheric Halogens Based on Measurements of Inorganic Species

This section focuses on the contributions of VSL halocarbons to the stratospheric budgets of bromine, chlorine, and iodine, based on measurements of inorganic species. For chlorine and bromine, the material is focused mainly on studies that compare the total halogen content of inorganic species with the halogen content of organics. Typically the difference between the inorganic and organic budgets is computed for an organic budget containing just long-lived SGs. The resulting difference is then interpreted as being the contribution to the stratospheric

VERY SHORT-LIVED SUBSTANCES

halogen loading by VSLS. This method is unable to distinguish between SGI and PGI, and would also include contributions from product gases that do not originate from VSLS. For bromine the long-lived SG budget is defined by the total bromine content of CH_3Br and the three or four halons that are commonly used to define baseline halogen scenarios for this and previous Assessments. For chlorine species the long-lived SG budget is defined by the 12 species (CFC-11, CFC-12, CFC-113, CFC-114, CFC-115, CCl_4 , CH_3CCl_3 , HCFC-22, HCFC-141b, HCFC-142b, halon-1211, and CH_3Cl ; see Chapter 1) used to define the baseline halogen loading scenarios in this and prior Assessments. As defined in the introduction, the terms $\text{Br}_y^{\text{VSLS}}$ and $\text{Cl}_y^{\text{VSLS}}$ refer to the component of stratospheric Br_y and Cl_y , respectively, due to SGI and PGI of sources other than these long-lived SGs. For iodine, the discussion is focused on quantification of total stratospheric inorganic iodine (I_y) based on measurements of IO, since supply is thought to be exclusively from VSL SGs. These approaches represent the present state of knowledge regarding quantification of the contribution of VSLS on the stratospheric halogen loadings.

2.5.2.1 BROMINE

Prior to this Assessment, balloonborne observations of BrO in the middle stratosphere at midlatitudes were shown to be consistent with stratospheric Br_y of 21.5 ± 3 ppt (Pfeilsticker et al., 2000). The total amount of organic bromine in the upper troposphere reported in this study was $18.4 (+1.8 / -1.5)$ ppt, based on measurements of CH_3Br , four halons, and a variety of VSL SGs. The higher levels of Br_y inferred from BrO, compared with Br_y inferred from the suite of organics, suggested either direct transport of VSL PGs or inorganic bromine across the tropopause, or perhaps larger abundances of VSL SGs in the tropics compared with midlatitudes where the balloon observations were obtained. Ground-based observations of column BrO from many stations were shown to be consistent with a total stratospheric bromine abundance of 20 ± 4 ppt, reflecting a ~ 5 ppt contribution from VSLS (Sinnhuber et al., 2002). Also in the last Assessment, a time series of Br_y inferred from BrO measurements in the middle stratosphere over several years was shown to exceed Br_y from CH_3Br + halons by an amount consistent with supply of 4 to 5 ppt of Br_y from VSLS (Figure 1-8, WMO, 2003). However, the interpretation of these data in the last Assessment was tentative, with the possibility of “calibration errors either in the measurements of BrO or the organic source gases” being noted as a possible explanation of the observations.

Since the last Assessment, there have been many studies, described below, that quantify $\text{Br}_y^{\text{VSLS}}$. Most of these studies, based on measurements of BrO by many techniques, conclude that stratospheric Br_y exceeds the amount of bromine that can be supplied solely by CH_3Br and halons. Therefore, since the last Assessment, we have gained greater confidence that the stratospheric bromine budget is affected by cross-tropopause transport of brominated VSLS, by either the SGI and/or PGI routes, and that the difference noted in the last Assessment is not due to “calibration errors.”

Figure 2-3 updates the time series of stratospheric and tropospheric bromine shown in the last Assessment (Figure 1-8, WMO, 2003). Observations of BrO using balloonborne differential optical absorption spectroscopy (DOAS) have been used to estimate stratospheric Br_y (Dorf, 2005; Dorf et al., 2006a). The most accurate analysis is based on estimating the mixing ratio of BrO for the middle stratosphere from the slope of BrO slant column versus air column above the balloon float altitude (the “Langley” method) and then using a photochemical model to deduce Br_y from measured BrO. Results for five flights, from 1996 to 2005, are illustrated (points labeled “DOAS BrO Langley obs.”) in Figure 2-3. Numerical values are also given in Table 2-7. Estimates of $\text{Br}_y^{\text{VSLS}}$ are based on the difference between Br_y inferred from BrO and the bromine content of CH_3Br and halons ($\text{Br}_y^{\text{CH}_3\text{Br}+\text{Halogns}}$). The estimate of $\text{Br}_y^{\text{CH}_3\text{Br}+\text{Halogns}}$ considers age of air, inferred from measured tracers, and neglects tropospheric gradients (i.e., it assumes that the sum of bromine from source and associated product gases at the tropical tropopause, notably in the case of CH_3Br , is represented by the mean of observed global surface mixing ratios). The difference between Br_y inferred from BrO and $\text{Br}_y^{\text{CH}_3\text{Br}+\text{Halogns}}$ yields the estimated value for $\text{Br}_y^{\text{VSLS}}$ (bottom row, Table 2-7). The mean and standard deviation for $\text{Br}_y^{\text{VSLS}}$, considering all five flights, is 4.1 ± 1 ppt. The overall uncertainty of this estimate, which is dominated by the accuracy of the BrO measurements and by the kinetics used to estimate Br_y from BrO, is ± 2.5 ppt (see Table 2-7 for discussion of uncertainties). Values of $\text{Br}_y^{\text{VSLS}}$ are illustrated in Figure 2-3 by the difference between the time series of Br_y inferred from BrO and $\text{Br}_y^{\text{CH}_3\text{Br}+\text{Halogns}}$.

Other DOAS-based estimates of Br_y are also shown in Figure 2-3. These estimates, labeled “DOAS BrO profiles,” are derived from model interpretation of BrO profiles in the lower stratosphere. The DOAS BrO profile estimate is considered to be a less reliable method for inferring $\text{Br}_y^{\text{VSLS}}$ compared with the Langley method (Dorf, 2005). It is reassuring that the two methods give good agreement, since this shows an overall level of con-

Table 2-7. Contribution to stratospheric Br_y^{VLSL} based on DOAS balloon BrO profiles.

	Leon, Spain 1996	Kiruna, Sweden 1999	Aire sur l'Adour, France 2003	Kiruna, Sweden 2003	Teresina, Brazil 2005
Br _y from BrO (ppt) ^a	17.8	19.9	20.1	20.4	21.5
Age (yrs)	5	6	5	5	5
CH ₃ Br (ppt) ^b	9.2	9.3	9.6	9.5	8.8
Halons (ppt) ^b	5.2	5.8	7.2	7.2	7.5
Br _y ^{VLSL} (ppt) ^c	3.4	4.8	3.3	3.7	5.2

^a The 1σ precision of Br_y estimated using the Langley method is about 0.7 ppt. The total uncertainty is 2.5 ppt, which represents the precision as well as uncertainties in the BrO cross section (±8%) and the photochemical correction used to convert BrO to Br_y (±8%).

^b Estimates of Br_y^{CH₃Br+Halons} are obtained from Montzka et al. (2003), assuming no tropospheric gradient of CH₃Br.

^c The mean and standard deviation of the 5 estimates of Br_y^{VLSL} are 4.1 ± 1 ppt. The standard deviation is consistent with the estimated precision in Br_y. Considering the overall uncertainty in Br_y from BrO, and assuming that Br_y^{CH₃Br+Halons} is well known, leads to a range for Br_y^{VLSL} of 4.1 ± 2.5 ppt, which is the value for DOAS given in Table 2-8. From Dorf (2005).

sistency between the two methods that sample different parts of the atmosphere. DOAS BrO profile estimates are also available for more flights than the estimates based on the Langley method, resulting in a more complete time series for stratospheric Br_y. The fact that values of Br_y in the lower and middle stratosphere are similar lends credence to the notion that VLSL contribute significantly to stratospheric Br_y.

The values of Br_y inferred from the balloon observations of BrO shown in Figure 2-3 imply, by an amount that is larger than the overall uncertainty, a significant contribution to stratospheric Br_y from VLSL. In addition, the values of Br_y observed during the past few years indicate a “leveling off” that appears to be consistent with the behavior of Br_y^{CH₃Br+Halons} (Dorf et al., 2006b). This suggests that Br_y^{VLSL} has not changed dramatically between 1996 and 2005, the time period of the stratospheric observations, and that changes in the surface emissions of CH₃Br and halons are being reflected in the stratospheric abundance of Br_y.

As noted above, Figure 2-3 neglects tropospheric gradients of CH₃Br that may, at least partly, result from its tropospheric degradation. The mixing ratios of CH₃Br in the TTL may be about 7% smaller than the globally averaged surface value (Schaufler et al., 1999; Montzka et al., 2003). If the bromine compounds resulting from tropospheric decomposition of CH₃Br do not reach the stratosphere, then estimates of Br_y^{VLSL} that rely on surface mixing ratios of CH₃Br may consequently be too low by up to 0.6 ppt.

Salawitch et al. (2005) examined GOME column BrO as well as measurements of BrO from aircraft and balloons. Their study suggested Br_y^{VLSL} between 4 and 10 ppt; best agreement with aircraft data was achieved for a

value of 6.9 ppt, while a balloon profile of BrO in the summer tropics (Pundt et al., 2002) suggested a value closer to 10 ppt. Sinnhuber et al. (2002, 2005) showed that the gas-phase reaction of bromine nitrate (BrONO₂) with oxygen atom triplet (O(³P)) proceeds quickly enough (Soller et al., 2001) to affect the partitioning of Br_y species. Nearly all of the studies presented here consider this reaction, even though it is not included in any of the past JPL or IUPAC evaluations. The exception is the study of Salawitch et al. (2005), who relied solely on JPL kinetics. Had they included this reaction, their values of Br_y^{VLSL} from the aircraft and balloon data would have been ~6 ppt and ~8 ppt, respectively. The Salawitch et al. (2005) values of Br_y^{VLSL} are a little higher than those derived from the DOAS measurements, but are generally consistent with the picture presented in Figure 2-3.

Since the last Assessment, attention has also focused on the interpretation of satellite observations of BrO. As noted previously, observations of column BrO from GOME reveal abundances of total column BrO, throughout the global atmosphere, that are much larger than expected based on simulations that assume supply of atmospheric bromine from only CH₃Br and halons (Figure 2-8, top panel). Measurements of column BrO from the Scanning Imaging Absorption Spectrometer for Atmospheric Cartography (SCIAMACHY) satellite instrument confirm the accuracy of the GOME observations of column BrO (Sinnhuber et al., 2005; Sioris et al., 2006). Recent scientific studies have focused on quantifying whether the much higher than expected levels of BrO reported by GOME reside in the stratosphere, the troposphere, or perhaps in both layers at levels important for the photochemical environment. Evidence for and against a global, background tropospheric level of BrO large

VERY SHORT-LIVED SUBSTANCES

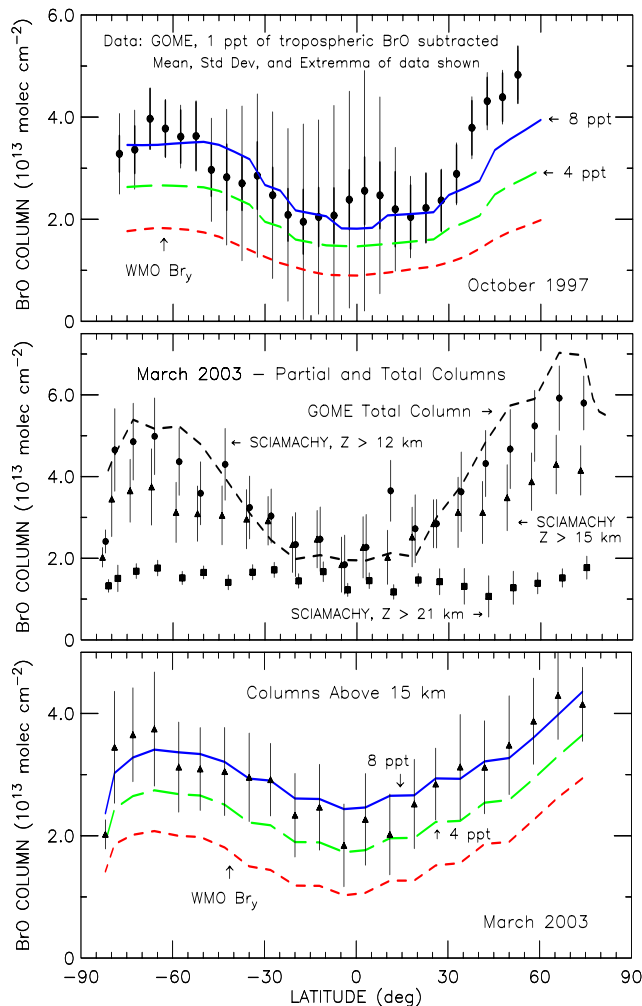


Figure 2-8. Top panel: Comparison of estimated stratospheric column BrO from GOME, October 1997, assuming a uniform 1 ppt distribution of BrO in the troposphere (close to the upper limit of 0.9 reported by Schofield et al., 2004) with stratospheric column BrO from the AER 2-D model, for the WMO (2003) “best guess” scenario Ab (labeled WMO Br_y) and for simulations assuming Br_y^{VLS} of 4 and 8 ppt, respectively. Plotted points show mean, standard deviation (thick error bars) and extreme values (thin error bars) of GOME data in 5°-wide latitude bins. The reasonably good agreement between the 8 ppt curve and the data suggest the BrO signal measured by GOME may be due to the presence of higher amounts of BrO in both the stratosphere and troposphere than is assumed in most models. After Chance (1998) and Salawitch et al. (2005). Middle panel: Comparison of total column BrO measured by GOME (March, 2003) vs. latitude and partial column BrO above various altitudes, based on BrO profiles from SCIAMACHY limb radiances. The comparison suggests a large component of the GOME total column resides between ~12 and 21 km. Bottom panel: Comparison of total column BrO above 15 km from SCIAMACHY with BrO partial columns from the AER 2-D model, found for the WMO Br_y and for model simulations assuming Br_y^{VLS} of 4 and 8 ppt. Model simulations from Salawitch et al. (2005); SCIAMACHY BrO from Sioris et al. (2006).

enough to account for excess BrO revealed by GOME and SCIAMACHY are described in Section 2.5.1.2. Clearly, a better definition of tropospheric BrO would clarify the stratospheric implications of the column BrO measurements, from both satellite and ground-based instruments.

Measurements of BrO profiles from SCIAMACHY provide new insight on the global stratospheric distribution of BrO. However, retrievals of BrO have been conducted by two groups and the scientific interpretations differ considerably. Retrievals by Sioris et al. (2006) show large abundances in the tropical tropopause layer and lowermost stratosphere, consistent with large abundances of stratospheric Br_y, ~24 to 25 ppt, and Br_y^{VLS} = 8.4 ± 2 ppt (Sioris et al., 2006) (Figure 2-8, middle and bottom panels). Retrievals of SCIAMACHY BrO by Sinnhuber et al. (2005) suggest stratospheric Br_y = 18 ± 3 ppt, implying a smaller value for Br_y^{VLS} of 3 ± 3 ppt (Figure 2-9). The BrO retrievals of Sinnhuber et al. (2005) show a deficit in the tropical lower stratosphere compared with calculations, particularly for model simulations that

include Br_y from VLS (Figure 2-9, panel labeled “18.5 km”). This deficit is contrary to the expectation of a significant perturbation to stratospheric Br_y from VLS. Conversely, partial BrO columns retrieved by Sioris et al. (2006) show large abundances in the tropical LMS, consistent with supply of Br_y from VLS (Figure 2-8, middle).

The retrievals of BrO in these two studies also offer different views on tropospheric BrO. Comparison of the Sinnhuber et al. (2005) stratospheric BrO profiles (based on limb radiances) and total column BrO measurements (based on nadir radiances) suggests the presence of 1 ± 0.5 ppt of tropospheric BrO (Figure 2-9, bottom). On the other hand, the consistency of BrO columns integrated above 12 km (limb) from SCIAMACHY and total column BrO from GOME (nadir) shown by Sioris et al. (2006) suggests a much smaller level of global tropospheric BrO (Figure 2-8, middle). The reason for these alternate interpretations of SCIAMACHY radiances is due to differences in the BrO retrievals computed by the two groups and does not appear to be related to either the methods used to infer

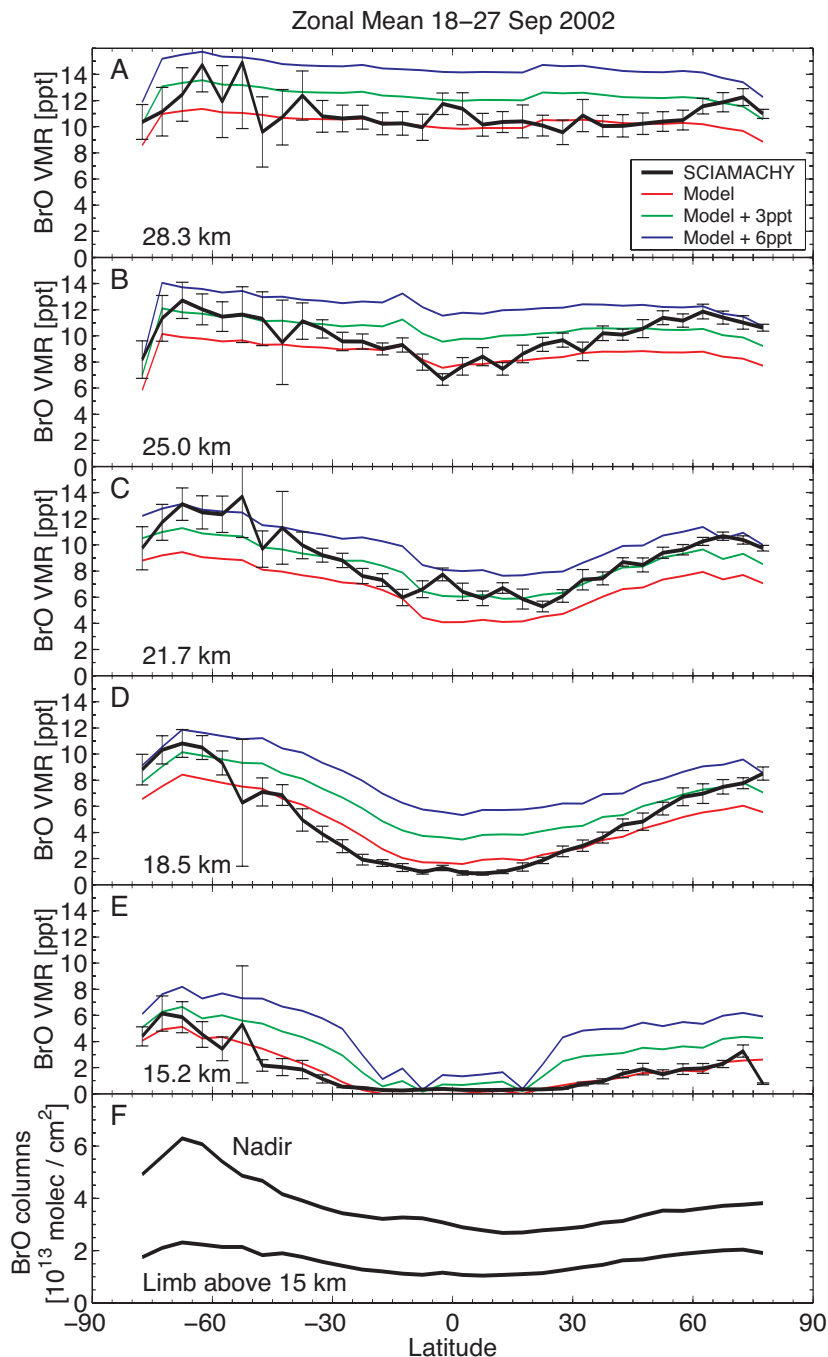


Figure 2-9. SCIAMACHY BrO observations. Panels A-E: Comparison between BrO volume mixing ratios (VMR) retrieved from SCIAMACHY limb radiances and model calculations for different altitudes. SCIAMACHY error bars are derived from the standard deviation of BrO measurements within each latitude bin. The modeled BrO was calculated from an estimate of Br_y derived from Michelson Interferometer for Passive Atmospheric Sounding (MIPAS) measurements of CFC-11 and the Wamsley et al. (1998) relation between Br_y and CFC-11 (scaled to the time of observation) and a photochemical model estimate of BrO/Br_y . Three model runs are shown: Br_y from only CH_3Br and halons (i.e., WMO Br_y) (red line), and using Br_y^{VSLs} of 3 ppt of Br_y (green line) and 6 ppt (blue line). Panel F: Total BrO column from SCIAMACHY nadir measurements compared with the integrated vertical BrO column above 15 km from SCIAMACHY limb observations. The difference between the integrated limb and the nadir column implies the presence of a significant amount of BrO below 15 km, corresponding to an average BrO mixing ratio of about 1.0 ± 0.5 ppt between the surface and 15 km. Adapted from Sinnhuber et al. (2005).

VERY SHORT-LIVED SUBSTANCES

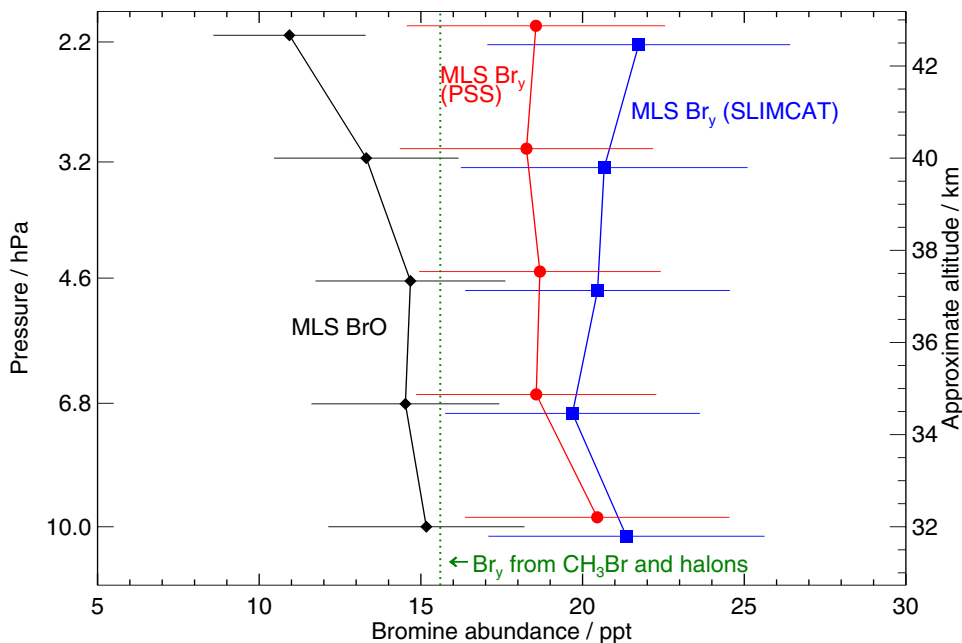
Br_y from BrO, or to assumptions regarding $\text{Br}_y^{\text{CH}_3\text{Br}+\text{Halons}}$. The SCIAMACHY BrO retrievals are sensitive to the determination of the tangent height of the limb radiances and methods used to account for spectral residuals (Sioris et al., 2006). Efforts are underway to compare balloon profiles of BrO with the SCIAMACHY retrievals (Dorf et al., 2006a). However, much work remains to understand the differences between the various retrievals of BrO and to reduce the uncertainty in the global distribution of BrO retrieved from SCIAMACHY radiances, which is perhaps best reflected by the contrasting results of Sinnhuber et al. (2005) and Sioris et al. (2006).

Measurements of BrO from the Microwave Limb Sounder (MLS) have also been used to quantify $\text{Br}_y^{\text{VLSL}}$ (Livesey et al., 2006). These observations, shown in Figure 2-10, imply a value for Br_y of 18.6 ± 5.5 ppt for the upper stratosphere (~30 to 42 km), between 55°S and 55°N , from September 2004 to August 2005. The uncertainty reflects the accuracy of the MLS measurements of BrO and possible errors in kinetic parameters used to infer Br_y from BrO. Livesey et al. (2006) inferred Br_y from BrO using two modeling approaches, but place greater confidence in the approach that uses a model constrained by MLS measurements of O_3 and nitrous oxide (N_2O) (PSS results in Figure 2-10). Their value of $\text{Br}_y^{\text{VLSL}}$ is 3.0 ± 5.5 ppt.

Observations of BrO in the polar vortices provide an opportunity to examine the bromine budget in an environment where all of the organic precursors have decomposed, and where the low levels of reactive nitrogen oxides ($\text{NO} + \text{NO}_2 = \text{NO}_x$) imply that nearly all of Br_y is contained in the two species BrO and bromine chloride (BrCl). These observations, discussed in Chapter 4, also support a significant, non-zero value for $\text{Br}_y^{\text{VLSL}}$. As discussed in Chapter 4, the 6 to 8 ppt enhancement of BrO_x (BrO+BrCl) in the Arctic vortex (Frieler et al., 2006), presumably from VLSL, relative to standard models (see Figure 4-16 in Chapter 4) may account for the discrepancy between measured and modeled chemical loss rates for Arctic ozone that was noted in the last Assessment.

Table 2-8 shows estimates of $\text{Br}_y^{\text{VLSL}}$ from nine studies. The central value from each study is given, as well as a range. For most studies, the uncertainty of $\text{Br}_y^{\text{VLSL}}$ was explicitly calculated while, for a few, it has been estimated by this Assessment based on information in each paper (see Table 2-8). The range was estimated using different methods by the various studies; the original papers should be consulted for details. Estimates of $\text{Br}_y^{\text{VLSL}}$ from ground-based studies are included. The Sinnhuber et al. (2002) study, discussed in the last Assessment, has been described above. Schofield et al. (2004, 2006) examined direct and scattered sunlight to

Figure 2-10. Measurement of BrO from Aura MLS versus pressure, for limb scans covering 55°S to 55°N , September 2004 to August 2005, and values of Br_y inferred from MLS BrO using estimates of BrO/ Br_y from the SLIMCAT model (blue) and from a photochemical steady state (PSS) model (red) constrained by MLS BrO, O_3 , and H_2O , and values of NO_y and CH_4 derived from MLS N_2O . The value of Br_y due to CH_3Br and halons during the time of measurement is shown by the dotted line. Error bars reflect the accuracy of MLS BrO and uncertainties in the model estimate of Br_y . The analysis using the PSS simulation was considered to be a more reliable estimate for stratospheric Br_y because this model is constrained by measured O_3 and exhibits a profile for NO_2 that agrees well with Halogen Occultation Experiment (HALOE) satellite measurements. The stratospheric bromine loading is estimated to be 18.6 ± 5.5 ppt, implying $\text{Br}_y^{\text{VLSL}} = 3.0 \pm 5.5$ ppt. From Livesey et al. (2006).



retrieve BrO profiles over Lauder, New Zealand (45°S), and Arrival Heights, Antarctica (78°S). They concluded that stratospheric column BrO was consistent with Br_y^{VLSL} of 6 ± 3 ppt at both locations.

Estimates of the Br_y^{VLSL} given in Table 2-8 range from lows of 3.0 ± 5.5 ppt (MLS data: Livesey et al., 2006) and 3 ± 3 ppt (SCIAMACHY retrievals: Sinnhuber et al., 2005) to highs of 4 to 10 ppt (aircraft and balloon data: Salawitch et al., 2005) and 8.4 ± 2 ppt (SCIAMACHY retrievals: Sioris et al., 2006). Dorf (2005) report a value of 4.1 ± 2.5 ppt from many years of balloon observations. Sheode et al. (2006) report a value of 3.5 ± 4 ppt, based on analysis of two years of SCIAMACHY data. This study is an update to Sinnhuber et al. (2005), who considered SCIAMACHY data over a 10-day period; the slightly larger uncertainty given by Sheode et al. (2006) is due to increased atmospheric variability over the longer time period.

The mean of the central values of Br_y^{VLSL} given in Table 2-8 is 5 ppt. This is the “ensemble” value reported at the bottom of the table. It is difficult to ascribe a true uncertainty to this ensemble value, given that uncertainties in Br_y^{VLSL} were determined using different methods, and in some cases were estimated by this Assessment. As a result, we place greater confidence in the range of central values in the Table (3 to 8 ppt) as an estimate of the uncertainty in Br_y^{VLSL}. While three of the studies could not rule out a zero contribution from VLSL, the majority of studies pointed to a positive value for Br_y^{VLSL} large enough to affect ozone photochemistry in the LMS (Section 2.6).

2.5.2.2 CHLORINE

Measurements of HCl in the subtropics typically exceed 50 ppt (Marcy et al., 2004). As noted above, these

Table 2-8. Contribution to stratospheric Br_y^{VLSL}.

Data Source	Br _y ^{VLSL} Central Value (ppt)	Br _y ^{VLSL} Range (ppt)	Reference
Ground-based BrO 11 sites, 78°S-79°N	5	1-9 ^a	Sinnhuber et al. (2002)
Ground-based BrO Lauder, New Zealand, 45°S	6	3-9	Schofield et al. (2004)
Ground-based BrO Arrival Heights, Antarctica, 78°S	6	3-9	Schofield et al. (2006)
DOAS Balloon BrO Profiles 5°S-68°N, 0-35 km	4.1	1.6-6.6	Dorf, 2005
Aircraft & Balloon BrO Profiles, 22°S-35°N, 17-32 km and GOME Satellite Column BrO, 60°S-60°N	7	4-10 ^a	Salawitch et al. (2005)
SCIAMACHY Satellite BrO Profiles 80°S-80°N, 15-28 km	8.4	6.4-10.4	Sioris et al. (2006)
SCIAMACHY Satellite BrO Profiles 80°S-80°N, 15-28 km	3	0-6	Sinnhuber et al. (2005)
SCIAMACHY Satellite BrO Profiles 80°S-80°N, 15-28 km	3.5	0-7.5	Sheode et al. (2006)
MLS Satellite BrO Profiles 55°S-55°N, 30-42 km	3.0	0-8.5	Livesey et al. (2006)
Ensemble	5 (3-8)^b		

DOAS, Differential Optical Absorption Spectroscopy; GOME, Global Ozone Monitoring Experiment; SCIAMACHY, Scanning Imaging Absorption Spectrometer for Atmospheric Cartography; MLS, Microwave Limb Sounder.

^a Range estimated by this Assessment, based on the uncertainty in stratospheric Br_y inferred from BrO that was stated in the reference.

^b Average and range of the central values of the 9 estimates of Br_y^{VLSL}.

VERY SHORT-LIVED SUBSTANCES

data have been interpreted as being evidence for supply of HCl from the stratosphere, rather than being due to the decomposition of VSL SGs. There have been no studies, since the last Assessment, quantifying the influence of VSL SGs on measured HCl in the tropical TTL or LMS. Such a study would require accurate and precise measurement of HCl and a suite of organic chlorine species, including long-lived SGs and VSL SGs, plus either detailed model analysis and/or observations of dynamical tracers to be able to isolate the effects on chlorine of transport from above (where the longer lived SGs decompose) and from below (where VSL SGs potentially contribute).

Another avenue for assessing the role of VSL compounds on stratospheric chlorine, which has received some attention since the last Assessment, is quantification of stratospheric chlorine either by measurements of a suite of compounds in the middle stratosphere or by measurement of HCl in the upper stratosphere. Nassar et al. (2006) quantified total stratospheric chlorine (Cl_{TOT} , the sum of simultaneous measurements of organic and inorganic species; see Figure 1-12 of Chapter 1) based primarily on data from the Atmospheric Chemistry Experiment Fourier Transform Spectrometer (ACE-FTS). They report a value of Cl_{TOT} of 3.65 ppb over the period February 2004 to January 2005, for both Southern and Northern Hemisphere midlatitudes. The 1σ precision of Cl_{TOT} is 0.09 ppb and the estimated accuracy is 0.13 ppb. The estimated contribution of just long-lived species to Cl_y during this time period is 3.41 ppb (this estimate is based on a mean age for stratospheric air of 5 years and an age of air spectrum width of 3 years, applied to the WMO 2002 baseline scenario Ab (see Chapters 1 and 3 of this Assessment) for the 12 long-lived chlorine species). The fact that the ACE-FTS value of Cl_{TOT} exceeds this value of Cl_y could be indicative of a contribution from VSLS. On the other hand, the combined uncertainty of the ACE-FTS value of Cl_{TOT} (accuracy + precision) nearly overlaps with the expected value of Cl_y from just long-lived species.

Time series of HCl near 55 km from the ATMOS (Atmospheric Trace Molecule Spectroscopy experiment), HALOE (Halogen Occultation Experiment), MLS, and ACE-FTS instruments are shown in Figure 1-12 of Chapter 1, where it is discussed in terms of trends of Cl_y in the stratosphere. In the Figure these measurements are compared with modeled stratospheric abundances of HCl due to long-lived chlorinated gases alone (dashed line), and enhanced by the addition of 100 ppt of chlorine to represent a possible contribution from VSLS and phosgene (solid lines). Because of the level of uncertainty in the respective satellite measurements (note the error bars in Figure 1-12, which represent 2-sigma uncertainty), it is

difficult to discriminate between the model runs with and without enhanced chlorine. The model run based on long-lived source gases alone appears closer to the HALOE measurements of HCl, which are lower than those obtained by the other instruments (although within their reported error limits). The MLS, ATMOS, and ACE-FTS measurements are suggestive of a contribution of chlorine from VSLS. The contribution of VSLS to stratospheric Cl_y cannot be quantified definitively given the current level of accuracy of the satellite HCl measurements.

2.5.2.3 IODINE

Solomon et al. (1994) suggested that if stratospheric inorganic iodine (I_y) levels were close to 1.0 ppt, catalytic cycles involving $IO + BrO$ and $IO + ClO$ could be responsible for a significant component of midlatitude ozone trends. That suggestion has led to considerable effort to better understand the photochemistry of inorganic iodine species (e.g., Bösch et al., 2003, and references therein) and to define the stratospheric iodine budget.

Wennberg et al. (1997), based on analysis of ground-based spectra, reported an upper limit for I_y of 0.2 ppt. Pundt et al. (1998) reported a similar upper limit, based on analysis of balloonborne spectra. Both studies were summarized in the last Assessment. Since the last Assessment, several additional studies of the I_y budget have appeared. Bösch et al. (2003), based on balloonborne solar occultation spectra in the UV/visible region from flights at middle and high latitudes, report an upper limit for I_y of 0.1 ppt. Recent measurements of IO in the tropics, using the same technique, also show very low levels of IO (Butz, 2006) (Figure 2-11). These observations suggest that either much less iodine enters the stratosphere than expected based on levels of CH_3I near the surface, or that stratospheric iodine resides either in gaseous species besides IO or perhaps in particulate form (see Section 2.3.5). As noted above, the tropospheric lifetime of the dominant iodine VSL SGs is much smaller (i.e., ~5 days) than the tropospheric lifetime of many brominated VSLS (>100 days). This could account for SGI of bromine and little or no SGI of iodine. Furthermore, observations of self-nucleation of iodine oxides (Hoffmann et al., 2001) and iodine uptake on tropospheric aerosols (Murphy and Thomson, 2000) could account for inefficient transfer of I_y to the stratosphere via PGI.

The only evidence of significant levels of stratospheric iodine is provided by ground-based observations of spectra recorded at 79°N that show, on some days, signs of elevated column IO (Wittrock et al., 2000). The SZA variation of slant column density of IO was used to suggest that the elevated IO lies in the stratosphere, with an

abundance of I_y as high as 0.8 ppt. The considerable variation in I_y for different days is difficult to reconcile in terms of a large stratospheric contribution, particularly for high-latitude air masses that should lack any residual CH_3I . Higher levels of IO were seen in February 1997 compared with March 1997, associated with lower levels of NO_x in February. Similar observations of the SZA variation of slant column IO in the Antarctic have been used to argue for a burden located primarily in the troposphere (Frieß et al., 2001). The observation of highly elevated IO on some days by Wittrock et al. (2000) is presently the only piece of observational evidence supporting a large source of I_y from VLS. It should be recalled, however, that the ozone destruction efficiency of iodine is large compared with that of both bromine and chlorine, and IO abundances in the stratosphere of several tenths of 1 ppt could be potentially significant (Figure 2-2).

2.6 POTENTIAL IMPACT OF VLSL ON OZONE

In WMO (2003) the focus of this topic was on (1) the theoretical basis for estimating the change in column ozone from emissions of organic VSL SGs, and (2) the theoretical basis for estimating Ozone Depletion Potentials (ODPs), including the differences (Wuebbles and Ko, 1999; Wuebbles et al., 2001) from the standard ODP definition, and initial analyses of location-dependent ODPs for one VSL SG, n-propyl bromide. WMO (2003) gave a comprehensive evaluation of the theoretical basis and procedures

for estimating ozone column effects and ODPs of VSL SGs; the discussion here is intended to update that evaluation.

2.6.1 Effects of Halogenated VLSL on Column Ozone

Halogens supplied by the decomposition of VLSL have the potential to significantly alter the photochemistry of ozone in the upper troposphere (UT) and lowermost stratosphere (LMS). Within models that consider supply of bromine solely from CH_3Br plus halons, pure odd-hydrogen radical (HO_x) photochemistry is the dominant loss process for odd oxygen in the LMS (Salawitch et al., 2005; see Figure 2-2). As discussed in Section 2.5, Br_y^{VLSL} in the LMS, maintained by the SGI and PGI pathways, can potentially cause significant local perturbation to the Br_y budget. Inorganic tropospheric bromine may also be transported in the LMS and contribute to additional Br_y^{VLSL} (as discussed in Section 2.5). Enhanced levels of bromine lead to greater efficiency for ozone loss by the $BrO + ClO$ catalytic cycle, particularly during times of high aerosol loading following major volcanic eruptions (Salawitch et al., 2005; Sinnhuber et al., 2006). Because of this cycle, Br_y^{VLSL} enhances ozone depletion due to CFCs and other chlorocarbons. If Br_y^{VLSL} is 5 ppt, as suggested by the assessment presented in Section 2.5, and if the majority of this bromine is present in the LMS, then ozone loss by the $BrO + HO_2$ cycle becomes greatly enhanced (Salawitch et al., 2005). Indeed, at Br_y^{VLSL} between 4 to 8 ppt, ozone loss by bromine cycles through-

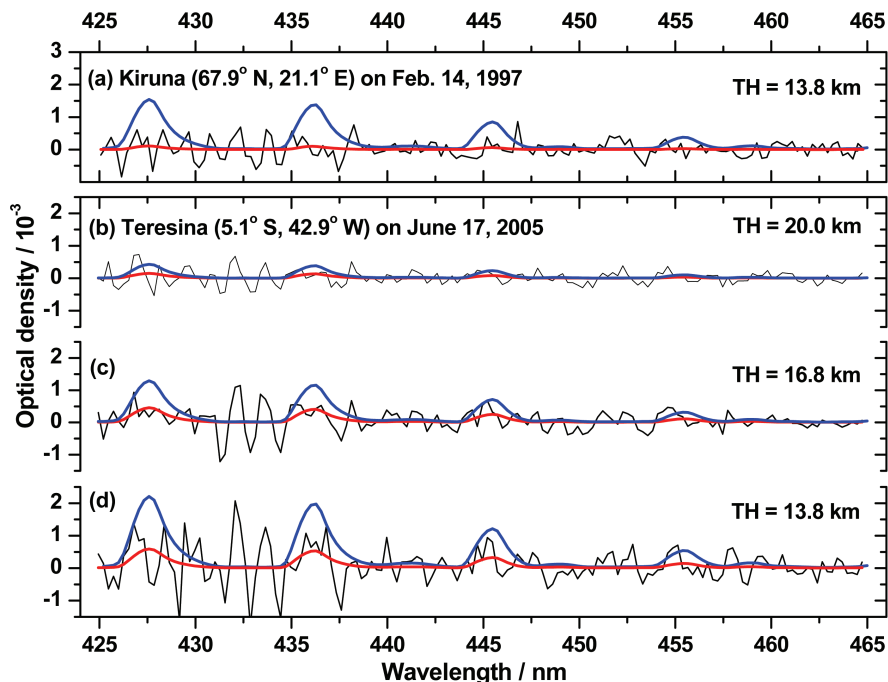


Figure 2-11. Comparison of measured and expected IO absorption by balloonborne UV/visible solar occultation spectroscopy at high and low latitudes (black line: measured IO + residual absorption; red line: inferred IO absorption; blue line: the expected IO absorption assuming $[IO] = 0.5$ ppt for the 0 to 20 km altitude range). Panels (a) and (b) are for observations within the lowermost stratosphere, and panels (c) and (d) for observations within the tropical tropopause layer. TH = tangent height. Panel (a) is adopted from Bösch et al. (2003), and panels (b) to (d) are from Butz (2006).

VERY SHORT-LIVED SUBSTANCES

out the lowermost stratosphere can approach ozone loss by HO_x cycles alone (Figure 2-2).

In the last Assessment, a value of 45 was given for the relative effectiveness of stratospheric ozone depletion by bromine; the so-called α parameter (Section 1.4.4, WMO, 2003). This value has been reassessed in Chapter 8 of this Assessment (Section 8.2.2), and the recommendation made that the value of α be increased to 60 (65 for the Antarctic stratosphere). As a consequence, the semi-empirically determined values of ODPs for all brominated source gases have now increased. Some models that also include VSLs in their calculations suggest even larger values for α . For example, Sinnhuber et al. (2006), using the University of Bremen two-dimensional model (Chipperfield and Feng, 2003), derive values for α of 66 without Br_y^{VSLs} and 69 including Br_y^{VSLs}, suggesting an impact on α from halogenated VSLs. Updated versions of the Atmospheric and Environmental Research, Inc., (AER) (U.S.) and University of Illinois at Urbana-Champaign (UIUC) (U.S.) models that include Br_y^{VSLs} from gases discussed earlier in this chapter (i.e., CH₂Cl₂, CHCl₃, C₂HCl₃, C₂Cl₄, CH₂BrCl, CH₂Br₂, CHBr₂Cl, CHBrCl₂, and CHBr₃) both derive an α of 61. More work is needed to assess the importance of Br_y^{VSLs} on α .

There was no attempt in WMO (2003) to quantify the effects of halogenated VSLs on past trends, or on future changes in stratospheric ozone or ozone columns. Since then, there has been increasing awareness that VSLs have a potentially important effect on chlorine and bromine in the lower stratosphere. As discussed in Section 2.5 of this report, halogenated VSLs appear to add about 5 ppt, on average, of reactive bromine (Br_y) to the lower stratosphere. Although significant uncertainties remain, analyses with the AER 2-D chemical transport model in Salawitch et al. (2005) suggest that this constant amount of Br_y added to the lower stratosphere has a noticeable impact on past trends in column ozone, as shown in Figure 2-12. Similar results were found using the University of Bremen 2-D model (Sinnhuber et al., 2006). Indeed, the inclusion of additional Br_y^{VSLs} may lead to better agreement between modeled and observed stratospheric ozone trends, particularly during times of perturbed aerosol loading, especially in the Northern Hemisphere (Salawitch et al., 2005; Sinnhuber et al., 2006). (Similar findings are discussed in Chapter 3, Section 3.4.3.2, and shown in Figure 3-25.) Both of these simulations assumed that Br_y^{VSLs} was constant over time, due to primarily natural sources. Increased ozone depletion due to Br_y^{VSLs} was caused by the ability of bromine to enhance ozone loss by ClO derived from CFCs, as outlined above (Chapter 3 also discusses impacts of Br_y^{VSLs} on ozone trends). The effect of anthropogenic emissions of Br_y^{VSLs} or possible long-

term changes in Br_y^{VSLs} due to climate change or natural variability, have yet to be studied (see Section 2.7).

Several recent studies (e.g., von Glasow et al., 2004; Yang et al., 2005) suggest that inorganic bromine from halogenated VSLs could lead to reductions in tropospheric ozone. The effect on tropospheric ozone should largely be regional in nature, but may have implications on global-scale ozone concentrations. Reductions in ozone occur due to a direct effect (increased loss by the BrO + HO₂ cycle) and an indirect effect (reduced production due to decreased levels of NO) that is ultimately driven by increased efficiency of the BrONO₂ hydrolysis sink of NO_x (Lary, 2005). More accurate evaluations will be dependent on improved knowledge about the bromine budget in the troposphere. If anthropogenic production of brominated VSLs becomes important in the future, the effect of inorganic product gas on tropospheric ozone will have to be evaluated to quantify the impact of these compounds on total column ozone.

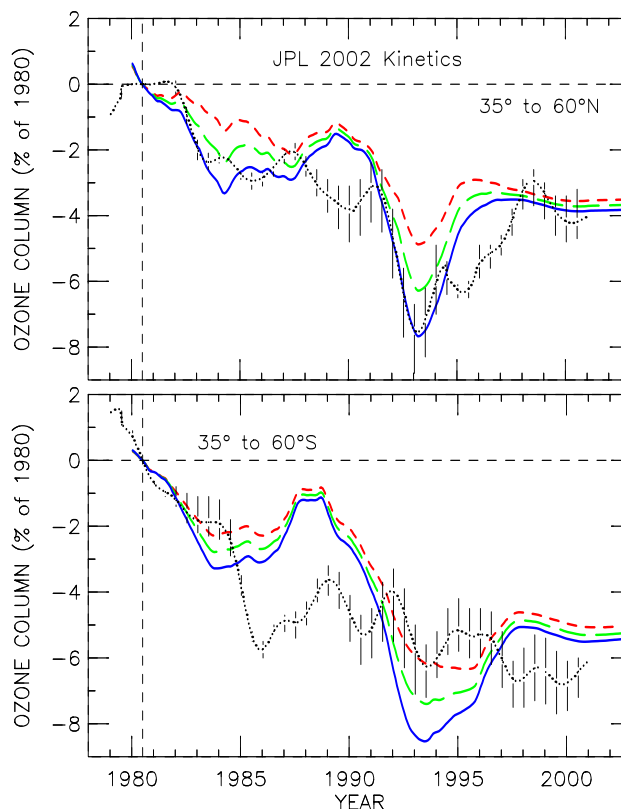


Figure 2-12. Calculated change in column ozone relative to 1980 levels using the AER 2-D model for stratospheric Br_y^{VSLs} of 0 (red), 4 (green), and 8 (blue) ppt for 35°N-60°N (top) and for 35°S-60°S (bottom), compared with observed trends in total ozone (black line). Based on Salawitch et al. (2005).

2.6.2 ODPs for Halogenated VSLS

There have been only a few new reported studies of the ODPs for VSL SGs since the last Assessment. The additional model estimates of SGI and PGI fluxes provide an opportunity to update the estimates for ODP using Equation 2.15 from Ko and Poulet et al. (2003). Using the results discussed in Section 2.5.1 as a guideline, it is reasonable to assume that for a source gas with a local tropospheric lifetime of about 25 days and uniform landmass emissions, 1% of the emitted flux enters the stratosphere via the SGI and PGI pathways. We make the additional assumption that the residence time of the Br_y introduced by either pathway is similar to that of the Br_y produced by long-lived SGs. The order of magnitude estimate for the ODP of a species with molecular weight comparable to that of CFC-11, and a local lifetime of about 25 days, can be determined to be c. 0.003 if it contains 1 chlorine atom, and c. 0.18 if it contains 1 bromine atom (assuming an alpha factor of 60 for bromine). A simple scaling for iodinated compounds is not possible because of their shorter lifetimes and the uncertainty of the alpha factor for iodine. The resulting ODP for any given compound with the above characteristics would be linearly dependent on the number of chlorine or bromine atoms.

Using the UIUC zonally averaged 2-D model, Li et al. (2006) have re-evaluated the ODPs for surface emissions of trifluoroiodomethane (CF_3I), a compound that is proposed as a replacement for bromotrifluoromethane (halon-1301, CBrF_3) in firefighting and inhibition applications. The model used an updated representation of iodine chemistry relative to an earlier study of the ODP of CF_3I (Solomon et al., 1994). They found an ODP of 0.013 for emissions evenly distributed over the Northern Hemisphere (compared with <0.008 from Solomon et al. (1994)), 0.011 for emissions distributed over 30°N to 60°N, and 0.018 for emissions distributed over 5°S to 30°N. Li et al. (2006) also consider the effects of potentially using CF_3I in aircraft. The resulting ODPs depend heavily on the altitude and latitude of the emissions. For example, emissions peaking at 6-9 km were calculated to give an ODP of 0.084 for emissions occurring at 30°N-40°N and 0.25 for emissions occurring at 0-10°N. Another proposed replacement for halon-1301 in aircraft engine fire applications, phosphorus tribromide (PBr_3), has not been evaluated, but should also have non-zero ODPs.

The ODP of n-propyl bromide was considered at length in WMO (2003), but there have been no new evaluations since that date.

2.7 POTENTIAL FUTURE CONSIDERATIONS

The impact of halogenated VSLS on stratospheric halogen loading and ozone depletion is, as discussed in Sections 2.5.1 and 2.6.1, currently thought to be relatively small (but significant) compared with that from the long-lived halocarbons. The present-day impact arises principally from the brominated VSLS, whereas the contributions from chlorinated and iodinated gases (for instance, to EESC) are small.

This situation could potentially change in the future. Small anthropogenic emissions of halogenated VSLS already exist (e.g., $n\text{-C}_3\text{H}_7\text{Br}$, CHCl_3 , CH_2Cl_2 , C_2Cl_4 , etc.; see Section 2.2.4). These could increase in the future (although several of these have evidently decreased in the last decade, as previously discussed), or new products could enter commercial use (e.g., CF_3I ; Sections 2.2.4.3 and 2.6.2). However, as noted previously, the majority of halogenated VSLS have partly or wholly natural origins, and therefore contribute to the natural background halogen loading of the stratosphere. This is set against a future trend of declining concentrations of long-lived anthropogenic halogenated gases, and hence a potentially larger relative impact from halogenated VSLS.

The exact sources and intensities of natural VSLS emissions are largely linked to biogenic activity in both the marine and terrestrial biospheres (there is also evidence of some abiotic marine emissions; see Section 2.2.3.2). It is conceivable that biogenic emissions could change in response to, for example, changing global temperatures, atmospheric CO_2 , rainfall, land use, vegetative cover, and oceanic productivity. Evidence for this is presently sparse (Section 2.2). In one study (Butler et al., 2006), positive correlations between open ocean flux rates of CHBr_3 and CH_3I with sea surface temperature (SST) were reported. The authors noted, however, that SST might simply be a proxy for some other driver (e.g., incident radiation, latitude, etc.). They further noted that while SST (and also wind speed) largely dictate sea-air flux rates, other significant parameters, such as nutrient supply and stratification of surface waters, are also affected by SST and wind speed, and may have important modifying effects (both positive and negative) on overall emission rates. Another study, reported in Section 2.2.2, showed that measurements of organo-halogen emissions from rice paddies indicate an apparent positive correlation between temperature and CH_3I emissions (Redeker and Cicerone, 2004). On the other hand, firn records of the atmospheric abundance of several halogenated VSLS suggest minimal

VERY SHORT-LIVED SUBSTANCES

long-term changes throughout the second half of the 20th century, other than small changes in the Northern Hemisphere atmosphere for a few gases with evident anthropogenic sources (Worton et al., 2006; Sturges et al., 2001).

It is noted that inorganic VSLS in the boundary layer, notably BrO from halogen activation reactions (Sections 2.2.5 and 2.5.1.2), might be sensitive to climatic changes. Hollwedel et al. (2004), for instance, suggest a link between observed increases in springtime BrO column density with increased annual sea ice coverage, but we do not consider it likely that boundary layer VSLS from high latitudes will be transported to the stratosphere. There might, however, be a potential link between inorganic halogen released from sea salt in the free troposphere and wind speed-dependent generation of marine aerosol (see also Section 2.2.5).

It is significant that several of the limited studies to date point toward maximum flux rates of halogenated VSLS in the tropics (Section 2.2). This coincides with the region where strong convection can most effectively and quickly transport VSLS to the tropopause region (Section 2.4). Changes in circulation and meteorology in the tropics might also exert a powerful modifying influence on the contribution of VSLS to stratospheric halogen loading. These effects could be either positive or negative. For example, a stronger future Brewer-Dobson circulation (as suggested by Butchart et al., 2006) could increase the rate of vertical transport of VSLS from the TTL into the stratosphere, whereas enhanced precipitation could decrease the efficiency of the PGI route (Section 2.3.4.1). Changes in the latitudes of the subtropical jets, or equivalently the extent of the tropospheric Hadley circulation (Fu et al., 2006), might be associated with changes in quasi-horizontal transport of VSLS from the TTL into the lowermost stratosphere.

Future changes in the chemical processing of VSLS and their product gases could also influence their atmospheric concentrations (Section 2.3), for example, through changes in OH abundance.

Our understanding of these many processes is presently too poor to allow any quantitative prediction of possible future halogenated VSLS trends.

REFERENCES

Abbatt, J.P.D., Interactions of atmospheric trace gases with ice surfaces: Adsorption and reaction, *Chem. Rev.*, 103 (12), 4783-4800, 2003.

Afe, O.T., A. Richter, B. Sierk, F. Wittrock, and J.P. Burrows, BrO emission from volcanoes: A survey using GOME and SCIAMACHY measurements, *Geophys. Res. Lett.*, 31, L24113, doi: 10.1029/

2004GL020944, 2004.

Arakawa, A., and W.H. Schubert, Interaction of a cumulus cloud ensemble with the large-scale environment, Part 1, *J. Atmos. Sci.*, 31 (3), 674-701, 1974.

Arnaud, P., *Cours de Chimie Organique*, 3rd ed., Gauthier-Villars, Paris, 1966.

Atkinson, R., D.L. Baulch, R.A. Cox, J.N. Crowley, R.F. Hampson, R.G. Hynes, M.E. Jenkin, J.A. Kerr, M.J. Rossi, and J. Troe, *Summary of Evaluated Kinetic and Photochemical Data for Atmospheric Chemistry*, Available: <http://www.iupac-kinetic.ch.cam.ac.uk>, 2005.

Bale, C.S.E., C.E. Canosa-Mas, D.E. Shallcross, and R.P. Wayne, A discharge-flow study of the kinetics of the reactions of IO with CH₃O₂ and CF₃O₂, *Phys. Chem. Chem. Phys.*, 7 (10), 2164-2172, 2005.

Barnes, D.H., S.C. Wofsy, B.P. Fehla, E.W. Gottlieb, J.W. Elkins, G.S. Dutton, and S.A. Montzka, Urban/industrial pollution for the New York City-Washington, D.C., corridor, 1996-1998: 1. Providing independent verification of CO and PCE emissions inventories, *J. Geophys. Res.*, 108 (D6), 4185, doi: 10.1029/2001JD001116, 2003.

Barth, M.C., A.L. Stuart, and W.C. Skamarock, Numerical simulations of the July 10, 1996, Stratospheric-Tropospheric Experiment: Radiation, Aerosols, and Ozone (STERAO)-deep convection experiment storm: Redistribution of soluble tracers, *J. Geophys. Res.*, 106 (D12), 12381-12400, 2001.

Bayes, K.D., R.R. Friedl, S.P. Sander, and D.W. Toohey, Measurements of quantum yields of bromine atoms in the photolysis of bromoform from 266 to 324 nm, *J. Geophys. Res.*, 108 (D3), 4095, doi: 10.1029/2002JD002877, 2003.

Bell, N., L. Hsu, D.J. Jacob, M.G. Schultz, D.R. Blake, J.H. Butler, D.B. King, J.M. Lobert, and E. Maier-Reimer, Methyl iodide: Atmospheric budget and use as a tracer of marine convection in global models, *J. Geophys. Res.*, 107 (D17), 4340, doi: 10.1029/2001/JD001151, 2002.

Blake, D., Methane, nonmethane hydrocarbons, alkyl nitrates, and chlorinated carbon compounds including 3 chlorofluorocarbons (CFC-11, CFC-12, and CFC-113) in whole-air samples, in *Trends: A Compendium of Data on Global Change*, Carbon Dioxide Information Analysis Center, Oak Ridge National Laboratory, U.S. Department of Energy, Oak Ridge, Tenn., U.S.A., Available: <http://cdiac.esd.ornl.gov/trends/otheratg/blake/blake.html>, 2005.

Blake, N.J., D.R. Blake, O.W. Wingenter, B.C. Sive, L.M. McKenzie, J.P. Lopez, I.J. Simpson, H.E. Fuelberg,

- G.W. Sachse, B.E. Anderson, G.L. Gregory, M.A. Carroll, G. Albercook, and F.S. Rowland, Influence of southern hemispheric biomass burning on mid-tropospheric distributions of nonmethane hydrocarbons and selected halocarbons over the remote South Pacific, *J. Geophys. Res.*, *104* (D13), 16213-16232, doi: 10.1029/1999JD900067, 1999a.
- Blake, N.J., D.R. Blake, O.W. Wingenter, B.C. Sive, C.H. Kang, D.C. Thornton, A.R. Bandy, E. Atlas, F. Flocke, J.M. Harris, and F.S. Rowland, Aircraft measurements of the latitudinal, vertical, and seasonal variations of NMHCs, methyl nitrate, methyl halides, and DMS during the First Aerosol Characterization Experiment (ACE 1), *J. Geophys. Res.*, *104* (D17), 21803-21818, doi: 10.1029/1999JD900238, 1999b.
- Blake, N.J., D.R. Blake, I.J. Simpson, J.P. Lopez, N.A.C. Johnston, A.L. Swanson, A.S. Katzenstein, S. Meinardi, B.C. Sive, J.J. Colman, E. Atlas, F. Flocke, S.A. Vay, M.A. Avery, and F.S. Rowland, Large-scale latitudinal and vertical distributions of NMHCs and selected halocarbons in the troposphere over the Pacific Ocean during the March-April 1999 Pacific Exploratory Mission (PEM-Tropics B), *J. Geophys. Res.*, *106* (D23), 32627-32644, 2001.
- Blake, N.J., D.R. Blake, I.J. Simpson, S. Meinardi, A.L. Swanson, J.P. Lopez, A.S. Katzenstein, B. Barletta, T. Shirai, E. Atlas, G. Sachse, M. Avery, S. Vay, H.E. Fuelberg, C.M. Kiley, K. Kita, F.S. Rowland, NMHCs and halocarbons in Asian continental outflow during TRACE-P: Comparison to PEM-West B, *J. Geophys. Res.*, *108* (D20), 8806, doi: 10.1029/2002JD003367, 2003a.
- Blake, N.J., D.R. Blake, A.L. Swanson, E. Atlas, F. Flocke, and F.S. Rowland, Latitudinal, vertical, and seasonal variations of C1-C4 alkyl nitrates in the troposphere over the Pacific Ocean during PEM-Tropics A and B: Oceanic and continental sources, *J. Geophys. Res.*, *108* (D2), 8242, doi: 10.1029/2001JD001444, 2003b.
- Bloss, W.J., D.M. Rowley, R.A. Cox, and R.L. Jones, Kinetics and products of the IO self-reaction, *J. Phys. Chem. A*, *105* (33), 7840-7854, 2001.
- Bobrowski, N., G. Honninger, B. Galle, and U. Platt, Detection of bromine monoxide in a volcanic plume, *Nature*, *423* (6937), 273-276, 2003.
- Bösch, H., C. Camy-Peyret, M.P. Chipperfield, R. Fitzenberger, H. Harder, U. Platt, and K. Pfeilsticker, Upper limits of stratospheric IO and OIO inferred from center-to-limb-darkening-corrected balloon-borne solar occultation visible spectra: Implications for total gaseous iodine and stratospheric ozone, *J. Geophys. Res.*, *108* (D15), 4455, doi: 10.1029/2002JD003078, 2003.
- Brunner, D., J. Staehelin, H.L. Rogers, M.O. Köhler, J.A. Pyle, D. Hauglustaine, L. Jourdain, T.K. Berntsen, M. Gauss, I.S.A. Isaksen, E. Meijer, P. van Velthoven, G. Pitari, E. Mancini, V. Grewe, and R. Sausen, An evaluation of the performance of chemistry transport models by comparison with research aircraft observations. Part 1: Concepts and overall model performance, *Atmos. Chem. Phys.*, *3*, 1609-1631, 2003.
- Bureau, H., H. Keppler, and N. Métrich, Volcanic degassing of bromine and iodine: Experimental fluid/melt partitioning data and applications to stratospheric chemistry, *Earth Planet. Sci. Lett.*, *183* (1-2), 51-60, 2000.
- Butchart, N., A.A. Scaife, M. Bourqui, J. de Grandpré, S.H.E. Hare, J. Kettleborough, U. Langematz, E. Manzini, F. Sassi, K. Shibata, D. Shindell, and M. Sigmond, Simulations of anthropogenic change in the strength of the Brewer-Dobson circulation, *Clim. Dyn.*, *27* (7-8), 727-741, 2006.
- Butler, J.H., D.B. King, S.A. Montzka, J.M. Lobert, S.A. Yvon-Lewis, and N.J. Warwick, Oceanic fluxes of CHBr₃, CH₂Br₂, and CH₃I into the marine boundary layer, *Global Biogeochem. Cycles*, *21*, doi: 10.1029/2006GB002732, in press, 2006.
- Butz, A., Case studies of stratospheric nitrogen, chlorine, and iodine photochemistry based on balloon borne UV/visible and IR absorption spectroscopy, Ph.D. thesis, University of Heidelberg, Heidelberg, Germany, Available: <http://www.ub.uni-heidelberg.de/archiv/6696>, 2006.
- Carpenter, L.J., Iodine in the marine boundary layer, *Chem. Rev.*, *103* (12), 4953-4962, 2003.
- Carpenter, L.J., and P.S. Liss, On temperate sources of bromoform and other reactive organic bromine gases, *J. Geophys. Res.*, *105* (D16), 20539-20548, 2000.
- Carpenter, L.J., G. Malin, P.S. Liss, and F.S. Küpper, Novel biogenic iodine-containing trihalomethanes and other short-lived halocarbons in the coastal East Atlantic, *Global Biogeochem. Cycles*, *14* (4), 1191-1204, 2000.
- Carpenter, L.J., P.S. Liss, and S.A. Penkett, Marine organohalogens in the atmosphere over the Atlantic and Southern Oceans, *J. Geophys. Res.*, *108* (D9), 4256, doi: 10.1029/2002JD002769, 2003.
- Carpenter, L.J., D.J. Wevill, S. O'Doherty, G. Spain, and P.G. Simmonds, Atmospheric bromoform at Mace Head, Ireland: seasonality and evidence for a peatland source, *Atmos. Chem. Phys.*, *5*, 2927-2934, 2005.

VERY SHORT-LIVED SUBSTANCES

- Chance, K., Analysis of BrO measurements from the Global Ozone Monitoring Experiment, *Geophys. Res. Lett.*, 25 (17), 3335-3338, 1998.
- Chen, P., Isentropic cross-tropopause mass exchange in the extratropics, *J. Geophys. Res.*, 100 (D8), 16661-16674, 1995.
- Chipperfield, M.P., and W. Feng, Comment on: Stratospheric ozone depletion at northern mid-latitudes in the 21st century: The importance of future concentrations of greenhouse gases nitrous oxide and methane, *Geophys. Res. Lett.*, 30 (7), 1389, doi: 10.1029/2002GL016353, 2003.
- Choi, Y., S. Elliott, I.J. Simpson, D.R. Blake, J.J. Colman, M.K. Dubey, S. Meinardi, F.S. Rowland, T. Shirai, and F.A. Smith, Survey of whole air data from the second airborne Biomass Burning and Lightning Experiment using principal component analysis, *J. Geophys. Res.*, 108 (D5), 4163, doi: 10.1029/2002JD002841, 2003.
- Chuck, A.L., S.M. Turner, and P.S. Liss, Oceanic distributions and air-sea fluxes of biogenic halocarbons in the open ocean, *J. Geophys. Res.*, 110, C10022, doi: 10.1029/2004JC002741, 2005.
- Cohan, D.S., G.A. Sturrock, A.P. Biazar, and P.J. Fraser, Atmospheric methyl iodide at Cape Grim, Tasmania, from AGAGE observations, *J. Atmos. Chem.*, 44 (2), 131-150, 2003.
- Collins, W.J., R.G. Derwent, C.E. Johnson, and D.S. Stevenson, A comparison of two schemes for the convective transport of chemical species in a Lagrangian global chemistry model, *Quart. J. Roy. Meteorol. Soc.*, 128 (581), 991-1009, 2002.
- Considine, D.B., D.J. Bergmann, and H. Liu, Sensitivity of Global Modeling Initiative chemistry and transport model simulations of radon-222 and lead-210 to input meteorological data, *Atmos. Chem. Phys.*, 5, 3389-3406, 2005.
- Cox, M.L., G.A. Sturrock, P.J. Fraser, S.T. Siems, and P.B. Krummel, Identification of regional sources of methyl bromide and methyl iodide from AGAGE observations at Cape Grim, Tasmania, *J. Atmos. Chem.*, 50 (1), 59-77, 2005.
- Crutzen, P.J., and M.G. Lawrence, The impact of precipitation scavenging on the transport of trace gases: A 3-dimensional model sensitivity study, *J. Atmos. Chem.*, 37 (1), 81-112, 2000.
- Davis, D., J. Crawford, S. Liu, S. McKeen, A. Bandy, D. Thornton, F. Rowland, and D. Blake, Potential impact of iodine on tropospheric levels of ozone and other critical oxidants, *J. Geophys. Res.*, 101 (D1), 2135-2147, 1996.
- Deiber, G., C. George, S. Le Calvé, F. Schweitzer, and P. Mirabel, Uptake study of ClONO₂ and BrONO₂ by halide containing droplets, *Atmos. Chem. Phys.*, 4 (5), 1291-1299, 2004.
- Dessler, A.E., and S.C. Sherwood, Effect of convection on the summertime extratropical lower stratosphere, *J. Geophys. Res.*, 109, D23301, doi: 10.1029/2004JD005209, 2004.
- Dessler, A.E., E.J. Hints, E.M. Weinstock, J.G. Anderson, and K.R. Chan, Mechanisms controlling water vapor in the lower stratosphere: "A tale of two stratospheres," *J. Geophys. Res.*, 100 (D11), 23167-23172, 1995.
- Donner, L.J., C.J. Seman, R.S. Hemler, and S. Fan, A cumulus parameterization including mass fluxes, convective vertical velocities, and mesoscale effects: Thermodynamic and hydrological aspects in a general circulation model, *J. Clim.*, 14 (16), 3444-3463, 2001.
- Dorf, M., Investigation of inorganic stratospheric bromine using balloon-borne DOAS measurements and model simulations, Ph.D. thesis, University of Heidelberg, Heidelberg, Germany, Available: <http://www.ub.uni-heidelberg.de/archiv/6093>, 2005.
- Dorf, M., H. Bösch, A. Butz, C. Camy-Peyret, M.P. Chipperfield, A. Engel, F. Goutail, K. Grunow, F. Hendrick, S. Hrechanyy, B. Naujokat, J.-P. Pommereau, M. Van Roozendaal, C. Sioris, F. Stroh, F. Weidner, and K. Pfeilsticker, Balloon-borne stratospheric BrO measurements: comparison with Envisat/SCIAMACHY BrO limb profiles, *Atmos. Chem. Phys.*, 6 (9), 2483-2501, 2006a.
- Dorf, M., J.H. Butler, A. Butz, C. Camy-Peyret, M.P. Chipperfield, L. Kritten, S.A. Montzka, B. Simmes, F. Weidner, and K. Pfeilsticker, Long-term observations of stratospheric bromine reveal slow down in growth, *Geophys. Res. Lett.*, 33, doi: 10.1029/2006GL027714, in press, 2006b.
- Dvortsov, V.L., M.A. Geller, V.A. Yudin, and S.P. Smyshlyaev, Parameterization of the convective transport in a two-dimensional chemistry-transport model and its validation with radon 222 and other tracer simulations, *J. Geophys. Res.*, 103 (D17), 22047-22062, 1998.
- Dvortsov, V.L., M.A. Geller, S. Solomon, S.M. Schauffler, E.L. Atlas, and D.R. Blake, Rethinking reactive halogen budgets in the midlatitude lower stratosphere, *Geophys. Res. Lett.*, 26 (12), 1699-1702, 1999.
- Ekman, A.M.L., C. Wang, J. Wilson, and J. Ström, Explicit simulations of aerosol physics in a cloud-resolving model: a sensitivity study based on an observed convective cloud, *Atmos. Chem. Phys.*,

- 4, 773-791, 2004.
- Engel, A., H. Bönisch, D. Brunner, H. Fischer, H. Franke, G. Günther, C. Gurk, M. Hegglin, P. Hoor, R. Königstedt, M. Krebsbach, R. Maser, U. Parchatka, T. Peter, D. Schell, C. Schiller, U. Schmidt, N. Spelten, T. Szabo, U. Weers, H. Wernli, T. Wetter, and V. Wirth, Highly resolved observations of trace gases in the lowermost stratosphere and upper troposphere from the Spurt project: An overview, *Atmos. Chem. Phys.*, *6*, 283-301, 2006.
- Fernandez, M.A., R.A. Cox, and R.G. Hynes, Kinetics of ClONO₂ reactive uptake on ice surfaces at temperatures of the upper troposphere, *J. Phys. Chem. A*, *109* (44), 9986-9996, 2005.
- Fischer, H., F.G. Wienhold, P. Hoor, O. Bujok, C. Schiller, P. Siegmund, M. Ambaum, H.A. Scheeren, and J. Lelieveld, Tracer correlations in the northern high latitude lowermost stratosphere: Influence of cross-tropopause mass exchange, *Geophys. Res. Lett.*, *27* (1), 97-100, 2000.
- Fischer, H., M. de Reus, M. Traub, J. Williams, J. Lelieveld, J. de Gouw, C. Warneke, H. Schlager, A. Minikin, R. Scheele, and P. Siegmund, Deep convective injection of boundary layer air into the lowermost stratosphere at midlatitudes, *Atmos. Chem. Phys.*, *3*, 739-745, 2003.
- Fitzenberger, R., H. Bösch, C. Camy-Peyret, M.P. Chipperfield, H. Harder, U. Platt, B.-M. Sinnhuber, T. Wagner, and K. Pfeilsticker, First profile measurements of tropospheric BrO, *Geophys. Res. Lett.*, *27* (18), 2921-2924, 2000.
- Folkins, I., and R.V. Martin, The vertical structure of tropical convection and its impact on the budgets of water vapor and ozone, *J. Atmos. Sci.*, *62* (5), 1560-1573, 2005.
- Folkins, I., M. Loewenstein, J. Podolske, S.J. Oltmans, and M. Proffitt, A barrier to vertical mixing at 14 km in the tropics: Evidence from ozonesondes and aircraft measurements, *J. Geophys. Res.*, *104*, (D18), 22095-22102, 1999.
- Fraser, P.J., D.E. Oram, C.E. Reeves, S.A. Penkett, and A. McCulloch, Southern hemispheric halon trends (1978-1998) and global halon emissions, *J. Geophys. Res.*, *104* (D13), 15985-15999, 1999.
- Frieler, K., M. Rex, R.J. Salawitch, T. Canty, M. Streibel, R.M. Stimpfle, K. Pfeilsticker, M. Dorf, D.K. Weisenstein, S. Godin-Beekmann, and P. von der Gathen, Toward a better quantitative understanding of polar stratospheric ozone loss, *Geophys. Res. Lett.*, *33*, L10812, doi: 10.1029/2005GL025466, 2006.
- Frieß, U., T. Wagner, I. Pundt, K. Pfeilsticker, and U. Platt, Spectroscopic measurements of tropospheric iodine oxide at Neumayer Station, Antarctica, *Geophys. Res. Lett.*, *28* (10), 1941-1944, 2001.
- Fromm, M.D., and R. Servranckx, Transport of forest fire smoke above the tropopause by supercell convection, *Geophys. Res. Lett.*, *30* (10), 1542, doi: 10.1029/2002GL016820, 2003.
- Fromm, M., R. Bevilacqua, R. Servranckx, J. Rosen, J.P. Thayer, J. Herman, and D. Larko, Pyro-cumulonimbus injection of smoke to the stratosphere: Observations and impact of a super blowup in northwestern Canada on 3-4 August 1998, *J. Geophys. Res.*, *110*, D08205, doi: 10.1029/2004JD005350, 2005.
- Fu, Q., C.M. Johanson, J.M. Wallace, and T. Reichler, Enhanced mid-latitude tropospheric warming in satellite measurements, *Science*, *312* (5777), 1179-1179, doi: 10.1126/science.1125566, 2006.
- Füeglistaler, S., H. Wernli, and T. Peter, Tropical troposphere-to-stratosphere transport inferred from trajectory calculations, *J. Geophys. Res.*, *109*, D03108, doi: 10.1029/2003JD004069, 2004.
- Gottelman, A., and P.M.F. Forster, A climatology of the tropical tropopause layer, *J. Meteorol. Soc. Japan*, *80* (4B), 911-924, 2002.
- Gottelman, A., P.M.F. Forster, M. Fujiwara, Q. Fu, H. Vömel, L.K. Gohar, C. Johanson, and M. Ammerman, Radiation balance of the tropical tropopause layer, *J. Geophys. Res.*, *109*, D07103, doi: 10.1029/2003JD004190, 2004.
- Harder, H., C. Camy-Peyret, F. Ferlemann, R. Fitzenberger, T. Hawat, H. Osterkamp, M. Schneider, D. Perner, U. Platt, P. Vradelis, and K. Pfeilsticker, Stratospheric BrO profiles measured at different latitudes and seasons: Atmospheric observations, *Geophys. Res. Lett.*, *25* (20), 3843-3846, 1998.
- Haynes, P., and E. Shuckburgh, Effective diffusivity as a diagnostic of atmospheric transport 2. Troposphere and lower stratosphere, *J. Geophys. Res.*, *105* (D18), 22795-22810, 2000.
- Hegels, E., P.J. Crutzen, T. Klüpfel, D. Perner, and J.P. Burrows, Global distribution of atmospheric bromine-monoxide from GOME on earth observing satellite ERS-2, *Geophys. Res. Lett.*, *25* (16), 3127-3130, 1998.
- Hegglin, M.I., D. Brunner, H. Wernli, C. Schwierz, O. Martius, P. Hoor, H. Fischer, U. Parchatka, N. Spelten, C. Schiller, M. Krebsbach, U. Weers, J. Staehelin, and T. Peter, Tracing troposphere-to-stratosphere transport above a mid-latitude deep convective system, *Atmos. Chem. Phys.*, *4*, 741-

VERY SHORT-LIVED SUBSTANCES

- 756, 2004.
- Hintsa, E.J., K.A. Boering, E.M. Weinstock, J.G. Anderson, B.L. Gary, L. Pfister, B.C. Daube, S.C. Wofsy, M. Loewenstein, J.R. Podolske, J.J. Margitan, and T.P. Bui, Troposphere-to-stratosphere transport in the lowermost stratosphere from measurements of H₂O, CO₂, N₂O and O₃, *Geophys. Res. Lett.*, 25 (14), 2655-2658, 1998.
- Hoffmann, T., C.D. O'Dowd, and J.H. Seinfeld, Iodine oxide homogeneous nucleation: An explanation for coastal new particle production, *Geophys. Res. Lett.*, 28 (10), 1949-1952, 2001.
- Hollwedel, J., M. Wenig, S. Beirle, S. Kraus, S. Kühl, W. Wilms-Grabe, U. Platt, and T. Wagner, Year-to-year variations of spring time polar tropospheric BrO as seen by GOME, *Adv. Space Res.*, 34 (4), 804-808, 2004.
- Holton, J.R., P.H. Haynes, M.E. McIntyre, A.R. Douglass, R.B. Rood, and L. Pfister, Stratosphere-troposphere exchange, *Rev. Geophys.*, 33 (4), 403-439, 1995.
- Hoor, P., H. Fischer, L. Lange, J. Lelieveld, and D. Brunner, Seasonal variations of a mixing layer in the lowermost stratosphere as identified by the CO-O₃ correlation from in situ measurements, *J. Geophys. Res.*, 107 (D5), 4044, doi: 10.1029/2000JD000289, 2002.
- Hoor, P., C. Gurk, D. Brunner, M.I. Hegglin, H. Wernli, and H. Fischer, Seasonality and extent of extra-tropical TST derived from in-situ CO measurements during SPURT, *Atmos. Chem. Phys.*, 4, 1427-1442, 2004.
- Hoor, P., H. Fischer, and J. Lelieveld, Tropical and extra-tropical tropospheric air in the lowermost stratosphere over Europe: A CO-based budget, *Geophys. Res. Lett.*, 32, L07802, doi: 10.1029/2004GL022018, 2005.
- Iraci, L.T., R.R. Michelsen, S.F.M. Ashbourn, T.A. Rammer, and D.M. Golden, Uptake of hypobromous acid (HOBr) by aqueous sulfuric acid solutions: Low-temperature solubility and reaction, *Atmos. Chem. Phys.*, 5, 1577-1587, 2005.
- Joseph, D.M., S.H. Ashworth, and J.M.C. Plane, The absorption cross-section and photochemistry of OIO, *J. Photochem. Photobiol. A*, 176 (1-3 Spec. Iss.), 68-77, 2005.
- Kärcher, B., and M.M. Basko, Trapping of trace gases in growing ice crystals, *J. Geophys. Res.*, 109, D22204, doi: 10.1029/2004JD005254, 2004.
- Kärcher, B., and U. Lohmann, A parameterization of cirrus cloud formation: Heterogeneous freezing, *J. Geophys. Res.*, 108 (D14), 4402, doi: 10.1029/2002JD003220, 2003.
- Keene, W.C., M.A.K. Khalil, D.J. Erickson III, A. McCulloch, T.E. Graedel, J.M. Lobert, M.L. Aucott, S.L. Gong, D.B. Harper, G. Kleiman, P. Midgley, R.M. Moore, C. Seuzaret, W.T. Sturges, C.M. Benkovitz, V. Koropalov, L.A. Barrie, and Y.F. Li, Composite global emissions of reactive chlorine from anthropogenic and natural sources: Reactive Chlorine Emissions Inventory, *J. Geophys. Res.*, 104 (D7), 8429-8440, 1999.
- Khalil, M.A.K., Reactive chlorine compounds in the atmosphere, Chapter 2 in *Reactive Halogen Compounds in the Atmosphere, Vol. 4, Part E of The Handbook of Environmental Chemistry*, edited by P. Fabian, and O.N. Singh, 45-79, Springer-Verlag, Heidelberg, Germany, 1999.
- Khalil, M.A.K., and R.A. Rasmussen, Atmospheric chloroform, *Atmos. Environ.*, 33 (7), 1151-1158, 1999.
- Khalil, M.A.K., R.M. Moore, D.B. Harper, J.M. Lobert, D.J. Erickson, V. Koropalov, W.T. Sturges, and W.C. Keene, Natural emissions of chlorine-containing gases: Reactive Chlorine Emissions Inventory, *J. Geophys. Res.*, 104 (D7), 8333-8346, 1999.
- Kindler, T.P., W.L. Chameides, P.H. Wine, D.M. Cunnold, F.N. Alyea, and J.A. Franklin, The fate of atmospheric phosgene and the stratospheric chlorine loadings of its parent compounds: CCl₄, C₂Cl₄, C₂HCl₃, CH₃CCl₃, and CHCl₃, *J. Geophys. Res.*, 100 (D1), 1235-1252, 1995.
- Knight, G.P., and J.N. Crowley, The reactions of IO with HO₂, NO and CH₃SCH₃: Flow tube studies of kinetics and product formation, *Phys. Chem. Chem. Phys.*, 3, 393-401, 2001.
- Ko, M.K.W., and G. Poulet (Lead Authors), D.R. Blake, O. Boucher, J.H. Burkholder, M. Chin, R.A. Cox, C. George, H.-F. Graf, J.R. Holton, D.J. Jacob, K.S. Law, M.G. Lawrence, P.M. Midgley, P.W. Seakins, D.E. Shallcross, S.E. Strahan, D.J. Wuebbles, and Y. Yokouchi, Very short-lived halogen and sulfur substances, Chapter 2 in *Scientific Assessment of Ozone Depletion: 2002, Global Ozone Research and Monitoring Project-Report No. 47*, World Meteorological Organization, Geneva, Switzerland, 2003.
- Ko, M.K.W., N.D. Sze, C.J. Scott, and D.K. Weisenstein, On the relation between stratospheric chlorine/bromine loading and short-lived tropospheric source gases, *J. Geophys. Res.*, 102 (D21), 25507-25518, 1997.
- Kondo, Y., M. Koike, K. Kita, H. Ikeda, N. Takegawa, S. Kawakami, D. Blake, S.C. Liu, M. Ko, Y. Miyazaki, H. Irie, Y. Higashi, B. Liley, N. Nishi, Y. Zhao, and T. Ogawa, Effects of biomass burning, lightning,

- and convection on O₃, CO, and NO_y over the tropical Pacific and Australia in August–October 1998 and 1999, *J. Geophys. Res.*, *108* (D3), 8402, doi: 10.1029/2001JD000820, 2002.
- Krämer, M., C. Schiller, H. Ziereis, J. Ovarlez, and H. Bunz, Nitric acid partitioning in cirrus clouds: The role of aerosol particles and relative humidity, *Tellus*, *58B* (2), 141-147, 2006.
- Krebsbach, M., C. Schiller, D. Brunner, G. Günther, M.I. Hegglin, D. Mottaghy, M. Riese, N. Spelten, and H. Wernli, Seasonal cycles and variability of O₃ and H₂O in the UT/LMS during SPURT, *Atmos. Chem. Phys.*, *6*, 109-125, 2006.
- Küpper, C., J. Thuburn, G.C. Craig, and T. Birner, Mass and water transport into the tropical stratosphere: A cloud-resolving simulation, *J. Geophys. Res.*, *109*, D10111, doi: 10.1029/2004JD004541, 2004.
- Kurylo, M.J., and J.M. Rodríguez (Lead Authors), M.O. Andreae, E.L. Atlas, D.R. Blake, J.H. Butler, S. Lal, D.J. Lary, P.M. Midgley, S.A. Montzka, P.C. Novelli, C.E. Reeves, P.G. Simmonds, L.P. Steele, W.T. Sturges, R.F. Weiss, and Y. Yokouchi, Short-lived ozone-related compounds, Chapter 2 in *Scientific Assessment of Ozone Depletion: 1998, Global Ozone Research and Monitoring Project—Report No. 44*, World Meteorological Organization, Geneva, Switzerland, 1999.
- Lary, D.J., Halogens and the chemistry of the free troposphere, *Atmos. Chem. Phys.*, *5*, 227-237, 2005.
- Laternus, F., C. Wiencke, and H. Kloser, Antarctic macroalgae – Sources of volatile halogenated organic compounds, *Mar. Environ. Res.*, *41* (2), 169-181, 1996.
- Lawrence, M.G., and P.J. Rasch, Tracer transport in deep convective updrafts: Plume ensemble versus bulk formulations, *J. Atmos. Sci.*, *62* (8), 2880-2894, 2005.
- Lee-Taylor, J., and K.R. Redeker, Reevaluation of global emissions from rice paddies of methyl iodide and other species, *Geophys. Res. Lett.*, *32*, L15801, doi: 10.1029/2005GL022918, 2005.
- Leser, H., G. Hönninger, and U. Platt, MAX-DOAS measurements of BrO and NO₂ in the marine boundary layer, *Geophys. Res. Lett.*, *30* (10), 1537, doi: 10.1029/2002GL015811, 2003.
- Levine, J.G., P. Braesicke, N.R.P. Harris, N.H. Savage, and J.A. Pyle, Pathways and timescales for troposphere-to-stratosphere transport via the tropical tropopause layer and their relevance for very short lived substances, *J. Geophys. Res.*, in press, 2006.
- Li, Y., K.O. Patten, D. Youn, and D.J. Wuebbles, Potential impacts of CF₃I on ozone as a replacement for CF₃Br in aircraft applications, *Atmos. Chem. Phys.*, *6*, 4559-4568, 2006.
- Libuda, H.G., Spektroskopische und kinetische Untersuchungen an halogenierten Carbonylverbindungen von atmosphärischem Interesse, Ph.D. thesis, University of Wuppertal, Germany, 1992.
- Liss, P.S., and P.G. Slater, Flux of gases across the air-sea interface, *Nature*, *247* (5438), 181-184, 1974.
- Livesey, N.J., L.J. Kovalenko, R.J. Salawitch, I.A. MacKenzie, M.P. Chipperfield, W.G. Read, R.F. Jarnot, and J.W. Waters, EOS Microwave Limb Sounder observations of upper stratospheric BrO: Implications for bromine, *Geophys. Res. Lett.*, *33*, L20817, doi: 10.1029/2006GL026930, 2006.
- Lobert, J.M., W.C. Keene, J.A. Logan, and R. Yevich, Global chlorine emissions from biomass burning: Reactive Chlorine Emission Inventory, *J. Geophys. Res.*, *104* (D7), 8373-8390, 1999.
- Low, J.C., N.Y. Wang, J. Williams, and R.J. Cicerone, Measurements of ambient atmospheric C₂H₅Cl and other ethyl and methyl halides at coastal California sites and over the Pacific Ocean, *J. Geophys. Res.*, *108* (19), 4608, doi: 10.1029/2003JD003620, 2003.
- Marcy, T.P., D.W. Fahey, R.S. Gao, P.J. Popp, E.C. Richard, T.L. Thompson, K.H. Rosenlof, E.A. Ray, R.J. Salawitch, C.S. Atherton, D.J. Bergmann, B.A. Ridley, A.J. Weinheimer, M. Loewenstein, E.M. Weinstock, and M.J. Mahoney, Quantifying stratospheric ozone in the upper troposphere with in situ measurements of HCl, *Science*, *304* (5668), 261-265, 2004.
- Mari, C., D.J. Jacob, and P. Bechtold, Transport and scavenging of soluble gases in a deep convective cloud, *J. Geophys. Res.*, *105* (D17), 22255-22268, 2000.
- Marsh, A.R.W., and W.J. McElroy, The dissociation constant and Henry's law constant of HCl in aqueous solution, *Atmos. Environ.*, *19* (7), 1075-1080, 1985.
- Martino, M., P.S. Liss, and J.M.C. Plane, The photolysis of dihalomethanes in surface seawater, *Environ. Sci. Technol.*, *39* (18), 7097-7101, 2005.
- McCulloch, A., Chloroform in the environment: Occurrence, sources, sinks and effects, *Chemosphere*, *50* (10), 1291-1308, 2003.
- McCulloch, A., M.L. Aucott, T.E. Graedel, G. Kleiman, P.M. Midgley, and Y.-F. Li, Industrial emissions of trichloroethene, tetrachloroethene, and dichloromethane: Reactive Chlorine Emissions Inventory, *J. Geophys. Res.*, *104* (D7), 8417-8427, 1999.
- McElroy, C.T., C.A. McLinden, and J.C. McConnell, Evidence for bromine monoxide in the free troposphere during the Arctic polar sunrise, *Nature*, *397* (6717), 338-341, 1999.

VERY SHORT-LIVED SUBSTANCES

- McFiggans, G., H. Coe, R. Burgess, J. Allan, M. Cubison, M.R. Alfarra, R. Saunders, A. Saiz-Lopez, J.M.C. Plane, D. Wevill, L. Carpenter, A.R. Rickard, and P.S. Monks, Direct evidence for coastal iodine particles from *Laminaria* macroalgae – Linkage to emissions of molecular iodine, *Atmos. Chem. Phys.*, *4* (3), 701-713, 2004.
- Misra, A., and P. Marshall, Computational investigations of iodine oxides, *J. Phys. Chem. A*, *102* (45), 9056-9060, 1998.
- Montzka, S.A., J.H. Butler, B.D. Hall, D.J. Mondeel, and J.W. Elkins, A decline in tropospheric organic bromine, *Geophys. Res. Lett.*, *30* (15), 1826, doi: 10.1029/2003GL017745, 2003.
- Moore, R.M., Dichloromethane in North Atlantic waters, *J. Geophys. Res.*, *109*, C09004, doi: 10.1029/2004JC002397, 2004.
- Moore, R.M., and W. Groszko, Methyl iodide distribution in the ocean and fluxes to the atmosphere, *J. Geophys. Res.*, *104* (C5), 11163-11172, 1999.
- Mössinger, J.C., R.G. Hynes, and R.A. Cox, Interaction of HOBr and HCl on ice surfaces in the temperature range 205-227 K, *J. Geophys. Res.*, *107* (D24), 4740, doi: 10.1029/2002JD002151, 2002.
- Mullendore, G.L., D.R. Durran, and J.R. Holton, Cross-tropopause tracer transport in midlatitude convection, *J. Geophys. Res.*, *110*, D06113, doi: 10.1029/2004JD005059, 2005.
- Müller, R.W., H. Bovensmann, J.W. Kaiser, A. Richter, A. Rozanov, F. Wittrock, and J.P. Burrows, Consistent interpretation of ground based and GOME BrO slant column data, *Adv. Space Res.*, *29* (11), 1655-1660, 2002.
- Muramatsu, Y., and S. Yoshida, Volatilization of methyl iodide from the soil-plant system, *Atmos. Environ.*, *29* (1), 21-25, 1995.
- Murphy, D.M., and D.S. Thomson, Halogen ions and NO⁺ in the mass spectra of aerosols in the upper troposphere and lower stratosphere, *Geophys. Res. Lett.*, *27* (19), 3217-3220, 2000.
- Murphy, D.M., D.S. Thomson, and T.J. Mahoney, In situ measurements of organics, meteoritic material, mercury, and other elements in aerosols at 5 to 19 kilometers, *Science*, *282* (5394), 1664-1669, 1998.
- Nassar, R., P.F. Bernath, C.D. Boone, C. Clerbaux, P.F. Coheur, G. Dufour, L. Froidevaux, E. Mahieu, J.C. McConnell, S.D. McLeod, D.P. Murtagh, C.P. Rinsland, K. Semeniuk, R. Skelton, K.A. Walker, and R. Zander, A global inventory of stratospheric chlorine in 2004, *J. Geophys. Res.*, *111*, D22312, doi: 10.1029/2006JD007073, 2006.
- Nedelec, P., V. Thouret, J. Brioude, B. Sauvage, J.-P. Cammas, and A. Stohl, Extreme CO concentrations in the upper troposphere over northeast Asia in June 2003 from the in situ MOZAIC aircraft data, *Geophys. Res. Lett.*, *32*, L14807, doi: 10.1029/2005GL023141, 2005.
- Nielsen, J.E., and A.R. Douglass, A simulation of bromoform's contribution to stratospheric bromine, *J. Geophys. Res.*, *106* (D8), 8089-8100, 2001.
- Nober, F.J., H.F. Graf, and D. Rosenfeld, Sensitivity of the global circulation to the suppression of precipitation by anthropogenic aerosols, *Global Planet. Change*, *37* (1), 57-80, 2003.
- O'Connor, F.M., G. Vaughan, and H. De Backer, Observations of subtropical air in the European mid-latitude lower stratosphere, *Quart. J. Roy. Meteorol. Soc.*, *125* (560), 2965-2986, 1999.
- O'Dowd, C.D., and T. Hoffmann, Coastal new particle formation: A review of the current state-of-the-art, *Environ. Chem.*, *2*, 245-255, 2005.
- Pan, L., S. Solomon, W. Randel, J.F. Lamarque, P. Hess, J. Gille, E.W. Chiou, and M.P. McCormick, Hemispheric asymmetries and seasonal variations of the lowermost stratospheric water vapor and ozone derived from SAGE II data, *J. Geophys. Res.*, *102* (D23), 28177-28184, 1997.
- Pan, L.L., W.J. Randel, B.L. Gary, M.J. Mahoney, and E.J. Hintsa, Definitions and sharpness of the extratropical tropopause: A trace gas perspective, *J. Geophys. Res.*, *109*, D23103, doi: 10.1029/2004JD004982, 2004.
- Peters, C., S. Pechtl, J. Stutz, K. Hebestreit, G. Hönninger, K.G. Heumann, A. Schwarz, J. Winterlik, and U. Platt, Reactive and organic halogen species in three different European coastal environments, *Atmos. Chem. Phys.*, *5*, 3357-3375, 2005.
- Pfeilsticker, K., W.T. Sturges, H. Bösch, C. Camy-Peyret, M.P. Chipperfield, A. Engel, R. Fitzenberger, M. Müller, S. Payan, and B.-M. Sinnhuber, Lower stratospheric organic and inorganic bromine budget for the Arctic winter 1998/99, *Geophys. Res. Lett.*, *27* (20), 3305-3308, 2000.
- Plane, J.M.C., D.M. Joseph, B.J. Allan, S.H. Ashworth, and J.S. Francisco, An experimental and theoretical study of the reactions of OIO + NO and OIO + OH, *J. Phys. Chem. A*, *110* (1), 93-100, 2006.
- Platt, U., and G. Hönninger, The role of halogen species in the troposphere, *Chemosphere*, *52* (2), 325-338, 2003.
- Popp, P.J., R.S. Gao, T.P. Marcy, D.W. Fahey, P.K. Hudson, T.L. Thompson, B. Kärcher, B.A. Ridley, A.J. Weinheimer, D.J. Knapp, D.D. Montzka, D.

- Baumgardner, T.J. Garrett, E.M. Weinstock, J.B. Smith, D.S. Sayres, J.V. Pittman, S. Dhaniyala, T.P. Bui, and M.J. Mahoney, Nitric acid uptake on subtropical cirrus cloud particles, *J. Geophys. Res.*, *109*, D06302, doi: 10.1029/2003JD004255, 2004.
- Poulida, O., R.R. Dickerson, and A. Heymsfield, Stratosphere-troposphere exchange in a midlatitude mesoscale convective complex 1. Observations, *J. Geophys. Res.*, *101* (D3), 6823-6836, 1996.
- Prados, A.I., G.E. Nedoluha, R.M. Bevilacqua, D.R. Allen, K.W. Hoppel, and A. Marenco, POAM III ozone in the upper troposphere and lowermost stratosphere: Seasonal variability and comparisons to aircraft observations, *J. Geophys. Res.*, *108* (D7), 4218, doi: 10.1029/2002JD002819, 2003.
- Prinn, R.G., R.F. Weiss, P.J. Fraser, P.G. Simmonds, D.M. Cunnold, F.N. Alyea, S. O'Doherty, P. Salameh, B.R. Miller, J. Huang, R.H.J. Wang, D.E. Hartley, C. Harth, L.P. Steele, G. Sturrock, P.M. Midgley, and A. McCulloch, A history of chemically and radiatively important gases in air deduced from ALE/GAGE/AGAGE, *J. Geophys. Res.*, *105* (D14), 17751-17792, 2000.
- PRTR, *Pollutant Release and Transfer Register 2002-Japan*, PRTR Data, (in Japanese), 197 pp., Minist. Econ. Trade Ind., Tokyo, Available at: <http://www.chem.unep.ch/prtr/>, 2004.
- Pundt, I., J.P. Pommereau, C. Phillips, and E. Lateltin, Upper limit of iodine oxide in the lower stratosphere, *J. Atmos. Chem.*, *30* (1), 173-185, 1998.
- Pundt, I., M. Van Roozendaal, T. Wagner, A. Richter, M. Chipperfield, J.P. Burrows, C. Fayt, F. Hendrick, K. Pfeilsticker, U. Platt, and J.-P. Pommereau, Simultaneous UV-vis measurements of BrO from balloon, satellite and ground: implications for tropospheric BrO, in *Stratospheric Ozone 1999, Proc. 5th European Symp.*, 27 September-1 October 1999, St. Jean de Luz, France, edited by N.R.P. Harris, M. Guirlet, and G.T. Amanatidis, *Air Pollution Research Rep. 73, EUR 19340*, 316-319, European Commission, Luxembourg, 2000.
- Pundt, I., J.-P. Pommereau, M.P. Chipperfield, M. Van Roozendaal, and F. Goutail, Climatology of the stratospheric BrO vertical distribution by balloon-borne UV-visible spectrometry, *J. Geophys. Res.*, *107* (D24), 4806, doi: 10.1029/2002JD002230, 2002.
- Qiu, L.X., S.H. Shi, S.B. Xing, and X.G. Chen, Rate constants for the reactions of hydroxyl with five halogen-substituted ethanes from 292 to 366 K, *J. Phys. Chem.*, *96* (2), 685-689, 1992.
- Quack, B., and D.W.R. Wallace, Air-sea flux of bromoform: Controls, rates, and implications, *Global Biogeochem. Cycles*, *17* (1), 1023, doi: 10.1029/2002GB001890, 2003.
- Quack, B., E. Atlas, G. Petrick, V. Stroud, S. Schauffler, and D.W.R. Wallace, Oceanic bromoform sources for the tropical atmosphere, *Geophys. Res. Lett.*, *31*, L23S05, doi: 10.1029/2004GL020597, 2004.
- Randel, W.J., F. Wu, A. Gettelman, J.M. Russell III, J.M. Zawodny, and S.J. Oltmans, Seasonal variation of water vapor in the lower stratosphere observed in Halogen Occultation Experiment data, *J. Geophys. Res.*, *106* (D13), 14313-14325, 2001.
- Randel, W.J., F. Wu, S.J. Oltmans, K. Rosenlof, and G.E. Nedoluha, Interannual changes of stratospheric water vapor and correlations with tropical tropopause temperatures, *J. Atmos. Sci.*, *61* (17), 2133-2148, 2004.
- Randel, W.J., F. Wu, H. Vömel, G.E. Nedoluha, and P. Forster, Decreases in stratospheric water vapor after 2001: Links to changes in the tropical tropopause and the Brewer-Dobson circulation, *J. Geophys. Res.*, *111*, D12312, doi: 10.1029/2005JD006744, 2006.
- Ray, E.A., K.H. Rosenlof, E.C. Richard, P.K. Hudson, D.J. Cziczo, M. Loewenstein, H.-J. Jost, J. Lopez, B. Ridley, A. Weinheimer, D. Montzka, D. Knapp, S.C. Wofsy, B.C. Daube, C. Gerbig, I. Xueref, and R.L. Herman, Evidence of the effect of summertime mid-latitude convection on the subtropical lower stratosphere from CRYSTAL-FACE tracer measurements, *J. Geophys. Res.*, *109*, D18304, doi: 10.1029/2004JD004655, 2004.
- Redeker, K.R., and R.J. Cicerone, Environmental controls over methyl halide emissions from rice paddies, *Global Biogeochem. Cycles*, *18*, GB1027, doi: 10.1029/2003GB002092, 2004.
- Redeker, K.R., N.-Y. Wang, J.C. Low, A. McMillan, S.C. Tyler, and R.J. Cicerone, Emissions of methyl halides and methane from rice paddies, *Science*, *290* (5493), 966-969, 2000.
- Redeker, K.R., S. Meinardi, D. Blake, and R. Sass, Gaseous emissions from flooded rice paddy agriculture, *J. Geophys. Res.*, *108* (D13), 4386, doi: 10.1029/2002JD002814, 2003.
- Reeves, C.E., W.T. Sturges, G.A. Sturrock, K. Preston, D.E. Oram, J. Schwander, R. Mulvaney, J.-M. Barnola, and J. Chappellaz, Trends of halon gases in polar firn air: Implications for their emission distributions, *Atmos. Chem. Phys.*, *5* (8), 2055-2064, 2005.
- Richter, A., F. Wittrock, A. Ladstätter-Weissenmayer, and J.P. Burrows, GOME measurements of strato-

VERY SHORT-LIVED SUBSTANCES

- spheric and tropospheric BrO, *Adv. Space Res.*, 29 (11), 1667-1672, 2002.
- Richter, U., and D.W.R. Wallace, Production of methyl iodide in the tropical Atlantic Ocean, *Geophys. Res. Lett.*, 31, L23S03, doi: 10.1029/2004GL020779, 2004.
- Ridley, B., E. Atlas, H. Selkirk, L. Pfister, D. Montzka, J. Walega, S. Donnelly, V. Stroud, E. Richard, K. Kelly, A. Tuck, T. Thompson, J. Reeves, D. Baumgardner, W.T. Rawlins, M. Mahoney, R. Herman, R. Friedl, F. Moore, E. Ray, and J. Elkins, Convective transport of reactive constituents to the tropical and mid-latitude tropopause region: I. Observations, *Atmos. Environ.*, 38 (9), 1259-1274, 2004.
- Rinsland, C.P., D.K. Weisenstein, M.K.W. Ko, C.J. Scott, L.S. Chiou, E. Mahieu, R. Zander, and P. Demoulin, Post-Mount Pinatubo eruption ground-based infrared stratospheric column measurements of HNO₃, NO, and NO₂ and their comparison with model calculations, *J. Geophys. Res.*, 108 (D15), 4437, doi: 10.1029/2002JD002965, 2003.
- Rosenlof, K.H., Seasonal cycle of the residual mean meridional circulation in the stratosphere, *J. Geophys. Res.*, 100 (D3), 5173-5191, 1995.
- Rowley, D.M., W.J. Bloss, R.A. Cox, and R.L. Jones, Kinetics and products of the IO + BrO reaction, *J. Phys. Chem. A*, 105 (33), 7855-7864, 2001.
- Saiz-Lopez, A., and J.M.C. Plane, Novel iodine chemistry in the marine boundary layer, *Geophys. Res. Lett.*, 31, L04112, doi: 10.1029/2003GL019215, 2004.
- Saiz-Lopez, A., J.M.C. Plane, and J.A. Shillito, Bromine oxide in the mid-latitude marine boundary layer, *Geophys. Res. Lett.*, 31, L03111, doi: 10.1029/2003GL018956, 2004a.
- Saiz-Lopez, A., R.W. Saunders, D.M. Joseph, S.H. Ashworth, and J.M.C. Plane, Absolute absorption cross-section and photolysis rate of I₂, *Atmos. Chem. Phys.*, 4 (5), 1443-1450, 2004b.
- Saiz-Lopez, A., J.M.C. Plane, G. McFiggans, P.I. Williams, S.M. Ball, M. Bitter, R.L. Jones, C. Hongwei, and T. Hoffmann, Modelling molecular iodine emissions in a coastal marine environment: the link to new particle formation, *Atmos. Chem. Phys.*, 6 (4), 883-895, 2006.
- Salawitch, R.J., D.K. Weisenstein, L.J. Kovalenko, C.E. Sioris, P.O. Wennberg, K. Chance, M.K.W. Ko, and C.A. McLinden, Sensitivity of ozone to bromine in the lower stratosphere, *Geophys. Res. Lett.*, 32 (5), L05811, doi: 10.1029/2004GL021504, 2005.
- Saltzman, E.S., M. Aydin, W.J. De Bruyn, D.B. King, and S.A. Yvon-Lewis, Methyl bromide in preindustrial air: Measurements from an Antarctic ice core, *J. Geophys. Res.*, 109 (5), D05301, doi: 10.1029/2003JD004157, 2004.
- Sander, R., W.C. Keene, A.A.P. Pszenny, R. Arimoto, G.P. Ayers, E. Baboukas, J.M. Caine, P.J. Crutzen, R.A. Duce, G. Hönninger, B.J. Huebert, W. Maenhaut, N. Mihalopoulos, V.C. Turekian, and R. Van Dingenen, Inorganic bromine in the marine boundary layer: A critical review, *Atmos. Chem. Phys.*, 3 (5), 1301-1336, 2003.
- Sander, S.P., R.R. Friedl, D.M. Golden, M.J. Kurylo, G.K. Moortgat, H. Keller-Rudek, P.H. Wine, A.R. Ravishankara, C.E. Kolb, M.J. Molina, B.J. Finlayson-Pitts, R.E., Huie, and V.L. Orkin, *Chemical Kinetics and Photochemical Data for Use in Atmospheric Studies: Evaluation No. 15, JPL Publication 06-2*, Jet Propulsion Laboratory, Pasadena, Calif., 2006.
- Schaffler, S.M., E.L. Atlas, F. Flocke, R.A. Lueb, V. Stroud, and W. Travnicek, Measurements of bromine containing organic compounds at the tropical tropopause, *Geophys. Res. Lett.*, 25 (3), 317-320, 1998.
- Schaffler, S.M., E.L. Atlas, D.R. Blake, F. Flocke, R.A. Lueb, J.M. Lee-Taylor, V. Stroud, and W. Travnicek, Distributions of brominated organic compounds in the troposphere and lower stratosphere, *J. Geophys. Res.*, 104 (D17), 21513-21535, 1999.
- Scheeren, H.A., J. Lelieveld, J.A. de Gouw, C. van der Veen, and H. Fischer, Methyl chloride and other chlorocarbons in polluted air during INDOEX, *J. Geophys. Res.*, 107 (D19), 8015, doi: 10.1029/2001JD001121, 2002.
- Schofield, R., K. Kreher, B.J. Connor, P.V. Johnston, A. Thomas, D. Shooter, M.P. Chipperfield, C.D. Rodgers, and G.H. Mount, Retrieved tropospheric and stratospheric BrO columns over Lauder, New Zealand, *J. Geophys. Res.*, 109, D14304, doi: 10.1029/2003JD004463, 2004.
- Schofield, R., P.V. Johnston, A. Thomas, K. Kreher, B.J. Connor, S. Wood, D. Shooter, M.P. Chipperfield, A. Richter, R. von Glasow, and C.D. Rodgers, Tropospheric and stratospheric BrO columns over Arrival Heights, Antarctica, 2002, *J. Geophys. Res.*, 111, D22310, doi: 10.1029/2005JD007022, 2006.
- Schweitzer, F., P. Mirabel, and C. George, Uptake of hydrogen halides by water droplets, *J. Phys. Chem. A*, 104 (1), 72-76, 2000.
- Sheode, N., B.-M. Sinnhuber, A. Rozanov, and J.P. Burrows, Towards a climatology of stratospheric bromine monoxide from SCIAMACHY limb observations, *Atmos. Chem. Phys. Discuss.*, 6, 6431-

- 6466, 2006.
- Sherwood, S.C., and A.E. Dessler, A model for transport across the tropical tropopause, *J. Atmos. Sci.*, *58* (7), 765-779, 2001.
- Simmonds, P.G., A.J. Manning, D.M. Cunnold, A. McCulloch, S. O'Doherty, R.G. Derwent, P.B. Krummel, P.J. Fraser, B. Dunse, L.W. Porter, R.H.J. Wang, B.R. Grealley, B.R. Miller, P. Salameh, R.F. Weiss, and R.G. Prinn, Global trends, seasonal cycles, and European emissions of dichloromethane, trichloroethene, and tetrachloroethene from the AGAGE observations at Mace Head, Ireland, and Cape Grim, Tasmania, *J. Geophys. Res.*, *111*, D18304, doi: 10.1029/2006JD007082, 2006.
- Simpson, I.J., O.W. Wingenter, D.J. Westberg, H.E. Fuelberg, C.M. Kiley, J.H. Crawford, S. Meinardi, D.R. Blake, and F.S. Rowland, Airborne measurements of cirrus-activated C₂Cl₄ depletion in the upper troposphere with evidence against Cl reactions, *Geophys. Res. Lett.*, *30* (20), 2025, doi: 10.1029/2003GL017598, 2003.
- Simpson, I.J., S. Meinardi, N.J. Blake, F.S. Rowland, and D.R. Blake, Long-term decrease in the global atmospheric burden of tetrachloroethene (C₂Cl₄), *Geophys. Res. Lett.*, *31*, L08108, doi: 10.1029/2003GL019351, 2004.
- Singh, H.B., L.J. Salas, and R.E. Stiles, Methyl halides in and over the eastern Pacific (40°N-32°S), *J. Geophys. Res.*, *88* (C6), 3684-3690, 1983.
- Sinnhuber, B.-M., and I. Folkins, Estimating the contribution of bromoform to stratospheric bromine and its relation to dehydration in the tropical tropopause layer, *Atmos. Chem. Phys.*, *6*, 4755-4761, 2006.
- Sinnhuber, B.-M., D.W. Arlander, H. Bovensmann, J.P. Burrows, M.P. Chipperfield, C.-F. Enell, U. Frieß, F. Hendrick, P.V. Johnston, R.L. Jones, K. Kreher, N. Mohamed-Tahrin, R. Müller, K. Pfeilsticker, U. Platt, J.-P. Pommereau, I. Pundt, A. Richter, A.M. South, K.K. Tørnkvist, M. Van Roozendael, T. Wagner, and F. Wittrock, Comparison of measurements and model calculations of stratospheric bromine monoxide, *J. Geophys. Res.*, *107* (D19), 4398, doi: 10.1029/2001JD000940, 2002.
- Sinnhuber, B.-M., A. Rozanov, N. Sheode, O.T. Afe, A. Richter, M. Sinnhuber, F. Wittrock, J.P. Burrows, G.P. Stiller, T. von Clarmann, and A. Linden, Global observations of stratospheric bromine monoxide from SCIAMACHY, *Geophys. Res. Lett.*, *32*, L20810, doi: 10.1029/2005GL023839, 2005.
- Sinnhuber, B.-M., N. Sheode, M. Sinnhuber, M.P. Chipperfield, and W. Feng, The contribution of anthropogenic bromine emissions to past stratospheric ozone trends: A modelling study, *Atmos. Chem. Phys. Discuss.*, *6*, 6497-6524, 2006.
- Sioris, C.E., L.J. Kovalenko, C.A. McLinden, R.J. Salawitch, M. Van Roozendael, F. Goutail, M. Dorf, K. Pfeilsticker, K. Chance, C. von Savigny, X. Liu, T.P. Kurosu, J.-P. Pommereau, H. Bösch, and J. Frerick, Latitudinal and vertical distribution of bromine monoxide in the lower stratosphere from Scanning Imaging Absorption Spectrometer for Atmospheric Chartography limb scattering measurements, *J. Geophys. Res.*, *111*, D14301, doi: 10.1029/2005JD006479, 2006.
- Smythe-Wright, D., S.M. Boswell, C.H. Lucas, A.L. New, and M.S. Varney, Halocarbon and dimethyl sulphide studies around the Mascarene Plateau, *Phil. Trans. R. Soc. Lond. A*, *363* (1826), 169-185, 2005.
- Soller, R., J.M. Nicovich, and P.H. Wine, Temperature-dependent rate coefficients for the reactions of Br(²P_{3/2}), Cl(²P_{3/2}), and O(³P_J) with BrONO₂, *J. Phys. Chem. A*, *105* (9), 1416-1422, 2001.
- Solomon, S., R.R. Garcia, and A.R. Ravishankara, On the role of iodine in ozone depletion, *J. Geophys. Res.*, *99* (D10), 20491-20499, 1994.
- Sprenger, M., and H. Wernli, A northern hemispheric climatology of cross-tropopause exchange for the ERA15 time period (1979-1993), *J. Geophys. Res.*, *108* (D12), 8521, doi: 10.1029/2002JD002636, 2003.
- Stohl, A., A 1-year Lagrangian "climatology" of airstreams in the Northern Hemisphere troposphere and lowermost stratosphere, *J. Geophys. Res.*, *106* (D7), 7263-7279, 2001.
- Stohl, A., P. Bonasoni, P. Cristofanelli, W. Collins, J. Feichter, A. Frank, C. Forster, E. Gerasopoulos, H. Gäggeler, P. James, T. Kentarchos, H. Kromp-Kolb, B. Krüger, C. Land, J. Meloen, A. Papayannis, A. Priller, P. Seibert, M. Sprenger, G.J. Roelofs, H.E. Scheel, C. Schnabel, P. Siegmund, L. Tobler, T. Trickl, H. Wernli, V. Wirth, P. Zanis, and C. Zerefos, Stratosphere-troposphere exchange: A review, and what we have learned from STACCATO, *J. Geophys. Res.*, *108* (D12), 8516, doi: 10.1029/2002JD002490, 2003.
- Stuart, A.L., and M.Z. Jacobson, A timescale investigation of volatile chemical retention during hydrometeor freezing: Nonrime freezing and dry growth riming without spreading, *J. Geophys. Res.*, *108* (D6), 4178, doi: 10.1029/2001JD001408, 2003.
- Sturges, W.T., D.E. Oram, L.J. Carpenter, S.A. Penkett, and A. Engel, Bromoform as a source of stratospheric bromine, *Geophys. Res. Lett.*, *27* (14), 2081-

VERY SHORT-LIVED SUBSTANCES

- 2084, 2000.
- Sturges, W.T., H.P. McIntyre, S.A. Penkett, J. Chappellaz, J.-M. Barnola, R. Mulvaney, E. Atlas, and V. Stroud, Methyl bromide, other brominated methanes and methyl iodide in polar firn air, *J. Geophys. Res.*, *106* (D2), 1595-1606, 2001.
- Stutz, J., R. Ackermann, J.D. Fast, and L. Barrie, Atmospheric reactive chlorine and bromine at the Great Salt Lake, Utah, *Geophys. Res. Lett.*, *29* (10), 1380, doi: 10.1029/2002GL014812, 2002.
- Thompson, T.M. (Ed.), J.H. Butler, B.C. Daube, G.S. Dutton, J.W. Elkins, B.D. Hall, D.F. Hurst, D.B. King, E.S. Kline, B.G. LaFleur, J. Lind, S. Lovitz, D.J. Mondeel, S.A. Montzka, F.L. Moore, J.D. Nance, J.L. Neu, P.A. Romashkin, A. Scheffer, and W.J. Snible, Halocarbons and other atmospheric trace species, in *Climate Monitoring and Diagnostics Laboratory: Summary Report No. 27, 2002-2003*, edited by R.C. Schnell, A.-M. Bugge, and R.M. Rosson, 115-135, NOAA/Climate Monitoring and Diagnostics Laboratory, Boulder, Colo., 2004.
- Thornton, B.F., D.W. Toohey, L.M. Avallone, H. Harder, M. Martinez, J.B. Simpas, W.H. Brune, and M.A. Avery, In situ observations of ClO near the winter polar tropopause, *J. Geophys. Res.*, *108* (D8), 8333, doi: 10.1029/2002JD002839, 2003.
- Thuburn, J., and G.C. Craig, On the temperature structure of the tropical stratosphere, *J. Geophys. Res.*, *107* (D2), 4017, doi: 10.1029/2001JD000448, 2002.
- Tiedtke, M., A comprehensive mass flux scheme for cumulus parameterization in large-scale models, *Mon. Wea. Rev.*, *117* (8), 1779-1800, 1989.
- Toon, G.C., J.-F. Blavier, B. Sen, and B.J. Drouin, Atmospheric COCl₂ measured by solar occultation spectrometry, *Geophys. Res. Lett.*, *28* (14), 2835-2838, 2001.
- Trudinger, C.M., D.M. Etheridge, G.A. Sturrock, P.J. Fraser, P.B. Krummel, and A. McCulloch, Atmospheric histories of halocarbons from analysis of Antarctic firn air: Methyl bromide, methyl chloride, chloroform, and dichloromethane, *J. Geophys. Res.*, *109*, D22310, doi: 10.1029/2004JD004932, 2004.
- Tucceri, M.E., D. Holscher, A. Rodriguez, T.J. Dillon, and J.N. Crowley, Absorption cross section and photolysis of OIO, *Phys. Chem. Chem. Phys.*, *8* (7), 834-846, 2006.
- Tuck, A.F., S.J. Hovde, K.K. Kelly, S.J. Reid, E.C. Richard, E.L. Atlas, S.G. Donnelly, V.R. Stroud, D.J. Cziczo, D.M. Murphy, D.S. Thomson, J.W. Elkins, F.L. Moore, E.A. Ray, M.J. Mahoney, and R.R. Friedl, Horizontal variability 1-2 km below the tropical tropopause, *J. Geophys. Res.*, *109*, D05310, doi: 10.1029/2003JD003942, 2004.
- Van Roozendaal, M., T. Wagner, A. Richter, I. Pundt, D.W. Arlander, J.P. Burrows, M. Chipperfield, C. Fayt, P.V. Johnston, J.-C. Lambert, K. Kreher, K. Pfeilsticker, U. Platt, J.-P. Pommereau, B.-M. Sinnhuber, K.K. Tørnkvist, and F. Wittrock, Intercomparison of BrO measurements from ERS-2 GOME, ground-based and balloon platforms, *Adv. Space Res.*, *29* (11), 1661-1666, 2002.
- Vaughan, G., and C. Timmis, Transport of near-tropopause air into the lower midlatitude stratosphere, *Quart. J. Roy. Meteorol. Soc.*, *124* (549), 1559-1578, 1998.
- von Glasow, R., R. Sander, A. Bott, and P.J. Crutzen, Modeling halogen chemistry in the marine boundary layer 2. Interactions with sulfur and the cloud-covered MBL, *J. Geophys. Res.*, *107* (D17), 4323, doi: 10.1029/2001JD000943, 2002.
- von Glasow, R., R. von Kuhlmann, M.G. Lawrence, U. Platt, and P.J. Crutzen, Impact of reactive bromine chemistry in the troposphere, *Atmos. Chem. Phys.*, *4*, 2481-2497, 2004.
- Wagner, T., and U. Platt, Satellite mapping of enhanced BrO concentrations in the troposphere, *Nature*, *395* (6701), 486-490, 1998.
- Wagner, T., C. Leue, M. Wenig, K. Pfeilsticker, and U. Platt, Spatial and temporal distribution of enhanced boundary layer BrO concentrations measured by the GOME instrument aboard ERS-2, *J. Geophys. Res.*, *106* (D20), 24225-24235, 2001.
- Wamsley, P.R., J.W. Elkins, D.W. Fahey, G.S. Dutton, C.M. Volk, R.C. Myers, S.A. Montzka, J.H. Butler, A.D. Clarke, P.J. Fraser, L.P. Steele, M.P. Lucarelli, E.L. Atlas, S.M. Schauffler, D.R. Blake, F.S. Rowland, W.T. Sturges, J.M. Lee, S.A. Penkett, A. Engel, R.M. Stimpfle, K.R. Chan, D.K. Weisenstein, M.K.W. Ko, and R.J. Salawitch, Distribution of halon-1211 in the upper troposphere and lower stratosphere and the 1994 total bromine budget, *J. Geophys. Res.*, *103* (D1), 1513-1526, 1998.
- Wang, P.K., Moisture plumes above thunderstorm anvils and their contributions to cross-tropopause transport of water vapor in midlatitudes, *J. Geophys. Res.*, *108* (D6), 4194, doi: 10.1029/2002JD002581, 2003.
- Warwick, N.J., G. Carver, X. Yang, N. Savage, F. O'Connor, R.A. Cox, and J.A. Pyle, Global modeling of natural bromocarbons, *J. Geophys. Res.*, in press, 2006.
- Wennberg, P.O., J.W. Brault, T.F. Hanisco, R.J. Salawitch,

- and G.H. Mount, The atmospheric column abundance of IO: Implications for stratospheric ozone, *J. Geophys. Res.*, *102* (D7), 8887-8898, 1997.
- Wernli, H., and M. Bourqui, A Lagrangian “1-year climatology” of (deep) cross-tropopause exchange in the extratropical Northern Hemisphere, *J. Geophys. Res.*, *107* (D2), 4021, doi: 10.1029/2001JD000812, 2002.
- Wittrock, F., R. Müller, A. Richter, H. Bovensmann, and J.P. Burrows, Measurements of iodine monoxide (IO) above Spitsbergen, *Geophys. Res. Lett.*, *27* (10), 1471-1474, 2000.
- WMO (World Meteorological Organization), *Scientific Assessment of Ozone Depletion: 1994, Global Ozone Research and Monitoring Project-Report No. 37*, Geneva, Switzerland, 1995.
- WMO (World Meteorological Organization), *Scientific Assessment of Ozone Depletion: 1998, Global Ozone Research and Monitoring Project-Report No. 44*, Geneva, Switzerland, 1999.
- WMO (World Meteorological Organization), *Scientific Assessment of Ozone Depletion: 2002, Global Ozone Research and Monitoring Project-Report No. 47*, Geneva, Switzerland, 2003.
- Worton, D.R., W.T. Sturges, J. Schwander, R. Mulvaney, J.-M. Barnola, and J. Chappellaz, 20th century trends and budget implications of chloroform and related tri- and dihalomethanes inferred from firn air, *Atmos. Chem. Phys.*, *6* (10), 2847-2863, 2006.
- Wuebbles, D.J., and M.K.W. Ko, *Summary of EPA/NASA Workshop on the Stratospheric Impacts of Short-Lived Gases*, March 30-31, 1999, Washington D.C., available through the U.S. Environmental Protection Agency, Stratospheric Protection Division, Washington D.C., 1999.
- Wuebbles, D.J., K.O. Patten, M.T. Johnson, and R. Kotamarthi, New methodology for Ozone Depletion Potentials of short-lived compounds: n-Propyl bromide as an example, *J. Geophys. Res.*, *106* (D13), 14551-14571, 2001.
- Yang, X., R.A. Cox, N.J. Warwick, J.A. Pyle, G.D. Carver, and F.M. O’Connor, Tropospheric bromine chemistry and its impacts on ozone: A model study, *J. Geophys. Res.*, *110*, D23311, doi: 10.1029/2005JD006244, 2005.
- Yano, J.I., F. Guichard, J.P. Lafore, J.L. Redelsperger, and P. Bechtold, Estimations of mass fluxes for cumulus parameterizations from high-resolution spatial data, *J. Atmos. Sci.*, *61* (7), 829-842, 2004.
- Yin, Y., D.J. Parker, and K.S. Carslaw, Simulation of trace gas redistribution by convective clouds – Liquid phase processes, *Atmos. Chem. Phys.*, *1*, 19-36, 2001.
- Yin, Y., K.S. Carslaw, and D.J. Parker, Redistribution of trace gases by convective clouds – Mixed-phase processes, *Atmos. Chem. Phys.*, *2*, 293-306, 2002.
- Yokouchi, Y., T. Inagaki, K. Yazawa, T. Tamaru, T. Enomoto, and K. Izumi, Estimates of ratios of anthropogenic halocarbon emissions from Japan based on aircraft monitoring over Sagami Bay, Japan, *J. Geophys. Res.*, *110*, D06301, doi: 10.1029/2004JD005320, 2005a.
- Yokouchi, Y., F. Hasebe, M. Fujiwara, H. Takashima, M. Shiotani, N. Nishi, Y. Kanaya, S. Hashimoto, P. Fraser, D. Toom-Saunty, H. Mukai, and Y. Nojiri, Correlations and emission ratios among bromoform, dibromochloromethane, and dibromomethane in the atmosphere, *J. Geophys. Res.*, *110*, D23309, doi: 10.1029/2005JD006303, 2005b.
- Zhou, Y., R.K. Varner, R.S. Russo, O.W. Wingenter, K.B. Haase, R. Talbot, and B.C. Sive, Coastal water source of short-lived halocarbons in New England, *J. Geophys. Res.*, *110*, D21302, doi: 10.1029/2004JD005603, 2005.
- Zingler, J., and U. Platt, Iodine oxide in the Dead Sea Valley: Evidence for inorganic sources of boundary layer IO, *J. Geophys. Res.*, *110*, D07307, doi: 10.1029/2004JD004993, 2005.

CHAPTER 3

Global Ozone: Past and Present

Lead Authors:

M.P. Chipperfield
V.E. Fioletov

Coauthors:

B. Bregman
J. Burrows
B.J. Connor
J.D. Haigh
N.R.P. Harris
A. Hauchecorne
L.L. Hood
S.R. Kawa
J.W. Krzyścin
J.A. Logan
N.J. Muthama
L. Polvani
W.J. Randel
T. Sasaki
J. Stähelin
R.S. Stolarski
L.W. Thomason
J.M. Zawodny

Contributors:

G. Bodeker
P. Demoulin
W. Feng
L. Flynn
S. Frith
S. Guillas
M. Ilyas
B. Knudsen
B. Liley
R. McPeters
A.J. Miller
R. Müller
S. Oltmans
Y. Orsolini
I. Petropavlovskikh
W. Steinbrecht
H. Struthers
D. Tarasick
Y. Terao

Final Release: February 2007

From *Scientific Assessment of Ozone Depletion: 2006*

CHAPTER 3

GLOBAL OZONE: PAST AND PRESENT

Contents

SCIENTIFIC SUMMARY	3.1
3.1 INTRODUCTION	3.5
3.2 UPDATE OF OZONE CHANGES	3.5
3.2.1 Statistical Methods	3.5
3.2.2 Changes in Total Ozone	3.7
3.2.3 Changes in the Vertical Distribution of Ozone	3.8
3.2.3.1 Upper Stratosphere	3.10
3.2.3.2 Lower Stratosphere	3.13
3.2.3.3 Consistency of Column and Profile Trends	3.17
3.2.4 Tropospheric Ozone	3.18
3.3 SUMMARY OF OTHER OBSERVATIONS	3.19
3.3.1 Stratospheric Aerosol and Its Precursors	3.19
3.3.2 Nitrogen Dioxide (NO ₂)	3.20
3.4 UNDERSTANDING AND INTERPRETATION OF OZONE CHANGES	3.21
3.4.1 Models	3.21
3.4.2 Dynamical Processes	3.22
3.4.3 Chemical Processes	3.25
3.4.3.1 Update of Relevant Kinetics	3.25
3.4.3.2 Lower Stratosphere	3.26
3.4.3.3 Upper Stratosphere	3.30
3.4.4 Solar Cycle Variations	3.30
3.4.5 Assessment Model Simulations	3.32
REFERENCES	3.41
APPENDIX 3A: DESCRIPTION OF THE OZONE DATASETS	3.55
3A.1 Column Ozone Data	3.55
3A.2 Ozone Profile Measurements	3.57

SCIENTIFIC SUMMARY

Total Column Ozone

- **Global mean total column ozone values for 2002-2005 were approximately 3.5% below 1964-1980 average values.** The 2002-2005 values are similar to the 1998-2001 values and this indicates that ozone is no longer decreasing. These changes are evident in all available global datasets, although differences of up to 1% between annual averages exist between some individual sets.
- **Averaged for the period 2002-2005, total column ozone for the Northern Hemisphere (NH) and Southern Hemisphere (SH) midlatitudes (35°-60°) are about 3% and 5.5%, respectively, below their 1964-1980 average values and are similar to their 1998-2001 values.** However, as noted in previous Assessments, the behavior of column ozone in the two hemispheres during the 1990s was different. The NH shows a minimum around 1993, followed by an increase. The SH shows an ongoing decrease through the late 1990s, followed by the recent leveling off.
- **There are seasonal differences in ozone changes over midlatitudes between the NH and the SH.** Changes since the pre-1980 period over northern midlatitudes (35°N-60°N) are larger in spring, while those over southern midlatitudes (35°S-60°S) are nearly the same throughout the year.
- **Total column ozone over the tropics (25°S-25°N) remains essentially unchanged.** Total ozone trends in this region for the period 1980-2004 are not statistically significant. These findings are consistent with the findings of the previous Assessments.

Vertical Ozone Distribution

- **Upper stratospheric ozone declined during 1979-1995, but has been relatively constant during the last decade.** Measurements from the Stratospheric Aerosol and Gas Experiment (SAGE I+II) and Solar Backscatter Ultraviolet (SBUV(2)) satellite instruments show significant declines through 1995 when averaged over 60°N-60°S and altitudes of 35 to 50 kilometers (km). The net ozone decrease was ~10-15% over midlatitudes; smaller but significant changes occurred over the tropics. Available independent Umkehr, lidar, and microwave ozone measurements confirm these findings.
- **Lower stratospheric ozone declined over the period 1979-1995, but has been relatively constant with significant variability over the last decade.** At midlatitudes of both the Northern and Southern Hemispheres, measurements by SAGE I+II and SBUV(2) showed declines of up to 10% by 1995 between 20 and 25 km altitude. These decreases did not continue in the last decade.
- **In the lowermost stratosphere, between 12 and 15 km in the Northern Hemisphere, a strong decrease in ozone was observed from ozonesonde data between 1979 and 1995, followed by an overall increase from 1996 to 2004, leading to no net long-term decrease at this level.** These changes in the lowermost stratosphere have a substantial influence on the column. The Southern Hemisphere midlatitude data do not show a similar increase since 1995 at these altitudes.
- **Significant ozone decreases of ~3% between the tropopause and 25 km are found in the SAGE satellite measurements between 1979 and 2004 at 25°S-25°N.** Since no change is found in total ozone over the tropics, this could be explained by significant increases in tropospheric ozone in the tropics. While regional increases in tropical tropospheric ozone have been seen, not all tropical regions or datasets show an increase.

GLOBAL OZONE

Understanding Past Changes in Ozone

- **There has been no change in our basic understanding that, analyzed over all latitudes and seasons, halogen increases have been the principal driver of ozone depletion over the past few decades.** There is good overall agreement between observed long-term changes in extrapolar ozone and model simulations that include the effects of increasing halogens. The models generally reproduce the observed ozone changes as a function of altitude, latitude, and season, confirming our understanding that halogen changes are the main driver of global ozone changes. This link is supported by the statistical fit of globally averaged ozone observations with Equivalent Effective Stratospheric Chlorine (EESC).
- **Empirical and model studies have shown that changes in tropospheric and stratospheric dynamics have been partially responsible for the observed NH midlatitude winter ozone decline from 1979 to the mid-1990s and ozone increase thereafter.** Whether this is due to dynamical variability or results from a long-term trend in stratospheric circulation is not yet clear. Estimates of these dynamical effects on long-term trends range from ~20% up to 50% for the winter period.
- **The impact of aerosols (dynamical and chemical) on midlatitude ozone was greatest in the early 1990s after the eruption of Mt. Pinatubo in 1991.** The observed decrease in NH column ozone in 1993 agrees with chemical-dynamical models that include these effects. An outstanding issue is the absence of an effect of the Mt. Pinatubo eruption on the observed SH ozone column, which contrasts with model predictions.
- **Several independent modeling studies covering periods in the 1990s confirm that dilution of ozone-depleted polar air makes a substantial contribution to midlatitude ozone depletion, especially in the Southern Hemisphere (due to the much larger polar ozone loss there).** Long-term annually averaged model-based estimates indicate that dilution by polar air contributes about one-third of the midlatitude ozone depletion in the Northern Hemisphere, with large interannual variation; in the Southern Hemisphere midlatitudes, the contribution is estimated to be about one-half.
- **The inclusion of additional inorganic bromine (Br_y) from very short-lived substances (VSLS) in models leads to larger ozone destruction at midlatitudes, compared with studies including only long-lived bromine source gases.** The enhanced ozone loss occurs in the lower stratosphere via interactions of this bromine with anthropogenic chlorine. Midlatitude ozone loss is most enhanced during periods of high aerosol loading. Ozone loss through cycles involving bromine and odd-hydrogen (HO_x) is also enhanced at midlatitudes under all conditions. The impact on long-term midlatitude ozone trends (1980-2004), assuming constant VSLS Br_y , is calculated to be small because aerosol loading was low at the start and end of this time period.
- **The profile shape of upper stratospheric ozone trends from 1980-2004 is generally consistent with our understanding of gas-phase chlorine chemistry as the cause, modulated by changes in temperature and other gases such as methane (CH_4).** However, global dynamical-chemical models have not demonstrated that they can simultaneously reproduce realistic trends in all relevant parameters, although observations over the full time period are limited. Non-interactive models obtain ozone change that peak at about 14% for 1980-2004 (in altitude coordinates), consistent with SAGE observations. Interactive models, which calculate their own temperatures, obtain ozone trends that are nearly half in magnitude.
- **Both two-dimensional (2-D) and three-dimensional (3-D) models perform better in reproducing observed past changes in the NH than in the SH.** Consistent with results presented in the previous Assessment, 2-D models show large model-model differences in the SH due to different treatments of the Antarctic ozone loss. Off-line 3-D chemical transport models (CTMs) are now also routinely available to study past changes. These models are inherently better in simulating the polar regions and this leads to relatively small model-model differences, especially in the SH. CTMs also clearly perform better at reproducing long-term changes in the NH than in the SH. The ongoing disagreement between model-observation comparisons in the NH versus the SH indicates that we do not yet have a full understanding of the processes controlling ozone changes at midlatitudes.

Solar Cycle

- **Identification of the solar cycle signal in observed ozone has been improved due to the absence of major volcanic eruptions over the past 15 years.** The deduced solar cycle variation in column ozone has a mean amplitude of 2-3% (from minimum to maximum) in low to midlatitudes from the extended data series.
- **Model estimates and measurements suggest that the amplitude of the solar cycle in ozone concentration is less than 4% throughout the stratosphere, although there are apparent differences between the models and observations at some altitudes.** The vertical structure of the ozone solar cycle variation is subject to observational uncertainties (e.g., short record lengths, instrument intercalibration problems) that make it difficult to test models critically.

3.1 INTRODUCTION

The abundance of stratospheric ozone is determined by a combination of chemical and dynamical processes. The importance of these processes changes with location (particularly altitude and latitude) and with time. These processes also act on different time scales. For example, the influence of the solar cycle on total column ozone varies over its 11-year cycle, the quasi-biennial oscillation (QBO) over an approximately 27-month cycle, and strong volcanic eruptions have an effect lasting a few years.

The long-term changes in global ozone were last reviewed in Chapter 4 of WMO (2003). At that time, global total ozone values were about 3% below the pre-1980 levels. This reduction had occurred primarily in the mid- to high latitudes of both hemispheres, with no significant trends reported in the tropics. Clear differences between the two hemispheres were noted. Annually averaged total ozone over the northern midlatitudes was 3% lower than pre-1980 levels, with twice as much decline in winter than in summer. Over the southern midlatitudes, by contrast, a long-term decrease of 6% had occurred, roughly constant through the year.

WMO (2003) concluded that models including observed changes in halocarbons, other source gases, and aerosols captured the long-term behavior in midlatitudes. At that time, the differences between the Northern and Southern Hemispheres were not explained. However, the report did conclude that there was increased evidence that the observed changes in atmospheric dynamics had a significant influence on ozone over northern midlatitudes on decadal time scales. It also noted that the magnitude of these influences, largest in the lower stratosphere, had not been quantified unambiguously. At higher altitudes (35–50 kilometers (km)), ozone trends were up to 8%/decade over midlatitudes in both hemispheres, consistent with expectation due to the observed changes in chlorine concentrations.

In this chapter, the same issues are examined with the benefit of an additional four years of measurements and a number of new analyses and interpretations. Equivalent effective stratospheric chlorine (EESC) peaked in the late 1990s to early 2000s, and so there are now several years of observations since that peak. There is an encouraging consistency between the observations of ozone and the behavior expected from EESC changes. Major emphases of this chapter are whether the gradual reduction in EESC, described in Chapter 1, can be found in the observational record when broken down by latitude and altitude, and whether the observational record can be reproduced by models. The decadal influence of the changes in dynamical processes is again an important issue

for Northern Hemisphere midlatitudes, and one that is critical for a complete understanding of total ozone changes over the last decades.

Both dynamical and chemical processes may contribute to decadal ozone (O_3) changes in the lower stratosphere. There is no single cause and the relative contributions of different processes will change with time period considered and between the hemispheres. Chemical changes in midlatitudes may result from changes in O_3 loss processes occurring locally or those at polar latitudes (see Chapter 4), whose effects are subsequently transported to midlatitudes. Both gas-phase and heterogeneous chemical processes are important in these processes. A major chemical driver for long-term lower stratospheric ozone changes is increases in chlorine and bromine.

Previous Assessments described long-term ozone changes in terms of linear trends, estimated using regression analysis. The decision to fit a linear trend was based on the expected response to the approximately linear increase in ozone-depleting substances (ODSs). However, it has become clear that the change of ODSs after the mid-1990s is no longer linear with time. In addition, ozone data in the late 1990s to early 2000s do not follow the trend line drawn by fitting the past data to a linear function. Recent studies of long-term changes in ozone are focused on detection of the ODS-related signal in the available data. Typically this is done by including a term in statistical models that is proportional to the stratospheric burden of ODSs, such as EESC or a similar function.

In this chapter, Section 3.2 presents the basic observations of ozone, with particular emphasis on behavior over the past 4 years and a statistical interpretation. Section 3.3 presents observations of long-term changes in aerosols and nitrogen dioxide (NO_2) that are relevant to stratospheric ozone. Finally, Section 3.4 discusses the dynamical and chemical processes that lead to ozone changes and summarizes the use of “physical” models for quantifying the contributions of the key processes to these changes.

3.2 UPDATE OF OZONE CHANGES

3.2.1 Statistical Methods

The general purpose of the use of statistical models is to characterize and quantify the relationship between “predictor” or “explanatory” variables and ozone. Some of the explanatory variables describe natural variations in ozone, while others are included in the model to reflect possible anthropogenic changes in ozone. Multiple linear regression is typically used to estimate statistical model

GLOBAL OZONE

parameters (e.g., SPARC, 1998; Weatherhead et al., 1998, 2000; Reinsel et al., 2002, 2005; Svenby and Dahlback, 2004; Krzyścin, 2006).

Seasonal cycle, solar flux (see Section 3.4.4), and quasi biennial oscillation (QBO) indices are commonly used as proxies for natural ozone variability. Characteristics of volcanic aerosols, such as aerosol optical depth, are used in some models to account for effects of volcanic eruptions, particularly for the El Chichón and Mt. Pinatubo eruptions (see Section 3.3.1).

The way proxies are included in a regression model can be an issue. Steinbrecht et al. (2004a) used harmonic oscillations to describe ozone variations related to the 11-year solar cycle, while Newchurch et al. (2003) assume strict proportionality to the 10.7-cm solar radio flux with no seasonal variation. Debate over the accuracy, robustness, and physical meaning of such choices of proxies is found in Steinbrecht et al. (2004b) and Cunnold et al. (2004). Stolarski et al. (2006) used the 10.7-cm solar radio flux proxy and allowed for possible seasonal variations. Harris et al. (2003) and Malanca et al. (2005) used a polynomial fit to separate long-term ozone changes from natural variability.

A linear function was used in earlier ozone Assessments (WMO, 1995; 1999) to describe long-term changes in ozone due to ODSs. As noted above, the increase of ODSs is not approximated well by a linear function over the time period from the late 1970s through the 1990s and beyond. The piecewise linear trend concept, in which different linear fits are used before and after a turning point, has been incorporated in several recent trend analyses (e.g., Newchurch et al., 2003; Reinsel et al., 2005; Miller et al., 2006). The turnaround date has been chosen to be January 1996 (Reinsel et al., 2002; 2005) or 1994 (Krzyścin et al., 2005).

Instead of fitting a linear (or piecewise) trend to the ozone time series, the changes in ozone can be analyzed using the EESC function (Chapter 1). The EESC is an index reflecting the amount of ozone-depleting chlorine and bromine in the stratosphere (Chapter 8). Daniel et al. (1995) suggested that a change in total column ozone can be assumed to be generally proportional to the EESC. The EESC trend model has been used in several recent statistical analyses of ozone (e.g., Newman et al., 2004; Guillas et al., 2004; Yang et al., 2005; Fioletov and Shepherd, 2005; Dhomse et al., 2006; Stolarski et al., 2006). This chapter is focused on detection of the EESC-related signals in available ozone records and so we use this method. Piecewise trends and other methods used for the detection of ozone recovery are discussed further in Chapter 6.

The contribution of different explanatory variables to ozone fluctuations is illustrated in Figure 3-1 (upper

panel). It shows area-weighted seasonal mean total ozone values for the region 60°S-60°N estimated from ground-based data, and the contribution (in Dobson units, DU) of major components of the ozone variability to the total integral: the seasonal cycle, solar cycle-related signal, QBO, and an estimated volcanic-related component. The EESC-related term included in the regression model allows for possible seasonal variations. The residuals are also shown. Possible anthropogenic changes in ozone are isolated by removing known natural components of ozone variability. Total ozone for the region 60°S-60°N, with seasonal components and volcanic-, solar cycle-, and QBO-related components removed, are shown in Figure 3-1 (lower panel). The seasonal component of the EESC-related signal is also removed from the data to reduce seasonal variations of the residuals. The plot illustrates the good agreement between the long-term changes in ozone and the EESC.

For trends derived as a regression onto the EESC time series as shown in Figure 3-1, the results can be expressed in several ways:

- (a) The results can be simply expressed as ozone change per unit of EESC (e.g., % per 0.1 parts per billion by volume (ppbv) EESC).
- (b) The EESC time series is nearly linear for 1979-1989 (see Figure 3-1), with a net change of approximately 1.0 ppbv of chlorine. Thus the EESC fit to ozone can be expressed in terms of linear changes for this time period, with results reported in ozone changes (% or DU) per decade (as in Stolarski et al., 2006).
- (c) Ozone changes associated with EESC can also be expressed as simple differences between two time periods.

Here we follow (b) and show results expressed as percent per decade for 1979-1989. The net change in ozone between 1979 and 2005 is approximately 1.4 times these linear trend values (i.e., a -5% per decade trend corresponds to approximately a -7% net change for 1979-2005). Approach (b) also makes it easier to compare EESC-related trends discussed here with linear ozone trends reported in the earlier Assessments.

There are certain issues related to the use of EESC as a regressor. The EESC calculation depends on the age of air spectrum, which varies with altitude and latitude (see Newman et al. (2006) and Box 8-1 of Chapter 8 for details). The age of air is about 3 years in the midlatitude lower stratosphere. It is longer, about 6 years, over the poles and in the upper stratosphere. Ozone dilution from the Antarctic, and to a lesser degree from the Arctic, affects lower stratospheric ozone over midlatitudes (Section 3.4.3) and, strictly speaking, the “polar” EESC should also

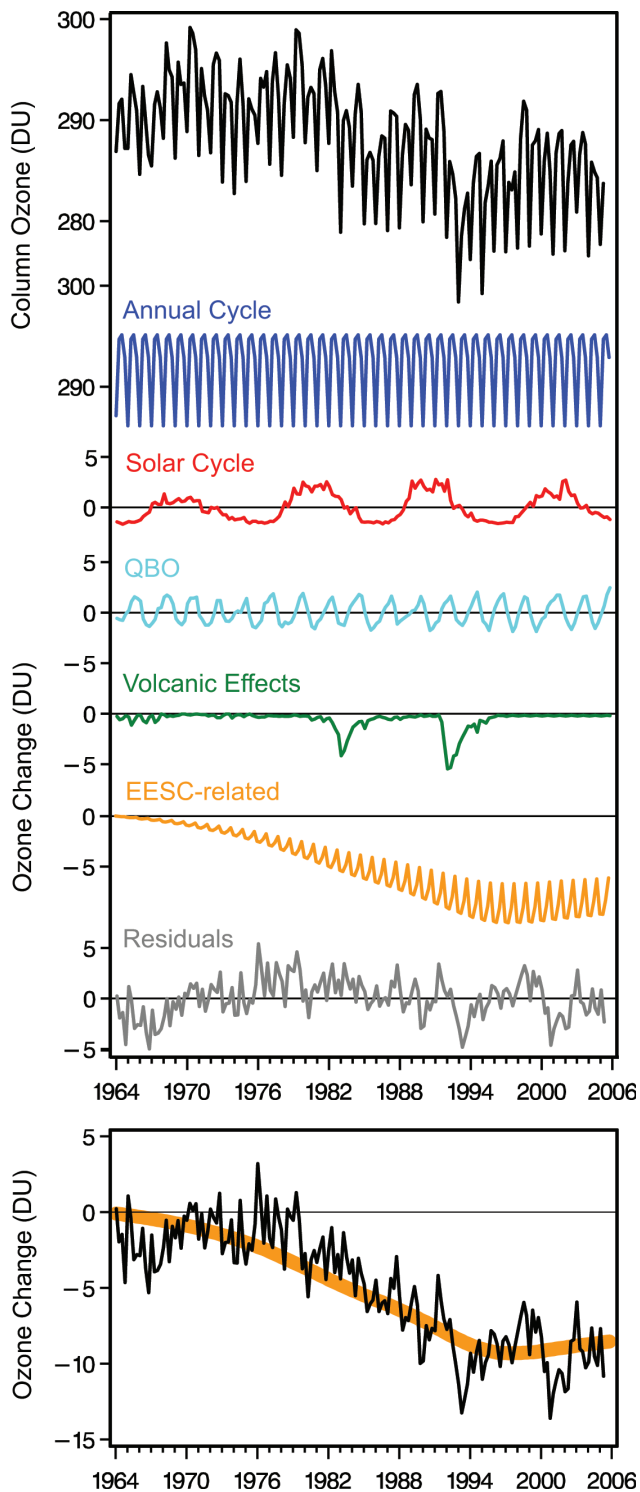


Figure 3-1. Top: Ozone variations for 60°S-60°N estimated from ground-based data and individual components that comprise ozone variations. Bottom: Deseasonalized, area-weighted total ozone deviations estimated from ground-based adjusted for solar, volcanic, and QBO effects, for 60°S-60°N. The thick yellow line represents the EESC curve scaled to fit the data from 1964-2005.

be used as a contributing factor when midlatitude trends are considered. However, due to the shape of the EESC curve, a 3-year difference in the age of air has limited effect on the estimated EESC-related regression coefficient. For example, the annual trend for 60°S-60°N is $-1.6\% \pm 0.17\%$ and $-1.3\% \pm 0.15\%$ per decade (2σ uncertainties here and elsewhere in this chapter) for EESC calculated with an age of air of 3 and 6 years, respectively. However, the age of air plays a major role when ozone recovery is considered (see Chapter 8).

Care must be used when comparing trends derived from data in different vertical coordinate systems. In the presence of a temperature trend, the various representations of the changes in ozone profiles will give different trends because of the changing altitudes of pressure surfaces and the changing air density on pressure surfaces with time. These trend differences will depend on the magnitude of the temperature trend and are important only in the upper stratosphere. Rosenfield et al. (2005) demonstrated that between 1979 and 1997, ozone trend differences at 3 hectoPascals (hPa) are as large as 1-2%/decade depending on how ozone changes are reported, with the largest differences in the southern high latitudes. The most negative trend is computed when ozone profiles are given as number densities on geometric altitude, while the least negative trend is computed for number densities on pressure levels. The Stratospheric Aerosol and Gas Experiment (SAGE) instrument measures ozone profiles as number densities on geometric altitude, while Solar Backscatter Ultraviolet (SBUV) data are provided as mixing ratios on a pressure grid. Thus, upper stratospheric ozone trends computed from SAGE data will be larger than those computed from SBUV data when the trends are computed in the natural vertical coordinate for each instrument. For comparison with SBUV, SAGE data are typically converted from number density on altitude levels to mixing ratio on pressure levels (e.g., Wang et al., 1996; McPeters et al., 1994). However, errors in the temperature data used to carry out this conversion can then affect the computed trends. Li et al. (2002) estimated that adjustment for the temperature trends would reduce differences in SBUV trends relative to SAGE by about 1%/decade, in agreement with Rosenfield et al. (2005).

3.2.2 Changes in Total Ozone

Since the previous Assessment (WMO, 2003), satellite data from Total Ozone Mapping Spectrometer (TOMS) and SBUV(2) instruments have been reprocessed with the new version 8 algorithm (Bhartia et al., 2004). This has resulted in better agreement between satellite and ground-based datasets, particularly in the 1980s and early 1990s. The version 8 algorithm was also

GLOBAL OZONE

applied to 1970-1977 measurements from the Nimbus 4 Backscatter Ultraviolet (BUV) instrument, and these data are shown in figures below. A new version of Global Ozone Monitoring Experiment (GOME) data was also used here. Details of the instruments and datasets can be found in Appendix 3A.

The approach used in WMO (2003) is again used here (Fioletov et al., 2002). Five datasets of 5°-wide zonal averages of total ozone values are analyzed in this Assessment and described in the Appendix. Area-weighted seasonal (3-month) averages are calculated for different latitude belts and for the globe. Each dataset has been deseasonalized with respect to the period 1979-1987, followed by subtraction of the average of the monthly mean anomalies for 1964-1980, estimated from ground-based data. Deviations are expressed as percentages of the ground-based time average for the period 1964-1980.

As a part of the deseasonalizing process, the long-term trends for individual seasons have been removed and replaced by the average of seasonal trends, as was previously done in WMO (1999). Unlike WMO (1999), where the trend was approximated by a straight line, the EESC curve is used here as a proxy for the trend function. For regions with missing data, ozone deviations are assumed to be identical to the surrounding latitude belts where data are available.

The total ozone deviations for the 90°S-90°N, 60°S-60°N, 35°-60°N, and 35°-60°S latitude belts are shown in Figures 3-2 and 3-3. These plots differ slightly from those of WMO (2003) because the satellite data processing algorithms have changed. The ozone deviations in the most recent years are similar to those in the late 1990s-early 2000s, with no clear change in magnitude. A decadal periodic component related to the 11-year solar cycle is discussed in Section 3.4.4. Another distinct feature seen in the unsmoothed data plot is a periodic structure with a period of 2-3 years that is likely associated with the QBO. These components are estimated and removed using statistical models as described above. Furthermore, to remove short-term fluctuations, annual averages were calculated (Figure 3-2 and 3-3, bottom). Comparing hemispheres, midlatitude ozone values in 2002-2005 are about 3% lower than the pre-1980 level in the Northern Hemisphere (NH) and about 5.5% lower in the Southern Hemisphere (SH) (Figure 3-3), i.e., they are similar to those reported in WMO (2003).

Figure 3-4 shows the total ozone deviations in the tropics (25°S-25°N), where about 40% of global ozone is located. No long-term changes in total column ozone have been observed over the equator (e.g., Reinsel et al., 2005). Outside the equatorial region, total ozone at 10°-25°S and 10°-25°N shows some signs of decline, but the trends are

not statistically significant. As discussed in Section 3.4.4, there is a strong decadal periodic component in tropical total ozone variations, probably related to the solar cycle. The solar flux at 10.7 cm is shown at the top of Figure 3-4. Pre-1980 ozone deviation estimates from ground-based data for the tropics are less reliable because the number of stations in that region was very limited and there were no regular Dobson instrument intercomparisons prior to 1974 (Bojkov and Fioletov, 1996). Ground-based data do seem to agree with Nimbus 4 BUV measurements; however, BUV measurements were very sparse after 1972 (Stolarski et al., 1997).

Total ozone changes in different seasons (DJF, MAM, JJA, and SON) from 35°-60°S and 35°-60°N are shown in Figure 3-5 for the period 1979-2005. The variability is high during the seasonal ozone buildup period in winter and spring and is less through summer and autumn. Long-term ozone declines in winter and spring seasons are similar between hemispheres; ozone values are 5-6% lower than the pre-1980 values. Summertime ozone deviations from the pre-1980 level are smaller in the NH (about 2%) than in the SH (about 5%).

Figure 3-5 shows that there is a clear difference in long-term ozone variations over NH and SH midlatitudes. Ozone variations over northern midlatitudes have a minimum in 1992-1995 (see also Figure 3-3 for annual averages). The large anomalies in winter-spring of 1992 and 1993 have been associated with the Mt. Pinatubo volcanic eruption in June 1991 (Gleason et al., 1993; Bojkov et al., 1993; Kerr et al., 1993; Hofmann et al., 1994). Low values in the mid-1990s were followed by increases in the late 1990s-early 2000s (Reinsel et al., 2005; Yang et al., 2006). This increase in column ozone is associated with the rise in ozone content in the lower stratosphere below 18 km, as described in Section 3.2.3 and further discussed in Section 3.4.5. Similar features are not seen over southern midlatitudes, where strong ozone minima occurred in 1985 and 1997 (Brinksma et al., 1998; Connor et al., 1999; Cordero and Nathan, 2002). Differences in the seasonal cycle of long-term ozone loss between NH and SH midlatitudes are partly caused by the export of ozone-depleted air from the polar vortex (see Section 3.4.3.2). This effect exists in both hemispheres, but its effect on spring- and summertime ozone is stronger in the SH due to the larger and more regular springtime ozone depletion over the Antarctic.

3.2.3 Changes in the Vertical Distribution of Ozone

There are a number of sources of vertically resolved ozone data. Ozonesondes make in-situ measurements up

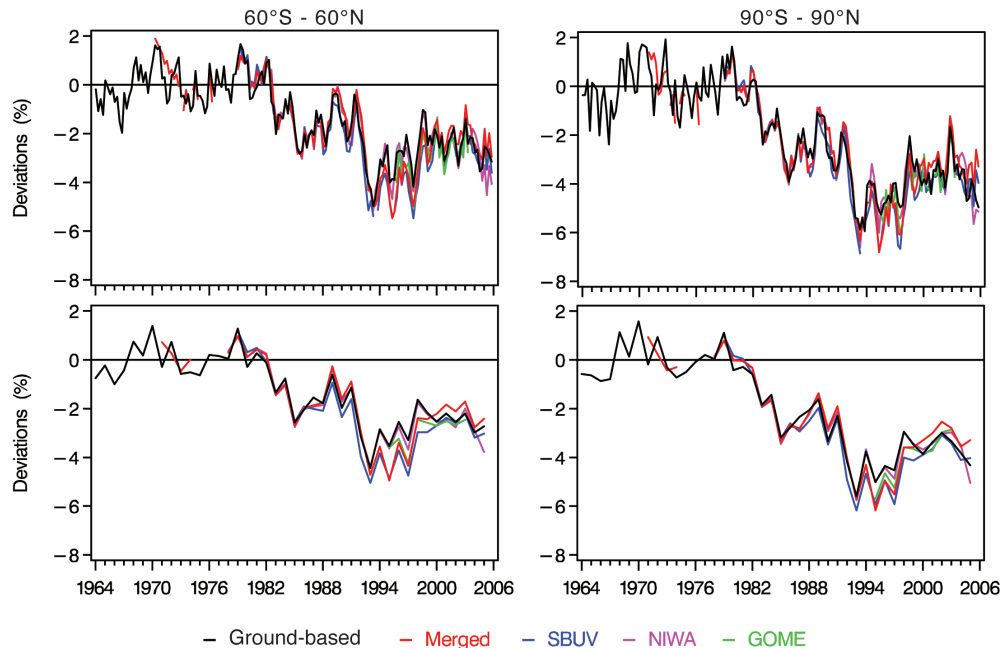


Figure 3-2. Top: Deseasonalized, area-weighted seasonal (3-month average) total ozone deviations, estimated from different global datasets: ground-based, merged satellite dataset, National Institute of Water and Atmospheric Research (NIWA) assimilated dataset, SBUV(/2), and GOME total ozone data. See Appendix 3A for details. Each dataset was deseasonalized with respect to the period 1979-1987, the average of the monthly mean anomalies for 1964-1980 estimated from ground-based data was then subtracted from each anomaly time series, and deviations are expressed as percentages of the ground-based time average for the period 1964-1980. Results are shown for the region 60°S-60°N (left) and the entire globe (90°S-90°N) (right). Updated from Fioletov et al. (2002) and WMO (2003). Bottom: The same plot, but for annual averages.

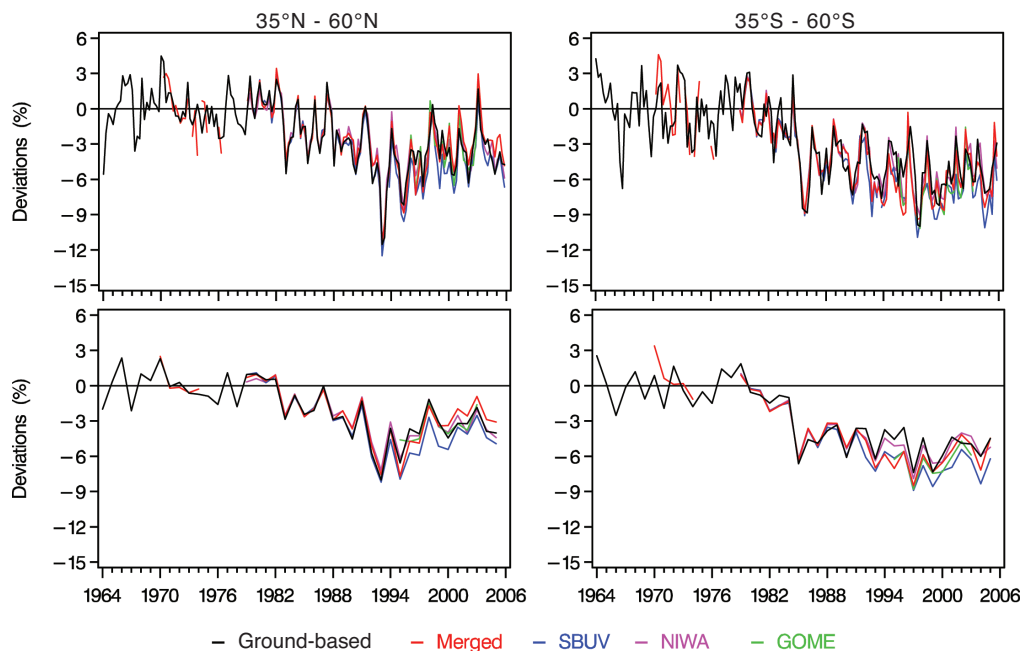


Figure 3-3. Top: Deseasonalized, area-weighted total ozone deviations from datasets for the latitude bands 35°N-60°N (left) and 35°S-60°S (right). Anomalies were calculated with respect to the time average for the period 1964-1980. Updated from Fioletov et al. (2002) and WMO (2003). Bottom: The same plot, but for annual averages.

GLOBAL OZONE

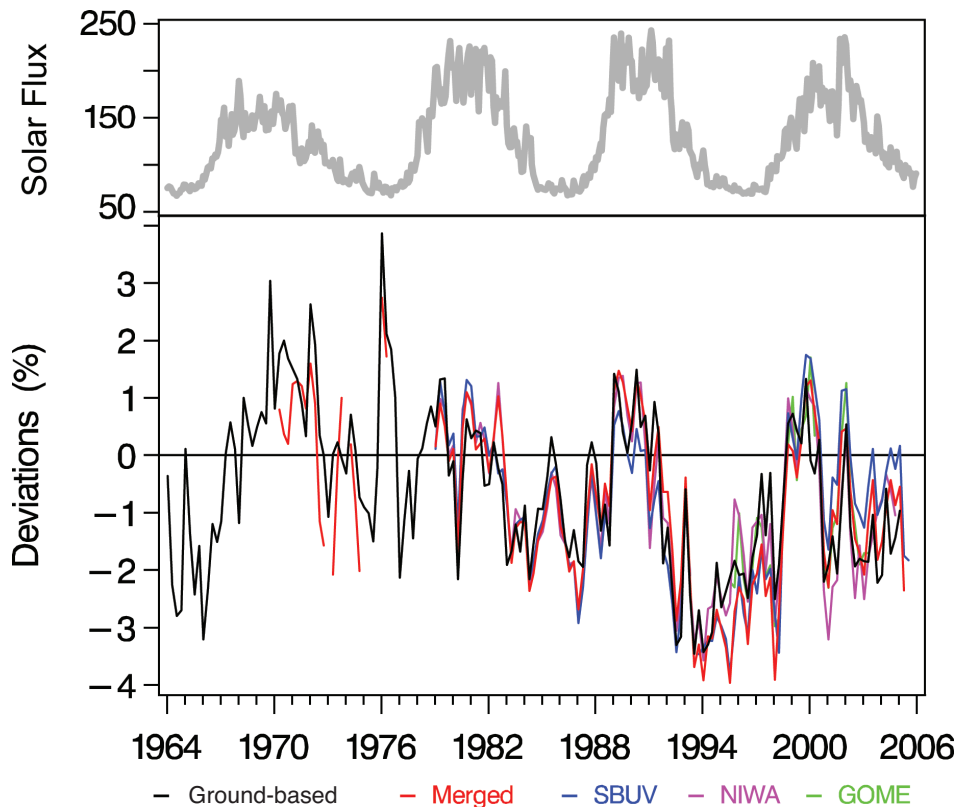


Figure 3-4. Deseasonalized, area-weighted total ozone deviations from five datasets for the latitude bands 25°S-25°N. The solar flux at 10.7 cm is shown as a proxy for solar variability.

to 30-35 km. Lidar and microwave instruments measure ozone vertical profiles from the lower stratosphere to about 50 km (higher for microwave) and their records are now long enough to assess long-term ozone changes (e.g., Schneider et al., 2003; Hartogh et al., 2004; Steinbrecht et al., 2006). The Umkehr method provides profile data to about 50 km from ground-based observations by Dobson and Brewer instruments. A new version of the Umkehr algorithm, UMK04, has been developed recently (Petrovavlovskikh et al., 2005a, b). Long records of ozone profile retrieval from satellite observations are available from the SAGE and SBUV and SBUV/2 series of instruments, although there are also satellite instruments with shorter records, such as the Halogen Occultation Experiment (HALOE) (e.g., Nazaryan et al., 2005). The SBUV and SBUV/2 instruments have been in operation since 1978, with six SBUV(2) instruments having flown since then. A new version 8 of SBUV(2) data has recently been released (Bhartia et al., 2004). First results have demonstrated a significant improvement of the SBUV(2) data quality (McPeters et al., 2004). While there are some differences between the SBUV and SAGE time series, they both demonstrate similar features of long-term changes in the vertical distribution of ozone. The biases between the SAGE II and the SBUV record vary with time, according to which of the individual SBUV(2) sensors are used in

the long-term record (Nazaryan and McCormick, 2005; Fioletov et al., 2006; Terao and Logan, 2006). These biases, of several percent, are largest in the upper stratosphere and will contribute to differences in trends derived from SAGE II and SBUV data. Data sources are discussed in detail in the Appendix.

3.2.3.1 UPPER STRATOSPHERE

Figure 3-6 shows the evolution of upper stratospheric ozone relative anomalies, averaged between 35 and 45 km altitude, from lidar and microwave measurements, for five stations (Steinbrecht et al., 2006). The corresponding zonal averages from satellite data (SAGE, SBUV, and HALOE) are also plotted. Anomalies are defined as the deviation of individual monthly means from the average climatological annual cycle. All records starting before 1990 clearly show the long-term decline of ozone in the upper stratosphere. Steinbrecht et al. (2006) estimated that ozone in the upper stratosphere shows a long-term decline of 10 to 15% since 1980. Upper stratospheric ozone trends before 1997 were about $-6\%/decade$ at the northern midlatitude stations, almost $-8\%/decade$ at Lauder in southern midlatitudes, and only $-4.5\%/decade$ at subtropical Hawaii (Steinbrecht et al., 2006). This confirms similar findings of interhemispheric and latitudinal

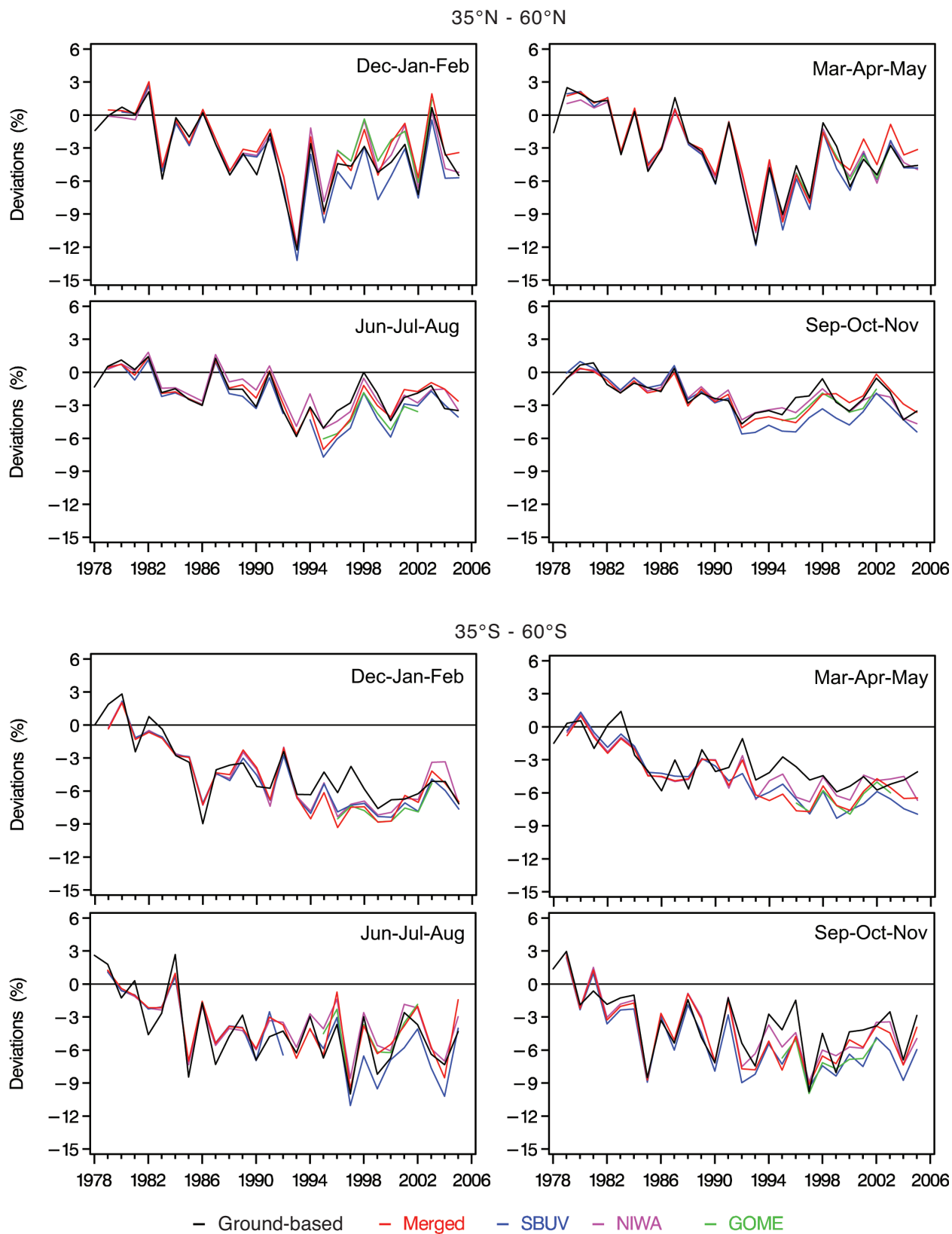


Figure 3-5. Seasonal area-weighted total ozone deviations from the 1964-1980 means, calculated for four seasonal averages, for the latitude bands 35°N-60°N (top) and 35°S-60°S (bottom). Updated from WMO (2003).

GLOBAL OZONE

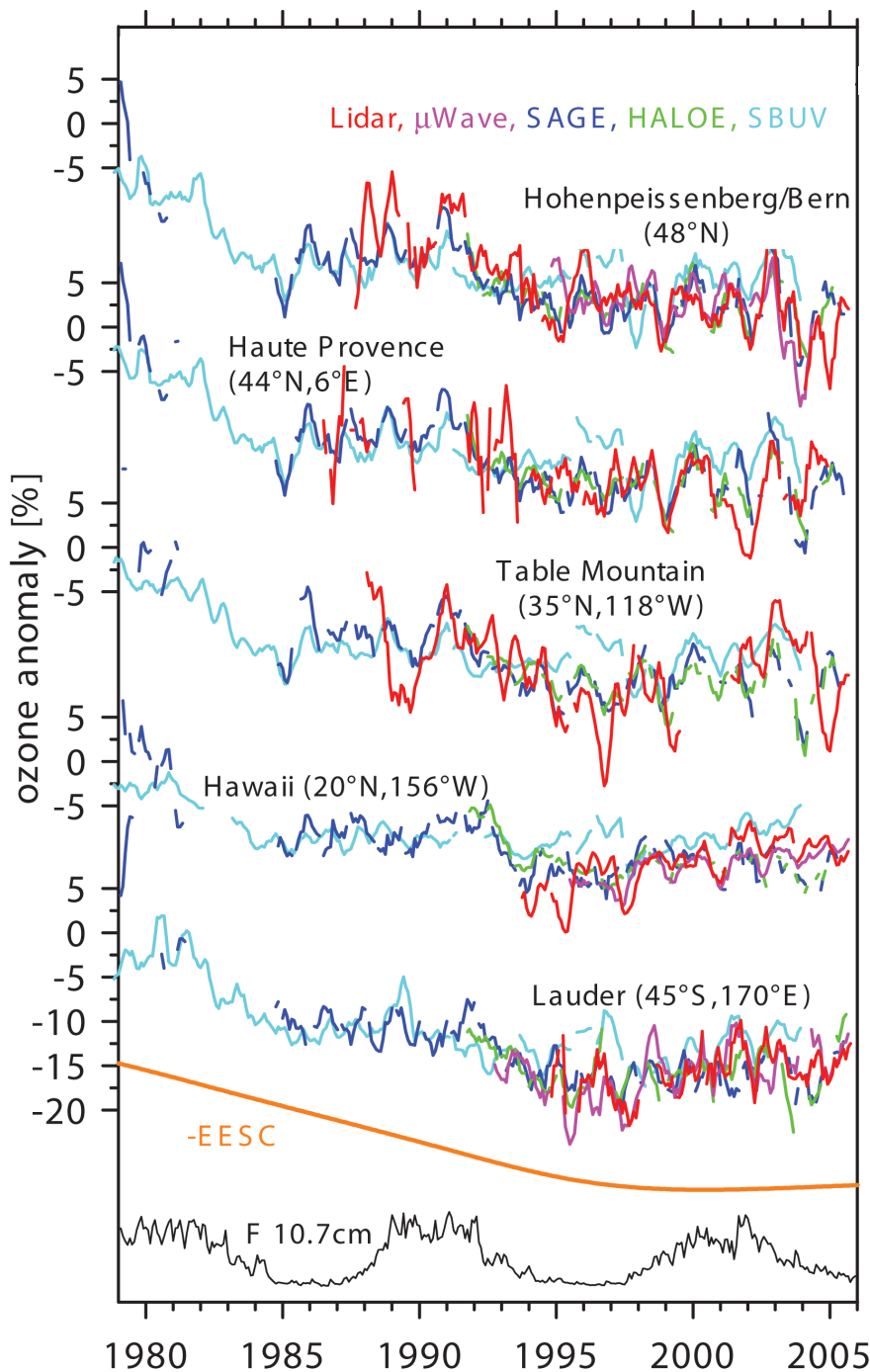


Figure 3-6. Upper stratospheric ozone anomalies as measured by ground-based lidars and microwave radiometers at selected stations of the Network for the Detection of Atmospheric Composition Change (NDACC), and by the corresponding zonal means from the satellite-borne Stratospheric Aerosol and Gas Experiments (SAGE, v6.20), Halogen Occultation Experiment (HALOE, v19), and Solar Backscatter Ultraviolet instruments (SBUV). Anomalies are averaged over the altitude range from 35 to 45 km, or the pressure range from 6.4 to 1.6 hPa for SBUV (V8-merged dataset). For clarity, 5-month running means are plotted. The EESC in the figure is for the age of air spectrum with mean age of 6 years and width of 3 years, and zero bromine (see Box 8-1 of Chapter 8). Thin black curve at the bottom shows the solar flux at 10.7 cm. Adapted from Steinbrecht et al. (2006).

differences reported from SAGE data by Li et al. (2002) and from SBUV(/2) data by Rosenfield et al. (2005). Figure 3-6 also shows that ozone levels seem to be inversely following the chlorine curve, and at many stations the previously steep ozone decline has not continued in the last five years. Newchurch et al. (2003), using SAGE data, also emphasized the lack of decline of ozone in the upper stratosphere since 1997.

The vertical structure of ozone trends has been derived from SAGE data (Wang et al., 2002; Li et al., 2002; Randel and Wu, 2006) and SBUV data (Rosenfield et al., 2005). Updated ozone trend estimates attributed to the changes in the EESC as a function of latitude and altitude estimated using SAGE I+II data and SBUV(/2) data for 1979-2004 are shown in Figure 3-7. Values are given in % per decade for the period of linear change of the EESC, and were calculated in the native units of each instrument.

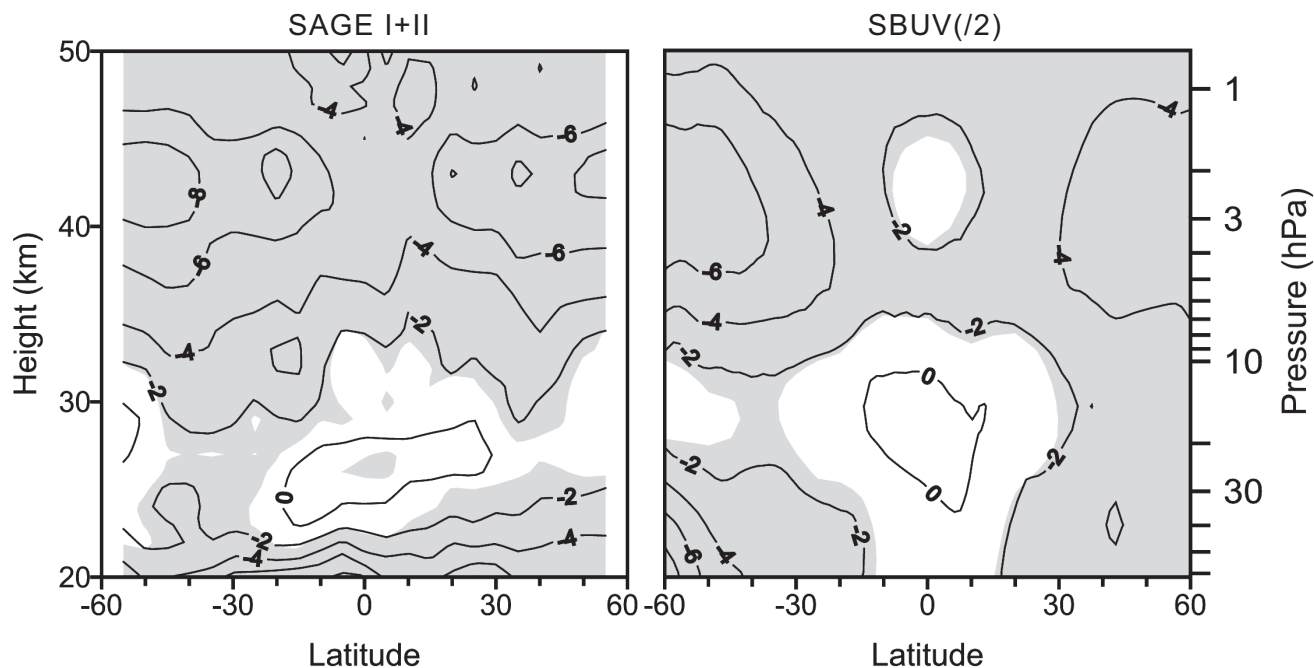


Figure 3-7. SAGE I+II and SBUV(/2) annual trends in percent per decade as a function of latitude and altitude for the period 1979-2004. The trends were estimated using regression to an EESC curve and converted to %/decade using the variation of EESC with time in the 1980s. The SAGE trends were calculated in geometric altitude coordinates, and the SBUV(/2) trends were calculated in pressure coordinates. Shadings indicate that the changes are statistically significant at the 2σ level.

Also, as noted in Section 3.2.1, the SAGE data give larger trends than SBUV data in the upper stratosphere due to the temperature trend and the use of pressure (SBUV) rather than geometric altitude (SAGE) coordinates. Some of the differences are also likely caused by different biases between ozone measured by SAGE and by the different SBUV(/2) instruments. The strongest decline (7-9% per decade, or 10-15% since 1979) occurred at 40-45 km over midlatitudes. The overall pattern of upper stratosphere ozone trends shown in Figure 3-7 is similar to that reported in WMO (2003) from SAGE data for a shorter period and using a linear trend function.

The vertical profiles of trends in ozone over northern midlatitudes (35° - 60° N) derived from SAGE, SBUV, and Umkehr instruments are very similar for 30-38 km. SAGE trends are larger than the SBUV and Umkehr trends above 40 km (Figure 3-8). Similarly, over 35° - 60° S, SAGE and SBUV trends are essentially the same for 30-38 km and the SAGE trends are larger above 40 km. Despite the difference in the magnitude of the trend, both SAGE and SBUV show that the decline at 40 km over SH midlatitudes is slightly larger than that over NH midlatitudes, but the difference is within the error bars. A slightly stronger decline over the SH was previously reported from SAGE data in WMO (2003).

Upper stratospheric negative trends are generally largest in winter and smallest in summer (Hood et al., 1993; Hollandsworth et al., 1995). Ozone trends for four seasons estimated using the EESC from version 8 SBUV data for 1979-1997 are shown in Figure 3-9 (Rosenfield et al., 2005). In both hemispheres the winter decline is larger (maximum of $-5.7 \pm 2.8\%$ /decade in the NH and $-6.9 \pm 2.8\%$ /decade in the SH) than the summer decline ($-3.1 \pm 1.5\%$ /decade and $-4.9 \pm 1.6\%$ /decade, respectively). Spring and autumn negative trends are also larger in the SH than in the NH. The spring and autumn upper stratospheric trends lie in between the winter and summer trends.

3.2.3.2 LOWER STRATOSPHERE

Ozone values in the lower stratosphere from the late 1970s to the present from measurements made by sondes, SAGE, SBUV(/2), and HALOE are shown over Europe (Figure 3-10a) and over Lauder, New Zealand (Figure 3-10b) (updated from WMO, 2003 for sondes; Terao and Logan, 2006). There is good agreement among the various datasets. Ozone reached minimum values in 1993 in the NH from 13 to 25 km (158-25 hPa) in the NH. Since then, from 13 to 16 km (158-100 hPa), ozone values have increased and are about the same as in the early 1980s,

GLOBAL OZONE

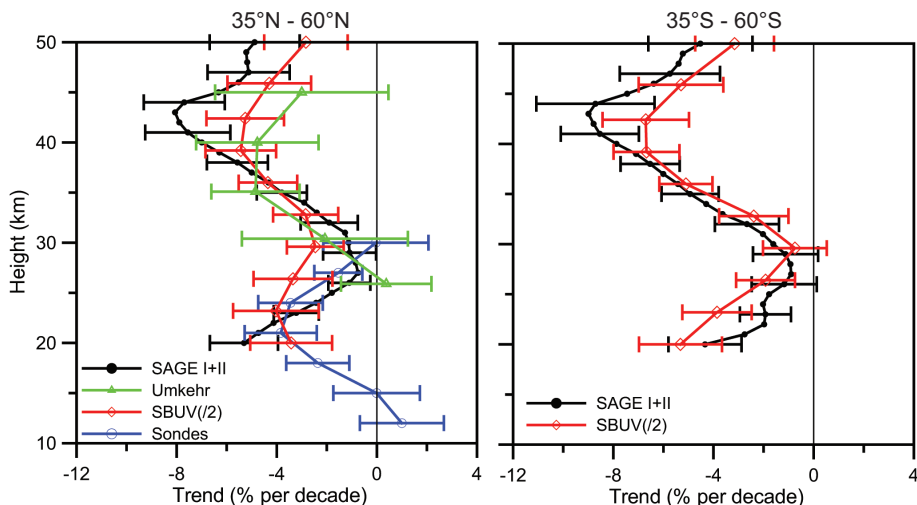
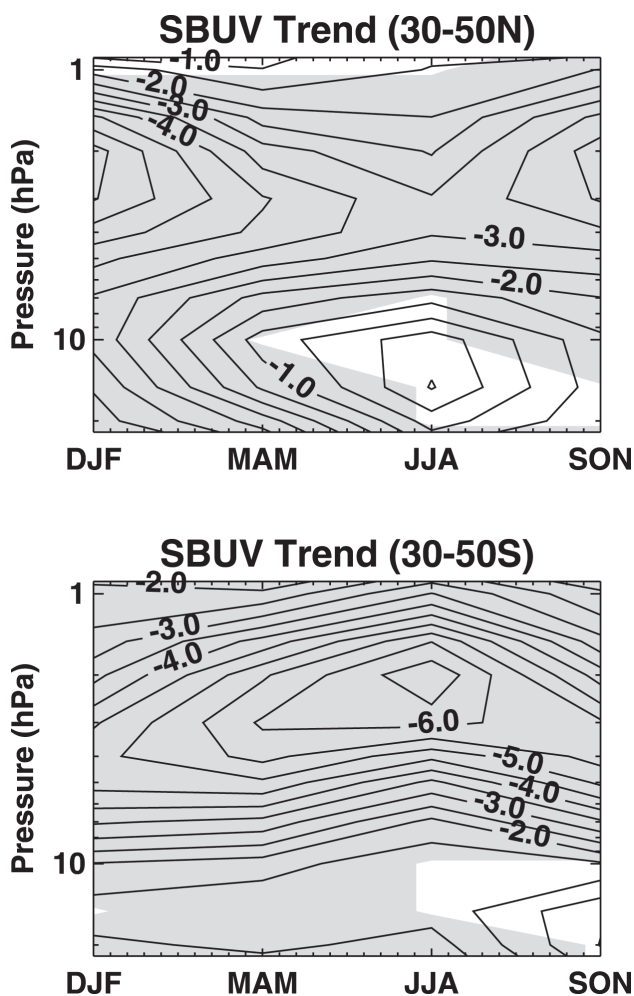


Figure 3-8. Vertical profile of ozone trends over northern and southern midlatitudes estimated from ozonesondes, Umkehr, SAGE I+II, and SBUV(/2) for the period 1979-2004. The trends were estimated using regression to an EESC curve and converted to %/decade using the variation of EESC with time in the 1980s. The trends were calculated in geometric altitude coordinates for SAGE and in pressure coordinates for SBUV(/2), sondes, and Umkehr data, and then converted to altitude coordinates using the standard atmosphere. The 2σ error bars are shown.



while from 22 to 25 km (40-25 hPa), they are about 5-8% lower than in the early 1980s.

Estimating long-term ozone changes below 20 km from satellite data is still a challenge. SBUV(/2) version 8 Layer 1 data represent the partial ozone column from approximately 7 to 19 km. However, it is a fairly new data product and more validation is required. The use of SAGE data is limited in this altitude range because the present version of SAGE I data is not reliable below 20 km. The ozone amount below a certain level in the lower stratosphere can be estimated by subtracting SAGE I and II partial column ozone above that level from total column measured by TOMS. Figure 3-11 shows estimates of partial column ozone below 19 km from satellite data for northern and southern midlatitudes from SBUV(/2) and SAGE/TOMS data. (The SAGE partial column above 19 km is derived from a regression analysis of the SAGE profile measurements, as described in Randel and Wu, 2006.) Figure 3-11 demonstrates that ozone levels below 19 km in the NH in the 2000s are similar to these from the early 1980s but are ~10% lower in 1992-1995. In the SH, the data also show a decline between 1980 and the mid-1990s; however levels in the 2000s remain ~10% lower than the levels of the late 1970s to early 1980s.

Figure 3-9. Season-pressure sections of SBUV mid-latitude linear ozone trends for (top) Northern Hemisphere and (bottom) Southern Hemisphere for 1979-1997 in % per decade (Rosenfield et al., 2005). Shaded areas are significant at the 2σ level.

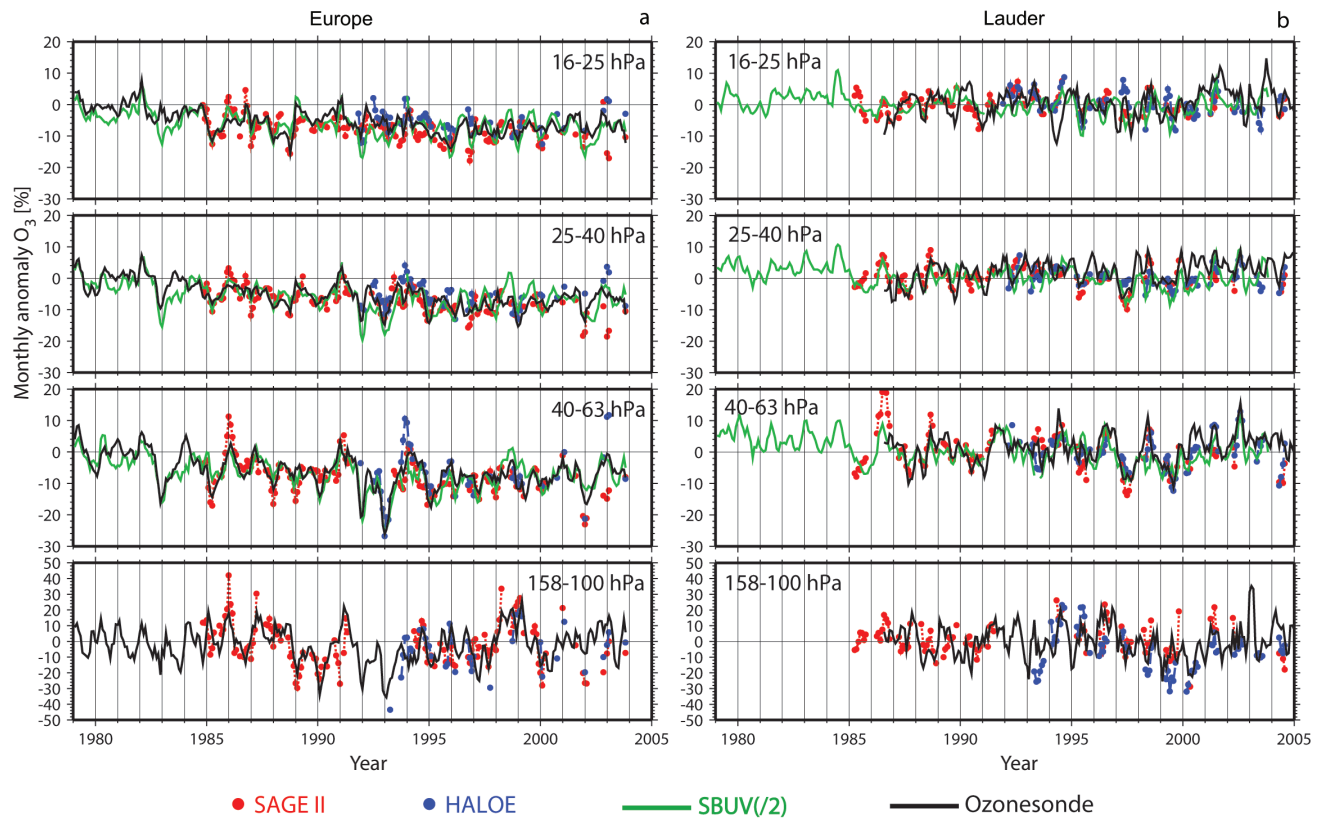


Figure 3-10. (a) Monthly ozone anomalies for Europe as measured by ozonesondes (black line), SAGE II (red circles), HALOE (blue circles), and SBUV(2) (green line) at four pressure layers. The monthly anomalies were calculated as the difference between a given monthly mean and the average of monthly means for 1985–1990 for each dataset, except for HALOE where 1994–1999 was used; the average of the monthly mean ozonesonde anomalies for 1979–1981 was then subtracted from each anomaly time series. The ozonesonde data are the average of measurements at three European stations: Hohenpeissenberg, Payerne, and Uccle. The satellite data were selected within a grid box of 45°N–55°N and 10°W–30°E. A 3-month running mean was applied to the data. For SAGE II and HALOE, results are shown when the number of observations is larger than 4 per month. (b) Same as (a), but for Lauder, New Zealand. The monthly anomalies were calculated using the 1987–1991 monthly means for each dataset, except for HALOE where 1994–1999 was used. The satellite data were selected within a grid box of 40°S–50°S and 150°E–170°W. Adapted from Terao and Logan (2006).

Earlier Assessments reported a large negative trend (more than 5%/decade) in the lower stratosphere below 18 km (WMO, 1992, 1999; SPARC, 1998; Logan et al., 1999) over northern midlatitudes for the period up to the mid-1990s. A maximum decline of about –10% per decade was reported at 15 km (see Figure 3-12). However, the ozonesonde trends reported by WMO (2003) for 1980–2000 at 12–18 km (200–63 hPa) are half as large as those for 1980–1996. A similar reduction of the trend magnitude is shown by Umkehr data analysis (Bojkov et al., 2002). Recent trend estimates over northern midlatitudes for the period up to 2004 show no decline at 15 km (Figures 3-8, 3-12) and ozone values at 13–16 km are similar to those in the early 1980s (Figure 3-10).

The dramatic change in ozone trend estimates at 12–18 km results from a decline in ozone during the 1980s and early 1990s followed by a rapid increase thereafter (see Figure 3-10). This behavior can be partially attributed to low ozone values in the lower stratosphere in 1992 and 1993 (Figure 3-10) when the stratosphere was influenced by the Mt. Pinatubo eruption. Miller et al. (2006) fit the sonde data from 13 NH stations for 1970–2003 with a piecewise linear trend, with the change in trend specified at January 1996. They removed two years of data after June 1991 to reduce the influence of the Mt. Pinatubo eruption. Nevertheless, they found that the trend is about –3 to –4%/decade at 15–18 km for 1970–1995, with a statistically significant change in trend of +9 to +13%/decade

GLOBAL OZONE

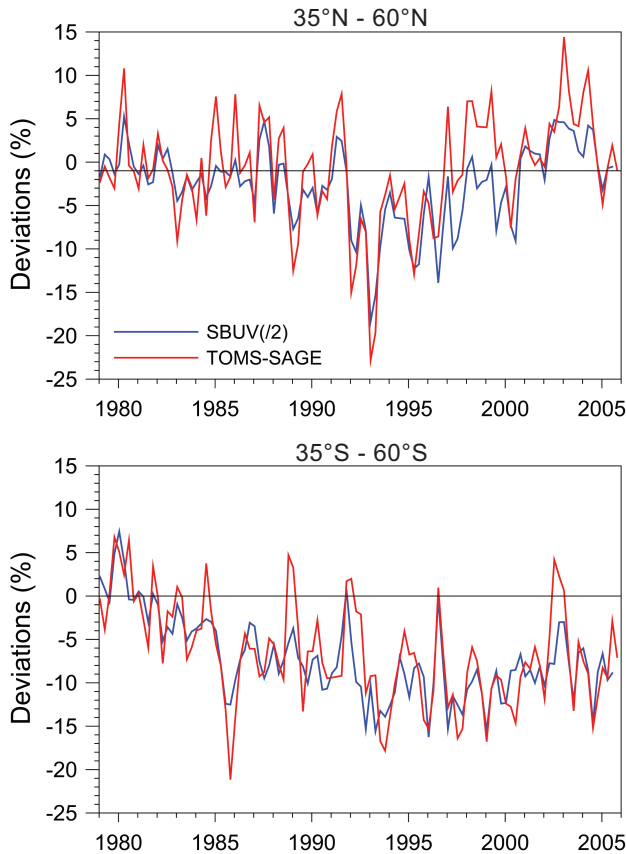


Figure 3-11. Deseasonalized, seasonal (3-month average) ozone deviations from SBUV and SAGE II data for the latitude bands 35°N-60°N (top) and 35°S-60°S (bottom) below 19 km. Anomalies were calculated with respect to the time average during 1979-1982. The blue line represents SBUV(/2) Layer 1 data (1000-63 hPa). The red line represents the difference between TOMS column ozone and SAGE I+II data vertically integrated above 19 km. The SAGE partial column above 19 km is derived from a regression analysis of the SAGE profile measurements, as described in Randel and Wu (2006).

after January 1996, i.e., there was a positive trend of 6 to 11% per decade in 1996-2003. Similar results are reported by Yang et al. (2006) and their study is discussed in detail in Chapter 6. The piecewise method gives an increase in ozone after 1996 because of the low ozone values in the first half of the 1990s and the higher values in the early 2000s (Figure 3-10a). The pre-1996 trends for 12-18 km are largest in spring, as in earlier studies (Logan et al., 1999), and the trend change is also largest in spring (Miller et al., 2006).

Ozonesonde data from Lauder, New Zealand (45°S), show no significant trends at 12-19 km (Figure 3-

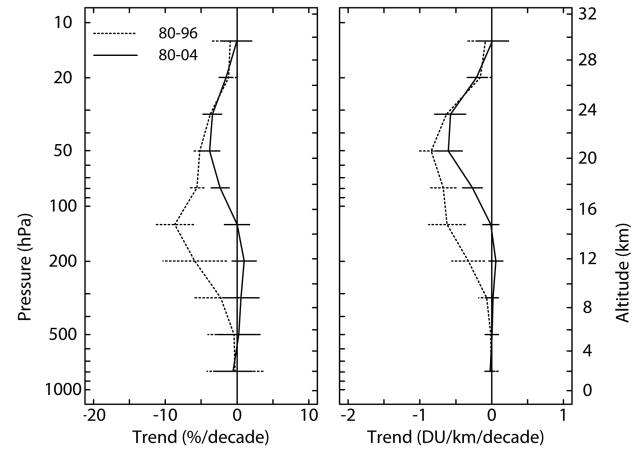


Figure 3-12. Ozone trends over northern midlatitudes (36°N-59°N) as a function of altitude in %/decade and DU/km/decade estimated from ozonesonde data for 1980-1996 (dotted line) and 1980-2004 (solid line). The trends were estimated using regression to an EESC curve and converted to %/decade and DU/decade using the variation of EESC with time in the 1980s. The error bars represent the 95% confidence limits. Updated from Logan et al. (1999).

10b). The lack of trend in the Lauder record, which begins in late 1986, is not inconsistent with the satellite data in Figure 3-11, because much of the ozone decline over southern midlatitudes occurred before 1986. An ozonesonde record from earlier years is available from Melbourne, Australia. It demonstrates a significant decline of about 10% per decade at 100 hPa (~16 km) for 1970-1990 (Logan, 1994; WMO, 1995). However, the record is affected by infrequent measurements for many years, as well as changes in sonde type and site location, and further analysis is required for trend studies.

At 18-25 km, ozone values have been relatively flat in the NH since the late 1990s, as shown in Figure 3-10. According to Miller et al. (2006), at 20-22 km, the trend is -4.5%/decade for 1970-1995, with a change in trend of 2-4%/decade after January 1996. Yang et al. (2006) suggested that the cessation of ozone depletion at 18-25 km is consistent with a leveling of the EESC curve. The ozone trend estimated using the EESC curve is about -3 to -4%/decade at 18-24 km (Figures 3-7 and 3-8) in the both hemispheres. In the past five years, ozone values at 22-25 km (40-25 hPa) were about 5% below those in the early 1980s. As shown by the ozone time series discussed above and the EESC curve, this decrease occurred prior to about 1996.

As was previously reported by SPARC (1998) and WMO (1999, 2003), the trend magnitude over midlati-

tudes has its minimum near 30 km. The SAGE I+II data and the ozonesonde data give almost no trend related to EESC at 30 km in northern midlatitudes, while the SBUV data give a small negative trend (-2 to -3% /decade) (Figures 3-7 and 3-8).

In the tropics, the SAGE data in Figure 3-7 show negative trends in the lower stratosphere, while the SBUV data show no significant trends in tropical ozone from 22 to 30 km. WMO (2003) showed significant negative trends in the tropical lower stratosphere below 22 km based on SAGE I+II data, and these changes have been accentuated by several recent years of low ozone (Figure 3-7; Randel et al., 2006). However, these results should be viewed with caution as there are no other long-term records for ozone in the tropical lower stratosphere. This is a region of small ozone concentrations and large vertical gradients, which present challenges for satellite observations. On the other hand, interannual changes in SAGE II data show good agreement with tropical ozonesonde data from the SHADOZ (Southern Hemisphere Additional Ozonesondes) network (Thompson et al., 2003) for 1998-2004 (Randel et al., 2006).

3.2.3.3 CONSISTENCY OF COLUMN AND PROFILE TRENDS

The vertical profile trends over midlatitudes discussed in Section 3.2.3 are in general consistent with column ozone trends there. Less than 10% of the midlatitude total column ozone is located above 35 km, and a 10-15% decline there accounts for a total column decline of about 1%. The lower stratosphere between 20 and 25 km contains 20-25% of the total column ozone, and an 8-10% decline in this layer contributes a total column decline of about 2%. Ozone located below 18 km contributes about 30% to the total column. As shown in Figure 3-11, there is no ozone decline below 19 km over northern midlatitudes and about a 10% decline at southern midlatitudes, yielding a total column decline of about 3%. Thus, the overall total column decline from the vertically integrated profiles is about 3% over northern midlatitudes and about 6% over southern midlatitudes; these are similar to the declines in column ozone described in Section 3.2.2.

As mentioned in Appendix 3A, SBUV(2) total ozone used in Section 3.2.2 is the vertically integrated SBUV(2) ozone profiles. Therefore, SBUV(2) column ozone and integrated profile trends are necessarily consistent. Section 3.2.2 shows that SBUV(2) column ozone data agree with total ozone data from the other sources.

Figure 3-13 shows a latitudinal profile of the vertically integrated SAGE I+II ozone changes for 1979-2005 compared with corresponding changes in column ozone,

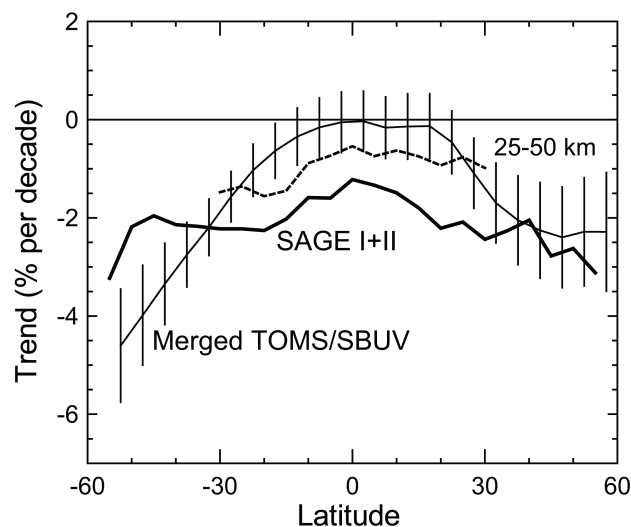


Figure 3-13. Latitudinal profile of ozone trends derived from the vertically integrated SAGE I+II data, compared with results from the merged TOMS/SBUV column ozone dataset. The trends were estimated using regression to an EESC curve and converted to %/decade using the variation of EESC with time in the 1980s. The SAGE I+II results are a vertical integral of the changes in Figure 3-7, integrated between the tropopause and 50 km. For comparison, the dashed line shows the SAGE results integrated over a limited range of 25-50 km (for 30°N-30°S). Adapted from Randel and Wu (2006).

derived from the merged satellite ozone data. The SAGE results represent a vertical integral of the profile trends from the tropopause to 50 km. Results from both datasets show reasonable agreement for net ozone decreases over the extratropics. There are significant differences, however, in the magnitude of changes in the tropics, with the integrated SAGE results giving larger changes than the column measurements (which are near zero in the equatorial region). This difference could have several implications. There could be compensating positive trends in tropical tropospheric column ozone, with increases of ~ 6 DU over 1979-2005 ($\sim 15\%$ of background levels). Tropical tropospheric ozone trends for this period are not well known. Lelieveld et al. (2004) have reported substantial increases in near-surface ozone in the tropical Atlantic ocean for 1972-2002, and Bortz et al. (2006) suggest a 20% increase in tropical upper tropospheric ozone during 1994-2003, based on aircraft measurements. On the other hand, Ziemke et al. (2005) suggested that there have not been significant trends in tropical tropospheric ozone for this period based on satellite observations. An alternative explanation of the tropical differences in

GLOBAL OZONE

Figure 3-13 is that the ozone changes derived from SAGE data are simply too large, particularly the lower stratospheric maximum (as discussed above). For comparison, Figure 3-13 also includes the SAGE I+II changes integrated over the limited altitude range of 25-50 km (for 30°N-30°S), and this produces smaller trends that border on the statistical uncertainty levels for the tropical column trends.

3.2.4 Tropospheric Ozone

A recent analysis of long-term changes in tropospheric ozone emphasizes that trends vary regionally and that within a given region, trends have changed over the past 25-35 years (Oltmans et al., 2006). This section updates the discussion in WMO (2003) and focuses on ozonesonde data and surface data at remote, or relatively remote, sites.

Tarasick et al. (2005) showed that tropospheric ozone over Canada (53°-75°N) decreased from 1980 to around 1994 and then increased up to the present, with ozone values in the early 2000s similar to those in the early 1980s. They also found that annual average ozone anomalies in the troposphere at the Canadian sites are correlated with those in the lower stratosphere ($r \sim 0.65$). Ozone over the eastern U.S.A. (Wallops Island) shows relatively small changes from 1970 to the present (<5%), with highest ozone in the late 1980s (Oltmans et al., 2006). An analysis of short-term trends in MOZAIC (Measurements of Ozone and Water Vapor by In-service Airbus Aircraft) aircraft data finds an increase of 12%/decade in the middle troposphere over New York from mid-1994 to 2001; the increase is much larger in winter (20%/decade) than summer (6%/decade). Ozone was particularly high in 1998 and 1999 (Zbinden et al., 2006).

Over Europe, the sonde data from Hohenpeissenberg (the longest self-consistent record) show a steady increase from 1966 to the mid- to late 1980s, followed by a slow decrease and considerable interannual variability. Values in the past few years are similar to those in the early 1980s (Oltmans et al., 2006). Sonde data from Payerne and Uccle show little change in ozone in the mid-troposphere in the last decade. Oltmans et al. (2006) compare mean values for 1995-2004 to those for 1985-1994 for Hohenpeissenberg and the nearby mountain station of Zugspitze (~3000 m). The sonde data show little change except a small decrease in May-July, while the Zugspitze data show a small increase in summer, and a larger increase in winter. Simmonds et al. (2004) report an increase in ozone of 13%/decade in background air at Mace Head (Ireland) from 1987 to 2003, with highest values in 1998 and 1999. The MOZAIC data over Frankfurt and Paris also give an increase in ozone, 7 and

15%/decade, for 1994 to 2001, with the largest trend in winter and spring and almost no trend in summer (Zbinden et al., 2006).

Jonson et al. (2006) recently summarized reports on trends over Europe and noted that the differences between the trends given by sondes, and those from MOZAIC, mountain sites, and Mace Head cannot easily be reconciled. They also note that surface sites within Europe generally show substantial downward trends in high ozone (95th or 98th percentiles) over the past 10-15 years, as well as increases in ozone at polluted surface sites. Both these features are caused by substantial decreases in emissions of ozone precursors in Europe, leading to less ozone formation in summer, and a reduction in titration of ozone by nitric oxide (NO) in winter (e.g., Jonson et al., 2006).

Long-term ozonesonde measurements over Japan (32°-43°N) show an overall increase since 1970, but most of this occurs early in the record, and the last few years show a downturn in ozone (Oltmans et al., 2006). Naja and Akimoto (2004) find that ozone below 3 km in regionally polluted air over Japan increased by 11-22% from the 1970s to the 1990s. The MOZAIC data over Japan give an increase of 8%/decade for 1994-2001, with no trend in summer and an increase of ~10%/decade in other seasons (Zbinden et al., 2006).

In summary, the sonde data for northern midlatitudes for the last decade show increases in ozone over Canada and slight decreases over Europe and Japan. The average trend for the sonde data for 1980 to 2004 is zero (Figure 3-12).

There has been a long-term increase in ozone over Hawaii of $3.5 \pm 1.5\%$ /decade during autumn and winter, in both surface data at 3.4 km and sonde data at 3-6 km, that appears to be related to shifts in transport patterns (Oltmans et al., 2006). There is little change in ozone since 1985 in spring, when transport events from Asia occur.

Indian ozonesonde data demonstrate a statistically significant increase of tropospheric ozone ($43\% \pm 25\%$ per decade at 800-1000 hPa and more than 50% per decade at 200-500 hPa) over Delhi for the period 1972-2001 (Saraf and Beig, 2004). However, Indian sondes have demonstrated large, more than 30%, uncertainties in the troposphere during international ozonesonde intercomparisons (Attmanspacher and Dütsch, 1970; SPARC, 1998) and these trend results should be interpreted with caution.

Analysis of MOZAIC data indicates that that tropical ozone at cruise altitudes (7.7-11.3 km) has increased by ~1 ppb/year, or by ~20%/decade, from 1994 to 2003 (Bortz et al., 2006). This is twice as large as the increase reported for surface ozone over the tropical Atlantic from shipboard data by Lelieveld et al. (2004). Surface and

sonde data up to the mid-troposphere from Samoa (14°S) show a small decrease from the late 1980s to the most recent decade in austral winter, and no change the rest of the year (Oltmans et al., 2006). Unfortunately, the longest tropical sonde record from Natal (Brazil) suffers from changes in sonde types and procedures, as well as data gaps, and the record is not suitable at present for deriving reliable trends.

The Samoa sonde data since 1995 do not show the increase seen in the MOZAIC data for the southern tropics. The MOZAIC data are from South America, the Atlantic, and Africa, while the sonde data are from the Pacific. Ziemke et al. (2005) found no trend in the tropospheric column of ozone derived from TOMS data in the tropics from 1979 to 2003. There appear to be inconsistencies among the various data records for tropospheric ozone.

In southern midlatitudes, ozone at Lauder (45°S) increased from 1986 to present by ~5%/decade below 3 km, with a marginally significant increase of 2%/decade at 3-6 km, and no trend at 6-9 km (Oltmans et al., 2006). Sonde data from the South Pole show a small increase in ozone of 0.5%/decade since 1986 in the mid-troposphere, primarily in spring and summer. No such increase is seen at Syowa (69°S) (Oltmans et al., 2006).

It appears that the short-term trends from MOZAIC data for both the midlatitudes and the tropics may be inconsistent with sonde data, but more analysis is needed.

3.3 SUMMARY OF OTHER OBSERVATIONS

The observed long-term changes in temperature and water vapor are discussed in Chapter 5. In addition, observations of past changes in long-lived source gases and halogen-containing species are discussed in Chapter 1. In this subsection we therefore focus on the remaining parameters that are important for long-term changes in ozone and for which there are relevant data records.

3.3.1 Stratospheric Aerosol and Its Precursors

The source of stratospheric aerosol observed since the late 1970s has been dominated by the injection of sulfur dioxide (SO₂) from a few major volcanic events including El Chichón in 1982 and Mt. Pinatubo in 1991. The inference of a nonvolcanic stratospheric background is hampered by very limited periods without volcanic influence since systematic measurements began; however, the best indications are that there is no long-term trend in the background aerosol level (Deshler et al., 2006). For background periods, observed since the late 1990s, the dominant stratospheric aerosol precursor gases

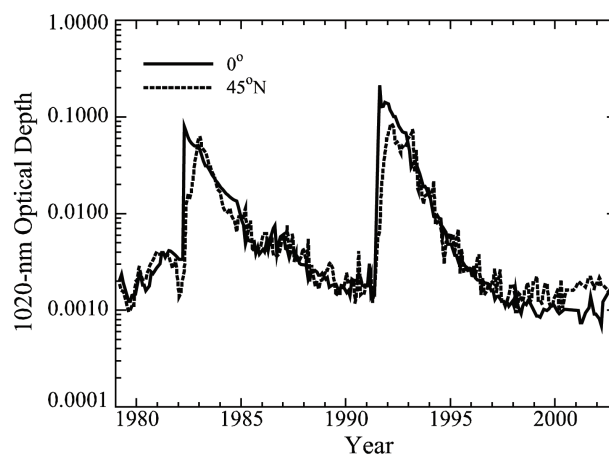


Figure 3-14. The Assessment of Stratospheric Aerosol Particles (ASAP) reconstruction of the tropical (solid line) and northern midlatitude (dotted) 1020-nm aerosol optical depth from 1979 through 2002 based on a combination of SAGE, SAGE II, and ground-based and airborne lidar data. From SPARC, 2006.

are carbonyl sulfide (OCS) and SO₂. Through SO₂, human-related activities may influence the observed background stratospheric aerosol. There is general agreement between measured OCS and modeling of its transformation to sulfate aerosol, and observed aerosols. However, there is a significant dearth of SO₂ measurements, and the role of tropospheric SO₂ in the stratospheric aerosol budget, while significant, remains a matter of some guesswork. In addition, it is not well understood whether global human-derived SO₂ emissions, which are decreasing, or emissions in low latitude developing countries, such as China, which are increasing, dominate the human component of SO₂ transport across the tropical tropopause (e.g., Notholt et al., 2005).

As shown in Figure 3-14, aerosol loading during the past 20 years has varied by as much as 2 orders of magnitude. As a result, the quality of the measurements and the agreement among diverse measure systems varies strongly as a function of the level of aerosol loading. For instance, results from the SPARC *Assessment of Stratospheric Aerosol Properties* (ASAP) (SPARC, 2006) demonstrate that space-based and in situ measurements of aerosol parameters, in particular surface area density (SAD), tend to be consistent following significant volcanic events like El Chichón and Mt. Pinatubo. However, during periods of very low aerosol loading, this consistency breaks down and significant differences exist between systems for inferred parameters like SAD and directly measured parameters like aerosol extinction coefficient (SPARC, 2006). Although integrated aerosol

GLOBAL OZONE

quantities such as surface area density and effective radius can be calculated without approximation from a known size distribution, the satellite and in situ observational bases for size distributions are controlled by a priori assumptions regarding the distribution itself or by having coarse size resolution, respectively. ASAP showed that during volcanically quiescent periods, models and observations disagree significantly mainly because of the modeled fraction of the surface area density that resides in particles too small to be measured, especially near nucleation regions. While there are some model shortcomings relative to observations, particularly in the lower stratosphere, it seems likely that space-based datasets underestimate, perhaps significantly, aerosol surface area density in the lower stratosphere during low loading periods.

In the past, the effect on ozone variability of stratospheric aerosol driven by sporadic volcanic events (primarily the El Chichón and Mt. Pinatubo eruptions) has given concern that it could mimic the effects of the 11-year solar cycle. However, since stratospheric aerosol has remained near nonvolcanic background levels since the late 1990s through much of the recent solar maximum, such concerns have been greatly mitigated (see Section 3.4.4).

3.3.2 Nitrogen Dioxide (NO₂)

Long-term ground-based observations of column NO₂ have been made at Lauder, New Zealand (45°S), since late 1980, by UV/visible observations of sunlight scattered from the zenith. Trends in the observations were discussed in Liley et al. (2000) and WMO (2003). Here the observations and analysis are updated through early 2006. A statistical analysis of geophysical cycles (solar cycle, QBO, El Niño-Southern Oscillation), trends, and volcanic eruptions was done to assess correlations with the observed NO₂. Linear increases of $6.2 \pm 1.8\%$ per decade (am) and $5.7 \pm 1.1\%$ per decade (pm) are inferred. These are not significantly different from those reported in Liley et al. (2000). Figure 3-15 shows the time series for monthly averages of morning and afternoon column NO₂ at Lauder, after subtraction of the seasonal cycle.

NO₂ columns have also been measured at the Jungfraujoch (47°N) since 1985 (Mahieu et al., 2000). The Jungfraujoch measurements are made by Fourier transform spectroscopy (FTS) in solar absorption in the infrared. The monthly averaged vertical column densities from 1985-2005 are also shown in Figure 3-15. Analysis of these data using the same algorithm applied to the Lauder data produces a linear trend of $1.5 \pm 1.0\%$ per decade. The trend reported by Mahieu et al. for 1986-1998 ($7 \pm 3\%$ per decade) may have been significantly affected

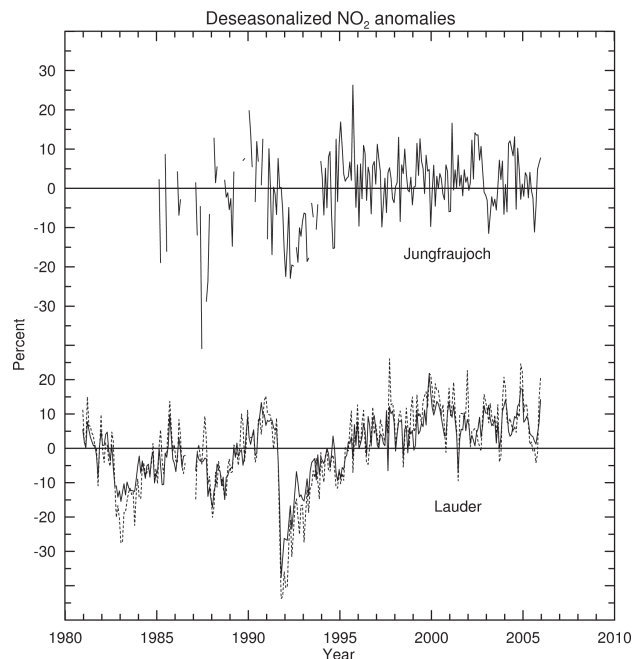


Figure 3-15. Deseasonalized anomalies of the NO₂ slant column measured at two sites, the Jungfraujoch, Switzerland (47°N), and Lauder, New Zealand (45°S). The Jungfraujoch data are measured in direct, solar absorption in the infrared, at a wide range of zenith angles, while the Lauder data are UV/visible absorption of sunlight scattered from the zenith at solar zenith angles of 90°. Sunrise measurements are shown as dashed lines, and sunset measurements as solid lines.

by not explicitly accounting for the effect of the Mt. Pinatubo eruption from 1992-1994. SAGE II satellite observations of profile NO₂ (Cunnold et al., 1991) are consistent with the Lauder data and show that the bulk of the increase occurs in the lower stratosphere. The SAGE II data also show a large hemispheric asymmetry, with no significant trend at Northern Hemisphere midlatitudes.

Thus, the available evidence suggests that the trend of NO₂ in the Southern Hemisphere is significantly larger than that in the Northern Hemisphere. The trend at the Jungfraujoch is consistent with the 2.4%/decade increase in tropospheric N₂O reported in WMO (2003). Other factors may be required to explain the larger increase at Lauder. WMO (2003) concluded that observed nitrous oxide (N₂O) increases and decreases in ozone explained a trend in NO₂ of $5 \pm 1\%$ /decade. The origin of the apparent hemispheric difference in trend remains unexplained, although uncertainties in the analysis due to the relatively short data records should be noted.

3.4 UNDERSTANDING AND INTERPRETATION OF OZONE CHANGES

3.4.1 Models

In order to quantify the effect of certain processes on long-term ozone changes, we need to describe these processes by numerical models. These models can either be “physical” models, which solve the governing equations of the physics/chemistry of the atmosphere, or “statistical” models, in which changes in the long-term ozone time series are linked with forcing terms, typically by multiple regression (see Section 3.2.1).

In this chapter, we use the term “physical model” to describe a numerical model that integrates the relevant equations of the chemistry and dynamics of the atmosphere to predict the evolution of the atmosphere with time. These models are a mathematical representation of our current understanding of the chemistry and physics of the atmosphere. These models can be 0-D (box), 1-D (column), 2-D (latitude-height), or 3-D models. The 3-D models can be classified as “off-line” chemical transport models (CTMs), which are forced by specified winds, or general circulation models (GCMs), which calculate their own winds and temperatures. The components of such models were described in Chapter 4 of WMO (2003). GCMs that contain interactive, detailed chemistry schemes are called coupled Chemistry-Climate Models (CCMs). The various types of models are also described in more detail in Chapter 5 (Box 5-1).

Aside from increased computer power allowing more 3-D simulations, and therefore a better understanding of the performance of these models, a major development in these tools over the past four years for understanding past ozone changes has been the new availability of long-term, whole-stratosphere meteorological reanalyses that can be used to force CTMs.

The European Centre for Medium-range Weather Forecasts (ECMWF) and the National Centers for Environmental Prediction (NCEP) have extended the upper boundary of their operational meteorological analyses to the lower mesosphere (0.1 hPa, more recently 0.01 hPa) and upper stratosphere (1 hPa), respectively. The United Kingdom Met Office (UKMO) has provided meteorological analyses extending to 0.3 hPa since 1991 (Swinbank et al., 2002). The Global Modeling and Assimilation Office (GMAO) of the National Aeronautics and Space Administration (NASA) also produces meteorological analyses for the troposphere and stratosphere. The Goddard Earth Observing System, version 4 (GEOS-4) data assimilation system (Bloom et al., 2005) has an upper

boundary near 80 km (0.01 hPa), with data constraints up to about 55 km. Furthermore, both ECMWF and NCEP have performed 40- and 50-year reanalyses labeled ERA-40 (Simmons et al., 2005; Uppala et al., 2005) and REAN or NCEP-50 (Kanamitsu et al., 2002), respectively. ERA-40 extends to 0.1 hPa, although REAN only extends up to 10 hPa. These reanalyses have been performed with a 3-D variational analysis (3D-VAR), while the operational analyses are performed with the computationally more expensive 4-D variational analysis (4D-VAR), which is regarded as more accurate, due to the re-integration in time.

Some general issues relating to the quality of wind datasets used to force CTMs have been identified. Schoeberl et al. (2003), Strahan and Douglass (2004), and Tan et al. (2004) showed that GMAO and UKMO winds are too dispersive as a result of the assimilation procedure. The procedure causes excessive mixing in the tropical lower stratosphere, forcing large-scale meridional tracer circulation in the stratosphere. The consequence is that the mean residence time of air in the stratosphere becomes too short, which has a negative impact on long-term tracer integrations. Schoeberl et al. (2003) showed that winds from GCMs are much less dispersive and contain a weaker residual circulation, leading to a mean age of air closer to observations.

The ERA-40 reanalyses extend from 1957 to 2001 and, because they cover the whole stratosphere, were expected to provide a much better representation than previous analyses, which extended only up to 10 hPa. Such analyses (e.g., ECMWF ERA-15 reanalyses for the period 1978 to 1993) were used in studies discussed in WMO (2003). These ERA-40 reanalyses have now been quite extensively tested in long-term transport studies and the winds have been applied for ozone integrations. These studies have shown that the reanalyses are a very important resource for diagnosing past ozone changes but, due to some clear problems, some caution is needed in their use. The ERA-40 data has a much stronger circulation than the operational data, due to the less balanced assimilation procedure in 3D-VAR, which has been shown by ozone integrations (Laat et al., 2006). In addition, ERA-40 suffers from inhomogeneity, introduced by the use of spaceborne observations in the data assimilation as well as by changes in the satellite instrumentation. This was illustrated from different diagnoses, e.g., downward ozone fluxes (Van Noije et al., 2004) and water vapor distributions (Bengtsson et al., 2004). They showed significant discontinuities in the strength of the ozone flux at 100 hPa.

Different datasets of assimilated winds and temperature (operational and reanalyses) have been evaluated for the Arctic winter (Manney et al., 2003) and the 2002

Antarctic polar vortex (Manney et al., 2005) by comparisons with observations. The large-scale dynamical structures were well represented in all datasets, but noticeable differences appeared in several diagnoses. The REAN and NCEP show warm biases in the temperatures, while the ERA-40 dataset shows unrealistic spurious temperature oscillations, which were also reported by Simmons et al. (2005). Manney et al. (2005) also show that between the different meteorological datasets, there is little consensus in mixing of vortex air with midlatitudes. Overall, they concluded that caution must be taken when applying a certain assimilated wind dataset, and that the use of some reanalysis data for detailed studies of polar dynamics and chemistry is not recommended. Additional evidence of inhomogeneities in the reanalysis datasets was given by temperature and tropopause height trends analyses (Santer et al., 2004). However, they also concluded that the ERA-40 reanalysis has much improved compared with the earlier ERA-15 and NCEP-50 reanalyses. Birner et al. (2006) also noted the effect of data inhomogeneities on tropopause characteristics. Despite the caveats, the interannual variability of tracers using ERA-40 is simulated quite well (Hadjinicolaou et al., 2005; Feng et al., 2006).

Even when applying the operational 4D-VAR ECMWF data, the large-scale circulation in pressure-coordinate CTMs remains too strong (Meijer et al., 2004; Van Noije et al., 2006). However, there are different approaches to the use of analyzed winds to force an off-line CTM. For example, the use of an isentropic vertical coordinate results in less noisy vertical motion, shown by a reduction of air parcel dispersion in the tropical lower stratosphere and increased mean age of air (Mahowald et al., 2002; Schoeberl et al., 2003; Chipperfield, 2006). Another approach to reducing the noise in the wind data uses forecasts instead of analyses (Meijer et al., 2004; Scheele et al., 2005; Laat et al., 2006). In addition, the use of 3-hourly instead of the usual 6-hourly analyses has been shown to improve stratospheric tracer distribution at northern midlatitudes (Berthet et al., 2005).

Nevertheless, the apparent dispersive character of assimilated winds remains, and it seems inherently connected to the assimilation procedure. In addition, reducing present spurious variability and inhomogeneity as a result of temporal changes in spaceborne instrumentation and inter-instrumental biases is a major challenge for future improvements of reanalyses datasets. Data assimilation for the stratosphere is the subject of ongoing development. Improvements in the 3D-VAR and 4D-VAR assimilation procedures are currently being evaluated (Polavarapu et al., 2005; Monge Sanz et al., 2006), which may lead to improved reanalyses datasets. In the meantime, despite its shortcomings, the ERA-40 dataset is the best descrip-

tion we have of the meteorological state of the stratosphere over the past few decades (Randel et al., 2004). These reanalyses have been used in chemical and dynamical attribution studies discussed below (Sections 3.4.2 and 3.4.5).

3.4.2 Dynamical Processes

As reviewed in Section 4.6 of WMO (2003), changes in two specific dynamical transport processes can significantly influence midlatitude ozone trends. These are:

- (1) interannual and long-term changes in the strength of the stratospheric mean meridional (Brewer-Dobson) circulation, which is responsible for the winter-spring buildup of extratropical ozone (e.g., Fusco and Salby, 1999; Randel et al., 2002; Weber et al., 2003; Salby and Callaghan, 2004; Hood and Soukharev, 2005); and
- (2) changes in tropospheric circulation, particularly changes in the frequency of local nonlinear synoptic wave forcing events, which lead to the formation of extreme ozone minima (“mini-holes”) and associated large increases in tropopause height (Steinbrecht et al., 1998; Hood et al., 1997, 1999, 2001; Reid et al., 2000; Orsolini and Limpasuvan, 2001; Brönnimann and Hood, 2003; Hood and Soukharev, 2005; Koch et al., 2005).

It is therefore important to consider interannual changes in both the Brewer-Dobson circulation and the nonlinear synoptic wave forcing when estimating the component of interannual ozone variability and trends that can be attributed to dynamical transport processes. The bulk of the studies on this subject have looked at the northern midlatitudes, and this is reflected in the following discussion. The lack of published studies for the Southern Hemisphere is partly due to the apparently weaker signal of dynamical changes on ozone trends compared with the Northern Hemisphere.

When the stratospheric polar vortex is strong (positive North Atlantic Oscillation or Arctic Oscillation index), tropospheric wave forcing is weaker, the Brewer-Dobson circulation is weaker, and less ozone is transported to the extratropics in winter and spring. Also, when the polar vortex is strong, the zonal wind field in the midlatitude lower stratosphere is less cyclonic, implying a greater frequency of anticyclonic, poleward wave breaking events that lead to ozone mini-holes and localized tropopause height increases (Peters and Waugh, 1996; Hood et al., 1999; Orsolini and Limpasuvan, 2001). Therefore, at northern midlatitudes in winter-spring, these two dynamical transport mechanisms tend to reinforce one another.

During a period of increasing AO and NAO indices, such as the 1980s and early 1990s (Appenzeller et al., 2000; Hurrell, 1995; Graf et al., 1998; Zhou et al., 2001), a negative dynamically induced contribution to column ozone trends at northern midlatitudes is to be expected. As assessed below, several studies aimed at estimating empirically the contribution to ozone trends at northern midlatitudes due to one or both of the above transport mechanisms have been published during the past four years.

Reinsel et al. (2005) reported a multiple regression analysis of the version 7 TOMS and SBUV/SBUV(2) total ozone dataset over the 1979 to 2002 period. The statistical model included terms proportional to the Eliassen-Palm (EP) planetary wave flux averaged between 30° and 90° latitude in each hemisphere as well as the Arctic/Antarctic Oscillation (AO/AAO) indices. It was found that both dynamical variables had a substantial influence on total ozone at latitudes higher than ~40° in both hemispheres. Evidence was also obtained for a “large positive and significant” change in trend after 1996. The latter result was obtained both with and without the inclusion of dynamical index terms in the regression model. For the Southern Hemisphere, Malanca et al. (2005) found a sizeable, latitude-dependent slowdown in the ozone loss from the early 1990s, with significant longitudinal variations in the size of the change in trends. Although the zonal mean behavior is strongly linked to variations in chemical loss in the Antarctic vortex, the longitudinal asymmetry is due to dynamical influences.

Inclusion of AO/AAO or NAO indices alone in a regression model does not necessarily account completely for ozone variability associated with synoptic wave forcing. Also, the EP flux is more a measure of the ozone tendency associated with changes in the Brewer-Dobson circulation (e.g., Fusco and Salby, 1999; Randel et al., 2002) than of ozone itself. So this statistical analysis could not definitively determine whether or not the change in trend after 1996 was caused by dynamical transport contributions. Nevertheless, the statistical evidence for a change in trend after 1996 is not affected by these issues. A similar statistical analysis of total ozone from ground-based observations in Europe by Krzyścin et al. (2005) has also concluded that a positive change in ozone trend in this region has occurred since 1994.

Continuing the earlier work of Fusco and Salby (1999), Salby and Callaghan (2002, 2004) showed that total ozone interannual variability and trends in the Northern Hemisphere are both characterized by an out-of-phase relationship between low latitudes and high latitudes. This relationship is consistent with that expected from changes in the Brewer-Dobson circulation. It was therefore argued that a “systematic weakening” of the

latter transport influence was responsible for a major portion of the ozone decline between the 1980s and 1990s. Randel et al. (2002) also used correlative and regression relationships to estimate more specifically that net decreases in strength of the Brewer-Dobson circulation may have caused 20% to 30% of the column ozone trend at northern midlatitudes over the 1979 to 2000 period.

The importance of nonlinear synoptic wave forcing for ozone interannual variability and trends at northern midlatitudes has been indicated by several recent studies. Wohltmann et al. (2005) analyzed total ozone variability measured at European ground-based Dobson stations using a multiple regression statistical model that included an explanatory variable based on the equivalent latitude (i.e., potential vorticity or PV) profile at a given station. Their technique takes advantage of the near conservation of both ozone and PV on isentropic surfaces on a time scale less than a few weeks in order to transform the PV profile into a synthetic ozone profile using an ozone climatology. The resulting synthetic ozone column is then used as the explanatory variable. It accounts for both vertical lifting (sinking) of isentropes by tropospheric pressure systems and for horizontal isentropic advection of ozone. It was concluded that 30% to 50% of the observed long-term trend over Europe during the 1970 to 2002 period was attributable to long-term changes in tropospheric pressure systems. The latter consist primarily of increases in the number and amplitudes of anticyclonic systems associated with poleward planetary and synoptic wave events (e.g., Hood et al., 1999). Consistent with their results, Brönnimann and Hood (2003) analyzed historical data to show that low-ozone events over northwestern Europe in winter were much more frequent in 1990-2000 than in 1952-1963 and that changing atmospheric circulation strongly contributed to the observed increase in frequency. In an analysis of balloonborne ozonesonde data at several Canadian stations, Tarasick et al. (2005) report evidence for a positive change in ozone trends at all levels below 63 hPa after about 1993. Interannual variability was found to correlate well with the wintertime frequency of laminae in the ozone profile (defined here as a thin layer bounded by sudden changes in the ozone profile of at least 20 hPa), which represent southward excursions of ozone-rich Arctic, or polar vortex, air. It was suggested that much of the positive change in trends after the early 1990s could result from changes in circulation, since both the laminae time series and the ozone time series show a similar change in trend (see also Krizan and Lastovicka, 2005).

As also reviewed in the previous Assessment (Section 4.6.3.3 of WMO, 2003), it may be reasonably questioned whether the separate influences of the Brewer-Dobson circulation and tropospheric synoptic wave

GLOBAL OZONE

forcing on zonal mean ozone trends at a given latitude can simply be added together, because these two dynamical processes may not be entirely independent of one another. For example, tropospheric planetary-scale waves that are dominantly responsible for driving the Brewer-Dobson circulation are also associated with synoptic wave events and local tropopause height changes.

Hood and Soukharev (2005) used correlative and regression methods to estimate separately and in combination the portion of ozone interannual variability and trends over the 1979 to 2002 period that can be attributed to long-term changes in both the Brewer-Dobson circulation and nonlinear synoptic wave forcing. In approximate agreement with Randel et al. (2002), it was estimated that 18% to 25% of the observed maximum negative trend in February and March is due to long-term changes in the Brewer-Dobson circulation. In addition, 27% to 31% of the observed maximum midlatitude trend was estimated to be caused by synoptic wave forcing. No significant correlations were found between monthly mean EP flux variations (representing changes in Brewer-Dobson circulation strength) and monthly mean PV variations (representing changes in synoptic wave forcing) at northern midlatitudes. A significantly higher correlation, up to 0.7, was obtained using both the time-integrated EP flux and zonal mean PV as predictor variables than using either predictor variable alone. This indicates that contributions to total ozone variability from these processes are, at least to first order, independent and summable at northern midlatitudes. Together, these transport components could explain almost 50% of the observed interannual variance and maximum negative trend at northern midlatitudes in February and March (Figure 3-16). The empirical regression model was able to simulate approximately the leveling off and slight increase in column ozone anomalies that have been observed for some months and latitudes since the middle 1990s (Figure 3-16). Furthermore, Brönnimann et al. (2004a, b) provided evidence for dynamic coupling of strong and long-lasting El Niño-Southern Oscillation events with stratospheric ozone in the NH by analyzing the record high total ozone values observed in northern midlatitudes in the early 1940s.

Changes in dynamical processes also affect the polar vortex conditions and, as a result, polar ozone loss. The midlatitude ozone is influenced by polar loss via air-mass mixing after the polar vortex breakup in early spring, as discussed in Section 3.4.3.2. Using regression analysis, Dhomse et al. (2006) concluded that this mechanism is one of the main factors responsible for the recent increase in NH total ozone.

Finally, estimates of the dynamically induced contributions to ozone interannual variability and trends can

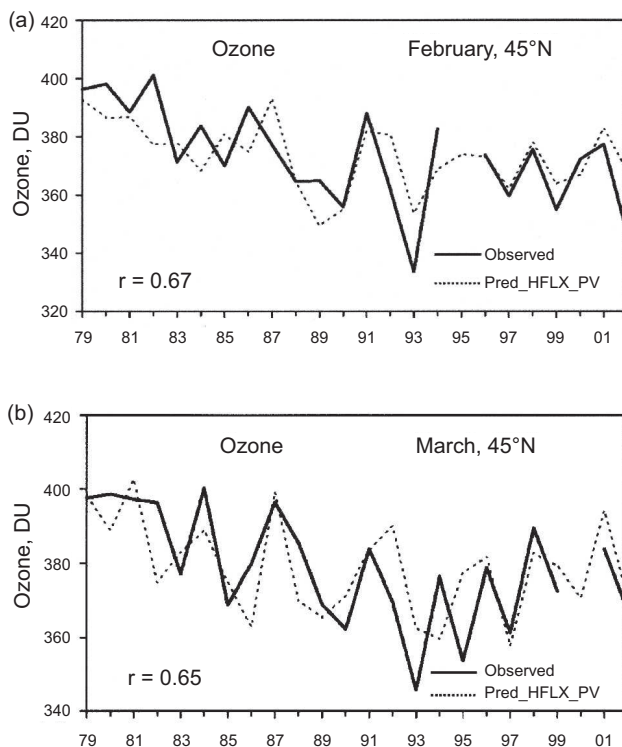


Figure 3-16. (a) Comparison of observed and empirically estimated column ozone at 45°N for February when both 350 K PV and EP flux, averaged over the 40°N to 70°N latitude band and integrated over January and February, are considered as predictor variables in the empirical model. (b) As in (a) but for March. In this case, EP flux is integrated over the January to March period. From Hood and Soukharev (2005).

be derived by using CTMs driven by observed temperature and wind fields (Hadjinicolaou et al., 1997, 2002, 2005). Most recently, Hadjinicolaou et al. (2005) have reported further integrations of the SLIMCAT 3-D chemical transport model with a parameterized ozone tracer and using the ECMWF ERA-40 meteorological analyses for 1979-2002. They find that the model simulates a large part of the observed ozone changes at northern midlatitudes (represented by the merged satellite dataset (see the Appendix 3A.1) averaged over the 35°N to 60°N latitude range), including the positive tendency after the mid-1990s. A linear regression analysis indicated that about one-third of the observed ozone trend from 1979 to 1993 at these latitudes and, within uncertainties, all of the positive trend thereafter could be explained by the model, which includes only transport-related changes. They argue that these changes are consistent with the changes in the Brewer-Dobson circulation in the observed positive tendency after the mid-1990s, but emphasized that this trans-

port process alone is unlikely to explain the relatively large change in slope of the ozone trend (modeled and observed) and that synoptic wave forcing may contribute significantly. Results from this study are included with full chemistry CTM studies, which also quantify the important role for halogen forcing, in the discussion of assessment models (Section 3.4.5 below).

The direct effects of dynamical factors on ozone described above are mainly limited to winter and spring. Through the summer season the total ozone changes from month to month are mainly controlled by nitrogen oxides (NO_x) abundance and photochemistry (Brühl et al., 1998). While the photochemical lifetime does not vary from year to year (e.g., Randel et al., 2002), the initial conditions for summertime ozone vary and depend on the winter-spring ozone abundance. As a result, ozone anomalies observed in late summer and early autumn are highly correlated with winter-spring anomalies (Fioletov and Shepherd, 2003; Dhomse et al., 2006). This suggests that summertime ozone is also indirectly influenced by dynamical processes in the preceding winter-spring.

In summary, both empirical and model studies using observed circulation changes continue to indicate that a major fraction (almost 50% in February-March) of the observed column ozone trends at northern midlatitudes from 1979 to the mid-1990s can be attributed to long-term changes in lower stratospheric circulation. Such circulation changes may also have been responsible, at least in part, for the increase that has been observed at these latitudes since the mid-1990s. The primary dynamical transport processes are (1) interannual and long-term changes in the strength of the mean meridional (Brewer-Dobson) circulation and (2) interannual and long-term changes in nonlinear synoptic wave forcing. Contributions from these two forcings appear to be comparable in amplitude and are, at least to first order, independent of one another. Zonal mean ozone decreases at northern midlatitudes in winter-spring caused by both forcings are larger when the tropospheric AO/NAO circulation indices are positive. The causes of the observed long-term trends in lower stratospheric circulation (including trends in the AO/NAO indices) are unclear. This question can be answered ultimately only with the aid of GCMs. Such models have so far indicated that it is unlikely that radiative changes from chemically induced ozone losses are responsible (e.g., Langematz et al., 2003). Remaining possibilities include long-term natural climate variability and greenhouse-gas-induced climate change.

3.4.3 Chemical Processes

3.4.3.1 UPDATE OF RELEVANT KINETICS

Based on the Jet Propulsion Laboratory (JPL) 2002 recommendation (Sander et al., 2003), updates to stratospheric reaction kinetics since the previous Assessment have generally been minor. No major new reaction pathways or rate changes have been uncovered since WMO (2003), which relied primarily on the *JPL 2000* evaluation (Sander et al., 2000). Several open issues from the previous Assessment have been resolved and some relatively minor updates are discussed here. Note that here we do not discuss any results from the very recent *JPL 2006* recommendation (Sander et al., 2006), which appeared after this Assessment was finalized.

Gas Phase

The *JPL 2002* recommendation (Sander et al., 2003) highlights several noteworthy changes from the previous stratospheric evaluation. Rates of some hydrocarbon reactions in the upper troposphere are considered, although their effect on the lower stratosphere is probably small. Reactions with hydroxyl radical (OH) and photolysis cross sections and quantum yields have been updated and added for numerous halocarbons. These will affect halocarbon lifetimes to some degree but do not have a major impact on stratospheric ozone.

Progress has been made in resolving several kinetics issues that were raised in WMO (2003). Regarding the product pernitrous acid (HOONO) in the reaction $\text{OH} + \text{NO}_2 + \text{M}$, *JPL 2002* recommends neglecting this channel in stratospheric models. The $\text{OH} + \text{ClO} \rightarrow \text{HCl}$ product channel has increased from 5 to 7% at 298 K in *JPL 2002*, and the $\text{HO}_2 + \text{ClO}$ updates discussed in WMO (2003) are included in *JPL 2002*, however, the impacts of these changes in models have not been published specifically. Peroxynitric acid (HO_2NO_2) overtone photolysis has been tested in comparison with aircraft and balloon data by Salawitch et al. (2002) and in a global model by Evans et al. (2003). This process significantly changes the model abundance of HO_2NO_2 globally and odd hydrogen (HO_x) particularly near sunrise/sunset, and improves comparison with observations. The maximum change of O_3 in the lower stratosphere is 1-2%. This process is not included in *JPL 2002*. Data on HO_x reactions with O_3 discussed in WMO (2003) are now included in *JPL 2002*, which is consistent with atmospheric measurements of OH/ HO_x .

GLOBAL OZONE

More recently, the reaction $\text{NO} + \text{HO}_2 \rightarrow \text{OH} + \text{NO}_2$ (a) has been found to have a second channel at low temperatures: $\text{NO} + \text{HO}_2 \rightarrow \text{HNO}_3$ (b), branching ratio (k_b/k_a) = 0.18 (298 K) and 0.87 (223 K) (Butkovskaya et al., 2005). Inclusion of this product channel will produce a HO_x sink in the upper troposphere and decrease NO_x/HNO_3 partitioning in the lower stratosphere, perhaps by as much as 10-15%. Global impacts have yet to be tested in models.

Low-temperature oxidation rates for several hydrocarbon species have been updated, including: $\text{CH}_3\text{CHO} + \text{OH} \rightarrow \text{CH}_3\text{CO} + \text{H}_2\text{O}$ (Sivakumaran and Crowley, 2003), $\text{H}_2\text{CO} + \text{OH}$ (Sivakumaran et al., 2003), and $\text{CH}_3\text{OH} + \text{OH} \rightarrow \text{products}$ (Dillon et al., 2005). These changes will affect upper troposphere calculations but are not expected to have a significant impact on stratospheric chemistry.

The assessment models discussed in Section 3.4.5 use an updated version of the *JPL 2002* kinetics. No significant differences from simulations using the standard *JPL 2002* are found.

Heterogeneous Chemistry

JPL 2002 provides updates to several heterogeneous processes, with particular focus on liquid binary $\text{H}_2\text{SO}_4 \cdot \text{H}_2\text{O}$ uptake, i.e., $\text{HOCl} + \text{HBr}$, $\text{HO}_2\text{NO}_2 + \text{HCl}$, and α (HOI), as well as $\text{HCl} + \text{HNO}_3$ on liquid ternary solution. None of these updates is expected to have a significant impact on global ozone, although a specific test has not been published.

Recent laboratory experiments yielded new information regarding uptake of gases on ice surfaces under atmospheric conditions corresponding to the upper troposphere/lower stratosphere (UT/LS). So far the knowledge of gas uptake on ice particles was primarily based on clouds in cold polar stratospheric conditions and no information was available for competitive and reactive uptake. Hynes et al. (2002) and Cox et al. (2005) found that the uptake of HCl was suppressed when HNO_3 was present on the ice surface at temperatures higher than 208 K (Hynes et al.) or 218 K (Cox et al.). Hence for temperatures greater than 208 K, there is a tendency to reduce uptake of hydrochloric acid (HCl) when competitive uptake is considered, which will reduce the potential for chlorine activation on cirrus clouds. Fernandez et al. (2005) found significant uptake of chlorine nitrate (ClONO_2) on pure and doped (HNO_3 , HCl) ice surfaces. No model study has included this information to estimate the effect of heterogeneous chemistry on aerosol and ice particles on ozone.

3.4.3.2 LOWER STRATOSPHERE

The major chemical processes expected to contribute to global ozone depletion were reviewed in previous Assessments (e.g., WMO 2003). There have been no significant changes to the understanding of these processes, although studies have provided new quantification. There have been relatively minor refinements in chemical rate constants and uncertainties (Section 3.4.3.1) but no major changes in our understanding of chemical processes. However, some new observations, related to likely minor processes of cirrus activation and pyroconvection, are discussed here. Then we discuss recent findings related to the more established and important process of aerosol chemistry, the role of bromine in the lower stratosphere, and export from the polar vortex.

Cirrus (Including Subvisible Cirrus)

In addition to the observed cirrus climatologies in the tropopause region reported earlier (see WMO, 2003), there is new observational evidence of thin cirrus clouds in the cold tropical (Peter et al., 2003) and midlatitude tropopause region (Ström et al., 2003; Keckhut et al., 2005a). Supporting these findings, there is further observational evidence of supersaturation with respect to ice in the same altitude range (Ovarlez et al., 2002; Spichtinger et al., 2004), though it is likely that the thin “ice” clouds consist of nitric acid trihydrate (NAT) (Popp et al., 2006). Gao et al. (2004) found observational evidence for a new HNO_3 -containing ice particle (delta-ice). However, the laboratory results from Delval and Rossi (2005) do not support the Gao et al. findings and suggest that small NAT particles, even H_2O -rich, can survive much longer in a subsaturated atmosphere than previously thought.

Following the first observations of possible chlorine activation in the lowermost stratosphere (Keim et al., 1996; Borrmann et al., 1997), Solomon et al. (1997) showed that these findings could lead to significant chemical ozone loss in the midlatitude lowermost stratosphere, but Bregman et al. (2002) calculated considerably less loss (see WMO, 2003). More recent observations by Thornton et al. (2003) showed much more in-situ observational evidence of chlorine monoxide (ClO) of several tens of parts per trillion by volume (pptv) in the lowermost stratosphere in the northern extratropics. The observed mixing ratios are significantly higher than can be explained by background gas-phase and heterogeneous chemistry on aerosols (Thornton et al., 2005). The observations were primarily performed during wintertime in the Northern Hemisphere and the enhancements were found between 55°N - 70°N . These observed levels of ClO were in very

close agreement with those calculated by Bregman et al. (2002), although no evaluation could be made regarding the temporal and spatial distribution of the ClO enhancements. However, the modeled bromine monoxide (BrO) levels in Bregman et al. were 2-4 pptv, which is a factor of two too small, according to recent estimates from Salawitch et al. (2005), implying that the calculated ozone loss is likely too small; consequently, this process may need further study.

The chemical composition of the ice cloud particles is important for their potential to activate halogens. In the tropical tropopause region there is ongoing discussion about the existence and occurrence frequency of the HNO₃-containing particles (Gao et al., 2004; Popp et al., 2006; Delval and Rossi., 2005).

Pyroconvection

It is well known that the presence of enhanced aerosols in the stratosphere can cause significant chemical ozone loss through heterogeneous chemical reactions, as demonstrated by many studies of the impact of the eruption of Mt. Pinatubo (see WMO, 2003). Apart from volcanic eruptions, a recently identified process, pyroconvection, may also cause enhanced stratospheric aerosol concentrations. Pyroconvection is induced by boreal fires or biomass burning, likely in combination with strong convective activity (Fromm and Servranckx, 2003; Jost et al., 2004; Fromm et al., 2005). The aerosol enhancements have been found in the lower stratosphere over all longitudes in the northern mid- and high latitudes. The particles likely consist of soot and smoke (Fromm and Servranckx, 2003).

Blumenstock et al. (2006) observed chlorine activation in the lower stratosphere in late Arctic winter under conditions well above the NAT temperatures. This was attributed to heterogeneous chemistry on an enhanced aerosol plume, originating from forest fires and injected by strong convection, as described in Gerding et al. (2003).

Ray et al. (2004) and Jost et al. (2004) attribute enhanced carbon monoxide (CO) and aerosol observed by aircraft measurements in the subtropical stratosphere to pyroconvection. Livesey et al. (2004) found enhanced acetonitrile (CH₃CN) in stratospheric data from the spaceborne Microwave Limb Sounder (MLS), associated with forest fires and thunderstorm lofting. Injection of aerosol and other fire-produced chemical species will affect ozone locally.

The occurrence frequency of pyroconvection remains an open issue, as does a quantification of its impact on ozone. However, given the impact of other established processes included in models that can gener-

ally reproduce past ozone changes, we can surmise that any effect will be relatively small.

Aerosol Effects

Sulfate aerosol in the lower stratosphere provides surfaces for the activation of chlorine. The distribution of sulfate surface area depends on background sulfur emissions and volcanic eruptions. The atmosphere is currently (since about 1999) near a background minimum (Section 3.3.1) and this sets the minimum for the nonvolcanic aerosol loading. Thus, the Mt. Pinatubo-to-present period gives a good span of potential heterogeneous effects, barring a huge future volcanic eruption. The reactions, as reviewed in previous Assessments, do not suggest significant missing processes or inaccurate rates. Sulfate surface area in models can be, and usually is, specified from observations for past-to-present runs.

A large chemical effect from volcanoes has been quantified in 2-D models (e.g., Tie et al., 1994; WMO 2003, Section 4.5.3.4) and 3-D models (e.g., Chipperfield, 1999; 2003; Stolarski et al., 2006). The volcanic effect on column ozone results from heterogeneous suppression of NO_x, via N₂O₅ + H₂O(l), which then interferes less with the halogen and HO_x ozone loss cycles in the lower stratosphere. Thus, chemical ozone losses from volcanic sulfate injection are largest at times of peak chlorine and bromine, and volcanic impact on ozone at preindustrial halogen levels is small or even positive (Tie and Brasseur, 1995).

Dynamical changes resulting from the Mt. Pinatubo eruption also contribute to ozone change and are present in meteorological analyses (Hadjinicolaou et al., 2005; see Sections 3.4.2, 3.4.5). An outstanding puzzle is the lack of a Pinatubo effect on observed ozone in the SH while the effect on NO₂ there is clear. Models all show a SH effect as large, or larger than, the NH effect. Stolarski et al. (2006) show that much of this apparent hemispheric discrepancy may be the result of interannual variability masking the volcanic effect in the ozone time series analysis.

Inorganic Bromine

A variety of observations have shown that that inorganic bromine in the stratosphere is underestimated when based on release from methyl bromide (CH₃Br), halons, and other long-lived source gases (see Chapter 2), as is usually assumed in global models. Although full resolution of this issue awaits further study (Sinnhuber et al., 2005), the potential impact of increased background stratospheric Br on O₃ loss is significant (Salawitch et al.,

GLOBAL OZONE

2005). Assuming the purported additional Br is of biogenic origin, and thus is constant with time, it contributes slightly to the O₃ column change from 1979 to present through reaction with Cl at low background aerosol amounts. The effect of the additional Br is large, however, during periods of volcanically enhanced stratospheric aerosol following El Chichón and Mt. Pinatubo (see Figures 3-14 and 3-25). Ozone loss via the BrO + ClO catalytic cycle is enhanced by a factor of two or more by the additional Br during periods of relatively high Cl resulting from heterogeneous reactions on volcanic sulfate. This enhancement generally improves the global model simulation of decadal O₃ change in comparison to observations (Chapter 2 Figure 2-12; see also 3-D results in Figure 3-25 below). This potential additional source of stratospheric Br is important to resolve and characterize because it will impact O₃ future projections as Cl decreases and if the Br source and/or transport processes change with climate.

Export from Vortex

The export of ozone-depleted or activated polar vortex air may have a significant contribution to observed ozone loss at midlatitudes in spring-summer. This effect exists in both hemispheres but is expected to be larger in the Southern Hemisphere due to the larger and more regular ozone depletion in the Antarctic vortex. Although transport is clearly involved in this process, the ultimate cause is chemical O₃ loss in the polar regions by Cl and Br species (see Chapter 4). Figure 3-17 shows that the mass of “missing” ozone in the ozone hole has the same order of magnitude as the mass deficit over southern middle and high latitudes in summer, and illustrates the strong correlation between loss in the ozone hole and in summer.

Konopka et al. (2003) investigated the fate of Arctic vortex remnants, and the chemistry occurring in those remnants, during the spring of 1997 and 2000 using a Lagrangian CTM. They found a different behavior in the lower and in the mid-stratosphere. Above 20 km, vortex remnants (Orsolini, 2001) remain long-lived in the summer westward circulation. Using balloonborne in-situ measurements of water vapor and methane, Durry and Hauchecorne (2005) indeed found evidence for such vortex remnants in the midlatitude summer stratosphere. Below 20 km, the subtropical jet bounds the meridional propagation of those remnants (Piani et al., 2002), and the remnants' lifetime is considerably reduced due to enhanced stirring by synoptic eddies. This picture is corroborated by satellite measurements of the breakup of the Antarctic polar vortex in 2004. Manney et al. (2005)

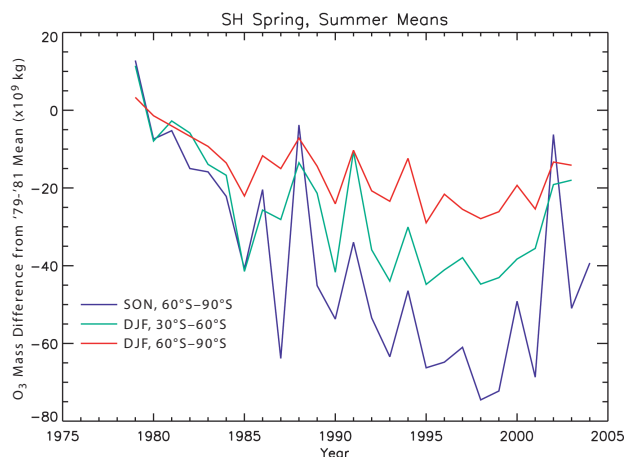


Figure 3-17. The change in mean ozone mass from the average of 1979-1981 over southern polar latitudes in spring (September-November; blue curve) and summer (December-February; red curve) compared with that over southern midlatitudes in summer (green curve). Derived from the NIWA Assimilated Dataset (see Appendix 3A).

reported that vortex remnants persisted in tracer measurements for over a month in the mid-stratosphere, but no more than a week in the lower stratosphere.

Seasonal model studies have been conducted to quantify the impact of the export of polar air on midlatitudes in particular years. Knudsen and Grooß (2000) found that about 40% of the observed midlatitude depletion in May 1995 and 1997 is due to dilution with polar-processed air. Including all years with large Arctic ozone depletion (1993, 1995, 1996, 1997, and 2000) Andersen and Knudsen (2002) found that the dilution explains 33% of the 1979-2002 midlatitude trend in the April-May period. The dilution has a tendency to occur mainly over the Eurasian continent, which helps to explain why ozone trends are larger over this region (Knudsen and Andersen, 2001). Using a high resolution CTM, Marchand et al. (2003) estimated that the dilution of polar vortex air during the cold winter 1999-2000 contributed up to 50% of ozone depletion at northern midlatitudes (45°-55°N) over the period from December 10 to April 30. Millard et al. (2003) studied the connection between polar and midlatitude ozone loss with a series of seasonal 3-D CTM simulations. During years 1994 to 2000, they found a large interannual variability (from -25 DU to almost 0) in the contribution of polar vortex air (90°-70°N) to midlatitude (60°-30°N) ozone loss from December 1 to May 31.

For the Southern Hemisphere, Ajtić et al. (2004) quantified the seasonal dilution effect of the Antarctic ozone hole by calculating ensemble diabatic trajectories

of ozone-depleted air parcels from October 15 to January 15 for a series of years. The mean calculated ozone reduction in 1998, 1999, and 2000 was 16-19 DU (5-6% of total column) between 30°S-60°S. This is 83-95% of the change observed by TOMS between 1979-1980 and 1998-2000. Part of this overestimate is due to the fact that photochemistry was not included. Based on Prather et al. (1990), who suggested there would be 20-30% production during this period, the dilution may therefore account for 58-76% of the summertime ozone depletion at southern midlatitudes

Multiannual model studies have been performed to investigate the accumulated effect of polar processing on midlatitudes. Hadjinicolaou and Pyle (2004) investigated the dilution of polar ozone loss in the 1990s using a decadal 3-D CTM run with parameterized ozone. They found a large interannual variability in the north related to winter-spring planetary wave activity and calculated a year-round midlatitude depletion of about 1% between 40°N-60°N,

compared with 2-4% in the south. Chipperfield (2003) used a full chemistry 3-D CTM for 1979-1995 and reported that for the overall modeled decrease of midlatitude ozone due to halogens, about 30% (NH) to 50% (SH) of the change is caused by ozone loss within the polar vortex.

Once the vortex breaks down, ozone is rapidly mixed throughout the extratropics, which makes summertime year-to-year ozone variations outside the tropics homogeneous in latitude. This holds for both short-term variations and long-term trends (Fioletov and Shepherd, 2005). Figure 3-18 (top) shows that the magnitudes of the summertime trends over middle and polar latitudes are nearly identical, while the corresponding springtime trends are quite different. Polar ozone depletion and export of depleted air from the vortex thus affects the seasonal structure of midlatitude ozone trends, and thereby accounts for the different seasonality of the midlatitude trends in the two hemispheres. Over 35°-60°N, the long-

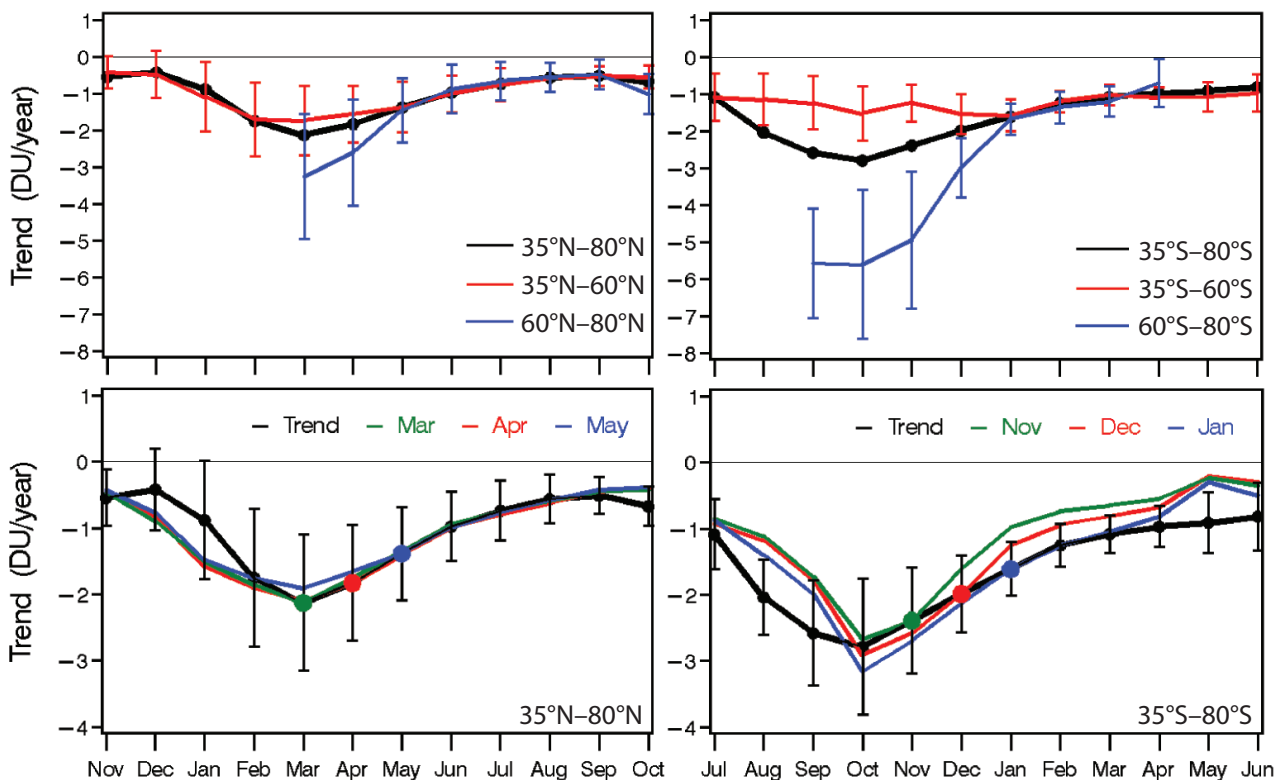


Figure 3-18. Top: The observed total ozone trends for 35°-60° (red), 60°-80° (blue), and 35°-80° (black) latitudinal belts for the Northern Hemisphere (left) and Southern Hemisphere (right). Bottom: The observed ozone trends for 35°-80°N and S (black line), and the trends estimated from the March, April, and May trends for the NH (November, December, and January trends for the SH) and regression coefficients estimated from detrended data. The trends were estimated for the period 1979-2003 using regression to an EESC curve and converted to DU/year using the variation of EESC with time in the 1980s. The error bars represent the 95% confidence intervals. From Fioletov and Shepherd (2005).

GLOBAL OZONE

term trends are in line with interannual variability, with a maximum in spring and a minimum in autumn. In particular, the trend magnitudes from late spring through to early autumn are related to the trend in April in the same way that the corresponding monthly ozone anomalies are related to the April anomaly in the detrended data (Fioletov and Shepherd, 2003). In contrast, the summer ozone long-term decline over 35°-60°S is stronger than one would expect purely from photochemical decay of the spring trend there, and is in fact of comparable magnitude to the spring trend. However for the entire 35°-80° belt, the long-term trends in SH ozone have a clear seasonal structure and are in line with interannual variability, as shown in Figure 3-18 (bottom). The implication is that the near constancy of the SH midlatitude trends throughout the year, in striking contrast to the behavior in the NH, reflects the much greater influence of polar processes in the SH compared with the NH. Indeed, Fioletov and Shepherd (2005) estimated from total ozone observations that about 39% of the observed southern midlatitude long-term ozone decline in December can be attributed to the polar ozone depletion achieved up to November. In the Northern Hemisphere, the corresponding contribution is about 15%, but the statistical uncertainty is too large to make an accurate estimate.

3.4.3.3 UPPER STRATOSPHERE

There have been no changes in our understanding that ozone trends in the upper stratosphere (around 40 km) are caused by changes in chlorine acting through the ClO + O cycle. The chemistry of the upper stratosphere will be affected by the trend in temperature (Chapter 5) and the partitioning of ClO and HCl, which will affect loss via the ClO + O cycle, will also be affected by changes in methane (CH₄) (Chapter 1). Trends in these quantities also need to be observed and compared with models for a rigorous test of our understanding. Overall, our understanding, as expressed in current models, is qualitatively consistent with observations, though as discussed in Section 3.4.5, there appears to be quantitative discrepancies in the simultaneous modeling of all relevant trends. This, however, should be considered as a problem for these models to simulate realistically the distribution of the precursors and species that control ozone, rather than a measure of uncertainty in the upper stratosphere chemical processes for which we have a good understanding (e.g., WMO, 1999). Chapter 6 (Section 6.5.1) summarizes observations of recent changes in ozone in the upper stratosphere, in the context of EESC levels, and discusses the implications for recovery from halogen-induced loss.

3.4.4 Solar Cycle Variations

A decadal variation of total column ozone is observed to be in phase with the solar cycle, with an amplitude of 2-3% from solar minimum to maximum in the tropics (Figure 3-4) and over the 60°S-60°N band (Figure 3-1). The detailed vertical structure of the ozone variation is still a topic of current research (for a review, see Hood, 2004) but, despite some uncertainty due to the limited record length (see discussion below), this decadal variation appears to be a dominant form of long-term ozone variability and should be carefully considered when evaluating anthropogenic trends at all latitudes and altitudes (Steinbrecht et al., 2004a, b; Cunnold et al., 2004).

The stratospheric ozone response to 11-year solar forcing has been estimated as a function of altitude, latitude, and season by a number of analysts based mainly on long-term, near-global satellite remote sensing datasets (Chandra and McPeters, 1994; McCormack and Hood, 1996; McCormack et al., 1997; Hood, 1997; Wang et al., 1996; Lee and Smith, 2003; Soukharev and Hood, 2006). Figure 3-19 compares the annually averaged solar cycle response derived from two long-term satellite ozone profile datasets (SBUV and SAGE) with the predictions of four models that account for observed 11-year changes in solar ultraviolet spectral irradiance. The observed ozone change from solar minimum to maximum is estimated using a multiple regression statistical model containing QBO, volcanic aerosol, solar cycle, and linear trend explanatory variables as well as a first-order autoregressive term. Figure 3-19a presents the signal in ozone averaged over the 55°S-55°N band (essentially the whole region covered by the satellites), while Figure 3-19b shows only the tropical response (25°S-25°N). The satellite datasets used are SBUV(/2) version 8 from 1979-2003 (Frith et al., 2004; updated from Hood, 2004) and SAGE I+II version 6.20 from 1979 to 2005, excluding several years after the Mt. Pinatubo eruption (updated from Stolarski and Randel, 1998). Analyses of SAGE II and UARS HALOE data (Soukharev and Hood, 2006), as well as comparisons between SBUV and TOMS data (e.g., Hood, 1997), suggest that most or all of the apparent total ozone solar cycle variation originates primarily in the lower stratosphere. Thus the observed variation in the ozone column of 2-3% (as discussed above) can be taken to represent the integrated values below about 25 km and 30 km for the 55°S-55°N and 25°S-25°N bands.

The theoretical curves in Figure 3-19 include results from two 2-D radiative-chemical transport models (Brasseur, 1993; Haigh, 1994) and two fully interactive, 3-D Chemistry-Climate Models (Tourpali et al., 2003; Egorova et al., 2004). Although the models have very dif-

ferent dynamical formulations, their predictions for the ozone solar response in the low-to-middle stratosphere (15-35 km) are very similar, and also representative of the results from other published modeling studies. In the upper stratosphere the model predictions diverge, probably due to their different representations of photochemical processes in the mesosphere.

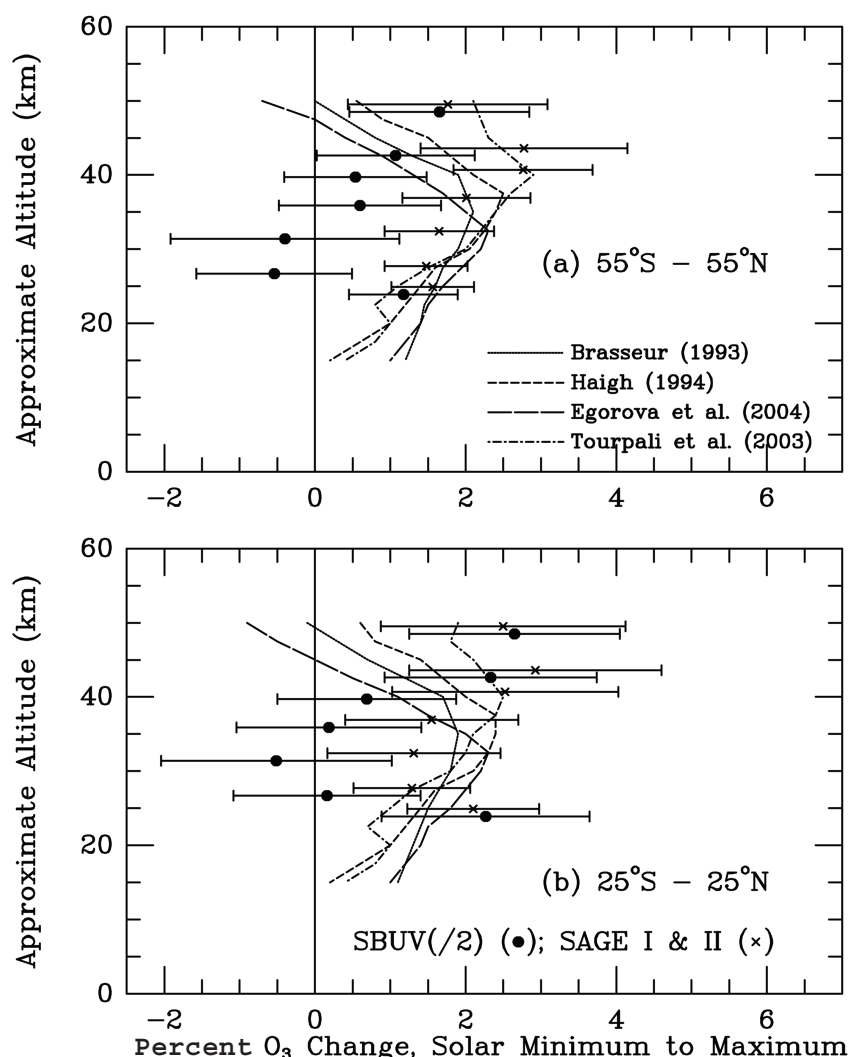
Over the 55°S-55°N band (Figure 3-19a), the model predictions lie within the error bars of the SAGE data analysis, and of the SBUV analysis in the upper and lower stratosphere, but tend to overestimate the signal found in the middle stratosphere in the SBUV data. The models are also generally consistent with the 1.5% lower stratospheric (ozone column) signal. However, in comparing the predicted model ozone responses to the observationally derived responses in the tropics (Figure 3-19b), some possible differences on the 11-year time scale are evident. Near the stratopause (~50 km altitude), the observed response appears to be larger than expected from the

models while in the middle stratosphere (~30 – 35 km), the reverse is true, especially relative to SBUV data. In the lower stratosphere, the mean observed response appears to increase again while the model responses decrease.

A number of possible explanations for the apparent differences between the observationally derived and model-predicted tropical ozone responses may be considered. First, it is possible that there are significant uncertainties in the observations because of problems in the cross-calibration of instruments (see Section 3.2.3), overall short record lengths, and the relative size of the solar effect (a few percent). Only after another several decades of data are acquired will these uncertainties be reduced.

One physical explanation suggested for the unexpected altitude dependence of the tropical ozone response is increased odd nitrogen in the upper stratosphere caused by enhanced precipitation of energetic electrons when the

Figure 3-19. Annual mean solar cycle response calculated from two long-term satellite ozone profile datasets with the predictions of four stratospheric models that account for observed 11-year changes in solar ultraviolet spectral irradiance, for (a) 55°S-55°N and (b) 25°S-25°N. Datasets are the monthly zonal mean version 8 SBUV/SBUV(2) ozone profile dataset of Frith et al. (2004) over the 1979 through 2003 period (updated from Hood, 2004) and version 6.20 SAGE I and II ozone profile data over the 1979 to 2005 period, except for several years following the Mt. Pinatubo eruption (updated from Stolarski and Randel, 1998). Model results are from the 3-D models of Tourpali et al. (2003) and Egorova et al. (2004) and the 2-D models of Brasseur (1993) and Haigh (1994).



GLOBAL OZONE

Sun is less active (Callis et al., 2000, 2001). Some model simulations (Langematz et al., 2005; Rozanov et al., 2005) have produced a response of opposite sign (a “self-healing effect”) in the mid-stratosphere but only in response to massive electron precipitation events producing very large NO_x signals, which have not been detected in satellite data (Hood and Soukharev, 2006). At this time, therefore, there is no evidence for particle-induced NO_x being responsible for the apparent difference between models and observations in the tropics.

Several possible explanations for the reduced solar cycle ozone response in the tropical middle stratosphere may be considered. First, it is possible that the multiple regression statistical analysis is being biased by interference from the QBO and major volcanic eruptions. Lee and Smith (2003) have applied a two-dimensional chemical-dynamical-radiative model with a prescribed QBO to show that such interference can occur, especially from the QBO, and can potentially lead to small or even negative solar cycle regression coefficients in the equatorial lower and middle stratosphere. It remains to be seen whether some of this response is an artifact due to the highly idealized form used by Lee and Smith for the QBO, but interference from the QBO should be carefully considered in future evaluations of the observed tropical response minimum. It is also possible that the QBO itself may be modulated slightly by the solar cycle (Salby and Callaghan, 2000; McCormack, 2003; but see also Hamilton, 2002). If so, then additional dynamical effects on the net ozone change over a solar cycle could be implied. Finally, one relatively simple possible explanation for the tropical ozone response minimum is that the unexpectedly large ozone response in the upper stratosphere effectively reduces the ozone production rate in the middle stratosphere through increased absorption of UV radiation (a form of “self-healing”), but this remains to be tested. On short time scales (i.e., that of the ~27-day solar rotation period), the observed ozone response to solar UV variations in the tropical middle and upper stratosphere agrees very well with photochemical model predictions (see, e.g., Chen et al., 1997).

The origin of the apparent solar cycle ozone variation in the lower stratosphere also remains uncertain. It has been questioned whether the lower stratospheric decadal ozone variation is of solar origin at all because of the occurrence of two major volcanic perturbations about 9 years apart in 1982 and 1991 (e.g., Solomon et al., 1996). However, the increase in tropical total ozone approaching the most recent solar maximum, when no major eruptions have occurred, supports the view that volcanic eruptions alone cannot explain this decadal variation. A remaining hypothesis is that the direct upper stratospheric effects of

solar ultraviolet radiation (and possibly particle precipitation) are able to modify the development of stratospheric circulation in such a way as to modify the effective upwelling rate in the tropical and subtropical lower stratosphere. Possible mechanisms for this, and for the subsequent transmission of a solar signal into the troposphere, are discussed in Section 5.2.1.1 of Chapter 5.

3.4.5 Assessment Model Simulations

A range of model runs have been performed for this Assessment to simulate both the past and future atmosphere. Different types of two-dimensional (2-D) latitude-height models and three-dimensional (3-D) models are described in Box 5-1 (Chapter 5). Simulations using 2-D models and 3-D coupled Chemistry-Climate Models (CCMs) are described in Chapter 6 (Appendix 6A), where they are used to investigate future changes in stratospheric ozone. These models were also used, in certain experiments, to simulate the past atmosphere. In this section we make use of these simulations of the recent past to understand the causes of past changes in ozone. Descriptions of the 2-D models and 3-D CCMs used in this chapter may be found in Tables 6-3 and 6-4 of Chapter 6. In addition to the 2-D models and CCMs, we also use results from off-line 3-D chemical transport models (CTMs). Because the CTM results are only used in this chapter, we summarize details of the runs available in Table 3-1. Generally, for the CTMs we have used existing, published simulations and reanalyzed the output to compare with recent observations. The NASA Goddard Space Flight Center (GSFC) CTM provided one simulation (Stolarski et al., 2006), which was forced by GCM winds. The Global Modeling Initiative (GMI) CTM, which is technically very similar to the GSFC CTM and is based on much of the same code, provided two simulations. These used repeating climatological GCM winds corresponding to a “cold” and a “warm” Arctic winter. The SLIMCAT CTM was forced by analyzed ECMWF winds. In one experiment the model used a parameterized ozone tracer (see Hadjinicolaou et al., 2005). The model was also used to perform three experiments with full chemistry: A run with time-dependent halogen loading, a similar run but without an assumed 5 pptv of inorganic bromine (Br_y) from short-lived species, and a run with fixed halogen loadings.

Two-dimensional models have been used extensively in previous Assessments and we use them again here for comparison with the 3-D CTM runs. We have used output from the P5 runs (see Chapter 6), as these have the most realistic bromine loadings. In addition to the basic model setups described in Appendix 6A, the non-interactive GSFC 2-D model also performed a run in

Table 3-1. Participating 3-D chemical transport models.

Model Name	Institution(s)	Investigators	Forcing Winds and Temperatures	Resolution and Domain	Chemistry / PSC Scheme	Reference
GSFC CTM	NASA Goddard, U.S.	A. Douglass S.R. Kawa R. Stolarski	GEOS-4 GCM	2° × 2.5° Surface to 0.4 hPa	Full chemistry / Considine et al. (2000)	Stolarski et al. (2006)
GMI CTM	Several institutions, U.S.	A. Douglass S. Strahan R. Stolarski	GEOS-4 GCM	2° × 2.5° Surface to 0.015 hPa (33 levels)	Full chemistry / Considine et al. (2000)	Douglass et al. (2004)
SLIMCAT	University of Leeds, U.K.	M.P. Chipperfield W. Feng	ECMWF (ERA-40, operational)	7.5° × 7.5° Surface to 55 km	Full chemistry / Equilibrium	Chipperfield (1999) Feng et al. (2006)
	University of Cambridge, U.K.	P. Hadjinicolaou J. A. Pyle	ECMWF (ERA-40, operational)	5.6° × 5.6° 8 to 55 km	Parameterized O ₃ tracer / (No time dependence)	Hadjinicolaou et al. (2005)

which the model was forced with an interannually varying circulation (run GSFC-IDV in discussion below). These 2-D models and the 3-D CTMs have been compared with observations for ozone column and profiles in both the Northern and Southern Hemispheres, which extends on published work. The status of CCMs is much less mature and for these simulations we show just a basic comparison of the range of models with column ozone.

Figure 3-20 shows the deseasonalized zonal mean column ozone for global (60°N-60°S), NH (60°N-35°N) and SH (35°S-60°S) regions for a selection of the 2-D models and 3-D CTMs. There is a wide range in the predicted absolute column O₃ from the different models, which is due mainly to differences in the model transport. Clearly, the 2-D models, with their climatological circulation, do not capture the interannual variability in the observations. The GSFC CTM, forced by GCM winds, does well in tracking the variations in global ozone (as shown in Stolarski et al., 2006) but overestimates the SH values by around 20 DU. The interannual variability in this model, driven by the GCM winds, would not be expected to correlate with observed variations. For the 2-D models (except GSFC-IDV, not shown in Figure 3-20), the weak interannual variations will be driven by only aerosol changes and source gas trends. The SLIMCAT CTM, which is forced by analyzed winds, does capture more variability. This was demonstrated for the NH by Hadjinicolaou et al. (2005), who ran the model for the stratosphere with parameterized O₃ and showed the very

good agreement for 35°N-60°N. The full chemistry SLIMCAT run extends to the surface and tends to have larger columns due to overestimating O₃ in the lowermost stratosphere. However, these model runs are characterized by a large, spurious positive deviation in O₃ in the late 1980s that is caused by inaccurate interannual variability in the forcing (ERA-40) analyzed winds.

Figure 3-21 shows the global, equatorial, NH mid-latitude, and SH midlatitude anomalies of the annual average O₃ from the 2-D models and 3-D CTMs. As seen in WMO (2003), the 2-D models perform better in reproducing the observed variations in the NH, although there is still a spread in model results. In particular, the decrease in these models around 1992 is due to enhanced aerosol from the Mt. Pinatubo eruption. In the SH and globally, the 2-D models produce a wider spread of results, likely reflecting different treatments of the Antarctic ozone hole. The 3-D CTMs also appear more successful in simulating the NH midlatitudes than the SH midlatitudes. Aside from the large positive (late 1980s) and negative (early 1990s) deviations in the SLIMCAT runs, which use ERA-40 winds, the CTMs perform well in capturing the overall variations, which will be dominated by changes in aerosol loading and halogens. The SLIMCAT parameterized O₃ run is that discussed in Hadjinicolaou et al. (2005), where they show results for 35°N-60°N (see Section 3.4.2). This run has no time-dependence in the chemistry parameterization and clearly does not capture the overall trend from 1980-2004. However, the run does produce an increase in

GLOBAL OZONE

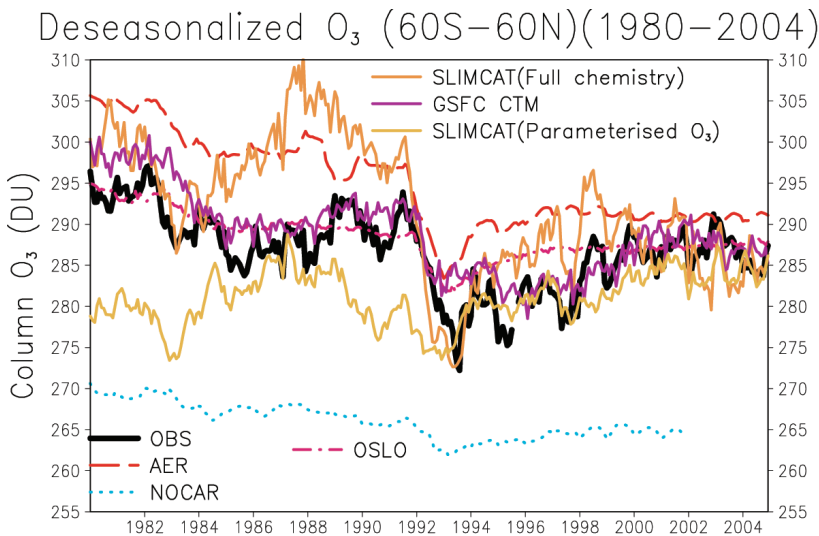


Figure 3-20. Time series of deseasonalized mean column O_3 for (top panel) 60°S - 60°N , (middle panel) 35°N - 60°N , and (bottom panel) 60°S - 35°S from 1980-2004 for three selected 2-D models and three 3-D CTMs. Also shown are the observations from the merged satellite data-set (black line). See Tables 6-3 and 6-4 of Chapter 6 for information about the models.

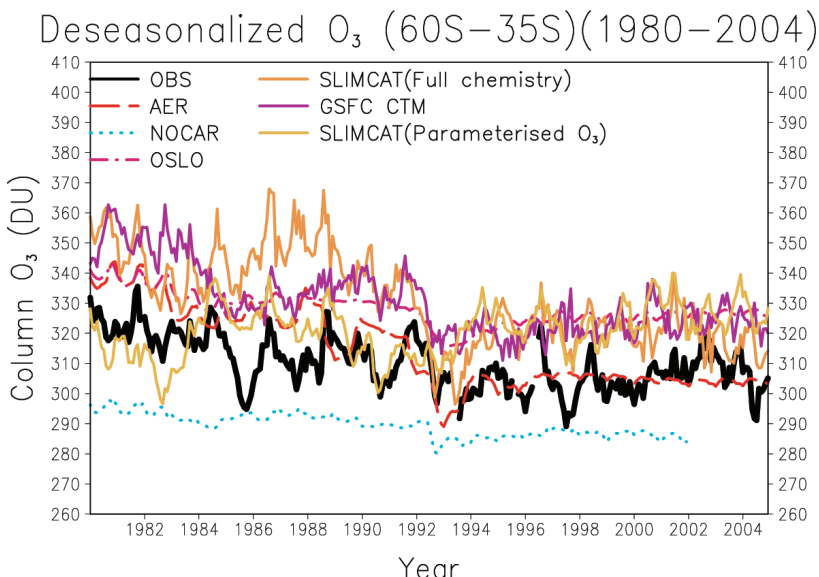
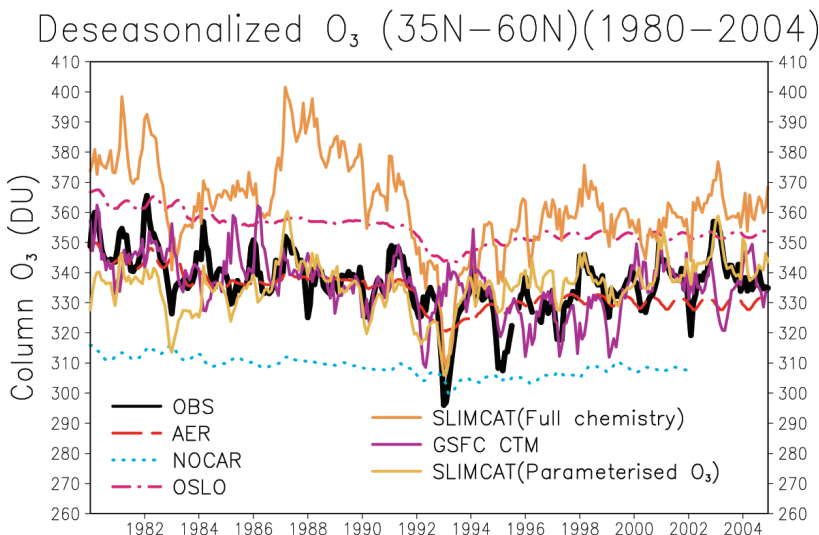
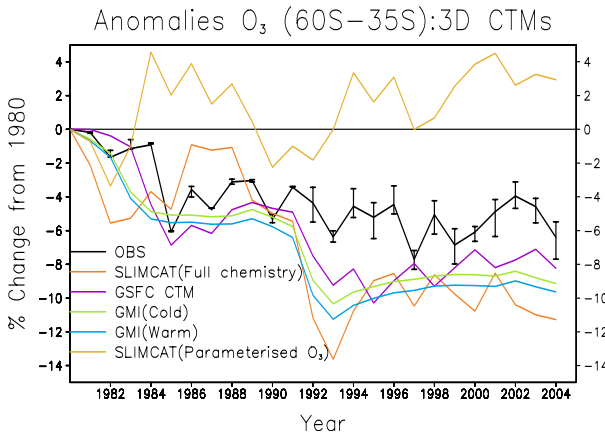
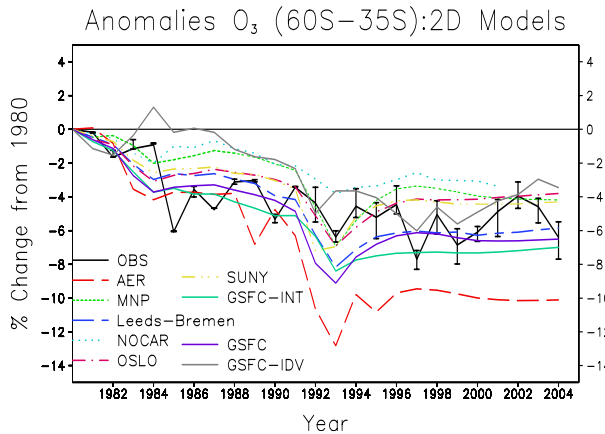
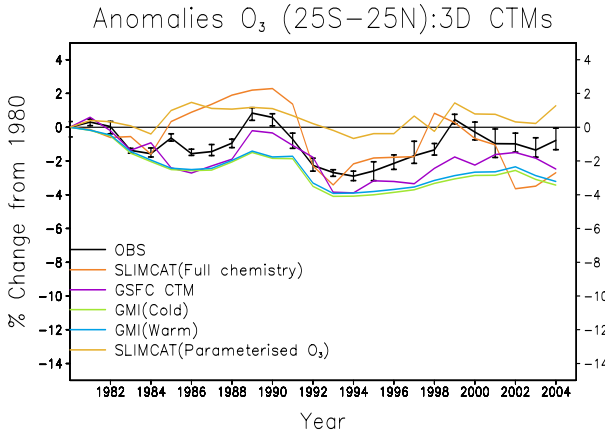
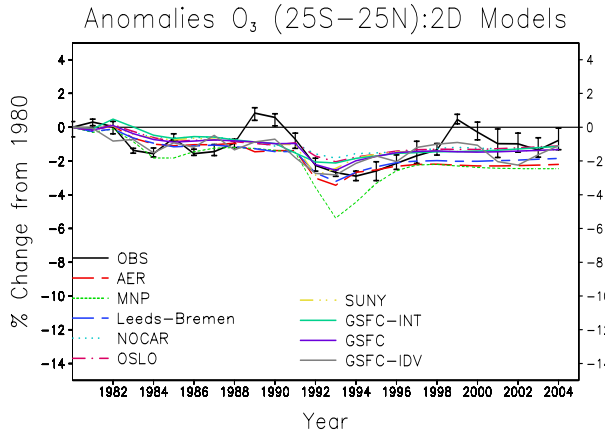
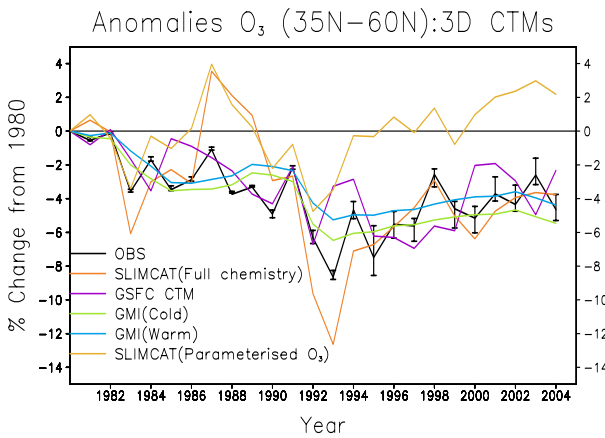
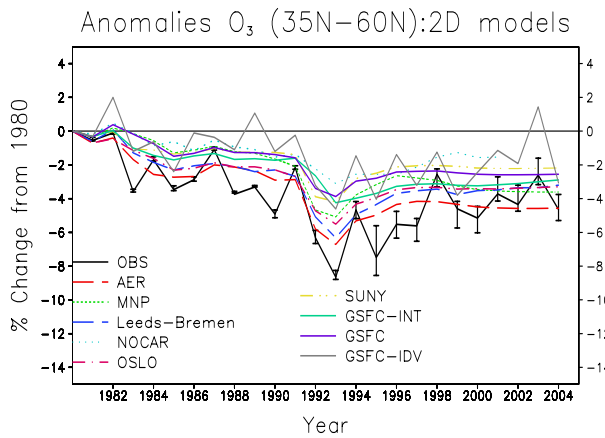
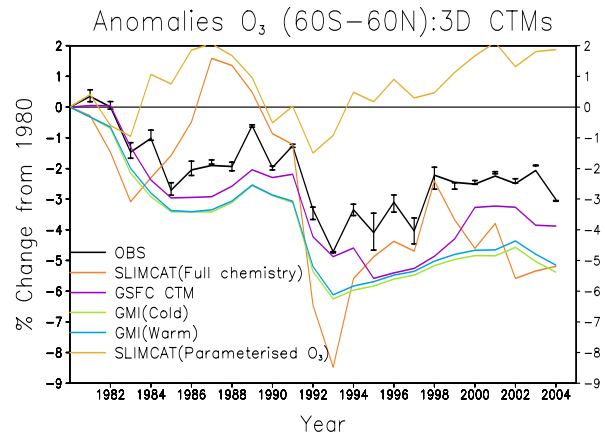
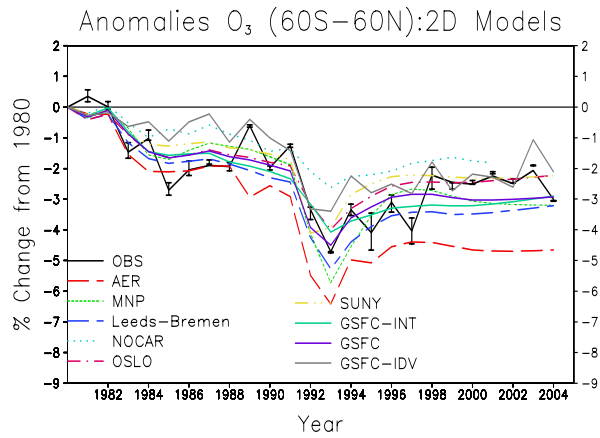


Figure 3-21. (On the right.) Time series of annual mean column ozone variations from observations (black line) and from eight 2-D model runs (left) and five 3-D CTM runs (right) for latitude bands of (top) 60°S - 60°N , 35°N - 60°N , 25°N - 25°S , and (bottom) 60°S - 35°S . Changes are calculated in percent with respect to 1980 values for each time series. Observations are from the merged satellite dataset; see Appendix 3A. The error bars on the observations represent the spread of different datasets, which provides a minimum estimate of their uncertainty. The SLIMCAT run with parameterized O_3 does not include any chemical changes and is therefore not expected to follow the other model curves. See Tables 6-3 and 6-4 of Chapter 6 for information about the models.



GLOBAL OZONE

NH column O_3 after the mid-1990s and this was presented as evidence that circulation changes are leading to O_3 increases. Interestingly, the GMI CTM runs with repeating meteorology also model an increase in O_3 during this period, which, like any changes in the 2-D models except GSFC-IDV, is related to aerosol trends. The GMI run with “cold” Arctic meteorology gives around 1% lower O_3 than the run with “warm” meteorology, which is a measure of the impact of different polar loss in this run. The different CTM runs give similar simulations for the SH, again with more variability in the SLIMCAT run, but the full chemistry CTMs clearly underestimate the observed O_3 from the early 1990s on. These models produce a realistically large O_3 hole and this appears to be having a large impact on the model SH midlatitudes. The models shown here are a mixture of those that include feedback between chemistry and dynamics (e.g., some of the 2-D models) and models without any coupling (e.g., the off-line 3-D CTMs). However, the impact of the modeled midlatitude O_3 loss on dynamics is not likely to be important. Using a GCM with parameterized O_3 chemistry, Braesicke and Pyle (2003) showed the impact of an imposed midlatitude O_3 loss did not produce an additional feedback on the O_3 distribution. The effect of dynamical changes on ozone is discussed in Section 3.4.2.

Results from the 2-D models and 3-D CTMs have been analyzed for ozone trends. This was done with a similar statistical model to that used in Section 3.2.1 and the trend term was regressed onto an EESC curve. Figure 3-22 shows the modeled O_3 trends from 1980-2004 (fitted using EESC and converted to %/decade using the EESC-time variation in the 1980s) as a function of latitude. As shown in WMO (2003) the 2-D models tend to reproduce the observed trends in the NH midlatitudes but show a wide variation in the SH. The 2-D models also produce a negative trend of 1-2%/decade in the tropics where the observations indicate a zero trend. The 3-D CTMs also fall in the range of observations in the NH and produce a negative trend in the tropics with the exception of the SLIMCAT run forced by analyzed winds. This run produces a zero trend in the tropics (see also Figure 3-21), which may indicate that the ECMWF analyzed winds succeed in isolating this region more efficiently (see Monge Sanz et al., 2006). In the SH, the CTMs are quite consistent with each other but again tend to overestimate the observed midlatitude trend.

Figure 3-23 shows the modeled and observed column ozone trends versus month for the NH and SH. The NH observations show a seasonality with the largest trend of around -4%/decade in March and a minimum

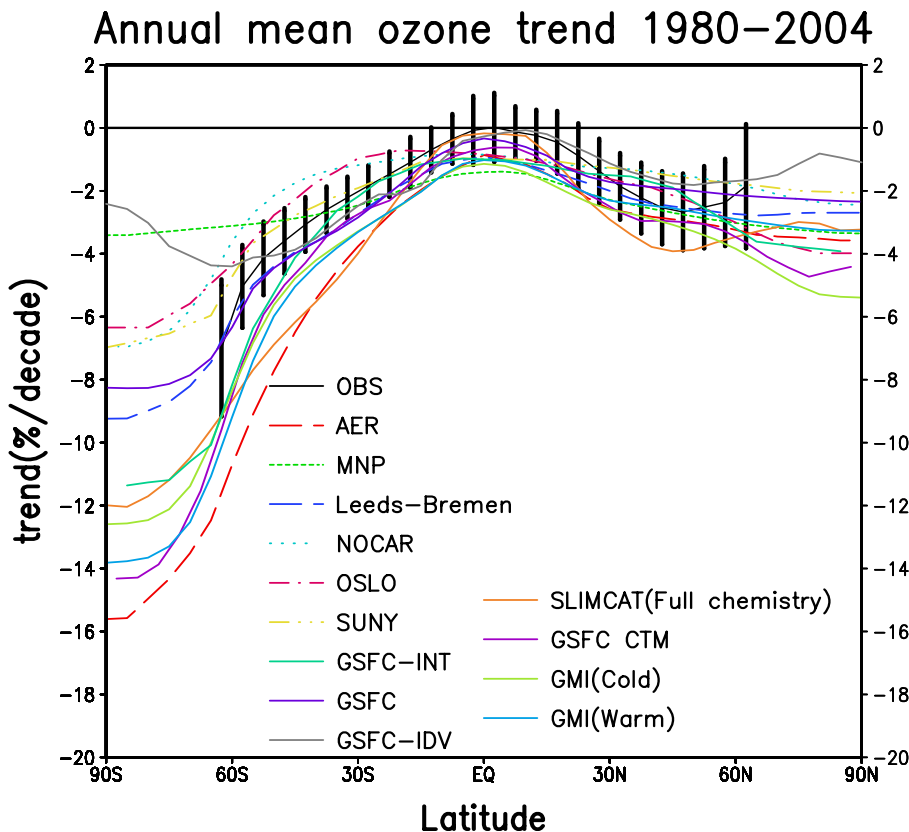


Figure 3-22. Latitudinal profile of annual mean column ozone trends from observations (black line) compared with results from 2-D models and 3-D CTMs for 1980-2004. The trends were estimated using regression to an EESC curve and converted to %/decade using the variation of EESC with time in the 1980s. Observations are from the merged satellite dataset; see Appendix 3A. The error bars for the observations indicate the 2σ uncertainties.

trend in late summer. The models generally capture the magnitude of this trend and its seasonal variation. There is a wide variation in the 2-D model results, which is similar to WMO (2003); this is expected, as these models will not have evolved substantially over this period. The CTMs capture the seasonal variations but tend to overestimate the trend in late spring. In contrast, the comparison in the SH is very poor. The observations show a trend of -4% decade with only a small seasonal variation. This lack of seasonal variation is produced by some 2-D models but there is a wide range in magnitude of trend, reflecting the extent of the models' SH polar loss. The 3-D CTMs, with their expected more realistic treatment of the SH polar loss and vortex dynamics, produce a trend which is larger than observed and shows a clear seasonal cycle. In these runs the formation of the Antarctic ozone hole in August-September seems to impact midlatitudes and increase the trend there. Given the better physical basis for the 3-D models, the apparently better agreement for the seasonality of the trend from some 2-D models should not be taken to mean that this modeling approach is better.

The trends in the vertical profile of O_3 from the models and observations are shown in Figure 3-24. The observations show a characteristic double peak with loss around 40 km due to the $ClO + O$ cycle and loss in the lower stratosphere due to halogen/aerosol chemistry and the impact of loss at higher latitudes. In the upper stratosphere the 3-D CTMs and model 2-D models produce trends similar to the observations, with a peak around 40-45 km. The Leeds-Bremen, NOCAR, and GSFC-INT 2-D models produce a trend that is about a factor of two less than observed. These three models, in contrast to the other 2-D models and CTMs, calculate interactive temperatures in the upper stratosphere. On this basis they might be expected to be more realistic than models that use fixed temperatures, although yearly varying analyses should also be realistic. However, this depends on the accuracy of the modeled temperature trends and any trends that causes in circulation. The interactive 2-D models produce a peak upper stratospheric cooling over the same time period of around 1-1.4 K/decade (not shown), which is in reasonable agreement with observations (Chapter 5) and clearly better than models that assume no trend. These interactive 2-D models also produce the largest CH_4 trend in the upper stratosphere, indicating a feedback in these models that increases the meridional circulation (not shown). Both of these factors act to reduce the magnitude of the ozone trend. Overall these comparisons shown that while we have a reasonable understanding of upper stratospheric ozone depletion, we still do not have full quantitative agreement between models and observations. Around 20 km in the NH lower stratosphere, the models again

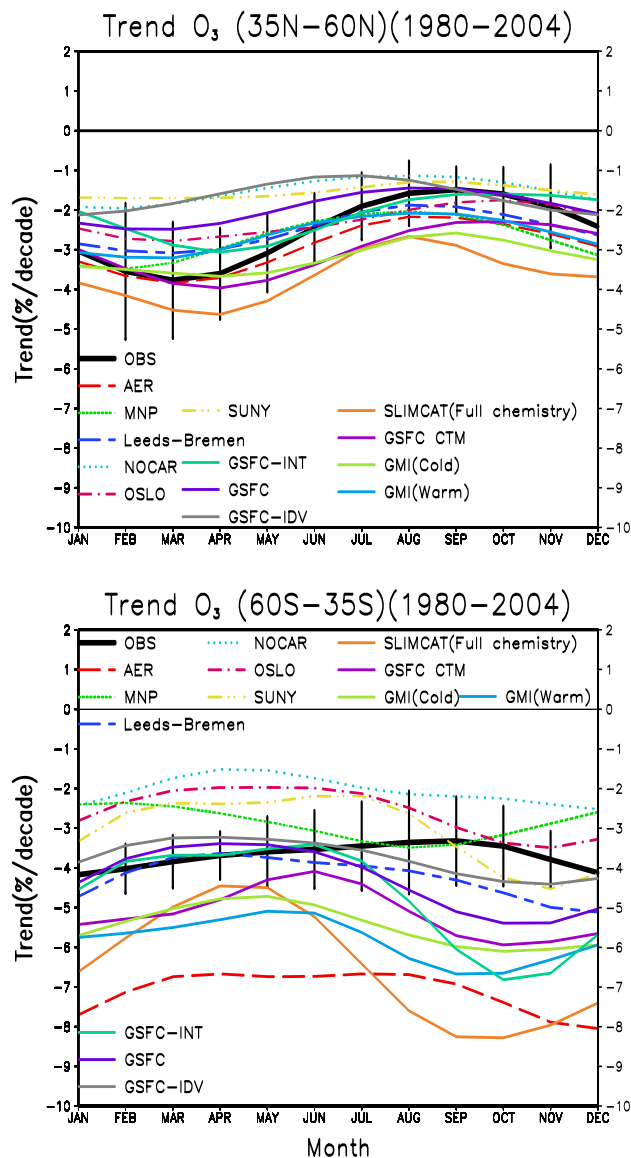


Figure 3-23. Seasonal variation of observed (black line) and modeled column ozone trends at (top) 35°N-60°N and (bottom) 35°S-60°S. The model results are from 2-D models and 3-D CTMs. The trends were estimated using regression to an EESC curve and converted to %/decade using the variation of EESC with time in the 1980s. Observed trends were estimated from the merged satellite dataset, with error bars denoting 2σ uncertainties.

overall produce a similar trend to that observed. There are no trend estimates from observations below 20 km in the SH but, consistent with the SH comparisons shown above, there is a large variation between the models. The CTMs give similar results while the 2-D models can give very small trends, or in the case of the AER model, a large trend between 10-15 km.

GLOBAL OZONE

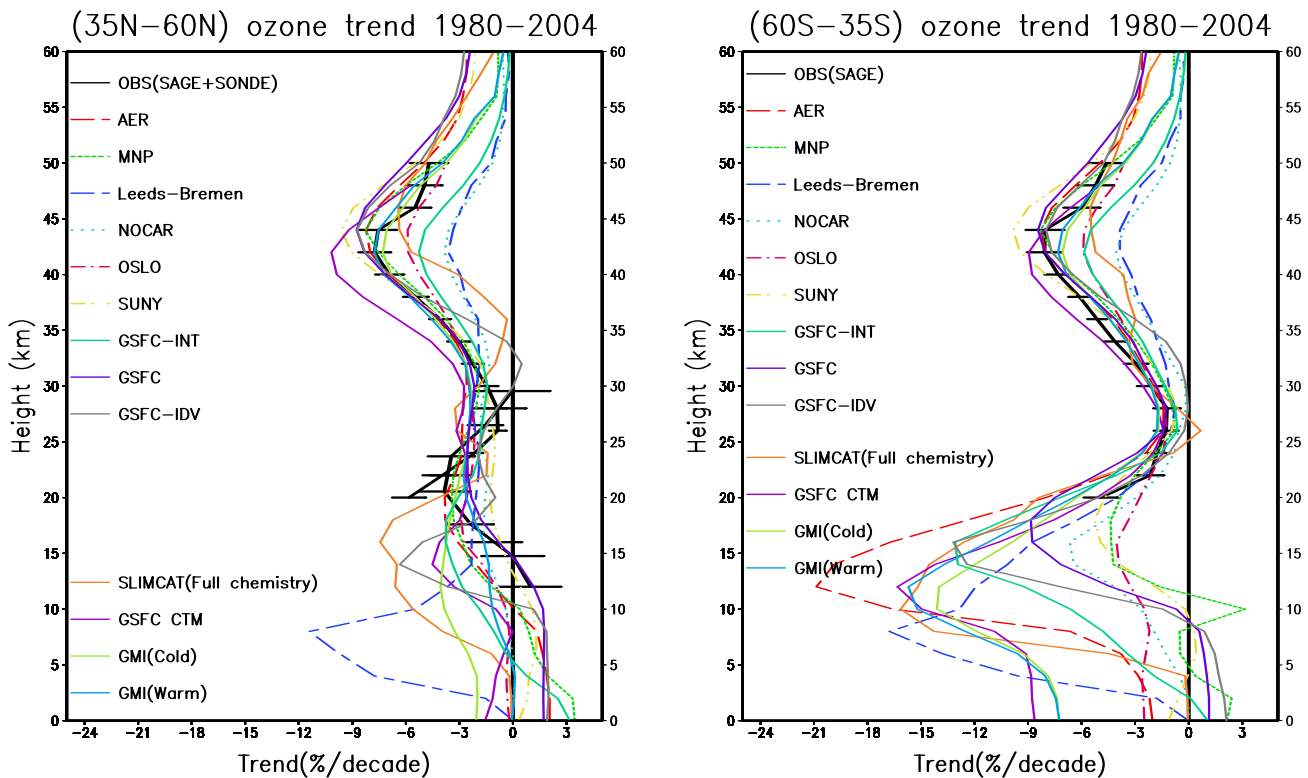


Figure 3-24. Vertical profiles of ozone trends over the period 1980-2004 from observations compared with 2-D models and 3-D CTMs for (left) 60°N-35°N and (right) 35°S-60°S. The trends were estimated using regression to an EESC curve and converted to %/decade using the variation of EESC with time in the 1980s. The observations are from SAGE I+II in the upper stratosphere and from ozonesondes in the lower stratosphere (NH only).

On the basis of these comparisons, it is evident that many broad features of the observed ozone trends are consistent with models that are forced with observed variations in halogens and aerosols. The models generally perform better in the Northern Hemisphere than in the south. Overall, the 3-D CTMs perform as least as well as the 2-D models, although there are fewer of them to compare. In particular, the behavior of the models in the SH is more similar, though they do show a significant discrepancy with the observed magnitude and seasonality of the trend.

We now use results from the SLIMCAT CTM runs to diagnose the roles of chemistry and dynamics in past ozone changes in more detail. As discussed in Section 3.4.2, CTMs forced by meteorological analyses have been used to estimate the role of dynamics on (NH) midlatitude ozone. Full chemistry CTMs can also be used to quantify the effect of different chemical forcings. For example, Chipperfield (2003) reported a similar SLIMCAT CTM integration to Hadjinicolaou et al. (2002) but including detailed chemistry for cases with and without the inclusion of halogen loading and time-dependent aerosol. For most months and latitudes, the run with halogen loading and aerosol data yielded a better agreement with observed

ozone time series. Moreover, the magnitude of the modeled halogen effect was similar to the observed long-term decrease. It was therefore concluded that the modeled ozone decrease at all latitudes up to the early 1990s, including northern midlatitudes, was dominantly caused by halogen-related trends in combination with heterogeneous chemistry on lower stratospheric polar stratospheric clouds (PSCs)/aerosols. The runs discussed above (Table 3-1) update these studies using ERA-40 winds (Hadjinicolaou et al., 2005; Feng et al., 2006). Feng et al. (2006) ran the CTM from 1977 until 2005, using ERA-40 winds until the end of 2001 followed by operational analyses. In addition to the basic model run with time-dependent source gases, they performed a run with fixed (1980 troposphere) halogen loadings and a run without a 6 pptv contribution of Br_y from very short-lived substances (VSLS). As shown in Figure 3-25, the comparison of the basic model runs with the TOMS/SBUV anomaly is similar to that shown in Hadjinicolaou et al. (2005) (Figure 3-21), where the model captures some observed variability but, through the use of ERA-40 winds, produces some features (variability) which are not observed. As discussed in Section 3.4.1, the use of meteorological analyses for

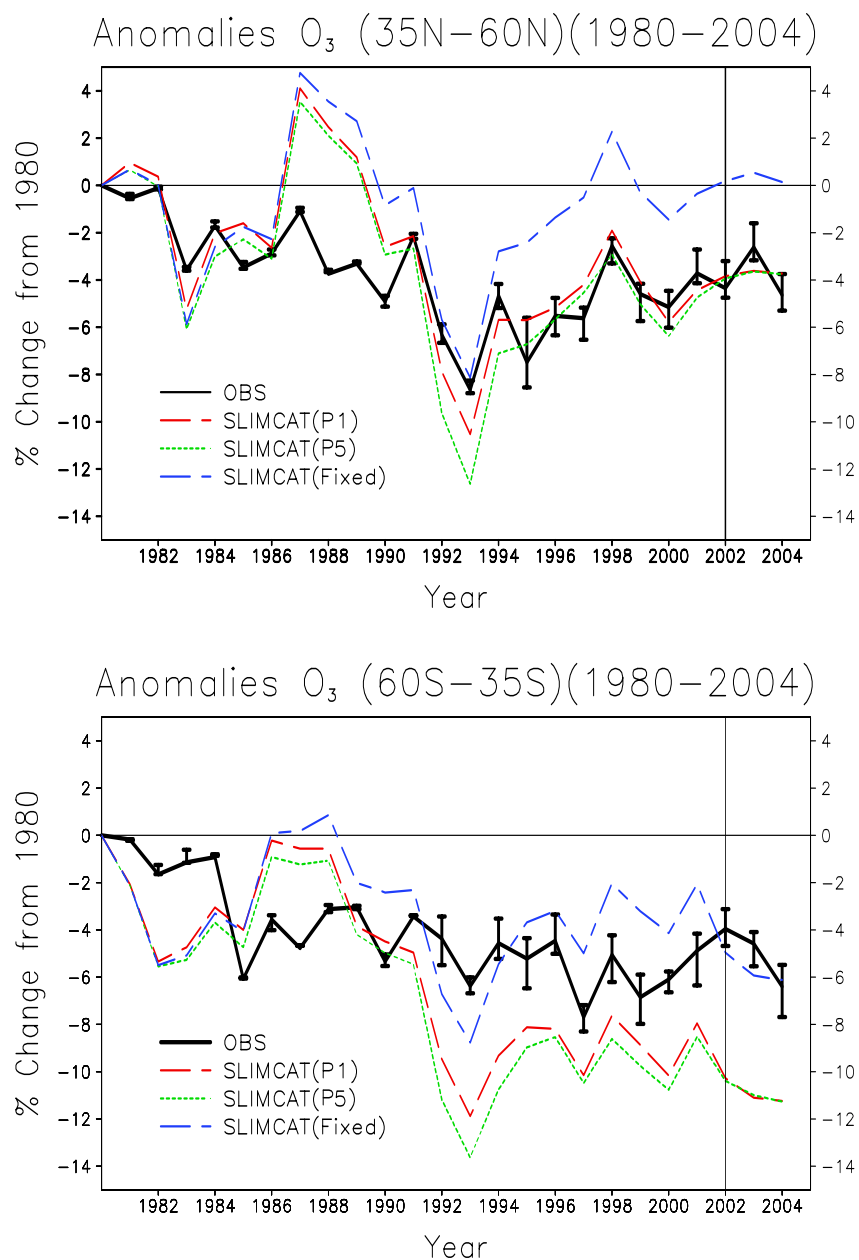
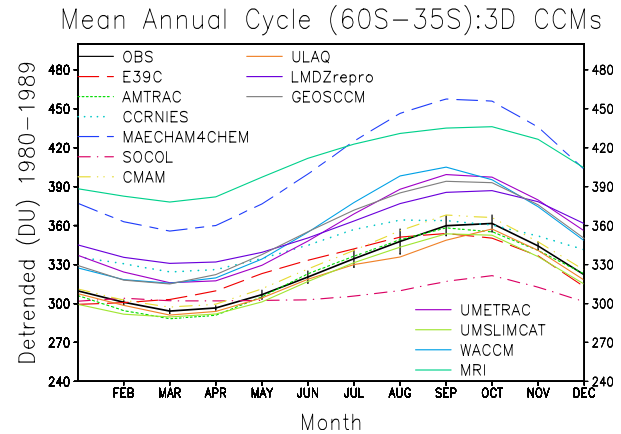
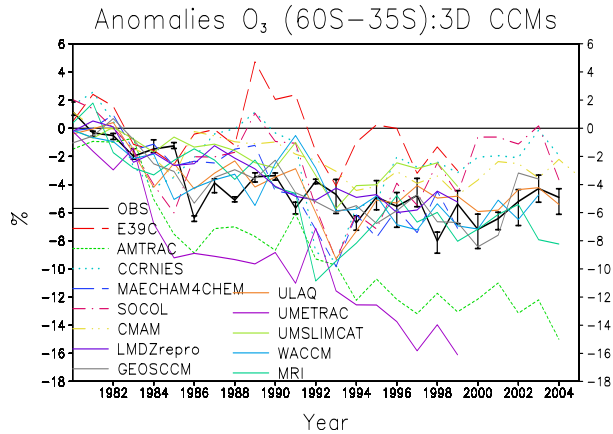
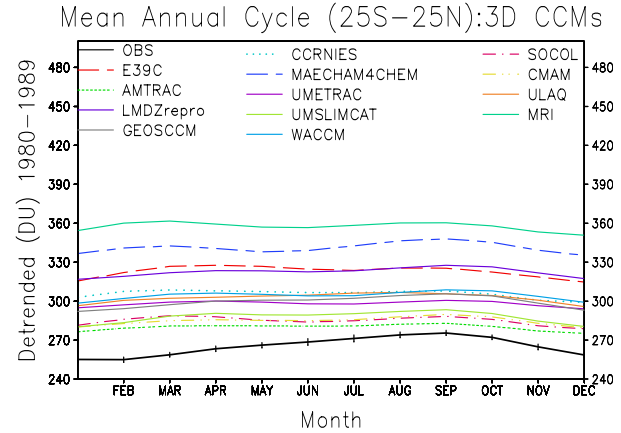
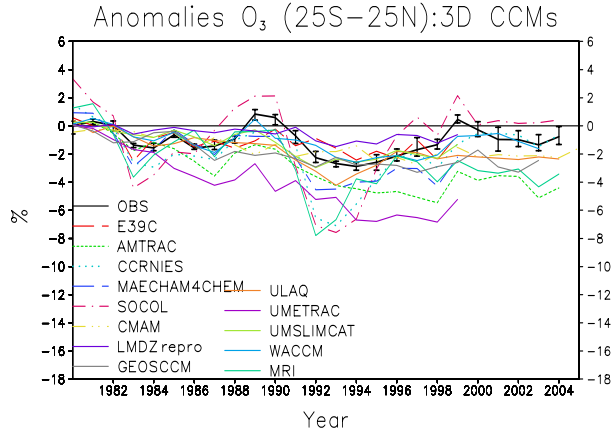
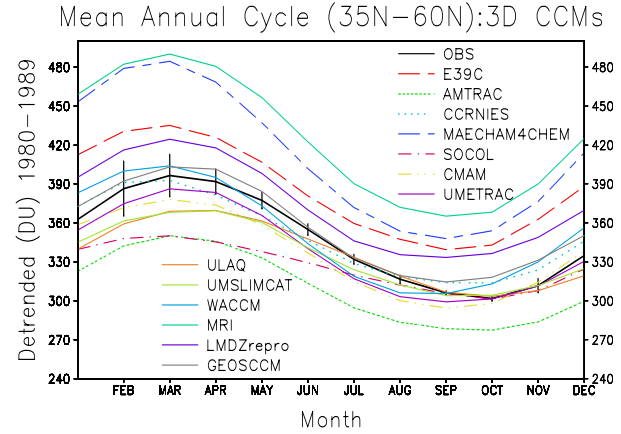
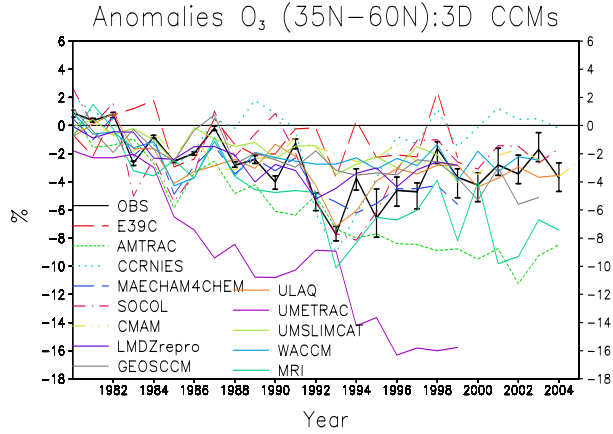
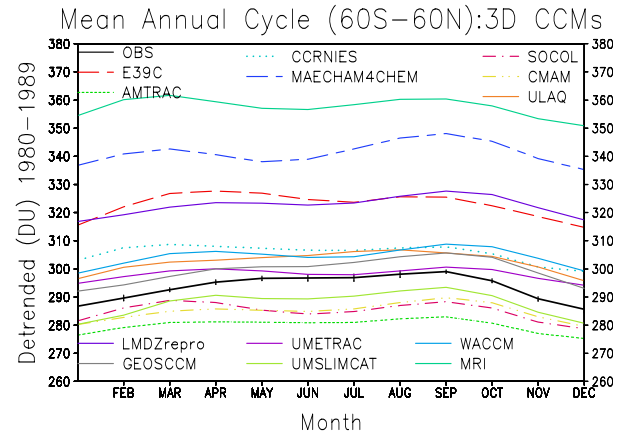
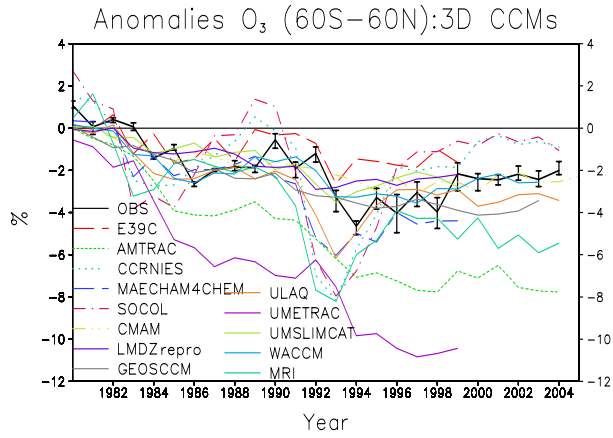


Figure 3-25. Time series of annual mean anomalies (with respect to 1980) for three simulations of the SLIMCAT 3-D CTM compared with observations (black line). The SLIMCAT simulations considered full time-dependent halogen chemistry (run P5, green dotted line), a simulation without 6 pptv Br_y from short-lived species (run P1, red dashed line), and a simulation with fixed (1980 tropospheric) halogen loadings (blue dashed line). The vertical line at the start of 2002 indicates where the CTM forcing changed from ECMWF ERA-40 analyses to ECMWF operational.

trend studies needs to be treated with caution. Assuming that the analyses are able to give a realistic circulation in the model, then the CTM can be used for chemical experiments, although these are not coupled (i.e., any indirect circulation effect of a chemical forcing will not be captured). Figure 3-25 shows that when the model is run with fixed halogen loadings, there is a difference of about 4–7% in the NH and SH anomalies, or 20–22 DU of the column, in the model ozone by 2000 relative to the run with time-varying halogens, confirming the important overall role of the halogen trends. The 3-D CTM results in Figure 3-25 also confirm the 2-D results of Salawitch et al. (2005) (see Section 3.4.3). An additional 6 pptv of Br_y

in the lower stratosphere decreases the model O_3 column by about 10 DU (Feng et al., 2006) but, when expressed as an anomaly relative to 1980 (a low aerosol period), an additional relative depletion is only noticeable around the time of the Mt. Pinatubo eruption. Finally, we can note that by about 2000, and before the model results are affected by the switch of analyses, the modeled contribution from halogens to midlatitude ozone loss is starting to decrease slightly, i.e., there is only a small contribution of halogen changes to recent changes in ozone. Using a photochemical box model, Yang et al. (2006) argued that the increase in ozone for altitudes below 18 km is most likely driven by changes in transport (see Section 3.4.2), rather

GLOBAL OZONE



than by declining chlorine and bromine, but the cessation of ozone depletion between 18-25 km altitude is consistent with a leveling off of stratospheric abundances of chlorine and bromine.

As discussed in Chapter 6, there are now many coupled Chemistry-Climate Models (CCMs) that have been developed to study past and future changes in the stratosphere. These models have chemistry schemes similar to those in 2-D models and CTMs, but they calculate their own interactive circulation, which will be much more variable than interactive 2-D models. The models are also computationally expensive and often can only run one scenario either as a single simulation or as a few-member ensemble. Hence, these models have not yet been applied to diagnosing past changes in midlatitude ozone; rather the models themselves are still at the validation stage. Andersen et al. (2006) presented results of three CCMs compared with the 2-D models used in WMO (2003); the CCM results varied significantly. More recently, Eyring et al. (2006) compared results from 13 CCMs that ran with the same external forcings. These were the REF1 simulations described in Chapter 6 of this Assessment. The CCMs produce a good simulation of the global temperature fields. Results of the stratospheric age of air and tropical tape recorder signal showed a large spread of results, although about half of the models were realistic; this shows an improvement compared with CCMs used in previous Assessments. Eyring et al. (2006) also discussed the performance of these models in reproducing polar ozone depletion. Overall the differences in modeled transport, and likely the treatment of lower stratospheric chemical processes at all latitudes, leads to a range in modeled global ozone trends over the past 20 years.

Figure 3-26 shows the results from 13 CCMs for the seasonal cycle in column ozone and its anomaly for various latitude bands (see Chapter 6 for model details), extending on the analysis of Eyring et al. (2006). At NH and SH midlatitudes the models all capture the expected seasonal cycle but the modeled column varies by up to 160 DU. The models also all tend to overestimate the tropical column ozone. In the tropics some CCMs capture the

Figure 3-26. Time series of mean annual anomalies, expressed as a % deviation from the detrended 1980-1989 mean annual cycle (left), and mean 1980-1989 detrended seasonal cycle (right) for latitude bands 60°N-60°S, 60°N-35°N, 25°N-25°S, and 35°S-60°S for the REF1 simulations of 13 coupled Chemistry-Climate Models (CCMs) described in Chapter 6 (Table 6-4 and Appendix 6A). Also shown are the merged satellite observations. (Note: observations in right panels are mean over years 1980-2004.)

observed small long-term change but many, as in the case of 2-D models and 3-D CTMs, produce a large long-term decrease. Note that only some of the CCM simulations include a treatment of the solar cycle (see Chapter 6). For the midlatitude anomalies, the models generally show a decreasing trend through to the 1990s, in response to the imposed halogen and aerosol variations, but again there is a wide range in the model predictions. However, as noted in Chapter 6, some of the outlying simulations should be ignored due to unrealistic levels of inorganic chlorine in the lower stratosphere. Still, given the expected dynamical variability in the models, it is not possible to draw robust conclusions from this range of model runs.

REFERENCES

- Ajtić, J., B.J. Connor, B.N. Lawrence, G.E. Bodeker, K.W. Hoppel, J.E. Rosenfield, and D.N. Heuff, Dilution of the Antarctic ozone hole into southern midlatitudes, 1998-2000, *J. Geophys. Res.*, *109*, D17107, doi: 10.1029/2003JD004500, 2004.
- Andersen, S.B., and B.M. Knudsen, The influence of vortex ozone depletion on Arctic ozone trends, *Geophys. Res. Lett.*, *29* (21), 2013, doi: 10.1029/2001GL014595, 2002.
- Andersen, S.B., E.C. Weatherhead, A. Stevermer, J. Austin, C. Brühl, E.L. Fleming, J. de Grandpré, V. Grewe, I. Isaksen, G. Pitari, R.W. Portmann, B. Rognerud, J.E. Rosenfield, S. Smyshlyaev, T. Nagashima, G.J.M. Velders, D.K. Weisenstein, and J. Xia, Comparison of recent modeled and observed trends in total column ozone, *J. Geophys. Res.*, *111*, D02303, doi: 10.1029/2005JD006091, 2006.
- Appenzeller, C., A.K. Weiss, and J. Staehelin, North Atlantic Oscillation modulates total ozone winter trends, *Geophys. Res. Lett.*, *27* (8), 1131-1134, 2000.
- Attmanspacher, W., and H.U. Dütsch, International ozone sonde; intercomparison at the observatory Hohenpeissenberg, 19 January - 5 February 1970, *Berichte des Deutschen Wetterdienstes, Nr. 120 (Bd. 16)*, 74p., 1970.
- Bengtsson, L., S. Hagemann, and K.I. Hodges, Can climate trends be calculated from reanalysis data?, *J. Geophys. Res.*, *109*, D11111, doi: 10.1029/2004JD004536, 2004.
- Berthet, G., N. Huret, F. Lefèvre, G. Moreau, C. Robert, M. Chartier, V. Catoire, B. Barret, I. Pissot, and L. Pomathiod, On the ability of chemical transport models to simulate the vertical structure of the N₂O, NO₂ and HNO₃ species in the mid-latitude stratosphere, *Atmos. Chem. Phys.*, *6*, 1599-1609, 2005.
- Bhartia, P.K., C.G. Wellemeyer, S.L. Taylor, N. Nath, and

GLOBAL OZONE

- A. Gopalan, Solar Backscatter Ultraviolet (SBUV) version 8 profile algorithm, in *Ozone Vol. I, Proceedings of the XX Quadrennial Ozone Symposium*, 1-8 June 2004, Kos, Greece, edited by C.S. Zerefos, 295-296, Int. Ozone Comm., Athens, Greece, 2004.
- Birner, T., D. Sankey, and T.G. Shepherd, The tropopause inversion layer in models and analyses, *Geophys. Res. Lett.*, *33*, L14804, doi: 10.1029/2006GL026549, 2006.
- Bloom, S., A. de Silva, D. Dee (Senior Authors), M. Bosilovich, J-D. Chern, S. Pawson, S. Schubert, M. Sienkiewicz, I. Stajner, W-W. Tan, and M-L. Wu, Documentation and Validation of the Goddard Earth Observing System (GEOS) Data Assimilation System – Version 4, NASA/TM-2005-104606, 26, 2005.
- Blumenstock, T., G. Kopp, F. Hase, G. Hochschild, S. Mikuteit, U. Raffalski, and R. Ruhnke, Observation of unusual chlorine activation by ground-based infrared and microwave spectroscopy in the late Arctic winter 2000/01, *Atmos. Chem. Phys.*, *6*, 897-905, 2006.
- Bodeker, G.E., J.C. Scott, K. Kreher, and R.L. McKenzie, Global ozone trends in potential vorticity coordinates using TOMS and GOME intercompared against the Dobson network: 1978-1998, *J. Geophys. Res.*, *106* (D19), 23029-23042, 2001.
- Bodeker, G.E., H. Shiona, and H. Struthers, The NIWA assimilated total column ozone data base and assimilated trace gas profile data base for validation of CCMs, paper presented at *CCMVal 2005 Workshop*, October 2005, Boulder, Colo. Available: http://www.pa.op.dlr.de/workshops/CCMVal2005/CCMVal2005_abstract.html, 2005.
- Bojkov, R.D., and V.E. Fioletov, Total ozone variations in the tropical belt: An application for quality of ground based measurements, *Meteorol. Atmos. Phys.*, *58* (1-4), 223-240, 1996.
- Bojkov, R.D., C.S. Zerefos, D.S. Balis, I.C. Ziomas, and A.F. Bais, Record low total ozone during northern winters of 1992 and 1993, *Geophys. Res. Lett.*, *20* (13), 1351-1354, 1993.
- Bojkov, R.D., E. Kosmidis, J.J. DeLuisi, I. Petropavlovskikh, V.E. Fioletov, S. Godin, and C. Zerefos, Vertical ozone distribution characteristics deduced from ~44,000 re-evaluated Umkehr profiles (1957-2000), *Meteorol. Atmos. Phys.*, *79* (3-4), 127-158, 2002.
- Borrmann, S., S. Solomon, L. Avallone, D. Toohey, and D. Baumgardner, On the occurrence of ClO in cirrus clouds and volcanic aerosol in the tropopause region, *Geophys. Res. Lett.*, *24* (16), 2011-2014, 1997.
- Bortz, S.E., M.J. Prather, J.-P. Cammas, V. Thouret, and H. Smit, Ozone, water vapor, and temperature in the upper tropical troposphere: Variations over a decade of MOZAIC measurements, *J. Geophys. Res.*, *111*, D05305, doi: 10.1029/2005JD006512, 2006.
- Braesicke, P., and J.A. Pyle, Changing ozone and changing circulation in northern mid-latitudes: Possible feedbacks?, *Geophys. Res. Lett.*, *30* (2), 1059, doi: 10.1029/2002GL015973, 2003.
- Brasseur, G., The response of the middle atmosphere to long-term and short-term solar variability: A two-dimensional model, *J. Geophys. Res.*, *98* (D12), 23079-23090, 1993.
- Bregman, B., P.-H. Wang, and J. Lelieveld, Chemical ozone loss in the tropopause region on subvisible ice clouds, calculated with a chemistry-transport model, *J. Geophys. Res.*, *107* (D3), 4032, doi: 10.1029/2001JD000761, 2002.
- Brinksma, E.J., Y.J. Meijer, B.J. Connor, G.L. Manney, J.B. Bergwerff, G.E. Bodeker, I.S. Boyd, J.B. Liley, W. Hogervorst, J.W. Hovenier, N.J. Livesey, and D.P.J. Swart, Analysis of record-low ozone values during the 1997 winter over Lauder, New Zealand, *Geophys. Res. Lett.*, *25* (15), 2785-2788, 1998.
- Brönnimann, S., and L.L. Hood, Frequency of low-ozone events over northwestern Europe in 1952-1963 and 1990-2000, *Geophys. Res. Lett.*, *30* (21), 2118, doi: 10.1029/2003GL018431, 2003.
- Brönnimann, S., J. Staehelin, S.F.G. Farmer, J.C. Cain, T. Svendby, and T. Svenøe, Total ozone observations prior to the IGY. I: A history, *Quart. J. Roy. Meteorol. Soc.*, *129* (593), 2797-2817, 2003a.
- Brönnimann, S., J.C. Cain, J. Staehelin, and S.F.G. Farmer, Total ozone observations prior to the IGY. II: Data and quality, *Quart. J. Roy. Meteorol. Soc.*, *129* (593), 2819-2843, 2003b.
- Brönnimann, S., J. Luterbacher, J. Staehelin, and T. Svendby, An extreme anomaly in stratospheric ozone over Europe in 1940-1942, *Geophys. Res. Lett.*, *31*, L08101, doi: 10.1029/2004GL019611, 2004a.
- Brönnimann, S., J. Luterbacher, J. Staehelin, T.M. Svendby, G. Hansen, and T. Svenøe, Extreme climate of the global troposphere and stratosphere in 1940-42 related to El Niño, *Nature*, *431* (7011), 971-974, 2004b.
- Brühl, C., P.J. Crutzen, and J.U. Groöb, High-latitude, summertime NO_x activation and seasonal ozone decline in the lower stratosphere: Model calculations based on observations by HALOE on UARS,

- J. Geophys. Res.*, 103 (D3), 3587-3597, 1998.
- Brunner, D., J. Staehelin, H.-R. Künsch, and G.E. Bodeker, A Kalman filter reconstruction of the vertical ozone distribution in an equivalent latitude – potential temperature framework from TOMS/GOME/SBUV total ozone observations, *J. Geophys. Res.*, 111, D12308, doi: 10.1029/2005JD006279, 2006.
- Burrows, J.P., M. Weber, M. Buchwitz, V. Rozanov, A. Ladstaeetter-Weissenmayer, A. Richter, R. de Beek, R. Hoogen, K. Bramstedt, K.U. Eichmann, and M. Eisinger, The Global Ozone Monitoring Experiment (GOME): mission concept and first scientific results, *J. Atmos. Sci.*, 56 (2), 151-175, 1999.
- Butkovskaya, N.I., A. Kukui, N. Pouvesle, and G. Le Bras, Formation of nitric acid in the gas-phase HO₂ + NO reaction: effects of temperature and water vapor, *J. Phys. Chem. A*, 109 (29), 6509-6520, 2005.
- Calisesi, Y., R. Stübi, N. Kämpfer, and P. Viatte, Investigation of systematic uncertainties in Brewer-Mast ozone soundings using observations from a ground-based microwave radiometer, *J. Atmos. Oceanic Technol.*, 20 (11), 1543-1551, 2003.
- Callis, L.B., M. Natarajan, and J.D. Lambeth, Calculated upper stratospheric effects of solar UV flux and NO_y variations during the 11-year solar cycle, *Geophys. Res. Lett.*, 27 (23), 3869-3872, 2000.
- Callis, L.B., M. Natarajan, and J.D. Lambeth, Solar-atmospheric coupling by electrons (SOLACE): 3. Comparisons of simulations and observations, 1979-1997, issues and implications, *J. Geophys. Res.*, 106 (D7), 7523-7539, 2001.
- Chandra, S., and R.D. McPeters, The solar cycle variation of ozone in the stratosphere inferred from Nimbus-7 and NOAA-11 satellites, *J. Geophys. Res.*, 99 (D10), 20665-20671, 1994.
- Chen, L., J. London, and G. Brasseur, Middle atmospheric ozone and temperature responses to solar irradiance variations over 27-day periods, *J. Geophys. Res.*, 102 (D25), 29957-29980, 1997.
- Chipperfield, M.P., Multiannual simulations with a three-dimensional chemical transport model, *J. Geophys. Res.*, 104 (D1), 1781-1805, 1999.
- Chipperfield, M.P., A three-dimensional model study of long-term mid-high latitude lower stratosphere ozone changes, *Atmos. Chem. Phys.*, 3, 1253-1265, 2003.
- Chipperfield, M.P., New version of the TOMCAT/SLIMCAT off-line chemical transport model: Intercomparison of stratospheric tracer experiments, *Quart. J. Roy. Meteorol. Soc.*, 132 (617), 1179-1203, 2006.
- Clancy, R.T., and D.O. Muhleman, Ground-based microwave spectroscopy of the Earth's stratosphere and mesosphere, Chapter 7 in *Atmospheric Remote Sensing by Microwave Radiometry*, edited by M.A. Janssen, 335-381, John Wiley & Sons, Inc., New York, 1993.
- Coldewey-Egbers, M., M. Weber, L.N. Lamsal, R. de Beek, M. Buchwitz, and J.P. Burrows, Total ozone retrieval from GOME UV spectral data using the weighting function DOAS approach, *Atmos. Chem. Phys.*, 5, 1015-1025, 2005.
- Connor, B.J., G.E. Bodeker, R.L. McKenzie, and I.S. Boyd, The total ozone anomaly at Lauder, NZ in 1997, *Geophys. Res. Lett.*, 26 (2), 189-192, 1999.
- Considine, D.B., A.R. Douglass, P.S. Connell, D.E. Kinnison, and D.A. Rotman, A polar stratospheric cloud parameterization for the global modeling initiative three-dimensional model and its response to stratospheric aircraft, *J. Geophys. Res.*, 105 (D3), 3955-3974, 2000.
- Cordero, E.C., and T.R. Nathan, An examination of anomalously low column ozone in the Southern Hemisphere midlatitudes during 1997, *Geophys. Res. Lett.*, 29 (7), 1123, doi: 10.1029/2001GL013948, 2002.
- Cox, R.A., M.A. Fernandez, A. Symington, M. Ullerstam, and J.P.D. Abbatt, A kinetic model for uptake of HNO₃ and HCl on ice in a coated wall flow system, *Phys. Chem. Chem. Phys.*, 7 (19), 3434-3442, 2005.
- Cunnold, D.M., J.M. Zawodny, W.P. Chu, J.P. Pommereau, F. Goutail, J. Lenoble, M.P. McCormick, R.E. Veiga, D. Murcray, N. Iwagami, K. Shibasaki, P.C. Simon, and W. Peetermans, Validation of SAGE II NO₂ measurements, *J. Geophys. Res.*, 96 (D7), 12913-12925, 1991.
- Cunnold, D.M., E.-S. Yang, M.J. Newchurch, G.C. Reinsel, J.M. Zawodny, and J.M. Russell III, Comment on "Enhanced upper stratospheric ozone: Sign of recovery or solar cycle effect?" by W. Steinbrecht et al., *J. Geophys. Res.*, 109, D14305, doi: 10.1029/2004JD004826, 2004.
- Daniel, J.S., S. Solomon, and D.L. Albritton, On the evaluation of halocarbon radiative forcing and global warming potentials, *J. Geophys. Res.*, 100 (D1), 1271-1285, 1995.
- Delval, C., and M.J. Rossi, Influence of monolayer amounts of HNO₃ on the evaporation rate of H₂O over ice in the range 179 to 208 K: A quartz crystal microbalance study, *J. Phys. Chem. A*, 109 (32), 7151-7165, 2005.
- Deshler, T., R. Anderson-Sprecher, H. Jäger, J. Barnes, D.J. Hofmann, B. Clemesha, D. Simonich, M. Osborn, R.G. Grainger, and S. Godin-Beekmann,

GLOBAL OZONE

- Trends in the nonvolcanic component of stratospheric aerosol over the period 1971-2004, *J. Geophys. Res.*, *111*, D01201, doi: 10.1029/2005JD006089, 2006.
- Dhomse, S., M. Weber, I. Wohltmann, M. Rex, and J.P. Burrows, On the possible causes of recent increases in NH total ozone from a statistical analysis of satellite data from 1979 to 2003, *Atmos. Chem. Phys.*, *6*, 1165-1180, 2006.
- Dillon, T.J., D. Hölscher, V. Sivakumaran, A. Horowitz, and J.N. Crowley, Kinetics of the reactions of HO with methanol (210-351 K) and with ethanol (216-368 K), *Phys. Chem. Chem. Phys.*, *7* (2), 349-355, 2005.
- Donovan, D.P., H. Fast, Y. Makino, J.C. Bird, A.I. Carswell, J. Davies, T.J. Duck, J.W. Kaminski, C.T. McElroy, R.L. Mittermeier, S.R. Pal, V. Savastiouk, D. Velkov, and J.A. Whiteway, Ozone, column ClO, and PSC measurements made at the NDSC Eureka observatory (80°N, 86°W) during the spring of 1997, *Geophys. Res. Lett.*, *24* (22), 2709-2712, 1997.
- Douglass, A.R., R.S. Stolarski, S.E. Strahan, and P.S. Connell, Radicals and reservoirs in the GMI chemistry and transport model: Comparison to measurements, *J. Geophys. Res.*, *109*, D16302, doi: 10.1029/2004JD004632, 2004.
- Durry, G., and A. Hauchecorne, Evidence for long-lived polar vortex air in the mid-latitude summer stratosphere from in situ laser diode CH₄ and H₂O measurements, *Atmos. Chem. Phys.*, *5*, 1467-1472, 2005.
- Dütsch, H.U., and J. Staehelin, Results of the new and old Umkehr algorithm compared with ozone soundings, *J. Atmos. Terr. Phys.*, *54* (5), 557-569, 1992.
- Egorova, T., E. Rozanov, E. Manzini, M. Haberer, W. Schmutz, V. Zubov, and T. Peter, Chemical and dynamical response to the 11-year variability of the solar irradiance simulated with a chemistry-climate model, *Geophys. Res. Lett.*, *31*, L06119, doi: 10.1029/2003GL019294, 2004.
- Eskes, H.J., R.J. van der A, E.J. Brinksma, J.P. Veefkind, J.F. de Haan, and P.J.M. Valks, Retrieval and validation of ozone columns derived from measurements of SCIAMACHY on Envisat, *Atmos. Chem. Phys. Discuss.*, *5* (4), 4429-4475, 2005.
- Evans, J.T., M.P. Chipperfield, H. Oelhaf, M. Stowasser, and G. Wetzell, Effect of near-IR photolysis of HO₂NO₂ on stratospheric chemistry, *Geophys. Res. Lett.*, *30* (5), 1223, doi: 10.1029/2002GL016470, 2003.
- Eyring, V., N. Butchart, D.W. Waugh, H. Akiyoshi, J. Austin, S. Bekki, G.E. Bodeker, B.A. Boville, C. Brühl, M.P. Chipperfield, E. Cordero, M. Dameris, M. Deushi, V.E. Fioletov, S.M. Frith, R.R. Garcia, A. Gettelman, M.A. Giorgetta, V. Grewe, L. Jourdain, D.E. Kinnison, E. Mancini, E. Manzini, M. Marchand, D.R. Marsh, T. Nagashima, P.A. Newman, J.E. Nielsen, S. Pawson, G. Pitari, D.A. Plummer, E. Rozanov, M. Schraner, T.G. Shepherd, K. Shibata, R.S. Stolarski, H. Struthers, W. Tian, and M. Yoshiki, Assessment of temperature, trace species, and ozone in chemistry-climate model simulations of the recent past, *J. Geophys. Res.*, *111*, D22308, doi: 10.1029/2006JD007327, 2006.
- Feng, W., M.P. Chipperfield, M. Dorf, and K. Pfeilsticker, Mid-latitude ozone changes: Studies with a 3-D CTM forced by ERA-40 analyses, *Atmos. Chem. Phys. Discuss.*, *6*, 6695-6722, 2006.
- Fernandez, M.A., R.G. Hynes, and R.A. Cox, Kinetics of ClONO₂ reactive uptake on ice surfaces at temperatures of the upper troposphere, *J. Phys. Chem. A*, *109* (44), 9986-9996, 2005.
- Fioletov, V.E., and T.G. Shepherd, Seasonal persistence of midlatitude total ozone anomalies, *Geophys. Res. Lett.*, *30* (7), 1417-1420, 2003.
- Fioletov, V.E., and T.G. Shepherd, Summertime total ozone variations over middle and polar latitudes, *Geophys. Res. Lett.*, *32*, L04807, doi: 10.1029/2004GL022080, 2005.
- Fioletov, V.E., G.E. Bodeker, A.J. Miller, R.D. McPeters, and R. Stolarski, Global and zonal total ozone variations estimated from ground-based and satellite measurements: 1964-2000, *J. Geophys. Res.*, *107* (D22), 4647, doi: 10.1029/2001JD001350, 2002.
- Fioletov, V.E., J.B. Kerr, C.T. McElroy, D.I. Wardle, V. Savastiouk, and T.S. Grajnar, The Brewer reference triad, *Geophys. Res. Lett.*, *32*, L20805, doi: 10.1029/2005GL024244, 2005.
- Fioletov, V.E., D.W. Tarasick, and I. Petropavlovskikh, Estimating ozone variability and instrument uncertainties from SBUV(2), ozonesonde, Umkehr, and SAGE II measurements: Short-term variations, *J. Geophys. Res.*, *111*, D02305, doi: 10.1029/2005JD006340, 2006.
- Frith, S., R. Stolarski, and P.K. Bhartia, Implications of Version 8 TOMS and SBUV data for long-term trend analysis, in *Ozone Vol. I, Proceedings of the XX Quadrennial Ozone Symposium*, 1-8 June 2004, Kos, Greece, edited by C.S. Zerefos, 65-66, Int. Ozone Comm., Athens, Greece, 2004.
- Fromm, M.D., and R. Servranckx, Transport of forest fire smoke above the tropopause by supercell convection, *Geophys. Res. Lett.*, *30* (10), 1542, doi: 10.1029/2002GL016820, 2003.
- Fromm, M., R. Bevilacqua, R. Servranckx, J. Rosen, J.P.

- Thayer, J. Herman, and D. Larko, Pyrocumulonimbus injection of smoke to the stratosphere: Observations and impact of a super blowup in northwestern Canada on 3-4 August 1998, *J. Geophys. Res.*, *110*, D08205, doi: 10.1029/2004JD005350, 2005.
- Fusco, A.C., and M.L. Salby, Interannual variations of total ozone and their relationship to variations of planetary wave activity, *J. Clim.*, *12* (6), 1619-1629, 1999.
- Gao, R.S., P.J. Popp, D.W. Fahey, T.P. Marcy, R.L. Herman, E.M. Weinstock, D.G. Baumgardner, T.J. Garrett, K.H. Rosenlof, T.L. Thompson, P.T. Bui, B.A. Ridley, S.C. Wofsy, O.B. Toon, M.A. Tolbert, B. Karcher, T. Peter, P.K. Hudson, A.J. Weinheimer, and A.J. Heymsfield, Evidence that nitric acid increases relative humidity in low-temperature cirrus clouds, *Science*, *303* (5657), 516-520, 2004.
- Gerding, M., G. Baumgarten, U. Blum, J.P. Thayer, K.-H. Fricke, R. Neuber, and J. Fiedler, Observations of an unusual mid-stratospheric aerosol layer in the Arctic: possible sources and implications for polar vortex dynamics, *Ann. Geophys.*, *21* (4), 1057-1069, 2003.
- Gleason, J.F., P.K. Bhartia, J.R. Herman, R. McPeters, P. Newman, R.S. Stolarski, L. Flynn, G. Labow, D. Larko, C. Seftor, C. Wellemeyer, W.D. Komhyr, A.J. Miller, and W. Planet, Record low global ozone in 1992, *Science*, *260* (5107), 523-526, 1993.
- Godin, S., V. Bergeret, S. Bekki, C. David, and G. Mégie, Study of the interannual ozone loss and the permeability of the Antarctic polar vortex from aerosol and ozone lidar measurements in Dumont d'Urville (66.4°S, 140°E), *J. Geophys. Res.*, *106* (D1), 1311-1330, 2001.
- Godin, S., M. Marchand, A. Hauchecorne, and F. Lefèvre, Influence of Arctic polar ozone depletion on lower stratospheric ozone amounts at Haute-Provence Observatory (43.92°N, 5.71°E), *J. Geophys. Res.*, *107* (D20), 8272, doi: 10.1029/2001JD000516, 2002.
- Graf, H.-F., I. Kirchner, and J. Perlwitz, Changing lower stratospheric circulation: The role of ozone and greenhouse gases, *J. Geophys. Res.*, *103* (D10), 11251-11261, 1998.
- Griffin, R.E.M., V. Fioletov, and J.C. McConnell, Measurements of historical total ozone from the Chalonge-Divan stellar spectrum program: A reanalysis of the 1953-1972 data and a comparison with simultaneous Dobson Arosa measurements, *J. Geophys. Res.*, *111*, D12309, doi: 10.1029/2005JD006476, 2006.
- Guillas, S., M.L. Stein, D.J. Wuebbles, and J. Xia, Using chemistry transport modeling in statistical analysis of stratospheric ozone trends from observations, *J. Geophys. Res.*, *109*, D22303, doi: 10.1029/2004JD005049, 2004.
- Guirlet, M., P. Keckhut, S. Godin, and G. Mégie, Description of the long-term ozone data series obtained from different instrumental techniques at a single location: the Observatoire de Haute-Provence (43.9°N, 5.7°E), *Ann. Geophys.*, *18* (10), 1325-1339, 2000.
- Hadjinicolaou, P., and J.A. Pyle, The impact of Arctic ozone depletion on northern middle latitudes: interannual variability and dynamical control, *J. Atmos. Chem.*, *47* (1), 25-43, 2004.
- Hadjinicolaou, P., J.A. Pyle, M.P. Chipperfield, and J.A. Kettleborough, Effect of interannual meteorological variability on mid-latitude O₃, *Geophys. Res. Lett.*, *24* (23), 2993-2996, 1997.
- Hadjinicolaou, P., A. Jrrar, J.A. Pyle, and L. Bishop, The dynamically driven long-term trend in stratospheric ozone over northern middle latitudes, *Quart. J. Roy. Meteorol. Soc.*, *128* (583), 1393-1412, 2002.
- Hadjinicolaou, P., J.A. Pyle, and N.R.P. Harris, The recent turnaround in stratospheric ozone over northern middle latitudes: A dynamical modeling perspective, *Geophys. Res. Lett.*, *32*, L12821, doi: 10.1029/2005GL022476, 2005.
- Haigh, J.D., The role of stratospheric ozone in modulating the solar radiative forcing of climate, *Nature*, *370* (6490), 544-546, 1994.
- Hamilton, K., On the quasi-decadal modulation of the stratospheric QBO period, *J. Clim.*, *15* (17), 2562-2565, 2002.
- Hansen, G., and T. Svenøe, Multilinear regression analysis of the 65-year Tromsø total ozone series, *J. Geophys. Res.*, *110*, D10103, doi: 10.1029/2004JD005387, 2005.
- Harris, J.M., S.T. Oltmans, G.E. Bodeker, R. Stolarski, R.D. Evans, and D.M. Quincy, Long-term variations in total ozone derived from Dobson and satellite data, *Atmos. Environ.*, *37* (23), 3167-3175, 2003.
- Hartogh, P., C. Jarchow, G.R. Sonnemann, and M. Grygalashvyly, On the spatiotemporal behavior of ozone within the upper mesosphere/mesopause region under nearly polar night conditions, *J. Geophys. Res.*, *109*, D18303, doi: 10.1029/2004JD004576, 2004.
- Hofmann, D.J., S.J. Oltmans, W.D. Komhyr, J.M. Harris, J.A. Lathrop, A.O. Langford, T. Deshler, B.J. Johnson, A. Torres, and W.A. Matthews, Ozone loss in the lower stratosphere over the United States in

GLOBAL OZONE

- 1992-1993: Evidence for heterogeneous chemistry on the Pinatubo aerosol, *Geophys. Res. Lett.*, 21 (1), 65-68, 1994.
- Hollandsworth, S.M., R.D. McPeters, L.E. Flynn, W. Planet, A.J. Miller, and S. Chandra, Ozone trends deduced from combined Nimbus-7 SBUV and NOAA-11 SBUV/2 data, *Geophys. Res. Lett.*, 22 (8), 905-908, 1995.
- Hood, L.L., The solar cycle variation of total ozone: Dynamical forcing in the lower stratosphere, *J. Geophys. Res.*, 102 (D1), 1355-1370, 1997.
- Hood, L.L., Effects of solar UV variability on the stratosphere, in *Solar Variability and its Effect on the Earth's Atmospheric and Climate System*, edited by J. Pap, P. Fox, C. Frohlich, H. Hudson, J. Kuhn, J. McCormack, G. North, W. Sprigg, and S.T. Wu, 283-304, American Geophysical Union, Washington, D.C., 2004.
- Hood, L.L., and B.E. Soukharev, Interannual variations of total ozone at northern midlatitudes correlated with stratospheric EP flux and potential vorticity, *J. Atmos. Sci.*, 62 (10), 3724-3740, 2005.
- Hood, L.L., and B.E. Soukharev, Solar induced variations of odd nitrogen: Multiple regression analysis of UARS HALOE data, *Geophys. Res. Lett.*, 33, L22805, doi: 10.1029/2006GL028122, 2006.
- Hood, L.L., R.D. McPeters, J.P. McCormack, L.E. Flynn, S.M. Hollandsworth, and J.F. Gleason, Altitude dependence of stratospheric ozone trends based on Nimbus-7 SBUV data, *Geophys. Res. Lett.*, 20 (23), 2667-2670, 1993.
- Hood, L.L., J.P. McCormack, and K. Labitzke, An investigation of dynamical contributions to midlatitude ozone trends in winter, *J. Geophys. Res.*, 102 (D11), 13079-13093, 1997.
- Hood, L.L., S. Rossi, and M. Beulen, Trends in lower stratospheric zonal winds, Rossby wave breaking behavior, and column ozone at northern midlatitudes, *J. Geophys. Res.*, 104 (D20), 24321-24339, 1999.
- Hood, L.L., B.E. Soukharev, M. Fromm, and J. McCormack, Origin of extreme ozone minima at middle to high northern latitudes, *J. Geophys. Res.*, 106 (D18), 20925-20940, 2001.
- Hurrell, J.W., Decadal trends in the North Atlantic Oscillation regional temperatures and precipitation, *Science*, 269 (5224), 676-679, 1995.
- Hynes, R.G., M.A. Fernandez, and R.A. Cox, Uptake of HNO₃ on water-ice and coadsorption of HNO₃ and HCl in the temperature range 210-235 K, *J. Geophys. Res.*, 107 (D24), 4797, doi: 10.1029/2001JD001557, 2002.
- Jonson, J.E., D. Simpson, H. Fagerli, and S. Solberg, Can we explain the trends in European ozone levels?, *Atmos. Chem. Phys.*, 6, 51-66, 2006.
- Jost, H.-J., K. Drdla, A. Stohl, L. Pfister, M. Loewenstein, J.P. Lopez, P.K. Hudson, D.M. Murphy, D.J. Cziczo, M. Fromm, T.P. Bui, J. Dean-Day, C. Gerbig, M.J. Mahoney, E.C. Richard, N. Spichtinger, J.V. Pittman, E.M. Weinstock, J.C. Wilson, and I. Xueref, In-situ observations of mid-latitude forest fire plumes deep in the stratosphere, *Geophys. Res. Lett.*, 31, L11101, doi: 10.1029/2003GL019253, 2004.
- Kanamitsu, M., W. Ebisuzaki, J. Woollen, S.K. Yang, J.J. Hnilo, M. Fiorino, and G.L. Potter, NCEP-DOE AMIP-II reanalysis (R-2), *Bull. Amer. Meteorol. Soc.*, 83 (11), 1631-1643, 2002.
- Keckhut, P., A. Hauchecorne, S. Bekki, A. Colette, C. David, and J. Jumelet, Indications of thin cirrus clouds in the stratosphere at mid-latitudes, *Atmos. Chem. Phys.*, 5, 3407-3414, 2005a.
- Keckhut, P., I. McDermid, D. Swart, T. McGee, S. Godin-Beekmann, A. Adriani, J. Barnes, J.L. Baray, H. Bencherif, H. Claude, A.G. di Sarra, G. Fiocco, G. Hansen, A. Hauchecorne, T. Leblanc, C.H. Lee, S. Pal, G. Mégie, H. Nakane, R. Neuber, W. Steinbrecht, and J. Thayer, Review of ozone and temperature lidar validations performed within the framework of the Network for the Detection of Stratospheric Change, *J. Environ. Monit.*, 6 (9), 721-733, 2005b.
- Keim, E.R., D.W. Fahey, L.A. DelNegro, E.L. Woodbridge, R.S. Gao, P.O. Wennberg, R.C. Cohen, R.M. Stimpfle, K.K. Kelly, E.J. Hints, J.C. Wilson, H.H. Jonsson, J.E. Dye, D. Baumgardner, S.R. Kawa, R.J. Salawitch, M.H. Proffitt, M. Loewenstein, J.R. Podolske, and K.R. Chan, Observations of large reductions in the NO/NO_y ratio near the mid-latitude tropopause and the role of heterogeneous chemistry, *Geophys. Res. Lett.*, 23 (22), 3223-3226, 1996.
- Kerr, J.B., C.T. McElroy, and R.A. Olafson, Measurements of ozone with the Brewer spectrophotometer, in *Proceedings of the Quadrennial International Ozone Symposium*, 4-9 August 1980, Boulder, Colo., edited by J. London, 74-79, National Center for Atmospheric Research, 1981.
- Kerr, J.B., D.I. Wardle, and D.W. Tarasick, Record low ozone values over Canada in early 1993, *Geophys. Res. Lett.*, 20 (18), 1979-1982, 1993.
- Klein, U., K. Lindner, S. Bagdohn, I. Wohltmann, and K.F. Kuenzi, Microwave measurements of arctic chlorine monoxide and computed chemical ozone loss in

- spring 2000, *Adv. Space Res.*, 29, 1719-1723, 2002.
- Knudsen, B.M., and S.B. Andersen, Geophysics: Longitudinal variation in springtime ozone trends, *Nature*, 413 (6857), 699-700, 2001.
- Knudsen, B.M., and J.-U. Grooß, Northern midlatitude stratospheric ozone dilution in spring modeled with simulated mixing, *J. Geophys. Res.*, 105 (D5), 6885-6890, doi: 10.1029/1999JD901076, 2000.
- Koch, G., H. Wernli, C. Schwierz, J. Staehelin, and T. Peter, A composite study on the structure and formation of ozone miniholes and minihighs over central Europe, *Geophys. Res. Lett.*, 32, L12810, doi: 10.1029/2004GL022062, 2005.
- Konopka, P., J.U. Grooß, S. Bausch, R. Müller, D.S. McKenna, O. Morgenstern, and Y. Orsolini, Dynamics and chemistry of vortex remnants in late Arctic spring 1997 and 2000: Simulations with the Chemical Lagrangian Model of Stratosphere (CLaMS), *Atmos. Chem. Phys.*, 3 (3), 839-849, 2003.
- Krizan, P., and J. Lastovicka, Trends in positive and negative ozone laminae in the Northern Hemisphere, *J. Geophys. Res.*, 110, D10107, doi: 10.1029/2004JD005477, 2005.
- Krzyżcin, J.W., Change in ozone depletion rates beginning in the mid 1990s: Trend analyses of the TOMS/SBUV merged total ozone data, 1978-2003, *Ann. Geophys.*, 24 (2), 493-502, 2006.
- Krzyżcin, J.W., J. Jaroslawski, and B. Rajewska-Wiech, Beginning of the ozone recovery over Europe? Analysis of the total ozone data from the ground-based observations, 1964-2004, *Ann. Geophys.*, 23 (5), 1685-1695, 2005.
- Laat, J. de, J. Landgraf, O. Hasekamp, I. Aben, and B. Bregman, Assimilated winds for global modelling: Evaluation with space- and balloon-borne ozone observations, *J. Geophys. Res.*, in press, 2006.
- Langematz, U., M. Kunze, K. Krüger, K. Labitzke, and G.L. Roff, Thermal and dynamical changes of the stratosphere since 1979 and their link to ozone and CO₂ changes, *J. Geophys. Res.*, 108 (D1), 4027, doi: 10.1029/2002JD002069, 2003.
- Langematz, U., J.L. Grenfell, K. Matthes, P. Mieth, M. Kunze, B. Steil, and C. Brühl, Chemical effects in 11-year solar cycle simulations with the Freie Universität Berlin Climate Middle Atmosphere Model with online chemistry (FUB-CMAM-CHEM), *Geophys. Res. Lett.*, 32, L13803, doi: 10.1029/2005GL022686, 2005.
- Leblanc, T., and I.S. McDermid, Stratospheric ozone climatology from lidar measurements at Table Mountain (34.4°N, 117.7°W) and Mauna Loa (19.5°N, 155.6°W), *J. Geophys. Res.*, 105 (D11), 14613-14623, 2000.
- Leblanc, T., and I.S. McDermid, Quasi-biennial oscillation signatures in ozone and temperature observed by lidar at Mauna Loa, Hawaii (19.5°N, 155.6°W), *J. Geophys. Res.*, 106 (D14), 14869-14874, 2001.
- Lee, H., and A.K. Smith, Simulation of the combined effects of solar cycle, quasi-biennial oscillation, and volcanic forcing on stratospheric ozone changes in recent decades, *J. Geophys. Res.*, 108 (D2), 4049, doi: 10.1029/2001JD001503, 2003.
- Lelieveld, J., J. van Aardenne, H. Fischer, M. de Reus, J. Williams, and P. Winkler, Increasing ozone over the Atlantic Ocean, *Science*, 304 (5676), 1483-1487, 2004.
- Li, J.L., D.M. Cunnold, H.J. Wang, E.S. Yang, and M.J. Newchurch, A discussion of upper stratospheric ozone asymmetries and SAGE trends, *J. Geophys. Res.*, 107 (D23), 4705, doi: 10.1029/2001JD001398, 2002.
- Liley, J.B., P.V. Johnston, R.L. McKenzie, A.J. Thomas, and I.S. Boyd, Stratospheric NO₂ variations from a long time series at Lauder, New Zealand, *J. Geophys. Res.*, 105 (D9), 11633-11640, 2000.
- Livesey, N., M.D. Fromm, J.W. Waters, G.L. Manney, M.L. Santee, and W.G. Read, Enhancements in lower stratospheric CH₃CN observed by the Upper Atmosphere Research Satellite Microwave Limb Sounder following boreal forest fires, *J. Geophys. Res.*, 109, D06308, doi: 10.1029/2003JD004055, 2004.
- Logan, J.A., Trends in the vertical distribution of ozone: An analysis of ozonesonde data, *J. Geophys. Res.* 99 (D12), 25553-25585, 1994.
- Logan, J.A., I.A. Megretskaja, A.J. Miller, G.C. Tiao, D. Choi, L. Zhang, R.S. Stolarski, G.J. Labow, S.M. Hollandsworth, G.E. Bodeker, H. Claude, D. De Muer, J.B. Kerr, D.W. Tarasick, S.J. Oltmans, B. Johnson, F. Schmidlin, J. Staehelin, P. Viatte, and O. Uchino, Trends in the vertical distribution of ozone: A comparison of two analyses of ozonesonde data, *J. Geophys. Res.*, 104 (D21), 26373-26399, 1999.
- Mahieu, E., R. Zander, P. Demoulin, M. De Mazière, F. Mélen, C. Servais, G. Roland, L. Delbouille, J. Poels, and R. Blomme, Fifteen years-trend characteristics of key stratospheric constituents monitored by FTIR above the Jungfraujoch, in *Stratospheric Ozone 1999, Proc. 5th European Symp.*, 27 September-1 October 1999, St. Jean de Luz, France, edited by N.R.P. Harris, M. Guirlet, and G.T. Amanatidis, *Air Pollution Research Rep. 73, EUR 19340*, 99-102, European Commission, Luxembourg, 2000.
- Mahowald, N.M., R.A. Plumb, P.J. Rasch, J. del Corral, F.

GLOBAL OZONE

- Sassi, and W. Heres, Stratospheric transport in a three-dimensional isentropic coordinate model, *J. Geophys. Res.*, 107 (D15), 4254, doi: 10.1029/2001JD001313, 2002.
- Malanca, F.E., P.O. Canziani, and G.A. Arguello, Trends evolution of ozone between 1980 and 2000 at mid-latitudes over the Southern Hemisphere: Decadal differences in trends, *J. Geophys. Res.*, 110, D05102, doi:10.1029/2004JD004977, 2005.
- Manney, G.L., L. Froidevaux, M.L. Santee, N.J. Livesey, J.L. Sabutis, and J.W. Waters, Variability of ozone loss during Arctic winter (1991-2000) estimated from UARS Microwave Limb Sounder measurements, *J. Geophys. Res.*, 108 (D4), 4149, doi: 10.1029/2002JD002634, 2003.
- Manney, G.L., D.R. Allen, K. Krueger, B. Naujokat, M.L. Santee, J.L. Sabutis, S. Pawson, R. Swinbank, C.E. Randall, A.J. Simmons, and C. Long, Diagnostic comparison of meteorological analyses during the 2002 Antarctic winter, *Mon. Wea. Rev.*, 133 (5), 1261-1278, 2005.
- Marchand, M., S. Godin, A. Hauchecorne, F. Lefèvre, S. Bekki, and M. Chipperfield, Influence of polar ozone loss on northern midlatitude regions estimated by a high-resolution chemistry transport model during winter 1999/2000, *J. Geophys. Res.*, 108 (D5), 8326, doi: 10.1029/2001JD000906, 2003.
- Mateer, C.L., H.U. Dutsch, and J. Staehelin, Influence of a priori profiles on trend calculations from Umkehr data, *J. Geophys. Res.*, 101 (D11), 16779-16787, 1996.
- McCormack, J.P., The influence of the 11-year solar cycle on the quasi-biennial oscillation, *Geophys. Res. Lett.*, 30 (22), 2162, doi: 10.1029/2003GL018314, 2003.
- McCormack, J.P., and L.L. Hood, Apparent solar cycle variations of upper stratospheric ozone and temperature: Latitude and seasonal dependences, *J. Geophys. Res.*, 101 (D15), 20933-20944, 1996.
- McCormack, J.P., L.L. Hood, R. Nagatani, A.J. Miller, W.G. Planet, and R.D. McPeters, Approximate separation of volcanic and 11-year signals in the SBUV-SBUV/2 total ozone record over the 1979-1995 period, *Geophys. Res. Lett.*, 24 (22), 2729-2732, 1997.
- McCormick, M.P., J.M. Zawodny, R.E. Viegas, J.C. Larsen, and P.-H. Wang, An overview of SAGE I and II ozone measurements, *Planet. Space Sci.*, 37 (12), 1567-1586, 1989.
- McPeters, R.D., T. Miles, L.E. Flynn, C.G. Wellemeyer, and J.M. Zawodny, Comparison of SBUV and SAGE II ozone profiles: Implications for ozone trends, *J. Geophys. Res.*, 99 (D10), 20513-20524, 1994.
- McPeters, R.D., J.A. Logan, and G.J. Labow, Ozone climatological profiles for version 8 TOMS and SBUV retrievals, *Eos Trans. Amer. Geophys. Union*, 84, Abstract A21D-0998, 2003.
- McPeters, R., C. Wellemeyer, and A. Ahn, The validation of version 8 ozone profiles: Is SBUV ready for prime time?, in *Ozone Vol. I, Proceedings of the XX Quadrennial Ozone Symposium*, 1-8 June 2004, Kos, Greece, edited by C.S. Zerefos, 113-114, Int. Ozone Comm., Athens, Greece, 2004.
- Meijer, E.W., B. Bregman, A. Segers, and P.F.J. van Velthoven, The influence of data assimilation on the age of air calculated with a global chemistry-transport model using ECMWF wind fields, *Geophys. Res. Lett.*, 31, L23114, doi: 10.1029/2004GL021158, 2004.
- Millard, G.A., A.M. Lee, and J.A. Pyle, A model study of the connection between polar and midlatitude ozone loss in the Northern Hemisphere lower stratosphere, *J. Geophys. Res.*, 108 (D5), 8323, doi: 10.1029/2001JD000899, 2003.
- Miller, A.J., R.M. Nagatani, L.E. Flynn, S. Kondragunta, E. Beach, R. Stolarski, R.D. McPeters, P.K. Bhartia, M.T. DeLand, C.H. Jackman, D.J. Wuebbles, K.O. Patten, and R.P. Cebula, A cohesive total ozone data set from the SBUV(/2) satellite system, *J. Geophys. Res.*, 107 (D23), 4701, doi: 10.1029/2001JD000853, 2002.
- Miller, A.J., A. Cai, G. Taio, D.J. Wuebbles, L.E. Flynn, S.-K. Yang, E.C. Weatherhead, V. Fioletov, I. Petropavlovskikh, X.-L. Meng, S. Guillas, R.M. Nagatani, and G.C. Reinsel, Examination of ozone-sonde data for trends and trend changes incorporating solar and Arctic oscillation signals, *J. Geophys. Res.*, 111, D13305, doi: 10.1029/2005JD006684, 2006.
- Monge Sanz, B., M.P. Chipperfield, A. Simmons, and S. Uppala, Mean age of air and transport in a CTM: Comparison of different ECMWF analyses, *Geophys. Res. Lett.*, in press, 2006.
- Nagahama, T., H. Nakane, Y. Fujinuma, H. Ogawa, A. Mizuno, and Y. Fukui, A semiannual variation of ozone in the middle mesosphere observed with the millimeter-wave radiometer at Tsukuba, Japan, *J. Geophys. Res.*, 108 (D21), 4684, doi: 10.1029/2003JD003724, 2003.
- Naja, M., and H. Akimoto, Contribution of regional pollution and long-range transport to the Asia-Pacific region: Analysis of long-term ozonesonde data over Japan, *J. Geophys. Res.*, 109, D21306, doi:

- 10.1029/2004JD004687, 2004.
- Nazaryan, H., and M.P. McCormick, Comparisons of Stratospheric Aerosol and Gas Experiment (SAGE II) and Solar Backscatter Ultraviolet Instrument (SBUV/2) ozone profiles and trend estimates, *J. Geophys. Res.*, *110*, D17302, doi: 10.1029/2004JD005483, 2005.
- Nazaryan, H., M.P. McCormick, and J.M. Russell III, New studies of SAGE II and HALOE ozone profile and long-term change comparisons, *J. Geophys. Res.*, *110*, D09305, doi: 10.1029/2004JD005425, 2005.
- Newchurch, M.J., E.-S. Yang, D.M. Cunnold, G.C. Reinsel, J.M. Zawodny, and J.M. Russell III, Evidence for slowdown in stratospheric ozone loss: First stage of ozone recovery, *J. Geophys. Res.*, *108* (D16), 4507, doi: 10.1029/2003JD003471, 2003.
- Newman, P.A., S.R. Kawa, and E.R. Nash, On the size of the Antarctic ozone hole, *Geophys. Res. Lett.*, *31*, L21104, doi: 10.1029/2004GL020596, 2004.
- Newman, P.A., E.R. Nash, S.R. Kawa, S.A. Montzka, and S.M. Schauffler, When will the Antarctic ozone hole recover?, *Geophys. Res. Lett.*, *33*, L12814, doi: 10.1029/2005GL025232, 2006.
- Notholt, J., B.P. Luo, S. Füglistaler, D. Weisenstein, M. Rex, M.G. Lawrence, H. Bingemer, I. Wohltmann, T. Corti, T. Warneke, R. von Kuhlmann, and T. Peter, Influence of tropospheric SO₂ emissions on particle formation and the stratospheric humidity, *Geophys. Res. Lett.*, *32*, L07810, doi: 10.1029/2004GL022159, 2005.
- Oltmans, S.J., A.S. Lefohn, J.M. Harris, I. Galbally, H.E. Scheel, G. Bodeker, E. Brunke, H. Claude, D. Tarasick, B.J. Johnson, P. Simmonds, D. Shadwick, K. Anlauf, K. Hayden, F. Schmidlin, T. Fujimoto, K. Akagi, C. Meyer, S. Nichol, J. Davies, A. Redondas, and E. Cuevas, Long-term changes in tropospheric ozone, *Atmos. Environ.*, *40* (17), 3156-3173, 2006.
- Orsolini, Y.J., Long-lived tracer patterns in the summer polar stratosphere, *Geophys. Res. Lett.*, *28* (20), 3855-3858, 2001.
- Orsolini, Y.J., and V. Limpasuvan, The North Atlantic Oscillation and the occurrences of ozone miniholes, *Geophys. Res. Lett.*, *28* (21), 4099-4102, 2001.
- Ovarlez, J., J.F. Gayet, K. Gierens, J. Strom, H. Ovarlez, F. Auriol, R. Busen, and U. Schumann, Water vapour measurements inside cirrus clouds in Northern and Southern hemispheres during INCA, *Geophys. Res. Lett.*, *29* (16), 1813-1817, 2002.
- Parrish, A., Millimeter-wave remote sensing of ozone and trace constituents in the stratosphere, *Proc. IEEE.*, *82* (12), 1915-1929, 1994.
- Peter, T., B.P. Luo, M. Wirth, C. Kiemle, H. Flentje, V.A. Yushkov, V. Khattatov, V. Rudakov, A. Thomas, S. Borrmann, G. Toci, P. Mazzinghi, J. Beuermann, C. Schiller, F. Cairo, G. Di Donfrancesco, A. Adriani, C.M. Volk, J. Strom, K. Noone, V. Mitev, R.A. MacKenzie, K.S. Carslaw, T. Trautmann, V. Santacesaria, and L. Stefanutti, Ultrathin Tropical Tropopause Clouds (UTTCS): I. Cloud morphology and occurrence, *Atmos. Chem. Phys.*, *3*, 1083-1091, 2003.
- Peters, D., and D. Waugh, Influence of barotropic shear on the poleward advection of upper-tropospheric air, *J. Atmos. Sci.*, *53* (21), 3013-3031, 1996.
- Petropavlovskikh, I., C. Ahn, P.K. Bhartia, and L.E. Flynn, Comparison and covalidation of ozone anomalies and variability observed in SBUV(2) and Umkehr northern midlatitude ozone profile estimates, *Geophys. Res. Lett.*, *32*, L06805, doi: 10.1029/2004GL022002, 2005a.
- Petropavlovskikh, I., P.K. Bhartia, and J.J. DeLuisi, New Umkehr ozone profile retrieval algorithm optimized for climatological studies, *Geophys. Res. Lett.*, *32*, L16808, doi: 10.1029/2005GL023323, 2005b.
- Piani, C., W.A. Norton, A.M. Iwi, E.A. Ray, and J.W. Elkins, Transport of ozone-depleted air on the breakup of the stratospheric polar vortex in spring/summer 2000, *J. Geophys. Res.*, *107* (D20), 8270, doi: 10.1029/2001JD000488, 2002.
- Polavarapu, S., S.Z. Ren, Y. Rochon, D. Sankey, N. Ek, J. Koshyk, and D. Tarasick, Data assimilation with the Canadian Middle Atmosphere Model, *Atmos. Ocean*, *43* (1), 77-100, 2005.
- Popp, P.J., T.P. Marcy, E.J. Jensen, B. Karcher, D.W. Fahey, R.S. Gao, T.L. Thompson, K.H. Rosenlof, E.C. Richard, R.L. Herman, E.M. Weinstock, J.B. Smith, R.D. May, H. Vomel, J.C. Wilson, A.J. Heymsfield, M.J. Mahoney, and A.M. Thompson, The observation of nitric acid-containing particles in the tropical lower stratosphere, *Atmos. Chem. Phys.*, *6*, 610-611, 2006.
- Prather, M.J., M.M. Garcia, A.R. Douglass, C.H. Jackman, M.K.W. Ko, and N.D. Sze, The space shuttle's impact on the stratosphere, *J. Geophys. Res.*, *95* (D11), 18583-18590, 1990.
- Randel, W.J., and F. Wu, A stratospheric ozone profile data set for 1979-2005: variability, trends, and comparisons with column ozone data, *J. Geophys. Res.*, *111*, doi:10.1029/2006JD007339, in press, 2006.
- Randel, W.J., F. Wu, and R. Stolarski, Changes in column ozone correlated with the stratospheric EP flux, *J. Meteorol. Soc. Japan*, *80* (4B), 849-862, 2002.
- Randel, W., P. Udelhofen, E. Fleming, M. Geller, M.

GLOBAL OZONE

- Gelman, K. Hamilton, D. Karoly, D. Ortland, S. Pawson, R. Swinbank, F. Wu, M. Baldwin, M.L. Chanin, P. Keckhut, K. Labitzke, E. Remsberg, A. Simmons, and D. Wu, The SPARC intercomparison of middle atmosphere climatologies, *J. Clim.*, 17 (5), 986-1003, 2004.
- Randel, W.J., F. Wu, H. Vömel, G.E. Nedoluha, and P. Forster, Decreases in stratospheric water vapor after 2001: Links to changes in the tropical tropopause and the Brewer-Dobson circulation, *J. Geophys. Res.*, 111, D12312, doi:10.1029/2005JD006744, 2006.
- Ray, E.A., K.H. Rosenlof, E.C. Richard, P.K. Hudson, D.J. Cziczo, M. Loewenstein, H.J. Jost, J. Lopez, B. Ridley, A. Weinheimer, D. Montzka, D. Knapp, S.C. Wofsy, B.C. Daube, C. Gerbig, I. Xueref, and R.L. Herman, Evidence of the effect of summertime midlatitude convection on the subtropical lower stratosphere from CRYSTAL-FACE tracer measurements, *J. Geophys. Res.*, 109, D18304, doi: 10.1029/2004JD004655, 2004.
- Reid, S.J., A.F. Tuck, and G. Kiladis, On the changing abundance of ozone minima at northern midlatitudes, *J. Geophys. Res.*, 105 (D10), 12169-12180, 2000.
- Reinsel, G.C., E.C. Weatherhead, G.C. Tiao, A.J. Miller, R.M. Nagatani, D.J. Wuebbles, and L.E. Flynn, On detection of turnaround and recovery in trend for ozone, *J. Geophys. Res.*, 107 (D10), 4078, doi: 10.1029/2001JD000500, 2002.
- Reinsel, G.C., A.J. Miller, E.C. Weatherhead, L.E. Flynn, R. Nagatani, G.C. Tiao, and D.J. Wuebbles, Trend analysis of total ozone data for turnaround and dynamical contributions, *J. Geophys. Res.*, 110, D16306, doi: 10.1029/2004JD004662, 2005.
- Ricaud, P., P. Baron, and J. De La Noë, Quality assessment of ground-based microwave measurements of chlorine monoxide, ozone, and nitrogen dioxide from the NDSC radiometer at the Plateau de Bure, *Ann. Geophys.*, 22 (6), 1903-1915, 2004.
- Rind, D., J. Lerner, and J. Zawodny, A complementary analysis for SAGE II data profiles, *Geophys. Res. Lett.*, 32, L07812, doi: 10.1029/2005GL022550, 2005.
- Rosenfield, J.E., S.M. Frith, and R.S. Stolarski, Version 8 SBUV ozone profile trends compared with trends from a zonally averaged chemical model, *J. Geophys. Res.*, 110, D12302, doi: 10.1029/2004JD005466, 2005.
- Rozanov, E., L. Callis, M. Schlesinger, F. Yang, N. Andronova, and V. Zubov, Atmospheric response to NO_y source due to energetic electron precipitation, *Geophys. Res. Lett.*, 32, L14811, doi: 10.1029/2005GL023041, 2005.
- Salawitch, R.J., P.O. Wennberg, G.C. Toon, B. Sen, and J.F. Blavier, Near IR photolysis of HO₂NO₂: Implications for HO_x, *Geophys. Res. Lett.*, 29 (16), 1762, doi: 10.1029/2002GL015006, 2002.
- Salawitch, R.J., D.K. Weisenstein, L.J. Kovalenko, C.E. Sioris, P.O. Wennberg, K. Chance, M.K.W. Ko, and C.A. McLinden, Sensitivity of ozone to bromine in the lower stratosphere, *Geophys. Res. Lett.*, 32, L05811, doi: 10.1029/2004GL021504, 2005.
- Salby, M., and P. Callaghan, Connection between the solar cycle and the QBO: The missing link, *J. Clim.*, 13 (14), 2652-2662, 2000.
- Salby, M.L., and P.F. Callaghan, Interannual changes of the stratospheric circulation: Relationship to ozone and tropospheric structure, *J. Clim.*, 15 (24), 3673-3685, 2002.
- Salby, M.L., and P.F. Callaghan, Systematic changes of Northern Hemisphere ozone and their relationship to random interannual changes, *J. Clim.*, 17 (23), 4512-4521, 2004.
- Sander, S.P., R.R. Friedl, W.B. DeMore, D.M. Golden, M.J. Kurylo, R.F. Hampson, R.E. Huie, G.K. Moortgat, A.R. Ravishankara, C.E. Kolb, and M.J. Molina, *Chemical Kinetics and Photochemical Data for Use in Stratospheric Modeling, Evaluation No. 13, JPL Publication 00-03*, Jet Propulsion Laboratory, Pasadena, Calif., 2000.
- Sander, S.P., R.R. Friedl, D.M. Golden, M.J. Kurylo, R.E. Huie, V.L. Orkin, G.K. Moortgat, A.R. Ravishankara, C.E. Kolb, M.J. Molina, and B.J. Finlayson-Pitts, *Chemical Kinetics and Photochemical Data for Use in Atmospheric Studies: Evaluation Number 14, JPL Publication 02-25*, Jet Propulsion Laboratory, Pasadena, Calif., 2003.
- Sander, S.P., R.R. Friedl, D.M. Golden, M.J. Kurylo, G.K. Moortgat, H. Keller-Rudek, P.H. Wine, A.R. Ravishankara, C.E. Kolb, M.J. Molina, B.J. Finlayson-Pitts, R.E. Huie, and V.L. Orkin, *Chemical Kinetics and Photochemical Data for Use in Atmospheric Studies: Evaluation Number 15, JPL Publication 06-2*, Jet Propulsion Laboratory, Pasadena, Calif., 2006.
- Santer, B.D. T.M.L. Wigley, A.J. Simmons, P.W. Kallberg, G.A. Kelly, S.M. Uppala, C. Ammann, J.S. Boyle, W. Bruggemann, C. Doutriaux, M. Fiorino, C. Mears, G.A. Meehl, R. Sausen, K.E. Taylor, W.M. Washington, M.F. Wehner, and F.J. Wentz, Identification of anthropogenic climate change using a second-generation reanalysis, *J. Geophys. Res.*,

- 109, D21104, doi: 10.1029/2004JD005075, 2004.
- Saraf, N., and G. Beig, Long-term trends in tropospheric ozone over the Indian tropical region, *Geophys. Res. Lett.*, *31*, L05101, doi: 10.1029/2003GL018516, 2004.
- Scheele, M.P., P.C. Siegmund, and P.F.J. van Velthoven, Stratospheric age of air computed with trajectories based on various 3D-var and 4D-var datasets, *Atmos. Chem. Phys.*, *5*, 1-7, 2005.
- Schneider, N., O. Lezeaux, J. La Noe, J. Urban, and P. Ricaud, Validation of ground-based observations of stratomesospheric ozone, *J. Geophys. Res.*, *108* (D17), 4540, doi: 10.1029/2002JD002925, 2003.
- Schoeberl, M.R., A.R. Douglass, Z.X. Zhu, and S. Pawson, A comparison of the lower stratospheric age spectra derived from a general circulation model and two data assimilation systems, *J. Geophys. Res.*, *108* (D3), 4113, doi: 10.1029/2002JD002652, 2003.
- Shalomyanskij, A.M., I.L. Karol, L.P. Klyagina, and K.I. Romashkina, Total ozone over regions of the Russian Federation and adjacent countries from measurements at surface stations for 30 years, *Russ. Meteorol. Hydrol.*, *8*, 24-36, 2004.
- Simmonds P.G., R.G. Derwent, A.L. Manning, and G. Spain, Significant growth in surface ozone at Mace Head, Ireland, 1987-2003, *Atmos. Env.*, *38* (28), 4769-4778, 2004.
- Simmons, A.J., M. Hortal, G. Kelly, A. McNally, A. Untch, and S. Uppala, ECMWF analyses and forecasts of stratospheric winter polar vortex breakup: September 2002 in the Southern Hemisphere and related events, *J. Atmos. Sci.*, *62* (3), 668-689, 2005.
- Sinnhuber, B.-M., A. Rozanov, N. Sheode, O.T. Afe, A. Richter, M. Sinnhuber, F. Wittrock, J.P. Burrows, G.P. Stiller, T. von Clarmann, and A. Linden, Global observations of stratospheric bromine monoxide from SCIAMACHY, *Geophys. Res. Lett.*, *32*, L20810, doi: 10.1029/2005GL023839, 2005.
- Sivakumaran, V., and J.N. Crowley, Reaction between OH and CH₃CHO, Part 2. Temperature dependent rate coefficients (201-348 K), *Phys. Chem. Chem. Phys.*, *5* (1), 106-111, 2003.
- Sivakumaran, V., D. Holscher, T.J. Dillon, and J.N. Crowley, Reaction between OH and HCHO: temperature dependent rate coefficients (202-399K) and product pathways (298 K), *Phys. Chem. Chem. Phys.*, *5* (21), 4821-4827, 2003.
- Solomon, S., R.W. Portmann, R.R. Garcia, L.W. Thomason, L.R. Poole, and M.P. McCormick, The role of aerosol variations in anthropogenic ozone depletion at northern midlatitudes, *J. Geophys. Res.*, *101* (D3), 6713-6727, 1996.
- Solomon, S., S. Bormann, R.R. Garcia, R. Portmann, L. Thomason, L.R. Poole, D. Winker, and M.P. McCormick, Heterogeneous chlorine chemistry in the tropopause region, *J. Geophys. Res.*, *102* (D17), 21411-21430, 1997.
- Soukharev, B.E., and L.L. Hood, Solar cycle variation of stratospheric ozone: Multiple regression analysis of long-term satellite data sets and comparisons with models, *J. Geophys. Res.*, *111* (D20314), doi: 10.1029/2006JD007107, 2006.
- SPARC (Stratospheric Processes And their Role in Climate), *SPARC/IOC/GAW Assessment of Trends in the Vertical Distribution of Ozone*, edited by N. Harris, R. Hudson, and C. Phillips, *SPARC Report No. 1, WMO Global Ozone Research and Monitoring Project Report No. 43*, 289 pp., Verrières le Buisson, France, 1998.
- SPARC (Stratospheric Processes And their Role in Climate), *SPARC Assessment of Stratospheric Aerosol Properties*, edited by L. Thomason, and Th. Peter, *World Climate Research Program Report 124, SPARC Report 4*, 346 pp., Verrières le Buisson, France, 2006.
- Spichtinger, P., K. Gierens, H.G.J. Smit, J. Ovarlez, and J.F. Gayet, On the distribution of relative humidity in cirrus clouds, *Atmos. Chem. Phys.*, *4*, 639-647, 2004.
- Stahelin, J., J. Kerr, R. Evans, and K. Vanicek, *Comparison of Total Ozone Measurements of Dobson and Brewer Spectrophotometers and Recommended Transfer Functions*, WMO/TD No. 1147, World Meteorological Organization, Geneva, Switzerland, 2003.
- Steinbrecht, W., H. Claude, and U. Köhler, Correlations between tropopause height and total ozone: Implications for long-term changes, *J. Geophys. Res.*, *103* (D15), 19183-19192, 1998.
- Steinbrecht, W., H. Claude, and P. Winkler, Enhanced upper stratospheric ozone: Sign of recovery or solar cycle effect?, *J. Geophys. Res.*, *109*, D14305, doi: 10.1029/2004JD004826, 2004a.
- Steinbrecht, W., H. Claude, and P. Winkler, Reply to comment by D.M. Cunnold et al. on "Enhanced upper stratospheric ozone: Sign of recovery or solar cycle effect?" *J. Geophys. Res.*, *109*, D14306, doi: 10.1029/2004JD004948, 2004b.
- Steinbrecht, W., H. Claude, F. Schöenborn, I.S. McDermid, T. Leblanc, S. Godin, T. Song, D.P.J. Swart, Y.J. Meijer, G.E. Bodeker, B.J. Connor, N. Kämpfer, K. Hocke, Y. Calisesi, N. Schneider, J. de la Noë, A.D. Parrish, I.S. Boyd, C. Brühl, B. Steil, M.A. Giorgetta, E. Manzini, L.W. Thomason, J.M.

GLOBAL OZONE

- Zawodny, M.P. McCormick, J.M. Russell III, P.K. Bhartia, R.S. Stolarski, and S.M. Hollandsworth-Frith, Long-term evolution of upper stratospheric ozone at selected stations of the Network for the Detection of Stratospheric Change (NDSC), *J. Geophys. Res.*, *111*, D10308, doi: 10.1029/2005JD006454, 2006.
- Stolarski, R.S., and S. Frith, Search for evidence of trend slow-down in the long-term TOMS/SBUV total ozone data record: the importance of instrument drift uncertainty and fingerprint detection, *Atmos. Chem. Phys. Discuss.*, *6*, 3883-3912, 2006.
- Stolarski, R., and W. Randel, Ozone change as a function of altitude, Chapter 3 in *SPARC/IOC/GAW Assessment of Trends in the Vertical Distribution of Ozone*, edited by N. Harris, R. Hudson, and C. Phillips, *SPARC Report No. 1, WMO Global Ozone Research and Monitoring Project Report No. 43*, 289 pp., Verrières le Buisson, France, 1998.
- Stolarski, R.S., G.J. Labow, and R.D. McPeters, Springtime Antarctic total ozone measurements in the early 1970s from the BUUV instrument on Nimbus 4, *Geophys. Res. Lett.*, *24* (5), 591-594, 1997.
- Stolarski, R.S., A.R. Douglass, S. Steenrod, and S. Pawson, Trends in stratospheric ozone: Lessons learned from a 3D Chemical Transport Model, *J. Atmos. Sci.*, *63* (3), 1028-1041, 2006.
- Strahan, S.E., and A.R. Douglass, Evaluating the credibility of transport processes in simulations of ozone recovery using the Global Modeling Initiative three-dimensional model, *J. Geophys. Res.*, *109*, D05110, doi: 10.1029/2003JD004238, 2004.
- Ström, J., M. Seifert, B. Kärcher, J. Ovarlez, A. Minikin, J.-F. Gayet, R. Krejci, A. Petzold, F. Auriol, W. Haag, R. Busen, U. Schumann, and H.C. Hansson, Cirrus cloud occurrence as a function of ambient relative humidity: A comparison of observations obtained during the INCA experiment, *Atmos. Chem. Phys.*, *3*, 1807-1816, 2003.
- Svenby, T.M., and A. Dahlback, Statistical analysis of total ozone measurements in Oslo, Norway, 1978-1998, *J. Geophys. Res.*, *109*, D16107, doi: 10.1029/2004JD004679, 2004.
- Swinbank, R., N.B. Ingleby, P.M. Boorman, and R.J. Renshaw, *A 3D Variational Data Assimilation System for the Stratosphere and Troposphere*, Forecasting Research Division Scientific Paper No. 71, U.K. Met. Office, NWP Division, Berkshire, U.K., 2002.
- Tan, W.W., M.A. Geller, S. Pawson, and A. da Silva, A case study of excessive subtropical transport in the stratosphere of a data assimilation system, *J. Geophys. Res.*, *109*, D11102, doi: 10.1029/2003JD004057, 2004.
- Tarasick, D.W., V.E. Fioletov, D.I. Wardle, J.B. Kerr, and J. Davies, Changes in the vertical distribution of ozone over Canada from ozonesondes: 1980-2001, *J. Geophys. Res.*, *110*, D02304, doi: 10.1029/2004JD004643, 2005.
- Terao, Y., and J.A. Logan, Consistency of time series and trends of stratospheric ozone as seen by ozone-sonde, SAGE II, HALOE, and SBUV (/2), *J. Geophys. Res.*, in press, 2006.
- Thompson, A.M., J.C. Witte, R.D. McPeters, S.J. Oltmans, F.J. Schmidlin, J.A. Logan, M. Fujiwara, V.W.J.H. Kirchhoff, F. Posny, G.J.R. Coetzee, B. Hoegger, S. Kawakami, T. Ogawa, B.J. Johnson, H. Vömel, and G. Labow, Southern Hemisphere Additional Ozonesondes (SHADOZ) 1998-2000 tropical ozone climatology 1. Comparison with Total Ozone Mapping Spectrometer (TOMS) and ground-based measurements, *J. Geophys. Res.*, *108* (D2), 8238, doi: 10.1029/2001JD000967, 2003.
- Thornton, B.F., D.W. Toohey, L.M. Avallone, H. Harder, M. Martinez, J.B. Simpas, W.H. Brune, and M.A. Avery, In situ observations of ClO near the winter polar tropopause, *J. Geophys. Res.*, *108* (D8), 8333, doi: 10.1029/2002JD002839, 2003.
- Thornton, B.F., D.W. Toohey, L.M. Avallone, A.G. Hallar, H. Harder, M. Martinez, J.B. Simpas, W.H. Brune, M. Koike, Y. Kondo, N. Takegawa, B.E. Anderson, and M.A. Avery, Variability of active chlorine in the lowermost Arctic stratosphere, *J. Geophys. Res.*, *110*, D22304, doi: 10.1029/2004JD005580, 2005.
- Tie, X.X., and G.P. Brasseur, The response of stratospheric ozone to volcanic eruptions: Sensitivity to atmospheric chlorine loading, *Geophys. Res. Lett.*, *22* (22), 3035-3038, 1995.
- Tie, X.X., G.P. Brasseur, B. Briegleb, and C. Granier, Two-dimensional simulation of Pinatubo aerosol and its effect on stratospheric ozone, *J. Geophys. Res.*, *99* (D10), 20545-20562, 1994.
- Tourpali, K., C.J.E. Schuurmans, R. van Dorland, B. Steil, and C. Brühl, Stratospheric and tropospheric response to enhanced solar UV radiation: A model study, *Geophys. Res. Lett.*, *30* (5), 1231, doi: 10.1029/2002GL016650, 2003.
- Tsou, J.J., B.J. Connor, A. Parrish, R.B. Pierce, I.S. Boyd, G.E. Bodeker, W.P. Chu, J.M. Russell III, D.P.J. Swart, and T.J. McGee, NDSC millimeter wave ozone observations at Lauder, New Zealand, 1992-1998: Improved methodology, validation, and variation study, *J. Geophys. Res.*, *105* (D19), 24263-24281, 2000.

- Uppala, S.M., P.W. Kallberg, A.J. Simmons, U. Andrae, V.D. Bechtold, M. Fiorino, J.K. Gibson, J. Haseler, A. Hernandez, G.A. Kelly, X. Li, K. Onogi, S. Saarinen, N. Sokka, R.P. Allan, E. Andersson, K. Arpe, M.A. Balmaseda, A.C.M. Beljaars, L. Van De Berg, J. Bidlot, N. Bormann, S. Caires, F. Chevallier, A. Dethof, M. Dragosavac, M. Fisher, M. Fuentes, S. Hagemann, E. Holm, B.J. Hoskins, L. Isaksen, P. Janssen, R. Jenne, A.P. McNally, J.F. Mahfouf, J.J. Morcrette, N.A. Rayner, R.W. Saunders, P. Simon, A. Sterl, K.E. Trenberth, A. Untch, D. Vasiljevic, P. Viterbo, and J. Woollen, The ERA-40 re-analysis, *Quart. J. Roy. Meteorol. Soc.*, *131* (612), 2961-3012, 2005.
- Van Noije, T.P.C., H.J. Eskes, M. van Weele, and P.F.J. van Velthoven, Implications of the enhanced Brewer-Dobson circulation in European Centre for Medium-Range Weather Forecasts reanalysis ERA-40 for the stratosphere-troposphere exchange of ozone in global chemistry transport models, *J. Geophys. Res.*, *109*, D19308, doi: 10.1029/2004JD004586, 2004.
- Van Noije, T.P.C., A.J. Segers, and P.F.J. van Velthoven, Time series of the stratosphere-troposphere exchange of ozone simulated with reanalyzed and operational forecast data, *J. Geophys. Res.*, *111*, D03301, doi: 10.1029/2005JD006081, 2006.
- Van Roozendaal, M., D. Loyola, R. Spurr, D. Balis, J.-C. Lambert, Y. Livschitz, P. Valks, T. Ruppert, P. Kenter, C. Fayt, and C. Zehner, Ten years of GOME/ERS2 total ozone data—The new GOME Data Processor (GDP) Version 4 1. Algorithm description, *J. Geophys. Res.*, *111*, D14311, doi: 10.1029/2005JD006375, 2006.
- Vogler, C., S. Brönnimann, and G. Hansen, Re-evaluation of the 1950-1962 total ozone record from Longyearbyen, Svalbard, *Atmos. Chem. Phys. Discuss.*, *6*, 3913-3943, 2006.
- Wang, H.J., D.M. Cunnold, and X. Bao, A critical analysis of Stratospheric Aerosol and Gas Experiment ozone trends, *J. Geophys. Res.*, *101* (D7), 12495-12514, 1996.
- Wang, H.J., D.M. Cunnold, L.W. Thomason, J.M. Zawodny, and G.E. Bodeker, Assessment of SAGE version 6.1 ozone data quality, *J. Geophys. Res.*, *107* (D23), 4691, doi: 10.1029/2002JD002418, 2002.
- Weatherhead, E.C., G.C. Reinsel, G.C. Tiao, X.L. Meng, D.S. Choi, W.K. Cheang, T. Keller, J. DeLuisi, D.J. Wuebbles, J.B. Kerr, A.J. Miller, S.J. Oltmans, and J.E. Frederick, Factors affecting the detection of trends: Statistical considerations and applications to environmental data, *J. Geophys. Res.*, *103* (D14), 17149-17161, 1998.
- Weatherhead, E.C., G.C. Reinsel, G.C. Tiao, C.H. Jackman, L. Bishop, S.M. Hollandsworth, J. Frith, T. DeLuisi, S.J. Keller, S.J. Oltmans, E.L. Fleming, D.J. Wuebbles, J.B. Kerr, A.J. Miller, J. Herman, R. McPeters, R.M. Nagatani, and J.E. Frederick, Detecting the recovery of total column ozone, *J. Geophys. Res.*, *105* (D17), 22201-22210, 2000.
- Weber, M., S. Dhomse, F. Wittrock, A. Richter, B.-M. Sinnhuber, and J.P. Burrows, Dynamical control of NH and SH winter/spring total ozone from GOME observations in 1995-2002, *Geophys. Res. Lett.*, *30* (11), 1583, doi: 10.1029/2002GL016799, 2003.
- Weber, M., L.N. Lamsal, M. Coldewey-Egbers, K. Bramstedt, and J. Burrows, Pole-to-pole validation of GOME WFOAS total ozone with groundbased data, *Atmos. Chem. Phys.*, *5*, 1341-1355, 2005.
- Wohltmann, I., M. Rex, D. Brunner, and J. Mader, Integrated equivalent latitude as a proxy for dynamical changes in ozone column, *Geophys. Res. Lett.*, *32*, L09811, doi: 10.1029/2005GL022497, 2005.
- WMO (World Meteorological Organization), *Scientific Assessment of Ozone Depletion: 1991, Global Ozone Research and Monitoring Project—Report No. 25*, Geneva, Switzerland, 1992.
- WMO (World Meteorological Organization), *Scientific Assessment of Ozone Depletion: 1994, Global Ozone Research and Monitoring Project—Report No. 37*, Geneva, Switzerland, 1995.
- WMO (World Meteorological Organization), *Scientific Assessment of Ozone Depletion: 1998, Global Ozone Research and Monitoring Project—Report No. 44*, Geneva, Switzerland, 1999.
- WMO (World Meteorological Organization), *Scientific Assessment of Ozone Depletion: 2002, Global Ozone Research and Monitoring Project—Report No. 47*, Geneva, Switzerland, 2003.
- Yang, E.S., D.M. Cunnold, M.J. Newchurch, and R.J. Salawitch, Change in ozone trends at southern high latitudes, *Geophys. Res. Lett.*, *32*, L12812, doi: 10.1029/2004GL022296, 2005.
- Yang, E.S., D.M. Cunnold, R.J. Salawitch, M.P. McCormick, J.M. Russell III, J.M. Zawodny, S. Oltmans, and M.J. Newchurch, Attribution of recovery in lower-stratospheric ozone, *J. Geophys. Res.*, *111*, D17309, doi: 10.1029/2005JD006371, 2006.
- Zanis, P., E. Maillard, J. Staehelin, C. Zerefos, E. Kosmidis, K. Tourpali, and I. Wohltmann, On the turnaround of stratospheric ozone trends deduced from the reevaluated Umkehr record of Arosa, Switzerland, *J. Geophys. Res.*, *111*, D22307, doi:

GLOBAL OZONE

10.1029/2005JD006886, 2006.

- Zbinden, R.M., J.-P. Cammas, V. Thouret, P. Nedelec, F. Karcher, and P. Simon, Mid-latitude tropospheric ozone columns from the MOZAIC program: climatology and interannual variability, *Atmos. Chem. Phys.*, *6*, 1053-1073, 2006.
- Zhou, S., A.J. Miller, J. Wang, and J. Angell, Trends of NAO and AO and their associations with strato-

spheric processes, *Geophys. Res. Lett.*, *28* (21), 4107-4110, 2001.

- Ziemke, J.R., S. Chandra, and P.K. Bhartia, A 25-year data record of atmospheric ozone in the Pacific from Total Ozone Mapping Spectrometer (TOMS) cloud slicing: Implications for ozone trends in the stratosphere and troposphere, *J. Geophys. Res.*, *110*, D15105, doi: 10.1029/2004JD005687, 2005.

Appendix 3A

DESCRIPTION OF THE OZONE DATASETS

3A.1 Column Ozone Data

Ground-Based Data

Three types of ground-based instruments are used for long-term monitoring of total ozone content. Their characteristics and performance have been discussed in numerous WMO Assessments (e.g., WMO, 1995, 1999, 2003), and therefore only a brief description of new developments is provided here. The longest records of continuous reliable measurements are available from stations equipped with Dobson spectrophotometers. The first regular Dobson measurements started in the 1920s. The quality of total ozone data available from 17 Dobson sites prior to 1957 was assessed by Brönnimann et al. (2003a, b). About half of these pre-1957 datasets are reliable for analysis of total ozone variability; however, uncertainties in the absolute calibrations make all sets unsuitable for trend analysis. Several old Dobson records have been recently re-evaluated: from Tromsø, Norway, 1935-1972 (Hansen and Svenøe, 2005); Svalbard, Spitzbergen, Norway, 1950-1962 (Vogler et al., 2006); and Hradec Kralove, Czech Republic, 1962-2003. Griffin et al. (2006) reanalyzed datasets of 1953-1972 astronomical observations from Haute Provence, France, and Jungfrauoch, Switzerland, to calculate nightly column ozone. The retrieved values agree well with Arosa Dobson observations, but with a bias of 6-7%. The Brewer spectrophotometer was developed in the early 1980s (Kerr et al., 1981). There are now about 200 instruments installed around the world. They are regularly calibrated against a traveling standard. The traveling standard itself is calibrated against the set of three Brewer instruments located in Toronto and known as the Brewer Reference Triad (Fioletov et al., 2005). Small systematic differences between Dobson and Brewer total ozone measurements have been reported (Staehelin et al., 2003). Filter ozonometers are widely used in the former Soviet Union countries, and long-term reliable records are available from 1972 (Shalomyanskij et al., 2004). This instrument is less accurate than the Dobson and Brewer instruments, and the calibration is traceable to the Dobson reference. Dobson, Brewer, and filter ozonometer data are available from the World Ozone and UV Data Centre (WOUDC) at <http://www.woudc.org>. The ground-based dataset used in the Assessment is an updated version of the ground-based zonal mean dataset (Fioletov et al., 2002).

Total Ozone Mapping Spectrometer (TOMS)

Data from a series of TOMS instruments (on Nimbus 7, Meteor 3, and Earth Probe) have been reprocessed using a new version 8 algorithm (Bhartia, et al., 2004). The calibration was reviewed and updated during this process to be consistent from instrument to instrument. The TOMS version 8 algorithm uses a more detailed, improved a priori in the retrieval. The Nimbus 7 TOMS calibration has a slightly different time dependence than in version 7 because of a reassessment of how to handle the uncertainties in noise when TOMS started exhibiting occasional chopper non-synchronization effects in the mid-1980s. The Earth Probe TOMS data began to have a scan-mirror problem starting in about year 2000 that could not be corrected. The data should probably not be used for trend determination beyond year 2000. By 2002, there were latitude-dependent errors of 4% to 10%. TOMS data prior to July 1999 were included in the Merged satellite dataset described below. Data are available from the TOMS web site at <http://toms.gsfc.nasa.gov/>.

Backscatter Ultraviolet (BUV)

The BUV instrument launched on Nimbus 4 in April of 1970 provided the first global measurements of ozone from space (Stolarski et al., 1997). Data from this instrument are valuable for extending the satellite data record into the pre-ozone depletion period. Data from 1970 through 1972 provide good global coverage, but thereafter coverage is more sparse after the partial failure of the solar power array. Data from BUV were recently processed through the latest (version 8) SBUV algorithm (Bhartia et al., 2004). The calibration of BUV has always been questionable because of very rapid degradation of its solar diffuser plate. For the recent reprocessing, Umkehr data were used to establish the basic long-term calibration. The soft calibration techniques that were developed to calibrate SBUV instruments were used to establish the absolute accuracy of BUV. Comparison with Dobson data from that period shows that the resulting data were reasonably well calibrated.

GLOBAL OZONE

Solar Backscatter Ultraviolet (SBUV, SBUV/2)

The SBUV data have also been reprocessed using a new profile retrieval algorithm (Bhartia et al., 2004). This one is also designated version 8, and while there are some similarities, it is not the same algorithm as used for TOMS. The SBUV algorithm, in contrast to TOMS, now has a time-independent a priori to remove the possibility that a trend in the a priori could contribute to the deduced trend in ozone. The calibrations for the SBUV instrument on Nimbus 7 and for the SBUV/2 instruments on the sequence of NOAA satellites (9, 11, 14, 16, 17, and 18) have now been put on a consistent scale. The data for upper stratosphere profile can now be used for trend analyses directly without adjustment (though with some associated uncertainties). Data are available from <http://www.cpc.ncep.noaa.gov/products/stratosphere/sbuv2to>. The observational data used for this Assessment are zonally averaged, integrated vertical profile SBUV/2 data (version 8) from the period from 1979 to 2005 (updated from Miller et al., 2002).

Global Ozone Monitoring Experiment (GOME)

The GOME on board the European Space Agency's ERS-2 satellite is the first European experiment dedicated to global ozone measurements (Burrows et al., 1999). ERS-2 was launched in April 1995. GOME has been operational since June 1995, but spatial coverage has been limited since July 2003 due to problems with tape storage on ERS-2. GOME measures the backscattered radiances from 240-790 nm in the nadir-viewing geometry. In the relevant region for total ozone retrieval (320-340 nm), the spectral resolution is about 0.17 nm. The maximum scan width in the nadir is 960 km across track on the ground and global coverage is achieved within three days.

Three algorithms were developed for GOME applications in 2003 and used to reprocess the GOME total ozone data. These algorithms are all based on the DOAS (Differential Optical Absorption Spectroscopy) technique. They are (1) the WFDOS algorithm (Coldewey-Egbers et al., 2005; Weber et al., 2005; <http://www.iup.uni-bremen.de/gome/wfdoas/>); (2) the TOGOMI/TOSOMI algorithm (Eskes et al., 2005; <http://www.temis.nl/protocols/O3total.html>); and (3) the GDOAS algorithm (Van Roozendaal et al., 2006; <http://wdc.dlr.de/sensors/gome/gdp4.html>). For all three algorithms, retrieved GOME total ozone show excellent agreement with each other and with ground-based Brewer and Dobson measurements at midlatitudes, so only one GOME dataset is shown in Figures 3-2, 3-3, 3-4, and 3-5 (WFDOS version 1 algorithm).

Merged TOMS+SBUV/2

The merged dataset consists of monthly-mean zonal and gridded average datasets constructed by merging individual TOMS and SBUV/2 satellite datasets (Frith et al., 2004). An external calibration adjustment has been applied to each satellite dataset in an effort to calibrate all the instruments to a common standard. All data in the present version of the merged dataset have been derived using the TOMS version 8 and SBUV version 8 algorithms. A recent manuscript (Stolarski and Frith, 2006) evaluates the instrument record uncertainty for one of these datasets and shows that the variations among them are within the uncertainties. For this Assessment, SBUV total ozone data are also included in the merged dataset without any adjustments. There are inherent uncertainties in the possible drift of each instrument and in the offset of overlapping instruments. For the merged dataset, Stolarski and Frith (2006) estimated an overall drift uncertainty of a little more than 1%/decade due to instrument effects. This corresponds to about 8 DU over the 25-year period of the measurements. The data, and information about how they were constructed, can be found at http://hyperion.gsfc.nasa.gov/Data_services/merged/mod_data.public.html.

National Institute of Water and Atmospheric Research (NIWA) Assimilated Dataset

The assimilated database combines satellite-based ozone measurements from 4 Total Ozone Mapping Spectrometer (TOMS) instruments, 3 different retrievals from the Global Ozone Monitoring Experiment (GOME), and data from 4 Solar Backscatter Ultraviolet (SBUV) instruments (Bodeker et al., 2005). The dataset used in this analysis is an update and extension of the homogenized total column ozone dataset developed by Bodeker et al. (2001). Specific changes include: version 8 Nimbus 7 and Earth Probe TOMS data are used rather than version 7 (<http://toms.gsfc.nasa.gov/>). GOME data from the European Space Agency (ESA) are updated from version 2.4 (used in Bodeker et al., 2001) to version 3.1. Assimilated total column ozone fields from the Royal Netherlands Meteorological Institute (KNMI) (<http://www.knmi.nl/goa>) based on GOME measurements are included. Total column ozone fields from the KNMI total ozone algorithm from GOME using the Ozone Monitoring Instrument algorithm (<http://www.temis.nl/protocols/O3total.html>) are included. Version 8 SBUV (Solar Backscatter Ultraviolet) data from the NASA Nimbus 7, NOAA 9, NOAA 11, and NOAA 16 satellites (<http://www.cpc.ncep.noaa.gov/products/stratosphere/sbuv2to/>) are included. The analysis period is extended to the end of 2004.

3A.2 Ozone Profile Measurements

Stratospheric Aerosol and Gas Experiment (SAGE)

The SAGE measurement technique (McCormick et al., 1989) is based on solar occultation, with ozone profile measurements obtained at sunrise and sunset on each of 14 orbits per day. This technique provides high vertical resolution (~1 km) and very small long-term drifts resulting from instrument calibration. However, spatial sampling is limited, and it takes approximately one month to sample the latitude range 60°N to 60°S. SAGE I ozone profile data cover the time period February 1979 to November 1981. A difficulty in combining the SAGE I and SAGE II data for trend studies arises from an apparent error in the reference altitude for SAGE I. An empirical altitude correction has been applied to the SAGE I data in an attempt to remove this bias (Wang et al., 1996). SAGE II ozone profile data commenced in November 1984 and the science mission ended in August 2005. The analysis here used SAGE II version 6.2 (v6.2), which was released in its entirety in September 2005. In mid-2000, SAGE II experienced a failure of the azimuth gimbal in the pointing system. After an approximate two-month interruption in science data gathering, normal science operation resumed at a reduced duty-cycle. The failure precluded the ability to take both sunrise and sunset observations on each orbit. Events of only one type occur in blocks of approximately 35 days. The event type switched from one type to the other after each spacecraft yaw-maneuver (performed in order to maintain proper illumination of the spacecraft's fixed solar panels). The spatial and temporal sampling in the reduced mode of operation does not introduce any new significant gaps or biases in the latitudinal and seasonal coverage. The species profiles have a vertical resolution of 1 km or better and are placed on a 0.5 km altitude grid. The species separation and inversion in v6.2 is similar to that used in v6.1 (the basis for the SAGE II ozone data in WMO (2003)), but v6.2 incorporates an improved spectral characterization of the 940 nm channel optical properties that results in significantly improved water vapor retrievals. In general, the ozone results are of good quality down to the tropopause. As in previous Assessments, the data analyzed here exclude time periods of enhanced aerosol extinction following the eruption of Mt. Pinatubo in June 1991. A small percentage of SAGE II data is affected by errors caused by interference from aerosol (including stratospheric aerosol from major volcanic eruptions), clouds, and other, not always known, factors and should be removed (Rind et al., 2005). The data are available from <http://eosweb.larc.nasa.gov/>.

Solar Backscatter Ultraviolet (SBUV, SBUV/2)

The SBUV/2 instrument is a scanning double monochromator measuring backscattered solar radiation in 12 discrete wavelength bands ranging from 252.0 to 339.8 nm. In previous SBUV algorithms, total column ozone was retrieved using the longest 4 wavelengths, and then a profile was retrieved using the shortest 8 wavelengths. In the version 8 algorithm released in 2004, an ozone profile is retrieved using all 12 wavelengths, and total column ozone is the integral of the profile (Bhartia et al., 2004). The version 8 algorithm is optimized to provide a self-consistent long-term ozone record. The SBUV(2) satellite data used here are reprocessed with the version 8 algorithm and are available at <http://daac.gsfc.nasa.gov/data/dataset/TOMS/DVD-ROMs> and from <http://www.cpc.ncep.noaa.gov/products/stratosphere/sbuv2to>. The data are available as column ozone in Dobson units (DU) for 13 layers, each 3.2 km thick except for Layer 1, which is about 18 km in depth, and as ozone mixing ratios at 15 levels. To avoid errors related to volcanic aerosols, it is recommended to exclude from the analysis data between 40°S and 40°N for the 1-year periods following the major volcanic eruptions in 1982 and 1991 (SPARC, 1998). Results of SBUV(2) ozone profile comparisons with other data sources are discussed by Petropavlovskikh, et al. (2005a), Nazaryan and McCormick (2005), Fioletov et al. (2006), and Terao and Logan (2006). Combined datasets are now becoming available for profile data. Stolarski and Frith have put together the SBUV series from the version 8 results (http://hyperion.gsfc.nasa.gov/Data_services/merged/mod_data.public.html). Brunner et al. (2006) reconstructed the vertical ozone distribution in equivalent latitude coordinates.

Ozonesonde Data

A network of stations provides ozone profile information from balloonborne sondes, which measure ozone from the ground to about 33 km, with a vertical resolution of ~150 m. Details of ozonesonde measurements and data processing are discussed in SPARC (1998). Data are available from the WMO World Ozone and UV Data Centre (WOUDC) (<http://www.woudc.org>). Data from many sonde stations are normalized to the overhead ozone column measured on the same day by a Dobson or Brewer instrument. The normalizing factor (called the correction factor) is commonly used to screen the data, as described in Logan et al. (1999). Data are available from about 1970 for stations in North America, Europe, and Japan. The European stations make measurements 2-3 times a week, while other stations make weekly

GLOBAL OZONE

measurements. The long-term records from Payerne and Uccle have been reprocessed since the SPARC (1998) assessment, and the Japanese sonde data since 1994 are now available with much higher vertical resolution than previously.

Umkehr Data

The Umkehr technique is used to derive the vertical distribution of ozone from ground-based measurements of zenith sky radiation. The method is based on principles of differential absorption of solar UV light by atmospheric ozone and molecular scattering. The ratio of zenith blue sky radiation at two UV wavelengths is measured over a range of solar zenith angles between 60° and 90°. A representative total ozone measurement is required as part of the data input. The resulting profile is reported as mean partial pressure values for ten pressure layers, where the pressure at the top of the layer is half of the pressure at the bottom of the layer, and layer 10 contains ozone integrated above the ~1 hPa pressure level. The analysis is based on a climatological first guess and an iterative solution is reached. The dependence of Umkehr retrievals on a priori information becomes a serious issue for trend analysis. (Dütsch and Staehelin, 1992; Mateer et al., 1996). In the presently used operational UMK92 algorithm, the a priori profiles are constructed using total ozone column measured by the same instrument. This makes it difficult to ascertain whether the retrieved long-term changes are forced by a priori or whether they reflect information contained in the measurements. The new UMK04 algorithm includes revised a priori profiles based on the new ozone climatology (McPeters et al., 2003) that vary with season and latitude, but have no day-to-day or long-term variability. It also uses new look-up tables and an improved forward model. In addition, the impacts of both algorithm smoothing and measurement errors on the retrieved ozone profiles have been further optimized (Petrovavlovskikh et al., 2005a, b). The overall accuracy of the Umkehr method (1σ) is estimated to be $\pm 25\%$ for the troposphere (layers 0 and 1), $\pm 15\%$ for low stratosphere (layers 3 and 2), less than $\pm 10\%$ for the middle stratosphere (layers 4 to 6), less than $\pm 10\%$ for the upper stratosphere (layers 7 and 8), and errors slightly increase in ozone integrated above layer 7. The algorithm description and the data are available at <http://www.srrb.noaa.gov/research/umkehr/>. Zanis et al. (2006) described re-evaluation of the 1956-2003 Umkehr series from Arosa, Switzerland. The vertical profiles of ozone trends from Umkehr data shown in Figure 3-8 are the average of trends derived from measurements at Arosa (1979-2004), Haute-Provence (1984-2004), Boulder (1979-2004), and Belsk (1979-2004), processed with the new UMK04 algorithm.

Lidar Data

The Differential Absorption Lidar (DIAL) ozone measurement technique retrieves the vertical profile of ozone absorption by comparing atmospheric return at two UV wavelengths, one absorbed by ozone (usually 308 nm) and one much less absorbed (353 or 355 nm) (Donovan et al., 1997; Guirlet et al., 2000; Leblanc and McDermid, 2000, 2001; Godin et al., 2001, 2002). The DIAL method is differential in wavelength and altitude, which makes it self-calibrating and ideally suitable for long-term routine measurements. Altitude resolution of the measurements ranges from 1 km (below 30 km) to 5 km (at 45-50 km), and the altitude range is typically from 15 to 45-50 km, with accuracies of approximately 3% below 35 km and 10% above 40 km. Observations are made during clear nights. High quality, continuous time series are available since the late 1980s (Keckhut et al., 2005b). The data are available from the Network for the Detection of Atmospheric Composition Change (NDACC) site at <http://www.ndacc.org/>.

Microwave Ozone Measurements

The method is based on measurements of microwave thermal radiation in the ~100-200 GHz range, emitted by ozone and measured at high spectral resolution. As the observed emission line is broadened by pressure, information about the vertical distribution of ozone in the atmosphere can be retrieved from the measured spectra by means of an inversion algorithm. Individual rotational spectral lines with frequencies most often either 100 or 142 GHz, are used. A review of the methodology and instrumentation used for ozone observations in the microwave frequency range is given, for example, in Parrish (1994) and Clancy and Muhleman (1993). Ground-based microwave radiometers allow unattended, continuous observations of the atmosphere that are nearly independent of weather conditions. A vertical resolution is typically ~10 km and the temporal resolution is 1-2 hours. The altitude range is typically 20-70 km, with accuracies of ~5%. High quality, continuous time series are available since 1992 (Tsou et al., 2000; Klein et al., 2002; Calisesi et al., 2003; Nagahama et al., 2003; Ricaud et al., 2004). The data are available from the NDACC site at <http://www.ndacc.org/>.

CHAPTER 4

Polar Ozone: Past and Present

Lead Authors:

P.A. Newman

M. Rex

Coauthors:

P.O. Canziani

K.S. Carslaw

K. Drdla

S. Godin-Beekmann

D.M. Golden

C.H. Jackman

K. Kreher

U. Langematz

R. Müller

H. Nakane

Y.J. Orsolini

R.J. Salawitch

M.L. Santee

M. von Hobe

S. Yoden

Contributors:

G.E. Bodeker

K. Frieler

F. Goutail

M. López-Puertas

G.L. Manney

E.R. Nash

C.E. Randall

H.J. Singer

C.S. Singleton

R.M. Stimpfle

S. Tilmes

M. Weber

Final Release: February 2007

From *Scientific Assessment of Ozone Depletion: 2006*

CHAPTER 4

POLAR OZONE: PAST AND PRESENT

Contents

SCIENTIFIC SUMMARY	4.1
4.0 INTRODUCTION	4.3
4.1 POLAR STRATOSPHERIC OBSERVATIONS UPDATE	4.4
4.1.1 Polar Stratospheric Dynamics and Transport	4.4
4.1.1.1 Temperatures and PSC Formation Potential	4.4
4.1.1.2 Vortex Parameters	4.7
4.1.1.3 Transport	4.9
4.1.2 Polar Ozone	4.11
4.1.2.1 Ozone and Other Constituents	4.11
4.1.2.2 Polar Ozone Loss Studies	4.14
4.2 PROGRESS IN OUR UNDERSTANDING OF THE PHYSICAL AND CHEMICAL PROCESSES	4.20
4.2.1 Polar Ozone Chemistry	4.20
4.2.1.1 Chlorine	4.21
4.2.1.2 Bromine	4.24
4.2.1.3 Ozone Loss Rates	4.25
4.2.2 PSC Processes	4.28
4.3 RECENT POLAR OZONE CHANGES	4.30
4.3.1 2002 Antarctic Ozone Hole	4.30
4.3.1.1 Observations	4.30
4.3.1.2 Modeling of the Warming	4.31
4.3.1.3 Theoretical Understanding	4.33
4.3.2 Is Polar Ozone Getting Worse?	4.34
4.3.2.1 Arctic	4.34
4.3.2.2 Antarctic	4.34
4.4 THE INFLUENCE OF PRECIPITATING CHARGED PARTICLES ON POLAR OZONE	4.35
4.4.1 Odd Nitrogen (NO _y) Enhancements	4.36
4.4.2 Ozone Decreases	4.37
REFERENCES	4.37

SCIENTIFIC SUMMARY

Arctic

- **Arctic spring total ozone values over the last decade were lower than values observed in the 1980s. In addition, spring Arctic ozone is highly variable depending on dynamical conditions.** For current halogen levels, anthropogenic chemical loss and variability in ozone transport are about equally important for year-to-year Arctic ozone variability. Colder-than-average vortex conditions result in larger halogen-driven chemical ozone losses. Variability of temperatures and ozone transport are correlated because they are both driven by dynamic variability.
- **For the coldest Arctic winters, the volume of air with temperatures low enough to support polar stratospheric clouds (V_{PSC}) increased significantly since the late 1960s.** This change of climate conditions is much larger than expected from the direct radiative effect of increasing greenhouse gas concentrations. The reason for the change is not clear and it could be due to long-term natural variability or an unknown dynamical mechanism.
- **Column ozone loss in the 2004/2005 Arctic winter was among the largest ever observed.** The 2004/2005 Arctic stratosphere was exceptionally cold, particularly below 18 kilometers (km), leading to a value of V_{PSC} 25% larger than the previous record value. Various independent studies and methods suggest that the chemical column ozone loss in 2004/2005 was among the largest ever observed. However, dynamical processes resulted in March-average Arctic total ozone amounts being comparable to those in other recent winters, while the large losses contributed to low total column ozone over parts of Europe during March 2005.

Antarctic

- **Over the last decade (1995-2005), Antarctic ozone depletion has stabilized.** Most ozone hole diagnostics show a leveling off after the mid-1990s. Saturation of ozone loss inside the ozone hole due to complete ozone destruction over a broad vertical layer plays a role in this leveling off. Ozone hole area, ozone mass deficit, and higher minimum column amounts were observed to be below average in some recent winter years. These improvements in the ozone hole resulted from higher levels of dynamical forcing, and not decreases in equivalent effective stratospheric chlorine levels.
- **In September 2002, the first ever observed Antarctic major stratospheric warming occurred. This early-spring warming caused a drastic reduction of the ozone hole area and resulted in a less severe ozone hole.** This warming resulted from anomalously strong dynamical wave activity in the Southern Hemisphere. The triggers of these very unusual waves are unknown, and it is not clear whether the 2002 warming is a random event due to internal atmospheric variability or whether it can be related to long-term changes in climate. The Antarctic winter 2004 was also dynamically very active and had less ozone mass deficit than previous years. The higher levels of ozone in these two years were dynamically driven and not related to halogen chemical reductions.

General

- **Large interannual variability in polar stratospheric temperatures complicates the interpretation of trends.** Previously reported estimates of temperature trends in polar regions have differed from assessment to assessment. It now is evident that trends determined over a time scale of one to two decades, though they may appear statistically significant, are not robust because of large interannual and decadal variability in observed temperatures. Therefore, changes in reported trends do not necessarily indicate systematic changes in physical or chemical processes.
- **There are indications that the chlorine monoxide (ClO) dimer cycle may be a more efficient process for polar ozone loss than previously thought.** Uncertainties in the laboratory absorption cross section of the chlorine

POLAR OZONE

monoxide dimer (ClOOCl) are large. Good overall consistency between in situ observations of ClO and the ClOOCl and model calculations can be achieved if it is assumed that ClOOCl photolyzes faster than assumed in the previous Assessment. Faster photolysis of ClOOCl, combined with recent laboratory studies indicating more rapid formation of ClOOCl by the ClO self-reaction, leads to more efficient ozone loss by this catalytic cycle.

- **Recent measurements suggest that bromine may play a more important role in polar ozone depletion than previously thought.** Profiles of bromine monoxide (BrO) measured in the Arctic vortex suggest that inorganic bromine levels may be 3 to 8 parts per trillion by volume larger than the amount of bromine carried to the stratosphere by methyl bromide (CH₃Br) and halons. This observation indicates the BrO + ClO cycle is likely to be a more efficient ozone loss process than considered in the previous Assessment. The BrO + ClO cycle is now estimated to contribute up to half of total chemical loss of polar ozone, even considering the more efficient ozone loss by the ClO dimer cycle. However, the polar stratospheric bromine budget is a significant source of uncertainty.
- **Calculated chemical loss rates of polar ozone substantially increased in models that assume: (1) more efficient ozone destruction by the ClO dimer cycle and (2) higher levels of bromine.** These changes improve the comparison between measured and modeled Arctic ozone loss rates for cold Januaries that was noted in the past Assessment. These two changes also improve the comparison between theory and observation of Antarctic ozone loss rates.
- **The chemical loss of column ozone for Arctic winters exhibits a near linear relation with V_{PSC} during each winter.** A similar relation between ozone loss and V_{PSC} is now seen for two independent analyses of chemical ozone loss, increasing our confidence in the robustness of this relation. Observations of the large Arctic ozone loss in 2004/2005 are in line with the relationship established for prior winters. The slope of this relation provides an empirical measure of the sensitivity of chemical loss of Arctic ozone to changes in stratospheric temperature (for contemporary levels of chlorine and bromine) and provides an important metric for chemical transport models (CTMs) and coupled Chemistry-Climate Models (CCMs) that are used in both diagnostic and prognostic studies of polar ozone loss.
- **For the first time, measurements show unambiguously that nitric acid trihydrate (NAT) polar stratospheric cloud particles can nucleate above the ice frost point, and there is additional evidence of their widespread occurrence.** Widespread low number density NAT clouds can lead to denitrification and enhanced ozone loss. Incorporating NAT nucleation above the ice frost point into chemical transport models has improved denitrification simulations, but discrepancies in interannual variability remain, probably because the NAT nucleation mechanisms are not fully understood.
- **The most recent solar cycle was associated with frequent and exceptionally strong episodes of charged particle precipitation. This caused only small decreases in total column ozone in the polar region (<3%, <10 Dobson units).** However, the measured ozone reduction in the mid-to-upper stratosphere (30-50 km) exceeded 30% for weeks following certain episodes of intense particle precipitation.

4.0 INTRODUCTION

Since the discovery of the Antarctic ozone hole by Farman et al. (1985), considerable effort has been focused on observing these ozone losses, understanding the chemical, dynamical, and radiative processes, and predicting the future of polar ozone. This chapter builds upon a sequence of polar ozone chapters in the World Meteorological Organization (WMO) Assessment series.

The first publication of large Antarctic ozone losses by Farman et al. (1985) sparked scattered discussion of polar ozone in the 1985 Ozone Assessment (WMO, 1986). Chapter 14 of that Assessment (Ozone and Temperature Trends) showed the Farman et al. (1985) results and included Total Ozone Mapping Spectrometer (TOMS) total ozone images (subsequently published in Stolarski et al., 1986). These early satellite data confirmed the findings of Farman et al. and moreover displayed the horizontal dimensions of the ozone hole. The Ozone Trends Panel's 1988 report (WMO, 1990a) followed with an entire chapter on Antarctic ozone (Chapter 11) including an extensive discussion of both Antarctic observations and of the three competing theories of the ozone hole that were proposed originally in the mid-1980s. In particular, this WMO (1990a) chapter focused on (1) the drastic reduction in nitrogen dioxide (NO_2) abundance resulting from the formation of polar stratospheric clouds (PSC) consisting of nitric acid trihydrate (NAT) (Crutzen and Arnold, 1986; Toon et al., 1986), (2) the conversion of hydrogen chloride (HCl) and chlorine nitrate (ClONO_2) to active chlorine on PSC surfaces as a mechanism for freeing chlorine from reservoir species into radical species (McElroy et al., 1986; Solomon et al., 1986), (3) the two catalytic cycles involving chlorine monoxide (ClO) and bromine monoxide (BrO) that destroy Antarctic ozone (McElroy et al., 1986; Molina and Molina, 1987), and (4) observations from field campaigns that supported the theory that the ozone hole is caused by elevated ClO and BrO levels in the lower stratosphere from human-produced chlorofluorocarbons and halons (de Zafra et al., 1987; P. Solomon et al., 1987; S. Solomon et al., 1987; Farmer et al., 1987). This WMO (1990a) polar ozone chapter also discussed in situ observations of ClO and BrO (subsequently published in Brune et al., 1989a; Brune et al., 1989b; Anderson et al., 1989). The 1989 Ozone Assessment (WMO, 1990b) included a chapter on polar ozone (Chapter 1) that presented extensive observations from field campaigns that overwhelmingly established human-produced chlorine and bromine chemicals as responsible for the ozone hole. The 1991 Ozone Assessment (WMO, 1992) did not include a specific chapter on polar ozone, but it updated polar ozone science in various sections of the report. WMO (1995) included a Polar Processes chapter (Chapter 3) that confirmed chlorine- and

bromine-catalyzed ozone loss in the Antarctic and the Arctic from both in situ (Anderson et al., 1991; Toohey et al., 1993) and satellite observations (Waters et al., 1993). WMO (1999) included a chapter on lower stratospheric processes (Chapter 7), noting a number of very low Arctic ozone years and stating that the Antarctic ozone losses were continuing.

This chapter provides an update to Chapter 3 of the WMO (2003) Assessment on Polar Ozone: Past, Present, and Future. This chapter is derived from research over the last 4 years, other reports, and recent and updated observations from various field campaigns and new satellite instrumentation. Discussion of the recovery of polar ozone can be found in Chapter 6 (The Ozone Layer in the 21st Century), and polar chemistry-climate interactions can be found in Chapter 5 (Climate-Ozone Connections).

The WMO (2003) polar ozone chapter reported that in the Antarctic, springtime ozone depletion has been large throughout the 1990s, and that the area of the ozone hole varies from one year to another, but that it was not yet possible to say whether the area of the ozone hole had maximized. It was also reported that the polar vortex and ozone hole were persisting into early summer, increasing the impact on ultraviolet radiation.

In the Arctic, the WMO (2003) polar ozone chapter reported that there were a number of cold Arctic winters in the 1990s in which maximum total column ozone losses due to halogens had been quite large. In particular, Arctic chemical ozone loss for the 1999/2000 winter/spring season was extensively discussed, and an ozone loss was observed that reached 70% near 20 kilometers (km) by early spring, and total column ozone losses greater than 80 Dobson units (DU) (~20 to 25%) by early spring. The large 1999/2000 ozone losses were a result of the colder than average stratospheric vortex, consistent with our understanding. It was also reported that the magnitude of chemical loss of ozone for all Arctic winters during the 1990s showed generally good agreement between different analyses for quantifying losses. For the 1999/2000 winter, agreement was better than 20% in the Arctic stratosphere around 20 km.

This chapter is divided into 4 basic sections. Section 1 provides an update of observations of polar stratospheric conditions. Section 2 provides an update of theoretical progress on understanding polar ozone processes. Section 2 is divided into subsections on chemical processes and polar stratospheric clouds and aerosols. Section 3 provides a discussion of our current observations and also a description of an unprecedented splitting of the ozone hole that was observed in September 2002 just prior to the publishing of WMO (2003). A number of large solar particle events have occurred in the last few years and they are described, together with their impacts, in Section 4.

POLAR OZONE

4.1 POLAR STRATOSPHERIC OBSERVATIONS UPDATE

4.1.1 Polar Stratospheric Dynamics and Transport

Variability in the dynamical conditions in the troposphere/stratosphere system results in variability of ozone transport and temperatures in the stratosphere. Previous Assessments and Section 4.2.1 of this document show that on short time scales, interannual variability in polar ozone chemistry is mainly driven by temperature variability, which in turn is the result of variable dynamical conditions. The combined effect of dynamically induced variability in both chemistry and transport is the main driver of interannual variability of the abundance of ozone in the polar stratosphere. This section gives an update of the dynamical conditions, temperatures, and transport of the polar winter stratosphere since the previous Assessment.

4.1.1.1 TEMPERATURES AND PSC FORMATION POTENTIAL

WMO (1999) and WMO (2003) have dealt at length with the observed temperature changes detected over the polar regions using observations (radiosondes and satellite sensors) as well as objective analysis products (e.g., Ramaswamy et al., 2001). During the period 1979-1998, satellite measurements showed a cooling of 3 K/decade in the Arctic and Antarctic middle stratosphere and significant coolings of 1.8 K/decade at 70°N and 1.1 K/decade at 70°S in the lower stratosphere during spring.

Following the mostly cold stratospheric winter and spring seasons of the early to mid-1990s, polar regions in both hemispheres were characterized by an alternation of cold and warm winter seasons since the late 1990s. As seen in Figure 4-1, Arctic lower stratospheric temperatures show considerable interannual variability. The variability is strongest during winter and spring due to the occurrence of midwinter and final sudden stratospheric warmings. Although several recent northern winters were cold (e.g., 1999/2000, 2002/2003, and in particular 2004/2005; see Figure 4-1), the northern winters 1998/1999, 2000/2001, 2001/2002, 2003/2004, and 2005/2006 were disturbed by stratospheric warmings and thus exhibited periods with high temperatures. In the Antarctic, interannual variability is much weaker than in the Arctic and is strongest during spring due to the timing of the Antarctic vortex breakup. In the Antarctic, an anomalously warm spring season was observed in 2002 (see Section 4.3.1), and relatively high temperatures also

occurred in the years 2000 and 2004 in the lower stratosphere (100 hPa) (see Figure 4-2).

Given the interannual variability of stratospheric temperatures in winter and spring, determining statistically significant trends requires both sufficient temporal and spatial coverage and a careful choice of the applied trend model. As discussed in Section 5.2.6 of Chapter 5, different temperature datasets are available to derive trends. All of them have their own advantages and limitations. Long-term stratospheric temperature trends (since the late 1950s) are usually derived from radiosonde measurements or radiosonde-based gridded datasets such as the United Kingdom Meteorological Office (UKMO) adjusted dataset (RAOB) or the Freie Universität Berlin (FUB) stratospheric analyses. Radiosonde limitations due to instrumental and other operational discontinuities could be eliminated by applying new adjustment methods, e.g., as in the radiosonde atmospheric temperature products for assessing climate (RATPAC) (Lanzante et al., 2003; Free et al., 2005) and Hadley Centre Radiosonde Temperature 2 (HadAT2) (Thorne et al., 2005) datasets. However, radiosonde data are biased toward Northern Hemisphere (NH) continental locations due to data scarcity in the Southern Hemisphere (SH) and over extended oceanic regions. Satellite data provide better spatial and altitude coverage than radiosondes, but are only available since 1979. Their vertical resolution is limited, and they have to be composed from different instruments to build continuous time series (see Section 5.2.6 of Chapter 5). Recent assessments of the uncertainties of radiosonde- and satellite-derived temperature trends revealed disagreement in the lower stratosphere, with an overestimation of the stratospheric cooling in the radiosonde data (Seidel et al., 2004). The bias was confined to the tropics, and thus polar temperature trends should not be affected (Randel and Wu, 2006).

Reanalysis products that result from the assimilation of radiosonde and satellite data provide an alternative source for long-term trend estimates. They are, however, affected by changes in the input data and the assimilation systems and therefore are not generally suited for trend estimates (Bengtsson et al., 2004; Santer et al., 2004). Labitzke and Kunze (2005) compared North Pole temperature trends for the lower and middle stratosphere derived from the National Centers for Environmental Prediction/National Center for Atmospheric Research (NCEP/NCAR) and European Centre for Medium-Range Weather Forecasts (ECMWF) Re-Analysis 40 (ERA40) reanalyses with those derived from subjective FUB stratospheric analyses that are closely matched to direct radiosonde measurements. They confirmed that largest discrepancies between ERA40 and FUB data exist during the winter months in

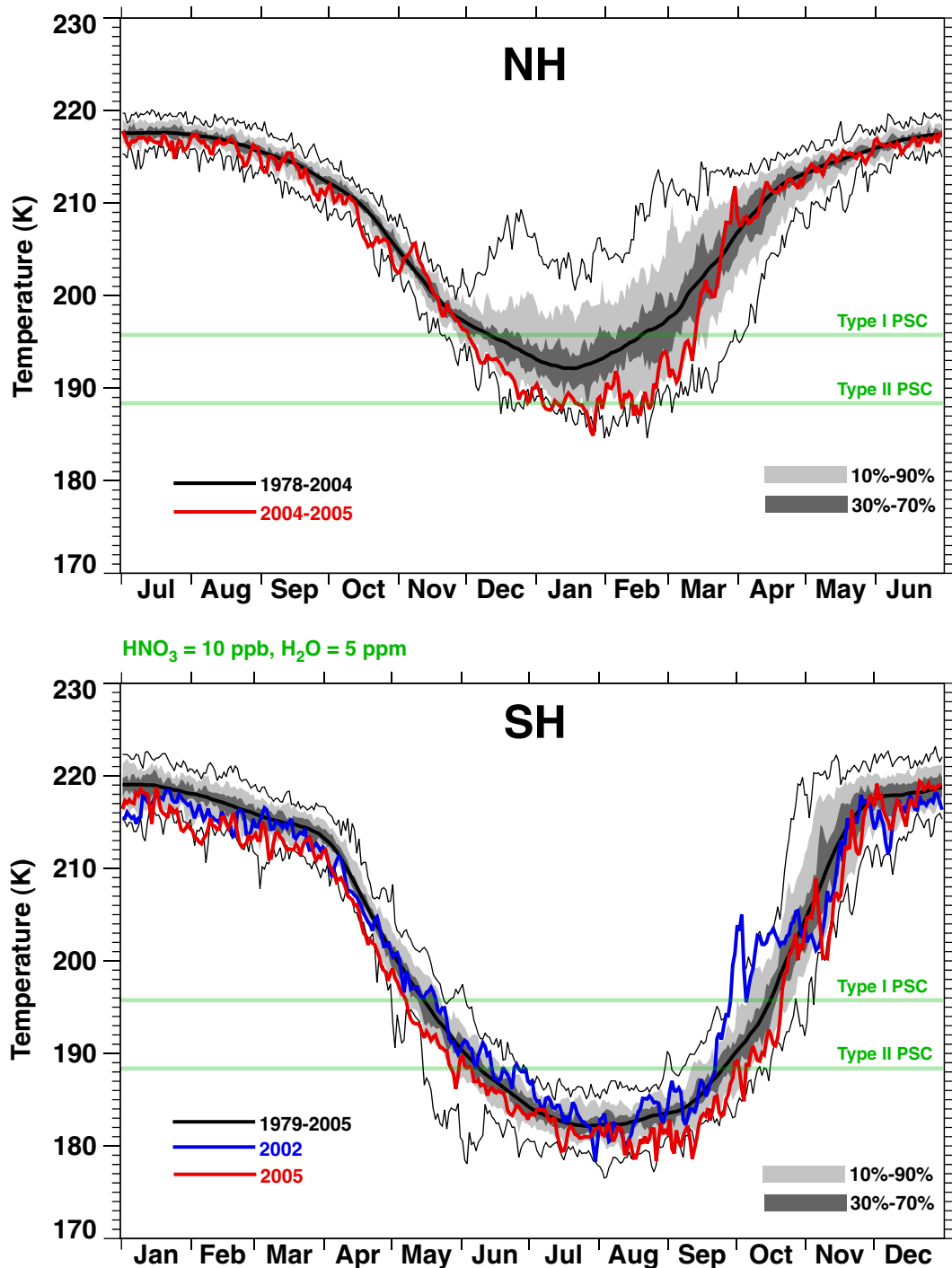


Figure 4-1. Annual temperature cycle and variability at 50 hPa for minimum temperature between 50°N and 90°N (top), and between 50°S and 90°S (bottom) from the National Centers for Environmental Prediction/National Center for Atmospheric Research (NCEP/NCAR) reanalysis data. The black line shows the mean annual cycle for the periods 1978-2004 (Northern Hemisphere, NH) and 1979-2005 (Southern Hemisphere, SH). The red line shows the evolution during 2004/2005 (NH) and 2005 (SH). In the case of the SH, the blue line shows the evolution during 2002, i.e., the year with the anomalous Antarctic vortex behavior. Dark gray shading shows the 30 to 70% probability of observations, light gray shading shows the 10 to 90% probabilities, and the lower and upper thin black lines show the record values for the 27 years of observations. Green lines indicate the thresholds for PSC formation (nitric acid (HNO₃) = 10 ppb and H₂O = 5 ppm). Updated from Figure 3-13 in WMO (2003).

POLAR OZONE

the middle stratosphere, when the enhanced cold polar bias of the pre-satellite era in ERA40 affects the long-term trends (1958-2001) (Bengtsson et al., 2004). The use of reanalyses for polar spring temperature trends is justified because the discrepancies between the ERA40, NCEP/NCAR, and FUB datasets are negligible.

Figure 4-2 shows spring stratospheric temperature trends derived from NCEP/NCAR reanalyses for the period 1958-2005 at the altitudes of maximum cooling for the Arctic polar cap (60°N-90°N) at 30 hPa in March (Figure 4-2a) and for the Antarctic polar cap (60°S-90°S) at 100 hPa in October (Figure 4-2b) (updated from Labitzke and Kunze, 2005). Post-volcanic periods (24 months) following the three eruptions of Mt. Agung in 1963, El Chichón in 1982, and Mt. Pinatubo in 1991 were excluded to avoid a contamination of the trend.

During the past 25 years, Arctic temperatures showed a clear downward trend of -1.70 ± 0.20 K/decade in March. Compared with the trend estimates for the period 1979-1998 (WMO, 2003) however, the magnitude of the stratospheric temperature trend in Arctic spring has decreased by about 50%. For the full period 1958-2005, only a very small, non-significant trend of -0.25 ± 0.20 K/decade can be detected due to a warming of the Arctic stratosphere during the 1960s and early 1970s (Figure 4-2a), which nearly compensates the cooling of the later decades. The dependence of the trends on the underlying time period demonstrates the strong impact of low-frequency dynamical variability on polar temperatures. Multidecadal time series are thus required to minimize the effect of low-frequency dynamical variability in trend calculations, in particular in the Arctic. This observational result is further supported by idealized model experiments (Nishizawa and Yoden, 2005).

In the Antarctic lower stratosphere (100 hPa), the cooling trend since the late 1970s is substantially smaller than that reported in WMO (2003) due to increased dynamical variability of the Antarctic polar vortex that led to unusually high spring temperatures of the polar cap in the years 2000, 2002, and 2004. Consistently, the temperature change in October between 1979 and 2005 is very small at 100 hPa (-0.23 ± 0.20 K/decade) (Figure 4-2b) and becomes even positive at higher altitudes ($+1.01 \pm 0.25$ K/decade at 50 hPa and $+2.02 \pm 0.24$ K/decade at 30 hPa). On the long-term scale, a small warming of 0.36 ± 0.18 K/decade occurred at 100 hPa.

As in Figure 4-2, long-term atmospheric changes are usually described in terms of linear trends per decade using multiyear time series, or the derivation of differences between averaged sub-periods, e.g., the temperature difference between 1990s and the 1970s. The magnitude and the statistical significance of the calculated changes in both methods strongly depend on the

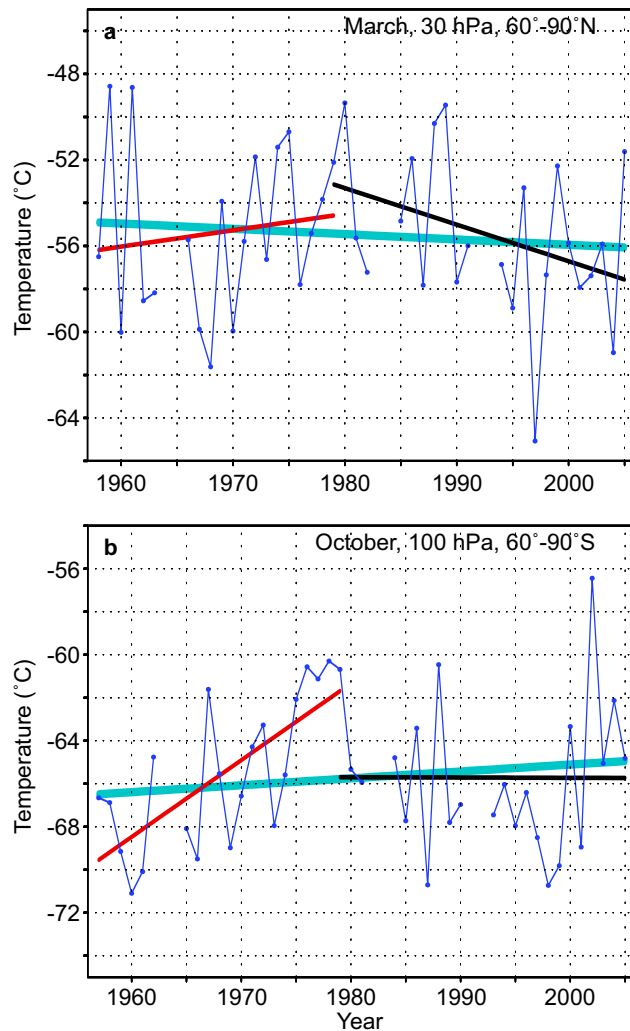


Figure 4-2. Arctic 30-hPa March (a) and Antarctic 100-hPa October (b) temperatures (°C) derived from the NCEP/NCAR reanalysis data. Trend lines were added for the periods 1958-1979 (red), 1979-2005 (black), and 1958-2005 (turquoise). Updated from Labitzke and Kunze (2005).

data period, as seen in Figure 4-2. For the purpose of understanding the nature of the observed changes, new statistical approaches were suggested in which trends may occur in flat or sloped steps including breakpoints with abrupt changes (Seidel and Lanzante, 2004) or the use of polynomials (Malanca et al., 2005). A comparison of the methods showed that a description of stratospheric cooling by a gradual linear change since the late 1950s (without considering the singular volcanic eruptions) is as equally valid as a description by a more step-like downward trend concentrated in the two-year periods after the three major volcanic eruptions (Seidel and Lanzante, 2004), which was also suggested by Pawson

et al. (1998). Climate model simulations suggest that the stratospheric cooling since 1979 was driven by anthropogenic factors (i.e., ozone depletion and increases in well-mixed greenhouse gases) but modulated by natural factors (i.e., solar variability and volcanic aerosols) (Ramaswamy et al., 2006).

In summary, the Arctic stratosphere has cooled over the past 27 years, however due to stronger dynamical variability in a number of recent winters and springs, the negative temperature trend is only about half the magnitude of the estimate in WMO (2003). In the Antarctic lower stratosphere, the cooling trend since the late 1970s has become less negative than that reported in WMO (2003) due to increased dynamical variability.

Estimating the overall trend of the polar stratospheric temperatures is not sufficient to assess the impact of long-term temperature changes on ozone chemistry. The large Arctic ozone losses are driven by the evolution of conditions during cold winters. Warm winters are much less relevant for ozone chemistry, because chemical loss of ozone is very limited and the chemistry is not very sensitive to small changes in temperature. Section 4.2.1 shows that the interannual variability in Arctic chemical ozone loss mainly follows the volume of temperatures cold enough to activate chlorine on particle surfaces (i.e., V_{PSC}). Figure 4-3 shows the long-term evolution of V_{PSC} derived from stratospheric temperature analyses for the Arctic (updated from Rex et al., 2004). Over the past 40 years, the cold Arctic winters became colder, resulting in larger values for V_{PSC} and chemical ozone loss. The long-term data shown in Figure 4-3 relies on the FU-Berlin subjective radiosonde analysis. Hence, the dataset is rel-

atively independent of the introduction of satellite observations or assimilation system changes (e.g., Manney et al., 2003b). A linear fit through the solid points in Figure 4-3, which represents maximum values of V_{PSC} for 5-year intervals, has a slope of $9.9 \pm 1.1 \times 10^6 \text{ km}^3$ per decade, with very similar results if 4- to 10-year intervals are chosen to select the maximum values (update of Rex et al., 2004). Rex et al. (2006) also have shown that it is unlikely (well below 1% probability) that this estimated tendency toward colder Arctic winters is a purely random event or is caused by inconsistencies in the meteorological datasets.

The tendency of decreasing temperatures during cold winters is in contrast to the clustering of a series of warmer than average winters during recent years. Hence, the temperature trend during the cold winters is different from the overall temperature trend. The change in temperature during the cold winters is much larger than expected from the direct radiative effect of increasing greenhouse gas concentrations. The reason for the change is not clear and it could be due to long-term natural climate variability or an unknown dynamical feedback mechanism.

4.1.1.2 VORTEX PARAMETERS

The mean structure and seasonal evolution of the polar vortices and their hemispheric differences were discussed in detail in WMO (2003). The Arctic polar vortex is much more perturbed by planetary wave activity propagating upward from the troposphere than the Antarctic vortex. It is important to assess such dynamical variations and their changes as they determine, together with

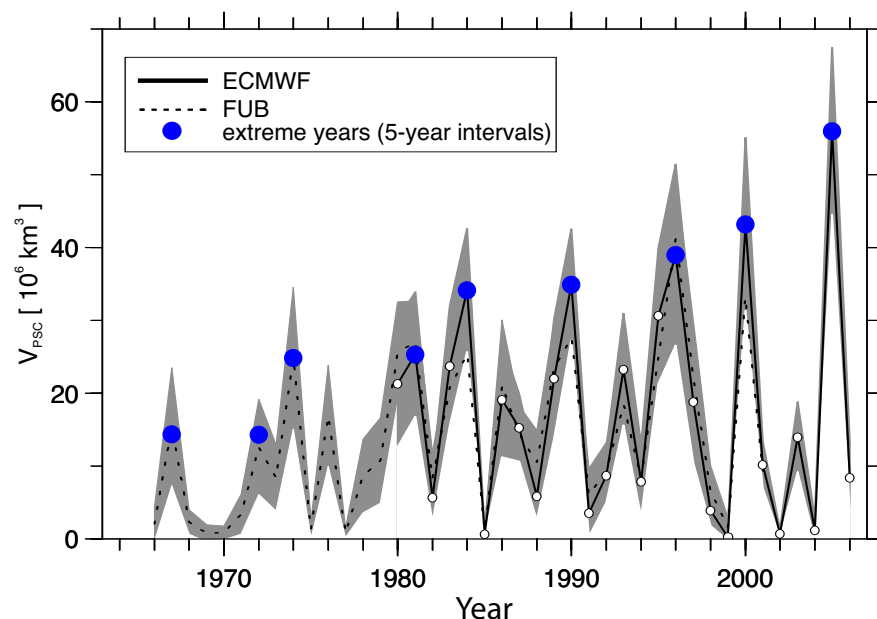


Figure 4-3. Evolution of V_{PSC} for the Arctic over the past four decades, composed from ECMWF and FUB data. The blue dots represent the maximum values of V_{PSC} during five-year intervals. The dotted line is based on radiosonde analyses of the FUB, and the solid line is ECMWF ERA-15 data extended by operational analyses. The gray shading represents the uncertainty of V_{PSC} based on a 1-K uncertainty of the long-term stability of radiosonde temperatures. Updated from Rex et al. (2004).

POLAR OZONE

chemical processes, the ozone column at polar latitudes during spring (Randel et al., 2002; Huck et al., 2005).

The breakup dates of the Arctic and Antarctic vortices (Figure 4-4) as determined by the wind average along the vortex edge vary from year to year in both hemispheres (WMO, 2003). For the Arctic vortex, no discernible long-term trend in the breakup date appears since the 1960s (Langematz and Kunze, 2006). The period between the mid-1980s to the mid-1990s however showed a tendency toward later breakdown dates. These years were characterized by a reduced dynamical variability, with nine consecutive winters without major stratospheric warmings from 1989/1990 to 1997/1998 (Labitzke et al., 2002; Manney et al., 2005c). In contrast, since 1998/1999, the Arctic exhibited a clustering of warmer than average and dynamically disturbed winters. Major warmings took place in the winters 1998/1999, 2000/2001, 2001/2002, 2002/2003, 2003/2004 and 2005/2006, leading to weak or split vortices. Consistent with these changes in dynamical variability, the vortex breakup date varied between mid-February 2001 and early May 1997, with three late breakups since 2002. However, this recent delay in the breakup date is not statistically significant and does not indicate a trend (Langematz and Kunze, 2006). The described alternation of cold (1989/1990-1997/1998) and warm (1998/1999-2005/2006) clusters may be interpreted as shifts between warmer/weaker and colder/stronger vortex regimes (Perlwitz and Graf, 2001; Perlwitz and Harnik, 2003). These shifts may be caused by anthropogenic processes (i.e., ozone depletion and greenhouse gases) that nonlinearly force natural modes of variability (Corti et al., 1999; Pawson et al., 1998; Christiansen, 2003). Such a clustering also could be a random occurrence, as shown in model simulations by Taguchi and Yoden (2002).

The Antarctic vortex exhibited a delay of the breakup date from late November into mid-December which is consistent with an intensification of the vortex (Huth and Canziani, 2003; Renwick, 2004) caused by additional radiative cooling following strong Antarctic ozone loss in spring (Shine, 1986; Jones and Shanklin, 1995). However, since the late 1990s, there is larger variability in the breakup date over Antarctica with the process taking place sometime between the second half of November (1997, 2000, and 2002) and late December (1999, 2001). The tendency toward a later vortex breakup date has stopped and perhaps reversed (Langematz and Kunze, 2006). This means that, compared with the 1960s and 1970s, the Antarctic vortex is still more persistent; however, compared with the 1980s/early 1990s, the Antarctic vortex broke down earlier in recent years. This is probably the result of the large interannual variability in recent Antarctic winters and springs (see Section 4.1.2).

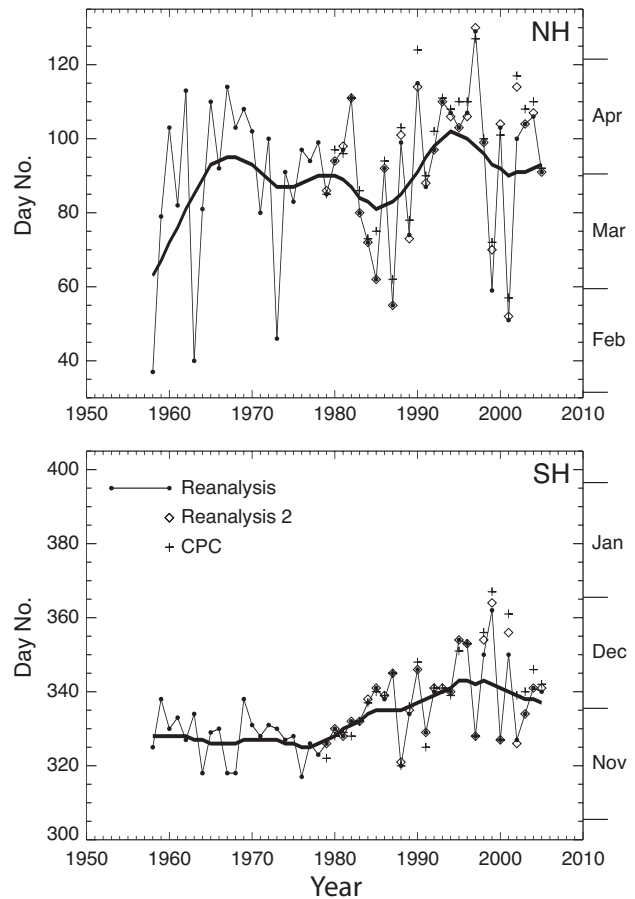


Figure 4-4. Vortex breakup dates from 1958 to 2005 on the 500-K isentropic surface over the NH (top) and the SH (bottom) using the method described in Nash et al. (1996). The filled lines with dots are the dates calculated from the NCEP/NCAR reanalysis data. The thick lines are the same data, time-filtered to remove interannual fluctuations. The crosses are the breakup dates calculated from NCEP/Climate Prediction Center analyses for the period 1979-2005. Updated from Figure 3-10, WMO (2003).

Summing up, since the previous Assessment (WMO, 2003) changes in the interannual behavior of both polar vortices have been observed. The Arctic vortex continues to show large variability with a shift from a period of dynamically undisturbed winters between 1989/1990 and 1997/1998 to a period of more dynamically disturbed winters from 1998/1999 to 2005/2006. The Antarctic vortex has shown an enhanced variability since the late 1990s compared with previous decades, which culminated in the anomalous vortex split in 2002. The reasons for the observed changes in the interannual variability in both hemispheres are not yet understood.

4.1.1.3 TRANSPORT

Besides chemistry, transport is the main driver for ozone variability at high latitudes. Chemical and transport-related causes for polar ozone variability are closely coupled, particularly in the Arctic. Transport contributions to polar ozone variability are closely controlled by the strength of the middle atmospheric residual circulation that, in turn, is driven by tropospheric (planetary and gravity) wave forcing; strong winter planetary wave forcing leads to larger transport of ozone to high latitudes due to a stronger residual circulation and a higher-than-average Arctic lower stratosphere temperature and a weaker vortex in early spring, whereas weak winter forcing leads to less transport and lower Arctic temperatures in spring and to a stronger vortex (Fusco and Salby 1999; Newman et al., 2001). For the Arctic, Rex et al. (2004) find that for the current halogen loading, about one-half of the year-to-year variability in total ozone is caused by variability in anthropogenic chemical ozone loss and one-half by variability in transport with the variable residual circulation. Because temperatures influence chemistry, both terms are correlated.

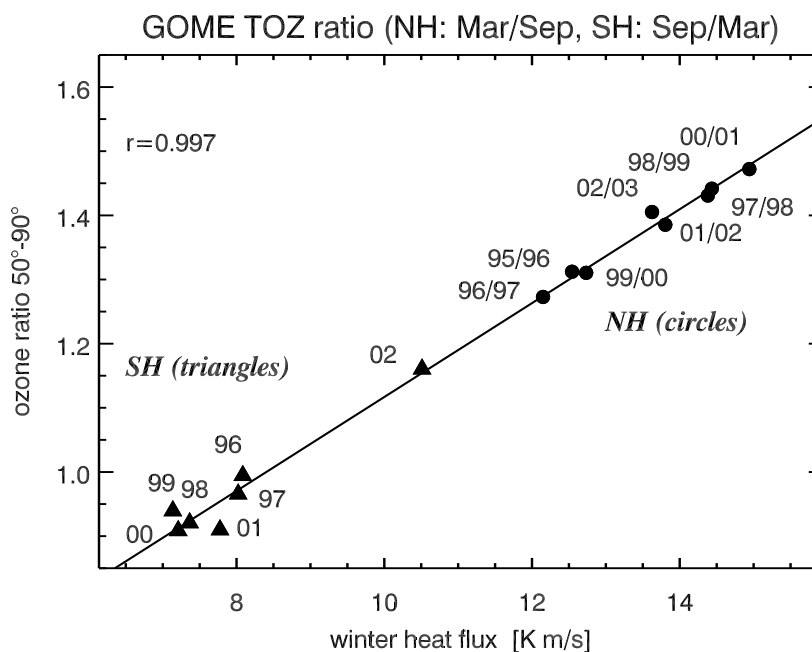
Although the variability is larger in the Arctic compared with the Antarctic, wave activity has been shown to correlate well with the observed change of polar column ozone over the course of winter for both hemispheres

(Randel et al., 2002; Weber et al., 2003; see also Figure 4-5). It has been shown that in the Antarctic, this is due to the same co-action of transport and chemistry as in the Arctic. Newman et al. (2004) and Huck et al. (2005) showed that the year-to-year variability of Antarctic ozone depletion is driven by the year-to-year variability of the polar vortex temperatures. Huck et al. (2005) also showed that interannual variability in Antarctic stratospheric temperatures and ozone loss are affected by midlatitude wave activity, while the decadal increase in Antarctic ozone loss is driven by the increase in halogens.

In climate models, planetary wave activity has been shown to partially depend on sea surface temperatures, among other forcings (Schnadt et al., 2002). It is therefore susceptible to climate change. The external factors determining stratospheric wave forcing and its interannual variability (i.e., stochastic tropospheric dynamics, quasi-biennial oscillation (QBO), sea surface temperatures (SSTs), solar variability, and volcanic eruptions) are difficult to quantify; Chapter 6 discusses the impact of these uncertainties for the predictability of future changes of polar ozone.

Besides the systematic transport of ozone to high latitudes with the residual circulation, another important aspect of transport is mixing. Although mixing across the vortex edge is relatively weak, it has an effect on the distribution of ozone within the polar vortices. The Antarctic vortex is divided into two distinct regions of approximately

Figure 4-5. Increase of ozone over the winter as a function of planetary wave activity. Planetary wave activity is measured as winter eddy heat flux in the respective hemisphere. The ozone ratio of the zonal mean between 50° and 90° latitudes from March over that from September is shown for the NH, and September over March for the SH. Circles are NH values, and triangles represent SH values. Total ozone is from weighting function differential optical absorption spectroscopy (WFDOS) V1 (Weber et al., 2005). The monthly mean eddy heat flux at 100 hPa averaged from 40 to 75 degrees latitude is derived from ECMWF ERA40/operational analysis, and has been averaged from fall to spring in each hemisphere. SH winter eddy heat flux is negative, but is shown here as absolute values. Updated from Weber et al. (2003).



POLAR OZONE

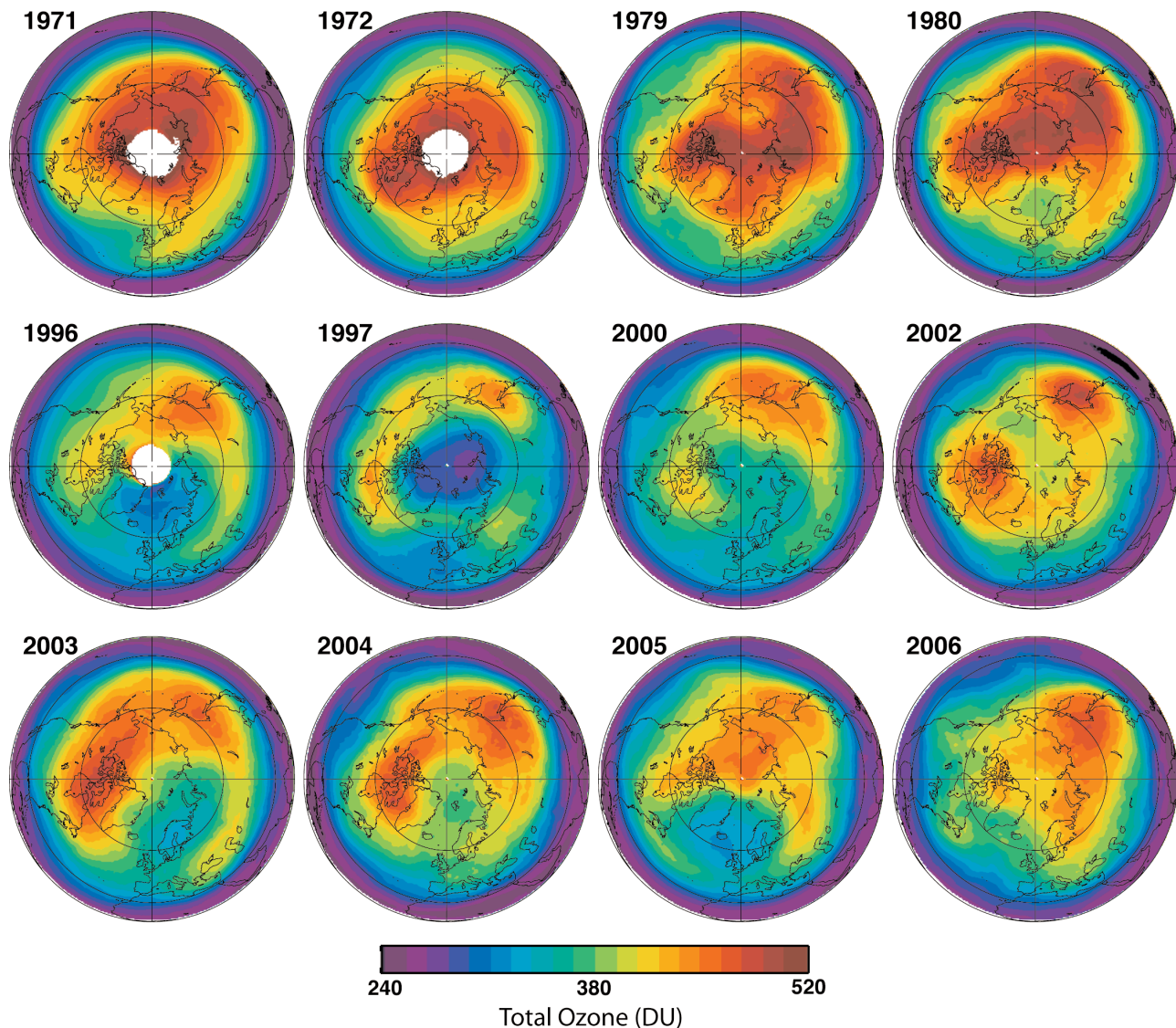


Figure 4-6. March monthly averaged total ozone for the Arctic. The 1971 and 1972 images are from the Nimbus-4 Backscatter Ultraviolet (BUV) instrument; the 1979 and 1980 images are from the Nimbus-7 TOMS instrument; the 1996 image is from the NOAA-9 SBUV/2 instrument; the 1997, 2000, 2002, 2003, and 2004 images are from the Earth Probe TOMS instrument; and the 2005 and 2006 images are from the Aura Ozone Monitoring Instrument (OMI). This figure is updated from Figure 7-21 of WMO (1999).

equal area: a strongly mixed vortex core and, separated from the core, a broad ring of weakly mixed air extending to the vortex boundary (Lee et al., 2001). This division was deduced from an analysis of a mixing diagnostic (the so-called “equivalent length”) based on transport calculations of an artificial tracer field on an isentropic surface (480 K) for the period from July to November. A transport barrier within the Antarctic vortex between July and November, is likewise apparent for the altitude range between 475 and 650 K in the potential vorticity field (Tilmes et al., 2006b) and, moreover, extends to the setup

phase of the Antarctic vortex in March and April (Tilmes et al., 2006a). During March and April, ozone-tracer relations in the two vortex regions are clearly distinct (Tilmes et al., 2006a). Further, measurements of ozone and volcanic aerosol show rather different vertical profiles within the vortex core and in the edge region (Godin et al., 2001). A better understanding of the dynamical mechanisms responsible for the occurrence of transport barriers within the vortex is important, because temperature variations in the weakly mixed air mass between the vortex boundary and the vortex core drive the year-to-year variability of

about 10-20% in the area of the ozone hole (measured as the area enclosed in the 220-DU contour) (Newman et al., 2004).

4.1.2 Polar Ozone

This section presents observations of ozone and diagnoses of ozone destruction in both polar regions. Section 4.1.2.1 gives an update of observations of ozone and the primary chlorine species involved in stratospheric ozone destruction, along with a discussion of various indicators that capture different aspects of ozone hole area and severity. A discussion of other trace gas species such as BrO and chlorine dioxide (OCIO) can be found in Section 4.2.1 and Chapter 2 (Section 2.5.1), and nitrogen dioxide (NO_2) is discussed in Chapter 3 (Section 3.3.2). In Section 4.1.2.2, refinements since the previous Assessment (WMO, 2003) of various methods for quantifying chemical ozone loss in the Arctic polar vortex are presented. Near-record ozone losses during the Arctic 2004/2005 winter are discussed. Finally, recent progress in quantifying ozone loss rates in the Antarctic is discussed.

4.1.2.1 OZONE AND OTHER CONSTITUENTS

The ozone content in the Arctic stratosphere is dependent on chemical and dynamical conditions and shows great interannual variability. This section discusses resulting interannual variability of ozone and other constituents, which is due to the combined effect of transport and chemistry. Section 4.1.2.2 isolates the impact of anthropogenic chemical loss on polar ozone variability from the variability in transport.

As noted in the previous section, the formation, evolution, and breakup of the polar vortex and the occurrence of stratospheric warmings are subject to large year-to-year variations. Figure 4-3 shows that the variability in amplitude of V_{PSC} (PSC formation potential derived from stratospheric temperature analyses) in the Arctic has clearly increased over the last 40 years, with 1995/1996, 1999/2000 and 2004/2005 standing out as cold winters with high PSC formation potential, whereas 1998/1999, 2001/2002, and 2003/2004 were warm winters with very low PSC formation potential. As discussed in the previous section, this variability in dynamical conditions has a correlated impact on ozone transport and chemistry and is therefore reflected in the total ozone column over the polar regions.

Total Ozone Average

Arctic total ozone has remained low over the last few years in comparison with pre-1982 observations.

Figure 4-6 displays a series of March averages for selected years from 1971 to 2006 (updated from Figure 7-21 in WMO, 1999). The 60°N latitude circle generally encloses the region of low ozone, but in some years (e.g., 2005) the vortex and low-ozone region are displaced from the pole, extending southward of 60°N . Nevertheless, Arctic ozone levels during March of recent years are low in comparison with the observations prior to 1980, as shown in the top row of Figure 4-6.

The springtime average total ozone values in the Arctic and Antarctic poleward of 63° latitude are shown in Figure 4-7 in comparison with the average total ozone for the years 1970-1982 (gray lines). The difference between the observed values and the 1970-1982 average indicates the combined changes in ozone due to chemistry and dynamics. In the last 9 years, Arctic column ozone exceeded the low values of the mid-1990s, except in the cold and chemically active winter of 1999/2000, when a large decrease of 63° - 90° NH total ozone was observed. The record-cold winter of 2004/2005, however, showed a less pronounced impact on the March polar average total ozone. Although NH polar column ozone averages are in general a good indicator of Arctic ozone depletion (WMO, 2003), the March average in 2004/2005 reflects the strong influence of dynamics (e.g., vortex fragments moved outside the 63° - 90° region during March, see Figure 4-6) and is consequently high relative to those of other recent cold winters even though the magnitude of chemical ozone

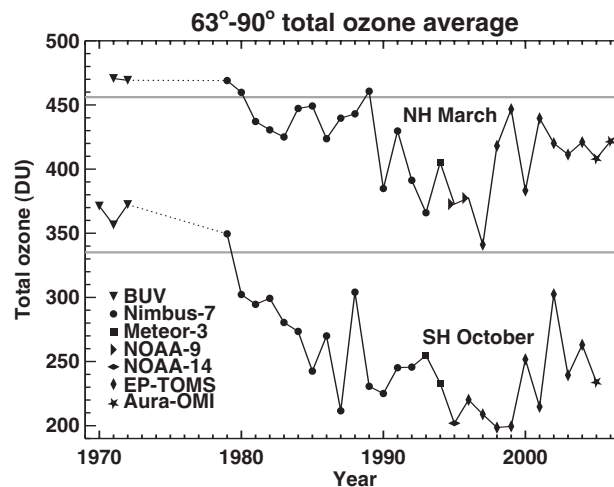


Figure 4-7. Total ozone average of 63° - 90° latitude in March (NH) and October (SH). Symbols indicate the satellite data that have been used in different years. The horizontal gray lines represent the average total ozone in March for the years prior to 1983 for the NH and SH. Updated from Figure 3-2, WMO (2003).

POLAR OZONE

loss in the lower stratospheric vortex was as high as or higher than in those years (cf. Section 4.1.2.2).

In the SH polar region, the lowest average October total ozone values were observed in the late 1990s (Figure 4-7, bottom panel). The last 6 years have shown an increase in polar column ozone averages, with a high degree of variability and notably higher ozone values in 2000, 2002, and 2004 resulting from greater dynamical activity.

To aid the detection of the recovery of the Antarctic ozone hole (discussed in detail in Chapter 6), various metrics that capture different aspects of the ozone hole are used to describe the severity of ozone depletion, such as ozone hole area, ozone minimum, ozone mass deficit, and date of ozone hole appearance and disappearance. Figure 4-8 displays ozone hole area (top panel), ozone hole minimum (middle), and ozone mass deficit (bottom). Following Newman et al. (2006), we have added a fit of these metrics (gray line) to a quadratic function of Antarctic equivalent effective stratospheric chlorine (EESC) (see Box 8.1 for a description of Antarctic EESC).

Ozone Hole Area

A primary estimate of the severity of the Antarctic ozone hole is its geographic area (WMO, 2003). Figure 4-8 (top panel) shows the ozone hole area calculated from the area contained by total column ozone values less than 220 DU during 21-30 September from Total Ozone Mapping Spectrometer (TOMS) and Ozone Monitoring Instrument (OMI) observations. The value 220 DU was chosen to define the ozone hole because it is almost always a middle value in a strong gradient of total ozone, and because it is lower than pre-1980 observed ozone values. The average ozone hole area currently reaches approximately 25 million km² each spring, while the single largest daily value reached nearly 30 million km² in September 2000 (Newman et al., 2004). Ozone depletion can be enhanced by volcanic perturbations (e.g., Hofmann and Oltmans, 1993) as could be seen in the very strong ozone depletion (or “deep ozone holes”) observed in the 1990s after the Mt. Pinatubo eruption (e.g., 1994). The area growth of the ozone hole slowed during the mid-1990s, with a large dip in 2002.

Ozone Minimum

The daily total column ozone minimum value is a widely used measure of the state of the ozone hole. Average minimum ozone columns calculated over Antarctica for the period 21 September to 16 October show a clear decrease from 1979 to the mid-1990s, with the

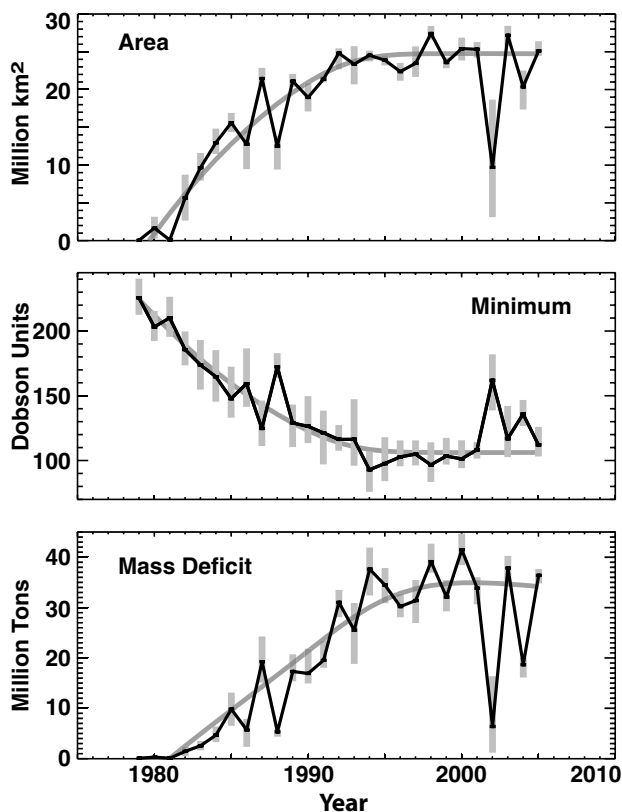


Figure 4-8. Top panel: Area of the Antarctic ozone hole for 1979-2005, averaged from daily total ozone area values contained by the 220-DU contour for 21-30 September. The gray bars indicate the range of values over the same time period. The gray line shows the fit to these area values as was shown in Newman et al. (2004), and now using EESC, as derived in Newman et al. (2006) (see also Box 8.1 in Chapter 8). The EESC has a mean age of 5.5 years, an age spectrum width of 2.75 years, and a bromine-scaling factor of 50. The fit is quadratic in EESC. Middle panel: An average of daily minimum ozone values over Antarctica during the period from 21 September to 16 October. The gray bars indicate the range of ozone values over the same time period. The gray line is the fit as described for the top panel. Bottom panel: Ozone mass deficit (OMD) average over the 21-30 September period. The gray bars indicate the range of values over the same time period. The gray line is the fit as described for the top panel. This figure was generated using the merged ozone data courtesy of Greg Bodeker (NIWA) and NCEP/NCAR reanalysis 2 data. Updated from Figures 3-5 and 3-7 from WMO (2003).

lowest minimum value observed in 1994 (Figure 4-8, middle panel).

Ozone Mass Deficit

The ozone mass deficit (OMD) combines the effects of changes in ozone hole area and depth, and provides a direct measure of the deficit relative to the mass present for a value of 220 DU (e.g., Uchino et al., 1999). Figure 4-8 (bottom panel) shows the OMD averaged over the period 21-30 September. While the long-term evolution of the OMD follows the halogen loading, there is higher frequency year-to-year variability; years with anomalously high wave activity (1988, 2002, and 2004) show weak Antarctic ozone depletion, and years with suppressed wave activity show severe depletion (Huck et al., 2005, and references therein).

Daily values of OMD over Antarctica for the years 2002-2005 are compared with the range of values over the period 1990-2001 in Figure 4-9. This plot shows that, apart from 2002, the year 2004 also stands out as having a weak ozone hole, while the OMD in the 2003 and 2005 Antarctic winters is more comparable to those observed during the 1990s. Although lower stratospheric (50 hPa) minimum temperatures were below average over much of the 2004 Antarctic winter, they increased and remained near average after mid-August

(Santee et al., 2005). The lower stratosphere warmed rapidly in September, halting further heterogeneous processing of vortex air by the end of the month. This resulted in a slow increase in OMD and a leveling off in late September (see Figure 4-9). At the end of September, a large increase in mixing accompanied by a weakening vortex transport barrier signaled vortex erosion leading to the breakup (Manney et al., 2005b).

Hoppel et al. (2005b) used measurements from both the Polar Ozone and Aerosol Measurement (POAM) instrument and South Pole ozonesondes to investigate changes in the ozone mixing ratio near the top (20-22 km) of the ozone hole, comparing the years 2001-2004 with the previous six years of POAM observations (1994-1996; 1998-2000). They found that in this altitude range, the year 2004 was distinguished by the highest minimum vortex temperatures throughout August and September, the lowest observed PSC frequency, and the smallest photochemical ozone loss.

Chlorine Partitioning

The evolution of chlorine partitioning in the winter polar vortices of both hemispheres is shown in Figure 4-10. In this figure, contemporaneous measurements from two recent satellite missions are used to update the conceptual sketch of wintertime chlorine par-

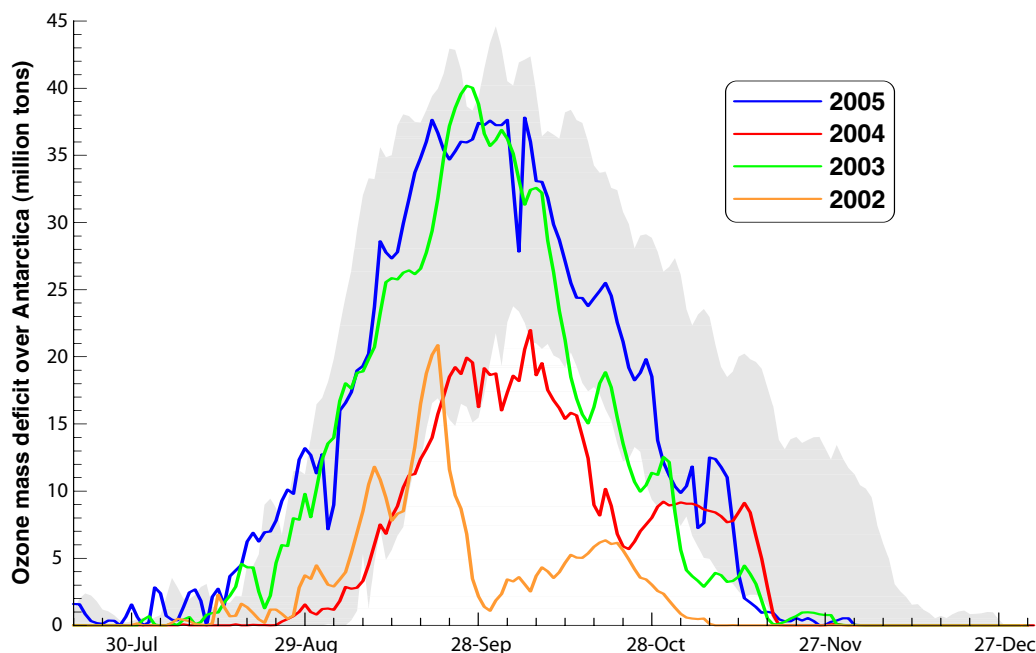


Figure 4-9. Daily OMD over Antarctica for the years 2002-2005 compared with the range of values over the period 1990-2001. The grayed area shows the daily range from 1990 to 2001. Adapted from Bodeker et al. (2005).

POLAR OZONE

tioning presented in a previous WMO Assessment (WMO, 1995; Figure 3-1). Although several studies based on satellite, aircraft, balloon, and ground-based measurements over the last decade have provided insight into both the relative abundances of the main chlorine reservoirs prior to activation and the interhemispheric differences in their recovery at the end of winter, the new data from the Atmospheric Chemistry Experiment Fourier Transform Spectrometer (ACE-FTS) (e.g., Dufour et al., 2006) and the Aura Microwave Limb Sounder (MLS) (e.g., Santee et al., 2005) are of unprecedented scope for studying seasonal changes in chlorine partitioning. In particular, the dominant chlorine reservoir before the onset of PSC processing is confirmed to be HCl, not ClONO₂ as indicated in the schematic shown in WMO (1995).

In the Antarctic (Figure 4-10, left panel), chlorine is converted into the active form ClO by early June; elevated abundances of ClO then persist through mid-September. In the severely denitrified and ozone-depleted conditions characteristic of late Antarctic winter, HCl production is highly favored and ClONO₂ production is suppressed.

In the Arctic (Figure 4-10, right panel), the magnitude and duration of chlorine activation are much smaller than the Antarctic, even in a relatively cold winter. The ACE-FTS and Aura MLS measurements clearly support the canonical picture of initial chlorine deactivation in the Arctic, with the primary pathway the reformation of ClONO₂, followed by slow repartitioning between ClONO₂ and HCl.

4.1.2.2 POLAR OZONE LOSS STUDIES

Quantifying Arctic Ozone Loss

Diagnosing chlorine-catalyzed ozone destruction requires distinguishing the effects of chemical processes from those of transport and mixing, especially in the Arctic, where ozone abundances are strongly controlled by dynamics. WMO (2003) presented an overview of the methods commonly used to estimate chemical ozone loss and discussed the limitations and sources of uncertainty of each, as well as the degree of consistency between them. Most of these techniques have been significantly refined since the previous Assessment, with a particular emphasis

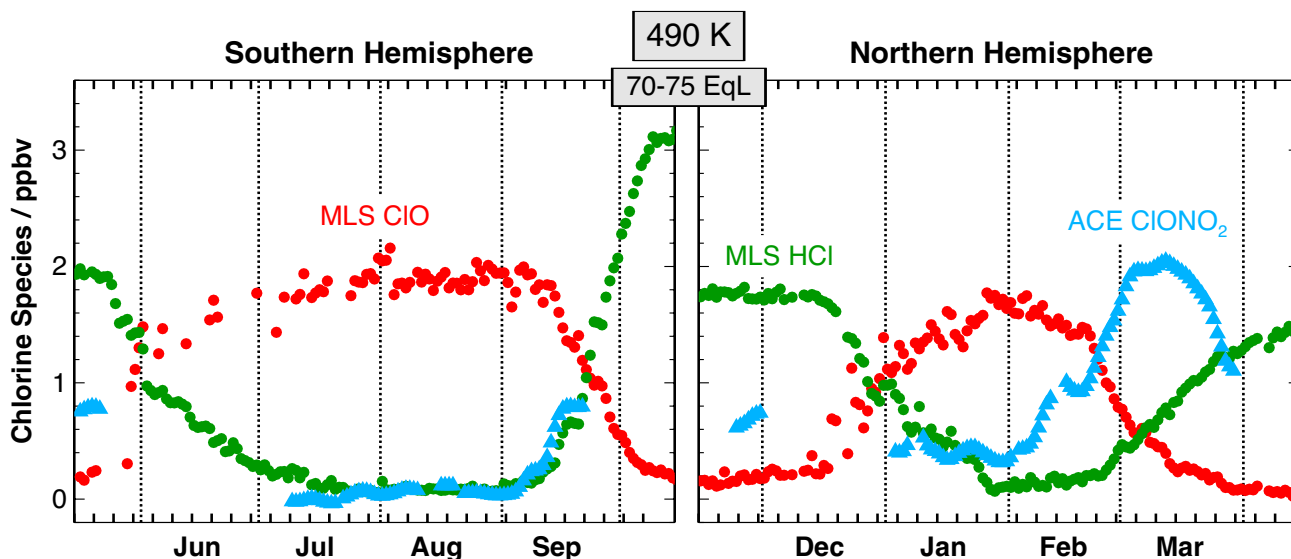


Figure 4-10. Left panel: Daily averages of ClO (red dots) and HCl (green dots) observed by Aura MLS, and ClONO₂ (cyan triangles) observed by ACE-FTS at 490 K (~20 km) during the 2005 Antarctic winter/spring period, calculated over the 70°-75° equivalent latitude band using the Global Modeling and Assimilation Office Goddard Earth Observing System (GEOS-4) temperatures and potential vorticity. Only daytime measurements are included in the averages for ClO; ClO data appear sparser because measurements in sunlight are not always available at high equivalent latitudes, especially in early winter. The sampling pattern of ACE-FTS, a solar occultation instrument, does not provide coverage of this equivalent latitude band at all times throughout the winter. Right panel: As in the left panel, for the 2004/2005 Arctic winter/spring period.

on quantifying the uncertainties in the loss estimates. This section presents an update of recent progress in separating chemical and dynamical effects and quantifying ozone destruction, mainly in the context of the 2002/2003 Arctic winter. In 2002/2003, an unusually cold early winter promoted an earlier inception of significant ozone destruction than in most other recent cold winters (e.g., Goutail et al., 2005; Streibel et al., 2006). The mid- to late winter was very dynamically active and warmer than average, but with a series of stratospheric warming events that limited cumulative ozone loss. Aircraft and ground field campaigns in the 2002/2003 winter provided an excellent opportunity to assess understanding of polar ozone loss processes, especially under the high solar zenith angle conditions of early winter. The different approaches to calculating chemical ozone loss generally agree well, lending confidence in the estimates.

Ozone/Tracer Correlation Method. In this technique, changes in the compact correlations between ozone and long-lived tracers over the winter are ascribed to chemical loss. This approach assumes that a reference ozone/tracer relation representative of the early-winter polar vortex can be established and that transport and mixing processes do not significantly alter it, assumptions that had been questioned at the time of the previous Assessment (e.g., Harris et al., 2002; WMO, 2003; Sankey and Shepherd, 2003). The technique was refined in recent applications (Müller et al., 2002; Tilmes et al., 2003), and a comprehensive re-evaluation of ozone loss in the Arctic winters 1991–2003 was performed (Tilmes et al., 2004). Ozone loss estimates generally agreed well with those based on other approaches, with the smallest estimated errors obtained in the coldest winters with greatest loss; the major contribution to the error in the calculated loss remained the uncertainty in the reference relation. Müller et al. (2005) confirmed the validity of ozone-tracer relations for quantifying chemical loss, provided that a reliable early vortex reference is obtained and vortex and midlatitude air masses are well separated by a strong transport barrier at the vortex edge.

Match Method. “Match” is a pseudo-Lagrangian technique involving identification (through trajectory calculations) of air parcels sampled two or more times in a prescribed interval; differences in the observed ozone mixing ratios are attributed to chemical loss. Match has received substantial attention since the previous Assessment. Morris et al. (2005) revisited the January–March periods in 1992 and 2000 using a different trajectory code and meteorological analyses than in the original Match studies (Rex et al., 1998, 2002). They confirmed the statistical error bars published previously, but concluded that actual uncertainties in the calculated ozone loss

rates are larger because of additional systematic errors, consistent with earlier discussions of systematic Match uncertainties (e.g., Rex et al., 1998; Harris et al., 2002). Morris et al. (2005) recommended that future Match studies employ extended (14-day) trajectory calculations and suggested that some of the filter criteria built into the approach may be unnecessary. In contrast, Grooß and Müller (2003) carried out a virtual Match campaign in the Chemical Lagrangian Model of the Stratosphere (CLaMS) three-dimensional (3-D) chemical transport model and found that these filter criteria reduce the statistical uncertainty of the estimated ozone loss rates and remove a systematic bias induced by mixing across the vortex edge, particularly during periods of strong vortex disturbances.

Lehmann et al. (2005) developed a statistical approach to take into account the error correlation between matches that share a common ozone measurement and found that it depends nearly linearly on the “oversampling rate” (i.e., the average number of matches to which an ozone measurement contributes). For ozonesonde Match studies, the oversampling rate is low and the average increase in the error bars is 15%. For satellite Match studies, however, the oversampling rate is typically much higher and uncertainties increase by more than 50% compared with those estimated assuming uncorrelated errors. This updated approach to estimating uncertainties was used for the 2002/2003 Match study (Streibel et al., 2006), which also included the use of higher-resolution wind fields for the trajectory calculations, the imposition of a backward match radius in addition to the criterion along the forward trajectory, and the earliest start of a Match campaign, allowing investigation of ozone loss starting in December.

Vortex-Average Method. In this method, the difference between an initial profile altered using diabatic descent rates (estimated using a radiation code) and a final observed profile yields an estimate of chemical loss. Grooß and Müller (2003) used CLaMS simulations to quantify the influence of intrusions of midlatitude air into the vortex on ozone loss estimates derived with this method and showed that, although cross-vortex transport may often be insignificant, in some dynamically active periods neglecting it may introduce significant error in the estimated ozone loss rate. Christensen et al. (2005) applied the vortex-average method, corrected to account for transport into the vortex, to ozonesonde data from the 2002/2003 Arctic winter and compared the results with ozone loss estimates from other techniques, finding generally good agreement. A variant on the vortex-average method uses the evolution of a long-lived tracer, rather than trajectory calculations and a radiation code, to deduce diabatic descent. For example, Odin SubMillimeter

POLAR OZONE

Radiometer (SMR) measurements of nitrous oxide (N_2O) were used to account for the effects of subsidence in estimating chemical loss during the 2002/2003 winter from both Odin/SMR (Urban et al., 2004) and ground-based millimeter-wave (Raffalski et al., 2005) ozone observations. This approach has been greatly facilitated by the availability of simultaneous global ozone and tracer measurements from recent satellite missions such as Odin, Envisat, and Aura (e.g., Manney et al., 2006).

Passive Subtraction Method. In this technique, differences between measured ozone and results from model runs in which ozone is treated as a passive dynamical tracer are assumed to arise from chemical changes. Recent refinements in 3-D chemical transport models (see Section 4.2.1.3) have improved estimates of chemical loss derived in this manner. Feng et al. (2005b) showed that seasonal runs of the updated Single-Layer Isentropic Model of Chemistry and Transport (SLIMCAT) model (Chipperfield, 2006) produced realistic representations of tracer transport and ozone loss for selected warm and cold Arctic winters, including 2002/2003. Goutail et al. (2005) compared ground-based total ozone columns from the 2002/2003 winter with modeled passive ozone columns from the Reactive Processes Ruling the Ozone Budget in the Stratosphere (REPROBUS) and updated SLIMCAT models; although both models indicated significant early-winter loss, full-chemistry simulations from REPROBUS did not reproduce all of the inferred loss. Singleton et al. (2005) compared the updated SLIMCAT with Polar Ozone and Aerosol Measurement (POAM) III ozone observations from 2002/2003, examining a “pure passive” ozone advected as an inert tracer with no chemical changes and a “pseudo passive” ozone for which only heterogeneous reactions on PSCs were switched off in order to explore the influence of gas-phase chemistry on inferred ozone loss. The timing, morphology, and magnitude of modeled (full chemistry) ozone loss agreed well with that deduced from POAM observations, with the largest differences (<1 parts per million by volume (ppmv)) in the two passive ozone fields, attributed to nitrogen oxides (NO_x) chemistry in the “pseudo passive” run, occurring above 450 K. Finally, Grooß et al. (2005b) showed that ozone loss inferred using CLaMS compared well with other estimates.

Lagrangian Transport Calculation Method. A method frequently applied to ozone measurements from the Upper Atmosphere Research Satellite (UARS) Microwave Limb Sounder (MLS) involves the use of a Lagrangian transport (LT) model advecting trace gases passively along parcel trajectories; departures from the observed ozone provide an estimate of chemical loss. Previous studies covered only the late-winter period for a

subset of Arctic winters observed by UARS MLS and used different LT models and MLS data versions. Manney et al. (2003a) performed a comprehensive reanalysis that encompassed the entire Arctic winter for all years with sufficient data and used a consistent LT model and the definitive UARS MLS dataset, facilitating evaluation of interannual variability.

Chemical Loss in the 2004/2005 Arctic Winter

The potential for severe ozone depletion will exist so long as stratospheric chlorine loading remains well above natural levels. The degree of chlorine activation and consequent ozone destruction in the Arctic is primarily controlled by dynamical variability. Winters in which the polar vortex is cold and isolated are expected to experience large ozone losses, whereas ozone losses should be minimal in warmer than average, disturbed winters. The 2004/2005 Arctic winter was especially interesting in this context. The lower stratosphere was exceptionally cold, particularly below 400 K (~ 15 km), with temperatures below PSC existence thresholds on more days and over a broader region than previously observed (Manney et al., 2006; Rex et al., 2006). But the lower stratosphere was also dynamically active, with frequent intrusions of lower-latitude or vortex edge air into the vortex interior throughout the winter (Manney et al., 2006; Schoeberl et al., 2006). Moreover, the initial morphology of ozone in early winter, prior to the onset of chemical loss, exhibited a strong gradient in mixing ratio between low values in the vortex core and high values at the edge (Manney et al., 2006; Rex et al., 2006). Thus mixing processes may have masked or mimicked chemical loss, depending on the location in the vortex. A major final warming in early-March 2005 halted PSC processing, terminating ozone destruction earlier than in other recent cold winters. These effects made disentangling chemical and dynamical processes particularly difficult this year, possibly causing some analyses to be more sensitive to sampling biases and increasing uncertainties in the estimated losses. Nevertheless, a suite of studies using a variety of datasets and techniques provided fairly consistent ozone loss estimates for this winter.

Manney et al. (2006) deduced chemical ozone loss from Aura MLS measurements by using N_2O to account for the effects of diabatic descent in the vortex edge and core regions, and estimated loss of up to 2 ppmv in the outer vortex and ~ 1.5 ppmv averaged over the entire vortex, with maximum losses in both regions between 450 and 500 K. Manney et al. (2006) also applied the vortex-average method, using trajectory calculations and a radiation code, to both Aura MLS and POAM measurements (Figure 4-11) and found maximum vortex-averaged chemical loss near

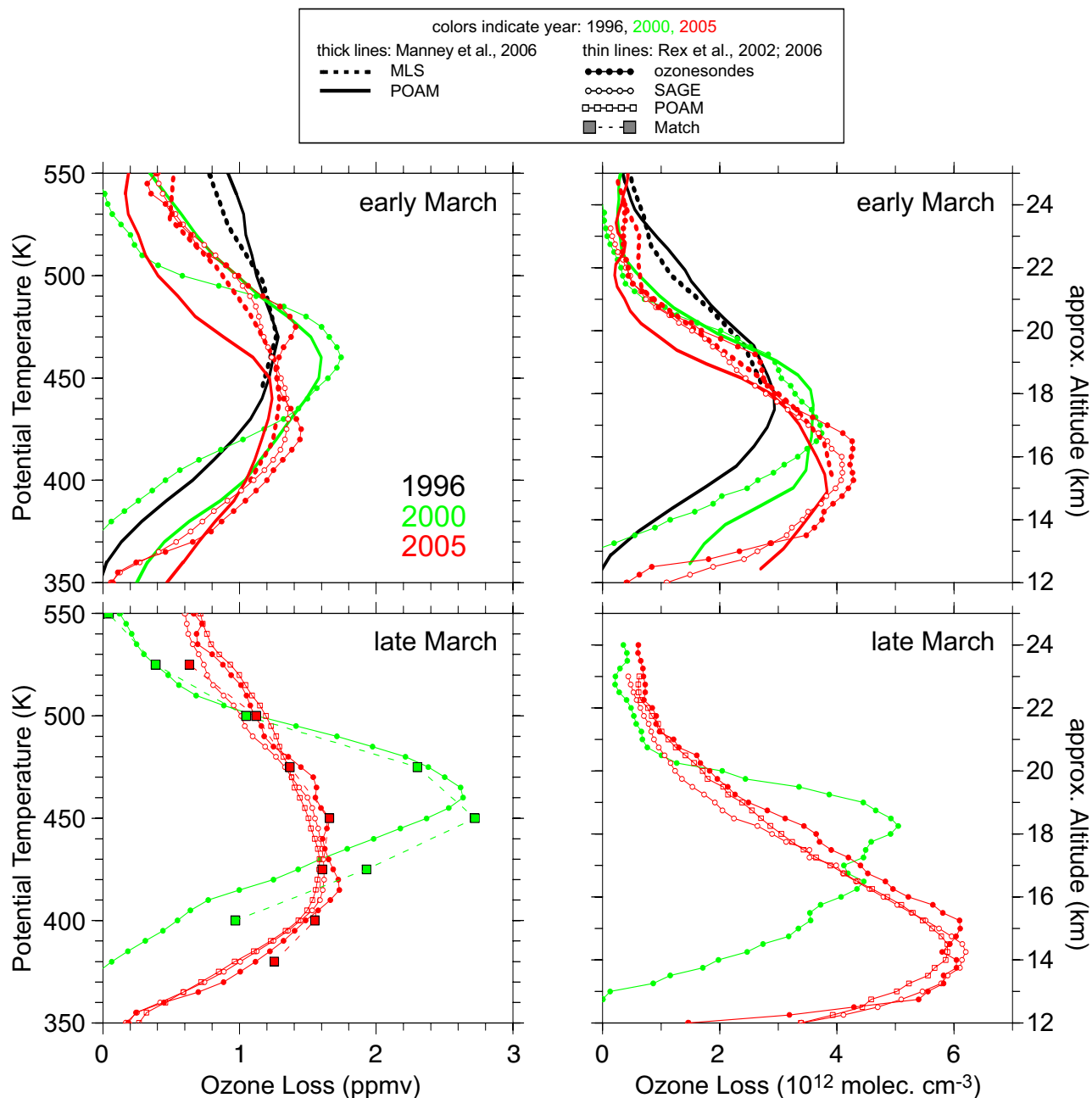


Figure 4-11. Profiles of chemical ozone loss in terms of mixing ratio versus potential temperature (left panels) and concentration versus altitude (right panels), over the intervals from 5 January to 10 March (top panels) and 5 January to 25 March (bottom panels) for three cold Arctic winters, estimated using various data sources and techniques. Although different line styles and symbols have been used to denote the different datasets and approaches, in most cases it is not necessary to clearly distinguish the curves, as the derived ozone loss values are generally in quite good agreement. All lines represent results from the vortex-average descent method. Thick lines without symbols are from Manney et al. (2006), with solid lines based on POAM II/III and dotted lines based on UARS MLS (1996) and Aura MLS (2005). Thin lines with small symbols are from Rex et al. (2002) and Rex et al. (2006), with lines marked by filled dots based on ozonesonde data, lines marked by open circles based on SAGE III data, and lines marked by open squares based on POAM II/III data. Large square symbols (connected by dashed lines) show results from Match (Rex et al., 2002, 2006). Ozone loss in 2005 terminated earlier and was smaller in terms of mixing ratios compared with 2000. But, because the 2005 loss extended to lower altitudes where ozone concentrations are high, it was larger in terms of concentration, which is the relevant quantity for total column loss.

POLAR OZONE

450 K of 1.2-1.3 ppmv, slightly less than the estimates based on MLS N_2O . These results imply that, in terms of mixing ratios, chemical loss in 2004/2005 was slightly less than that in 1999/2000 and comparable to that in 1995/1996, but with maximum loss occurring at a lower altitude.

Singleton et al. (2006) used the updated SLIMCAT model to infer chemical ozone loss from POAM III, Aura MLS, ACE-FTS, Measurement of Aerosol Extinction in the Stratosphere and Troposphere Retrieved by Occultation (MAESTRO), and Stratospheric Aerosol and Gas Experiment (SAGE) III measurements; all instruments provided similar results, with a maximum inferred loss of 2-2.3 ppmv near 450 K (Figure 4-12). Jin et al. (2006) also examined ACE-FTS measurements, using correlations between ozone and methane (CH_4) (modified to account for mixing processes), correlations between ozone and an artificial tracer constructed to have a linear correlation with ozone in early winter, and the vortex-averaged descent method to diagnose an average maximum loss of ~ 2.1 ppmv near 500 K, with an average column loss of 119 DU over the region 375-800 K (14-30 km).

Results from Match (Rex et al., 2006; Figure 4-11) indicated chemical loss characterized by a broad peak of ~ 1.5 ppmv from ~ 400 -450 K, smaller than the maximum mixing ratio loss in 1999/2000, but with more loss occurring at lower altitudes. However, Rex et al. (2006) showed that, in terms of concentration (rather than mixing ratio), ozone loss in 2004/2005 was considerably more severe than that in 1999/2000, particularly below about 16 km. For the total column and, hence, the ultraviolet (UV) reaching the surface, the large concentration losses at lower altitude have the biggest impact. Therefore, total

column losses during 2004/2005 were at least on the order of the largest losses recorded previously (Rex et al., 2006).

The 2004/2005 winter stands out as having the largest V_{PSC} and partial column ozone loss ($\Delta O_3 = 121 \pm 20$ DU over 380-550 K) of the last 14 years, although the differences between column ozone losses in 1995/1996, 1999/2000, and 2004/2005 are within the uncertainties in the calculation. The compact and nearly linear relationship between the influence of chemical ozone loss on ΔO_3 and the winter average of V_{PSC} reported by Rex et al. (2004) and confirmed by Tilmes et al. (2004) was maintained in 2004/2005 (Figure 4-13; Rex et al., 2006). In contrast, comparisons of ground-based total ozone measurements with passive ozone from REPROBUS (e.g., Goutail et al., 2005) indicated that the total column loss in 2004/2005 rivaled that in 1999/2000 but was smaller than that in 1995/1996. The various partial and total column ozone loss estimates for the 2004/2005 Arctic winter discussed here are compared with those available from previous years in Figure 4-14.

The March 2005 averaged total ozone in Figure 4-6 clearly shows a distinct minimum (near $60^\circ N$) that is comparable to that in other years with strong depletions. As discussed in Section 4.1.2.1, total column ozone (data from the OMI on Aura; Figure 4-7) averaged over the Arctic region in March 2005 was below normal but comparable to that in other recent winters, even though the magnitude of chemical ozone destruction in the lower stratospheric vortex was substantially larger. The March 2005 average in Figure 4-6 clearly shows a distinct minimum (near $60^\circ N$) that is comparable to other years with strong depletions. Several factors account for these apparent discrepancies.

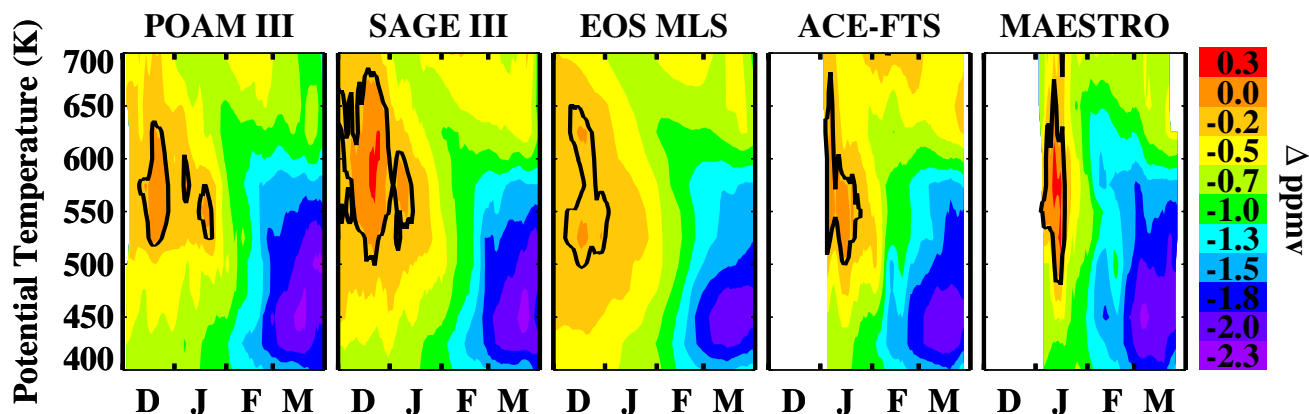


Figure 4-12. Daily average chemical ozone loss (ppmv) inside the vortex during the 2004/2005 Arctic winter inferred by differencing passive ozone calculated by the updated SLIMCAT chemical transport model, and ozone measured by the POAM III, SAGE III, Aura MLS, ACE-FTS, and MAESTRO instruments. Days on which data are missing or an instrument did not sample the vortex have been interpolated in time. Data have been smoothed with a seven-day running average. The solid black line denotes the zero contour.

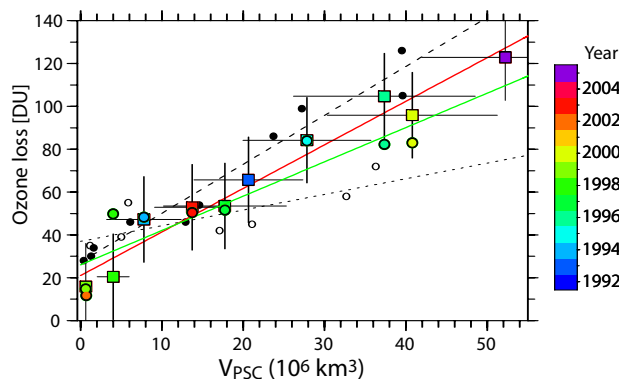


Figure 4-13. Scatter plot of vortex-average chemical loss of column ozone (ΔO_3 , calculated over the range 380 to 550 K) versus V_{PSC} inferred from ozonesonde observations for the 1991/1992 to 2004/2005 Arctic winters (update from Rex et al., 2004). Colored squares and the red fit line show results based on ozonesonde analyses; colored circles and the green fit line show results from tracer correlation studies based on Halogen Occultation Experiment (HALOE) data (update from Tilmes et al., 2004). Also shown are results from SLIMCAT model simulations. Open black circles and the dotted fit line show results from an older version of the model, run at a resolution of 7.5° for the 1990/1991 to 1999/2000 winters (same model results as shown in Figure 2 of Rex et al., 2004). Closed black circles and the dashed fit line show results from a new version of the model, run at higher resolution (2.8°) for the 1994/1995 to 2003/2004 winters (same model results as shown in Figure 1 of Chipperfield et al., 2005). See Section 4.2.1 for descriptions of the old and newly updated versions of the SLIMCAT model. Adapted from Rex et al. (2006), Rex et al. (2004), Tilmes et al. (2004), and Chipperfield et al. (2005).

In previous years with later final warmings, the March average reflected primarily winter vortex values that, for dynamical reasons, were much lower than the spring values dominating the 2005 average. Even before the final warming, the 2005 vortex had become highly distorted and shifted off the pole (Manney et al., 2006). The monthly average over the entire Arctic region, therefore, encompassed air from both inside and outside the vortex; together with the vigorous mixing following the vortex breakup, this effect muted the signature of chemical depletion in the average ozone north of $63^\circ N$. As a consequence, the average total column ozone over the Arctic in March 2005 was strongly influenced by dynamics and was not representative of chemical loss inside the polar vortex remnants.

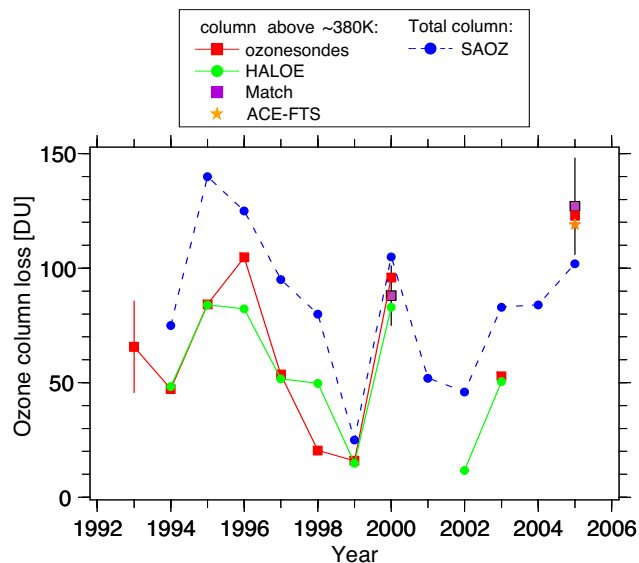


Figure 4-14. Interannual variation of the ozone column losses in the Arctic since the early 1990s based on Système d'Analyse par Observation Zénithale (SAOZ) satellite data (blue, update of Goutail et al., 2005); ozonesonde analyses (red, typical uncertainty illustrated by the single error bar, update from Rex et al., 2004); HALOE data (green, Tilmes et al., 2004); Match (purple, Rex et al., 2002, 2006); and ACE-FTS data (orange, Jin et al., 2006). The sonde, HALOE, and Match analyses represent partial column losses between 380 and 550 K potential temperature. The other studies represent estimates of the total column losses, which can result in slightly larger estimates in some winters. Therefore, the loss estimates from the SAOZ data have been plotted with a dashed line to signify that they should not be directly compared with the results from the other two long-term studies.

As a result of dynamical processes during the warming in combination with the large chemical depletion, total ozone over large parts of Europe was very low (reaching values below 250 DU) for several days during late March of 2005. This led to elevated levels of UV at the ground over Europe during those days.

Quantifying Antarctic Ozone Loss

Over the past two decades, numerous studies have compared modeled and measured ozone in the Antarctic ozone hole region. Although in most cases the models were shown to be successful in simulating the general features of ozone hole development, such as the timing of the onset and the cumulative amount of ozone loss, these

POLAR OZONE

did not provide a stringent test of theoretical understanding. Until recently, few studies have undertaken the kind of detailed quantitative estimations of ozone loss that have become routine in the Arctic. The inability to accurately model ozone loss during cold Arctic winters (e.g., WMO, 2003; Rex et al., 2003), however, has renewed interest in the Antarctic, where ozone losses are larger, the vortex is more isolated, and, consequently, transport and mixing processes are less important in controlling ozone abundances. Several recent studies have applied methods described above to quantify ozone loss using measurements from satellites and the first coordinated Antarctic ozonesonde Match campaign, conducted in 2003.

Hoppel et al. (2005b) used the vortex-average descent method with 10 years of ozone measurements from the POAM II and III instruments to deduce chemical loss, with a particular emphasis on the 20-22 km region near the top of the ozone hole (see 4.1.2.1 for further details). Hoppel et al. (2005a) used the satellite Match technique to calculate ozone loss rates at four potential temperature levels over the range ~450-520 K from five years of POAM III data and compared them with rates from a photochemical box model. Measured loss rates at the high solar zenith angles characteristic of the POAM-Match trajectories were found to increase slowly from late June to early August, and then increase rapidly until mid-September. The Match loss rates were also found to be highly sensitive to the meteorological analyses used for the trajectory calculations. Frieler et al. (2006) compared modeled ozone loss rates with those estimated for the 2003 ozonesonde Match campaign, as well as several Arctic winters. Detailed discussion of the implications of both the Hoppel et al. (2005a) and Frieler et al. (2006) studies for various model parameters is given in Section 4.2.1.3.

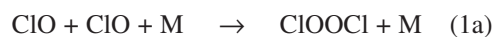
Tilmes et al. (2006b) used the tracer/tracer correlation technique with Improved Limb Atmospheric Sounder (ILAS)-II measurements to examine the temporal evolution of ozone loss throughout the 2003 Antarctic winter. Chemical loss began in July for all altitudes considered (380-620 K), and the accumulated ozone loss and loss rates were shown to be highly dependent on altitude. Ozone loss rates increased strongly during September throughout the lower stratosphere; half of the entire column ozone loss of 157 DU occurred during September, with virtually all ozone between 380 and 470 K destroyed by the end of the month. Simulations by the CLaMS box model confirmed that increasing solar illumination and persistent low temperatures led to enhanced ozone loss rates in mid-September.

4.2 PROGRESS IN OUR UNDERSTANDING OF THE PHYSICAL AND CHEMICAL PROCESSES

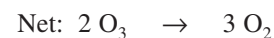
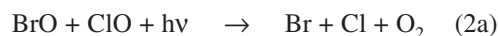
4.2.1 Polar Ozone Chemistry

The chemical loss of polar ozone during winter and spring occurs primarily by two gas-phase catalytic cycles that involve chlorine oxide radicals (Molina and Molina, 1987) and bromine and chlorine oxides (McElroy et al., 1986):

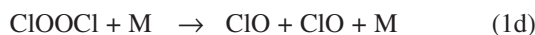
Cycle 1



Cycle 2



If loss of ClOOC occurs by thermal decomposition:



rather than photolysis (1b), a null cycle results that recycles ClO but leads to no change in ozone. Small contributions to polar ozone loss also occur due to cycles limited by the reactions ClO + O and ClO + HO₂.

Abundances of ClO in the polar vortex are greatly elevated by reactions of inactive chlorine reservoir species on various types of PSCs that form when temperatures drop below about 195 K (see Section 4.2.2). Abundances of BrO determine the removal rate by cycle (2), which may contribute almost half of the total chemical loss rate of Antarctic and Arctic ozone (e.g., Frieler et al., 2006). The abundance of BrO, in contrast to ClO, is not strongly affected by reactions involving PSCs (Pundt et al., 2002). The emerging issue involving BrO, important also for our understanding of polar ozone loss, is quantification of total inorganic bromine (Br_y) supplied to the stratosphere by very short-lived (VSL) bromocarbons (see Chapter 2).

Since the previous Assessment, numerous field and laboratory studies have provided advances in our

quantitative understanding of ozone destruction by cycles (1) and (2). These advances include the first measurements of the abundance of the chlorine monoxide dimer (ClOOCl) (Stimpfle et al., 2004; von Hobe et al., 2005); observations of BrO in the polar vortices (Fitzenberger, 2000; Pfeilsticker et al., 2000; Pundt et al., 2002; Canty et al., 2005; Giovanelli et al., 2005; Dorf et al., 2006; Sinnhuber et al., 2005b; Frieler et al., 2006; Schofield et al., 2006; Sioris et al., 2006); better representation of denitrification in models (Groß et al., 2005b; Chipperfield et al., 2005); recognition that formation of ClOOCl likely occurs faster than previously assumed (Boakes et al., 2005); and better constraints on the equilibrium constant between ClO and ClOOCl from both laboratory studies (Plenge et al., 2005) and field observations (von Hobe et al., 2005; Stimpfle et al., 2004). As detailed below, these findings lead to better model representation of two key processes: (1) the apparent discrepancies between measured and modeled chemical loss rates of Arctic ozone during cold Januaries of specific winters (e.g., Rex et al., 2003) that was noted in Section 3.3 of the previous Assessment (Frieler et al., 2006), and (2) the relation between chemical ozone loss and the volume of air exposed to PSCs, based on more than a decade of observations, that was introduced in the previous Assessment (Rex et al., 2004; Chipperfield et al., 2005). These advances suggest better predictive capability for future ozone loss due to anthropogenic halogens is achievable in general circulation models (GCMs) and coupled Chemistry-Climate Models (CCMs), provided certain fundamental characteristics of the atmosphere (e.g., chlorine and bromine loading; photolysis and thermal decomposition of ClOOCl; denitrification) are well represented. However, as discussed below, certain aspects of polar chemistry are still subject to considerable uncertainty, due to differences in various laboratory measurements of the absorption cross section of ClOOCl (σ_{ClOOCl}) (Section 4.2.1.1) and uncertainty in the atmospheric abundance of BrO (Chapter 2).

4.2.1.1 CHLORINE

Attention since the previous Assessment has continued to be focused on reducing uncertainties in the parameters that control ozone loss by Cycle 1, such as the rate constant for formation of ClOOCl (k_{1a}), the photolysis rate of ClOOCl (J_{1b}), and the equilibrium constant between the concentrations of ClO and ClOOCl (denoted [ClO] and [ClOOCl], respectively) established if loss of ClOOCl occurs via thermal decomposition:

$$K_{\text{EQ}} = k_{1a}/k_{1d} = [\text{ClOOCl}] / [\text{ClO}]^2 \quad (3)$$

This section begins with a description of recent laboratory measurements of reactions that affect polar ozone loss by chlorine. Then, we describe analyses of field studies that focus on consistency between measured and modeled representation of ClO and ClOOCl photochemistry.

Laboratory Studies

Boakes et al. (2005) reported a laboratory measurement of k_{1a} that is ~20% larger, over the temperature range 206 to 298 K, than the measurements of Bloss et al. (2001) and the Jet Propulsion Laboratory (JPL) Publication 02-25 compendium (Sander et al., 2003; hereafter referred to as *JPL 02-25*) recommendation for this rate constant. This new study suggests that ozone loss by Cycle 1 is faster than previously thought, which has implications for the partitioning between ClO and ClOOCl (see below). Boakes et al. (2005) support the upward revision in the recommended value of k_{1a} by *JPL 02-25* that followed the study of Bloss et al. (2001). The Bloss et al. (2001) and Boakes et al. (2005) values for k_{1a} are fast enough to pose a challenge to the theoretical understanding of this reaction (Golden, 2003).

Plenge et al. (2004) is the only published laboratory study of ClOOCl photolysis since the previous Assessment. They found complete production of chlorine atoms and chloroperoxy radicals (ClOO) upon photolysis of ClOOCl at 250 and 308 nm, leading to $2\text{Cl} + \text{O}_2$ upon the rapid thermal decomposition of ClOO at polar temperatures, resulting in catalytic loss of ozone by Cycle 1. This contrasts with an earlier study, described in the previous Assessment, that indicated a ~10% yield of 2 ClO at 308 nm (Moore et al., 1999) (this branch leads to a null cycle for ozone). Most ozone depletion models assume production of only ClOO + Cl upon photolysis of ClOOCl. Thus, Plenge et al. (2004) increase our confidence in the accuracy of this assumption. However, the primary contribution to photolysis of ClOOCl occurs longward of 308 nm, and there remains a need to define the product yields of ClOOCl photolysis for the atmospherically relevant spectral region.

Many of the ozone loss simulations described below use a value for σ_{ClOOCl} based on measurements by Burkholder et al. (1990) out to 410 nm, with a log-linear extrapolation to 450 nm using a formula given by Stimpfle et al. (2004). This Burkholder et al. (1990) photolysis rate of ClOOCl is 40 to 50% faster than J_{1b} based on the *JPL 02-25* cross section and results in a good overall description of measured ClO and ClOOCl, if the *JPL 02-25* value of k_{1a} is also used (Stimpfle et al., 2004; see below). The JPL Publication 06-2 compendium (Sander et al., 2006;

POLAR OZONE

hereafter referred to as *JPL 06-2*) recommendation for σ_{ClOOCl} is the same as in the previous recommendation.

The correctness of a log-linear extrapolation relies on the assumption of a single dissociative state in the wavelength region of interest. The primary photolytic pathway for ClOOCl is excitation to a singlet electronic excited state. Peterson and Francisco (2004) suggested the existence of a weakly absorbing, dissociative triplet state, predicted to have an absorption maximum at about 385 ± 25 nm, based on an ab initio calculation of the structure of the ClOOCl molecule. This study calls into question the appropriateness of log-linear extrapolations of ClOOCl cross-section data.

Present uncertainty in J_{1b} underscores the need for laboratory studies able to quantify σ_{ClOOCl} to wavelengths as high as ~ 450 nm. Existing laboratory studies are based on spectra measured in the presence of other molecules, such as molecular chlorine (Cl_2), ozone, and/or dichlorine monoxide (Cl_2O). The ClOOCl cross sections must be determined by analysis of a composite spectrum that includes absorptions from multiple species. Large uncertainties in laboratory determinations of σ_{ClOOCl} persist at atmospherically important wavelengths because the procedures to correct for interfering species can be qualitative in nature and prone to error (e.g., Huder and DeMore, 1995).

Plenge et al. (2005) recently reported values of K_{EQ} based on the bond strength of ClOOCl determined using photoionization mass spectrometry. Their values of K_{EQ} are smaller than the *JPL 02-25* recommendation and the earlier laboratory study of Nickolaisen et al. (1994), but agree well with the laboratory measurement of Cox and Hayman (1988). The range of uncertainty for the *JPL 02-25* value of K_{EQ} encompasses results from all of these laboratory studies. A lower value of K_{EQ} implies that loss of ClOOCl by thermal decomposition occurs faster than previously thought, leading to higher levels of ClO during nighttime. Bröske and Zabel (2006) report a value for K_{EQ} , determined from a laboratory kinetics study over the temperature range 243 to 261 K, that lies between the values of Cox and Hayman (1988) and Plenge et al. (2005) but also exhibits a possible pressure dependence. The high-pressure ($p > 30$ hPa) value for K_{EQ} of Bröske and Zabel (2006) is similar to the *JPL 06-2* recommendation. The low-pressure result, considered to be more reliable by Bröske and Zabel (2006), leads to a value of K_{EQ} quite similar to the Plenge et al. (2005) value.

Ultimately, consistency between laboratory thermodynamic determinations of the heat of formation of ClOOCl and kinetic measurements of k_{1a} and the reverse of k_{1a} is desired. Determinations of K_{EQ} from kinetics studies are affected by uncertainties in k_{1a} . Bröske and Zabel (2006)

note that the apparent pressure dependence of K_{EQ} points to inconsistencies between dissociation and recombination data, since K_{EQ} is independent of pressure on theoretical grounds. Consistency between thermodynamic and kinetic measurements has yet to be achieved, especially for temperatures relevant for the winter polar stratosphere.

Field Observations

Stimpfle et al. (2004) reported the first measurements of ClOOCl, acquired from an instrument aboard the NASA ER-2 aircraft in the Arctic stratosphere during the winter of 1999/2000. These observations, analyzed with simultaneous measurements of ClO from the same instrument, were used to test the understanding of k_{1a} , J_{1b} , and K_{EQ} . Assuming the *JPL 02-25* recommendation for k_{1a} , measurements made during daylight, over a wide range of solar zenith angles, indicate best agreement with a value for J_{1b} based on absorption cross sections from Burkholder et al. (1990) (Figure 4-15). The JPL Publication 00-3 (Sander et al., 2000; hereafter referred to as *JPL 00-3*) rate for k_{1a} is most consistent with a value of J_{1b} based on ClOOCl cross sections that lie between those given by *JPL 02-25* and Burkholder et al. (1990), while the Boakes et al. (2005) rate for k_{1a} implies faster photolysis of ClOOCl than given by any of the available cross section measurements. Figure 4-15 highlights the fact, emphasized by Stimpfle et al. (2004), that daytime measurements of ClO and ClOOCl constrain only the ratio k_{1a}/J_{1b} . The value of J_{1b} decreases by more than an order of magnitude as solar zenith angle (SZA) increases from 70° to 92° (Figure 4-15), so analysis of $[\text{ClO}]^2/[\text{ClOOCl}]$ provides a test of the partitioning of these species for a wide range of photolytic conditions (Stimpfle et al., 2004). This ratio is important because models adopting J_{1b} based on Burkholder as well as k_{1a} from *JPL 02-25* will calculate more rapid ozone loss than models using *JPL 02-25* kinetics, since photolysis of ClOOCl is the rate-limiting step for ozone loss by Cycle 1. Considering the $\pm 25\%$ (1σ) uncertainty in the observations used to define β (see caption of Figure 4-15), a model based solely on *JPL 02-25* kinetics is not consistent with the observations at the 1σ uncertainty level (Stimpfle et al., 2004).

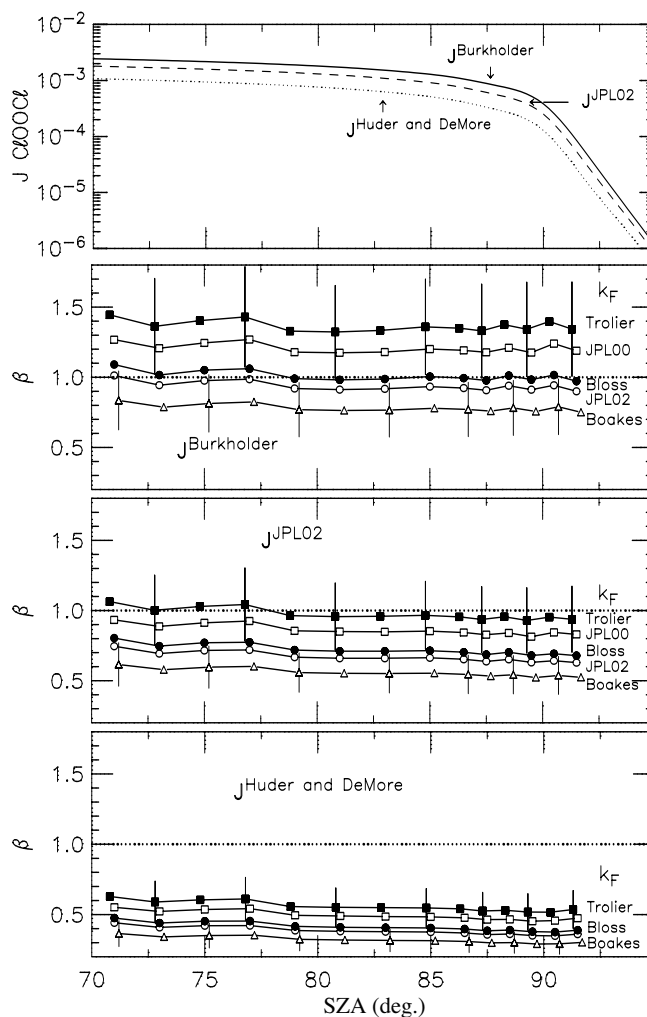
Field observations of nighttime ClO and in some cases ClOOCl abundances by several groups suggest that the equilibrium constant K_{EQ} may be smaller than the *JPL 02-25* recommendation. Observations of ClO and ClOOCl by Stimpfle et al. (2004), obtained during nighttime when thermal equilibrium (e.g., equation (3)) can be assumed, indicate better overall agreement with values of K_{EQ} from the laboratory study of Cox and Hayman

(1988) compared with values from either *JPL 02-25* or Nikolaisen et al. (1994). Nighttime observations of ClO and ClOOCl abundances in the Arctic stratosphere during the winter of 2002/2003 reported by von Hobe et al. (2005) were used to determine an empirical value for K_{EQ} that implies faster thermal decomposition for ClOOCl than the *JPL 02-25* value, and somewhat faster decomposition than the Cox and Hayman (1988) and Plenge et al. (2005) values. Berthet et al. (2005) analyzed nighttime observations of ClO in the Arctic vortex during the winter of 2002/2003, obtained from a microwave radiometer onboard the Odin satellite. They concluded that K_{EQ} lies between the laboratory determination of Cox and Hayman (1988) and the empirical value of von Hobe et al. (2005) and that their data are not consistent with the *JPL 02-25* value for K_{EQ} . Finally, an analysis of daytime and nighttime field measurements together with thermodynamic calculations and unimolecular rate theory reveals that overall best consistency between theory and observation is obtained using the Plenge et al.

(2005) value for K_{EQ} , the Nikolaisen et al. (1994) value for k_{1a} , and σ_{ClOOCl} that lies between *JPL 02-25* and the value given by Burkholder et al. (1990) (von Hobe et al., 2006). The uncertainty in the *JPL 02-25* recommendation for K_{EQ} encompasses all of the field observations as well as the recent laboratory determination based on measurement of the ClOOCl bond dissociation energy, so none of the recent results are outside of the range of prior expectation.

All of these recent results are in basic agreement with earlier analyses of nighttime atmospheric measurements of ClO (Avallone and Toohey, 2001, and references therein). Vogel et al. (2006) examined chemistry related to ClO-radical complexes, and concluded that this chemistry, while still highly uncertain, might be important for regulating the ratio of ClO and ClOOCl at night, which might complicate atmospheric, empirical determinations of K_{EQ} . However, the effect of uncertainty in K_{EQ} on ozone loss is small compared with other uncertainties, such as the abundance of BrO and

Figure 4-15. Daytime analysis of all SAGE III Ozone Loss and Validation Experiment (SOLVE) flights, β versus solar zenith angle (SZA), where $\beta = ([ClOOCl] / [ClO]^2)_{OBSERVED} / ([ClOOCl] / [ClO]^2)_{MODEL}$. Data selected for $SZA < 92^\circ$ and $M < 3.0 \times 10^{18}$ molec cm^{-3} . Average values of β are shown for 2° -wide SZA bins for $70^\circ < SZA < 86^\circ$, and for 1° -wide bins for $SZA > 86^\circ$. The top panel shows calculated values of J_{1b} versus SZA at 60 hPa for a model albedo of 0.24, using values of the ClOOCl cross section from Burkholder et al. (1990), *JPL 02-25*, and Huder and DeMore (1995), as indicated. Observed albedos are used for the calculations of β . The bottom three panels show results for using three values of the absorption cross section of ClOOCl: Huder and DeMore (1995), *JPL 02-25*, and Burkholder et al. (1990). Within each panel, results are shown for model simulations using five values of the rate constant of ClO + ClO + M: Trolier et al. (1990), *JPL 00-3*, Bloss et al. (2001), *JPL 02-25*, and Boakes et al. (2005). Error bars depict the $\pm 25\%$ uncertainty (1σ) in β attributable to the uncertainties in the observations of ClO and ClOOCl; error bars are shown only for simulations using the Trolier et al. (1990) and Boakes et al. (2005) rate constants. Points associated with these two model runs have been displaced slightly with respect to the actual mean SZA, for clarity of the error bars. After Stimpfle et al. (2004).



POLAR OZONE

the photolysis rate of ClOOCl. Perhaps the most important reason to reduce uncertainties in K_{EQ} is that accurate knowledge of this parameter will enable better determination of ClO_x (ClO + 2 × ClOOCl) from nighttime observations of ClO.

4.2.1.2 BROMINE

Measurements of BrO profiles in the Arctic vortex have been obtained for a number of winters using a balloonborne spectrometer (e.g., Pfeilsticker et al., 2000; Fitzenberger, 2000; Pundt et al., 2002; Dorf et al., 2006). Model studies that deduce BrO_x (BrO + BrCl) or Br_y from these BrO profiles estimate a total bromine loading of 20 to 24 parts per trillion by volume (pptv) (Canty et al., 2005; Dorf et al., 2006; Frieler et al., 2006), significantly larger than the abundance of bromine that can be delivered to the stratosphere by methyl bromide (CH₃Br) + halons alone (see Chapter 2). Most chemical transport models (CTMs), GCMs, and CCMs used to assess polar ozone loss use estimates of Br_y based only on supply of bromine from CH₃Br + halons. A value of bromine radicals (BrO_x) inferred from BrO in the Arctic vortex on 18 February 2000 is 40 to 60% higher (e.g., 6 to 9 pptv larger) than values of BrO_x (BrO + BrCl) used in typical simulations of the Modèle Isentropique de transport Mésoéchelle de l'Ozone Stratosphérique par Advection avec CHIMie (MIMOSA-CHIM) 3-D CTM and the Atmospheric and Environmental Research, Inc. (AER) two-dimensional (2-D) model (Figure 4-16), resulting in a larger relative contribution from bromine to polar ozone loss (Frieler et al., 2006). The BrO_x profile shown in Figure 4-16 provides additional and independent support to the results to the analyses shown in Chapter 2 because the chemistry used to infer BrO_x from BrO at high latitude (involving only bromine chloride (BrCl) and BrO) is distinct from the chemistry used to infer Br_y from BrO at midlatitudes (involving mainly BrO and bromine nitrate (BrONO₂), and hypobromous acid (HOBr) and hydrogen bromide (HBr) to a lesser degree).

Retrievals of BrO profiles from Scanning Imaging Absorption Spectrometer for Atmospheric Chartography (SCIAMACHY) limb scattered radiances, which provide near-global coverage and hence include the polar vortices, have been conducted by two research groups. Sinnhuber et al. (2005b) report a modest contribution, 3 ± 3 pptv, to Br_y from VSL compounds, whereas Sioris et al. (2006) deduce a much larger contribution, 8.4 ± 2 pptv. As discussed in Chapter 2, these discordant findings are driven by differences in the retrievals of BrO. Schofield et al. (2006) report ground-based observations of BrO over Arrival Heights, Antarctica (77.8°S), that are consistent

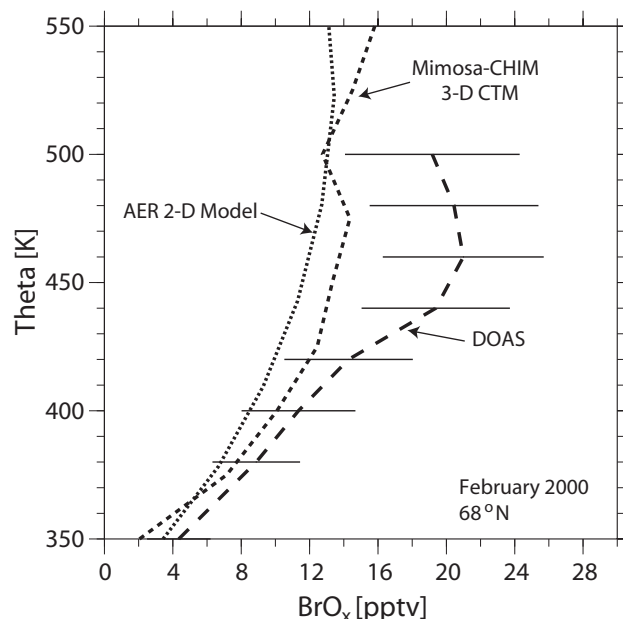
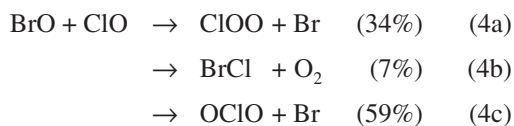


Figure 4-16. Profile of BrO_x (= BrO + BrCl) inferred from a DOAS measurement of BrO over Kiruna, Sweden (68°N), on 18 February 2000 (Canty et al., 2005; Fitzenberger, 2000) compared with a profile of BrO_x found for this region by the AER two-dimensional model assuming supply of stratospheric bromine from only CH₃Br and halons (Salawitch et al., 2005). Also shown is an estimate of Br_y from the MIMOSA-CHIM three-dimensional chemical transport model, assuming again stratospheric supply of Br_y only by CH₃Br + halons. Adapted from Frieler et al. (2006).

with Br_y of ~21.2 pptv at 20 km, suggesting again a significant role for the presence of more bromine in the polar regions than can be supplied solely by CH₃Br and halons. Giovanelli et al. (2005) obtained aircraft measurements of BrO over Antarctica that range from 4 to 10.3 pptv. Chapter 2 provides an extensive discussion on the quantification of the role of VSL compounds on the stratospheric bromine budget.

The reaction of BrO + ClO has three product channels:



The percentage yields for the three branches at 195 K using JPL 02-25 kinetics are noted. Channels 4a and 4b lead to

ozone loss (following thermal decomposition of ClOO or photolysis of BrCl), which is generically represented by process 2a in the depiction of Cycle 2. Channel 4c, the most efficient branch, results in a null cycle, since the O-O bond is not reformed upon loss of OCIO.

The only direct determination of the yield of BrCl from BrO + ClO, a laboratory study conducted at room temperature (Poulet et al., 1990), resulted in a yield of ~12%, larger than the *JPL 02-25* room temperature recommendation of $9 \pm 2\%$. Considerable uncertainty exists in the branching ratios at temperatures characteristic of the polar vortices, owing mainly to the lack of direct laboratory determinations at low temperature. Nighttime abundances of OCIO are particularly sensitive to the branching ratios of BrO + ClO, since the twilight formation of BrCl as a nighttime reservoir of bromine affects the efficiency of OCIO production. An analysis of nighttime OCIO measurements, obtained by lunar and stellar occultation, suggests a higher yield for BrCl and a smaller yield for OCIO from the BrO + ClO reaction at low temperature than is given by *JPL 02-25* (Canty et al., 2005). This result could imply a ~10% increase in the rate of ozone loss by the BrO + ClO cycle (Canty et al., 2005). While numerous uncertainties complicate the interpretation of nighttime OCIO, the study of Canty et al. (2005) underscores the need for better definition of the branching ratios of the BrO + ClO reaction.

The precise level of BrO and Br_y in the polar vortices remains an area of active research. Many measurements are emerging from satellite, balloon, and in situ aircraft instruments. Quantification of the contribution of VSL bromocarbons to the Br_y budget of the polar vortices and of the branching ratios of the BrO + ClO reaction at low temperature are needed to improve future quantification of the polar ozone loss rates and to better quantify the relative contribution of bromine to polar ozone loss.

4.2.1.3 OZONE LOSS RATES

This section focuses on studies that examine the consistency of modeled and measured chemical loss rates of polar ozone. The discussion is organized around two key concepts: (1) that models, using rate constants from *JPL 02-25* and estimates of bromine based on supply of bromine from only CH₃Br + halons, tend to underestimate measured chemical ozone loss rates, particularly during cold Arctic Januaries (e.g., Rex et al., 2003 and references therein); and (2) that the overall amount of chemical loss of column ozone, for specific Arctic winters, exhibits a tight correlation with the volume of air in the vortex that has been exposed to PSCs throughout winter (Rex et al., 2004; Tilmes et al., 2004).

Ozone Loss Rates: Measurement Overview

The estimates of ozone loss rates in Rex et al. (2003) are based on the Match technique applied to a series of ozone-sonde measurements. This study showed that measured chemical loss rates of Arctic ozone exceed the maximum possible calculated rates, assuming complete chlorine activation and *JPL 00-3* kinetics, for four cold Januaries (1992, 1995, 1996, and 2000). A number of other studies, some of which have been discussed in previous assessments, also have documented similar discrepancies between measured and calculated chemical ozone loss rates during cold Arctic Januaries (e.g., Hansen et al., 1997; Becker et al., 1998). The estimates of ozone loss rates in Rex et al. (2004), which examine processes over longer time scales than Rex et al. (2003), are based on the “vortex-averaged descent” technique applied to temporal averages of ozonesonde profiles inside the polar vortex. Rex et al. (2004) showed a tight, near-linear relation between chemical loss of column ozone (ΔO_3) and the volume of air exposed to PSC conditions (V_{PSC}) in the Arctic vortex for data collected during 10 Arctic winters that span 12 years (Figure 4-13, previous section). A preliminary version of this relation was presented in the previous Assessment. The relation between ΔO_3 and V_{PSC} was poorly simulated by the 3-D CTM simulations of SLIMCAT shown in Rex et al. (2004). These SLIMCAT simulations exhibit a slope that is considerably less steep than the observations (Figure 4-13), implying the model might be underestimating the sensitivity of future polar ozone depletion to climate change. However, as shown below, updated runs of SLIMCAT result in an improved simulation of the relation between ΔO_3 and V_{PSC} .

Tilmes et al. (2004) conducted an independent analysis of the relation between ΔO_3 and V_{PSC} that was based on chemical loss rates deduced from analyses of Halogen Occultation Experiment (HALOE) data. Their study supports the linear relationship between ΔO_3 and V_{PSC} reported by Rex et al. (2004). They also showed that, if V_{PSC} is averaged over the same time period as ΔO_3 , then solar illumination of the cold vortex is a factor that impacts ozone loss rates.

Ozone Loss Rates: Theory and Observation

A number of studies using various models have shown considerable improvement in our understanding of polar ozone loss rates since the previous Assessment. Feng et al. (2005b) reported 3-D CTM calculations using the SLIMCAT model of Arctic ozone for the winters of 1999/2000, 2002/2003, and 2003/2004. In their model, they assumed an extra 100 pptv of chlorine and an extra 6 pptv of bromine reaches the stratosphere, due to short-

POLAR OZONE

lived halocarbons (these values are consistent with estimates given in Chapter 2). They used *JPL 02-25* kinetics, except the value for σ_{ClOOCl} was based on Burkholder et al. (1990), extrapolated to 450 nm as described by Stimpfle et al. (2004). They used a simple nitric acid trihydrate (NAT)-based denitrification scheme, described by Davies et al. (2002). Overall, the model calculations provided a realistic representation of chemical ozone loss for the three winters. Some discrepancies between observed and calculated ozone are noted during times of vortex disturbance, but overall these simulations provide a quantitative advance in the ability to accurately simulate chemical ozone loss rates using the SLIMCAT model. Groöb et al. (2005b) reported improvements in the agreement between modeled and measured ozone loss rates upon use of a more realistic denitrification scheme within the CLaMS Lagrangian trajectory model for the Arctic winter of 2002/2003. A study using the MIMOSA-CHIM CTM found that denitrification contributed about 23% and 17% more ozone depletion for the Arctic winters of 1999-2000 and 2002-2003, respectively, compared with model calculations that did not include denitrification (Tripathi et al., 2006). They also found best agreement between measured and modeled chemical loss of column ozone for Arctic winters of 1999/2000 and 2002/2003 for a simulation that used the Burkholder et al. (1990) cross section, allowed for supply of bromine from CH_3Br and halons as well as short-lived species methylene bromide (CH_2Br_2) and bromochloromethane (CH_2BrCl), and an adjustment to cooling rates that improved agreement with measured N_2O (i.e., that led to more realistic vortex descent).

Chipperfield et al. (2005) examined the relation between ΔO_3 and V_{PSC} using runs of the SLIMCAT CTM updated relative to results shown in Rex et al. (2004). These runs used the Burkholder et al. (1990) extrapolated value for σ_{ClOOCl} , an extra 100 pptv of inorganic chlorine (Cl_y) and an extra 6 pptv of Br_y due to VSL halocarbons (Chapter 2), and a treatment of denitrification by large nitric acid trihydrate (NAT) particles (Davies et al., 2002) that results in denitrification for the cold winters that was largely absent from earlier ice-based denitrification schemes. The new denitrification scheme increased modeled ozone depletion by ~30% for cold winters, such as 1999/2000 (Davies et al., 2002; Chipperfield et al., 2005). Also, the new SLIMCAT runs were at higher spatial resolution ($2.8^\circ \times 2.8^\circ$) than the older simulations ($7.5^\circ \times 7.5^\circ$) shown in Rex et al. (2004) and used a new radiation scheme; these improvements lead to stronger descent and a more isolated vortex. The new SLIMCAT runs simulate quite well the empirical relation between ΔO_3 and V_{PSC} (Figure 4-13). Improvements relative to the SLIMCAT results shown in Rex et al. (2004) are due to all three chem-

ical factors as well as the improved model representation of vortex descent and isolation.

Douglass et al. (2006) simulated ΔO_3 versus V_{PSC} using a CTM driven by winds from a 50-year integration of the Goddard Earth Observing System (GEOS-4) GCM. Their calculations were conducted at a resolution of 2.5° (longitude) by 2.0° (latitude). They concluded that use of winds from a GCM tends to result in a more realistic simulation of vortex isolation than found using assimilated winds. Douglass et al. (2006) were able to simulate well the empirical relation between ΔO_3 and V_{PSC} for standard photochemistry (e.g., *JPL 02-25*) and for Br_y assuming no contribution from VSL halocarbons. They also reported that use of the Burkholder et al. (1990) value for σ_{ClOOCl} and extra bromine from VSL compounds resulted in excess ozone loss compared with observations. Hence, it is presently unclear whether changes in ClO_x photochemistry and representation of Br_y from VSL compounds are needed to achieve accurate representation of the ΔO_3 versus V_{PSC} relation within CTMs. Finally, Tripathi et al. (2006) examined the sensitivity of ozone loss to CTM resolution, and concluded that their model required a resolution of $1.0^\circ \times 1.0^\circ$ to properly represent ozone loss at the edge of the vortex at low solar illumination (i.e., during January in the Arctic).

Hoppel et al. (2005a) compared measured ozone loss rates in the Antarctic vortex, found using the Match approach applied to POAM III satellite data, with Lagrangian box model estimates of calculated ozone loss rates. They reported that agreement between modeled and measured ozone loss rates is improved if the model employs larger values of σ_{ClOOCl} (e.g., Burkholder et al., 1990) and a total bromine loading of 24 pptv, reflecting an ~8 pptv contribution from VSL bromocarbons. This amount of bromine from VSL species is near the upper limit of estimates based on satellite and aircraft data (Section 2.5, Chapter 2). Tripathi et al. (2006) concluded that a CTM simulation using *JPL 02-25* kinetics and bromine from CH_3Br , halons, CH_2Br_2 , and CH_2BrCl tended to underestimate observed Antarctic ozone loss rates for several winters. Slightly better agreement was obtained using Burkholder et al. (1990) cross sections.

Frieler et al. (2006) examined measured and modeled ozone loss rates for the Arctic and Antarctic vortices, with the measured loss rates based on Match estimates applied to ozonesonde data, and the modeled loss rates based on Lagrangian box model calculations. Their reference simulation used *JPL 02-25* kinetics and a value for BrO_x based on supply of Br_y from only CH_3Br + halons. Using the maximum amount of ClO_x available, the reference simulation underestimates observed ozone loss rates for several Arctic winters, particularly during cold Januaries, such as in 2000 (Figure 4-17, top panel), consistent

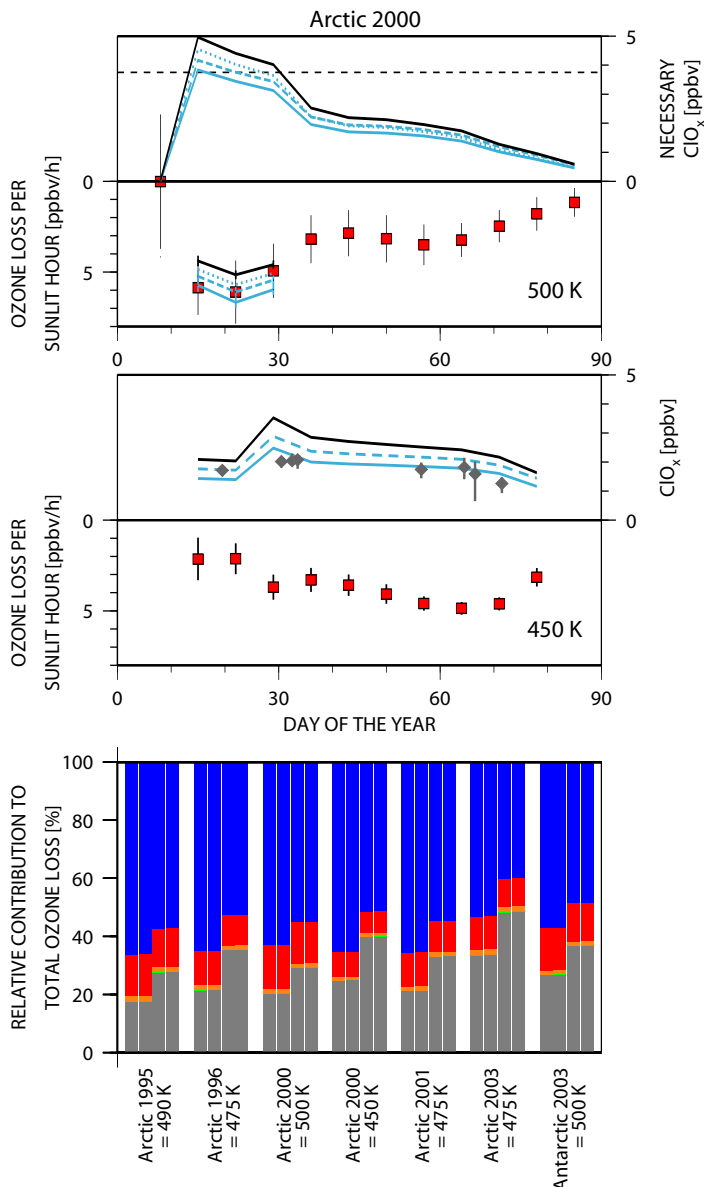


Figure 4-17. Top two panels: All results are for the Arctic winter 1999/2000. Gray diamonds represent the mean value of ClO_x measured at 450 ± 10 K potential temperature for 8 ER-2 flights that remained entirely inside the vortex; vertical bars represent the range between maximum and minimum ClO_x (Stimpfle et al., 2004). The lines represent the amount of ClO_x necessary to account for the measured ozone loss rate and the modeled ozone loss assuming $\text{ClO}_x = 3.7$ ppbv (“maximum possible ozone loss”), for the following four model runs:

- Run 1 (black): *JPL 02-25* kinetics and modeled BrO_x from CH_3Br and halons
- Run 2 (blue dashed): Burkholder et al. (1990) σ_{ClOOCl} and modeled BrO_x from CH_3Br + halons
- Run 3 (blue dotted): *JPL 02-25* kinetics and measured BrO_x
- Run 4 (blue solid): Burkholder et al. (1990) σ_{ClOOCl} and measured BrO_x

Red boxes show the observed chemical ozone loss rate per sunlit hour from Match (error bars denote 1σ uncertainty), used to constrain model estimates of necessary ClO_x . Bottom panel: Relative importance of ozone loss due to the $\text{BrO} + \text{ClO}$ cycle (gray), the HOCl cycle (orange), the $\text{ClO} + \text{O}$ cycle (red), and the $\text{ClO} + \text{ClO}$ cycle (blue), for various Arctic winters (as indicated). Each grouping shows model results, in order, for the four model runs described above (e.g., run 4 has highest contribution of $\text{BrO} + \text{ClO}$ to ozone loss). Adapted from Frieler et al. (2006).

POLAR OZONE

with previous results (e.g., Rex et al., 2003). They show that the discrepancy between measured and maximum possible ozone loss rates in January (i.e., rates based on an assumption of complete chlorine activation) is largely resolved in a second model run that assumed a profile for BrO_x based on differential optical absorption spectroscopy (DOAS) balloon BrO that is considerably higher than BrO_x found assuming supply of Br_y from only CH_3Br + halons (Figure 4-16), and a value for J_{1b} based on the Burkholder et al. (1990) value for σ_{ClOOCl} (extrapolated to 450 nm). The largest effects on ozone removal rates were the faster value of J_{1b} (~20% effect) and the higher value of BrO_x (~15% effect). The relative contribution of Cycle 2 (BrO + ClO) to overall chemical loss for various winters increases from 17 to 33% for the reference run to 27 to 48% for the model run that agrees best with overall measured ozone loss rates (Figure 4-17, bottom panel).

Most important, Frieler et al. (2006) were able to examine ClO_x (Stimpfle et al., 2004), BrO_x (Fitzenberger, 2000; Canty et al., 2005), and measured and modeled ozone loss rates for the Arctic winter of 1999/2000. They showed good overall consistency between all of these quantities for the second model run (Figure 4-17, middle panel), suggesting a good quantitative explanation of the chemical loss rates of Arctic ozone for this winter at 450 K, the highest level where sufficient in situ measurements of ClO_x species are available. This finding relies on the validity of the larger value of J_{1b} and higher levels of stratospheric bromine. These aspects of polar chemistry are still subject to considerable uncertainty, due to differences in various laboratory measurements of σ_{ClOOCl} (Section 4.2.1.1) and uncertainty in the atmospheric abundance of BrO (Chapter 2). Also, quantitative consistency between observation of polar ozone loss rates and measured ClO_x and BrO has yet to be demonstrated at other altitudes and for other years.

In summary, numerous recent studies have shown that models are better able to capture the observed degree of chemical loss of polar ozone for a wide range of meteorological conditions that occurred during the past decade. This is an important advancement since the previous Assessment. The improvements of simulated ozone depletion are driven in part by the use of global models that are able to better capture the isolation of the polar vortices, due to improved horizontal resolution and/or winds that minimize excessive horizontal mixing across vortex boundaries. Previously noted discrepancies between measured and modeled ozone loss rates are largely resolved, within Lagrangian trajectory box models, assuming a faster rate of ClOOCl photolysis, higher levels of BrO that may be consistent with a sig-

nificant source from VSL bromocarbons, and improved representation of denitrification that appears to be consistent with available observations (see Section 4.2.2). While the faster rate of ClOOCl photolysis appears to be consistent with atmospheric observations of ClO and ClOOCl , it is important to stress that daytime observations of these species constrain only the ratio k_{1a} / J_{1b} , and that considerable uncertainty exists in present laboratory determinations of k_{1a} and the cross sections used to calculate J_{1b} . Nighttime observations of ClO provide an important test of the consistency of our understanding of polar ozone photochemistry. However, field observations reveal inconsistencies with many laboratory studies. Also, we have yet to achieve consistency between thermodynamic and kinetic laboratory studies of ClO/ClOOCl photochemistry, in part due to the challenges associated with laboratory work at temperatures near 200 K. Finally, quantification of BrO and Br_y levels in the polar vortices, and the role of VSL bromocarbons, presents an additional source of uncertainty that is an active area of research.

4.2.2 PSC Processes

Polar stratospheric clouds (PSCs) influence ozone loss through two main processes: (1) chlorine activation on PSC particles leading to ozone losses and (2) sedimentation of PSCs causing denitrification and exacerbating ozone loss. Our understanding of denitrification in particular continues to evolve, mainly in response to research into the characteristics and formation of solid-phase nitric acid hydrate particles. WMO (2003) described the unexpectedly low ($\sim 10^{-4} \text{ cm}^{-3}$) concentrations of large nitric acid particles that were first observed during the 1999/2000 Arctic winter with the introduction of improved instrumentation (Fahey et al., 2001). Several studies have now concluded that such particles are widespread, both from in situ observations during the 2002/2003 Arctic winter (Larsen et al., 2004; Voigt et al., 2005) and from updated analyses of remote measurements (Poole et al., 2003; Adriani et al., 2004). Using multiple simultaneous PSC measurements, Larsen et al. (2004) have demonstrated that a low concentration of nitric acid trihydrate (NAT) particles can be masked when the coexisting liquid particles become optically dominant. Therefore, a background population of solid particles may be more pervasive than is apparent in remote sensing observations, requiring the introduction of new PSC formation mechanisms.

Synoptic-scale ice formation below the frost point (T_{ice}), which was considered to be a primary mechanism for solid nitric acid formation, is much too infre-

quent to account for the widespread formation of solid nitric acid particles in the Arctic. In contrast, mesoscale temperatures below T_{ice} may provide a NAT formation mechanism, through nucleation of nitric acid hydrates on mountain wave-induced ice clouds. High concentrations of mesoscale solid nitric acid particles have been unambiguously identified in multiple studies (Carslaw et al., 1999; Wirth et al., 1999; Hu et al., 2002; Fueglistaler et al., 2003; Luo et al., 2003). Modeling studies have demonstrated that sedimentation from the base of a NAT cloud with high particle concentrations (the “mother cloud”) allows selective growth of a few NAT particles in the underlying supersaturated, cloud-free air (Fueglistaler et al., 2002a; Dhaniyala et al., 2002). Over several days, low concentrations (10^{-2} - 10^{-5} cm^{-3}) of large NAT particles are generated over a wide vertical and horizontal extent. This mechanism can successfully explain observations of low NAT particle concentrations from clouds assumed to initially contain much higher solid particle concentrations (Fueglistaler et al., 2002b). Mann et al. (2005) have shown that including this mechanism in a 3-D model can produce large NAT particles in up to 60% of the NAT supersaturated region in the Arctic. Most studies have focused on the Arctic, but some Antarctic NAT PSC observations have also been attributed to mesoscale nucleation (Höpfner et al., 2006).

Other Arctic PSC observations, however, cannot be explained by mesoscale cloud formation (Pagan et al., 2004; Larsen et al., 2004; Voigt et al., 2005). Pagan et al. (2004) examined the role of mountain wave ice clouds in generating solid-phase nitric acid PSCs that were observed on three dates. Using satellite observations and model results to identify any regions with ice cloud formation, Pagan et al. (2004) concluded that none of the observed PSCs could have originated in an ice cloud. In situ measurements of large nitric acid particles at low concentrations made by Voigt et al. (2005) in the Arctic also cannot be attributed to ice formation, at either the synoptic scale or mesoscale. The observed particles formed within one day of the temperature dropping below the NAT temperature, T_{NAT} , with temperatures at most 3.1 K below T_{NAT} (implying NAT supersaturation ratios less than ten). The narrow range of environmental conditions strictly constrains the formation mechanism and the NAT freezing rate. Voigt et al. (2005) show that heterogeneous freezing of NAT, specifically triggered by meteoritic particles, could explain the observations. Homogeneous freezing of NAT is unlikely, because laboratory data show that such freezing is very slow under the observed conditions (Knopf et al., 2002). Alternative interpretations of the

homogeneous freezing rates have been proposed (Tabazadeh, 2003). However, in a study of several proposed homogeneous freezing rates, Drdla and Browell (2004) concluded that none yielded model results consistent with observations of denitrification and PSC onset for the 1999/2000 Arctic winter. Heterogeneous freezing currently appears to be the most likely mechanism for producing nitric acid hydrate particles at synoptic scales in the Arctic. However, the specifics remain poorly defined, such as the nuclei involved, the factors that control the freezing rate, and the extent to which heterogeneous freezing also occurs in the Antarctic.

Based on these PSC formation mechanisms, new denitrification schemes for CTMs have been developed. Previous denitrification schemes that required synoptic scale temperatures below T_{ice} frequently failed to get any Arctic denitrification; the new schemes produce much more widespread denitrification. Revised denitrification has contributed to improvements in modeling ozone loss (see Section 4.2.1.3). Synoptic-scale particle formation has been approximated by applying a slow, uniform NAT particle-formation rate whenever NAT is supersaturated. Using this approach and an assumed rate of 8×10^{-10} $\text{cm}^{-3}\text{s}^{-1}$, Davies et al. (2005) have simulated several Arctic winters with the SLIMCAT CTM. Generally good agreement was found between model denitrification and observations (both satellite and in situ), but interannual variability in denitrification was not fully captured. The CLaMS has introduced a similar denitrification scheme (Groß et al., 2005b); for the Arctic winter studied by Groß et al. (2005b), a prescribed rate of 2×10^{-9} $\text{cm}^{-3}\text{s}^{-1}$ best reproduced observed denitrification. A single, constant particle formation rate appears insufficient to simulate interannual variability, but refinements will require a more detailed understanding of PSC formation mechanisms and their rates.

Alternatively, denitrification may be caused by mesoscale NAT PSCs. This mechanism has been studied with the SLIMCAT CTM (Mann et al., 2005) by introducing mountain wave-induced ice clouds that generate NAT “mother clouds.” They concluded that approximately 80% of the denitrification observed in the 1999/2000 Arctic winter could have been caused by sedimentation of particles out of mountain wave-induced NAT mother clouds. Further quantification of this mechanism is limited by the requirement for accurate mountain wave information spanning the polar vortex. Therefore, the relative importance of synoptic scale and mesoscale processes for denitrification remains uncertain.

In summary, the mechanisms responsible for NAT PSC formation and thus denitrification have been refined

POLAR OZONE

over the last four years, with increasing evidence that key processes occur above the ice frost point. However, specifics of PSC formation remain uncertain, forcing model denitrification to rely upon empirical freezing rates that are unable to fully capture interannual variability. Recent findings are primarily based on Arctic observations. Whether these PSC formation processes and denitrification mechanisms are equally applicable in the Antarctic remains to be evaluated.

4.3 RECENT POLAR OZONE CHANGES

4.3.1 2002 Antarctic Ozone Hole

In September 2002, a SH major stratospheric warming split the polar vortex and ozone hole for the first time in the observational record. Major warmings cause dramatic stratospheric circulation changes. Warmings are caused by planetary waves propagating up from the troposphere. These waves decelerate the polar night jet, increase polar temperatures, and distort and/or split the vortex. Warmings are classified as major if the 10 hPa zonal-mean temperatures increase poleward of 60° and 10 hPa zonal-mean winds turn easterly (Julian, 1967; Labitzke, 1968). Major warmings are distinguished from final warmings, where final warmings mark the transition from the cold vortex in winter to the warm anticyclone in summer.

The September 2002 major warming was puzzling because it was previously thought they only happened in the NH, where the tropospheric forced planetary wave activity is much stronger (see WMO, 1986, Section 6.1.7). The Arctic polar vortex is regularly disturbed by waves, with major warmings occurring every two to three years. The difference in planetary wave activity between the hemispheres is due to various factors: less orographic forcing and weaker longitudinal land-sea contrast in the SH, and the presence of the cold elevated Antarctic continent at the pole. As a consequence, Antarctic winter stratospheric temperatures are much colder than the Arctic and exhibit much less variability (see midwinter period in Figure 4-1). Furthermore, temperature records from 1940 do not show evidence of any major Antarctic warmings (Roscoe et al., 2005; Naujokat and Roscoe, 2005).

This unprecedented event induced a dramatic reduction of the ozone hole area to less than 5 million km² as compared with more than 20 million km² in the previous years (Stolarski et al., 2005). Its occurrence triggered numerous investigations using meteorological analyses, observations of chemical species from various satellite and ground-based instruments, and model simulations.

4.3.1.1 OBSERVATIONS

Chemistry

The major warming had a dramatic impact on total ozone (Stolarski et al., 2005). On 23 September, the ozone hole elongated and split in two pieces (Figure 4-18). One piece drifted over South America and dissipated, while the other drifted back over the pole as a significantly weakened ozone hole. The 2002 total ozone daily minimum value did not reach values lower than 150 DU, as compared with around 100 DU in the preceding decade. Higher total ozone values were observed in the polar region from mid-September to mid-October. Ozone hole metrics (Figures 4-7 and 4-8) all show remarkable deviations from averages over the last decade.

Ozone profiles showed that the vortex was not vertically aligned during the major warming. Solar Backscatter Ultraviolet (SBUV) measurements show an increase of ozone in the 70°-80°S region of about 200

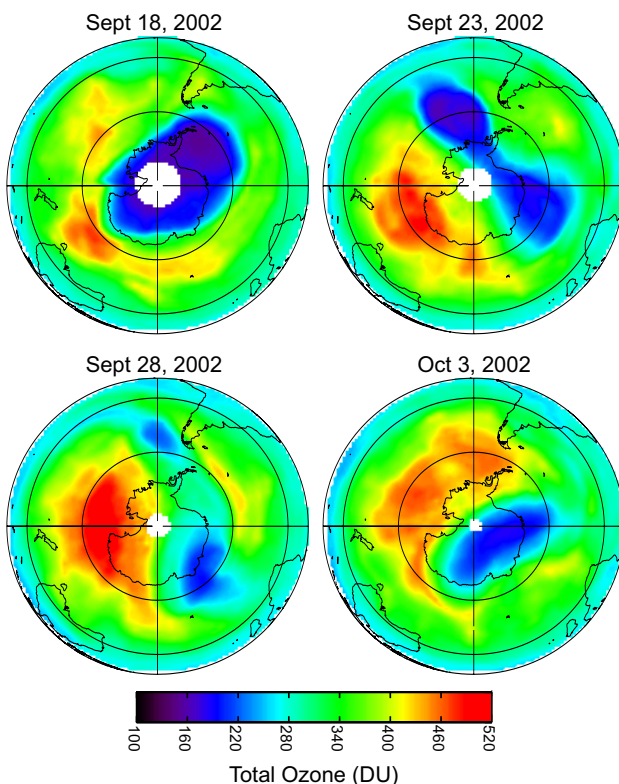


Figure 4-18. TOMS total ozone maps for four days during September and October 2002. The white space around the South Pole is polar night, where no measurements are made. Adapted from Stolarski et al. (2005).

DU due to the influx of low latitude air (Kondragunta et al., 2005). Upper levels of the vortex were displaced from the pole so that the ozone-depleted lower stratosphere region was overlaid by ozone-rich extra-vortex air (Allen et al., 2003; Randall et al., 2005a; Yela et al., 2005). POAM measurements showed that below 22 km, the chemical ozone loss was similar to previous years up to the major warming (Hoppel et al., 2003).

Measurements of minor chemical species provide further insights into the 2002 ozone hole. Most measurements showed that prior to the warming, the vortex was denitrified, with near-complete chlorine activation and extensive PSC areas up to 24 km (Ricaud et al., 2005; von Savigny et al., 2005). The large temperature increase during the warming induced rapid PSC disappearance and deactivation of chlorine radicals. Faster decay of the OCIO slant column was measured by satellite and ground observations in September as compared with the same period in 1996-2001 (Richter et al., 2005; Frieß et al., 2005). The re-establishment in October of a weak vortex in the lowermost polar stratosphere was confirmed by satellite observations that showed low ozone mixing ratios below 20 km (Ricaud et al., 2005; von Savigny et al., 2005). As the middle stratosphere remained strongly perturbed, rapid NO₂ recovery above 25 km was observed, inducing larger than usual total NO₂ columns in the polar regions in October (Frieß et al., 2005; Richter et al., 2005; Yela et al., 2005).

Dynamics

Meteorological conditions in 2002 showed that the early winter was already unusually disturbed (Hio and Yoden, 2005; Newman and Nash, 2005; Allen et al., 2003). Figure 4-19 (second panel) displays the vertical distribution of the 2002 zonal-mean temperature departure from the 1979-2001 mean in the 55°-75°S latitude band. From June, temperatures steadily increased with respect to the climatological average until the September major warming. Temperature increases are associated with decreases of the zonal-mean wind intensity at 60°S and 10hPa (Figure 4-19, panels 1 and 3). In August, the zonal wind dropped below the 1979-2001 range of values and turned easterly during the warming. The temperature increase in the polar vortex collar is directly controlled by the planetary waves propagating upward from the troposphere to the stratosphere. The black line in the bottom panel of Figure 4-19 is the time series of midlatitude eddy heat flux in 2002 at 100 hPa for waves 1-3 (heat flux is proportional to the vertically propagating wave activity). The 2002 times series is compared with the climatological average over the 1979-

2001 period (gray shading). There are several significant wave events from May to October. After each wave event, the stratosphere warmed by a few degrees until the major warming in late September. During this event, the eddy heat flux reached twice the largest value in the 1979-2001 period.

The synoptic development of the vortex split in September 2002 is described in several studies (e.g., Charlton et al., 2005; Krüger et al., 2005). The vortex began to split on 24 September. By 26 September, it had split completely at 10 hPa into two vortices of similar intensity with a tongue of anticyclonic circulation stretching across the pole and a region of high temperature between each vortex and the anticyclone. By 8 October, a single weakened vortex was re-established over the pole. The vortex split extended up to 1 hPa. In the lower stratosphere, the vortex did not split but formed two distinct cyclonic systems. During the major warming, polar temperatures south of 60° increased by about 25 K at 10 hPa and local temperature at several Antarctic stations showed an increase of up to 50 K at 30 and 10 hPa. The 60°S mean zonal wind reversed from ~60 m/s westerly to ~15 m/s easterly at 10 hPa until 30 September, when it switched back to westerlies. Much weaker westerly winds were re-established in October as one of the cyclonic remnants of the polar vortex moved back toward the pole. The final warming of the vortex occurred in late October, much earlier than in previous years.

4.3.1.2 MODELING OF THE WARMING

The 2002 warming was simulated by mechanistic models for reproducing the event's dynamics, and by CTMs for a detailed evaluation of the vortex chemical evolution. The UK stratosphere-mesosphere model (USMM) reproduced the warming's dynamical features (Manney et al., 2005a). This simulation was initialized on 14 September 2002 and forced at 100 hPa by analyzed geopotential heights. The model produced a good simulation of the vortex recovery phase, suggesting that the warming's evolution was largely determined by the initial conditions and the prescribed 100 hPa geopotential heights. The modeled transport during the warming showed enhanced diabatic descent in the vortex below ~700 K and strong poleward transport and mixing in mid- to high-latitude regions. The strong vortex vertical tilt during the warming was well reproduced, showing low-latitude air surrounding and overlying the vortices after the split in the middle stratosphere. Sensitivity tests indicate a strong dependence on the boundary forcing, especially the amplitude and upward propagation of planetary wave-2.

POLAR OZONE

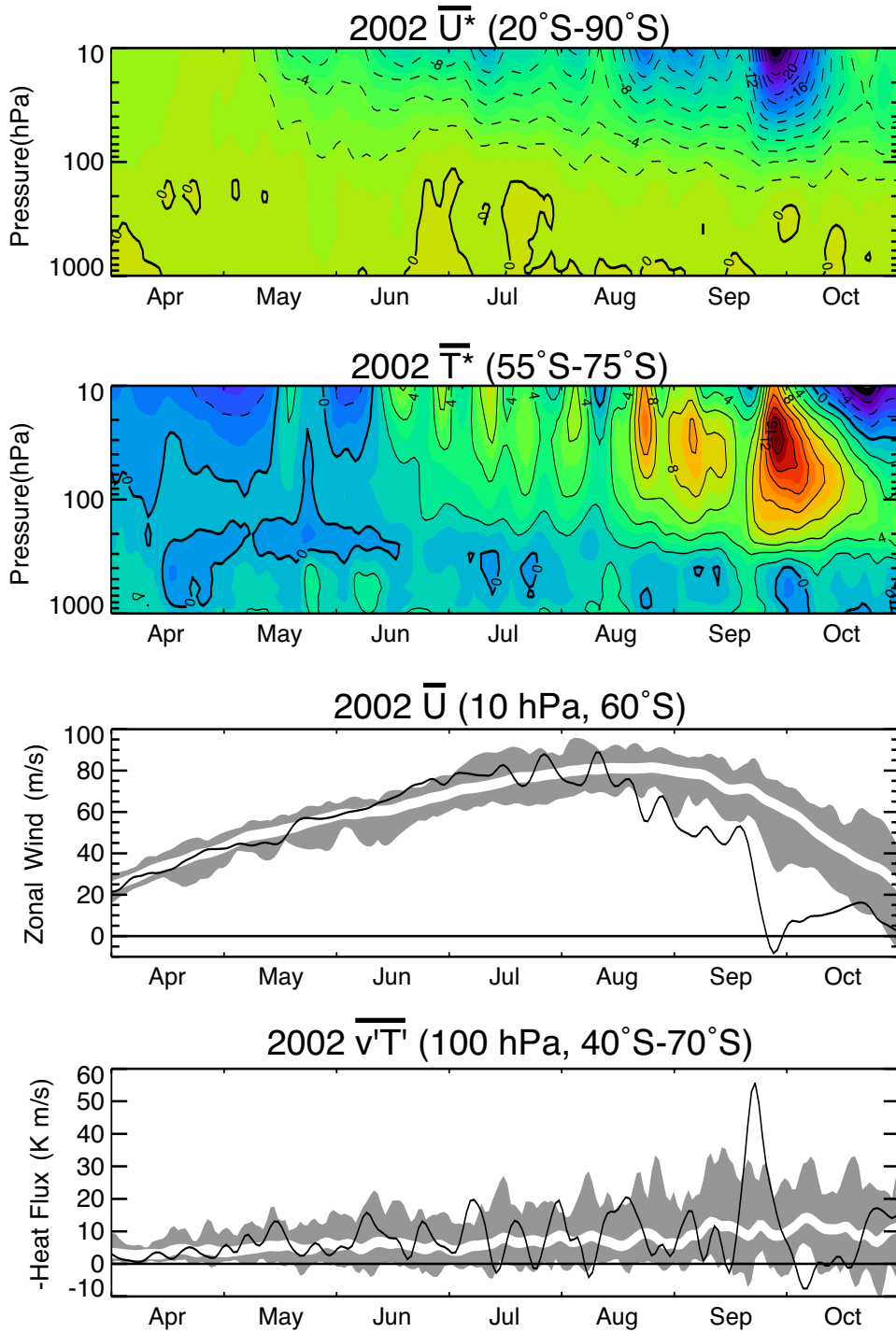


Figure 4-19. From top to bottom: (1) Daily zonal-mean zonal wind departures from the 1979-2001 mean for 1 April to 31 October 2002, averaged for 20°S to 90°S. Contour intervals are 2 m s⁻¹ with dashed negative contours. (2) Daily zonal-mean temperature departures, averaged for 55°S to 75°S. Contour intervals are 2 K with dashed negative contours. (3) Daily zonal-mean zonal wind at 10 hPa and 60°S. Units are in m s⁻¹. (4) Daily zonal-mean eddy heat flux at 100 hPa, averaged for 40°S to 70°S. Units are in K m s⁻¹. In the two bottom panels, the black line shows 2002 values, which have been smoothed with a 1–2–1 filter applied three times. The white line displays the 23-year average (1979-2001), smoothed with a 15-day boxcar. The gray shading indicates the range of values (also 1–2–1 filtered) observed between 1979 and 2001. Adapted from Newman and Nash (2005) and Allen et al. (2003).

Several CTMs simulated the chemical polar ozone loss during the 2002 winter and spring. Using ECMWF or United Kingdom Meteorological Office (UKMO) analyses, the simulations successfully reproduced the main features of the 2002 Antarctic ozone hole (e.g., Ricaud et al., 2005; Konopka et al., 2005; Grooß et al., 2005a; Sinnhuber et al., 2003). Feng et al. (2005a) compared simulations of the 2002 Antarctic ozone hole with calculations for 2000. While large ozone losses were observed in 2002, the warmer than average 2002 vortex temperatures led to smaller amounts of ClO_x that induced smaller chemical ozone loss (Richter et al., 2005; Frieß et al., 2005). The accumulated chemical loss in the polar lower stratosphere was about 20 DU less than in 2000. Significant contributions to the larger September 2002 ozone column were caused by enhanced descent at the vortex edge and increased horizontal transport associated with the distorted vortex. Grooß et al. (2005a) showed that the rapid chlorine deactivation after the major warming depended on the ozone mixing ratio. Very low ozone mixing ratios favored formation of HCl, while larger ozone mixing ratios and less denitrification led to formation of ClONO_2 . At higher altitudes (above 700 K), the midlatitude air masses transported to the polar region during the major warming experienced very large ozone depletion rates caused by NO_x catalytic cycles typical of polar summer chemistry. Several model simulations showed enhanced ozone loss in the midlatitudes due to the dilution of ozone-poor vortex air during the major warming (Grooß et al., 2005a; Feng et al., 2005a; Marchand et al., 2005). The polar vortex remnant that survived the major warming was strongly isolated from the extra vortex air until late November and did not experience any significant dilution with the midlatitude air (Konopka et al., 2005).

4.3.1.3 THEORETICAL UNDERSTANDING

Several studies examined the conditions that led to the major warming in 2002 in order to explain this unprecedented event. Scaife et al. (2005) and Newman and Nash (2005) both argued that the stratosphere had been preconditioned throughout the preceding months by stratospheric vacillations in the zonal-mean winds. Scaife et al. (2005) further argued that the large September tropospheric wave pulse that caused the warming was also dependent on this preconditioning. Numerical simulations of the stratospheric flow show distinct stratospheric regimes that are either steady or vacillating. Vacillations are found for high levels of planetary wave forcing emanating from the troposphere (Scaife and James, 2000). The SH stratosphere flow is generally in quasi-steady state or in vacillating regimes for a short period of time. The 2002

winter was in a vacillating regime beginning in June. This vacillation induced a systematic weakening of the polar-night jet that ultimately allowed a strong pulse of planetary wave to propagate into the stratosphere.

Gray et al. (2005) examined the influence of the QBO on the major warming. Contrary to expectations, the warming event occurred during the QBO west phase in the lower stratosphere. NH major warmings are likelier in the QBO easterly phase when a zero wind line confines planetary wave propagation to higher latitudes, closer to the polar vortex. However, meteorological analyses indicated the presence of anomalously strong easterly equatorial winds above 10 hPa from January to September 2002. The influence of these anomalous winds was investigated in idealized model experiments where equatorial winds were relaxed to observations obtained in several years. It was shown that the 2002 equatorial winds hurried the simulated warming event. Harnik et al. (2005) also suggested that the low latitude, middle stratosphere easterly wind was a main factor in the warming. They showed that the zonal wind at 30°S and 10 hPa turned easterly in May 2002, due to a large burst of upward wave activity into the stratosphere. The primary effect of this event was the deceleration of the low-latitude winds in the upper stratosphere. The zero wind line was shifted significantly farther poleward than normal and the resulting enhanced poleward wave focusing is likely to have contributed to the erosion of the vortex.

Moreover the vortex preconditioning was connected with the persistence of large wave-2 amplitudes through the winter. The warming itself occurred when a large wave-1 disturbance combined with a traveling wave-2. Such a simultaneous combination was not observed during the period 1979-2001. Through a detailed study of the wave activity in both the troposphere and stratosphere in the winter 2002, Newman and Nash (2005) confirmed that the major warming could be explained by two main factors: (1) stronger than usual tropospheric wave forcing that propagated upward into the stratosphere and (2) a propagation state in the stratosphere that favored upward propagation of waves. They showed that for April-September, the heat flux at 200 hPa for wave 1-3 between 40°S and 70°S was 50% larger than climatology. The stronger wave-1 in the lower stratosphere was found to be statistically related to wave-1 in the lower troposphere, itself highly correlated with wave-1 in the tropics. The 2002 winter average wave-1 amplitudes in both the midlatitude lower troposphere and tropical upper troposphere were the largest observed over the 1979-2002 record.

During the 2002 winter, larger-than-normal planetary-scale wave events occurred regularly in the

POLAR OZONE

midlatitude troposphere. The zonal-mean flow at the tropopause and in the tropical upper stratosphere was conducive to wave propagation, and these waves in the troposphere were efficiently refracted upward into the stratosphere. Each wave event warmed the polar lower stratosphere and weakened the jet stream. By mid-September the cumulative effect of wave activity had efficiently preconditioned the stratosphere. The major warming was preceded by an extraordinary strong pulse of eddy heat flux in the upper troposphere/lower stratosphere, much stronger than what is typically observed in the SH and even in a NH major warming (Harnik et al., 2005; Manney et al., 2005a).

4.3.2 Is Polar Ozone Getting Worse?

Observed total ozone columns in the polar regions have been larger in recent winters than in the 1990s, as emphasized in Section 4.1.2. The stabilization of ozone-depleting substances (ODSs) in the stratosphere has raised the question of its impact on observed ozone levels in the polar regions. This topic is discussed throughout the Assessment; see Chapter 1 for past and present ODS levels, Section 6.5.3 of Chapter 6 for attribution of recent changes in polar ozone as they pertain to changes in halogen loadings, Section 6.6.4 of Chapter 6 for projected future changes in polar ozone, and Chapter 8 for future ODS levels. The effect of anthropogenic elevated halogen levels in the stratosphere on polar ozone is different in both hemispheres due to differences in meteorological conditions. The Antarctic winter stratosphere is characterized by cold and stable meteorological conditions. The large chlorine activation induced by the very low temperatures in the vortex core leads to a nearly complete ozone destruction in the lower stratosphere by the end of September, which indicates that the Antarctic ozone depletion is saturated. The effects of ODS leveling off and saturation are difficult to discriminate. In contrast, Arctic chemical ozone loss is not saturated, due to much warmer conditions in the winter stratosphere. Arctic year-to-year variation is primarily controlled by the year-to-year variability in stratospheric temperatures. These temperature variations are much larger in the NH than in the SH. The large NH variability makes it difficult to establish long-term trends in Arctic ozone.

4.3.2.1 ARCTIC

Recent winters (since 1997/1998) have been characterized by higher than average temperatures than in the 1990s, although 1999/2000 and 2004/2005 stand out as being particularly cold, with record ozone chemical deple-

tion (see Section 4.1.2). Major stratospheric warmings were more frequent prior to 1990, while the 1990s were remarkable by the absence of such events (except during the winter 1998/1999). Studies of Arctic chemical ozone loss over this range of years and meteorological conditions have shown that a near-linear relationship can be found between the vortex average chemical ozone loss and V_{PSC} , the stratospheric volume of potential PSC as shown in Figure 4-13 (Rex et al., 2004, 2006). Arctic ozone losses since 2000 are in line with the relationship based on data collected prior to 2000, with very low (as in 2001/2002) and very large (as in 2004/2005) chemical ozone loss that is clearly due to differences in V_{PSC} for these years. No specific change in the behavior of Arctic ozone loss can be detected from these observations, which is consistent with present understanding given the similar halogen loadings over the time period for which this relationship can be defined from observations.

4.3.2.2 ANTARCTIC

Several studies have analyzed the evolution of the ozone hole since its appearance in the early 1980s. Newman et al. (2004) investigated the ozone hole area (OHA), while Bodeker et al. (2005) investigated OHA, annual minimum, and ozone mass deficit (OMD) (see Section 4.1.2 and Figure 4-8). The OHA and minimum ozone showed modest increases in severity in the 1990s, while OMD increased greatly in severity in the 1990s. The trend of monthly averaged OHA was analyzed by Alvarez-Madrigal and Pérez-Peraza (2005) in the period 1982-2003. After continuous growth since the eighties, the trend in October and November over 6-year subsets became negative since 2002. However, this trend did not account for temperature effects, or for dynamical effects during the breakup phase of the ozone hole.

Other studies investigated the relationship between the evolution of the Antarctic ozone hole and stratospheric chlorine and bromine levels over the last two decades. Newman et al. (2004) have shown that OHA is mainly controlled by catalytic ozone loss with stratospheric chlorine and bromine, and secondarily by the year-to-year variations in temperature in the collar region, near the edge of the polar vortex. Newman et al. (2004) fit the OHA to equivalent effective stratospheric chlorine (EESC, see Chapter 8, Box 8.1) with a 6-year time lag, and showed that OHA is currently decreasing at a very slow rate of 0.4% per year in response to halogen decreases. Huck et al. (2005) also fit the annual mean OMD to EESC with a 3-year time lag, the eddy heat flux anomalies at 20 hPa and 60°S, and South Pole 100 hPa temperature anomalies. In both studies, EESC and temperature explain almost all

of the variability of ozone-hole diagnostics. The residuals of the OHA fit to EESC and temperature have year-to-year variations of a few millions km² (compared with a current area of 23-24 millions km²). This variance masks the area response to the small halogen decreases over Antarctica since 2000.

An increase of ozone due to ODS decreases can also be looked for in regions where the chemical loss is still the main factor affecting ozone variations but without saturation, as in the upper edge (above 20 km) or in the collar region (60°S-70°S) of the Antarctic ozone hole. Using measurements from ozonesondes and the satellite-borne POAM instrument, Hoppel et al. (2005b) showed that the ozone mixing ratio near the top of the ozone hole at 20-22 km in early October was higher in the period 2001-2004 than in the previous years of POAM measurements (1994-1996; 1998-2000). However, this increase was accompanied by higher temperatures and reduced PSC occurrence frequency, which indicates that the ozone changes were linked to temperature variability associated with changes in dynamical processes rather than a decline in ODSs. The relationship between ozone mixing ratios and temperature in recent years also was noted by Solomon et al. (2005) from the analysis of four decades of ozonesondes over Antarctica. Yang et al. (2005) studied the evolution of ozone in the extra-vortex collar region (60°S-70°S), but this study is not completely representative of ozone hole conditions.

The latest studies on polar ozone thus show no further increase of the severity of the polar ozone depletion both in the Arctic and the Antarctic stratosphere. The Antarctic ozone hole shows a clear leveling off since the beginning of the century. The leveling off is primarily due to saturation of losses because of ODSs. Both 2002 and 2004 were weak ozone holes, giving the appearance of a downward trend. However, these weak holes directly resulted primarily from active SH dynamical forcing. Interannual variability of the SH is currently masking the expected ozone hole improvement as ODSs decrease. Arctic losses also appear to be decreasing, but the very large interannual variability of the Arctic masks the improvement as ODSs decrease.

4.4 THE INFLUENCE OF PRECIPITATING CHARGED PARTICLES ON POLAR OZONE

Precipitating charged particles influence ozone and other constituents. Processes on the Sun and in Earth's magnetosphere, the interaction of the solar wind with Earth's magnetosphere, and the interplanetary magnetic field ultimately drive the flux of charged particles into the atmosphere and have led to observed and predicted strato-

spheric and mesospheric constituent changes in the past few years. Some of these natural charged-particle-driven variations have been measured to cause significant increases in odd nitrogen and odd hydrogen constituents, with corresponding significant ozone decreases. These effects are transient as ozone recovers to quiescent levels within days (middle to upper mesosphere) to several years (middle and lower stratosphere) after these natural impacts. Since the previous Ozone Assessment, a wealth of new satellite measurements have become available that have helped to better quantify the charged particle atmospheric influences.

The charged particle effects that influence the atmosphere can roughly be grouped into three types of perturbations: (1) solar particle events, which are primarily protons entering the polar regions and thereby often are referred to as solar proton events (SPEs); (2) energetic electrons precipitating in the auroral zone and lower latitudes; and (3) galactic cosmic rays. Galactic cosmic rays (GCRs) continually create odd nitrogen and odd hydrogen constituents in the lower stratosphere and upper troposphere but play a small role in polar ozone variations.

SPEs and energetic precipitating electrons influence polar ozone levels. The most recent solar cycle period (solar cycle 23) was very active, with both SPEs and periods of enhanced fluxes of energetic electrons. In particular, six of the nine largest SPEs in the past 40 years occurred in the most recent solar cycle. The precipitating particles associated with these solar-driven events produced ionizations, excitations, dissociations, and dissociative ionizations of the background constituents in both the polar cap (reaching to 60° geomagnetic latitude or lower during strong geomagnetic storms) and lower latitudes, including the auroral oval region. The solar protons primarily deposited their energy in the mesosphere and stratosphere, whereas the energetic electrons primarily deposited their energy in the thermosphere and upper mesosphere.

HO_x (odd hydrogen, atomic hydrogen (H), hydroxyl radical (OH), hydroperoxyl radical (HO₂)) constituents are created by a series of ion chemistry reactions (e.g., Solomon et al., 1981) as a result of the charged particle precipitation. The solar particles and associated secondary electrons (produced in ionization events) also create atomic nitrogen through dissociation-producing collisions with molecular nitrogen (N₂). Atomic nitrogen then leads to the production of other odd nitrogen constituents, NO_y (total reactive nitrogen; usually includes atomic nitrogen (N), nitric oxide (NO), NO₂, nitrogen trioxide (NO₃), dinitrogen radical (N₂O₅), nitric acid (HNO₃), peroxyxynitric acid (HNO₄), BrONO₂, ClONO₂) through chemical reactions.

POLAR OZONE

The HO_x increases cause short-lived ozone decreases in the polar mesosphere and upper stratosphere due to the short lifetimes of the HO_x constituents. This HO_x -caused ozone effect was first observed in Weeks et al. (1972) and explained in Swider and Keneshea (1973). The NO_y increases lead to both short- and long-lived polar stratospheric ozone changes because of the long lifetime of the NO_y family in this region. This NO_y -caused ozone impact was first suggested by Crutzen et al. (1975) and observed in Heath et al. (1977). Since these early works, a number of papers have been published that document these solar-caused polar changes (recently reviewed in Jackman and McPeters, 2004). Although HO_x -driven short-lived decreases are useful for understanding the mesosphere and upper stratosphere, the NO_y enhancements cause the more important charged-particle-induced polar ozone decreases.

4.4.1 Odd Nitrogen (NO_y) Enhancements

Substantial increases in odd nitrogen (NO_y) constituents in the mesosphere and upper stratosphere as a direct result of SPEs have been measured by several satellite instruments during solar cycle 23. Very large fluxes of solar protons in July 2000 produced huge increases (>50 parts per billion by volume (ppbv) in the mesosphere) in Arctic NO_x ($\text{NO} + \text{NO}_2$) (Jackman et al., 2001). The large SPEs in late October and early November 2003 also caused very large proton fluxes that created substantial amounts of NO_x (Jackman et al., 2005a; López-Puertas et al., 2005a; Seppälä et al., 2004). Other NO_y constituents also were elevated as a result of huge SPEs that occurred in October/November 2003, including HNO_3 (Orsolini et al., 2005; López-Puertas et al., 2005b) and N_2O_5 and ClONO_2 (López-Puertas et al., 2005b).

Solar protons also caused long-term NO_y enhancements. For example, Randall et al. (2001) showed that Antarctic middle stratospheric NO_x in September 2000 was enhanced as a result of the transport of huge NO_x enhancements from the lower mesosphere and upper stratosphere, which were originally produced by the solar protons during the July 2000 SPE. Large enhancements of polar stratospheric NO_2 through November and into early December of 2003 probably were caused by the solar protons from the October/November 2003 SPEs (Seppälä et al., 2004; López-Puertas et al., 2005a).

High Arctic NO_x was observed in January to July 2004 by several satellite instruments (Natarajan et al., 2004; Randall et al., 2005b; Rinsland et al., 2005; López-Puertas et al., 2005a, 2006). Figure 4-20 (top, adapted from Randall et al., 2005b) shows NO_2 at 40 km for years 1994-1996 and 1998-2004. Very significant NO_2 enhance-

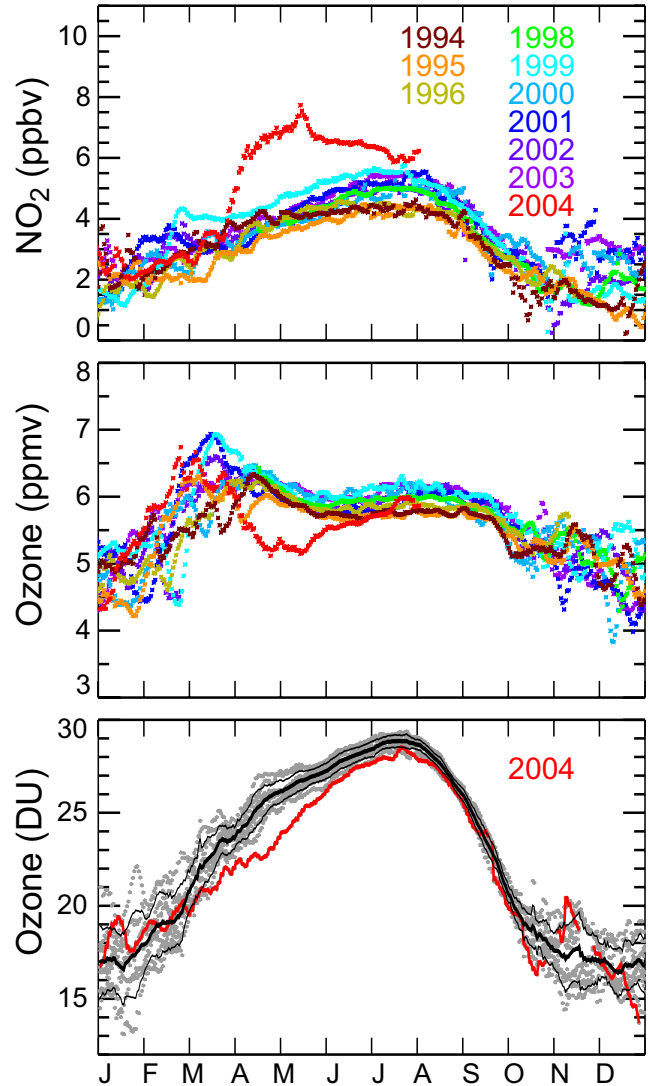


Figure 4-20. Seven-day running means of POAM II (1994-1996) and POAM III (1998-2004) NO_2 (top) and ozone (middle) mixing ratios in the NH at 40 km. The NO_2 enhancements and ozone reductions in the spring of 2004 resulted from transport to the stratosphere of NO_x produced by energetic particles precipitating in the mesosphere and thermosphere during the winter. The bottom panel shows 7-day running means of POAM partial column ozone over the vertical region from 35 to 50 km. Black lines represent the average (thick) $\pm 1\sigma$ standard deviation (thin) for column measurements from 1994 to 1996 and 1998 to 2004 (gray dots), excluding 2004. The red curve shows results for 2004 in all three panels. POAM II measurements have been corrected for instrument biases as determined by comparisons with independent satellite measurements. Adapted from Randall et al. (2005b).

ments are observed from March through July in 2004. It is unclear when these enhanced Northern Hemisphere NO_x levels were generated, although it is likely that energetic particle precipitation was the cause. The energetic electron fluxes associated with the geomagnetic storms of October/November 2003 were large and probably generated significant mesospheric and thermospheric NO_x (Natarajan et al., 2004), which could have been transported to lower levels. Other active geomagnetic periods in late November and December 2003 and even January 2004 could have been the main sources of the NO_x observed in the stratosphere and mesosphere (Randall et al., 2005b; López-Puertas et al., 2005a, 2006).

Funke et al. (2006) found high levels of Antarctic upper stratospheric NO_x during May to August 2003. This NO_x enhancement was attributed to precipitating electrons in the lower thermosphere and subsequent descent during polar night.

4.4.2 Ozone Decreases

Substantial mesospheric and upper stratospheric ozone decreases during and shortly after the July 2000, October/November 2003, and January 2005 SPEs were measured by several satellite instruments (see Jackman et al., 2001, 2005a, b; Seppälä et al., 2004, 2006; Verronen et al., 2005; Degenstein et al., 2005; López-Puertas et al., 2005a; Rohen et al., 2005). The transported NO_y enhancements from SPEs also resulted in observed ozone decreases. Randall et al. (2001) used POAM III observations to show middle stratospheric ozone decreases in September 2000 up to 45% (at 33 km) as a result of the solar proton precipitation in July 2000.

The long-lasting polar upper stratospheric ozone depletion was measured to be >30% for late November through December 2003 (Seppälä et al., 2004) and conjectured to be from the SPEs of October/November 2003. The polar upper stratospheric ozone depletion of more than 60% measured in the spring of 2004 (Natarajan et al., 2004; Randall et al., 2005b; López-Puertas et al., 2005a) is likely connected with the huge enhancements of geomagnetic storm-generated NO_x in November/December 2003 and January 2004 (see Section 4.4.1). Figure 4-20 (middle and bottom, adapted from Randall et al., 2005b) shows the measured variations in ozone at 40 km (middle plot) and partial column ozone between 35 and 50 km (bottom plot). Total ozone decreases were measured to be ~0.5-1% (~1.5-3 DU, compared with unperturbed levels of ~300 DU) in the spring and early summer of 2004 and are correlated with the NO_2 enhancements.

Models have been used to predict the impact of the solar protons in solar cycle 23. Krivolutsky et al.

(2005) predicted significant short-term ozone changes as a result of SPEs in July and November 2000, November 2001, and October/November 2003 with the use of a one-dimensional (1-D) photochemical model. Jackman et al. (2005b) simulated the influences of all the solar proton fluxes between 2000 and 2003 with a two-dimensional (2-D) CTM and predicted polar total ozone decreases of ~0.5-3% (~2-10 DU). These computed depletions resulted from the large solar proton fluxes in 2000, 2001, and 2003. The ozone decreases last beyond the SPEs and gradually diminish over several years as the NO_y (mainly in the form of nitric acid (HNO_3)) is transported to the troposphere and rained out from the atmosphere through wet deposition or sedimentation.

The electron impacts associated with geomagnetic storms are more difficult to simulate, since the magnitude of the precipitating electrons is hard to measure. However, Rozanov et al. (2005) and Langematz et al. (2005) simulated the impact of energetic electron precipitation with 3-D CCMs and suggest that the solar cycle variation of the electron flux could cause polar middle stratospheric ozone changes of 20% or more. Sinnhuber et al. (2005a) analyzed polar ozonesonde measurements with the use of a 3-D CTM, which includes measured temperatures and wind fields. They find that the residual ozone (modeled minus measured) at 800 K correlates very well with Geostationary Operational Environmental Satellite (GOES)-measured electron fluxes greater than 2 MeV, which are not in phase with 10.7-cm solar radio flux. Precipitating electrons may be somewhat important in determining long-term stratospheric ozone variability in both the SH and in the NH during years when there is a strong polar vortex accompanied by significant downward transport from the mesosphere to the stratosphere (e.g., early 2004 in the NH) (Manney et al., 2005a; Semeniuk et al., 2005).

REFERENCES

- Adriani, A., P. Massoli, G. Di Donfrancesco, F. Cairo, M.L. Moriconi, and M. Snels, Climatology of polar stratospheric clouds based on lidar observations from 1993 to 2001 over McMurdo Station, Antarctica, *J. Geophys. Res.*, 109, D24211, doi: 10.1029/2004JD004800, 2004.
- Allen, D.R., R.M. Bevilacqua, G.E. Nedoluha, C.E. Randall, and G.L. Manney, Unusual stratospheric transport and mixing during the 2002 Antarctic winter, *Geophys. Res. Lett.*, 30 (12), 1599, doi: 10.1029/2003GL017117, 2003.
- Alvarez-Madrigal, M., and J. Pérez-Peraza, Analysis of the evolution of the Antarctic ozone hole size, *J.*

POLAR OZONE

- Geophys. Res.*, 110, D02107, doi: 10.1029/2004JD004944, 2005.
- Anderson, J.G., W.H. Brune, S.A. Lloyd, D.W. Toohey, S.P. Sander, W.L. Starr, M. Loewenstein, and J.R. Podolske, Kinetics of O₃ destruction by ClO and BrO within the Antarctic vortex: An analysis based on in situ ER-2 data, *J. Geophys. Res.*, 94 (D9), 11480-11520, 1989.
- Anderson, J.G., D.W. Toohey, and W.H. Brune, Free radicals within the Antarctic vortex: The role of CFCs in Antarctic ozone loss, *Science*, 251 (4989), 39-46, 1991.
- Avallone, L.M., and D.W. Toohey, Tests of halogen photochemistry using in situ measurements of ClO and BrO in the lower polar stratosphere, *J. Geophys. Res.*, 106 (D10), 10411-10422, 2001.
- Becker, G., R. Müller, D.S. McKenna, M. Rex, and K.S. Carslaw, Ozone loss rates in the Arctic stratosphere in the winter 1991/92: Model calculations compared with Match results, *Geophys. Res. Lett.*, 25 (23), 4325-4328, 1998.
- Bengtsson, L., S. Hagemann, and K.I. Hodges, Can climate trends be calculated from reanalysis data?, *J. Geophys. Res.*, 109, D11111, doi: 10.1029/2004JD004536, 2004.
- Berthet, G., P. Ricaud, F. Lefèvre, E. Le Flochmoën, J. Urban, B. Barret, N. Lauté, E. Dupuy, J. De La Noë, and D. Murtagh, Nighttime chlorine monoxide observations by the Odin satellite and implications for the ClO/Cl₂O₂ equilibrium, *Geophys. Res. Lett.*, 32, L11812, doi: 10.1029/2005GL022649, 2005.
- Bloss, W.J., S.L. Nickolaisen, R.J. Salawitch, R.R. Friedl, and S.P. Sander, Kinetics of the ClO self reaction and 210 nm absorption cross section of the ClO dimer, *J. Phys. Chem. A*, 105, 11226-11239, 2001.
- Boakes, G., W.H. Hindy Mok, and D.M. Rowley, Kinetic studies of the ClO + ClO association reaction as a function of temperature and pressure, *Phys. Chem. Chem. Phys.*, 7 (24), 4102-4113, 2005.
- Bodeker, G.E., H. Shiona, and H. Eskes, Indicators of Antarctic ozone depletion, *Atmos. Chem. Phys.*, 5, 2603-2615, 2005.
- Bröske, R. and F. Zabel, Thermal decomposition of ClOOC1, *J. Phys. Chem. A*, 110 (9), 3280-3288, 2006.
- Brune, W.H., J.G. Anderson, and K.R. Chan, In situ observations of BrO over Antarctica: ER-2 aircraft results from 54°S to 72°S latitude, *J. Geophys. Res.*, 94 (D14), 16639-16647, 1989a.
- Brune, W.H., J.G. Anderson, and K.R. Chan, In situ observations of ClO in the Antarctic: ER-2 aircraft results from 54°S to 72°S latitude, *J. Geophys. Res.*, 94 (D14), 16649-16663, 1989b.
- Burkholder, J.B., J.J. Orlando, and C.J. Howard, Ultraviolet absorption cross sections of chlorine oxide (Cl₂O₂) between 210 and 410 nm, *J. Phys. Chem.*, 94 (2), 687-695, 1990.
- Canty, T., E.D. Rivière, R.J. Salawitch, G. Berthet, J.-B. Renard, K. Pfeilsticker, M. Dorf, A. Butz, H. Bösch, R.M. Stimpfle, D.M. Wilmouth, E.C. Richard, D.W. Fahey, P.J. Popp, M.R. Schoeberl, L.R. Lait, and T.P. Bui, Nighttime OCIO in the winter Arctic vortex, *J. Geophys. Res.*, 110, D01301, doi: 10.1029/2004JD005035, 2005.
- Carslaw, K.S., T. Peter, J.T. Bacmeister, and S.D. Eckermann, Widespread solid particle formation by mountain waves in the Arctic stratosphere, *J. Geophys. Res.*, 104 (D1), 1827-1836, 1999.
- Charlton, A.J., A. O'Neill, W.A. Lahoz, and P. Berrisford, The splitting of the stratospheric polar vortex in the Southern Hemisphere, September 2002: Dynamical evolution, *J. Atmos. Sci.*, 62 (3), 590-602, 2005.
- Chipperfield, M.P., New version of the TOMCAT/SLIMCAT off-line chemical transport model: Intercomparison of stratospheric tracer experiments, *Quart. J. Roy. Meteorol. Soc.*, 132 (617), 1179-1203, 2006.
- Chipperfield, M.P., W. Feng, and M. Rex, Arctic ozone loss and climate sensitivity: Updated three-dimensional model study, *Geophys. Res. Lett.*, 32, L11813, doi: 10.1029/2005GL022674, 2005.
- Christensen, T., B.M. Knudsen, M. Streibel, S.B. Andersen, A. Benesova, G. Braathen, H. Claude, J. Davies, H. De Backer, H. Dier, V. Dorokhov, M. Gerding, M. Gil, B. Henchoz, H. Kelder, R. Kivi, E. Kyrö, Z. Litynska, D. Moore, G. Peters, P. Skrivankova, R. Stübi, T. Turunen, G. Vaughan, P. Viatte, A.F. Vik, P. von der Gathen, and I. Zaitcev, Vortex-averaged Arctic ozone depletion in the winter 2002/2003, *Atmos. Chem. Phys.*, 5, 131-138, 2005.
- Christiansen, B., Evidence for nonlinear climate change: Two stratospheric regimes and a regime shift, *J. Clim.*, 16 (22), 3681-3690, 2003.
- Corti, S., F. Molteni, and T.N. Palmer, Signature of recent climate change in frequencies of natural atmospheric circulation regimes, *Nature*, 398 (6730), 799-802, 1999.
- Cox, R.A., and G.D. Hayman, The stability and photochemistry of dimers of the ClO radical and implications for Antarctic ozone depletion, *Nature*, 332 (6167), 796-800, 1988.
- Crutzen, P.J., and F. Arnold, Nitric-acid cloud formation in the cold Antarctic stratosphere: A major cause

- for the springtime 'ozone hole', *Nature*, 324, 651-655, 1986.
- Crutzen, P.J., I.S.A. Isaksen, and G.C. Reid, Solar proton events: Stratospheric sources of nitric oxide, *Science*, 189 (4201), 457-459, 1975.
- Davies, S., M.P. Chipperfield, K.S. Carslaw, B.M. Sinnhuber, J.G. Anderson, R.M. Stimpfle, D.M. Wilmouth, D.W. Fahey, P.J. Popp, E.C. Richard, P. von der Gathen, H. Jost, and C.R. Webster, Modeling the effect of denitrification on Arctic ozone depletion during winter 1999/2000, *J. Geophys. Res.*, 108 (D5), 8322, doi: 10.1029/2001JD000445, 2002.
- Davies, S., G.W. Mann, K.S. Carslaw, M.P. Chipperfield, J.A. Kettleborough, M.L. Santee, H. Oelhaf, G. Wetzell, Y. Sasano, and T. Sugita, 3-D microphysical model studies of Arctic denitrification: Comparison with observations, *Atmos. Chem. Phys.*, 5, 347-393, 2005.
- Degenstein, D.A., N.D. Lloyd, A.E. Bourassa, R.L. Gattinger, and E.J. Llewellyn, Observations of mesospheric ozone depletion during the October 28, 2003 solar proton event by OSIRIS, *Geophys. Res. Lett.*, 32, L03S11, doi: 10.1029/2004GL021521, 2005.
- de Zafra, R.L., M. Jaramillo, A. Parrish, P. Solomon, B. Connor, and J. Barrett, High concentrations of chlorine monoxide at low altitudes in the Antarctic spring stratosphere: Diurnal variation, *Nature*, 328 (6129), 408-411, 1987.
- Dhaniyala, S., K.A. McKinney, and P.O. Wennberg, Lee-wave clouds and denitrification of the polar stratosphere, *Geophys. Res. Lett.*, 29 (9), 1322, doi: 10.1029/2001GL013900, 2002.
- Dorf, M., H. Bösch, A. Butz, C. Camy-Peyret, M.P. Chipperfield, A. Engel, F. Goutail, K. Grunow, F. Hendrick, S. Hrechanyy, B. Naujokat, J.-P. Pommereau, M. Van Roozendaal, C. Sioris, F. Strohm, F. Weidner, and K. Pfeilsticker, Balloon-borne stratospheric BrO measurements: Comparison with ENVISAT/SCIAMACHY BrO limb profiles, *Atmos. Chem. Phys.*, 6, 2483-2501, 2006.
- Dougllass, A.R., R.S. Stolarski, S.E. Strahan, and B.C. Polansky, Sensitivity of Arctic ozone loss to polar stratospheric cloud volume and chlorine and bromine loading in a chemistry and transport model, *Geophys. Res. Lett.*, 33, L17809, doi: 10.1029/2006GL026492, 2006.
- Drdla, K., and E.V. Browell, Microphysical modeling of the 1999-2000 Arctic winter: 3. Impact of homogeneous freezing on polar stratospheric clouds, *J. Geophys. Res.*, 109, D10201, doi: 10.1029/2003JD004352, 2004.
- Dufour, G., R. Nassar, C.D. Boone, R. Skelton, K.A. Walker, P.F. Bernath, C.P. Rinsland, K. Semeniuk, J.J. Jin, J.C. McConnell, and G.L. Manney, Partitioning between the inorganic chlorine reservoirs, HCl and ClONO₂, during the Arctic winter 2005 derived from ACE-FTS, *Atmos. Chem. Phys.*, 6, 2355-2366, 2006.
- Fahey, D.W., R.S. Gao, K.S. Carslaw, J. Kettleborough, P.J. Popp, M.J. Northway, J.C. Holecek, S.C. Ciciora, R.J. McLaughlin, T.L. Thompson, R.H. Winkler, D.G. Baumgardner, B. Gandrud, P.O. Wennberg, S. Dhaniyala, K. McKinney, Th. Peter, R.J. Salawitch, T.P. Bui, J.W. Elkins, C.R. Webster, E.L. Atlas, H. Jost, J.C. Wilson, R.L. Herman, A. Kleinböhl, and M. von König, The detection of large HNO₃-containing particles in the winter Arctic stratosphere, *Science*, 291 (5506), 1026-1031, 2001.
- Farman, J.C., B.G. Gardiner, and J.D. Shanklin, Large losses of total ozone in Antarctica reveal seasonal ClO_x/NO_x interaction, *Nature*, 315, 207-210, 1985.
- Farmer, C.B., G.C. Toon, P.W. Schaper, J.-F. Blavier, and L.L. Lowes, Stratospheric trace gases in the spring 1986 Antarctic atmosphere, *Nature*, 329 (6135), 126-130, doi: 10.1038/329126a0, 1987.
- Feng, W., M.P. Chipperfield, H.K. Roscoe, J.J. Remedios, A.M. Waterfall, G.P. Stiller, N. Glatthor, M. Höpfner, and D.-Y. Wang, Three-dimensional model study of the Antarctic ozone hole in 2002 and comparison with 2000, *J. Atmos. Sci.*, 62 (3), 822-837, 2005a.
- Feng, W., M.P. Chipperfield, S. Davies, B. Sen, G. Toon, J.-F. Blavier, C.R. Webster, C.M. Volk, A. Ulanovsky, F. Ravagnani, P. von der Gathen, H. Jost, E.C. Richard, and H. Claude, Three-dimensional model study of the Arctic ozone loss in 2002/2003 and comparison with 1999/2000 and 2003/2004, *Atmos. Chem. Phys.*, 5, 139-152, 2005b.
- Fitzenberger, R., Investigation of the stratospheric inorganic bromine budget for 1996-2000: Balloon-borne measurements and model comparison, Ph.D. thesis, University of Heidelberg, Germany, 2000.
- Free, M., S.J. Seidel, J.K. Angell, J. Lanzante, I. Durre, and T.C. Peterson, Radiosonde Atmospheric Temperature Products for Assessing Climate (RATPAC): A new data set of large-area anomaly time series, *J. Geophys. Res.*, 110, D22101, doi: 10.1029/2005JD006169, 2005.
- Frieler, K., M. Rex, R.J. Salawitch, T. Canty, M. Streibel, R.M. Stimpfle, K. Pfeilsticker, M. Dorf, D.K. Weisenstein, S. Godin-Beekmann, and P. von der Gathen, Toward a better quantitative understanding

POLAR OZONE

- of polar stratospheric ozone loss, *Geophys. Res. Lett.*, 33, L10812, doi: 10.1029/2005GL025466, 2006.
- Frieß, U., K. Kreher, P.V. Johnston, and U. Platt, Ground-based DOAS measurements of stratospheric trace gases at two Antarctic stations during the 2002 ozone hole period, *J. Atmos. Sci.*, 62 (3), 765-777, 2005.
- Fueglistaler, S., B.P. Luo, C. Voigt, K.S. Carslaw, and Th. Peter, NAT-rock formation by mother clouds: A microphysical model study, *Atmos. Chem. Phys.*, 2, 93-98, 2002a.
- Fueglistaler, S., B.P. Luo, S. Buss, H. Wernli, C. Voigt, M. Müller, R. Neuber, C.A. Hostetler, L.R. Poole, H. Flentje, D.W. Fahey, M.J. Northway, and Th. Peter, Large NAT particle formation by mother clouds: Analysis of SOLVE/THESEO-2000 observations, *Geophys. Res. Lett.*, 29 (12), 1610, doi: 10.1029/2001GL014548, 2002b.
- Fueglistaler, S., S. Buss, B.P. Luo, H. Wernli, H. Flentje, C.A. Hostetler, L.R. Poole, K.S. Carslaw, and Th. Peter, Detailed modeling of mountain wave PSCs, *Atmos. Chem. Phys.*, 3, 697-712, 2003.
- Funke, B., M. López-Puertas, S. Gil-López, T. von Clarmann, G.P. Stiller, H. Fischer, and S. Kellmann, Downward transport of upper atmospheric NO_x into the polar stratosphere and lower mesosphere during Antarctic 2003 and Arctic 2002/2003 winters, *J. Geophys. Res.*, 110, D24308, doi: 10.1029/2005JD006463, 2005.
- Fusco, A.C., and M.L. Salby, Interannual variations of total ozone and their relationship to variations of planetary wave activity, *J. Clim.*, 12 (6), 1619-1629, 1999.
- Giovanelli, G., D. Bortoli, A. Petritoli, E. Castelli, I. Kostadinov, F. Ravegnani, G. Redaelli, C.M. Volk, U. Cortesi, G. Bianchini, and B. Carli, Stratospheric minor gas distribution over the Antarctic Peninsula during the APE-GAIA campaign, *Int. J. Remote Sens.*, 26 (16), 3343-3360, 2005.
- Godin, S., V. Bergeret, S. Bekki, C. David, and G. Mégie, Study of the interannual ozone loss and the permeability of the Antarctic polar vortex from aerosol and ozone lidar measurements in Dumont d'Urville (66.4°S, 140°E), *J. Geophys. Res.*, 106 (D1), 1311-1330, 2001.
- Golden, D.M., Reaction ClO + ClO → Products: Modeling and parameterization for use in atmospheric models, *Int. J. Chem. Kinet.*, 35 (5), 206-211, 2003.
- Goutail, F., J.-P. Pommereau, F. Lefèvre, M. Van Roozendaal, S.B. Andersen B.-A. Kåstad Høiskar, V. Dorokhov, E. Kyrö, M.P. Chipperfield, and W. Feng, Early unusual ozone loss during the Arctic winter 2002/2003 compared to other winters, *Atmos. Chem. Phys.*, 5, 665-677, 2005.
- Gray, L., W. Norton, C. Pascoe, and A. Charlton, A possible influence of equatorial winds on the September 2002 Southern Hemisphere sudden warming event, *J. Atmos. Sci.*, 62 (3), 651-667, 2005.
- Groß, J.-U., and R. Müller, The impact of mid-latitude intrusions into the polar vortex on ozone loss estimates, *Atmos. Chem. Phys.*, 3, 395-402, 2003.
- Groß, J.-U., P. Konopka, and R. Müller, Ozone chemistry during the 2002 Antarctic vortex split, *J. Atmos. Sci.*, 62 (3), 860-870, 2005a.
- Groß, J.-U., G. Günther, R. Müller, P. Konopka, S. Bausch, H. Schlager, C. Voigt, C.M. Volk, and G.C. Toon, Simulation of denitrification and ozone loss for the Arctic winter 2002/2003, *Atmos. Chem. Phys.*, 5, 1437-1448, 2005b.
- Hansen, G., T. Svenøe, M.P. Chipperfield, A. Dahlback, and U.-P. Hoppe, Evidence of substantial ozone depletion in winter 1995/96 over northern Norway, *Geophys. Res. Lett.*, 24 (7), 799-802, 1997.
- Harnik, N., R.K. Scott, and J. Perlwitz, Wave reflection and focusing prior to the major stratospheric warming of September 2002, *J. Atmos. Sci.*, 62 (3), 640-650, 2005.
- Harris, N.R.P., M. Rex, F. Goutail, B.M. Knudsen, G.L. Manney, R. Müller, and P. von der Gathen, Comparison of empirically derived ozone losses in the Arctic vortex, *J. Geophys. Res.*, 107 (D20), 8264, doi: 10.1029/2001JD000482, 2002.
- Heath, D.F., A.J. Krueger, and P.J. Crutzen, Solar proton event: Influence on stratospheric ozone, *Science*, 197 (4306), 886-889, 1977.
- Hio, Y., and S. Yoden, Interannual variations of the seasonal March in the Southern Hemisphere stratosphere for 1979-2002 and characterization of the unprecedented year 2002, *J. Atmos. Sci.*, 62 (3), 567-580, 2005.
- Hofmann, D.J., and S.J. Oltmans, Anomalous Antarctic ozone during 1992: Evidence for Pinatubo volcanic aerosol effects, *J. Geophys. Res.*, 98 (D10), 18555-18562, 1993.
- Höpfner, M., N. Larsen, R. Spang, B.P. Luo, J. Ma, S.H. Svendsen, S.D. Eckermann, B. Knudsen, P. Massoli, F. Cairo, G. Stiller, T.v. Clarmann, and H. Fischer, MIPAS detects Antarctic stratospheric belt of NAT PSCs caused by mountain waves, *Atmos. Chem. Phys.*, 6, 1221-1230, 2006.
- Hoppel, K., R. Bevilacqua, D. Allen, G. Nedoluha, and C. Randall, POAM III observations of the anomalous 2002 Antarctic ozone hole, *Geophys. Res. Lett.*, 30

- (7), 1394, doi: 10.1029/2003GL016899, 2003.
- Hoppel, K., R. Bevilacqua, T. Canty, R. Salawitch, and M. Santee, A measurement/model comparison of ozone photochemical loss in the Antarctic ozone hole using Polar Ozone and Aerosol Measurement observations and the Match technique, *J. Geophys. Res.*, *110*, D19304, doi: 10.1029/2004JD005651, 2005a.
- Hoppel, K., G. Nedoluha, M. Fromm, D. Allen, R. Bevilacqua, J. Alfred, B. Johnson, and G. König-Langlo, Reduced ozone loss at the upper edge of the Antarctic ozone hole during 2001-2004, *Geophys. Res. Lett.*, *32*, L20816, doi: 10.1029/2005GL023968, 2005b.
- Hu, R.-M., K.S. Carslaw, C. Hostetler, L.R. Poole, B. Luo, T. Peter, S. Fueglistaler, T.J. McGee, and J.F. Burris, Microphysical properties of wave polar stratospheric clouds retrieved from lidar measurements during SOLVE/THESEO 2000, *J. Geophys. Res.*, *107* (D20), 8294, doi: 10.1029/2001JD001125, 2002.
- Huck, P.E., A.J. McDonald, G.E. Bodeker, and H. Struthers, Interannual variability in Antarctic ozone depletion controlled by planetary waves and polar temperature, *Geophys. Res. Lett.*, *32*, L13819, doi: 10.1029/2005GL022943, 2005.
- Huder, K.J., and W.B. DeMore, Absorption cross sections of the ClO dimer, *J. Phys. Chem.*, *99*, 3905-3908, 1995.
- Huth, R., and P.O. Canziani, Classification of hemispheric monthly mean stratospheric potential vorticity fields, *Ann. Geophys.*, *21*, 805-817, 2003.
- Jackman, C.H., and R.D. McPeters, The effect of solar proton events on ozone and other constituents, in *Solar Variability and its Effects on Climate*, edited by J.M. Pap, P.A. Fox, and C. Frohlich, *AGU Monograph 141*, 305-319, Washington, D.C., 2004.
- Jackman, C.H., R.D. McPeters, G.J. Labow, E.L. Fleming, C.J. Praderas, and J.M. Russell, Northern Hemisphere atmospheric effects due to the July 2000 solar proton event, *Geophys. Res. Lett.*, *28* (15), 2883-2886, 2001.
- Jackman, C.H., M.T. DeLand, G.J. Labow, E.L. Fleming, D.K. Weisenstein, M.K.W. Ko, M. Sinnhuber, and J.M. Russell, Neutral atmospheric influences of the solar proton events in October-November 2003, *J. Geophys. Res.*, *110*, A09S27, doi: 10.1029/2004JA010888, 2005a.
- Jackman, C.H., M.T. DeLand, G.J. Labow, E.L. Fleming, D.K. Weisenstein, M.K.W. Ko, M. Sinnhuber, J. Anderson, and J.M. Russell, The influence of the several very large solar proton events in years 2000-2003 on the neutral middle atmosphere, *Adv. Space Res.*, *35*, 445-450, 2005b.
- Jin, J.J., K. Semeniuk, G.L. Manney, A.I. Jonsson, S.R. Beagley, J.C. McConnell, G. Dufour, R. Nassar, C.D. Boone, K.A. Walker, P.F. Bernath, and C.P. Rinsland, Severe Arctic ozone loss in the winter 2004/2005: Observations from ACE-FTS, *Geophys. Res. Lett.*, *33*, L15801, doi: 10.1029/2006GL026752, 2006.
- Jones, A.E., and J.D. Shanklin, Continued decline of total ozone over Halley, Antarctica since 1985, *Nature*, *376*, 409-411, 1995.
- Julian, P.R., Midwinter stratospheric warmings in the Southern Hemisphere: General remarks and a case study, *J. Appl. Meteorol.*, *6* (3), 557-563, 1967.
- Knopf, D.A., T. Koop, B.P. Luo, U.G. Weers, and T. Peter, Homogeneous nucleation of NAD and NAT in liquid stratospheric aerosols: Insufficient to explain denitrification, *Atmos. Chem. Phys.*, *2*, 207-214, 2002.
- Kondragunta, S., L.E. Flynn, A. Neuendorffer, A.J. Miller, C. Long, R. Nagatani, S. Zhou, T. Beck, E. Beach, R. McPeters, R. Stolarski, P.K. Bhartia, M.T. DeLand, and L.-K. Huang, Vertical structure of the anomalous 2002 Antarctic ozone hole, *J. Atmos. Sci.*, *62* (3), 801-811, 2005.
- Konopka, P., J.-U. Groö, K.W. Hoppel, H.-M. Steinhörst, and R. Müller, Mixing and chemical ozone loss during and after the Antarctic polar vortex major warming in September 2002, *J. Atmos. Sci.*, *62* (3), 848-859, 2005.
- Krivolutsky, A., A. Kuminov, and T. Vyushkova, Ionization of the atmosphere caused by solar protons and its influence on ozonosphere of the Earth during 1994-2003, *J. Atmos. Sol.-Terr. Phys.*, *67* (1-2), 105-117, 2005.
- Krüger, K., B. Naujokat, and K. Labitzke, The unusual midwinter warming in the Southern Hemisphere stratosphere 2002: A comparison to Northern Hemisphere phenomena, *J. Atmos. Sci.*, *62* (3), 603-613, 2005.
- Labitzke, K., Midwinter warmings in the stratosphere and lower mesosphere and the behavior of ionospheric absorption, *Zeitschr. Geophys.*, *34*, 555-566, 1968.
- Labitzke, K., and collaborators, *The Berlin Stratospheric Data Series* CD from Meteorological Institute, Freie Universität Berlin, Germany, 2002.
- Labitzke, K., and M. Kunze, Stratospheric temperatures over the Arctic: Comparison of three data sets, *Meteorol. Z.*, *14* (1), 65-74, 2005.
- Langematz, U., and M. Kunze, An update on dynamical changes in the Arctic and Antarctic stratospheric polar vortices, *Clim. Dyn.*, *27* (6), 647-660, doi:

POLAR OZONE

- 10.1007/s00382-006-0156-2, 2006.
- Langematz, U., J.L. Grenfell, K. Matthes, P. Mieth, M. Kunze, B. Steil, and C. Brühl, Chemical effects in 11-year solar cycle simulations with the Freie Universität Berlin Climate Middle Atmosphere Model with online chemistry (FUB-CMAM-CHEM), *Geophys. Res. Lett.*, *32*, L13803, doi: 10.1029/2005GL022686, 2005.
- Lanzante, J.R., S.A. Klein, and D.J. Seidel, Temporal homogenization of monthly radiosonde temperature data. Part I: Methodology, *J. Clim.*, *16* (2), 224-240, 2003.
- Larsen, N., B.M. Knudsen, S.H. Svendsen, T. Deshler, J.M. Rosen, R. Kivi, C. Weisser, J. Schreiner, K. Mauerberger, F. Cairo, J. Ovarlez, H. Oelhaf, and R. Spang, Formation of solid particles in synoptic-scale Arctic PSCs in early winter 2002/2003, *Atmos. Chem. Phys.*, *4*, 2001-2013, 2004.
- Lee, A.M., H.K. Roscoe, A.E. Jones, P.H. Haynes, E.F. Shuckburgh, M.W. Morrey, and H.C. Pumphrey, The impact of the mixing properties within the Antarctic stratospheric vortex on ozone loss in spring, *J. Geophys. Res.*, *106* (D3), 3203-3212, doi: 10.1029/2000JD900398, 2001.
- Lehmann, R., P. von der Gathen, M. Rex, and M. Streibel, Statistical analysis of the precision of the Match method, *Atmos. Chem. Phys.*, *5*, 2713-2727, 2005.
- López-Puertas, M., B. Funke, S. Gil-López, T. von Clarmann, G.P. Stiller, M. Höpfner, S. Kellman, H. Fischer, and C.H. Jackman, Observation of NO_x enhancement and ozone depletion in the Northern and Southern Hemispheres after the October-November 2003 solar proton events, *J. Geophys. Res.*, *110*, A09S43, doi: 10.1029/2005JA011050, 2005a.
- López-Puertas, M., B. Funke, S. Gil-López, T. von Clarmann, G.P. Stiller, M. Höpfner, S. Kellman, G.M. Tsidu, H. Fischer, and C.H. Jackman, HNO₃, N₂O₅, and ClONO₂ enhancements after the October-November 2003 solar proton events, *J. Geophys. Res.*, *110*, A09S44, doi: 10.1029/2005JA011051, 2005b.
- López-Puertas, M., B. Funke, T.V. Clarmann, H. Fischer, and G.P. Stiller, The variability of stratospheric and mesospheric NO_y in the Arctic and Antarctic 2002-2004 polar winters, *Space Sci. Rev.*, in press, 2006.
- Luo, B.P., C. Voigt, S. Fueglistaler, and T. Peter, Extreme NAT supersaturations in mountain wave ice PSCs: A clue to NAT formation, *J. Geophys. Res.*, *108* (D15), 4441, doi: 10.1029/2002JD003104, 2003.
- Malanca, F.E., P.O. Canziani, and G.A. Argüello, Trends evolution of ozone between 1980 and 2000 at mid-latitudes over the Southern Hemisphere. Decadal differences in trends, *J. Geophys. Res.*, *110*, D05102, doi: 10.1029/2004JD004977, 2005.
- Mann, G.W., K.S. Carslaw, M.P. Chipperfield, S. Davies, and S.D. Eckermann, Large nitric acid trihydrate particles and denitrification caused by mountain waves in the Arctic stratosphere, *J. Geophys. Res.*, *110*, D08202, doi: 10.1029/2004JD005271, 2005.
- Manney, G.L., L. Froidevaux, M.L. Santee, N.J. Livesey, J.L. Sabutis, and J.W. Waters, Variability of ozone loss during Arctic winter (1991-2000) estimated from UARS Microwave Limb Sounder measurements, *J. Geophys. Res.*, *108* (D4), 4149, doi: 10.1029/2002JD002634, 2003a.
- Manney, G.L., J.L. Sabutis, S. Pawson, M.L. Santee, B. Naujokat, R. Swinbank, M.E. Gelman, and W. Ebisuzaki, Lower stratospheric temperature differences between meteorological analyses in two cold Arctic winters and their impact on polar processing studies, *J. Geophys. Res.*, *108* (D5), 8328, doi: 10.1029/2001JD001149, 2003b.
- Manney, G.L., J.L. Sabutis, D.R. Allen, W.A. Lahoz, A.A. Scaife, C.E. Randall, S. Pawson, B. Naujokat, and R. Swinbank, Simulations of dynamics and transport during the September 2002 Antarctic major warming, *J. Atmos. Sci.*, *62* (3), 690-707, 2005a.
- Manney, G.L., M.L. Santee, N.J. Livesey, L. Froidevaux, W.G. Read, H.C. Pumphrey, J.W. Waters, and S. Pawson, EOS Microwave Limb Sounder observations of the Antarctic polar breakup in 2004, *Geophys. Res. Lett.*, *32*, L12811, doi: 10.1029/2005GL022823, 2005b.
- Manney, G.L., K. Krüger, J.L. Sabutis, S.A. Sena, and S. Pawson, The remarkable 2003-2004 winter and other recent warm winters in the Arctic stratosphere since the late 1990s, *J. Geophys. Res.*, *110*, D04107, doi: 10.1029/2004JD005367, 2005c.
- Manney, G.L., M.L. Santee, L. Froidevaux, K. Hoppel, N.J. Livesey, and J.W. Waters, EOS MLS observations of ozone loss in the 2004-2005 Arctic winter, *Geophys. Res. Lett.*, *33*, L04802, doi: 10.1029/2005GL024494, 2006.
- Marchand, M., S. Bekki, A. Pazmino, F. Lefèvre, S. Godin-Beekmann, and A. Hauchecorne, Model simulations of the impact of the 2002 Antarctic ozone hole on the midlatitudes, *J. Atmos. Sci.*, *62* (3), 871-884, 2005.
- McElroy, M.B., R.J. Salawitch, S.C. Wofsy, and J.A. Logan, Reductions of Antarctic ozone due to synergistic interactions of chlorine and bromine, *Nature*, *321*, 759-762, 1986.

- Molina, L.T., and M.J. Molina, Production of Cl_2O_2 from the self-reaction of the ClO radical, *J. Phys. Chem.*, *91*, 433-436, 1987.
- Moore, T.A., M. Okumura, J.W. Seale, and T.K. Minton, UV photolysis of ClOOCl, *J. Phys. Chem. A*, *103* (12), 1691-1695, 1999.
- Morris, G.A., B.R. Bojkov, L.R. Lait, and M.R. Schoeberl, A review of the Match technique as applied to AASE-2/EASOE and SOLVE/THESEO 2000, *Atmos. Chem. Phys.*, *5*, 2571-2592, 2005.
- Müller, R., S. Tilmes, J.-U. Grooß, D.S. McKenna, M. Müller, U. Schmidt, G.C. Toon, R.A. Stachnik, J.J. Margitan, J.W. Elkins, J. Arvelius, and J.M. Russell III, Chlorine activation and chemical ozone loss deduced from HALOE and balloon measurements in the Arctic during the winter of 1999-2000, *J. Geophys. Res.*, *108* (D5), 8302, doi: 10.1029/2001JD001423, 2002.
- Müller, R., S. Tilmes, P. Konopka, J.-U. Grooß, and H.-J. Jost, Impact of mixing and chemical change on ozone-tracer relations in the polar vortex, *Atmos. Chem. Phys.*, *5*, 3139-3151, 2005.
- Nash, E.R., P.A. Newman, J.E. Rosenfield, and M.R. Schoeberl, An objective determination of the polar vortex using Ertel's potential vorticity, *J. Geophys. Res.*, *101* (D5), 9471-9478, 1996.
- Natarajan, M., E.E. Remsberg, L.E. Deaver, and J.M. Russell III, Anomalously high levels of NO_x in the polar upper stratosphere during April, 2004: Photochemical consistency of HALOE observations, *Geophys. Res. Lett.*, *31*, L15113, doi: 10.1029/2004GL020566, 2004.
- Naujokat, B., and H.K. Roscoe, Evidence against an Antarctic stratospheric vortex split during the periods of pre-IGY temperature measurements, *J. Atmos. Sci.*, *62* (3), 885-889, 2005.
- Newman, P.A., and E.R. Nash, The unusual Southern Hemisphere stratosphere winter of 2002, *J. Atmos. Sci.*, *62* (3), 614-628, 2005.
- Newman, P.A., E.R. Nash, and J.E. Rosenfield, What controls the temperature of the Arctic stratosphere during the spring?, *J. Geophys. Res.*, *106* (D17), 19999-20010, 2001.
- Newman, P.A., S.R. Kawa, and E.R. Nash, On the size of the Antarctic ozone hole, *Geophys. Res. Lett.*, *31*, L21104, doi: 10.1029/2004GL020596, 2004.
- Newman, P.A., E.R. Nash, S.R. Kawa, S.A. Montzka, and S.M. Schauffler, When will the Antarctic ozone hole recover?, *Geophys. Res. Lett.*, *33*, L12814, doi: 10.1029/2005GL025232, 2006.
- Nickolaisen, S.L., R.R. Friedl, and S.P. Sander, Kinetics and mechanism of the ClO + ClO reaction – pressure and temperature dependences of the bimolecular and termolecular channels and thermal-decomposition of chlorine peroxide, *J. Phys. Chem.*, *98* (1), 155-169, 1994.
- Nishizawa, S., and S. Yoden, Distribution functions of a spurious trend in a finite length data set with natural variability: Statistical considerations and a numerical experiment with a global circulation model, *J. Geophys. Res.*, *110*, D12105, doi: 10.1029/2004JD005714, 2005.
- Orsolini, Y.J., G.L. Manney, M.L. Santee, and C.E. Randall, An upper stratospheric layer of enhanced HNO_3 following exceptional solar storms, *Geophys. Res. Lett.*, *32*, L12S01, doi: 10.1029/2004GL021588, 2005.
- Pagan, K.L., A. Tabazadeh, K. Drdla, M.E. Hervig, S.D. Eckermann, E.V. Browell, M.J. Legg, and P.G. Foschi, Observational evidence against mountain-wave generation of ice nuclei as a prerequisite for the formation of three solid nitric acid polar stratospheric clouds observed in the Arctic in early December 1999, *J. Geophys. Res.*, *109*, D04312, doi: 10.1029/2003JD003846, 2004.
- Pawson, S., K. Labitzke, and S. Leder, Stepwise changes in stratospheric temperature, *Geophys. Res. Lett.*, *25* (12), 2157-2160, 1998.
- Perlwitz, J., and H.-F. Graf, Troposphere-stratosphere dynamic coupling under strong and weak polar vortex conditions, *Geophys. Res. Lett.*, *28* (2), 271-274, 2001.
- Perlwitz, J., and N. Harnik, Observational evidence of a stratospheric influence on the troposphere by planetary wave reflection, *J. Clim.*, *16* (18), 3011-3026, 2003.
- Peterson, K.A., and J.S. Francisco, Does chlorine peroxide absorb below 250 nm?, *J. Chem. Phys.*, *121* (6), 2611-2616, 2004.
- Pfeilsticker, K., W.T. Sturges, H. Bösch, C. Camy-Peyret, M.P. Chipperfield, A. Engel, R. Fitzenberger, M. Müller, S. Payan, and B.-M. Sinnhuber, Lower stratospheric organic and inorganic bromine budget for the arctic winter 1998/99, *Geophys. Res. Lett.*, *27* (20), 3305-3308, 2000.
- Plenge, J., R. Flesch, S. Köhl, B. Vogel, R. Müller, F. Stroh, and E. Rühl, Ultraviolet photolysis of the ClO dimer, *J. Phys. Chem., A*, *108* (22), 4859-4863, 2004.
- Plenge, J., S. Köhl, B. Vogel, R. Müller, F. Stroh, M. von Hobe, R. Flesch, and E. Rühl, Bond strength of chlorine peroxide, *J. Phys. Chem. A*, *109* (30), 6730-6734, doi: 10.1021/jp044142h, 2005.
- Poole, L.R., C.R. Trepte, V.L. Harvey, G.C. Toon, and R.L. Van Valkenburg, SAGE III observations of Arctic

POLAR OZONE

- polar stratospheric clouds – December 2002, *Geophys. Res. Lett.*, *30* (23), 2216, doi: 10.1029/2003GL018496, 2003.
- Poulet, G., I.T. Lancar, G. Laverdet, and G. Le Bras, Kinetics and products of the BrO + ClO reaction, *J. Phys. Chem.*, *94* (1), 278-284, 1990.
- Pundt, I., J.-P. Pommereau, M.P. Chipperfield, M. Van Roozendael, and F. Goutail, Climatology of the stratospheric BrO vertical distribution by balloon-borne UV-visible spectrometry, *J. Geophys. Res.*, *107* (24), 4806, doi: 10.1029/2002JD002230, 2002.
- Raffalski, U., G. Hochschild, G. Kopp, and J. Urban, Evolution of stratospheric ozone during winter 2002/2003 as observed by a ground-based millimetre wave radiometer at Kiruna, Sweden, *Atmos. Chem. Phys.*, *5*, 1399-1407, 2005.
- Ramaswamy, V., M.L. Chanin, J. Angell, J. Barnett, D. Gaffen, M. Gelman, P. Keckhut, Y. Koshelkov, K. Labitzke, J.J.R. Lin, A. O'Neill, J. Nash, W. Randel, R. Rood, K. Shine, M. Shiotani, and R. Swinbank, Stratospheric temperature trends: Observations and model simulations, *Rev. Geophys.*, *39* (1), 71-122, 2001.
- Ramaswamy, V., M.D. Schwarzkopf, W.J. Randel, B.D. Santer, B.J. Soden, and G.L. Stenchikov, Anthropogenic and natural influences in the evolution of lower stratospheric cooling, *Science*, *311* (5764), 1138-1141, 2006.
- Randall, C.E., D.E. Siskind, and R.M. Bevilacqua, Stratospheric NO_x enhancements in the Southern Hemisphere vortex in winter/spring of 2000, *Geophys. Res. Lett.*, *28* (12), 2385-2388, 2001.
- Randall, C.E., G.L. Manney, D.R. Allen, R.M. Bevilacqua, J. Hornstein, C. Trepte, W. Lahoz, J. Ajtic, and G. Bodeker, Reconstruction and simulation of stratospheric ozone distributions during the 2002 Austral winter, *J. Atmos. Sci.*, *62* (3), 748-764, 2005a.
- Randall, C.E., V.L. Harvey, G.L. Manney, Y. Orsolini, M. Codrescu, C. Sioris, S. Brohede, C.S. Haley, L.L. Gordley, J.M. Zawodny, and J.M. Russell III, Stratospheric effects of energetic particle precipitation in 2003-2004, *Geophys. Res. Lett.*, *32*, L05802, doi: 10.1029/2004GL022003, 2005b.
- Randel, W.J., and F. Wu, Biases in stratospheric and tropospheric temperature trends derived from historical radiosonde data, *J. Clim.*, *19* (10), 2094-2104, 2006.
- Randel, W.J., F. Wu, and R. Stolarski, Changes in column ozone correlated with EP flux, *J. Meteorol. Soc. Japan*, *80* (4B), 849-862, 2002.
- Renwick, J.A., Trends in the Southern Hemisphere polar vortex in NCEP and ECMWF reanalyses, *Geophys. Res. Lett.*, *31*, L07209, doi: 10.1029/2003GL019302, 2004.
- Rex, M., P. von der Gathen, N.R.P. Harris, D. Lucic, B.M. Knudsen, G.O. Braathen, S.J. Reid, H. De Backer, H. Claude, R. Fabian, H. Fast, M. Gil, E. Kyrö, I.S. Mikkelsen, M. Rummukainen, H.G. Smit, J. Stähelin, C. Varotsos, and I. Zaitcev, In situ measurements of stratospheric ozone depletion rates in the Arctic winter of 1991/1992: A Lagrangian approach, *J. Geophys. Res.*, *103* (D5), 5843-5854, 1998.
- Rex, M., R.J. Salawitch, N.R.P. Harris, P. von der Gathen, G.O. Braathen, A. Schulz, H. Deckelmann, M. Chipperfield, B.M. Sinnhuber, E. Reimer, R. Alfier, R. Bevilacqua, K. Hoppel, M. Fromm, J. Lumpe, H. Küllmann, A. Kleinböhl, H. Bremer, M. von König, K. Künzi, D. Toohey, H. Vömel, E. Richard, K. Aikin, H. Jost, J.B. Greenblatt, M. Loewenstein, J.R. Podolske, C.R. Webster, G.J. Flesch, D.C. Scott, R.L. Herman, J.W. Elkins, E.A. Ray, F.L. Moore, D.F. Hurst, P. Romashkin, G.C. Toon, B. Sen, J.J. Margitan, P. Wennberg, R. Neuber, M. Allart, B.R. Bojkov, H. Claude, J. Davies, W. Davies, H. De Backer, H. Dier, V. Dorokhov, H. Fast, Y. Kondo, E. Kyrö, Z. Litynska, I.S. Mikkelsen, M.J. Molyneux, E. Moran, T. Nagai, H. Nakane, C. Parrondo, F. Ravagnani, P. Skrivankova, P. Viatte, and V. Yushkov, Chemical depletion of Arctic ozone in winter 1999/2000, *J. Geophys. Res.*, *107* (D20), 8276, doi: 10.1029/2001JD000533, 2002.
- Rex, M., R.J. Salawitch, M.L. Santee, J.W. Waters, K. Hoppel, and R. Bevilacqua, On the unexplained stratospheric ozone losses during cold Arctic Januaries, *Geophys. Res. Lett.*, *30* (1), 1008, doi: 10.1029/2002GL016008, 2003.
- Rex, M., R.J. Salawitch, P. von der Gathen, N.R.P. Harris, M.P. Chipperfield, and B. Naujokat, Arctic ozone loss and climate change, *Geophys. Res. Lett.*, *31*, L04116, doi: 10.1029/2003GL018844, 2004.
- Rex, M., R.J. Salawitch, H. Deckelmann, P. von der Gathen, N.R.P. Harris, M.P. Chipperfield, B. Naujokat, E. Reimer, M. Allaart, S.B. Andersen, R. Bevilacqua, G.O. Braathen, H. Claude, J. Davies, H. De Backer, H. Dier, V. Dorokhov, H. Fast, M. Gerding, S. Godin-Beekmann, K. Hoppel, B. Johnson, E. Kyrö, Z. Litynska, D. Moore, H. Nakane, M.C. Parrondo, A.D. Risley Jr., P. Skrivankova, R. Stübi, P. Viatte, V. Yushkov, and C. Zerefos, Arctic winter 2005: Implications for stratospheric ozone loss and climate change, *Geophys. Res. Lett.*, *33*, L23808, doi: 10.1029/2006GL026731, 2006.
- Ricaud, P., F. Lefèvre, G. Berthet, D. Murtagh, E.J.

- Llewellyn, G. Mégie, E. Kyrölä, G.W. Leppelmeier, H. Auvinen, C. Boone, S. Brohede, D.A. Degenstein, J. de La Noë, E. Dupuy, L. El Amraoui, P. Eriksson, W.F.J. Evans, U. Frisk, R.L. Gattinger, F. Girod, C.S. Haley, S. Hassinen, A. Hauchecorne, C. Jimenez, E. Kyrö, N. Lautié, E. Le Flochmoën, N.D. Lloyd, J.C. McConnell, I.C. McDade, L. Nordh, M. Olberg, A. Pazmio, S.V. Petelina, A. Sandqvist, A. Seppälä, C.E. Sioris, B.H. Solheim, J. Stegman, K. Strong, P. Taalas, J. Urban, C. von Savigny, F. von Scheele, and G. Witt, Polar vortex evolution during the 2002 Antarctic major warming as observed by the Odin satellite, *J. Geophys. Res.*, *110*, D05302, doi: 10.1029/2004JD005018, 2005.
- Richter, A., F. Wittrock, M. Weber, S. Beirle, S. Kühl, U. Platt, T. Wagner, W. Wilms-Grabe, and J.P. Burrows, GOME observations of stratospheric trace gas distributions during the splitting vortex event in the Antarctic winter of 2002, Part I: Measurements, *J. Atmos. Sci.*, *62* (3), 778-785, 2005.
- Rinsland, C.P., C. Boone, R. Nassar, K. Walker, P. Bernath, J.C. McConnell, and L. Chiou, Atmospheric Chemistry Experiment (ACE) Arctic stratospheric measurements of NO_x during February and March 2004: Impact of intense solar flares, *Geophys. Res. Lett.*, *32*, L16S05, doi: 10.1029/2005GL022425, 2005.
- Rohen, G., C. von Savigny, M. Sinnhuber, E.J. Llewellyn, J.W. Kaiser, C.H. Jackman, M.-B. Kallenrode, J. Schröter, K.-U. Eichmann, H. Bovensmann, and J.P. Burrows, Ozone depletion during the solar proton events of October/November 2003 as seen by SCIAMACHY, *J. Geophys. Res.*, *110*, A09S39, doi: 10.1029/2004JA010984, 2005.
- Roscoe, H.K., J.D. Shanklin, and S.R. Colwell, Has the Antarctic vortex split before 2002?, *J. Atmos. Sci.*, *62* (3), 581-588, 2005.
- Rozañov, E., L. Callis, M. Schlesinger, F. Yang, N. Andronova, and V. Zubov, Atmospheric response to NO_y source due to energetic electron precipitation, *Geophys. Res. Lett.*, *32*, L14811, doi: 10.1029/2005GL023041, 2005.
- Salawitch, R.J., D.K. Weisenstein, L.J. Kovalenko, C.E. Sioris, P.O. Wennberg, K. Chance, M.K.W. Ko, and C.A. McLinden, Sensitivity of ozone to bromine in the lower stratosphere, *Geophys. Res. Lett.*, *32*, L05811, doi: 10.1029/2004GL021504, 2005.
- Sander, S.P., R.R. Friedl, W.B. DeMore, D.M. Golden, M.J. Kurylo, R.F. Hampson, R.E. Huie, G.K. Moortgat, A.R. Ravishankara, C.E. Kolb, and M.J. Molina, *Chemical Kinetics and Photochemical Data for Use in Stratospheric Modeling, Evaluation No. 13, JPL Publication 00-03*, Jet Propulsion Laboratory, Pasadena, Calif., 2000.
- Sander, S.P., R.R. Friedl, D.M. Golden, M.J. Kurylo, R.E. Huie, V.L. Orkin, G.K. Moortgat, A.R. Ravishankara, C.E. Kolb, M.J. Molina, and B.J. Finlayson-Pitts, *Chemical Kinetics and Photochemical Data for Use in Atmospheric Studies, Evaluation No. 14, JPL Publication 02-25*, Jet Propulsion Laboratory, Pasadena, Calif., 2003.
- Sander, S.P., R.R. Friedl, D.M. Golden, M.J. Kurylo, G.K. Moortgat, H. Keller-Rudek, P.H. Wine, A.R. Ravishankara, C.E. Kolb, M.J. Molina, B.J. Finlayson-Pitts, R.E. Huie, and V.L. Orkin, *Chemical Kinetics and Photochemical Data for Use in Atmospheric Studies, Evaluation Number 15, JPL Publication 06-02*, Jet Propulsion Laboratory, Pasadena, Calif., [Available: <http://jpldataeval.jpl.nasa.gov/>], 2006.
- Sankey, D., and T.G. Shepherd, Correlations of long-lived chemical species in a middle atmosphere general circulation model, *J. Geophys. Res.*, *108* (D16), 4494, doi: 10.1029/2002JD002799, 2003.
- Santee, M.L., G.L. Manney, N.J. Livesey, L. Froidevaux, I.A. MacKenzie, H.C. Pumphrey, W.G. Read, M.J. Schwartz, J.W. Waters, and R.S. Harwood, Polar processing and development of the 2004 Antarctic ozone hole: First results from MLS on Aura, *Geophys. Res. Lett.*, *32*, L12817, doi: 10.1029/2005GL022582, 2005.
- Santer, B.D., T.M.L. Wigley, A.J. Simmons, P.W. Kållberg, G.A. Kelly, S.M. Uppala, C. Ammann, J.S. Boyle, W. Brüggemann, C. Doutriaux, M. Fiorino, C. Mears, G.A. Meehl, R. Sausen, K.E. Taylor, W.M. Washington, M.F. Wehner, and F.J. Wentz, Identification of anthropogenic climate change using a second-generation reanalysis, *J. Geophys. Res.*, *109*, D21104, doi: 10.1029/2004JD005075, 2004.
- Scaife, A.A., and I.N. James, Response of the stratosphere to interannual variability of tropospheric planetary waves, *Quart. J. Roy. Meteorol. Soc.*, *126* (562), 275-297, 2000.
- Scaife, A.A., D.R. Jackson, R. Swinbank, N. Butchart, H.E. Thornton, M. Keil, and L. Henderson, Stratospheric vacillations and the major warming over Antarctica in 2002, *J. Atmos. Sci.*, *62* (3), 629-639, 2005.
- Schnadt, C., M. Dameris, M. Ponater, R. Hein, V. Grewe, and B. Steil, Interaction of atmospheric chemistry and climate and its impact on stratospheric ozone, *Clim. Dyn.*, *18* (6), 501-517, 2002.
- Schoeberl, M.R., S.R. Kawa, A.R. Douglass, T.J. McGee, E.V. Browell, J. Waters, N. Livesey, W. Read, L. Froidevaux, M.L. Santee, H.C. Pumphrey, L.R. Lait,

POLAR OZONE

- and L. Twigg, Chemical observations of a polar vortex intrusion, *J. Geophys. Res.*, *111*, D20306, doi: 10.1029/2006JD007134, 2006.
- Schofield, R., P.V. Johnston, A. Thomas, K. Kreher, B.J. Connor, S. Wood, D. Shooter, M.P. Chipperfield, A. Richter, R. von Glasow, and C.D. Rodgers, Tropospheric and stratospheric BrO columns over Arrival Heights, Antarctica, 2002, *J. Geophys. Res.*, *111*, D22310, doi: 10.1029/2005JD007022, 2006.
- Seidel, D.J., and J.R. Lanzante, An assessment of three alternatives to linear trends for characterizing global atmospheric temperature changes, *J. Geophys. Res.*, *109*, D14108, doi: 10.1029/2003JD004414, 2004.
- Seidel, D.J., J.K. Angell, M. Free, J. Christy, R. Spencer, S.A. Klein, J.R. Lanzante, C. Mears, M. Schabel, F. Wentz, D. Parker, P. Thorne, and A. Sterin, Uncertainty in signals of large-scale climate variations in radiosonde and satellite upper-air temperature data sets, *J. Clim.*, *17* (11), 2225-2240, 2004.
- Semeniuk, K., J.C. McConnell, and C.H. Jackman, Simulation of the October-November 2003 solar proton events in the CMAM GCM: Comparison with observations, *Geophys. Res. Lett.*, *32*, L15S02, doi: 10.1029/2004GL022392, 2005.
- Seppälä, A., P.T. Verronen, E. Kyrölä, S. Hassinen, L. Backman, A. Hauchecorne, J.L. Bertaux, and D. Fussen, Solar proton events of October-November 2003: Ozone depletion in the Northern Hemisphere polar winter as seen by GOMOS/Envisat, *Geophys. Res. Lett.*, *31*, L19107, doi: 10.1029/2004GL021042, 2004.
- Seppälä, A., P.T. Verronen, V.F. Sofieva, J. Tamminen, E. Kyrölä, C.J. Rodger, and M.A. Clilverd, Destruction of the tertiary ozone maximum during a solar proton event, *Geophys. Res. Lett.*, *33*, L07804, doi: 10.1029/2005GL025571, 2006.
- Shine, K.P., On the modeled thermal response of the Antarctic stratosphere to a depletion of ozone, *Geophys. Res. Lett.*, *13*, 1331-1334, 1986.
- Singleton, C.S., C.E. Randall, M.P. Chipperfield, S. Davies, W. Feng, R.M. Bevilacqua, K.W. Hoppel, M.D. Fromm, G.L. Manney, and V.L. Harvey, 2002-2003 Arctic ozone loss deduced from POAM III satellite observations and the SLIMCAT chemical transport model, *Atmos. Chem. Phys.*, *5*, 597-609, 2005.
- Singleton, C.S., C.E. Randall, V.L. Harvey, M.P. Chipperfield, W. Feng, L. Froidevaux, G.L. Manney, P.F. Bernath, K.A. Walker, C.D. Boone, and T. McElroy, Quantifying Arctic ozone loss during the 2004-2005 winter using satellite observations and a chemical transport model, *J. Geophys. Res.*, in press, 2006.
- Sinnhuber, B.-M., M. Weber, A. Amankwah, and J.P. Burrows, Total ozone during the unusual Antarctic winter of 2002, *Geophys. Res. Lett.*, *30* (11), 1580, doi: 10.1029/2002GL016798, 2003.
- Sinnhuber, B.-M., P. von der Gathen, M. Sinnhuber, M. Rex, G. König-Langlo, and S.J. Oltmans, Large decadal scale changes of polar ozone suggest solar influence, *Atmos. Chem. Phys. Discuss.*, *5*, 12103-12117, 2005a.
- Sinnhuber, B.-M., A. Rozanov, N. Sheode, O.T. Afe, A. Richter, M. Sinnhuber, F. Wittrock, J.P. Burrows, G.P. Stiller, T. von Clarmann, and A. Linden, Global observations of stratospheric bromine monoxide from SCIAMACHY, *Geophys. Res. Lett.*, *32*, L20810, doi: 10.1029/2005GL023839, 2005b.
- Sioris, C.E., L.J. Kovalenko, C.A. McLinden, R.J. Salawitch, M. Van Roozendaal, F. Goutail, M. Dorf, K. Pfeilsticker, K. Chance, C. von Savigny, X. Liu, T.P. Kurosu, J.-P. Pommereau, H. Bösch, and J. Frerick, Latitudinal and vertical distribution of bromine monoxide in the lower stratosphere from Scanning Imaging Absorption Spectrometer for Atmospheric Chartography limb scattering measurements, *J. Geophys. Res.*, *111*, D14301, doi: 10.1029/2005JD006479, 2006.
- Solomon, P.M., B. Connor, R.L. de Zafra, A. Parrish, J. Barrett, and M. Jaramillo, High concentrations of chlorine monoxide at low altitudes in the Antarctic spring stratosphere: Secular variation, *Nature*, *328* (6129), 411-413, 1987.
- Solomon, S., D.W. Rusch, J.-C. Gérard, G.C. Reid, and P.J. Crutzen, The effect of particle precipitation events on the neutral and ion chemistry of the middle atmosphere, 2, Odd hydrogen, *Planet. Space Sci.*, *29* (8), 885-893, 1981.
- Solomon, S., R.R. Garcia, F.S. Rowland, and D.J. Wuebbles, On the depletion of Antarctic ozone, *Nature*, *321*, 755-758, 1986.
- Solomon, S., G.H. Mount, R.W. Sanders, and A.L. Schmeltekopf, Visible spectroscopy at McMurdo Station, Antarctica, 2. Observations of OCIO, *J. Geophys. Res.*, *92* (D7), 8329-8338, 1987.
- Solomon, S., R.W. Portmann, T. Sasaki, D.J. Hofmann, and D.W.J. Thompson, Four decades of ozonesonde measurements over Antarctica, *J. Geophys. Res.*, *110*, D21311, doi: 10.1029/2005JD005917, 2005.
- Stimpfle, R., D.M. Wilmouth, R.J. Salawitch, and J.G. Anderson, First measurements of ClOOC1 in the stratosphere: The coupling of ClOOC1 and ClO in the Arctic polar vortex, *J. Geophys. Res.*, *109*, D03301, doi: 10.1029/2003JD003811, 2004.

- Stolarski, R.S., A.J. Kreuger, M.R. Schoeberl, R.D. McPeters, P.A. Newman, and J.C. Alpert, Nimbus-7 satellite measurements of the springtime Antarctic ozone decrease, *Nature*, 322 (6082), 808-811, 1986.
- Stolarski, R.S., R.D. McPeters, and P.A. Newman, The ozone hole of 2002 as measured by TOMS, *J. Atmos. Sci.*, 62 (3), 716-720, 2005.
- Streibel, M., M. Rex, P. von der Gathen, R. Lehmann, N.R.P. Harris, G.O. Braathen, E. Reimer, H. Deckelmann, M. Chipperfield, G. Millard, M. Allaart, S.B. Andersen, H. Claude, J. Davies, H. De Backer, H. Dier, V. Dorokov, H. Fast, M. Gerding, E. Kyrö, Z. Litynska, D. Moore, E. Moran, T. Nagai, H. Nakane, C. Parrondo, P. Skrivankova, R. Stübi, G. Vaughan, P. Viatte, and V. Yushkov, Chemical ozone loss in the Arctic winter 2002/2003 determined with Match, *Atmos. Chem. Phys.*, 6, 2783-2792, 2006.
- Swider, W., and T.J. Keneshea, Decrease of ozone and atomic oxygen in the lower mesosphere during a PCA event, *Planet. Space Sci.*, 21 (11), 1969-1973, 1973.
- Tabazadeh, A., Commentary on "Homogeneous nucleation of NAD and NAT in liquid stratospheric aerosols: Insufficient to explain denitrification" by Knopf et al., *Atmos. Chem. Phys.*, 3, 827-833, 2003.
- Taguchi, M., and S. Yoden, Internal interannual variability of the troposphere-stratosphere coupled system in a simple global circulation model, Part II: Millennium integrations, *J. Atmos. Sci.*, 59 (21), 3037-3050, 2002.
- Thorne, P.W., D.E. Parker, S.F.B. Tett, P.D. Jones, M. McCarthy, H. Coleman, and P. Brohan, Revisiting radiosonde upper air temperatures from 1958 to 2002, *J. Geophys. Res.*, 110, D18105, doi: 10.1029/2004JD005753, 2005.
- Tilmes, S., R. Müller, J.-U. Groöf, D.S. McKenna, J.M. Russell III, and Y. Sasano, Calculation of chemical ozone loss in the Arctic winter 1996-1997 using ozone-tracer correlations: Comparison of Improved Limb Atmospheric Spectrometer (ILAS) and Halogen Occultation Experiment (HALOE) results, *J. Geophys. Res.*, 108 (D2), 4045, doi: 10.1029/2002JD002213, 2003.
- Tilmes, S., R. Müller, J.-U. Groöf, and J.M. Russell III, Ozone loss and chlorine activation in the Arctic winters 1991-2003 derived with the tracer-tracer correlations, *Atmos. Chem. Phys.*, 4 (8), 2181-2213, 2004.
- Tilmes, S., R. Müller, J.-U. Groöf, H. Nakajima, and Y. Sasano, Development of tracer relations and chemical ozone loss during the setup phase of the polar vortex, *J. Geophys. Res.*, in press, 2006a.
- Tilmes, S., R. Müller, J.-U. Groöf, R. Spang, T. Sugita, H. Nakajima, and Y. Sasano, Chemical ozone loss and related processes in the Antarctic winter 2003 based on improved limb atmospheric spectrometer (ILAS)-II observations, *J. Geophys. Res.*, 111, D11S12, doi: 10.1029/2005JD006260, 2006b.
- Toohey, D.W., L.M. Avallone, L.R. Lait, P.A. Newman, M.R. Schoeberl, D.W. Fahey, E.L. Woodbridge, and J.G. Anderson, The seasonal evolution of reactive chlorine in the Northern-Hemisphere stratosphere, *Science*, 261 (5125), 1134-1136, 1993.
- Toon, O.B., P. Hamill, R.P. Turco, and J. Pinto, Condensation of HNO₃ and HCl in the winter polar stratospheres, *Geophys. Res. Lett.*, 13 (12), 1284-1287, 1986.
- Tripathi, O.P., S. Godin-Beekmann, F. Lefèvre, M. Marchand, A. Pazmiño, A. Hauchecorne, F. Goutail, H. Schlager, C.M. Volk, B. Johnson, G. König-Langlo, S. Balestri, F. Stroh, T.P. Bui, H.J. Jost, T. Deshler, and P. von der Gathen, High resolution simulation of recent Arctic and Antarctic stratospheric chemical ozone loss compared to observations, *J. Atmos. Chem.*, 55 (3), doi: 10.1007/s10874-006-9028-8, 2006.
- Trolier, M., R.L. Mauldin III, and A.R. Ravishankara, Rate coefficient for the termolecular channel of the self-reaction of ClO, *J. Phys. Chem.*, 94, 4896-4907, 1990.
- Uchino, O., R.D. Bojkov, D.S. Balis, K. Akagi, M. Hayashi, and R. Kajihara, Essential characteristics of the Antarctic-spring ozone decline: Update to 1998, *Geophys. Res. Lett.*, 26 (10), 1377-1380, 1999.
- Urban, J., N. Lautié, E. Le Flochmoën, D. Murtagh, P. Ricaud, J. De La Noë, E. Dupuy, A. Drouin, L. El Amraoui, P. Eriksson, U. Frisk, C. Jiménez, E. Kyrölä, E.J. Llewellyn, G. Mégie, L. Nordh, and M. Olberg, The northern hemisphere stratospheric vortex during the 2002-03 winter: Subsidence, chlorine activation, and ozone loss observed by the Odin Sub-Millimetre Radiometer, *Geophys. Res. Lett.*, 31, L07103, doi: 10.1029/2003GL019089, 2004.
- Verronen, P.T., A. Seppälä, M.A. Clilverd, C.J. Rodger, E. Kyrölä, C.-F. Enell, T. Ulich, and E. Turunen, Diurnal variation of ozone depletion during the October-November 2003 solar proton events, *J. Geophys. Res.*, 110, A09S32, doi: 10.1029/2004JA010932, 2005.
- Vogel, B., W. Feng, M. Streibel, and R. Müller, The potential impact of ClO_x radical complexes on polar stratospheric ozone loss processes, *Atmos. Chem. Phys.*, 6, 3099-3114, 2006.
- Voigt, C., H. Schlager, B.P. Luo, A.D. Dornbrack, A.

POLAR OZONE

- Roiger, P. Stock, J. Curtius, H. Vossing, S. Borrmann, S. Davies, P. Konopka, C. Schiller, G. Shur, and T. Peter, Nitric acid trihydrate (NAT) formation at low NAT supersaturation in polar stratospheric clouds (PSCs), *Atmos. Chem. Phys.*, 5, 1371-1380, 2005.
- von Hobe, M., J.-U. Grooß, R. Müller, S. Hrechanyy, U. Winkler, and F. Stroh, A re-evaluation of the ClO/Cl₂O₂ equilibrium constant based on stratospheric in-situ observations, *Atmos. Chem. Phys. Discuss.*, 4 (5), 5075-5102, 2004.
- von Hobe, M., R.J. Salawitch, T. Canty, H. Keller-Rudek, G. Moortgat, J.-U. Grooß, R. Müller, and F. Stroh, Understanding the kinetics of the ClO dimer cycle, *Atmos. Chem. Phys. Discuss.*, 6, 7905-7944, 2006.
- von Savigny, C., A. Rozanov, H. Bovensmann, K.-U. Eichmann, S. Noël, V. Rozanov, B.-M. Sinnhuber, M. Weber, J.P. Burrows, and J.W. Kaiser, The ozone hole breakup in September 2002 as seen by SCIAMACHY on ENVISAT, *J. Atmos. Sci.*, 62 (3), 721-734, 2005.
- Waters, J.W., L. Froidevaux, W.G. Read, G.L. Manney, L.S. Elson, D.A. Flower, R.F. Jarnot, and R.S. Harwood, Stratospheric ClO and ozone from the Microwave Limb Sounder on the Upper Atmosphere Research Satellite, *Nature*, 362, 597-602, 1993.
- Weber, M., S. Dhomse, F. Wittrock, A. Richter, B.-M. Sinnhuber, and J.P. Burrows, Dynamical control of NH and SH winter/spring total ozone from GOME observations in 1995-2002, *Geophys. Res. Lett.*, 30 (11), 1583, doi: 10.1029/2002GL016799, 2003.
- Weber, M., L.N. Lamsal, M. Coldewey-Egbers, K. Bramstedt, and J.P. Burrows, Pole-to-pole validation of GOME WFOAS total ozone with ground-based data, *Atmos. Chem. Phys.*, 5, 1341-1355, 2005.
- Weeks, L.H., R.S. Cuikay, and J.R. Corbin, Ozone measurements in the mesosphere during the solar proton event of 2 November 1969, *J. Atmos. Sci.*, 29 (6), 1138-1142, 1972.
- Wirth, M., A. Tsias, A. Dörnbrack, V. Weiß, K.S. Carslaw, M. Leutbecher, W. Renger, H. Volkert, and T. Peter, Model-guided Lagrangian observation and simulation of mountain polar stratospheric clouds, *J. Geophys. Res.*, 104 (D19), 23971-23982, 1999.
- WMO (World Meteorological Organization), *Atmospheric Ozone: 1985, Global Ozone Research and Monitoring Project-Report No. 16*, Geneva, Switzerland, 1986.
- WMO (World Meteorological Organization), *International Ozone Trends Panel: 1988, Global Ozone Research and Monitoring Project-Report No. 18*, Geneva, Switzerland, 1990a.
- WMO (World Meteorological Organization), *Scientific Assessment of Stratospheric Ozone: 1989, Global Ozone Research and Monitoring Project-Report No. 20*, Geneva, Switzerland, 1990b.
- WMO (World Meteorological Organization), *Scientific Assessment of Ozone Depletion: 1991, Global Ozone Research and Monitoring Project-Report No. 25*, Geneva, Switzerland, 1992.
- WMO (World Meteorological Organization), *Scientific Assessment of Ozone Depletion: 1994, Global Ozone Research and Monitoring Project-Report No. 37*, Geneva, Switzerland, 1995.
- WMO (World Meteorological Organization), *Scientific Assessment of Ozone Depletion: 1998, Global Ozone Research and Monitoring Project-Report No. 44*, Geneva, Switzerland, 1999.
- WMO (World Meteorological Organization), *Scientific Assessment of Ozone Depletion: 2002, Global Ozone Research and Monitoring Project-Report No. 47*, Geneva, Switzerland, 2003.
- Yang, E.-S., D.M. Cunnold, M.J. Newchurch, and R.J. Salawitch, Change in ozone trends at southern high latitudes, *Geophys. Res. Lett.*, 32, L12812, doi: 10.1029/2004GL022296, 2005.
- Yela, M., C. Parrondo, M. Gil, S. Rodríguez, J. Araujo, H. Ochoa, G. Deferrari, and S. Díaz, The September 2002 Antarctic vortex major warming as observed by visible spectroscopy and ozonesoundings, *Int. J. Remote Sens.*, 26 (16), 3361-3376, 2005.

CHAPTER 5

Climate-Ozone Connections

Lead Authors:

M. Baldwin
M. Dameris

Coauthors:

J. Austin
S. Bekki
B. Bregman
N. Butchart
E. Cordero
N. Gillett
H.-F. Graf
C. Granier
D. Kinnison
S. Lal
T. Peter
W. Randel
J. Scinocca
D. Shindell
H. Struthers
M. Takahashi
D. Thompson

Contributors:

D. Battisti
P. Braesicke
R. Garcia
P. Haynes
E. Manzini
K. Matthes
G. Pitari
V. Ramaswamy
K. Rosenlof
B. Santer
R. Scott
A. Stenke
C. Timmreck

Final Release: February 2007
From *Scientific Assessment of Ozone Depletion: 2006*

CHAPTER 5

CLIMATE-OZONE CONNECTIONS

Contents

SCIENTIFIC SUMMARY	5.1
5.1 INTRODUCTION	5.3
5.2 COUPLING OF THE STRATOSPHERE AND TROPOSPHERE	5.3
5.2.1 Radiation	5.3
5.2.2 Dynamics	5.6
5.2.2.1 Role of Waves	5.6
5.2.2.2 How the Stratosphere Affects Its Own Variability	5.6
5.2.2.3 Transport of Air into the Stratosphere	5.7
5.2.2.4 Modeling and Parameterization of Small-Scale Waves	5.7
5.2.2.5 Annular Modes	5.8
5.2.2.6 Effects of Stratospheric Variability on the Troposphere	5.8
5.2.3 Tropospheric Composition	5.8
5.2.4 Stratospheric Aerosols	5.10
5.2.5 Past Changes in Stratospheric Water Vapor	5.12
5.2.6 Past Changes in Stratospheric Temperature	5.13
5.2.7 Impact of Ozone Changes on Surface Climate	5.16
5.2.7.1 Southern Hemisphere	5.16
5.2.7.2 Northern Hemisphere	5.18
5.3 EFFECTS OF ANTHROPOGENIC CLIMATE CHANGE AND OF EMISSIONS ON STRATOSPHERIC OZONE	5.18
5.3.1 Stratospheric Temperature Changes Due to Shifts in Radiative Forcing	5.18
5.3.2 Stratospheric Temperature Changes Due to Additional Effects	5.23
5.3.3 Troposphere-Stratosphere Exchange and the Brewer-Dobson Circulation	5.26
5.3.4 Changes in the Tropical and Extratropical Tropopause Layer	5.29
5.3.4.1 The Tropical Tropopause Layer (TTL)	5.29
5.3.4.2 The Extratropical Tropopause Layer (ExTL)	5.31
5.3.5 Impact of Future Water Vapor Changes on Ozone Chemistry	5.31
5.3.6 Impact of Temperature Changes on Ozone Chemistry	5.32
5.3.6.1 Upper Stratosphere	5.32
5.3.6.2 Polar Lower Stratosphere	5.33
5.3.7 Impact of Climate Change on Ozone Recovery	5.34
REFERENCES	5.38
APPENDIX 5A: AOGCMs Used in Chapter 5	5.49

SCIENTIFIC SUMMARY

Climate change will affect the evolution of the ozone layer through changes in transport, chemical composition, and temperature. In turn, changes to the ozone layer will affect climate through radiative processes, and consequential changes in temperature gradients will affect atmospheric dynamics. Therefore, climate change and the evolution of the ozone layer are coupled. Understanding all of the processes involved is made more complex by the fact that many of the interactions are nonlinear.

Impact of Climate Change

- **The stratospheric cooling observed during the past two decades has slowed in recent years.** Satellite and radiosonde measurements reveal an overall cooling trend in the global-mean lower stratosphere of approximately 0.5 K/decade over the 1979-2005 period, with a slowdown in the temperature decline since the late 1990s. The overall temperature decrease is punctuated by transient warmings of the stratosphere associated with the major volcanic eruptions in 1982 and 1991. Model calculations suggest that the observed ozone loss is the predominant cause of the cooling observed over this period. The lower stratospheric cooling is evident at all latitudes, in particular in both Arctic and Antarctic winter/spring lower stratosphere but with considerable interannual variability. Satellite observations show larger temperature trends in the upper stratosphere, with values of -1 to -2 K/decade, but little additional decline since the middle 1990s. Model calculations suggest that the upper stratosphere trends are due, roughly equally, to decreases in ozone and increases in CO_2 .
- **Future increases of greenhouse gas concentrations will contribute to the average cooling in the stratosphere.** Estimates derived from climate models (AOGCMs, coupled ocean-atmosphere general circulation models) and Chemistry-Climate Models (CCMs) with interactive ozone consistently predict continued cooling of the global average stratosphere. The predicted cooling rate within the next two decades is dependent on the prescribed scenario and the type of model used for the assessment. At 50 hPa an average of all AOGCMs gives approximately 0.1 K/decade, while CCMs predict a larger cooling of about 0.25 K/decade caused by the interactive consideration of ozone changes. All models calculate a stronger cooling at 10 hPa, averaging approximately 0.5 K/decade. Polar temperatures in the future are less certain than global mean temperatures because of greater natural variability.
- **Chemical reaction rates in the atmosphere are dependent on temperature, and thus the concentration of ozone is sensitive to temperature changes.** Decreases in upper stratospheric temperature slow the rate of photochemical ozone destruction in this region. Hence the concentration of upper stratospheric ozone increases in response to cooling. Cooling of the polar lower stratosphere would lead to more efficient chlorine activation on aerosol and polar stratospheric clouds and enhanced ozone destruction. Therefore, the concentration of ozone in the springtime polar lower stratosphere would decrease in response to cooling.
- **Greenhouse-gas-induced temperature and circulation changes are expected to accelerate global ozone increases in the next decades.** Two-dimensional latitude-height models, as well as CCMs, show that 1980 global mean total ozone values will be reached several years earlier than in a constant-temperature stratospheric environment.

Impact on the Troposphere

- **Changes to the temperature and circulation of the stratosphere affect weather and climate of the troposphere.** The response is seen largely as changes to the strength of the surface westerly winds in midlatitudes, and is found in both observations and model results. The strongest evidence for coupling is seen in the Northern Hemisphere during winter and in the Southern Hemisphere during spring. We do not have a complete understanding of the mechanisms that cause the stratosphere to affect the troposphere.
- **Stratospheric ozone depletion in the Southern Hemisphere appears to have caused circulation changes not only in the stratosphere, but in the troposphere as well.** The observed cooling of the Antarctic lower stratosphere has led to an increase in the speed of the stratospheric westerly winds and an associated delay in the seasonal breakdown of the stratospheric polar vortex. Observations and model results suggest that the changes to the lower

CLIMATE-OZONE CONNECTIONS

stratosphere have contributed to the observed strengthening of midlatitude tropospheric winds and to cooling over the interior of Antarctica during December-February. As ozone recovers, tropospheric changes due to ozone loss are expected to reverse. However, temperature changes due to increasing greenhouse gas concentrations may offset this reversal.

Importance of Tropospheric Changes

- **Human activities are expected to affect stratospheric ozone through changes in emissions of trace gases.** Enhanced methane (CH_4) emission (from wetter and warmer soils) is expected to enhance ozone production in the lower stratosphere, whereas a climate-driven increase in nitrous oxide (N_2O) emission is expected to reduce ozone in the middle and high stratosphere. Also, changes in nonmethane hydrocarbons and nitrogen oxide (NO_x) emissions are expected to affect the tropospheric concentrations of hydroxyl radical (OH) and, hence, impact the lifetime and concentration of stratospheric trace gases such as CH_4 and organic halogen species.
- **The exchange of air between the troposphere and the stratosphere is predicted to increase due to climate change.** Model studies predict that the annual mean troposphere-to-stratosphere mass exchange rate is expected to increase significantly, which will also decrease the average time that air remains within the stratosphere. Another possible consequence is a counterbalance of the stratospheric cooling associated with increasing greenhouse gases by an increase in the descent and adiabatic heating in the polar stratosphere during winter and spring. The net effect could result in local stratospheric temperature increases confined to high northern latitudes during winter and spring.

Importance of Water Vapor

- **Updated datasets of stratospheric water vapor concentrations now show differences in long-term behavior.** Recent trend analyses, which are based on only two available multiyear datasets, casts doubt on the positive stratospheric water vapor trend that was noted in the previous Assessment. Balloonborne measurements at Boulder, Colorado, for the period 1980-2005 show a significant increase of 5-10% per decade over altitudes of 15-28 km. Global measurements from the Halogen Occultation Experiment (HALOE) satellite instrument for 1991-2005 do not show corresponding positive lower stratospheric trends. Interannual water vapor changes derived from HALOE data exhibit quantitative agreement with temperature variations near the tropical tropopause. In contrast, the long-term increases inferred from the Boulder data are larger than can be explained by observed tropopause temperature changes or past increases in tropospheric methane.
- **Future changes of stratospheric water vapor concentrations are uncertain.** If water vapor concentration increases in the future, there will be both radiative and chemical effects. Modeling studies suggest increased water vapor concentrations will enhance odd hydrogen (HO_x) in the stratosphere and subsequently influence ozone depletion. Increases in water vapor in the polar regions would raise the temperature threshold for the formation of polar stratospheric clouds, potentially increasing springtime ozone depletion.

Importance of Volcanoes

- **If a major volcanic eruption occurs while stratospheric halogen loading is elevated, ozone will temporarily be depleted.** Strong volcanic eruptions enhance stratospheric aerosol loading for two to three years. A global average increase of lower stratospheric temperature (about 1 K at 50 hPa) was observed following the eruptions of El Chichón and Mt. Pinatubo, and globally averaged total ozone significantly decreased by about 2% before recovering after about two to three years. Ozone destruction via heterogeneous reactions depends on halogen loading, so the effects on ozone of a major eruption are expected to decrease in the coming decades. For sufficiently low halogen loading, a large volcanic eruption would temporarily increase ozone. Long-term ozone recovery would not be significantly affected.

5.1 INTRODUCTION

The purpose of this chapter is to assess the effects of human-induced climate change and greenhouse gases on stratospheric ozone. Investigations of the relationships and feedbacks between ozone depletion and climate change processes have demonstrated that it is not possible to achieve a complete understanding of ozone changes without the consideration of climate change. This chapter primarily concentrates on how climate change affects stratospheric ozone. The effect of stratospheric ozone depletion on climate was a focus of the Intergovernmental Panel on Climate Change/Technology and Economic Assessment Panel special report (IPCC/TEAP, 2005).

An increase of well-mixed greenhouse gas concentrations in the atmosphere leads to higher tropospheric temperatures (the greenhouse effect) and lower stratospheric temperatures. The rates of many chemical reactions are temperature dependent, and these reaction rates affect the chemical composition of the atmosphere. Reduced stratospheric temperatures lead to a slowing of some gas-phase reactions that destroy ozone, but also lead to intensified depletion of ozone in the lower polar stratosphere due to increased activation of halogens on polar stratospheric clouds (PSCs).

Since climate change processes influence the dynamics of the troposphere and the stratosphere, dynamically induced temperature changes could locally reinforce or oppose the temperature changes caused by radiative processes. These future changes are highly uncertain, with some models projecting that temperature will increase in the polar regions during northern winter and spring. The net effect of radiative, chemical, and dynamical interactions and feedbacks (many of which are nonlinear) is poorly understood and quantified at present.

Results of investigations presented in this chapter are based on observations and numerical modeling studies. Although atmospheric models have improved in recent years, they are still subject to uncertainties due to an incomplete description of atmospheric processes, their forcing, and their feedbacks. Weaknesses of models must be considered when evaluating calculated future changes, in particular for the assessment of the future evolution of the stratospheric ozone layer, as discussed in Chapter 6.

A summary description of the types of models used in this Assessment is given in Box 5-1. Section 5.2 provides an overview of stratospheric processes and a basic description of the coupling of the stratosphere and the troposphere. It contains background information about mechanisms and key processes that are relevant to describe and explain climate-ozone connections and feedbacks. In addition, it describes the influences of water vapor and of

its changes, sulfate aerosol, changes in source gases, temperature trends, their feedbacks on both chemistry and dynamics, and comparisons to results derived from numerical models describing atmospheric processes. Section 5.3 focuses on interactions between human-induced climate change and ozone depletion. At the end a detailed discussion of results derived from Chemistry-Climate Models is presented, which specifically addresses the question of how climate change will affect the evolution of the ozone layer.

5.2 COUPLING OF THE STRATOSPHERE AND TROPOSPHERE

5.2.1 Radiation

Greenhouse gases (GHGs), mainly carbon dioxide (CO_2) and water vapor, warm the troposphere by absorbing outgoing infrared (IR) radiation from the Earth in the well-known greenhouse effect. The dominant balance in the troposphere is between latent heating and radiative cooling by greenhouse gases. In the stratosphere, however, increased greenhouse gases lead to a net cooling as they emit more IR radiation out to space than they absorb. IR emission increases with local temperature, so the cooling effect increases with altitude, maximizing near the stratopause, where stratospheric temperatures are highest. The stratospheric cooling effect of greenhouse gases varies with latitude, as it depends on the balance between absorption of IR from below and local emission. The net cooling effect of greenhouse gases extends to lower levels at high latitudes, roughly following the tropopause.

Any change in radiatively active gas concentrations will change the balance between incoming solar (shortwave) and outgoing terrestrial (longwave) radiation in the atmosphere. The change of this balance due solely to the species in question, keeping other climate variables fixed, is termed radiative forcing (WMO, 2003; IPCC/TEAP, 2005). Radiative forcing is conventionally given as the net change in radiative fluxes at the tropopause, which can be a reasonable indicator of the surface temperature response.

Ozone absorbs both shortwave and longwave radiation. To determine radiative forcing from stratospheric ozone changes, it is important to distinguish between instantaneous effects and the effects after the stratospheric temperature has adjusted. Depletion of ozone in the lower stratosphere causes an instantaneous increase in the shortwave solar flux at the tropopause and a slight reduction of the downwelling longwave radiation. The net instantaneous effect is a positive radiative forcing. However, the

Box 5-1. Atmospheric Models

Numerical models are useful for investigations of the composition and the thermal and dynamical structure of Earth's atmosphere. They allow evaluation of different processes and mechanisms as well as feedbacks. Scientific progress can be achieved by understanding the discrepancies between observations and results derived from model simulations. Assessments of the future development of atmospheric dynamics and chemistry are typically based on scenario simulations and sensitivity studies. In this 2006 Assessment, results of the following model systems have been used:

- **Two-Dimensional (2-D) Photochemical Model:** *Zonally averaged representation of the atmosphere, with detailed chemistry but simplified transport and mixing.* Chemical reactions are included in the model according to the physical characteristics: pressure, temperature and incident solar radiation. In each model box, the movement of air into and out of each box is simulated, representing advection and dispersion. Advection by three-dimensional (3-D) motion and sub-grid scale mixing are parameterized. Some models include emissions from different sources, particularly for tropospheric pollutants, otherwise they use imposed tropospheric concentrations. In an "interactive" model, changes in the chemical composition of the atmosphere cause changes in temperatures and hence transport, whereas in a "non-interactive" model, this feedback is missing and temperatures are unaffected by changes in chemical composition.
- **Chemical Transport Model (CTM):** *Simulation of chemical processes in the atmosphere employing meteorological analyses derived from observations or climate models.* A CTM is a non-interactive model that does not consider the feedback of chemistry to dynamical and radiative processes. It uses winds and temperatures from meteorological analyses or predictions to specify the atmospheric transport and temperatures and to calculate the abundances of chemical species in the troposphere and stratosphere. A CTM can be used to simulate the evolution of atmospheric composition and help interpret observations.
- **Atmospheric General Circulation Model (AGCM):** *Three-dimensional model of large-scale (spatial resolution of a few hundred km) physical, radiative, and dynamical processes in the atmosphere over years and decades.* An AGCM is used to study changes in natural variability of the atmosphere and for investigations of climate effects of radiatively active trace gases (greenhouse gases) and aerosols (natural and anthropogenic), along with their interactions and feedbacks. Usually, AGCM calculations employ prescribed concentrations of radiatively active gases, e.g., carbon dioxide (CO₂), methane (CH₄), nitrous oxide (N₂O), chlorofluorocarbons (CFCs), and ozone (O₃). Changes of water vapor (H₂O) concentrations due to the hydrological cycle are directly simulated by an AGCM. Sea surface temperatures (SSTs) are prescribed. An AGCM coupled to an ocean model, commonly referred to as an AOGCM or a climate model, is used for investigation of climate change. More recently, climate models may also include other feedback processes (e.g., carbon cycle, interaction with the biosphere).
- **Chemistry-Climate Model (CCM):** *An AGCM that is interactively coupled to a detailed chemistry module (see Figure 5-1).* In a CCM, the simulated concentrations of the radiatively active gases are used in the calculations of net heating rates. Changes in the abundance of these gases due to chemistry and advection influence heating rates and, consequently, variables describing atmospheric dynamics such as temperature and wind. This gives rise to a dynamical-chemical coupling in which the chemistry influences the dynamics (via radiative heating) and vice versa (via temperature and advection). Not all CCMs have full coupling for all chemical constituents; some radiatively active gases are specified in either the climate or chemistry modules. Ozone is always fully coupled, as it represents the overwhelmingly dominant radiative-chemical feedback in the stratosphere. *Transient* simulations consider observed or predicted gradual changes in concentrations of radiatively active gases and other boundary conditions (e.g., emissions). The temporal development of source gas emissions and SSTs are prescribed for a specific episode (years to decades). In *time-slice* simulations, the internal variability of a CCM can be investigated under fixed conditions, e.g., for greenhouse gas (GHG) concentrations and SSTs, to estimate the significance of specific changes.

decrease in ozone causes less absorption of solar and long-wave radiation, leading to a local cooling. After the stratosphere has adjusted, the net effect of ozone depletion in the lower stratosphere is a negative radiative forcing (IPCC/TEAP, 2005). In contrast, ozone depletion in the middle and upper stratosphere causes a slight positive radiative forcing (IPCC/TEAP, 2005). The maximum sensitivity of radiative forcing for ozone changes is found in the tropopause region, and the maximum sensitivity of surface temperatures to ozone changes also peaks near the tropopause (Forster and Shine, 1997).

Quantifying the impact of stratospheric ozone changes on surface temperatures is less straightforward than estimating radiative forcing (RF). This is because a climate sensitivity term, λ , has to be introduced to translate radiative forcing to changes in surface temperatures (T_{surf}). The relationship between λ and T_{surf} changes is generally given by $\Delta T_{\text{surf}} = \lambda \text{ RF}$ (see Box 1.3 in IPCC/TEAP, 2005), where λ is in units of $\text{K} (\text{W m}^{-2})^{-1}$. ΔT_{surf} is the equilibrium response of global mean surface temperature and RF is the radiative perturbation. The assumption of linearity between radiative forcing and the surface temperature change made in this equation is found to hold well for ozone depletion (Forster and Shine, 1999).

λ is poorly constrained by observations and is conventionally evaluated in climate models as the equilibrium global mean temperature response to a radiative forcing change equivalent to a doubling of CO_2 . λ is dependent on the strength of climate feedbacks, such as those associated with clouds, water vapor, and ice albedo, and its magnitude varies considerably from model to model. Its value is likely to lie in the range 1.5 to $4.5 \text{ K} (\text{W m}^{-2})^{-1}$ (IPCC, 2001). λ can depend significantly on the nature of the forcing, particularly in the case of stratospheric ozone changes, and can differ from that for a doubling of CO_2 . Section 5.2.7 discusses dynamic responses in more detail.

Eleven-year solar ultraviolet (UV) irradiance variations have a direct impact on the radiation and ozone budget of the middle atmosphere (e.g., Haigh, 1994; see also Chapter 3, Section 3.4.4). During years with maximum solar activity, the solar UV irradiance is enhanced, which leads to additional ozone production and heating in the stratosphere and above. By modifying the meridional temperature gradient, the heating can alter the propagation of planetary and smaller-scale waves that drive the global circulation. Although the direct radiative forcing of the solar cycle in the upper stratosphere is relatively weak, it could lead to a large indirect dynamical response in the lower atmosphere through a modulation of the polar night jet and the Brewer-Dobson circulation (Kodera and Kuroda, 2002). Such dynamical changes can feed back on the chemical budget of the atmosphere because of the

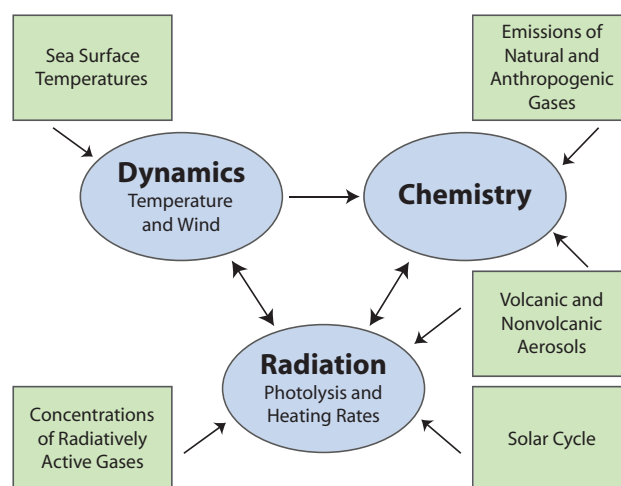


Figure 5-1. Schematic of a Chemistry-Climate Model (CCM). The core of a CCM (oval symbols) consists of an atmospheric general circulation model (AGCM) that includes calculation of the heating and cooling rates and a detailed chemistry module. They are interactively coupled. Photolysis rates are calculated online or are determined from a lookup table. Arrows indicate the direction of effect. Rectangular boxes denote external impacts. In current CCMs, sea surface temperatures (SSTs) are prescribed based on observations or are adopted from calculations with a climate model. Natural and anthropogenic emissions of gases are considered. Tropospheric and stratospheric aerosol loading (especially after volcanic eruptions) can be taken into account. CCMs often consider the changes of solar radiation caused by the 11-year activity cycle of the Sun.

temperature dependence of both the chemical reaction rates and the transport of chemical species.

The Arctic lower and middle stratosphere tend to be cold and undisturbed during west-wind phases of the equatorial quasi-biennial oscillation (QBO; Section 5.2.2.1), while they are warm and disturbed during QBO east-wind phases (Holton and Tan, 1980; 1982). Further analysis (Labitzke, 1987; Labitzke and van Loon, 1988) showed that this relationship is strong during solar minimum conditions, while during solar maximum years the relationship does not hold. This solar-QBO interaction has remained robust in the observations since its discovery. Equatorial upper stratospheric winds during the early winter appear to be important for the evolution of the Northern Hemisphere winter, especially the timing of stratospheric sudden warmings (Gray et al., 2001a; 2001b; Gray, 2003; Gray et al., 2004).

CLIMATE-OZONE CONNECTIONS

Some modeling studies have confirmed the modulation of the polar night jet and the Brewer-Dobson circulation by the solar cycle (e.g., Matthes et al., 2004). The transfer of the solar signal from the stratosphere to the troposphere is the subject of ongoing research and includes the possibility of the modulation of the Northern Hemisphere Annular Mode (NAM; Section 5.2.2.5) (Kodera, 2002; Matthes et al., 2006) and changes in vertical motion and precipitation in the tropics (e.g., Kodera, 2004; Haigh et al., 2005; Matthes et al., 2006). It is also possible that a “wave-ozone feedback” mechanism communicates the solar signal to the QBO (Cordero and Nathan, 2005), although Mayr et al. (2006) found a solar modulation of the QBO even though there is no wave-ozone feedback in their model.

5.2.2 Dynamics

Although the stratosphere and troposphere are in many ways distinct, the atmosphere is continuous, allowing vertical wave propagation and a variety of other dynamical interactions between these regions. A complete description of atmospheric dynamics requires an understanding of both of these layers. The dynamical coupling of the stratosphere and troposphere is primarily mediated by wave dynamics. A variety of waves originate in the troposphere, propagate upward into the stratosphere and above, and then dissipate, shaping the spatial and temporal structure of the stratospheric flow. This traditional view of a passive stratosphere has more recently given way to a greater appreciation of the stratosphere’s ability to shape not only its own evolution but that of the troposphere as well.

5.2.2.1 ROLE OF WAVES

The climatological temperature structure of the stratosphere, as well as its seasonal cycle and variability, depend crucially on the dynamics of waves that are generated in the troposphere. Wave dynamics can be divided broadly into three processes: generation mechanisms, propagation characteristics, and dissipation (primarily due to wave breaking and thermal damping, with thermal damping important for planetary wave dissipation at high latitudes, outside the surf zones; it is also likely to be important for the dissipation of equatorial waves). In the extratropics, the temperature structure of the stratosphere depends on a balance between diabatic radiative heating and adiabatic heating from induced vertical motion due to planetary wave dissipation (Andrews et al., 1987). Planetary wave breaking in the winter stratosphere (and mesosphere) generally produces a westward force that decelerates the polar

stratospheric jet, resulting in ascent (adiabatic cooling) in the tropics, and descent (adiabatic warming) over the poles (Holton et al., 1995). This response pattern describes a meridional mass circulation that is called the Brewer-Dobson circulation.

The basic climatology of the extratropical stratosphere is broadly understood in terms of wave dynamics together with the seasonal cycle of radiative heating. For example, the easterly winds of the summer stratosphere inhibit upward propagation of planetary waves (Charney and Drazin, 1961) and so the summer stratosphere is much less disturbed than the winter stratosphere. Asymmetries in the continental land mass between the Northern Hemisphere (NH) and Southern Hemisphere (SH) imply asymmetries in the efficiency of planetary wave generation mechanisms. Consequently in winter, planetary wave disturbances in the stratosphere of the NH are significantly larger than those in the SH. In the tropical stratosphere, the dominant form of variability is a quasi-periodic (2-3 year) wave-driven descending zonal mean wind reversal, called the quasi-biennial oscillation (QBO). The peak-to-peak amplitude of the wind QBO is ~55 m/s at 25-30 km (Baldwin and Gray, 2005), while the temperature QBO amplitude is ~8 K. The QBO affects the global stratospheric circulation, and extends to ~20° north and south with an amplitude of about 10 m/s (Dunkerton and Delisi, 1985). It affects a variety of extratropical phenomena including the strength and stability of the wintertime polar vortex, and the distribution of ozone and other gases (see Baldwin et al., 2001 for a review). The QBO is driven by the dissipation of a variety of equatorial waves (Lindzen and Holton, 1968; Dunkerton, 2001) that are primarily forced by deep cumulus convection in the tropics.

5.2.2.2 HOW THE STRATOSPHERE AFFECTS ITS OWN VARIABILITY

Although stratospheric variability has long been viewed as being caused directly by variability in tropospheric wave sources, it is by now widely accepted that the configuration of the stratosphere itself also plays an important role in determining the vertical flux of wave activity from the troposphere. The original theory of Charney and Drazin (1961) states that it is only when the winds are westerly that the longest waves (mainly waves 1, 2, and 3) can propagate vertically. This theory has been extended to account for the strongly inhomogeneous nature of the stratospheric background state and the steep potential vorticity gradients at the polar vortex edge (e.g., Scott et al., 2004). Given a steady source of waves in the troposphere, any changes in the stratospheric background potential vorticity (PV) gradient will change the vertical

wave fluxes, giving rise to the possibility of internally driven variability of the stratosphere, as modeled by Holton and Mass (1976). Similar internal variability has also been demonstrated in more comprehensive AGCMs (see Box 5-1) (e.g., Christiansen, 1999). Modeling studies suggest that realistic stratospheric variability can arise in the absence of tropospheric variability (Scott and Polvani, 2004; 2006).

The modulation of vertical wave flux into the stratosphere by the stratospheric configuration may be related to the extent to which the stratosphere can act as a resonant cavity, involving downward reflection of stationary planetary waves (McIntyre, 1982; Smith, 1989). Further, through these processes, the tropospheric circulation itself is also influenced by the stratospheric configuration. Reflection of stationary planetary wave energy takes place when the polar vortex exceeds a critical threshold in the lower stratosphere, leading to structural changes of the leading tropospheric variability patterns (Perlwitz and Graf, 2001; Castanheira and Graf, 2003; Walter and Graf, 2005).

There exists also an external or barotropic mode whose potential impact on the stratospheric circulation (in terms of its deceleration of the polar night vortex) is significantly larger than that of upward propagating waves. Esler and Scott (2005) demonstrated the relevance of this mode in wavenumber-2 major warmings in which the vortex is split throughout the full depth of the stratosphere.

5.2.2.3 TRANSPORT OF AIR INTO THE STRATOSPHERE

Planetary waves breaking in the stratosphere are also important for the transport of species from the troposphere to and within the stratosphere. The mean circulation of the stratosphere is essentially a “wave-driven pump” (see Holton et al., 1995, for a review) in which stratospheric wave drag moves air poleward and downward over the polar cap. As a consequence, the air in the tropical lower stratosphere rises slowly (0.2 to 0.3 mm/s) and carries ozone-poor air from the troposphere higher into the stratosphere. There, with increasing altitude, photochemical production becomes more effective. The upwelling in the tropics is modulated by the seasonal cycle and the tropical QBO phase (Baldwin et al., 2001). When the QBO is westerly at 40-50 hPa, the ascent rate is lower, there is more time for ozone production, and the tropical ozone column is enhanced. In the subtropics and extratropics, transport of chemical species from the troposphere to the lowermost stratosphere occurs through quasi-isentropic motion associated with synoptic-scale and mesoscale circulations (e.g., baroclinic eddies, frontal circulations). In the same circulations, there is substantial

transport from stratosphere to troposphere. Quantification of this two-way (troposphere-to-stratosphere and stratosphere-to-troposphere) transport has improved significantly over the last few years through modeling and observations. (See, e.g., Stohl et al., 2003 for a review.) However, significant quantitative uncertainty remains over the role of small-scale circulations, e.g., convective systems, in transport from troposphere to stratosphere or vice versa. The transport of air in the tropopause region is discussed in greater detail in Chapter 2, Section 2.4.

5.2.2.4 MODELING AND PARAMETERIZATION OF SMALL-SCALE WAVES

The consideration of wave dynamics in determining the climatology of the stratosphere is very important. Any systematic change in the generation, propagation, or dissipation of waves (both resolved and parameterized) will result in systematic changes in the temperature structure of the stratosphere. The capability to simulate the climatology and space-time changes of stratospheric properties hinges critically on our ability to simulate highly nonlinear wave dynamics in a reliable way. Atmospheric models generally have inadequate horizontal resolution (for baroclinic eddies, interaction with ocean and land surface) and vertical resolution (for the planetary wave propagation characteristics and cross-tropopause transport). Another issue is that deep convection (an important excitation mechanism for waves that propagate into the stratosphere) is a sub-grid-scale process that must be parameterized.

One of the most challenging aspects of modeling the dynamical coupling of the troposphere and stratosphere is the parameterization of unresolved waves (in particular, non-orographic gravity waves) and their feedback on the resolved flow. There are limited observational data to constrain the tropospheric sources and basic middle-atmosphere climatology of gravity waves (e.g., see reviews by Fritts and Alexander, 2003 and Kim et al., 2003). Parameterizations of ever-increasing complexity are being developed to more realistically model the dynamics of these waves, and the free parameters are used to reproduce present-day climate. This raises a credibility issue when these gravity-wave parameterizations are employed for the purpose of climate change simulations (but see Section 5.3.2). With the advent of newer satellite temperature and wind observations of global extent and higher spatial resolution (e.g., Wu, 2004; Eckermann et al., 2006), it is anticipated that current parameterizations of gravity waves will be better constrained and more objectively validated. There are also current efforts to specify gravity wave source spectra in terms of fields calculated by the underlying

CLIMATE-OZONE CONNECTIONS

AGCM, such as frontal zones and convective heating (e.g., Charron and Manzini, 2002; Beres et al., 2005).

5.2.2.5 ANNULAR MODES

Annular modes are hemispheric spatial patterns of climate variability characterized by north-south shifts in mass between polar and lower latitudes (Thompson and Wallace, 2000). Tropospheric signatures of stratospheric variability are often well described by annular mode patterns (e.g., Baldwin and Dunkerton, 2001; Gillett and Thompson, 2003). In both the stratosphere and troposphere, the annular modes explain a larger fraction of variance than any other pattern of climate variability in their respective hemisphere. On month-to-month time scales, annular variability at tropospheric levels is strongly coupled with annular variability at stratospheric levels (Baldwin and Dunkerton, 1999; Thompson and Wallace, 2000). Thus, as noted in Section 5.2.2.6, time series of the annular modes provide a convenient way to describe some aspects of stratosphere-troposphere coupling. The Northern Hemisphere Annular Mode (NAM) near Earth's surface is alternatively known as the Arctic Oscillation (AO; Thompson and Wallace, 1998) and the North Atlantic Oscillation (NAO; Hurrell, 1995). The Southern Hemisphere Annular Mode (SAM) is also referred to as the Antarctic Oscillation and High Latitude Mode.

Recent studies suggest the annular modes reflect feedbacks between the eddies and the zonal flow at middle latitudes (Lorenz and Hartmann, 2001; 2003). Other studies imply the annular modes are expected in any rotating planetary fluid system that conserves momentum and mass, and that has some smoothness property (Gerber and Vallis, 2005). The key dynamics that underlie the annular modes are still under investigation.

5.2.2.6 EFFECTS OF STRATOSPHERIC VARIABILITY ON THE TROPOSPHERE

Observational analysis suggests that stratospheric processes affect surface weather and climate (e.g., Scaife et al., 2005). Figure 5-2 shows composites of indices of the Northern Hemisphere Annular Mode (NAM) during periods when the stratospheric vortex rapidly changes strength. It reveals that within the winter season when the stratospheric flow is westerly, changes to the strength of the northern polar vortex are, on average, accompanied by similarly signed and similarly persistent changes to the tropospheric flow (Baldwin and Dunkerton, 1999; 2001). The illustration would be similar if high-latitude zonal winds ($\sim 60^\circ\text{N}$) were used instead of the annular mode index. The figure thus suggests that changes to the strength

of the polar vortex—especially in the lowermost stratosphere—may affect the tropospheric flow.

Despite the apparent robustness of the above evidence, the principal mechanisms whereby stratospheric variability may influence the tropospheric circulation remain unclear. A complete explanation of the observed coupling likely lies in one or more of the following physical processes:

- 1) Geostrophic and hydrostatic adjustment of the tropospheric flow to anomalous wave drag (Haynes et al., 1991; Thompson et al., 2006) and anomalous diabatic heating at stratospheric levels (Thompson et al., 2006);
- 2) The impact of anomalous shear in the lower stratospheric zonal flow on the momentum flux by baroclinic eddies (Shepherd, 2002; Kushner and Polvani, 2004; Wittman et al., 2004);
- 3) Amplification due to internal tropospheric dynamics (Song and Robinson, 2004);
- 4) The impact of anomalous shear at the tropopause level on vertically propagating waves (Chen and Robinson, 1992; Shindell et al., 1999; Limpasuvan and Hartmann, 2000);
- 5) The reflection of planetary waves (Hartmann et al., 2000; Perlwitz and Harnik, 2004).

Through such mechanisms, long-term changes in temperature and circulation of the stratosphere (e.g., radiative heating anomalies due to a GHG increase or changes to the ozone distribution) may affect surface weather patterns, at least during winter, spring, and early summer.

5.2.3 Tropospheric Composition

Many of the chemical constituents present in the stratosphere have sources that originate in the troposphere. Any changes in the chemical composition of the troposphere can affect the composition of the stratosphere. The chemical constituents are either directly emitted in the troposphere, mostly at or near the surface, or they are oxidation products of emitted species. The predominant source gases for stratospheric hydrogen, halogen, and nonvolcanic sulfur are long-lived species (water vapor, methane (CH_4), nitrous oxide (N_2O), organic halogen gases such as chlorofluorocarbons (CFCs), halons, and carbonyl sulfide (COS)). Surface emissions of short-lived species (sulfur dioxide (SO_2), dimethyl sulfide (DMS)) are also important sources of sulfur to the stratosphere, as are occasional large volcanic eruptions.

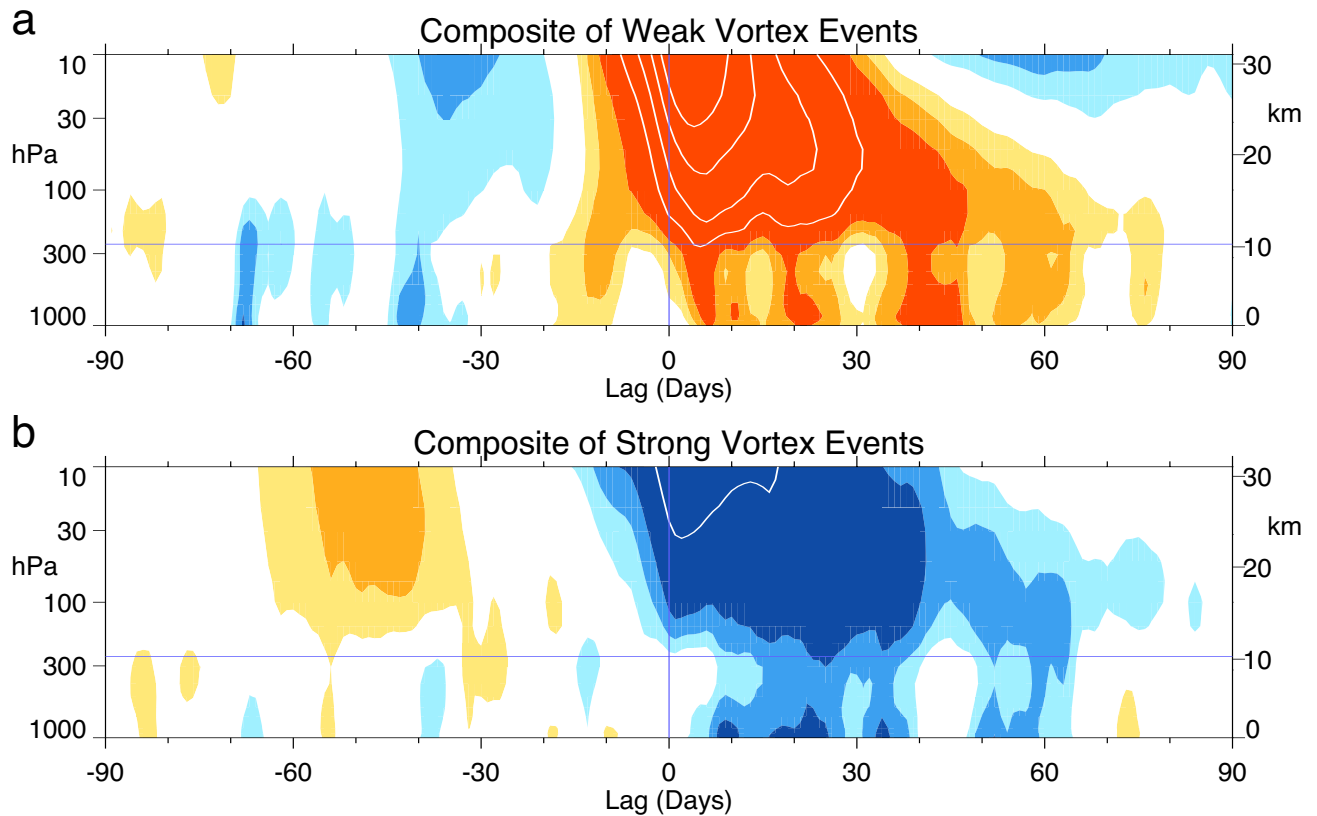


Figure 5-2. Composites of time-height development of the Northern Hemisphere Annular Mode (NAM) for: (a) 22 weak vortex events; and (b) 35 strong vortex events during 1958 to 2006. Updated from Baldwin and Dunkerton (2001). The events are determined by the dates on which the 10 hPa NAM values crossed -3.0 and $+1.5$, respectively. The indices are non-dimensional; the contour interval for the color shading is 0.25, with values between -0.25 and 0.25 unshaded. The white contours begin at ± 1.25 with a contour interval of 0.5. The thin horizontal lines indicate the approximate tropopause. The diagrams illustrate that large anomalies in the strength of the polar vortex at 10 hPa tend to descend to the lowermost stratosphere, where they last, on average, more than two months. After the stratospheric events occur, the tropospheric NAM anomaly is of the same sign as the stratospheric anomaly.

Long-term increases in CH_4 , N_2O , and CFCs brought about by increasing anthropogenic emissions are discussed in Chapter 1. However, with the exception of CFCs and halons, emissions of most stratospheric source gases have a substantial natural component. For instance, natural emissions represent more than a third of the CH_4 source, more than half of the N_2O source (IPCC, 2001), and are the dominant source of carbonyl sulfide (COS) (SPARC, 2006). As natural emissions are very likely to be affected by climate changes and, in particular, changes in precipitation, vegetation, and temperature, it is important to assess their sensitivity to climate changes, taking into account this effect when forecasting their future evolution and their overall impact on ozone recovery. Natural emissions also represent a large source of key short-lived species, such as nitric oxide (NO) emissions from soil and

lightning, or emissions of nonmethane hydrocarbons such as isoprene. Sources, transport, and stratospheric impact of halogenated short-lived species, many of which have predominantly natural origins, are dealt with in Chapter 2. The lifetimes of such short-lived compounds in relation to transport time scales are such that only a fraction of surface emissions reach the stratosphere (see Chapter 2). They may also affect the chemical composition of the troposphere, and hence potentially the lifetimes of other trace gases, through changes in atmospheric hydroxyl radical (OH).

Some progress has been made in estimating the sensitivity of natural sources to various climate parameters. For example, process modeling suggests that CH_4 emissions from wetlands could increase by 20% for a temperature increase of 1 K (Walter and Heimann, 2000). The

CLIMATE-OZONE CONNECTIONS

emissions of short-lived species such as biogenic hydrocarbons also increase with temperature. However, it is difficult to quantify climate-driven changes in natural sources because the temperature is not the only driving factor. Other factors such as water table level, soil moisture, vegetation cover, photosynthetically active radiation, biogenic productivity, or exposure to atmospheric pollutants can play a role, depending on the emitting substrate and the emitted species. Ignoring changes in land use, most natural emissions are expected to increase as Earth's surface warms. The changes that are most relevant to the stratosphere are climate-driven increases in CH₄ and N₂O emissions. An increase in CH₄ would accelerate the ozone recovery whereas an increase in N₂O would delay it (Randeniya et al., 2002; Chipperfield and Feng, 2003).

Climate changes can also alter other key processes in the exchange of chemical constituents between the troposphere and stratosphere. The vertical transport of surface emissions to the tropopause is largely dependent on the intensity of convective activity, and the flux of tropospheric air into the stratosphere is mostly determined by the strength of the upwelling from the troposphere that is linked to the strength of the Brewer-Dobson circulation (see Section 5.2.2.3).

5.2.4 Stratospheric Aerosols

Non-explosive volcanic surface emissions of sulfur species (SO₂, COS) are important sources of stratospheric aerosol loading mainly through tropical stratosphere/troposphere exchange (Notholt et al., 2005). Stratospheric aerosols have a direct radiative impact that decreases the surface temperature, since more shortwave radiation is reflected. Although there has been no significant change in the background (nonvolcanic) stratospheric aerosols for the period 1970 to 2004 (Deshler et al., 2006; see also SPARC, 2006), the non-volcanic aerosol loading could increase in the future if convection increases (Pitari et al., 2002), because convection is a key process that transports the short-lived species SO₂ from the surface to the upper troposphere and lower stratosphere.

Volcanic SO₂ injected into the stratosphere is oxidized to sulfuric acid that condenses and forms aerosols, on which heterogeneous reactions occur. Volcanic eruptions have strong impacts on the lower stratospheric thermal structure because the volcanic aerosols scatter back incoming solar radiation and absorb solar near-infrared and terrestrial infrared radiation (e.g., Stenchikov et al., 1998; Al-Saadi et al., 2001; Rozanov et al., 2002; Timmreck et al., 2003). Heterogeneous chemistry occurring on aerosol surfaces affects ozone concentrations, producing an additional indirect radiative impact depending on the concentration of atmospheric chlorine. In addition,

the modified meridional temperature profile in the stratosphere may result in colder polar vortices in winter (Chapter 3 in WMO, 2003).

The ozone impact of a given volcano depends on the amount of material, in particular sulfur, injected by the volcanic eruption and on whether the material reaches the stratosphere, as well as the phase of the QBO and the latitude of the eruption. The height reached by ejecta depends on the explosivity of the eruption, not on its location. Ejecta from tropical eruptions will be carried upward and poleward by the Brewer-Dobson circulation and, therefore, they will spread throughout much of the stratosphere with a long residence time, whereas ejecta from mid- to high-latitude eruptions will more quickly be returned to the troposphere by the descending branch of the Brewer-Dobson circulation.

The effect of a future major volcanic eruption will depend on chlorine levels. For low-chlorine conditions, heterogeneous chemistry can lead to ozone increases in the stratosphere, whereas for high chlorine conditions, as observed in recent years, volcanic aerosols lead to additional ozone depletion (Tie and Brasseur, 1995). Moreover, volcanic aerosol affects photolysis rates and therefore ozone concentrations (Timmreck et al., 2003).

The results of several CCM simulations (see Box 5-1) are consistent with the Tie and Brasseur study. After the eruption of Mt. Agung in 1963, the total amount of ozone was reduced, particularly in the tropics (see Chapter 3, Figure 3-4). Since the chlorine loading of the atmosphere was low at that time, the solar cycle influences were of particular importance (see Chapter 3, Section 3.4.4). For example, the CCM E39C simulated reasonably well the observed decrease of tropical ozone around 1965, since the influence of the 11-year solar cycle was considered, which was minimal around 1965 (Dameris et al., 2005). Following the major eruptions of El Chichón (1982) and Mt. Pinatubo (1991), when atmospheric chlorine amounts were much higher and solar activity was near maximum, the total ozone significantly decreased in subsequent months in both observations and models, before recovering after two to three years. The simulated globally averaged total ozone decreases for many models in the Eyring et al. (2006) assessment were about 2%, similar to what was observed (cf. Fioletov et al., 2002; WMO, 2003).

In AOGCM and CCM simulations, the temperature perturbations after the eruptions of El Chichón and Mt. Pinatubo are often larger than 1 K (annually averaged) in the lower stratosphere (see Figures 5-3 and 5-11), whereas observations indicate an increase of about 1 K. The temperature impact is important since this will determine to a large extent the water vapor perturbation. In turn, this will

Simulated and Observed Stratospheric Temperature Changes

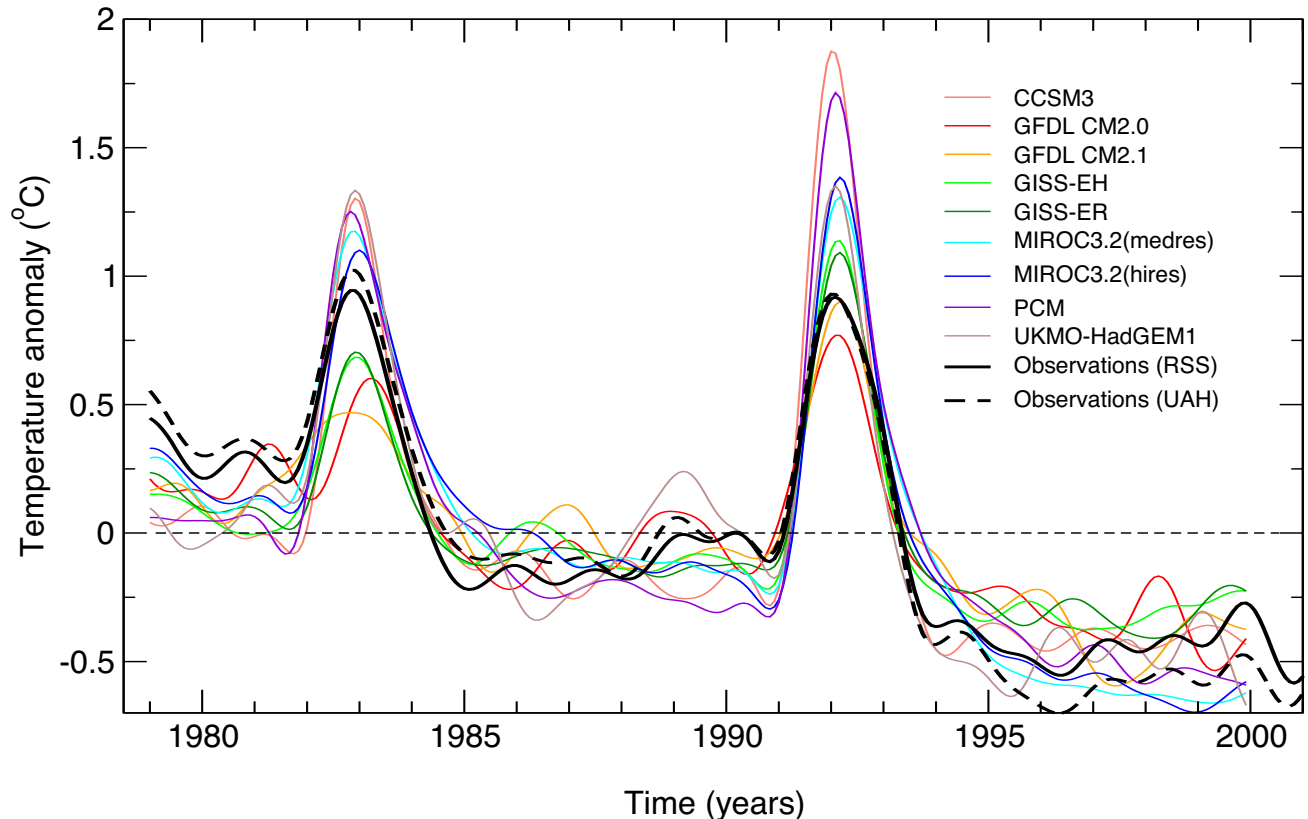


Figure 5-3. Globally averaged temperature anomalies in the lower stratosphere from a range of climate models (Santer et al., 2006) in comparison with Microwave Sounding Unit MSU4 channel temperatures. The MSU4 observations are from two independent analyses by the Remote Sensing Systems (RSS) and the University of Alabama at Huntsville (UAH) groups. See Appendix 5A for information about the models.

influence the ozone chemistry in the lower stratosphere (Section 5.3.5) and lower stratospheric cooling rates (Section 5.2.6). Figure 5-3 shows the globally averaged temperature from a range of tropospheric climate models (Santer et al., 2006; see also Ramaswamy et al., 2006), vertically averaged by the Microwave Sounding Unit MSU4 weighting function, together with MSU4 data. The variations due to volcanic eruptions are clear for several years, with an overall slow cooling. The CCM and climate model studies indicate that the strength of the volcanic signal varies substantially between the models (see also Figures 3-26 and 5-11, and Eyring et al., 2006).

The sulfate aerosols and ash injected into the stratosphere from volcanic eruptions can cause tropospheric cooling (e.g., Hansen et al., 1992; Robock, 2000; Santer et al., 2001; Wigley et al., 2005; Yokohata et al., 2005), although ash particles have a short residence time because

of gravitational settling. The tropospheric cooling would be expected to change the tropospheric circulation, as well as the interaction between the stratosphere and the troposphere (Stenchikov et al., 2002).

Based on the historical volcanic record, a major eruption of similar atmospheric impact to that of Mt. Pinatubo is likely to occur during the next 30 years (Roscoe, 2001). The previous 50-year period, with three such eruptions, appears to be unusual. Much larger eruptions, such as Toba 74,000 years ago, are a remote possibility, with recovery times of a decade (Bekki et al., 1996). Model studies by Rosenfield (2003), assuming a Pinatubo-sized eruption every 10 years from 2010 to 2050, suggest that the long-term recovery of ozone would not be strongly affected by infrequent large volcanic eruptions. The impacts on ozone of all except the largest eruptions would be expected to last only a few years, and not significantly

CLIMATE-OZONE CONNECTIONS

affect long-term ozone recovery, because ozone recovery depends primarily on halogen levels.

5.2.5 Past Changes in Stratospheric Water Vapor

Water vapor is the most important greenhouse gas, and it plays an important role in chemistry-climate interactions. Previous studies reported in WMO (2003) showed that ozone perturbations are amplified in the upper troposphere and lower stratosphere as a result of feedback processes with water vapor. Any increase in stratospheric water vapor could lead to an increase in the level of odd-hydrogen radicals (HO_x), which could affect the nitrogen oxide radicals (NO_x) and chlorine oxide radicals (ClO_x) cycles, leading to ozone depletion (see Section 5.3.5). A change in water vapor concentration could also change the temperature thresholds for polar stratospheric cloud formation over the polar caps (see Section 5.3.5).

Air enters the stratosphere mostly in the tropics, and stratospheric water vapor is primarily controlled by temperatures near the tropical tropopause. The associated processes have been studied in detail over the past few years, for example using trajectory studies (Bonazzola and Haynes, 2004; Fueglistaler et al., 2005). Water vapor is also produced in the stratosphere by the photochemical oxidation of methane, producing approximately two molecules of water vapor per molecule of methane. The increase in the concentration of tropospheric methane since the 1950s (0.55 parts per million by volume (ppmv)) is responsible for part of the increase in stratospheric water vapor over this time period (SPARC, 2000).

Measurements of stratospheric water vapor content are available from ground-based instruments and aircraft observations, plus balloonborne and satellite datasets. The longest continuous dataset is from a single location (Boulder, Colorado, USA), based on balloonborne frost point hygrometer measurements (approximately one per month), beginning in 1980 (Oltmans et al., 2000; see updated data in Figure 5-4). Over the period 1980-2005, a statistically significant linear trend of ~5-10% per decade is observed at all levels between approximately 15 and 26 km. However, although a linear trend can be fitted to this 25-year long record, there is a high degree of variability in the infrequent sampling, and the increases seen are neither continuous nor steady. In particular, stratospheric water vapor concentrations have decreased since 2001. Long-term increases in stratospheric water vapor content are also inferred from a number of other datasets covering the years 1980-2000 (Rosenlof et al., 2001), although the time series are short and the sampling uncertainty is high in many cases.

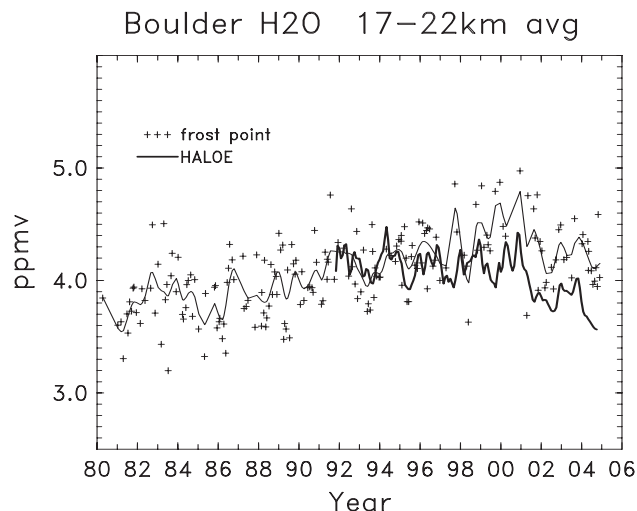


Figure 5-4. Evolution of stratospheric water vapor mixing ratio (in ppmv, averaged over 17-22 km) at Boulder, Colorado (40°N, 105°W), derived from balloonborne frost point hygrometer measurements covering 1980-2005. The thin line shows a smooth fit through the data points, using a running Gaussian window with a half-width of three months. The heavy line shows HALOE satellite water vapor data during 1992-2005 for the same altitude region, using measurements near Boulder (over latitudes 35°N-45°N, and longitudes 80°W-130°W). Note the difference between the two datasets after about 1997. Updated from Randel et al., 2004a.

Recent work has focused on the interannual and long-term evolution of the water vapor distribution using near-global observations from the satellite-based Halogen Occultation Experiment (HALOE). These measurements span more than a decade (late 1991 to 2005). Interannual changes in water vapor derived from HALOE data show excellent agreement with the Polar Ozone and Aerosol Measurement (POAM) satellite data (Randel et al., 2004b) and also with the Stratospheric Aerosol and Gas Experiment II (SAGE II) water vapor data (Thomason et al., 2004; Chiou et al., 2006). An updated comparison of the HALOE measurements with the Boulder balloon data for the period 1992-2005 is shown in Figure 5-4. The Boulder and HALOE data show reasonable agreement for the early part of the record (1992-1996), but the Boulder data are about 5% to 8% higher after 1997. These differences are within the accuracies of both types of observations (reported to be around 10-20% in SPARC, 2000). Year-to-year water vapor changes in each dataset appear to be correlated, and both time series show the persistent decreases after 2001. However, as a result of the differences after 1997, changes

derived from the two datasets over the (short) overlap period 1992-2005 are very different, with net decreases in the HALOE data but not in the Boulder record. These differences seem statistically significant, as Randel et al. (2004b) report a statistical uncertainty of linear fits of the 1992-2002 record of less than $\pm 0.5\%$ /year. The reason for the differences between the balloon and satellite datasets (for the same time period and location) is unclear.

Interannual changes in the HALOE stratospheric water vapor data during 1992-2005 are in quantitative agreement with observed changes in tropical tropopause temperatures for this period (Randel et al., 2004a; Fueglistaler and Haynes, 2005). Tropopause temperature variations associated with the QBO (and to a lesser degree the El Niño-Southern Oscillation, ENSO) are echoed in observed water vapor changes for this period, consistent with the modeling studies of Giorgetta and Bengtsson (1999) and Geller et al. (2002). Furthermore, the persistent decreases in stratospheric water vapor concentrations since 2001 are associated with anomalously low tropopause temperatures (Randel et al., 2004a, 2006; Fueglistaler and Haynes, 2005; see also Figure 5-21). This agreement suggests a reasonable level of understanding for interannual water vapor changes during the HALOE time period (and ability to project future values based on tropical tropopause temperatures). In contrast, the long-term water vapor increases inferred from the Boulder balloon data since 1980 (and from combined datasets beginning in the 1960s; Rosenlof et al., 2001) are difficult to reconcile with observed long-term decreases in tropical tropopause temperatures (e.g., Seidel et al., 2001). Only a fraction of the changes can be attributed to increasing tropospheric methane, as discussed in detail in Fueglistaler and Haynes (2005). Thus, while the HALOE record appears quantitatively well understood, the long-term increases inferred from the Boulder data over 1980-2005 (and combined datasets since the 1960s) are larger than can be explained by observed tropopause temperature changes or past increases in tropospheric methane.

5.2.6 Past Changes in Stratospheric Temperature

Stratospheric temperature changes are closely coupled to ozone changes. Ozone is a key radiatively active constituent in the stratosphere, and it is important to assess the consistency between observed changes in ozone and temperature. Also, the halogen-related ozone destruction rate is generally reduced by lower temperatures in the upper stratosphere, but increased by lower temperatures in the polar lower stratosphere.

Estimates of past temperature changes in the stratosphere have been derived from several different types of data. Most of these datasets were not designed for climate monitoring purposes, and each has strengths and limitations that require careful evaluation and scrutiny. An important advance during the last several years is increased quantification of trend uncertainties, accomplished by comparisons of independent datasets and analyses. Temperature trends can also be derived from meteorological analysis and reanalysis datasets, but evidence suggests these can be influenced by artificial changes related to data inhomogeneity effects (e.g., Santer et al., 2004; Randel et al., 2004a; Birner et al., 2006), and hence may not be reliable in all applications.

Optimal detection and attribution techniques have been widely used to attribute observed changes in surface and tropospheric temperatures to particular external climate influences (Chapter 12 in IPCC, 2001). However, while some detection and attribution studies have identified an anthropogenic influence in variables incorporating stratospheric temperature, such as radiosonde temperature trends in the troposphere and stratosphere (e.g., Tett et al., 2002; Thorne et al., 2002), or tropospheric height (Santer et al., 2003, 2004), none has focused exclusively on stratospheric temperature. One reason may be that the coupled ocean-atmosphere models (AOGCMs; see Box 5-1) required for such studies generally have limited stratospheric resolution, and they underestimate stratospheric variability (Tett et al., 2002). A realistic estimate of internal variability is required in order to distinguish an externally forced response.

A nearly continuous record of stratospheric temperature measurements from satellites is available from the series of operational NOAA satellites beginning in 1979. These are based on the Microwave Sounding Unit (MSU) and Stratospheric Sounding Unit (SSU) instruments, which have flown on ten individual operational satellites over 1979-2005. These data represent mean temperatures for 10- to 15-km thick layers covering the lower to upper stratosphere. The SSU data are available for three fundamental channels (25, 26, and 27), together with several synthetic channels derived by differencing nadir and off-nadir measurements, which provide increased vertical resolution (Nash, 1988). Records of stratospheric temperatures for 1979-2005 are derived by combining data from the individual instruments, adjusted for calibration effects using periods of overlap between adjacent satellites. Effects of orbital drift and decay, and the influence of aliasing atmospheric tides also need to be considered in constructing long-term stratospheric datasets. There are

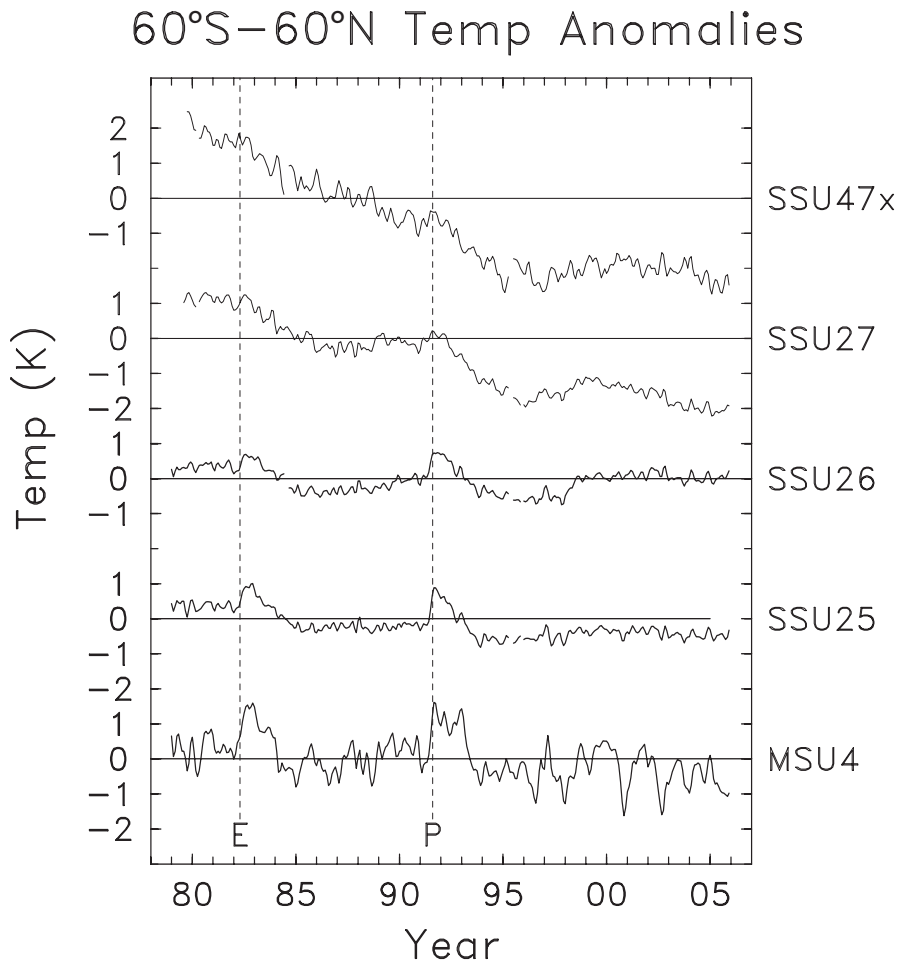


Figure 5-5. Time series of near-global mean (60°N-60°S) temperature anomalies for 1979-2005 derived from satellite radiance measurements. Results are shown for MSU Channel 4 (representing the layer mean temperature over ~13-22 km), and SSU channels 25 (~18-37 km), 26 (~25-44 km), 27 (~34-51 km), and 47x (~44-58 km). Vertical dashed lines mark the occurrence of volcanic eruptions of El Chichón (E) and Mt. Pinatubo (P).

several independent analyses of the MSU Channel 4 data, which covers the lower stratosphere, including results from the University of Alabama at Huntsville (UAH, Christy et al., 2003) and Remote Sensing Systems (RSS, Mears et al., 2003). At present there are two analyses of the combined SSU dataset, with data details discussed in Scaife et al. (2000) and Ramaswamy et al. (2001).

Long-term temperature changes can also be evaluated from historical radiosonde data, for which stratospheric measurements (up to ~25-30 km) are available since approximately 1960. Uncertainties in radiosonde-based temperature trends are associated with spatial sampling (the majority of measurements occur over NH midlatitudes), and more importantly with changes (improvements) in instrumentation over time, which can result in artificial cooling biases (Gaffen, 1994; Luers and Eskridge, 1998). Temperature trends calculated from ensemble radiosonde datasets exhibit strong cooling in the lower stratosphere (Lanzante et al., 2003b; Thompson and Solomon, 2005; Free et al., 2005). However, these

trends are substantially larger than corresponding trends derived from satellite measurements (Seidel et al., 2004) or estimates from current model simulations (Santer et al., 2005), and a recent U.S. Climate Change Science Program Assessment (CCSP, 2006) concludes that the ensemble radiosonde trends are probably influenced by artificial cooling biases.

There is strong evidence for a large and significant cooling in most of the stratosphere since 1980. Figure 5-5 shows near-global average temperature anomalies derived from satellite datasets for 1979-2005, spanning a range of altitudes from the lower to upper stratosphere. The vertical profile of near-global temperature trends during 1979-2005 derived from these satellite data are shown in Figure 5-6, in addition to trends derived from radiosonde data, and a synthesis of model results (taken from Shine et al., 2003). Both the satellite and radiosonde datasets reveal an overall cooling of the stratosphere, with trend values of about 0.5 K/decade in the lower stratosphere, increasing to larger values of about 1 to 2 K/decade in the upper stratosphere. There is reasonable

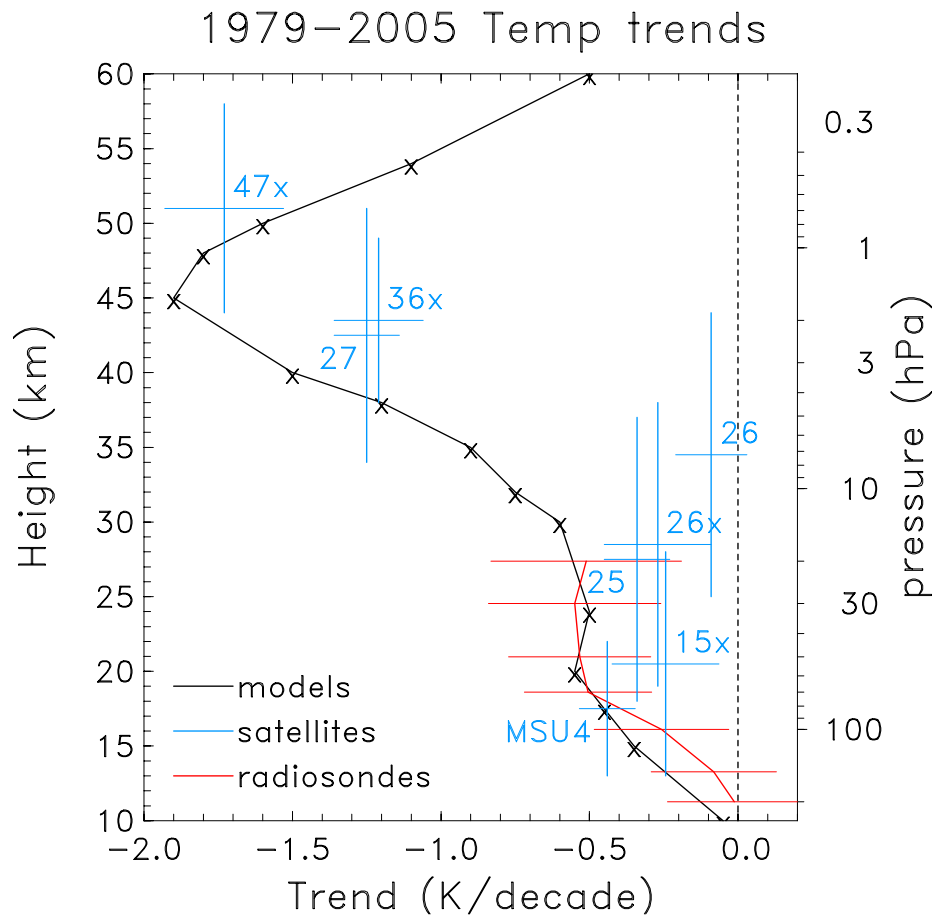


Figure 5-6. Vertical profile of temperature trends derived from satellite and radiosonde data over 60°N-60°S for the period 1979-2005, together with a synthesis of model results taken from Shine et al. (2003). The satellite results are shown for each individual SSU channel (as noted) and MSU Channel 4. For each channel the vertical bar denotes the approximate altitude range sampled by that channel, and the horizontal bar denotes the (two sigma) statistical trend uncertainty. Radiosonde results are shown for individual pressure levels (200-20 hPa), and are derived from a subset of stations described in Lanzante et al. (2003a), updated as described in Randel and Wu (2006). The subset of stations is chosen to omit stations with large artificial cooling biases, in particular stations where MSU4 minus radiosonde trends are greater than 0.3 K/decade (taken from Table 1 of Randel and Wu, 2006). Note that the Shine et al. (2003) results refer to model calculations and observations for the period 1979-1997, whereas the observed trends in the figure are for the longer period 1979-2005.

agreement between the lower stratospheric trends derived from satellite data and radiosondes, although note that the radiosonde results in Figure 5-6 are derived from a subset of one particular homogenized dataset (see Figure 5-6 caption). The radiosonde data suggest there has been significant cooling of the lower stratosphere (70-30 hPa) over most of the globe for 1979-2005, including the tropics.

Temperature trends derived from both the MSU4 (Randel and Wu, 2006) and radiosonde datasets (Thompson and Solomon, 2005; Free et al., 2005; Randel

and Wu, 2006) suggest the cooling of the lower stratosphere spans tropical and extratropical latitudes. However, temperature trends derived from the SSU data (as shown in WMO, 2003) suggest the cooling of the lower stratosphere is restricted to the extratropics. The differences between temperature trends derived from the SSU, MSU4, and radiosonde data are currently under investigation.

The time series in Figure 5-5 show that the observed cooling is not a simple linear trend. A strong imprint of transient warming (for 1-2 years) is observed in the lower

CLIMATE-OZONE CONNECTIONS

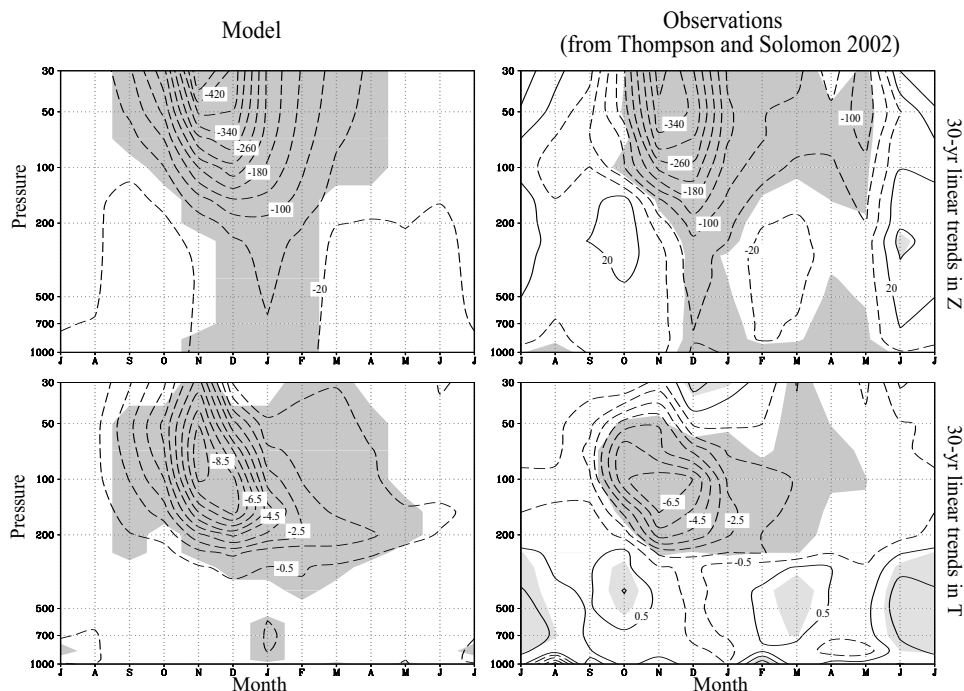


Figure 5-7. Antarctic geopotential height (in m, top) and temperature trends (in K, bottom) by month and pressure level in radiosonde observations over the period 1969-1998 (right) and a simulation of the response to stratospheric ozone depletion (left). Shading indicates regions of significant change based on (left panels) exceedance of one standard deviation of the monthly anomalies and (right panels) a two-sample t-test at the 5% level. From Gillett and Thompson, 2003.

and middle stratosphere following the volcanic eruptions of El Chichón (1982) and Mt. Pinatubo (1991). In the lower stratosphere, the long-term cooling manifests itself as more of a step-like change following the volcanic warming events (Pawson et al., 1998; Seidel and Lanzante, 2004). The overall lower stratospheric cooling is primarily a response to ozone decreases (Shine et al., 2003; Langematz et al., 2003), with a possible but much less certain contribution from changes in stratospheric water vapor. Ramaswamy et al. (2006) suggest that the step-like time series behavior is due to a combination of volcanic, solar cycle, and ozone influences. There is a substantial flattening of these trends evident in Figure 5-5 after approximately 1995; the latter aspect agrees with small global trends in the upper stratosphere and lower mesosphere observed in HALOE data for 1992-2004 (Remsberg et al., 2005). Although some flattening might be expected in response to changes in the ozone trends, the strength of this behavior is curious in light of continued increases in well-mixed greenhouse gases during this decade.

5.2.7 Impact of Ozone Changes on Surface Climate

5.2.7.1 SOUTHERN HEMISPHERE

The largest stratospheric ozone depletion is observed in the austral spring in the Antarctic stratosphere, and therefore it is here that one might expect any effect of stratospheric ozone depletion on tropospheric

climate to be largest. While the largest stratospheric temperature and geopotential height trends over the Antarctic have been observed in November, coincident in space with the maximum ozone depletion, significant decreases in geopotential height also extend to the troposphere 1-2 months later (Thompson and Solomon, 2002) (Figure 5-7).

Several modeling studies have examined the tropospheric response to prescribed changes in stratospheric ozone. Two studies using atmospheric models with prescribed sea surface temperatures demonstrated that a tropospheric response similar to the positive phase of the SAM is simulated in the austral summer in response to prescribed changes in stratospheric ozone (Kindem and Christiansen, 2001; Sexton, 2001). Using a model with high vertical resolution in the stratosphere and a mixed-layer ocean, Gillett and Thompson (2003) simulated a significant tropospheric geopotential height response to prescribed stratospheric ozone changes (Figure 5-7) with no greenhouse gas (GHG) changes. The simulated and observed geopotential height and temperature changes agreed well, both in magnitude and in seasonality, supporting the hypothesis that the observed trends were largely induced by stratospheric ozone depletion.

Transient simulations with coupled ocean-atmosphere models (AOGCMs) also indicate that ozone depletion has played an important role in inducing SAM trends, particularly in the summer (Marshall et al., 2004; Shindell and Schmidt, 2004; Arblaster and Meehl, 2006),

although all three studies found that GHG changes have played at least as large a role in inducing trends in the annual mean SAM.

The observed trend toward the positive phase of the SAM in December to May has been associated with a surface cooling of the Antarctic interior of ~1 K, and a warming of the Antarctic Peninsula, the Scotia Sea, and the southern tip of South America (Thompson and Solomon, 2002) (Figure 5-8). A similar pattern of warming

and cooling has been simulated in response to stratospheric ozone depletion (Gillett and Thompson, 2003) and combined stratospheric ozone depletion and GHG increases (Shindell and Schmidt, 2004; Arblaster and Meehl, 2006) (Figure 5-8). Thompson and Solomon (2002) also identified an associated strengthening of the westerlies over the Southern Ocean, corresponding to a poleward shift of the storm track, which is also simulated in response to stratospheric ozone depletion (Gillett and Thompson, 2003;

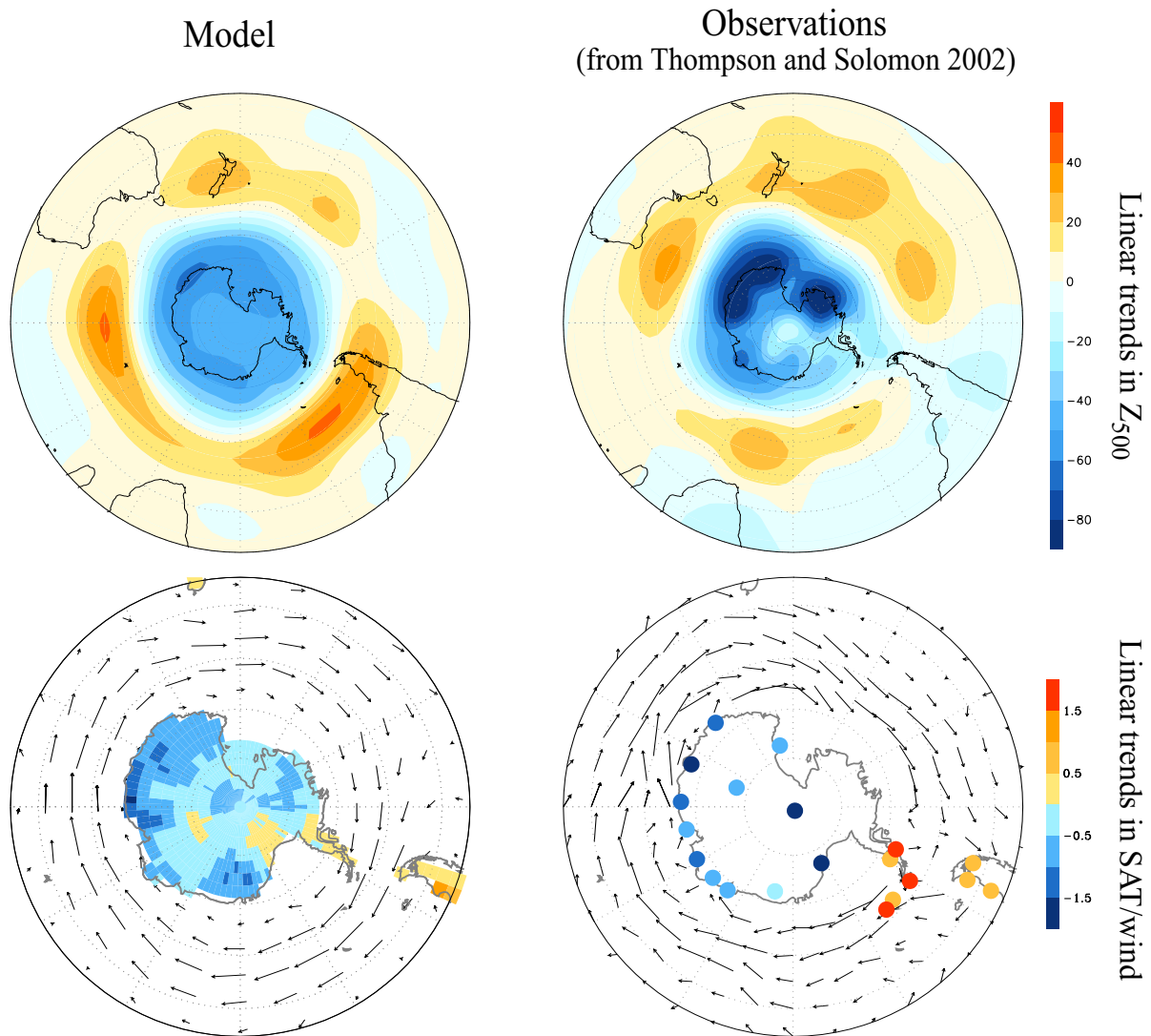


Figure 5-8. Simulated (left column) and observed (right column) changes in (upper row) 500 hPa geopotential height (in m) and (lower row) near-surface temperature (in K) and winds. Observed changes (Thompson and Solomon, 2002) are 22-year linear trends in 500 hPa geopotential height and 925 hPa winds (1979 to 2000), and 32-year linear trends in surface temperature (1969 to 2000) averaged over December to May. Simulated changes are differences between the perturbed and control integrations in 500 hPa geopotential height, 950 hPa winds, and land surface temperature averaged over December to February. The longest wind vector corresponds to ~4 m/s. From Gillett and Thompson, 2003.

CLIMATE-OZONE CONNECTIONS

Shindell and Schmidt, 2004) (see also Figure 5-8). Simulated and observed wind changes of ~1 m/s extend to 30°S (Gillett and Thompson, 2003).

Stratospheric ozone depletion likely influences tropospheric climate through both radiative and dynamical processes. Idealized model simulations indicate that a perturbation to the diabatic heating in the stratosphere gives an annular-mode response in sea level pressure over intraseasonal time scales (Polvani and Kushner, 2002; Kushner and Polvani, 2004; see also Section 5.2.2.6). Recent results suggest that the tropospheric response to stratospheric perturbations may result directly from wave driving and radiative forcing changes in the stratosphere (Thompson et al., 2006; see Section 5.2.2.6), although this direct forcing effect cannot explain the latitudinal structure of the tropospheric response. Antarctic stratospheric ozone depletion acts as a direct radiative cooling influence at the surface. Indeed, an early study of the response to stratospheric ozone depletion with a radiative-convective model found a surface cooling over Antarctica in response to stratospheric ozone depletion (Lal et al., 1987).

Maximum stratospheric ozone depletion close to the tropopause occurs in December to January, more than a month after the maximum ozone depletion at 70 hPa, due to the downward transport of ozone-depleted air (Solomon et al., 2005). Since surface temperature is particularly sensitive to changes in ozone concentration close to the tropopause (Forster and Shine, 1997), this suggests that surface cooling is radiatively induced, and that the apparent lag between stratospheric and tropospheric responses is due to the downward transport of ozone-depleted air toward the tropopause, rather than any dynamical effect.

Most studies suggest that Antarctic ozone depletion is likely to peak sometime in the current decade, and that a recovery is likely to follow over the next 50 years (Chapter 6). Therefore, over the coming decades, increases in stratospheric ozone should drive a decrease in the SAM index toward values seen before ozone depletion. However, increasing GHGs will likely have the opposite effect, contributing an increase in the SAM index (Shindell and Schmidt, 2004; Arblaster and Meehl, 2006). The magnitudes of the future ozone and GHG effects on the SAM are therefore uncertain.

5.2.7.2 NORTHERN HEMISPHERE

Stratospheric ozone depletion has also occurred in the Northern Hemisphere, where it has led to a smaller cooling of the Arctic polar vortex, maximizing in the spring, although model studies indicate that only part of the cooling observed in the Northern Hemisphere stratosphere can be explained by ozone depletion (Section 3.4.3.1 in WMO,

2003). Some studies have suggested that ozone depletion has contributed to the observed trend toward the positive phase of the NAO or NAM (Graf et al., 1998; Volodin and Galin, 1999; Hartmann et al., 2000). Ozone was found to contribute a small trend toward the positive phase of the NAM in model simulations, albeit one rather smaller than that due to GHGs, or indeed that observed (Graf et al., 1998; Shindell et al., 2001). However, while the largest response to stratospheric ozone depletion is simulated in the spring (Graf et al., 1998), the largest trends have been observed in the winter months (Thompson et al., 2000), when no significant trends are simulated in response to ozone depletion (Gillett et al., 2003; Gillett, 2005). Overall, therefore, based on theoretical considerations and some modeling studies, it can be concluded that Arctic ozone depletion has likely contributed to the weak positive trend in the NAM in the spring, but that it cannot explain the observed winter trends.

5.3 EFFECTS OF ANTHROPOGENIC CLIMATE CHANGE AND OF EMISSIONS ON STRATOSPHERIC OZONE

5.3.1 Stratospheric Temperature Changes Due to Shifts in Radiative Forcing

Long-term changes in radiative forcing over the next few decades will continue to impact global mean temperatures in both the troposphere and stratosphere. Over the past three decades, increases in well-mixed greenhouse gas (WMGHG) concentrations and declines in stratospheric ozone have been the primary forcing mechanisms affecting stratospheric climate.

Global concentrations of WMGHGs will continue to rise in the next half century, although significant uncertainties remain as to the exact rate of increase. These changes will act, on average, to cool the stratosphere (see Section 5.2.1), but there can still be a seasonal warming, particularly at high latitudes, due to changes in planetary wave activity. Therefore, the assessment of the future evolution of polar temperatures is uncertain. Future changes in stratospheric water vapor are also difficult to predict, in part because the changes observed over the last four decades are still not fully understood (e.g., Randel et al., 2004b, 2006; see also Section 5.2.5). While declines in stratospheric ozone also act to cool the stratosphere, within this decade global ozone levels will likely begin to rise (Chapter 6). Higher ozone levels will increase stratospheric ozone heating, which will at least partially offset the cooling due to increases in WMGHG concentrations. Because ozone concentrations are so sensitive to the background temperature field, understanding the complex

interaction between changing constituent concentrations and temperature requires an evaluation of the coupling between chemistry, radiation, and atmospheric dynamics.

The primary method used for quantifying the interaction between changing chemistry and dynamics is the Chemistry-Climate Model (CCM). With advances in CCMs, the nonlinear coupled evolution of chemistry and dynamics can be studied. One of the continuing challenges for climate models (AOGCMs, coupled ocean-atmosphere general circulation models) is predicting future changes in tropospheric and stratospheric wave dynamics, which in turn affect the structure and evolution of lower and upper atmospheric temperature (see Section 5.2.2). Improvements in CCMs (Eyring et al., 2006; see also Section 6.6) are providing valuable insight into how temperatures will evolve in the future.

Model simulations for doubled CO₂ conditions with and without interactive ozone chemistry show a substantial temperature decrease throughout most of the middle atmosphere, with a maximum cooling of 10-12 K near the stratopause (Jonsson et al., 2004; Sigmond et al., 2004; Fomichev et al., 2006; see Figure 5-13a). In these calculations, stratospheric ozone increases are associated with lower temperatures, which partially modulate the CO₂-induced cooling through enhanced ozone heating. While simulations using CCMs demonstrate how the inclusion of interactive chemistry alters model meteorology (Austin and Butchart, 2003; Manzini et al., 2003; Tian and Chipperfield, 2005), more fundamental dynamical processes such as the parameterization of gravity waves and propagation characteristics of planetary waves remain significant modeling challenges (see also Section 5.2.2.4).

AOGCMs (i.e., AGCM coupled with an ocean model) whose output will be used in the Intergovernmental Panel on Climate Change (IPCC) Fourth Assessment Report (AR4; IPCC, in preparation for 2007) represent the most advanced and comprehensive set of climate simulations so far produced. To better represent the many physical processes responsible for climate variability and change, enhanced horizontal and vertical resolution has been used in these models compared with earlier IPCC Assessments. While the AOGCMs used for the IPCC were not specifically designed for stratospheric simulations, it is becoming increasingly apparent that accurate simulations of the stratosphere are important in determining the evolution of the surface climate, as well as other aspects of climate change. It is for this reason that the assumptions that have been chosen in the IPCC AOGCM simulations for the 21st century (i.e., future greenhouse gas (GHG) concentrations are only specified by different scenarios from the Special Report on Emissions Scenarios (IPCC, 2000) that differ primarily in

the emissions of WMGHGs) constitute a restriction for an assessment of climate change within the next few decades. In the high (A2) scenario, concentrations of CO₂ increase from today's value (~380 ppmv) to approximately 850 ppmv by 2100, while the low (B1) scenario reaches 550 ppmv by 2100 (IPCC, 2001). In these AOGCM simulations, ozone concentrations are prescribed and not interactively computed during the 21st century, which is an obvious restriction and has an impact on the assessment of the future development of lower stratospheric temperature (see below).

Figure 5-9 shows a time series of global-mean temperature anomalies between 2000 and 2100 at 50 hPa from fifteen AOGCMs adopting the A2 emission scenario used for the IPCC AR4. See Appendix 5A for information concerning the specific AOGCMs. While all simulations show 50 hPa global temperatures declining over the 21st century, the range of predictions for temperature change varies from -0.5 to -3.5 K by 2100. Differences in model ozone concentrations over the 21st century are likely responsible for some of the range in model predictions, while variations in model dynamics, the limited vertical extent of many of the AOGCMs, and differences in radiation schemes are also likely contributors.

The relative uncertainty in model predictions of future stratospheric temperature is further illustrated in Figure 5-10, which shows the globally averaged temperature trend computed during the 21st century using the models submitted to the IPCC AR4 for low (B1) and high (A2) emission scenarios. In the troposphere, temperatures rise during the next century, ranging between 0.2 K/decade (low) to 0.5 K/decade (high) for the different emission scenarios. In the stratosphere, the rate of cooling is also strongly dependent on the emission scenario, ranging from 0.07 ± 0.20 K/decade (low) to 0.18 ± 0.20 K/decade (high) at 50 hPa and 0.38 ± 0.09 K/decade (low) to 0.72 ± 0.47 K/decade (high) at 10 hPa. However, it should be reemphasized that in the present set of IPCC AOGCM simulations, the ozone forcing in the 21st century varies from constant ozone to a slow recovery by 2050, and thus contributes to the large model-to-model variability (Hare et al., 2004).

A similar analysis of global-mean temperature trends from CCMs (Eyring et al., 2006) that consider interactive ozone feedback (see Box 5-1) generally shows less model-to-model variability compared with the AOGCM results submitted to the IPCC AR4. See Chapter 6, Table 6-4 for information concerning the specific CCMs. Figure 5-11 (bottom panel) shows that global temperature trends at 50 hPa from CCMs are in reasonable agreement with ERA-40 (European Centre for Medium-Range Weather Forecasts (ECMWF) 40-year Reanalysis) and radiosonde data (Radiosonde

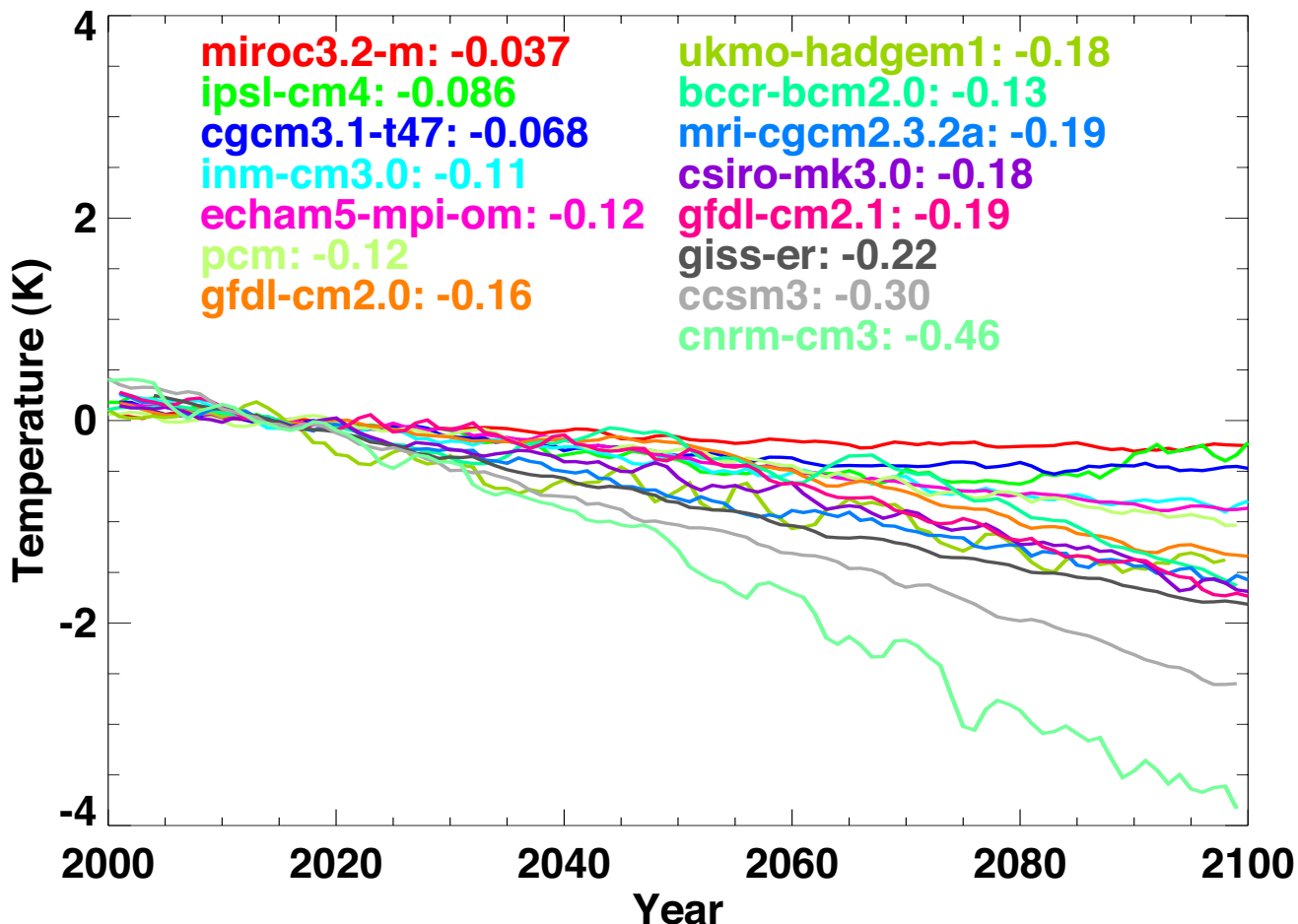


Figure 5-9. Evolution of global-mean temperature anomaly at 50 hPa between 2000 and 2100 as estimated from AOGCMs for the A2 emission scenario. The temperature trend in K/decade is given next to the name of each participating model. Anomalies are computed with respect to temperatures between 2010 and 2020. For clarity, models are labeled in order from weakest to strongest temperature variation. Information about the AOGCMs is given in Appendix 5A.

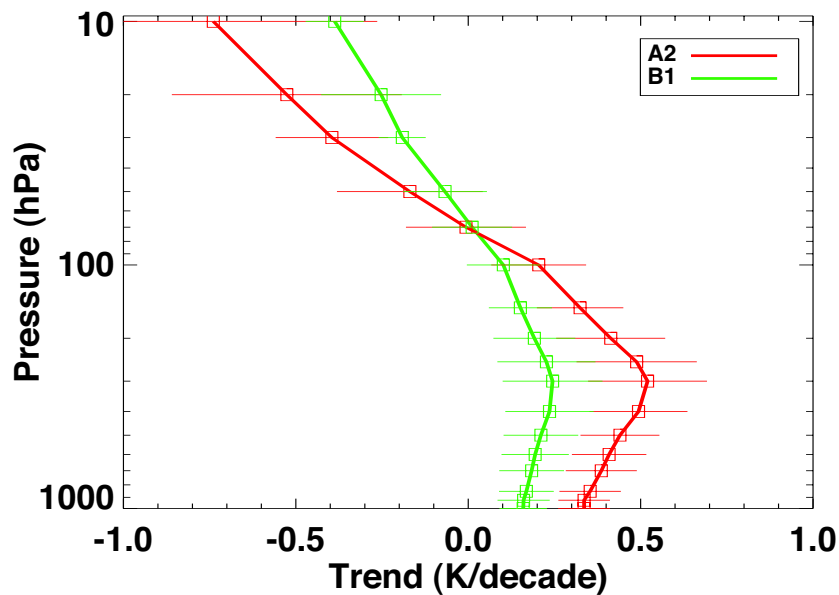


Figure 5-10. Global and annual mean 21st century temperature trends from AOGCMs using A2 (high) and B1 (low) emission scenarios. The boxes indicate the average trend computed for all models, while the thin horizontal lines indicate the range of model-calculated trends. Information about the AOGCMs is given in Appendix 5A.

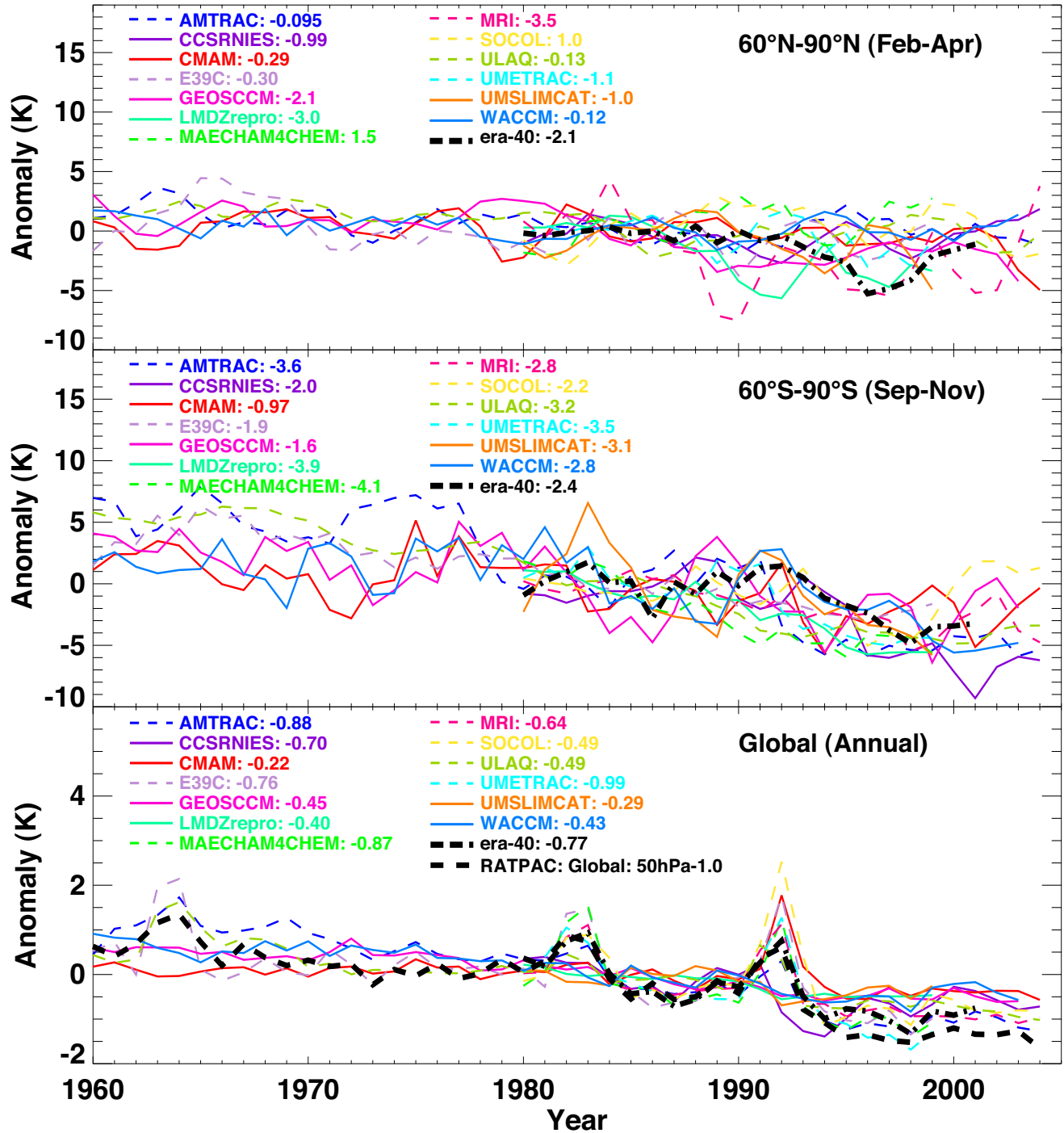


Figure 5-11. Time series of temperature anomalies for Arctic spring (top), Antarctic spring (middle), and the annual global mean (bottom) at 50 hPa derived from the REF1 (20th century climate) CCM simulations and from observations (i.e., ECMWF 40-year reanalysis, ERA-40, and Radiosonde Atmospheric Temperature Products for Assessing Climate, RATPAC). The temperature anomalies are calculated with respect to a mean reference period between 1980 and 1989. A linear temperature trend in K/decade is calculated for each model using data between 1980 and 1999. AMTRAC, MAECHAM4CHEM, MRI, UMETRAC, SOCOL, ULAQ, and E39C are shown with dashed lines, all other CCMs with solid lines. The temperature trend is given next to the name of each participating model (from Eyring et al., 2006). See Table 6-4 and Appendix 6A of Chapter 6 for information about the CCMs and the model runs.

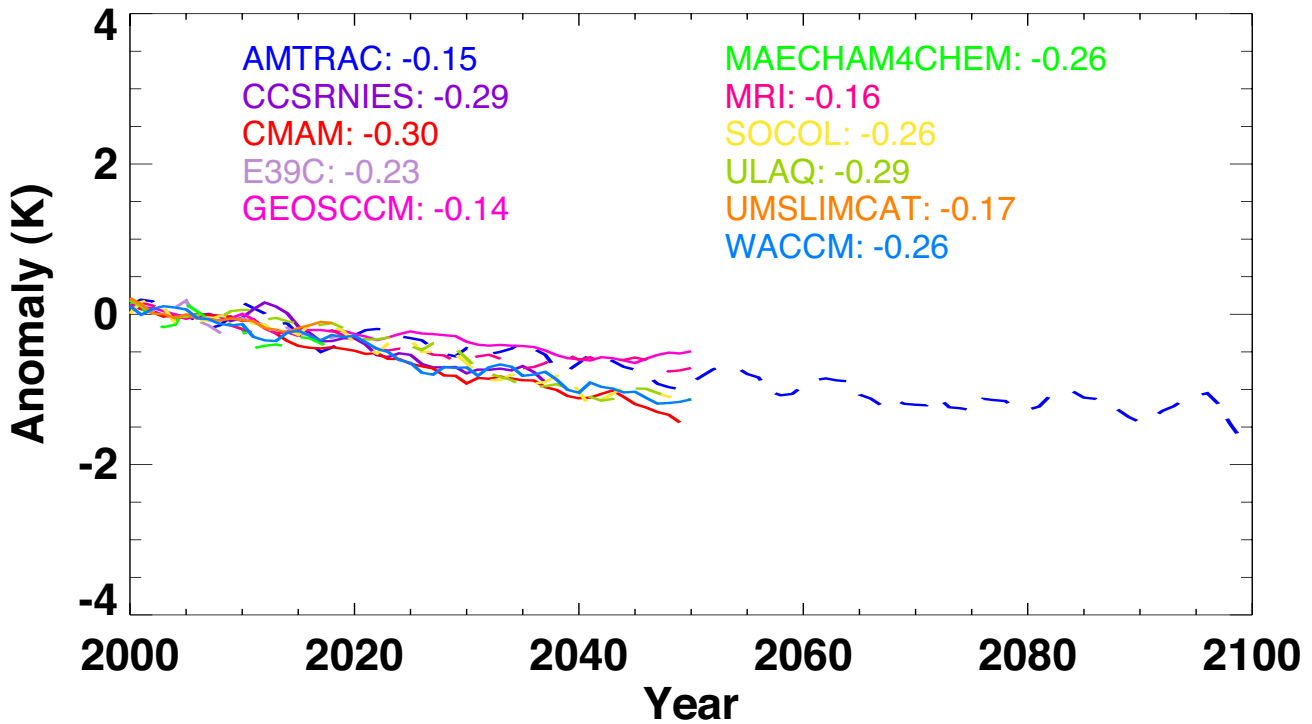


Figure 5-12. Time series of global-mean annual temperature anomalies at 50 hPa from the REF2 (21st century climate, A1B scenario; IPCC, 2001) CCM simulations (see Chapter 6, Appendix 6A). The temperature anomalies are calculated with respect to a mean reference period between 2000 and 2010. AMTRAC, E39C, MAECHAM4CHEM, MRI, SOCOL, and ULAQ are shown with dashed lines, all others CCMs with solid lines. A linear temperature trend in K/decade is calculated for each model using data after 2000 and is shown next to the name of each participating model. See Chapter 6, Table 6-4 and Appendix 6A for information about the CCMs and the model runs.

Atmospheric Temperature Products for Assessing Climate, RATPAC; Free et al., 2005) and display an obvious cooling from 1980 to present day. The model temperature trends range from -0.22 K/decade to -0.99 K/decade (average = -0.64 K/decade), with 7 out of 13 CCMs showing statistically significant trends, compared

with the ERA-40 (-0.77 K/decade; not significant) and RATPAC (-1.0 K/decade; significant) data. Corresponding AOGCM results show model temperature trends ranging from -0.03 to -0.97 (average = -0.38 K/decade). Perturbations by volcanic eruptions are well captured in many of the CCMs, but generally the temperature response is over-predicted (see Section 5.2.4; Figure 5-3). A similar over-prediction of the warming effect at 50 hPa from volcanic aerosols was also found with the AOGCMs. The evolution of lower stratospheric (50 hPa) springtime temperatures in the polar regions (Figure 5-11, top and middle panel) indicates a much greater inter-annual variability, which is caused by the specific impact of wave dynamics (Section 5.2.2.1; see also Chapter 4, Section 4.1.1.1). This is another reason for larger uncertainties in the assessment of the future evolution of stratospheric springtime temperatures in these geographical regions.

Table 5-1. Mean linear temperature trend in K/decade calculated from different types of models and for different emission scenarios using model data after year 2000. See text for detailed description.

Pressure Level	Emission Scenario (Model Employed)		
	B1 (AOGCM)	A1B (CCM)	A2 (AOGCM)
50 hPa	-0.07 ± 0.20	-0.23 ± 0.09	-0.18 ± 0.20
10 hPa	-0.38 ± 0.09	-0.63 ± 0.23	-0.72 ± 0.47

Figure 5-12 shows that there is good agreement between the CCM results showing a global cooling trend at 50 hPa through the first half of the 21st century. The

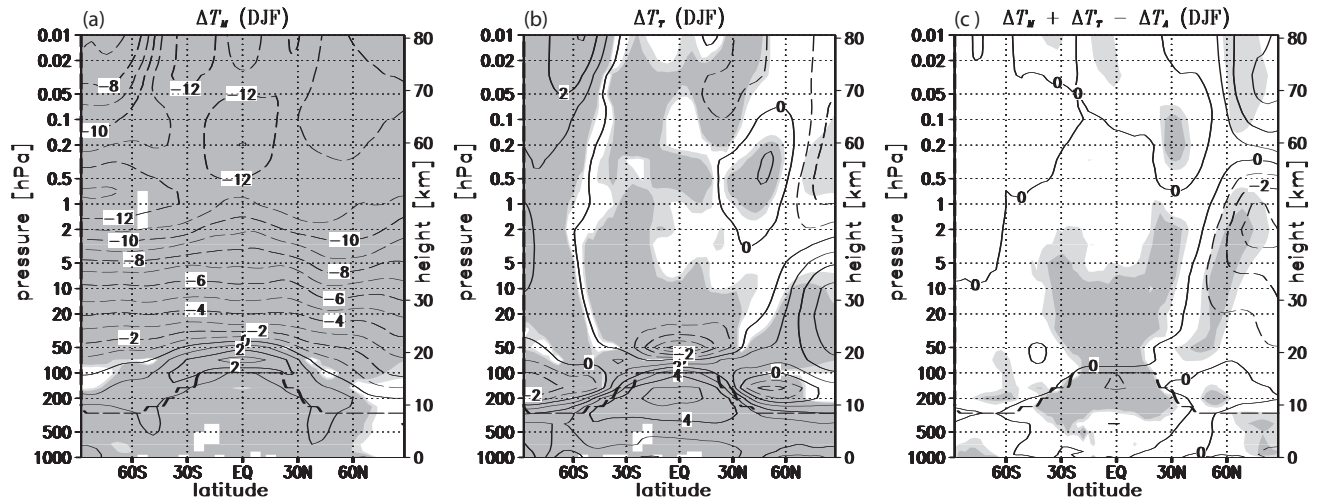


Figure 5-13. Changes in the middle atmosphere resulting from different doubling CO_2 model runs for the months of December-January-February: (a) The change in the zonally averaged temperature due to a doubling of CO_2 in the middle atmosphere, ΔT_M ; (b) the change due to a doubling of CO_2 in the troposphere, ΔT_T ; and (c) the degree of non-additivity, i.e., the sum of the temperature changes due to a doubling of CO_2 separately in middle atmosphere and troposphere, minus the temperature change resulting from a doubling of CO_2 in all the atmosphere ($\Delta T_M + \Delta T_T - \Delta T_A$). Light (dark) shading denotes significance at 95% (99%) level of the changes in (a) and (b) and of the non-additivity in (c). The contour interval is 1 K. The thick dashed line denotes the position of the tropopause. From Sigmond et al., 2004.

CCMs adopted a medium (A1B) emission scenario used for the IPCC AR4, which reaches 720 ppmv by 2100. Considering the CCM results up to the year 2050, the cooling trend ranges from 0.14 to 0.30 K/decade. In the lower stratosphere, the temperature trends derived from the CCM simulations using the medium (A1B) emission scenario are larger compared with the AOGCM results which are related to the high (A2) emission scenario (cp. Table 5-1). At 10 hPa, where ozone changes are expected to be weak, AOGCM and CCM simulations are in line, i.e., the calculated trends derived from the AOGCM A2 simulations are stronger than those derived from the CCM A1B simulations (see Table 5-1). The fact that the different CCM results are more tightly constrained may be due to the smaller range in the prescribed forcing (see Chapter 6, Appendix 6A). Both results from AOGCMs and CCMs point to the changing nature of the stratosphere and troposphere and the important role that emission of WMGHGs has in the prediction of future temperature in the stratosphere.

5.3.2 Stratospheric Temperature Changes Due to Additional Effects

Future changes in radiative forcing will have both a direct in-situ effect on stratospheric temperatures (Section 5.3.1) and an indirect effect resulting from changes in the

wave forcing from the troposphere. For the stratosphere, to a first approximation, the effects of in-situ radiative changes and those of changes in wave forcing from the troposphere are additive and therefore can be assessed separately (Sigmond et al., 2004; Fomichev et al., 2006). Figure 5-13 illustrates the response of the middle atmosphere (10-80 km) to a doubling of CO_2 in the troposphere and middle atmosphere separately, as well as together (Sigmond et al., 2004). Anthropogenic climate change is likely to have an impact on sea surface temperatures (SSTs), land-sea temperature differences, tropospheric jets, and synoptic scale activity, which in turn are likely to have an impact on the planetary wave forcing originating in the troposphere, as well as their regional effects in the lower stratosphere. Climate change can also affect the propagation of planetary waves into the stratosphere (Rind et al., 2005a; 2005b; Scott and Polvani, 2004; Scott et al., 2004). Changes in planetary wave forcing and propagation in the polar winter are a major source of uncertainty for predicting future levels of Arctic ozone loss (Austin et al., 2003). CCM (see Box 5-1) results used for WMO (2003) did not agree on the sign of the trend in the planetary wave flux from the troposphere. Recently, Fomichev et al. (2006) found that the response in the polar winter stratosphere to a doubling of CO_2 in the first 15 years of a 30-year simulation differed from the response in the last 15 years, which also supports earlier findings (e.g.,

CLIMATE-OZONE CONNECTIONS

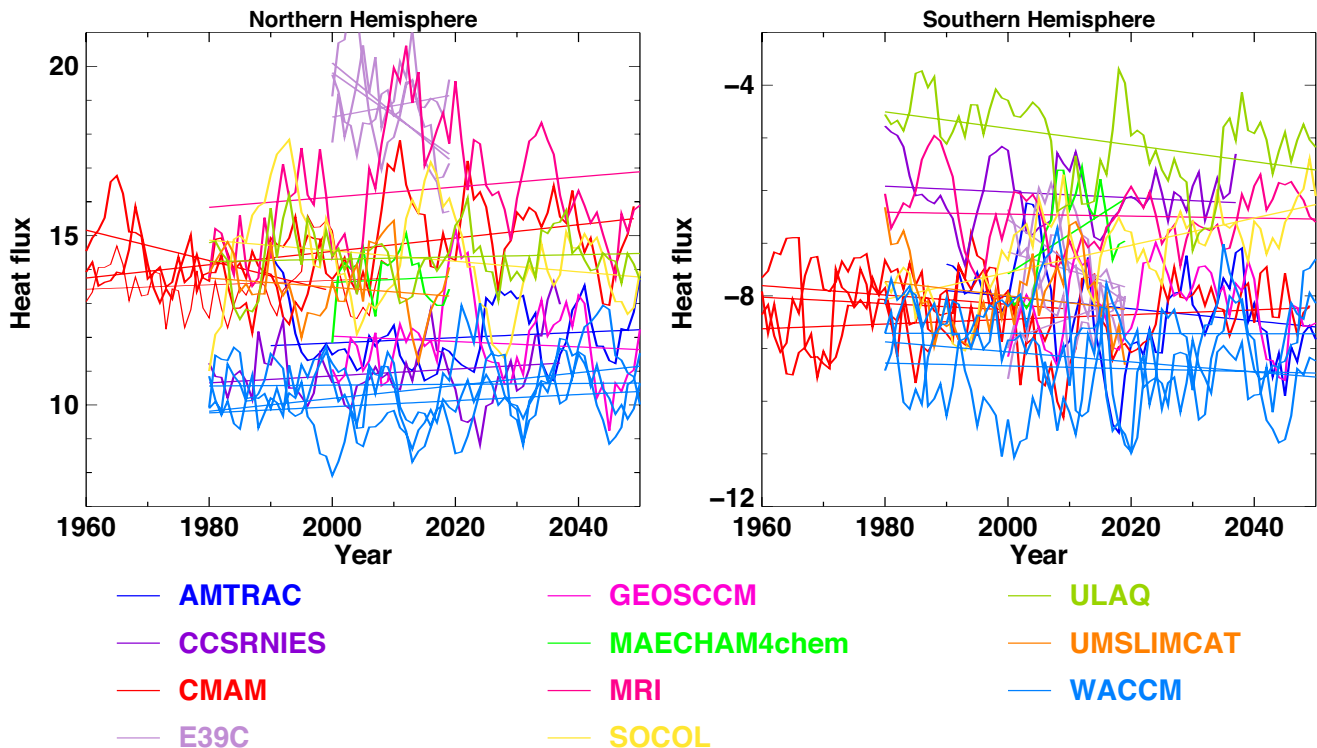


Figure 5-14. Evolution of the heat flux (K m/s) at 100 hPa as derived from CCM calculations. The analysis is based on model data derived from the REF2 and SCN2 simulations (see Chapter 6, Appendix 6A). Left panel: Heat flux averaged over 40°N to 80°N in January and February. Right panel: Heat flux averaged over 40°S to 80°S in July and August. Results are shown for each year of the simulations but have been smoothed with a 5-year running mean. The straight lines represent the least squares linear fit for the individual model runs. The heat flux at 100 hPa provides a measure of the wave flux propagating from the troposphere to the stratosphere. A negative heat flux in the SH corresponds to an upward planetary wave flux.

Butchart et al., 2000) that on a decadal time scale, the dynamics of the polar winter stratosphere are unpredictable due to internal variability.

Since WMO (2003), a number of transient CCM simulations have been run into the 21st century using the same climate forcing and halogen loadings (see Chapter 6, Table 6-4 and Appendix 6A). Eyring et al. (2006) assessed the CCMs used for these simulations and found that temperature biases in the northern winter in the polar lower stratosphere were quite small, and most of the models exhibited the correct temperature sensitivity to variations in the wave forcing from the troposphere. These are both notable improvements relative to the CCMs used by Austin et al. (2003). In contrast, there was little improvement in the Southern Hemisphere, with most of the CCMs still predicting Antarctic cold biases in spring, and the polar vortex breaking down much later than observed. Again, these latest CCM simulations do not provide any consensus as to what will happen to the planetary wave forcing from the troposphere in a future cli-

mate (see Figure 5-14), despite each model using the same amounts of greenhouse gases and halogens.

The reasons why the models continue to fail to provide a consensus are unclear. In part it could be due to model deficiencies, especially in the SH where many of the models are unable to reproduce the correct polar temperature sensitivity to the wave forcing from the troposphere. On the other hand, as argued in WMO (2003, Chapter 3), it could reflect true atmospheric behavior: in a truly chaotic system, planetary wave forcing from the troposphere may not be inherently predictable, and so models are giving a range of results reflecting that unpredictability. Clarification is strongly required because the assessment of the evolution of the ozone layer depends on the ability of CCMs to predict wave changes.

The most important SST factor affecting the troposphere and the stratosphere is tropical SST gradients, as found during El Niño-Southern Oscillation (ENSO) events. Anomalous tropical SST gradients are also known to have an impact on planetary wave forcing. The strato-

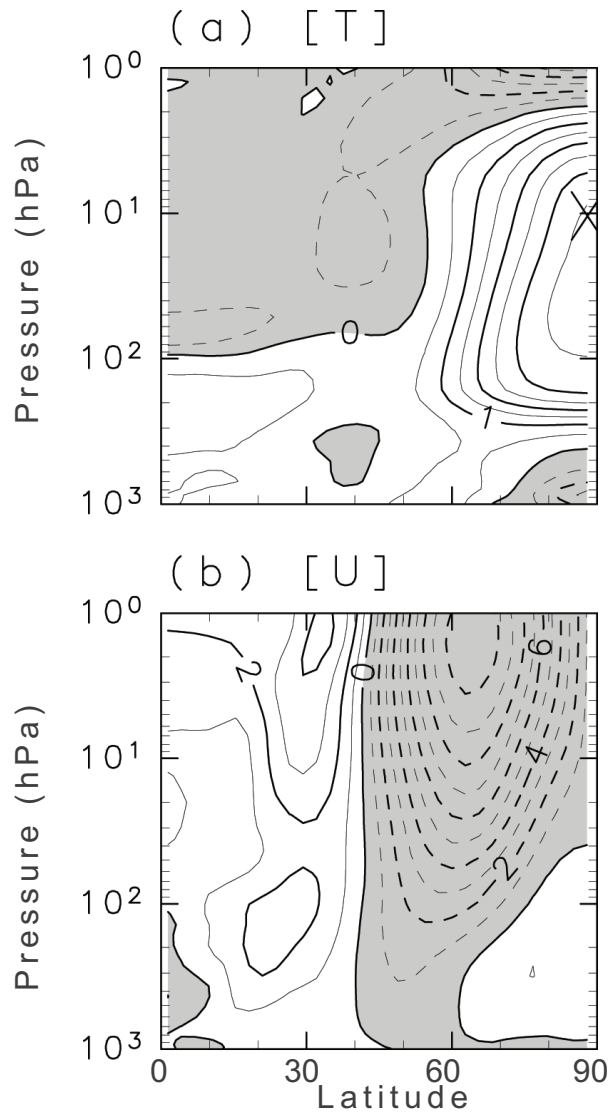


Figure 5-15. Climatological differences between WACCM (Whole Atmosphere Community Climate Model) simulations forced with high and low SSTs in the eastern tropical Pacific: (a) zonal mean temperature [T] in K and (b) zonal mean zonal wind [U] in m/s. Both panels display results for the Northern Hemisphere, with the equator on the left and the North Pole on the right. From Taguchi and Hartmann, 2006.

spheric polar vortex tends to be weaker than average during warm ENSO years, when SSTs are anomalously warm in the eastern tropical Pacific (van Loon and Labitzke, 1987), while cold ENSO years are associated with suppressed incidences of stratospheric sudden warmings (Limpasuvan et al., 2005). Similar relationships have been noted in several numerical simulations (Hamilton, 1993; Sassi et al., 2004; Manzini et al., 2006). Moreover,

there are indications of increased incidences of sudden stratospheric warmings in CCM simulations run with high SST anomalies in the eastern tropical Pacific (Taguchi and Hartmann, 2006; see Figure 5-15). Hoerling et al. (2001; 2004) and Hurrell et al. (2004) argued that changes in Indian Ocean SSTs have a demonstrable impact on the Northern Hemisphere Annular Mode/North Atlantic Oscillation (NAO/NAM) on decadal time scales, but the extent to which these changes extend to stratospheric levels remains unclear.

Outside the polar regions in winter, changes in the tropospheric forcing are also expected to have an impact on lower stratospheric temperatures throughout the year. There are indications from model assessments that anthropogenic climate change will increase the upwelling across the tropical tropopause and downwelling in the extratropics (see Sections 5.3.3 and 5.3.7). The associated adiabatic heating will then lead to a cooling of the tropical lower stratosphere and warmer extratropics in all months (Figure 5-16), but it is more pronounced during the boreal winter and spring, which is consistent with the asymmetry in the SST change between the NH and SH in the adopted model (Fomichev et al., 2006). Other climate change simulations (Butchart et al., 2006) also indicate that, on average, the increase in planetary wave driving is greater during the northern winter than during the southern winter.

All CCMs and AOGCMs used to predict stratospheric temperature changes (see Section 5.3.1) parameterize the effects of small-scale gravity waves. The more sophisticated of these schemes parameterize the vertical propagation and breaking of the waves in terms of the large-scale flow, and therefore are able to respond to climate perturbations in the stratosphere resulting from radiative or planetary wave forcing. Moreover, research by Shaw and Shepherd (2007) suggests that, provided the parameterizations are implemented to conserve momentum, the climate response will be robust to differences in the gravity wave source spectrum, background flow, gravity wave-breaking criterion, and model upper boundary. McLandress and Scinocca (2005) also showed that the response is not very dependent on the choice of gravity wave drag parameterization, at least among those schemes that have been developed to represent the propagation and breaking. It is not clear what proportion of the change in gravity wave forcing will result from the indirect effect of climate change modifying the propagation and breaking of the waves, and how much will result directly from a change in the source. The greatest uncertainty is in knowing how the source spectrum will evolve in a changing climate. Unfortunately, the spectrum is rather poorly constrained by observations for the present climate, and it will be difficult to quantify the effects of

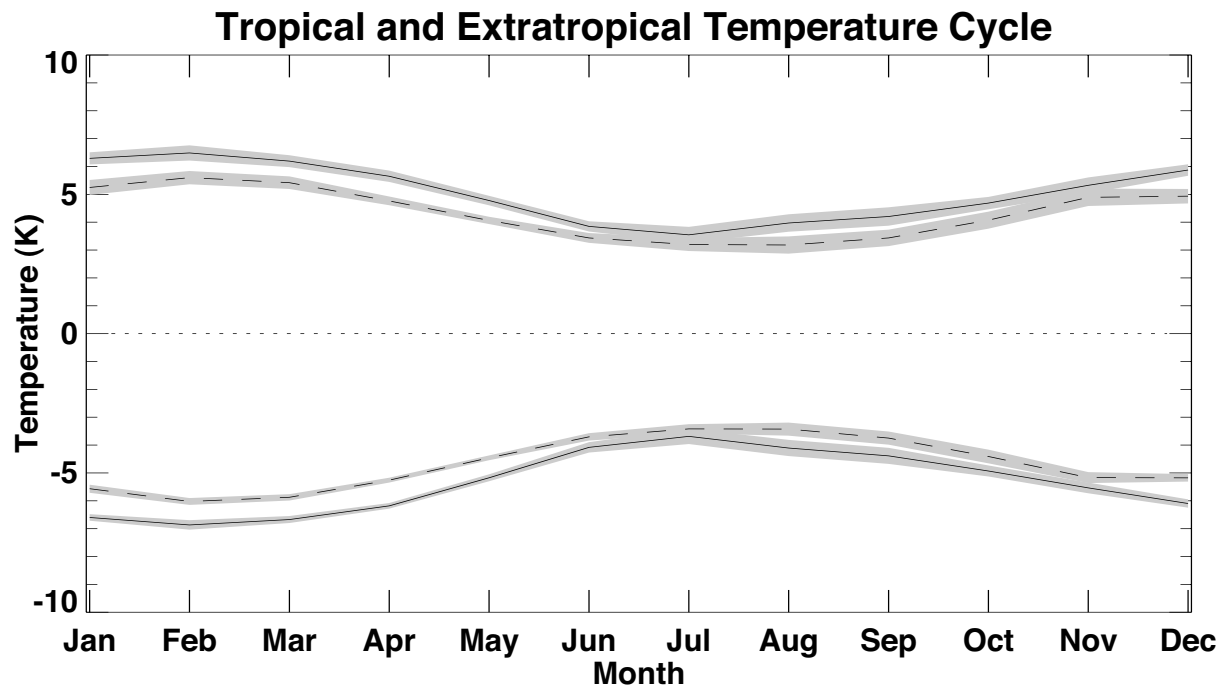


Figure 5-16. Annual cycle of the tropical (30°S - 30°N ; negative curves) and extratropical (positive curves) mean temperature, with global mean subtracted, at 50 hPa. The dashed curve results from a model simulation in which the atmospheric CO_2 was doubled, but the SSTs were not adjusted for the doubled CO_2 conditions. The solid curve is from a simulation with both the CO_2 doubling and adjusted SSTs, and therefore includes an additional effect on the temperatures due to changes in wave forcing from the troposphere. From Fomichev et al., 2006.

changes in gravity wave forcing on the stratospheric temperatures without further progress toward specifying sources in terms of other flow parameters to allow for climate feedbacks.

5.3.3 Troposphere-Stratosphere Exchange and the Brewer-Dobson Circulation

The net mass exchange between the troposphere and stratosphere is associated with the large-scale Brewer-Dobson circulation (Holton et al., 1995; Shepherd, 2002), with a net upward flux in the tropics balanced by a net downward flux in the extratropics. However, near the tropopause itself, the picture is more complex, with two-way mixing across the extratropical tropopause at and below synoptic scales, and vertical mixing in the tropical-tropopause layer (TTL) resulting from convective processes (see Section 5.3.4). Nonetheless, above the lowermost extratropical stratosphere and at the top of the TTL, the exchange is more one-way with, in particular, air slowly rising into the stratosphere above the TTL. Model studies indicate that climate change will impact the mass exchange across the tropopause. Rind et al.

(2001) estimated a 30% increase in the mass flux due to a doubling of atmospheric CO_2 amounts, and Butchart and Scaife (2001) estimated that the net upward mass flux above the TTL would increase by about 3% per decade due to climate change. In both of these studies, the changes in the mass flux resulted from more vigorous wave propagation from the troposphere into the stratosphere. Modeling studies of tropospheric ozone (Collins et al., 2003; Zeng and Pyle, 2003; Sudo et al., 2003) also found that climate change caused a comparable percentage increase in the extratropical stratosphere-to-troposphere ozone flux.

For a doubled CO_2 concentration, all 14 climate-change model simulations in Butchart et al. (2006) resulted in an increase in the annual mean troposphere-to-stratosphere mass exchange rate (Figure 5-17), with a mean trend of $11 \text{ Gg s}^{-1} \text{ year}^{-1}$, or about 2% per decade. The predicted increase occurred throughout the year but was, on average, larger during the boreal winter than during the austral winter. The Butchart et al. study was unable to conclude whether stratospheric ozone changes or ozone feedbacks had a significant impact on the underlying trend in the mass exchange rate. Other simulations

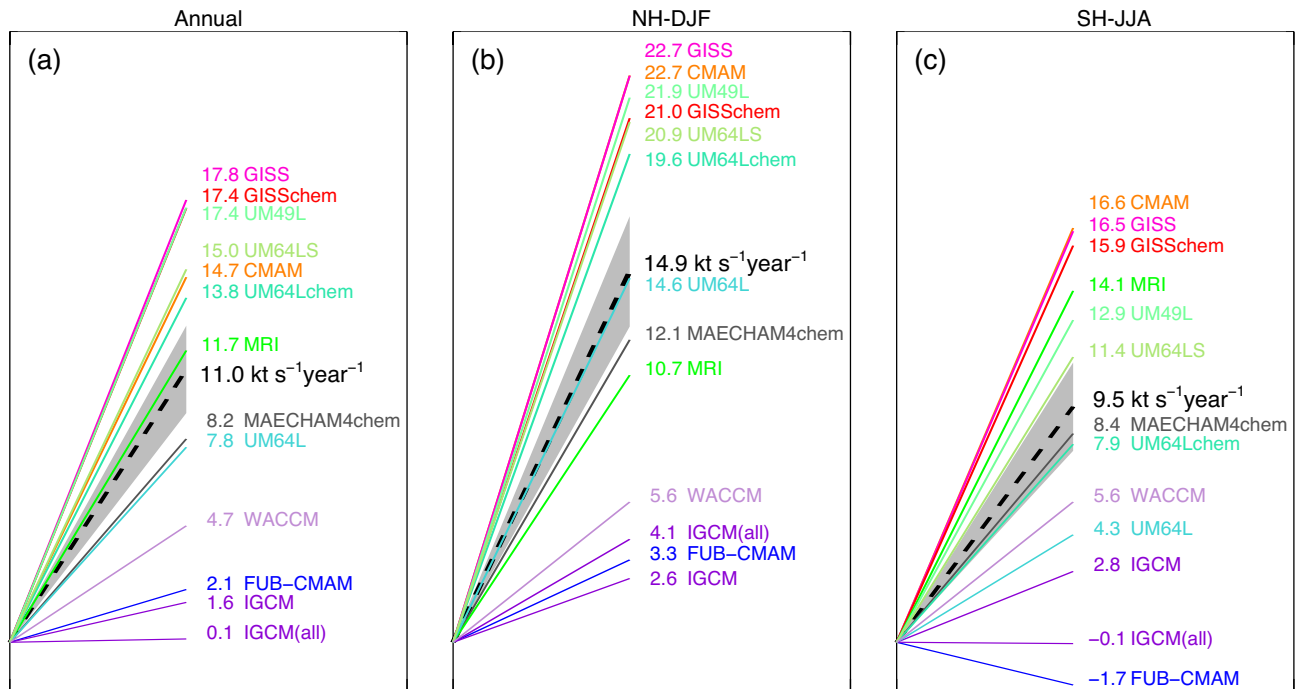


Figure 5-17. Schematic representation of the trends in troposphere-to-stratosphere mass exchange rate computed in a set of 14 CCMs and climate models that consider the complete stratosphere (from Butchart et al., 2006). The trends ($\text{Gg s}^{-1} \text{ year}^{-1}$) are given by the slope of the lines. For the transient simulations, trends were calculated from a least squares fit to the mass flux data. For the time-slice simulations (see Box 5-1) the difference in flux was converted to a mean mass flux trend, assuming a doubling time of 70 years for CO_2 . The dashed line is the multi-model mean; the standard error is given by the gray shading.

(e.g., Austin et al., 2006) suggest that the trend in tropical upwelling is not constant. Periods of enhanced upwelling coincide with periods of significant ozone depletion.

The calculation of tropical upwelling (or of mean age of air¹; see below) from measurements or assimilated datasets is challenging, and it is not possible to calculate reliable trends. Calculations of age of air using a transport model and meteorological fields (Schoeberl et al., 2003; Meijer et al., 2004; Scheele et al., 2005) gave values that were lower than those determined using observations of long-lived tracers (e.g., Boering et al., 1996; Andrews et al., 2001; Schoeberl et al., 2005). Similar results have been obtained recently from a suite of CCMs (Eyring et al., 2006; see Chapter 6).

Tropical upwelling is inversely related to model age of air (Austin and Li, 2006), so that the age of air changes as the stratospheric climate changes. As noted for the tropical upwelling, the age of air does not change steadily

(Figures 5-18 and 5-19). In both CCMs AMTRAC (e.g., Austin et al., 2006) and WACCM (e.g., Beres et al., 2005), age of air decreased significantly from about 1975 to 2000, consistent with an increase in tropical upwelling, which in AMTRAC was identified as due in part to ozone depletion (Austin et al., 2006). As shown in Figure 5-19, WACCM also indicates that age of air remains constant for conditions of fixed GHG concentrations and sea surface temperatures (SSTs) (see also Section 5.3.7), indicating that changes in GHG concentrations and SSTs are major influences for age of air changes in the future. The overall decrease of age of air and increase in tropical upwelling on climate time scales implies a more rapid removal of the long-lived CFCs from the entire atmosphere (Butchart and Scaife, 2001), as well as source species such as CH_4 and N_2O . Once enhanced CH_4 concentrations reached the stratosphere, enhanced CH_4 oxidation would occur, leading to a faster increase in water

¹ Age of air: The length of time that a stratospheric air mass has been out of contact with the well-mixed troposphere. The content of a unit element of air at a particular location and particular time of year in the stratosphere can be thought of as a mixture of different air parcels that have taken different routes from the tropopause to arrive at that location. The mean age of air at a specific location is defined as the average transit times of the elements since their last contact with the tropopause.

Age of Air 20°N-20°S, 1.3 hPa

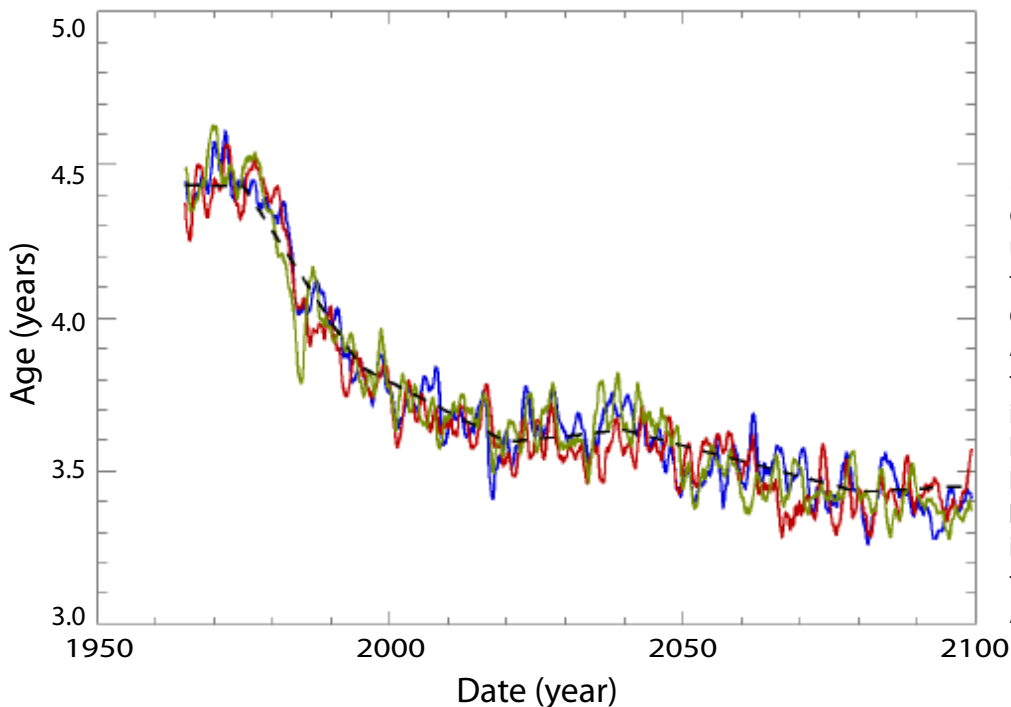


Figure 5-18. Mean age of air in the tropical upper stratosphere for the period 1960-2100 computed from the CCM AMTRAC. The three different colored curves indicate individual simulations. A piecewise linear curve (black broken line) is included to illustrate changes in trends. Modified from Austin and Li, 2006.

Age of Air 22°N-22°S, 1.24 hPa

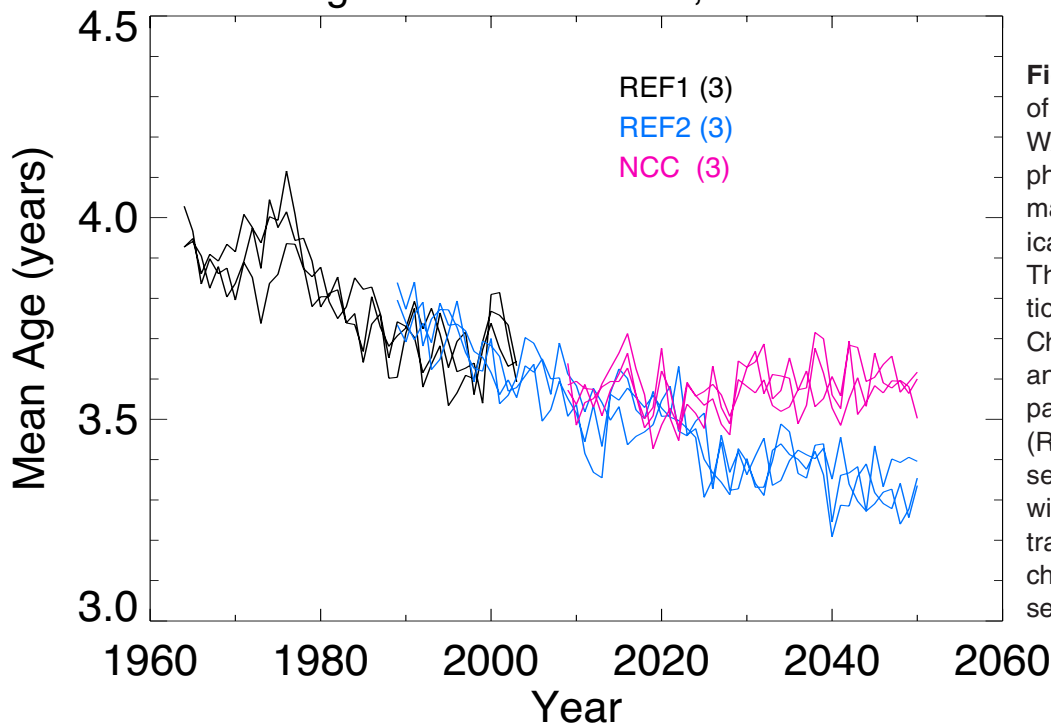


Figure 5-19. Mean age of air for the CCM WACCM (Whole Atmosphere Community Climate Model) in the tropical upper stratosphere. The individual simulations are described in Chapter 6 (Appendix 6A) and cover the recent past (REF1), the future (REF2), and an ensemble of simulations with fixed GHG concentrations (“no climate change” scenario (NCC); see also Section 5.3.7).

vapor amounts than would be anticipated on the basis of the tropospheric CH_4 concentrations alone.

5.3.4 Changes in the Tropical and Extratropical Tropopause Layer

5.3.4.1 THE TROPICAL TROPOPAUSE LAYER (TTL)

The TTL (Sherwood and Dessler, 2001) is typically defined as the body of air extending from the level of the temperature lapse rate minimum at 11-13 km (Gettelman and Forster, 2002) to the level of highest convective overshoot, slightly above the cold point tropopause (CPT) at 16-17 km (see Chapter 2, Section 2.4.1 for other definitions). This encompasses the level of zero net radiative heating (z_0) that marks the transition from radiative cooling to radiative heating, divides the TTL into the lower and upper TTL (Section 2.4.1), and depends on the presence of clouds (Corti et al., 2005). Below z_0 , the cooling air sinks back into the troposphere, whereas above z_0 the warming air rises and eventually enters the stratosphere. The chemical state of this air depends on its residence time in the TTL (Folkens et al., 1999; Thuburn and Craig, 2002; Bonazzola and Haynes, 2004; Fueglistaler et al., 2004). In addition, the minimum temperature experienced by this air is crucial for dehydration along the transport pathway in the TTL, and thus for stratospheric humidity (see Sections 5.2.5 and 5.3.5).

The TTL has undergone changes within the last few decades that are not well known or understood, and our predictive capabilities remain extremely limited. There is no merged reference dataset of long-term global temperature observations for this height region.

The TTL is sandwiched between a warming troposphere and a cooling stratosphere, which makes it difficult to produce a theoretical estimate of the response of the CPT and stratospheric humidity. A simple conceptual picture is shown in Figure 5-20. If one assumes a convectively controlled troposphere with a constant lapse rate, then tropospheric warming raises and warms the tropopause (cold point temperature increasing from T_1 to T_2). A cooling of the stratosphere further raises the tropopause but leads to a cooling (from T_2 to T_3). It seems likely that the tropospheric warming should be the dominant effect, because the enhanced infrared cooling by enhanced greenhouse gas concentrations is weak due to the very low temperatures close to the tropopause (e.g., Clough and Iacono, 1995). The observed temperature trends just above the tropical tropopause correspond to a cooling of less than 0.4 K/decade but are not statistically significant (Chapter 4 in WMO, 2003). The general con-

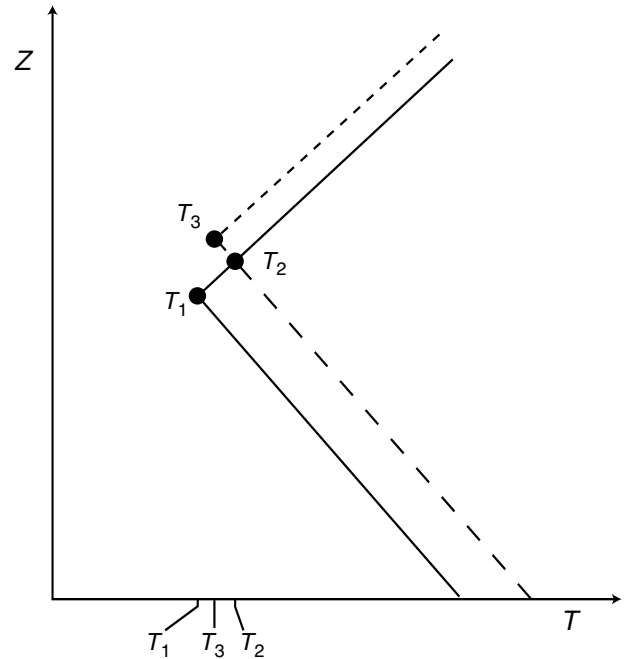


Figure 5-20. Simplified sketch of the sensitivity of the tropopause temperature and height with regard to changes of temperature in the stratosphere and troposphere. Solid lines: reference profile with cold point T_1 . Long-dashed line with solid line: perturbed profile reflecting tropospheric warming with cold point T_2 . Long-dashed line with short-dashed line: perturbed profile reflecting tropospheric warming and stratospheric cooling with cold point T_3 . After Shepherd, 2002.

cept behind Figure 5-20 has been corroborated by AGCM time-slice (Shepherd, 2002) and transient simulations (Santer et al., 2003) (see Box 5-1).

The evolution of TTL temperatures is further complicated by the fact that there is a tropospheric amplification of surface warming (Santer et al., 2005). Conversely, a strengthening of the Brewer-Dobson circulation, as suggested by model climate studies with enhanced CO_2 (Butchart and Scaife, 2001; Rind et al., 2002a, b; Sigmond et al., 2004; Eichelberger and Hartmann, 2005), would imply a lowering of TTL temperatures.

Seidel et al. (2001) obtained an increase in CPT height of about 40 meters and a decrease in pressure of about 1 hPa during 1978-1997. Both Seidel et al. (2001) and Zhou et al. (2001) have also noted a decrease of tropical tropopause temperatures by about 1 K during this period, resulting in a decrease in the saturation volume mixing ratio of water of about 0.5 ppmv during 1978-1997. These temperatures are therefore at odds with tropospheric warming dominating the response of the CPT. Rather, they

CLIMATE-OZONE CONNECTIONS

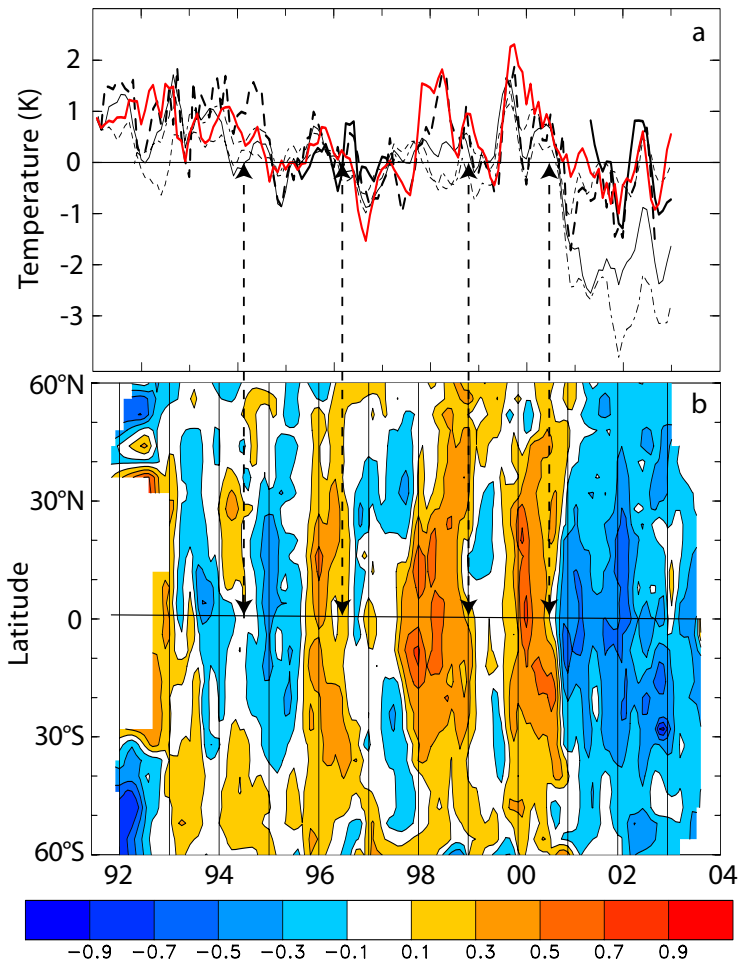


Figure 5-21. (a) Time series of deseasonalized 100 hPa temperature anomalies over 10°N-10°S, showing results from six different datasets (red = radiosondes, thick black = GPS, and various model results). (b) Latitude-time cross sections at 82 hPa of deseasonalized anomalies in $H_2O + 2 \times CH_4$ from HALOE measurements. Contours are $\pm 0.1, 0.3$, etc., ppmv. Dashed vertical lines show the onsets of various cold phases ascribed to the quasi-biennial oscillation and El Niño-Southern Oscillation. From Randel et al., 2004a.

suggest that the CPT is being largely controlled by increases in the Brewer-Dobson circulation and by increased convection as suggested by Zhou et al. (2001). Zhou et al. (2004) have also shown how the QBO and El Niño-Southern Oscillation effects produce extremely high and low tropical CPT temperatures.

Figure 5-21a indicates a very small negative trend of tropical temperatures on the 100 hPa level over the past decade, which merges into an enhanced negative evolution during 2001-03. The reasons for the most recent development are not clear at present. Figure 5-21b shows stratospheric total water content. Large anomalies are centered in the tropics and are in phase with the 100 hPa tropical temperatures. The low 2001-03 water vapor anomaly covers nearly the entire globe. The observed strong seasonal and interannual T- H_2O correlations suggest stratospheric total water content to be strongly controlled by temperatures between the 100 hPa level and the CPT, which is in agreement with recent trajectory calculations (Hatsushika and Yamazaki, 2003; Bonazzola and Haynes,

2004; Fueglistaler et al., 2005; Fueglistaler and Haynes, 2005).

Changes in the TTL may also affect the abundance of many other species in the stratosphere. This may concern short-lived chemical species, such as biogenic bromine compounds that may be carried to the stratosphere via deep convection followed by transport through the TTL (see Chapter 2, Section 2.4.1). Changes in deep convection may further affect the transport of longer-lived species produced by biomass burning, such as methyl bromide (Andreae and Merlet, 2001). Finally, species may be transported in particulate form across the tropical tropopause, e.g., organic sulfur-containing species (Notholt et al., 2005). Little is known about these processes, and even less is known about climate-induced changes.

In summary, given the uncertainties in our understanding of mechanisms in the TTL and of their previous changes, predictions of future changes in TTL morphology, processes, or transport are rendered difficult. A future atmosphere with increasing greenhouse gas load-

ings is expected to develop a warmer troposphere with enhanced deep convection. But for the reasons mentioned above, it remains speculative that this will be reflected in a warmer tropopause, higher water mixing ratios, and as a consequence, a moister stratosphere with less rapid recovery of ozone. The past decades suggest the dominance of other processes, possibly related to changes in the Brewer-Dobson circulation, which may give rise to surprises.

5.3.4.2 THE EXTRATROPICAL TROPOPAUSE LAYER (ExTL)

As described in Section 2.4.2 of Chapter 2, the ExTL is a layer of air adjacent to the local extratropical (thermal) tropopause, which has been interpreted as the result of irreversible mixing of tropospheric air into the lowermost stratosphere (Hoor et al., 2004; Hegglin et al., 2005) or as the result of two-way stratosphere-troposphere exchanges (Pan et al., 2004; Bischoff et al., 2006).

The origin of ozone in the ExTL changes markedly with season, with photochemical production dominating in summer and transport from the stratosphere dominating in winter and spring. A general upward trend of the extratropical tropopause height has been identified and has been related to ozone column changes (Steinbrecht et al., 1998; Varotsos et al., 2004). This long-term change provides a sensitive indicator of human effects on climate (Santer et al., 2004) and may be related to changes such as are sketched in Figure 5-20. However, it is presently not clear how these changes have affected, or will affect, the dominant transport pathways of air between the troposphere and the stratosphere on the synoptic scale or mesoscale.

Possible future changes in midlatitude circulation—increased strength of Brewer-Dobson circulation (e.g., Butchart and Scaife, 2001), changes in synoptic eddies (e.g., Schneider, 2004), changes in midlatitude convection (e.g., IPCC, 2001)—are all likely to change ozone concentration in the upper troposphere and lower stratosphere. However, limitations of our knowledge regarding the ExTL prevent any firm predictions on the future of the ExTL. In particular, the relative contribution of isentropic (quasi-horizontal) and convective (vertical) transport of tropospheric air into the lowermost stratosphere is not well established, though there is evidence that vertical mixing (both convectively and radiatively driven) might have a significant influence on the large-scale trace gas distributions in the lowermost stratosphere (Hegglin et al., 2005). If the frequency or intensity of midlatitudinal deep convection were to change in a future warmer climate, this could affect the lowermost stratosphere and, thus, the midlatitudinal ozone layer. Simulations of the 20th century in

the IPCC climate models (AOGCMs) generally show a decrease in the total number of extratropical storms in both hemispheres, but an increase in the number of the most intense storms (Lambert and Fyfe, 2006). Predictions of implications for ExTL dynamics and chemistry will require further investigations.

5.3.5 Impact of Future Water Vapor Changes on Ozone Chemistry

It is difficult to assess the magnitude of recent changes to stratospheric water vapor concentrations (Section 5.2.5), and future changes are uncertain. Water vapor concentrations may remain similar to current values, or possibly increase. For example, most of the CCM future simulations (i.e., REF2; see Chapter 6, Appendix 6A) show increasing stratospheric water vapor concentrations in the stratosphere. In this section, the implications for ozone of possible future increases in water vapor concentrations are discussed.

A positive trend in stratospheric water vapor concentrations would affect stratospheric ozone production and loss chemistry. Increases in water vapor would cause increases in hydrogen oxide (HO_x) radicals, affecting ozone loss processes. HO_x chemistry is the primary ozone loss process in the lower stratosphere (Wennberg et al., 1994; 1998), except over the polar caps. In addition, balloon constituent data, in conjunction with a photochemical box model, have highlighted the important role that HO_x plays in the stratosphere and lower mesosphere (Osterman et al., 1997; Jucks et al., 1998).

Evans et al. (1998) examined the effect of increased water vapor concentrations on ozone; they found that increased humidity slightly increased ozone in the middle stratosphere, and decreased ozone in the upper stratosphere. The decrease in upper stratospheric ozone was primarily from increased loss by the HO_x catalytic cycles. Dvortsov and Solomon (2001) modeled past and future changes in greenhouse gas concentrations and atmospheric chlorine and bromine loading. The model was forced to have an annual stratospheric H_2O increase of 1% per year. The water vapor trend in the model intensified the Northern Hemisphere midlatitude ozone trends, primarily due to increased ozone loss in the lower stratosphere from enhanced HO_x , and subsequent HO_x -amplified ClO_x ozone loss. The study suggests that a 1% per year stratospheric humidity trend during this century would enhance ozone loss via the HO_x catalytic cycles and delay the ozone recovery by approximately 10 years. Shindell (2001), using a CCM, also showed that including a similar future trend in water vapor may delay the ozone recovery time by approximately 15 years.

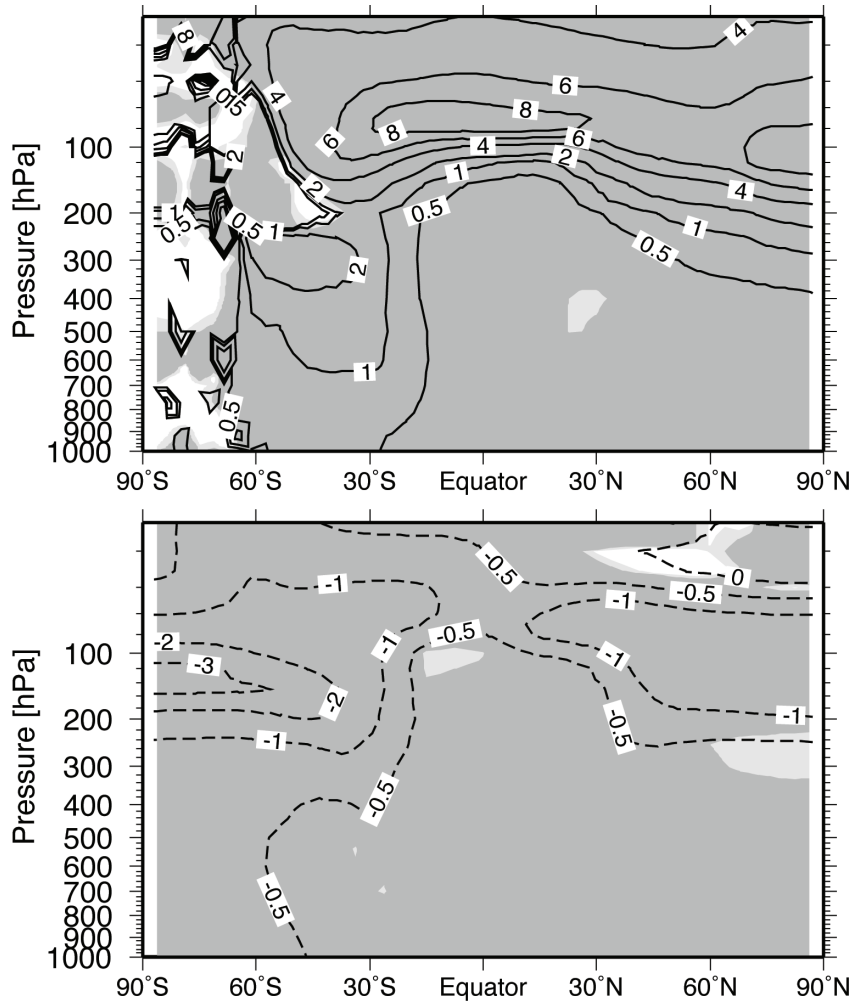


Figure 5-22. Impact of 1 ppmv water vapor perturbation above a baseline simulation in the CCM E39C. The top panel shows the percentage change in zonally and monthly averaged local OH. The bottom panel shows the percentage change in zonally and monthly averaged local O₃. Light (dark) shading indicates regions in which differences are statistically significant at the 95% (99%) level (t-test). From Stenke and Grewe, 2005.

The CCM study of Stenke and Grewe (2005) found that an increase of 1 ppmv in stratospheric water vapor would result in a 5-10% hydroxyl radical (OH) increase in the tropical lower stratosphere between 100 and 30 hPa (Figure 5-22, top panel). In the model, the OH increase caused an increase in the HO_x ozone destruction cycle of about 6%. Ozone in the lower stratosphere decreased by 1-3% (Figure 5-22, bottom panel), reducing the column by less than 1% in nonpolar latitudes (Figure 5-23).

Increases in water vapor concentration can also affect polar ozone depletion on polar stratospheric clouds (PSCs). Enhanced water vapor concentrations would increase the critical temperature below which heterogeneous reaction on liquid aerosols become important (Kirk-Davidoff et al., 1999). Tabazadeh et al. (2000) estimated that the enhancement of PSC formation for an addition of 1 ppmv water vapor is approximately the same as the PSC enhancement from a 1 K radiative cooling. Stenke and Grewe (2005) concluded that increased humidity will enhance heterogeneous ozone depletion in the Antarctic spring due to a longer PSC- existence period (Figure 5-23).

5.3.6 Impact of Temperature Changes on Ozone Chemistry

The assessment of ozone chemistry’s sensitivity to changes in temperature in the atmosphere is complicated by the concomitant changes that occur in the dynamics, transport, and radiation as the temperature changes. In addition, the chemical state of the atmosphere will change as the concentration of trace species change and ozone-depleting substances (ODSs) decrease over the coming decades. This in turn will alter the sensitivity of the stratospheric chemical system to temperature changes.

5.3.6.1 UPPER STRATOSPHERE

There is a relatively solid understanding of the sensitivity of ozone chemistry in the upper stratosphere to changes in temperature. In this region the chemical system is generally under photochemical control and is constrained by gas-phase reaction cycles that are well understood. The largest stratospheric cooling associated with

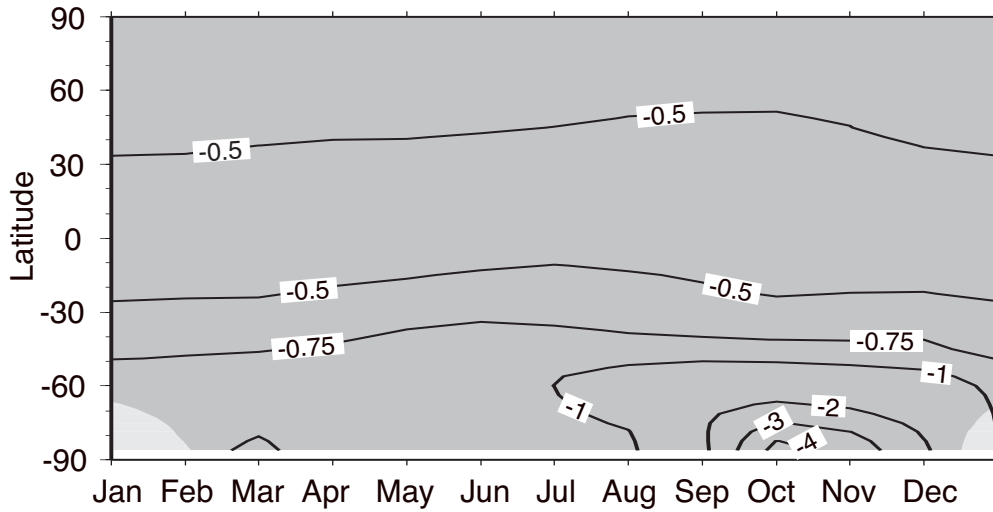


Figure 5-23. Impact of 1 ppmv water vapor perturbation above baseline simulation in the CCM E39C. This figure shows the percentage change in zonally averaged total column ozone. Light (dark) shading indicates regions in which differences are statistically significant at the 95% (99%) level (t-test). From Stenke and Grewe, 2005.

increased greenhouse gas concentrations (see Sections 5.2.6 and 5.3.1) has been observed in the upper stratosphere and mesosphere. The dominant ozone loss cycles in the upper stratosphere (NO_x , ClO_x , and HO_x) are expected to slow with decreasing temperatures (e.g., Haigh and Pyle, 1982). CCM simulations for doubled- CO_2 conditions presented by Jonsson et al. (2004) indicated an increase of 15-20% in the ozone mixing ratios in the upper stratosphere associated with a 10-12 K temperature decrease (see Section 5.3.1). In the lower mesosphere, the ozone increase is primarily due to the negative temperature dependence of the $\text{O} + \text{O}_2 + \text{M} \rightarrow \text{O}_3 + \text{M}$ reaction. The situation is more complex in the upper stratosphere, with different loss cycles having greater influence on ozone concentrations at different altitude ranges (50-60 km: HO_x ; 45-50 km: all cycles; below 45 km: NO_x). The slower loss rates are controlled by the temperature dependence of the reaction rate constants and by the reduction in the abundance of atomic oxygen (change in O_x partitioning). The rate-limiting reactions for all the loss cycles are proportional to the atomic oxygen number density. The atomic oxygen number density, in turn, is strongly determined by the reaction $\text{O} + \text{O}_2 + \text{M} \rightarrow \text{O}_3 + \text{M}$ (Jonsson et al., 2004).

5.3.6.2 POLAR LOWER STRATOSPHERE

In the springtime polar lower stratosphere, the gas-phase loss cycles described above play a similar role in determining the ozone concentration. Any decrease in temperature is expected to slow the rate of ozone loss (Zeng and Pyle, 2003). Counteracting this effect, chlorine- and bromine-containing reservoir species are activated via heterogeneous processes on cloud and cold aerosol particles, leading to markedly increased ClO_x

and BrO_x concentrations. This in turn leads to significant ozone loss via ClO_x and BrO_x catalytic cycles in the presence of sunlight. The rate of chlorine and bromine activation on the surface of cloud and aerosol particles is strongly temperature dependent, increasing sharply below approximately 195 K.

For the current polar lower stratosphere with elevated ODS concentrations, halogen activation, and consequent ozone losses at lower temperatures, offset any effect of ozone increases through reduction in NO_x and HO_x gas-phase ozone loss. This is clear from comparisons of the Antarctic and Arctic spring ozone concentrations (see Chapter 4). The Antarctic stratosphere routinely experiences temperatures below the threshold for heterogeneous halogen activation during the winter and early spring, with the consequent significant loss of ozone. The Arctic lower stratosphere, on the other hand, is highly variable and lies close to the halogen activation threshold. This means that a significant change in Arctic stratospheric temperatures would strongly influence springtime ozone concentrations in this region.

Arctic Spring

Chapter 4 discusses the compact linear relationship between chemical ozone loss in the Arctic winter and the vortex-averaged volume of air that is below the PSC threshold temperature (V_{PSC}) introduced by Rex et al. (2004). They deduce a linear relationship of approximately 15 DU of additional chemical ozone loss per Kelvin of cooling of the lower stratosphere, on the basis of ozonesonde soundings. This result is supported by a similar study by Tilmes et al. (2004). The V_{PSC} , as defined by Rex et al. (2004), is essentially a temperature metric and thus the relationship they derive indicates the temperature

CLIMATE-OZONE CONNECTIONS

sensitivity of chemical Arctic ozone loss, but other factors (e.g., vortex isolation) are also coupled to vortex temperature and influence the chemical ozone loss over the Arctic vortex period.

The ozone loss vs. V_{PSC} linear relationship determined by Rex et al. (2004) is compact and robust for recent winters. This is surprising given the highly nonlinear nature of some processes within the system being described. Their relationship was derived by averaging over the Arctic vortex for the period mid-December to the end of March, which concatenates a number of complex nonlinear processes (microphysical details of PSC formation, denitrification and dehydration, and chemical activation on PSC surfaces).

It should be noted that the ozone loss vs. V_{PSC} relationship is valid for current conditions of elevated ODSs. As concentrations of ODSs in the stratosphere decrease through the early part of this century, it is likely that the ozone loss vs. V_{PSC} relationship will change. Also, vortex conditions (e.g., size) may change, so it is unclear whether the ozone loss vs. V_{PSC} relationship has any use as a predictive tool.

Antarctic Spring

In contrast to the Arctic polar vortex, the extent of ozone loss within the Antarctic polar vortex during winter and spring is primarily dictated by the amount of stratospheric halogen present.

A major predictor for ozone mass deficit over the Antarctic vortex period for the years 1979 to 2003 is the lagged equivalent effective stratospheric chlorine (EESC); it explains 82% of the variance in the ozone mass deficit (Huck et al., 2005). The 100 hPa polar temperatures modulate the interannual variability in the ozone mass deficit anomaly. The Antarctic ozone hole size is primarily sensitive to EESC and secondarily to temperatures near the edge of the vortex (collar temperature) (Newman et al., 2004). Changes in sulfate aerosol particle surface area and surface reactivity were used to explain the correlation between the residual ozone hole size and collar temperature. Using the residuals from a quadratic fit of the ozone hole size to the EESC amounts, they estimated that a 1 K decrease in collar temperature leads to an increase in size of the late September ozone hole of 1.1 million km².

Both Huck et al. (2005) and Newman et al. (2004) used regression analysis based on data from recent (1979-2003) years to derive empirical models of Antarctic ozone loss. The models can only be expected to remain valid for descriptions of near-future ozone losses when stratospheric conditions remain broadly similar to the 1979-2003 period used to construct the models. Both models' ozone hole indices will become less meaningful as meas-

ures of Antarctic ozone levels as the ozone hole begins to close from the middle of this century.

5.3.7 Impact of Climate Change on Ozone Recovery

As discussed in the previous sections, the long-term evolution of stratospheric ozone concentrations depends not only on changes of many stratospheric constituents (including ozone-depleting substances (ODSs), greenhouse gases (GHGs), water vapor, and aerosols), but also on changes in the climate of the troposphere and stratosphere caused by natural variability and anthropogenic forcing. While it is expected that the reduction of ODSs in the next years to decades will lead to an increase in ozone, this increase could be affected by changes in temperature (Section 5.3.6) and in chemical composition and transport (Sections 5.3.3 through 5.3.5). This section discusses results of sensitivity studies that use CCMs to elucidate how climate change could affect formation and destruction of future stratospheric ozone.

Recent Assessment reports (Section 12.2.1.3 in WMO, 1999; Section 4.8 in WMO, 2003) presented results derived from an ensemble of two-dimensional (2-D) models (see Box 5-1) that calculated the evolution of total ozone through the year 2050. For some models, near-global mean (60°N-60°S) column ozone remained up to 1% below 1980 levels even in 2050, while for others the ozone column amounts in 2050 were 3.5% higher than in 1980. Several of the 2-D models did not include the impact of greenhouse gas-induced stratospheric cooling on ozone. Temperatures affect ozone by changing the reaction rates that determine O_x abundance, primarily in the middle and upper stratosphere. Moreover, in the polar lower stratosphere, in addition to gas-phase photochemistry, chlorine and bromine reservoir species are activated via heterogeneous processes on cloud and cold aerosol particles (see Section 5.3.6). For example, in the 2-D models of Rosenfield et al. (2002) and Chipperfield and Feng (2003), ozone recovers to 1980 values 10-20 years earlier in many latitudes and seasons, due to the inclusion of the stratospheric cooling effect from enhanced GHG concentrations (e.g., Figure 6-11 of Chapter 6).

The aforementioned 2-D model studies illustrate that the future evolution of ozone is sensitive to changes in both chemical constituents *and* climate. Although a few 2-D models include some of the effects of changes in dynamics, they do not consider any variability in tropospheric wave forcing due to climate change and the impact this may have on the stratosphere (see Sections 5.2.2 and 5.3.2). Another weak point of 2-D models is that they are simply not useful for investigations of polar regions (WMO, 2003). Nowadays CCMs offer a more complete possibility to fur-

ther investigate the impact of climate change on ozone, since these models do consider interactions and feedbacks of radiative, dynamical, and chemical processes. Recently a number of CCMs (see Chapter 6, Table 6-4) have been used to simulate the past and future evolution of ozone (see Chapter 6, Appendix 6A). The following discussion highlights some results of additional CCM sensitivity studies (using the “no climate change” scenario, NCC) that enable a more detailed investigation of the impact of fixed greenhouse gas concentrations on the recovery of the stratospheric ozone layer. The results derived from these model sensitivity studies provide useful and supplementary information to better understand the expected evolution of the ozone layer in the 21st century (Chapter 6).

Three CCMs (E39C, ULAQ, WACCM) were employed to carry out long-term sensitivity simulations (through 2050), wherein concentrations of well-mixed greenhouse gases (CO₂, CH₄, and N₂O) are held constant after a given date (E39C: 1980; ULAQ: 1970; WACCM: 2000), whereas the evolution of halocarbon is based on the “Ab” scenario from WMO (2003). Additionally, in E39C and ULAQ, the sea surface temperatures (SSTs) were prescribed according to observations of the years 1970 to 1979. This SST dataset was used again for every succeeding decade in the model simulation (E39C: 1980 to 2020; ULAQ: 1960 to 2050). The methods used to prescribe SSTs in the NCC simulations are a bit simplified, but reasonable for this kind of sensitivity study. In reality, the thermal inertia of the oceans must be considered. A mixed-layer ocean model needs approximately 20 to 30 years to reach a new equilibrium, and a deep-ocean model even several hundred years (e.g., Hansen et al., 2005). For this kind of sensitivity study, the neglect of this effect is expected to be of small significance. Nonetheless, this effect was considered in the WACCM NCC simulations using SSTs from a coupled ocean-atmosphere model (AOGCM) that was run in support of the most recent IPCC Assessment (IPCC CCSM/CAM3). The CCSM/CAM3 simulation was run with IPCC emissions for 2000 held constant from 2000 to 2100, i.e., the same GHG scenario as adopted for the NCC simulations.

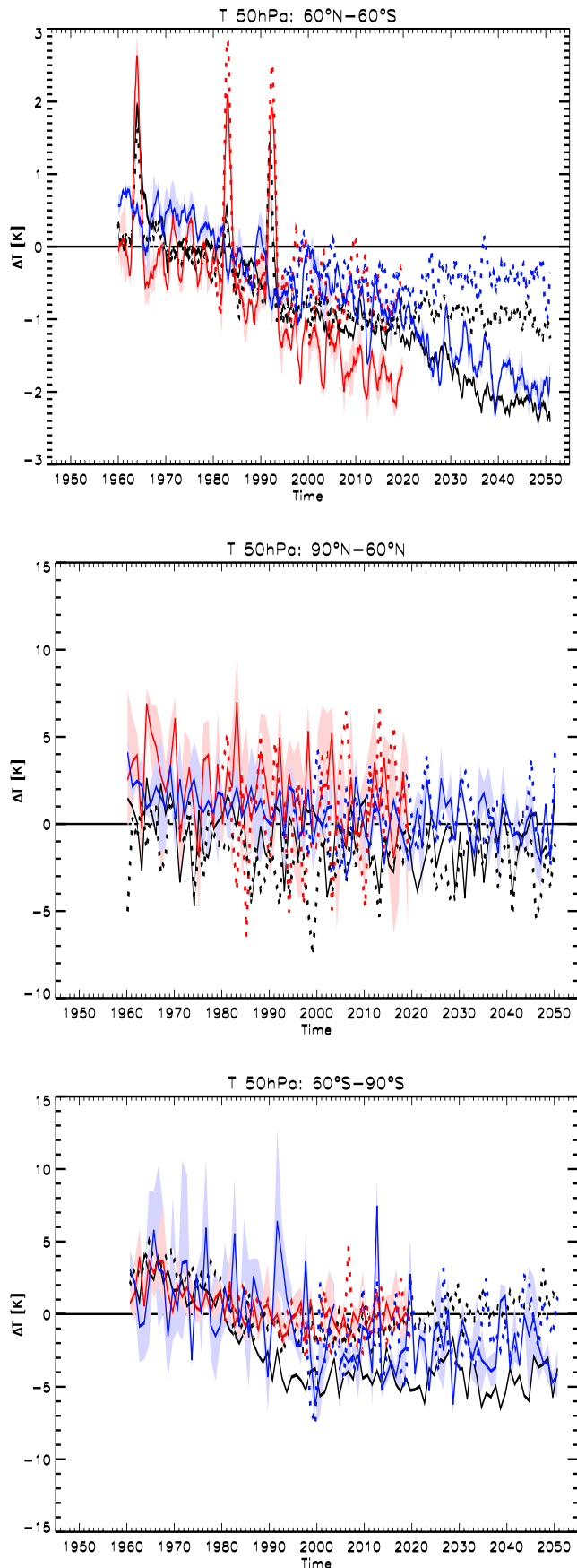
In all three CCMs, ozone and water vapor are prognostic variables, i.e., the radiative feedback of ozone and water vapor changes is considered. A direct comparison of results from the NCC simulations with results from reference simulations (prescribing past and expected future changes, i.e., REF1 and REF2/SCN2; see Chapter 6, Appendix 6A) allows a qualitative estimation of the future impact of climate change on ozone. Figure 5-24 (top) displays the evolution of the near-global (60°N-60°S) mean temperature deviations of the lower stratosphere at 50 hPa. The results derived from the reference simulations

show an obvious cooling trend because of increasing GHG concentrations (see Section 5.3.1). Nearly zero trends are calculated by all three CCMs when fixed GHG concentrations are assumed. It takes about 20 years before a difference is apparent between curves derived from the reference and the sensitivity simulations. This statement is not valid for mean temperatures (at 50 hPa) over the Northern Hemisphere polar region (i.e., 60°-90°N, Figure 5-24 middle panel), which does not show statistically significant differences between the reference and the sensitivity simulations. The picture is unclear for the Southern Hemisphere polar region (i.e., 60°-90°S, Figure 5-24 bottom panel). E39C shows no obvious differences between the two simulations, whereas WACCM results indicate slightly higher and ULAQ much higher temperatures in the NCC simulations.

Investigations of the CCM results do not indicate a clear impact of climate (temperature) change on metrics like minimum ozone column values in the polar stratosphere or “maximum ozone hole area,” either in the Northern Hemisphere or the Southern Hemisphere (not shown). These metrics are evidently insensitive to temperature changes of less than about 1 K. But the results shown in Figure 5-25 demonstrate that the recovery of near-global mean (60°N-60°S) column ozone is accelerated in a changing climate: since the global stratosphere is under photochemical control (constrained by gas-phase reaction cycles), the ozone loss cycles in the stratosphere (primarily O_x) slow down with decreasing temperature. When climate change is included, ULAQ and WACCM show a return to the 1980 global ozone amount approximately 10 to 15 years earlier than without climate change. This is in agreement with former estimates derived from 2-D model studies (see above). The results derived from the CCM E39C are not as clear in this sense, but here it must be considered that in contrast to ULAQ and WACCM, E39C has a low uppermost layer which is centered at 10 hPa, and therefore neglects the impact of dynamical and photochemical effects on ozone in the upper part of the stratosphere. In any case, the E39C simulations were not long enough for the difference between NCC and REF simulations to become apparent.

Results derived from ULAQ and WACCM show that by 2050, the middle to upper stratosphere is 5-10 K colder in the reference runs than in corresponding NCC simulations (not shown). As a result of this cooling, ozone mixing ratios in the middle and upper stratosphere are higher in the reference cases than in NCC (up to 15% below the stratopause). The most important impact is through the effect of temperature on the ozone loss rate. Below 10 hPa, all three CCMs show a consistent behavior. These results indicate a delay in the recovery of ozone in

CLIMATE-OZONE CONNECTIONS



the Antarctic lower stratosphere (not shown) due to “intensified” heterogeneous chemistry that is caused by reduced temperatures in the lower polar stratosphere. The changes are not statistically significant in the Arctic lower stratosphere. Interestingly, all models very clearly show less ozone in the tropical lower stratosphere in the reference simulations, which may point to an enhanced updraft in the tropics (intensified Brewer-Dobson circulation) in the reference simulations.

Qualitatively, the evolution of column ozone and lower stratospheric temperatures (50 hPa) in the polar regions (60°-90°) is very similar in the reference and NCC simulations (Figure 5-26). The results seem to indicate that the net impact of changes of well-mixed greenhouse gas concentrations and SSTs on total ozone is perhaps slightly larger in the Arctic stratosphere than in the Antarctic stratosphere. Differences in ozone column between results derived from reference simulations and NCC are not apparent in the polar SH. In the polar NH, the WACCM model indicates that after the year 2020, the ozone column is systematically larger in the reference simulations. So, lower temperatures in the ozone loss regions of high latitudes have the opposite effect of lower temperatures in the ozone production region in the tropics. Notwithstanding, it may be that in the NH the transport of air with enhanced ozone mixing ratios to high latitudes by an intensified Brewer-Dobson circulation dominates the effect of enhanced chlorine/bromine catalysis of ozone destruction in the polar region. The fact that it takes at least until 2020 for a noticeable difference to emerge between the reference simulations and NCC in the NH may be consistent with this conjecture.

Figure 5-24. Time series of zonally averaged near-global (top panel, 60°N-60°S) temperature deviations at 50 hPa between 1960 and 2050 relative to the year 1980 (in K). Data have been smoothed with a 13-month running mean. Respective time series are shown for the northern polar region (middle panel, 60°N-90°N) and the southern polar region (lower panel, 60°S-90°S). Here, data have been considered only for springtime months, i.e., 3-month mean values of February, March, and April in the NH, and August, September, and October in the SH. For each model, i.e., E39C (red lines), ULAQ (black lines), and WACCM (blue lines), the solid curves show results derived from the reference simulations (REF). Since WACCM and E39C have performed ensemble simulations, the envelope of results is shown for each model. The dotted curves indicate the results derived from the “no climate change runs” (NCC).

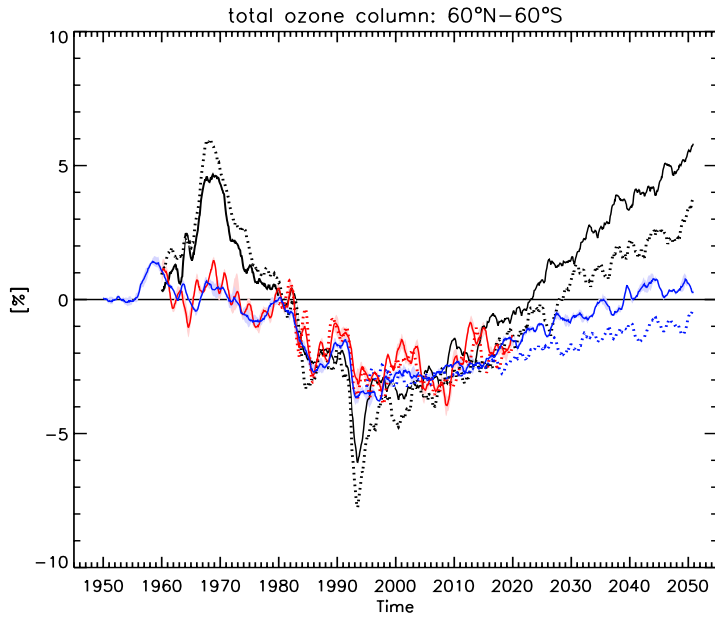


Figure 5-25. Time series of zonally averaged near-global (60°N-60°S) total ozone deviations between 1960 and 2050 with regard to the year 1980 (in %). For each model, i.e., E39C (red lines), ULAQ (black lines), and WACCM (blue lines), the solid curves show results derived from the reference simulations (REF). Since WACCM and E39C have performed ensemble simulations, the envelope of results is shown for each model. The dotted curves indicate the results derived from the “no climate change runs” (NCC). All data are smoothed with a 13-month running mean.

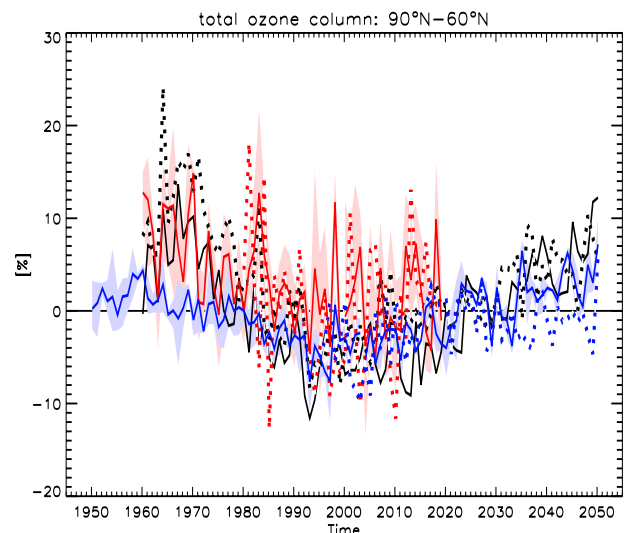
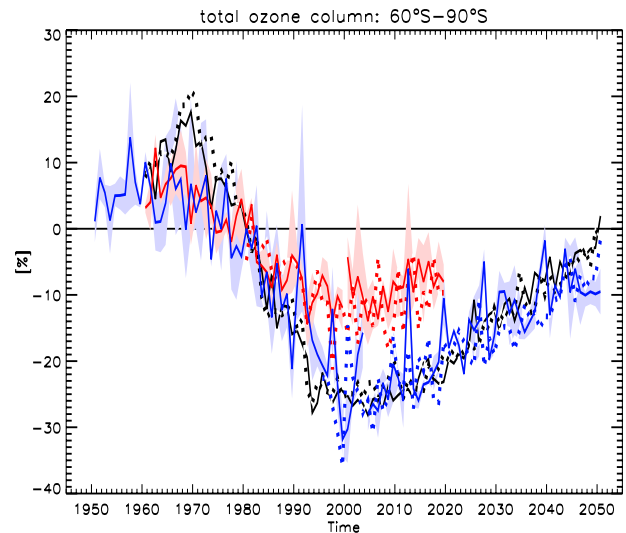


Figure 5-26. Time series of zonally averaged total ozone deviations at southern polar latitudes (top panel, 60°S-90°S) and northern polar latitudes (lower panel, 60°N-90°N) between 1960 and 2050 with regard to the year 1980 (in %). For each model, i.e., E39C (red lines), ULAQ (black lines), and WACCM (blue lines), the solid curves show results derived from the reference simulations (REF). Since WACCM and E39C have performed ensemble simulations, the envelope of results is shown for each model. The dotted curves indicate the results derived from the “no climate change runs” (NCC). Data have been considered only for springtime months, i.e., 3-month mean values of February, March, and April in the NH, and August, September, and October in the SH.

REFERENCES

- Al-Saadi, J.A., R.B. Pierce, T.D. Fairlie, M.M. Kleb, R.S. Eckman, W.L. Grose, M. Natarajan, and J.R. Olson, Response of middle atmosphere chemistry and dynamics to volcanically elevated sulfate aerosol: Three-dimensional coupled model simulations, *J. Geophys. Res.*, 106 (D21), 27255-27275, doi: 10.1029/2000JD000185, 2001.
- Andreae, M.O., and P. Merlet, Emission of trace gases and aerosols from biomass burning, *Global Biogeochem. Cycles*, 15 (4), 955-966, 2001.
- Andrews, A.E., K.A. Boering, B.C. Daube, S.C. Wofsy, M. Loewenstein, H. Jost, J.R. Podolske, C.R. Webster, R.L. Herman, D.C. Scott, G.J. Flesch, E.J. Moyer, J.W. Elkins, G.S. Dutton, D.F. Hurst, F.L. Moore, E.A. Ray, P.A. Romashkin, and S.E. Strahan, Mean ages of stratospheric air derived from in situ observations of CO₂, CH₄, and N₂O, *J. Geophys. Res.*, 106 (D23), 32295-32314, 2001.
- Andrews, D.G., J.R. Holton, and C.B. Leovy, *Middle Atmosphere Dynamics*, Academic Press, 489 pp., Orlando, Fla., 1987.
- Arblaster, J.M., and G.A. Meehl, Contributions of external forcings to Southern Annular Mode trends, *J. Clim.*, 19 (12), 2896-2905, doi: 10.1175/JCL13774.1, 2006.
- Austin, J., and N. Butchart, Coupled chemistry-climate model simulations for the period 1980 to 2020: Ozone depletion and the start of ozone recovery, *Quart. J. Roy. Meteorol. Soc.*, 129 (595), 3225-3249, 2003.
- Austin, J., and F. Li, On the relationship between the strength of the Brewer-Dobson circulation and the age of stratospheric air, *Geophys. Res. Lett.*, 33, L17807, doi: 10.1029/2006GL026867, 2006.
- Austin, J., D. Shindell, S.R. Beagley, C. Brühl, M. Dameris, E. Manzini, T. Nagashima, P. Newman, S. Pawson, G. Pitari, E. Rozanov, C. Schnadt, and T.G. Shepherd, Uncertainties and assessments of chemistry-climate models of the stratosphere, *Atmos. Chem. Phys.*, 3 (1), 1-27, 2003.
- Austin, J., J. Wilson, F. Li, and H. Vömel, Evolution of water vapor and age of air in coupled chemistry climate model simulations of the stratosphere, *J. Atmos. Sci.*, 33, L17807, doi:10.1029/2006GL026867, 2006.
- Baldwin, M.P., and T.J. Dunkerton, Propagation of the Arctic Oscillation from the stratosphere to the troposphere, *J. Geophys. Res.*, 104 (D24), 30937-30946, doi: 10.1029/1999JD900445, 1999.
- Baldwin, M.P., and T.J. Dunkerton, Stratospheric harbingers of anomalous weather regimes, *Science*, 244 (5542), 581-584, 2001.
- Baldwin, M.P., and L.J. Gray, Tropical stratospheric zonal winds in ECMWF ERA-40 reanalysis, rocketsonde data, and rawinsonde data, *Geophys. Res. Lett.*, 32 (9), L09806, doi: 10.1029/2004GL022328, 2005.
- Baldwin, M.P., L.J. Gray, T.J. Dunkerton, K. Hamilton, P.H. Haynes, W.J. Randel, J.R. Holton, M.J. Alexander, I. Hirota, T. Horinouchi, D.B.A. Jones, J.S. Kinnerson, C. Marquardt, K. Sato, and M. Takahashi, The Quasi-Biennial Oscillation, *Rev. Geophys.*, 39 (2), 179-229, 2001.
- Bekki, S., J.A. Pyle, W. Zhong, R. Toumi, J.D. Haigh, and D.M. Pyle, The role of microphysical and chemical processes in prolonging the climate forcing of the Toba eruption, *Geophys. Res. Lett.*, 23 (19), 2669-2672, 1996.
- Beres, J.H., R.R. Garcia, B.A. Boville, and F. Sassi, Implementation of a gravity wave source spectrum parameterization dependent on the properties of convection in the Whole Atmosphere Community Climate Model (WACCM), *J. Geophys. Res.*, 110, D10108, doi: 10.1029/2004JD005504, 2005.
- Birner, T., D. Sankey, and T.G. Shepherd, The tropopause inversion layer in models and analyses, *Geophys. Res. Lett.*, 33, L14804, doi: 10.1029/2006GL026549, 2006.
- Bischoff, S.A., P.O. Canziani, A.E. Yuchechechen, The tropopause at southern extratropical latitudes: Argentine operational rawinsonde climatology, *Int. J. Climatol.*, doi:10.1002/joc.1385, in press, 2006.
- Boering, K.A., S.C. Wofsy, B.C. Daube, H.R. Schneider, M. Loewenstein, and J.R. Podolske, Stratospheric mean ages and transport rates from observations of CO₂ and N₂O, *Science*, 274 (5291), 1340-1343, 1996.
- Bonazzola, M., and P.H. Haynes, A trajectory-based study of the tropical tropopause region, *J. Geophys. Res.*, 109, D20112, doi: 10.1029/2003JD004356, 2004.
- Butchart, N., and A.A. Scaife, Removal of chlorofluorocarbons by increased mass exchange between the stratosphere and the troposphere in a changing climate, *Nature*, 410 (6830), 799-802, 2001.
- Butchart, N., J. Austin, J.R. Knight, A.A. Scaife, and M.L. Gallani, The response of the stratospheric climate to projected changes in the concentrations of well-mixed greenhouse gases from 1992 to 2051, *J. Clim.*, 13 (13), 2142-2159, 2000.
- Butchart, N., A.A. Scaife, M. Bourqui, J. de Grandpre, S.H.E. Hare, J. Kettleborough, U. Langematz, E. Manzini, F. Sassi, K. Shibata, D. Shindell, and M. Sigmund, Simulations of anthropogenic change in the strength of the Brewer-Dobson circulation,

- Clim. Dyn.*, 27 (7-8), 727-741, doi:10.1007/s00382-006-0162-4, 2006.
- Castanheira, J.M., and H.-F. Graf, North Pacific-North Atlantic relationships under stratospheric control?, *J. Geophys. Res.*, 108 (D1), 4036, doi: 10.1029/2002JD002754, 2003.
- CCSP (U.S. Climate Change Science Program), *Temperature Trends in the Lower Atmosphere: Steps for Understanding and Reconciling Differences*, edited by T.R. Karl, S.J. Hassol, C.D. Miller, and W.L. Murray, A Report by the Climate Change Science Program and the Subcommittee on Global Change Research, 164 pp., Washington, D.C., 2006.
- Charney, J.G., and P.G. Drazin, Propagation of planetary-scale disturbances from the lower into the upper atmosphere, *J. Geophys. Res.*, 66 (1), 83-109, 1961.
- Charron, M., and E. Manzini, Gravity waves from fronts: Parameterization and middle atmosphere response in a general circulation model, *J. Atmos. Sci.*, 59 (5), 923-941, 2002.
- Chen, P., and W.A. Robinson, Propagation of planetary waves between the troposphere and stratosphere, *J. Atmos. Sci.*, 49 (24), 2533-2545, 1992.
- Chiou, E.W., L.W. Thomason, and W.P. Chu, Variability of stratospheric water vapor inferred from SAGE II, HALOE and Boulder (Colorado) balloon measurements, *J. Clim.*, 19 (16), 4121-4133, doi: 10.1175/JCL13841.1, 2006.
- Chipperfield, M.P., and W. Feng, Comment on: Stratospheric Ozone Depletion at northern mid-latitudes in the 21st century: The importance of future concentrations of greenhouse gases nitrous oxide and methane, *Geophys. Res. Lett.*, 30 (7), 1389, doi: 10.1029/2002GL016353, 2003.
- Christiansen, B., Stratospheric vacillations in a general circulation model, *J. Atmos. Sci.*, 56 (12), 1858-1872, 1999.
- Christy, J.R., R.W. Spencer, W.B. Norris, W.D. Braswell, and D.E. Parker, Error estimates of version 5.0 of MSU-AMSU bulk atmospheric temperatures, *J. Atmos. Oceanic Technol.*, 20 (5), 613-629, 2003.
- Clough, S.A., and M.J. Iacono, Line-by-line calculation of atmospheric fluxes and cooling rates 2. Application to carbon dioxide, ozone, methane, nitrous oxide and the halocarbons, *J. Geophys. Res.*, 100 (D8), 16519-16535, 1995.
- Collins, W.D., P.J. Rasch, B.A. Boville, J.R. McCaa, D.L. Williamson, J.T. Kiehl, B. Briegleb, C. Bitz, S.-J. Lin, M. Zhang, and Y. Dai, *Description of the NCAR Community Atmosphere Model (CAM3.0)*, Technical Note TN-464+STR, National Center for Atmospheric Research, 214 pp., Boulder, Colo., 2004.
- Collins, W.J., R.G. Derwent, B. Garnier, C.E. Johnson, M.G. Sanderson, and D.S. Stevenson, Effect of stratosphere-troposphere exchange on the future tropospheric ozone trend, *J. Geophys. Res.*, 108 (D12), 8528, doi: 10.1029/2002JD002617, 2003.
- Cordero, E.C., and T.R. Nathan, A new pathway for communicating the 11-year solar cycle signal to the QBO, *Geophys. Res. Lett.*, 32, L18805, doi: 10.1029/2005GL023696, 2005.
- Corti, T., B.P. Luo, T. Peter, H. Vömel, and Q. Fu, Mean radiative energy balance and vertical mass fluxes in the equatorial upper troposphere and lower stratosphere, *Geophys. Res. Lett.*, 32 (6), L06802, doi: 10.1029/2004GL021889, 2005.
- Dameris, M., V. Grewe, M. Ponater, R. Deckert, V. Eyring, F. Mager, S. Matthes, C. Schnadt, A. Stenke, B. Steil, C. Brühl, and M.A. Giorgetta, Long-term changes and variability in a transient simulation with a chemistry-climate model employing realistic forcing, *Atmos. Chem. Phys.*, 5, 2121-2145, 2005.
- Déqué, M., C. Dreveton, A. Braun, and D. Cariolle, The ARPEGE/IFS atmosphere model: A contribution to the French community climate modeling, *Clim. Dyn.*, 10, 249-266, 1994.
- Deshler, T., R. Anderson-Sprecher, H. Jäger, J. Barnes, D.J. Hofmann, B. Clemesha, D. Simonich, M. Osborn, R.G. Grainger, and S. Godin-Beekmann, Trends in nonvolcanic component of stratospheric aerosol over the period 1971-2004, *J. Geophys. Res.*, 111, D01201, doi: 10.1029/2005JD006089, 2006.
- Dunkerton, T.J., Quasi-biennial and sub-biennial variations of stratospheric trace constituents derived from HALOE observations, *J. Atmos. Sci.*, 58 (1), 7-25, 2001.
- Dunkerton, T.J., and D.P. Delisi, Climatology of the equatorial lower stratosphere, *J. Atmos. Sci.*, 42 (4), 376-396, 1985.
- Dvortsov, V.L., and S. Solomon, Response of the stratospheric temperatures and ozone to past and future increases in stratospheric humidity, *J. Geophys. Res.*, 106 (D7), 7505-7514, 2001.
- Eckermann, S.D., D.L. Wu, J.D. Doyle, J.F. Burris, T.J. McGee, C.A. Hostetler, L. Coy, B.N. Lawrence, A. Stephens, J.P. McCormack, and T.F. Hogan, Imaging gravity waves in lower stratospheric AMSU-A radiances, Part 2: Validation case study, *Atmos. Chem. Phys.*, 6, 3343-3362, 2006.
- Eichelberger, S.J., and D.L. Hartmann, Changes in the strength of the Brewer-Dobson circulation in a simple AGCM, *Geophys. Res. Lett.*, 32, L15807, doi: 10.1029/2005GL022924, 2005.
- Esler, J.G., and R.K. Scott, Excitation of transient Rossby

CLIMATE-OZONE CONNECTIONS

- waves on the stratospheric polar vortex and the barotropic sudden warming, *J. Atmos. Sci.*, *62* (10), 3661-3682, 2005.
- Evans, S.J., R. Toumi, J.E. Harries, M.P. Chipperfield, and J.M. Russell III, Trends in stratospheric humidity and the sensitivity of ozone to these trends, *J. Geophys. Res.*, *103* (D8), 8715-8725, 1998.
- Eyring, V., N. Butchart, D.W. Waugh, H. Akiyoshi, J. Austin, S. Bekki, G.E. Bodeker, B.A. Boville, C. Brühl, M.P. Chipperfield, E. Cordero, M. Dameris, M. Deushi, V.E. Fioletov, S.M. Frith, R.R. Garcia, A. Gettelman, M.A. Giorgetta, V. Grewe, L. Jourdain, D.E. Kinnison, E. Mancini, E. Manzini, M. Marchand, D.R. Marsh, T. Nagashima, P.A. Newman, S. Pawson, G. Pitari, D.A. Plummer, E. Rozanov, M. Schraner, T.G. Shepherd, K. Shibata, R.S. Stolarski, H. Struthers, W. Tian, and M. Yoshiki, Assessment of temperature, trace species, and ozone in chemistry-climate model simulations of the recent past, *J. Geophys. Res.*, *111* (D22308), doi: 10.1029/2006JD007327, 2006.
- Fioletov, V.E., G.E. Bodeker, A.J. Miller, R.D. McPeters, and R. Stolarski, Global and zonal total ozone variations estimated from ground-based and satellite measurements: 1964-2000, *J. Geophys. Res.*, *107* (D22), 4647, doi: 10.1029/2001JD001350, 2002.
- Flato, G.M., The Third Generation Coupled Global Climate Model (CGCM3) (and included links to the description of the AGCM3 atmospheric model), <http://www.cccma.bc.ec.gc.ca/models/cgcm2.shtml>, 2005.
- Folkins, I., M. Loewenstein, J. Podolske, S.J. Oltmans, and M. Proffitt, A barrier to vertical mixing at 14 km in the tropics: Evidence from ozonesondes and aircraft measurements, *J. Geophys. Res.*, *104* (D18), 22095-22102, 1999.
- Fomichev, V.I., A.I. Jonsson, J. de Grandpré, S.R. Beagley, C. McLandress, K. Semeniuk, and T.G. Shepherd, Response of the middle atmosphere to CO₂ doubling: Results from the Canadian Middle Atmosphere Model, *J. Clim.*, in press, 2006.
- Forster, P.M. de F., and K.P. Shine, Radiative forcing and temperature trends from stratospheric ozone changes, *J. Geophys. Res.*, *102* (D9), 10841-10855, 1997.
- Forster, P.M. de F., and K.P. Shine, Stratospheric water vapour changes as a possible contributor to observed stratospheric cooling, *Geophys. Res. Lett.*, *26* (21), 3309-3312, 1999.
- Free, M., D.J. Seidel, J.K. Angell, J. Lanzante, I. Dure, and T.C. Peterson, Radiosonde Atmospheric Temperature Products for Assessing Climate (RATPAC): A new data set of large-area anomaly time series, *J. Geophys. Res.*, *110*, D22101, doi: 10.1029/2005JD006169, 2005.
- Fritts, D.C., and M.J. Alexander, Gravity wave dynamics and effects in the middle atmosphere, *Rev. Geophys.*, *41* (1), 1003, doi: 10.1029/2001RG000106, 2003.
- Fueglistaler, S., and P.H. Haynes, Control of interannual and longer-term variability of stratospheric water vapor, *J. Geophys. Res.*, *110*, D24108, doi: 10.1029/2005JD006019, 2005.
- Fueglistaler, S., H. Wernli, and T. Peter, Tropical troposphere-to-stratosphere transport inferred from trajectory calculations, *J. Geophys. Res.*, *109*, D03108, doi: 10.1029/2003JD004069, 2004.
- Fueglistaler, S., M. Bonazzola, P.H. Haynes, and T. Peter, Stratospheric water vapor predicted from the Lagrangian temperature history of air entering the stratosphere in the tropics, *J. Geophys. Res.*, *110*, D08107, doi: 10.1029/2004JD005516, 2005.
- Gaffen, D.J., Temporal inhomogeneities in radiosonde temperature records, *J. Geophys. Res.*, *99* (D2), 3667-3676, 1994.
- Galin, V. Ya., E.M. Volodin, and S.P. Smyshliaev, Atmospheric general circulation model of INM RAS with ozone dynamics, *Russian Meteorol. Hydro.*, *5*, 13-22, 2003.
- Geller, M.A., X.L. Zhou, and M.H. Zhang, Simulations of the interannual variability of stratospheric water vapor, *J. Atmos. Sci.*, *59* (6), 1076-1085, 2002.
- Gerber, E.P., and G.K. Vallis, A stochastic model for the spatial structure of annular patterns of variability and the North Atlantic oscillation, *J. Clim.*, *18* (12), 2102-2118, 2005.
- Gettelman, A., and P.M. de F. Forster, A climatology of the tropical tropopause layer, *J. Meteorol. Soc. Japan*, *80* (4B), 911-924, 2002.
- Gillett, N.P., Northern Hemisphere circulation, *Nature*, *437* (7058), 496, doi: 10.1038/437496a, 2005.
- Gillett, N.P., and D.W.J. Thompson, Simulation of recent Southern Hemisphere climate change, *Science*, *302* (5643), 273-275, 2003.
- Gillett, N.P., M.R. Allen, and K.D. Williams, Modelling the atmospheric response to doubled CO₂ and depleted stratospheric ozone using a stratosphere-resolving coupled GCM, *Quart. J. Roy. Meteorol. Soc.*, *129* (589), 947-966, 2003.
- Giorgetta, M.A., and L. Bengtsson, The potential role of the quasi-biennial oscillation in the stratosphere-troposphere exchange as found in water vapour in general circulation model experiments, *J. Geophys. Res.*, *104* (D6), 6003-6019, 1999.
- Gordon, H.B., L.D. Rotstayn, J.L. McGregor, M.R.

- Dix, E.A. Kowalezyk, S.P. O'Farrell, L.J. Waterman, A.C. Hirst, S.G. Wilson, M.A. Collier, I.G. Watterson, and T.I. Elliott, *The CSIRO Mk3 Climate System Model, CSIRO Atmospheric Research Technical Paper No. 60*, 130 pp., Aspendale, Victoria, Australia, 2002, (http://www.dar.csiro.au/publications/gordon_2002a.pdf).
- Graf, H.-F., I. Kirchner, and J. Perlwitz, Changing lower stratospheric circulation: The role of ozone and greenhouse gases, *J. Geophys. Res.*, *103* (D10), 11251-11261, 1998.
- Gray, L.J., The influence of the equatorial upper stratosphere on stratospheric sudden warmings, *Geophys. Res. Lett.*, *30* (4), 1166, doi: 10.1029/2002GL016430, 2003.
- Gray, L.J., E.F. Drysdale, T.J. Dunkerton, and B.N. Lawrence, Model studies of the interannual variability of the northern hemisphere stratospheric winter circulation: the role of the Quasi Biennial Oscillation, *Quart. J. Roy. Meteorol. Soc.*, *127* (578), 1413-1432, 2001a.
- Gray, L.J., S.J. Phipps, T.J. Dunkerton, M.P. Baldwin, E.F. Drysdale, and M.R. Allen, A data study of the influence of the equatorial upper stratosphere on northern hemisphere stratospheric sudden warmings, *Quart. J. Roy. Meteorol. Soc.*, *127* (576), 1985-2003, 2001b.
- Gray, L.J., S. Crooks, C. Pascoe, S. Sparrow, and M. Palmer, Solar and QBO influences on the timing of stratospheric sudden warmings, *J. Atmos. Sci.*, *61* (23), 2777-2796, 2004.
- Haigh, J.D., The role of stratospheric ozone in modulating the solar radiative forcing of climate, *Nature*, *370* (6490), 544-546, 1994.
- Haigh, J.D., and J.A. Pyle, Ozone perturbation experiments in a two-dimensional circulation model, *Quart. J. Roy. Meteorol. Soc.*, *108*, 551-574, 1982.
- Haigh, J.D., M. Blackburn, and R. Day, The response of tropospheric circulation to perturbations in lower-stratospheric temperature, *J. Clim.*, *18* (17), 3672-3685, 2005.
- Hamilton, K., An examination of observed Southern Oscillation effects in the Northern Hemisphere stratosphere, *J. Atmos. Sci.*, *50* (20), 3468-3473, 1993.
- Hansen, J., A. Lacis, R. Ruedy, and M. Sato, Potential climate impact of Mount Pinatubo eruption, *Geophys. Res. Lett.*, *19* (2), 215-218, doi: 10.1029/91GL02788, 1992.
- Hansen, J., M. Sato, R. Ruedy, L. Nazarenko, A. Lacis, G.A. Schmidt, G. Russell, I. Aleinov, M. Bauer, S. Bauer, N. Bell, B. Cairns, V. Canuto, M. Chandler, Y. Cheng, A. Del Genio, G. Faluvegi, E. Fleming, A. Friend, T. Hall, C. Jackman, M. Kelley, N. Kiang, D. Koch, J. Lean, J. Lerner, K. Lo, S. Menon, R. Miller, P. Minnis, T. Novakov, V. Oinas, Ja. Perlwitz, Ju. Perlwitz, D. Rind, A. Romanou, D. Shindell, P. Stone, S. Sun, N. Tausnev, D. Thresher, B. Wielicki, T. Wong, M. Yao, and S. Zhang, Efficacy of climate forcings, *J. Geophys. Res.*, *110*, D18104, doi: 10.1029/2005JD005776, 2005.
- Hare, S.H.E., L.J. Gray, W.A. Lahoz, A. O'Neill, and L. Steenman-Clark, Can stratospheric temperature trends be attributed to ozone depletion?, *J. Geophys. Res.*, *109*, D05111, doi: 10.1029/2003JD003897, 2004.
- Hartmann, D.L., J.M. Wallace, V. Limpasuvan, D.W.J. Thompson, and J.R. Holton, Can ozone depletion and global warming interact to produce rapid climate change?, *Proc. Natl. Acad. Sci.*, *97* (4), 1412-1417, 2000.
- Hatsushika, H., and K. Yamazaki, Stratospheric drain over Indonesia and dehydration within the tropical tropopause layer diagnosed by air parcel trajectories, *J. Geophys. Res.*, *108* (D19), 4610, doi: 10.1029/2002JD002986, 2003.
- Haynes, P.H., C.J. Marks, M.E. McIntyre, T.G. Shepherd, and K.P. Shine, On the "downward control" of extratropical diabatic circulations by eddy-induced mean zonal forces, *J. Atmos. Sci.*, *48* (4), 651-678, 1991.
- Hegglin, M.I., D. Brunner, T. Peter, J. Staehelin, V. Wirth, P. Hoor, and H. Fischer, Determination of eddy diffusivity in the lowermost stratosphere, *Geophys. Res. Lett.*, *32*, L13812, doi:10.1029/2005GL022495, 2005.
- Hoerling, M.P., J.W. Hurrell, and T. Xu, Tropical origins for recent North Atlantic climate change, *Science*, *292* (5514), 90-92, 2001.
- Hoerling, M.P., J.W. Hurrell, T. Xu, G.T. Bates, and A.S. Phillips, Twentieth century North Atlantic climate change. Part II: Understanding the effect of Indian Ocean warming, *Clim. Dyn.*, *23* (3-4), 391-405, 2004.
- Holton, J.R., and C. Mass, Stratospheric vacillation cycles, *J. Atmos. Sci.*, *33* (11), 2218-2225, 1976.
- Holton, J.R., and H.-C. Tan, The influence of the equatorial quasi-biennial oscillation on the global circulation at 50 mb, *J. Atmos. Sci.*, *37* (10), 2200-2208, 1980.
- Holton, J.R., and H.-C. Tan, The quasi-biennial oscillation in the Northern Hemisphere lower stratosphere, *J. Meteorol. Soc. Japan*, *60*, 140-148, 1982.
- Holton, J.R., P.H. Haynes, M.E. McIntyre, A.R. Douglass, R.B. Rood, and L. Pfister, Stratosphere-troposphere

CLIMATE-OZONE CONNECTIONS

- exchange, *Rev. Geophys.*, 33 (4), 403-440, 1995.
- Hoor, P., C. Gurk, D. Brunner, M.I. Hegglin, H. Wernli, and H. Fischer, Seasonality and extent of extratropical TST derived from in-situ CO measurements during SPURT, *Atmos. Chem. Phys.*, 4, 1427-1442, 2004.
- Hourdin, F., I. Musat, S. Bony, P. Braconnot, F. Codron, J.-L. Dufresne, L. Fairhead, M.-A. Filiberti, P. Friedlingstein, J.-Y. Grandpeix, G. Krinner, P. LeVan, Z.-X. Li, and F. Lott, The LMDZ4 general circulation model: Climate performance and sensitivity to parameterized physics with emphasis on tropical convection, *Clim. Dyn.*, 27 (7-8), 787-813, doi:10.1007/s00382-006-0158-0, 2006.
- Huck, P.E., A.J. McDonald, G.E. Bodeker, and H. Struthers, Interannual variability in Antarctic ozone depletion controlled by planetary waves and polar temperatures, *Geophys. Res. Lett.*, 32, L13819, doi: 10.1029/2005GL022943, 2005.
- Hurrell, J.W., Decadal trend in the North Atlantic Oscillation: Regional temperatures and precipitation, *Science*, 269 (5224), 676-679, 1995.
- Hurrell, J.W., M.P. Hoerling, A.S. Phillips, and T. Xu, Twentieth century North Atlantic climate change. Part I: assessing determinism, *Clim. Dyn.*, 23 (3-4), 371-389, 2004.
- IPCC (Intergovernmental Panel on Climate Change), *Emissions Scenarios. A Special Report of Working Group III of the Intergovernmental Panel on Climate Change*, edited by N. Nakicenovic and R. Swart, 570 pp., Cambridge University Press, Cambridge, U.K., and New York, N.Y., 2000.
- IPCC (Intergovernmental Panel on Climate Change), *Climate Change 2001: The Scientific Basis: Contribution of Working Group I to the Third Assessment Report of the Intergovernmental Panel on Climate Change*, edited by J.T. Houghton, Y. Ding, D.J. Griggs, M. Noguer, P.J. van der Linden, X. Dai, K. Maskell, and C.A. Johnson, 881 pp., Cambridge University Press, Cambridge, U.K., 2001.
- IPCC/TEAP (Intergovernmental Panel on Climate Change/Technology and Economic Assessment Panel), *IPCC/TEAP Special Report on Safeguarding the Ozone Layer and the Global Climate System: Issues Related to Hydrofluorocarbons and Perfluorocarbons*. Prepared by Working Group I and III of the IPCC, and the TEAP. Edited by B. Metz, L. Kuijpers, S. Solomon, S.O. Andersen, O. Davidson, J. Pons, D. de Jager, T. Kestin, M. Manning, and L.A. Meyers, 488 pp., Cambridge University Press, Cambridge, U.K. and New York, NY, USA, 2005.
- IPCC (Intergovernmental Panel on Climate Change), *Climate Change 2007: The Physical Science Basis*, in preparation, 2007.
- Jonsson, A.I., J. de Grandpré, V.I. Fomichev, J.C. McConnell, and S.R. Beagley, Doubled CO₂-induced cooling in the middle atmosphere: Photochemical analysis of the ozone radiative feedback, *J. Geophys. Res.*, 109, D24103, doi: 10.1029/2004JD005093, 2004.
- Jucks, K.W., D.G. Johnson, K.V. Chance, W.A. Traub, J.J. Margitan, G.B. Osterman, R.J. Salawitch, and Y. Sasano, Observations of OH, HO₂, H₂O, and O₃ in the upper stratosphere: Implications for HO_x photochemistry, *Geophys. Res. Lett.*, 25 (21), 3935-3938, 1998.
- K-1 Model Developers, *K-1 Coupled Model (MIROC) Description. K-1 Technical Report 1*, edited by H. Hasumi and S. Emori, 34 pp., Center for Climate System Research, University of Tokyo, Tokyo, Japan, 2004, (<http://www.ccsr.u-tokyo.ac.jp/kyosei/hasumi/MIROC/tech-repo.pdf>).
- Kiehl, J.T., J.J. Hack, G. Bonan, B.A. Boville, D. Williamson, and P. Rasch, The National Center for Atmospheric Research Community Climate Model: CCM3, *J. Clim.*, 11, 1131-1149, 1998.
- Kim, Y.-J., S.D. Eckermann, and H.-Y. Chun, An overview of the past, present and future of gravity-wave drag parameterization for numerical climate and weather prediction models, *Atmos. Ocean*, 41 (1), 65-98, 2003.
- Kindem, I.T., and B. Christiansen, Tropospheric response to stratospheric ozone loss, *Geophys. Res. Lett.*, 28 (8), 1547-1550, 2001.
- Kirk-Davidoff, D.B., E.J. Hintsa, J.G. Anderson, and D.W. Keith, The effect of climate change on ozone depletion through changes in stratospheric water vapour, *Nature*, 402 (6760), 399-401, 1999.
- Kodera, K., Solar cycle modulation of the North Atlantic Oscillation: Implication in the spatial structure of the NAO, *Geophys. Res. Lett.*, 29 (8), 1218, doi: 10.1029/2001GL014557, 2002.
- Kodera, K., Solar influence on the Indian Ocean Monsoon through dynamical processes, *Geophys. Res. Lett.*, 31, L24209, doi: 10.1029/2004GL020928, 2004.
- Kodera, K., and Y. Kuroda, Dynamical response to the solar cycle, *J. Geophys. Res.*, 107 (D24), 4749, doi: 10.1029/2002JD002224, 2002.
- Kushner, P.J., and L.M. Polvani, Stratosphere-troposphere coupling in a relatively simple AGCM: The role of eddies, *J. Clim.*, 17 (3), 629-639, 2004.
- Labitzke, K., Sunspots, the QBO and the stratospheric temperature in the north polar region, *Geophys. Res.*

- Lett.*, 14 (5), 535-537, 1987.
- Labitzke, K., and H. van Loon, Associations between the 11-year solar cycle, the QBO, and the atmosphere, Part I: Troposphere and stratosphere in the Northern Hemisphere in winter, *J. Atmos. Terr. Phys.*, 50, 197-206, 1988.
- Lal, M., A.K. Jain, and M.C. Sinha, Possible climatic implications of depletion of Antarctic ozone, *Tellus*, 39B, 326-328, 1987.
- Lambert, S.J., and J.C. Fyfe, Changes in winter cyclone frequencies and strengths simulated in enhanced greenhouse warming experiments: Results from the models participating in the IPCC diagnostic exercise, *Clim. Dyn.*, 26 (7-8), 713-728, doi: 10.1007/s00382-006-0110-3, 2006.
- Langematz, U., M. Kunze, K. Krüger, K. Labitzke, and G.L. Roff, Thermal and dynamical changes of the stratosphere since 1979 and their link to ozone and CO₂ changes, *J. Geophys. Res.*, 108 (D1), 4027, doi: 10.1029/2002JD002069, 2003.
- Lanzante, J.R., S.A. Klein, and D.J. Seidel, Temporal homogenization of monthly radiosonde temperature data. Part I: Methodology, *J. Clim.*, 16 (2), 224-240, 2003a.
- Lanzante, J.R., S.A. Klein, and D.J. Seidel, Temporal homogenization of monthly radiosonde temperature data. Part II: Trends, sensitivities, and MSU comparisons, *J. Clim.*, 16 (2), 241-262, 2003b.
- Limpasuvan, V., and D.L. Hartmann, Wave-maintained annular modes of climate variability, *J. Clim.*, 13 (24), 4414-4429, 2000.
- Limpasuvan, V., D.L. Hartmann, D.W.J. Thompson, K. Jeev, and Y.L. Yung, Stratosphere-troposphere evolution during polar vortex intensification, *J. Geophys. Res.*, 110, D24101, doi: 10.1029/2005JD006302, 2005.
- Lindzen, R.S., and J.R. Holton, A theory of the Quasi-Biennial Oscillation, *J. Atmos. Sci.*, 25 (6), 1095-1107, 1968.
- Lorenz, D.J., and D.L. Hartmann, Eddy-zonal flow feedback in the Southern Hemisphere, *J. Atmos. Sci.*, 58 (21), 3312-3327, 2001.
- Lorenz, D.J., and D.L. Hartmann, Eddy-zonal flow feedback in the Northern Hemisphere winter, *J. Clim.*, 16 (8), 1212-1227, 2003.
- Luers, J.K., and R.E. Eskridge, Use of radiosonde temperature data in climate studies, *J. Clim.*, 11 (5), 1002-1019, 1998.
- Manzini, E., B. Steil, C. Brühl, M.A. Giorgetta, and K. Krüger, A new interactive chemistry climate model: 2. Sensitivity of the middle atmosphere to ozone depletion and increase in greenhouse gases and implications for recent stratospheric cooling, *J. Geophys. Res.*, 108 (D14), 4429, doi: 10.1029/2002JD002977, 2003.
- Manzini, E., M.A. Giorgetta, M. Esch, L. Kornblueh, and E. Roeckner, The influence of sea surface temperatures on the Northern winter stratosphere: Ensemble simulations with the MAECHAM5 model, *J. Clim.*, 19, 3863-3881, 2006.
- Marshall, G.J., P.A. Stott, J. Turner, W.M. Connolley, J.C. King, and T.A. Lachlan-Cope, Causes of exceptional atmospheric circulation changes in the Southern Hemisphere, *Geophys. Res. Lett.*, 31, L14205, doi: 10.1029/2004GL019952, 2004.
- Martin, G.M., C. Dearden, C. Greeves, T. Hinton, P. Inness, P. James, V.D. Pope, M.A. Ringer, R.A. Stratton, and G.Y. Yang, *Evaluation of the Atmospheric Performance of HadGAM/GEM1*. Hadley Centre Technical Note No. 54, Hadley Centre for Climate Prediction and Research/Met Office, Exeter, U.K., 2004, (<http://www.metoffice.gov.uk/research/hadleycentre/pubs/HCTN/index.html>).
- Matthes, K., U. Langematz, L.L. Gray, K. Kodera, and K. Labitzke, Improved 11-year solar signal in the Freie Universität Berlin Climate Middle Atmosphere Model (FUB-CMAM), *J. Geophys. Res.*, 109, D06101, doi: 10.1029/2003JD004012, 2004.
- Matthes, K., Y. Kuroda, K. Kodera, and U. Langematz, Transfer of the solar signal from the stratosphere to the troposphere: Northern winter, *J. Geophys. Res.*, 111, D06108, doi: 10.1029/2005JD006283, 2006.
- Mayr, H.G., J.G. Mengel, C.L. Wolff, and H.S. Porter, QBO as potential amplifier of solar cycle influence, *Geophys. Res. Lett.*, 33, L05812, doi: 10.1029/2005GL025650, 2006.
- McIntyre, M.E., How well do we understand the dynamics of stratospheric warmings?, *J. Meteorol. Soc. Japan*, 60 (1), 37-65, 1982.
- McLandress, C., and J.F. Scinocca, The GCM response to current parameterizations of nonorographic gravity wave drag, *J. Atmos. Sci.*, 62 (7), 2394-2413, 2005.
- Mears, C.A., M.C. Schabel, and F.J. Wentz, A reanalysis of the MSU Channel 2 tropospheric temperature record, *J. Clim.*, 16 (22), 3650-3664, 2003.
- Meijer, E.W., B. Bregman, A. Segers, and P.F.J. van Velthoven, The influence of data assimilation on the age of air calculated with a global chemistry-transport model using ECMWF wind fields, *Geophys. Res. Lett.*, 31, L23114, doi: 10.1029/2004GL021158, 2004.
- Nash, J., Extension of explicit radiance observations by the Stratospheric Sounding Unit into the lower

CLIMATE-OZONE CONNECTIONS

- stratosphere and lower mesosphere, *Quart. J. Roy. Meteorol. Soc.*, *114*, 1153-1171, 1988.
- Newman, P.A., S.R. Kawa, and E.R. Nash, On the size of the Antarctic ozone hole, *Geophys. Res. Lett.*, *31*, L21104, doi: 10.1029/2004GL020596, 2004.
- Notholt, J., B.P. Luo, S. Fueglistaler, D. Weisenstein, M. Rex, M.G. Lawrence, H. Bingemer, I. Wohltmann, T. Corti, T. Warneke, R. von Kuhlmann, and T. Peter, Influence of tropospheric SO₂ emissions on particle formation and the stratospheric humidity, *Geophys. Res. Lett.*, *32*, L07810, doi: 10.1029/2004GL022159, 2005.
- Oltmans, S.J., H. Vömel, D.J. Hofmann, K.H. Rosenlof, and D. Kley, The increase in stratospheric water vapor from balloonborne frostpoint hygrometer measurements at Washington D.C., and Boulder, Colorado, *Geophys. Res. Lett.*, *27* (21), 3453-3456, 2000.
- Osterman, G.B., R.J. Salawitch, B. Sen, G.C. Toon, R.A. Stachnik, H.M. Pickett, J.J. Margitan, J.-F. Blavier, and D.B. Peterson, Balloon-borne measurements of stratospheric radicals and their precursors: Implications for the production and loss of ozone, *Geophys. Res. Lett.*, *24* (9), 1107-1110, 1997.
- Pan, L.L., W.J. Randel, B.L. Gary, M.J. Mahoney, and E.J. Hints, Definitions and sharpness of the extratropical tropopause: A trace gas perspective, *J. Geophys. Res.*, *109*, D23103, doi: 10.1029/2004JD004982, 2004.
- Pawson, S., K. Labitzke, and S. Leder, Stepwise changes in stratospheric temperature, *Geophys. Res. Lett.*, *25* (12), 2157-2160, 1998.
- Perlwitz, J., and H.-F. Graf, Troposphere-stratosphere dynamic coupling under strong and weak polar vortex conditions, *Geophys. Res. Lett.*, *28* (2), 271-274, doi: 10.1029/2000GL012405, 2001.
- Perlwitz, J., and N. Harnik, Downward coupling between the stratosphere and troposphere: The relative roles of wave and zonal mean processes, *J. Clim.*, *17* (24), 4902-4909, 2004.
- Pitari, G., E. Mancini, V. Rizi, and D.T. Shindell, Impact of future climate and emission changes on stratospheric aerosols and ozone, *J. Atmos. Sci.*, *59* (3), 414-440, 2002.
- Polvani, L.M., and P.J. Kushner, Tropospheric response to stratospheric perturbations in a relatively simple general circulation model, *Geophys. Res. Lett.*, *29* (7), 1114, doi: 10.1029/2001GL014284, 2002.
- Ramaswamy, V., M.-L. Chanin, J. Angell, J. Barnett, D. Gaffen, M. Gelman, P. Keckhut, Y. Koshelkov, K. Labitzke, J.-J.R. Lin, A. O'Neill, J. Nash, W. Randel, R. Rood, K. Shine, M. Shiotani, and R. Swinbank, Stratospheric temperature trends: Observations and model simulations, *Rev. Geophys.*, *39* (1), 71-122, 2001.
- Ramaswamy, V., M.D. Schwarzkopf, W.J. Randel, B.D. Santer, B.J. Soden, and G.L. Stenchikov, Anthropogenic and natural influences in the evolution of lower stratospheric cooling, *Science*, *311* (5764), 1138-1141, doi: 10.1126/science.1122587, 2006.
- Randel, W.J., and F. Wu, Biases in stratospheric and tropospheric temperature trends derived from historical radiosonde data, *J. Clim.*, *19*, 2094-2104, 2006.
- Randel, W.J., F. Wu, S.J. Oltmans, K. Rosenlof, and G.E. Nedoluha, Interannual changes of stratospheric water vapor and correlations with tropical tropopause temperatures, *J. Atmos. Sci.*, *61* (17), 2133-2148, 2004a.
- Randel, W., P. Udelhofen, E. Fleming, M. Geller, M. Gelman, K. Hamilton, D. Karoly, D. Ortland, S. Pawson, R. Swinbank, F. Wu, M. Baldwin, M. Chanin, P. Keckhut, K. Labitzke, E. Remsberg, A. Simmons, and D. Wu, The SPARC intercomparison of middle-atmosphere climatologies, *J. Clim.*, *17* (5), 986-1003, 2004b.
- Randel, W.J., F. Wu, H. Vömel, G.E. Nedoluha, and P. Forster, Decreases in stratospheric water vapor after 2001: Links to changes in the tropical tropopause and the Brewer-Dobson circulation, *J. Geophys. Res.*, *111*, D12312, doi: 10.1029/2005JD006744, 2006.
- Randeniya, L.K., P.F. Vohralik, and I.C. Plumb, Stratospheric ozone depletion at northern mid latitudes in the 21st century: The importance of future concentrations of greenhouse gases nitrous oxide and methane, *Geophys. Res. Lett.*, *29* (4), 1051, doi: 10.1029/2001GL014295, 2002.
- Remsberg, E.E., and L.E. Deaver, Interannual, solar cycle, and trend terms in middle atmospheric temperature time series from HALOE, *J. Geophys. Res.*, *110*, D06106, doi: 10.1029/2004JD004905, 2005.
- Rex, M., R.J. Salawitch, P. von der Gathen, N.R.P. Harris, M.P. Chipperfield, and B. Naujokat, Arctic ozone loss and climate change, *Geophys. Res. Lett.*, *31*, L04116, doi: 10.1029/2003GL018844, 2004.
- Rind, D., J. Lerner, and C. McLinden, Changes of tracer distributions in the doubled CO₂ climate, *J. Geophys. Res.*, *106* (D22), 28061-28080, doi: 10.1029/2001JD000439, 2001.
- Rind, D., J. Lerner, J. Perlwitz, C. McLinden, and M. Prather, Sensitivity of tracer transports and stratospheric ozone to sea surface temperature patterns in the doubled CO₂ climate, *J. Geophys. Res.*, *107* (D24), 4800, doi: 10.1029/2002JD002483, 2002a.
- Rind, D., P. Lonergan, N.K. Balachandran, and D. Shindell,

- 2 x CO₂ and solar variability influences on the troposphere through wave-mean flow interactions, *J. Meteorol. Soc. Japan*, 80 (4B), 863-876, 2002b.
- Rind, D., J. Perlwitz, and P. Lonergan, AO/NAO response to climate change: 1. Respective influences of stratospheric and tropospheric climate changes, *J. Geophys. Res.*, 110, D12107, doi: 10.1029/2004JD005103, 2005a.
- Rind, D., J. Perlwitz, P. Lonergan, and J. Lerner, AO/NAO response to climate change: 2. Relative importance of low- and high-latitude temperature changes, *J. Geophys. Res.*, 110, D12108, doi: 10.1029/2004JD005686, 2005b.
- Robock, A., Volcanic eruptions and climate, *Rev. Geophys.*, 38 (2), 191-219, 2000.
- Roeckner, E., G. Bäuml, L. Bonaventur, R. Brokopf, M. Esch, M. Giorgetta, S. Hagemann, I. Kirchner, L. Kornblueh, E. Manzini, A. Rhodin, U. Schlese, U. Schulzweida, and A. Tompkins, *The Atmospheric General Circulation Model ECHAM5: Part I, Model Description. Max Planck Institute for Meteorology Report 349*, 127 pp., Max Planck Institute for Meteorology, Bundesstrasse, Hamburg, Germany, 2003.
- Roscoe, H.K., The risk of large volcanic eruptions and the impact of this risk on future ozone depletion, *Nat. Hazards*, 23 (2-3), 231-246, 2001.
- Rosenfield, J.E., Effects of volcanic eruptions on stratospheric ozone recovery, in *Volcanism and the Earth's Atmosphere*, edited by A. Robock, and C. Oppenheimer, *Geophysical Monograph 139*, American Geophysical Union, 227-236, 2003.
- Rosenfield, J.E., A.R. Douglass, and D.B. Considine, The impact of increasing carbon dioxide on ozone recovery, *J. Geophys. Res.*, 107 (D6), 4049, doi: 10.1029/2001JD000824, 2002.
- Rosenlof, K.H., S.J. Oltmans, D. Kley, J.M. Russell III, E.-W. Chiou, W.P. Chu, D.G. Johnson, K.K. Kelly, H.A. Michelsen, G.E. Nedoluha, E.E. Remsberg, G.C. Toon, and M.P. McCormick, Stratospheric water vapor increases over the past half-century, *Geophys. Res. Lett.*, 28 (7), 1195-1198, 2001.
- Rozanov, E.V., M.E. Schlesinger, N.G. Andronova, F. Yang, S.L. Malyshev, V.A. Zubov, T.A. Egorova, and B. Li, Climate/chemistry effects of the Pinatubo volcanic eruption simulated by the UIUC stratosphere/troposphere GCM with interactive photochemistry, *J. Geophys. Res.*, 107 (D21), 4594, doi: 10.1029/2001JD000974, 2002.
- Santer, B.D., T.M.L. Wigley, C. Doutriaux, J.S. Boyle, J.E. Hansen, P.D. Jones, G.A. Meehl, E. Roeckner, S. Sengupta, and K.E. Taylor, Accounting for the effects of volcanoes and ENSO in comparisons of modeled and observed temperature trends, *J. Geophys. Res.*, 106 (D22), 28033-28059, 2001.
- Santer, B.D., M.F. Wehner, T.M.L. Wigley, R. Sausen, G.A. Meehl, K.E. Taylor, C. Ammann, J. Arblaster, W.M. Washington, J.S. Boyle, and W. Brüggemann, Contributions of anthropogenic and natural forcing to recent tropopause height changes, *Science*, 301 (5632), 479-483, doi: 10.1126/science.1084123, 2003.
- Santer, B.D., T.M.L. Wigley, A.J. Simmons, P.W. Kållberg, G.A. Kelly, S.M. Uppala, C. Ammann, J.S. Boyle, W. Brüggemann, C. Doutriaux, M. Fiorino, C. Mears, G.A. Meehl, R. Sausen, K.E. Taylor, W.M. Washington, M.F. Wehner, and F.J. Wentz, Identification of anthropogenic climate change using a second-generation reanalysis, *J. Geophys. Res.*, 109, D21104, doi: 10.1029/2004JD005075, 2004.
- Santer, B.D., T.M.L. Wigley, C. Mears, F.J. Wentz, S.A. Klein, D.J. Seidel, K.E. Taylor, P.W. Thorne, M.F. Wehner, P.J. Gleckler, J.S. Boyle, W.D. Collins, K.W. Dixon, C. Doutriaux, M. Free, Q. Fu, J.E. Hansen, G.S. Jones, R. Ruedy, T.R. Karl, J.R. Lanzante, G.A. Meehl, V. Ramaswamy, G. Russell, and G.A. Schmidt, Amplification of surface temperature trends and variability in the tropical atmosphere, *Science*, 309 (5740), 1551-1556, doi: 10.1126/science.1114867, 2005.
- Santer, B.D., J.E. Penner, and P.W. Thorne, How well can the observed vertical temperature changes be reconciled with our understanding of the causes of these changes?, in *Temperature Trends in the Lower Atmosphere: Steps for Understanding and Reconciling Differences*, A Report by the U.S. Climate Change Science Program and the Subcommittee on Global Change Research, edited by T.R. Karl, S.J. Hassol, C.D. Miller, and W.L. Murray, 89-118, NOAA, National Climatic Data Center, Asheville, North Carolina, USA, 2006.
- Sassi, F., D. Kinnison, B.A. Boville, R.R. Garcia, and R. Roble, Effect of El Niño-Southern Oscillation on the dynamical, thermal, and chemical structure of the middle atmosphere, *J. Geophys. Res.*, 109, D17108, doi: 10.1029/2003JD004434, 2004.
- Scaife, A.A., J. Austin, N. Butchart, S. Pawson, M. Keil, J. Nash, and I.N. James, Seasonal and interannual variability of the stratosphere diagnosed from UKMO TOVS analyses, *Quart. J. Roy. Meteorol. Soc.*, 126 (568), 2585-2604, 2000.
- Scaife, A.A., J.R. Knight, G.K. Vallis, and C.K. Folland, A stratospheric influence on the winter NAO and North Atlantic surface climate, *Geophys. Res. Lett.*,

CLIMATE-OZONE CONNECTIONS

- 32, L18715, doi: 10.1029/2005GL023226, 2005.
- Scheele, M.P., P.C. Siegmund, and P.F.J. van Velthoven, Stratospheric age of air computed with trajectories based on various 3D-Var and 4D-Var data sets, *Atmos. Chem. Phys.*, 5, 1-7, 2005.
- Schmidt, G.A., R. Ruedy, J.E. Hansen, I. Aleinov, N. Bell, M. Bauer, S. Bauer, B. Cairns, V. Canuto, Y. Cheng, A. DelGenio, G. Faluvegi, A.D. Friend, T.M. Hall, Y. Hu, M. Kelley, N.Y. Kiang, D. Koch, A.A. Lacis, J. Lerner, K.K. Lo, R.L. Miller, L. Nazarenko, V. Oinas, Ja. Perlwitz, Ju. Perlwitz, D. Rind, A. Romanou, G.L. Russell, M. Sato, D.T. Shindell, P.H. Stone, S. Sun, N. Tausnev, D. Thresher, and M.-S. Yao, Present day atmospheric simulations using GISS ModelE: Comparison to in-situ, satellite and reanalysis data, *J. Clim.*, 19, 153-192, 2006.
- Schneider, T., The tropopause and the thermal stratification in the extratropics of a dry atmosphere, *J. Atmos. Sci.*, 61 (12), 1317-1340, 2004.
- Schoeberl, M.R., A.R. Douglass, Z. Zhu, and S. Pawson, A comparison of lower stratospheric age spectra derived from a general circulation model and two data assimilation systems, *J. Geophys. Res.*, 108 (D3), 4113, doi: 10.1029/2002JD002652, 2003.
- Schoeberl, M.R., A.R. Douglass, B. Polansky, C. Boone, K.A. Walker, and P. Bernath, Estimation of stratospheric age spectrum from chemical tracers, *J. Geophys. Res.*, 110, D21303, doi: 10.1029/2005JD006125, 2005.
- Scott, R.K., and L.M. Polvani, Stratospheric control of upward wave flux near the tropopause, *Geophys. Res. Lett.*, 31, L02115, doi: 10.1029/2003GL017965, 2004.
- Scott, R.K., and L.M. Polvani, Internal variability of the winter stratosphere. Part I: Time independent forcing, *J. Atmos. Sci.*, 63 (11), 2758-2776, doi: 10.1175/JAS3797.1, 2006.
- Scott, R.K., D.G. Dritschel, L.M. Polvani, and D.W. Waugh, Enhancement of Rossby wave breaking by steep potential vorticity gradients in the winter stratosphere, *J. Atmos. Sci.*, 61 (8), 904-918, 2004.
- Seidel, D.J., and J.R. Lanzante, An assessment of three alternatives to linear trends for characterizing global atmospheric temperature changes, *J. Geophys. Res.*, 109, D14108, doi: 10.1029/2003JD004414, 2004.
- Seidel, D.J., R.J. Ross, J.K. Angell, and G.C. Reid, Climatological characteristics of the tropical tropopause as revealed by radiosondes, *J. Geophys. Res.*, 106 (D8), 7857-7878, 2001.
- Seidel, D.J., J.K. Angell, J. Christy, M. Free, S.A. Klein, J.R. Lanzante, C. Mears, D. Parker, M. Schabel, R. Spencer, A. Sterin, P. Thorne, and F. Wentz, Uncertainty in signals of large-scale climate variations in radiosonde and satellite upper-air temperature datasets, *J. Clim.*, 17 (11), 2225-2240, 2004.
- Sexton, D.M.H., The effect of stratospheric ozone depletion on the phase of the Antarctic Oscillation, *Geophys. Res. Lett.*, 28 (19), 3697-3700, 2001.
- Shaw, T.A., and T.G. Shepherd, Angular momentum conservation and gravity wave drag parameterization: Implications for climate models, *J. Atmos. Sci.*, 64 (1), 190-203, 2007.
- Shepherd, T.G., Issues in stratosphere-troposphere coupling, *J. Meteorol. Soc. Japan*, 80 (4B), 769-792, 2002.
- Sherwood, S.C., and A.E. Dessler, A model for transport across the tropical tropopause, *J. Atmos. Sci.*, 58 (7), 765-779, 2001.
- Shibata, K., H. Yoshimura, M. Ohizumi, M. Hosaka, and M. Sugi, A simulation of troposphere, stratosphere and mesosphere with an MRI/JMA98 GCM. Papers in *Meteorol. Geophys.*, 50, 15-53, 1999. (Available from Meteorological Research Institute, Nagamine 1-1, Tsukuba, Ibaraki, 305-0052, Japan.)
- Shindell, D.T., Climate and ozone response to increased stratospheric water vapor, *Geophys. Res. Lett.*, 28 (8), 1551-1554, 2001.
- Shindell, D., and G.A. Schmidt, Southern Hemisphere climate response to ozone changes and greenhouse gas increases, *Geophys. Res. Lett.*, 31, L18209, doi: 10.1029/2004GL020724, 2004.
- Shindell, D.T., D. Rind, N. Balachandran, J. Lean, and P. Lonergan, Solar cycle variability, ozone, and climate, *Science*, 284 (5412), 305-308, 1999.
- Shindell, D.T., G.A. Schmidt, R.L. Miller, and D. Rind, Northern Hemisphere winter climate response to greenhouse gas, ozone solar and volcanic forcing, *J. Geophys. Res.*, 106 (D7), 7193-7210, 2001.
- Shine, K.P., M.S. Bourqui, P.M.F. Forster, S.H.E. Hare, U. Langematz, P. Braesicke, V. Grewe, M. Ponater, C. Schnadt, C.A. Smith, J.D. Haigh, J. Austin, N. Butchart, D.T. Shindell, W.J. Randel, T. Nagashima, R.W. Portmann, S. Solomon, D.J. Seidel, J. Lanzante, S. Klein, V. Ramaswamy, and M.D. Schwarzkopf, A comparison of model-simulated trends in stratospheric temperatures, *Quart. J. Roy. Meteorol. Soc.*, 129 (590), 1565-1588, 2003.
- Sigmond, M., P.C. Siegmund, E. Manzini, and H. Kelder, A simulation of the separate climate effects of middle-atmospheric and tropospheric CO₂ doubling, *J. Clim.*, 17 (12), 2352-2367, 2004.
- Smith, A.K., An investigation of resonant waves in a numer-

- ical model of an observed sudden stratospheric warming, *J. Atmos. Sci.*, 46 (19), 3038-3054, 1989.
- Solomon, S., R.W. Portmann, T. Sasaki, D.J. Hofmann, and D.W.J. Thompson, Four decades of ozonesonde measurements over Antarctica, *J. Geophys. Res.*, 110, D21311, doi: 10.1029/2005JD005917, 2005.
- Song, Y., and W.A. Robinson, Dynamical mechanisms for stratospheric influences on the troposphere, *J. Atmos. Sci.*, 61 (14), 1711-1725, 2004.
- SPARC (Stratospheric Processes And their Role in Climate), *SPARC Assessment of Upper Tropospheric and Stratospheric Water Vapour*, edited by D. Kley, J.M. Russell III, and C. Phillips, *World Climate Research Program Report 113*, SPARC Report No. 2, 312 pp., Verrières le Buisson, France, 2000.
- SPARC (Stratospheric Processes And their Role in Climate), *SPARC Assessment of Stratospheric Aerosol Properties (ASAP)*, edited by L. Thomason, and Th. Peter, *World Climate Research Program Report 124*, SPARC Report No. 4, 346 pp., Verrières le Buisson, France, 2006.
- Steinbrecht, W., H. Claude, U. Köhler, and K.P. Hoinka, Correlations between tropopause height and total ozone: Implications for long-term changes, *J. Geophys. Res.*, 103 (D15), 19183-19192, 1998.
- Stenchikov, G., I. Kirchner, A. Robock, H.-F. Graf, J.C. Artuña, R.G. Grainger, A. Lambert, and L. Thomason, Radiative forcing from the 1991 Mount Pinatubo volcanic eruption, *J. Geophys. Res.*, 103 (D12), 13837-13857, 1998.
- Stenchikov, G.L., A. Robock, V. Ramaswamy, M.D. Schwarzkopf, K. Hamilton, and S. Ramachandran, Arctic Oscillation response to the 1991 Mount Pinatubo eruption: Effects of volcanic aerosols and ozone depletion, *J. Geophys. Res.*, 107 (D24), 4803, doi: 10.1029/2002JD002090, 2002.
- Stenke, A., and V. Grewe, Simulation of stratospheric water vapor trends: impact on stratospheric ozone chemistry, *Atmos. Chem. Phys.*, 5, 1257-1272, 2005.
- Stohl, A., H. Wernli, P. James, M. Bourqui, C. Forster, M.A. Liniger, P. Seibert, and M. Sprenger, A new perspective of stratosphere-troposphere exchange, *Bull. Amer. Meteorol. Soc.*, 84 (11), 1565-1573, 2003.
- Sudo, K., M. Takahashi, and H. Akimoto, Future changes in stratosphere-troposphere exchange and their impacts on future tropospheric ozone simulations, *Geophys. Res. Lett.*, 30 (24), 2256, doi: 10.1029/2003GL018526, 2003.
- Tabazadeh, A., M.L. Santee, M.Y. Danilin, H.C. Pumphrey, P.A. Newman, P.J. Hamill, and J.L. Mergenthaler, Quantifying denitrification and its effect on ozone recovery, *Science*, 288 (5470), 1407-1411, 2000.
- Taguchi, M., and D.L. Hartmann, Increased occurrence of stratospheric sudden warmings during El Niño as simulated by WACCM, *J. Clim.*, 19 (3), 324-332, 2006.
- Tett, S.F.B., G.S. Jones, P.A. Stott, D.C. Hill, J.F.B. Mitchell, M.R. Allen, W.J. Ingram, T.C. Johns, C.E. Johnson, A. Jones, D.L. Roberts, D.M.H. Sexton, and M.J. Woodage, Estimation of natural and anthropogenic contributions to twentieth century temperature change, *J. Geophys. Res.*, 107 (D16), 4306, doi: 10.1029/2000JD000028, 2002.
- The GFDL Global Atmospheric Model Development Team (GAMDT), The new GFDL global atmosphere and land model AM2-LM2: Evaluation with prescribed SST simulations. *J. Clim.*, 17, 4641-4673, 2004.
- Thomason, L.W., S.P. Burton, N. Iyer, J.M. Zawodny, and J. Anderson, A revised water vapor product for the Stratospheric Aerosol and Gas Experiment (SAGE) II version 6.2 data set, *J. Geophys. Res.*, 109, D06312, doi: 10.1029/2003JD004465, 2004.
- Thompson, D.W.J., and S. Solomon, Interpretation of recent Southern Hemisphere climate change, *Science*, 296 (5569), 895-899, 2002.
- Thompson, D.W.J., and S. Solomon, Recent stratospheric climate trends as evidenced in radiosonde data: Global structure and tropospheric linkages, *J. Clim.*, 18 (22), 4785-4795, 2005.
- Thompson, D.W.J., and J.M. Wallace, The Arctic Oscillation signature in the wintertime geopotential height and temperature fields, *Geophys. Res. Lett.*, 25 (9), 1297-1300, 1998.
- Thompson, D.W.J., and J.M. Wallace, Annular modes in the extratropical circulation. Part I: Month-to-month variability, *J. Clim.*, 13 (5), 1000-1016, 2000.
- Thompson, D.W.J., J.M. Wallace, and G.C. Hegerl, Annular modes in the extratropical circulation. Part II: Trends, *J. Clim.*, 13 (5), 1018-1036, 2000.
- Thompson, D.W.J., J.C. Furtado, and T.G. Shepherd, On the tropospheric response to anomalous stratospheric wave drag and radiative heating, *J. Atmos. Sci.*, 63 (10), 2616-2629, 2006.
- Thorne, P.W., P.D. Jones, T.J. Osborn, T.D. Davies, S.F.B. Tett, D.E. Parker, P.A. Stott, G.S. Jones, and M.R. Allen, Assessing the robustness of zonal mean climate change detection, *Geophys. Res. Lett.*, 29 (19), 1920, doi: 10.1029/2002GL015717, 2002.
- Thuburn, J., and G.C. Craig, On the temperature structure of the tropical stratosphere, *J. Geophys. Res.*, 107 (D2), 4017, doi:10.1029/2001JD000448, 2002.

CLIMATE-OZONE CONNECTIONS

- Tian, W., and M.P. Chipperfield, A new coupled chemistry-climate model for the stratosphere: The importance of coupling for future O₃-climate prediction, *Quart. J. Roy. Meteorol. Soc.*, 131 (605), 281-303, 2005.
- Tie, X., and G. Brasseur, The response of stratospheric ozone to volcanic eruptions: Sensitivity to atmospheric chlorine loading, *Geophys. Res. Lett.*, 22 (22), 3035-3038, 1995.
- Tilmes, S., R. Müller, J.-U. Grooß, and J.M. Russell III, Ozone loss and chlorine activation in the Arctic winters 1991-2003 derived with the tracer-tracer correlations, *Atmos. Chem. Phys.*, 4, 2181-2213, 2004.
- Timmreck, C., H.-F. Graf, and B. Steil, Aerosol chemistry interactions after the Mt. Pinatubo eruption, in *Volcanism and the Earth's Atmosphere*, edited by A. Robock and C. Oppenheimer, *Geophysical Monograph 139*, 214-225, American Geophysical Union, Washington, D.C., 2003.
- van Loon, H., and K. Labitzke, The Southern Oscillation, Part V: The anomalies in the lower stratosphere of the Northern Hemisphere in winter and a comparison with the Quasi-Biennial Oscillation, *Mon. Wea. Rev.*, 115 (2), 357-369, 1987.
- Varotsos, C., C. Cartalis, A. Vlamakis, C. Tzanis, and I. Keramitsoglou, The long-term coupling between column ozone and tropopause properties, *J. Clim.*, 17 (19), 3843-3854, 2004.
- Volodin, E.M., and V.Y. Galin, Interpretation of winter warming on Northern Hemisphere continents in 1977-94, *J. Clim.*, 12 (10), 2947-2955, 1999.
- Walter, B.P., and M. Heimann, A process-based, climate-sensitive model to derive methane emissions from natural wetlands: Application to five wetland sites, sensitivity to model parameters, and climate, *Global Biogeochem. Cycles*, 14 (3), 745-766, 2000.
- Walter, K., and H.-F. Graf, The North Atlantic variability structure, storm tracks, and precipitation depending on the polar vortex strength, *Atmos. Chem. Phys.*, 5, 239-248, 2005.
- Wennberg, P.O., R.C. Cohen, R.M. Stimpfle, J.P. Koplów, J.G. Anderson, R.J. Salawitch, D.W. Fahey, E.L. Woodbridge, E.R. Keim, R.S. Gao, C.R. Webster, R.D. May, D.W. Toohey, L.M. Avallone, M.H. Proffitt, M. Loewenstein, J.R. Podolske, K.R. Chan, and S.C. Wofsy, Removal of stratospheric O₃ by radicals: In situ measurements of OH, H₂O, NO, NO₂, ClO, and BrO, *Science*, 266 (5184), 398-404, 1994.
- Wennberg, P.O., T.F. Hanisco, L. Jaeglé, D.J. Jacob, E.J. Hints, E.J. Lanzendorf, J.G. Anderson, R.-S. Gao, E.R. Keim, S.G. Donnelly, L.A. Del Negro, D.W. Fahey, S.A. McKeen, R.J. Salawitch, C.R. Webster, R.D. May, R.L. Herman, M.H. Proffitt, J.J. Margitan, E.L. Atlas, S.M. Schauffler, F. Flocke, C.T. McElroy, and T.P. Bui, Hydrogen radicals, nitrogen radicals, and the production of O₃ in the upper troposphere, *Science*, 279 (5347), 49-53, 1998.
- Wigley, T.M.L., C.M. Amman, B.D. Santer, and S.C.B. Raper, Effect of climate sensitivity on the response to volcanic forcing, *J. Geophys. Res.*, 110, D09107, doi: 10.1029/2004JD005557, 2005.
- Wittman, M.A.H., L.M. Polvani, R.K. Scott, and A.J. Charlton, Stratospheric influence on baroclinic life-cycles and its connection to the Arctic Oscillation, *Geophys. Res. Lett.*, 31, L16113, doi: 10.1029/2004GL020503, 2004.
- WMO (World Meteorological Organization), *Scientific Assessment of Ozone Depletion: 1998, Global Ozone Research and Monitoring Project-Report No. 44*, Geneva, Switzerland, 1999.
- WMO (World Meteorological Organization), *Scientific Assessment of Ozone Depletion: 2002, Global Ozone Research and Monitoring Project-Report No. 47*, Geneva, Switzerland, 2003.
- Wu, D.L., Mesoscale gravity wave variances from AMSU-A radiances, *Geophys. Res. Lett.*, 31, L12114, doi: 10.1029/2004GL019562, 2004.
- Yokohata, T., S. Emori, T. Nozawa, Y. Tsusima, T. Ogura, and M. Kimoto, Climate response to volcanic forcing: Validation of climate sensitivity of a coupled atmosphere-ocean circulation model, *Geophys. Res. Lett.*, 32, L21710, doi: 10.1029/2005GL023542, 2005.
- Zeng, G., and J.A. Pyle, Changes in tropospheric ozone between 2000 and 2100 modeled in a chemistry-climate model, *Geophys. Res. Lett.*, 30 (7), 1392, doi: 10.1029/2002GL016708, 2003.
- Zhou, X.-L., M.A. Geller, and M. Zhang, Cooling trend of the tropical cold point tropopause temperatures and its implications, *J. Geophys. Res.*, 106 (D2), 1511-1522, 2001.
- Zhou, X.-L., M.A. Geller, and M. Zhang, Temperature fields in the tropical tropopause transition layer, *J. Clim.*, 17 (15), 2901-2908, 2004.

Appendix 5A

AOGCMs USED IN THIS CHAPTER

The coupled atmosphere-ocean general circulation models (AOGCMs) used in this chapter, and the country of the sponsoring organization. The model simulations were completed to support the Fourth Assessment Report of the Intergovernmental Panel on Climate Change (IPCC, in preparation for 2007). The models submitted 21st century simulations using the A2 (high) and B1 (low) emission scenarios. Also listed is the key reference for the atmospheric model, the approximate altitude in kilometers of the model top, and the number of stratospheric levels at or above 16 km. The experiments include various emission scenarios of the 20th and 21st century and focus on simulating the surface and tropospheric climate. The stratosphere of most of these models tends to be poorly resolved. While all models include changes in well-mixed greenhouse gases, other forcings such as changes in ozone, volcanic and other aerosols, and changes in solar radiation are only included in a subset of the models. This set of experiments was produced by 15 modeling groups from 9 countries and represents one of the most comprehensive international climate model efforts ever attempted.

Model	Key Reference	Model Top	Stratospheric Levels
BCCR-BCM2.0, Norway	Déqué et al., 1994	33	5
CCSM3, USA	Collins et al., 2004	40	7
CGCM3.1(T47), Canada	Flato, 2005	49	11
CNRM-CM3, France	Déqué et al., 1994	76	17
CSIRO-Mk3.0, Australia	Gordon et al., 2002	38	3
ECHAM5/MPI-OM, Germany	Roeckner et al., 2003	29	4
GFDL-CM2.0, USA	GFDL GAMDT, 2004	35	3
GFDL-CM2.1, USA	GFDL GAMDT, 2004	35	3
GISS-ER, USA	Schmidt et al., 2006	67	9
INM-CM3.0, Russia	Galim et al., 2003	32	6
IPSL-CM4, France	Hourdin et al., 2006	32	7
MIROC3.2-M, Japan	K-1 Developers, 2004	67	6
MRI-CGCM2.3.2, Japan	Shibata et al., 1999	54	8
PCM, USA	Kiehl et al., 1998	43	7
UKMO-HadGEM1, UK	Martin et al., 2004	39	10

CHAPTER 6

The Ozone Layer in the 21st Century

Lead Authors:

G.E. Bodeker
D.W. Waugh

Coauthors:

H. Akiyoshi
P. Braesicke
V. Eyring
D.W. Fahey
E. Manzini
M.J. Newchurch
R.W. Portmann
A. Robock
K.P. Shine
W. Steinbrecht
E.C. Weatherhead

Contributors:

J. Austin
S. Bekki
C. Brühl
N. Butchart
M. Chipperfield
M. Dameris
T. Egorova
V. Fioletov
A. Gettelman
M.A. Giorgetta
D. Kinnison
E. Mancini
M. Marchand
P.A. Newman
S. Pawson
G. Pitari
D. Plummer
B. Rognerud
E. Rozanov
R.J. Salawitch
T.G. Shepherd
K. Shibata
B.-M. Sinnhuber
M. Sinnhuber
S. Smyshlyaev
R. Stolarski
H. Struthers
W. Tian
G. Velders
D. Weisenstein
E.-S. Yang

CHAPTER 6

THE OZONE LAYER IN THE 21ST CENTURY

Contents

SCIENTIFIC SUMMARY	6.1
6.1 INTRODUCTION	6.5
6.2 A FRAMEWORK FOR EVALUATING CHANGES IN OZONE ABUNDANCES	6.5
6.2.1 Ozone Changes in the Near and Long Term	6.5
6.2.2 Stages in the Evolution of the Ozone Layer	6.6
6.2.3 Milestones in the Evolution of the Ozone Layer	6.7
6.2.4 Using Data and Models to Evaluate Ozone Milestones and Milestone Parameters	6.8
6.3 FACTORS AFFECTING THE DETECTION, ATTRIBUTION, AND TIMING OF MILESTONES	6.8
6.3.1 Stratospheric Halogen Loading	6.8
6.3.2 Atmospheric Chemical Composition	6.9
6.3.3 Stratospheric Temperatures	6.9
6.3.4 Atmospheric Transport	6.10
6.3.5 The Solar Cycle	6.10
6.3.6 Volcanic Eruptions	6.11
6.4 STATISTICAL METHODS FOR DETECTION OF MILESTONES	6.11
6.4.1 Change in Linear Trends	6.12
6.4.2 Cumulative Sum of Residuals	6.12
6.5 ATTRIBUTION OF THE RECENT BEHAVIOR OF OZONE	6.13
6.5.1 Upper Stratospheric Ozone	6.13
6.5.2 Lower Stratospheric and Total Column Ozone	6.15
6.5.3 Polar Ozone	6.18
6.6 PROJECTIONS OF THE FUTURE BEHAVIOR OF OZONE	6.20
6.6.1 Model Descriptions and Scenarios	6.20
6.6.2 Model Evaluation	6.22
6.6.3 Midlatitude and Tropical Ozone	6.27
6.6.4 Polar Ozone	6.30
6.6.4.1 The Antarctic	6.31
6.6.4.2 The Arctic	6.33
6.6.5 Uncertainties in Model Projections and Open Questions	6.36
REFERENCES	6.37
APPENDIX 6A: MODEL SCENARIOS	6.43

SCIENTIFIC SUMMARY

Global ozone levels are now no longer declining as they were from the late 1970s until the mid-1990s, and some increases in ozone have been observed. These improvements in the ozone layer have occurred during a period when stratospheric halogen abundances reached their peak and started to decline. These declining halogen abundances clearly reflect the success of the Montreal Protocol and its Amendments and Adjustments in controlling the global production and consumption of ozone-depleting substances (ODSs).

Stratospheric ozone abundances are affected by a number of natural and anthropogenic factors in addition to the atmospheric abundance of ODSs, e.g., temperatures, transport, volcanoes, solar activity, and hydrogen and nitrogen oxides (Chapter 3). Separating the effects of these factors is complex because of nonlinearities and feedbacks in the atmospheric processes affecting ozone. For the purposes of this Assessment, we consider specifically the recovery of ozone from the effects of ODSs, because the primary audience is the group of Parties to the Montreal Protocol, whose purview is ozone-depleting compounds. In this Assessment, the metric used to gauge the overall burden of ozone-depleting halogens in the stratosphere from the ODSs is equivalent effective stratospheric chlorine (EESC).

The Process of Ozone Recovery from the Effects of ODSs

- In this Assessment, the recovery of ozone from depletion caused by increases in ODSs is discussed as a process involving three stages:
 - (i) The **slowing of ozone decline**, identified as the occurrence of a statistically significant reduction in the rate of decline in ozone due to changing EESC.
 - (ii) The **onset of ozone increases (turnaround)**, identified as the occurrence of statistically significant increases in ozone above previous minimum values due to declining EESC.
 - (iii) The **full recovery of ozone from ODSs**, identified as when ozone is no longer significantly affected by ODSs. In the absence of changes in the sensitivity of ozone to ODSs, this is likely to occur when EESC returns to pre-1980 levels.

The first two stages of recovery either have already occurred or are expected to occur within the next two decades. The third stage is expected to occur around the middle of the century. Because of changes in atmospheric composition and dynamics, this third stage may or may not be accompanied by the actual return of ozone to pre-1980 levels, and it is possible that ozone could return to 1980 levels before the effects of ODSs disappear.

- In reaching full recovery of ozone, the milestone of **the return of ozone to pre-1980 levels** is considered important because ozone was not significantly affected by ODSs prior to 1980. As a consequence, this milestone is useful, for example, to gauge when the adverse impacts of enhanced surface ultraviolet (UV) radiation on human health and ecosystems caused by ozone depletion are likely to become negligible. However, as mentioned above, the return of ozone to pre-1980 levels may not occur at the same time as the return of EESC to pre-1980 levels, and in fact may never occur because of changes in the atmosphere since 1980 that are not caused by ODSs. Therefore, this milestone alone cannot be used to identify the recovery of ozone from the effects of ODSs.

The Role of ODSs in Recent Ozone Trends

- **The slowing of the decline and leveling off of midlatitude upper stratospheric (35-45 km) ozone over the past decade has very likely been dominated by changes in EESC.** Gas-phase chemistry, modulated by changes in temperature and other gases such as methane (CH₄), directly controls ozone in this region, and observed ozone changes are similar to those modeled from EESC decreases.
- **Over the past decade, changes in EESC have likely contributed to the slowing of the midlatitude total column ozone decline and the leveling off of ozone.** However, evidence suggests that changes in transport have also played an important role, particularly in the lowermost stratosphere, making attribution of specific ozone changes to EESC more complicated. For northern midlatitudes, increases in ozone have been greater than expected from

21st CENTURY OZONE LAYER

EESC decreases alone, while over southern midlatitudes the observed ozone changes are broadly consistent with the expectations from EESC decreases alone.

- **Inside the Antarctic vortex, the interannual variations in ozone depletion observed from 2001 to 2005 have not been caused by changes in EESC.** At current EESC concentrations, nearly total loss of ozone occurs in the lowermost stratosphere inside the ozone hole in September and October, and EESC concentrations often exceed those necessary to cause total loss. The Antarctic ozone hole, therefore, has low sensitivity to moderate decreases in EESC and the unusually small ozone holes in some recent years (e.g., 2002 and 2004) are strongly attributable to a dynamically driven warmer Antarctic stratosphere.
- **In the collar region of the Antarctic vortex (60°S-70°S), where ozone destruction is not complete, reductions in EESC have likely contributed to the slowing of ozone decline observed over the past decade.** However, uncertainty in the estimation of EESC in the collar region and the ozone response to temperature changes confound the attribution of observed ozone changes to reductions in EESC.
- **The decline in EESC has not caused the large interannual variations observed in Arctic ozone depletion.** Indeed there has been no detection of any ozone recovery stages in the Arctic. The large interannual variations in ozone are driven by changes in meteorology and are likely to delay the detection of the first stage of recovery.

Expected Future Changes in Ozone

Two-dimensional (2-D) models and three-dimensional (3-D) coupled Chemistry-Climate Models (CCMs), both of which have achieved significant successes in simulating many or nearly all of the factors that affect ozone and their feedbacks, have been used to project the evolution of ozone throughout the 21st century. The evolution of tropical and midlatitude ozone was examined in all models. CCMs are generally believed to better represent key processes relating to three-dimensional transport in the polar regions and, therefore, only CCMs were used for polar regions. The projected total column ozone was examined for three periods:

- (i) The beginning of the century (2000-2020), when EESC is expected to start decreasing or continue to decrease
- (ii) Mid-century (2040-2050 in extrapolar regions, 2060-2070 in polar regions), when EESC is expected to reach and fall below 1980 values
- (iii) End of the century (2090-2100), when changes in factors other than ODSs are expected to control changes in stratospheric ozone

Because modeled changes in column ozone to 2100 are not specifically attributable to changes in EESC, ozone column amounts when EESC returns to pre-1980 levels and the timing of the return of ozone to pre-1980 levels are examined in the model projections.

- **The CCMs used to project future ozone abundances have been critically evaluated, and more emphasis has been given to those models that best represent the processes known to strongly affect column ozone abundances.** The CCMs vary in their skill in representing different processes and characteristics of the atmosphere. However, there is sufficient agreement between the majority of the CCMs and the observations that some confidence can be placed in their projections.

BEGINNING OF THE CENTURY

- **Averaged between 60°S and 60°N, total column ozone is projected to increase in all models between 2000 and 2020, with most of the increase of 1 to 2.5% occurring after 2010.** The small interannual variability shown in 2-D models allows more precise identification of key ozone change dates compared with CCMs that show large interannual variability, similar to that seen in observations. Nonetheless, both the 2-D models and CCMs suggest that minimum total column ozone values have already occurred in this latitude region.

- **Over the Antarctic, most CCMs predict column ozone increases in spring of around 5 to 10% between 2000 and 2020. Different diagnostics of ozone depletion show different sensitivities to EESC.** The most rapid change (decrease) occurs in the ozone mass deficit and the slowest change (increase) in ozone minimum values and October ozone anomalies. Minimum ozone values remain roughly constant between 2000 and 2010 in many models. The projected onset of decreases in the ozone mass deficit occurs between 2000 and 2005, whereas the projected onset of increases in minimum Antarctic ozone does not occur until after 2010 in many models.
- **Over the Arctic, most CCMs predict that springtime column ozone in 2020 will be 0 to 10% above 2000 levels and that ozone turnaround in the Arctic will occur before 2020.** Over the Arctic, the large interannual variability in the CCM projections obscures the year when the ozone turnaround due to decreasing EESC occurs.

MID-CENTURY

- **Averaged between 60°S and 60°N, total column ozone is projected to be close to or above 1980 values when EESC in that region of the stratosphere declines to 1980 values (2040-2050).** This occurs in nearly all models that include coupling between well-mixed greenhouse gases (WMGHGs; carbon dioxide (CO₂), methane (CH₄), and nitrous oxide (N₂O)) and temperature (interactive 2-D models and the CCMs). Thus, outside polar regions, ozone is projected to reach 1980 values at about the same time or before EESC returns to 1980 values.
- **Two-dimensional models that include coupling between WMGHGs and temperature (interactive 2-D models) predict that column ozone averaged over 60°S to 60°N will in general exceed 1980 values up to 15 years earlier than models that do not include these feedbacks (non-interactive 2-D models).** This suggests that the earlier return to 1980 values is caused mainly by response to stratospheric cooling linked to increased WMGHGs. The response results from the temperature dependence of the gas-phase photochemistry of ozone. In some non-interactive 2-D models, column ozone never increases to 1980 values throughout the 21st century in some regions.
- **Over the Antarctic, most models predict that ozone amounts will increase to 1980 values close to the time when Antarctic EESC decreases to 1980 values.** That time is later than at midlatitudes due to the delay associated with transport of stratospheric air to polar regions. A new empirical model, based on observations, indicates a return of Antarctic EESC to 1980 values between 2060 and 2075.
- **Over the Arctic, CCMs show ozone values exceeding 1980 values before EESC decreases to 1980 values, with ozone increasing to 1980 values between 2020 and 2040.** The increases in ozone do not follow the decreases in EESC as closely as in the Antarctic, and in the majority of CCMs Arctic ozone exceeds 1980 values before the Antarctic. There is no indication of future severe reductions in Arctic column ozone in any of the model simulations. There is large uncertainty in projections of Arctic ozone because of the smaller ozone depletion and the larger interannual variability in the Arctic stratosphere in comparison with the Antarctic.

END OF THE CENTURY

- **Averaged between 60°S and 60°N, total column ozone is projected to be around 2 to 5% above 1980 values between 2090 and 2100.** This result is obtained in all 2-D models that include coupling between WMGHGs and temperature and in one CCM that extends to 2100. This CCM predicts that from 2090 to 2100, Arctic ozone will be substantially above 1980 values, while Antarctic ozone will be close to or just below 1980 values.
- **Projected ozone amounts in 2100 are sensitive to future levels of WMGHGs.** For example, expected future increases in N₂O will increase stratospheric nitrogen oxides (NO_x), which may exacerbate ozone depletion. However, the expected stratospheric cooling induced by increasing concentrations of greenhouse gases, primarily CO₂, is expected to slow gas-phase ozone depletion reactions and, thereby, increase ozone. The net effect on ozone amounts will depend on future levels of the different WMGHGs. The importance of this temperature feedback is demonstrated by the non-interactive 2-D models, which predict that extrapolar column ozone will be less than or near 1980 values through the latter half of the century.

6.1 INTRODUCTION

It is now clear that the depletion of the ozone layer, both globally and in the polar regions, is attributable to an atmospheric halogen burden that is strongly enhanced compared with natural levels by anthropogenic emissions of ozone-depleting substances (ODSs). Over the past decade, as a consequence of adherence to the Montreal Protocol and its Amendments and Adjustments, equivalent effective stratospheric chlorine (EESC; see Chapter 8), a commonly used measure of the stratospheric halogen burden, has peaked and begun to decline (Chapter 1). However, owing to the long lifetime of the most important halogen source gases, the removal of ODSs from the atmosphere will take many decades even with continued compliance with the Montreal Protocol (Chapter 8). Ozone is expected to continue to respond to these changes in ODSs but the timing and sensitivity of the response will depend on other changes in the atmosphere, e.g., increases in well-mixed greenhouse gases (WMGHGs) that have occurred since the onset of significant ozone depletion in 1980.

Chapters 3 and 4 discuss ozone changes observed to date and interpret the underlying causes of the changes, while Chapter 5 examines the mechanisms connecting ozone depletion with climate change. This chapter builds on the material presented in these three chapters, with a focus on two overarching themes:

- (1) Analysis of recent ozone measurements for the first signs of ozone recovery attributable to decreasing ODS concentrations
- (2) Projections of how the global ozone layer will evolve during the 21st century and how this evolution will depend on ODSs and other concomitant changes in the atmosphere

The first of these two themes uses the observational time series presented in Chapters 3 and 4 to assess whether ozone recovery (defined in Section 6.2) has been detected. The interpretation of observations presented in the two earlier chapters is extended by applying different statistical tools (Section 6.4) to the detection of the first stage of ozone recovery, i.e., a slowing of the ozone decline attributable to decreasing ODSs. This chapter also examines when increases in ozone due to decreases in ODSs are likely to occur, i.e., the second stage in the ozone recovery process.

The second theme builds on the discussion of the feedbacks between ozone depletion and climate change presented in Chapter 5. A group of two-dimensional (2-D) models and coupled Chemistry-Climate Models (CCMs), incorporating climate feedback processes, is used

to predict the evolution of the ozone layer throughout the 21st century. While Chapter 5 discusses ozone depletion/climate change interactions, this chapter uses models to investigate the effects of those interactions and addresses how they may affect the evolution of ozone throughout this century. The resulting ozone projections are then used in Chapter 7 to show how surface clear-sky ultraviolet (UV) radiation is expected to change in the future.

Section 6.2 describes the framework for assessing ozone changes through the 21st century. Specifically it discusses the time scales of the expected changes, stages in the recovery process and the milestones defining those stages. Section 6.3 includes a discussion of how factors other than ODSs affect the detection and timing of milestones in the ozone recovery process and the attribution to changing EESC. Section 6.4 presents how least squares regression models (also discussed in Chapter 3) can be used to evaluate the role of ODSs and other factors in ozone recovery. The interpretation of recent observations of ozone in the context of ozone recovery is presented in Section 6.5. The longer-term perspective of the evolution of global ozone through the 21st century is provided in Section 6.6, where the results from the 2-D models and CCMs are assessed.

6.2 A FRAMEWORK FOR EVALUATING CHANGES IN OZONE ABUNDANCES

In considering the ozone layer in the 21st century, two topics are prominent in the scientific and policy communities. The first is obtaining evidence as soon as possible that the ozone layer is responding to the decline in EESC. As ODSs are removed from the atmosphere, the destruction of ozone attributed to ODSs is also expected to decline. The second topic is the projection of changes that might occur in the ozone layer by mid-century and by the end of the century. By approximately mid-century, substantial or full recovery of the ozone layer is expected globally. By the end of the century, other changes in atmospheric chemistry and transport become a prominent consideration in projected ozone amounts. Here, we have adopted a specific framework, described below, to evaluate changes in ozone over the recent past and until the end of the century. This framework is conceptual in design and is intended to encompass both ozone changes that have already occurred as well as potential future changes.

6.2.1 Ozone Changes in the Near and Long Term

The discussion of ozone changes in the 21st century is divided into those in the “near term,” which includes

21st CENTURY OZONE LAYER

the recent past, the present day, and the first decades of the century, and those in the “long term,” which includes the remaining decades of this century. In the near term, when ozone observations and model simulations can be compared, the first changes in the ozone layer attributable to the ongoing removal of ODSs can be detected. In contrast, changes in the last decades of this century can only be discussed as model projections and, hence, are associated with large uncertainties.

Within each time period, the analyses of ozone changes will focus separately on changes that occur, for example, in global average total column ozone, midlatitude and tropical column ozone, as well as springtime polar ozone amounts. The role of ODSs in ozone changes is of particular importance, but the role of other factors, such as changes in abundances of other gases and of sulfate aerosols, stratospheric temperatures, atmospheric transport, solar output, and volcanic emissions, will also be carefully examined (see Section 6.3). Without a compre-

hensive examination of all factors that significantly influence ozone amounts, the contribution of ODSs cannot be quantified with sufficient confidence.

6.2.2 Stages in the Evolution of the Ozone Layer

Ozone changes in the 21st century are expected to encompass the period of the “recovery” of ozone from the influence of ODSs that have been released in anthropogenic activities. ODSs have led to the decline in global ozone amounts, with measurable changes beginning in the 1980s and the largest changes found in the winter/spring polar stratospheres (see Chapters 3 and 4). The total abundance of ODSs is in decline in the troposphere and stratosphere as a result of the effective actions undertaken as part of the Montreal Protocol (see Chapter 1). The start of the decline in EESC marks the conceptual start of the ozone recovery process. The continued analysis of ozone measurements

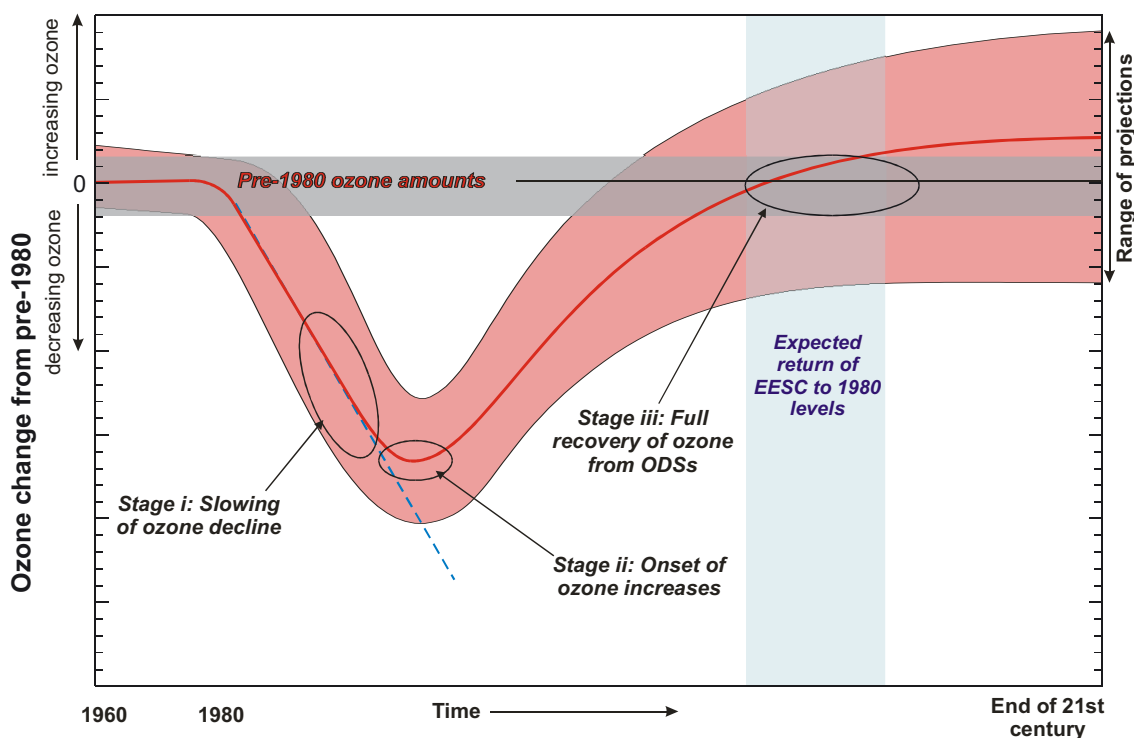


Figure 6-1. A schematic diagram of the temporal evolution of global ozone amounts beginning with pre-1980 values, which represent amounts before significant depletion due to anthropogenic ODS emissions, and stopping at the end of the 21st century. Observed and expected ozone amounts (solid red line) show depletion from pre-1980 values and the three stages of recovery from this depletion (see Section 6.2). The red-shaded region represents the range of observations and model results for both near-term and long-term ozone changes. The blue-shaded region represents the time period when declining global ODS concentrations are expected to reach 1980 values. The full recovery of ozone from ODSs may be delayed beyond the return of ODSs to 1980 levels by factors (e.g., a volcanic eruption close to that time) that could change the sensitivity of ozone to ODSs.

during the 21st century is expected to reveal and confirm three key stages in the recovery process:

- (i) The **slowing of ozone decline**, identified as the occurrence of a statistically significant reduction in the rate of decline in ozone due to changing EESC
- (ii) The **onset of ozone increases (turnaround)**, identified as the occurrence of statistically significant increases in ozone above previous minimum values due to declining EESC
- (iii) The **full recovery of ozone from ODSs**, identified as when ozone is no longer affected by ODSs. In the absence of changes in the sensitivity of ozone to ODSs, this is likely to occur when EESC returns to pre-1980 levels

As illustrated in Figure 6-1, the first two stages of recovery are expected to occur in the near term and the last stage in the long-term future. These three stages apply to both total column ozone and ozone at a specific altitude. However, the timing of the stages may be different for these different measures of ozone. Documenting how and when each of these stages of ozone layer recovery is reached will be of interest to both the scientific and policy communities.

The focus of this chapter is how, and to what extent, observed and projected changes in ozone during the recovery process will be attributable to changes in ODSs and to other contributing factors as noted above.

The role of contributing factors in the recovery process is important because the physical and chemical environment of the atmosphere has changed significantly since the onset of observable ozone depletion in the 1980s. A key aspect of ozone recovery is whether or not ozone abundances in stage (iii) will be greater than or less than

those present in 1980 before significant depletion by ODSs occurred. As shown in Figure 6-1, projections of ozone abundances show a range of values during the full recovery stage because of uncertainties in the role of contributing factors in controlling ozone in the coming decades. At present there is no standard definition of stages in the ozone recovery process and no standard framework that can be used to analyze ozone observations for signs of recovery. Authors of previous studies have used terms such as “recovery” with a range of different meanings. For example, not all studies have incorporated the concept of attribution in the definition of ozone recovery. The framework presented here with three defined stages of ozone recovery will provide a more rigorous basis for future analyses of ozone changes.

6.2.3 Milestones in the Evolution of the Ozone Layer

The stages of recovery outlined above apply to the overall response of the ozone layer. As an aid to monitoring and documenting each stage of recovery, *milestones* can be defined within the recovery stages. A milestone is a point in a recovery stage that a specific change in a specific ozone parameter can be said to have occurred. Milestones and milestone parameters reflect that ozone changes during the recovery process will vary with geographic region and altitude, following in large part the known variations and differences in ozone depletion. Primary geographic regions are the Antarctic and Arctic regions, midlatitudes, and the tropics. Primary altitude regions are the upper and lower stratosphere. Table 6-1 summarizes a number of possible milestone parameters, some of which will be discussed in the following sections.

Table 6-1. Examples of milestone parameters in ozone recovery stages.

Stratospheric Region	Milestone Parameters
Antarctic during winter/early spring (60°S-90°S)	Daily minimum column ozone values Minimum values of the ozone partial column between 12 and 20 km above the South Pole Area of the 220 DU contour of the ozone hole Vortex average daily ozone mass deficit Seasonal trend in average column ozone
Arctic during winter/early spring (60°N-90°N)	Daily minimum column ozone values Seasonal trend in average column ozone
Midlatitudes (35°-60°)	Trend in column ozone Trend in upper stratospheric column ozone (35-45 km) Trend in lower stratospheric ozone (15-20 km)
Tropics (25°N-25°S)	Trend in column ozone

21st CENTURY OZONE LAYER

Milestone parameters are all quantifiable from observational datasets. A milestone derives directly from a parameter by choosing a quantitative threshold or limit value. Reaching or passing a milestone then has a quantitative and statistical basis that can be objectively evaluated. For example, milestones derive easily from parameters associated with trends in Table 6-1:

Milestone 1: the year(s) when the negative ozone trends seen in the 1980s and 1990s begin to weaken (related to Stage (i))

Milestone 2: the year(s) that there is a trend reversal (related to Stage (ii))

Milestone 3: the year(s) that EESC returns to pre-1980 values

Milestone 4: the year(s) that the parameter reaches pre-1980 values (related to Stage (iii))

Clearly, many milestones can be defined using the parameters listed and the expectations of the stages of ozone recovery as outlined above and as temporally displayed in Figure 6-1. Of greatest interest and importance are those milestones that primarily result from changes in ODS amounts, that will occur soonest, and that will have the largest statistical significance using available observational datasets. Also of interest are those milestones that can be simulated in global models of ozone recovery using known changes in ODSs.

6.2.4 Using Data and Models to Evaluate Ozone Milestones and Milestone Parameters

The principal tools to evaluate ozone milestone parameters are statistical analyses of ozone observations, the results of global models for past ozone amounts, and the model projections of future amounts. Observational time series are available from multiple sources, including satellite-, ground-, aircraft-, and balloon-based instruments. Each has a role in documenting ozone parameters over time in profile and column amounts, and each has value in establishing accurate ozone trends. Statistical tools are required to derive ozone trends because ozone amounts are subject to significant natural variability throughout the available time series and the quality of ozone data is not uniform. The variability arises because ozone amounts reflect transport as well as chemical production and loss processes that are affected by a wide range of factors as noted in Sections 6.2.1 and 6.3, and Section 3.4 of Chapter 3.

Models and statistical methods are key tools in the attribution of changes in milestone parameters to the various controlling factors. Statistical analyses of time series

are used to derive trends and their uncertainties (see Chapter 3). Photochemical box models constrained by observations of chemical composition are useful for quantifying the role of ODS changes in observed parameter changes. More complex models are needed to address global ozone changes caused by the full range of contributing factors; namely, changes in atmospheric composition, stratospheric temperatures, atmospheric transport, solar output, and volcanic emissions. Those relied upon in this Assessment are 2-D models and CCMs. Descriptions of these models are provided in Chapter 5 while the role of each model in this chapter is detailed in the following sections. An important challenge for these models is to represent the atmospheric processes sufficiently well that observed changes can be understood and attribution of changes can be discussed. A large source of uncertainty in model projections of ozone is the scenarios that must be adopted by the models to account for changes in atmospheric parameters related to climate change.

6.3 FACTORS AFFECTING THE DETECTION, ATTRIBUTION, AND TIMING OF MILESTONES

In this section we discuss to what extent different factors contributing to the variability in stratospheric ozone are likely to affect the detection, attribution, and timing of milestones. A major issue is the variability in ozone induced by these factors that masks or resembles the expected ozone change due to halogen loading (see Figure 3-1 of Chapter 3). For projections over the rest of the century, the issue is how factors other than ODSs may change the expected increases in ozone from decreasing halogen loading.

6.3.1 Stratospheric Halogen Loading

The evolution of stratospheric halogen loading is an obvious factor impacting ozone. Correctly estimating stratospheric halogen loading is important for attributing observed changes in ozone to decreases in EESC. The global mean EESC from WMO (2003) is generally used in such studies. However, if the estimated EESC is incorrect or not appropriate for the region being considered, then the attribution or inferred timing of a milestone may be incorrect. Possible causes of incorrect EESC include using an inappropriate mean age of air, neglecting mixing processes in the atmosphere (i.e., neglect of age spectra), or incorrectly accounting for the bromine contribution (see Chapter 1). The effect of errors in EESC estimation is most likely largest for the detection of milestones in polar regions, where the EESC from WMO (2003) peaks too

early and decays too rapidly because of the older mean age of air in polar regions and the neglect of the age spectra (see Newman et al., 2006, and the figure in Box 8-1 of Chapter 8).

Future stratospheric halogen concentrations will depend on future emissions of ODSs and on transport into and through the stratosphere. Model simulations suggest that increases in WMOGHGs (carbon dioxide (CO₂), nitrous oxide (N₂O), and methane (CH₄)) may lead to an increased stratospheric circulation and to reduced transport time scales (e.g., Butchart and Scaife, 2001; Butchart et al., 2006; Section 5.3.3 of Chapter 5). A reduction in transport time scales will result in a reduction of EESC, which could affect the timing of long-term milestones.

6.3.2 Atmospheric Chemical Composition

Apart from changing ODSs, changes in other gases could affect the evolution of ozone and the timing of ozone recovery by changing the background chemical composition of the atmosphere. In particular, increases in gases producing radicals that catalytically destroy ozone (e.g., N₂O, CH₄, molecular hydrogen (H₂), and water (H₂O)) are likely to change ozone. As discussed in Section 6.3.3, temperature changes due to WMOGHGs are also important. Section 1.4 of Chapter 1 discusses the possible long-term changes in gases other than ODSs that may affect ozone and Section 6.6 discusses model estimates of ozone evolution based on emission scenarios of these gases.

Catalytic ozone loss in the stratosphere occurs from the reactive nitrogen (NO_x), hydrogen (HO_x), oxygen (O_x), chlorine (ClO_x), and bromine (BrO_x) families. Ozone loss through these families is strongly altitude and latitude dependent (see Figure 1.11 of IPCC/TEAP, 2005), with NO_x dominating in the middle stratosphere (approximately 25-40 km), and HO_x dominating in the lower and upper stratosphere. Under conditions of high chlorine loading, ClO_x is important in the upper stratosphere (peak impact near 40 km) and in regions where heterogeneous reaction rates are large, such as in the polar regions during spring. However, in many regions of the stratosphere, these changes are strongly buffered by induced changes on the other chemical families, which can reduce the primary impact (Nevison et al., 1999). For example, NO_x increases in the lower stratosphere cause decreases in HO_x and ClO_x catalyzed losses, along with increases in “tropospheric” ozone production mechanisms. In the middle stratosphere, NO_x induced changes are reduced by interactions with chlorine species. On the other hand, in some cases coupling between different chemical processes can amplify the effects of source gas emissions, e.g., nitrogen dioxide (NO₂) concentrations over southern midlatitudes have

risen at approximately twice the rate of its source gas N₂O as a result of changes in ozone (Section 3.3.2 of Chapter 3; McLinden et al., 2001).

Another compositional change that could affect ozone is a change in stratospheric water vapor. An increase in water vapor would increase HO_x and thus cause ozone decreases in the upper and lower stratosphere (Kirk-Davidoff et al., 1999; Dvortsov and Solomon, 2001), although these changes are reduced by complex buffering interactions. In the polar regions, increases in water vapor would cause an increase in heterogeneous reaction rates (e.g., hydrogen chloride (HCl) plus chlorine nitrate (ClONO₂)) and an increase in the surface areas of polar stratospheric cloud (PSC) particles. Both effects are likely to lead to an increase in chlorine activation and ozone loss. The effects of water vapor increases on ozone (via HO_x), induced by increases in methane, are partially offset by the reaction of methane with atomic chlorine, which deactivates ClO_x and reduces ClO_x-driven ozone loss (this could be important throughout the stratosphere). The coupling of water vapor and methane with ClO_x induced ozone loss will be eliminated by decreasing ODS levels during the 21st century.

While the Assessment does not deal with tropospheric ozone per se, it should be noted that increases in tropospheric ozone in some regions might have masked stratospheric decreases (such as in the tropics, where stratospheric decreases are relatively small). In such regions, total column ozone measurements cannot be used for detection and attribution of recovery milestones, and vertical ozone profile data are required. Vertically resolved observations in the stratosphere allow separation of regions controlled by ODSs and those dominated by transport (see Section 6.5).

6.3.3 Stratospheric Temperatures

As discussed in Chapter 5, the rates of chemical reactions, and the formation of PSCs, depend on temperature. Thus, changes in temperature can have a large influence on ozone. Temperature changes need to be accounted for when attributing observed ozone variations to changes in halogen loading and when predicting future ozone levels. This is especially important for attribution in polar regions, where interannual variations in ozone are closely coupled to variations in polar temperatures; in the Arctic, ozone loss rates are related to the volume of PSCs (e.g., Rex et al., 2004), whereas in the Antarctic, the size of the ozone hole depends on the temperature in the vortex “collar region” (60°S-70°S) (e.g., Newman et al., 2004).

Future stratospheric temperatures are a major source of uncertainty when predicting future ozone levels.

21st CENTURY OZONE LAYER

They are a key parameter for the questions of whether and when ozone will return to pre-1980 levels. As discussed in Chapter 5, stratospheric temperatures depend on stratospheric dynamics, radiation, and composition. Future changes in temperature, and hence ozone, are not likely to be uniform throughout the stratosphere. Cooling due to increased CO₂ (and other WMGHGs), particularly in the upper stratosphere, is expected to slow gas-phase ozone loss reactions. When EESC decreases to pre-1980 levels, and if there are no other changes, the cooling will lead to an increase in ozone to values higher than in 1980. However, as noted in the previous subsection, increases in WMGHGs will also alter the chemical composition of the stratosphere and possibly the Brewer-Dobson circulation. These effects are also likely to affect ozone; see Section 6.6 for further discussion. The impact of stratospheric cooling on ozone might be the opposite in polar regions. Here, cooling could result in increases in PSCs, which, given enough halogens, would increase ozone loss.

6.3.4 Atmospheric Transport

Atmospheric transport is a major factor contributing to stratospheric ozone variability. Accounting for this variability is an important issue both for detecting and attributing ozone recovery milestones. As discussed in Chapters 3 and 4, changes in the stratospheric meridional circulation, in the stratospheric polar vortices, and in tropospheric weather systems, all have a strong influence on stratospheric ozone and can produce variability on a wide range of time scales. Some of these changes can be linked to waves propagating from the troposphere, but internal stratospheric dynamics also play a role.

The detection of recovery milestones is essentially a signal-to-noise ratio problem, and much of the “noise” in the ozone signal results from variability in transport. Geographical differences in the variability in ozone induced by this factor will affect where and when certain recovery milestones can best be detected. Alternatively, it determines the number of years of measurements required to detect a milestone. Reinsel et al. (2002) found that for midlatitudes (30°-60°), a statistically significant change in total column ozone trend can be detected with ~7-8 years of data following the period of linear decline, whereas detection of ozone turnaround (the second stage in the ozone recovery process) can require ~15-20 years for southern midlatitude zonal average column ozone and ~20-25 years for northern midlatitude zonal average column ozone. This result is in agreement with earlier findings (Weatherhead et al., 2000). Analyzing vertically resolved atmospheric regions is an effective technique to increase the signal-to-noise ratio because of the vertical

separation of the forcing functions (Yang et al., 2006; Weatherhead and Andersen, 2006).

Statistical regression models are often used to remove competing drivers of ozone variability in the attribution of ozone changes to ODSs. They are based on the assumption that proxies describing the dynamical state of the atmosphere and resultant effects on ozone can be provided as model basis functions. Commonly used dynamical proxies are equatorial zonal winds to capture the effects of the quasi-biennial oscillation (QBO), the Arctic Oscillation or Antarctic Oscillation (AO or AAO), the North Atlantic Oscillation (NAO), the El Niño Southern Oscillation (ENSO) index, and measures of wave activity (e.g., latitudinally averaged tropopause Eliassen-Palm fluxes). However, because such preselected proxies are not necessarily independent (they are not orthogonal within the regression model), the partitioning of the ozone variance among the different proxies by the model requires some interpretation. It is difficult to establish how much of the transport-driven ozone variability is appropriately accounted for. An alternative approach is to use idealized modeling studies to quantify the impact of different circulation regimes on ozone. For example, the magnitude of ozone changes related to a strong warm ENSO event was investigated by Brönnimann et al. (2004) and Pyle et al. (2005).

Changes in temperatures and transport not only complicate the detection and attribution of recovery milestones, they also affect ozone projections over the rest of this century (see Chapter 5).

6.3.5 The Solar Cycle

When attributing recent changes in stratospheric ozone to changes in ODSs, it is important to consider ozone variations related to the 11-year solar cycle because the timing of the most recent maximum in solar activity, between 1999 and 2003, was around the time when EESC peaked in the stratosphere. As discussed in Chapter 3, observations continue to indicate a statistically significant solar variation of ozone, with ozone in phase with solar activity. This suggests that an increase in solar activity during the 1999-2003 solar maximum will have contributed to the slowing of the decline and increase of ozone (e.g., Dameris et al., 2006). Proper attribution of the cause of the ozone changes in recent years requires the separation of ozone increases due to changes in solar irradiance from those due to changes in halogen levels. However, this is difficult, as the magnitude of the solar influence on ozone is somewhat uncertain.

The amplitude of ozone changes due to solar activity varies with altitude and latitude. In the upper strat-

osphere, ozone during solar maximum is 2 to 5% higher than in solar minimum, with an uncertainty around 2% (McCormack and Hood, 1996; Steinbrecht et al., 2004a; Figure 3-19 of Chapter 3). Sensitivity studies by Cunnold et al. (2004) indicate that current estimates of the solar cycle effect on ozone are probably sufficiently accurate to allow the separation of halogen decrease-related ozone increases from solar cycle effects in the upper stratosphere. Recent data from 2004 and 2005, i.e., from the beginning of the solar minimum, confirm this result (Steinbrecht et al., 2006a).

The situation is less clear for total column ozone. Depending on latitude and location, total column ozone is between 2 and 10 Dobson units (DU) higher during solar maximum, both in observations and model simulations, with uncertainty ranging from 2 to over 5 DU (McCormack et al., 1997; Steinbrecht et al., 2006b; Reinsel et al., 2005). One reason for this large uncertainty in the magnitude of the solar cycle variation in total ozone is the fact that the two solar maxima before 1999-2003 coincided with large volcanic eruptions. It is difficult to separate the impacts of eruptions and solar cycle on observed ozone (Solomon et al., 1996). There were no major volcanic eruptions during the 1999-2003 solar maximum. However, in this case, the ozone response is contaminated by the ozone changes related to the turnaround of ODSs, that we are trying to quantify. It is further unlikely that the solar cycle signal in ozone exactly follows the simple proxies used in most analyses, such as the Mg II core-to-wing ratio, 10.7 cm radio flux, or an 11-year harmonic function (Steinbrecht et al., 2004a,b). The response may inherently vary from one solar maximum to the next (Ruzmaikin et al., 2003). All of the above factors add uncertainty to estimates of ozone increases in all three past solar maxima. In particular, they complicate the separation of recent or near-term increases in ozone due to the EESC turnaround from increases due to the 1999 to 2003 solar maximum. It is likely that observations at least to the end of the next solar minimum in 2008 will be required to allow better separation of solar cycle effects from possible ozone increases due to decreases in EESC.

6.3.6 Volcanic Eruptions

As discussed in the previous Ozone Assessment (WMO, 2003) and in Chapter 5, volcanic eruptions can have a large impact on stratospheric ozone by changing heterogeneous chemistry, thermal structure, and circulation in the stratosphere. Because of this, it is necessary to consider volcanic eruptions both when interpreting observed changes and when making projections of future changes of ozone.

There have been no large volcanic eruptions since the 1991 Mt. Pinatubo eruption, and the stratospheric aerosol loading in the four years since the previous Ozone Assessment has remained at low, nonvolcanic levels. However, the impact of the Mt. Pinatubo eruption still needs to be considered when attributing changes in ozone in the last decade of the 20th century to changes in ODSs (or any other factor). The Mt. Pinatubo eruption contributed to a large decline in Northern Hemisphere ozone, which was followed by an increase in ozone as stratospheric aerosols decayed back to low, nonvolcanic levels. This decrease in aerosol levels occurred at around the same time that the growth in EESC slowed and reached its peak value. Both the changes in aerosols and EESC led to changes in ozone levels, and it is difficult to separate their impact on ozone.

If one or more large volcanoes erupt in the next 50 years, it is likely to impact the ozone recovery process. The overall impact of volcanic eruptions varies with halogen levels (see Chapter 5). Outside the polar regions, the primary effect of an increased rate of heterogeneous reactions is to cause a reduction of nitrogen oxides. In the current high-chlorine conditions, this causes an increase in reactive chlorine and increased ozone depletion, as observed following the Mt. Pinatubo eruption (Brasseur and Granier, 1992). However, in low-chlorine conditions, a large volcanic eruption could cause a small ozone increase due to the suppression of nitrogen oxides (e.g., Tie and Brasseur, 1995). Hence, a large, Pinatubo-like eruption within the next 20 years, when there will still be significant amounts of halogens in the stratosphere, may lead to an increase in ozone destruction by ODSs and a temporary delay in ozone recovery; whereas a similar eruption in the more distant future, when EESC has decreased to around or below 1980 values, may lead to an increase in ozone levels. In both cases, the exact impact will depend on the latitude and size of the volcanic eruption, and ozone may also be impacted by changes in the stratospheric thermal structure and circulation caused by the eruption.

6.4 STATISTICAL METHODS FOR DETECTION OF MILESTONES

Detection of recovery milestones, and in particular the detection of the onset of ozone recovery (i.e., a slowing of the ozone decline), cannot be achieved simply by examining raw measurement time series. Statistical methods are required to distill the subtle changes in trend from an observed ozone time series. Typically, multiple linear regression fits are used with various proxies accounting for different contributions to the ozone variation, which

have been described in Section 6.3. Autocorrelation in the residual time series also needs to be considered (Tiao et al., 1990). Several different approaches have been used on model output, total column data, and vertically resolved data, to test the last few years of data for an increase in values: the change in linear trend (“change-in-trend”) method (Reinsel et al., 2002), the multivariate adaptive regression splines method (Krzyścin et al., 2005), the flexible tendency method (Harris et al., 2001), or the cumulative sum of residuals (CUSUM) method (Reinsel, 2002; Newchurch et al., 2003). Each has its merits, offers slightly different information, and tests different hypotheses with the data. The change-in-trend and CUSUM approaches have been used extensively to examine recent data and test for early signs of changes in ozone trends. They are discussed in more detail below. Both of these methods assume linear trends in ozone between the start of the analysis period (usually 1980) and a selected “turnaround date” (usually 1996). Over this period, when EESC increased approximately linearly, the expectation is, therefore, that ozone loss is linearly proportional to EESC. This assumption has been shown to be valid over midlatitudes (Yang et al., 2006), over the Arctic (Douglass et al., 2006), and over the Antarctic when ozone destruction is incomplete (Jiang et al., 1996).

6.4.1 Change in Linear Trends

In the change-in-trend method (Reinsel et al., 2002), the standard least-squares regression model (see Chapter 3) is extended by adding a second basis function, set to zero before a selected turnaround date and proportional to time thereafter (Figure 6-2). The turnaround date is preselected and its choice can affect the results. Such a regression model gives an estimate of the magnitude of the trend before the turnaround date (m_1), the slope change at the turnaround date (m_2), and the magnitude of the trend after the specified turnaround date (m_1+m_2). The statistical significance of m_2 can be tested and a change-in-trend milestone is reached when m_2 is significantly different from zero at the 2σ level. This method assumes that the ozone record exhibits a discrete change from a downward trend to a less steep trend or an upward trend across the turnaround date (Reinsel et al., 2002). Calculations indicate that the actual shift from upward trend to downward trend in EESC may take a few years, but includes a near linear trend prior to the turnaround and a near linear trend for a few years after this turnaround (WMO, 2003). If the underlying trend in ozone follows this EESC pattern, the piecewise linear and contiguous approach may be appropriate. Each data point, in most cases monthly and regionally averaged data, is weighted

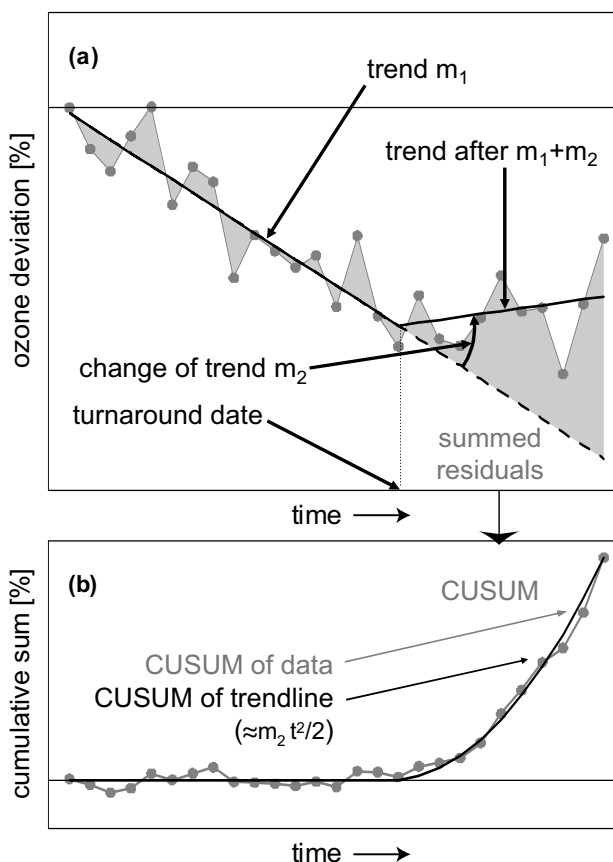


Figure 6-2. A schematic representation of (a) the change-in-trend method, and (b) the CUSUM method. See Section 6.4 for discussion.

by the square of the distance from the fit, resulting in large deviations having a strong influence on the final trend estimates. Anomalous years either near the turnaround or near the beginning or end of the record have particularly high leverage on the trend estimates.

6.4.2 Cumulative Sum of Residuals

The CUSUM approach (Reinsel, 2002; Newchurch et al., 2003) assumes that the data, after accounting for various non-ODS influences, follow a near-linear downward trend until some preselected specified date, analogous to the turnaround date of the change-in-trend method. After that date, all later data are evaluated to determine if they represent a likely deviation from that downward trend. This evaluation is made by examining the cumulative sum of residual deviations from the extrapolated trend after the specified point (see Figure 6-2). The choice of the turnaround date is not very important provided it is not too far from the physically appropriate point (e.g., the date at which EESC maximizes). In contrast to the change-in-

trend approach, CUSUM makes no assumptions about the temporal path of the deviation. Data shifts, gradual reductions in trend, and slow changes to an extrapolated trend are all detected. However, little information is provided on the temporal shape of a change. Because the cumulative sum of deviations is considered, as opposed to the minimum of the sum of the squares as in the change-in-trend method, highly unusual points are somewhat less influential. The explanatory variables, such as the QBO, solar cycle, and an underlying trend, are fit for the entire time series and removed from the data to create the monthly ozone residuals. These residuals are used to form the trend estimate calculated over the period up to the turnaround date and extrapolated thereafter for the CUSUM calculation.

The CUSUM approach detects arbitrary deviations from the extrapolated trend, whereas the change-in-trend method looks for a specific temporal path. Comparison between the change-in-trend and CUSUM approaches is possible using the fact that if there is a change of trend by m_2 per unit time, the CUSUM value after the turnaround increases with time approximately as $m_2 t^2/2$ (Yang et al., 2006). For example, a representative change of trend m_2 for total ozone at northern midlatitudes is 2 DU per year, or 0.166 DU per month (see Figure 6-4, panel b). When accumulated over 84 months from January 1997 to December 2004, this change of trend corresponds to a CUSUM value of 595 cumulative DU by the end of 2004. This compares very well with the CUSUMs given in panels (d) and (f) of Figure 6-3 for partial ozone columns. By the end of 2004, these CUSUMs amount to 250 and 350 DU, or 600 DU combined for the total column.

6.5 ATTRIBUTION OF THE RECENT BEHAVIOR OF OZONE

To attribute the recent changes in ozone to changes in ODSs, we require more than the observation of a slowing of the ozone decline or an increase in ozone. We require that the observed changes in ozone occur at approximately the right time to be associated with ODS concentrations, that the magnitude of change in ozone trend be of the appropriate magnitude expected due to changes in ODS concentrations, and that the latitudinal, altitudinal, and seasonal changes are in agreement with the changes expected due to a turnaround in ODS concentrations. Even if all of the above are observed, scientific judgment is involved in assessing whether the recent changes in ozone are appropriately linked with the changes in ODS concentrations. Scientific judgment in this assessment process takes into account statistical studies, a variety of models involving a range of appropriate assumptions, an under-

standing of the time scales of relevance in the atmosphere, possible uncertainties in mechanisms governing ozone concentrations, as well as uncertainties in available ozone measurements.

Attribution is fundamentally difficult because, as discussed in Section 6.3, many factors other than ODSs can affect ozone on time scales of a few years. The separation of these other factors from any underlying ODS signal in ozone is further complicated by the fact that the quantification of the many factors affecting ozone is uncertain, can be nonlinear, and involves feedbacks through a variety of mechanisms. Furthermore, attribution requires analyzing data with high natural variability and using models that cannot represent atmospheric processes at arbitrary degrees of spatial and temporal resolution. Several approaches have been used to assess whether the changes in ozone can be attributed to changes in ODSs. These include using statistical methods to separate effects of transport and temperature from chemical effects of ODSs, and modeling efforts to partition the past changes into those due to ODS changes and those due to known transport and temperature effects.

6.5.1 Upper Stratospheric Ozone

As described in Section 6.2, the first stage of the ozone recovery process is defined as a statistically significant deviation above the previous linear decline in ozone that must be attributable to changes in EESC. We expect that this stage of ozone recovery will be passed first in those regions of the atmosphere where ozone changes are most closely controlled by changes in EESC. One such region is the upper stratosphere, where the largest ozone decline due to gas-phase chemical reactions has been recorded (WMO, 2003) and where few factors other than gas-phase chemistry directly control ozone. Reinsel (2002) and Newchurch et al. (2003) showed that a statistically significant deviation in the ozone decline can be found in observations of ozone in this altitude region. This deviation is illustrated in Figure 6-3(a), which shows ozone residuals for northern midlatitudes and the altitude range from 35 to 45 km. Residuals were defined by subtracting the mean annual cycle and estimated variations due to the solar cycle and QBO. Up to about the end of 1996, ozone residuals closely followed a linear decline of approximately -7% per decade, and since then, this steep decline has not continued and ozone levels have been essentially constant or may have even increased. This behavior is quantified in Figure 6-3(b), where the CUSUMs from the extrapolated 1979 to 1996 trend are shown. The CUSUM increases with time since 1996, demonstrating that the residuals lie significantly above the

21st CENTURY OZONE LAYER

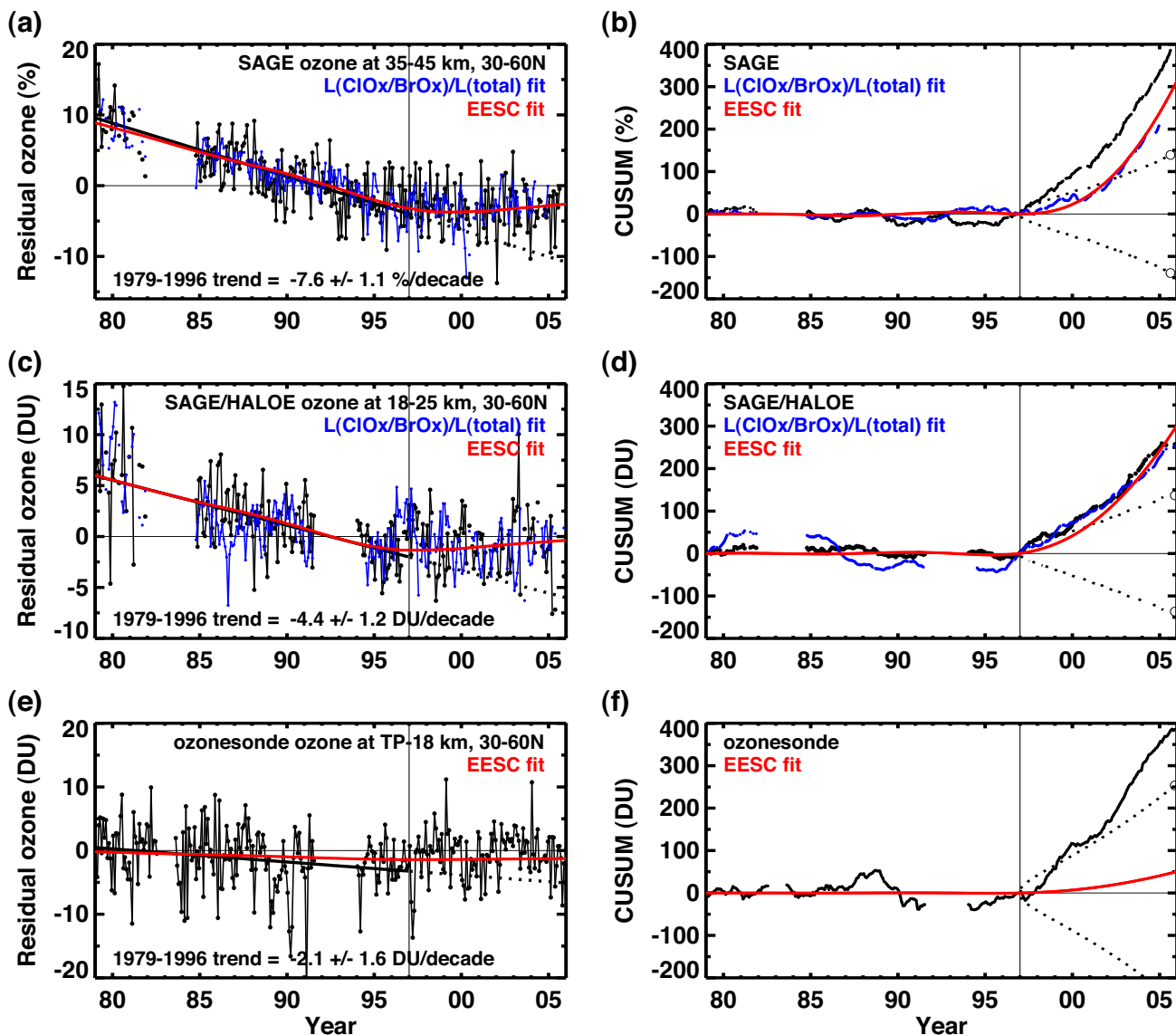


Figure 6-3. Time series of monthly average ozone residuals plus linear trend (left panels) and cumulative sum (CUSUM) of residuals (right panels) in percent or DU. Panels on the left show ozone column residuals between 30°N and 60°N, at 35-45 km from SAGE (top), at 18-25 km from SAGE and HALOE (middle), and from the tropopause (TP) to 18 km from ozonesondes (bottom). Ozone residuals, calculated over the period 1979-2005, have annual cycle, QBO, and solar cycle effects removed. In all left panels, EESC fits to the residuals are shown in red. The solid black lines on the left panels indicate the ozone trend calculated from observations for 1979-1996 and forecasted linearly afterward (dotted). The blue lines in the top and middle panels show the ozone evolution expected from photochemical model calculations. Cumulative sums of residuals of traces in the left hand panels are shown in the panels on the right together with the 95% confidence envelopes of departure from natural variability and model uncertainty as dotted lines. Updated from Newchurch et al. (2003) and Yang et al. (2006).

extrapolated trend line, and since about 1999 the CUSUM has exceeded the 2-sigma error envelope (95% confidence level) of a continuing decline. Similar behavior is found for equatorial latitudes and Southern Hemisphere midlatitudes (Newchurch et al., 2003).

The significant positive deviation of upper-stratospheric ozone levels from the previous linear decline shown in Figure 6-3(a,b) is corroborated by Petropavlovskikh et al. (2005) using Umkehr and SBUV(2) data, and by Steinbrecht et al. (2006a) using

ground-based and satellite records for four stations between 45°S and 44°N and the change-in-trend method. The latter showed an increase in ozone residuals over the last few years for some of the stations (see also Figure 3-6 of Chapter 3). The lessening of the trends in the residuals depends to some degree on the estimates of the solar-cycle and QBO amplitude in ozone (Steinbrecht et al., 2004a; Cunnold et al., 2004), as discussed in Section 6.3. Also, the reduction in trend in upper stratospheric ozone was not significant at the most northerly station (48°N) considered by Steinbrecht et al. (2006a), see Figure 3-6. At northern midlatitudes, other unquantified factors seem to mask the reduction of the ozone decline expected from the beginning of the decline of EESC. A general problem is the lack of long-term upper stratospheric ozone records at latitudes north of 60°N. Nevertheless there is now conclusive evidence for a reduction in the negative trend in upper-stratospheric ozone over a wide region between southern and northern midlatitudes.

The observations of a slowing of the ozone decline discussed above do not alone constitute the first stage of recovery as these changes need to be attributed to changes in ODS amounts. While the ozone changes are in general consistent with those expected from changes in EESC, we recognize that we do not have a full quantitative understanding of ozone loss in the upper stratosphere (Chapter 3). The smooth curves in Figure 6-3(a,b) show fits to the ozone residuals using the EESC (red curve) and ozone loss fraction due to chlorine and bromine (blue curves). The latter was calculated using a photochemical model constrained by observations of total reactive nitrogen (NO_y), inorganic chlorine (Cl_y), CH_4 , and H_2O (Yang et al., 2006). As quantified by the CUSUMs, these fits show a significant deviation from the previous decline up to 1997. The good fit to the observed ozone residuals by 1) EESC and 2) the calculated ozone loss fraction due to EESC, as well as the fact that most other sources of ozone variability have been removed, provides strong evidence that the slowing of the ozone decline in the midlatitudes in the upper stratosphere can be attributed to changes in ODSs.

6.5.2 Lower Stratospheric and Total Column Ozone

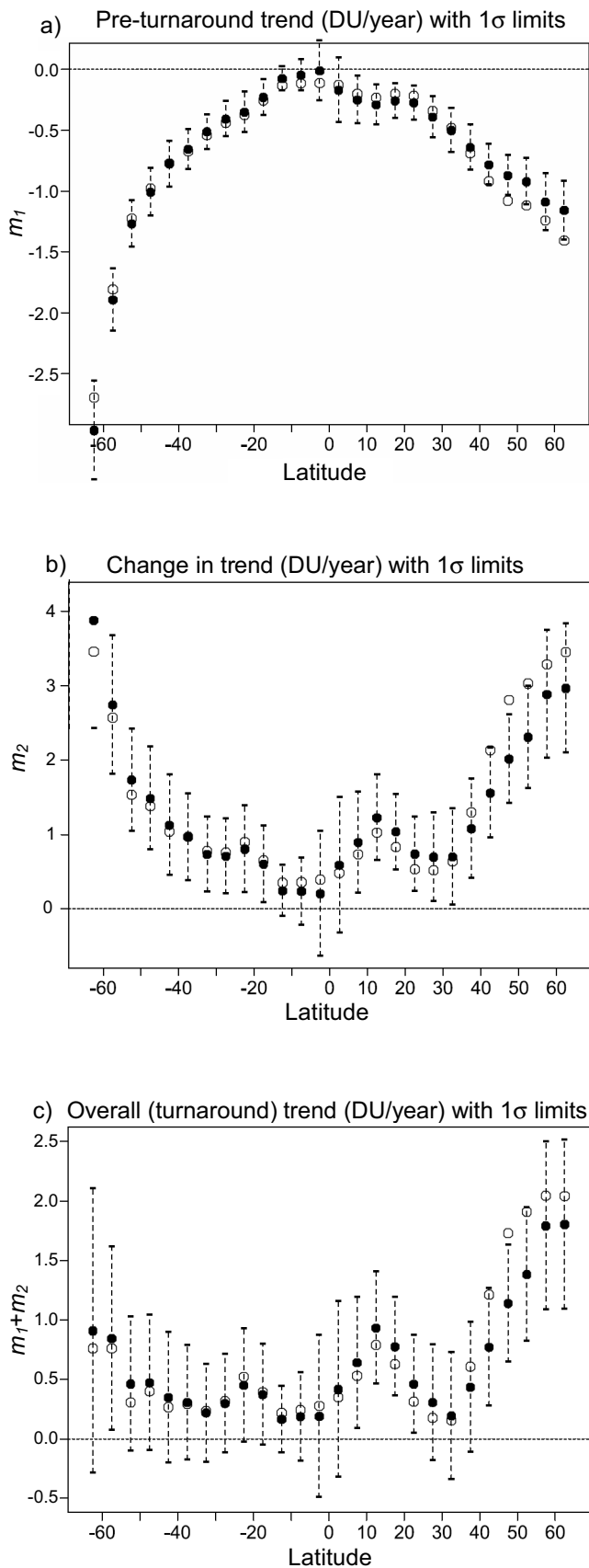
A similar slowing of the decline since 1997 has also been observed in total column ozone, and in some regions of the globe, column ozone has even increased since 1997 (Chapter 3). This deviation from the previous decline is, in general, statistically significant (e.g., Reinsel et al., 2005; Krzyścin et al., 2005; Dhomse et al., 2006; Miller et al., 2006; Krzyścin, 2006; Yang et al., 2006).

The change in total column ozone evolution is illustrated in Figure 6-4, which shows calculations of the overall trend and the change in trend (see Section 6.4) of column ozone as a function of latitude (Reinsel et al., 2005). The change-in-trend term is statistically significant at the 95% confidence level between 40°N and 60°N, and between 50°S and 60°S. At lower latitudes the change in trend is not statistically significant. The trends and changes in trends shown in Figure 6-4 are representative of the range of results obtained in Chapter 3 for various total column ozone datasets. Furthermore, several other studies (Krzyścin et al., 2005; Dhomse et al., 2006; Krzyścin, 2006; Yang et al., 2006) came to a similar conclusion based, in part, on additional data and using somewhat different approaches. A statistically significant slowing of the decline is also found for ozone in different altitude regions. For example, Figures 6-3(c) and (e) show residuals for ozone between 18 and 25 km and between the tropopause and 18 km, respectively. The corresponding CUSUMs (Figures 6.3(d) and (f)) indicate a similarly significant deviation from the previous decline.

The above studies have shown that there is now substantial evidence that a slowing of ozone decline has occurred not only for upper stratospheric ozone (Section 6.5.1), but also for lower-stratospheric and total column ozone over substantial parts of the globe. However, it is still necessary to attribute these ozone deviations to changes in EESC in order to label this as stage (i) of ozone recovery. This attribution can be done by estimating changes in chemical ozone destruction (Yang et al., 2006), by eliminating as many non-chemical ozone variations as possible (e.g., Hadjinicolaou et al., 2005; Reinsel et al., 2005; Miller et al., 2006; Dhomse et al., 2006), or by comparisons with multidimensional models (e.g., Anderson et al., 2006; Weatherhead and Andersen, 2006).

Yang et al. (2006) compared the changes in ozone residuals for column ozone, ozone between 18 to 25 km, and ozone between the tropopause and 18 km with changes in EESC and those in the chemical ozone loss fraction due to chlorine and bromine (using the same model as described in Section 6.5.1). As shown in Figures 6-3(c) and (d), the ozone residuals in the 18 to 25 km altitude range closely follow both the EESC and the model-calculated ozone loss fraction due to chlorine and bromine, and CUSUM calculations indicate statistical significance above the 95% confidence level. This result is robust for both northern and southern midlatitudes. It is a strong indication that the beginning of the reduction in EESC is mirrored in photochemical ozone loss rates and that this is the major contributor to the recent leveling off of ozone residuals in the 18 to 25 km range (Yang et al., 2006). The situation is however different for the lower altitude range

21st CENTURY OZONE LAYER



from the tropopause to 18 km (Figure 6-3(e) and (f)). Although ozone residuals between the tropopause and 18 km have increased, the low cumulative sum of residuals for the EESC fit (red curve in Figure 6-3(f)) suggests that these changes have not been driven by declining EESC. Because ozone is significantly controlled by transport in this region, the low CUSUM for EESC indicates that dynamical and transport changes likely account for the major part of the ozone increases between the tropopause and 18 km.

The altitude partitioning of total column ozone changes before and after 1997, according to Yang et al. (2006), is summarized in Table 6-2. About 80% of the total ozone decline between 1979 and 1996 occurred above 18 km, and, as discussed above, this is largely due to increasing EESC. The remaining 20% of the total ozone decline occurred below 18 km, where transport changes played a major role. For the recent total ozone increases, however, only about half comes from altitudes above 18 km, and can be attributed to changes in EESC. The other half comes from altitudes between the tropopause and 18 km, and must largely be due to dynamical and transport changes. The error bars on this partitioning are substantial, of the order of $\pm 30\%$; nonetheless, the CUSUM statistics are well above the 2σ level.

Numerous other studies, using a variety of approaches, have also concluded that changes in transport make a major contribution to the recent increase of total column ozone. Multilinear regression studies by Dhomse et al. (2006), Reinsel et al. (2005), or Krzyściński (2006) show that dynamical factors account for a major fraction, but not all, of the recent increases in total ozone. Figure 6-4, for example, indicates that for northern lati-

Figure 6-4. Trends in zonal mean (5°) total column ozone from the merged Total Ozone Mapping Spectrometer/Solar Backscatter Ultraviolet spectrometer (TOMS/SBUV) satellite dataset (see Chapter 3). (a) Pre-turnaround trends calculated over the period 1979-1996; m_1 as shown in Figure 6-2. (b) The change in trend at the turnaround date, calculated using data over the period 1979 to 2002; m_2 as shown in Figure 6-2. (c) the overall trend; $m_1 + m_2$ as shown in Figure 6-2. All trends are shown with 1σ error bars. Trends from a regression model incorporating basis functions to account for changes in ozone driven by the Arctic Oscillation, Antarctic Oscillation, and wave activity are shown using filled circles, while trends calculated using a traditional regression model incorporating trend, QBO, and solar cycle terms are shown using open circles. From Reinsel et al. (2005).

Table 6-2. Total column ozone trends and trend changes, and contributions from different altitude ranges. The column ozone is obtained from the Dobson/Brewer (total), Stratospheric Aerosol and Gas Experiment (SAGE) satellite (above 25 km), SAGE (18 to 25 km), and ozonesonde (tropopause (TP) to 18 km) measurements. The fractions with respect to the ozone column above the tropopause are listed in percent. Results are for the 30° to 60°N latitude band. Uncertainties given are 2 σ . Adapted from Yang et al. (2006).

Altitude Range	Trend 1979-1996 (DU/decade)	Fraction of Total Trend 1979-1996 (%)	Change of Trend 1997-2005 (DU/decade)	Fraction of Change of Trend 1997-2005 (%)
Total column	-8.7 \pm 2.3		17.4 \pm 8.2	
Above 25 km	-4.3 \pm 1.0	42 \pm 10	4.9 \pm 2.9	30 \pm 18
18 to 25 km	-3.9 \pm 0.9	38 \pm 9	3.4 \pm 2.8	21 \pm 17
TP to 18 km	-2.1 \pm 1.6	20 \pm 16	8.0 \pm 5.3	49 \pm 3

tudes, trends before and after 1996 are comparable in magnitude. Since EESC is declining at a rate three times slower than the previous increase, this is a strong indication for a major contribution from transport to the post-turnaround trend, at least in the Northern Hemisphere. Chemical transport model simulations using the European Centre for Medium-Range Weather Forecasts ERA 40 meteorological reanalyses with chlorine fixed at 1980 levels can reproduce the total ozone increase from 1996 to 2003 (Hadjinicolaou et al., 2005; see also Chapter 3). Analysis of Canadian ozonesondes indicates significant increases in ozone below 60 hPa (20 km), mostly related to dynamical changes in the occurrence of ozone laminae (Tarasick et al., 2005). Furthermore, studies suggest that changes in the mean meridional Brewer-Dobson circulation, e.g., inferred by 100 hPa Eliassen Palm flux, and in lower tropospheric wave forcing, e.g., described by potential vorticity, can account for a substantial fraction of the pre-1997 total ozone decline outside the polar regions and also for the recent increases in northern midlatitude spring (e.g., Salby and Callaghan, 2004; Malanca et al., 2005; Hood and Soukharev, 2005; see also Section 3.4.2 of Chapter 3).

Andersen et al. (2006) compared the recent changes in total column ozone with fourteen 2-D and 3-D model estimates of recovery rates. The comparison showed that for most areas, the changes in long-term trends were in agreement with the range of model expectations for the long-term trends. However, the change in trend was larger than any of the models predicted for the same short time period (1996-2003). In particular, they showed that the large changes observed in the high northern latitudes were larger than any of the models predicted, indicating that much of the change observed north of 50°N may be nat-

ural variability and such trends will not continue into the future at the same rate. Weatherhead and Andersen (2006) extended this analysis and showed that the latitudinal, altitudinal, and seasonal signatures of change in ozone from 1996 through 2005 are in rough agreement with what models are predicting for long-term ozone change (between 1996 and 2050 for the 2-D models and for periods of time-slice runs for 3-D models); see Figure 6-5. The models and measurements agree well in the Southern Hemisphere, and in the Northern Hemisphere show rough agreement for past trends but significant disagreement for the magnitude of trends since 1996. Some of this disagreement could be due to the different time periods considered for observations and models.

All of the above approaches suffer from methodological and statistical uncertainties. Multilinear regression methods are limited by the simplicity of the underlying assumptions, and are only an attempt to describe very complex processes in the atmosphere with a simple set of indices. Not all effects, e.g., solar cycle effects, may be correctly removed on the basis of these simple indices. The reconstruction of chemical ozone loss may require substantial data extrapolation to include periods before measurements of key species (e.g., methane) were available (Yang et al., 2006). Also, bromine may be more important in the lower stratosphere, and lead to higher ozone loss than previously thought (Salawitch et al., 2005). Estimations on the basis of chemical transport models and reanalysis datasets (National Centers for Environmental Prediction (NCEP) or ERA-40), e.g., Hadjinicolaou et al. (2005), suffer from uncertainty regarding the long-term consistency of the reanalysis datasets and their ability to correctly describe the slow mean meridional circulation (see Chapter 3). Also, the meteorological data may inherently contain effects from

21st CENTURY OZONE LAYER

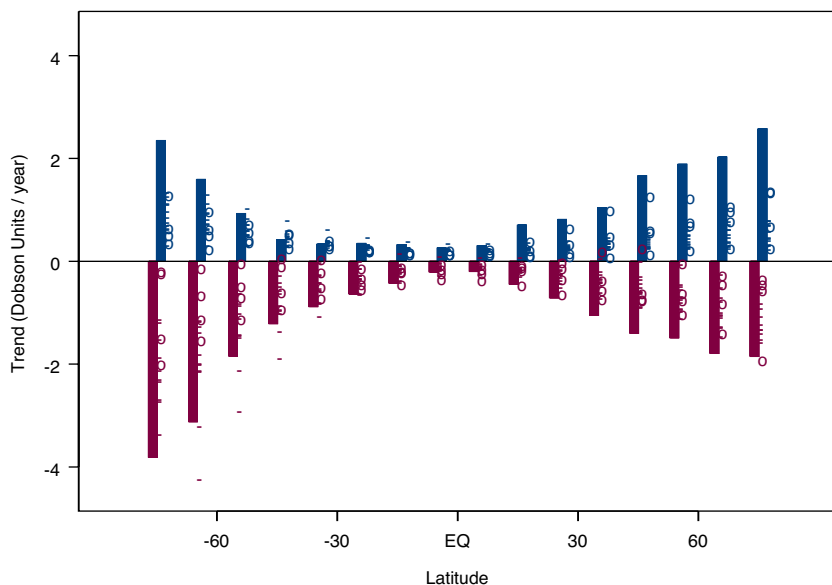


Figure 6-5. Measured and modeled column ozone trends by latitude for 1979-1995 (in red) and 1996-2005 (in blue). Increases in ozone during the past eight years coincide with the regions in which past depletion has occurred. Analyses of the measurements are represented by the solid bars; analyses of 2-D models are shown with horizontal dashes, and results of 3-D models are shown with circles. The model estimates for 1979-1995 are shown in red; projections for long-term recovery are shown in blue. Trends before 1995 are statistically significant (2σ) for middle and high latitudes. Data are from version 8 of the merged TOMS/SBUV2 dataset. Eq., equator; negative latitudes are degrees south. From Weatherhead and Andersen (2006).

the true ozone changes, making it difficult to separate chemical and transport processes.

Even though all approaches have uncertainties, the complementary approaches come to similar conclusions: that changes in transport have contributed a major fraction to the leveling off and increase in midlatitude total ozone since 1997, particularly in the lower stratosphere over northern midlatitudes. However the changes in trends are in agreement, on a number of criteria, with changes in EESC. It is likely that we have passed the “slowing of ozone decline” stage for total ozone over large parts of the globe and in the middle and upper stratosphere. However, at this time, due to the described statistical and methodological uncertainties, an unambiguous attribution to changes in EESC, with a high level of confidence, is not possible.

6.5.3 Polar Ozone

The sustained increase in the severity of Antarctic ozone depletion from the early 1980s to the later 1990s has not continued. Recent changes in metrics of the severity of Antarctic ozone depletion have ranged from little or no change over the past 10 years (ozone hole area), to small (minimum ozone levels) and moderate (ozone mass deficit) signs of ozone increases (Bodeker et al., 2005; Section 4.3.2 and Figure 4-8 of Chapter 4). The cessation of ozone hole growth can be ascribed to the fact that at current ODS levels, all or most of the ozone is destroyed between 12 and 24 km (e.g., WMO, 2003).

Recent reductions in Antarctic ozone loss can be explained by anomalously high stratospheric temperatures and reduced frequency of PSCs in recent years (Solomon et al., 2005; Hoppel et al., 2005). Therefore, although recent stabilization and reduction of Antarctic ozone depletion has occurred at approximately the same time as the growth in EESC has slowed and passed its peak, this ozone change cannot be attributed solely to changes in EESC. It is therefore not possible to conclude that either the first or second stage of Antarctic ozone hole recovery has occurred. The near total destruction of ozone inside the ozone hole means that there is low sensitivity to moderate reductions in EESC. ODS amounts in the Antarctic vortex are expected to decrease only slowly over the next decade (polar EESC is decreasing at around 0.6%/year, see figure in Box 8-1 of Chapter 8). Therefore, in the near future, only small changes in Antarctic ozone area are expected as EESC declines, and these changes will be masked by interannual variability due to temperature and transport variations (Newman et al., 2004; Solomon et al., 2005).

Larger sensitivity to changes in EESC is expected at the upper altitudes of the ozone hole (20-22 km) where ozone depletion is not complete, and this has been identified as a possible region to detect Antarctic ozone recovery (Hofmann et al., 1997). Hoppel et al. (2005) analyzed measurements of ozone mixing ratios in the 20-22 km altitude range for October, and showed that the values for 2001-2004 were higher than for 1994-1996 and 1998-

2000. However, the higher ozone mixing ratios were accompanied by higher temperatures and reduced frequency of PSCs. Although ozone is more sensitive to ODS changes in the 20-22 km region, there is more dynamical activity in this region, and changes in ozone due to ODS changes cannot be clearly distinguished from those due to changes in meteorological conditions. It is therefore not possible to conclude that the first (or second) stage of ozone recovery has occurred at 20-22 km in the Antarctic.

Another region where detection of the first stages of ozone recovery may be possible is the polar vortex collar region (60°S to 70°S). Yang et al. (2005) examined the evolution of ozone in this region using several different datasets. They accounted for dynamical variability using the observed correlation between ozone and 100 hPa temperatures, and showed that temperature-adjusted ozone

anomalies were roughly constant since 1997 (see Figure 6-6). The change in the trend of these anomalies is significant at greater than 95% confidence limits. Yang et al. also showed that complete ozone loss is infrequent in the collar region and was not responsible for the slowing of the ozone decline. As shown in Figure 6-6, the variation in the ozone anomalies is similar to that of midlatitude EESC, and fits to EESC can explain most of the long-term variations in the ozone anomalies. This high correlation and the limited role of complete ozone loss provide evidence that the first stage of ozone recovery may have occurred in the stratospheric collar region surrounding the Antarctica vortex. However, there is some uncertainty in the EESC in the collar region, and the resulting fit with temperature-adjusted ozone anomalies. For example, the polar EESC shown in Box 8-1 continues to increase until

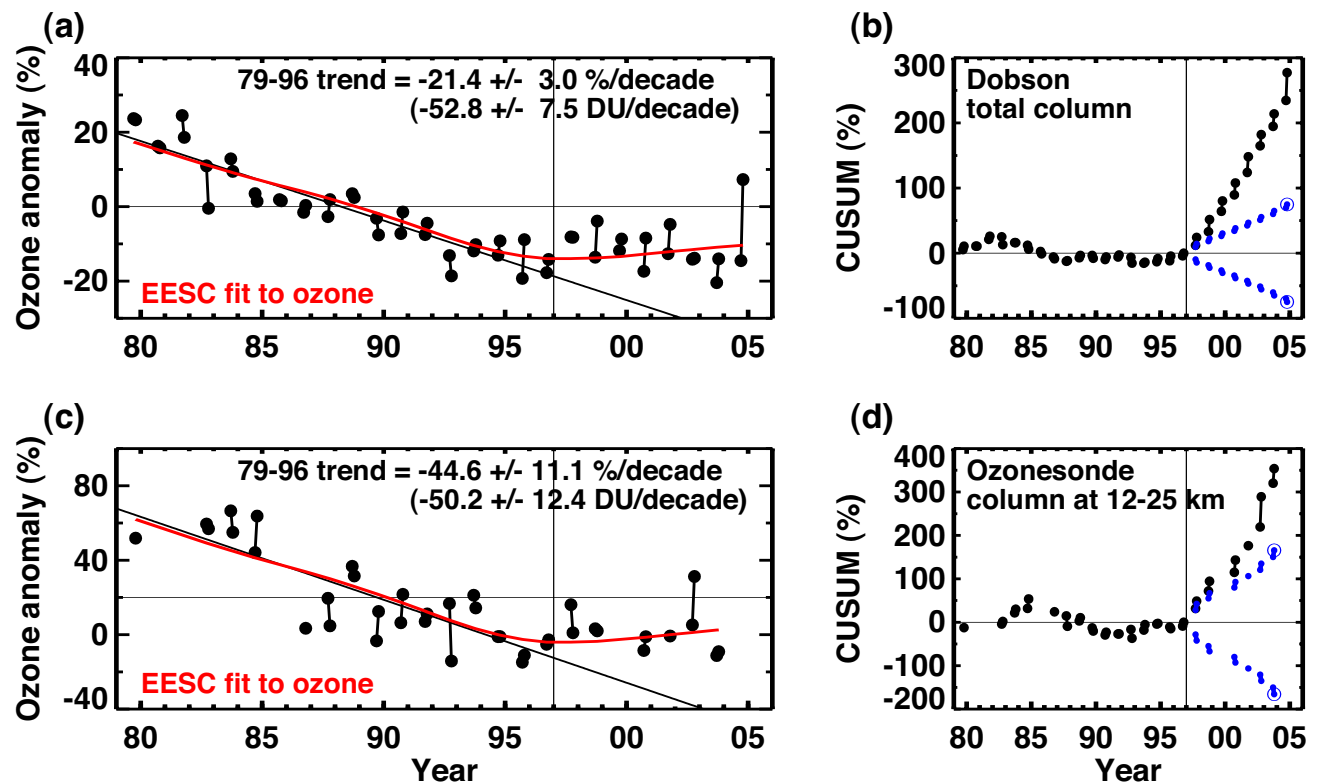


Figure 6-6. September and October temperature-adjusted ozone monthly anomalies (left panels) and CUSUM of ozone residuals (right panels) in percent for Dobson spectrophotometer total ozone columns at Vernadsky (65°S) and Syowa (69°S) (top) and ozonesonde ozone columns from 12-25 km at Syowa (bottom). The ozone anomalies are calculated from a regression model fit to the data over the full period. The temperature-adjusted ozone anomalies are obtained by subtracting the ozone equivalent temperatures from the ozone anomalies (see Yang et al., 2005, for details). The black line indicates the ozone trend calculated from observations for 1979-1996 and forecasted linearly afterward. Linear trends and 95% confidence intervals for 1979-1996 are listed in %/decade and DU/decade. The red line shows the EESC fits to the temperature-adjusted ozone. The blue lines indicate the 95% confidence envelopes of departure from natural variability and trend model uncertainty. Adapted from Yang et al. (2005).

21st CENTURY OZONE LAYER

2001, in contrast to the ozone anomalies in the collar that peak around 1997. It is unclear whether the midlatitude or polar EESC is more representative for the collar region which is outside the ozone hole. These uncertainties cast some doubt on using EESC to quantify the role of ODSs in the stabilization of ozone in the collar region.

The expected slow improvement of Antarctic ozone over the next decade (e.g., Newman et al., 2004, 2006) means that variability will continue to complicate detection of the first and second stages of ozone hole recovery, even after accounting for temperature variations. Solomon et al. (2005) have suggested that the return of (1) the relationship between temperature and ozone and (2) the variance in ozone abundances to historical values may provide early signals of the beginning of recovery inside the ozone hole. However, after a stage of recovery has occurred, it is unclear how long it will take to achieve the detection of the stage using either diagnostic.

The issue of identifying recovery in the Arctic springtime is even more difficult than in the Antarctic. Arctic ozone depletion occurs in most years, but there is substantial interannual variability (see Chapter 4). The larger meteorological variability in the Arctic compared with the Antarctic (e.g., Langematz and Kunze, 2006) and smaller ozone depletion means that it will likely take many years to detect any changes in ozone due to decreases in EESC. Furthermore, it is likely that the first stage of recovery (slowing of decline) cannot be detected for the Arctic. As with the Antarctic, the first signals of recovery might be found by looking at the relationship between ozone and temperature. As discussed in Chapter 4, one relationship that reduces the variability is the compact relationship between vortex average ozone loss and V_{PSC} , the volume of air potentially containing PSCs (Rex et al., 2004). It may be possible to detect the recovery of polar ozone in the Northern Hemisphere from a statistically significant and persistent deviation from this relationship. However, no such deviation has been detected, and there has been no detection of any ozone recovery stages in the Arctic.

6.6 PROJECTIONS OF THE FUTURE BEHAVIOR OF OZONE

As discussed above (and in Chapter 5), the process of recovery of the ozone layer will depend not only on the decline of ODSs but also on many other factors. Although some of these factors can be accounted for empirically when projecting future ozone (e.g., Knudsen et al., 2004), coupling between the different chemical, dynamical, and radiative processes involved requires the use of models that include these interdependencies to make well-founded

projections. In particular, models used for prognostic studies should incorporate the effects of changes in temperature and transport that are likely to occur as the concentrations of WMGHGs rise. This section addresses how changes in ODSs couple with other atmospheric changes to influence the long-term evolution of ozone.

The framework introduced in Section 6.2 is used to examine the ozone recovery process in the model simulations. In particular, projections of total column ozone are examined for three periods:

- (i) The beginning of the century (2000-2020), when EESC is expected to start to decrease or continue to decrease
- (ii) Mid-century (2040-2050 in extrapolar regions, 2060-2070 in polar regions), when EESC is expected to fall below 1980 values
- (iii) End of the century (2090-2100), when factors other than ODSs are expected to control stratospheric ozone

Confidence in projections near the beginning of the century is higher than near the middle or end of the century because the former can be supported by observations, empirical studies, and extrapolations while the latter are more influenced by uncertainties in the emissions scenarios and other boundary conditions. In general, a separation of the different factors contributing to the ozone variability in the model output has not been performed. Therefore the modeled ozone time series presented below cannot be used for attribution of ozone changes to changes in ODSs.

6.6.1 Model Descriptions and Scenarios

In this Assessment both two-dimensional chemical transport models (2-D models) and three-dimensional coupled Chemistry-Climate Models (CCMs) are used to make projections of the ozone layer in the 21st century. By using both classes of models, with their respective advantages and disadvantages, the conclusions drawn from the model projections are likely to be more robust.

2-D models have been used extensively in previous Assessments. Their relative computational efficiency allows long integrations and a large number of sensitivity studies. This capability makes these models a valuable tool for understanding and quantifying the long-term changes in ozone. However, due to the inherent zonal averaging within these models, they are not well suited for modeling polar processes. The 2-D models used in this Assessment (see Table 6-3 for a summary of their characteristics) vary in the extent to which they incorporate interactions between model components. Most of the 2-D models use prescribed temperatures and transport, and therefore do not include the well-known temperature feed-

Table 6-3. A summary of the 2-D models used in this chapter.

Model	Institution(s)	Investigators	Temperature	PSC Scheme	Solar Cycle	Reference
AER	AER, Inc., U.S.	D. Weisenstein	Specified from NCEP analyses	Based on model T	No	Rinsland et al. (2003)
GSFC-INT	NASA/Goddard Space Flight Center	E. Fleming, C. Jackman	Interactive	Based on observed T	No	Rosenfield et al. (1997)
GSFC	NASA/Goddard Space Flight Center	E. Fleming, C. Jackman	Specified from UKMO analyses	Distribution based on NCEP	No	Fleming et al. (1999)
Leeds-Bremen	University of Leeds, U.K.; University of Bremen, Germany	M. Chipperfield, M. Sinnhuber, B.-M. Sinnhuber	Interactive	Based on model T	No	Chipperfield and Feng (2003)
MNP¹	Netherlands Environmental Assessment Agency	G. Velders	Climatology	No solid PSCs	No	Velders (1995)
MPIC	MPI for Chemistry, Mainz, Germany	C. Brühl	Specified from CIRA data	Based on model and observed T deviation	No	Grooß et al. (1998)
NOCAR	NOAA/NCAR	R. Portmann	Interactive	Based on NCEP T, Liquid aerosols	No	Portmann et al. (1999)
OSLO	University of Oslo, Norway	B. Rognerud	Specified	Based on climatology	No	Stordal et al. (1985); Isaksen et al. (1990)
SUNY	SUNY, U.S.; St. Petersburg, Russia	S. Smyshlyaev	Specified from NCEP analyses	Based on NCEP T	Yes	Smyshlyaev et al. (1998)

AER, Atmospheric and Environmental Research Inc.; MPIC, Max-Planck Institute for Chemistry; NOAA, National Oceanic and Atmospheric Administration; NCAR, National Center for Atmospheric Research; SUNY, State University of New York; NCEP, National Centers for Environmental Prediction; UKMO, United Kingdom Meteorological Office; CIRA, COSPAR (Committee on Space Research) International Reference Atmosphere.

¹ This was referred to as the RIVM model in the 2002 Ozone Assessment (WMO, 2003).

back from changes in WMGHGs, or the ozone radiative-dynamical feedback, in which changes in ozone also affect the radiative balance of the stratosphere and hence temperatures and transport. Three of the models (NOCAR, Leeds-Bremen, and GSFC-INT) calculate temperatures from the modeled atmospheric composition, and capture some of the feedback on the circulation and transport. However, these so-called “interactive” models do not include changes in the wave forcing.

CCMs have a much more limited history in the Ozone Assessments. WMO (2003) was the first time

CCMs were fully integrated into an Assessment. These simulations focused on the polar regions and, due to computational limitations, were largely restricted to the recent past and near future (roughly 1980 to 2020). Transient simulations (see Box 5-1 in Chapter 5) are preferred for predicting future ozone because in these simulations, ozone responds interactively to the gradual secular trends in WMGHGs, ODSs, and other boundary conditions. For this Assessment we consider only transient simulations from CCMs, and we examine global as well as polar ozone. Since WMO (2003), several new CCMs have been devel-

21st CENTURY OZONE LAYER

oped, significantly deepening the pool of model simulations of future ozone.

An additional improvement over the approach used in WMO (2003) is the use of two standard simulations, defined as part of the CCM Validation Activity (CCMVal; Eyring et al., 2005). One “past” simulation (REF1) is designed to reproduce ozone changes from 1980 to the present when global ozone observations are available. It allows a detailed investigation of the role of natural variability and other atmospheric changes important for ozone trends. All forcing fields in this simulation are based on observations (Appendix 6A). The “future” simulation (REF2) is a self-consistent simulation from the past into the future. In this simulation the surface time series of halocarbons is based on the “Ab” scenario from WMO (2003); see Appendix 6A. The new halogen scenario A1 from this Assessment (Chapter 8) has not been applied because the computational requirements of the CCMs meant that these simulations had to be started well before the scenarios in Chapter 8 were finalized. The WMGHG concentrations for the future simulations are taken from the IPCC (2000) “A1B” scenario, while sea surface temperatures (SSTs) are taken from different coupled ocean model simulations, either from simulations with the ocean coupled to the underlying general circulation models, or from the U.K. Meteorological Office HadGEM1 simulations using IPCC (2000) scenario “A1B.” Some CCMs ran multiple future simulations with the same boundary conditions but different initial conditions (see Table 6-4). In general, the variability between ensembles from a single model is much smaller than the inter-model differences (see also Austin and Wilson, 2006; Dameris et al., 2006).

For consistency, the 2-D model simulations used the same halogen and WMGHG scenarios as the CCMs. Additional sensitivity runs with different scenarios were also performed by some 2-D models (see discussion below and Table 6-3). In this chapter, the focus is on the “future” simulations out to 2100, whereas the “past” simulations (up to 2004) are discussed in Chapter 3. Of the 13 CCMs available (see Table 6-4 for a summary of their characteristics), all but UMETRAC and LMDZrepro provided simulations of future ozone changes, and their results form the basis for the projections discussed in Sections 6.6.3 and 6.6.4.

6.6.2 Model Evaluation

Most of the 2-D models listed in Table 6-3 have been used in earlier Assessments. Their use in the past has often been accompanied by model intercomparisons and comparisons with measurements to characterize their

capabilities and deficiencies. For example, Park et al. (1999) assessed the chemistry and transport in a large number of 2-D and 3-D chemical transport models (CTMs) (including the AER, GSFC-INT, GSFC, and NOCAR 2-D models considered here). This study showed that there was a large variation in the transport in the models, and most models produced air that was too young in the stratosphere and did not correctly simulate the tropical “tape recorder” (Mote et al., 1996). Also, there were significant differences in the NO_y and Cl_y in the lower stratosphere. Here, 2-D models are used to predict ozone changes in the midlatitudes and tropics. More emphasis has been given to interactive 2-D models because non-interactive 2-D models neglect the important effects of temperature feedback from changes in WMGHGs and the ozone radiative-dynamical feedback.

An evaluation of the CCMs used here is reported in Eyring et al. (2006). They compared simulations of the recent past (1960 to 2004) with meteorological analyses and trace gas observations. This CCM evaluation provides guidance on the level of confidence that can be placed on each model simulation.

The comparisons in Eyring et al. (2006) showed that the models reproduce the global, annual mean temperature fairly well, but most CCMs still have a cold bias in winter-spring in the Antarctic resulting in later polar vortex breakup (most severe in LMDZrepro and E39C). Most models display the correct stratospheric response to wave forcing in the Northern Hemisphere, but in the Southern Hemisphere several of the models (e.g., CCSRNIES, E39C, MAECHAM4CHEM, MRI, ULAQ, and LMDZrepro) have temperatures that are rather unresponsive to changes in the heat fluxes, with the ULAQ model having the incorrect sign. These biases indicate problems in the simulation of the dynamical response of the Southern Hemisphere stratosphere in winter in these models.

Eyring et al. (2006) also evaluated the transport in the CCMs by comparing simulated methane, mean age of air, and the water vapor “tape recorder” with observations. They found a wide spread in the model results for each diagnostic, indicating large differences in the transport. However, the majority of the spread is due to only a small subset of models (E39C, MAECHAM4CHEM, MRI, SOCOL, and ULAQ) where large deviations from observations are apparent in several, if not all, of the transport diagnostics. This is illustrated for methane and mean age of air at 50 hPa in Figure 6-7(a) and (b), where the above models are shown as dashed curves. The cause of significant biases in the tracer fields in these models is generally not known, but in some cases it can be attributed to specific model

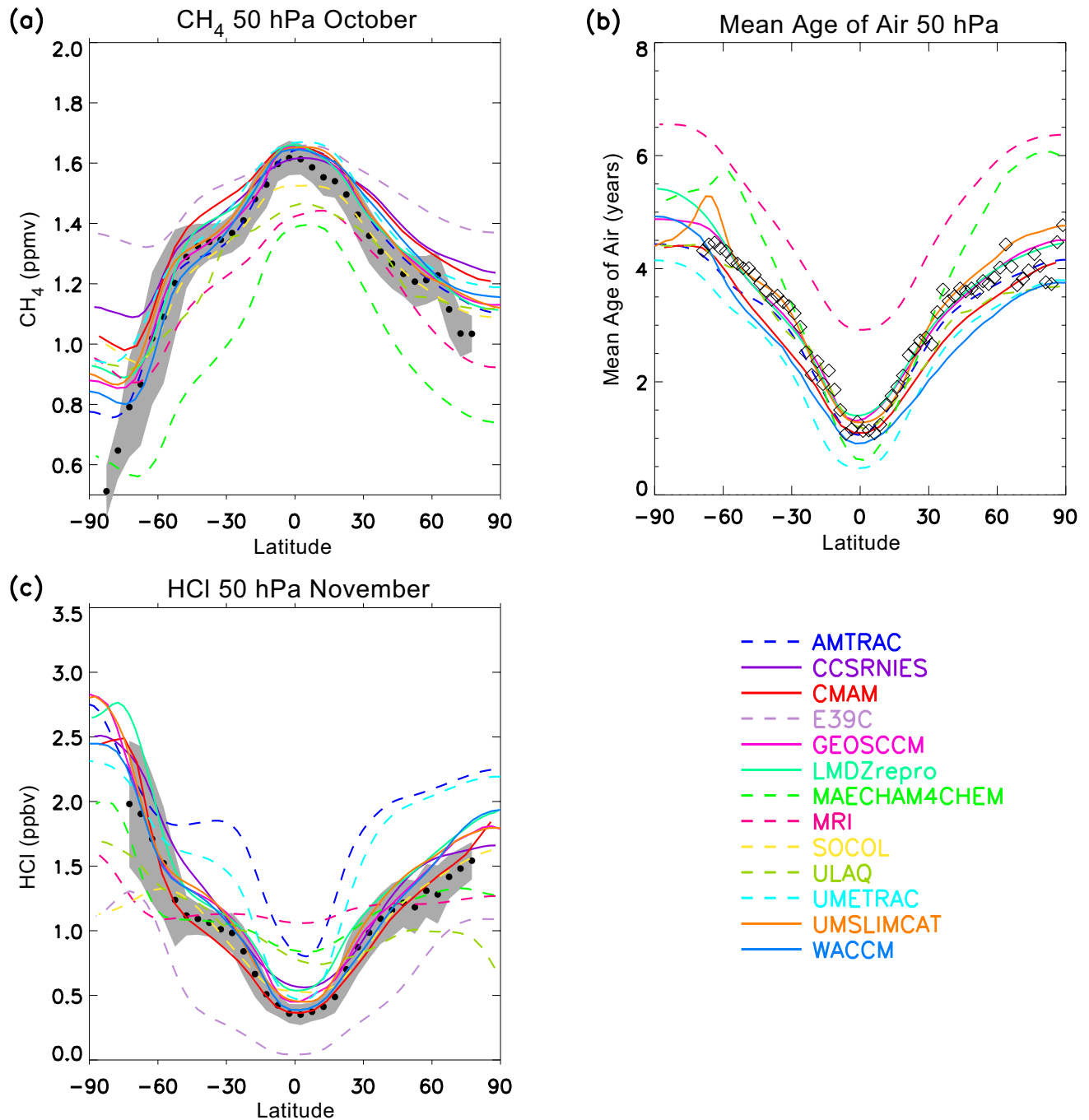


Figure 6-7. Comparison of climatological zonal-mean (a) methane in October, (b) annual mean of the mean age of air, and (c) HCl in November, at 50 hPa from CCMs and observations. Observations in (a) and (c) are from HALOE: Black dots are values averaged in latitudes (zonal means) and the gray area shows plus and minus 1 standard deviation about the climatological zonal mean HALOE. Observations in (b) are based on ER-2 aircraft measurements of CO_2 from many different years and months (Andrews et al., 2001). Adapted from Eyring et al. (2006).

21st CENTURY OZONE LAYER

Table 6-4. A summary of the CCMs used in this Assessment. See Appendix 6A for descriptions of the model runs. All CCMs have a comprehensive range of stratospheric chemical reactions, except E39C and MAECHAM4CHEM, which do not include bromine chemistry.

Model	Institution(s)	Investigators	Horizontal Resolution	No. Levels/ Upper Boundary	Runs	Reference
AMTRAC	GFDL, U.S.	J. Austin R. Wilson	2° × 2.5°	48 / 0.0017 hPa	3×REF1 ^a 3×SCN2 ^b	Austin et al. (2006); Austin and Wilson (2006)
CCSRNIES	NIES, Tsukuba, Japan	H. Akiyoshi T. Nagashima M. Yoshiki	2.8° × 2.8° (T42)	34 / 0.01 hPa	REF1 REF2	Akiyoshi et al. (2004); Kurokawa et al. (2005)
CMAM	MSC, Univ. of Toronto and York Univ., Canada	J. McConnell N. McFarlane D. Plummer J. Scinocca T. Shepherd	3.75° × 3.75° (T32)	71 / 0.0006 hPa	3×REF2 ^c	Beagley et al. (1997); de Grandpré et al. (2000)
E39C	DLR Oberpfaffenhofen, Germany	M. Dameris V. Eyring V. Grewe M. Ponater	3.75° × 3.75° (T30)	39 / 10 hPa	3×REF1 4×SCN2 2×NCC	Dameris et al. (2005, 2006)
GEOSCCM	NASA/GSFC, U.S.	A. Douglass P. Newman S. Pawson R. Stolarski	2° × 2.5°	55 / 0.01 hPa	REF1 ^c REF2	Bloom et al. (2005); Stolarski et al. (2006)
LMDZrepro	IPSL, France	S. Bekki F. Lott F. Lefèvre M. Marchand	2.5° × 3.75°	50 / 0.07 hPa	REF1 REF2	Chemistry part: Lefèvre et al. (1994)
MAECHAM4 CHEM	MPI Mainz, Hamburg, Germany	C. Brühl M. Giorgetta E. Manzini B. Steil	3.75° × 3.75° (T30)	39 / 0.01 hPa	REF1 REF2 SCN2	Manzini et al. (2003); Steil et al. (2003)
MRI	MRI, Tsukuba, Japan	K. Shibata M. Deushi	2.8° × 2.8° (T42)	68 / 0.01 hPa	REF1 REF2	Shibata and Deushi (2005); Shibata et al. (2005)
SOCOL	PMOB/WRC and ETHZ, Switzerland	E. Rozanov M. Schraner	3.75° × 3.75° (T30)	39 / 0.01 hPa	REF1 REF2	Egorova et al. (2005); Rozanov et al. (2005)
ULAQ	Univ. of L'Aquila, Italy	E. Mancini G. Pitari	10° × 22.5°	26 / 0.04 hPa	REF1 ^d REF2 NCC	Pitari et al. (2002)
UMETRAC	Met Office, U.K.; NIWA, New Zealand	N. Butchart H. Struthers	2.5° × 3.75°	64 / 0.01 hPa	REF1	Austin (2002); Struthers et al. (2004)

Table 6-4, continued.

UMSLIMCAT	University of Leeds, U.K.	M. Chipperfield W. Tian	2.5° × 3.75°	64 / 0.01 hPa	REF1 REF2	Tian and Chipperfield (2005)
WACCM (v.3)	NCAR, U.S.	B. Bovillei R. Garcia A. Gettelman D. Kinnison D. Marsh F. Sassi	4° × 5°	66 / 4.5×10 ⁻⁶ hPa	3×REF1 ^a 3×REF2 2×NCC	Park et al. (2004); Richter and Garcia (2006)

GFDL, Geophysical Fluid Dynamics Laboratory; NIES, National Institute for Environmental Studies; MSC, Meteorological Service of Canada; DLR, Deutschen Zentrum für Luft- und Raumfahrt; NASA, National Aeronautics and Space Administration; GSFC, Goddard Space Flight Center; IPSL, Institut Pierre Simon Laplace; MPI, Max-Planck-Institut; MRI, Meteorological Research Institute; PMOB/WRC, Physical-Meteorological Observatory/World Radiation Center; ETHZ, Eidgenössische Technische Hochschule Zurich; NIWA, National Institute of Water and Atmospheric Research; NCAR, National Center for Atmospheric Research.

^a REF1 but with SSTs from the Smith/Reynolds dataset (J. Hurrell, private communication) and without QBO

^b SCN2 without QBO

^c REF1 without QBO, solar cycle, and volcanic eruptions

^d REF1 without QBO and solar cycle

^e Different SSTs were used in each simulation

features, e.g., very low horizontal resolution (ULAQ) or a low upper boundary (E39C). For the remaining CCMs there is, in general, reasonable agreement with observations. In the upper stratosphere, the model agreement with age of air observations is poorer, with most models underestimating the age (not shown). However, in general the mean age of air and the tape recorder are in better agreement than reported in the Hall et al. (1999) assessment of 2-D and 3-D CTMs.

The ability of CCMs to reproduce past stratospheric chlorine and bromine concentrations clearly affects the confidence that we can place in their projections of future ozone changes, particularly in the Antarctic. Eyring et al. (2006) examined modeled HCl and inorganic Cl_y fields, and again found a large model spread, with some large deviations from observations, see Figure 6-7(c) and Figure 6-8(a). The differences are most pronounced in the polar lower stratosphere, where peak Cl_y varies from around 1 ppb to over 3.5 ppb. Measurements of Cl_y in the Antarctic lower stratosphere (symbols in Figure 6-8(a)) clearly show that peak values of Cl_y close to or less than 2.5 ppb, as simulated by several CCMs, are unrealistic. Transport deficiencies are a major contributor to deficiencies in the simulated HCl and Cl_y, and the models discussed above that did not perform well for transport diagnostics also showed differences from observed HCl. In the MRI model, the age of air decreases significantly with time and, unlike in all other models and observations, Cl_y does not peak around 2000 but continues to increase until after 2015. This unrealistic continued

increase of Cl_y lowers the confidence we can place in this simulation. Transport deficiencies do not, however, explain all of the differences. The initial decrease in Cl_y in UMSLIMCAT is due to wrong initial conditions used in this simulation. AMTRAC and UMETRAC have higher HCl and Cl_y than other models but similar CH₄ and mean age of air, and presumably similar transport (Figure 6-7 and 6-8). The additional Cl_y results from photolysis rates of organic chlorine species being artificially increased by 25% in AMTRAC and UMETRAC so that the Cl_y in the upper stratosphere is in close agreement with observed Cl_y. Although this adjustment of the photolysis rates improves the agreement with observed Cl_y in the upper stratosphere and polar lower stratosphere (Figure 6-8(a)), HCl (and also Cl_y) in the extrapolar lower stratosphere is unrealistically large (Figure 6-7(c)). It is not clear whether the 25% increase in the photolysis rates is responsible for the enhanced extrapolar Cl_y.

The CCMs are generally able to reproduce the observed amplitude and phase of the mean annual cycle in total column ozone, except over southern high latitudes (see right panels in Figure 3-26, Chapter 3). However, most models exhibit large offset biases in the mean annual cycle, with the majority overestimating total column ozone. Although it is not possible to trace all differences in the simulated ozone to deficiencies in the simulated temperature and tracers, in some cases a link can be made. For example, the models with low tropical and midlatitude CH₄ have high ozone (MAECHAM4CHEM and MRI), those with low Cl_y in polar regions have smaller

21st CENTURY OZONE LAYER

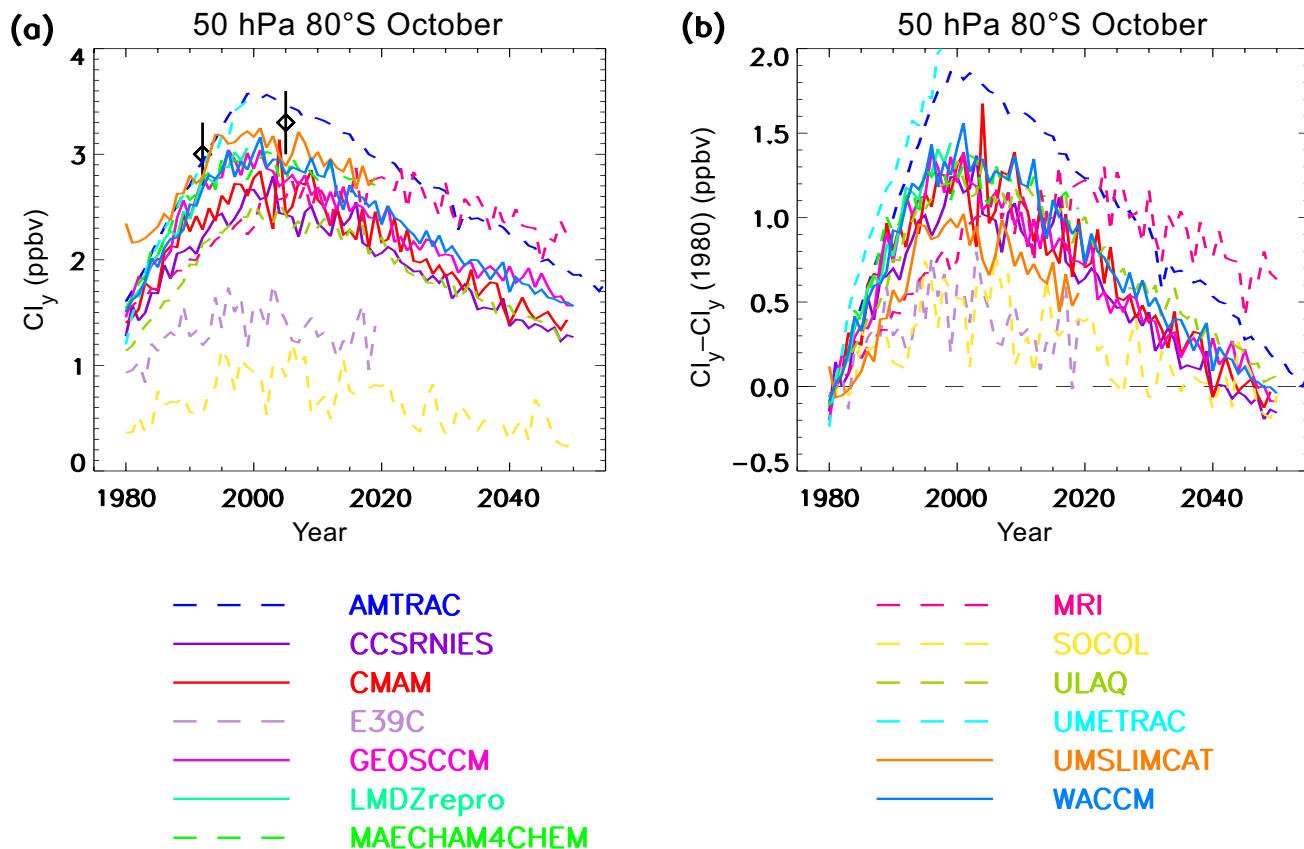


Figure 6-8. October zonal mean values of total inorganic chlorine (Cl_y in ppbv) at 50 hPa and 80°S from CCMs. Panel (a) shows Cl_y and panel (b) difference in Cl_y from that in 1980. The symbols in (a) show estimates of Cl_y in the Antarctic lower stratosphere in spring from measurements from the UARS satellite in 1992 and the Aura satellite in 2005, yielding values around 3 ppb (Douglass et al., 1995; Santee et al., 1996) and around 3.3 ppb (see Figure 4-8), respectively.

ozone reductions there (SOCOL and E39C), and the model with the largest cold bias in the Antarctic lower stratosphere in spring (LMDZrepro) simulates very low ozone.

CCMs show a large range of ozone trends over the past 25 years (see left panels in Figure 3-26 of Chapter 3) and large differences from observations. Some of these differences may in part be related to differences in the simulated Cl_y , e.g., E39C and SOCOL show a trend smaller than observed, whereas AMTRAC and UMETRAC show a trend larger than observed in extrapolar area weighted mean column ozone. However, other factors also contribute, e.g., biases in tropospheric ozone (Austin and Wilson, 2006).

The CCM evaluation discussed above and in Eyring et al. (2006) has guided the level of confidence we place on each model simulation. The CCMs vary in their skill in representing different processes and characteristics of the atmosphere. Because the focus here is on ozone

recovery due to declining ODSs, we place importance on the models' ability to correctly simulate stratospheric Cl_y as well as the representation of transport characteristics and polar temperatures. Therefore, more credence is given to those models that realistically simulate these processes. Figure 6-7 shows a subset of the diagnostics used to evaluate these processes and CCMs shown with solid curves in Figures 6-7, 6-8, 6-10 and 6-12 to 6-14 are those that are in good agreement with the observations in Figure 6-7. However, these line styles should not be over-interpreted as both the ability of the CCMs to represent these processes as well as the relative importance of Cl_y , temperature, and transport vary between different regions and altitudes. Also, analyses of model dynamics in the Arctic, and differences in the chlorine budget/partitioning in these models, when available, might change this evaluation for some regions and altitudes.

6.6.3 Midlatitude and Tropical Ozone

Figures 6-9 and 6-10 show the time evolution through the 21st century of annual means of monthly total column ozone anomalies from the 2-D models and CCMs, respectively, for four different regions: extrapolar (60°S to 60°N), tropics (25°S to 25°N), northern midlatitudes (35° to 60°N), and southern midlatitudes (35° to 60°S). For the 2-D models, ozone from the P1 and F1 simulations is shown, while for the CCMs the ozone is from REF1 and REF2 or SCN2 (depending on the CCM) simulations (see Table 6-4 for description of simulations). Multiple curves are shown for CCMs that ran multiple simulations with the same forcing. The method used to calculate the ozone anomalies is detailed in Eyring et al. (2006).

The evolution of the ozone anomalies is qualitatively similar for both the 2-D models and the CCMs: the lowest ozone occurs around 2000 within a broad minimum after which ozone increases, as expected from decreasing EESC beyond 2000. A clear difference between the 2-D model and CCM projections is the year-to-year fluctuations in the ozone anomalies. The 2-D models show a smooth ozone evolution, whereas the CCMs show large interannual variability. The variability in the CCMs arises from internal dynamics and variations in prescribed sea surface temperatures with time. Variability associated with the QBO and 11-year solar cycle is also included in some CCM simulations (see Table 6-4) and contributes to the interannual and longer time variations. Since the focus is on decadal changes, the ozone anomalies plotted in Figure 6-10 have been smoothed using a 1:2:1 filter applied 5 times iteratively. There is a large spread in projected ozone anomalies during the beginning of the 21st century (2000 to 2020). Two CCMs (AMTRAC and MRI) show much larger ozone anomalies than the other models. These two models also have much larger HCl and Cl_y during this period (AMTRAC because of increased CFC photolysis rates, and MRI because of slower circulation; see discussion in Section 6.6.2), which may explain part of the larger ozone anomalies.

Averaged between 60°N and 60°S, total column ozone is projected to increase between 2000 and 2020 in all models except MRI (see above discussion), with most of the increase of 1% to 2.5% occurring after 2010. Over midlatitudes, the majority of the models predict an increase of 1.5% to 3.5%, while over the tropics smaller ozone increases of less than 2% are projected. The evaluation of the timing of ozone minima is biased by the large response to Mt. Pinatubo in the 2-D models, and obscured by interannual variability in the CCMs. If smoothed CCM anomalies are used (as shown in Figure 6-10) and, to avoid local ozone minima caused by Mt. Pinatubo, only minima after

1996 are considered, both classes of model predict that minimum ozone values have already occurred between 60°S and 60°N. In midlatitudes, 2-D models predict ozone minima between 1997 and 2001 while the CCMs (again with the exception of MRI) predict ozone minima between 1997 and 2007 with no clear hemispheric differences. Because the exact timing of minimum ozone in some of the CCM simulations might be affected by the solar cycle (e.g., Dameris et al., 2006) or other factors, the ozone minima detected in the CCMs are not synonymous with ozone turnaround and should not be interpreted as stage (ii) of ozone recovery.

It is expected that EESC in the midlatitude lower stratosphere will decrease to its 1980 value between 2040 and 2050 (see box 8-1). If no other factors played a role, it would be expected that ozone would increase to its 1980 values at the same time. However, if there are changes in temperature, transport, or the abundance of other gases, ozone may return to 1980 values earlier or later than EESC. Figure 6-9 shows that total column ozone in the interactive 2-D models that include temperature feedbacks from changes in WMGHGs (GSFC-INT, LeedsBremen, NOCAR) is above 1980 values between 2040 and 2050. Ozone averaged between 60°S and 60°N in these models returns to 1980 values between 2025 and 2035, so that by the time EESC returns to 1980 values, ozone is 0.5% to 3.0% above 1980 values. In the tropics and northern midlatitudes, ozone returns to 1980 values between 2020 and 2030, while over southern midlatitudes this happens somewhat later, between 2025 and 2040. The increase in ozone to levels higher than would be expected from ODS concentrations alone results from stratospheric cooling due to increased concentrations of WMGHGs. In contrast to the interactive 2-D models, the non-interactive 2-D models predict that column ozone will be less than or around 1980 values in 2040, and averaged between 60°S and 60°N, column ozone returns to 1980 values about 5 years (but up to 15 years) later than in the interactive models. This is consistent with temperature changes playing a major role in the increases in ozone.

The CCM simulations that extend to 2050 show a similar recovery process over midlatitudes as the interactive 2-D models. Most CCMs (all but one/two in northern/southern midlatitudes) predict midlatitude ozone to be on average higher than 1980 values between 2040 and 2050, with increases to 1980 values generally occurring between 2005 and 2035 over northern midlatitudes and over southern midlatitudes somewhat later between 2025 and 2040, in agreement with the interactive 2-D models (Figure 6-10). The earlier return of northern midlatitude ozone to pre-1980 values is echoed in the hemispheric differences in ozone anomalies between 2040 and

21st CENTURY OZONE LAYER

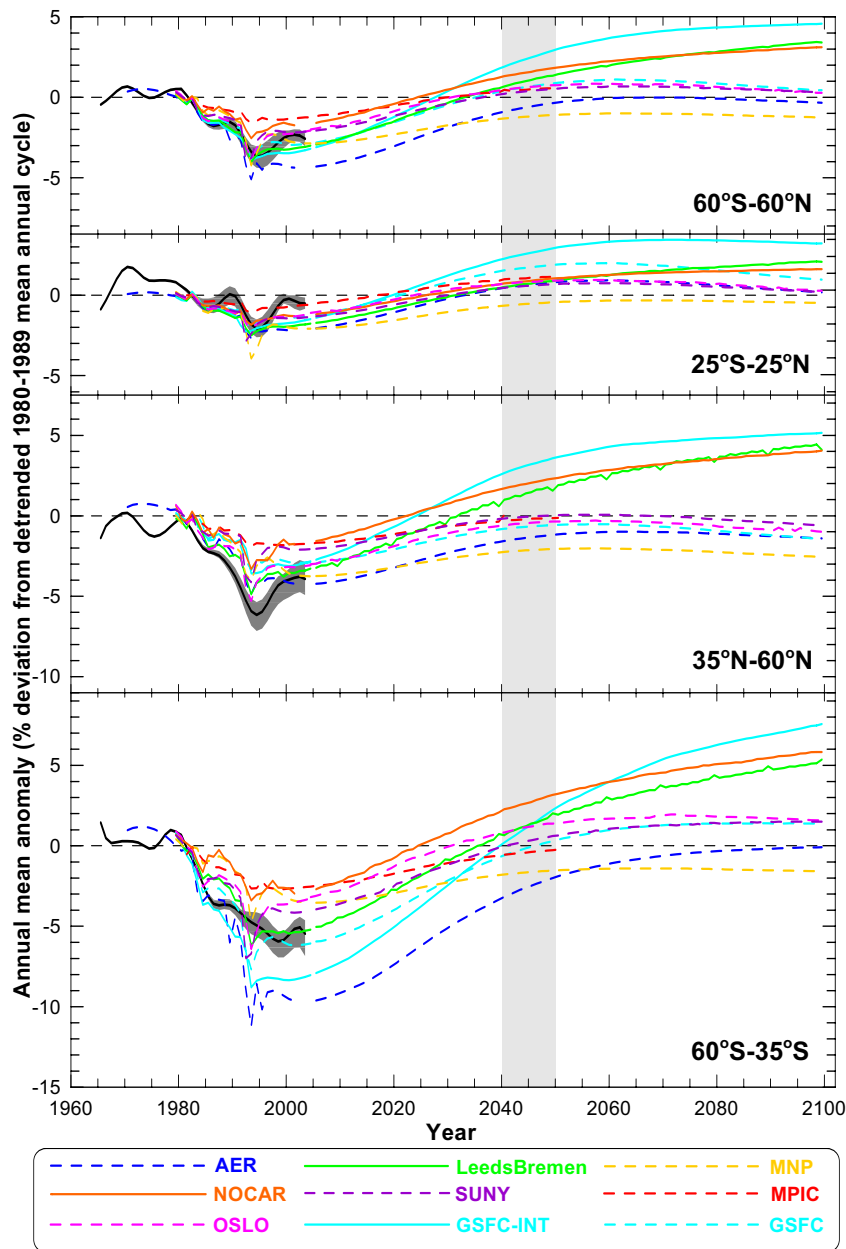


Figure 6-9. Annual mean zonal mean total column ozone anomalies from the P1 (1980-2004) and F1 (2005-2100) runs (Appendix 6A) from all of the 2-D models (colored lines; solid for interactive models and dashed for non-interactive models) and from four observational datasets (thick black line and gray shaded area show the mean and range of observed anomalies; see Chapter 3). Area-weighted zonal mean time series are shown for the global region (60°S to 60°N), the equatorial region (25°S to 25°N), the northern midlatitude region (35°N to 60°N), and the southern midlatitude region (60°S to 35°S) to match the analysis regions used in Chapter 3. The observational time series have been smoothed by applying a 1:2:1 filter iteratively five times. The filter width is reduced to 1 at the ends of the time series, effectively reproducing the original data and avoiding anomalous edge effects. The light gray shading between 2040 and 2050 shows the period when EESC is expected to return to 1980 values. Monthly anomalies were calculated by subtracting a detrended mean annual cycle, calculated over the period 1980-1989, from each time series. The annual cycle was detrended by fitting a regression model with seasonally dependent trends to the data and then reconstructing the “1980” mean annual cycle using the stationary components of the regression model. For further details on the method for calculating the anomalies, see Eyring et al. (2006).

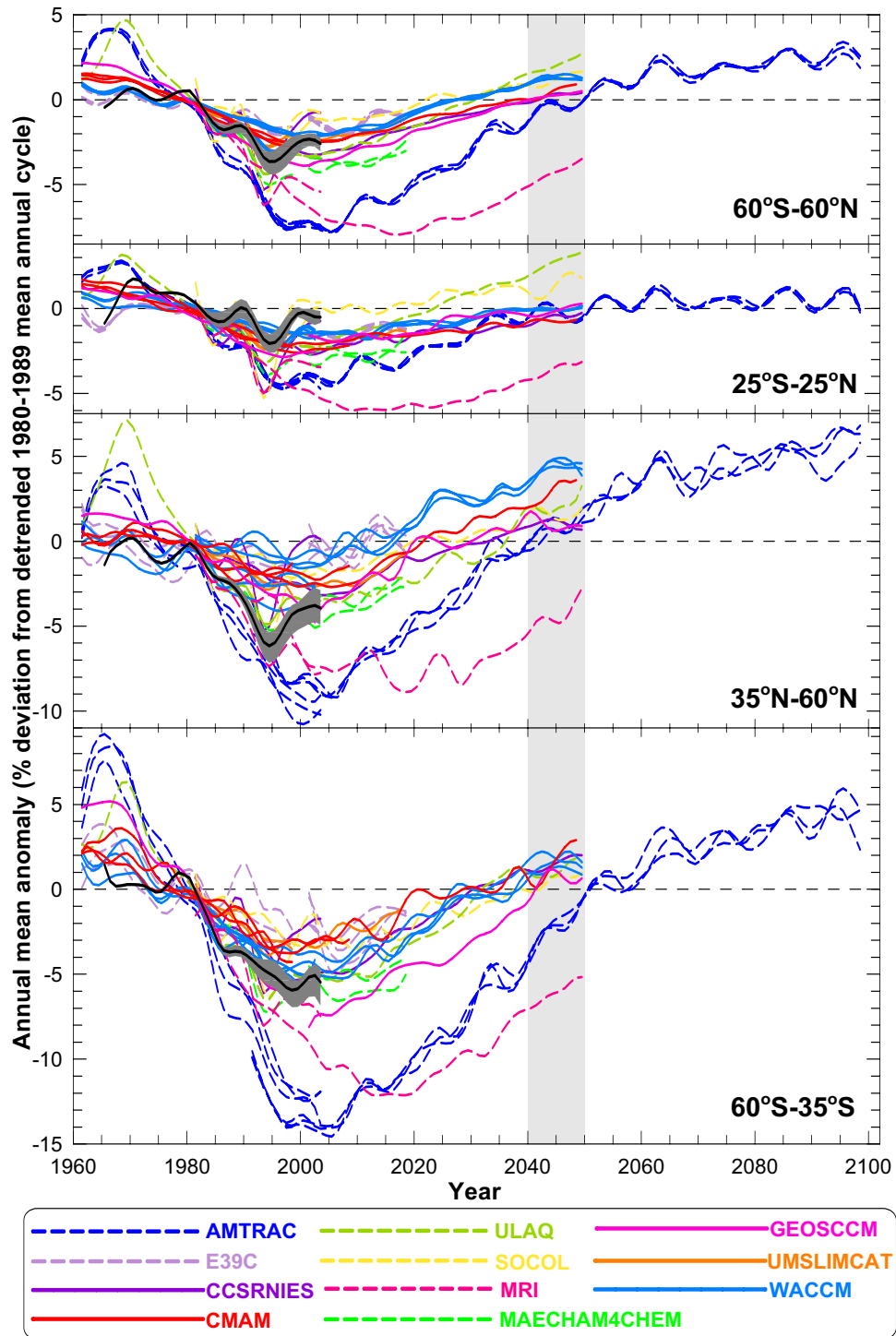


Figure 6-10. Annual mean zonal mean total column ozone anomalies from CCMs (colored lines) and from four observational datasets (thick black line and gray shaded area show the mean and range of observed anomalies; see Chapter 3). The time series are formed using the REF1 and REF2 or SCN2 simulations of each model (see Table 6-4). The time series have been smoothed as in Figure 6-9. The light gray shading between 2040 and 2050 shows the period when EESC is expected to return to 1980 values. As for the 2-D model results, the anomalies were calculated by subtracting the detrended 1980-1989 mean annual cycle. The mean annual cycles subtracted from the raw monthly means to calculate these anomalies are shown in Figure 3-26. For further details on the method for calculating the anomalies, see Eyring et al. (2006).

21st CENTURY OZONE LAYER

2050 (NH value of 0.5 to 5%; SH value of -0.5 to 3%). The two exceptions to the above are AMTRAC and MRI, which show a slower return of ozone to 1980 values such that ozone is below 1980 values in 2040. The later return of ozone to pre-1980 values in AMTRAC and MRI is consistent with the later decrease of Cl_y to 1980 values in these models (although other factors, such as biases in the troposphere (Austin and Wilson, 2006), may also contribute).

The recovery process of tropical ozone differs between the CCMs and interactive 2-D models. As discussed above, the interactive 2-D models predict tropical ozone to be above pre-1980 levels by 2040. In contrast, the majority of the CCMs predict ozone around or less than 1980 values in 2040. The cause of this difference is not known. Austin and Wilson (2006) noted that during northern spring, tropical ozone remained below 1980 levels out to 2100 in a narrow band around the equator. Rosenfield and Schoeberl (2005), using the GSFC-INT interactive 2-D model, showed that ozone at 51 hPa and 5°N remains low out to 2050 in their model as a result of increasing CO_2 , which cools the upper stratosphere, slows ozone gas-phase destruction reactions, and increases ozone there, which in turn reduces the penetration of UV to the lower stratosphere, which reduces ozone production there (a reverse of the “self-healing” effect). However, given that the GSFC-INT model also shows ozone exceeding pre-1980 levels between 25°S and 25°N (Figure 6-9), these suppressed ozone concentrations in the tropical lower stratosphere must not dominate column ozone changes.

After 2050, the ozone changes primarily reflect changes in WMGHGs. In the non-interactive 2-D models, the ozone is roughly constant or declines. In contrast, in the interactive 2-D models and in the one CCM that ran beyond 2050 (Austin and Wilson, 2006), ozone continues to slowly increase (except tropical ozone in AMTRAC and in the GSFC-INT model). By the end of the 21st century, these models predict that ozone averaged between 60°S and 60°N will be 2% to 5% above 1980 values.

In the simulations presented above, only a single scenario for WMGHG emissions has been considered. However, the sensitivity to temperatures and/or composition caused by WMGHG increases has been examined in other simulations. For example, Rosenfield et al. (2002) used an interactive 2-D model to examine the impact of CO_2 increase-induced cooling on ozone recovery and found that ozone returns to 1980 values 10 to 20 years earlier in many latitudes and seasons. Randeniya et al. (2002) used a non-interactive 2-D model to examine the impact of WMGHG-induced atmospheric composition changes on ozone through the 21st century and showed that in

northern midlatitudes, the ozone recovery depended greatly on the emissions scenarios used to drive the model. After 2050, NO_x increases due to N_2O increases caused stratospheric ozone levels to start to fall, and this loss was exacerbated if future methane levels remained approximately constant, rather than growing, as assumed in many scenarios.

The combined impact of CO_2 -induced cooling and changes in N_2O was subsequently examined by Chipperfield and Feng (2003), using the Leeds-Bremen interactive 2-D model. They performed two simulations, one with and the other without temperature changes due to increasing CO_2 , for three different WMGHG scenarios (one with high emissions (A1FI), one with low emissions (B1), and a third with A1FI emissions except with reduced CH_4 emissions). As shown in Figure 6-11, these calculations indicate that the inclusion of the CO_2 -induced cooling overcomes the N_2O chemical effect and leads to ozone reaching 1980 levels or above between 2030 and 2050, depending on the WMGHG scenario used. Similar results were obtained in NOCAR simulations performed for this Assessment (not shown). Consistent with Randeniya et al. (2002), Figure 6-11 also shows that for the cases where the CO_2 -induced cooling is excluded, ozone does not return to pre-1980 values in the 21st century. Therefore, the CO_2 -induced cooling and the N_2O chemical effect oppose each other, with the net effect dependent on the WMGHG scenario chosen.

The sensitivity of ozone recovery to WMGHG scenarios has also been examined using CCMs that include a more complete representation of climate-ozone feedbacks (e.g., the variability in tropospheric wave forcing due to climate change). As discussed in Chapter 5, simulations were also repeated for several CCMs with fixed WMGHGs, rather than increasing WMGHGs as in the “A1B” scenario. These simulations show higher stratospheric temperatures and slower increases in midlatitude ozone than in the simulations with increasing WMGHGs (see Figure 5-25 of Chapter 5).

6.6.4 Polar Ozone

As discussed in Chapter 5, the processes affecting ozone recovery in the polar regions are different from those influencing extrapolar recovery. For example, WMGHG-induced cooling of the stratosphere reduces ozone destruction in extrapolar regions, but enhances it in the polar lower stratosphere where heterogeneous chemistry dominates. To investigate the evolution of polar ozone through the 21st century, we focus on the CCMs as 2-D models do not include the three-dimensional processes that play a key role in polar ozone depletion and recovery. Several dif-

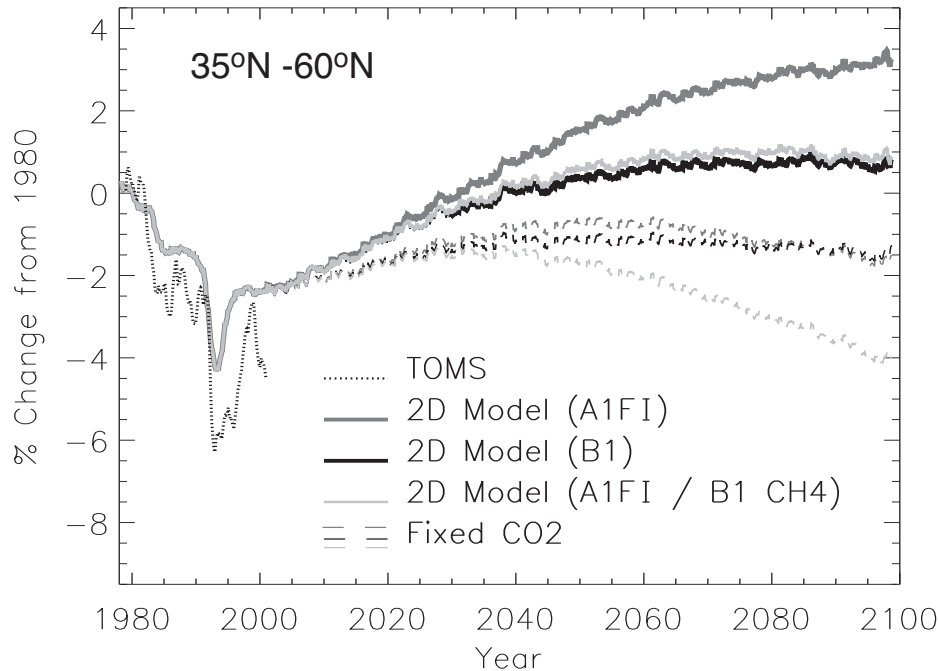


Figure 6-11. Variation in Northern Hemisphere midlatitude total column ozone (% change since 1980) from six runs of a 2-D model. The simulations used three different WMGHG scenarios (A1FI, B1, and A1FI with B1 CH₄ emissions), with results shown with (solid lines) and without (dashed lines) stratospheric cooling due to CO₂ increases. Also shown are observed past changes from satellite data. From Chipperfield and Feng (2003).

ferent diagnostics of polar ozone from the CCMs are considered, including:

- springtime total column ozone anomalies for the Arctic (March, 60°N-90°N) and Antarctic (October, 60°S-90°S), Figure 6-12;
- the minimum total column ozone poleward of 60°N for March-April (Arctic) and 60°S for September-October (Antarctic), Figure 6-13;
- the ozone mass deficit (Bodeker et al., 2005) from September to October, Figure 6-14; and
- the maximum Antarctic ozone hole area between September and October, Figure 6-14.

A discussion of the Antarctic ozone hole indices is provided in Chapter 4.

We examine these diagnostics for the same time periods as above: the beginning of the century (2000-2020) when EESC declines substantially, mid-century (2060-2070) when EESC is expected to decrease to 1980 values, and the end of the century (2090-2100) when ODSs are not expected to play a role in controlling polar ozone.

6.6.4.1 THE ANTARCTIC

In the Antarctic, the general characteristics of the ozone recovery are similar in all models and similar to the CCM projections shown in Austin et al. (2003) and WMO (2003), namely, the peak depletion occurs around 2000 within a broad minimum, followed by a slow increase in ozone values. All CCMs show Antarctic ozone increasing between 2000 and 2020, although the evolution varies

between models and between diagnostics. In general, column ozone increases by around 5% to 10% during this period. In nearly all models, the year of lowest October column ozone anomalies occurs between 1997 and 2010 but, as shown in Figures 6-12, 6-13, and 6-14, the response of the ozone diagnostic to changes in ODSs varies between the diagnostics. The increase in 60°-90°S October ozone anomalies and minimum Antarctic ozone is relatively slow, with values remaining constant between 2000 and 2010 in many models, whereas there is a relatively fast decrease in the ozone mass deficit. This behavior matches the differences in response between different Antarctic ozone hole indices seen in observations (Bodeker et al., 2005). The fact that some of the CCMs suggest that minimum October ozone anomalies have already occurred in the Antarctic may appear to contradict the conclusion made in Section 6.5.3 that neither the first, nor second stage of Antarctic ozone recovery has been detected in observations. It should be noted that the availability of model results beyond 2005, as opposed to measurements that terminate in 2005, facilitates the detection of the minimum. Ozone turnaround in measurements may have already occurred but lack of data beyond 2005 precludes its statistical detection. Nevertheless, because the turnaround in ozone as simulated in the CCMs has not been attributed here to changes in EESC, this behavior cannot be interpreted as stage (ii) of ozone recovery.

There is a wide range in the simulated peak ozone depletion in the CCMs. For example, the smoothed wintertime minimum Antarctic ozone values in the CCMs vary

21st CENTURY OZONE LAYER

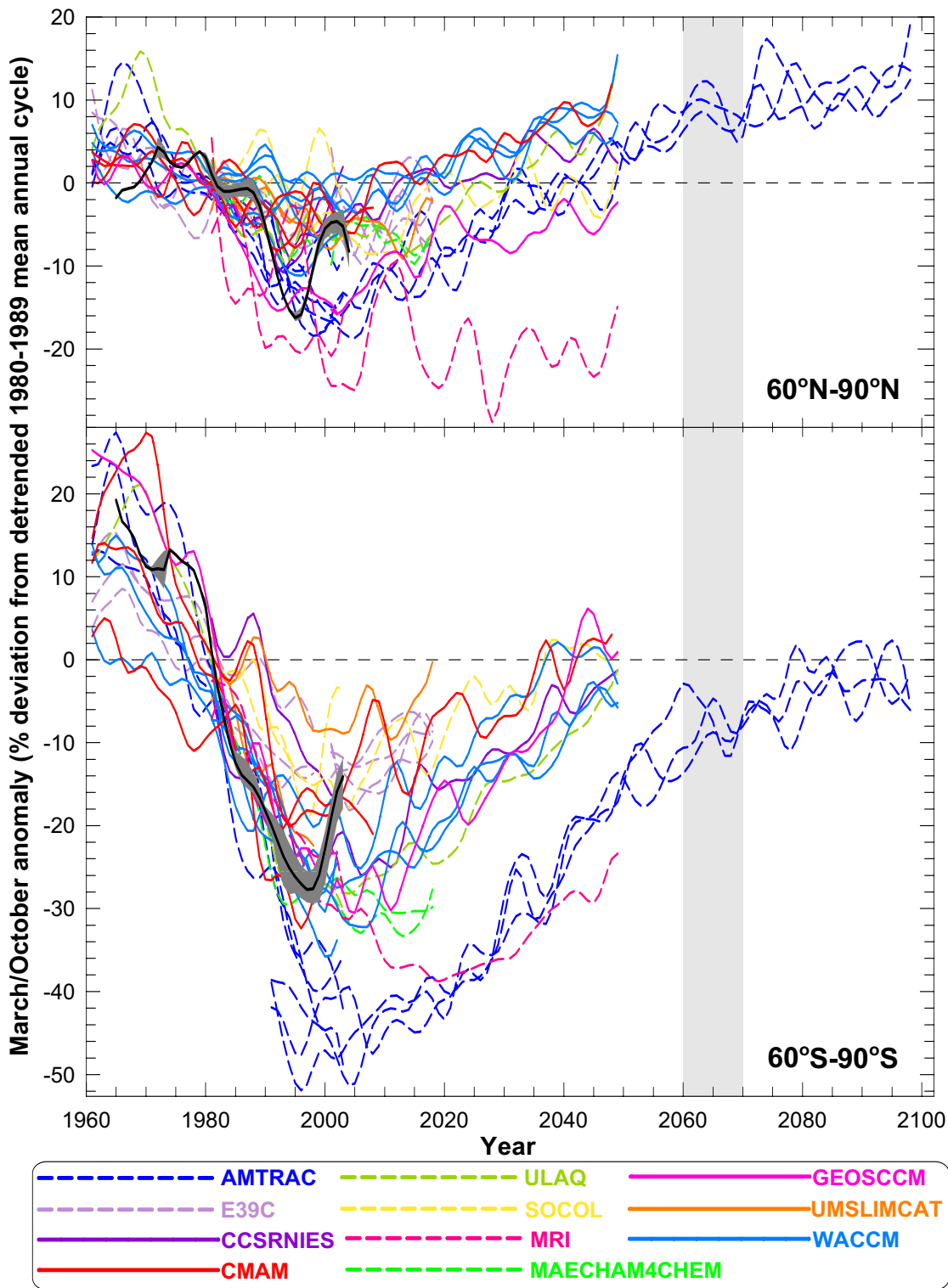


Figure 6-12. Upper panel: March Arctic (60°N to 90°N) total column ozone anomalies from CCMs (colored lines) and from 4 observational datasets (thick black line and gray shaded area show the mean and range of observed anomalies; see Chapter 3). Lower panel: as for the upper panel but October Antarctic (60°S to 90°S) total column ozone anomalies. Model simulations are as in Figure 6-10. The time series have been smoothed as in Figure 6-10. The light gray shading between 2060 and 2070 shows the period when EESC is expected to return to 1980 values.

between around 60 DU and 120 DU compared with observed values around 80 DU (Figure 6-13(b)), while the peak smoothed ozone mass deficit varies between 5 and 33 million tons compared with observed values around 31 million tons (Figure 6-14(a)). These variations highlight the deficiencies in some of the CCM simulations of the present-day ozone hole. Note, however, that because both the ozone hole area and the ozone mass deficit are based on 220 DU thresholds, a general high bias in the global-mean total ozone fields will generate a bias in these two diagnostics (e.g., most pronounced in MAECHAM-4CHEM).

There is a wide spread in the projected Antarctic ozone anomalies in 2050 and in the projected date when Antarctic ozone increases to or around 1980 values. The anomalies in 60°-90°S ozone in 2050 (see Figure 6-12) vary from around -24% to 3%, while the date for Antarctic ozone to increase to 1980 values varies between 2035 and 2095. However, this wide spread is mainly due to a few models (AMTRAC, MRI; see further discussion); in the majority of the CCMs, ozone is around 1980 values between 2040 and 2050.

There is no simple relationship in the CCMs between the date that Antarctic ozone increases to 1980 values and either the date of the minimum in Antarctic ozone or the ozone anomaly at this date. Hence, comparison of the simulated ozone hole with observations (as shown in Figures 6-13 and 6-14) does not provide a good indicator of differences in the CCM projections of the future ozone hole, and the wide spread shown in Figures 6-12 to 6-14.

However, some insight into the model differences can be obtained from comparisons of inorganic chlorine (Cl_y) in the models. A relationship is expected between the decrease in Cl_y and increase in ozone, and, in general, the increase in Antarctic ozone follows the decrease in Cl_y in the CCMs. As shown in Figure 6-8, there is a large spread in the simulated Antarctic Cl_y , including in the peak value and the date at which the Cl_y decreases to 1980 values. Models with a smaller peak have an earlier return of Cl_y to pre-1980 levels (e.g., SOCOL and E39C) and those with a larger peak have a later return (e.g., AMTRAC). Comparison with observations showed that peak Cl_y in several models is unrealistically low (see Section 6.6.2), and the above analysis indicates that the return to pre-1980 values of both Cl_y and ozone will be too early in these models. We thus put more weight on results from CCMs with higher, and more realistic, Cl_y . These models predict Cl_y and ozone back to pre-1980 values around or later than 2050. The MRI model simulates a later return of ozone to pre-1980 values due to an

unrealistic too slow decrease of Cl_y after 2000 and we put less weight on this model simulation. The Cl_y in AMTRAC matches the observations best, and predicts the latest return to pre-1980 values (Figure 6-8). The better agreement of polar Cl_y with observations gives support for this late return, but the justification for altering CFC photolysis rates has to be questioned (see Section 6.6.2).

The late return to pre-1980 values in the AMTRAC model is, nevertheless, consistent with the parametric modeling study of Newman et al. (2006). Using a parametric model of spring Antarctic ozone amounts that includes EESC levels over Antarctica (see Box 8.1 of Chapter 8) and analyzed Antarctic stratospheric temperatures, they predicted that the ozone hole area will remain constant until around 2010, that a decrease of the ozone hole area would not be statistically detectable until around 2024, and that return to pre-1980 levels in the Antarctic would not occur until around 2068; see Figure 6-14(b).

AMTRAC is the only CCM to run past 2050. This model predicts that springtime Antarctic ozone will be close to or just below (-7% to 3%) 1980 values by the end of the century (2090-2100). However, uncertainties in the projection are high because they are based on a single model and single WMGHG concentration scenario.

6.6.4.2 THE ARCTIC

As in the other regions, Arctic ozone is projected to increase from 2000 to 2020 (see Figures 6-12 and 6-13). The increases range between 0% and 10% and there is large interannual variability. Using the smoothed minimum Arctic ozone or 60°-90°N ozone anomalies, where the smoothing reduces the large variability, the date of minimum ozone occurs between 1997 and 2015 in nearly all of the models. This time range is similar to that for the Antarctic. As in the Antarctic, although the timing of the minimum anomaly is similar between models, there is a substantial variation in the magnitude of the ozone when this occurs, with the smoothed minimum Arctic ozone varying from around 200 DU to over 300 DU, compared with around 220 DU in the observations. This again highlights some substantial biases in many of the models.

Most CCMs that have been run to 2050 show Arctic ozone values larger than 1980 values in 2050. In other words, all CCMs show Arctic ozone increasing to pre-1980 values before 2050 (and before EESC returns to 1980 concentrations; 2060-2070). There is a wide range of dates for Arctic ozone to increase to 1980 values, with the date that smoothed minimum Arctic ozone increases to 1980 values varying between around 2010 and 2040. Although there are large differences in the CCM simulations of Arctic ozone, all, except MRI, show an increase to pre-

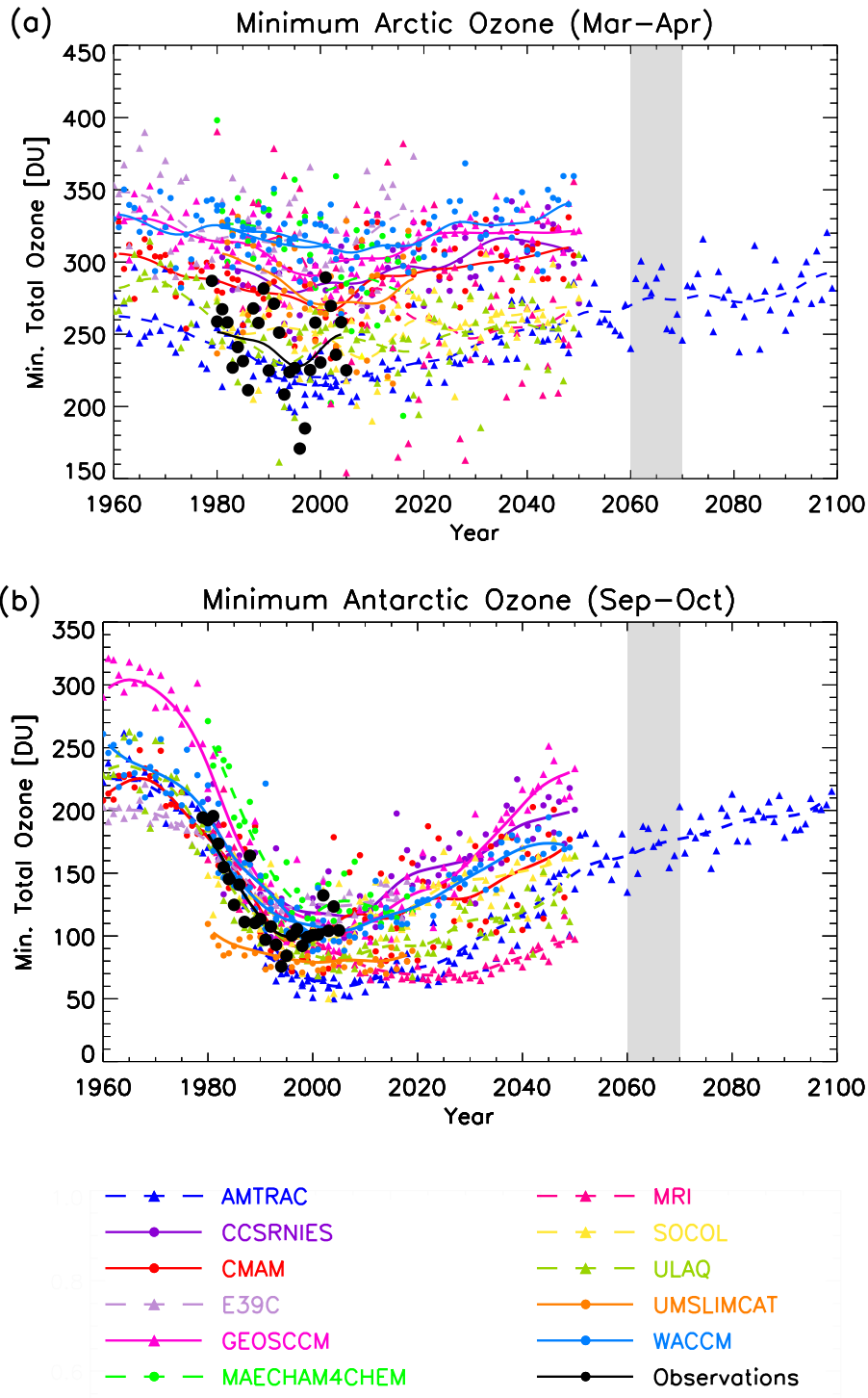


Figure 6-13. (a) Minimum Arctic total column ozone for March to April and (b) minimum Antarctic total column ozone for September to October for various transient CCM simulations. Model simulations are as in Figure 6-10, except a single ensemble simulation is shown for each model. Model results are compared with observations calculated using the National Institute of Water and Atmospheric Research (NIWA) combined total column ozone database (Bodeker et al., 2005). Solid and dashed curves show smoothed data derived by applying a 1:2:1 filter iteratively 30 times. The filter width is reduced to 1 at the ends of the time series, effectively reproducing the original data and avoiding anomalous edge effects. The light gray shading between 2060 and 2070 shows the period when EESC is expected to return to 1980 values.

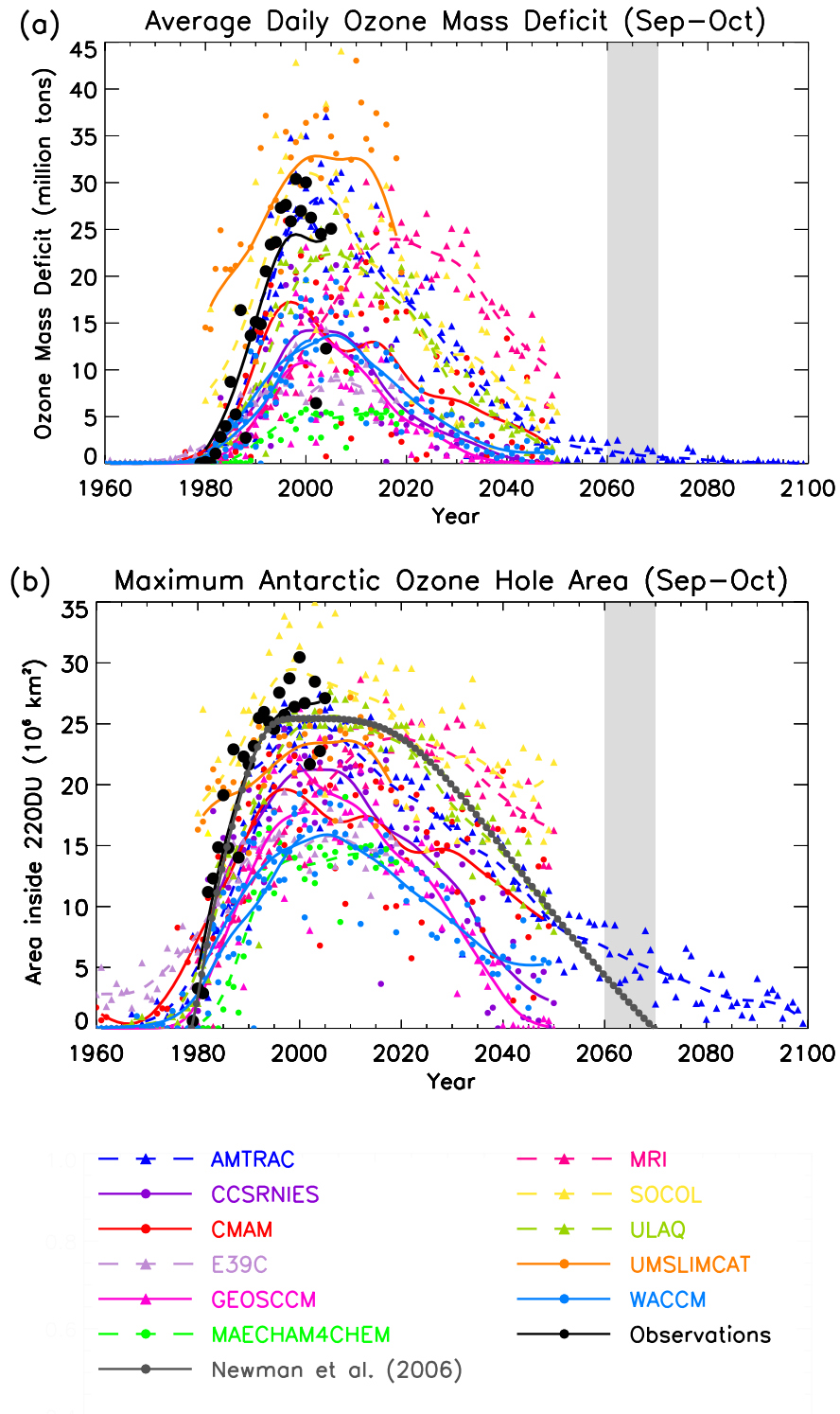


Figure 6-14. (a) The Antarctic September to October average daily ozone mass deficit for each year from each CCM and (b) the maximum Antarctic ozone hole area between September and October. Model simulations are as in Figure 6-10, except a single ensemble simulation is shown for each model. Model results are compared with observations calculated using the National Institute of Water and Atmospheric Research (NIWA) combined total column ozone database (Bodeker et al., 2005). The curves show the data smoothed as in Figure 6-13. Gray circles show the projection from Newman et al. (2006). The light gray shading between 2060 and 2070 shows the period when EESC is expected to return to 1980 values.

21st CENTURY OZONE LAYER

1980 ozone before or around 2050 with no indication of severe Arctic ozone loss over this time.

In all CCMs that have been run long enough, Arctic ozone increases to 1980 values before Antarctic ozone does. In some models the difference is only a few years, but in others the difference is over 25 years. The projected evolution of Arctic ozone does not follow the evolution of halogens as closely as in the Antarctic, i.e., the spread of the projected Arctic ozone is not strongly related to the spread in simulated Cl_y (the simulated Arctic Cl_y is similar to that shown in Figure 6-8). This indicates that changes in other factors (e.g., temperature and transport) play a significant role in determining when Arctic ozone returns to pre-1980 values. Austin and Wilson (2006) reported that the earlier return to pre-1980 values in the Arctic in AMTRAC results from both an increased Brewer-Dobson circulation and reduced gas-phase ozone depletion in a cooler stratosphere. However, it is unclear whether this is occurring in all models. For example, in the E39C, ULAQ, and WACCM simulations with fixed WMGHGs discussed in Chapter 5, the return to pre-1980 values is very similar to that in simulations with increasing WMGHGs presented here (see Figure 5-26 of Chapter 5). This suggests that in these models, there is little impact of increased WMGHGs on Arctic ozone recovery before 2050.

Projections from AMTRAC, the only CCM to run past 2050, suggest that Arctic ozone in 2090 to 2100 will be substantially above (8% to 19%) 1980 values. This is in contrast to Antarctic ozone in this model, which is close to or just below 1980 values by the end of the century.

The increase in the Arctic column ozone minima in the above CCM simulations is much faster than the empirical estimation of Knudsen et al. (2004), where the Arctic ozone losses would increase until 2010-2015 and decrease only slightly afterwards. However there are large uncertainties in the Knudsen et al. calculations: the observed temperature and water vapor trends used in the analysis are uncertain, and most important, it is unlikely that the past trends will (as they assumed) continue unchanged into the future (see Austin, 2004; Pitari, 2004). Given the likelihood of changes in trends in the Arctic, we put more weight on the CCM projections, which attempt to capture these changes, than the Knudsen empirical predictions.

6.6.5 Uncertainties in Model Projections and Open Questions

Sources of uncertainty in model projections of future ozone range from those intrinsic to the models, such as uncertainties in parameterizations and adequate incorporation of feedbacks, to those external, such as uncertainties in the emissions scenarios and sea surface temperature

datasets used to drive the models. Many of the intrinsic sources of uncertainties in CCMs are discussed in Chapter 5 and the uncertainties resulting from projections of future ODS emissions are discussed in Chapter 8. The purpose of this section is to discuss some of the processes that are not included in the models that may contribute to uncertainty in ozone projections.

The model results presented above have focused on one WMGHG emissions scenario (see Appendix 6A). The IPCC Special Report on Emissions Scenarios (SRES) (IPCC, 2000) A1B scenario is by no means the most likely scenario, and the use of different, but possibly equally likely, scenarios is expected to cause different projections of future ozone, see Figure 6-11. Furthermore, the SRES scenarios define only changes in anthropogenic emissions and not concurrent changes in natural emissions due, for example, to changes in surface climate. Climate change-induced increases in emissions of halogenated very short-lived sources gases, changes to their transport to the tropical tropopause layer (TTL), and their degradation to bromine, chlorine, and iodine (see Section 2.4 of Chapter 2) have the potential to change tropical ozone abundances in the future. Given the current resolution of the TTL region in CCMs, we cannot fully assess this question. Currently our understanding from transport studies would indicate that only a small fraction of air is directly lifted vertically through the TTL into the lower tropical stratosphere, but there are indications that the “sideways” transport into the extratropical stratosphere might be significant and sometimes fast (Levine et al., 2006).

At present, the prescribed model boundary conditions are not the emissions scenarios themselves but concentration scenarios derived from the emissions scenarios (Prather and Ehhalt et al., 2001). This decoupling of the processes linking changes in emissions to changes in concentrations of WMGHGs and ODSs neglects feedbacks that could be important, e.g., future increases in stratospheric ozone may change tropospheric photolysis rates through enhanced absorption of solar UV, and change tropospheric ozone levels by increasing the stratosphere-troposphere exchange source of ozone (Hauglustaine et al., 2005). These in turn affect tropospheric oxidizing capacity, which affects WMGHG and ODS lifetimes. The effects of such changes on lifetimes have been ignored in the construction of ODS and WMGHG concentration scenarios; see Section 8.3.1 of Chapter 8 and Prather and Ehhalt et al. (2001), respectively. Natural processes, such as volcanic eruptions (see Section 6.3.6), could also affect tropospheric oxidizing capacity and/or change the effectiveness of stratospheric ODSs in depleting ozone.

New anthropogenic source gases, currently excluded from emissions scenarios, may become impor-

tant in the future, e.g., fugitive emissions of hydrogen from a hydrogen economy. Tromp et al. (2003) estimated that a hydrogen economy could cause stratospheric water vapor increases of up to 35% and decrease ozone by up to 10% in polar regions during spring. However, Warwick et al. (2004) found a much reduced effect on stratospheric ozone on the order of 0.5% or less. This reduced estimate is the result of an assumed smaller leakage rate of hydrogen combined with the inclusion of reduced CO, NO_x, CH₄, and nonmethane hydrocarbons due to the reduction of fossil fuel usage. Furthermore, the timing of the conversion to a hydrogen economy with respect to the reduction of halogen loading is a major factor, because the coupling to chlorine chemistry causes most of the ozone loss. If the shift to a hydrogen economy occurs primarily after 2020 (Kammen and Lipman, 2003), the potential harm due to the increase in anthropogenic hydrogen emission can be prevented.

REFERENCES

- Akiyoshi, H., T. Sugita, H. Kanzawa, and N. Kawamoto, Ozone perturbations in the Arctic summer lower stratosphere as a reflection of NO_x chemistry and planetary scale wave activity, *J. Geophys. Res.*, *109*, D03304, doi: 10.1029/2003JD003632, 2004.
- Andersen, S.B., E.C. Weatherhead, A. Stevermer, J. Austin, C. Brühl, E.L. Fleming, J. de Grandpré, V. Grewe, I. Isaksen, G. Pitari, R.W. Portmann, B. Rognerud, J.E. Rosenfield, S. Smyshlyayev, T. Nagashima, G.J.M. Velders, D.K. Weisenstein, and J. Xia, Comparison of recent modeled and observed trends in total column ozone, *J. Geophys. Res.*, *111*, D02303, doi: 10.1029/2005JD006091, 2006.
- Andrews, A.E., K.A. Boering, B.C. Daube, S.C. Wofsy, M. Loewenstein, H. Jost, J.R. Podolske, C.R. Webster, R.L. Herman, D.C. Scott, G.J. Flesch, E.J. Moyer, J.W. Elkins, G.S. Dutton, D.F. Hurst, F.L. Moore, E.A. Ray, P.A. Romashkin, and S.E. Strahan, Mean ages of stratospheric air derived from in situ observations of CO₂, CH₄, and N₂O, *J. Geophys. Res.*, *106* (D23), 32295-32314, doi: 10.1029/2001JD000465, 2001.
- Austin, J., A three-dimensional coupled chemistry-climate model simulation of past stratospheric trends, *J. Atmos. Sci.*, *59* (2), 218-232, 2002.
- Austin, J., Is there really an alternative to the use of coupled chemistry-climate models? Part 1, Interactive comment on "Extrapolating future Arctic ozone losses" by B.M. Knudsen et al., *Atmos. Chem. Phys. Discuss.*, *4*, S1068-S1072, 2004.
- Austin, J., and R.J. Wilson, Ensemble simulations of the decline and recovery of stratospheric ozone, *J. Geophys. Res.*, *111*, D16314, doi: 10.1029/2005JD006907, 2006.
- Austin, J., D. Shindell, S.R. Beagley, C. Brühl, M. Dameris, E. Manzini, T. Nagashima, P. Newman, S. Pawson, G. Pitari, E. Rozanov, C. Schnadt, and T.G. Shepherd, Uncertainties and assessments of chemistry-climate models of the stratosphere, *Atmos. Chem. Phys.*, *3*, 1-27, 2003.
- Austin, J., J. Wilson, F. Li, and H. Vömel, Evolution of water vapor and age of air in coupled chemistry climate model simulations of the stratosphere, *J. Atmos. Sci.*, in press, 2006.
- Beagley, S.R., J. de Grandpré, J.N. Koshyk, N.A. McFarlane, and T.G. Shepherd, Radiative-dynamical climatology of the first-generation Canadian Middle Atmosphere Model, *Atmos. Ocean*, *35* (3), 293-331, 1997.
- Bloom, S., A. da Silva, D. Dee, M. Bosilovich, J.-D. Chern, S. Pawson, S. Schubert, M. Sienkiewicz, I. Stajner, W.-W. Tan, and M.-L. Wu, *Documentation and Validation of the Goddard Earth Observing System (GEOS) Data Assimilation System, Version 4, NASA/TM-2005-104606*, 26, 187 pp., NASA Goddard Space Flight Center, Greenbelt, Md., 2005.
- Bodeker, G.E., H. Shiona, and H. Eskes, Indicators of Antarctic ozone depletion, *Atmos. Chem. Phys.*, *5*, 2603-2615, 2005.
- Brasseur, G., and C. Granier, Mount Pinatubo aerosols, chlorofluorocarbons, and ozone depletion, *Science*, *257* (5074), 1239-1242, 1992.
- Brönnimann, S., J. Luterbacher, J. Staehelin, T.M. Svendby, G. Hansen, and T. Svenøe, Extreme climate of the global troposphere and stratosphere in 1940-42 related to El Niño, *Nature*, *431* (7011), 971-974, 2004.
- Butchart, N., and A.A. Scaife, Removal of chlorofluorocarbons by increased mass exchange between the stratosphere and troposphere in a changing climate, *Nature*, *410* (6830), 799-802, 2001.
- Butchart, N., A.A. Scaife, M. Bourqui, J. de Grandpré, S.H.E. Hare, J. Kettleborough, U. Langematz, E. Manzini, F. Sassi, K. Shibata, D. Shindell, and M. Sigmond, Simulations of anthropogenic change in the strength of the Brewer-Dobson circulation, *Clim. Dyn.*, *27* (7-8), 727-741, 2006.
- Chipperfield, M.P., and W. Feng, Comment on: "Stratospheric Ozone Depletion at northern mid-latitudes in the 21st century: The importance of future concentrations of greenhouse gases nitrous oxide and methane," *Geophys. Res. Lett.*, *30* (7), 1389, doi: 10.1029/2002GL016353, 2003.
- Cunnold, D.M., E.-S. Yang, M.J. Newchurch, G.C.

- Reinsel, J.M. Zawodny, and J.M. Russell III, Comment on "Enhanced upper stratospheric ozone: Sign of recovery or solar cycle effect?" by W. Steinbrecht et al., *J. Geophys. Res.*, *109*, D14305, doi: 10.1029/2004JD004826, 2004.
- Dameris, M., V. Grewe, M. Ponater, R. Deckert, V. Eyring, F. Mager, S. Matthes, C. Schnadt, A. Stenke, B. Steil, C. Brühl, and M.A. Giorgetta, Long-term changes and variability in a transient simulation with a chemistry-climate model employing realistic forcing, *Atmos. Chem. Phys.*, *5*, 2121-2145, 2005.
- Dameris, M., S. Matthes, R. Deckert, V. Grewe, and M. Ponater, Solar cycle effect delays onset of ozone recovery, *Geophys. Res. Lett.*, *33*, L03806, doi: 10.1029/2005GL024741, 2006.
- de Grandpré, J., S.R. Beagley, V.I. Fomichev, E. Griffioen, J.C. McConnell, A.S. Medvedev, and T.G. Shepherd, Ozone climatology using interactive chemistry: Results from the Canadian Middle Atmosphere Model, *J. Geophys. Res.*, *105* (D21), 26475-26491, 2000.
- Dhomse, S., M. Weber, I. Wohltmann, M. Rex, and J.P. Burrows, On the possible causes of recent increases in northern hemispheric total ozone from a statistical analysis of satellite data from 1979 to 2003, *Atmos. Phys. Chem.*, *6*, 1165-1180, 2006.
- Douglass, A.R., M.R. Schoeberl, R.S. Stolarski, J.W. Waters, J.M. Russell III, A.E. Roche, and S.T. Massie, Interhemispheric differences in springtime production of HCl and ClONO₂ in the polar vortices, *J. Geophys. Res.*, *100* (D7), 13967-13978, 1995.
- Douglass, A.R., R.S. Stolarski, S.E. Strahan, and B.C. Polansky, Sensitivity of Arctic ozone loss to polar stratospheric cloud volume and chlorine and bromine loading in a chemistry and transport model, *Geophys. Res. Lett.*, *33*, L17809, doi: 10.1029/2006GL026492, 2006.
- Dvortsov, V.L., and S. Solomon, Response of the stratospheric temperatures and ozone to past and future increases in stratospheric humidity, *J. Geophys. Res.*, *106* (D7), 7505-7514, 2001.
- Egorova, T., E. Rozanov, V. Zubov, E. Manzini, W. Schmutz, and T. Peter, Chemistry-climate model SOCOL: a validation of the present-day climatology, *Atmos. Chem. Phys.*, *5*, 1557-1576, 2005.
- Eyring, V., N.R.P. Harris, M. Rex, T.G. Shepherd, D.W. Fahey, G.T. Amanatidis, J. Austin, M.P. Chipperfield, M. Dameris, P.M. de F. Forster, A. Gattelman, H.F. Graf, T. Nagashima, P.A. Newman, S. Pawson, M.J. Prather, J.A. Pyle, R.J. Salawitch, B.D. Santer, and D.W. Waugh, A strategy for process-oriented validation of coupled chemistry-climate models, *Bull. Amer. Meteorol. Soc.*, *86* (8), 1117-1133, 2005.
- Eyring, V., N. Butchart, D.W. Waugh, H. Akiyoshi, J. Austin, S. Bekki, G.E. Bodeker, B.A. Boville, C. Brühl, M.P. Chipperfield, E. Cordero, M. Dameris, M. Deushi, V.E. Fioletov, S.M. Frith, R.R. Garcia, A. Gattelman, M.A. Giorgetta, V. Grewe, L. Jourdain, D.E. Kinnison, E. Mancini, E. Manzini, M. Marchand, D.R. Marsh, T. Nagashima, P.A. Newman, J.E. Nielsen, S. Pawson, G. Pitari, D.A. Plummer, E. Rozanov, M. Schraner, T.G. Shepherd, K. Shibata, R.S. Stolarski, H. Struthers, W. Tian, and M. Yoshiki, Assessment of temperature, trace species, and ozone in chemistry-climate model simulations of the recent past, *J. Geophys. Res.*, *111*, D22308, doi: 10.1029/2006JD007327, 2006.
- Fleming, E.L., C.H. Jackman, R.S. Stolarski, and D.B. Considine, Simulation of stratospheric tracers using an improved empirically based two-dimensional model transport formulation, *J. Geophys. Res.*, *104* (D19), 23911-23934, 1999.
- Giorgetta, M.A., and L. Bengtsson, The potential role of the quasi-biennial oscillation in the stratosphere-troposphere exchange as found in water vapor in general circulation model experiments, *J. Geophys. Res.*, *104* (D6), 6003-6019, 1999.
- Groß, J.-U., C. Brühl, and T. Peter, Impact of aircraft emissions on tropospheric and stratospheric ozone. Part I: Chemistry and 2-D model results, *Atmos. Environ.*, *32* (18), 3173-3184, 1998.
- Hadjinicolaou, P., J.A. Pyle, and N.R.P. Harris, The recent turnaround in stratospheric ozone over northern middle latitudes: A dynamical modeling perspective, *Geophys. Res. Lett.*, *32*, L12821, doi: 10.1029/2005GL022476, 2005.
- Hall, T.M., D.W. Waugh, K.A. Boering, and R.A. Plumb, Evaluation of transport in stratospheric models, *J. Geophys. Res.*, *104* (D15), 18815-18840, 1999.
- Harris, J.M., S.J. Oltmans, P.P. Tans, R.D. Evans, and D.L. Quincy, A new method for describing long-term changes in total ozone, *Geophys. Res. Lett.*, *28* (24), 4535-4538, 2001.
- Hauglustaine, D.A., J. Lathière, S. Szopa, and G.A. Folberth, Future tropospheric ozone simulated with a climate-chemistry-biosphere model, *Geophys. Res. Lett.*, *32*, L24807, doi: 10.1029/2005GL024031, 2005.
- Hofmann, D.J., S.J. Oltmans, J.M. Harris, B.J. Johnson, and J.A. Lathrop, Ten years of ozonesonde measurements at the south pole: Implications for recovery of springtime Antarctic ozone, *J. Geophys. Res.*, *102* (D7), 8931-8943, 1997.

- Hood, L.L., and B.E. Soukharev, Interannual variations of total ozone at northern midlatitudes correlated with stratospheric EP flux and potential vorticity, *J. Atmos. Sci.*, 62 (10), 3724-3740, 2005.
- Hoppel, K., R. Bevilacqua, T. Canty, R.J. Salawitch, and M.L. Santee, A measurement/model comparison of ozone photochemical loss in the Antarctic ozone hole using Polar Ozone and Aerosol Measurement observations and the Match technique, *J. Geophys. Res.*, 110, D19304, doi: 10.1029/2004JD005651, 2005.
- IPCC (Intergovernmental Panel on Climate Change), *Emissions Scenarios. A Special Report of Working Group III of the Intergovernmental Panel on Climate Change*, edited by N. Nakicenovic and R. Swart, 570 pp., Cambridge University Press, Cambridge, U.K. and New York, N.Y., 2000.
- IPCC/TEAP (Intergovernmental Panel on Climate Change/Technology and Economic Assessment Panel), *IPCC/TEAP Special Report on Safeguarding the Ozone Layer and the Global Climate System: Issues Related to Hydrofluorocarbons and Perfluorocarbons*. Prepared by Working Groups I and III of the Intergovernmental Panel on Climate Change, and the Technical and Economic Assessment Panel, Cambridge University Press, U.K. and New York, N.Y., 2005.
- Isaksen, I.S.A., B. Rognerud, F. Stordal, M.T. Coffey, and W.G. Mankin, Studies of Arctic stratospheric ozone in a 2-D model including some effects of zonal asymmetries, *Geophys. Res. Lett.*, 17, 557-560, 1990.
- Jiang, Y., Y.L. Yung, and R.W. Zurek, Decadal evolution of the Antarctic ozone hole, *J. Geophys. Res.*, 101, 8985-8999, 1996.
- Kammen, D.M., and T.E. Lipman, Assessing the future hydrogen economy, *Science*, 302 (5643), 226-229, 2003.
- Kirk-Davidoff, D.B., E.J. Hints, J.G. Anderson, and D.W. Keith, The effect of climate change on ozone depletion through changes in stratospheric water vapour, *Nature*, 402 (6760), 399-401, 1999.
- Knudsen, B.M., N.R.P. Harris, S.B. Andersen, B. Christiansen, N. Larsen, M. Rex, and B. Naujokat, Extrapolating future Arctic ozone losses, *Atmos. Chem. Phys.*, 4, 1849-1856, 2004.
- Krzyścin, J.W., Change in ozone depletion rates beginning in the mid 1990s: Trend analyses of the TOMS/SBUV merged total ozone data, 1978-2003, *Ann. Geophys.*, 24, 493-502, 2006.
- Krzyścin, J.W., J. Jaroslowski, and B. Rajewska-Wiech, Beginning of the ozone recovery over Europe? - Analysis of the total ozone data from the ground-based observations, 1964-2004, *Ann. Geophys.*, 23, 1685-1695, 2005.
- Kurokawa, J., H. Akiyoshi, T. Nagashima, H. Masunaga, T. Nakajima, M. Takahashi, and H. Nakane, Effects of atmospheric sphericity on stratospheric chemistry and dynamics over Antarctica, *J. Geophys. Res.*, 110, D21305, doi: 10.1029/2005JD005798, 2005.
- Langematz, U., and M. Kunze, An update on dynamical changes in the Arctic and Antarctic stratospheric polar vortices, *Clim. Dyn.*, 27 (6), 647-660, 2006.
- Lean, J., G.J. Rottman, H.L. Kyle, T.N. Woods, J.R. Hickey, and L.C. Puga, Detection and parameterization of variations in solar mid and near ultraviolet radiation (200-400 nm), *J. Geophys. Res.*, 102 (D25), 29939-29956, 1997.
- Lefèvre, F., G.P. Brasseur, I. Folkins, A.K. Smith, and P. Simon, Chemistry of the 1991-1992 stratospheric winter: Three dimensional model simulations, *J. Geophys. Res.*, 99 (D4), 8183-8195, 1994.
- Levine, J.G., P. Braesicke, N.R.P. Harris, N.H. Savage, and J.A. Pyle, Pathways and timescales for troposphere-to-stratosphere transport via the tropical tropopause layer and their relevance for very short lived substances, *J. Geophys. Res.*, in press, 2006.
- Malanca, F.E., P.O. Canziani, and G.A. Argüello, Trends evolution of ozone between 1980 and 2000 at mid-latitudes over the Southern Hemisphere: Decadal differences in trends, *J. Geophys. Res.*, 110, D05102, doi: 10.1029/2004JD004977, 2005.
- Manzini, E., B. Steil, C. Brühl, M.A. Giorgetta, and K. Krüger, A new interactive chemistry-climate model: 2. Sensitivity of the middle atmosphere to ozone depletion and increase in greenhouse gases and implications for recent stratospheric cooling, *J. Geophys. Res.*, 108 (D14), 4429, doi: 10.1029/2002JD002977, 2003.
- McCormack, J.P., and L.L. Hood, Apparent solar cycle variations of upper stratospheric ozone and temperature: Latitude and seasonal dependences, *J. Geophys. Res.*, 101 (D15), 20933-20944, 1996.
- McCormack, J.P., L.L. Hood, R. Nagatani, A.J. Miller, W.G. Planet, and R.D. McPeters, Approximate separation of volcanic and 11-year signals in the SBUV-SBUV/2 total ozone record over the 1979-1995 period, *Geophys. Res. Lett.*, 24 (22), 2729-2732, doi: 10.1029/97GL02900, 1997.
- McLinden, C.A., S.C. Olsen, M.J. Prather, and J.B. Liley, Understanding trends in stratospheric NO_y and NO₂, *J. Geophys. Res.*, 106 (D21), 27787-27793, 2001.

21st CENTURY OZONE LAYER

- Miller, A.J., A. Cai, G.C. Tiao, D.J. Wuebbles, L.E. Flynn, S.-K. Yang, E.C. Weatherhead, V. Fioletov, I. Petropavlovskikh, X.-L. Meng, S. Guillas, R.M. Nagatani, and G.C. Reinsel, Examination of ozone-sonde data for trends and trend changes incorporating solar and Arctic oscillation signals, *J. Geophys. Res.*, *111*, D13305, doi: 10.1029/2005JD006684, 2006.
- Mote, P.W., K.H. Rosenlof, M.E. McIntyre, E.S. Carr, J.C. Gille, J.R. Holton, J.S. Kinnersley, H.C. Pumphrey, J.M. Russell, and J.W. Waters, An atmospheric tape recorder: The imprint of tropical tropopause temperatures on stratospheric water vapor, *J. Geophys. Res.*, *101* (D2), 3989-4006, 1996.
- Nevison, C.D., S. Solomon, and R.S. Gao, Buffering interactions in the modeled response of stratospheric O₃ to increased NO_x and HO_x, *J. Geophys. Res.*, *104* (D3), 3741-3754, 1999.
- Newchurch, M.J., E.-S. Yang, D.M. Cunnold, G.C. Reinsel, J.M. Zawodny, and J.M. Russell III, Evidence for slowdown in stratospheric ozone loss: First stage of ozone recovery, *J. Geophys. Res.*, *108* (D16), 4507, doi: 10.1029/2003JD003471, 2003.
- Newman, P.A., S.R. Kawa, and E.R. Nash, On the size of the Antarctic ozone hole, *Geophys. Res. Lett.*, *31*, L21104, doi: 10.1029/2004GL020596, 2004.
- Newman, P.A., E.R. Nash, S.R. Kawa, S.A. Montzka, and S.M. Schauffler, When will the Antarctic ozone hole recover?, *Geophys. Res. Lett.*, *33*, L12814, doi: 10.1029/2005GL025232, 2006.
- Park, J.H., M.K.W. Ko, C.H. Jackman, R.A. Plumb, J.A. Kaye, and K.H. Sage, *Models and Measurements Intercomparison II, NASA/TM-1999-209554*, 502 pp., NASA Langley Research Center, Hampton, Va., 1999.
- Park, M., W.J. Randel, D.E. Kinnison, R.R. Garcia, and W. Choi, Seasonal variation of methane, water vapor, and nitrogen oxides near the tropopause: Satellite observations and model simulations, *J. Geophys. Res.*, *109*, D03302, doi: 10.1029/2003JD003706, 2004.
- Petropavlovskikh, I., C. Ahn, P.K. Bhartia, and L.E. Flynn, Comparison and covalidation of ozone anomalies and variability observed in SBUV(2) and Umkehr northern midlatitude ozone profile estimates, *Geophys. Res. Lett.*, *32*, L06805, doi: 10.1029/2004GL022002, 2005.
- Pitari, G., Interactive comment on "Extrapolating future Arctic ozone losses" by B.M. Knudsen et al., *Atmos. Chem. Phys. Discuss.*, *4*, S1214-S1215, 2004.
- Pitari, G., E. Mancini, V. Rizi, and D.T. Shindell, Impact of future climate change and emission changes on stratospheric aerosols and ozone, *J. Atmos. Sci.*, *59* (3), 414-440, 2002.
- Portmann, R.W., S.S. Brown, T. Gierczak, R.K. Talukdar, J.B. Burkholder, and A.R. Ravishankara, Role of nitrogen oxides in the stratosphere: A reevaluation based on laboratory studies, *Geophys. Res. Lett.*, *26* (15), 2387-2390, 1999.
- Prather, M., and D. Ehhalt (Co-ordinating Lead Authors), F. Dentener, R. Derwent, E. Dlugokencky, E. Holland, I. Isaksen, J. Katima, V. Kirchhoff, P. Matson, P. Midgley, and M. Wang, Atmospheric chemistry and greenhouse gases, Chapter 4 in *Climate Change 2001: The Scientific Basis: Contribution of Working Group I to the Third Assessment Report of the Intergovernmental Panel on Climate Change*, edited by J.T. Houghton, Y. Ding, D.J. Griggs, M. Noguer, P.J. van der Linden, X. Dai, K. Maskell, and C.A. Johnson, 881 pp., Cambridge University Press, Cambridge, U.K., 2001.
- Pyle, J.A., P. Braesicke, and G. Zeng, Dynamical variability in the modelling of chemistry-climate interactions, *Faraday Discuss.*, *130*, 27-39, doi: 10.1039/b417947c, 2005.
- Randeniya, L.K., P.F. Vohralik, and I.C. Plumb, Stratospheric ozone depletion at northern mid latitudes in the 21st century: The importance of future concentrations of greenhouse gases nitrous oxide and methane, *Geophys. Res. Lett.*, *29* (4), 1051, doi: 10.1029/2001GL014295, 2002.
- Rayner, N.A., D.E. Parker, E.B. Horton, C.K. Folland, L.V. Alexander, D.P. Rowell, E.C. Kent, and A. Kaplan, Global analyses of sea surface temperature, sea ice, and night marine air temperature since the late nineteenth century, *J. Geophys. Res.*, *108* (D14), 4407, doi: 10.1029/2002JD002670, 2003.
- Reinsel, G.C., Trend analysis of upper stratospheric Umkehr ozone data for evidence of turnaround, *Geophys. Res. Lett.*, *29* (10), 1451, doi: 10.1029/2002GL014716, 2002.
- Reinsel, G.C., E. Weatherhead, G.C. Tiao, A.J. Miller, R.M. Nagatani, D.J. Wuebbles, and L.E. Flynn, On detection of turnaround and recovery in trend for ozone, *J. Geophys. Res.*, *107* (D10), 4078, doi: 10.1029/2001JD000500, 2002.
- Reinsel, G.C., A.J. Miller, E.C. Weatherhead, L.E. Flynn, R.M. Nagatani, G.C. Tiao, and D.J. Wuebbles, Trend analysis of total ozone data for turnaround and dynamical contributions, *J. Geophys. Res.*, *110*, D16306, doi: 10.1029/2004JD004662, 2005.
- Rex, M., R.J. Salawitch, P. von der Gathen, N.R.P. Harris, M.P. Chipperfield, and B. Naujokat, Arctic ozone loss and climate change, *Geophys. Res. Lett.*, *31*,

- L04116, doi: 10.1029/2003GL018844, 2004.
- Richter, J.H., and R.R. Garcia, On the forcing of the mesospheric semi-annual oscillation in the Whole Atmosphere Community Climate Model, *Geophys. Res. Lett.*, *33*, L01806, doi: 10.1029/2005GL024378, 2006.
- Rinsland, C.P., D.K. Weisenstein, M.K.W. Ko, C.J. Scott, L.S. Chiou, E. Mahieu, R. Zander, and P. Demoulin, Post-Mount Pinatubo eruption ground-based infrared stratospheric column measurements of HNO₃, NO, and NO₂ and their comparison with model calculations, *J. Geophys. Res.*, *108* (D15), 4437, doi: 10.1029/2002JD002965, 2003.
- Rosenfield, J.E., and M.R. Schoeberl, Recovery of the tropical lower stratospheric ozone layer, *Geophys. Res. Lett.*, *32*, L21806, doi: 10.1029/2005GL023626, 2005.
- Rosenfield, J.E., D.B. Considine, P.E. Meade, J.T. Bacmeister, C.H. Jackman, and M.R. Schoeberl, Stratospheric effects of Mount Pinatubo aerosol studied with a coupled two-dimensional model, *J. Geophys. Res.*, *102* (D3), 3649-3670, 1997.
- Rosenfield, J.E., A.R. Douglass, and D.B. Considine, The impact of increasing carbon dioxide on ozone recovery, *J. Geophys. Res.*, *107* (D6), 4049, doi: 10.1029/2001JD000824, 2002.
- Rozanov, E., M. Schraner, C. Schnadt, T. Egorova, M. Wild, A. Ohmura, V. Zubov, W. Schmutz, and Th. Peter, Assessment of the ozone and temperature variability during 1979-1993 with the chemistry-climate model SOCOL, *Adv. Space Res.*, *35* (8), 1375-1384, 2005.
- Ruzmaikin, A., J. Lawrence, and C. Cadavid, A simple model of stratospheric dynamics including solar variability, *J. Clim.*, *16* (10), 1593-1600, 2003.
- Salawitch, R.J., D.K. Weisenstein, L.J. Kovalenko, C.E. Sioris, P.O. Wennberg, K. Chance, M.K.W. Ko, and C.A. McLinden, Sensitivity of ozone to bromine in the lower stratosphere, *Geophys. Res. Lett.*, *32*, L05811, doi: 10.1029/2004GL021504, 2005.
- Salby, M.L., and P.F. Callaghan, Systematic changes of Northern Hemisphere ozone and their relationship to random interannual changes, *J. Clim.*, *17* (23), 4512-4521, 2004.
- Santee, M.L., G.L. Manney, W.G. Read, L. Froidevaux, and J.W. Waters, Polar vortex conditions during the 1995-96 Arctic winter: MLS ClO and HNO₃, *Geophys. Res. Lett.*, *23* (22), 3207-3210, 1996.
- Shibata, K., and M. Deushi, Radiative effect of ozone on the quasi-biennial oscillation in the equatorial stratosphere, *Geophys. Res. Lett.*, *32*, L24802, doi: 10.1029/2005GL023433, 2005.
- Shibata, K., M. Deushi, T.T. Sekiyama, and H. Yoshimura, Development of an MRI chemical transport model for the study of stratospheric chemistry, *Pap. Meteorol. Geophys.*, *55* (3/4), 75-119, 2005.
- Smyshlyaev, S.P., V.L. Dvortsov, M.A. Geller, and V.A. Yudin, A two-dimensional model with input parameters from a general circulation model: Ozone sensitivity to different formulations for the longitudinal temperature variation, *J. Geophys. Res.*, *103* (D21), 28373-28387, 1998.
- Solomon, S., R.W. Portmann, R.R. Garcia, L.W. Thomason, L.R. Poole, and M.P. McCormick, The role of aerosol variations in anthropogenic ozone depletion at northern midlatitudes, *J. Geophys. Res.*, *101*, 6713-6728, doi: 10.1029/95JD03353, 1996.
- Solomon, S., R.W. Portmann, T. Sasaki, D.J. Hofmann, and D.W.J. Thompson, Four decades of ozonesonde measurements over Antarctica, *J. Geophys. Res.*, *110*, D21311, doi: 10.1029/2005JD005917, 2005.
- Steil, B., C. Brühl, E. Manzini, P.J. Crutzen, J. Lelieveld, P.J. Rasch, E. Roeckner, and K. Krüger, A new interactive chemistry climate model: 1. Present-day climatology and interannual variability of the middle atmosphere using the model and 9 years of HALOE/UARS data, *J. Geophys. Res.*, *108* (D9), 4290, doi: 10.1029/2002JD002971, 2003.
- Steinbrecht, W., H. Claude, and P. Winkler, Enhanced upper stratospheric ozone: Sign of recovery or solar cycle effect?, *J. Geophys. Res.*, *109*, D02308, doi: 10.1029/2003JD004284, 2004a.
- Steinbrecht, W., H. Claude, and P. Winkler, Reply to comment by D. M. Cunnold et al. on "Enhanced upper stratospheric ozone: Sign of recovery or solar cycle effect?", *J. Geophys. Res.*, *109*, D14306, doi: 10.1029/2004JD004948, 2004b.
- Steinbrecht, W., H. Claude, F. Schöenborn, I.S. McDermid, T. Leblanc, S. Godin, T. Song, D.P.J. Swart, Y.J. Meijer, G.E. Bodeker, B.J. Connor, N. Kämpfer, K. Hocke, Y. Calisesi, N. Schneider, J. de la Nöe, A.D. Parrish, I.S. Boyd, C. Brühl, B. Steil, M.A. Giorgetta, E. Manzini, L.W. Thomason, J.M. Zawodny, M.P. McCormick, J.M. Russell, P.K. Bhartia, R.S. Stolarski, and S.M. Hollandsworth-Frith, Long-term evolution of upper stratospheric ozone at selected stations of the Network for the Detection of Stratospheric Change (NDSC), *J. Geophys. Res.*, *111*, D10308, doi: 10.1029/2005JD006454, 2006a.
- Steinbrecht, W., B. Haßler, C. Brühl, M. Dameris, M.A. Giorgetta, V. Grewe, E. Manzini, S. Matthes, C. Schnadt, B. Steil, and P. Winkler, Interannual variation patterns of total ozone and lower stratospheric

21st CENTURY OZONE LAYER

- temperature in observations and model simulations, *Atmos. Chem. Phys.*, *6*, 349-374, 2006b.
- Stolarski, R.S., A.R. Douglass, S. Steenrod, and S. Pawson, Trends in stratospheric ozone: Lessons learned from a 3D chemical transport model, *J. Atmos. Sci.*, *63* (3), 1028-1041, 2006.
- Stordal, F., I.S.A. Isaksen, and K. Horntveth, A diabatic circulation two-dimensional model with photochemistry: Simulations of ozone and long-lived tracers with surface sources, *J. Geophys. Res.*, *90*, 5757-5776, 1985.
- Struthers, H., K. Kreher, J. Austin, R. Schofield, G.E. Bodeker, P.V. Johnston, H. Shiona, and A. Thomas, Past and future simulations of NO₂ from a coupled chemistry-climate model in comparison with observations, *Atmos. Chem. Phys.*, *4*, 2227-2239, 2004.
- Tarasick, D.W., V.E. Fioletov, D.I. Wardle, J.B. Kerr, and J. Davies, Changes in the vertical distribution of ozone over Canada from ozonesondes: 1980-2001, *J. Geophys. Res.*, *110*, D02304, doi: 10.1029/2004JD004643, 2005.
- Tian, W., and M.P. Chipperfield, A new coupled chemistry-climate model for the stratosphere: The importance of coupling for future O₃-climate predictions, *Quart. J. Roy. Meteorol. Soc.*, *131* (605), 281-303, 2005.
- Tiao, G.C., D. Xu, J.H. Pedrick, X. Zhu, and G.C. Reinsel, Effects of autocorrelation and temporal sampling schemes on estimates of trend and spatial correlation, *J. Geophys. Res.*, *95*, 20507-20517, 1990.
- Tie, X.X., and G. Brasseur, The response of stratospheric ozone to volcanic eruptions: Sensitivity to atmospheric chlorine loading, *Geophys. Res. Lett.*, *22* (22), 3035-3038, 1995.
- Tromp, T.K., R.-L. Shia, M. Allen, J.M. Eiler, and Y.L. Yung, Potential environmental impact of a hydrogen economy on the stratosphere, *Science*, *300* (5626), 1740-1742, 2003.
- Velders, G.J.M., *Scenario Study of the Effects of CFC, HCFC, and HFC Emissions on Stratospheric Ozone*, RIVM Report 722201006, 99 pp., National Institute of Public Health and the Environment, Bilthoven, The Netherlands, 1995.
- Warwick, N.J., S. Bekki, E.G. Nisbet, and J.A. Pyle, Impact of a hydrogen economy on the stratosphere and troposphere studied in a 2-D model, *Geophys. Res. Lett.*, *31*, L05107, doi: 10.1029/2003GL019224, 2004.
- Weatherhead, E.C., and S.B. Andersen, The search for signs of recovery of the ozone layer, *Nature*, *441* (7089), 39-45, doi: 10.1038/nature04746, 2006.
- Weatherhead, E.C., G.C. Reinsel, G.C. Tiao, C.H. Jackman, L. Bishop, S.M. Hollandsworth Frith, J. DeLuisi, T. Keller, S.J. Oltmans, E.L. Fleming, D.J. Wuebbles, J.B. Kerr, A.J. Miller, J. Herman, R.D. McPeters, R.M. Nagatani, and J.E. Frederick, Detecting the recovery of total column ozone, *J. Geophys. Res.*, *105* (D17), 22201-22210, 2000.
- WMO (World Meteorological Organization), *Scientific Assessment of Ozone Depletion: 2002, Global Ozone Research and Monitoring Project-Report No. 47*, Geneva, Switzerland, 2003.
- Yang, E.-S., D.M. Cunnold, M.J. Newchurch, and R.J. Salawitch, Change in ozone trends at southern high latitudes, *Geophys. Res. Lett.*, *32*, L12812, doi: 10.1029/2004GL022296, 2005.
- Yang, E.-S., D.M. Cunnold, R.J. Salawitch, M.P. McCormick, J. Russell III, J.M. Zawodny, S. Oltmans, and M.J. Newchurch, Attribution of recovery in lower-stratospheric ozone, *J. Geophys. Res.*, *111*, D17309, doi: 10.1029/2005JD006371, 2006.

Appendix 6A

MODEL SCENARIOS

Table 6A-1 lists the forcings used in the 2-D model and Chemistry-Climate Model (CCM) simulations. Two reference and two sensitivity simulations along with a set of model forcings have been proposed as part of the CCM Validation Activity for the Stratospheric Processes and their Role in Climate (SPARC) project of the World Climate Research Programme (Eyring et al., 2005) to assess the near-term and long-term evolution of stratospheric ozone. Unless otherwise stated, both types of models used changes in halocarbons as prescribed in Table 4B-2 of WMO (2003), WMGHGs based on the IPCC (2000) Special Report on Emissions Scenarios (SRES) A1B scenario, and sulfate aerosols for 1979 to 1999 based on the climatology of David Considine (NASA Langley Research Center; see http://www.pa.op.dlr.de/CCMVal/Forcings/CCMVal_Forcing.html) with background values thereafter.

The sea surface temperatures (SSTs) in the CCMs are prescribed from observations (HadSST1) in past simulations (Rayner et al., 2003). For REF2/SCN2 simulations they come either from the underlying IPCC coupled-ocean model simulation or from the UK Meteorological Office HadGEM1 simulations using IPCC SRES scenario A1B. In the reference past simulations (REF1), the quasi-biennial oscillation (QBO) is either prescribed (Giorgetta and Bengtsson, 1999) or internally generated, and the influence of the 11-year solar cycle on photolysis rates is parameterized according to the intensity of the 10.7 cm radiation of the Sun (Lean et al., 1997). In future runs, the solar cycle and an external QBO forcing are only considered in SCN2, but not in REF2.

In the CCMVal halogen file (i) The data from Table 4B-2 of WMO (2003), which were given every 5 years, were linearly interpolated into monthly values; (ii) The data for each year in Table 4B-2 were interpreted as the midpoint of each year rather than the correct 1st of the year; and (iii) Halon-2402 was mistakenly not included. Assumptions (i) and (ii) result in a slightly smaller peak organic chlorine (CCl_y) than observed (3.56 ppb instead of 3.58 ppb) and the peak occurs 2.4 years too late, while assumption (iii) results in organic bromine (CBr_y) that is around 1 ppt too low at the peak. To test the sensitivity of these assumptions on ozone, one 2-D model has been used to rerun the simulation with a corrected Ab halogen scenario. The difference between the two simulations is very small (especially compared with the differences between models), and none of the conclusions from the analysis of the 2-D models or CCMs are affected by the differences in the halogen forcing.

Table 6A-1. Model simulations.

Run ¹	Period	Motivation	Halocarbons	WMGHGs	SSTs ²	Solar Variability	QBO
P1	1979-2004	Past Trends	WMO (2003) Table 4B-2	IPCC (2000) A1B	N/A	None	None
F1	2005-2100	Future, Control	WMO (2003) Table 4B-2	IPCC (2000) B1	N/A	None	None
REF1	1960/1980-2004	Past Trends	WMO (2003) Table 4B-2	IPCC (2000) A1B	Observed (HadISST1)	Observed (MAVER)	Forced or internally generated
REF2	1960/1980-2100	Future, Control	WMO (2003) Table 4B-2	IPCC (2000) A1B	Modeled	None	Only internally generated
SCN2	1980-2025	Solar Cycle and QBO	WMO (2003) Table 4B-2	IPCC (2000) A1B	Modeled	Observed + repeating in future	Forced or internally generated
NCC	1970-2050	Fixed GHGs	WMO (2003) Table 4B-2	Fixed at start of simulation	Observed 1970-79 repeating or modeled	As in REF1/REF2/SCN2	Forced or internally generated

¹ P1 and F1 runs are for 2-D models, and remainder are for CCMs.

² Applies to CCM simulations only.

CHAPTER 7

Surface Ultraviolet Radiation: Past, Present, and Future

Lead Authors:

A.F. Bais

D. Lubin

Coauthors:

A. Arola

G. Bernhard

M. Blumthaler

N. Chubarova

C. Erlick

H.P. Gies

N. Krotkov

K. Lantz

B. Mayer

R.L. McKenzie

R.D. Piacentini

G. Seckmeyer

J.R. Slusser

C.S. Zerefos

Contributors:

U. Feister

V. Fioletov

J. Gröbner

E. Kyrö

H. Slaper

Final Release: February 2007

From *Scientific Assessment of Ozone Depletion: 2006*

SURFACE ULTRAVIOLET RADIATION

- **New methods to quantify the aerosol optical properties have been developed.** These properties have important influences on UV radiation. By combining spectral irradiance and radiance measurements, the effective single scattering albedo and optical depth of aerosols can be derived with reasonable accuracy at locations with moderate to high aerosol optical depth. Under low aerosol conditions, accurate determination of the wavelength dependence of the aerosol optical depth in the UV-B is restricted by calibration uncertainties and by the interference of ozone and SO₂.
- **Although the Total Ozone Mapping Spectrometer (TOMS) instrument is no longer available, continuity of satellite-derived global UV data is maintained.** The new Ozone Monitoring Instrument (OMI) onboard the National Aeronautics and Space Administration (NASA) Earth Observing System (EOS) Aura spacecraft was launched in July 2004 for continued global monitoring of ozone, other trace gases, and surface UV irradiance.
- **Tropospheric aerosols are responsible for the overestimation of UV irradiance from satellite instruments (e.g., TOMS) that use solar backscattered ultraviolet radiation to derive surface UV irradiance.** Although at clean sites the agreement with ground-based measurements is good, over more polluted locations the bias can be as large as 40% because the lowermost atmosphere containing the absorbing aerosols is not adequately probed. The presence of clouds, and snow or ice cover, can also lead to significant biases. New algorithms have been developed to improve the parameterization of aerosol and snow and ice effects on satellite-derived surface UV irradiance, as well as of cloud effects using Advanced Very High Resolution Radiometer (AVHRR) and METEOSAT images, showing on average good agreement with ground-based UV observations.
- **Further improvements have been made in UV measuring instruments and techniques.** For example, a transportable spectroradiometer was compared with instruments at more than 25 sites in Europe. The uncertainty of well-maintained spectroradiometers, however, could not be significantly reduced in recent years, mainly due to the remaining difficulties with lamp calibrations. Diode array and CCD spectrographs record the entire spectrum in a fraction of a second, allowing for better spectral characterization of cloud effects of UV radiation, but their intrinsic stray-light problem limits their use in the UV-B. Narrowband multifilter radiometers are now used in several networks providing more information than broadband radiometers and are a useful supplement to well-maintained spectroradiometers. Those that include rotating shadow-bands provide, in addition, estimates of the aerosol optical properties.
- **Algorithms have been developed for converting spectral irradiance to actinic flux, which is more relevant to atmospheric chemistry.** This enables us to derive historic actinic fluxes from the 1990s, when the irradiance measurements became widely available. The resulting uncertainties in the actinic fluxes are between 5% and 15% under all sky conditions.
- **Model calculations incorporating only ozone projections show that UV levels will decrease over the next few decades.** These calculations imply that UV irradiance is currently close to maximum and under this scenario they will revert to pre-1980 levels at midlatitudes between about 2040 and 2070, but later at southern high latitudes. However, other factors that influence UV are likely to dominate over these time scales.
- **Climate change will also influence surface UV irradiance through changes induced mainly to clouds and surface reflectivity.** Aerosols and air pollutants are also expected to change in the future. These factors may lead to either increases or decreases in surface UV radiation, through absorption or scattering. If the projections for future ozone are correct, these factors are likely to dominate future changes in UV radiation.

CHAPTER 7

SURFACE ULTRAVIOLET RADIATION: PAST, PRESENT, AND FUTURE

Contents

SCIENTIFIC SUMMARY	7.1
7.1 INTRODUCTION	7.3
7.2 FACTORS AFFECTING UV RADIATION: NEW FINDINGS	7.3
7.2.1 The Extraterrestrial Solar Spectrum	7.4
7.2.2 Stratospheric Ozone	7.5
7.2.3 Clouds	7.5
7.2.4 Aerosol Scattering and Absorption	7.7
7.2.5 Tropospheric Ozone and Other Gaseous Air Pollutants	7.8
7.2.6 Surface Albedo	7.9
7.2.7 Altitude	7.10
7.2.8 UV Irradiances on Inclined Surfaces	7.11
7.2.9 UV Under Water, Ice, and Snow	7.11
7.3 RESOURCES FOR STUDYING SURFACE UV RADIATION	7.13
7.3.1 Ground-Based Measurements	7.13
7.3.1.1 Spectroradiometers	7.13
7.3.1.2 Broadband Filter Radiometers	7.14
7.3.1.3 Narrowband Multifilter Radiometers	7.14
7.3.1.4 Advancements in Instrumentation	7.15
7.3.1.5 Data Quality and Databases	7.15
7.3.2 Satellite-Derived UV Estimates	7.16
7.3.2.1 Differences Between Ground-Based and TOMS-Derived UV Irradiances	7.16
7.3.2.2 UV Retrieval Algorithms and Related Uncertainties	7.17
7.3.3 Advancements in UV Radiation Modeling	7.17
7.3.4 Short-Term UV Forecasting	7.20
7.4 UV CLIMATOLOGY	7.21
7.4.1 Derived from Ground-Based UV Measurements	7.21
7.4.1.1 Long-Term Changes	7.21
7.4.1.2 Short-Term and Spatial UV Variability	7.25
7.4.2 Estimates from Satellite Data	7.26
7.4.3 Reconstruction of Past UV Records	7.26
7.4.4 Polar UV Variability	7.28
7.5 EXPECTATIONS FOR THE FUTURE	7.29
7.5.1 Links with the Recovery of the Ozone Layer	7.29
7.5.2 Predictions of UV Long-Term Changes	7.29
7.5.3 Factors Related to Climate Change	7.30
7.6 REMAINING QUESTIONS AND UNCERTAINTIES	7.32
REFERENCES	7.32
APPENDIX 7A: SPECTRAL DATA AVAILABLE FROM DATABASES	
7A.1 World Ozone and Ultraviolet Radiation Data Centre (WOUDC)	7.49

7A.2 European Ultraviolet Database (EUUVDB) 7.51
7A.3 U.S. National Science Foundation UV Monitoring Network 7.52

APPENDIX 7B: INTERNET ADDRESSES FOR UV SITES

7B.1 General UV Information 7.53
7B.2 International UV Projects 7.53
7B.3 Radiative Transfer Codes 7.53
7B.4 Extraterrestrial Spectra 7.53
7B.5 Internet Sites with UV Information 7.54

SCIENTIFIC SUMMARY

- **Ultraviolet (UV) measurements from some stations in unpolluted locations indicate that the Montreal Protocol is working, because at these locations further increases have not been observed since the late 1990s.** Outside polar regions, increases in UV due to ozone depletion have been relatively small and in many places they are difficult to separate from those due to other causes, such as changes in cloud and aerosol. In unpolluted locations, especially in the Southern Hemisphere, UV irradiances have been decreasing in recent years, as expected from the observed increases in ozone.
- **At most midlatitude stations in the Northern Hemisphere, surface UV irradiance continued to increase at rates of a few percent per decade.** The observed increases and their significance depend on location, wavelength range, and the period of measurements. These increases cannot be explained solely by ozone depletion and could be attributed to a decreasing tendency in aerosol extinction and air pollution since the beginning of the 1990s and partly to decreasing cloudiness, as estimated from satellites. The longest reconstructed series of erythemal irradiance (in Switzerland back to 1920s) revealed that high UV levels occurred in the mid-1940s and early 1960s due to reduction in cloudiness. Increased cloudiness in the mid-1970s resulted in reduced erythemal irradiance over several locations in Europe.
- **In polar regions, high UV irradiances lasting for a few days have been observed, associated with low total ozone episodes.** Erythemal irradiance averaged over several days has been increased by ~70% over southern Argentina during vortex overpasses in October. Instantaneous enhancements up to a factor of 6 have been observed over Antarctica. Over northern Europe and Alaska, the observed enhancements were smaller.
- **At present, clouds generally influence surface UV irradiance more strongly than any other atmospheric variable, including ozone.** Further studies that quantify cloud effects on surface UV irradiance are now available. Under overcast conditions, reductions can exceed 90%. Reductions of UV irradiance by clouds are 15-45% smaller than in the visible part of the spectrum. Recent measurements have shown intermittent enhancements of up to 40% in UV actinic flux over clear-sky values for cloudy conditions when the solar disk is unoccluded, whereas enhancements of 25% were found for irradiance under similar conditions.
- **Cloud variability is the major factor limiting our ability to detect long-term changes in surface UV radiation due to ozone.** At most sites, even if ozone trends were linear, at least 10-15 years of measurements would be needed to detect a trend in UV radiation.
- **The high surface reflectivity (close to unity) in Antarctica can lead to enhancements in clear-sky UV irradiance up to 50%.** Under such conditions, the high albedo compensates the UV attenuation by clouds, resulting in surface irradiance similar to clear skies, while zenith radiance is strongly enhanced (even tripled). For the first time the UV surface albedo was measured in Antarctica with high spectral resolution, confirming that albedo in the UV is slightly lower than in the visible, but still close to unity. New observations in the European Alps showed that a snow-covered terrain may increase the clear-sky erythemal and UV-A irradiance by up to 22% and 15% respectively, with respect to low-albedo conditions. Spatial variations of snow coverage may result in large (up to 40%) variations in sky radiance from different directions. The effect of snow albedo is stronger on tilted surfaces.
- **Air pollutants may counterbalance the UV radiation increases resulting from ozone depletion.** Observations confirmed that surface UV irradiance at locations near the emission sources of ozone (O₃), nitrogen dioxide (NO₂), or sulfur dioxide (SO₂) in the lower troposphere is attenuated by up to ~20%. Air pollution exerts stronger attenuation in UV compared with total solar irradiance.
- **Three-dimensional radiative transfer models have improved the ability to model UV radiation under broken cloud and over complex terrains.** For most measuring sites, these are the prevailing conditions. However, the realization of this improved capability is still limited by the lack of the necessary input parameters.

SURFACE ULTRAVIOLET RADIATION

- **New methods to quantify the aerosol optical properties have been developed.** These properties have important influences on UV radiation. By combining spectral irradiance and radiance measurements, the effective single scattering albedo and optical depth of aerosols can be derived with reasonable accuracy at locations with moderate to high aerosol optical depth. Under low aerosol conditions, accurate determination of the wavelength dependence of the aerosol optical depth in the UV-B is restricted by calibration uncertainties and by the interference of ozone and SO₂.
- **Although the Total Ozone Mapping Spectrometer (TOMS) instrument is no longer available, continuity of satellite-derived global UV data is maintained.** The new Ozone Monitoring Instrument (OMI) onboard the National Aeronautics and Space Administration (NASA) Earth Observing System (EOS) Aura spacecraft was launched in July 2004 for continued global monitoring of ozone, other trace gases, and surface UV irradiance.
- **Tropospheric aerosols are responsible for the overestimation of UV irradiance from satellite instruments (e.g., TOMS) that use solar backscattered ultraviolet radiation to derive surface UV irradiance.** Although at clean sites the agreement with ground-based measurements is good, over more polluted locations the bias can be as large as 40% because the lowermost atmosphere containing the absorbing aerosols is not adequately probed. The presence of clouds, and snow or ice cover, can also lead to significant biases. New algorithms have been developed to improve the parameterization of aerosol and snow and ice effects on satellite-derived surface UV irradiance, as well as of cloud effects using Advanced Very High Resolution Radiometer (AVHRR) and METEOSAT images, showing on average good agreement with ground-based UV observations.
- **Further improvements have been made in UV measuring instruments and techniques.** For example, a transportable spectroradiometer was compared with instruments at more than 25 sites in Europe. The uncertainty of well-maintained spectroradiometers, however, could not be significantly reduced in recent years, mainly due to the remaining difficulties with lamp calibrations. Diode array and CCD spectrographs record the entire spectrum in a fraction of a second, allowing for better spectral characterization of cloud effects of UV radiation, but their intrinsic stray-light problem limits their use in the UV-B. Narrowband multifilter radiometers are now used in several networks providing more information than broadband radiometers and are a useful supplement to well-maintained spectroradiometers. Those that include rotating shadow-bands provide, in addition, estimates of the aerosol optical properties.
- ^a **Algorithms have been developed for converting spectral irradiance to actinic flux, which is more relevant to atmospheric chemistry.** This enables us to derive historic actinic fluxes from the 1990s, when the irradiance measurements became widely available. The resulting uncertainties in the actinic fluxes are between 5% and 15% under all sky conditions.
- ^a **Model calculations incorporating only ozone projections show that UV levels will decrease over the next few decades.** These calculations imply that UV irradiance is currently close to maximum and under this scenario they will revert to pre-1980 levels at midlatitudes between about 2040 and 2070, but later at southern high latitudes. However, other factors that influence UV are likely to dominate over these time scales.
- **Climate change will also influence surface UV irradiance through changes induced mainly to clouds and surface reflectivity.** Aerosols and air pollutants are also expected to change in the future. These factors may lead to either increases or decreases in surface UV radiation, through absorption or scattering. If the projections for future ozone are correct, these factors are likely to dominate future changes in UV radiation.

7.1 INTRODUCTION

The potential for increased solar ultraviolet (UV) radiation reaching the Earth's surface in response to ozone (O_3) reduction has been a major concern since the first signs of ozone depletion in the early 1980s. Although UV is a small fraction of the total radiant solar energy, it may produce detrimental effects on the ecosystem and degrading effects on materials, and therefore knowledge of its variability in time and space has high priority in scientific research. Oxygen, ozone, and nitrogen molecules in the upper atmosphere absorb the UV-C (wavelength < 280 nanometers (nm)) part of the spectrum effectively, whereas ozone in the stratosphere strongly absorbs the UV-B (280-315 nm) part and consequently determines the spectral shape of UV radiation at the surface. UV-B is of great biological importance because photons in this region may damage deoxyribonucleic acid (DNA) molecules and some proteins of living organisms. On the other hand, UV-B is essential for the synthesis of vitamin D in the human body, which has beneficial health effects and helps in prevention of some diseases. Vitamin D can not be produced in sufficient amounts when incident UV-B radiation is very low. UV-A (315-400 nm) is less affected by ozone and may also contribute to some biological effects, especially if received in high doses. UV in both spectral ranges is important for tropospheric chemistry because it is involved in important photochemical reactions, such as the photolysis of nitrogen dioxide (NO_2), ozone, and formaldehyde. Changes in tropospheric composition induced by UV changes may be important for the stratosphere through interactions between the troposphere and stratosphere. Finally, there are linkages between changes in UV-A radiation and climate change.

Monitoring of UV radiation has been a challenging task because of the great difficulties in conducting accurate measurements and proper quality control, and because UV is highly variable both in time and space. Assessment of the UV levels in the last two decades is addressed through a limited number of measurement records from instruments operating at the ground or onboard satellites.

Most of the unresolved issues that were pointed out in the previous Assessment (Kerr and Seckmeyer et al., 2003) have been further studied. Some progress has been made with respect to the effects of absorbing aerosols on satellite UV retrievals, and different methods have been proposed for determining the aerosol single scattering albedo from radiation measurements and modeling. Improvements have also been made in quantifying the cloud effects and the influence of high surface albedo on the ground-based and satellite-derived measurements. Effects from inhomogeneities in the surface reflectivity of

the terrain surrounding a monitoring site have also been studied, although marginal progress has been made in investigating the representativeness of measurements made at a monitoring site for the surrounding areas.

While propagating through the atmosphere, solar UV radiation is influenced by complex processes of scattering and absorption before reaching the Earth's surface. Sufficient understanding and quantification of the effects of these processes, particularly the tropospheric, are essential for the simulation of the UV radiation field and for explaining its variations in time and space. Improvement of our knowledge and more quantitative information on these processes since the previous Assessment (WMO, 2003) are presented in Section 7.2. In particular this section describes effects arising from the Sun-Earth geometry, clouds, atmospheric gases and aerosols, as well as effects from the surface albedo and altitude. Finally, new findings about the transfer of UV under water and ice are also included. Section 7.3 discusses the progress made in instruments and procedures that are used to measure solar UV radiation and other relevant parameters, from the ground and space. The differences between ground-based and satellite-derived surface UV measurements are also discussed in connection with further developments in satellite UV retrieval algorithms. The section also includes developments in radiative transfer (RT) modeling and other modeling approaches. Finally, this section discusses the short-term predictions of surface UV and the use of these predictions to construct the UV index. Changes in surface UV irradiance on different time scales derived from ground-based and satellite instruments, as well as from reconstructed past UV records are discussed in Section 7.4. Particular emphasis is given to long-term changes and to the attribution of these changes to different atmospheric parameters. The link between surface UV and climate change, and prediction of future UV levels in relation to ozone changes, are discussed in Section 7.5. Finally, open issues that need further investigation are outlined in Section 7.6.

7.2 FACTORS AFFECTING UV RADIATION: NEW FINDINGS

The non-uniform distribution of the predominant factors that interact with UV radiation (clouds, ozone, aerosols, and surface albedo) makes detailed calculations of UV radiation a nontrivial task. The impact of these factors cannot always be treated independently, since in most cases they act synergistically (e.g., Kerr, 2005). The following sections describe the progress that has been achieved during the last four years toward understanding and quantifying the role of these factors in modifying the

SURFACE ULTRAVIOLET RADIATION

solar UV radiation received at the surface. Due to the large natural variability of surface UV, ground-based measurements that are made in many locations worldwide provide results that are valid mainly locally, and cannot be easily extrapolated to global scales (see also Figure 7-4). On the other hand, satellite estimates of surface UV radiation provide global coverage, but the sampling frequency is typically only once per day, with a coarse spatial resolution that represents average conditions over large areas. Further, these estimates are based on model calculations that include assumptions that are not always realistic.

7.2.1 The Extraterrestrial Solar Spectrum

UV radiation entering the Earth's atmosphere is primarily controlled by the variations in the Sun's emittance and in the orbital position of the Earth. Uncertainties in the spectral solar irradiance at the top of the atmosphere translate directly into uncertainties in the spectral radiance (and irradiance) at all levels in the atmosphere and at the surface due to the linearity of the radiative transfer equation. Thus, accurate knowledge of the solar spectrum at the top of the atmosphere (see Appendix 7B.4) is very important for accurate prediction of the radiation levels at the surface with radiative transfer models.

Variations in the orbit of the Earth, the so-called Milankovitch cycles (obliquity, eccentricity, and precession), have very long periods and produce changes in radiation at the top of the atmosphere of up to ~30% on time scales of hundreds of thousands of years. Shaffer and Cerveny (2004) calculated surface irradiance changes in the UV band 300-325 nm taking into account variations in the extraterrestrial radiation reaching the atmosphere and the solar zenith angle (SZA), but assuming invariant latitudinal ozone concentrations (see example in Figure 7-1). Although over such long time scales there should have been significant changes in oxygen, Segura et al. (2003) showed that even for large changes in oxygen, changes in ozone are relatively small. Variations in surface UV radiation caused by these orbital changes are expected to be very small (less than ~1%) in the next few centuries. Thus solar activity (sunspots, and 11-year and 27-day cycles) is the dominant factor responsible for the variability in the extraterrestrial irradiance spectrum in the near future.

Solar activity in the last 70 years has been exceptionally strong, and the previous period of equally strong activity occurred more than 8,000 years ago, as suggested by Solanki et al. (2004) based on dendrochronologically dated radiocarbon concentrations. This strong solar activity marginally influences the UV radiation that reaches the surface (UV-B and longer wavelengths), but it

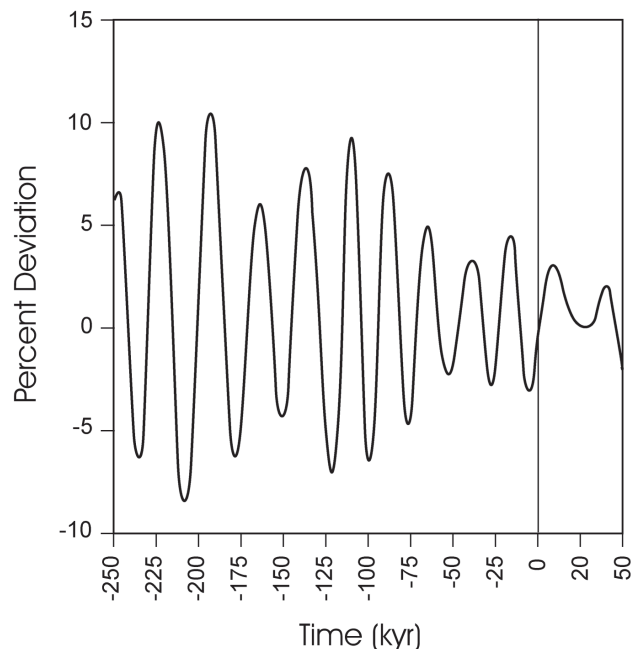


Figure 7-1. Percent deviations in daily near-UV (300-325 nm) solar irradiance on the March equinox at 60°N between 250,000 before present and 50,000 after present, caused by Milankovitch cycles. Larger variations, ranging between about ±30%, have been calculated for different latitudes and for the solstices. Reprinted from Shaffer and Cerveny, 2004, with permission from Elsevier.

is important for the UV-C wavelengths that are involved in stratospheric ozone production.

Spectroradiometers onboard Earth-orbiting satellites allow investigations of temporal variations of solar irradiance in different wavelength ranges. Two new composite solar irradiance reference spectra extending from 0.1 to 2400 nm were constructed using recent space measurements for two distinct time periods during solar cycle 22 (1985-1997). From data gathered with instruments onboard the Atmospheric Laboratory for Applications and Science (ATLAS) 1 and 2 and the Upper Atmosphere Research Satellite (UARS), the accuracy of the measured solar spectra was determined to be ~3% in the UV and visible ranges (Thuillier et al., 2004). Gurlit et al. (2005) presented a moderate resolution solar irradiance spectrum in the spectral range 316.7-652 nm derived from the azimuth-controlled Limb Profile Monitor of the Atmosphere/Differential Optical Absorption Spectroscopy (LPMA/DOAS) balloon gondola at around 32 km float altitude. This spectrum is in very good agreement with previously reported spectra (Kurucz et al., 1984; Thuillier et al., 1997, 1998; Harder et al., 2000) in the visible, but it

is 1.4 to 6.2% lower in the UV-A. In agreement with Skupin et al. (2003), this study emphasizes that the present level 1 calibration of the Scanning Imaging Absorption Spectrometer for Atmospheric Chartography (SCIAMACHY) of the European Space Agency (ESA) is systematically 15% higher in this wavelength range (316.7-652 nm) with respect to all other available solar irradiance measurements, and suggests using the recalibration proposed by the University of Bremen for SCIAMACHY. Finally, a new reference solar spectrum (given in steps of 0.5 nm) was constructed by combining measurements derived from different satellite platforms and from the ground, and this spectrum was compared with historical reference spectra (Gueymard, 2004, 2006). It was concluded that reference solar irradiance spectra in the UV-B and UV-A that were published after 1985 are in very good agreement (within a few percent) and that the ATLAS 3 spectrum is probably the most suitable one for radiative transfer calculations. The latter is in agreement with the conclusion of Bais et al. (2003) that was derived from comparison of measured and modeled surface UV spectra.

The variability of the solar irradiance spectrum for the duration of solar cycle 23 has been investigated using data from different satellites. Several studies quantified the amplitude of the solar cycle in the wavelength band 245-250 nm and found that it ranged between 6% and 8%: DeLand et al. (2004a) used data in the period from March 1985 to May 1997 from the Solar Backscatter Ultraviolet Radiometer 2 (SBUV/2) onboard the National Oceanic and Atmospheric Administration (NOAA) 9 satellite; DeLand et al. (2004b) used data from the Solar Ultraviolet Spectral Irradiance Monitor (SUSIM) and the Solar Stellar Irradiance Comparison Experiment (SOLSTICE) instruments aboard UARS; and Floyd et al. (2003) used the SUSIM dataset alone. In the band 200-205 nm, the amplitude is larger (~9%). All three analyses reveal that no irradiance variations due to solar cycle variability could be detected in the UV-B and UV-A ranges at these spectral resolutions. Therefore surface UV radiation is not expected to respond directly to solar variations, but only indirectly through changes in stratospheric ozone induced by the variability of solar irradiance in the far ultraviolet (see Chapter 3, Section 3.4.4). A weaker solar activity will result in less ozone in the stratosphere and thus in more UV-B radiation at the surface, but also in less risk of sudden ozone decreases due to solar flares.

7.2.2 Stratospheric Ozone

The influence of stratospheric ozone on the transmission of UV radiation through the atmosphere is well understood and has been extensively discussed in previous

Assessments (Herman and McKenzie et al., 1999). The community now has access to better measurements and radiative transfer models; and the effects of molecular absorptions are now better quantified through field measurements and supporting model calculations (e.g., Burrows et al., 1999; Mohamed-Tahrin et al., 2001). New evidence for increases of surface UV-B radiation due to stratospheric ozone depletion in Antarctica, particularly during the period of the ozone hole in spring, has been reported from observations (Bernhard et al., 2004, 2006). Summertime enhancements of surface UV were reported also at northern high latitudes during episodes of low ozone in the stratosphere caused by chemical destruction and transport processes (Orsolini et al., 2003).

Surface UV radiation depends on the vertical profile of ozone and on the vertical profile of temperature because of the temperature dependence of the molecular absorption cross sections. McKenzie et al. (2003) showed that differences in the shape of the vertical profile of ozone amplify the seasonal differences in UV irradiance between the northern (NH) and southern (SH) hemispheres. The summertime UV irradiance at southern midlatitudes greatly exceeds that at northern midlatitudes. Kazantzidis et al. (2005) quantified the differences in surface UV irradiances that are calculated by RT models when substituting the standard Air Force Geophysics Laboratory (AFGL) ozone and temperature profiles with measured ones. The differences in the UV-B irradiance are ~2-3% at small SZA, increasing by a few percent at larger SZA. Krzyścin (2004) reported that for large SZA, the UV irradiance at the surface is more sensitive to the ozone changes in the midstratosphere than to changes in the lower stratosphere, while the opposite occurs for small SZA. Under the current state of the atmosphere, the dependence of surface UV on the vertical profiles of temperature and ozone is relatively weak, but it might become stronger in the future, if the temperature of the lower stratosphere (where the bulk of ozone resides and most of the UV absorption occurs) changes (see Chapter 5, Section 5.3). Generally, the effect of changes in the ozone profile on surface UV radiation is larger than that of changes in the profile of temperature.

7.2.3 Clouds

Clouds dominate any other atmospheric variable as a source of surface UV variability, resulting in either a reduction or an increase in UV radiation. Indirectly, clouds may affect absorption of UV by other atmospheric constituents, while their variability usually masks the effects of other variables. For example, clouds are the major factor that limits the detectability of ozone-induced trends

SURFACE ULTRAVIOLET RADIATION

in UV radiation (den Outer et al., 2005; Glandorf et al., 2005). The higher the variability of clouds, the longer the record of ground-based UV data required for detecting an ozone-induced trend in UV radiation. Cloud effects on UV radiation are complex, thus restricting our ability to describe and predict accurately the UV radiation field at the ground. In practice, the necessary parameters needed to calculate local cloud effects are rarely available. Even if they were, the complexity of cloud geometry would require three dimensional (3-D) model calculations. Climate modeling suggests that the temporal and spatial distribution of clouds is likely to change in the future (IPCC, 2001 and Section 7.5.2). If ozone changes are small, the anticipated changes in cloudiness will have a much greater impact on UV radiation than changes in ozone. Despite the inherent difficulties in investigating the effects of clouds on surface UV, new case studies have been published and have broadened our understanding.

Results from different studies of cloud effects (e.g., Calbó et al., 2005) can be compared using the cloud modification factor (CMF), which is defined as the ratio between the measured UV radiation in a cloudy sky and the calculated radiation for a cloudless sky. Typical CMF values for overcast skies range from 0.3 to 0.8, depending both on cloud type and characteristics (Cede et al., 2002; Calbó et al., 2005). Den Outer et al. (2005) have investigated the effects of clouds on UV and visible solar radiation in the Netherlands by comparing measurements with model calculations. These studies confirm that clouds attenuate UV radiation by 15-45% less than total solar radiation, as a result of Rayleigh scattering that redirects toward the surface more efficiently the UV part of the radiation reflected by the clouds. Nichol et al. (2003) found a tendency toward greater cloud attenuation with increasing solar zenith angle.

Clouds may also have an enhancement effect, manifested by increased UV irradiance at the surface when the solar disk is unoccluded. Recent studies show enhancements of up to 25% and reconfirm earlier findings that the enhancements are significant (Herman and McKenzie et al., 1999; Kerr and Seckmeyer et al., 2003) and can last for hours (Cede et al., 2002). The enhancements were found to be most pronounced for large cloud cover of 5 to 7 octas (Cede et al., 2002) and were smaller in the UV than in the visible and infrared (Pfister et al., 2003). Simultaneous occurrence of a small solar zenith angle and a cumulus cloud close to the Sun's position in the sky at a high-altitude inter-tropical desert region produces very high erythemal doses. Piacentini et al. (2003) reported mean percentage increases due to the cloud effect of 6% for UV and 12% for total solar irradiance, relative to no clouds near the Sun. Cloud enhancements in UV actinic

flux can be up to 40% over clear-sky values when the solar disk is unoccluded (Crawford et al., 2003). When the solar disk is occluded, reductions in actinic flux below the cloud appear to vary inversely with cloud fraction in some instances. Wavelength dependence has been observed under broken clouds, with shorter wavelengths generally exhibiting lower variability in irradiance for both enhancements and reductions (e.g., 20-30% less variability at 320 versus at 420 nm). For actinic fluxes, the wavelength dependence due to clouds is stronger for cloud-induced enhancements than for cloud-induced reductions with respect to clear skies. At large SZA, a wavelength dependence appears to occur even for overcast conditions. The observed behavior (reductions, enhancements, and wavelength dependences) could be explained through the difference in the impact of clouds on the direct and diffuse components of actinic flux. Integration over longer periods results in weaker wavelength dependence, suggesting that differences in wavelength response may be localized phenomena with impacts that are minimized when integrated over the surrounding area.

Simultaneous measurements of actinic flux, irradiance, and aerosol and cloud properties were made from four ground stations and by aircraft (Kylling et al., 2005). The actinic flux above the cloud is increased by between 60-100% when compared with a cloudless sky, with the largest increase occurring for the optically thickest cloud. Similarly, the actinic flux below the cloud is decreased by about 55-65%. Just below the cloud top, the downwelling actinic flux reaches a maximum.

Mie scattering from cloud particles interacts with Rayleigh scattering in the atmosphere and produces a complex wavelength dependence in the top-of-the-atmosphere reflectances measured by satellite instruments that operate in the ultraviolet part of the spectrum (Ahmad et al., 2004). It was also shown that clouds can perturb the absorption by tropospheric ozone in complex ways that cannot be explained by models that treat them as reflecting surfaces rather than as volume scatterers. Winiiecki and Frederick (2005) confirmed that the cloud transmission in the ultraviolet decreases with decreasing wavelength as a consequence of increasing absorption by tropospheric ozone in the cloud, and they suggested that this mechanism results in enhanced production of excited-state oxygen atoms, O(¹D).

The UV-B sky radiance distribution under partial and overcast stratified cloud fields was studied using azimuthally averaged radiance measurements at Hobart, Australia (Kuchinke et al., 2004) and modeling. It was shown that inhomogeneities within realistic cloud fields have a significant effect on the radiation distribution at the ground, even on an overcast day.

7.2.4 Aerosol Scattering and Absorption

The influence of aerosols on the transmission of UV radiation has important consequences for stratospheric and tropospheric photochemistry, human and plant biology, remote sensing of column ozone, and surface UV mapping. There is a large variation in aerosol properties in both space and time caused either by natural or anthropogenic activities, and quantifying their effect remains a challenge. Uncertainties in aerosol particle microphysical data, particularly the particle number concentration, cause variability of up to 10% in predictions of actinic flux and UV irradiance (Früh et al., 2003). Advances in quantifying the effect of aerosols are being made from various fronts: laboratory and field measurements of aerosol optical properties in the UV, detection of aerosol amounts and optical properties from the ground and space, and theoretical modeling of scattering and absorption of UV radiation. Detecting and predicting aerosol absorption properties in the UV have received particular attention in recent years.

The optical properties of aerosols in the ultraviolet have been measured for different aerosol types in the laboratory and in the field. Black carbon/soot aerosols were characterized during the Aerosol Interactions and Dynamics in the Atmosphere (AIDA) Soot Aerosol Campaign (Schnaiter et al., 2003) using an optical technique based on the integrating sphere method (Mogo et al., 2005). Biomass burning aerosols were studied using a long path extinction spectrometer (LOPES) (Schnaiter et al., 2005) and fluorescence from a UV lidar (Immler et al., 2005). Desert dust, Arctic industrial pollution, and marine aerosols were investigated by Wetzal et al. (2003). Vaglieco et al. (2002) and Kirchstetter et al. (2004) found that organic carbon from motor vehicles and biomass burning contributes significantly to absorption of UV (and visible) radiation, although Myhre and Nielsen (2004) found that absorption of UV by organic acids is not significant. Kirchhoff et al. (2002) found a wavelength dependence of aerosol optical depth (AOD) in the UV-B that opposes the Angstrom law; they examined the possible influence of additional UV-absorbing species, such as formaldehyde, but found no influences on the AOD retrieval. On the other hand, Arola and Koskela (2004) studied various sources of errors in direct irradiance measurements due to the field of view of Brewer spectroradiometers that can partly explain this behavior. The properties of desert dust in the UV are also under debate. Some measurements have indicated enhanced absorption in the UV compared with the visible (Mattis et al., 2002; Meloni et al., 2004).

The optical properties of aerosol optical depth, single scattering albedo (SSA), and phase function are used to quantify the transmission of UV through turbid atmospheres and may be obtained by both satellite and ground radiometric data. Direct measurements of aerosol absorption present a great challenge even for ground-based remote sensing techniques, and the uncertainties have been recently discussed (e.g., Petters et al., 2003; Bais et al., 2005b; Goering et al., 2005; Krotkov et al., 2005a, 2005b). Using spectral direct irradiance measurements, AOD was retrieved by Lenoble et al. (2002) in the Bavarian Alps with absolute uncertainties of 0.03 to 0.05 and by Gröbner and Meleti (2004) in Ispra, Italy using a Brewer spectrophotometer. During the period 1991-2002, the AOD at 320 nm in Ispra varied between 0.05 and 2, showing a pronounced seasonal variability with high values (~ 0.6) in spring and summer and low values (~ 0.3) in winter. The AOD in the UV-A region determined from global and diffuse irradiance in the French Alps showed seasonal variations between 0.05 and 0.2 (Lenoble et al., 2004a). Techniques for retrieval of SSA have been developed using multiangle measurements of sky radiance (e.g., Dubovik et al., 2002; Qin et al., 2002), direct, diffuse, and global irradiance in conjunction with RT models (e.g., Petters et al., 2003; Bais et al., 2005b; Goering et al., 2005; Krotkov et al., 2005a, 2005b), and by combining Raman lidar, total ozone, and UV-B irradiance measurements with a RT model (Balis et al., 2004). The aerosol SSA is reported routinely by the Aerosol Robotic Network (AERONET) but only at visible wavelengths, so SSA at UV wavelengths can only be inferred by extrapolation. Petters et al. (2003) used an ultraviolet multifilter rotating shadowband radiometer (UVMFRSR) and RT model calculations to estimate the SSA, which ranged from 0.65 to 0.91 at 300 nm and 0.80 to 0.99 at 368 nm at Black Mountain, N.C. Bais et al. (2005b) estimated the SSA by combining Brewer irradiance measurements with a RT model and found that the ratio of direct to diffuse irradiance gives the highest accuracy compared with global irradiance, as long as the aerosol optical depth at 340 nm is greater than 0.2. From five years of irradiance measurements, the SSA in Thessaloniki, Greece, was determined to be between 0.85 and 0.99 when the AOD is larger than 0.8, and to cover the entire range from 0.64 to 0.99 for AOD between 0.2 and 0.8 (Bais et al., 2005b). The very low minimum SSA values (~ 0.65) reported in these two studies may have resulted from additional absorption by atmospheric gases, for example by NO_2 (Krotkov et al., 2005c) that was not taken into account in the retrieval of SSA.

Recently, an inversion technique has been developed to convert the unique Total Ozone Mapping Spectrometer (TOMS) spectral signature generated by the

SURFACE ULTRAVIOLET RADIATION

interaction of molecular scattering and aerosol absorption into a quantitative estimate of AOD and SSA, with accuracies of $\pm 30\%$ and ± 0.03 respectively (Torres et al., 2002, 2005).

New studies demonstrated the strong influences of variations in aerosol concentration and composition on long- and short-term variations in surface UV radiation: Chubarova et al. (2002) for Moscow, Russia; Barnard et al. (2003) for California, USA; Palancar and Toselli (2002) for Cordoba, Argentina; Micheletti et al., (2003) for Buenos Aires, Argentina; Ogunjobi and Kim (2004) for Kwangju, South Korea; Latha et al. (2004) for Northern India; Arola et al. (2003b) for Sodankylä, Finland, and Thessaloniki, Greece; Kambezidis et al. (2005) for Athens, Greece, and di Sarra et al. (2002) and Meloni et al. (2003a; 2003b; 2003c; 2005) for the island of Lampedusa in the Mediterranean. Jaroslowski and Krzyścin (2005) showed that aerosol forcing on the erythemally weighted UV at Belsk, Poland, under clear skies is as important as the forcing due to changes in ozone amount, both on long-term and short-term time scales.

The long-term variations of surface UV irradiance, which are discussed in Section 7.4, may strongly be influenced by temporal changes in the optical properties of aerosols, especially the SSA, which defines their absorption efficiency. In addition, the wavelength dependence of the two main aerosol optical properties, AOD and SSA, may result in different long-term variation of surface UV radiation at short and long wavelengths, if the type of aerosols over a particular site changes with time. Apart from their natural sources, aerosols are also a consequence of anthropogenic activities leading to atmospheric pollution, and thus they may change with time, depending on the effectiveness of pollution abatement measures. Finally, a reduction in SSA may result in less scattered radiation available for absorption by atmospheric gases, thus affecting indirectly the photochemistry in the troposphere.

7.2.5 Tropospheric Ozone and Other Gaseous Air Pollutants

UV radiation can be efficiently absorbed by man-made or natural gases in the troposphere, and at the same time it controls the concentration of some of them. For example, tropospheric concentrations of ozone may be significantly affected by changes in photodissociation rates induced by stratospheric ozone changes (Isaksen et al., 2005), which in turn affects the intensity of UV radiation at the surface. Under certain conditions, the concentration of gases resulting from photochemical reactions can increase simultaneously resulting in additional absorp-

tion of UV radiation near the Earth's surface. On the other hand, UV radiation is regulated by stratospheric ozone, as well as by the influence of aerosol and cloudiness. Thus, UV radiation interacts with tropospheric gases and aerosols in complex ways through a variety of atmospheric processes.

Tropospheric absorbers of UV radiation include ozone (O_3), sulfur dioxide (SO_2), nitrogen oxides (NO_2 , dinitrogen pentoxide (N_2O_5), NO_x), some bromine and chlorine compounds (e.g., chlorine dioxide (ClO), molecular chlorine (Cl_2), dichlorine monoxide (Cl_2O), bromine monoxide (BrO), hypobromous acid (HOBr)), and the oxygen dimer (O_2-O_2) (Atkinson et al., 1997; Sander et al., 2003). In addition, many organic species can also absorb UV radiation, including different types of aldehydes (i.e., formaldehyde, benzaldehyde, acetaldehyde), acetone, peroxyacetyl nitrate (PAN), propanal, glyoxal, nitrated aromatics, certain organic acids, and others (Atkinson et al., 1997; Jacobson, 1999; Sander et al., 2003; Myhre and Nielsen, 2004). The abundance of most of these substances in the troposphere usually is not large enough to produce measurable effects on surface UV, except near the sources of emission in polluted areas, or during natural hazards, like forest fires, volcanic eruptions, etc. For example, over large industrial centers on the eastern coast of the United States, the additional photochemically-produced ozone in the lower 2 km was up to 14 parts per billion by volume (ppb) (corresponding to a column contribution of 2.5 Dobson units) (Cooper et al., 2005) and was occasionally much higher (Jacobson, 1999). The content of NO_2 in the lower troposphere over polluted areas can be up to 1-2 DU, or even more (Richter and Burrows, 2002; Richter et al., 2005; Wang et al., 2005a; Cede et al., 2006a). Tropospheric SO_2 can be high in regions with volcanic activity and over industrial areas, with concentrations of 2 DU or more, as revealed from SCIAMACHY and ground measurements (Wang et al., 2005b). Finally, formaldehyde concentrations can exceed 0.6 DU (Heckel et al., 2005). The attenuation of UV radiation at the surface from these gases can be important, particularly if they coexist in the same area. Table 7-1 shows the effects of the main air pollutants in the boundary layer on the attenuation of UV irradiance, expressed by the absorption sensitivity (AS) parameter, defined as the relative change in UV irradiance due to 1 DU change in gas concentration. The absorption sensitivity of NO_2 and SO_2 can be even higher than for O_3 for the same change in concentration.

There is an increased awareness of the possible roles of these tropospheric trace gases on surface UV radiation, particularly in more polluted environments (Chubarova et al., 2002; Koronakis et al., 2002; Palancar

Table 7-1. The absorption sensitivity (AS) of different integrals of UV irradiance due to a 1-DU change in the column of O₃, SO₂, and NO₂ in the lower troposphere. Calculations are for local noon in January and July at 45°N, assuming 300 DU of ozone column (X) above 2 km. For a different ozone column, the absorption sensitivity for O₃ and SO₂ can be approximately estimated from the expression: $AS_X = AS_{300} \frac{300}{X}$, whereas NO₂ is practically unaffected. Adapted from Chubarova (2006).

	Absorption Sensitivity (%/DU)					
	O ₃		NO ₂		SO ₂	
	July	January	July	January	July	January
Erythema irradiance	-0.6	-0.4	-0.8	-1.8	-1.0	-0.9
UV-B (280 - 315 nm)	-0.3	-0.4	-0.8	-1.5	-0.6	-0.8
UV-A (315 - 400 nm)	Negligible		-1.6	-3.0	Negligible	
UV (280 - 400nm)	Negligible		-1.6	-2.9	Negligible	

and Toselli, 2002; Chubarova, 2004). Monitoring over several years of UV-B and total solar irradiance in Moscow and at a site located 50 km upwind to Moscow has revealed that in more than 75% of the cases, the monthly-mean UV-B values at the rural site are higher, with differences reaching 18% in winter and 9% in summer (Chubarova, 2002). For Moscow conditions, ozone and nitrogen dioxide are the most important gases in tropospheric UV-B absorption. For example, the observed attenuation of UV-B irradiance due to NO₂ is up to 6%, being ~2-3% on the average (Chubarova, 2004). During extremely high pollution episodes caused by forest fires near Moscow in 2002, the UV reduction only due to NO₂ was about 11-14%. Koronakis et al. (2002) reported reductions in UV-A irradiances of similar magnitude due to increased concentrations of tropospheric ozone and nitrogen oxides in Athens, Greece. Progress has also been made, using suites of ground-based instruments, to separate the effects of extinctions by NO₂ and aerosols (Krotkov et al., 2005c).

The future concentrations of tropospheric gases will depend on increased population, international agreements, such as the Kyoto Protocol and its successors, and the continued affordability of fuels. These changes in concentrations can affect UV radiation in various ways. Some gases, such as tropospheric ozone, can have a direct influence through absorption of UV. Others, such as nitrous oxide (N₂O) and methane (CH₄), can influence UV through their role in stratospheric chemistry, which results in changes to ozone concentrations. Further, all the greenhouse gases contribute to cooling of the stratosphere, which affects ozone chemistry, and to warming at the surface. The latter leads to changes in many variables that are capable of modifying directly the UV radiation at the surface. These include changes in glaciation, ice/snow cover, clouds,

rainfall, and run-off. Presently it is difficult to predict the future concentrations of tropospheric gases that attenuate UV radiation (Isaksen et al., 2005), and consequently their importance for surface UV in the future. It is clear, however, that UV is reduced under polluted atmospheric conditions and, in some cases, these reductions may balance, to a certain degree, the UV enhancements produced by stratospheric ozone depletion.

7.2.6 Surface Albedo

UV radiation is enhanced by surface albedo, particularly over strongly reflecting surfaces, such as snow, ice, or sand, and even more in the presence of cloud layers that trap the reflected radiation between the clouds and the surface. The wavelength-dependent scattering and absorption processes control the enhancement of UV radiation by surface albedo, and hence they determine the area around a site that can contribute to these enhancements. Changes in surface albedo due to global warming may thus become important for future surface UV radiation, through, for example, reduction of snow- and ice-covered areas, deforestation, or expansion of deserts. New studies have focused on quantifying the effects of high-albedo surfaces on UV irradiance under both clear skies and cloudy conditions, and on estimating surface albedo by combining measurements and modeling. Increases in erythema irradiance of up to ~20% were reported in these studies.

Variations of erythema and UV-A irradiances due to surface albedo changes were investigated during 15 cloudless days at Briançon (French Alps) in February 1998 with variable snow cover and a small snowfall in the middle of the campaign. The enhancement of erythema

SURFACE ULTRAVIOLET RADIATION

irradiance was found to change from 15% to 5% (7% to 5% for UV-A) as a result of changing surface albedo, with a jump to 22% (15% for UV-A) after the snowfall. The corresponding values of the effective surface albedo are respectively 0.4, 0.1, and 0.5 for erythemal, and 0.25, 0.1, and 0.4 for UV-A irradiances (Smolskaia et al., 2003). Measurements at the same station in winter/spring 2002 showed that the enhancement of surface UV irradiance depends more strongly on the snow distribution around the site than on the actual topography. The maximum enhancement of erythemal irradiance (~22%) for clear skies agrees with results of a 3-D RT model, assuming a snow albedo of 0.3 between the snow line and the tree line and of 0.8 above the tree line. Retrieving an effective surface albedo from the enhancement of UV irradiance measurements is challenging, because small uncertainties in the enhancement (e.g., $\pm 2\%$) lead to large uncertainties (± 0.05) in effective albedo (Lenoble et al., 2004b). Quantitative estimates of the enhancement of surface UV irradiance due to surface albedo changes were derived also for Sodankyla, Finland, by analyzing a time series of monthly erythemal dose measurements (Arola et al., 2003b). It has been shown that for this location the enhancement is largest in May, being 21% at its maximum and 7% on average.

The effect of surface albedo on UV sky radiance was investigated at the High Alpine Research Station Jungfrauoch, Switzerland, 3576 meters above mean sea level (amsl), located at the boundary between snow-covered and snow-free terrain (Huber et al., 2004). Toward the northwest, the effect of snow-free terrain causes a significant reduction of UV sky radiance (between 20% and 40% depending on SZA) relative to a modeled simulation assuming a homogeneous snow albedo of 0.4. Finally, at Neumayer, Antarctica, it was found that UV zenith sky radiance may increase by more than a factor of 2, relative to clear sky, due to the combined effect of clouds and high snow albedo (see example in Figure 7-2) (Wuttke and Seckmeyer, 2006). On the contrary, no change has been observed in the total irradiance, which was $\sim 670 \text{ W m}^{-2}$, both for overcast and clear-sky conditions.

Using model calculations, Parisi et al. (2003) estimated the increases in daily erythemal UV exposures on horizontal and on inclined planes over water, concrete, and sand relative to grassland. Under cloud-free skies, the estimated additional daily UV exposure on a horizontal plane was up to 3% higher over sand relative to grassland, while on a vertical plane the enhancement was up to 11%, for the range of SZA in the Australian sub-tropical location of this study.

Finally, measurements of spectral surface albedo from aircraft over flat arable land in East Anglia, Great

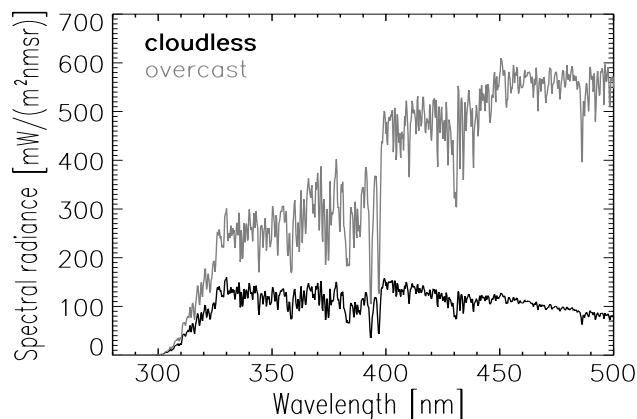


Figure 7-2. Spectra of zenith radiance measured under overcast and cloudless skies at the German Antarctic Neumayer Station (70.65°S , 8.25°W) on 19 December 2003 and 22 January 2004, respectively. The overcast spectrum exceeds the clear-sky spectrum by up to a factor of 10. In addition, the wavelength with maximum radiance is shifted from the UV (330 nm) for the clear-sky case to the visible (450 nm) for the overcast situation. Adapted from Wuttke and Seckmeyer, 2006.

Britain, show increasing albedo with increasing wavelength, from about 2% in the UV-B to about 5% at 500 nm (Webb et al., 2004). Effects of scattering and absorption within the layer beneath the flight level were removed by nonlinear extrapolation of the airborne albedo measurements to the ground (Wendisch et al., 2004).

7.2.7 Altitude

UV radiation increases with altitude, because of reduction of scattering and absorption by the less-dense overhead atmosphere, and, at high altitudes, because of additional reflections from the surface and the clouds below. At high altitudes, the surface is usually covered with snow, thus irradiance increases further due to enhanced surface albedo. As these processes are wavelength dependent, the increase of UV radiation varies also with wavelength.

New studies have investigated the altitude effect on UV-B irradiance using simultaneous measurements at different altitudes. The reported increases in erythemal irradiance are 7% per kilometer in Bolivia (Zaratti et al., 2003), 10.7% per kilometer in the Swiss Alps (Schmucki and Philipona, 2002), 7-16% per kilometer in Germany and between 5 and 23% per kilometer at different altitude pairs in Bolivia (Pfeifer et al., 2006), and $\sim 11\%$ per kilometer in the western Himalayas (Singh and Singh, 2004). The latter study also reported increases in direct and dif-

fuse irradiance, respectively, of 17.4 and 8.5% per kilometer. The variability in the estimates derived by these studies confirms that the altitude effect of UV irradiance is not linear, depending strongly on atmospheric and surface parameters, and varies also with wavelength.

Piacentini et al. (2003) measured extremely high values of solar irradiances at Cerro Cruz Azul (3900 m amsl) at the Puna of Atacama high-altitude inter-tropical desert, Argentina, under conditions favoring enhancements from reflections at the cloud edges and from multiple scattering in the cloud layer. The maximum short-wave (300-3000 nm) irradiance was 1528 W m^{-2} , about 8% higher than the solar constant, adjusted to the actual Sun-Earth distance, while the maximum UV irradiance integral (295-385 nm) was 69.5 W m^{-2} at 2.4° SZA.

Seasonal variations of the altitude effect on UV radiation are mainly influenced by changes in solar elevation, albedo, and turbidity. Allen and McKenzie (2005) measured with personal dosimeters the UV exposure of skiers at the ski field of Mount Hutt, New Zealand (2080 m amsl), and found the UV Index maxima greater by ~23% in mid-October and ~30% in mid-September than at sea level at the same time of year. Thus the exposure depends strongly on season.

7.2.8 UV Irradiances on Inclined Surfaces

Erythemal UV irradiance incident on a horizontal surface is not always the best way of estimating the real dose received by humans or animals, which is usually much higher, considering that nonhorizontal parts of their bodies may receive direct solar radiation at smaller angles of incidence. As solar radiation measurements are referenced traditionally on a horizontal surface, often personal UV radiation exposure studies and anatomical distributions of UV radiation relate the measured relative exposures to ambient UV radiation on a horizontal surface. A dataset of more than 3,000 days of irradiance measurements at 27 different orientations and on a horizontal plane reveals that irradiances on inclined surfaces are up to 1.7 times higher at the Schneefernerhaus high-altitude observatory (2650 m amsl) and 1.4 times higher in Munich (530 m amsl) compared with irradiances on a horizontal plane at the same locations (Oppenrieder et al., 2004, 2005). Simulations of these effects with a RT model were found to be in good agreement with measurements (Mech and Koepke, 2004). From clear-sky irradiance measurements with different detector inclinations in the plane of the Sun at Rosario, Argentina, it was found that the highest intensity of erythemal irradiance does not occur when the detector is pointed directly to the Sun, but at an angle larger than the solar elevation (i.e., closer to zenith). This

enhancement, which is stronger at large SZA (~30% at 80° SZA) and diminishes at solar zenith angles smaller than $\sim 50^\circ$, is attributed to differences in the contribution of diffuse and direct irradiances (Piacentini and Cede, 2004). The irradiance incident on inclined planes depends more strongly on ground reflectivity than irradiance on a horizontal plane (Koepke and Mech, 2005). Maximum increases of 57% in erythemal UV irradiance from horizontal to normal incidence were calculated by Weihs (2002) for altitudes above 3000 m.

7.2.9 UV Under Water, Ice, and Snow

Recent years have seen an expansion of research into UV under water, ice, and snow, along the lines of assessing variability in the context of climate change as well as ozone depletion, and in discovering the wide variability in UV penetration that exists among various types of aquatic ecosystems. Considerable new research has emerged on the dependence of UV in a wide variety of aquatic systems on bio-optical constituents such as dissolved organic matter (DOM), dissolved organic carbon (DOC), which is part of DOM, chromophoric (i.e., optically active) DOM (CDOM), particulate organic carbon (POC), and chlorophyll a, and on inorganic suspended particles. Table 7-2 summarizes many of these new results, listing the transmission depth, $Z(1\%)$, of UV-B radiation to 1% of the surface value for several aquatic systems. In addition, satellite methods for globally mapping UV penetration into oceanic waters have progressed from developmental stages to more viable algorithms (Vasilkov et al., 2005).

Häder et al. (2003) emphasize that for polar aquatic ecosystems, factors such as climate warming and changes in the sea ice season, surface albedo, and CDOM, may influence exposure to UV-B radiation even more than the springtime ozone depletion. As one example, Perovich (2002) reported that 10 cm of snow cover reduces UV-B transmittance by a factor of 40, thus protecting biota from UV-B while allowing a substantially larger fraction of PAR (i.e., Photosynthetically Active Radiation) to penetrate. During Arctic spring conditions, $Z(1\%)$ for UV-B radiation incident on bare sea ice may be as deep as 1.75 m, but with 5 cm of overlying snow, $Z(1\%)$ may be reduced to 30 cm. This implies a risk to non-UV-adapted organisms within and under the ice, if snowmelt were to occur earlier in the spring season as a result of climate warming. Similarly, Cockell and Córdoba-Jabonero (2004), who measured spectral UV transmittances through snow and ice on the Mars Oasis, a deglaciated section of Alexander Island, Antarctica, reported that an overlying snow depth of 4 cm is sufficient to offset a UV-B increase caused by

SURFACE ULTRAVIOLET RADIATION

Table 7-2. Values of the 1% transmission depth ($Z_{UV-B}(1\%)$) for solar radiation at single wavelengths and wavelength bands in the UV spectral region from recent studies in a variety of aquatic systems.

Location	$Z_{UV-B}(1\%)$ (m)	Wavelength Range	Source
N. Michigan stream, DOC = 2.0 mg l ⁻¹	0.45	305-320 nm	Frost et al., 2005
N. Michigan stream, DOC = 24 mg l ⁻¹	0.04	305-320 nm	Frost et al., 2005
Boreal forest lake, DOC = 3.0 mg l ⁻¹	2.00	300-320 nm	Donahue et al., 2003
Boreal forest lake, DOC = 6.7 mg l ⁻¹	0.40	300-320 nm	Donahue et al., 2003
Humic lake, Finland, DOC = 5.9 mg l ⁻¹	0.32	310-320 nm	Huovinen et al., 2003
Ultraoligotrophic high Arctic lake	7.00	308 nm	Ørbæk et al., 2002
Lake Huron, central	8.40	325 nm	Smith et al., 2004
Lake Erie and Lake Ontario, central	2.50	325 nm	Smith et al., 2004
Lake Huron tributaries	0.19	325 nm	Smith et al., 2004
Oceanic water, Jerlov type OI	30.50	310 nm	Piazena et al., 2002
Oceanic water, Jerlov type OIA	24.70	310 nm	Piazena et al., 2002
Oceanic water, Jerlov type OIB	20.60	310 nm	Piazena et al., 2002
Oceanic water, Jerlov type OII	12.40	310 nm	Piazena et al., 2002
Oceanic water, Jerlov type OIII	6.60	310 nm	Piazena et al., 2002
Atlantic water, Nordic Seas	31.00	310 nm	Aas et al., 2002
Northern Barents Sea	11.80	310 nm	Aas et al., 2002
Northern Greenland Sea	8.80	310 nm	Aas et al., 2002
Norwegian Coastal Current	7.80	310 nm	Aas et al., 2002
Kara Sea	3.60	310 nm	Aas et al., 2002
North Water Polynya, pre-bloom	9.40	320 nm	Vasseur et al., 2003
North Water Polynya, bloom	7.90	320 nm	Vasseur et al., 2003

60% ozone depletion. The penetration depth of UV radiation into snow may have also relevance for photochemical processes, through the release of NO₂ during the photolytic destruction of nitrate anions in the snow pack (Fisher et al., 2005). The expected decrease in snow cover in many areas due to climate warming suggests a strong linkage between climate change and UV-B variability at high latitudes.

Johannessen et al. (2003) have developed an empirical method to parameterize UV attenuation and CDOM absorption in oceanic waters using satellite ocean color measurements (i.e., SeaWiFS (Sea-viewing Wide Field-of-view Sensor) images of normalized water-leaving radiance). Their method is based on in situ measurements from a variety of sources, including the Mid-Atlantic and Georgia Bights, the Bering Sea, and inshore waters of the Delaware and Chesapeake Bays. Vasilkov et al. (2005) developed and validated a method for retrieving the radiation field in oceanic waters that uses backscatter UV (BUV) measurements from TOMS and OMI in conjunction with SeaWiFS data and full radiative transfer computations of irradiance at depth. Ocean Raman scattering, which is a function of absorption by particulate matter and

CDOM in the upper water column, contributes to the filling-in of Fraunhofer lines in space-based BUV measurements over cloud-free open ocean (Vasilkov et al., 2002). There is the potential to use BUV measurements to estimate chlorophyll and CDOM concentration for waters, where CDOM and particulate matter are well correlated. A BUV-based method would offer the advantages of (1) good sensitivity at low chlorophyll concentrations, and (2) a high-frequency spectral structure, thus being less affected by uncertainties associated with absolute calibration errors. However, complete development of such a method requires more in situ measurements of UV bio-optical properties throughout the world's oceans than presently exist.

From spectral transmission measurements in relatively transparent oceanic waters (characterized by small concentrations of particulate matter, such as silt, and yellow substance), Piazena et al. (2002) found that UV-B penetrates up to ~25% of the photic zone in these waters, while UV-A penetrates up to 93%. Rasmus et al. (2004) found that Southern Ocean waters are quite transparent to UV-B radiation during January, and that under an unperturbed ozone layer, 305 nm doses influence the first 4.0-

9.5 meters of the upper mixed layer, between 51°S and 65°S. They determined that the levels of UV and PAR were high enough that Southern Ocean phytoplankton is often not light limited.

Aas et al. (2002) synthesized several decades of in situ spectral UV attenuation measurements in Arctic marine waters and found considerable variability, related to particular classes of Arctic surface water, including Atlantic water, polar water influenced by river runoff, or Arctic water found in central gyres. Barron and Barron (2005) studied the waters of Prince William Sound, Alaska, in the context of glacial retreat due to climate warming, and reported that glacial melt water and suspended rock sediment cause a tenfold reduction in UV transmission at depth, compared with waters in the same basin distant from glacial influences.

In freshwater ecosystems, optical properties can vary widely due to factors such as water renewal time, the proportion of wetlands in the catchment, and the influence of tributaries, thus influencing the transmission of UV radiation in the water column (e.g., Frenette et al., 2003; Kjeldstad et al., 2003; Bracchini et al., 2005; Erga et al., 2005). Smith et al. (2004) found for the Great Lakes in the USA, much higher UV attenuation by CDOM in tributaries (89-94% of the attenuation) as compared with the lakes (37-77%). Arctic freshwater ecosystems are often characterized by low nutrient concentration and low DOC, implying particular vulnerability to UV stress (Häder et al., 2003). UV penetration in many boreal lakes is increasing, as DOC concentrations decrease due to influences of climate change and acidification. In Scandinavian humic lakes (60-63°N) and boreal forest lakes, DOC is a strong regulator of UV-B transmission (Donahue et al., 2003; Huovinen et al., 2003). In the shallowest aquatic ecosystems, there appears to be strong attenuation of UV radiation in the water column, correlated with DOM concentrations (e.g., Palen et al., 2002; Frost et al., 2005).

7.3 RESOURCES FOR STUDYING SURFACE UV RADIATION

The variability of surface UV irradiance in time and space is studied using measurements from ground-based instruments, as well as from estimates that are derived from a combination of satellite radiance measurements and radiative transfer modeling. Significant advancements have been reported in the last few years in measurement and calibration procedures of instruments and in algorithms used both in ground-based and satellite-borne platforms. Particular effort has been devoted to the determination and quantification of the errors and uncertainties involved.

7.3.1 Ground-Based Measurements

Quality control and quality assurance procedures have received considerable attention in the last decade, leading to significant improvements in instrument stability and data quality. Many monitoring stations have adapted widely accepted calibration and measurement procedures and protocols. In addition to irradiance, spectrally resolved measurements of actinic flux, direct irradiance, radiance, and polarization are now frequently made.

7.3.1.1 SPECTRORADIOMETERS

Spectroradiometers are still the most reliable type of instruments to measure solar UV radiation at the Earth's surface (Seckmeyer et al., 2001). In most cases, the measured quantity is the global irradiance, but in recent years, spectral measurements of actinic flux and of direct irradiance are gaining particular attention, for more accurate determination of photolysis frequencies, spectral aerosol optical depth, or column densities of different atmospheric constituents (e.g., Hofzumahaus et al., 2002; Webb et al., 2002a; Houët and Brogniez, 2004; Lenoble et al., 2004a; Kazadzis et al., 2005; Kylling et al., 2005).

Empirical and semi-empirical methods have been derived to determine actinic flux and photolysis frequencies from irradiance measurements, in experimental campaigns where the derived products could be validated by measurements (Webb et al., 2002a; Bais et al., 2003; Hofzumahaus et al., 2004; Monks et al., 2004). For clear-sky conditions, the conversion with empirical models agrees better than 10% with measurements (McKenzie et al., 2002; Webb et al., 2002b; Kazadzis et al., 2004; Topaloglou et al., 2005); for cloudy conditions the agreement is within ~15%. Use of model calculations yields a similar agreement under clear and overcast conditions, but is less accurate under broken clouds (Kylling et al., 2003b). A semi-empirical approach that combines measured actinic flux and irradiance spectra with model calculations results in similarly good agreement for all sky conditions (Schallhart et al., 2004). Considering that long-term measurements of actinic fluxes and photolysis frequencies are few and sparse, these methodologies constitute the only way to assess the variability of these quantities and their effects on tropospheric photochemistry in the last 10 to 15 years.

The distribution of actinic flux in the vertical dimension and through a cloud layer was measured during a field campaign and was well described by a RT model (Kylling et al., 2005). The interpretation of such measurements and simulations is important for improving our understanding of the radiative and chemical processes that

SURFACE ULTRAVIOLET RADIATION

occur in the troposphere, especially under and above the clouds.

7.3.1.2 BROADBAND FILTER RADIOMETERS

Broadband radiometers represent instruments that measure integrated irradiance over a large wavelength range, such as UV-A or UV-B, but typically have been designed to measure irradiance weighted by the action spectrum for erythema as defined by the Commission Internationale de l'Éclairage (CIE) (McKinlay and Diffey, 1987). These instruments are suitable for many applications because of their low cost and ease of operation in remote locations, but they do have limitations in terms of quality assurance and quality control (QA/QC). They are a major source of ultraviolet radiation information for larger geographical areas and have been in continual use for longer periods than many other types of UV instruments (Nunez et al., 2002; Hicke et al., 2004; Kimlin et al., 2005). The UV instrumentation working group of the World Meteorological Organization (WMO) prepared a report (Seckmeyer et al., 2005) which describes and defines the specifications of this type of instruments, provides guidelines for their calibration and characterization, and outlines QA/QC procedures based on current understanding of these instruments and UV science objectives. These guidelines have been applied, for example, in the Austrian UV monitoring network (Blumthaler, 2004). A detailed uncertainty analysis of broadband radiometers operating in Norrköping has been presented by Josefsson (2006).

A new method for calculating correction factors for the non-ideal angular response of the broadband radiometers was developed using actual measurements of the anisotropy of the UV-B sky (Kuchinke and Nunez, 2003). The usual assumption of isotropic sky distribution overestimates the diffuse component by 4-6% for clear skies.

Knowledge of the relative spectral response of erythemal radiometers is essential for correcting their measurements for column ozone and SZA variations. Measurements of the response of a sample of instruments at three different laboratories were found to agree within 20% with typical dynamic ranges of approximately 10^4 (Schreder et al., 2004). The dependence of the output signal of Solar Light Co. SL501 erythemal radiometers on ambient temperature and relative humidity was investigated (Huber et al., 2002, 2003). It was shown that despite the internal temperature stabilization at 25°C, increasing the ambient temperature by 20°C reduced the instrument's spectral response by up to 10% in the UV-B and by a factor of two in the UV-A, depending on the instrument and its internal relative humidity. By varying the relative

humidity from 9 to 70%, the instrument's sensitivity was reduced by 5% in the UV-B and by a factor of two in the UV-A. There is yet no evidence that such effects occur also in Yankee Environmental Systems, Inc. (YES) model UVB-1 radiometers that are stabilized above 40°C. The dependence of the SL501 radiometers on the ambient conditions calls for further investigation and quantification of the effects on the actual measurements and of this radiometer's suitability for long-term studies.

7.3.1.3 NARROWBAND MULTIFILTER RADIOMETERS

Narrowband multifilter radiometers measure solar radiation in several (typically 4 to 7) UV channels with bandwidths ranging from 2 to 10 nm. They provide more information than broadband radiometers and require less maintenance than spectroradiometers. All channels can be measured at high frequency, making the instruments well suited for investigating short-term variation of spectral UV irradiance caused, for example, by rapidly changing cloud conditions (Lovengreen et al., 2005). High sampling rates also allow deployment on balloons for measuring vertical profiles of UV (Kylling et al., 2003a). For accurate calibration, knowledge of the spectral response of the different channels is required (Høiskar et al., 2003; Bernhard et al., 2005; Lakkala et al., 2005) and corrections for the effect of ozone and SZA variation should be applied (Diaz et al., 2005). Methods for proper quality control of Norwegian Institute for Air Research NILU-UV multichannel radiometers, operating under harsh conditions in SH high latitudes, are described by Lakkala et al. (2005), who have also reported large (up to ~35%) drifts in their sensitivity.

Data from multifilter radiometers allow the calculation of secondary data products such as reconstructed high-resolution solar spectra, erythemal irradiance, total ozone, and cloud transmission, with the aid of empirical or RT models (Høiskar et al., 2003). Such products are regularly included in the UV-monitoring programs of Norway (Mikkelsen et al., 2000), the U.S. National Science Foundation (NSF) (Bernhard et al., 2005), and the U.S. Department of Agriculture (Davis and Slusser, 2005). Feister et al. (2005) use a neural network technique to reconstruct solar irradiance spectra. For solar zenith angles smaller than 80°, total ozone derived from multifilter radiometers can have accuracy similar to data obtained from Dobson spectrophotometers (Dahlback et al., 2005). Seroji et al. (2004) demonstrated the feasibility of calculating photolysis rates of O₃, NO₂, and formaldehyde (CH₂O) from filter instrument data.

If the instruments are equipped with an automated shadow band, direct solar irradiance can be retrieved,

which allows the calculation of aerosol optical depth (e.g., Krotkov et al., 2005a) and the optical depth of thin clouds (Min et al., 2004). By combining direct and diffuse measurements, single scattering albedo and other aerosol parameters can be derived (Petters et al., 2003; Goering et al., 2005; Krotkov et al., 2005b).

The improved technical characteristics of these instruments and the possibility to derive additional products constitute their main advantages and make them important supplements to spectral measurements of solar irradiance in the global UV monitoring system.

7.3.1.4 ADVANCEMENTS IN INSTRUMENTATION

Further progress has been made toward uncovering instrumental errors in solar UV radiation monitoring and in the development of methods for improving the measurement techniques and the quality of the data.

A temperature dependence in the transmission of polytetrafluoroethylene (PTFE), which is a widely used material in the diffusers of UV spectroradiometers, has been quantified by laboratory studies (Ylianttila and Schreder, 2005). At $\sim 19^\circ\text{C}$, the transmission of most types of PTFE increases abruptly by 2-3%, whereas below and above this point a temperature coefficient of about $-0.1\%/^\circ\text{C}$ is observed. The influence on UV irradiance was quantified through comparisons of measured and modeled UV irradiances at an unpolluted site in New Zealand, where all necessary modeling input parameters were available (McKenzie et al., 2005). These authors concluded that all data measured at ambient temperatures of less than 15°C are typically underestimated by $\sim 2\%$. The temperature sensitivity of PTFE diffusers introduces an additional uncertainty in the UV measurements, especially at sites where the ambient temperature fluctuates around this range of temperatures (i.e., $\sim 15\text{--}19^\circ\text{C}$), which may have also a seasonality. It is rather unlikely that long-term variations of surface irradiance at a particular site may be influenced, unless the ambient temperature has changed over a certain period from temperatures below this threshold to temperatures above it. Finally, during the calibration of the instruments, the diffuser is usually heated by the lamp; thus normally its temperature should be above this threshold.

Knowledge of the angular response error of a radiation instrument allows, with the aid of RT modeling, the calculation of correction factors. A transportable unit that was developed in the frame of the Quality Assurance of Spectral Solar UV Measurements in Europe (QASUME) project was used to measure the angular response of 11 spectroradiometers operating in Europe (Bais et al., 2005a), thus allowing back correction of datasets recorded

at these sites. Angular response errors of $\sim 2\%$ can now be reached in Brewer spectrophotometers by modifying their entrance optics (Gröbner, 2003), compared with errors of $\sim 10\%$ found in the standard Brewer configuration (e.g., Bais et al., 2005a).

Due to the combined effect of two polarization-sensitive elements, the entrance window and grating, the sensitivity of Brewer spectrophotometers for direct-Sun and sky-radiance measurements changes with solar zenith angle. This introduces systematic errors in Langley extrapolations, aerosol optical depth retrievals, and aerosol single scattering albedo retrievals. The need for appropriate corrections has been shown by Cede et al. (2006b). New methodologies were proposed for improving the measurements of O_3 , SO_2 , and NO_2 columns with Brewer spectrophotometers (Cede and Herman, 2005; Cede et al., 2006a).

In recent years, diode array and charged-coupled device (CCD) single monochromator instruments have become available, allowing measurement of the full solar spectrum from UV to infrared within seconds or milliseconds (Edwards and Monks, 2003; Jäkel et al., 2005). However, in the UV-B range, these instruments suffer from stray-light contamination, and many attempts are underway to reduce this problem.

7.3.1.5 DATA QUALITY AND DATABASES

The importance of quality assurance of UV measurements has been recognized since the beginning of the measurement records, although procedures for implementing quality assurance were developed later, mainly through intercomparison campaigns (e.g., Bais et al., 2001; Lantz et al., 2002; Metzdorf et al., 2003; Webb et al., 2003). Most of the spectroradiometers deployed today are radiometrically calibrated with tungsten halogen standard lamps that are traceable to standards maintained by National Metrology Institutes (NMI) (e.g., Gröbner and Sperfeld, 2005; Wuttke et al., 2006). Differences between the UV spectral irradiance scales realized and disseminated by different NMIs in the past are one of the most critical problems in UV radiometry (Kübarsepp et al., 2002; Metzdorf et al., 2003). Even standards of the same Institute may disagree beyond their stated accuracy, and deviations exceeding 4% in the UV have been observed (Bernhard and Seckmeyer, 1999; Kiedron et al., 1999; Gröbner et al., 2002). Alternative methods for reducing the uncertainties in the calibration standards and for improving the comparability of the irradiance scales of different NMIs are in progress (Yoon et al., 2002; Metzdorf et al., 2003; Sperfeld et al., 2003; Durak and Samadov, 2004).

SURFACE ULTRAVIOLET RADIATION

In the framework of the QASUME project, a transportable spectroradiometer was developed (Gröbner et al., 2005; Gröbner and Sperfeld, 2005). On-site comparisons with 26 spectroradiometers deployed at various locations in Europe revealed irradiance differences ranging between 4 and 14% (Gröbner and Sperfeld, 2005). Similarly, a new spectroradiometer to act as traveling standard for the Network for the Detection of Atmospheric Composition Change (NDACC) (formerly Network for the Detection of Stratospheric Change, NDSC) was developed (Wuttke et al., 2006).

The uncertainties in UV irradiance measurements vary between different instrument types and stations, depending on the availability of resources for achieving accurate characterization of instruments and for applying proper quality control procedures. These procedures are improving with time following the progress of the relevant technology. It is therefore expected that measurements conducted in early stages of monitoring have larger uncertainties, which in some cases are difficult to quantify. Different studies in the last 5-10 years have reported uncertainties between 5-7% for global or direct spectral irradiance measurements in the UV-B (Bernhard and Seckmeyer, 1999; Bernhard et al., 2004; Kazadzis et al., 2005; Bernhard et al., 2006), which are dominated by the uncertainty of the calibration standards and, for global irradiance, the cosine-error correction.

There are two major databases of spectral UV radiation measurements: the World Ozone and Ultraviolet Radiation Data Centre (WOUDC) in Toronto, Canada (<http://www.woudc.org>) with spectral irradiance data from 29 stations, and the European Ultraviolet Database (EUVDB) in Helsinki, Finland (<http://uv.fmi.fi/uvdb/>) containing data from 43 stations. A list of stations and currently available data are given in Appendix 7A. New techniques have been pursued to uncover errors in spectral measurements at the databases EUVDB and WOUDC, and tools have been developed (Slaper et al., 2004; Engelsen and Kylling, 2005) for this purpose. In EUVDB, all data are now automatically checked and flagged for their quality.

Several UV monitoring networks maintain independent UV databases. The U.S. National Science Foundation's UV monitoring network includes quality-controlled spectra measured between 1988 and 2006 at seven high-latitude sites located in Antarctica, South America, Alaska, and Greenland (see Appendix 7A.3). A new data edition named "Version 2" is currently in preparation; it will offer higher accuracy and additional data products such as total ozone, effective albedo, and cloud optical depth (Bernhard et al., 2004, 2006).

7.3.2 Satellite-Derived UV Estimates

Instruments onboard satellites provide global maps of surface UV irradiance by combining backscattered radiance measurements with RT models. The accuracy of the models is limited mostly by uncertainties in input parameters representing the atmosphere and the Earth's surface. Issues that require particular attention are the detection and correction of long-term calibration drifts and the establishment of interpolation methods when combining different satellite datasets.

7.3.2.1 DIFFERENCES BETWEEN GROUND-BASED AND TOMS-DERIVED UV IRRADIANCES

Surface UV retrievals from the measurements of the Total Ozone Mapping Spectrometer (TOMS) instruments onboard different satellites (1978-2002) is probably the only dataset that has been so extensively compared with ground-based measurements. Recently, the TOMS UV irradiance database (<http://toms.gsfc.nasa.gov>) has been expanded to include five new products (noon irradiance at 305, 310, 324, and 380 nm, and noon erythemally weighted irradiance), in addition to erythemal daily exposure, allowing direct comparisons with ground-based measurements from UV spectroradiometers (Krotkov et al., 2004).

Since the previous Assessment (WMO, 2003), advances have been made in understanding the factors causing differences between satellite- and ground-based UV data. Sabburg et al. (2002) compared TOMS daily erythemal doses on clear days against measurements at four sites of the Brewer network of the U.S. Environmental Protection Agency, and concluded that TOMS UV retrievals have a positive bias between 1.4 and 12.5%, with an average of ~5%. Fioletov et al. (2004) produced two UV Index climatologies over Canada and the United States for the period 1980-1990 using TOMS data, and these were validated against Brewer UV measurements from several sites. With snow on the ground, TOMS retrievals were up to ~60% lower, due to insufficient treatment of the snow albedo. In summer, the TOMS UV estimates were 10 to 30% higher, caused most likely by air pollution and absorbing aerosols. Differences between daily erythemal irradiances derived by TOMS (version 7 and 8) and by a Brewer spectrophotometer at Lampedusa have been found to increase with increasing aerosol optical depth, often associated with Saharan dust outbreaks (Meloni et al., 2005). Arola et al. (2005) found positive bias of 20-30% by comparing irradiance data over Thessaloniki, Greece, and Ispra, Italy, with TOMS version 8 products.

These studies confirmed that insufficient information on aerosols near the surface is responsible for the observed biases in satellite UV irradiances. Arola et al. (2005) and Krotkov et al. (2005b) have shown that knowledge of the absorbing properties of aerosols may reduce appreciably these biases, and suggested that taking into account even climatological estimates of AOD and SSA would greatly improve the satellite UV retrievals. Aerosol absorption corrections were found to improve TOMS-derived UV over Moscow during the period May–September (Chubarova et al., 2005). Erythral irradiances recorded at eight stations in Argentina agreed with TOMS estimates, which were first corrected for the effects of aerosols, to within $\pm 10\%$ under snow-free conditions (Cede et al., 2004). These newly reported differences are much smaller than those previously reported (Kerr and Seckmeyer et al., 2003). Therefore the use of satellite-derived UV estimates without accounting for effects from aerosols at locations with large aerosol abundances may lead to false conclusions.

New approaches have been suggested to model the effects of clouds over snow-covered terrain. The method proposed by Arola et al. (2003a) improved the agreement between TOMS-retrieved erythral daily doses and ground-based measurements over two Finnish and five Canadian sites. Tanskanen et al. (2003) developed a methodology by analyzing the TOMS Lambertian Equivalent Reflectivity (LER) data using a moving time-window technique, accounting also for autumn and spring transitions during snow accumulation and snow melt.

7.3.2.2 UV RETRIEVAL ALGORITHMS AND RELATED UNCERTAINTIES

Further studies were devoted to the development of new algorithms for producing global coverage of surface UV irradiances, involving information from other satellite products. Apart from the effect of aerosols (discussed in Section 7.3.2.1), the treatment of the cloud and surface reflectivity by the UV-retrieval algorithms is still a challenging issue.

The influence of clouds is one of the major sources of uncertainty in surface UV irradiances retrieved from satellite instruments, particularly over areas with high surface reflectivity, and different methodologies to parameterize the cloud transmittance have been proposed. Meerkötter et al. (2003) compared two independent approaches using data from the AVHRR instrument onboard the polar-orbiting NOAA satellites and from MVIRI (METEOSAT Visible and Infrared Instrument) onboard the geostationary METEOSAT satellite. The latter offers particularly good temporal resolution, but was

expected to be problematic at high latitudes where their study was focused. However, they found that METEOSAT (or the new METEOSAT Second Generation (MSG) satellite) may be used to account sufficiently for cloud effects in UV at latitudes up to 70° . By combining cloud information from METEOSAT, ozone column from TOMS and GOME (Global Ozone Monitoring Experiment), and RT modeling (Surface Irradiation Derived from a Range of Satellite-Based Sensors-SIDES), UV climatologies over Europe from 1984 to 2003 were generated by Verdehout (2004a; 2004b) with spatial resolution of ~ 5 km. Improvements to the Joint Research Center (JRC) algorithm SIDES were applied (Wuttke et al., 2003), resulting in better agreement with measurements in the UV-B. A new satellite UV algorithm for producing UV-B and UV-A irradiances and the UV Index using the Surface and Atmosphere Radiation Budget (SARB) products of Clouds and the Earth's Radiant Energy System (CERES) was developed (Su et al., 2005). Differences when compared with a high-resolution, multistream radiative transfer code range from -10% to $+4\%$ for UV-B and UV-A irradiances, and from -26% to $+16\%$ for the UV Index. Ciren and Li (2003) derived a long-term (1983–2000) global climatology of surface UV-B and erythral irradiance by combining TOMS ozone and International Satellite Cloud Climatology Project (ISCCP) D1 3-hour reflectance measurements, thus accounting more efficiently for the diurnal variability of clouds. On the other hand, Williams et al. (2004) have shown that using the ISCCP climatology for estimating surface UV irradiance results in significant bias, suggesting instead to use the TOMS reflectivity at 360 nm.

The TOMS UV algorithm (Krotkov et al., 1998; Herman and McKenzie et al., 1999; Krotkov et al., 2001) was successfully applied to the new Ozone Monitoring Instrument (OMI) onboard the Aura spacecraft for continued monitoring of ozone, other trace gases, and surface UV irradiance (Levelt et al., 2006; Tanskanen et al., 2006). OMI is a contribution of The Netherlands's Agency for Aerospace Programs (NIVR) in collaboration with the Finnish Meteorological Institute (FMI) to the NASA Earth Observing System (EOS) Aura mission and, among other products, provides global maps of surface UV irradiance (see example in Figure 7-3).

7.3.3 Advancements in UV Radiation Modeling

Considerable progress has been made in radiative transfer modeling, in particular on the interaction between clouds and radiation, the impact of aerosols, and three-dimensional radiative transfer. Important aspects for the ultraviolet spectral region are: (1) the strong Rayleigh scat-

SURFACE ULTRAVIOLET RADIATION

tering and absorption by ozone; (2) the approximately wavelength-independent optical properties of clouds and their negligible absorption unless they are polluted by absorbing aerosol; and (3) the importance of short wavelengths due to the strong biological and chemical effects of UV radiation, despite their small contribution to the total energy.

A variety of radiative transfer codes are freely available (see Appendix 7B.3) (Madronich and Flocke, 1997;

Evans, 1998; Ricchiazzi et al., 1998; Key, 1999; Koepke et al., 2005; Mayer and Kylling, 2005; Rozanov et al., 2005). In addition to being useful for calculating irradiance at the surface, most of them can be used to calculate other quantities, such as radiance and actinic flux, also at different altitudes. Some (e.g., LibRadTran) allow calculations throughout the whole solar and thermal spectral range.

OMUVB Erythemal Daily Dose

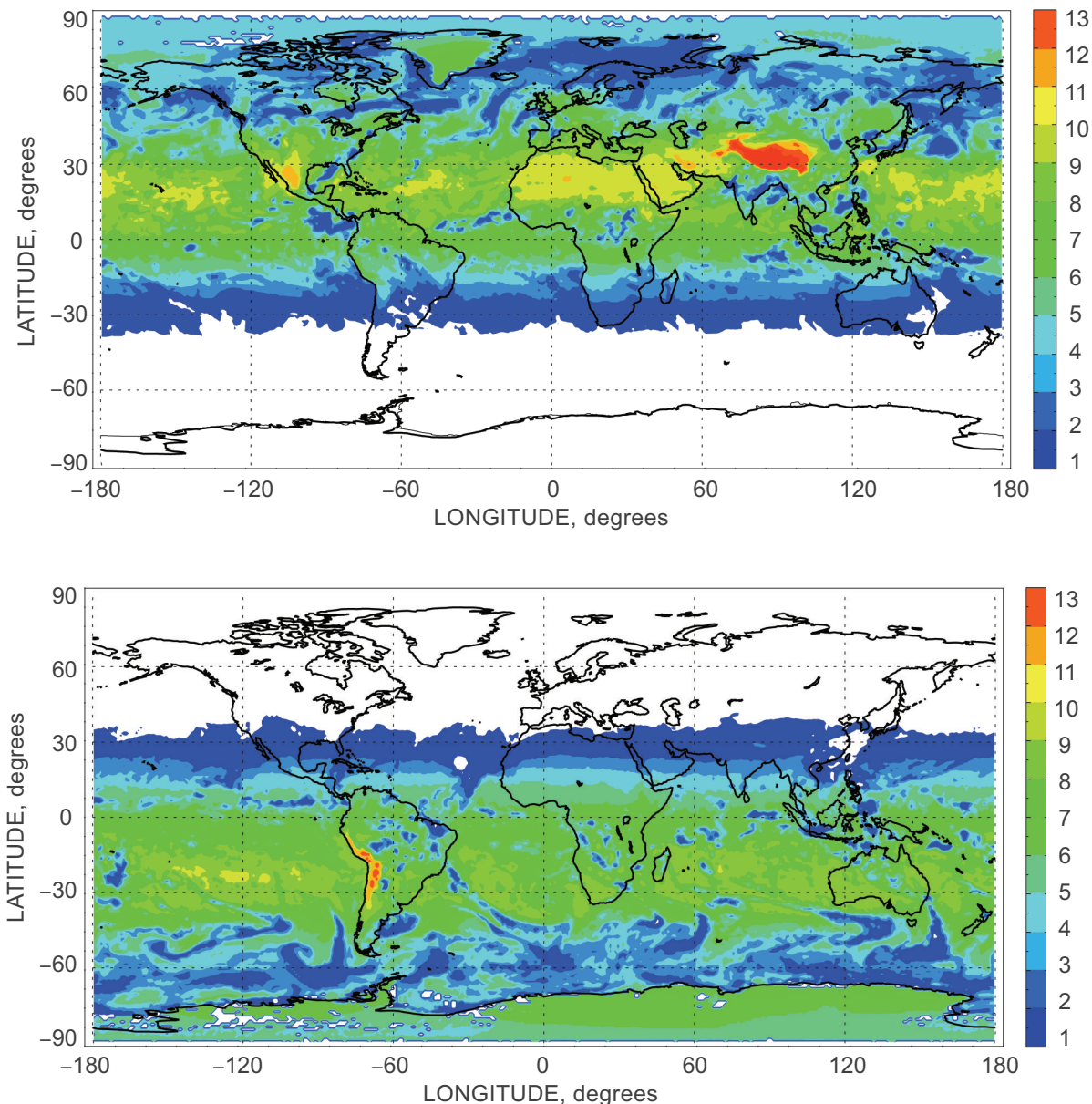


Figure 7-3. Global distribution of the cloud-corrected daily integral of erythemal irradiance in kJ m^{-2} for 28 June 2005 (upper panel) and 28 December 2005 (lower panel) derived from OMI measurements.

Radiative transfer is used in: (1) research applications, such as the interpretation of campaign data, requiring the highest degree of sophistication including, for example, three-dimensional solvers or spherical geometry; (2) routine applications, such as the quality control of observations or provision of cloudless-sky reference data to routinely estimate the influence of clouds from observed spectra; or (3) applications where large numbers of calculations are needed, such as the computation of photolysis frequencies in chemistry-transport models (CTMs) or the calculation of global time series of UV data. For most routine applications, the above-mentioned freely available codes are suitable, although they require significant computational power. The use of fast parameterizations like SMARTS2 (Gueymard, 2001) or lookup-table based approaches like FASTRT (Engelsen and Kylling, 2005) may be more appropriate whenever a large number of modeled spectra are required. The calculation of photolysis frequencies in chemistry or chemistry-transport models is probably one of the most demanding applications, in terms of the number of spectra to be calculated, requiring specially tailored solutions like Fast-J (Wild et al., 2000). Finally, statistical methods have been derived by relating a large number of observations at one or a few sites to a set of ancillary measurements, such as total ozone, cloud cover, or pyranometer observations (e.g., Fioletov et al., 2001; Schwander et al., 2002). While these are usually very good in predicting the radiation for a given location, it may be problematic to transfer the results to other locations or to calculate radiation for time periods other than the one used to build the statistical model.

After numerous model-model or model-measurement intercomparisons, the confidence in the results of radiative transfer codes in the UV is high if the input parameters are chosen carefully. Model-model intercomparisons have shown that different radiative transfer codes may agree to well below the 1% level if they are operated with identical optical properties. This is even true for complex three-dimensional codes, as has been shown in the Inter-comparison of 3-D Radiation Codes (I3RC) (Cahalan et al., 2005), where a core group of radiative transfer codes agreed to within 0.1-1% for a variety of complex cases, neglecting polarization, spherical geometry, and inelastic scattering.

Uncertainty of model calculations can have different sources. First, uncertainties in parameters like extra-terrestrial irradiance (Gueymard, 2004) and the absorption cross section of ozone (Orphal and Chance, 2003) translate directly to uncertainties in irradiance. The largest source of uncertainty is usually the lack of knowledge of the actual state of the atmosphere or surface, in particular for cloudy, polluted, or partially snow-covered conditions.

Clouds pose the most challenging modeling problem, due to their complex geometry and high variability in space and time. The effect of clouds on radiation is basically understood (at least for spherical droplets) and can be simulated with a 3-D radiative transfer code. For theoretical case studies, various cloud models have been used, including simple geometrical shapes, statistical assumptions (Cahalan et al., 1994), cloud-resolving models (Trautmann et al., 1999; Brasseur et al., 2002), and high-resolution observations by satellites and aircraft (Meerkötter and Degünther, 2001; Scheirer and Schmidt, 2005). However, the simulation of an actual situation is complicated because a sufficiently complete description of the clouds is generally not available. Information such as cloud cover or pictures by sky cameras give a first hint but are not sufficient to simulate the irradiance at the ground. The situation for aerosols is similar; while the optical depth is easily obtained by observations, the irradiance is critically determined by the single scattering albedo, which is not easily measured (see Section 7.2.4). Sometimes, the missing information is replaced by an effective parameter, such as an effective single scattering albedo (Kylling et al., 1998; Kazantzidis et al., 2001; Petters et al., 2003; Bais et al., 2005b). If more observations are available to constrain the actual situation, the concept of effective cloud parameters may fail (Kylling et al., 2005), but enough data are usually not available to verify that.

Three-dimensional radiative transfer effects in the ultraviolet spectral range caused by clouds have been recently studied both experimentally and theoretically (Brasseur et al., 2002; Kylling et al., 2005; Marshak and Davis, 2005). Topography also plays a role. For example, mountains may either block part of the diffuse-sky radiance, or cause an increase by reflection of extra radiation at snow-covered mountain slopes (see Sections 7.2.6 and 7.2.7). Moreover, air or clouds below an observation site enhance the backscattered radiation and lead to further increase in irradiance (McKenzie et al., 2001a). Considerable research efforts are spent on three-dimensional radiative transfer applications, to gain a detailed understanding of the processes that control the interaction of radiation with the atmosphere and the surface. The main objective of the Radiation Transfer Model Intercomparison (RAMI) was to improve understanding of the important interactions between radiation and vegetation (Pinty et al., 2004).

Validation campaigns have mostly concentrated on cloudless conditions. Comparisons of spectral irradiance (e.g., Mayer et al., 1997; van Weele et al., 2000) and actinic flux (Bais et al., 2003; Früh et al., 2003; Shetter et al., 2003; Hofzumahaus et al., 2004) for a cloudless sky

SURFACE ULTRAVIOLET RADIATION

generally found differences of about 5-10% between observations and simulations, which were usually within the combined uncertainty of measurement and model. Comparisons for cloudy sky are rare, due to the difficulty in obtaining cloud parameters independent of the irradiance observations. In the European project INSPECTRO (Influence of Clouds on the Spectral Actinic Flux in the Lower Troposphere), simultaneous observations of radiation and clouds using ground-based, aircraft, and satellite instrumentation provided a first dataset to evaluate three-dimensional radiative transfer calculations. Kylling et al. (2005) showed for a broken cloud case that the one-dimensional approach was not able to simultaneously reproduce the measured enhancement of the actinic flux above the cloud and the reduction below the cloud. Further evaluation of the campaign data is in progress.

In summary, radiative transfer in the ultraviolet spectral range has reached a mature state. If the input parameters are known, the radiation can be simulated with reasonable accuracy for many applications. However, some of these input parameters (e.g., a reasonable description of clouds or the single scattering albedo of the aerosol) are not easily attained. While satellite observations of clouds allow derivation of average radiation levels, they usually fail to provide information about the small-scale variability in space and time, which could be essential for biological systems. While the main aim of research in the ultraviolet spectral region remains the study of irradiance and actinic flux for applications in biology and chemistry, observations of radiance give much deeper insights into the interactions between radiation and the atmosphere or surface (Huber et al., 2004; Kuchinke et al., 2004). It may also help to validate and improve radiation codes and to decide which input parameters are required for specific applications.

7.3.4 Short-Term UV Forecasting

In the four years since the previous Assessment (WMO, 2003), the UV Index (WMO, 1994, 1998) has become the internationally accepted standard for disseminating information on solar UV levels to the general public. Forecasts, as well as measurements of the UV Index, now appear on numerous web-sites in many countries (Appendix 7B.5) and are used by TV, radio, and print media across the globe in an effort to change population behavior and moderate exposure to solar UV radiation. UV Index forecasts are a direct application of the scientific work on understanding the factors such as absorption and scattering affecting the transmission of UV radiation through the atmosphere to the Earth's surface.

Forecasts of the UV Index have been provided by numerous agencies since the 1990s using different computational methods (Austin et al., 1994; Burrows et al., 1994; Long et al., 1995; Burrows, 1997; Rikus, 1997; Bais et al., 1998; Staiger et al., 1998; Lemus-Deschamps et al., 1999; Renwick and McKenzie, 2001; Lemus-Deschamps et al., 2004; Staiger and Koepke, 2005). Forecasting the column ozone amount and estimating the atmospheric aerosol contribution to absorption remain the major difficulties in improving the accuracy of calculating the clear-sky surface UV irradiance and in subsequently forecasting UV indices. Computed UV irradiance for clear-sky conditions is generally overestimated in comparison to measurements (Kalliskota et al., 2000; McKenzie et al., 2001b), mainly due to lack of information on AOD (De Backer et al., 2001). Long-term correlations of aerosols with measured UV irradiance may improve AOD forecasts locally (Krzyścin et al., 2001; Petters et al., 2003; Gröbner and Meleti, 2004; Goering et al., 2005).

Including clouds in UV Index forecasting requires both accurate forecasts of cloud cover and cloud types, as well as more accurate data on cloud UV transmittance. Forecasts of UV Index have used empirical relations between forecast cloud types and measured UV radiation to adjust clear-sky forecasts. More recent approaches use information on cloud and surface albedo provided by numerical weather prediction (NWP) models (Staiger and Koepke, 2005). Work on improving agreement between calculations utilizing clouds and their effects on UV transmittance and surface measurements continues (Arola et al., 2003b; Krzyścin et al., 2003; Lane-Veron and Somerville, 2004; Su et al., 2005).

The major parameter affecting the forecast of the clear-sky UV Index is the estimated ozone amount, which can be determined either using the persistence of satellite-observed ozone or from a range of NWP meteorological variables via statistical regressions (e.g., Plets and Vynckier, 2000). Some forecasting centers such as the National Centers for Environmental Prediction (NCEP), the Koninklijk Nederlands Meteorologisch Instituut (KNMI), the European Centre for Medium-Range Weather Forecasts (ECMWF), and the Australian Bureau of Meteorology (BOM) assimilate ozone into their forecast models using satellite data to produce forecasts of the global (or continental) ozone fields a number of days in advance (Lemus-Deschamps et al., 2004). Research validating the results of the BOM numerical weather prediction (NWP) system's forecasts of UV Index continues with comparisons against surface observations (Gies et al., 2004; Lemus-Deschamps et al., 2004) in an effort to improve agreement. This ongoing validation study is coupled with research to improve the presentation of the UV

Index in communications to the public, with the aim of increasing its impact and making it more effective in changing behavior (Dixon and Armstrong, 1999; Dixon et al., 2002; Blunden et al., 2004). A range of different UV Index presentations utilizing the recommendations of the World Health Organization (WHO, 1994; Rehfuss, 2002) is being tested in Australia by the Cancer Councils, with planned follow-up assessments of their impact.

7.4 UV CLIMATOLOGY

Long- and short-term UV variability has been studied extensively during the last few years by analyzing measurements of surface UV irradiance that are now available for more than 10 years at several locations worldwide. Routine spectral measurements started only in the late 1980s and thus long-term changes that are calculated from these datasets should be smaller compared with what they would have been if UV records were available before the beginning of the ozone depletion in the early 1980s. Satellite estimates are also available for long periods (since 1979) and provide global coverage, which allows the derivation of UV estimates for any location on the Earth. However, gaps in the satellite records in the mid-1990s increase the uncertainty and complicate the calculation of long-term changes. In addition to the relative shortness of the UV records, surface UV exhibits a large variability from natural factors, such as clouds, ozone, aerosols, surface albedo, and UV-absorbing atmospheric constituents (e.g., SO₂ and NO₂), which reduce the significance of the estimated long-term changes. Extreme values of UV radiation at the surface as a consequence of these factors have been reported and were discussed in Section 7.2. The attribution of the causes for the observed changes is among the present research priorities, especially as it pertains to the response of surface UV to the recovery of the ozone layer.

7.4.1 Derived from Ground-Based UV Measurements

7.4.1.1 LONG-TERM CHANGES

The magnitude and statistical significance of the long-term changes in surface UV irradiance derived from analysis of ground-based measurements are of the order of a few percent per decade, depending on location, season, wavelength range, and the period of measurements. The sign of these changes varies also with location and depends strongly on the length of the measurements series. As measurements suitable for calculation of long-term changes are sparse, there are difficulties in projecting the

derived results to other time periods or other locations. An example is shown in Figure 7-4, which presents time series of monthly mean anomalies in noon erythemal irradiance under all-sky conditions at 11 UV monitoring sites distributed worldwide. Linear regressions over the period from the early 1990s to the mid-2000s indicate negative changes at stations in the Southern Hemisphere and in the Arctic. This pattern is especially evident if linear regressions are calculated since 1998, when the first signs of a slowdown in the ozone depletion were observed (see Chapter 3, Section 3.2), suggesting that surface UV radiation has responded to ozone increases, at least at these sites. In the northern midlatitudes, the observed UV irradiance changes are positive. The significance of the calculated changes is affected by the uncertainties of the measurements, which may range between 5% and 10%, depending on the site and the period. Data in the beginning of the records have usually higher uncertainties (see Section 7.3.1.5). Statistically significant linear changes (neglecting the measurement uncertainties) for the entire record of measurements were found only at Lauder and Palmer (−8.4% per decade at the 99% confidence level) and at Barrow (−4.4% per decade at 95% confidence level). Observations in Lauder prior to 1994 were performed only under fair-weather conditions, and this may have influenced the calculated linear changes. Statistically significant positive changes are found at all seasons in the station of Lindenberg, produced by two abrupt changes in UV irradiance that occurred in 1996 and 2003, respectively. The change in 2003 is shown also at Bilthoven. For the spring months the linear changes are insignificant and negative at all stations, except at Thessaloniki, Lindenberg, and Bilthoven. In the summer months, half of the stations show negative and the other half positive changes that are all insignificant, except from Lauder (−8.9% per decade at the 95% confidence level). The UV irradiance changes at these stations are dominated mainly by the variability in cloudiness and, to a lesser extent, by ozone and aerosols. The variability of clouds and aerosols has masked the detection of increases in surface UV irradiance that were expected to result from the observed decreases in total ozone in the early 1990s that were caused by stratospheric aerosols from the Mt. Pinatubo eruption. At most stations, the use of measurements made only under clear skies results in too little data to allow reliable statistical analysis.

Glandorf et al. (2005) analyzed in more detail 12 years of UV measurements at Thessaloniki, Greece, and 14 years of UV measurements at Sodankylä, Finland, and concluded that no unambiguous upward trend could be constituted at either station, due to the high natural variability of the data. It was suggested that for the given vari-

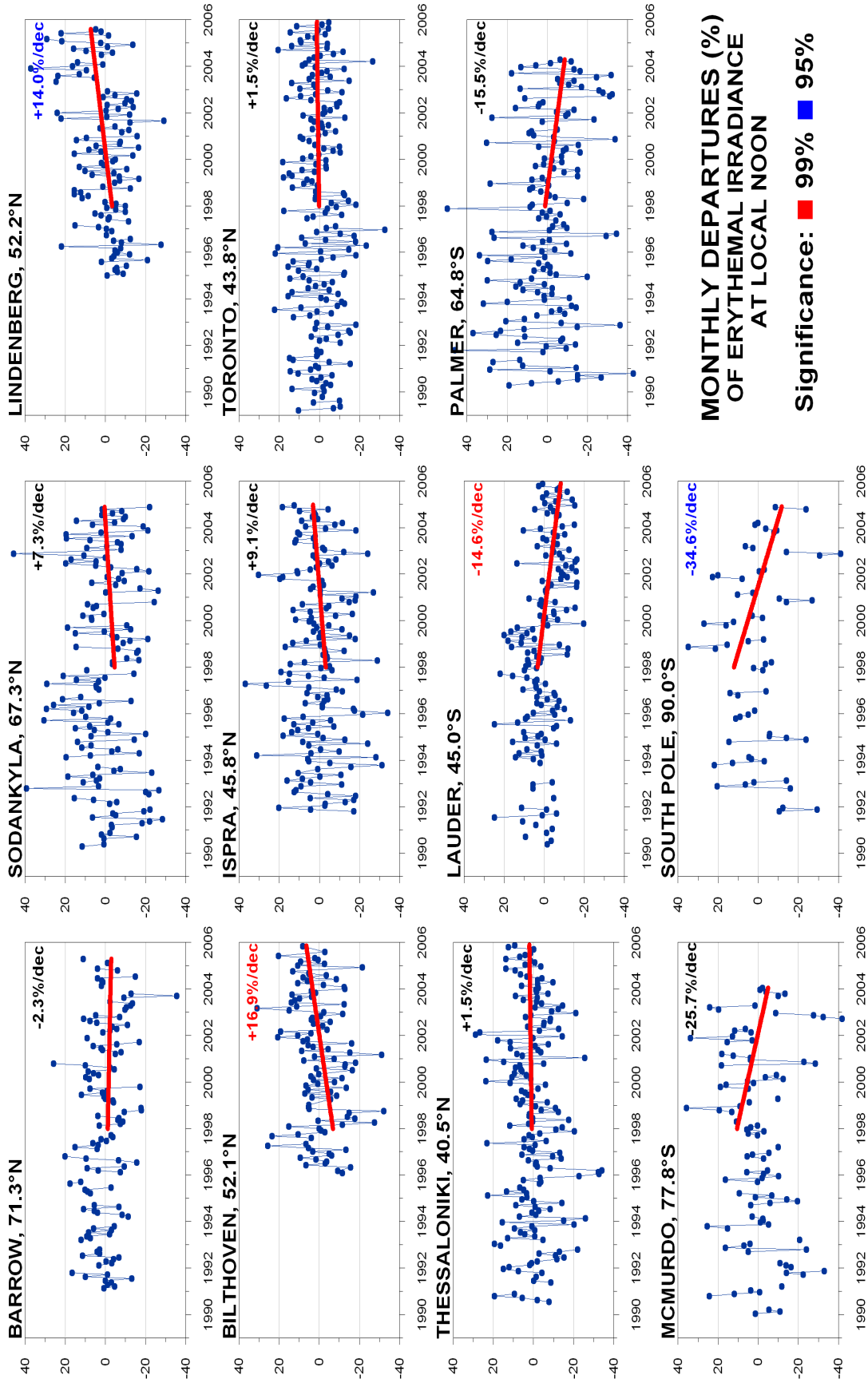


Figure 7-4. Long-term changes in monthly mean erythemal irradiance recorded by UV spectroradiometers within ± 1 hour around local noon at 11 sites distributed worldwide, shown as departures from the long-term averages. Linear regressions on the data (red lines) were used to estimate the corresponding linear changes after 1998, when the first indications of a slowdown in total ozone decreases have been observed. The trends are listed in the upper right of each plot, with color-coding to indicate the statistical significance (red = 99%; blue = negligible). This figure was prepared using updated series of published UV datasets. The statistical significance of the changes was calculated from the data variability only, neglecting the uncertainties in the measurements.

ability in total ozone and clouds at the two sites, more than 15 and 12 years of data, respectively, would have been needed for the detection of persistent statistically significant trends in surface UV radiation, in accordance with previous findings by Weatherhead et al. (1998). However, due to the complexity and the self-regulating mechanisms of our climate system, quasi-periodic changes in UV radiation are more likely to occur than long-lasting linear changes. Using two different periods of the Sodankylä dataset (1993-2001 vs. 1990-1997), Lakkala et al. (2003) calculated substantially different linear changes in spectral UV irradiance at 305 nm, even of opposite sign.

At northern midlatitude sites, surface UV irradiance was found to be increasing since the beginning of 1990s, while elsewhere there are signs of leveling. The updated record of clear-sky spectral UV irradiance at 305 nm and 325 nm and at 63° solar zenith angle over Thessaloniki (Kerr and Seckmeyer et al., 2003) indicates that UV has continuously increased since the beginning of the record (1990) at both wavelengths (Figure 7-5).

Although not very clear, there are indications that after about 2000, surface irradiance has increased with smaller rates or has even been constant, following the stabilization or a slight increase of total ozone over Thessaloniki. The upward trend during the 1990s at wavelengths unaffected by ozone absorption could only be explained by an increase in atmospheric transmission. Aerosol optical depth and SO₂ column over Thessaloniki have decreased since 1997 (Zerefos, 2002; Kazadzis et al., 2005), while a widespread brightening of the atmosphere has been observed since the late 1980s (Wild et al., 2005). Increasing tendencies of surface UV, unexplained by the total ozone decline alone, were reported also for Hohenpeissenberg, Germany (Trepte and Winkler, 2004). Reduced sunshine duration and increased cloudiness lead to a UV decrease that partially compensates for the UV increase caused by ozone loss in spring; in the autumn, these effects overcompensate for the effect of ozone loss.

The increasing peak values of UV irradiances that were reported in the previous Assessment (Kerr and

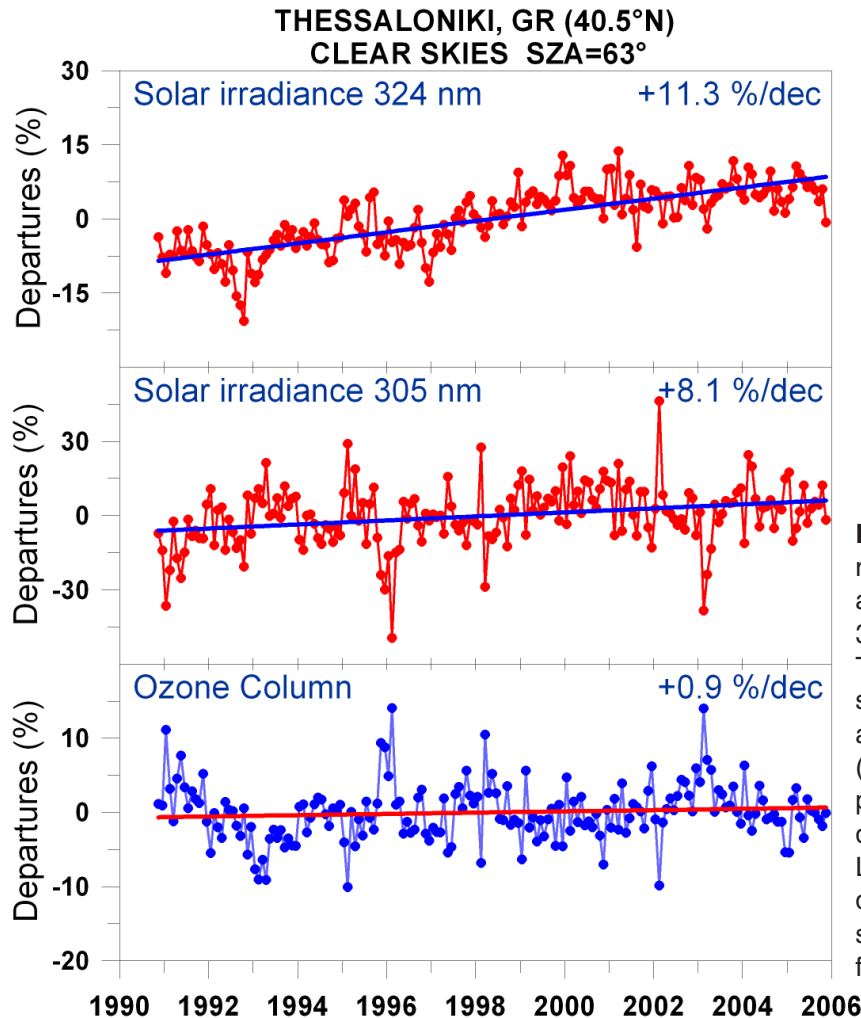


Figure 7-5. Long-term variability in monthly mean solar spectral irradiances at 324 nm (upper panel) and at 305 nm (middle panel) measured at Thessaloniki, Greece, under clear skies at 63° solar zenith angle, shown as departures from the long-term (1990-2006) averages. The lower panel shows the corresponding departures in the ozone column. Linear regressions on the data and the derived trends per decade are also shown for each parameter. Update from Zerefos et al., 2001.

SURFACE ULTRAVIOLET RADIATION

**Mean Summer Ozone and Estimated UV Index
Lauder, New Zealand**

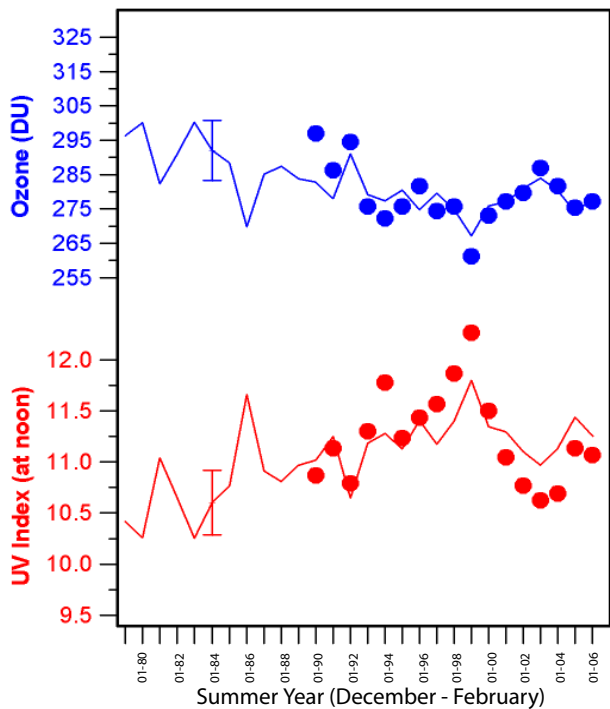


Figure 7-6. Long-term changes in summertime ozone (upper part) and in peak UV Index (lower part) deduced from assimilated ozone data (lines) and from UV spectral measurements at Lauder, New Zealand (symbols). Update from McKenzie et al., 2004.

Seckmeyer et al., 2003) in response to decreasing total ozone at New Zealand show a clear decreasing tendency in the recent four years (Figure 7-6). The magnitude of this decrease is larger than that expected by the increase in total ozone over the area, indicating that aerosol extinction may have also increased during this period. Aerosol data from GOME show increasing aerosol absorption between 45°S and 60°S over the period 1995 to 2000 (de Graaf et al., 2005).

Measurements of surface UV irradiance with broadband radiometers are available for longer periods compared with spectral measurements, although they usually have higher uncertainty (Seckmeyer et al., 2005). Ten years (1990-2000) of solar UV-B irradiance (290 to 320 nm) measurements at Hiratsuka, Japan (35.35°N, 139.27°E), show an increase at a rate of 15.7% per decade (Sasaki et al., 2002). After removing the effect of the Quasi-Biennial Oscillation (QBO) with a 26-month moving average filter, and removing the effect of cloudiness by normalizing with shortwave irradiance measurements, the rate of increase was reduced to 12.2% per

decade, corresponding to the observed total ozone changes at the same location. Statistically significant changes of monthly averages are found only for winter (16.7% per decade). Long-term (1968-2003) UV irradiance (300-380 nm) measurements at the Meteorological Observatory of Moscow State University (Figure 7-7) show a distinct interannual variability, with low levels in the 1970s and 1980s and an overall increase from late 1970s toward the late 1990s (Chubarova et al., 2005). This increase is believed to be due to the decrease in cloud amount and aerosol optical depth (since ~1994), with contributions of up to 10% and 2%, respectively. A decline in atmospheric turbidity of 8-10% during the period 1994-2002 as com-

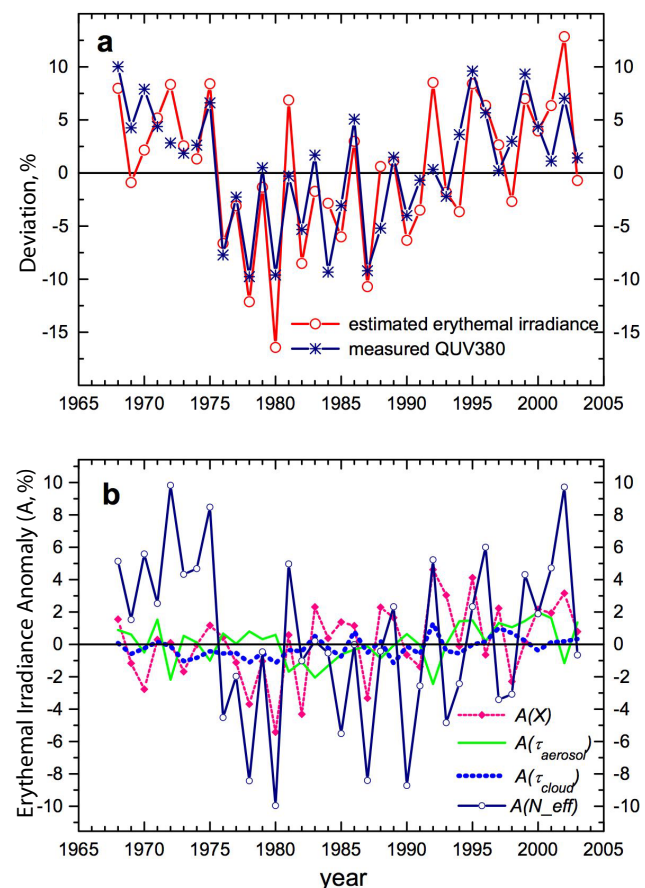


Figure 7-7. (a) Interannual variability of simulated erythemal irradiance and measured irradiance integral from 300 nm to 380 nm (QUV380) for the period May-September in Moscow, Russia, shown as deviations from the 1968-1997 mean. (b) Anomalies in erythemal irradiance (A) due to different atmospheric factors: effective cloud amount $A(N_{eff})$, total ozone $A(X)$, aerosol optical thickness $A(\tau_{aerosol})$, and cloud optical thickness $A(\tau_{cloud})$. Adapted from Chubarova and Nezval, 2000; Chubarova et al., 2005.

pared with the 1976-1995 period is observed at many other sites in Russia (Makhotkina et al., 2005). Increases in erythemal irradiance at Norrköping, Sweden, of ~5% per decade were reported by Josefsson (2006) for the period 1983-2003.

Increases in surface UV irradiances during the last decade are evident from several datasets. These changes are attributable to the increasing of atmospheric transmission because of ozone depletion, global reduction of cloud optical thickness, and reduction of the amount or nature of aerosols. Long-term satellite observations (World Climate Research Programme Global Energy and Water Cycle Experiment (GEWEX) International Satellite Cloud Climatology Project, ISCCP) reveal an overall increase of solar irradiance at the surface from 1983 to 2001 (Figure 7-8) at a rate of about 1% per decade, despite the finding that up to about 1990, solar irradiance measured at the surface was decreasing (Pinker et al., 2005). With respect to clouds, Meerkötter et al. (2004) found no significant long-term trend in cloud amount between 1990 and 2003 from the analysis of NOAA/AVHRR data and from Surface Synoptic Observations (SYNOP), although there are indications of decreasing cloud cover after 2000. Decreases in cloud cover of less than 1%/decade, increases in clear-sky days of ~0.6%/decade, and decreases in overcast days of ~0.8%/decade have been observed over most of China during the last half of the 20th century (Qian et al., 2006). For Barrow, Alaska, a statistically significant upward trend in cloud occurrence frequency, from 76 to 82% between

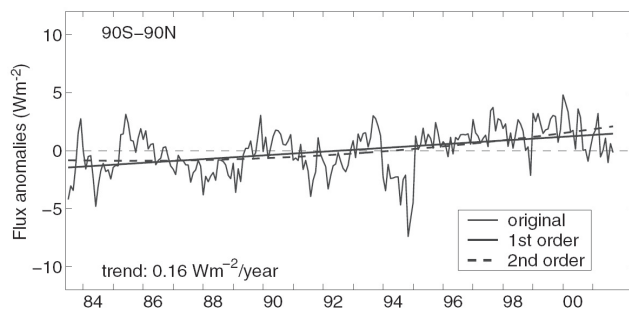


Figure 7-8. Satellite-derived surface solar irradiance (from 1983 to 2001) averaged over the globe, after removal of the mean annual cycle. The linear regression (solid line) on the data reveals a positive trend of ~0.1% per decade. The second-order polynomial (dashed line) indicates a small decrease from 1983 to 1992, with a reversal around 1992. Both fits are significant at the 99% level of confidence. Reprinted with permission from Pinker, R.T., B. Zhang, and E.G. Dutton, Do satellites detect trends in surface solar radiation? *Science*, 308 (5723), 850-854, 2005. Copyright 2005, AAAS.

1976 and 2001, was reported (Dutton et al., 2004). Evidently, only in some areas may an increase in atmospheric transmission be attributed to clouds.

An indication of cleaning of the atmosphere is supported by the long-term aerosol optical depth data at Uccle, Belgium (Cheymol and De Backer, 2003), which were retrieved from Brewer direct-Sun measurements. They reported a statistically significant negative trend of $24.6 \pm 3.7\%$ /decade over the period 1989-2002 for the aerosol optical depth at 306.3 nm; the annual mean was ~0.8 in 1992 and decreased to ~0.6 in 2002. Significant seasonal trends at all wavelengths (in the range 306.3-320.1 nm) were found only in winter months, while in the summer period only at 306.3 nm, a decrease in aerosol optical depth of $12.4 \pm 5.5\%$ /decade is significant at the 2σ level. Similarly, Jaroslowski and Krzyścin (2005) reported that aerosol optical depth in Belsk, Poland, shows a decreasing tendency in the beginning of 1990s followed by an increase in surface UV irradiance (UV Index) of about 4%.

7.4.1.2 SHORT-TERM AND SPATIAL UV VARIABILITY

Apart from the long-term changes, the variability of surface UV irradiance has been extensively studied using datasets measured all over the globe and at different periods. Some datasets are sufficiently long to be used for the establishment of a UV climatology that is representative for the region around the measurements site(s) (Tarasick et al., 2003; den Outer et al., 2005; Liao and Frederick, 2005). Most of the observed variability is caused by the influence of well-known factors, such as ozone, clouds, aerosols, surface albedo, SO_2 , and NO_2 , which were discussed in Section 7.2.

A climatology of surface erythemal irradiance, expressed as UV Index, was developed by Tarasick et al. (2003) using spectral measurements from 14 UV monitoring stations, spanning from 82.5°N to 69.0°S, but mainly distributed in Canada. The most prominent feature at all stations is the high degree of variability that is primarily due to clouds and thus is more pronounced at cloudy sites, such as Halifax and Goose Bay, and much less at Mauna Loa. Smaller, positive or negative, variations are due to ozone variability. Also apparent, at most of the Canadian sites as well as San Diego, is that maximum clear-sky UV Index values in the 1990s were higher than those calculated for the pre-1980 period, by about 10%, in accordance with the total ozone decline of about 6-7% during this period. Dramatically higher UV Index values are seen at Syowa during the Antarctic spring, due to the appearance of the ozone hole, with peak values similar to those in June at San Diego.

SURFACE ULTRAVIOLET RADIATION

Liao and Frederick (2005) presented a climatology of erythemal and DNA-damaging solar irradiance at high latitudes in the Southern Hemisphere, derived from data recorded between 1990 and 2001 by four spectroradiometers located between 55°S and 90°S. Monthly integrals show a distortion of the normal annual cycle in irradiance, with enhancements occurring in October and November due to the springtime ozone loss. In some cases, these irradiances exceed those near summer solstice in December. At Palmer Station, near 65°S, the monthly erythemal irradiance in November 1997 was more than double that observed five years earlier. The combined influence of the ozone column and cloudiness variability results in a large interannual variability of surface erythemal irradiance. Monthly averages vary between about ± 20 and $\pm 50\%$ for the period from October to December.

Geographical differences in surface UV irradiance were investigated using measurements from multifilter radiometers (Diaz et al., 2006) and from erythemal radiometers (Pazmiño et al., 2005) at stations located at different latitudes from tropical to sub-Antarctic regions. Extremely high UV-B irradiances were recorded when part of the polar vortex with low ozone moved over the measurement sites. McKenzie et al. (2006) have found that peak erythemal UV irradiances in New Zealand are $\sim 40\%$ higher than at locations of similar latitude in North America, as a result of the lower aerosol and ozone amounts in New Zealand and the smaller Earth-Sun separation during the Southern Hemisphere summer.

7.4.2 Estimates from Satellite Data

Global UV climatology and trends based on TOMS data for the period 1979-1991 were reported in the WMO (1999) Assessment, and since then no further studies on UV changes have been conducted using the extended dataset, although inferences can be made on the basis of the leveling off in ozone depletion reported by Reinsel et al. (2005). One of the problems for extending the satellite UV data in the recent years is the gap between Nimbus-7 and EP TOMS. Final EP/TOMS calibrations are not available after 2001, which currently prevents updating global TOMS UV climatology and trends. Updated global satellite UV trends will be a subject of future work, most likely combining TOMS, SeaWifs (Herman, 2004), SBUV/2 (Chapter 3, Appendix A1.1), and the new Ozone Monitoring Instrument (OMI) on NASA Aura spacecraft data (Tanskanen et al., 2006).

However, regional UV climatologies have been developed based on RT modeling and various input parameters. Daily maps of surface UV doses over Europe since 1984 were developed by Verdebout (2004a; 2004b) based

on total ozone from TOMS, Total Ozone Vertical Sounder (TOVS) and GOME, and taking into account cloud effects, using METEOSAT/MVIRI images, and effects from tropospheric aerosols, snow cover, and altitude. Fioletov et al. (2004) produced a regional UV climatology by calculating the UV Index over Canada and the United States for the period 1980-1990 using total ozone and reflectivity from TOMS and UV Index derived from ground-based global solar radiation, total ozone, snow, and dew point temperature measurements.

Similar climatologies were derived for Argentina (Luccini et al., 2006), revealing high values of UV irradiances at the northwestern tropical high-altitude Andean plateau. For December-January, the monthly mean UV Index was higher than 18 and the daily erythemal dose was higher than 10 kJ m^{-2} . For most of the continental region, clouds attenuate the clear-sky erythemal irradiance by less than 20% on the average throughout the year.

7.4.3 Reconstruction of Past UV Records

Assessment of UV radiation changes in the past is important because many biological and health-related effects depend on UV dose accumulation during long periods. Because reliable spectral UV measurements are only available since the end of the 1980s, several attempts have been made and various methods have been proposed to reconstruct past UV irradiance records.

Erythemal irradiances or irradiance integrals in other UV spectral ranges are calculated from statistical relationships between actual measurements and various geophysical parameters (e.g., ozone, total solar irradiance, snow cover, etc.) recorded in recent years (e.g., McArthur et al., 1999; Gantner et al., 2000; Fioletov et al., 2001; Diaz et al., 2003; Trepte and Winkler, 2004), or using neural-network techniques (Janouch, 2004). Another hybrid approach uses a radiative transfer model to estimate UV levels under cloud-free conditions, followed by correction for cloud effects based on either total solar irradiance (Kaurola et al., 2000; Bodeker et al., 2002; den Outer et al., 2005), or sunshine duration measurements (Lindfors et al., 2003; Lindfors and Vuilleumier, 2005). Reuder and Koepke (2005) used RT model calculations and algorithms for deriving the required input parameters, total ozone, surface albedo, and clouds from routine observations and aerosol properties from climatological information and the Optical Properties of Aerosols and Clouds (OPAC) database. Chubarova and Nezval (2000) reconstructed UV series by calculating UV anomalies due to different geophysical factors. Coupled Chemistry-Climate Models (CCMs) have also been used for deriving past UV series (Kaurola et al., 2004; Reuder et al., 2005).

In particular, UV trends since 1980 were obtained for the entire globe from the Unified Model with Eulerian Transport and Chemistry (UMETRAC) climate model, including coupled chemistry, and from the FinROSE chemistry-transport model; they demonstrated good agreement with TOMS UV estimates (Kaurola et al., 2004).

Reconstructed UV series allow the assessment of UV trends, as well the estimation of climatic UV irradiances over large areas and long periods. For example, the UV Index climatology over Canada and the United States has been derived from reconstructed UV data combined with TOMS UV estimates (Fioletov et al., 2004). The longest time series to date of UV irradiance reconstructed from total ozone and sunshine duration datasets has been obtained for Switzerland (Lindfors and Vuilleumier, 2005). In the period 1926-2003, distinct interannual changes in erythemal irradiance have been demonstrated, with high values in the middle 1940s, in the early 1960s, and in the 1990s (Figure 7-9). The irradiance changes prior to 1980 are mainly explained by variations in relative sunshine duration, caused mainly by changes in cloudiness, while the increase in the 1990s is due to the negative trend in total ozone. Reconstructed daily UV doses between 1968 and 2001 at Hohenpeissenberg, Germany, show positive changes of 2-5% in the summer months (between March and August) and negative changes of similar magnitude in winter (September to October) (Trepte and Winkler, 2004). The former are due to decreases in cloudiness and in ozone column, whereas the latter are attributable mainly to increases in cloud optical thickness.

Annual integrals of erythemally weighted UV doses were derived for the period 1979-2003 at Bilthoven, The Netherlands, based on model calculations, total ozone, and pyranometer data. These data show increasing UV to the mid-1990s followed by a small decrease, except for a relatively high value in 2003 due to smaller reductions by clouds. Linear regressions over the entire 25-year period revealed increases in UV dose by 3.1% per decade under clear skies and 5.5% per decade under all-sky conditions (den Outer et al., 2005; Lindfors and Vuilleumier, 2005). For the period 1936-2003 in Northern Norway, Engelsen et al. (2004) found trends in monthly reconstructed UV-B doses of 4.5%, 2.8%, and 1.3% per decade, respectively, for March, April, and May. UV-A and PAR doses, which are unaffected by total ozone, reveal smaller trends (1-2% per decade) in March and April, while in May the trend is comparable with that in the UV-B.

The reconstructed UV time series at European observatories in Central and Eastern Europe since the mid-1960s (Krzyściński et al., 2004; Chubarova et al., 2005) demonstrate a pronounced decrease in UV irradiance in

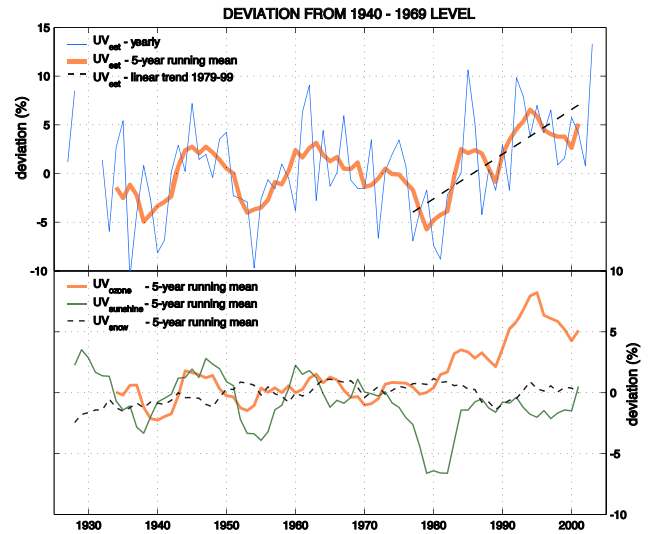


Figure 7-9. Upper panel: Time series of reconstructed erythemal irradiance over Switzerland shown as deviations (changes in %) from the 1940-1969 mean. Lower panel: Percentage contribution of changes in ozone, sunshine duration, and snow depth to the UV variability. Adapted from Lindfors and Vuilleumier, 2005.

the late 1970s and beginning of the 1980s and confirm the increase in the 1990s that is reported from measurement records (see Section 7.4.1). The decreases are mainly explained by negative UV anomalies, up to -10% due to increases in cloud amount, and up to -5% due to total ozone increases (Figure 7-7). It should be noted, however, that sometimes variations of clouds and total ozone are not completely decoupled, both being affected by circulation patterns. In such cases it is difficult to separate their influence on surface UV radiation.

Changes in surface UV radiation during the last century derived from reconstruction methods appear comparable in magnitude to those observed in the 1990s and 2000s. Although short-term UV irradiance variations imposed by different geophysical factors vary between regions, the similarity in the main features of reconstructed erythemal irradiance series confirms the prevalent effect of global processes, such as for example, the changes in atmospheric processes over Europe in the mid-1970s (IPCC, 2001) and the ozone decrease in the midlatitudes of the Northern Hemisphere in the 1990s. Surface UV radiation exhibits high values in the last 30 years, low values in the 1950s and 1960s, and high values again in the 1940s and early 1950s. Most of the past changes have been caused by changes in cloud amount and, to a certain extent, in aerosols; whereas ozone changes have been

SURFACE ULTRAVIOLET RADIATION

responsible for the increases of surface UV only in the 1980s and 1990s.

7.4.4 Polar UV Variability

Studies of polar UV variability have recently benefited from in situ measurement networks becoming more robust (Diaz et al., 2003; Bernhard et al., 2004; Lakkala et al., 2005; Pazmiño et al., 2005; Bernhard et al., 2006) and now provide regionally specific information about the effects of clouds and surface albedo. On the high Antarctic Plateau (Bernhard et al., 2004), most cloud cover is optically thin, and 71% of clouds sampled by the NSF UV Monitor at the South Pole had optical depth less than 1. Due to small optical depth and high surface albedo at the South Pole, the average cloud attenuation of UV radiation was only 5%, and the maximum observed UV cloud attenuation was 23%. This is consistent with radiative transfer studies and measurements by Nichol et al. (2003). Measurements reported by Luccini et al. (2003) for Almirante Brown Station (64.9°S, 62.9°W) show that the average cloud attenuation for erythemal UV was 46% under overcast skies without precipitation, and 73% under clouds with precipitation. Luccini et al. (2003) and Lubin et al. (2002), both studying summertime irradiance levels on the Antarctic Peninsula, show high (short-term) temporal variability for cloud UV attenuation in their measurements.

Liao and Frederick (2005) analyzed the interannual variability in springtime UV-A and UV-B irradiance at all four of the NSF UV monitoring program's high southern latitude sites over 1990-2001, and determined that Palmer Station exhibits the greatest interannual variability in both UV-A and erythemal irradiances due to cloud and albedo effects. They also examined trends in monthly integrated erythemal irradiance, and found upward trends during November and December at McMurdo and South Pole, but no upward trend during October. This result may reflect the springtime ozone decrease already reaching its maximum severity during October over the continent by 1990, but gradually increasing in duration since 1990. Diaz et al. (2003) used the NSF UV monitoring program data to develop an empirical model that allows estimation of historical trends in UV-B if total column ozone and ground-based pyranometer data are available. Their results show increases in UV-B at the South Pole during October since 1983, consistent with the beginning of the anthropogenic springtime ozone depletion.

Lubin et al. (2004) used satellite data to study the multidecadal variability and trends in Antarctic UV-B, in the context of exposure by Southern Ocean phytoplankton. These authors also confirm that elevated UV-B irradiances,

related to ozone depletion, had already occurred prior to the ozone "hole" discovery (before 1985), and that these enhanced irradiances had the potential to impact the most sensitive organisms years before dedicated biological field work began and before such damage could be detected. These authors also show that the most frequent occurrences of enhanced UV-B over waters containing significant phytoplankton biomass occurred in the Weddell Sea and Indian Ocean sectors of Antarctic waters, where there has historically been very little related biological field work. These two factors may help explain why reports of ecological impact due to the springtime ozone decrease have been modest compared with initial speculations.

When the polar vortex breaks up, the dilution of ozone-poor air from within the vortex can contribute to ozone decrease over midlatitudes, leading to enhancement of surface UV. Konopka et al. (2003) studied the fate of vortex remnants and the chemistry occurring within them during the spring of 1997 and 2000, using a Lagrangian chemical transport model, and found different behavior in the lower stratosphere and in the midstratosphere. Above 20 km, remnants from the polar vortex (Orsolini, 2001) remain long-lived in the summer westward circulation. Balloonborne in-situ measurements of water vapor and methane (Durry and Hauchecorne, 2005) provided evidence for such vortex remnants in the midlatitude summer stratosphere. Below 20 km, the subtropical jet bounds the meridional propagation of those remnants (Piani et al., 2002), and their lifetimes are considerably reduced due to enhanced stirring by synoptic eddies. Ajtić et al. (2004) noted that despite the regional differences observed in the springtime impact of Antarctic ozone depletion at midlatitudes, when the Antarctic polar vortex breaks down in late December and January, the resulting ozone reduction at southern midlatitudes is essentially zonally constant and decreases toward lower latitudes.

The expansion of the Antarctic polar vortex during the 1990s, both in spatial extent and temporal extent through early summer, has increased the frequency of elevated UV-B episodes over sub-Antarctic populated areas (Casaccia et al., 2003; Pazmiño et al., 2005). These episodes are no longer just small pockets of ozone-depleted stratospheric air coming from the breakup of the polar vortex, but now include occasional excursions of the polar vortex edge over Ushuaia and Punta Arenas. This occurred 44 times in the years 1997, 1998, and 2000 combined, and some episodes lasted 3-4 days. Surface measurements show average erythemal UV increases of 68% over Ushuaia since 1997, and episodic total UV-B increases of up to 80% over Punta Arenas.

Diaz et al. (2003) show that Barrow, Alaska, has experienced UV-B increases related to springtime ozone

depletion in March and April, but these increases are a factor of ten smaller than those observed at the South Pole. Summertime low-ozone episodes in the Arctic also affect surface UV-B irradiances (Orsolini et al., 2003). These summertime events result from gas-phase chemistry involving nitrogen and hydrogen cycles, which become very efficient during the 24-hour insolation that occurs in the Arctic summer. During summer 2000, two low-ozone episodes brought about erythemal UV increases of order 10-15%, each lasting more than five days.

7.5 EXPECTATIONS FOR THE FUTURE

7.5.1 Links with the Recovery of the Ozone Layer

All other UV modulating geophysical variables being stable, it is expected that decreases in stratospheric ozone will lead to increases in UV radiation at the surface. However, in practice it is difficult to detect such changes because of the high variability in UV radiation that is caused by factors other than ozone. During the period of most-rapid ozone decline (from ~1980 to ~1997), the situation was exacerbated by a lack of high-quality calibrated UV data. In recent years, data quality and quantity have improved. However, there are still only a few sites globally with sufficient long-term data to detect the effects of the observed changes in ozone. Spectroradiometric data from unpolluted NDACC sites located in regions of ozone depletion (e.g., Lauder, New Zealand, and Antarctica) offer the greatest hope for detecting these changes over the natural variability caused by clouds and aerosols. However, to date, no studies have clearly demonstrated any reductions in surface UV irradiance that may be attributable to possible increases in ozone since the late 1990s.

The most convincing studies to demonstrate these long-term changes all used some sort of filtering to minimize cloud effects (Calbó et al., 2005). Other confounding factors include systematic changes in surface albedo and air quality (aerosols and tropospheric ozone). Even with modern state-of-the-art equipment at our disposal, it remains a challenge to measure UV radiation to sufficient accuracy to unequivocally detect future changes in UV radiation that may result from future changes in ozone.

At Lauder, New Zealand, the observed increases in peak summer UV irradiance due to ozone depletion have ceased (McKenzie et al., 1999). Since 1999, the summer ozone levels have leveled off or started to increase, and in the most recent published update, it has been noted that the observed peak UV Index values now appear to be diminishing (McKenzie et al., 2004). Others factors may

also be important, because the UV reductions in recent years are larger than those expected from changes in ozone alone, and there are apparent reductions in UV-A that cannot be attributed to ozone changes. These reductions may therefore be due in part to increases in absorbing aerosols over this region, which have been inferred from satellite data (de Graaf et al., 2005). Satellite-derived ozone measurements show that the leveling off (or even turnaround) in summertime ozone occurs throughout the midlatitude region of the Southern Hemisphere (McKenzie et al., 2004; Reinsel et al., 2005).

7.5.2 Predictions of UV Long-Term Changes

Several attempts have been made to predict future changes of ultraviolet radiation. Such predictions are often based on radiative transfer simulations considering predicted changes of the relevant input parameters. All predictions made to date have concentrated on the effect of ozone changes, which is considered as the most prominent of these parameters, especially for the lowermost UV-B wavelengths and in the polar regions. One of the first estimates of how ultraviolet radiation might evolve in the 21st century was provided by Slaper et al. (1996), who based their calculations on ozone predictions for different scenarios under cloud-free conditions. Later studies included clouds, which were assumed to be constant in time, in the model calculations (Taalas et al., 2000; Reuder et al., 2001). While calculations including clouds are more realistic, any changes of UV radiation were still due to ozone, which is neither the only, nor the main, factor influencing ultraviolet radiation. Clouds, aerosols, and surface albedo are also very important (see Section 7.2). These are subject to change in a future climate, and they have already changed during the last decades. This is manifested by a worldwide decrease in total solar irradiance of ~4% between 1961 and 1990 (Liepert, 2002), which seems to have been followed by an increase in the 1990s (Wild et al., 2005). These changes are attributed to a modification in cloudiness and aerosol, which also affects ultraviolet radiation. A variation of this magnitude is comparable to the effect of ozone and may thus strongly reduce or enhance ozone-related trends. Based on the A2 and B2 IPCC emission scenarios, Giorgi et al. (2004) predicted decreases in the mean cloudiness over the period 2071-2100 in Europe, with respect to the period 1961-1990. For the summer months, these changes range from approximately -2 to -15%. This would result in an increase in the daily UV dose of ~10% instead of a reduction of ~5% due to the recovery of the ozone layer (Reuder et al., 2005). Another indirect effect on long-term trends in cloudiness

SURFACE ULTRAVIOLET RADIATION

involves ocean plankton and dimethyl sulfide (DMS) production, which feeds back to clouds via production of cloud condensation nuclei (CCN). Cloud formation depends on the availability of CCN, which may be produced locally through sea-to-air ventilation of DMS. PAR is important for DMS production, whereas UV photolysis leads to DMS loss (Deal et al., 2005). If long-term changes of clouds and aerosols cause an increase in surface UV irradiance, then any ozone reductions in the future will become more important for UV radiation levels.

Depending on the application, interest might be in either cloudless sky trends (e.g., if human exposure at the beach is investigated) or in all-sky changes (e.g., if exposure of the biosphere is investigated). Both are affected by changes in aerosol content, and the all-sky calculations must also take into account changes in cloudiness. Future scenario calculations should therefore also include the effect of clouds and aerosols. However, available data must be handled with care because predictions of clouds and aerosols are highly uncertain. In particular, IPCC (2001) states that “as has been the case since the first IPCC Assessment Report in 1990, probably the greatest uncertainty in future projections of climate arises from clouds and their interactions with radiation.” In fact, different climate models disagree about the magnitude and even the sign of the changes in cloudiness. As a consequence, the inclusion of clouds in UV predictions would at present add a large uncertainty range to the results. In any case, giving a range for the potential impact of changes in cloudiness on predictions of ultraviolet radiation is better than excluding them completely. If clouds, as predicted by climate models, are included into the analysis, great care must be taken in the UV calculation to treat them consistently with the cloud-radiation parameterization of the respective CCM.

The availability of CCM simulations for ozone column response to Montreal Protocol controls (Chapter 6) allows simulations of the corresponding multidecadal response in surface UV irradiance, assuming that the rest of the atmosphere and surface remain the same. By use of ozone simulations by the Atmospheric Model with Transport and Chemistry (AMTRAC) model (see Chapter 6 for details) as input to a UV radiative transfer algorithm designed for satellite UV mapping (Lubin et al., 1998), it is possible to estimate when biologically active UV irradiances might be expected to peak and to return to levels that existed prior to anthropogenic influences on the ozone layer. AMTRAC is currently the only Chemistry-Climate Model with results up to 2100 (Austin and Wilson, 2006). The ozone losses calculated by this model are larger than observed, especially in the Southern Hemisphere (see the blue dashed curves corresponding to the “AMTRAC”

model in Figures 6-10 and 6-12 of Chapter 6), and hence more emphasis is given on the timing of the projected changes of UV radiation, rather than on their absolute magnitude. Figure 7-10 shows an example of predicted erythemal irradiance at local noon for summertime at 45°N and 45°S, where a large part of the Earth’s population lives, and for October at 65°S. The UV calculations are based on the average ozone column, respectively, at the latitude bands 35°N-60°N, 35°S-60°S, and 60°S-90°S. Erythemal irradiance increases from a reference value (calculated as the average of the period 1970-1980) for twenty years beginning in 1980, and this increase reaches a maximum during ~2005. The predicted increases in erythemal irradiance are twice as large in the Southern Hemisphere, compared with the Northern Hemisphere. The return of the calculated irradiance to the pre-1980 levels is expected by about 2040 at the Northern Hemisphere and by about 2070 at the Southern Hemisphere, while at the southern high latitudes this return is expected to occur later. These simulations are focused on the effect of future ozone changes on surface UV radiation, thus it was assumed that all other UV-influencing parameters (Section 7.2) remain unchanged since 1980. In reality many other atmospheric variables (e.g., cloudiness, surface albedo, aerosols, and temperature) are expected to change during the period of study, as a result of climate change. Changes in the vertical profiles of ozone and temperature are also expected to influence the solar UV irradiance received at the surface. Therefore the changes shown in Figure 7-10 could be different in magnitude and shape when predictions of the other parameters become available and are included in the UV calculations.

7.5.3 Factors Related to Climate Change

If the ozone layer in the next ~50 years returns to its normal state, as predicted by models (in Chapter 6, see Figure 6-10 and Section 6.6), then climate change will likely dominate the surface UV variability in the future. While most of the discussion of climate forcing generally involves visible and infrared wavelengths, where most of the Sun’s energy lies, there are a number of linkages between ultraviolet radiation and climate change. Included among the elements that force the Earth’s climate on different time scales is the total solar irradiance incident at the top of the atmosphere, which varies by 0.08% or 1.1 W m⁻² in annual mean over the 11-year solar cycle (Section 6.11.2.1 in IPCC, 2001). The amplitude of variability in UV-C radiation is even higher, while in the UV-B and UV-A, only isolated spectral lines are modulated by the solar activity (see also Section 7.2.1). Such variations in UV irradiance cause a number of climate-

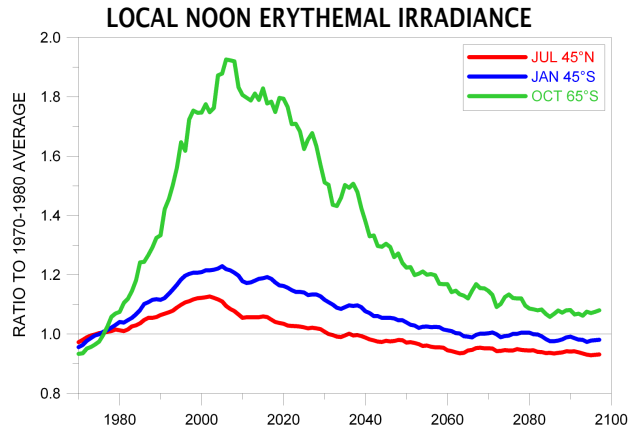


Figure 7-10. Estimated changes in erythemally weighted surface UV irradiance at local noon in response to projected changes in total column ozone for the period 1970-2099, using zonal-averages in total ozone in the latitude bands 35°N-60°N, 35°S-60°S, and 60°S-90°S, and the solar zenith angle corresponding to 45°N in July, 45°S in January, and 65°S in October, respectively. At each latitude, the irradiance is expressed as the ratio to the 1970-1980 average. The results have been smoothed with a 5-year running mean filter to remove some of the year-to-year variability in the ozone predictions in the model. The ozone losses calculated by this model are larger than observed, especially in the Southern Hemisphere (in Chapter 6, see the blue dashed curves corresponding to the “AMTRAC” model in Figures 6-10 and 6-12). Therefore, the corresponding increases in the calculated UV irradiance are overestimated. Surface UV irradiance is predicted to peak between about 2000 and 2010 and is expected to return to the pre-1980 levels between 2040 and 2070 at midlatitudes, but later at the southern high latitudes.

related changes: a change in downward shortwave flux at the tropopause; a change in stratospheric heating (Larkin et al. (2000) estimated the additional UV heating to be a factor of 8-10) leading to a change in downward infrared flux; or a change in ozone concentration (e.g., Tourpali et al., 2003; Egorova et al., 2004; Langematz et al., 2005) affecting also the balance of absorption of solar UV radiation in the troposphere. A change in the stratospheric heating may also affect stratospheric zonal wind structure and in turn affect vertically propagating planetary waves in the winter hemisphere. Such anomalies in zonal wind structure can propagate down into the troposphere in the same fashion as anomalies arising from heating in the lower stratosphere due to volcanic aerosol (e.g., Stenchikov et al., 2004). All of this may lead, for example,

to shifts in the positions of the sub-tropical jets in the troposphere. A change in ozone concentration feeds back on the downward shortwave flux at the tropopause and may thus force further changes in tropospheric dynamics (e.g., Shindell et al., 2001; Haigh, 2003; Labitzke and Matthes, 2003; Shindell et al., 2003) or may affect the lifetime of reactive greenhouse gases (IPCC/TEAP, 2005).

Soon et al. (2000) suggested that the climate may be particularly sensitive to changes in UV irradiance. They found a stronger climate response to an imposed UV radiative forcing, preferentially absorbed in the layer above 250 hPa, than to the radiative forcing induced by increases in CO₂ or total solar irradiance. The strong climate response to UV forcing is a coupled feedback involving vertical static stability, tropical thick cirrus ice clouds, and stratospheric ozone.

As discussed in Sections 7.2.3, 7.2.4, 7.2.5, and 7.4.4, forcing occurs in the other direction as well. Variations in atmospheric aerosols, air pollutants in urban areas (e.g., NO₂ and SO₂), and cloud content over long time scales, as well as variations in ozone concentration as a result of chemical processes, lead to significant variations in UV irradiance at the surface (see also Meloni et al. (2003c; 2004) and Hatzianastassiou et al. (2004a; 2004b) for radiative forcing by aerosols at UV wavelengths). Extreme UV irradiances that are expected in tropical high altitude regions are often mitigated by overcast skies in summertime during the rainy season. Changes of climate patterns in those regions linked to a decrease in cloud density, as it happens sometimes during El Niño-Southern Oscillation (ENSO) events, may become important for future surface UV radiation levels.

An indirect effect on the climate that works in this direction involves ocean plankton. Increased UV penetration to the troposphere also leads to increases in the concentration of tropospheric hydroxyl radicals (OH) and hence to decreases in the lifetime of CH₄, which influences ozone (IPCC, 2001). Such changes may play a role in future CO₂ and CH₄ trends and consequently in global warming due to greenhouse gases (e.g., Coale et al., 2004). Moreover, changes in UV radiation are inducing changes in biogenic emissions, some of which are important drivers of climate change. The overall scheme of such interactions is complicated, and our understanding of the effects on UV is still poor (EC, 2003). Although several mechanisms that couple UV radiation variations with climate variations can be identified, it is hard to determine the importance and magnitude of these couplings. Progress in simulating past and future UV radiation levels may be achieved through the combined use of CCMs, RT models, and measurements.

SURFACE ULTRAVIOLET RADIATION

7.6 REMAINING QUESTIONS AND UNCERTAINTIES

Despite the progress in the last four years, there are still open issues related to the transfer of UV radiation through the atmosphere and to interaction of UV radiation with climate change. These include:

- using assumptions in modeling aerosol effects on surface UV radiation (e.g., asymmetry parameter or phase function of aerosols);
- quantifying the effects of inhomogeneous clouds and inhomogeneous topography on UV irradiance and actinic flux at the surface;
- investigating the role of UV from the perspective of introducing changes in tropospheric photochemistry and, thus, indirectly affecting the stratospheric composition;
- advancing the state of knowledge concerning interactions of climate change and UV radiation in time and space, for example through changes in surface albedo (deforestation, decrease of snow-ice cover, etc) and cloudiness, which have not been extensively studied so far;
- developing a better understanding of the UV light penetration into the water, which may be underlying partially snow-covered ice, and is important for marine ecosystems;
- defining better the interaction of radiation and the surface, in particular the reflection of radiation by vegetation and the penetration into canopies; and
- better understanding and quantifying the effects of pollutant gases and aerosols on surface UV radiation.

With respect to tools and technological issues, research on UV radiation is expected to progress through further development in:

- three-dimensional radiative transfer modeling, which is becoming available but is not yet in widespread use and requires substantial computing resources and input parameters that are usually not available;
- more accurate UV radiation measurements that can help to validate radiative transfer models and satellite-derived UV estimates, while establishment of new stations, especially in the tropics, would provide better coverage;
- radiative transfer studies for large solar zenith angles and viewing angles, which are required for calculations for high latitudes and for the interpretation of remote sensing observations;

- retrieval of trace gas amounts and the optical properties of aerosols using combinations of measurements and modeling;
- correct consideration of polarization, which is important for the interpretation of radiance measurements; and
- quality control procedures of broadband and multi-channel narrowband radiometers deployed worldwide, which are not as good as required for addressing long-term changes and for studying radiative processes in detail.

REFERENCES

- Aas, E., J. Høkedal, N.K. Højerslev, R. Sandvik, and E. Sakshaug, Spectral properties and UV attenuation in Arctic marine waters, Chapter 2 in *UV Radiation and Arctic Ecosystems*, edited by D.O. Hessen, 23-56, Springer-Verlag, Heidelberg, Germany, 2002.
- Ahmad, Z., P.K. Bhartia, and N. Krotkov, Spectral properties of backscattered UV radiation in cloudy atmospheres, *J. Geophys. Res.*, *109*, D01201, doi: 10.1029/2003JD003395, 2004.
- Ajtić, J., B.J. Connor, B.N. Lawrence, G.E. Bodeker, K.W. Höppl, J.E. Rosenfield, and D.N. Heuff, Dilution of the Antarctic ozone hole into southern midlatitudes, 1998-2000, *J. Geophys. Res.*, *109*, D17107, doi: 10.1029/2003JD004500, 2004.
- Allen, M., and R. McKenzie, Enhanced UV exposure on a ski-field compared with exposures at sea level, *Photochem. Photobiol. Sci.*, *4* (5), 429-437, 2005.
- Arola, A., and T. Koskela, On the sources of bias in aerosol optical depth retrieval in the UV range, *J. Geophys. Res.*, *109*, D08209, doi: 10.1029/2003JD004375, 2004.
- Arola, A., J. Kaurola, L. Koskinen, A. Tanskanen, T. Tikkanen, P. Taalas, J.R. Herman, N. Krotkov, and V. Fioletov, A new approach to estimating the albedo for snow-covered surfaces in the satellite UV method, *J. Geophys. Res.*, *108* (D17), 4531, doi: 10.1029/2003JD003492, 2003a.
- Arola, A., K. Lakkala, A. Bais, J. Kaurola, C. Meleti, and P. Taalas, Factors affecting short- and long-term changes of spectral UV irradiance at two European stations, *J. Geophys. Res.*, *108* (D17), 4549, doi: 10.1029/2003JD003447, 2003b.
- Arola, A., S. Kazadzis, N. Krotkov, A. Bais, J. Gröbner, and J.R. Herman, Assessment of TOMS UV bias due to absorbing aerosols, *J. Geophys. Res.*, *110*, D23211, doi: 10.1029/2005JD005913, 2005.
- Atkinson, R., D.L. Baulch, R.A. Cox, R.F. Hampson Jr.,

- J.A. Kerr, M.J. Rossi, and J. Troe, Evaluated kinetic, photochemical and heterogeneous data for atmospheric chemistry: Supplement V. IUPAC Subcommittee on Gas Kinetic Data Evaluation for Atmospheric Chemistry, *J. Phys. Chem. Ref. Data*, 26 (3), 521-1011, 1997.
- Austin, J., and R.J. Wilson, Ensemble simulations of the decline and recovery of stratospheric ozone, *J. Geophys. Res.*, 111, D16314, doi: 10.1029/2005JD006907, 2006.
- Austin, J., B.R. Barwell, S.J. Cox, P.A. Hughes, J.R. Knight, G. Ross, P. Sinclair, and A.R. Webb, The diagnosis and forecast of clear sky ultraviolet levels at the Earth's surface, *Meteorol. Appl.*, 1 (4), 321-336, 1994.
- Bais, A.F., K. Tourpali, D. Balis, C. Meleti, and C.S. Zerefos, UV-B forecasting in Greece, in *Report of the WMO-WHO Meeting of Experts on Standardization of UV Indices and their Dissemination to the Public (Les Diablerets, Switzerland, 21-25 July 1997)*, *Global Atmosphere Watch, Report No. 127*, WMO/TD No. 921, 111-114, World Meteorological Organization, Geneva, Switzerland, 1998.
- Bais, A.F., B.G. Gardiner, H. Slaper, M. Blumthaler, G. Bernhard, R. McKenzie, A.R. Webb, G. Seckmeyer, B. Kjeldstad, T. Koskela, P.J. Kirsch, J. Gröbner, J.B. Kerr, S. Kazadzis, K. Leszczynski, D. Wardle, W. Josefsson, C. Brogniez, D. Gillotay, H. Reinen, P. Weihs, T. Svenøe, P. Eriksen, F. Kuik, and A. Redondas, SUSPEN intercomparison of ultraviolet spectroradiometers, *J. Geophys. Res.*, 106 (D12), 12509-12525, 2001.
- Bais, A.F., S. Madronich, J. Crawford, S.R. Hall, B. Mayer, M. van Weele, J. Lenoble, J.G. Calvert, C.A. Cantrell, R.E. Shetter, A. Hofzumahaus, P. Koepke, P.S. Monks, G. Frost, R. McKenzie, N. Krotkov, A. Kylling, W.H. Swartz, S. Lloyd, G. Pfister, T.J. Martin, E.-P. Roeth, E. Griffioen, A. Ruggaber, M. Krol, A. Kraus, G.D. Edwards, M. Mueller, B.L. Lefer, P. Johnston, H. Schwander, D. Flittner, B.G. Gardiner, J. Barrick, and R. Schmitt, International Photolysis Frequency Measurement and Model Intercomparison (IPMMI): Spectral actinic solar flux measurements and modeling, *J. Geophys. Res.*, 108 (D16), 8543, doi: 10.1029/2002JD002891, 2003.
- Bais, A.F., S. Kazadzis, K. Garane, N. Kouremeti, J. Gröbner, M. Blumthaler, G. Seckmeyer, A.R. Webb, T. Koskela, P. Görts, and J. Schreder, Portable device for characterizing the angular response of UV spectroradiometers, *Appl. Opt.*, 44 (33), 7136-7143, 2005a.
- Bais, A.F., A. Kazantzidis, S. Kazadzis, D.S. Balis, C.S. Zerefos, and C. Meleti, Deriving an effective aerosol single scattering albedo from spectral surface UV irradiance measurements, *Atmos. Environ.*, 39 (6), 1093-1102, 2005b.
- Balis, D.S., V. Amiridis, C. Zerefos, A. Kazantzidis, S. Kazadzis, A.F. Bais, C. Meleti, E. Gerasopoulos, A. Papayannis, V. Matthias, H. Dier, and M.O. Andreae, Study of the effect of different type of aerosols on UV-B radiation from measurements during EARLINET, *Atmos. Chem. Phys.*, 4, 307-321, 2004.
- Barnard, W.F., V.K. Saxena, B.N. Wenny, and J.J. DeLuisi, Daily surface UV exposure and its relationship to surface pollutant measurements, *J. Air Waste Manag. Assoc.*, 53 (2), 237-245, 2003.
- Barron, M.G., and K.J. Barron, Glacial influences on solar radiation in a subarctic sea, *Photochem. Photobiol.*, 81 (1), 187-189, 2005.
- Bernhard, G., and G. Seckmeyer, Uncertainty of measurements of spectral solar UV irradiance, *J. Geophys. Res.*, 104 (D12), 14321-14345, 1999.
- Bernhard, G., C.R. Booth, and J.C. Eshamjian, Version 2 data of the National Science Foundation's Ultraviolet Radiation Monitoring Network: South Pole, *J. Geophys. Res.*, 109, D21207, doi: 10.1029/2004JD004937, 2004.
- Bernhard, G., C.R. Booth, and J.C. Eshamjian, Real-time ultraviolet and column ozone from multichannel ultraviolet radiometers deployed in the National Science Foundation's ultraviolet monitoring network, *Opt. Eng.*, 44 (4), 041011, doi: 10.1117/1.1887195, 2005.
- Bernhard, G., C.R. Booth, J.C. Eshamjian, and S.E. Nichol, UV climatology at McMurdo Station, Antarctica, based on version 2 data of the National Science Foundation's Ultraviolet Radiation Monitoring Network, *J. Geophys. Res.*, 111, D11201, doi: 10.1029/2005JD005857, 2006.
- Blumthaler, M., Quality assurance and quality control methodologies used within the Austrian UV monitoring network, *Radiat. Prot. Dosim.*, 111 (4), 359-362, 2004.
- Blunden, A., T. Lower, and T. Slevin, Knowledge, awareness, and use of the UV index amongst the West Australian public, *J. Health Commun.*, 9 (3), 207-221, 2004.
- Bodeker, G., J. Burrows, R. Scott-Weekley, S.E. Nichol, and R.L. McKenzie, A UV Atlas for New Zealand, in *Workshop on UV Radiation and its Effects: An Update (2002)*, 26-28 March 2002, Christchurch,

SURFACE ULTRAVIOLET RADIATION

- New Zealand, 2002.
- Bracchini, L., A. Cózar, A.M. Dattilo, M.P. Picchi, C. Arena, S. Mazzuoli, and S.A. Loisselle, Modelling the components of the vertical attenuation of ultraviolet radiation in a wetland lake ecosystem, *Ecol. Model.*, 186 (1), 43-54, 2005.
- Brasseur, A.L., R. Ramarosan, A. Delannoy, W. Skamarock, and M. Barth, Three-dimensional calculation of photolysis frequencies in the presence of clouds and impact on photochemistry, *J. Atmos. Chem.*, 41 (3), 211-237, 2002.
- Burrows, J.P., M. Weber, M. Buchwitz, V. Rozanov, A. Ladstätter-Weißmayer, A. Richter, R. DeBeek, R. Hoogen, K. Bramstedt, K.-U. Eichmann, M. Eisinger, and D. Perner, The Global Ozone Monitoring Experiment (GOME): Mission concept and first scientific results, *J. Atmos. Sci.*, 56 (2), 151-175, 1999.
- Burrows, W.R., CART regression models for predicting UV radiation at the ground in the presence of cloud and other environmental factors, *J. Appl. Meteorol.*, 36 (5), 531-544, 1997.
- Burrows, W.R., M. Vallée, D.I. Wardle, J.B. Kerr, L.J. Wilson, and D.W. Tarasick, The Canadian operational procedure for forecasting total ozone and UV radiation, *Meteorol. Appl.*, 1 (3), 247-265, 1994.
- Cahalan, R.F., W. Ridgway, W.J. Wiscombe, T.L. Bell, and J.B. Snider, The albedo of fractal stratocumulus clouds, *J. Atmos. Sci.*, 51 (16), 2434-2455, 1994.
- Cahalan, R.F., L. Oreopoulos, A. Marshak, K.F. Evans, A.B. Davis, R. Pincus, K.H. Yetzer, B. Mayer, R. Davies, T.P. Ackerman, H.W. Barker, E.E. Clothiaux, R.G. Ellingson, M.J. Garay, E. Kassianov, S. Kinne, A. Macke, W. O'Hirok, P.T. Partain, S.M. Prigarin, A.N. Rublev, G.L. Stephens, F. Szczap, E.E. Takara, T. Várnai, G. Wen, and T.B. Zhuravleva, THE I3RC: Bringing together the most advanced radiative transfer tools for cloudy atmospheres, *Bull. Amer. Meteorol. Soc.*, 86 (9), 1275-1293, 2005.
- Calbó, J., D. Pagès, and J. González, Empirical studies of cloud effects on UV radiation: A review, *Rev. Geophys.*, 43, RG2002, doi: 10.1029/2004RG000155, 2005.
- Casaccia, C., V.W.J.H. Kirchhoff, and A. Torres, Simultaneous measurements of ozone and ultraviolet radiation: Spring 2000, Punta Arenas, Chile, *Atmos. Environ.*, 37 (3), 383-389, 2003.
- Cede, A., and J. Herman, Measurements of O₃, SO₂, NO₂ and HCHO column amounts using a Brewer spectrometer, *Proc. SPIE*, 5886, 588602, doi: 10.1117/12.620167, 2005.
- Cede, A., M. Blumthaler, E. Luccini, R.D. Piacentini, and L. Nuñez, Effects of clouds on erythral and total irradiance as derived from data of the Argentine Network, *Geophys. Res. Lett.*, 29 (24), 2223, doi: 10.1029/2002GL015708, 2002.
- Cede, A., E. Luccini, L. Nuñez, R.D. Piacentini, M. Blumthaler, and J.R. Herman, TOMS-derived erythral irradiance versus measurements at the stations of the Argentine UV Monitoring Network, *J. Geophys. Res.*, 109, D08109, doi: 10.1029/2004JD004519, 2004.
- Cede, A., J. Herman, A. Richter, N. Krotkov, and J. Burrows, Measurements of nitrogen dioxide total column amounts using a Brewer double spectrophotometer in direct Sun mode, *J. Geophys. Res.*, 111, D05304, doi: 10.1029/2005JD006585, 2006a.
- Cede, A., S. Kazadzis, M. Kowalewski, A. Bais, N. Kouremeti, M. Blumthaler, and J. Herman, Correction of direct irradiance measurements of Brewer spectrophotometers due to the effect of internal polarization, *Geophys. Res. Lett.*, 33, L02806, doi: 10.1029/2005GL024860, 2006b.
- Cheymol, A., and H. De Backer, Retrieval of the aerosol optical depth in the UV-B at Uccle from Brewer ozone measurements over a long time period 1984-2002, *J. Geophys. Res.*, 108 (D24), 4800, doi: 10.1029/2003JD003758, 2003.
- Chubarova, N.E., Monitoring of biologically active UV radiation in the Moscow region, *Izv. Atmos. Ocean. Phys.*, 38 (3), 312-322, 2002.
- Chubarova, N.E., Influence of aerosol and atmospheric gases on ultraviolet radiation in different optical conditions including smoky mist of 2002, *Dokl. Earth Sci.*, 394 (1), 62-67, 2004.
- Chubarova, N.E., Role of tropospheric gases in the absorption of UV radiation, *Dokl. Earth Sci.*, 407 (2), 294-297, 2006.
- Chubarova, N.Y., and Y.I. Nezval, Thirty year variability of UV irradiance in Moscow, *J. Geophys. Res.*, 105 (D10), 12529-12539, 2000.
- Chubarova, N.Y., A.Y. Yurova, N. Krotkov, J. Herman, and P.K. Bhartia, Comparisons between ground measurements of broadband ultraviolet irradiance (300 to 380 nm) and total ozone mapping spectrometer ultraviolet estimates at Moscow from 1979 to 2000, *Opt. Eng.*, 41 (12), 3070-3081, 2002.
- Chubarova, N.Y., Y.I. Nezval, J. Verdebout, N. Krotkov, and J. Herman, Long-term UV irradiance changes over Moscow and comparisons with UV estimates from TOMS and METEOSAT, *Proc. SPIE*, 5886, 58860A, doi: 10.1117/12.620303, 2005.
- Ciren, P., and Z. Li, Long-term global earth surface ultra-

- violet radiation exposure derived from ISCCP and TOMS satellite measurements, *Agric. For. Meteorol.*, 120 (1), 51-68, 2003.
- Coale, K.H., K.S. Johnson, F.P. Chavez, K.O. Buesseler, R.T. Barber, M.A. Brzezinski, W.P. Cochlan, F.J. Millero, P.G. Falkowski, J.E. Bauer, R.H. Wanninkhof, R.M. Kudela, M.A. Altabet, B.E. Hales, T. Takahashi, M.R. Landry, R.R. Bidigare, X. Wang, Z. Chase, P.G. Stratton, G.E. Friederich, M.Y. Gorbunov, V.P. Lance, A.K. Hilting, M.R. Hiscock, M. Demarest, W.T. Hiscock, K.F. Sullivan, S.J. Tanner, R.M. Gordon, C.N. Hunter, V.A. Elrod, S.E. Fitzwater, J.L. Jones, S. Tozzi, M. Koblizek, A.E. Roberts, J. Herndon, J. Brewster, N. Ladizinsky, G. Smith, D. Cooper, D. Timothy, S.L. Brown, K.E. Selph, C.C. Sheridan, B.S. Twining, and Z.I. Johnson, Southern Ocean iron enrichment experiment: Carbon cycling in high- and low-Si waters, *Science*, 304 (5669), 408-414, 2004.
- Cockell, C.S., and C. Córdoba-Jabonero, Coupling of climate change and biotic UV exposure through changing snow-ice covers in terrestrial habitats, *Photochem. Photobiol.*, 79 (1), 26-31, 2004.
- Cooper, O.R., A. Stohl, S. Eckhardt, D.D. Parrish, S.J. Oltmans, B.J. Johnson, P. Nédélec, F.J. Schmidlin, M.J. Newchurch, Y. Kondo, and K. Kita, A spring-time comparison of tropospheric ozone and transport pathways on the east and west coasts of the United States, *J. Geophys. Res.*, 110, D05S90, doi: 10.1029/2004JD005183, 2005.
- Crawford, J., R.E. Shetter, B. Lefer, C. Cantrell, W. Junkermann, S. Madronich, and J. Calvert, Cloud impacts on UV spectral actinic flux observed during the International Photolysis Frequency Measurement and Model Intercomparison (IPMMI), *J. Geophys. Res.*, 108 (D16), 8545, doi: 10.1029/2002JD002731, 2003.
- Dahlback, A., H.A. Eide, B.A.K. Høiskar, R.O. Olsen, F.J. Schmidlin, S.-C. Tsay, and K.H. Stamnes, Comparison of data for ozone amounts and ultraviolet doses obtained from simultaneous measurements with various standard ultraviolet instruments, *Opt. Eng.*, 44 (4), 041010, doi: 10.1117/1.1885473, 2005.
- Davis, J.M., and J.R. Slusser, New USDA UVB synthetic spectra algorithm, *Proc. SPIE*, 5886, 58860B, doi: 10.1117/12.620269, 2005.
- De Backer, H., P. Koepke, A. Bais, X. de Cabo, T. Frei, D. Gillotay, C. Haite, A. Heikkilä, A. Kazantzidis, T. Koskela, E. Kyrö, B. Lapeta, J. Lorente, K. Masson, B. Mayer, H. Plets, A. Redondas, A. Renaud, G. Schauburger, A. Schmalwieser, H. Schwander, and K. Vanicek, Comparison of measured and modelled UV indices for the assessment of health risks, *Meteorol. Appl.*, 8 (3), 267-277, 2001.
- de Graaf, M., P. Stammes, O. Torres, and R.B.A. Koelemeijer, Absorbing aerosol index: Sensitivity analysis, application to GOME and comparison with TOMS, *J. Geophys. Res.*, 110, D01201, doi: 10.1029/2004JD005178, 2005.
- Deal, C.J., D.J. Kieber, D.A. Toole, K. Stamnes, S. Jiang, and N. Uzuka, Dimethylsulfide photolysis rates and apparent quantum yields in Bering Sea seawater, *Continental Shelf Res.*, 25 (15), 1825-1835, 2005.
- DeLand, M.T., R.P. Cebula, and E. Hilsenrath, Observations of solar spectral irradiance change during cycle 22 from NOAA-9 Solar Backscattered Ultraviolet Model 2 (SBUV/2), *J. Geophys. Res.*, 109, D06304, doi: 10.1029/2003JD004074, 2004a.
- DeLand, M.T., L.E. Floyd, G.J. Rottman, and J.M. Pap, Status of UARS solar UV irradiance data, *Adv. Space Res.*, 34 (2), 243-250, 2004b.
- den Outer, P.N., H. Slaper, and R.B. Tax, UV radiation in the Netherlands: Assessing long-term variability and trends in relation to ozone and clouds, *J. Geophys. Res.*, 110, D02203, doi: 10.1029/2004JD004824, 2005.
- di Sarra, A., M. Cacciani, P. Chamard, C. Cornwall, J.J. DeLuisi, T. Di Iorio, P. Disterhoft, G. Fiocco, D. Fuá, and F. Monteleone, Effects of desert dust and ozone on the ultraviolet irradiance at the Mediterranean island of Lampedusa during PAUR II, *J. Geophys. Res.*, 107 (D18), 8135, doi: 10.1029/2000JD000139, 2002.
- Diaz, S., D. Nelson, G. Deferrari, and C. Camiliã, Estimated and measured DNA, plant-chromosphere and erythemal-weighted irradiances at Barrow and South Pole (1979-2000), *Agric. For. Meteorol.*, 120 (1), 69-82, 2003.
- Diaz, S., C.R. Booth, R. Armstrong, C. Brunat, S. Cabrera, C. Camiliã, C. Casiccia, G. Deferrari, H. Fuenzalida, C. Lovengreen, A. Paladini, J. Pedroni, A. Rosales, H. Zagarese, and M. Vernet, Multichannel radiometer calibration: a new approach, *Appl. Opt.*, 44 (26), 5374-5380, 2005.
- Diaz, S., C. Camiliã, G. Deferrari, H. Fuenzalida, R. Armstrong, C. Booth, A. Paladini, S. Cabrera, C. Casiccia, C. Lovengreen, J. Pedroni, A. Rosales, H. Zagarese, and M. Vernet, Ozone and UV radiation over southern South America: Climatology and anomalies, *Photochem. Photobiol.*, 82 (4), 834-843, doi: 10.1562/2005-09-26-RA-697, 2006.
- Dixon, H., and B. Armstrong, *The UV Index*, Report of a National Workshop on its Role in Sun Protection,

SURFACE ULTRAVIOLET RADIATION

- Sydney: NSW Cancer Council and Anti-Cancer Council of Victoria, Australia, 1999.
- Dixon, H., L. Lemus-Deschamps, and P. Gies, Meteorology meets public health: UV forecasts and reports for sun safety, *Health Prom. J. Austral.*, 13 (3), 252, 2002.
- Donahue, W.F., M.A. Turner, D.L. Findlay, and P.R. Leavitt, The role of solar radiation in structuring the shallow benthic communities of boreal forest lakes, *Limnol. Oceanogr.*, 48 (1), 31-47, 2003.
- Dubovik, O., B.N. Holben, T.F. Eck, A. Smirnov, Y.J. Kaufman, M.D. King, D. Tanré, and I. Slutsker, Variability of absorption and optical properties of key aerosol types observed in worldwide locations, *J. Atmos. Sci.*, 59 (3), 590-608, 2002.
- Durak, M., and F. Samadov, Realization of a filter radiometer-based irradiance scale with high accuracy in the region from 286 nm to 901 nm, *Metrologia*, 41 (6), 401-406, 2004.
- Durry, G., and A. Hauchecorne, Evidence for long-lived polar vortex air in mid-latitude summer stratosphere from in situ laser diode CH₄ and H₂O measurements, *Atmos. Chem. Phys.*, 5 (6), 1467-1472, 2005.
- Dutton, E.G., A. Farhadi, R.S. Stone, C.N. Long, and D.W. Nelson, Long-term variations in the occurrence and effective solar transmission of clouds as determined from surface-based total irradiance observations, *J. Geophys. Res.*, 109, D03204, doi: 10.1029/2003JD003568, 2004.
- EC (European Commission), *Ozone-Climate Interactions, Air Pollution Research Report No. 81, EUR 20623*, 143 pp., Luxembourg, Belgium, 2003.
- Edwards, G.D., and P.S. Monks, Performance of a single-monochromator diode array spectroradiometer for the determination of actinic flux and atmospheric photolysis frequencies, *J. Geophys. Res.*, 108 (D16), 8546, doi: 10.1029/2002JD002844, 2003.
- Egorova, T., E. Rozanov, E. Manzini, M. Haberreiter, W. Schmutz, V. Zubov, and T. Peter, Chemical and dynamical response to the 11-year variability of the solar irradiance simulated with a chemistry-climate model, *Geophys. Res. Lett.*, 31, L06119, doi: 10.1029/2003GL019294, 2004.
- Engelsen, O., and A. Kylling, Fast simulation tool for ultraviolet radiation at the earth's surface, *Opt. Eng.*, 44 (4), 041012, doi: 10.1117/1.1885472, 2005.
- Engelsen, O., G.H. Hansen, and T. Svenøe, Long-term (1936-2003) ultraviolet and photosynthetically active radiation doses at a north Norwegian location in spring on the basis of total ozone and cloud cover, *Geophys. Res. Lett.*, 31, L12103, doi: 10.1029/2003GL019241, 2004.
- Erga, S.R., K. Aursland, Ø. Frette, B. Hamre, J.K. Lotsberg, J.J. Stamnes, J. Aure, F. Rey, and K. Stamnes, UV transmission in Norwegian marine waters: Controlling factors and possible effects on primary production and vertical distribution of phytoplankton, *Mar. Ecol. Prog. Ser.*, 305, 79-100, 2005.
- Evans, K.F., The spherical harmonics discrete ordinate method for three-dimensional atmospheric radiative transfer, *J. Atmos. Sci.*, 55 (3), 429-446, 1998.
- Feister, U., A.K. Kaifel, R.-D. Grewe, J. Kaptur, O. Reutter, M. Wohlfart, and K. Gericke, Fast measurements of solar spectral UV irradiance – first performance results of two novel spectroradiometers, *Opt. Eng.*, 44 (4), 041007, doi: 10.1117/1.1886816, 2005.
- Fioletov, V.E., L.J.B. McArthur, J.B. Kerr, and D.I. Wardle, Long-term variations of UV-B irradiance over Canada estimated from Brewer observations and derived from ozone and pyranometer measurements, *J. Geophys. Res.*, 106 (D19), 23009-23027, 2001.
- Fioletov, V.E., M.G. Kimlin, N. Krotkov, L.J.B. McArthur, J.B. Kerr, D.I. Wardle, J.R. Herman, R. Meltzer, T.W. Mathews, and J. Kaurola, UV index climatology over the United States and Canada from ground-based and satellite estimates, *J. Geophys. Res.*, 109, D22308, doi: 10.1029/2004JD004820, 2004.
- Fisher, F.N., M.D. King, and J. Lee-Taylor, Extinction of UV-visible radiation in wet midlatitude (maritime) snow: Implications for increased NO_x emission, *J. Geophys. Res.*, 110, D21301, doi: 10.1029/2005JD005963, 2005.
- Floyd, L.E., J.W. Cook, L.C. Herring, and P.C. Crane, SUSIM's 11-year observational record of the solar UV irradiance, *Adv. Space Res.*, 31 (9), 2111-2120, 2003.
- Frenette, J.-J., M.T. Arts, and J. Morin, Spectral gradients of downwelling light in a fluvial lake (Lake Saint-Pierre, St-Lawrence River), *Aquat. Ecol.*, 37 (1), 77-85, 2003.
- Frost, P.C., J.H. Larson, L.E. Kinsman, G.A. Lamberti, and S.D. Bridgham, Attenuation of ultraviolet radiation in streams of northern Michigan, *J. North Am. Benthol. Soc.*, 24 (2), 246-255, 2005.
- Früh, B., E. Eckstein, T. Trautmann, M. Wendisch, M. Fiebig, and U. Feister, Ground-based measured and calculated spectra of actinic flux density and downward UV irradiance in cloudless conditions and their sensitivity to aerosol microphysical properties, *J. Geophys. Res.*, 108 (D16), 4509, doi: 10.1029/2002JD002933, 2003.
- Gantner, L., P. Winkler, and U. Köhler, A method to derive

- long-term time series and trends of UV-B radiation (1968-1997) from observations at Hohenpeissenberg (Bavaria), *J. Geophys. Res.*, *105* (D4), 4879-4888, 2000.
- Gies, P., C. Roy, J. Javorniczky, S. Henderson, L. Lemus-Deschamps, and C. Driscoll, Global solar UV index: Australian measurements, forecasts and comparison with the UK, *Photochem. Photobiol.*, *79* (1), 32-39, 2004.
- Giorgi, F., X. Bi, and J. Pal, Mean, interannual variability and trends in a regional climate change experiment over Europe. II: Climate change scenarios (2071-2100), *Clim. Dyn.*, *23* (7-8), 839-858, 2004.
- Glandorf, M., A. Arola, A. Bais, and G. Seckmeyer, Possibilities to detect trends in spectral UV irradiance, *Theor. Appl. Climatol.*, *81* (1-2), 33-44, 2005.
- Goering, C.D., T.S. L'Ecuyer, G.L. Stephens, J.R. Slusser, G. Scott, J. Davis, J.C. Barnard, and S. Madronich, Simultaneous retrievals of column ozone and aerosol optical properties from direct and diffuse solar irradiance measurements, *J. Geophys. Res.*, *110*, D05204, doi: 10.1029/2004JD005330, 2005.
- Gröbner, J., Improved entrance optic for global irradiance measurements with a Brewer spectrophotometer, *Appl. Opt.*, *42* (18), 3516-3521, 2003.
- Gröbner, J., and C. Meleti, Aerosol optical depth in the UVB and visible wavelength range from Brewer spectrophotometer direct irradiance measurements: 1991-2002, *J. Geophys. Res.*, *109*, D09202, doi: 10.1029/2003JD004409, 2004.
- Gröbner, J., and P. Sperfeld, Direct traceability of the portable QASUME irradiance scale to the primary irradiance standard of the PTB, *Metrologia*, *42* (2), 134-139, 2005.
- Gröbner, J., D. Rembges, A.F. Bais, M. Blumthaler, T. Cabot, W. Josefsson, T. Koskela, T.M. Thorseth, A.R. Webb, and U. Wester, Quality assurance of reference standards from nine European solar-ultraviolet monitoring laboratories, *Appl. Opt.*, *41* (21), 4278-4282, 2002.
- Gröbner, J., J. Schreder, S. Kazadzis, A.F. Bais, M. Blumthaler, P. Görts, R. Tax, T. Koskela, G. Seckmeyer, A.R. Webb, and D. Rembges, Traveling reference spectroradiometer for routine quality assurance of spectral solar ultraviolet irradiance measurements, *Appl. Opt.*, *44* (25), 5321-5331, 2005.
- Gueymard, C.A., Parameterized transmittance model for direct beam and circumsolar spectral irradiance, *Solar Energy*, *71* (5), 325-346, 2001.
- Gueymard, C.A., The sun's total and spectral irradiance for solar energy applications and solar radiation models, *Solar Energy*, *76* (4), 423-453, 2004.
- Gueymard, C.A., Reference solar spectra: Their evolution, standardization issues, and comparison to recent measurements, *Adv. Space Res.*, *37* (2), 323-340, 2006.
- Gurlit, W., H. Bösch, H. Bovensmann, J.P. Burrows, A. Butz, C. Camy-Peyret, M. Dorf, K. Gerilowski, A. Lindner, S. Noël, U. Platt, F. Weidner, and K. Pfeilsticker, The UV-A and visible solar irradiance spectrum: inter-comparison of absolutely calibrated, spectrally medium resolution solar irradiance spectra from balloon- and satellite-borne measurements, *Atmos. Chem. Phys.*, *5*, 1879-1890, 2005.
- Häder, D.P., H.D. Kumar, R.C. Smith, and R.C. Worrest, Aquatic ecosystems: effects of solar ultraviolet radiation and interactions with other climatic change factors, *Photochem. Photobiol. Sci.*, *2* (1), 39-50, 2003.
- Haigh, J.D., The effects of solar variability on the Earth's climate, *Phil. Trans. Roy. Soc. A*, *361* (1802), 95-111, 2003.
- Harder, H., H. Bösch, C. Camy-Peyret, M.P. Chipperfield, R. Fitzenberger, S. Payan, D. Perner, U. Platt, B.-M. Sinnhuber, and K. Pfeilsticker, Comparison of measured and modeled stratospheric BrO: Implications for the total amount of stratospheric bromine, *Geophys. Res. Lett.*, *27* (22), 3695-3698, 2000.
- Hatzianastassiou, N., B. Katsoulis, and I. Vardavas, Global distribution of aerosol direct radiative forcing in the ultraviolet and visible arising under clear skies, *Tellus*, *56B* (1), 51-71, 2004a.
- Hatzianastassiou, N., B. Katsoulis, and I. Vardavas, Sensitivity analysis of aerosol direct radiative forcing in ultraviolet-visible wavelengths and consequences for the heat budget, *Tellus*, *56B* (4), 368-381, 2004b.
- Heckel, A., A. Richter, T. Tarsu, F. Wittrock, C. Hak, I. Pundt, W. Junkermann, and J.P. Burrows, MAX-DOAS measurements of formaldehyde in the Po-Valley, *Atmos. Chem. Phys.*, *5*, 909-918, 2005.
- Herman, J.R., Estimations of the global distribution and time series of UV noontime irradiance (305, 310, 324, 380 nm, and erythema) from TOMS and SeaWiFS data, in *Ozone Vol. I, Proceedings of the XX Quadrennial Ozone Symposium*, 1-8 June 2004, Kos, Greece, edited by C.S. Zerefos, 253-253, Int. Ozone Comm., Athens, Greece, 2004.
- Herman, J.R., and R.L. McKenzie (Lead Authors), S.B. Diaz, J.B. Kerr, S. Madronich, and G. Seckmeyer, Ultraviolet radiation at the Earth's surface, Chapter 9 in *Scientific Assessment of Ozone Depletion: 1998, Global Ozone Research and Monitoring*

SURFACE ULTRAVIOLET RADIATION

- Project-Report No. 44*, World Meteorological Organization, Geneva, Switzerland, 1999.
- Hicke, J., J.R. Slusser, and K. Lantz, Long-term variability in surface UV-B radiation across the United States, *Proc. SPIE*, 5545, 7-16, 2004.
- Hofzumahaus, A., A. Kraus, A. Kylling, and C.S. Zerefos, Solar actinic radiation (280-420 nm) in the cloud-free troposphere between ground and 12 km altitude: Measurements and model results, *J. Geophys. Res.*, 107 (D18), 8139, doi: 10.1029/2001JD900142, 2002.
- Hofzumahaus, A., B.L. Lefer, P.S. Monks, S.R. Hall, A. Kylling, B. Mayer, R.E. Shetter, W. Junkermann, A. Bais, J.G. Calvert, C.A. Cantrell, S. Madronich, G.D. Edwards, A. Kraus, M. Müller, B. Bohn, R. Schmitt, P. Johnston, R. McKenzie, G.J. Frost, E. Griffioen, M. Krol, T. Martin, G. Pfister, E.P. Röth, A. Ruggaber, W.H. Swartz, S.A. Lloyd, and M. Van Weele, Photolysis frequency of O₃ to O(¹D): Measurements and modeling during the International Photolysis Frequency Measurement and Modeling Intercomparison (IPMMI), *J. Geophys. Res.*, 109, D08S90, doi: 10.1029/2003JD004333, 2004.
- Høiskar, B.A.K., R. Haugen, T. Danielsen, A. Kylling, K. Edvardsen, A. Dahlback, B. Johnsen, M. Blumthaler, and J. Schreder, Multichannel moderate-bandwidth filter instrument for measurement of the ozone-column amount, cloud transmittance, and ultraviolet dose rates, *Appl. Opt.*, 42 (18), 3472-3479, 2003.
- Houët, M., and C. Brogniez, Ozone column retrieval from solar UV irradiance measurements at ground level: Sensitivity tests and uncertainty estimation, *J. Geophys. Res.*, 109, D15302, doi: 10.1029/2004JD004703, 2004.
- Huber, M., M. Blumthaler, J. Schreder, A. Bais, and C. Topaloglou, Effect of ambient temperature on Robertson-Berger-type erythema dosimeters, *Appl. Opt.*, 41 (21), 4273-4277, 2002.
- Huber, M., M. Blumthaler, and J. Schreder, Solar UV measurements with Robertson-Berger type instruments: influence of the detector's internal humidity status, *Agric. For. Meteorol.*, 120 (1), 39-43, 2003.
- Huber, M., M. Blumthaler, J. Schreder, B. Schallhart, and J. Lenoble, Effect of inhomogeneous surface albedo on diffuse UV sky radiance at a high-altitude site, *J. Geophys. Res.*, 109, D08107, doi: 10.1029/2003JD004113, 2004.
- Huovinen, P.S., H. Penttila, and M.R. Soimasuo, Spectral attenuation of solar ultraviolet radiation in humic lakes in Central Finland, *Chemosphere*, 51 (3), 205-214, 2003.
- Immler, F., D. Engelbart, and O. Schrems, Fluorescence from atmospheric aerosol detected by a lidar indicates biogenic particles in the lowermost stratosphere, *Atmos. Chem. Phys.*, 5, 345-355, 2005.
- IPCC (Intergovernmental Panel on Climate Change), *Climate Change 2001: The Scientific Basis: Contribution of Working Group I to the Third Assessment Report of the Intergovernmental Panel on Climate Change*, edited by J.T. Houghton, Y. Ding, D.J. Griggs, M. Nogue, P.J. van der Linden, X. Dai, K. Maskell, and C.A. Johnson, 881 pp., Cambridge University Press, Cambridge, U.K., 2001.
- IPCC/TEAP (Intergovernmental Panel on Climate Change/Technology and Economic Assessment Panel), *Special Report on Safeguarding the Ozone Layer and the Global Climate System: Issues Related to Hydrofluorocarbons and Perfluorocarbons*, edited by B. Metz, L. Kuijpers, S. Solomon, S.O. Andersen, O. Davidson, J. Pons, D. de Jager, T. Kestin, M. Manning, and L.A. Meyer, 478 pp., Cambridge University Press, Cambridge, U.K., 2005.
- Isaksen, I.S.A., C. Zerefos, K. Kourtidis, C. Meleti, S.B. Dalsøren, J.K. Sundet, A. Grini, P. Zanis, and D. Balis, Tropospheric ozone changes at unpolluted and semipolluted regions induced by stratospheric ozone changes, *J. Geophys. Res.*, 110, D02302, doi: 10.1029/2004JD004618, 2005.
- Jacobson, M.Z., Isolating nitrated and aromatic aerosols and nitrated aromatic gases as sources of ultraviolet light absorption, *J. Geophys. Res.*, 104 (D3), 3527-3542, 1999.
- Jäkel, E., M. Wendisch, A. Kniffka, and T. Trautmann, Airborne system for fast measurements of upwelling and downwelling spectral actinic flux densities, *Appl. Opt.*, 44 (3), 434-444, 2005.
- Janouch, M., Modeling of UV-radiation by neural technologies, in *Ozone, Vol. II, Proceedings of the XX Quadrennial Ozone Symposium*, 1-8 June 2004, Kos, Greece, edited by C.S. Zerefos, 1097-1098, Int. Ozone Comm., Athens, Greece, 2004.
- Jaroslowski, J.P., and J.W. Krzyścin, Importance of aerosol variations for surface UV-B level: Analysis of ground-based data taken at Belsk, Poland, 1992-2004, *J. Geophys. Res.*, 110, D16201, doi: 10.1029/2005JD005951, 2005.
- Johannessen, S.C., W.L. Miller, and J.J. Cullen, Calculation of UV attenuation and colored dissolved organic matter absorption spectra from measurements of ocean color, *J. Geophys. Res.*, 108 (C9), 3301, doi: 10.1029/2000JC000514, 2003.

- Josefsson, W., UV-radiation 1983-2003 measured at Norrköping, Sweden, *Theor. Appl. Climatol.*, 83 (1), 59-76, 2006.
- Kalliskota, S., J. Kaurola, P. Taalas, J.R. Herman, E.A. Celarier, and N.A. Krotkov, Comparison of daily UV doses estimated from Nimbus 7/TOMS measurements and ground-based spectroradiometric data, *J. Geophys. Res.*, 105 (D4), 5059-5067, 2000.
- Kambezidis, H.D., A.D. Adamopoulos, and D. Zevgolis, Spectral aerosol transmittance in the ultraviolet and visible spectra in Athens, Greece, *Pure Appl. Geophys.*, 162 (3), 625-647, 2005.
- Kaurola, J., P. Taalas, T. Koskela, J. Borkowski, and W. Josefsson, Long-term variations of UV-B doses at three stations in northern Europe, *J. Geophys. Res.*, 105 (D16), 20813-20820, 2000.
- Kaurola, J., A. Arola, J. Damski, L. Backman, A. Tanskanen, L. Tholix, J. Austin, and N. Butchart, Surface UV trends derived from coupled chemistry-climate model simulations for the period 1980 to 2000, and 2000 to 2020, in *Ozone Vol. I, Proceedings of the XX Quadrennial Ozone Symposium*, 1-8 June 2004, Kos, Greece, edited by C.S. Zerefos, 255-256, Int. Ozone Comm., Athens, Greece, 2004.
- Kazadzis, S., C. Topaloglou, A.F. Bais, M. Blumthaler, D. Balis, A. Kazantzidis, and B. Schallhart, Actinic flux and O¹D photolysis frequencies retrieved from spectral measurements of irradiance at Thessaloniki, Greece, *Atmos. Chem. Phys.*, 4, 2215-2226, 2004.
- Kazadzis, S., A. Bais, N. Kouremeti, E. Gerasopoulos, K. Garane, M. Blumthaler, B. Schallhart, and A. Cede, Direct spectral measurements with a Brewer spectroradiometer: absolute calibration and aerosol optical depth retrieval, *Appl. Opt.*, 44 (9), 1681-1690, 2005.
- Kazantzidis, A., D.S. Balis, A.F. Bais, S. Kazadzis, E. Galani, E. Kosmidis, and M. Blumthaler, Comparison of model calculations with spectral UV measurements during the SUSPEN campaign: The effect of aerosols, *J. Atmos. Sci.*, 58 (12), 1529-1539, 2001.
- Kazantzidis, A., A.F. Bais, D.S. Balis, E. Kosmidis, and C.S. Zerefos, Sensitivity of solar UV radiation to ozone and temperature profiles at Thessaloniki (40.5°N, 23°E), Greece, *J. Atmos. Solar Terr. Phys.*, 67 (14), 1321-1330, 2005.
- Kerr, J.B., Understanding the factors that affect surface ultraviolet radiation, *Opt. Eng.*, 44 (4), 041002, doi: 10.1117/1.1886817, 2005.
- Kerr, J., and G. Seckmeyer (Lead Authors), A. Bais, M. Blumthaler, S.B. Diaz, N. Krotkov, D. Lubin, S. Madronich, R.L. McKenzie, A.-A. Sabzipavar, and J. Verdebout, Surface ultraviolet radiation: Past and future, Chapter 5 in *Scientific Assessment of Ozone Depletion: 2002, Global Ozone Research and Monitoring Project—Report No. 47*, World Meteorological Organization, Geneva, Switzerland, 2003.
- Key, J., *Streamer User's Guide*, Cooperative Institute for Meteorological Satellite Studies, University of Wisconsin, 96 pp., 1999.
- Kiedron, P.W., J.J. Michalsky, J.L. Berndt, and L.C. Harrison, Comparison of spectral irradiance standards used to calibrate shortwave radiometers and spectroradiometers, *Appl. Opt.*, 38 (12), 2432-2439, 1999.
- Kimlin, M.G., J.R. Slusser, K.A. Schallhorn, K. Lantz, and R.S. Meltzer, Comparison of ultraviolet data from colocated instruments from the U.S. EPA Brewer Spectrophotometer Network and the U.S. Department of Agriculture UV-B Monitoring and Research Program, *Opt. Eng.*, 44 (4), 041009, doi: 10.1117/1.1885470, 2005.
- Kirchhoff, V.W.J.H., A.A. Silva, and D.K. Pinheiro, Wavelength dependence of aerosol optical thickness in the UV-B band, *Geophys. Res. Lett.*, 29 (12), 1620, doi: 10.1029/2001GL014141, 2002.
- Kirchstetter, T.W., T. Novakov, and P.V. Hobbs, Evidence that the spectral dependence of light absorption by aerosols is affected by organic carbon, *J. Geophys. Res.*, 109, D21208, doi: 10.1029/2004JD004999, 2004.
- Kjeldstad, B., Ø. Frette, S.R. Erga, H.I. Browman, P. Kuhn, R. Davis, W. Miller, and J.J. Stamnes, UV (280 to 400 nm) optical properties in a Norwegian fjord system and an intercomparison of underwater radiometers, *Mar. Ecol. Prog. Ser.*, 256, 1-11, 2003.
- Koepke, P., and M. Mech, UV irradiance on arbitrarily oriented surfaces: Variation with atmospheric and ground properties, *Theor. Appl. Climatol.*, 81 (1-2), 25-32, 2005.
- Koepke, P., D. Anwender, M. Mech, A. Oppenrieder, J. Reuder, A. Ruggaber, M. Schreier, H. Schwander, and J. Schween, Actual state of the UV radiation transfer model package STAR, in *IRS 2004: Current Problems in Atmospheric Radiation, Proceedings of the International Radiation Symposium*, 23-28 August 2004, Busan, Korea, edited by H. Fischer and B.-J. Sohn, 71-74, 2006.
- Konopka, P., J.-U. Grooss, S. Bausch, R. Müller, D.S. McKenna, O. Morgenstern, and Y. Orsolini, Dynamics and chemistry of vortex remnants in late Arctic spring 1997 and 2000: Simulations with the Chemical Lagrangian Model of the Stratosphere (CLaMS), *Atmos. Chem. Phys.*, 3, 839-849, 2003.

SURFACE ULTRAVIOLET RADIATION

- Koronakis, P.S., G.K. Sfantos, A.G. Paliatsos, J.K. Kaldellis, J.E. Garofalakis, and I.P. Koronaki, Interrelations of UV-global/global/diffuse solar irradiance components and UV-global attenuation on air pollution episode days in Athens, Greece, *Atmos. Environ.*, 36 (19), 3173-3181, 2002.
- Krotkov, N.A., P.K. Bhartia, J.R. Herman, V. Fioletov, and J. Kerr, Satellite estimation of spectral surface UV irradiance in the presence of tropospheric aerosols 1. Cloud-free case, *J. Geophys. Res.*, 103 (D8), 8779-8794, 1998.
- Krotkov, N.A., J.R. Herman, P.K. Bhartia, V. Fioletov, and Z. Ahmad, Satellite estimation of spectral surface UV irradiance 2. Effects of homogeneous clouds and snow, *J. Geophys. Res.*, 106 (D11), 11743-11759, 2001.
- Krotkov, N.A., J. Herman, V. Fioletov, C. Seftor, D. Larko, A. Vasilikov, and G. Labow, Boundary layer absorbing aerosol correction of an expanded UV irradiance database from satellite Total Ozone Mapping Spectrometer, in Ozone Vol. I, *Proceedings of the XX Quadrennial Ozone Symposium*, 1-8 June 2004, Kos, Greece, edited by C.S. Zerefos, 267-268, Int. Ozone Comm., Athens, Greece, 2004.
- Krotkov, N., P.K. Bhartia, J. Herman, J. Slusser, G. Labow, G. Scott, G. Janson, T.F. Eck, and B. Holben, Aerosol ultraviolet absorption experiment (2002 to 2004), part 1: Ultraviolet multifilter rotating shadowband radiometer calibration and intercomparison with CIMEL sunphotometers, *Opt. Eng.*, 44 (4), 041004, doi: 10.1117/1.1886818, 2005a.
- Krotkov, N., P.K. Bhartia, J. Herman, J. Slusser, G. Scott, G. Labow, A.P. Vasilkov, T.F. Eck, O. Dubovik, and B.N. Holben, Aerosol ultraviolet absorption experiment (2002 to 2004), part 2: Absorption optical thickness, refractive index, and single scattering albedo, *Opt. Eng.*, 44 (4), 041005, doi: 10.1117/1.1886819, 2005b.
- Krotkov, N.A., J.R. Herman, A. Cede, and G. Labow, Partitioning between aerosol and NO₂ absorption in the UV spectral region, *Proc. SPIE*, 5886, 588601, doi:10.1117/12.615285, 2005c.
- Krzyścin, J.W., Ozone profile and aerosols forcing on the UV radiation: Analysis of the clear-sky UV measurements (1992-2002) at Belsk, Poland, in *Ozone Vol. II, Proceedings of the XX Quadrennial Ozone Symposium*, 1-8 June 2004, Kos, Greece, edited by C.S. Zerefos, 1110-1111, Int. Ozone Comm., Athens, Greece, 2004.
- Krzyścin, J.W., J. Jaroslowski, and P. Sobolewski, On an improvement of UV index forecast: UV index diagnosis and forecast for Belsk, Poland, in Spring/Summer 1999, *J. Atmos. Solar Terr. Phys.*, 63 (15), 1593-1600, 2001.
- Krzyścin, J.W., J. Jaroslowski, and P.S. Sobolewski, Effects of clouds on the surface erythral UV-B irradiance at northern midlatitudes: estimation from the observations taken at Belsk, Poland (1999-2001), *J. Atmos. Solar Terr. Phys.*, 65 (4), 457-467, 2003.
- Krzyścin, J.W., K. Eerme, and M. Janouch, Long-term variations of the UV-B radiation over Central Europe as derived from the reconstructed UV time series, *Ann. Geophys.*, 22 (5), 1473-1485, 2004.
- Kübarssepp, T., H.W. Yoon, S. Nevas, P. Kärhä, and E. Ikonen, Comparison of spectral irradiance scales between the NIST and the HUT, *Metrologia*, 39 (4), 399-402, 2002.
- Kuchinke, C., and M. Nunez, An anisotropy correction method for all-sky measurements of diffuse UV-B erythral irradiance, *J. Atmos. Ocean. Tech.*, 20 (11), 1523-1533, 2003.
- Kuchinke, C., K. Fienberg, and M. Nunez, The angular distribution of UV-B sky radiance under cloudy conditions: A comparison of measurements and radiative transfer calculations using a Fractal cloud model, *J. Appl. Meteorol.*, 43 (5), 751-761, 2004.
- Kurucz, R.L., I. Furenlid, J. Brault, and L. Testerman, Solar flux atlas from 296 to 1300 nm, in *National Solar Observatory Atlas No. 1*, National Solar Observatory, Sunspot, New Mexico, 1984.
- Kyilling, A., A.F. Bais, M. Blumthaler, J. Schreder, C.S. Zerefos, and E. Kosmidis, Effect of aerosols on solar UV irradiances during the Photochemical Activity and Solar Ultraviolet Radiation Campaign, *J. Geophys. Res.*, 103 (D20), 26051-26060, 1998.
- Kyilling, A., T. Danielsen, M. Blumthaler, J. Schreder, and B. Johnsen, Twilight tropospheric and stratospheric photodissociation rates derived from balloon borne radiation measurements, *Atmos. Chem. Phys.*, 3, 377-385, 2003a.
- Kyilling, A., A.R. Webb, A.F. Bais, M. Blumthaler, R. Schmitt, S. Thiel, A. Kazantzidis, R. Kift, M. Misslbeck, B. Schallhart, J. Schreder, C. Topaloglou, S. Kazadzis, and J. Rimmer, Actinic flux determination from measurements of irradiance, *J. Geophys. Res.*, 108 (D16), 4506, doi: 10.1029/2002JD003236, 2003b.
- Kyilling, A., A.R. Webb, R. Kift, G.P. Gobbi, L. Ammannato, F. Barnaba, A. Bais, S. Kazadzis, M. Wendisch, E. Jäkel, S. Schmidt, A. Kniffka, S. Thiel, W. Junkermann, M. Blumthaler, R. Silbernagl, B. Schallhart, R. Schmitt, B. Kjeldstad, T.M. Thorseth, R. Scheirer, and B. Mayer, Spectral

- actinic flux in the lower troposphere: measurement and 1-D simulations for cloudless, broken cloud and overcast situations, *Atmos. Chem. Phys.*, *5*, 1975-1997, 2005.
- Labitzke, K., and K. Matthes, Eleven-year solar cycle variations in the atmosphere: observations, mechanisms and models, *Holocene*, *13* (3), 311-317, 2003.
- Lakkala, K., E. Kyrö, and T. Turunen, Spectral UV measurements at Sodankylä during 1990-2001, *J. Geophys. Res.*, *108* (D19), 4621, doi: 10.1029/2002JD003300, 2003.
- Lakkala, K., A. Redondas, O. Meinander, C. Torres, T. Koskela, E. Cuevas, P. Taalas, A. Dahlback, G. Deferrari, K. Edvardsen, and H. Ochoa, Quality assurance of the solar UV network in the Antarctic, *J. Geophys. Res.*, *110*, D15101, doi: 10.1029/2004JD005584, 2005.
- Lane-Veron, D.E., and R.C.J. Somerville, Stochastic theory of radiative transfer through generalized cloud fields, *J. Geophys. Res.*, *109*, D18113, doi: 10.1029/2004JD004524, 2004.
- Langematz, U., J.L. Grenfell, K. Matthes, P. Mieth, M. Kunze, B. Steil, and C. Brühl, Chemical effects in 11-year solar cycle simulations with the Freie Universität Berlin Climate Middle Atmosphere Model with online chemistry (FUB-CMAM-CHEM), *Geophys. Res. Lett.*, *32*, L13803, doi: 10.1029/2005GL022686, 2005.
- Lantz, K., P. Disterhoft, E. Early, A. Thompson, J. DeLuisi, J. Berndt, L. Harrison, P. Kiedron, J. Ehranjian, G. Bernhard, L. Cabasug, J. Robertson, W. Mou, T. Taylor, J. Slusser, D. Bigelow, B. Durham, G. Janson, D. Hayes, M. Beaubien, and A. Beaubien, The 1997 North American interagency intercomparison of ultraviolet spectroradiometers including narrowband filter radiometers, *J. Res. Natl. Inst. Stand. Technol.*, *107* (1), 19-62, 2002.
- Larkin, A., J.D. Haigh, and S. Djavidnia, The effect of solar UV irradiance variations on the Earth's atmosphere, *Space Sci. Rev.*, *94* (1-2), 199-214, 2000.
- Latha, K.M., K.V.S. Badarinath, P.K. Gupta, A.B. Ghosh, S.L. Jain, B.S. Gera, R. Singh, A.K. Sarkar, N. Singh, R.S. Parmar, S. Koul, R. Kohli, S. Nath, V.K. Ojha, and G. Singh, Impact of biomass burning aerosols on UV erythema – a case study from northeast region of India, *J. Atmos. Solar Terr. Phys.*, *66* (11), 981-986, 2004.
- Lemus-Deschamps, L., L. Rikus, and P. Gies, The operational Australian ultraviolet index forecast 1997, *Meteorol. Appl.*, *6* (3), 241-251, 1999.
- Lemus-Deschamps, L., L. Rikus, S. Grainger, P. Gies, J. Sisson, and Z. Li, UV Index and UV dose distributions for Australia (1997-2001), *Aust. Meteorol. Mag.*, *53* (4), 239-250, 2004.
- Lenoble, J., T. Martin, M. Blumthaler, R. Philipona, A. Albold, T. Cabot, A. de La Casinière, J. Gröbner, D. Masserot, M. Müller, T. Pichler, G. Seckmeyer, D. Schmucki, M.L. Touré, and A. Yvon, Retrieval of the ultraviolet aerosol optical depth during a spring campaign in the Bavarian Alps, *Appl. Opt.*, *41* (9), 1629-1639, 2002.
- Lenoble, J., A. de la Casinière, and T. Cabot, Analysis of direct solar ultraviolet irradiance measurements in the French Alps. Retrieval of turbidity and ozone column amount, *Appl. Opt.*, *43* (15), 3133-3139, 2004a.
- Lenoble, J., A. Kylling, and I. Smolskaia, Impact of snow cover and topography on ultraviolet irradiance at the Alpine station of Briançon, *J. Geophys. Res.*, *109*, D16209, doi: 10.1029/2004JD004523, 2004b.
- Levelt, P.F., E. Hilsenrath, G.W. Leppelmeier, G.H.J. van der Oord, P.K. Bhartia, J. Tamminen, J.F. de Haan, and J.P. Veefkind, Science objectives of the ozone monitoring instrument, *IEEE Trans. Geosci. Rem. Sens.*, *44* (5), 1199-1208, 2006.
- Liao, Y., and J.E. Frederick, The ultraviolet radiation environment of high southern latitudes: Springtime behavior over a decadal timescale, *Photochem. Photobiol.*, *81* (2), 320-324, 2005.
- Liepert, B.G., Observed reductions of surface solar radiation at sites in the United States and worldwide from 1961 to 1990, *Geophys. Res. Lett.*, *29* (10), 1421, doi: 10.1029/2002GL014910, 2002.
- Lindfors, A., and L. Vuilleumier, Erythema UV at Davos (Switzerland), 1926-2003, estimated using total ozone, sunshine duration, and snow depth, *J. Geophys. Res.*, *110*, D02104, doi: 10.1029/2004JD005231, 2005.
- Lindfors, A.V., A. Arola, J. Kaurola, P. Taalas, and T. Svenøe, Long-term erythema UV doses at Sodankylä estimated using total ozone, sunshine duration, and snow depth, *J. Geophys. Res.*, *108* (D16), 4518, doi: 10.1029/2002JD003325, 2003.
- Long, C.S., A.J. Miller, H.-T. Lee, J.D. Wild, R.C. Przywarty, and D. Hufford, Ultraviolet index forecasts issued by the National Weather Service, *Bull. Amer. Meteorol. Soc.*, *77* (4), 729-748, 1995.
- Lovengreen, C., H.A. Fuenzalida, and L. Videla, On the spectral dependency of UV radiation enhancements due to clouds in Valdivia, Chile (39.8°S), *J. Geophys. Res.*, *110*, D14207, doi: 10.1029/2004JD005372, 2005.
- Lubin, D., E.H. Jensen, and H.P. Gies, Global surface ultraviolet radiation climatology from TOMS and ERBE

SURFACE ULTRAVIOLET RADIATION

- data, *J. Geophys. Res.*, *103* (D20), 26061-26091, 1998.
- Lubin, D., P. Ricchiazzi, A. Payton, and C. Gautier, Significance of multidimensional radiative transfer effects measured in surface fluxes at an Antarctic coastline, *J. Geophys. Res.*, *107* (D19), 4387, doi: 10.1029/2001JD002030, 2002.
- Lubin, D., K.R. Arrigo, and G.L. van Dijken, Increased exposure of Southern Ocean phytoplankton to ultraviolet radiation, *Geophys. Res. Lett.*, *31*, L09304, doi: 10.1029/2004GL019633, 2004.
- Luccini, E., A. Cede, and R.D. Piacentini, Effect of clouds on UV and total irradiance at Paradise Bay, Antarctic Peninsula, from a summer 2000 campaign, *Theor. Appl. Climatol.*, *75* (1-2), 105-116, 2003.
- Luccini, E., A. Cede, R. Piacentini, C. Villanueva, and P. Canziani, Ultraviolet climatology over Argentina, *J. Geophys. Res.*, *111*, D17312, doi: 10.1029/2005JD006580, 2006.
- Madronich, S., and S. Flocke, Theoretical estimation of biologically effective UV radiation at the earth's surface, in *Solar Ultraviolet Radiation Modelling, Measurements and Effects*, edited by C.S. Zerefos, and A.F. Bais, Springer-Verlag, Berlin, 1997.
- Makhotkina, E.L., I.N. Plakhina, and A.B. Lukin, Some features of atmospheric turbidity change over the Russian territory in the last quarter of the 20th century, *Russ. Meteorol. Hydrol.*, *1*, 20-27, 2005.
- Marshak, A., and A.B. Davis, *3D Radiative Transfer in Cloudy Atmospheres*, 686 pp., Springer-Verlag, Berlin, 2005.
- Mattis, I., A. Ansmann, D. Müller, U. Wandinger, and D. Althausen, Dual-wavelength Raman lidar observations of the extinction-to-backscatter ratio of Saharan dust, *Geophys. Res. Lett.*, *29* (9), 1306, doi: 10.1029/2002GL014721, 2002.
- Mayer, B., and A. Kylling, Technical note: The libRadtran software package for radiative transfer calculations – description and examples of use, *Atmos. Chem. Phys.*, *5*, 1855-1877, 2005.
- Mayer, B., G. Seckmeyer, and A. Kylling, Systematic long-term comparison of spectral UV measurements and UVSPEC modeling results, *J. Geophys. Res.*, *102* (D7), 8755-8767, 1997.
- McArthur, L.J.B., V.E. Fioletov, J.B. Kerr, C.T. McElroy, and D.I. Wardle, Derivation of UV-A irradiance from pyranometer measurements, *J. Geophys. Res.*, *104* (D23), 30139-30151, 1999.
- McKenzie, R., B. Connor, and G. Bodeker, Increased summertime UV radiation in New Zealand in response to ozone loss, *Science*, *285* (5434), 1709-1711, 1999.
- McKenzie, R.L., P.V. Johnston, D. Smale, B.A. Bodhaine, and S. Madronich, Altitude effects on UV spectral irradiance deduced from measurements at Lauder, New Zealand, and at Mauna Loa Observatory, Hawaii, *J. Geophys. Res.*, *106* (D19), 22845-22860, 2001a.
- McKenzie, R.L., G. Seckmeyer, A.F. Bais, J.B. Kerr, and S. Madronich, Satellite retrievals of erythemal UV dose compared with ground-based measurements at northern and southern midlatitudes, *J. Geophys. Res.*, *106* (D20), 24051-24062, 2001b.
- McKenzie, R.L., P.V. Johnston, A. Hofzumahaus, A. Kraus, S. Madronich, C. Cantrell, J. Calvert, and R. Shetter, Relationship between photolysis frequencies derived from spectroscopic measurements of actinic fluxes and irradiances during the IPMMI campaign, *J. Geophys. Res.*, *107* (D5), 4042, doi: 10.1029/2001JD000601, 2002.
- McKenzie, R., D. Smale, G. Bodeker, and H. Claude, Ozone profile differences between Europe and New Zealand: Effects on surface UV irradiance and its estimation from satellite sensors, *J. Geophys. Res.*, *108* (D6), 4179, doi: 10.1029/2002JD002770, 2003.
- McKenzie, R., G. Bodeker, M. Kotkamp, and P. Johnston, Long term changes in summertime UV radiation in New Zealand in response to ozone change, in *Ozone Vol. I, Proceedings of the XX Quadrennial Ozone Symposium*, 1-8 June 2004, Kos, Greece, edited by C.S. Zerefos, 257-258, Int. Ozone Comm., Athens, Greece, 2004.
- McKenzie, R., J. Badosa, M. Kotkamp, and P. Johnston, Effects of the temperature dependence in PTFE diffusers on observed UV irradiances, *Geophys. Res. Lett.*, *32*, L06808, doi: 10.1029/2004GL022268, 2005.
- McKenzie, R., G. Bodeker, G. Scott, J. Slusser, and K. Lantz, Geographical differences in erythemally-weighted UV measured at mid-latitude USDA sites, *Photochem. Photobiol. Sci.*, *5* (3), 343-352, 2006.
- McKinlay, A.F., and B.L. Diffey, A reference action spectrum for ultra-violet induced erythema in human skin, in *Human Exposure to Ultraviolet Radiation: Risks and Regulations: Proceedings of a Seminar Held in Amsterdam, 23-25 March 1987*, edited by W.F. Passchier and B.F.M. Bosnjakovic, 83-87, Elsevier, Amsterdam, 1987.
- Mech, M., and P. Koepke, Model for UV irradiance on arbitrarily oriented surfaces, *Theor. Appl. Climatol.*, *77* (3-4), 151-158, 2004.
- Meerkötter, R., and M. Degünther, A radiative transfer case study for 3-d cloud effects in the UV, *Geophys. Res. Lett.*, *28* (9), 1683-1686, 2001.
- Meerkötter, R., J. Verdebout, L. Bugliaro, K. Edvardsen,

- and G. Hansen, An evaluation of cloud affected UV radiation from polar orbiting and geostationary satellites at high latitudes, *Geophys. Res. Lett.*, 30 (18), 1956, doi: 10.1029/2003GL017850, 2003.
- Meerkötter, R., C. König, P. Bissolli, G. Gesell, and H. Mannstein, A 14-year European Cloud Climatology from NOAA/AVHRR data in comparison to surface observations, *Geophys. Res. Lett.*, 31, L15103, doi: 10.1029/2004GL020098, 2004.
- Meloni, D., A. di Sarra, J. DeLuisi, T. Di Iorio, G. Fiocco, W. Junkermann, and G. Pace, Tropospheric aerosols in the Mediterranean: 2. Radiative effects through model simulations and measurements, *J. Geophys. Res.*, 108 (D10), 4317, doi: 10.1029/2002JD002807, 2003a.
- Meloni, D., A. di Sarra, G. Fiocco, and W. Junkermann, Tropospheric aerosols in the Mediterranean: 3. Measurements and modeling of actinic radiation profiles, *J. Geophys. Res.*, 108 (D10), 4323, doi: 10.1029/2002JD003293, 2003b.
- Meloni, D., F. Marengo, and A. di Sarra, Ultraviolet radiation and aerosol monitoring at Lampedusa, Italy, *Ann. Geophys.*, 46 (2), 373-383, 2003c.
- Meloni, D., A. di Sarra, T. Di Iorio, and G. Fiocco, Direct radiative forcing of Saharan dust in the Mediterranean from measurements at Lampedusa Island and MISR space-borne observations, *J. Geophys. Res.*, 109, D08206, doi: 10.1029/2003JD003960, 2004.
- Meloni, D., A. di Sarra, J.R. Herman, F. Monteleone, and S. Piacentino, Comparison of ground-based and Total Ozone Mapping Spectrometer erythemal UV doses at the island of Lampedusa in the period 1998-2003: Role of tropospheric aerosols, *J. Geophys. Res.*, 110, D01202, doi: 10.1029/2004JD005283, 2005.
- Metzdorf, J., K.D. Stock, P. Sperfeld, A. Sperling, S. Winter, and T. Wittchen, Aspects of quality assurance in monitoring solar UV irradiance, *Metrologia*, 40 (1), S66-S69, 2003.
- Micheletti, M.I., E. Wolfram, R.D. Piacentini, A. Pazmiño, E. Quel, V. Orce, and A.A. Paladini, The incidence of erythemal and UV solar irradiance over Buenos Aires, Argentina, *J. Opt. A: Pure Appl. Opt.*, 5 (5), S262-S268, 2003.
- Mikkelsen, O., G. Saxebol, and B. Johnsen, Ultraviolet monitoring in Norway on the Web, *Radiat. Prot. Dosim.*, 91 (1), 165-167, 2000.
- Min, Q.-L., L.C. Harrison, P. Kiedron, J. Berndt, and E. Joseph, A high-resolution oxygen A-band and water vapor band spectrometer, *J. Geophys. Res.*, 109, D02202, doi: 10.1029/2003JD003540, 2004.
- Mogo, S., V.E. Cachorro, M. Sorribas, A. de Frutos, and R. Fernández, Measurements of continuous spectra of atmospheric absorption coefficients from UV to NIR via optical method, *Geophys. Res. Lett.*, 32, L13811, doi: 10.1029/2005GL022938, 2005.
- Mohamed-Tahrin, N., A.M. South, D.A. Newnham, and R.L. Jones, A new accurate wavelength calibration for the ozone absorption cross section in the near-UV spectral region, and its effect on the retrieval of BrO from measurements of zenith-scattered sunlight, *J. Geophys. Res.*, 106 (D9), 9897-9907, 2001.
- Monks, P.S., A.R. Rickard, S.L. Hall, and N.A.D. Richards, Attenuation of spectral actinic flux and photolysis frequencies at the surface through homogenous cloud fields, *J. Geophys. Res.*, 109, D17206, doi: 10.1029/2003JD004076, 2004.
- Myhre, C.E.L., and C.J. Nielsen, Optical properties in the UV and visible spectral region of organic acids relevant to tropospheric aerosols, *Atmos. Chem. Phys.*, 4, 1759-1769, 2004.
- Nichol, S.E., G. Pfister, G.E. Bodeker, R.L. McKenzie, S.W. Wood, and G. Bernhard, Moderation of cloud reduction of UV in the Antarctic due to high surface albedo, *J. Appl. Meteorol.*, 42 (8), 1174-1183, 2003.
- Nunez, M., C. Kuchinke, and P. Gies, Using broadband erythemal UV instruments to measure relative irradiance, *J. Geophys. Res.*, 107 (D24), 4789, doi: 10.1029/2001JD000738, 2002.
- Ogunjobi, K.O., and Y.J. Kim, Ultraviolet (0.280-0.400 μm) and broadband solar hourly radiation at Kwangju, South Korea: analysis of their correlation with aerosol optical depth and clearness index, *Atmos. Res.*, 71 (3), 193-214, 2004.
- Oppenrieder, A., P. Höpfe, and P. Koepke, Routine measurement of erythemally effective UV irradiance on inclined surfaces, *J. Photochem. Photobiol. B: Biol.*, 74 (2-3), 85-94, 2004.
- Oppenrieder, A., P. Höpfe, P. Koepke, and J. Reuder, Long term measurements of the UV irradiance of inclined surfaces and visualization of UV exposure of the human body, *Meteorol. Z.*, 14 (2), 285-290, 2005.
- Ørbæk, J.B., T. Svenøe, and D.O. Hessen, Spectral properties and UV attenuation in Arctic freshwater systems, Chapter 3 in *UV Radiation and Arctic Ecosystems*, edited by D.O. Hessen, 57-72, Springer, Heidelberg, 2002.
- Orphal, J., and K. Chance, Ultraviolet and visible absorption cross-sections for HITRAN, *J. Quant. Spectros. Radiat. Trans.*, 82 (1-4), 491-504, 2003.
- Orsolini, Y.J., Long-lived tracer patterns in the summer polar stratosphere, *Geophys. Res. Lett.*, 28 (20), 3855-3858, 2001.
- Orsolini, Y.J., H. Eskes, G. Hansen, U.P. Hoppe, A.

SURFACE ULTRAVIOLET RADIATION

- Kylling, E. Kyrö, J. Notholt, R. van der A, and P. von der Gathen, Summertime low-ozone episodes at northern high latitudes, *Quart. J. Roy. Meteorol. Soc.*, 129 (595), 3265-3275, 2003.
- Palancar, G.G., and B.M. Toselli, Erythematul ultraviolet irradiance in Córdoba, Argentina, *Atmos. Environ.*, 36 (2), 287-292, 2002.
- Palen, W.J., D.E. Schindler, M.J. Adams, C.A. Pearl, R.B. Bury, and S.A. Diamond, Optical characteristics of natural waters protect amphibians from UV-B in the U.S. Pacific Northwest, *Ecology*, 83 (11), 2951-2957, 2002.
- Parisi, A.V., J. Sabburg, M.G. Kimlin, and N. Downs, Measured and modelled contributions to UV exposures by the albedo of surfaces in an urban environment, *Theor. Appl. Climatol.*, 76 (3-4), 181-188, 2003.
- Pazmiño, A.F., S. Godin-Beekmann, M. Ginzburg, S. Bekki, A. Hauchecorne, R.D. Piacentini, and E.J. Quel, Impact of Antarctic polar vortex occurrences on total ozone and UVB radiation at southern Argentinean and Antarctic stations during 1997-2003 period, *J. Geophys. Res.*, 110, D03103, doi: 10.1029/2004JD005304, 2005.
- Perovich, D.K., UV and the optical properties of sea ice and snow, Chapter 4 in *UV Radiation and Arctic Ecosystems*, edited by D.O. Hessen, 73-89, Springer, Heidelberg, 2002.
- Petters, J.L., V.K. Saxena, J.R. Slusser, B.N. Wenny, and S. Madronich, Aerosol single scattering albedo retrieved from measurements of surface UV irradiance and a radiative transfer model, *J. Geophys. Res.*, 108 (D9), 4288, doi: 10.1029/2002JD002360, 2003.
- Pfeifer, M.T., P. Koepke, and J. Reuder, Effects of altitude and aerosol on UV radiation, *J. Geophys. Res.*, 111, D01203, doi: 10.1029/2005JD006444, 2006.
- Pfister, G., R.L. McKenzie, J.B. Liley, A. Thomas, B.W. Forgan, and C.N. Long, Cloud coverage based on all-sky imaging and its impact on surface solar irradiance, *J. Appl. Meteorol.*, 42 (10), 1421-1434, 2003.
- Piacentini, R.D., and A. Cede, Measurements of solar ultraviolet irradiance on inclined surfaces, *J. Opt. A: Pure Appl. Opt.*, 6 (9), 819-823, 2004.
- Piacentini, R.D., A. Cede, and H. Bárcena, Extreme solar total and UV irradiances due to cloud effect measured near the summer solstice at the high-altitude desertic plateau Puna of Atacama (Argentina), *J. Atmos. Solar Terr. Phys.*, 65 (6), 727-731, 2003.
- Piani, C., W.A. Norton, A.M. Iwi, E.A. Ray, and J.W. Elkins, Transport of ozone-depleted air on the breakup of the stratospheric polar vortex in spring/summer 2000, *J. Geophys. Res.*, 107 (D20), 8270, doi: 10.1029/2001JD000488, 2002.
- Piazena, H., E. Perez-Rodrigues, D.-P. Häder, and F. Lopez-Figueroa, Penetration of solar radiation into the water column of the central subtropical Atlantic Ocean – optical properties and possible biological consequences, *Deep Sea Res. (II Top. Stud. Oceanogr.)*, 49 (17), 3513-3528, 2002.
- Pinker, R.T., B. Zhang, and E.G. Dutton, Do satellites detect trends in surface solar radiation?, *Science*, 308 (5723), 850-854, 2005.
- Pinty, B., J.-L. Widlowski, M. Taberner, N. Gobron, M.M. Verstraete, M. Disney, F. Gascon, J.-P. Gastellu, L. Jiang, A. Kuusk, P. Lewis, X. Li, W. Ni-Meister, T. Nilson, P. North, W. Qin, L. Su, S. Tang, R. Thompson, W. Verhoef, H. Wang, J. Wang, G. Yan, and H. Zang, Radiation Transfer Model Intercomparison (RAMI) exercise: Results from the second phase, *J. Geophys. Res.*, 109, D06210, doi: 10.1029/2003JD004252, 2004.
- Plets, H., and C. Vynckier, A comparative study of statistical total column ozone forecasting models, *J. Geophys. Res.*, 105 (D21), 26503-26517, 2000.
- Qian, Y., D.P. Kaiser, L.R. Leung, and M. Xu, More frequent cloud-free sky and less surface solar radiation in China from 1955 to 2000, *Geophys. Res. Lett.*, 33, L01812, doi: 10.1029/2005GL024586, 2006.
- Qin, Y., M.A. Box, and D.L.B. Jupp, Inversion of multi-angle sky radiance measurements for the retrieval of atmospheric optical properties 1. Algorithm, *J. Geophys. Res.*, 107 (D22), 4652, doi: 10.1029/2001JD000945, 2002.
- Rasmus, K.E., W. Granéli, and S.-A. Wängberg, Optical studies in the Southern Ocean, *Deep Sea Res. (II Top. Stud. Oceanogr.)*, 51 (22-24), 2583-2597, 2004.
- Rehfuess, E., *Global Solar UV Index: A Practical Guide*, World Health Organization, 28 pp., Geneva, Switzerland, 2002.
- Reinsel, G.C., A.J. Miller, E.C. Weatherhead, L.E. Flynn, R.M. Nagatani, G.C. Tiao, and D.J. Wuebbles, Trend analysis of total ozone data for turnaround and dynamical contributions, *J. Geophys. Res.*, 110, D16306, doi: 10.1029/2004JD004662, 2005.
- Renwick, J., and R.L. McKenzie, Enhanced public UV index information: testing the skill of a simple ozone advection scheme, in *Communicating Meteorology, 2001: Conference of the New Zealand Meteorological Society*, 19-21 November 2001, Wellington, New Zealand, 2001.
- Reuder, J., and P. Koepke, Reconstruction of UV radiation over Southern Germany for the past decades, *Meteorol. Z.*, 14 (2), 237-246, 2005.

- Reuder, J., M. Dameris, and P. Koepke, Future UV radiation in Central Europe modelled from ozone scenarios, *J. Photochem. Photobiol. B: Biol.*, *61* (3), 94-105, 2001.
- Reuder, J., P. Koepke, and J. Schween, UV radiation in past and future modelling with all atmospheric parameters including cloudiness, in *IRS 2004: Current Problems in Atmospheric Radiation, Proceedings of the International Radiation Symposium*, 23-28 August 2004, Busan, Korea, edited by H. Fischer and B.-J. Sohn, 431-434, 2006.
- Ricchiuzzi, P., S. Yang, C. Gautier, and D. Sowle, SBDART: a research and teaching software tool for plane-parallel radiative transfer in the Earth's atmosphere, *Bull. Amer. Meteorol. Soc.*, *79* (10), 2101-2114, 1998.
- Richter, A., and J.P. Burrows, Tropospheric NO₂ from GOME measurements, *Adv. Space Res.*, *29* (11), 1673-1683, 2002.
- Richter, A., J.P. Burrows, H. Nüß, C. Granier, and U. Niemeier, Increase in tropospheric nitrogen dioxide over China observed from space, *Nature*, *437* (7055), 129-132, 2005.
- Rikus, L., Prediction of UV-B dosage at the surface, *Aust. Meteorol. Mag.*, *46* (3), 211-222, 1997.
- Rozanov, A., V. Rozanov, M. Buchwitz, A. Kokhanovsky, and J.P. Burrows, SCIATRAN 2.0 – A new radiative transfer model for geophysical applications in the 175-2400 nm spectral region, *Adv. Space Res.*, *36* (5), 1015-1019, 2005.
- Sabburg, J., J.E. Rives, R.S. Meltzer, T. Taylor, G. Schmalzle, S. Zheng, N. Huang, A. Wilson, and P.M. Udelhofen, Comparisons of corrected daily integrated erythemal UVR data from the US EPA/UGA network of Brewer spectroradiometers with model and TOMS-inferred data, *J. Geophys. Res.*, *107* (D23), 4676, doi: 10.1029/2001JD001565, 2002.
- Sander, S.P., R.R. Friedl, D.M. Golden, M.J. Kurylo, R.E. Huie, V.L. Orkin, G.K. Moortgat, A.R. Ravishankara, C.E. Kolb, M.J. Molina, and B.J. Finlayson-Pitts, *Chemical Kinetics and Photochemical Data for Use in Atmospheric Studies: Evaluation Number 14, JPL Publication 02-25*, Jet Propulsion Laboratory, Pasadena, Calif., 2003.
- Sasaki, M., S. Takeshita, T. Oyanagi, Y. Miyake, and T. Sakata, Increasing trend of biologically active solar ultraviolet-B irradiance in mid-latitude Japan in the 1990s, *Opt. Eng.*, *41* (12), 3062-3069, 2002.
- Schallhart, B., M. Huber, and M. Blumthaler, Semi-empirical method for the conversion of spectral UV global irradiance data into actinic flux, *Atmos. Environ.*, *38* (26), 4341-4346, 2004.
- Scheirer, R., and S. Schmidt, CLABAUTAIR: a new algorithm for retrieving three-dimensional cloud structure from airborne microphysical measurements, *Atmos. Chem. Phys.*, *5*, 2333-2340, 2005.
- Schmucki, D.A., and R. Philipona, Ultraviolet radiation in the Alps: the altitude effect, *Opt. Eng.*, *41* (12), 3090-3095, 2002.
- Schnaiter, M., H. Horvath, O. Möhler, K.-H. Naumann, H. Saathoff, and O.W. Schock, UV-VIS-NIR spectral optical properties of soot and soot-containing aerosols, *J. Aerosol Sci.*, *34* (10), 1421-1444, 2003.
- Schnaiter, M., O. Schmid, A. Petzold, L. Fritzsche, K.F. Klein, M.O. Andreae, G. Helas, A. Thielmann, M. Gimmmler, O.M. Möhler, C. Linke, and U. Schurath, Measurement of wavelength-resolved light absorption by aerosols utilizing a UV-VIS extinction cell, *Aerosol Sci. Technol.*, *39* (3), 249-260, 2005.
- Schreder, J., J. Gröbner, A. Los, and M. Blumthaler, Intercomparison of monochromatic source facilities for the determination of the relative spectral response of erythemal broadband filter radiometers, *Opt. Lett.*, *29* (13), 1455-1457, 2004.
- Schwander, H., P. Koepke, A. Kaifel, and G. Seckmeyer, Modification of spectral UV irradiance by clouds, *J. Geophys. Res.*, *107* (D16), 4296, doi: 10.1029/2001JD001297, 2002.
- Seckmeyer, G., A. Bais, G. Bernhard, M. Blumthaler, C.R. Booth, P. Disterhoft, P. Eriksen, R.L. McKenzie, M. Miyauchi, and C. Roy, *Instruments to Measure Solar Ultraviolet Irradiance. Part 1: Spectral Instruments, Global Atmospheric Watch, Report No. 125*, 30 pp., World Meteorological Organization, Geneva, Switzerland, 2001.
- Seckmeyer, G., A. Bais, G. Bernhard, M. Blumthaler, C.R. Booth, K. Lantz, and R.L. McKenzie, *Instruments to Measure Solar Ultraviolet Irradiance. Part 2: Broadband Instruments Measuring Erythemally Weighted Solar Irradiance, Global Atmospheric Watch, Report No. 164*, 54 pp., World Meteorological Organization, Geneva, Switzerland, 2005.
- Segura, A., K. Krellove, J.F. Kasting, D. Sommerlatt, V. Meadows, D. Crisp, M. Cohen, and E. Mlawer, Ozone concentrations and ultraviolet fluxes on earth-like planets around other stars, *Astrobiology*, *3* (4), 689-708, 2003.
- Seroji, A.R., A.R. Webb, H. Coe, P.S. Monks, and A.R. Rickard, Derivation and validation of photolysis rates of O₃, NO₂, and CH₂O from a GUV-541 radiometer, *J. Geophys. Res.*, *109*, D21307, doi: 10.1029/2004JD004674, 2004.
- Shaffer, J.A., and R.S. Cerveny, Long-term (250,000 BP

SURFACE ULTRAVIOLET RADIATION

- to 50,000 AP) variations in ultraviolet and visible radiation (0.175-0.690 μm), *Global Planet. Change*, 41 (2), 111-120, 2004.
- Shetter, R.E., W. Junkermann, W.H. Swartz, G.J. Frost, J.H. Crawford, B.L. Lefer, J.D. Barrick, S.R. Hall, A. Hofzumahaus, A. Bais, J.G. Calvert, C.A. Cantrell, S. Madronich, M. Müller, A. Kraus, P.S. Monks, G.D. Edwards, R. McKenzie, P. Johnston, R. Schmitt, E. Griffioen, M. Krol, A. Kylling, R.R. Dickerson, S.A. Lloyd, T. Martin, B. Gardiner, B. Mayer, G. Pfister, E.P. Röth, P. Koepke, A. Ruggaber, H. Schwander, and M. van Weele, Photolysis frequency of NO_2 : Measurement and modeling during the International Photolysis Frequency Measurement and Modeling Intercomparison (IPMMI), *J. Geophys. Res.*, 108 (D16), 8544, doi: 10.1029/2002JD002932, 2003.
- Shindell, D.T., G.A. Schmidt, R.L. Miller, and D. Rind, Northern Hemisphere winter climate response to greenhouse gas, ozone, solar, and volcanic forcing, *J. Geophys. Res.*, 106 (D7), 7193-7210, 2001.
- Shindell, D.T., G.A. Schmidt, R.L. Miller, and M.E. Mann, Volcanic and solar forcing of climate change during the preindustrial era, *J. Clim.*, 16 (24), 4094-4107, 2003.
- Singh, S., and R. Singh, High-altitude clear-sky direct solar ultraviolet irradiance at Leh and Hanle in the western Himalayas: Observations and model calculations, *J. Geophys. Res.*, 109, D19201, doi: 10.1029/2004JD004854, 2004.
- Skupin, J., S. Noël, M.W. Wuttke, H. Bovensmann, and J.P. Burrows, Calibration of SCIAMACHY in-flight measured irradiances and radiances—first results of level 1 validation, in *Proceedings of the Envisat Validation Workshop, Frascati, Italy, 9-13 December 2002, Report SP-531*, ESA Publications Division, 2003.
- Slaper, H., G.J.M. Velders, J.S. Daniel, F.R. de Groot, and J.C. van der Leun, Estimates of ozone depletion and skin cancer incidence to examine the Vienna convention achievements, *Nature*, 384 (6606), 256-258, 1996.
- Slaper, H., P.N. den Outer, J. Williams, A. Bais, J. Kaurola, T. Koskela, K. Lakkala, G. Seckmeyer, and P. Weihs, Towards a European UV-climatology utilising ground-based and satellite based analysis, in *Ozone Vol. I, Proceedings of the XX Quadrennial Ozone Symposium*, 1-8 June 2004, Kos, Greece, edited by C.S. Zerefos, 249-250, Int. Ozone Comm., Athens, Greece, 2004.
- Smith, R.E.H., C.D. Allen, and M.N. Charlton, Dissolved organic matter and ultraviolet radiation penetration in the Laurentian Great Lakes and tributary waters, *J. Great Lakes Res.*, 30 (3), 367-380, 2004.
- Smolskaia, I., D. Masserot, J. Lenoble, C. Brogniez, and A. de la Casinière, Retrieval of the ultraviolet effective snow albedo during 1998 winter campaign in the French Alps, *Appl. Opt.*, 42 (9), 1583-1587, 2003.
- Solanki, S.K., I.G. Usoskin, B. Kromer, M. Schüssler, and J. Beer, Unusual activity of the Sun during recent decades compared to the previous 11,000 years, *Nature*, 431 (7011), 1084-1087, 2004.
- Soon, W., E. Posmentier, and S. Baliunas, Climate hypersensitivity to solar forcing?, *Ann. Geophys.*, 18 (5), 583-588, 2000.
- Sperfeld, P., K.D. Stock, K.-H. Raatz, B. Nawo, and J. Metzendorf, Characterization and use of deuterium lamps as transfer standards of spectral irradiance, *Metrologia*, 40, S111-S114, 2003.
- Staiger, H., and P. Koepke, UV Index forecasting on a global scale, *Meteorol. Z.*, 14 (2), 259-270, 2005.
- Staiger, H., G. Vogel, U. Schubert, R. Kirchner, G. Lux, and G. Jendritzky, *UV Index Calculation by the Deutscher Wetterdienst and Dissemination of UV Index Products, (Report of the WMO-WHO Meeting of Experts on Standardization of UV Indices and their Dissemination to the Public, 21-24 July 1997)*, Global Atmosphere Watch, Report No. 127, 89-92, 1998.
- Stenchikov, G., K. Hamilton, A. Robock, V. Ramaswamy, and M.D. Schwarzkopf, Arctic oscillation response to the 1991 Pinatubo eruption in the SKYHI general circulation model with a realistic quasi-biennial oscillation, *J. Geophys. Res.*, 109, D03112, doi: 10.1029/2003JD003699, 2004.
- Su, W., T.P. Charlock, and F.G. Rose, Deriving surface ultraviolet radiation from CERES surface and atmospheric radiation budget: Methodology, *J. Geophys. Res.*, 110, D14209, doi: 10.1029/2005JD005794, 2005.
- Taalas, P., J. Kaurola, A. Kylling, D. Shindell, R. Sausen, M. Dameris, V. Grewe, J. Herman, J. Damski, and B. Steil, The impact of greenhouse gases and halogenated species on future solar UV radiation doses, *Geophys. Res. Lett.*, 27 (8), 1127-1130, 2000.
- Tanskanen, A., A. Arola, and J. Kujanpaa, Use of the moving time-window technique to determine surface albedo from TOMS reflectivity data, *Proc. SPIE*, 4896, 239-250, 2003.
- Tanskanen, A., N.A. Krotkov, J.R. Herman, and A. Arola, Surface ultraviolet irradiance from OMI, *IEEE Trans. Geosci. Rem. Sens.*, 44 (5), 1267-1271, 2006.
- Tarasick, D.W., V.E. Fioletov, D.I. Wardle, J.B. Kerr, L.J.B. McArthur, and C.A. McLinden, Climatology and trends of surface UV radiation, *Atmos. Ocean*,

- 41 (2), 121-138, 2003.
- Thuillier, G., M. Hersé, P.C. Simon, D. Labs, H. Mandel, and D. Gillotay, Observation of the UV solar spectral irradiance between 200 and 350 nm during the ATLAS I mission by the SOLSPEC spectrometer, *Sol. Phys.*, 171 (2), 283-302, 1997.
- Thuillier, G., M. Hersé, P.C. Simon, D. Labs, H. Mandel, and D. Gillotay, Observation of the solar spectral irradiance from 200 nm to 870 nm during the ATLAS 1 and ATLAS 2 missions by the SOLSPEC spectrometer, *Metrologia*, 35 (4), 689-695, 1998.
- Thuillier, G., L. Floyd, T.N. Woods, R. Cebula, E. Hilsenrath, M. Hersé, and D. Labs, Solar irradiance reference spectra for two solar active levels, *Adv. Space Res.*, 34 (2), 256-261, 2004.
- Topaloglou, C., S. Kazadzis, A.F. Bais, M. Blumthaler, B. Schallhart, and D. Balis, NO₂ and HCHO photolysis frequencies from irradiance measurements in Thessaloniki, Greece, *Atmos. Chem. Phys.*, 5, 1645-1653, 2005.
- Torres, O., P.K. Bhartia, J.R. Herman, A. Sinyuk, P. Ginoux, and B. Holben, A long-term record of aerosol optical depth from TOMS observations and comparison to AERONET measurements, *J. Atmos. Sci.*, 59 (3), 398-413, 2002.
- Torres, O., P.K. Bhartia, A. Sinyuk, E.J. Welton, and B. Holben, Total Ozone Mapping Spectrometer measurements of aerosol absorption from space: Comparison to SAFARI 2000 ground-based observations, *J. Geophys. Res.*, 110, D10S18, doi: 10.1029/2004JD004611, 2005.
- Tourpali, K., C.J.E. Schuurmans, R. van Dorland, B. Steil, and C. Brühl, Stratospheric and tropospheric response to enhanced solar UV radiation: A model study, *Geophys. Res. Lett.*, 30 (5), 1231, doi: 10.1029/2002GL016650, 2003.
- Trautmann, T., I. Podgorny, J. Landgraf, and P.J. Crutzen, Actinic fluxes and photodissociation coefficients in cloud fields embedded in realistic atmospheres, *J. Geophys. Res.*, 104 (D23), 30173-30192, 1999.
- Trepte, S., and P. Winkler, Reconstruction of erythemal UV irradiance and dose at Hohenpeissenberg (1968-2001) considering trends of total ozone, cloudiness and turbidity, *Theor. Appl. Climatol.*, 77 (3-4), 159-171, 2004.
- Vaglieco, B.M., S.S. Merola, A. D'Anna, and A. D'Alessio, Spectroscopic analysis and modeling of particulate formation in a diesel engine, *J. Quant. Spectrosc. Radiat. Transf.*, 73 (2-5), 443-450, 2002.
- van Weele, M., T.J. Martin, M. Blumthaler, C. Brogniez, P.N. den Outer, O. Engelsen, J. Lenoble, B. Mayer, G. Pfister, A. Ruggaber, B. Walravens, P. Weihs, B.G. Gardiner, D. Gillotay, D. Hafnerl, A. Kylling, G. Seckmeyer, and W.M.F. Wauben, From model intercomparison toward benchmark UV spectra for six real atmospheric cases, *J. Geophys. Res.*, 105 (D4), 4915-4925, 2000.
- Vasilkov, A.P., J. Joiner, J. Gleason, and P.K. Bhartia, Ocean Raman scattering in satellite backscatter UV measurements, *Geophys. Res. Lett.*, 29 (17), 1837, doi: 10.1029/2002GL014955, 2002.
- Vasilkov, A.P., J.R. Herman, Z. Ahmad, M. Kahru, and B.G. Mitchell, Assessment of the ultraviolet radiation field in ocean waters from space-based measurements and full radiative-transfer calculations, *Appl. Opt.*, 44 (14), 2863-2869, 2005.
- Vasseur, C., B. Mostajir, C. Nozais, M. Denis, E. Fouilland, B. Klein, and S. Demers, Effects of bio-optical factors on the attenuation of ultraviolet and photosynthetically available radiation in the North Water Polynya, northern Baffin Bay: ecological implications, *Mar. Ecol. Prog. Ser.*, 252, 1-13, 2003.
- Verdebot, J., A European satellite-derived UV climatology available for impact studies, *Radiat. Prot. Dosim.*, 111 (4), 407-411, 2004a.
- Verdebot, J., A satellite-derived UV radiation climatology over Europe to support impact studies, *Arct. Antarct. Alp. Res.*, 36 (3), 357-363, 2004b.
- Wang, P., A. Richter, M. Bruns, J.P. Burrows, W. Junkermann, K.-P. Heue, T. Wagner, U. Platt, and I. Pundt, Airborne multi-axis DOAS measurements of tropospheric SO₂ plumes in the Po-valley, Italy, *Atmos. Chem. Phys. Disc.*, 5, 2017-2045, 2005a.
- Wang, P., A. Richter, M. Bruns, V.V. Rozanov, J.P. Burrows, K.-P. Heue, T. Wagner, I. Pundt, and U. Platt, Measurements of tropospheric NO₂ with an airborne multi-axis DOAS instrument, *Atmos. Chem. Phys.*, 5, 337-343, 2005b.
- Weatherhead, E.C., G.C. Reinsel, G.C. Tiao, X.-L. Meng, D. Choi, W.-K. Cheang, T. Keller, J. DeLuisi, D.J. Wuebbles, J.B. Kerr, A.J. Miller, S.J. Oltmans, and J.E. Frederick, Factors affecting the detection of trends: Statistical considerations and applications to environmental data, *J. Geophys. Res.*, 103 (D14), 17149-17161, 1998.
- Webb, A.R., A.F. Bais, M. Blumthaler, G.P. Gobbi, A. Kylling, R. Schmitt, S. Thiel, F. Barnaba, T. Danielsen, W. Junkermann, A. Kazantzidis, P. Kelly, R. Kift, G.L. Liberti, M. Misslbeck, B. Schallhart, J. Schreder, and C. Topaloglou, Measuring spectral actinic flux and irradiance: Experimental results from the Actinic Flux Determination from Measurements of Irradiance (ADMIRA) project, *J. Atmos. Ocean. Tech.*, 19 (7),

SURFACE ULTRAVIOLET RADIATION

- 1049-1062, 2002a.
- Webb, A.R., R. Kift, S. Thiel, and M. Blumthaler, An empirical method for the conversion of spectral UV irradiance measurements to actinic flux data, *Atmos. Environ.*, *36* (27), 4397-4404, 2002b.
- Webb, A., B.G. Gardiner, K. Leszczynski, V.A. Mohnen, P. Johnston, N. Harrison, and D. Bigelow, *Quality Assurance in Monitoring Solar Ultraviolet Radiation: the State of the Art*, *Global Atmosphere Watch, Report No. 146*, Geneva, Switzerland, 2003.
- Webb, A.R., A. Kylling, M. Wendisch, and E. Jäkel, Airborne measurements of ground and cloud spectral albedos under low aerosol loads, *J. Geophys. Res.*, *109*, D20205, doi: 10.1029/2004JD004768, 2004.
- Weihls, P., Influence of ground reflectivity and topography on erythemal UV radiation on inclined planes, *Int. J. Biometeorol.*, *46* (2), 95-104, 2002.
- Wendisch, M., P. Pilewskie, E. Jäkel, S. Schmidt, J. Pommier, S. Howard, H.H. Jonsson, H. Guan, M. Schröder, and B. Mayer, Airborne measurements of areal spectral surface albedo over different sea and land surfaces, *J. Geophys. Res.*, *109*, D08203, doi: 10.1029/2003JD004392, 2004.
- Wetzel, M.A., G.E. Shaw, J.R. Slusser, R.D. Borys, and C.F. Cahill, Physical, chemical, and ultraviolet radiative characteristics of aerosol in central Alaska, *J. Geophys. Res.*, *108* (D14), 4418, doi: 10.1029/2002JD003208, 2003.
- WHO (World Health Organization), *Ultraviolet Radiation: An Authoritative Scientific Review of Environmental and Health Effects of UV, with Reference to Global Ozone Layer Depletion, Environmental Health Criteria 160*, 352 pp., Geneva, Switzerland, 1994.
- Wild, M., H. Gilgen, A. Roesch, A. Ohmura, C.N. Long, E.G. Dutton, B. Forgan, A. Kallis, V. Russak, and A. Tsvetkov, From dimming to brightening: Decadal changes in solar radiation at Earth's surface, *Science*, *308* (5723), 847-850, 2005.
- Wild, O., X. Zhu, and M.J. Prather, Fast-J: Accurate simulation of in- and below-cloud photolysis in tropospheric chemical models, *J. Atmos. Chem.*, *37* (3), 245-282, 2000.
- Williams, J.E., P.N. den Outer, H. Slaper, J. Matthijsen, and G. Kelfkens, Cloud induced reduction of solar UV-radiation: A comparison of ground-based and satellite based approaches, *Geophys. Res. Lett.*, *31*, L03104, doi: 10.1029/2003GL018242, 2004.
- Winiacki, S., and J.E. Frederick, Ultraviolet radiation and clouds: Couplings to tropospheric air quality, *J. Geophys. Res.*, *110*, D22202, doi: 10.1029/2005JD006199, 2005.
- WMO (World Meteorological Organization), *Report of the WMO Meeting of Experts on UV-B Measurements, Data Quality and Standardization of UV Indices, (Les Diablerets, Switzerland, 25-28 July 1994)*, *Global Atmosphere Watch, Report No. 95*, Geneva, Switzerland, 1994.
- WMO (World Meteorological Organization), *Report of the WMO Meeting of Experts on Standardization of UV Indices and their Dissemination to the Public, (Les Diablerets, Switzerland, 21-24 July 1997)*, *Global Atmosphere Watch, Report No. 127*, Geneva, Switzerland, 1998.
- WMO (World Meteorological Organization), *Scientific Assessment of Ozone Depletion: 1998, Global Ozone Research and Monitoring Project-Report No. 44*, Geneva, Switzerland, 1999.
- WMO (World Meteorological Organization), *Scientific Assessment of Ozone Depletion: 2002, Global Ozone Research and Monitoring Project-Report No. 47*, Geneva, Switzerland, 2003.
- Wuttke, S., and G. Seckmeyer, Spectral radiance and sky luminance in Antarctica: A case study, *Theor. Appl. Climatol.*, *85* (3-4), 131-148, doi: 10.1007/s00704-005-0188-2, 2006.
- Wuttke, S., J. Verdebout, and G. Seckmeyer, An improved algorithm for satellite-derived UV radiation, *Photochem. Photobiol.*, *77* (1), 52-57, 2003.
- Wuttke, S., G. Bernhard, J.C. Ehranjian, R. McKenzie, P. Johnston, G. Seckmeyer, M. O'Neil, and G. Seckmeyer, New spectroradiometers complying with the NDSC standards, *J. Atmos. Ocean. Tech.*, *23* (2), 241-251, 2006.
- Ylianttila, L., and J. Schreder, Temperature effects of PTFE diffusers, *Opt. Mater.*, *27* (12), 1811-1814, 2005.
- Yoon, H.W., C.E. Gibson, and P.Y. Barnes, Realization of the National Institute of Standards and Technology detector-based spectral irradiance scale, *Appl. Opt.*, *41* (28), 5879-5890, 2002.
- Zaratti, F., R.N. Forno, J. García Fuentes, and M.F. Andrade, Erythemally weighted UV variations at two high-altitude locations, *J. Geophys. Res.*, *108* (D9), 4623, doi: 10.1029/2001JD000918, 2003.
- Zerefos, C.S., Long-term ozone and UV variations at Thessaloniki, Greece, *Phys. Chem. Earth*, *27* (6), 455-460, 2002.
- Zerefos, C., D. Balis, M. Tzortziou, A. Bais, K. Tourpali, C. Meleti, G. Bernhard, and J. Herman, A note on the interannual variations of UV-B erythemal doses and solar irradiance from ground-based and satellite observations, *Ann. Geophys.*, *19* (1), 115-120, 2001.

Appendix 7A

SPECTRAL DATA AVAILABLE FROM DATABASES

7A.1 World Ozone and Ultraviolet Radiation Data Centre (WOUDC) ^a

Station	Name	Instrument	Country	Institute ^b	Lat. (°N)	Long. (°E)	Start Date
7	Kagoshima	Brewer	Japan	JMA	31.58	130.56	01/01/1991
12	Sapporo	Brewer	Japan	JMA	43.06	141.33	01/01/1991
14	Tateno / Tsukuba	Brewer	Japan	JMA	36.06	140.10	01/01/1990
18	Alert	Brewer	Canada	MSC	82.50	-62.32	09/06/1995
21	Edmonton / Stony Plain	Brewer	Canada	MSC	53.55	-114.10	19/03/1992
24	Resolute	Brewer	Canada	MSC	74.72	-94.98	14/03/1991
31	Mauna Loa	Brewer	United States	MSC	19.53	-155.57	24/03/1997
31	Mauna Loa	Brewer	United States	MSC-MLO	19.53	-155.57	01/01/1998
65	Toronto	Brewer	Canada	MSC	43.78	-79.47	01/03/1989
67	Boulder	Brewer	United States	EPA_UGA ^c	40.08	-105.25	01/01/1997
76	Goose Bay	Brewer	Canada	MSC	53.30	-60.36	01/01/1997
77	Churchill	Brewer	Canada	MSC	58.75	-94.07	30/03/1992
95	Taipei	Brewer	Taiwan	CWBT	25.02	121.47	06/03/1992
101	Syowa	Brewer	Japan	JMA	-69.00	39.58	01/01/1993
190	Naha	Brewer	Japan	JMA	26.20	127.68	01/01/1991
241	Saskatoon	Brewer	Canada	MSC	52.11	-106.71	01/01/1991
290	Saturna Island	Brewer	Canada	MSC	48.78	-123.13	03/10/1990
301	JRC Ispra (Varese)	Brewer	Italy	JRC_EU	45.80	8.63	01/01/2001
306	Chengkung	Brewer	Taiwan	CWBT	23.10	121.36	02/01/1992
307	Obninsk	Brewer	Russia	IEM-SPA	55.12	36.30	06/05/1993
315	Eureka	Brewer	Canada	MSC	80.04	-86.17	10/02/2001
319	Montreal (Dorval)	Brewer	Canada	MSC	45.48	-73.75	06/03/1993
320	Winnipeg	Brewer	Canada	MSC	49.90	-97.24	06/07/1992
321	Halifax (Bedford)	Brewer	Canada	MSC	44.70	-63.61	01/07/1992
331	Poprad-Ganovce	Brewer	Slovakia	SHMI	49.03	20.32	01/01/1994
332	Poyang	Brewer	Korea	KMA	36.03	129.38	27/01/1994
338	Bratts Lake (Regina)	Brewer	Canada	MSC	50.20	-104.70	01/01/1995
353	Reading	Optronic	United Kingdom	UMIST	51.45	0.93	27/01/1994
377	Research Triangle Park	Brewer	United States	EPA_UGA ^c	35.89	-78.87	10/09/1996
379	Gaithersburg	Brewer	United States	EPA_UGA	39.13	-77.21	01/01/1996
380	Atlanta	Brewer	United States	EPA_UGA	33.75	-84.41	30/05/1996
382	Riverside	Brewer	United States	EPA_UGA	34.00	-117.34	01/01/1996
383	Big Bend	Brewer	United States	EPA_UGA	29.31	-103.18	20/02/1997
384	Great Smokey Mountains	Brewer	United States	EPA_UGA	35.60	-83.78	03/01/1997
385	Canyonlands	Brewer	United States	EPA_UGA	38.47	-109.82	31/07/1997
386	Glacier	Brewer	United States	EPA_UGA	48.51	-113.99	18/09/1997
387	Everglades	Brewer	United States	EPA_UGA	25.39	-80.68	24/02/1997
388	Shenandoah	Brewer	United States	EPA_UGA	38.52	-78.44	05/03/1997
389	Acadia	Brewer	United States	EPA_UGA	44.38	-68.26	04/03/1998
390	Denali	Brewer	United States	EPA_UGA	63.73	-148.97	04/10/1997

SURFACE ULTRAVIOLET RADIATION

391	Virgin islands	Brewer	Virgin Islands	EPA_UGA	18.34	-64.79	25/05/1998
392	Rocky Mountain Natl. Park	Brewer	United States	EPA_UGA	40.03	-105.53	30/05/1998
393	Olympic	Brewer	United States	EPA_UGA	48.14	-123.40	11/12/1997
402	Theodore	Brewer	United States	EPA_UGA	46.90	-103.38	29/09/1998
463	Sequoia	Brewer	United States	EPA_UGA	36.49	-118.82	20/08/1998
465	Kilauea	Brewer	United States	EPA_UGA	19.42	-155.29	18/02/1999

^a Website: <http://www.msc-smc.ec.gc.ca/woudc/>

^b JMA, Japan Meteorological Agency; MSC, Meteorological Service of Canada; EPA_UGS, Environmental Protection Agency, University of Georgia, Athens, USA; CWBT, Central Weather Bureau of Taiwan; JRC_EU, Joint Research Centre of the European Union; IEM-SPA, Institute of Experimental Meteorology-Scientific Hydrometeorological Institute; SHMI, Slovakian Hydrometeorological Institute; KMA, Korean Meteorological Administration; UM, University of Manchester.

^c The Brewer spectrophotometers operated by EPA have ceased operation after 2004.

7A.2 European Ultraviolet Database (EUVDDB) ^a

No.	Station Name	Instrument	Country	Institute ^b	Lat. (°N)	Long. (°E)	Start Date
1	Sonnblick	Bentham	Austria	BOKU	47.05	12.97	Feb. 96
2	Vienna	Bentham	Austria	BOKU	48.23	16.35	Feb. 98
3	Uccle Brussels	Jobin Yvon	Belgium	IASB	50.80	4.36	Mar. 93
4	Hradec Kralove	Brewer	Czech Republic	CHI	50.19	15.83	Jan. 94
5	Jokioinen	Brewer	Finland	FMI	60.81	23.50	Mar. 95
6	Sodankylä	Brewer	Finland	FMI	67.37	26.63	Apr. 90
7	Briançon	Jobin Yvon	France	USTL	44.90	6.65	Sep. 99
8	Villeneuve d.Asq	Jobin Yvon	France	USTL	50.37	3.01	May 97
9	Neuherberg	Bentham	Germany	BfS	48.22	11.58	Mar. 00
10	Offenbach	Bentham	Germany	BfS	50.10	8.75	Jan. 00
11	Hohenpeissenberg	Brewer	Germany	DWD	47.80	11.02	Jan. 95
12	Lindenberg	Brewer	Germany	DWD	52.22	14.12	Jan. 95
13	Potsdam	Brewer	Germany	DWD	52.36	13.08	Jan. 95
14	Garmisch-Partenkirchen	Bentham	Germany	IFU	47.48	11.07	Apr. 94
15	Zugspitze	Bentham	Germany	IFU	47.42	10.98	Jul. 97
16	Thessaloniki	Brewer	Greece	LAP	40.52	22.97	Oct. 89
17	Lampedusa	Brewer	Italy	ENEA	35.50	12.60	Jan. 98
18	Ispira	Brewer	Italy	JRC	45.81	8.63	Aug. 91
19	Rome	Brewer	Italy	URO	41.90	12.52	Feb. 92
20	Andøya	Bentham	Norway	NILU	69.48	16.02	Feb. 98
21	Oesteraas	Bentham	Norway	NRPA	59.92	10.75	Jun. 99
22	Trondheim	Optronic	Norway	NTNU	64.43	10.47	Aug. 97
23	Tromsø	Brewer	Norway	UT	69.66	18.93	May 95
24	Belsk	Brewer	Poland	IGFPAS	51.83	20.78	Jan. 93
25	Azores Island	Brewer	Portugal	IM	38.66	-27.22	Jul. 92
26	Funchal (Madeira Is.)	Brewer	Portugal	IM	32.64	-16.89	Jan. 90
27	Lisbon	Brewer	Portugal	IM	38.77	-9.15	Jan. 90
28	Penhas Douradas	Brewer	Portugal	IM	40.42	-7.55	Oct. 94
29	Izana	Brewer	Spain	INM	28.49	-16.50	Jan. 95
30	Norrköping	Brewer	Sweden	SMHI	58.58	16.15	Sep. 91
31	Vindeln	Brewer	Sweden	SMHI	64.23	19.77	Jul. 96
32	De Bilt	Brewer	Netherlands	KNMI	52.10	5.18	Jan. 94
33	RIVM (Bilthoven)	Dilor XY-50	Netherlands	RIVM	52.12	5.20	Jan. 96
34	Reading	Optronics	United Kingdom	UM	51.45	0.93	Jan. 93

Only permanent stations are listed; campaign data are not included.

^a Website: <http://uvdb.fmi.fi/uvdb/index.html>

^b BOKU, Universität für Bodenkultur Wein; IASB, Institut d'Aéronomie Spatiale de Belgique; CHI, Czech Hydrometeorological Institute; FMI, Finnish Meteorological Institute; USTL, Université des Sciences et Technologies de Lille; BfS, Bundesamt für Strahlenschutz; DWD, Deutscher Wetterdienst; IFU, Atmosphärische Umweltforschung; LAP, Laboratory of Atmospheric Physics; ENEA, Ente per le Nuove Technologie, l'Energia e l'Ambiente; JRC, Joint Research Centre, European Union; URO, University of Rome; NILU, Norsk Institutt for Luftforskning; NRPA, Norwegian Radiation Protection Authority; NTNU, Norges Teknisk-Naturvitenskapelige Universitet; UT, University of Tromsø; IGFPAS, Institute of Geophysics, Polish Academy of Sciences; IM, Institute of Meteorology, Portugal; INM, Instituto Nacional de Meteorologia; SMHI, Swedish Meteorological and Hydrological Institute; KNMI, Koninklijk Nederlands Meteorologische Instituut; RIVM, Rijkinstituut voor Volksgezandheid en Milieu; UM, University of Manchester.

SURFACE ULTRAVIOLET RADIATION

7A.3 U.S. National Science Foundation UV Monitoring Network ^a

No.	Station Name	Instrument	Country	Institute ^b	Lat. (°N)	Long. (°E)	Start Date ^c
1	Arrival Heights	Biospherical	Antarctica	NSF	-77.83	166.67	13/12/1989
2	Palmer	Biospherical	Antarctica	NSF	-64.77	-64.05	14/03/1990
3	South Pole ^d	Biospherical	Antarctica	NSF	-90.00	80.00	31/01/1991
4	Ushuaia	Biospherical	Argentina	NSF	-54.82	-68.32	13/09/1990
5	San Diego	Biospherical	United States	NSF	32.77	-117.20	28/10/1992
6	Barrow	Biospherical	United States	NSF	71.32	-156.68	14/01/1991
7	Summit	Biospherical	Greenland	NSF	72.58	-38.46	15/08/2004

^a Website: <http://www.biospherical.com/NSF/>

^b Stations 1-6 are equipped with SUV-100 spectroradiometers. Station 7 (Summit) is equipped with a SUV-150B spectroradiometer.

^c Date from which data are available. Instruments may have been installed before this date.

^d The system at the South Pole was relocated by approximately 200 m in January 1997. Due to the proximity of the instrument to the geographic South Pole and the movement of the polar ice cap over the bedrock, the azimuth position of the instrument has changed from 84.5°E in January 1997 to 72.5°E in January 2006.

Appendix 7B

INTERNET ADDRESSES FOR UV SITES

7B.1 General UV Information

WMO UV radiation page	http://www.srrb.noaa.gov/UV/
TOMS (ozone and UV satellite data)	http://toms.gsfc.nasa.gov/
OMI (Ozone Monitoring Instrument)	http://aura.gsfc.nasa.gov/instruments/omi/index.html
NSF UV monitoring network, U.S.	http://www.biospherical.com/NSF/
USDA UV-B monitoring and research program	http://uvb.nrel.colostate.edu/
NIWA, New Zealand	http://www.niwascience.co.nz/services/uvozone/
EPA, U.S.	http://www.epa.gov/uvnet/
EPA SunWise School Program	http://www.epa.gov/sunwise/
WMO Ozone Bulletins	http://www.wmo.ch/web/arep/ozone.html
Center for International Earth Science	http://sedac.ciesin.columbia.edu/ozone/
World Radiation Centre	http://wrdc-mgo.nrel.gov/

7B.2 International UV Projects

World Ozone and UV Data Center	http://www.msc-smc.ec.gc.ca/woudc/
European Cooperation in the Field of Scientific and Technical Research (COST-726)	http://i115srv.vu-wien.ac.at/uv/COST726/Cost726.htm
EDUCE, European Commission	http://www.muk.uni-hannover.de/EDUCE/
Thematic Network For Ultraviolet Measurements	http://metrology.hut.fi/uvnet/
QASUME, European Communities	http://lap.physics.auth.gr/qasume/
Stratospheric-Climatic Links with Emphasis on the Upper Troposphere and Lower Stratosphere (SCOUT-O ₃)	http://www.ozone-sec.ch.cam.ac.uk/scout_o3/index.html
UV Index & UV dose based on GOME (TEMIS)	http://www.temis.nl/uvradiation/

7B.3 Radiative Transfer Codes

Tropospheric Ultraviolet Visible (TUV) (Madronich and Flocke, 1997)	http://cprm.acd.ucar.edu/Models/TUV/
Library for Radiative Transfer (libRadTran) (Mayer and Kylling, 2005)	http://www.libradtran.org/
System for Transfer of Atmospheric Radiation (STAR) (Koepke et al., 2005)	http://www.meteo.physik.uni-muenchen.de/strahlung/uvrad/Star/starprog.html
Fast and Easy Radiative Transfer (FASTRT)	http://zardoz.nilu.no/~olaeng/fastrt/fastrt.html
Santa Barbara Discrete-Ordinate Atmospheric Radiative Transfer (SBDART) (Ricchiazzi et al., 1998)	http://arm.mrcsb.com/sbdart/
Streamer model (Key, 1999)	http://stratus.ssec.wisc.edu/streamer/streamer.html
SCIATRAN code (Rozanov et al., 2005)	http://www.iup.physik.uni-bremen.de/sciatran/
3-D Spherical Harmonics Discrete Ordinate Method (SHDOM) model (Evans, 1998)	http://nit.colorado.edu/~evans/shdom.html

7B.4 Extraterrestrial Spectra

Solar Ultraviolet Spectral Irradiance Monitor (SUSIM)	http://wwwsolar.nrl.navy.mil/susim_atlas_data.html
Solar Stellar Irradiance Comparison Experiment (SOLSTICE)	http://lasp.colorado.edu/solstice/
McMath/Pierce at Kitt Peak	ftp://ftp.noao.edu/fts/fluxat/
The New Synthetic Gueymard Spectrum (Gueymard, 2004)	http://rredc.nrel.gov/solar/spectra/am0/special.html#newgueymard

SURFACE ULTRAVIOLET RADIATION

7B.5 Internet Sites with UV Information

Argentina	http://www.conae.gov.ar/uv/uv.html http://www.meteofa.mil.ar
Australia (BOM)	http://www.bom.gov.au/info/about_uv_b.shtml
Australia (ARPANSA)	http://www.arpansa.gov.au/is_uvindex.htm
Australia (SunSmart)	http://www.sunsmart.com.au/
Austria (University Vienna)	http://www-med-physik.vu-wien.ac.at/uv/uv_online.htm
Austria (University Innsbruck)	http://www.uv-index.at/
Belgium	http://ozone.meteo.be/uv/index.php
Brazil	http://www.master.iag.usp.br/ind.php?inic=00&prod=indiceuv
Canada	http://www.msc-smc.ec.gc.ca/education/uvindex/forecasts/index_e.html
Catalonia	http://www.meteocat.com/marcs/marcos_previsio/marcs_uvi.htm
Chile	http://www.meteochile.cl/
Czech Republic	http://www.chmi.cz/meteo/ozon/o3uvb-e.html
Denmark	http://www.dmi.dk/vejir/index_sol.html
European Commission (JRC)	http://ecuv.jrc.it/
Finland	http://www.fmi.fi/research_atmosphere/atmosphere_2.html
France	http://www.soleil.info/main.php
Germany (DWD)	http://www.uv-index.de/
Germany (BfS)	http://www.bfs.de/uv
Greece	http://www.uvnet.gr
Hong Kong	http://www.hko.gov.hk/wxinfo/uvfcst/uvfcst.htm
Israel	http://www.ims.gov.il/en2.htm#1
Italy	http://www.lamma.rete.toscana.it/previ/eng/uvhtm/uvnew0.html
Japan	http://www.jma.go.jp/en/uv/index.html
Luxembourg	http://www.restena.lu/meteo_lcd/
Netherlands	http://www.temis.nl/uvradiation/index.html
New Zealand	http://www.niwascience.co.nz/services/uvozone/
Norway	http://uvnett.nrpa.no/uv/
Poland	http://www.ingw.pl/wl/internet/zz/index.html
Portugal	http://www.meteo.pt/en/previsao/uv/prev_uv_d0.jsp
Slovenia	http://www.rzs-hm.si/zanimivosti/UV.htm
South Africa	http://www.weathersa.co.za/uv/uv.jsp
Spain	http://infomet.am.ub.es/uv_i_ozo/uvi.html
Sweden	http://www.smhi.se/weather/uvindex/index.htm
Switzerland	http://www.uv-index.ch/de/home.php
Taiwan	http://www.epa.gov.tw/monitoring/1-1/uv.htm
United Kingdom	http://www.m-office.gov.uk/weather/uv/
United States (NOAA)	http://www.cpc.ncep.noaa.gov/products/stratosphere/uv_index/
United States (EPA)	http://www.epa.gov/sunwise/uvindex.html
World Health Organization (WHO)	http://www.who.int/mediacentre/factsheets/fs271/en/index.html
Intersun (WHO)	http://www.who.int/uv/en/

CHAPTER 8

Halocarbon Scenarios, Ozone Depletion Potentials, and Global Warming Potentials

Lead Authors:

J.S. Daniel
G.J.M. Velders

Coauthors:

A.R. Douglass
P.M.D. Forster
D.A. Hauglustaine
I.S.A. Isaksen
L.J.M. Kuijpers
A. McCulloch
T.J. Wallington

Contributors:

P. Ashford
S.A. Montzka
P.A. Newman
D.W. Waugh

CHAPTER 8

HALOCARBON SCENARIOS, OZONE DEPLETION POTENTIALS, AND GLOBAL WARMING POTENTIALS

Contents

SCIENTIFIC SUMMARY	8.1
8.1 INTRODUCTION	8.5
8.2 HALOCARBON LIFETIMES, OZONE DEPLETION POTENTIALS, AND GLOBAL WARMING POTENTIALS	8.5
8.2.1 Introduction	8.5
8.2.2 Ozone Depletion Potentials	8.5
8.2.2.1 Atmospheric Lifetimes	8.6
8.2.2.2 Fractional Release Factors	8.6
8.2.2.3 Ozone Destruction Effectiveness	8.7
8.2.2.4 ODP Values	8.8
8.2.3 Direct Global Warming Potentials	8.8
8.2.4 Degradation Products and Their Implications for ODPs and GWPs	8.13
8.3 FUTURE HALOCARBON SOURCE GAS CONCENTRATIONS	8.13
8.3.1 Introduction	8.13
8.3.2 Baseline Scenario (A1)	8.15
8.3.2.1 Emissions	8.15
8.3.2.2 Mixing Ratios	8.21
8.3.2.3 Equivalent Effective Stratospheric Chlorine	8.25
8.3.3 Alternative Projections	8.28
8.3.3.1 Emissions	8.28
8.3.3.2 Mixing Ratios	8.28
8.3.3.3 Equivalent Effective Stratospheric Chlorine	8.30
8.3.4 Uncertainties in ODS Projections	8.32
8.4 OTHER PROCESSES RELEVANT TO FUTURE OZONE EVOLUTION	8.34
8.5 INDIRECT GWPS	8.35
REFERENCES	8.36

SCIENTIFIC SUMMARY

Ozone Depletion Potentials and Global Warming Potentials

- **The effectiveness of bromine compared with chlorine on a per-atom basis for global ozone depletion, typically referred to as α , has been re-evaluated upward from 45 to a value of 60.** The calculated values from three independent two-dimensional models range between 57 and 73, depending on the model used and depending on the assumed amount of additional bromine added to the stratosphere by very short-lived substances (VSLs).
- **Semi-empirical Ozone Depletion Potentials (ODPs) have been re-evaluated, with the most significant change being a 33% increase for bromocarbons due to the update in the estimate for the value of α .** A calculation error in the previous Assessment, which led to a 13% overestimate in the halon-1211 ODP, has been corrected.
- **Direct Global Warming Potentials (GWPs) have been updated to account for revised radiative efficiencies (HFC-134a, carbon tetrafluoride (CF₄), HFC-23, HFC-32, HFC-227ea, and nitrogen trifluoride (NF₃)) and revised lifetimes (trifluoromethylsulfurhexafluoride (SF₅CF₃) and methyl chloride (CH₃Cl)).** In addition, the direct GWPs for all compounds have been affected by slight decreases in the carbon dioxide (CO₂) absolute Global Warming Potentials for various time horizons.
- **Indirect GWPs have been updated primarily to reflect the later return of ozone-depleting substances (ODSs) to 1980 levels estimated in this Assessment and to account for the increased bromine efficiency factor.** Direct and indirect GWPs are presented separately due to concern over the appropriateness of combining them into net GWPs for application in certain climate change issues.

Projections of Halocarbon Abundances and Implications for Policy Formulation

- **Several of the options evaluated for accelerating the future reduction of ODS abundances demonstrate greater effectiveness than assessed previously.** These options are assessed using equivalent effective stratospheric chlorine (EESC) derived from projections of the atmospheric abundances of ODSs based on historic emissions, observations of concentrations, reported production, estimates of future production, and newly available estimates of the quantities of ODSs present in products in 2002 and 2015.
- **The date when EESC relevant to midlatitude ozone depletion returns to pre-1980 levels is 2049 for the baseline (A1) scenario, about 5 years later than projected in the previous Assessment.** This later return is primarily due to higher estimated future emissions of CFC-11, CFC-12, and HCFC-22. The increase in CFC emissions is due to larger estimated current bank sizes, while the increase in HCFC-22 emissions is due to larger estimated future production.
- **For the polar vortex regions, the return of EESC to pre-1980 conditions is projected to occur around 2065, more than 15 years later than the return of midlatitude EESC to pre-1980 abundances.** This later return is due to the older age of air in the lower stratosphere inside the polar vortex regions. This metric for the polar vortex regions has not been presented in previous ozone Assessments.
- **Three classes of hypothetical cases are presented here to illustrate the maximum potential for reducing midlatitude EESC if anthropogenic production or emission were eliminated after 2006 and if the existing banks at the end of 2006 were fully eliminated.** The sizes of the banks considered for elimination are equal to the total estimated production through 2006 minus all estimated emissions through 2006. These cases are not mutually exclusive, and separate effects of the elimination of production, emissions, and banks are not additive.

The table below shows the percentage reductions in integrated EESC relative to the baseline (A1) scenario that can be achieved in these hypothetical cases (see table footnote 1). EESC is integrated above the 1980 level from 2007 until it returns to the 1980 level (about 2050), and any potential contribution from VSLs is neglected.

HALOCARBON SCENARIOS, ODPs, AND GWPs

Compound or Compound Group	Reduction in Integrated EESC Relative to Baseline Scenario A1 (%)		
	Hypothetical Case A: All Emissions Eliminated from Production after 2006	Hypothetical Case B: All Emissions Eliminated from Existing Banks at End of 2006	Hypothetical Case C: All Emissions Eliminated after 2006
CFCs	0.3	11	11
Halons	0.5	14	14
CCl ₄	3	(a)	3
CH ₃ CCl ₃	0.2	(a)	0.2
HCFCs	12	4	16
CH ₃ Br (anthropogenic)	5	(a)	5

¹ Hypothetical case A corresponds to the elimination of all emissions from production after 2006. Hypothetical case B corresponds to the elimination of all emissions from banks existing at the end of 2006 (for example, capture and destruction). Hypothetical case C corresponds to the elimination of all emissions after 2006 and is approximately equal to the sum of columns A and B.

(a) For these compounds, banks are uncertain and therefore emissions are equated to production in these calculations.

- **The percentage reductions in EESC for halons and CFCs, integrated from 2007 until the 1980 level is reattained (shown in column B), are larger than previously reported.** This is because recent bank estimates from the Intergovernmental Panel on Climate Change/Technology and Economic Assessment Panel (IPCC/TEAP) 2005 Special Report are significantly larger and likely more reliable than values presented in previous Assessments for CFC-11, CFC-12, and halon-1211.
- **The percentage reductions in integrated EESC for HCFCs shown in hypothetical case A are larger than previously reported.** This is because of significantly larger estimates of future HCFC-22 production in Article-5 countries.
- **Evidence suggests that anthropogenic emissions have a stronger influence on atmospheric mixing ratios of CH₃Br than reported in the previous Assessment.** This enhanced sensitivity leads to a greater impact of an elimination of these emissions on EESC. The effect of an elimination of the anthropogenic methyl bromide emission on integrated EESC is about 50% larger than it would have been if the same fractional anthropogenic emission were used as was assumed in the previous Assessment.
- **The hypothetical elimination of all emissions of ODSs after 2006 (hypothetical case C) would accelerate the year EESC is expected to drop below the 1980 value by about 15 years, from 2049 to 2034.** The hypothetical elimination of all emissions from production of ODSs after 2006 (hypothetical case A) would accelerate it by about 6 years, to 2043.
- **Two additional hypothetical cases of critical and exempted (quarantine and pre-shipment, QPS) uses of methyl bromide were considered.** In the analysis of both cases, EESC is integrated above the 1980 level from 2007 until it returns to the 1980 level. A methyl bromide phase-out has been in effect since 2005 in developed countries, with critical-use exemptions granted in 2005 and 2006 at levels that are 30-40% of the 2003-2004 production levels. The size of the critical-use exemptions is similar to the estimated use of methyl bromide for QPS use.
 - **If critical-use exemptions continue indefinitely at the 2006 level compared with a cessation of these exemptions in 2010 or 2015, midlatitude integrated EESC would increase by 4.7% or 4.0%, respectively.**

- If production of methyl bromide for QPS use were to continue at present levels and cease in 2015, mid-latitude integrated EESC would decrease by 3.2% compared with the case of continued production at present levels.

Uncertainties and Sensitivities

- **Recent bank estimates from the IPCC/TEAP (2005) report are significantly larger and likely more reliable than values presented in previous Assessments for some compounds (CFC-11, CFC-12, halon-1211, and halon-1301).** However, there remain potential shortcomings in these new bank estimates that lead to uncertainties in assessing the potential for reducing integrated future EESC.
- **While the future evolution of the ozone layer depends largely on the abundances of ozone-depleting substances, changes in climate arising from natural and anthropogenic causes are likely to also play an important role.** Many of these changes are expected to induce spatially dependent chemical and dynamical perturbations to the atmosphere (Chapters 5 and 6), which could cause ozone to return to 1980 levels earlier or later than when EESC returns to 1980 levels. Furthermore, the changes may alter the lifetimes of the important ozone-depleting substances.

8.1 INTRODUCTION

This chapter provides an update of future halocarbon mixing ratio estimates and of Ozone Depletion Potentials and Global Warming Potentials. Future scenarios of halocarbons are constructed based on the current Montreal Protocol and build on the previous Scientific Assessments of Ozone Depletion (WMO, 1999, 2003) and on the recently published Intergovernmental Panel on Climate Change/Technology and Economic Assessment Panel (IPCC/TEAP) Special Report on *Safeguarding the Ozone Layer and the Global Climate System: Issues Related to Hydrofluorocarbons and Perfluorocarbons* (IPCC/TEAP, 2005). A number of hypothetical cases are presented to demonstrate how halocarbon production and emission, and halocarbons present in current applications, may contribute to the future ozone-depleting substance (ODS) loading of the atmosphere. Uncertainties in future emissions and atmospheric concentrations are discussed, as are the important differences from previous Assessments.

8.2 HALOCARBON LIFETIMES, OZONE DEPLETION POTENTIALS, AND GLOBAL WARMING POTENTIALS

8.2.1 Introduction

Halocarbons released from the Earth's surface become mixed in the lower atmosphere and are transported into the stratosphere by normal air circulation patterns. They are removed from the atmosphere by photolysis, reaction with hydroxyl (OH) radicals (for compounds containing carbon-hydrogen bonds), and for some compounds, uptake by the oceans. Halocarbon molecules that are transported to the stratosphere deposit their degradation products directly. A small fraction of the degradation products from halocarbons destroyed before leaving the troposphere can also be transported to the stratosphere (see Chapter 2). The final degradation products are inorganic halogen species containing fluorine, chlorine, bromine, and iodine atoms. A significant fraction of inorganic chlorine, bromine, and iodine are in the form of X (X = Cl, Br, or I) and XO that participate in efficient ozone destruction in the stratosphere. Fluorine atoms, in contrast, are rapidly converted into hydrogen fluoride (HF), which is a stable reservoir and prevents fluorine from contributing to ozone destruction to any significant degree. Iodine atoms participate in catalytic ozone destruction cycles, but rapid tropospheric loss of iodine-containing compounds limits the amount of iodine reaching the stratosphere (see Chapter 2).

All halocarbons also absorb terrestrial radiation (long-wavelength infrared radiation emitted from the

Earth's surface and by the atmosphere) and contribute to the radiative forcing of climate change. The relative contribution of individual compounds to stratospheric ozone depletion and global warming can be characterized by their Ozone Depletion Potentials (ODPs) and Global Warming Potentials (GWPs), respectively. ODPs and GWPs have been used in past ozone and climate Assessments (IPCC, 1990; 1995; 1996; 2001; 2005; WMO, 1995; 1999; 2003) and in international agreements such as the Montreal Protocol and the Kyoto Protocol.

8.2.2 Ozone Depletion Potentials

Ozone Depletion Potentials are indices that provide a simple way to compare the relative ability of various ODSs to destroy stratospheric ozone (Fisher et al., 1990; Solomon et al., 1992; Wuebbles, 1983). The concept of the ODP has been discussed extensively in previous WMO reports (WMO, 1995; 1999; 2003). ODPs are often calculated assuming steady-state conditions with constant emissions (for compounds that are removed by linear processes, this is equivalent to assuming an emission pulse and integrating over the entire decay of the compound (Prather, 1996; Prather, 2002)) and are not dependent on time. Time-dependent ODPs can also be calculated (Solomon and Albritton, 1992), which reflect the different time scales over which the compound and reference gas (the chlorofluorocarbon CFC-11) liberate chlorine and bromine into the stratosphere. Compounds that have shorter (longer) atmospheric lifetimes than CFC-11 have ODPs that decrease (increase) with increasing integration time.

The ODPs considered here are steady-state ODPs, integrated quantities that are distinct for each halocarbon species. The ODP of a well-mixed ozone-destroying species i is given by:

$$\text{ODP}_i = \frac{\text{global O}_3 \text{ loss due to unit mass emission of } i}{\text{global O}_3 \text{ loss due to unit mass emission of CFC-11}} \quad (8-1)$$

This quantity can be calculated using computer models, with the accuracy depending on the model's ability to simulate the distribution of the considered halocarbon and the ozone loss associated with it. Because ODPs are defined relative to the ozone loss caused by CFC-11, the ODP values demonstrate less sensitivity to photochemical modeling errors than do absolute ozone loss calculations.

Taking advantage of this reduced sensitivity, Solomon et al. (1992) proposed a semi-empirical approach to estimate ODPs that approximates and simplifies the accurate representation of ozone photochemistry and provides an observational constraint to the model-based

HALOCARBON SCENARIOS, ODPs, AND GWPs

results. In this approach, measurements of correlations between halocarbons are used to evaluate chlorine and bromine relative stratospheric release values. These release rates are used with lifetimes, molecular weights, and the number and type of halogen atoms per molecule to estimate the effect of a small source gas pulse emission on stratospheric ozone depletion. In the case of bromine and iodine, the catalytic efficiency for ozone destruction relative to chlorine is needed and differs from unity partly due to the different partitioning of the halogen chemical families. For long-lived chlorocarbons and bromocarbons that are well mixed in the troposphere, the semi-empirical ODP definition can be expressed by:

$$ODP_i = (\alpha n_{Br,i} + n_{Cl,i}) \frac{f_i}{f_{CFC-11}} \frac{\tau_i}{\tau_{CFC-11}} \frac{M_{CFC-11}}{M_i} \frac{1}{3} \quad (8-2)$$

where f is the fractional halogen release factor, α is the relative effectiveness of bromine compared with chlorine for ozone destruction, τ is the global lifetime, M is the molecular weight, and n_{Cl} (n_{Br}) is the number of chlorine (bromine) atoms contained in the compound. *CFC-11* subscripts indicate quantities for CFC-11, while i subscripts denote quantities pertaining to the compound for which the ODP is desired. This equation has been altered slightly from the form given in the previous Assessment (Equation 1-6, WMO, 2003) because it was less clear how to account for compounds with both chlorine and bromine atoms using the previous form. For very short-lived substances (VSLs), the location and season of emission affect the amount of halogen that can make it to the stratosphere, making Equation (8-2) an inappropriate choice for ODP estimates of these gases (see Chapter 2 of this Assessment, as well as Chapter 2 of WMO, 2003).

8.2.2.1 ATMOSPHERIC LIFETIMES

The lifetimes of atmospheric trace gases given in Tables 8-1 and 8-2 have been assessed in Chapter 1. A detailed explanation of global lifetimes can be found in WMO (2003). For these reported lifetimes, it is assumed that the gases are uniformly mixed throughout the troposphere. This assumption is less accurate for gases with lifetimes $< 1/2$ year, and is but one reason why single values for global lifetimes, ODPs, or GWPs are less appropriate for such short-lived gases (see Chapter 2). However, the majority of ozone-depleting substances and their replacements have atmospheric lifetimes greater than 2 years, much longer than tropospheric mixing times; hence their lifetimes, ODPs, and GWPs are not significantly altered by the location of sources within the troposphere.

8.2.2.2 FRACTIONAL RELEASE FACTORS

The distributions of species in the stratosphere depend on the competition between local photochemical removal processes and transport processes that carry the material from the entry point (mainly at the tropical tropopause) through, and out of, the stratosphere. Once a halogen source gas is in the stratosphere, release of a halogen atom from the source gas can occur through photolysis or chemical reaction. As already described in previous WMO reports (WMO, 2003), the fraction, f_i , of halocarbon i converted to an inorganic form by some time at a given location in the stratosphere can be given by:

$$f_i(x, y, z, t) = \frac{\rho_{i,entry} - \rho_i(x, y, z, t)}{\rho_{i,entry}} \quad (8-3)$$

where $\rho_i(x, y, z, t)$ denotes the mixing ratio of the halocarbon at a given stratospheric location (x, y, z) at time t , and $\rho_{i,entry}$ is the mixing ratio of species i in the air parcel when it entered the stratosphere. The value of $\rho_{i,entry}$ can be estimated from knowledge of the age (time since entering the stratosphere) of the parcel at location (x, y, z) and the tropospheric time series of species i . With Equation (8-3), measurements of the halocarbon distributions within the stratosphere then can be used to define $f_i(x, y, z, t)$. The relative fractional release term used in Equation (8-2) is the ratio f_i / f_{CFC-11} , which is a measure of the local fractional release of inorganic halogen compounds relative to the fractional release of CFC-11. Conceptually, the fractional release factor should be globally integrated. In practice, a more limited range of measured correlations representing mid- to high latitudes, where ozone is highly sensitive to changes in the local photochemical removal rate, is generally used (e.g., Schauffler et al., 2003). The fractional release factors used in this report are given in Table 8-1. Except for the value for CFC-114, which is taken from Schauffler et al. (2003), all values are taken from WMO (2003). Most of these values have been derived from stratospheric observations, with models used to estimate the fractional release factors for a few source gases (Solomon et al., 1992; WMO, 2003).

The fractional release factors for hydrochlorofluorocarbons HCFC-141b and HCFC-142b included in Table 8-1 and used in the previous Assessment differ from the values derived by Schauffler et al. (2003) from stratospheric observations. These observations suggest values smaller by a factor of 3.1 and 4.5 for HCFC-141b and HCFC-142b, respectively. Because of the large growth rates of these compounds at the time the measurements were made and the resulting sensitivity of the fractional release values to age-of-air estimates, the authors of the

Table 8-1. Lifetimes, relative fractional halogen release factors, and Ozone Depletion Potentials for halocarbons. ODPs recommended in this Assessment and ODPs adopted in the Montreal Protocol are included.

Halocarbon *	Lifetime (years)	Relative Fractional Release Factor ¹	Semi-Empirical ODP	ODP in Montreal Protocol
Annex A-I				
CFC-11	45	1	1.0	1.0
CFC-12	100	0.60	1.0	1.0
CFC-113	85	0.75	1.0	0.8
CFC-114	300	0.28 ± 0.02 ²	1.0	1.0
CFC-115	1700		0.44 [†]	0.6
Annex A-II				
Halon-1301	65	0.62	16	10.0
Halon-1211	16	1.18	7.1 ³	3.0
Halon-2402	20	1.22	11.5	6.0
Annex B-II				
Carbon tetrachloride	26	1.06	0.73	1.1
Annex B-III				
Methyl chloroform	5.0	1.08	0.12	0.1
Annex C-I				
HCFC-22	12.0	0.35	0.05	0.055
HCFC-123	1.3	1.11	0.02	0.02
HCFC-124	5.8	0.52	0.02	0.022
HCFC-141b	9.3	0.72	0.12	0.11
HCFC-142b	17.9	0.36	0.07	0.065
HCFC-225ca	1.9	1.1	0.02	0.025
HCFC-225cb	5.8	0.5	0.03	0.033
Annex E				
Methyl bromide	0.7	1.12	0.51	0.6
Others				
Halon-1202	2.9		1.7 ⁴	
Methyl iodide	see Chapter 2		see Chapter 2	
Methyl chloride	1.0	0.80	0.02	

* Chemical formulae for the halocarbons are listed in Table 8-2 and also in Appendix C of this Assessment.

[†] Model-derived value, WMO (2003).

¹ From WMO (2003), Table 1-4, except for the value for CFC-114. For the EESC calculations in Section 1.8 of WMO (2003), slightly different relative fractional release factors were used by mistake for the halons. The values given here are used for the calculations presented in this Assessment.

² From Schauffler et al. (2003).

³ The ODP of halon-1211 should have been reported as 5.3 in the previous Assessment (WMO, 2003), but was incorrectly reported as 6.0 due to a calculation error.

⁴ WMO (2003), with adjustment for updated α value.

previous Assessment did not adopt these new values. With no additional estimates available since this disagreement was discussed in the previous Assessment, the discrepancy remains an unresolved issue and we continue to use the older, model-derived values. Model estimates for all other gases agree with the values estimated from observations to within 2 times the quoted error bars of the observational estimates (Schauffler et al., 2003) except for

HCFC-22. The HCFC-22 value based on observations is about 17% lower than calculated in Solomon et al. (1992).

8.2.2.3 OZONE DESTRUCTION EFFECTIVENESS

Although the relative effectiveness of bromine compared with chlorine for ozone depletion, referred to as α , is treated as a single, fixed quantity in Equation 8-

HALOCARBON SCENARIOS, ODPs, AND GWPs

2 and in the calculation of EESC elsewhere in this Assessment Report, it represents a globally integrated result with sensitivity to many factors, including the kinetic parameters for chlorine and bromine species, the amount of inorganic bromine and inorganic chlorine in the background atmosphere, and atmospheric transport. The value of α was assumed to be 45 in the previous Assessment, based partly on the results from Daniel et al. (1999) and Ko et al. (1998).

The value of α has been recalculated for this Assessment with the Atmospheric Environmental Research, Inc. (AER), the Leeds-Bremen, and the University of Illinois two-dimensional models, which are discussed in Chapters 2 and 6. Using Jet Propulsion Laboratory (JPL) JPL-05 kinetics (preliminary version of Sander et al., 2006), the AER (D. Weisenstein, private communication) and Leeds-Bremen (B.-M. Sinnhuber, private communication) models calculate global values of 61 and 71, respectively. The University of Illinois (D. Wuebbles, private communication) model suggests a value of 57 using JPL-02 kinetics (Sander et al., 2002). The change in kinetics recommendations from 1997 are thought to play a relatively minor role in the increased estimates of the α value. The Leeds-Bremen model, when using JPL-97 rates (DeMore et al., 1997), calculates a reduced α value of 64 compared with the 71 with the JPL-05 kinetics. The AER model value is also higher than its previously calculated value when using JPL-97 rates; however, changes have been made in the model in addition to kinetic rates that also could have affected the α value. The AER value would have been 52 with the JPL-97 rates if a methyl bromide (CH_3Br) stratosphere fractional release value of 1.12 relative to CFC-11 was applied to the results of Ko et al. (1998); however, the calculated release value from the current AER model is larger than 1.12, perhaps implying a value for α lower than 52 (M. Ko, private communication). Thus, there is no simple way to be certain of the precise AER α value with JPL-97 kinetics.

The reasons for the variations in the calculated α values from these models apparently arise not from kinetics changes alone, but also from differences in other model processes, such as transport, the ozone loss spatial distribution, etc. The differences have not yet been explained in the literature. Nevertheless, due to the consistently larger values recently calculated with these well-documented models compared with the previously assumed value of 45, and because the Leeds-Bremen model suggests an even higher value when additional stratospheric bromine is considered to account for VSLs (a value of 73 for an additional 6 ppt of stratospheric bromine), we now recommend an α value of 60 for global ozone destruction. However, we emphasize the relatively

large model-dependent range of values discussed in the previous paragraph.

In Section 8.3, a value of 65 is used for α when simulating Antarctic conditions, based on the results of Chipperfield and Pyle (1998) for Arctic conditions. These calculations assumed DeMore et al. (1994) kinetic rates; a calculation using updated rates is not currently available.

For fluorine, the relative effectiveness compared with chlorine for ozone destruction is negligibly small based on the results from Ravishankara et al. (1994) and Wallington et al. (1995).

8.2.2.4 ODP VALUES

The most significant change in ODPs since the previous Assessment is for the bromocarbons, due to the increase in the recommended value of α from 45 to 60. This α increase leads directly to an increase in the semi-empirical ODPs of all bromocarbons of 33%. The ODP of halon-1211 was also incorrectly reported in the previous Assessment to be 6.0 due to a calculation error; it should have been reported as 5.3. The ODPs of the chlorocarbons remain the same as those reported in WMO (2003), except for CFC-114. In WMO (2003), the ODP for CFC-114 was derived from a model; because the fractional chlorine release and lifetime are available, the semi-empirical ODP is reported here. Although the recommended value of the methyl chloride (CH_3Cl) lifetime has been decreased from 1.3 to 1.0 (Chapter 1), the ODP remains unchanged to the reported precision.

8.2.3 Direct Global Warming Potentials

Halocarbons absorb terrestrial radiation (long wavelength infrared radiation emitted from the Earth's surface) and contribute to the radiative forcing of the climate system. They generally have strong absorption features in the atmospheric window region (at approximately 8-12 micrometers) where there is little absorption by atmospheric gases. This absorption reduces the amount of outgoing energy from the Earth-atmosphere system and leads to a direct radiative forcing. It is this forcing that plays an important role in the calculations of the direct GWPs discussed in this section.

The change in net radiation at the tropopause caused by a given change in greenhouse gas concentration or mass is referred to as radiative efficiency. Radiative efficiency has units of $\text{W m}^{-2} \text{ppb}^{-1}$ or $\text{W m}^{-2} \text{kg}^{-1}$; it is calculated using radiative transfer models of the atmosphere and depends upon the strength and spectral position of a compound's absorption bands. The Absolute Global Warming Potential (AGWP) has units of $\text{W m}^{-2} \text{ppb}^{-1} \text{yr}$ or $\text{W m}^{-2} \text{k}^{-1} \text{yr}$ and quantifies the future integrated radiative forcing of a unit

mass pulse emission of a greenhouse gas; it can be defined as:

$$AGWP_x(t') = \int_0^{t'} F_x[x(t)] dt \quad (8-4)$$

where F_x is the radiative forcing per unit mass of species x , $x(t)$ describes the decay with time of a unit pulse of compound x , and t' is the time horizon considered. To compare the relative integrated effects of various compounds on climate, the Global Warming Potential concept was developed. The Global Warming Potential (IPCC, 1990; 2001) can be defined as:

$$GWP_x(t') = \frac{\int_0^{t'} F_x \exp\left(-t/\tau_x\right) dt}{\int_0^{t'} F_{CO_2} R(t) dt} \quad (8-5)$$

where F_{CO_2} is the radiative forcing of carbon dioxide (CO_2), $R(t)$ is the response function that describes the decay of an instantaneous pulse of CO_2 , and the decay of the pulse of compound x has been rewritten assuming it obeys a simple exponential decay curve determined by a response time of τ_x . Both F_x and F_{CO_2} are generally given in units of $W m^{-2} kg^{-1}$. The unit pulse response terms lead to a dependence of GWPs on the integration time horizon; compounds that decay more quickly (slowly) than the reference (CO_2) have GWPs which decrease (increase) with increasing time horizon. As shown in Equations (8-4) and (8-5), the most common definition of GWPs applies to pulsed emissions. However, indices have also been developed to evaluate the effect of sustained emissions (Berntsen et al., 2005; Johnson and Derwent, 1996; Shine et al., 2005a).

The GWP index has three major advantages over other indices used to measure the contribution of halocarbons to global warming: transparency, simplicity, and widespread acceptance. Disadvantages of the GWP index include: (1) GWPs compare contributions with radiative forcing and not with the often more relevant factors of temperature change or economic damage; (2) impacts at different times in the future are given equal weight (for times between the time of the pulse and the time of the pulse plus the time horizon) (Fuglestad et al., 2000, 2003; Manne and Richels, 2001; O'Neill, 2000; Shine et al., 2005a; Smith and Wigley, 2000a, b; Wigley, 1998); and (3) GWPs are dependent on assumptions regarding other gas concentrations due to spectral overlaps of absorption bands (e.g., Hurley et al., 2005)). Various alternatives

have been presented to overcome some of these limitations, but discussions of these are beyond the scope of this chapter.

Direct GWPs are tabulated in Table 8-2. With the recent publication of the IPCC/TEAP (2005) Special Report and the soon to be released IPCC Fourth Assessment Report, we will limit additional discussion of GWPs to updates since the last Ozone Assessment. There are four reasons that updates have been made: (1) a change in F_{CO_2} due to an increase in the CO_2 atmospheric mixing ratio from 370 parts per million (ppm) to 378 ppm; (2) a new CO_2 response function; (3) updates to two atmospheric lifetimes; and (4) new radiative forcing recommendations.

The change in CO_2 mixing ratio reflects the continuing increase in the atmospheric concentration of this radiatively important gas. This increased atmospheric abundance of CO_2 results in a lower radiative efficiency due to the CO_2 bands becoming slightly more saturated. The formula used to calculate the forcing has also been changed to

$$5.35 \ln\left(\frac{c_0 + \Delta c}{c_0}\right) \quad (8-6)$$

where c_0 is 378 ppm and Δc is the added pulse. This formula is adopted because it is more consistent with current estimates of the radiative forcing associated with a doubling of CO_2 (IPCC, 2001). The mixing ratio used in Equation (8-6) in conjunction with a pulse of 1 ppm leads to a CO_2 radiative efficiency of $0.0141 W m^{-2} ppm^{-1}$ compared with a value of $0.0153 W m^{-2} ppm^{-1}$ from the previous Assessment. A new pulse response function for CO_2 was calculated with the Bern25CC model (Joos et al., 2001; Plattner et al., 2001) for a constant CO_2 background mixing ratio of 378 ppm and a pulse size of 40 GtC. The combination of this slightly changed response function and the smaller radiative forcing leads to CO_2 AGWPs of 0.192, 0.676, and 2.223 $W m^{-2} ppm^{-1} yr$ for time horizons of 20, 100, and 500 years, respectively (F. Joos, personal communication). These AGWPs are smaller than those of IPCC (2001) by 7.2%, 2.9%, and 0.8% for these same respective time horizons. GWPs are calculated relative to CO_2 so these lower CO_2 AGWPs result in increased GWP values by these same percentages in the absence of other changes.

Lifetimes have been updated for trifluoromethylsulfurpentafluoride (SF_5CF_3) and methyl chloride (CH_3Cl). A discussion of these updates can be found in Chapter 1. We also recommend updated radiative efficiencies of six compounds compared with WMO (2003):

HALOCARBON SCENARIOS, ODPs, AND GWPs

Table 8-2. Direct Global Warming Potentials for selected gases.

Industrial Designation or Common Name	Chemical Formula	Radiative Efficiency ¹ (W m ⁻² ppbv ⁻¹)	Lifetime (years)	Global Warming Potential for Given Time Horizon		
				20 years	100 years	500 years
Carbon dioxide	CO ₂	1.41 × 10 ^{-5 2}		1	1	1
Nitrous oxide	N ₂ O	3.03 × 10 ⁻³	114 ³	289	298	153
Chlorofluorocarbons						
CFC-11	CCl ₃ F	0.25	45	6,730	4,750	1,620
CFC-12	CCl ₂ F ₂	0.32	100	10,990	10,890	5,200
CFC-13	CClF ₃	0.25	640	10,800	14,420	16,430
CFC-113	CCl ₂ FCClF ₂	0.30	85	6,540	6,130	2,690
CFC-114	CClF ₂ CClF ₂	0.31	300	8,040	10,040	8,730
CFC-115	CClF ₂ CF ₃	0.18	1700	5,310	7,370	9,990
Hydrochlorofluorocarbons						
HCFC-21	CHCl ₂ F	0.14	1.7	530	151	46
HCFC-22	CHClF ₂	0.20	12.0	5,160	1,810	549
HCFC-123	CHCl ₂ CF ₃	0.14	1.3	273	77	24
HCFC-124	CHClF ₂ CF ₃	0.22	5.8	2,070	609	185
HCFC-141b	CH ₃ CCl ₂ F	0.14	9.3	2,250	725	220
HCFC-142b	CH ₃ CClF ₂	0.20	17.9	5,490	2,310	705
HCFC-225ca	CHCl ₂ CF ₂ CF ₃	0.20	1.9	429	122	37
HCFC-225cb	CHClF ₂ CClF ₂	0.32	5.8	2,030	595	181
Hydrofluorocarbons						
HFC-23	CHF ₃	0.19 ⁴	270	11,990	14,760	12,230
HFC-32	CH ₂ F ₂	0.11 ⁴	4.9	2,330	675	205
HFC-41	CH ₃ F	0.02	2.4	323	92	28
HFC-125	CHF ₂ CF ₃	0.23	29	6,340	3,500	1,100
HFC-134	CHF ₂ CHF ₂	0.18	9.6	3,400	1,100	335
HFC-134a	CH ₂ FCF ₃	0.16 ⁴	14.0	3,830	1,430	435
HFC-143	CH ₂ FCHF ₂	0.13	3.5	1,240	353	107
HFC-143a	CH ₃ CF ₃	0.13	52	5,890	4,470	1,590
HFC-152	CH ₂ FCH ₂ F	0.09	0.60	187	53	16
HFC-152a	CH ₃ CHF ₂	0.09	1.4	437	124	38
HFC-227ea	CF ₃ CHFCF ₃	0.26 ⁴	34.2	5,310	3,220	1,040
HFC-236cb	CH ₂ FCF ₂ CF ₃	0.23	13.6	3,630	1,340	407
HFC-236ea	CHF ₂ CHFCF ₃	0.30	10.7	4,090	1,370	418
HFC-236fa	CF ₃ CH ₂ CF ₃	0.28	240	8,100	9,810	7,660
HFC-245ca	CH ₂ FCF ₂ CHF ₂	0.23	6.2	2,340	693	211
HFC-245fa	CHF ₂ CH ₂ CF ₃	0.28	7.6	3,380	1,030	314
HFC-365mfc	CH ₃ CF ₂ CH ₂ CF ₃	0.21	8.6	2,520	794	241
HFC-43-10mee	CF ₃ CHFCHFCF ₂ CF ₃	0.40	15.9	4,140	1,640	499
Chlorocarbons						
Methyl chloroform	CH ₃ CCl ₃	0.06	5.0	506	146	45
Carbon tetrachloride	CCl ₄	0.13	26	2,700	1,400	435
Methyl chloride	CH ₃ Cl	0.01	1.0	45	13	4

Table 8-2, continued.

Industrial Designation or Common Name	Chemical Formula	Radiative Efficiency ¹ (W m ⁻² ppbv ⁻¹)	Lifetime (years)	Global Warming Potential for Given Time Horizon		
				20 years	100 years	500 years
Bromocarbons						
Methyl bromide	CH ₃ Br	0.01	0.7	17	5	1
Halon-1201	CHBrF ₂	0.14	5.8	1,380	404	123
Halon-1211	CBrClF ₂	0.30	16	4,750	1,890	574
Halon-1301	CBrF ₃	0.32	65	8,480	7,140	2,760
Halon-2402	CBrF ₂ CBrF ₂	0.33	20	3,680	1,640	503
Fully fluorinated species						
Sulfur hexafluoride	SF ₆	0.52	3200	16,260	22,810	32,600
Trifluoromethylsulfur- pentafluoride	SF ₅ CF ₃	0.57	650- 950	13,120- 13,180	17,540- 17,960	20,060- 22,360
Perfluoromethane	CF ₄	0.10 ⁴	50000	5,210	7,390	11,190
Perfluoroethane	C ₂ F ₆	0.26	10000	8,620	12,200	18,180
Perfluoropropane	C ₃ F ₈	0.26	2600	6,310	8,830	12,450
Perfluorobutane	C ₄ F ₁₀	0.33	2600	6,330	8,850	12,480
Perfluorocyclobutane	c-C ₄ F ₈	0.32	3200	7,310	10,250	14,660
Perfluoropentane	C ₅ F ₁₂	0.41	4100	6,510	9,150	13,260
Perfluorohexane	C ₆ F ₁₄	0.49	3200	6,620	9,290	13,280
Perfluorodecalin	C ₁₀ F ₁₈	0.56 ⁵	1000	5,500	7,510	9,440
Halogenated alcohols and ethers						
HFE-125	CHF ₂ OCF ₃	0.44	136	13,790	14,910	8,490
HFE-134	CHF ₂ OCHF ₂	0.45	26	12,190	6,320	1,960
HFE-143a	CH ₃ OCF ₃	0.27	4.3	2,630	756	230
HCFE-235da2	CHF ₂ OCHClCF ₃	0.38	2.6	1,230	349	106
HFE-245fa2	CHF ₂ OCH ₂ CF ₃	0.31	4.9	2,280	659	200
HFE-254cb2	CH ₃ OCF ₂ CHF ₂	0.28	2.6	1,260	359	109
HFE-7100 (HFE-44-9)	CH ₃ OC ₄ F ₉	0.31	5.0	1,390	404	123
HFE-7200 (HFE-56-9)	C ₂ H ₅ OC ₄ F ₉	0.30	0.77	200	57	17
HFE-245cb2	CH ₃ OCF ₂ CF ₃	0.32	5.1	2,440	708	215
HFE-347mcc3	CH ₃ OCF ₂ CF ₂ CF ₃	0.34	5.2	1,980	575	175
HFE-356pcc3	CH ₃ OCF ₂ CF ₂ CHF ₂	0.33	0.93	386	110	33
HFE-374pc2	CH ₃ CH ₂ OCF ₂ CHF ₂	0.25	5.0	1,930	557	169
	CH ₃ OCF(CF ₃) ₂	0.31	3.4	1,200	343	104
HFE-43-10pccc124 ^a	CHF ₂ OCF ₂ OC ₂ F ₄ OCHF ₂	1.37	6.3	6,320	1,870	569
	(CF ₃) ₂ CHOH	0.28	2.0	764	217	66
HFE-236ca12	CHF ₂ OCF ₂ OCHF ₂	0.66	12.1	8,040	2,820	859
HFE-338pcc13	CHF ₂ OCF ₂ CF ₂ OCHF ₂	0.87	6.2	5,070	1,500	456
Species whose lifetimes have a high uncertainty						
Nitrogen trifluoride	NF ₃	0.21 ⁴	740	13,370	18,000	21,270
Perfluorocyclopropane	c-C ₃ F ₆	0.42	>1000	>12,700	>17,340	>21,800
HFE-227ea	CF ₃ CHFOCF ₃	0.40	11	4,540	1,540	468
HFE-236ea2	CHF ₂ OCHF ₂ CF ₃	0.44	5.8	3,370	989	301
HFE-236fa	CF ₃ CH ₂ OCF ₃	0.34	3.7	1,710	487	148
HFE-245fa1	CHF ₂ CH ₂ OCF ₃	0.30	2.2	1,010	286	87

HALOCARBON SCENARIOS, ODPs, AND GWPs

Table 8-2, continued.

Industrial Designation or Common Name	Chemical Formula	Radiative Efficiency ¹ (W m ⁻² ppbv ⁻¹)	Lifetime (years)	Global Warming Potential for Given Time Horizon		
				20 years	100 years	500 years
HFE-329mcc2	CHF ₂ CF ₂ OCF ₂ CF ₃	0.49	6.8	3,060	919	279
HFE-338mcf2	CF ₃ CH ₂ OCF ₂ CF ₃	0.43	4.3	1,920	552	168
HFE-347mcf2	CHF ₂ CH ₂ OCF ₂ CF ₃	0.41	2.8	1,310	374	114
HFE-356mec3	CH ₃ OCF ₂ CHF ₂ CF ₃	0.30	0.94	355	101	31
HFE-356pcf2	CHF ₂ CH ₂ OCF ₂ CHF ₂	0.37	2.0	931	265	80
HFE-356pcf3	CHF ₂ OCH ₂ CF ₂ CHF ₂	0.39	3.6	1,760	502	153
	CHF ₂ OCH(CF ₃) ₂	0.41	3.1	1,330	379	115
	-(CF ₂) ₄ CH(OH)-	0.30	0.85	254	72	22

Note: Values are calculated for a CO₂ mixing ratio of 378 ppm, compared with 370 ppm in IPCC/TEAP (2005) and WMO (2003); this leads to slightly smaller CO₂ AGWPs.

^a Referred to as H-Galden 1040x in previous Assessments.

¹ All values from IPCC/TEAP (2005) unless otherwise noted.

² See Section 8.2.3.

³ This value is an adjustment time that includes feedbacks of emissions on the lifetime.

⁴ See Table 8-3.

⁵ From Shine et al. (2005b).

the hydrofluorocarbons HFC-134a (CFH₂CF₃), HFC-23 (CHF₃), HFC-32 (CH₂F₂), HFC-227ea (CF₃CHF₂CF₃), and CF₄ and NF₃. The radiative efficiency values used in the previous Assessment, the currently recommended values, and the values presented in the pertinent references are presented in Table 8-3.

Since the last Assessment (WMO, 2003), the radiative efficiency of HFC-134a has been studied by Forster et al. (2005). Various laboratory cross sections and radiative transfer models were used to assess the primary sensitivities of the radiative efficiency. The integrated absorption cross sections from six independent laboratory studies of the bands most significant to the radiative efficiency calculation differed by less

than 5%. While the models showed some difference in the cloudy-sky forcing for a single atmospheric profile, the best estimates of the radiative efficiency converged to a value of 0.16 W m⁻² ppbv⁻¹. This value is adopted; it is close to that used in the previous Assessment (0.15 W m⁻² ppbv⁻¹) (WMO, 2003).

The radiative efficiency of CF₄ has been studied by Hurley et al. (2005) since the previous ozone Assessment. There is good agreement (within 4%) in the absorption cross sections measured in two independent laboratory studies reported by Hurley et al. (2005) and in the study of Nemtchinov and Varanasi (2003). The radiative efficiency reported by Hurley et al. (2005), 0.102 W m⁻² ppbv⁻¹, is 15% greater than calculated by Myhre et al. (1998).

Table 8-3. Radiative efficiency estimates for six compounds whose recommended values have changed since the previous Assessment. All values are in units of W m⁻² ppbv⁻¹.

Species	WMO (2003)	Hurley et al. (2005)	Forster et al. (2005)	Jain et al. (2000)	Sihra et al. (2001)	Gohar et al. (2004)	This Assessment
HFC-134a	0.15		0.16	0.20	0.159	0.155-0.166	0.16
CF ₄	0.08	0.102		0.089 ¹	0.116		0.10
HFC-23	0.16			0.248	0.171	0.181-0.193	0.19
HFC-32	0.09			0.155	0.105	0.110-0.111	0.11
HFC-227ea	0.30			0.322	0.256	0.243-0.271	0.26
NF ₃	0.13						0.21 ²

¹ For a constant vertical mixing ratio profile.

² From Robson et al. (2006).

About a 10% increase is explained by the larger cross section and the remaining 5% is believed to be due to differing radiative transfer codes employed.

Since the last ozone Assessment, radiative efficiencies of HFC-23, HFC-32, and HFC-227ea have been studied by Gohar et al. (2004), using two independent sets of radiation codes. There is a greater than 20% difference in the calculated radiative efficiencies of these gases reported by Sihra et al. (2001) and Jain et al. (2000), both of which were considered in the previous Assessment. At the time of the previous Assessment, the reason for the differences was not clear and averages of the two datasets were used. While the reason for the differences between the Jain et al. and Sihra et al. values are still unknown, the results of Gohar et al. (2004) support the values given by Sihra et al. (2001), leading to an update of the recommendations given in Table 8-3. The calculations by Gohar et al. (2004) also illustrate the sensitivity of the radiative efficiency calculations to the particular model choice.

The radiative efficiency of NF_3 has been re-evaluated recently by Robson et al. (2006). The radiative efficiency used in previous Assessments (IPCC, 2001; WMO, 1999, 2003) was calculated from the absorption cross section data of Molina et al. (1995) by K.P. Shine using the simple radiative method given in Pinnock et al. (1995), as no radiative efficiency was provided in the Molina et al. (1995) work. The Robson et al. (2006) study suggests that the more intense infrared (IR) features reported by Molina et al. (1995) were saturated, causing the inferred radiative efficiency to be too small. Molina et al. (1995) did not report the precise conditions used to derive their absorption cross section values, making an unambiguous evaluation of the importance of saturation impossible. We adopt the radiative efficiency of $0.21 \text{ W m}^{-2} \text{ ppb}^{-1}$ from the more comprehensive study by Robson et al. (2006).

The 2σ uncertainty associated with the direct GWPs shown is estimated to be $\pm 35\%$. This value has been adopted from previous ozone and climate Assessments (IPCC, 2001; WMO, 2003; IPCC/TEAP, 2005) and is primarily due to uncertainties in the radiative efficiencies and lifetimes of the halocarbons and to uncertainties in our understanding of the carbon cycle (IPCC, 2001). However, because the uncertainties in the carbon cycle are thought to be an important part of this uncertainty, the error in the relative GWP values among halocarbons should be less than 35% (IPCC, 2001).

The indirect radiative forcing and indirect GWPs of a species quantify the radiative effects from changes in abundances of other greenhouse gases resulting from the

addition of the species considered. Because the indirect forcing and GWPs due to stratospheric ozone loss depend on the future evolution of stratospheric ozone and thus on the specific ODS emission scenario, these are presented in Section 8.5 of this chapter, after the halocarbon scenarios are discussed.

8.2.4 Degradation Products and Their Implications for ODPs and GWPs

Degradation products of CFCs, HCFCs, and HFCs have been discussed in IPCC/TEAP (2005). The main conclusion was that the intermediate degradation products of most long-lived CFCs, HCFCs, and HFCs have shorter lifetimes than the source gases, and therefore have lower atmospheric concentrations and smaller radiative forcings. Intermediate products and final products are removed from the atmosphere via deposition and washout processes and may accumulate in oceans, lakes, and other aquatic reservoirs. Trifluoroacetic acid is a persistent degradation product of some HCFCs and HFCs and is removed from the atmosphere mainly by wet deposition. Its sources (natural and anthropogenic), sinks, and potential environmental effects have been reviewed by Tang et al. (1998), Solomon et al. (2003), and IPCC/TEAP (2005). The available environmental risk assessment and monitoring data indicate that the source of trifluoroacetic acid from the degradation of HCFCs and HFCs will not result in environmental concentrations capable of significant ecosystem damage.

8.3 FUTURE HALOCARBON SOURCE GAS CONCENTRATIONS

8.3.1 Introduction

Projections of future atmospheric halocarbon mixing ratios require knowledge of future emissions and atmospheric/oceanic loss rates in addition to current atmospheric abundances. In this section, we use estimates of these quantities in a simple box model to calculate average future surface mixing ratios, which are assumed to be related to mean atmospheric mixing ratios by a fixed factor. These calculated mixing ratios are used to generate equivalent effective stratospheric chlorine (EESC) estimates, which are used to evaluate the effects of different halocarbon production/emission scenarios and hypothetical test cases. The lifetimes presented in Table 8-1 (see also Chapter 1) are estimated from the loss rates of the ODSs and are used in the box model. Any future changes in the hydroxyl radical (OH) amount (IPCC, 2001) and/or

HALOCARBON SCENARIOS, ODPs, AND GWPs

distribution, and any changes in circulation (see, e.g., Chapters 5 and 6) that might affect lifetimes, are neglected. To include more complicated atmospheric interactions such as these, more sophisticated two-dimensional (2-D) and three-dimensional (3-D) atmospheric models should be used.

The box model approach used here has also been used in previous Assessments (WMO, 1995; 1999; 2003). Global mean mixing ratios are calculated using the equation

$$\frac{d\rho_i}{dt} = F_i E_i - \frac{\rho_i}{\tau_i} \quad (8-7)$$

where ρ is the global mean mixing ratio (in ppt), τ is the total atmospheric lifetime, E is the emission rate (in kg/year), and F is the factor that relates the mass emitted to the global mean mixing ratio, given by

$$F_i = \frac{5.68 \times 10^{-9}}{M_i} \quad (8-8)$$

where F is in units of ppt/kg, and M is the molecular weight (in kg/mole). The i subscripts refer to the species considered in the calculation. As in the previous ozone Assessment, the calculated global mean mixing ratios are multiplied by a factor of 1.07 to represent surface mixing ratios. This factor is meant to account for the general decrease of the halocarbon mixing ratios with altitude above the tropopause. Using a constant factor such as this neglects the dependence of this factor on the particular species and neglects any change in this factor that could be caused by changes in circulation or by the variability of the surface emission (and the resulting variability in the atmospheric vertical distribution).

Accurate projections of emissions require an understanding of the amount of halocarbons in equipment and product banks, the rates of release from these banks, the quantity of equipment and products using ODSs that will be put into service, emissive uses, and the future production of ODSs. Banks here are defined as the quantity of ODSs produced but not yet emitted to the atmosphere. Due to the importance of policy decisions, energy cost, technological advancement, and economic growth rates in estimating future production and banks, the uncertainty level in future emissions remains high. However, with each passing year, as more years of emissions can be calculated from atmospheric abundance observations and fewer years remain for the legal consumption of ODSs under the Montreal Protocol, future projections should become more constrained.

Scenarios and test cases have been developed to describe the possible range of future atmospheric abundances of ODSs. These cases are generated using the current understanding of global production, emission, and banks of the most widely used halocarbons. Scenario A1 is meant to represent the current baseline or “best guess” scenario, analogous to the Ab scenario from the previous Assessment. An estimated “maximum” scenario, developed for previous Assessments, is not generated for this Assessment because developed and developing countries have produced less CFCs in 2000-2004 than allowed under the Montreal Protocol and the HCFC production in developing countries is not controlled before 2016. Hence, any attempt to develop such a scenario would be largely speculative on our part. Indeed, it is this uncertainty in future HCFC emission that represents a major reason for the difference that will be discussed later between the current A1 scenario and the comparable Ab scenario of the previous Assessment.

Consistent with past Assessments, our approach to relating annual production, emission, and banks sizes places most confidence on the emission values calculated from atmospheric observations and global lifetimes. Accurate estimates of yearly averaged ODS emissions from atmospheric observations are possible when global lifetimes are long and accurately known, and accurate global mixing ratio observations of ODSs are available. This approach, when used to estimate current bank sizes from historic production and emission data, is sometimes referred to as a top-down approach. In past Assessments, any inconsistency between mixing ratio observations and emission estimates based on the best knowledge of ODS production, sales, and application-specific release functions was eliminated by adjusting the bank size so the emissions would be consistent with the observations. The bank that remained after the sum of adjustments for all years was used in the future projections. Because the bank is an accumulating difference often between two large numbers, this method has an uncertainty that is difficult to quantify and can lead to unreasonable bank sizes; indeed the estimate of no bank in 2002 for CFC-12 in the previous ozone Assessment is such an example (IPCC/TEAP, 2005). One way an unreasonable bank could be attained is in a case in which annual production numbers are accurately known, but the atmospheric lifetime assumed is incorrect. In such a case, a lifetime that is too small (large) will result in an annual release from the bank that must be too large (small) for calculated mixing ratios to agree with observations. Such a situation would occur year after year and could result in a potentially significant error in the bank estimate today, depending on the compound (Daniel et al.,

2006). But without an independent estimate of bank size, such an error would be difficult to identify.

A different approach for determining bank sizes is taken in this Assessment because of the new independent estimates of bank sizes for several ODSs for the years 2002 and 2015 (Clodic and Palandre, 2004; IPCC/TEAP, 2005). These estimates are independent of atmospheric abundance observations and have been determined from the number of units of equipment that use a particular ODS and the amount of ODS in each unit. This is commonly referred to as a bottom-up approach. An extensive explanation of this methodology can be found in IPCC/TEAP (2005). Future emissions until 2015 estimated in this Assessment are calculated by beginning with the 2002 bottom-up bank from IPCC/TEAP (2005), and then by adding annual production and applying a constant annual bank emission factor needed to attain the bottom-up bank estimated in 2015 by IPCC/TEAP (2005). After 2015, emissions are calculated using the same constant bank emission factors as immediately before 2015. Thus, when bottom-up bank size estimates for 2002 and 2015 are available for a particular ODS, the scenarios in this chapter are consistent with them in most cases.

Bottom-up estimates are also not without problems; indeed bottom-up 2002 emission estimates for CFC-11, HCFC-141b, and HCFC-142b (IPCC/TEAP, 2005), which are dominated by emissions from foams, are smaller by more than a factor of two when compared with what is needed to be consistent with mixing ratio observations. Nevertheless, it is felt that these bottom-up bank estimates represent an important new constraint to current bank sizes that warrants a large role in the future projections in this chapter. In Sections 8.3.2.1 and 8.3.4, more discussion of the uncertainties involved with bottom-up and top-down emission estimates and their potential effects on the scenarios is presented.

8.3.2 Baseline Scenario (A1)

In this chapter, estimates of future banks and emissions have been calculated for most ODSs using annual production reported to the United Nations Environment Programme (UNEP, 2005), emissions estimated from atmospheric observations, and bank size estimates based on the bottom-up calculations of IPCC/TEAP (2005). The specific information used for each ODS considered is described in Table 8-4. Due to the uncertainty in the importance of and likely future trends in very short-lived ($\tau < \sim 0.5$ years) organic bromine and chlorine source gases, they are not considered in any of these scenarios. However, the bromocarbons considered in this chapter cannot explain the entire stratospheric inorganic bromine

abundance alone, so the very short-lived gases may prove to be important. Detailed information about these compounds can be found in Chapter 2.

It should be noted that the assumptions made in calculating the baseline scenario are critical to the interpretation of the reduced production and emission scenarios based on it. For example, if the production and/or bank sizes and/or future production rates are underestimated in the baseline scenario, the “no emission/production” results presented in the scenarios would be underestimates of the potential reduction benefit.

8.3.2.1 EMISSIONS

In Figure 8-1, the emission estimates from the 1-box model for the baseline scenario, A1, are compared with those of the Ab “best guess” scenario from the previous Assessment, with the IPCC/TEAP (2005) (business-as-usual (BAU) scenario) emissions, with the emissions of Clodic and Palandre (2004), and with the emissions calculated using the 12-box model discussed in Chapter 1. The emissions calculated with the 1-box model are calculated directly from mixing ratio observations (those shaded in Table 8-5) as are the emissions calculated with the 12-box model. The 12-box model, by having some vertical resolution, includes some changes in atmospheric lifetimes due to variations in atmospheric abundance distributions caused by increasing or decreasing trends; hence, the 12-box model can presumably better determine the relationship between surface mixing ratios and global averages and can better estimate changes in global lifetimes that arise from different atmospheric distributions. The comparisons between the A1 estimated emissions (1-box model) and the 12-box emissions are good most times, but do show some systematic differences. Throughout the measurement periods (shaded regions in the figure), the 12-box model consistently estimates more emission than the 1-box model, with the cumulative differences ranging from a 1.2% higher emission for HCFC-141b through the measurement period as calculated by the 12-box model, to a 6.3% higher emission for CFC-12. There are also noticeable differences between A1 and Ab emissions, many of which are due to the additional information acquired from continued measurements over the past 4 years. Important differences between A1 and Ab include the larger future emissions of CFC-11 and CFC-12, due to their larger estimated banks in A1. The CFC-11 increase in emission past 2010 is also due to a decrease of the bank release rate from plastic foams. The CFC-11 and CFC-12 bank size differences as calculated by the bottom-up method (IPCC/TEAP, 2005) and the top-down method of WMO (2003) have been shown by Daniel et al. (2006) to be large

HALOCARBON SCENARIOS, ODPs, AND GWPs

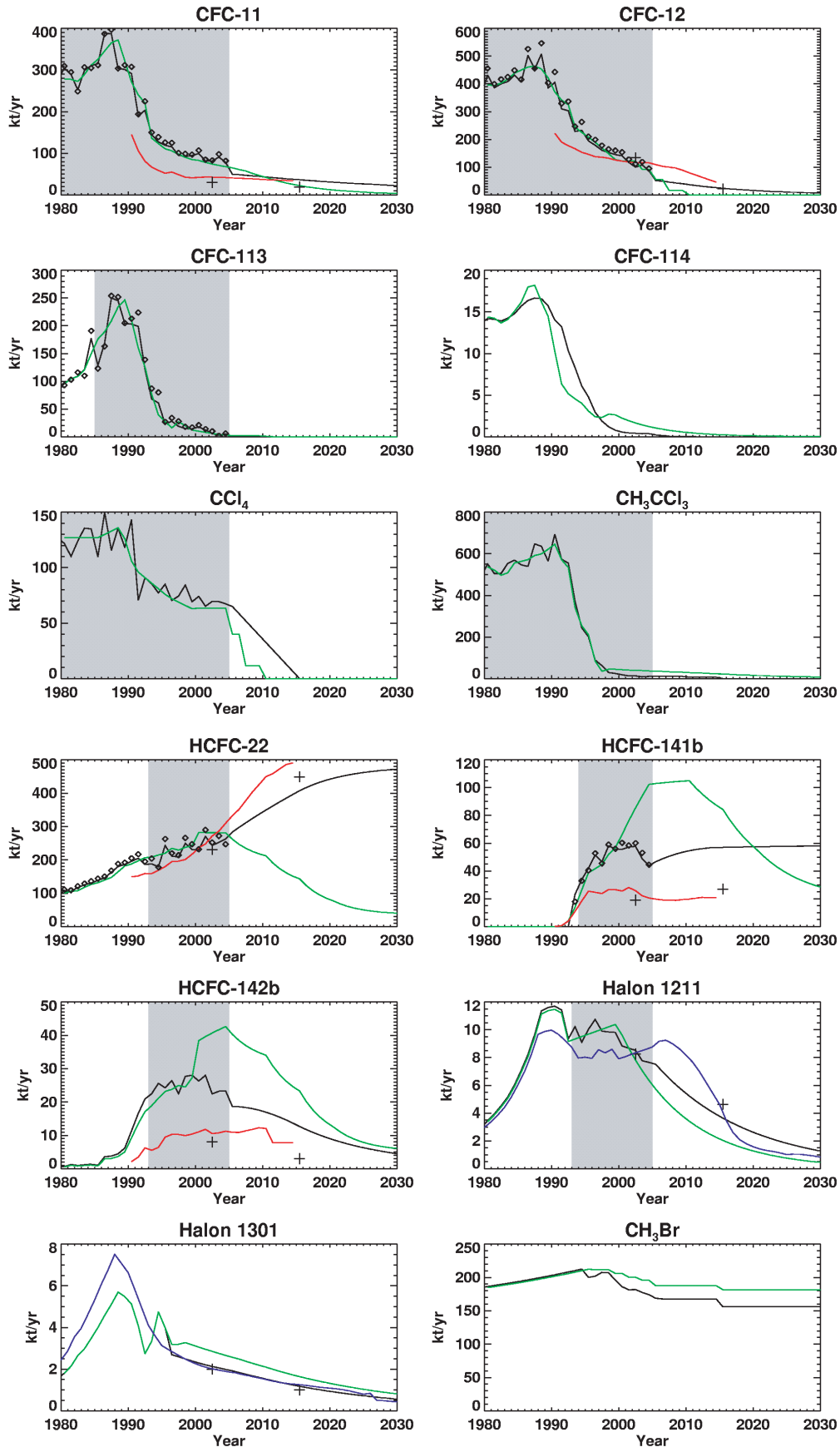


Figure 8-1. Comparison of scenario A1 emissions (black) with those of scenario Ab of the previous Assessment (green), the emissions of Clodic and Palandre (2004) (red), the IPCC/TEAP (2005) emissions (crosses), and emissions calculated from atmospheric abundance observations using a 12-box model (small diamonds), all in units of kilotons per year. Corrected data are used for emissions of halon-1211 according to TEAP (2005) and hence differ from the data reported in IPCC/TEAP (2005). Also shown for halon-1301 are the emissions estimates from the 2002 report of the Halons Technical Options Committee (HTOC) (UNEP, 2003) and, for halon-1211, updates to that report (blue curves). Shaded regions indicate years for which A1 emissions are determined with a 1-box model (see text) so that calculated mixing ratios are exactly equal to the observations. At times, the emissions from the two Assessments are identical, causing the green curve to obscure the black one.

Table 8-4. Assumptions made in obtaining production and emission estimates for the baseline A1 scenario.

General Approach for All Species

Production: For the years when production is reported to UNEP, reported values (or best estimates of production values for cases in which reporting is incomplete or reporting is made by classes of compounds) are used. Before this, WMO (2003) production values are generally used. In the future, annual figures are determined from the lesser of the Montreal Protocol limitations and the most recent annual estimates.

Emission: For the years when abundance observations are available, emissions are calculated using the box model described in Section 8.3.1 with the lifetimes of Table 8-1. Emissions before this are usually consistent with WMO (2003) but are also forced to yield mixing ratios that meld smoothly into the measurement record. Future emissions are determined in order to yield banks consistent with IPCC/TEAP (2005).

Bank: The bank assumed to be in place at the start of the measurement record is set at such a value that the IPCC/TEAP (2005) bank for 2002 is attained; the future annual fractional bank release is adjusted so that the IPCC/TEAP (2005) bank for 2015 is attained.

Approach for Specific Species

Species	Description
CFC-11	<p>Production:</p> <p>1950-1985: WMO (2003) 1986, 1989-2004: UNEP * 1987-1988: McCulloch et al. (2001) 2005-2006: Fixed at 2004 levels for Article 5(1) countries, with no other production 2007-2009: Protocol limits on Article 5(1) countries, with no other production 2010-on: No production</p> <p>Emission:</p> <p>1980-2004: Emissions calculated from observations 2005-on: Emission is a constant fraction of the bank, determined to give a bank in 2015 consistent with IPCC/TEAP (2005)</p>
CFC-12	<p>Production:</p> <p>Same as CFC-11 except: 1987-1988: Interpolated from 1986 and 1989 values 2005-2006: Protocol limits for Article 5(1) countries with no other production</p> <p>Emission:</p> <p>Same formalism as for CFC-11</p>

HALOCARBON SCENARIOS, ODPs, AND GWPs

Table 8-4, continued.

Approach for Specific Species	
CFC-113	<p>Production: Same formalism as for CFC-11</p> <p>Emission: 1986-2004: Emissions calculated from observations</p>
CFC-114	<p>Production: Same formalism as for CFC-11 except: 1987-1988: WMO (2003) 2005-2100: No production</p> <p>Emission: 1951-1959: WMO (2003) 1960-2100: Assume an annual fractional bank release of 0.4, chosen because it leads to bank results relatively close to those estimated by AFEAS (Alternative Fluorocarbons Environmental Acceptability Study) in the 1980s</p>
CFC-115	<p>Production: Same formalism as for CFC-11 except: 1987-1988: WMO (2003) 2005-2100: No production</p> <p>Emission: 1950-2100: Assume an annual fractional bank release of 0.25, chosen because it leads to bank results relatively close to those estimated by AFEAS in the 1980s</p>
CCl ₄	<p>Production: Not considered due to gaps in our understanding of where much of the global emission originates</p> <p>Emission: 1951-1979: WMO (2003) (except the mixing ratio at the beginning of 1951 is assumed to be 37.0 rather than 35.0 (WMO, 2003) to achieve slightly better continuity with the measurements beginning in 1980 1980-2004: Emissions calculated from observations 2005-2015: Linear decrease from 65 ktons in 2005 (compared with 67.4 ktons calculated for 2004) to 0 in 2015 2015-2100: No emission</p>
CH ₃ CCl ₃	<p>Production: Not considered</p> <p>Emission: 1950-1978: WMO (2003) 1979-2004: Emissions calculated from observations 2005-2009: Assume 2004 emissions because this value is lower than the limit in the Protocol (30% reduction relative to the 1998-2000 emission average; although the Protocol limits production and consumption and not emission, it is assumed that there is a negligibly small bank for this compound and that the limitations may be applied to emission) 2010-2014: Emission is 30% of the 1998-2000 average 2015-2100: No emission</p>
HCFC-22	<p>Production: 1950-1988: WMO (2003) 1989-2004: UNEP * 2005-2015: Linear interpolation of demand estimates from IPCC/TEAP (2005) for 2002 and 2015 2016-2030: Fixed at 2015 value</p>

Table 8-4, continued.

Approach for Specific Species

2030-2040: Linear interpolation from 2030 value to 0

Emission:

1950-1992: Emissions calculated to yield mixing ratios consistent with WMO (2003) but moved 1 year earlier (the 1-year offset is to make the mixing ratios meld smoothly with the observations)

1993-2004: Emissions calculated from observations

2005-2100: Assume a bank release fraction of 0.13 (average of 2002-2004)

Bank:

1993 WMO (2003) bank is reduced by 193 ktons from 1,036 ktons to obtain the IPCC/TEAP (2005) 2002 bank estimate; the bank in 2015 is 2,652 ktons compared with 1,879 ktons in IPCC/TEAP (2005); a much larger release fraction of 0.19 and increase in emissions in the near future would be needed to be consistent with the lower bank

HCFC-141b Production:

1989-2004: UNEP *

2005-2015: Linear interpolation of demand estimates from IPCC/TEAP (2005) for 2002 and 2015

2016-2030: Fixed at 2015 value

2030-2040: Linear interpolation from 2030 value to 0

Emission:

1993-2004: Emissions calculated from observations

2005-2100: Assume a bank release fraction of 0.05

Bank:

1993 bank from WMO (2003) is not increased in spite of an apparent need for a larger 1993 bank to attain the 2002 IPCC/TEAP (2005) bank; the increase is not applied because the increase needed would lead to a 1993 bank too large to be consistent with estimated global production before 1993; hence the 2002 bank is 674 ktons, while the IPCC/TEAP (2005) estimate is 836 ktons; the 2015 bank is in agreement with the IPCC/TEAP (2005) bank

HCFC-142b Production:

1992-2004: UNEP * (except for 1993)

1993: AFEAS data used because of unexplained drop in UNEP data for 1993

2005-2015: Linear interpolation of demand estimates from IPCC/TEAP (2005) for 2002 and 2015

2016-2030: Fixed at 2015 value

2030-2040: Linear interpolation from 2030 value to 0

Emission:

1971-1992: WMO (2003) multiplied by 1.225 to attain a mixing ratio consistent with the start of the measurements in 1993

1993-2004: Emissions calculated from observations

2005-2100: Assume a bank release fraction of 0.08

Bank:

1993 WMO (2003) bank is increased by 18 ktons to 103 ktons so the bank in 2002 is equal to the IPCC/TEAP (2005) 2002 bank; the bank release fraction of 0.08, which is consistent with the values estimated from 2002-2004 (0.085-0.089), leads to a bank in 2015 of 157 ktons, considerably lower than the 331 ktons estimated by IPCC/TEAP (2005)

Halon-1211 Production:

1989-2004: Corrected values from the Halons Technical Options Committee (HTOC) 2002 report (UNEP, 2003)

2005-2015: Linear interpolation of demand estimates from IPCC/TEAP (2005) for 2002 and 2015

2016-2030: Fixed at 2015 value

2030-2040: Linear interpolation from 2030 value to 0

HALOCARBON SCENARIOS, ODPs, AND GWPs

Table 8-4, continued.

Approach for Specific Species

	<p>Emission: 1950-1992: WMO (2003) multiplied by 1.02 to attain a mixing ratio in 1993 consistent with measurements 1993-2004: Emissions calculated from observations 2005-2100: Assume a bank release fraction of 0.07</p> <p>Bank: 2002 bank of 122 ktms is only 3 ktms below the IPCC/TEAP (2005) bank; the bank release fraction of 0.07, which is consistent with the release fraction from 1993-2004, leads to a bank in 2015 of 52 ktms compared with 31 ktms from IPCC/TEAP (2005); the 2002 bank of 125 ktms is larger than the 72 ktms in WMO (2003)</p> <p>Note that corrected data are used for banks and emissions of halon-1211 (TEAP, 2005) and hence differ from the data reported in IPCC/TEAP (2005). The 2002 emission data are changed from 17 to 8 ktms per year.</p>
Halon-1301	<p>Production: 1986-2009: HTOC 2002 report (UNEP, 2003) 2010-2100: No production</p> <p>Emission: 1950-1995: WMO (2003) 1996-2100: Assume a bank release fraction of 0.05 (leads to mixing ratios between NOAA/ESRL and AGAGE observations)</p> <p>Bank: 2002 and 2015 banks agree with IPCC/TEAP (2005)</p>
Halon-1202	Same as WMO (2003)
Halon-2402	Same as WMO (2003)
CH ₃ Br	<p>Production: Natural production/emission assumed to be 146 ktms 2005: Natural plus 10.7 ktms for quarantine/pre-shipment plus 14.1 ktms for critical uses plus 0.5 ktms for Article 5(1) production (same as 2004 reported to UNEP) 2006-2014: Same as 2005 but 13.0 ktms of critical uses 2015-2100: Natural plus 10.7 ktms for quarantine/pre-shipment</p> <p>Emission: 1950-2004: Emissions calculated from surface observations and South Pole firm observations (using global lifetime of 0.7 years, Table 8-1) 2005-2100: Emission equal to 0.88 times the anthropogenic production plus natural emissions; this combination of anthropogenic and natural emissions, constrained by the total emissions derived from observations of concentrations, leads to an anthropogenic fraction of the total production of 0.30 in 1992, in agreement with Montzka et al. (2003).</p> <p>Bank: No bank considered</p>
CH ₃ Cl	<p>Emission: Same as WMO (2003); assumed mostly natural (i.e., no future changes due to anthropogenic activity) 1950-1995: Emissions calculated from firm observations at the South Pole 1996-2100: Emissions held constant at 1995 levels</p>

* Estimated in cases in which reporting is not complete or reporting is made in compound classes rather than individually. The production data per species per year are obtained from UNEP (UNEP, 2005) and are consistent with the totals per class of species as usually reported by UNEP.

enough to have significant implications concerning the environmental benefits of reusing or destroying CFCs contained in existing equipment and products. Increases in the projected HCFC-22 emissions, due to larger reported (to UNEP) historic production in developing countries in 2000-2004 than projected in the Ab scenario, and expectations of greater future use based on IPCC/TEAP (2005), are also important.

While the historic emissions calculated with the 1-box model for this Assessment are completely constrained by the observations, emissions from Clodic and Palandre (2004) and IPCC/TEAP (2005) are based exclusively on estimates of the banks and bank release fractions and can be substantially different from those estimated from mixing ratio observations. As previously stated, for some species that have significant foam applications, i.e., CFC-11, HCFC-141b, and HCFC-142b, these emission differences are greater than a factor of two, with the estimated bottom-up emission underpredicting those derived from observed mixing ratio changes. In Table 1-7 of Chapter 1, an uncertainty range for the emissions in 2003 is given based on an uncertainty range in the lifetimes of the ODSs and calculations with the 12-box model. The uncertainty ranges of the inferred 2003 emissions are somewhat larger than those given in IPCC/TEAP (2005), but the IPCC ranges were due to model differences and to the variations in the trends of the different global networks, rather than different assumed lifetimes. Nevertheless, the top-down emissions in scenario A1 and bottom-up emissions of IPCC/TEAP (2005) for CFC-11, HCFC-141b, and HCFC-142b cannot be reconciled taking these uncertainties in emissions into account. These differences illustrate that there is a need for greater understanding regarding the possible shortcomings of the bottom-up approach and the differences between it and past approaches. The discrepancies are large enough to cast some doubt on projected future emissions that are based on the published bottom-up results alone. Section 8.3.4 contains a more extensive discussion of uncertainties.

8.3.2.2 MIXING RATIOS

The projected ODS mixing ratios for the baseline scenario are mostly consistent with those of the previous Assessment before the year 2002 because the previous Assessment's past mixing ratios were based on observations, and here observations are used as a direct constraint (see Figure 8-2). The observations are taken primarily from the Earth System Research Laboratory / Global

Monitoring Division (ESRL/GMD) (formerly Climate Monitoring and Diagnostics Laboratory, CMDL) (Montzka et al., 1999) and Advanced Global Atmospheric Gases Experiment (AGAGE) networks (Prinn et al., 2005) (and include the University of East Anglia observations for halon-1211), and the calibration factors were calculated in a similar manner as in Table 1-15 of WMO (2003). After correcting for calibration differences, the mean mixing ratios of the ESRL/GMD and AGAGE networks are used for temporally overlapping periods for the CFCs, CH_3CCl_3 , and for CCl_4 . For periods before any overlap exists, the ratios of the measurements are used to extend the record backward in time in a consistent manner. The average of the December and January observations are assumed to represent the mixing ratios at the start of the year, with the mixing ratios for the rest of the year calculated from estimated emissions and lifetimes. Although the model is run in 0.1-year time steps, yearly observations are used instead of monthly ones in order to avoid the impact of seasonal variability on the inferred emissions, which are assumed to be constant throughout each year. Calculated mixing ratios are tabulated in Table 8-5 for each of the considered halocarbons from 1955 through 2100. The yearly observations used are indicated in the table by the shaded regions.

Time series are shown in Figure 8-2 for the current A1 scenario and the previous Ab scenario. There are some differences between mixing ratios of this Assessment compared with the previous one for the period 2001-2004, but the greatest differences are found in the future projections. The HCFC-22 projection exhibits the most striking differences compared with the previous Assessment's scenario Ab projection with a peak mixing ratio over 150 ppt higher and peaking more than 20 years later. In contrast, HCFC-141b, HCFC-142b, and halon-1301 exhibit decreases in near-term projected mixing ratios compared with the Ab scenario, due to the decrease in observed growth rates from 2001 through 2004 and the expectation of lower future emissions for these species (Figure 8-1). Due to the increased emissions discussed in Section 8.3.2.1, future CFC-11 and CFC-12 mixing ratios also exhibit modest, but important, increases compared with the previous Assessment. Carbon tetrachloride decreases more slowly in A1 due to greater emission in the coming decade, with the increased emission based on the uncertain source of much of the global CCl_4 emission (see Chapter 1) and the slow decline of annual emissions over the past 15 years.

Table 8-5. Mixing ratios (ppt) of the ODSs considered in scenario A1. Values are for the beginning of the corresponding year. Potentially important short-lived gases that may currently contribute 3-8 ppt of stratospheric bromine and ~50 ppt of stratospheric chlorine (see Chapter 2) are not shown in the table.

	CFC-11	CFC-12	CFC-113	CFC-114	CFC-115	CCl ₄	CH ₃ CCl ₃	HCFC-22	HCFC-141b	Halon-142b	Halon-1211	Halon-1202	Halon-1301	Halon-2402	CH ₃ Br	CH ₃ Cl
	1955	3.3	14.3	1.3	2.6	0.0	42.4	0.1	1.0	0.0	0.0	0.00	0.00	0.00	0.00	7.13
1960	9.5	29.5	1.9	3.9	0.0	52.1	1.5	2.1	0.0	0.0	0.00	0.00	0.00	0.00	7.30	510.3
1965	23.5	58.8	3.1	5.1	0.0	64.4	4.7	4.9	0.0	0.0	0.00	0.00	0.00	0.00	7.49	528.1
1970	52.8	114.3	5.5	6.5	0.2	75.9	16.3	12.1	0.0	0.0	0.02	0.00	0.00	0.01	7.71	539.9
1975	106.1	203.1	10.4	8.2	0.6	85.5	40.0	23.8	0.0	0.1	0.12	0.00	0.04	0.04	7.97	545.8
1980	163.7	294.9	20.1	10.3	1.5	93.4	82.0	40.5	0.0	0.3	0.43	0.01	0.24	0.11	8.27	548.3
1981	173.4	313.6	22.9	10.8	1.8	94.6	89.9	44.4	0.0	0.3	0.53	0.01	0.31	0.12	8.34	548.6
1982	182.3	329.8	26.0	11.3	2.1	95.3	94.5	48.0	0.0	0.3	0.64	0.01	0.39	0.14	8.41	548.9
1983	189.3	346.5	29.2	11.7	2.4	96.5	98.2	52.0	0.0	0.4	0.76	0.02	0.49	0.16	8.48	549.1
1984	198.2	363.5	32.8	12.2	2.8	98.1	103.3	56.3	0.0	0.4	0.90	0.02	0.61	0.18	8.55	549.3
1985	207.5	381.5	38.1	12.7	3.2	99.6	108.1	60.6	0.0	0.5	1.06	0.02	0.74	0.20	8.62	549.4
1986	216.7	398.1	41.8	13.2	3.6	100.1	111.1	65.1	0.0	0.5	1.25	0.02	0.89	0.22	8.70	549.5
1987	228.9	419.2	46.8	13.7	4.0	102.1	113.2	69.7	0.0	0.7	1.46	0.02	1.06	0.24	8.78	549.6
1988	240.9	437.7	54.3	14.3	4.4	102.8	119.4	75.1	0.0	0.9	1.72	0.02	1.25	0.26	8.86	549.7
1989	248.9	458.8	61.6	14.8	4.8	104.1	124.0	81.3	0.0	1.1	2.02	0.03	1.46	0.29	8.94	549.8
1990	256.6	473.5	67.4	15.3	5.3	104.8	124.9	87.3	0.0	1.4	2.31	0.03	1.66	0.31	9.03	549.8
1991	263.7	489.1	73.2	15.8	5.8	106.4	130.9	93.5	0.0	2.0	2.59	0.03	1.84	0.34	9.12	549.9
1992	266.2	499.7	78.7	16.2	6.3	105.1	130.9	99.9	0.0	2.9	2.84	0.03	1.98	0.36	9.21	549.9
1993	269.3	509.9	81.7	16.5	6.7	104.7	130.1	104.4	0.0	3.9	3.00	0.03	2.06	0.38	9.30	549.9
1994	269.7	516.3	83.0	16.8	7.2	104.0	121.9	108.8	1.1	5.0	3.18	0.04	2.17	0.40	9.40	549.9
1995	269.3	522.8	84.0	16.9	7.6	103.1	109.9	112.1	2.7	6.3	3.31	0.04	2.33	0.42	9.50	550.0
1996	268.6	527.3	83.7	17.0	8.0	102.5	98.3	119.6	4.5	7.4	3.47	0.04	2.45	0.43	9.10	550.0
1997	267.8	531.0	83.6	17.1	8.2	101.4	84.2	124.3	6.6	8.5	3.64	0.05	2.52	0.43	9.06	550.0
1998	266.1	533.8	83.3	17.1	8.5	100.4	71.5	128.4	8.2	9.4	3.77	0.05	2.59	0.42	9.25	550.0
1999	264.3	536.1	82.8	17.1	8.6	99.9	59.7	135.0	10.2	10.5	3.90	0.05	2.65	0.42	9.27	550.0
2000	262.6	538.1	82.3	17.0	8.7	98.8	49.9	139.8	11.9	11.6	4.01	0.05	2.71	0.41	8.90	550.0
2001	261.2	539.7	81.9	17.0	8.8	98.0	41.6	144.1	13.5	12.5	4.08	0.04	2.76	0.41	8.48	550.0
2002	259.0	540.2	81.3	17.0	8.9	96.8	34.6	150.8	14.9	13.5	4.14	0.04	2.81	0.40	8.22	550.0

Table 8-5, continued.

	CFC-11		CFC-113		CFC-115		CH ₃ CCl ₃		HCFC-22		HCFC-141b		Halon-142b		Halon-1211		Halon-1202		Halon-1301		CH ₃ Br		CH ₃ Cl
	CFC-11	CFC-12	CFC-113	CFC-114	CFC-115	CCl ₄	CH ₃ CCl ₃	HCFC-22	HCFC-141b	HCFC-142b	Halon-1211	Halon-1202	Halon-1301	Halon-2402	CH ₃ Br	CH ₃ Cl							
2003	256.9	539.9	80.6	16.9	9.0	95.8	28.9	155.1	16.2	14.1	4.20	0.03	2.85	0.39	8.17	550.0							
2004	255.2	539.9	79.7	16.9	9.0	94.9	24.0	159.8	17.0	14.7	4.22	0.03	2.89	0.38	8.01	550.0							
2005	253.0	538.9	78.9	16.8	9.1	94.0	20.1	164.7	17.4	15.2	4.24	0.02	2.93	0.37	7.86	550.0							
2006	249.6	536.1	78.0	16.8	9.1	92.9	16.9	170.7	17.9	15.5	4.25	0.02	2.96	0.36	7.64	550.0							
2007	246.3	533.3	77.2	16.7	9.1	91.7	14.3	177.1	18.5	15.8	4.24	0.02	2.99	0.35	7.55	550.0							
2008	242.9	530.3	76.3	16.7	9.1	90.2	12.2	183.9	19.1	16.0	4.21	0.01	3.01	0.34	7.53	550.0							
2009	239.6	527.2	75.4	16.6	9.1	88.6	10.4	191.1	19.7	16.2	4.17	0.01	3.04	0.32	7.53	550.0							
2010	236.3	523.9	74.6	16.6	9.1	86.8	9.0	198.5	20.4	16.3	4.12	0.01	3.05	0.31	7.52	550.0							
2015	219.8	506.0	70.3	16.3	9.1	75.0	4.4	238.7	23.2	16.4	3.73	0.00	3.10	0.26	7.52	550.0							
2020	203.8	486.2	66.3	16.0	9.1	61.9	1.6	279.7	25.0	15.3	3.22	0.00	3.08	0.21	6.99	550.0							
2025	188.4	465.6	62.5	15.8	9.1	51.1	0.6	314.8	26.2	13.5	2.70	0.00	3.01	0.17	6.99	550.0							
2030	173.7	444.9	59.0	15.5	9.0	42.1	0.2	342.1	27.0	11.6	2.22	0.00	2.91	0.13	6.99	550.0							
2035	159.7	424.5	55.6	15.3	9.0	34.8	0.1	354.8	27.2	9.8	1.79	0.00	2.79	0.10	6.99	550.0							
2040	146.5	404.7	52.4	15.0	9.0	28.7	0.0	330.0	26.0	8.1	1.42	0.00	2.66	0.08	6.99	550.0							
2045	134.2	385.4	49.4	14.8	9.0	23.7	0.0	269.6	23.2	6.6	1.12	0.00	2.52	0.06	6.99	550.0							
2050	122.7	367.0	46.6	14.5	8.9	19.5	0.0	203.7	19.7	5.3	0.88	0.00	2.38	0.05	6.99	550.0							
2055	112.0	349.3	43.9	14.3	8.9	16.1	0.0	147.2	16.3	4.2	0.68	0.00	2.24	0.04	6.99	550.0							
2060	102.1	332.4	41.4	14.0	8.9	13.3	0.0	103.5	13.2	3.3	0.53	0.00	2.10	0.03	6.99	550.0							
2065	92.9	316.3	39.1	13.8	8.9	11.0	0.0	71.4	10.6	2.6	0.40	0.00	1.97	0.02	6.99	550.0							
2070	84.5	300.9	36.8	13.6	8.8	9.0	0.0	48.7	8.4	2.0	0.31	0.00	1.84	0.02	6.99	550.0							
2075	76.7	286.3	34.7	13.4	8.8	7.5	0.0	32.9	6.6	1.6	0.23	0.00	1.71	0.01	6.99	550.0							
2080	69.6	272.3	32.7	13.1	8.8	6.2	0.0	22.1	5.2	1.2	0.18	0.00	1.60	0.01	6.99	550.0							
2085	63.1	259.1	30.9	12.9	8.8	5.1	0.0	14.8	4.1	0.9	0.13	0.00	1.48	0.01	6.99	550.0							
2090	57.1	246.5	29.1	12.7	8.7	4.2	0.0	9.8	3.2	0.7	0.10	0.00	1.38	0.01	6.99	550.0							
2095	51.7	234.4	27.4	12.5	8.7	3.5	0.0	6.5	2.5	0.6	0.08	0.00	1.28	0.01	6.99	550.0							
2100	46.7	223.0	25.9	12.3	8.7	2.9	0.0	4.3	1.9	0.4	0.06	0.00	1.19	0.00	6.99	550.0							

Note: Areas are shaded for compounds in years when mixing ratio values are forced to equal global estimates calculated from observations. Global means for CH₃Br and CH₃Cl before 1996 were derived from South Pole firm air observations (Butler et al., 1999) and based on surface observations of CH₃Br after 1996 (Montzka et al., 2003). All other shaded areas are from atmospheric observations from one or more measurement networks (see text). Halon-1301 values used in this scenario fall between the global estimates made from observations of the NOAA/ESRL and AGAGE networks.

HALOCARBON SCENARIOS, ODPs, AND GWPs

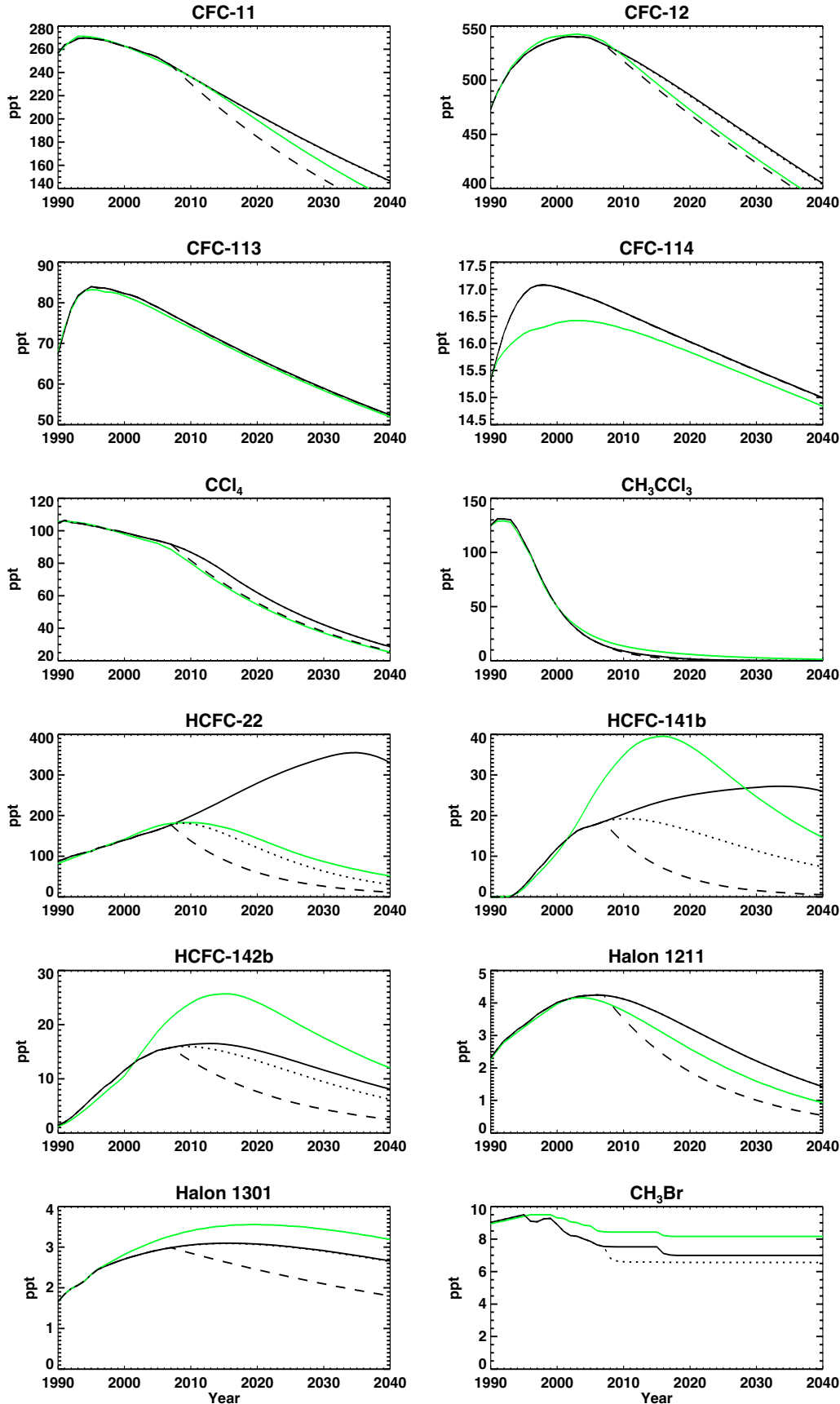


Figure 8-2. Projected mixing ratios of selected halocarbons for scenarios A1 (solid black), Ab (green, previous Assessment), E0 (dashed curve), and P0 (dotted curve). Note that for many of the gases, little or no future production is included in the A1 scenario, so the P0 curve is obscured by the A1 curve. For CH₃Br, the E0 and P0 curves are identical.

8.3.2.3 EQUIVALENT EFFECTIVE STRATOSPHERIC CHLORINE

The equivalent effective stratospheric chlorine (EESC) index (see Daniel et al., 1995; WMO, 2003) has been used in past Assessments and is summarized in Box 8-1. It is used as a measure of the amount of chlorine and bromine available in the stratosphere to destroy ozone. Here, we set f_{CFC-11} , the absolute fractional release value for CFC-11 (Equation 1 of Box 8-1), to be 0.84 as was done in the previous Assessment, with the ρ values assumed to be equal to the surface mixing ratios. This factor was incorrectly stated to be 0.8 in footnote “a” of Table 1-4 in the previous Assessment. It should also be noted that the CH_3Br mixing ratio at the tropopause may be less than the surface mixing ratio by a non-negligible amount due to its relatively large tropospheric loss (see Chapter 2); this would lead to

an additional reduction in the EESC contribution from CH_3Br that is not considered in this chapter. Newman et al. (2006) have extended the definition of EESC in order for it to correspond to the actual amount of inorganic chlorine and bromine in various stratospheric locations by applying location-appropriate age spectra, fractional release values, and “ f_{CFC-11} ” values. We do not consider the variation of EESC with stratospheric location, except in accounting for the older age of air in the Antarctic polar vortex as discussed below. Instead, we continue using EESC as an index that is only proportional to overall stratospheric inorganic chlorine and bromine. Very short-lived species are currently not included in the EESC calculation. In the future, as our knowledge of the very short-lived bromocarbon source gases improves (see Chapter 2), it may be warranted to link EESC directly with spatially varying inorganic chlorine and bromine in order to assess the importance of

Box 8-1. Equivalent Effective Stratospheric Chlorine (EESC)

Due to the established relationship between stratospheric ozone depletion and inorganic chlorine and bromine abundances, the temporal evolution of chlorine- and bromine-containing source gases is an important indicator of the potential effects of anthropogenic activity on the health of stratospheric ozone. Indices have been developed to demonstrate this halogen evolution in a simple manner. They account for the greater per-atom potency of stratospheric bromine (Br) compared with chlorine (Cl) in its ozone destructiveness with a constant factor, α (Section 8.2.2.3), and include the varying rates at which Cl and Br will be released in the stratosphere from different source gases.

EESC provides a simple index that relates the time evolution of long-lived surface abundances of ODSs with the ozone-destructive ability of stratospheric halogens that come from these long-lived source gases (WMO, 1995, 1999, 2003). Contributions of very short-lived chlorine- and bromine-containing sources gases and of tropospheric inorganic halogens generally have been neglected. EESC is defined as

$$EESC(t) = f_{CFC-11} \left[\sum_{\substack{\text{Cl-containing} \\ \text{halocarbons}}} n_i \frac{f_i}{f_{CFC-11}} \rho_{i,entry} + \alpha \sum_{\substack{\text{Br-containing} \\ \text{halocarbons}}} n_i \frac{f_i}{f_{CFC-11}} \rho_{i,entry} \right] \quad (1)$$

(Daniel et al., 1995), where n is the number of chlorine or bromine atoms in the source gas, f_i/f_{CFC-11} represents the efficiency of the stratospheric halogen release relative to that of CFC-11, denoted by f_{CFC-11} (Section 8.2.2.2), and $\rho_{i,entry}$ is the tropospheric mixing ratio of source gas i when it entered the stratosphere. Traditionally, $\rho_{i,entry}$ is calculated assuming a simple time lag Γ from the surface observations, i.e.,

$$\rho_{i,entry}(t) = \rho_i(t - \Gamma) \quad (2)$$

where $\rho_i(t)$ is the surface mixing ratio at time t . In WMO (2003), EESC was estimated assuming $\Gamma = 3$ years (typical of the lower, midlatitude stratosphere) to obtain a value appropriate for relating to midlatitude-averaged ozone loss. Effective equivalent chlorine (EECl) (Montzka et al., 1996) is a quantity similar to EESC, but includes no consideration of the transport lag time.

To retain the simplicity of the EESC index, several assumptions are generally made in its calculation. One such assumption is that the stratospheric entry mixing ratio for a given time is taken to be the surface mixing ratio at that time. This could be an overestimate of the EESC contribution for shorter-lived gases, like CH_3Br , whose abundance may be reduced before reaching the tropopause. In Montzka et al. (2003), this issue has been addressed by reducing the surface mixing ratio by 7% in the calculation of EESC. A second assumption generally made in EESC calculations

Continued, next page.

Box 8-1, continued.

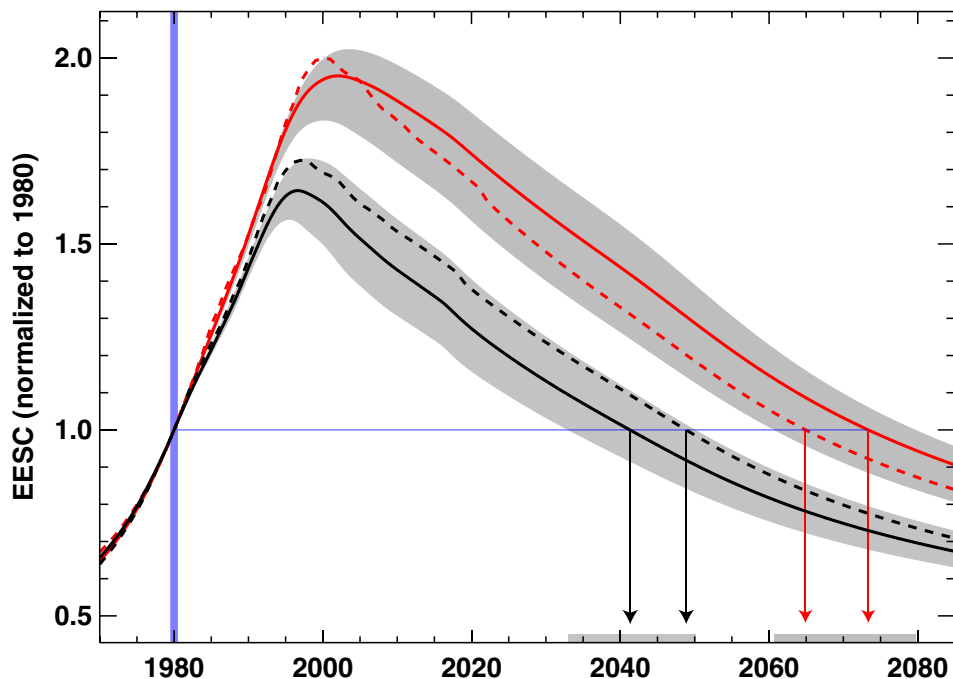
is the neglect of the transport time from the surface to the tropopause. Although the particular location of the surface emission affects the transport time to the tropopause, this is generally not considered.

Newman et al. (2006) extended the method of calculating EESC to account for the lack of a single transit time from the surface to a stratospheric location (i.e., stratospheric air is composed of air characterized by a range, or spectrum, of transit times, or ages) and that the fractional release values depend on the age of air. In Newman et al. (2006), $\rho_{i,entry}$ is calculated using

$$\rho_{i,entry}(t) = \int_{-\infty}^t \rho_i(t')G(t-t')dt' \tag{3}$$

where $G(t)$ is the age-spectrum, assumed to be an inverse Gaussian function with mean Γ and width Δ (see Equation 9 of Waugh and Hall, 2002), and $f_i = f_i(\Gamma)$. This reduces to the traditional EESC calculation if the mean age $\Gamma = 3$ yrs and the width $\Delta = 0$, i.e., (3) reduces to (2) when $\Delta = 0$. Including an age spectrum does not affect the EESC evolution when the temporal trend is constant, but acts to smooth changes over time when the trend is varying. Specifically, when an age spectrum is included, the period near when the maximum EESC occurs is characterized by a “flutter” or less peaked EESC time series.

The figure compares calculations of EESC, normalized by the 1980 value, for midlatitude and polar regions and illustrates some of the important sensitivities. The dashed lines show the EESC evolution used in Chapter 8 for midlatitudes (black) and inside the polar vortex in the lower stratosphere (red) (i.e., for $\Gamma = 3$ yrs and $\Delta = 0$ yrs for midlatitudes, and $\Gamma = 6$ yrs and $\Delta = 0$ yrs for the vortex). The solid lines show the same calculations using the fractional release values from Newman et al. (2006) and the same mean ages as the dashed lines, but with Δ equal to half the mean age in each case. The shaded regions show the sensitivity of the calculations using the Newman et al. fractional release values to a ± 1 -year mean age and with Δ always equal to half the mean age (e.g., for $\Gamma = 2$ yrs and $\Delta = 1$ yr, to $\Gamma = 4$ yrs and $\Delta = 2$ yrs for the midlatitude case). Using a larger value of Γ results in a shift in curves and leads to a much later recovery date, but does not change the EESC shape. Compared with the midlatitude recovery, the polar recovery time is delayed by much more than the 3-year older age of air because the magnitude of the slope of the EESC curve is projected to be much smaller in the mid-21st century than it was in 1980s. The inclusion of the age spectrum width in the polar calculation is the reason for the smoother EESC peak period but has little effect during periods when EESC is changing approximately linearly with time, and hence affects the time of return to 1980 levels only slightly.



these very short-lived species relative to long-lived source gases for ozone depletion.

As in previous Assessments, the year EESC returns to its 1980 levels is one metric used to compare different scenarios. The year 1980 is chosen because this is the approximate date when midlatitude and Antarctic ozone depletion has been observed to begin. It generally has been assumed that if all other atmospheric parameters and processes remain constant, ozone depletion relates linearly to EESC above a certain threshold level. An exception to this relationship is Antarctic ozone depletion. Springtime depletion became so great around 1990 that there was not enough ozone left in the lower stratosphere for the column

ozone amount to continue to follow a linear relationship with EESC. So it is assumed here (in the calculations of indirect GWPs, Section 8.5) that no additional Antarctic ozone destruction occurs for EESC values above 1990 levels. The second metric that has been used to compare scenarios is the integrated EESC value above the 1980 level, integrated from 1980 or the current time until EESC returns to the 1980 level. This metric is meant to represent the cumulative ozone depletion due to ODSs over the specified time frame.

The contributions of the various halocarbon groups to EESC for scenario A1, as well as for scenario Ab of the previous Assessment, are shown in Figure 8-3. The CFCs continue to be the dominant source of EESC, although as

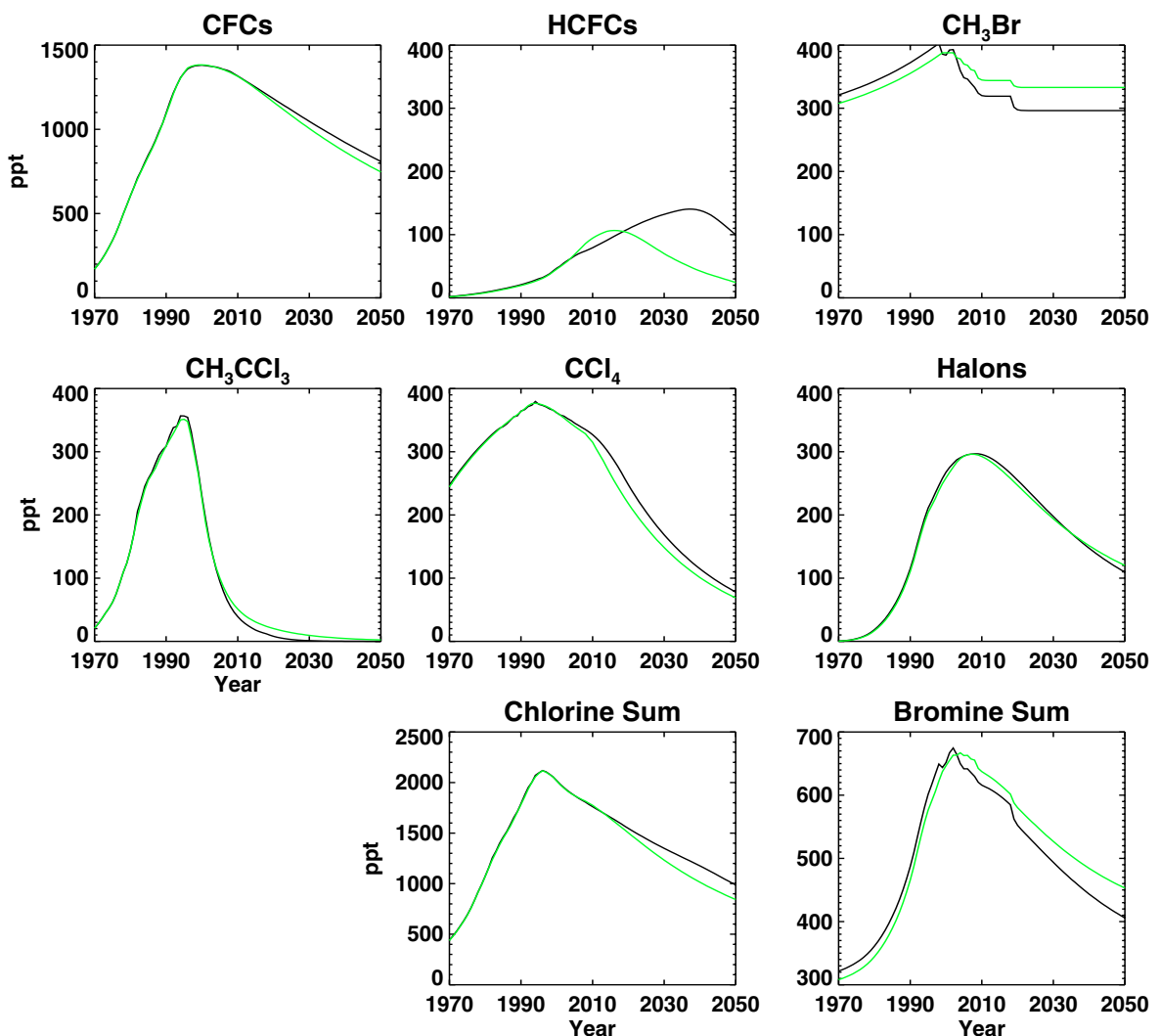


Figure 8-3. Contributions of halocarbon groups to global EESC for this Assessment (A1 scenario, black lines) and the previous Assessment (Ab scenario, green lines). The “chlorine sum” and “bromine sum” represent the total EESC from these particular chlorine and bromine long-lived source gases. EESC values for CH₃Br, the halons, and the bromine sum for this Assessment are scaled by 45/60 to eliminate the effect of the change in the α value, for easier comparison with the previous Assessment values.

HALOCARBON SCENARIOS, ODPs, AND GWPs

a group their contribution has begun to decrease, driven mostly by the decline of CFC-11. In terms of EESC, the most striking differences between the A1 and Ab scenarios are the HCFCs. As discussed in Sections 8.3.2.1 and 8.3.2.2, this increasing importance of the HCFCs is primarily due to the increase in expected future production and emission of HCFC-22 (Table 8-4). The updates to future emissions of CFCs and HCFCs lead to slight increases in the importance of these ODS groups to EESC in the future. Updates to the fractional halogen release values of the halons lead to a slightly larger contribution of these compounds. Estimated CH₃Br abundances are also noticeably different from WMO (2003). The differences from 1996 through 2004 arise because of the availability of new global surface data (Montzka et al., 2003, and updates). After that period, differences arise because of the larger assumed anthropogenic fraction of CH₃Br emission compared with WMO (2003) (30% compared with 20%), also based on Montzka et al. (2003). Overall, the updates to the future ODS emissions projections and the increase in the estimated value for α lead to a later “recovery” of midlatitude-relevant EESC, defined here as a return to pre-1980 values, by about 5 years.

In past Assessments, quantification of midlatitude-relevant EESC was used exclusively. These calculations assumed a lag of 3 years between surface and stratospheric mixing ratios and assumed a value for α of 45. However, it is known that the age of air in the wintertime polar vortex is greater than 3 years (Andrews et al., 2001; Daniel et al., 1996; Harnisch et al., 1999), and there are indications that the value of α should be larger, due to the stronger coupling of bromine monoxide (BrO) with chlorine monoxide (ClO) (Chipperfield and Pyle, 1998). Both of these points act to delay the halocarbon recovery of the polar vortex compared with midlatitudes. Consideration of the spectrum of ages that make up wintertime vortex air can further delay halocarbon recovery (Newman et al., 2006). The time lag increase is expected to be particularly important because of the fast increase in halocarbon abundances in the 1980s and the relatively slow decline expected in the future due to halocarbon lifetimes of decades. If a time lag is assumed to be 6 years and a value of α of 65 (Chipperfield and Pyle, 1998), the year of EESC recovery for Antarctic conditions is 2065, more than 15 years later compared with the midlatitude EESC recovery; the time lag increase is responsible for almost 13 of the 15 years, with the change in α responsible for the rest. Due to the large sensitivity of the EESC recovery to the age of air, all scenarios will be performed for midlatitude-relevant and polar vortex-relevant EESC. Newman et al. (2006) have also shown that the use of a simple lag can lead to

errors in estimated EESC, particularly near the peak period. However, because there is little difference in the recovery date when using a simple lag or a more complicated age spectrum, and because there is no agreement on a particular globally averaged age spectrum to use, we continue to use a simple time lag in this Assessment.

8.3.3 Alternative Projections

8.3.3.1 EMISSIONS

The alternative hypothetical cases used to examine the relative environmental effects of reducing future production and emissions of groups of halocarbons are compared in Table 8-6 and fall into three categories, each of which is based on the baseline A1 scenario: (1) “no future emission” cases (E0); (2) “no future production” cases (P0); and (3) cases of the full capture and destruction of the 2007 bank (B0). Assumptions of the alternative projections lead to various decreases in future emissions when compared with the baseline scenario. The hypothetical elimination of all future emissions (E0) represents the greatest possible reduction in future abundances. The hypothetical elimination of future production (P0) allows the ODSs currently residing in banks to continue to be released to the atmosphere as they would in the baseline scenario. The projections that consider the full capture and destruction of the 2007 bank (B0) complement the “no production” cases in that the full 2007 bank is destroyed in a manner that releases no ODS to the atmosphere; future production and the resulting future buildup of banks is allowed to continue, however. This expected future production is small for the CFCs and halons, but significant for the HCFCs. A case consistent with the mitigation scenario presented in IPCC/TEAP (2005) is assessed to illustrate the importance of emissions reductions from this carefully developed scenario on the future evolution of EESC. The mitigation scenario has a significant effect only on the banks of HCFC-22, HCFC-123, and HFCs in 2015 (the latter two are not considered in the cases or scenarios of this chapter).

8.3.3.2 MIXING RATIOS

The calculated mixing ratios from 1990 through 2040 are shown in Figure 8-2 for the E0 and P0 cases in addition to the previously discussed A1 and Ab scenarios. These calculations suggest that all ODSs considered here, except for the HCFCs and possibly halon-1301 have already reached their peak mixing ratios. The HCFCs are expected to reach peak abundances between 2010 and

Table 8-6. Comparison of scenarios and hypothetical cases ^a: the year when EESC drops below the 1980 value for both midlatitude and polar vortex cases, and integrated EESC differences (midlatitude case) relative to the baseline (A1) scenario. Note that the polar recovery times have not been given in previous Assessments; interpretation of any comparison between these numbers and recovery times given in previous Assessments requires an understanding of the large role played by the different transport times from the troposphere to the stratospheric midlatitude and polar vortex regions.

Scenario and Cases	Percent Difference in integrated EESC relative to baseline scenario for the midlatitude case		Year (x) when EESC is expected to drop below 1980 value	
	Midlatitude		Antarctic vortex ^b	
	$\int_{1980}^x EESC dt$	$\int_{2007}^x EESC dt$		
Scenarios				
A1: Baseline scenario			2048.9	2065.1
Cases ^a of zero production from 2007 onward of:				
P0: All ODSs	-8.0	-17.1	2043.1	2060.3
CFCs	-0.1	-0.3	2048.8	2065.0
Halons	-0.2	-0.5	2048.8	2065.1
HCFCs	-5.5	-11.8	2044.4	2062.2
Anthropogenic CH ₃ Br	-2.4	-5.1	2047.9	2063.7
Cases ^a of zero emissions from 2007 onward of:				
E0: All ODSs	-19.4	-41.7	2034.0	2049.9
CFCs	-5.3	-11.5	2045.0	2060.3
CH ₃ CCl ₃	-0.1	-0.2	2048.9	2065.1
Halons	-6.7	-14.4	2045.6	2061.9
HCFCs	-7.3	-15.7	2043.7	2061.8
CCl ₄	-1.3	-2.9	2048.5	2064.9
Anthropogenic CH ₃ Br	-2.4	-5.1	2047.9	2063.7
Cases ^a of full recovery of the 2007 banks of:				
B0: All ODS	-12.9	-27.8	2040.8	2056.7
CFCs	-5.2	-11.3	2045.1	2060.4
Halons	-6.7	-14.3	2045.7	2062.0
HCFCs	-1.9	-4.1	2048.4	2064.8
CH₃Br sensitivity:				
Same as A1, but CH ₃ Br anthropogenic emissions set to 20% in 1992 ^c	3.1	6.6	2050.6	2067.7
Same as A1, but zero QPS production from 2015 onward	-1.5	-3.2	2047.9	2063.7
Same as A1, but critical-use exemptions continued at 2006 level	1.9	4.0-4.7	2050.1	2067.0

^a Importance of ozone-depleting substances for future EESC were calculated in the hypothetical "cases" by setting production or emission to zero in 2007 and subsequent years or the bank of the ODS to zero in the year 2007 alone. These cases are not mutually exclusive, and separate effects of elimination of production, emissions, and banks are not additive.

^b This metric specifically for Antarctic polar vortex ozone depletion has not been shown in any previous ozone Assessment.

^c In the baseline scenario, this fraction was assumed to be 30% in 1992, with a corresponding emission fraction of 0.88 of production. In this alternative scenario, an anthropogenic fraction was assumed to be 20%, with an emission fraction of 0.56 of production. In both scenarios, the total historic emission was derived from atmospheric observations and a lifetime of 0.7 years.

HALOCARBON SCENARIOS, ODPs, AND GWPs

2035, with scenario A1 peak mixing ratios of HCFC-22 and HCFC-141b more than 50% higher than current values.

A comparison of the A1 curves with the P0 and the E0 curves illustrates the relative importance of the amount of an ODS already in existing equipment compared with what is expected to be produced and emitted in the future. For CFC-11 and CFC-12, for example, the amounts currently in the atmosphere and in the banks together dominate the future mixing ratio evolution. In contrast, for HCFC-22, the future production is expected to be far more important than the current bank. Gases like CH_3CCl_3 , CCl_4 , and CFC-113 are believed to have small banks in applications and are not expected to be produced much in the future; the future decline of these compounds is thus controlled almost exclusively by their lifetimes and can be accelerated little by any policy measures.

8.3.3.3 EQUIVALENT EFFECTIVE STRATOSPHERIC CHLORINE

Total midlatitude-relevant EESC time series projections are shown in Figure 8-4 for scenarios A1 (baseline); the zero production P0, zero emission E0, and full 2007 bank recovery B0 cases; and the no-Protocol scenario H1 (from WMO, 1999). The assumption of a 3-year time lag implies that any change in emission as early as 2007 will not affect EESC until 2010. Regions in the stratosphere characterized by younger (older) ages will respond more quickly (slowly). The EESC results illustrate that there is still a wide range in EESC projections before halocarbons recover to pre-1980 conditions. The calculated changes in EESC due to a cessation in future production and emission are shown for CFCs, HCFCs, and halon groups in Figure 8-5 (left column). These time series show the importance of future HCFC production (and associated emission) and the potential EESC reduction they can provide. For CFCs and halons, the amount of ODSs in the banks plays a larger role than does expected future production. This figure also shows the effect of the same scenarios on future radiative forcing. A comparison between the forcing and EESC estimates illustrates the greater relative importance of the HCFCs and the small significance of the halons when radiative forcing is considered. This large difference in significance of the halons for ozone depletion and climate change is due to the fact that the chemical enhancement of bromine's importance relative to chlorine for ozone depletion (α) plays no role in the direct radiative forcing of bromocarbons.

The times when midlatitude-relevant and Antarctic-relevant EESC values drop below the 1980 levels are shown

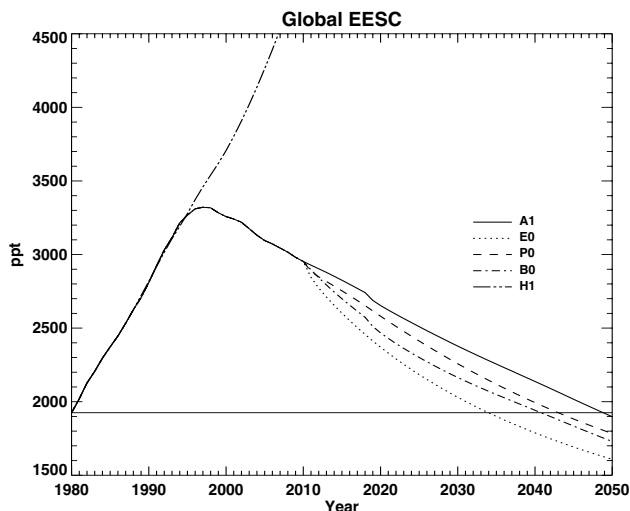


Figure 8-4. Midlatitude EESC projection calculated for 5 scenarios and cases: A1 (baseline), zero production P0, zero emission E0, full 2007 bank recovery B0, and the no-Protocol scenario H1 (from WMO, 1999). Any potential contributions of VSLs to EESC are not included.

in Table 8-6. Table 8-6 also includes the relative change in integrated midlatitude EESC for the various cases and scenarios when integrating from 1980 to the time of recovery and from 2007 to the time of recovery. For the midlatitudes, the quantity integrated from 1980 to the time of recovery can be thought of as a proxy for integrated ozone loss over the whole period of loss. The quantity integrated from 2007 can be thought of as a proxy for integrated future ozone loss (WMO, 1995, 1999, 2003). As stated earlier, such linear relationships break down in the Antarctic stratosphere due to the nearly complete loss of ozone over a range of altitudes, and the resulting saturation of halogen-caused ozone depletion (Chapter 3 of WMO, 2003).

For the baseline scenario, midlatitude EESC is expected to drop below the 1980 value in 2049. This is about 5 years later than assessed in WMO (2003), mainly because of larger future HCFC-22 production and emission and larger CFC-11 and CFC-12 banks and emissions from these banks compared with WMO (2003).

If all production of anthropogenic ODSs were to cease in 2007, the year EESC returns to the 1980 value would be 2043 for the midlatitude case, about 6 years earlier than for the baseline scenario, and 2060 for the Antarctic, almost 5 years earlier than for the baseline. HCFCs are responsible for the majority of this earlier recovery (Table 8-6). However, because the HCFC consumption in developing countries is not limited until

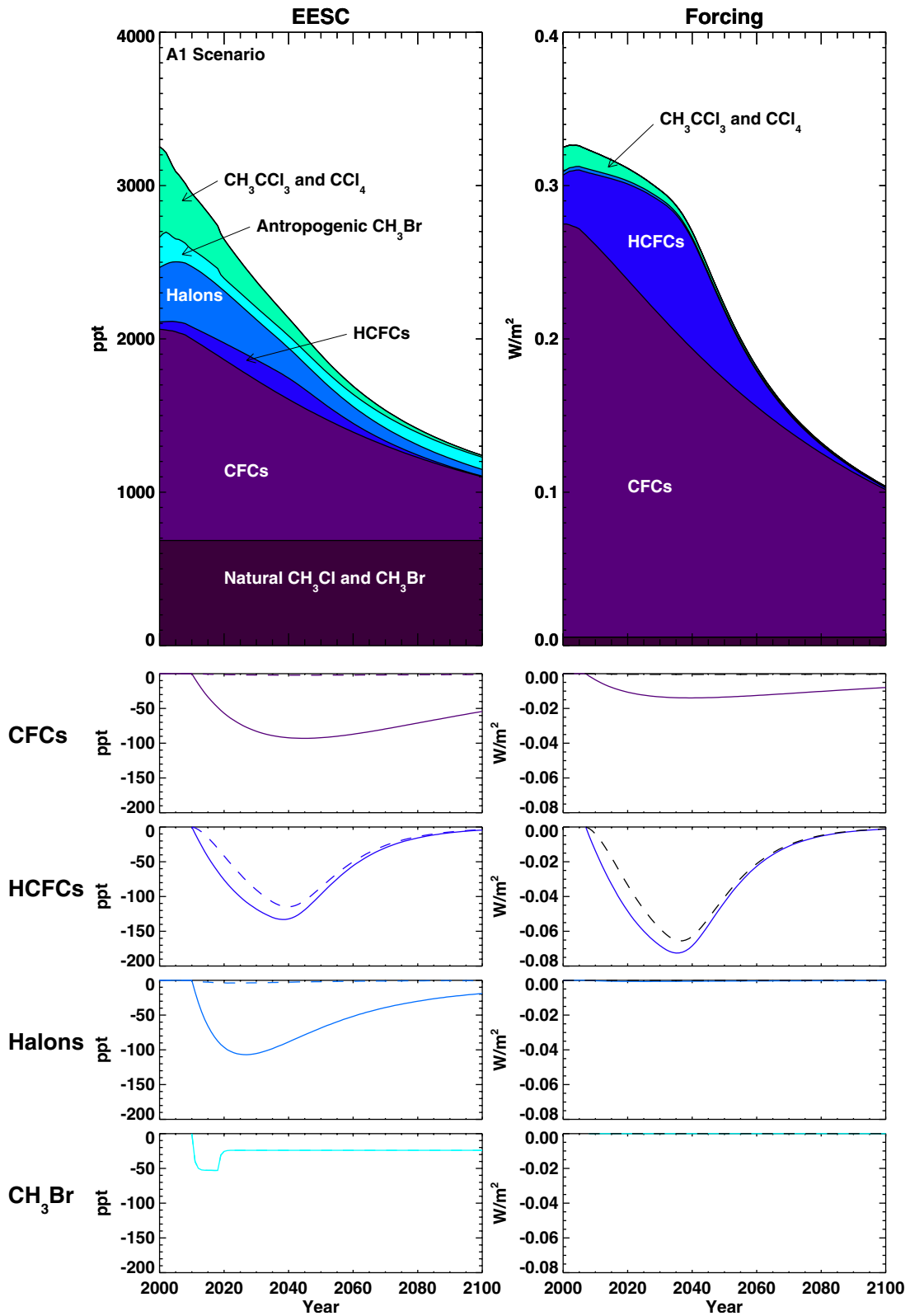


Figure 8-5. Projected EESC and radiative forcing decreases relative to the A1 scenario due to a cessation of emission (solid curves) and production (dashed curves) in 2007 for CFCs, HCFCs, halons, and anthropogenic CH_3Br . The forcing curves for the halons and CH_3Br are nearly indistinguishable from zero due to the much lower atmospheric abundances of halons and CH_3Br compared with CFC and HCFCs.

HALOCARBON SCENARIOS, ODPs, AND GWPs

2015, the assumptions regarding this consumption in the A1 scenario largely determine the magnitude of this earlier recovery. Smaller contributions come from the future production of CFCs, halons, and methyl bromide.

In the hypothetical case in which all anthropogenic emissions of ODSs were to cease in 2007, the future mixing ratios and EESC are governed entirely by the natural destruction in the atmosphere (and ocean/soil) of the ODSs. In this case the midlatitude EESC would drop below the 1980 value in 2034. The largest contributions to the zero emission cases come from HCFCs (especially HCFC-22), CFCs, and halons.

In the hypothetical case that the 2007 bank of CFCs, halons, and HCFCs were fully recovered and prevented from being emitted into the atmosphere, EESC would drop below the 1980 value 4, 3, and 0.5 years earlier, respectively, compared with the baseline scenario.

In the IPCC (IPCC/TEAP, 2005) "mitigation" scenario, economic, and technological analyses were performed in an attempt to determine reasonable reductions in future ODS emissions that could be accomplished using current best-practice emission reduction techniques. The mitigation scenario shows a decrease from 1879 to 1587 ktons in the bank of HCFC-22 in 2015. This decrease in the bank leads to a reduced emission over the period 2007-2050 from 15 to 11 Mt, contributing to an ODP-weighted decrease of the HCFCs from 1.0 to 0.8 Mt. The emission reduction in the mitigation scenario corresponds thereby to about 20% of the zero-emissions case of the HCFCs. Hence, the effects of the mitigation scenario, in terms of the length of time required for the ODSs to return to 1980 levels and the integrated EESC above the 1980 level, are also about 20% of the effects of the zero emissions case of the HCFCs (Table 8-6).

A few additional cases have been assessed for methyl bromide. There is uncertainty (see Section 1.2.1.7) regarding the fraction of anthropogenic emissions that comprise the sources needed to balance the sinks that are based on the observed surface mixing ratio and a global lifetime of 0.7 years. Montzka et al. (1999) estimated that the emission of CH₃Br resulting from industrial production is between 10% and 40% of the total emission in 1992. In the baseline scenario, this fraction is assumed to be 30%, higher than assumed in WMO (2003), but consistent with the discussions in Chapter 1. As a sensitivity study, an anthropogenic fraction of 20% was assumed in an alternative scenario. In our calculations, this 20% fraction is consistent with an emission fraction of 0.56 of the industrial production, meaning that 56% of the industrially produced CH₃Br is emitted to the atmosphere. This is, in turn, consistent with the range of 0.43-0.87 from agricultural and related uses as reported by UNEP (1998). The magnitude

of natural emissions for this case is 165 ktons, compared with 146 ktons in scenario A1, and compared with a total anthropogenic production of 73 ktons in 1992. In this alternative scenario, EESC drops below the 1980 value almost 2 years later than in the baseline scenario, demonstrating the expected effect of a smaller significance of anthropogenic CH₃Br emission reductions in a case in which natural emission plays a larger role.

A complete phase-out (except for critical and non-regulated uses) of the production and consumption of methyl bromide in developed countries (non-Article 5(1)) came into effect in 2005. Several countries have asked and obtained exemptions for critical uses of methyl bromide. In 2005, these exemptions totaled about 14 ktons and in 2006 about 13 ktons, which is 50-60% of the reported production in 2003-2004. In the baseline scenario, it is assumed that the critical-use exemptions continue at the 2006 level until 2015, when they are no longer granted and production in Article 5(1) countries is terminated. The existence of possible stockpiles of methyl bromide is not taken into account in the scenarios. If critical-use exemptions continue indefinitely at the 2006 level compared with a cessation of these exemptions in 2010 or 2015, midlatitude integrated EESC would increase by 4.7% or 4.0%, respectively.

Production of methyl bromide for quarantine and pre-shipment (QPS) is not controlled by the Montreal Protocol. In the baseline scenario, the QPS production, estimated at 10.7 ktons per year, is continued indefinitely. If the QPS production were to cease in 2015, the year EESC is expected to drop below the 1980 value is about a year earlier. This effect depends on the assumption of constant QPS emissions in the future in the baseline scenario and would be different if an alternative future QPS emission assumption were made. The estimated emissions of QPS are close to those of the critical-use exemptions and they have consequently similar contributions to the integrated EESC.

8.3.4 Uncertainties in ODS Projections

Numerous processes can affect the amount of ozone loss for a given halogen loading level. Many of these have been discussed in Chapters 5 and 6, and some will be mentioned in Section 8.4. Here we will focus on the uncertainties in the ODS projections themselves. Unfortunately, little work has been performed in this area, leading to a mostly qualitative assessment of the sensitivities of the projections presented here.

Before future emission projections based on the bottom-up analyses considered here can be considered fully reliable, the causes of the discrepancies with the top-down

estimates need to be better understood. Whether the missing emission from the bottom-up analysis is due to faster release from the bank than estimated, additional past production that has led to a larger bank and a correspondingly higher bank release, additional production and immediate release from use as solvent or aerosol propellant, or another factor, the particular assumptions made can lead to important differences in future ODS projections. A measure of the sensitivity of a particular gas's mixing ratio projection to the size of the bank, compared with future production uncertainties, can be obtained from Figures 8-2 and 8-5. For example, CFC-11 and the CFC group will have more sensitivity to uncertainties in the size of its bank, while HCFC-22 and the HCFC group will have more sensitivity to uncertainties in future production. While it is important to recognize the large emission discrepancies between these bottom-up analysis and observations for a few species, it is also important to consider the species that demonstrate relatively good agreement with emissions (CFC-12, HCFC-22, and halon-1211). Even for these species, there are important differences in the sizes of the estimated bank, depending on the method used to estimate this quantity. Table 8-7 shows a comparison of bank estimates from this Assessment, the previous Assessment (WMO, 2003), and IPCC/TEAP (2005). The large discrepancies between the CFC-11 and CFC-12 banks have been shown by Daniel et al. (2006) to have important implications for estimating the benefit of recycling/destroying the CFC banks. While the banks are calculated in this Assessment in a manner to agree best with the IPCC/TEAP (2005) estimates for many of the considered ODSs, the cause of this discrepancy has not been resolved.

Another potential explanation for some of the bank size discrepancy could be due to an error in the assumed factor of 1.07 that relates the surface mixing ratio to the globally averaged mixing ratio. A higher (lower) value for this factor would lead to smaller (larger) emissions estimated from atmospheric mixing ratio observations, and thus to larger (smaller) top-down bank sizes. Daniel et al. (2006) found, for example, that an increase in this factor to 1.10 from 1.07 would lead to an additional amount of banked CFC-11 in 2002 of 250 ktons, representing about 20% of the difference between the top-down estimate of WMO (2003) and the bottom-up estimate of IPCC/TEAP (2005).

Changes in atmospheric lifetimes, whether due to changing atmospheric dynamics or chemistry, can also affect future ODS projections. The recently published suggestion of an important soil sink that could reduce the carbon tetrachloride lifetime from 26 to 20 years (Happell and Roche, 2003), and its resulting implications for a quicker recovery of EESC to 1980 values, is one example

Table 8-7. Comparison of halocarbon banks (ktons) in 2002 used in this Assessment, the previous Assessment (WMO, 2003), and IPCC/TEAP (2005).

Species	WMO (2003) 2002 Bank	IPCC/TEAP (2005) 2002 Bank	This Assessment 2002 Bank
CFC-11	594	1,687	1,654
CFC-12	0	711	711
CFC-113	7	0	5
HCFC-22	1,317	1,531	1,531
HCFC-141b	753	836	674
HCFC-142b	210	224	224
Halon-1211	72	125	125
Halon-1301	58	42	42
CH ₃ CCl ₃	530		*

* Production and bank were not estimated; we assume emissions are equal to production, implying a zero bank. Protocol limitations are placed directly on emissions.

of the importance of lifetime uncertainties. Daniel et al. (2006) have shown that an increase in the CFC-11 lifetime by 10% would result in reduced annual emissions required to be consistent with observed mixing ratios that would lead to an increase in the 2002 bank by 300 ktons. The 12-box model emission estimates discussed in Section 8.3.2.1 can presumably account for changes in global lifetimes due to changing atmospheric distributions, as well as changes in the factor relating surface mixing ratio to the global mixing ratio average, better than the 1-box model. These differences likely play a role in the higher emissions estimates of the 12-box model (Section 8.3.2.1); however, these higher emissions would lead to smaller bank estimates using the top-down formalism in this chapter, and thus to even larger bank size discrepancies with the bottom-up analysis.

The release rate applied to the particular usage banks can affect the accuracy of future ODS projections. For example, there is a question as to how quickly ODSs are released from foam insulation once it is sent to a landfill (IPCC/TEAP, 2005). If foam ODSs were not released for 40 years, recycling these particular ODSs would have a much reduced benefit than if release were much sooner. This results because by the time the ODS would be finally released in the absence of recycling, EESC would have almost returned to pre-1980 levels in extrapolar regions of the lower stratosphere.

Sources of uncertainty in relating tropospheric mixing ratios to EESC include location- and time-dependent fractional chlorine/bromine release, age of air, and, α values.

HALOCARBON SCENARIOS, ODPs, AND GWPs

We have given examples of the potential significance of age of air and α variations, but there have been no studies examining the importance of the fractional halogen release variations with location. To the extent that much of the ozone depletion occurs in the lower stratosphere, where the release values remain relatively constant with location (Solomon et al., 1992), it has generally been assumed that any variability would represent a minor effect. The fractional chlorine release values of HCFC-141b and HCFC-142b represent two cases in which there is significant uncertainty regarding the correct value. The previous Assessment discussed the large differences between the previously assumed model-derived values and the values estimated from observations (Schauffler et al., 2003). The model-derived values were retained because of the large importance of the age-of-air correction in interpreting observations of gases with such a large growth rate. However, it is unlikely that the age-of-air correction could be responsible for such a large discrepancy. Unfortunately, no work has been performed since the previous Assessment to resolve these questions. Therefore, we continue to use the same values that were used in the previous Assessment, but caution that these values could be too large. While the ODPs of HCFC-141b and -142b are much larger than the ODP of HCFC-22, the effect of this fractional chlorine release uncertainty is limited by the lower projected mixing ratios of these two HCFCs compared with HCFC-22 (Figure 8-2). Nevertheless, uncertainties in the fractional release values for many of the ODSs do represent an important uncertainty in EESC calculations. These release values affect the relative importance of certain ODSs to total EESC and can thus affect future EESC evolution. If, for example, the Schauffler et al. release values (2- to 4.5-year means) were used instead of the ones assumed in this chapter, the EESC return to 1980 levels would occur about 3 years earlier.

It is important to recognize that errors in the accurate modeling of the baseline scenario can translate directly into errors in interpreting the alternative scenarios and test cases. For example, an error in the value of α will lead directly to an error in the assessment of the zero emission and production test cases for reducing EESC, particularly for the bromocarbons. As another example, any unreasonable assumption in the baseline scenario for future production of any species will necessarily affect the conclusions derived from both the “no production” and “no emission” test cases.

8.4 OTHER PROCESSES RELEVANT TO FUTURE OZONE EVOLUTION

To enable policy-relevant discussion of future scenarios, this chapter has made several simplifying assump-

tions. This chapter characterizes the complexities of ozone depletion using simple parameterizations based on ODPs. But perhaps more important, the scenarios are assumed to evolve within an unchanging background state. Given projections of climate change (e.g., IPCC, 2001), and our understanding of ozone and climate interactions (WMO, 2003; IPCC/TEAP, 2005; Chapter 5 and Chapter 6), this assumption is known to be inaccurate. This section qualitatively discusses a few possible consequences of a changing background state on the relationship between ODS emissions, EESC, and stratospheric ozone depletion. More details regarding the effects of climate change on the future ozone evolution can be found in Chapters 5 and 6.

Both natural and anthropogenic forcings of climate change have the potential to alter important chemistry related to future stratospheric ozone depletion for a given future evolution of ODSs and EESC. Two primary natural forcing mechanisms include solar changes and volcanic eruptions. Currently, solar changes are not expected to have a long-term effect on ozone recovery. However, a volcanic eruption that injects a large amount of sulfate aerosols into the stratosphere in the next few decades may enhance halogen ozone destruction. While this should perturb ozone chemistry for only a few years, the perturbations during that time could be substantial.

Future anthropogenic emissions of gases like carbon dioxide (CO_2), nitrous oxide (N_2O), and methane (CH_4) will also affect the chemical response of ozone depletion to ODS emissions and EESC. The expected stratospheric cooling induced by increasing concentrations, primarily of CO_2 , is expected to slow gas-phase ozone depletion reactions and increase global ozone; conversely, polar springtime ozone could be reduced by cooler temperatures and the resulting increase in heterogeneous ozone loss. The expected future increase in N_2O will increase stratospheric NO_x , which is expected to exacerbate globally averaged ozone depletion. However, increases in CH_4 abundances could accelerate ozone recovery. Hence, the globally averaged net effect of increases in these two important trace species depends on the specific future emission scenario. Emissions of hydrocarbons and NO_x are also expected to affect the lifetime and concentrations of stratospheric source gases, such as HCFCs, CH_3Br , CH_3Cl , and CH_4 , and thereby affect ozone.

Climate change by any cause (human, natural, or variability) can also be expected to affect atmospheric dynamics, which could lead to changes in ozone. These changes could be due, for example, to changes in the transport of ozone itself, or to changes in the lifetimes of the source gases.

So while this chapter examines the changes in EESC as a proxy for stratospheric ozone loss, it should be noted that neither total column amounts nor especially the latitudinal and vertical distribution of ozone are expected to return to their pre-1980 state at the same time that EESC returns to pre-1980 levels.

8.5 INDIRECT GWPS

ODSs can affect climate through their direct radiative forcing (Section 8.2) in a similar manner to other greenhouse gases. They also can uniquely affect climate by their destruction of lower stratospheric ozone, itself a greenhouse gas. This ozone destruction leads to a negative radiative forcing, and in the global mean acts in opposition to the ODSs' greenhouse warming. Potential implications of this offset have been discussed in Solomon and Daniel (1996) and include the possibility that the ozone destruction by the ODSs over the last 25 years may have offset part of the globally averaged surface warming due to the ODSs that would otherwise have been experienced. In past ozone Assessments, this indirect forcing offset has been combined with the direct Global Warming Potentials, to produce a "net" GWP. However, recent work suggests that the surface temperature response to recovering stratospheric ozone may be larger than suggested by radiative forcing alone (Joshi et al., 2003). As a potential remedy, it has been suggested that GWPs could be modified to account for the efficacy of any given forcing at modifying surface temperature (Berntsen et al., 2005; Fuglestedt et al., 2003). Studies also have shown that although it may be appropriate to combine these direct and indirect effects when evaluating long-term global mean surface temperature response, it may not be appropriate to simply offset these effects when evaluating other aspects of the climate response. Many physical characteristics of the direct and indirect climate change effects, especially in the stratosphere, do not act to offset each other (Forster and Joshi, 2005; IPCC/TEAP, 2005). Furthermore, GWP calculations for gases in the troposphere show that indirect GWPs vary with emission location (Berntsen et al., 2005). Due to these complications, in this report we follow the IPCC/TEAP (2005) formalism and do not present net GWPs, but keep direct and indirect GWPs separate.

The updated indirect GWP values for selected halocarbons are shown in Table 8-8. These values are calculated using a formalism similar to what was used in past Assessments and are based on discussions in Daniel et al. (1995). Specifically, a pulse of an ODS can lead to additional ozone depletion, which will be associated with a negative radiative forcing. For indirect GWP calculations, it is assumed that the ozone depletion occurs at

Table 8-8. Direct and indirect Global Warming Potentials of selected halocarbons calculated for a 100-year time horizon.

Gas	Direct GWP ¹	Indirect GWP ²
CFC-11	4,750 ± 1,660	-3,790 ± 2,620
CFC-12	10,890 ± 3,810	-2,160 ± 1,520
CFC-113	6,130 ± 2,150	-2,530 ± 1,780
HCFC-22	1,810 ± 630	-286 ± 192
HCFC-123	77 ± 27	-83 ± 55
HCFC-124	609 ± 213	-120 ± 81
HCFC-141b	725 ± 254	-667 ± 447
HCFC-142b	2,310 ± 810	-362 ± 244
CH ₃ CCl ₃	146 ± 51	-643 ± 431
CCl ₄	1,400 ± 490	-3,630 ± 2,470
CH ₃ Br	5 ± 2	-2,150 ± 1,440
Halon-1211	1,890 ± 660	-40,280 ± 27,120
Halon-1301	7,140 ± 2,500	-49,090 ± 34,280
Halon-2402	1,640 ± 570	-62,000 ± 41,930
HCFC-225ca	122 ± 43	-93 ± 50
HCFC-225cb	595 ± 208	-156 ± 85

¹ Direct GWP uncertainties represent 35% of the direct value.

² Indirect GWP uncertainties represent 1σ ranges, including a ±10-year 1σ ozone recovery uncertainty and a 67% 1σ ozone forcing uncertainty. The ozone forcing uncertainty is responsible for more than 90% of the total stated uncertainty.

midlatitudes when the total EESC amount is above the 1980 level. Below this level, it is assumed that no additional ozone loss occurs due to the pulse emission. In the stratosphere inside the polar vortex, additional loss from the pulse is assumed to occur when the EESC value is above the 1980 level and below the 1990 level. Above the 1990 level, it is assumed that due to ozone loss saturation over a large altitude range, no additional loss occurs due to the pulse emission. In past Assessments and here, all EESC values used in the indirect calculations have been generated with a 3-year time lag. If a 6-year time lag were used for the polar EESC calculations along with a value of 65 for α, the indirect GWPs would change by less than 20%.

For the purpose of calculating these indirect GWPs, the ozone radiative forcing assumed to be due to changes in chlorine and bromine from 1979 to 1997 is the same as discussed in IPCC (2001) and IPCC/TEAP (2005), which is $-0.15 \pm 0.10 \text{ W m}^{-2}$. Hansen et al. (2005) calculate a value of -0.06 W m^{-2} , but suggest that this may be a lower limit for the forcing due to chlorine- and bromine-induced ozone depletion because they do not consider tropospheric ozone trends outside the polar regions that may

HALOCARBON SCENARIOS, ODPs, AND GWPs

have arisen due to chlorine and bromine changes. A recent study that compares model calculations of ozone changes since preindustrial times suggests a range of -0.123 to $+0.066 \text{ W m}^{-2}$ for the forcing due to stratospheric ozone changes through the year 2000, when climate changes are neglected (Gauss et al., 2006). However, we have chosen to retain the previous forcing estimate because the Gauss et al. (2006) study does not quantify the mitigating forcing effects of tropospheric ozone and ozone precursor increases on stratospheric ozone, particularly in the lower stratosphere, where ozone changes are so important to radiative forcing calculations. It would be inappropriate to include the effect of tropospheric ozone chemistry not due to halogens in the indirect GWP estimates of chlorocarbons and bromocarbons.

The differences between the indirect GWP estimates in Table 8-8 and those in WMO (2003) (net GWPs minus direct GWPs of Table 1-8) are attributable to: a new ODS scenario that leads to a return to pre-1980 levels of EESC later; an updated CO_2 mixing ratio; a new CO_2 pulse response function; a change in the year of emission from 2002 to 2007; the updated value of α ; and different fractional bromine release values that are now consistent with Table 8-1 (and Table 1-4 in WMO, 2003) rather than the values used for CH_3Br , halon-1211, and halon-1301 of 1.08, 1.1, and 0.8, respectively, used in Table 1-8 of WMO (2003). Differences compared with IPCC/TEAP (2005) are due to the updated CO_2 mixing ratio and response function, to the new ODS scenario, and to the different value of α .

The direct GWP uncertainties represent 35% of the direct GWP values, consistent with Section 8.2.3. The indirect uncertainties represent a 1σ uncertainty due to a ± 10 -year 1σ error in the year of EESC recovery to 1980 levels and a 67% 1σ uncertainty in the ozone radiative forcing; this ozone forcing uncertainty accounts for nearly all of the quoted uncertainty total. It should be noted that these errors associated with GWPs are in addition to the potentially large difference in climate sensitivity (i.e., the amount of temperature change per change in radiative forcing, dT/dF) between stratospheric ozone loss and the well-mixed greenhouse gases (Joshi et al., 2003). While the climate sensitivity does not affect the GWP values, it does have relevance to the comparability of GWPs in assessing the impact of greenhouse gases on climate. There remains a large disparity in estimates of the variations of this climate sensitivity of ozone depletion in the upper troposphere and lower stratosphere; if this uncertainty can be reduced in the future, it may be advantageous to include this in assessing the relative climate impact of halocarbons (e.g., Berntsen et al., 2005; Fuglestedt et al., 2003).

REFERENCES

- Andrews, A.E., K.A. Boering, B.C. Daube, S.C. Wofsy, M. Loewenstein, H. Jost, J.R. Podolske, C.R. Webster, R.L. Herman, D.C. Scott, G.J. Flesch, E.J. Moyer, J.W. Elkins, G.S. Dutton, D.F. Hurst, F.L. Moore, E.A. Ray, P.A. Romashkin, and S.E. Strahan, Mean ages of stratospheric air derived from in situ observations of CO_2 , CH_4 , and N_2O , *J. Geophys. Res.*, 106 (D23), 32295-32314, 2001.
- Berntsen, T.K., J.S. Fuglestedt, M.M. Joshi, K.P. Shine, N. Stuber, M. Ponater, R. Sausen, D.A. Hauglustaine, and L. Li, Response of climate to regional emissions of ozone precursors: Sensitivities and warming potentials, *Tellus*, 57B (4), 283-304, 2005.
- Butler, J.H., M. Battle, M.L. Bender, S.A. Montzka, A.D. Clarke, E.S. Saltzman, C.M. Sucher, J.P. Severinghaus, and J.W. Elkins, A record of atmospheric halocarbons during the twentieth century in polar firn air, *Nature*, 399 (6738), 749-755, 1999.
- Chipperfield, M.P., and J.A. Pyle, Model sensitivity studies of Arctic ozone depletion, *J. Geophys. Res.*, 103 (D21), 28389-28404, 1998.
- Clodic, D., and L. Palandre, *Determination of Comparative HCFC and HFC Emission Profiles for the Foam and Refrigeration Sectors until 2015. Part 1: Refrigeration Emission Profiles*, 132 pp., Paris, France, 2004.
- Daniel, J.S., S. Solomon, and D.L. Albritton, On the evaluation of halocarbon radiative forcing and global warming potentials, *J. Geophys. Res.*, 100 (D1), 1271-1285, 1995.
- Daniel, J.S., S.M. Schauffler, W.H. Pollock, S. Solomon, A. Weaver, L.E. Heidt, R.R. Garcia, E.L. Atlas, and J.F. Vedder, On the age of stratospheric air and inorganic chlorine and bromine release, *J. Geophys. Res.*, 101 (D11), 16757-16770, 1996.
- Daniel, J.S., G.J.M. Velders, S. Solomon, M. McFarland, and S.A. Montzka, Present and future sources and emissions of halocarbons: Towards new constraints, *J. Geophys. Res.*, in press, 2006.
- DeMore, W.B., S.P. Sander, D.M. Golden, R.F. Hampson, M.J. Kurylo, C.J. Howard, A.R. Ravishankara, C.E. Kolb, and M.J. Molina, *Chemical Kinetics and Photochemical Data for Use in Stratospheric Modeling: Evaluation No. 12*, JPL Pub. 97-4, Jet Propulsion Laboratory, Pasadena, Calif., 1997.
- Fisher, D.A., C.H. Hales, D.L. Filkin, M.K.W. Ko, N.D. Sze, P.S. Connell, D.J. Wuebbles, I.S.A. Isaksen, and F. Stordal, Model calculations of the relative effects of CFCs and their replacements on stratospheric ozone, *Nature*, 344 (6266), 508-512, 1990.

- Forster, P.M.F., and M. Joshi, The role of halocarbons in the climate change of the troposphere and stratosphere, *Clim. Change*, 71 (1-2), 249-266, 2005.
- Forster, P.M.F., J.B. Burkholder, C. Clerbaux, P.F. Coheur, M. Dutta, L.K. Gohar, M.D. Hurley, G. Myhre, R.W. Portmann, K.P. Shine, T.J. Wallington, and D. Wuebbles, Resolution of the uncertainties in the radiative forcing of HFC-134a, *J. Quant. Spectrosc. Radiat. Transfer*, 93 (4), 447-460, 2005.
- Fuglestad, J.S., T.K. Berntsen, O. Godal, and T. Skodvin, Climate implications of GWP-based reductions in greenhouse gas emissions, *Geophys. Res. Lett.*, 27 (3), 409-412, 2000.
- Fuglestad, J.S., T.K. Berntsen, O. Godal, R. Sausen, K.P. Shine, and T. Skodvin, Metrics of climate change: Assessing radiative forcing and emission indices, *Clim. Change*, 58 (3), 267-331, 2003.
- Gauss, M., G. Myhre, I.S.A. Isaksen, V. Grewe, G. Pitari, O. Wild, W.J. Collins, F.J. Dentener, K. Ellingsen, L.K. Gohar, D.A. Hauglustaine, D. Iachetti, J.-F. Lamarque, E. Mancini, L.J. Mickley, M.J. Prather, J.A. Pyle, M.G. Sanderson, K.P. Shine, D.S. Stevenson, K. Sudo, S. Szopa, and G. Zeng, Radiative forcing since preindustrial times due to ozone change in the troposphere and the lower stratosphere, *Atmos. Chem. Phys.*, 6, 575-599, 2006.
- Gohar, L.K., G. Myhre, and K.P. Shine, Updated radiative forcing estimates of four halocarbons, *J. Geophys. Res.*, 109, D01107, doi: 10.1029/2003JD004320, 2004.
- Hansen, J., M. Sato, R. Ruedy, L. Nazarenko, A. Lacis, G.A. Schmidt, G. Russell, I. Aleinov, M. Bauer, S. Bauer, N. Bell, B. Cairns, V. Canuto, M. Chandler, Y. Cheng, A. Del Genio, G. Faluvegi, E. Fleming, A. Friend, T. Hall, C. Jackman, M. Kelley, N. Kiang, D. Koch, J. Lean, J. Lerner, K. Lo, S. Menon, R. Miller, P. Minnis, T. Novakov, V. Oinas, Ja. Perlwitz, Ju. Perlwitz, D. Rind, A. Romanou, D. Shindell, P. Stone, S. Sun, N. Tausnev, D. Thresher, B. Wielicki, T. Wong, M. Yao, and S. Zhang, Efficacy of climate forcings, *J. Geophys. Res.*, 110, D18104, doi: 10.1029/2005JD005776, 2005.
- Happell, J.D., and M.P. Roche, Soils: A global sink of atmospheric carbon tetrachloride, *Geophys. Res. Lett.*, 30 (2), 1088, doi: 10.1029/2002GL015957, 2003.
- Harnisch, J., R. Borchers, P. Fabian, and M. Maiss, CF₄ and the age of mesospheric and polar vortex air, *Geophys. Res. Lett.*, 26 (3), 295-298, 1999.
- Hurley, M.D., T.J. Wallington, G.A. Buchanan, L.K. Gohar, G. Marston, and K.P. Shine, IR spectrum and radiative forcing of CF₄ revisited, *J. Geophys. Res.*, 110, D02102, doi: 10.1029/2004JD005201, 2005.
- IPCC (Intergovernmental Panel on Climate Change), *Climate Change: The IPCC Scientific Assessment*, edited by J.T. Houghton, G.J. Jenkins, and J.J. Ephraums, 364 pp., Cambridge University Press, Cambridge, U.K., 1990.
- IPCC (Intergovernmental Panel on Climate Change), *Climate Change, 1994: Radiative Forcing of Climate Change and an Evaluation of the IPCC IS92 Emission Scenarios*, edited by J.T. Houghton, L.G. Meira Filho, J.P. Bruce, H. Lee, B.A. Callander, and E.F. Haites, 339 pp., Cambridge University Press, Cambridge, U.K., 1995.
- IPCC (Intergovernmental Panel on Climate Change), *Climate Change 1995: The Science of Climate Change*, edited by J.T. Houghton, L.G. Meira Filho, J. Bruce, H. Lee, B.A. Callander, E. Haites, N. Harris, and K. Maskell, 572 pp., Cambridge University Press, Cambridge, U.K., 1996.
- IPCC (Intergovernmental Panel on Climate Change), *Climate Change 2001: The Scientific Basis: Contribution of Working Group I to the Third Assessment Report of the Intergovernmental Panel on Climate Change*, edited by J.T. Houghton, Y. Ding, D.J. Griggs, M. Noguer, P.J. van der Linden, X. Dai, K. Maskell, and C.A. Johnson, 881 pp., Cambridge University Press, Cambridge, U.K., 2001.
- IPCC/TEAP (Intergovernmental Panel on Climate Change / Technology and Economic Assessment Panel), *IPCC/TEAP Special Report on Safeguarding the Ozone Layer and the Global Climate System: Issues Related to Hydrofluorocarbons and Perfluorocarbons*, edited by B. Metz, L. Kuijpers, S. Solomon, S.O. Andersen, O. Davidson, J. Pons, D. de Jager, T. Kestin, M. Manning, and L. Meyer, 478 pp., Cambridge University Press, New York, N.Y., 2005.
- Jain, A.K., B.P. Briegleb, K. Minschwaner, and D.J. Wuebbles, Radiative forcings and global warming potentials of 39 greenhouse gases, *J. Geophys. Res.*, 105 (D16), 20773-20790, 2000.
- Johnson, C.E., and R.G. Derwent, Relative radiative forcing consequences of global emissions of hydrocarbons, carbon monoxide and NO_x from human activities estimated with a zonally-averaged two-dimensional model, *Clim. Change*, 34 (3-4), 439-462, 1996.
- Joos, F., I.C. Prentice, S. Sitch, R. Meyer, G. Hooss, G. Plattner, S. Gerber, and K. Hasselmann, Global warming feedbacks on terrestrial carbon uptake

HALOCARBON SCENARIOS, ODPs, AND GWPs

- under the Intergovernmental Panel on Climate Change (IPCC) emission scenarios, *Global Biogeochem. Cycles*, 15 (4), 891-908, 2001.
- Joshi, M., K. Shine, M. Ponater, N. Stuber, R. Sausen, and L. Li, A comparison of climate response to different radiative forcings in three general circulation models: Towards an improved metric of climate change, *Clim. Dyn.*, 20 (7-8), 843-854, 2003.
- Ko, M.K.W., N.D. Sze, C. Scott, J.M. Rodriguez, D.K. Weisenstein, and S.P. Sander, Ozone depletion potential of CH₃Br, *J. Geophys. Res.*, 103 (D21), 28187-28195, 1998.
- Manne, A.S., and R.G. Richels, An alternative approach to establishing trade-offs among greenhouse gases, *Nature*, 410 (6829), 675-677, 2001.
- McCulloch, A. P. Ashford, and P.M. Midgley, Historic emissions of fluorotrichloromethane (CFC-11) based on a market survey, *Atmos. Environ.*, 35 (26), 4387-4397, 2001.
- Molina, L.T., P.J. Wooldridge, and M.J. Molina, Atmospheric reactions and ultraviolet and infrared absorptivities of nitrogen trifluoride, *Geophys. Res. Lett.*, 22 (14), 1873-1876, 1995.
- Montzka, S.A., J.H. Butler, R.C. Myers, T.M. Thompson, T.H. Swanson, A.D. Clarke, L.T. Lock, and J.W. Elkins, Decline in the tropospheric abundance of halogen from halocarbons: Implications for stratospheric ozone depletion, *Science*, 272 (5266), 1318-1322, 1996.
- Montzka, S.A., J.H. Butler, J.W. Elkins, T.M. Thompson, A.D. Clarke, and L.T. Lock, Present and future trends in the atmospheric burden of ozone-depleting halogens, *Nature*, 398 (6729), 690-694, 1999.
- Montzka, S.A., J.H. Butler, B.D. Hall, D.J. Mondeel, and J.W. Elkins, A decline in tropospheric organic bromine, *Geophys. Res. Lett.*, 30 (15), 1826, doi: 10.1029/2003GL017745, 2003.
- Myhre, G., E.J. Highwood, K.P. Shine, and F. Stordal, New estimates of radiative forcing due to well mixed greenhouse gases, *Geophys. Res. Lett.*, 25 (14), 2715-2718, 1998.
- Nemtchinov, V., and P. Varanasi, Thermal infrared absorption cross-sections of CCl₄ needed for atmospheric remote sensing, *J. Quant. Spect. and Rad. Transfer*, 82 (1-5), 473-481, 2003.
- Newman, P.A., E.R. Nash, S.R. Kawa, S.A. Montzka, and S.M. Schauffler, When will the Antarctic ozone hole recover?, *Geophys. Res. Lett.*, 33, L12814, doi: 10.1029/2005GL025232, 2006.
- O'Neill, B.C., The jury is still out on global warming potentials, *Clim. Change*, 44 (4), 427-443, 2000.
- Pinnock, S., M.D. Hurley, K.P. Shine, T.J. Wallington, and T.J. Smyth, Radiative forcing of climate by hydrochlorofluorocarbons and hydrofluorocarbons, *J. Geophys. Res.*, 100 (D11), 23227-23238, 1995.
- Plattner, G.-K., F. Joos, T.F. Stocker, and O. Marchal, Feedback mechanisms and sensitivities of ocean carbon uptake under global warming, *Tellus*, 53B (5), 564-592, 2001.
- Prather, M.J., Time scales in atmospheric chemistry: Theory, GWPs for CH₄ and CO, and runaway growth, *Geophys. Res. Lett.*, 23 (19), 2597-2600, 1996.
- Prather, M.J., Lifetimes of atmospheric species: Integrating environmental impacts, *Geophys. Res. Lett.*, 29 (22), 2063, doi: 10.1029/2002GL016299, 2002.
- Prinn, R.G., J. Huang, R.F. Weiss, D.M. Cunnold, P.J. Fraser, P.G. Simmonds, A. McCulloch, C. Harth, S. Reimann, P. Salameh, S. O'Doherty, R.H.J. Wang, L.W. Porter, B.R. Miller, and P.B. Krummel, Evidence for variability of atmospheric hydroxyl radicals over the past quarter century, *Geophys. Res. Lett.*, 32, L07809, doi: 10.1029/2004GL022228, 2005.
- Ravishankara, A.R., A.A. Turnipseed, N.R. Jensen, S. Barone, M. Mills, C.J. Howard, and S. Solomon, Do hydrofluorocarbons destroy stratospheric ozone?, *Science*, 263 (5143), 71-75, 1994.
- Robson, J.I., L.K. Gohar, M.D. Hurley, K.P. Shine, and T.J. Wallington, Revised IR spectrum, radiative efficiency and global warming potential of nitrogen trifluoride, *Geophys. Res. Lett.*, 33, L10817, doi: 10.1029/2006GL026210, 2006.
- Sander, S.P., R.R. Friedl, D.M. Golden, M.J. Kurylo, R.E. Huie, V.L. Orkin, G.K. Moortgat, A.R. Ravishankara, C.E. Kolb, M.J. Molina, and B.J. Finlayson-Pitts, *Chemical Kinetics and Photochemical Data for Use in Atmospheric Studies, Evaluation No. 14, JPL Publication 02-25*, Jet Propulsion Laboratory, Pasadena, Calif., 2003.
- Sander, S.P., R.R. Friedl, D.M. Golden, M.J. Kurylo, G.K. Moortgat, H. Keller-Rudek, P.H. Wine, A.R. Ravishankara, C.E. Kolb, M.J. Molina, B.J. Finlayson-Pitts, R.E. Huie, and V.L. Orkin, *Chemical Kinetics and Photochemical Data for Use in Atmospheric Studies, Evaluation Number 15, JPL Publication 06-02*, Jet Propulsion Laboratory, Pasadena, Calif., 2006. [Available: <http://jpldataeval.jpl.nasa.gov/>]
- Schauffler, S.M., E.L. Atlas, S.G. Donnelly, A. Andrews, S.A. Montzka, J.W. Elkins, D.F. Hurst, P.A. Romashkin, G.S. Dutton, and V. Stroud, Chlorine

- budget and partitioning during SOLVE, *J. Geophys. Res.*, 108 (D5), 4173, doi: 10.1029/2001JD002040, 2003.
- Shine, K.P., J.S. Fuglestedt, K. Hailemariam, and N. Stuber, Alternatives to the global warming potential for comparing climate impacts of emissions of greenhouse gases, *Clim. Change*, 68 (3), 281-302, 2005a.
- Shine, K.P., L.K. Gohar, M.D. Hurley, G. Marston, D. Martin, P.G. Simmonds, T.J. Wallington, and M. Watkins, Perfluorodecalin: Global warming potential and first detection in the atmosphere, *Atmos. Environ.*, 39 (9), 1759-1763, 2005b.
- Sihra, K., M.D. Hurley, K.P. Shine, and T.J. Wallington, Updated radiative forcing estimates of 65 halocarbons and nonmethane hydrocarbons, *J. Geophys. Res.*, 106 (D17), 20493-20505, 2001.
- Smith, S.J., and T.M.L. Wigley, Global warming potentials: 1. Climatic implications of emissions reductions, *Clim. Change*, 44 (4), 445-457, 2000a.
- Smith, S.J., and T.M.L. Wigley, Global warming potentials: 2. Accuracy, *Clim. Change*, 44 (4), 459-469, 2000b.
- Solomon, S., and D.L. Albritton, Time-dependent ozone depletion potentials for short- and long-term forecasts, *Nature*, 357 (6373), 33-37, 1992.
- Solomon, S., and J.S. Daniel, Impact of the Montreal protocol and its amendments on the rate of change of global radiative forcing, *Clim. Change*, 32 (1), 7-17, 1996.
- Solomon, S., A.F. Tuck, M. Mills, L.E. Heidt, and W.H. Pollock, On the evaluation of ozone depletion potentials, *J. Geophys. Res.*, 97, 825-842, 1992.
- Solomon, K.R., X. Tang, S.R. Wilson, P. Zanis, and A.F. Bais, Changes in tropospheric composition and air quality due to stratospheric ozone depletion, *Photochem. Photobiol. Sci.*, 2 (1), 62-67, 2003.
- Tang, X., S. Madronich, T. Wallington, and D. Calamari, Changes in tropospheric composition and air quality, *J. Photochem. Photobiol. B*, 46 (1-3), 83-95, 1998.
- TEAP (Technology and Economic Assessment Panel), *Report of the TEAP, November 2005: Supplement to the IPCC/TEAP Report*, 111 pp., UNEP Ozone Secretariat, Nairobi, Kenya, 2005.
- UNEP (United Nations Environment Programme), *Assessment of Alternatives to Methyl Bromide*, Methyl Bromide Technical Options Committee, 354 pp., UNEP Ozone Secretariat, Nairobi, Kenya, 1998.
- UNEP (United Nations Environment Programme), *2002 Report of the Halons Technical Options Committee (HTOC)*, 69 pp., UNEP Ozone Secretariat, Nairobi, Kenya, 2003.
- UNEP (United Nations Environment Programme), Ozone Secretariat, private communication of unpublished aggregated production data for CFC and HCFC chemicals 1986-2004, 2005.
- Wallington, T.J., W.F. Schneider, J. Sehested, and O.J. Nielsen, Hydrofluorocarbons and stratospheric ozone, *Faraday Discuss.*, 100, 55-64, 1995.
- Waugh, D., and T. Hall, Age of stratospheric air: Theory, observations, and models, *Rev. Geophys.*, 40 (4), 1010, doi: 10.1029/2000RG000101, 2002.
- Wigley, T.M.L., The Kyoto protocol: CO₂, CH₄ and climate implications, *Geophys. Res. Lett.*, 25 (13), 2285-2288, 1998.
- WMO (World Meteorological Organization), *Scientific Assessment of Ozone Depletion: 1994, Global Ozone Research and Monitoring Project—Report No. 37*, Geneva, Switzerland, 1995.
- WMO (World Meteorological Organization), *Scientific Assessment of Ozone Depletion: 1998, Global Ozone Research and Monitoring Project—Report No. 44*, Geneva, Switzerland, 1999.
- WMO (World Meteorological Organization), *Scientific Assessment of Ozone Depletion: 2002, Global Ozone Research and Monitoring Project—Report No. 47*, Geneva, Switzerland, 2003.
- Wuebbles, D.J., Chlorocarbon emission scenarios: Potential impact on stratospheric ozone, *Geophys. Res. Lett.*, 88 (C2), 1433-1443, 1983.

TWENTY QUESTIONS AND ANSWERS ABOUT THE OZONE LAYER: 2006 UPDATE

Lead Author:
D.W. Fahey

The update of this component of the Assessment was discussed by the 77 scientists who attended the Panel Review Meeting for the 2006 Ozone Assessment (Les Diablerets, Switzerland, 19-23 June 2006). In addition, subsequent contributions, reviews, or comments were provided by the following individuals: S.A. Montzka (special recognition), R.J. Salawitch (special recognition), D.L. Albritton, S.O. Andersen, P.J. Aucamp, M.P. Baldwin, A.F. Bias, G. Bodeker, J.F. Bornman, G.O. Braathen, J.P. Burrows, M.-L. Chanin, C. Clerbaux, M. Dameris, J.S. Daniel, S.B. Diaz, E.G. Dutton, C.A. Ennis, V. Eyring, V.E. Fioletov, N.P. Gillet, N.R.P. Harris, M.K.W. Ko, L. Kuijpers, G.L. Manney, R.L. McKenzie, R. Müller, E.R. Nash, P.A. Newman, T. Peter, A.R. Ravishankara, A. Robock, M.L. Santee, U. Schmidt, G. Seckmeyer, T.G. Shepherd, R.S. Stolarski, W.T. Sturges, J.C. van der Leun, G.J.M. Velders, D.W. Waugh, C.S. Zerefos.

TWENTY QUESTIONS AND ANSWERS ABOUT THE OZONE LAYER: 2006 UPDATE

Contents

	page
INTRODUCTION	Q.1
I. OZONE IN OUR ATMOSPHERE	
Q1. What is ozone and where is it in the atmosphere?	Q.3
Q2. How is ozone formed in the atmosphere?	Q.4
Q3. Why do we care about atmospheric ozone?	Q.5
Q4. Is total ozone uniform over the globe?	Q.6
Q5. How is ozone measured in the atmosphere?	Q.7
II. THE OZONE DEPLETION PROCESS	
Q6. What are the principal steps in stratospheric ozone depletion caused by human activities?	Q.9
Q7. What emissions from human activities lead to ozone depletion?	Q.11
Q8. What are the reactive halogen gases that destroy stratospheric ozone?	Q.14
Q9. What are the chlorine and bromine reactions that destroy stratospheric ozone?	Q.17
Q10. Why has an “ozone hole” appeared over Antarctica when ozone-depleting gases are present throughout the stratosphere?	Q.19
III. STRATOSPHERIC OZONE DEPLETION	
Q11. How severe is the depletion of the Antarctic ozone layer?	Q.22
Q12. Is there depletion of the Arctic ozone layer?	Q.26
Q13. How large is the depletion of the global ozone layer?	Q.28
Q14. Do changes in the Sun and volcanic eruptions affect the ozone layer?	Q.30
IV. CONTROLLING OZONE-DEPLETING GASES	
Q15. Are there regulations on the production of ozone-depleting gases?	Q.32
Q16. Has the Montreal Protocol been successful in reducing ozone-depleting gases in the atmosphere?	Q.34
V. IMPLICATIONS OF OZONE DEPLETION	
Q17. Does depletion of the ozone layer increase ground-level ultraviolet radiation?	Q.37
Q18. Is depletion of the ozone layer the principal cause of climate change?	Q.40
VI. STRATOSPHERIC OZONE IN THE FUTURE	
Q19. How will recovery of the ozone layer be identified?	Q.43
Q20. When is the ozone layer expected to recover?	Q.45
ADDITIONAL TOPICS	
• Global Ozone Dobson Network	Q.8
• Understanding Stratospheric Ozone Depletion	Q.10
• Heavier-Than-Air CFCs	Q.13
• Replacing the Loss of Ozone in the Stratosphere	Q.16
• The Discovery of the Antarctic Ozone Hole	Q.21
• The Anomalous 2002 Antarctic Ozone Hole	Q.25

INTRODUCTION

Ozone is a very small part of our atmosphere, but its presence is nevertheless vital to human well-being.

Most ozone resides in the upper part of the atmosphere. This region, called the stratosphere, is more than 10 kilometers (6 miles) above Earth's surface. There, about 90% of atmospheric ozone is contained in the "ozone layer," which shields us from harmful ultraviolet radiation from the Sun.

However, it was discovered in the mid-1970s that some human-produced chemicals could destroy ozone and deplete the ozone layer. The resulting increase in ultraviolet radiation at Earth's surface may increase the incidences of skin cancer and eye cataracts.

Following the discovery of this environmental issue, researchers focused on a better understanding of this threat to the ozone layer. Monitoring stations showed that the abundances of the ozone-depleting chemicals were steadily increasing in the atmosphere. These trends were linked to growing production and use of chemicals like chlorofluorocarbons (CFCs) for refrigeration and air conditioning, foam blowing, and industrial cleaning. Measurements in the laboratory and the atmosphere characterized the chemical reactions that were involved in ozone destruction. Computer models employing this information could predict how much ozone depletion was occurring and how much more could occur in the future.

Observations of the ozone layer showed that depletion was indeed occurring. The most severe and most surprising ozone loss was discovered to be recurring in springtime over Antarctica. The loss in this region is commonly called the "ozone hole" because the ozone depletion is so large and localized. A thinning of the ozone layer also has been observed over other regions of the globe, such as the Arctic and northern middle latitudes.

The work of many scientists throughout the world has provided a basis for building a broad and solid scientific understanding of the ozone depletion process. With this understanding, we know that ozone depletion is occur-

ring and why. And, most important, we know that if ozone-depleting gases were to continue to accumulate in the atmosphere, the result would be more depletion of the ozone layer.

In response to the prospect of increasing ozone depletion, the governments of the world crafted the 1987 United Nations Montreal Protocol as a global means to address this global issue. As a result of the broad compliance with the Protocol and its Amendments and Adjustments and, of great significance, industry's development of "ozone-friendly" substitutes for the now-controlled chemicals, the total global accumulation of ozone-depleting gases has slowed and begun to decrease. This has reduced the risk of further ozone depletion. Now, with continued compliance, we expect recovery of the ozone layer by the late 21st century. The International Day for the Preservation of the Ozone Layer, 16 September, is now celebrated on the day the Montreal Protocol was agreed upon.

This is a story of notable achievements: discovery, understanding, decisions, actions, and verification. It is a story written by many: scientists, technologists, economists, legal experts, and policymakers. And, dialogue has been a key ingredient.

To help foster continued interaction, this component of the *Scientific Assessment of Ozone Depletion: 2006* presents 20 questions and answers about the often-complex science of ozone depletion. The answers are updates of those first presented in the previous ozone Assessment, *Scientific Assessment of Ozone Depletion: 2002*. The questions address the nature of atmospheric ozone, the chemicals that cause ozone depletion, how global and polar ozone depletion occur, and what could lie ahead for the ozone layer. A brief answer to each question is first given in italics; an expanded answer then follows. The answers are based on the information presented in the 2006 and earlier Assessment reports. These reports and the answers provided here were all prepared and reviewed by a large international group of scientists.¹

¹ The update of this component of the Assessment was discussed by the 77 scientists who attended the Panel Review Meeting for the 2006 Ozone Assessment (Les Diablerets, Switzerland, 19-23 June 2006). In addition, subsequent contributions, reviews, or comments were provided by the following individuals: S.A. Montzka (special recognition), R.J. Salawitch (special recognition), D.L. Albritton, S.O. Andersen, P.J. Aucamp, M.P. Baldwin, A.F. Bias, G. Bodeker, J.F. Bornman, G.O. Braathen, J.P. Burrows, M.-L. Chanin, C. Clerbaux, M. Dameris, J.S. Daniel, S.B. Diaz, E.G. Dutton, C.A. Ennis, V. Eyring, V.E. Fioletov, N.P. Gillet, N.R.P. Harris, M.K.W. Ko, L. Kuijpers, G.L. Manney, R.L. McKenzie, R. Müller, E.R. Nash, P.A. Newman, T. Peter, A.R. Ravishankara, A. Robock, M.L. Santee, U. Schmidt, G. Seckmeyer, T.G. Shepherd, R.S. Stolarski, W.T. Sturges, J.C. van der Leun, G.J.M. Velders, D.W. Waugh, C.S. Zerefos.

I. OZONE IN OUR ATMOSPHERE

Q1: What is ozone and where is it in the atmosphere?

Ozone is a gas that is naturally present in our atmosphere. Each ozone molecule contains three atoms of oxygen and is denoted chemically as O₃. Ozone is found primarily in two regions of the atmosphere. About 10% of atmospheric ozone is in the troposphere, the region closest to Earth (from the surface to about 10-16 kilometers (6-10 miles)). The remaining ozone (90%) resides in the stratosphere, primarily between the top of the troposphere and about 50 kilometers (31 miles) altitude. The large amount of ozone in the stratosphere is often referred to as the “ozone layer.”

Ozone is a gas that is naturally present in our atmosphere. Ozone has the chemical formula O₃ because an ozone molecule contains three oxygen atoms (see Figure Q1-1). Ozone was discovered in laboratory experiments in the mid-1800s. Ozone’s presence in the atmosphere was later discovered using chemical and optical measurement methods. The word ozone is derived from the Greek word ὄζειν (*ozein* in Latin), meaning “to smell.” Ozone has a pungent odor that allows it to be detected even at very low amounts. Ozone will rapidly react with many chemical compounds and is explosive in concentrated amounts. Electrical discharges are generally used to produce ozone for industrial processes such as air and water purification and bleaching textiles and food products.

Ozone location. Most ozone (about 90%) is found in the stratosphere, a region that begins about 10-16 kilometers (6-10 miles) above Earth’s surface and extends up to about 50 kilometers (31 miles) altitude (see Figure Q1-2). Most ozone resides in the lower stratosphere in what is commonly known as the “ozone layer.” The remaining ozone, about 10%, is found in the troposphere, which is the lowest region of the atmosphere, between Earth’s surface and the stratosphere.

Ozone abundance. Ozone molecules have a relatively low abundance in the atmosphere. In the stratosphere near the peak of the ozone layer, there are up to 12,000 ozone molecules for every *billion* air molecules (1

billion = 1,000 million). Most air molecules are either oxygen (O₂) or nitrogen (N₂) molecules. In the troposphere near Earth’s surface, ozone is even less abundant, with a typical range of 20 to 100 ozone molecules for each billion air molecules. The highest surface values are a result of ozone formed in air polluted by human activities.

As an illustration of the low relative abundance of ozone in our atmosphere, one can imagine bringing all the ozone molecules in the troposphere and stratosphere down to Earth’s surface and uniformly distributing these molecules into a gas layer over the globe. The resulting layer of pure ozone would have a thickness of less than one-half centimeter (about one-quarter inch).



Figure Q1-1. Ozone and oxygen. A molecule of ozone (O₃) contains three oxygen (O) atoms bound together. Oxygen molecules (O₂), which constitute 21% of Earth’s atmosphere, contain two oxygen atoms bound together.

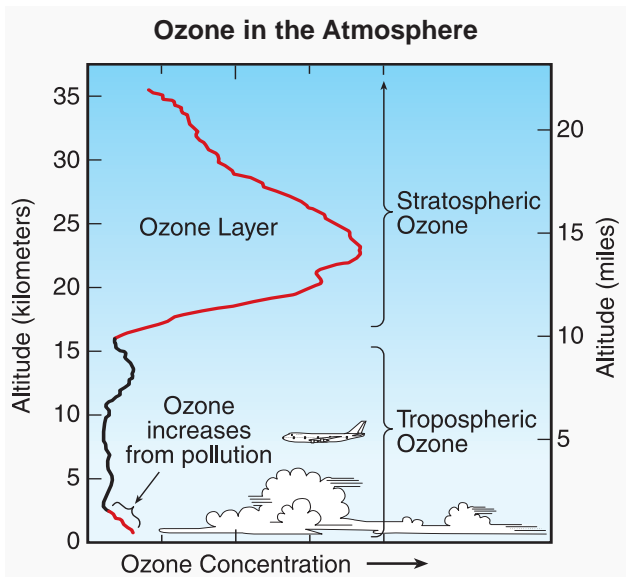


Figure Q1-2. Atmospheric ozone. Ozone is present throughout the lower atmosphere (troposphere and stratosphere). Most ozone resides in the stratospheric “ozone layer” above Earth’s surface. Increases in ozone occur near the surface as a result of pollution from human activities.

Q2: How is ozone formed in the atmosphere?

Ozone is formed throughout the atmosphere in multistep chemical processes that require sunlight. In the stratosphere, the process begins with an oxygen molecule (O₂) being broken apart by ultraviolet radiation from the Sun. In the lower atmosphere (troposphere), ozone is formed in a different set of chemical reactions involving hydrocarbons and nitrogen-containing gases.

Stratospheric ozone. Stratospheric ozone is naturally formed in chemical reactions involving ultraviolet sunlight and oxygen molecules, which make up 21% of the atmosphere. In the first step, sunlight breaks apart one oxygen molecule (O₂) to produce two oxygen atoms (2 O) (see Figure Q2-1). In the second step, each atom combines with an oxygen molecule to produce an ozone molecule (O₃). These reactions occur continually whenever ultraviolet sunlight is present in the stratosphere. As a result, the greatest ozone production occurs in the tropical stratosphere.

The production of stratospheric ozone is balanced by its destruction in chemical reactions. Ozone reacts continually with a wide variety of natural and human-

produced chemicals in the stratosphere. In each reaction, an ozone molecule is lost and other chemical compounds are produced. Important reactive gases that destroy ozone are those containing chlorine and bromine (see Q8).

Some stratospheric ozone is transported down into the troposphere and can influence ozone amounts at Earth's surface, particularly in remote, unpolluted regions of the globe.

Tropospheric ozone. Near Earth's surface, ozone is produced in chemical reactions involving naturally occurring gases and gases from pollution sources. Production reactions primarily involve hydrocarbon and nitrogen oxide gases and require sunlight. Fossil fuel combustion is a primary pollution source for tropospheric ozone production. The surface production of ozone does not significantly contribute to the abundance of stratospheric ozone. The amount of surface ozone is too small in comparison, and the transport of surface air to the stratosphere is not effective enough. As in the stratosphere, ozone in the troposphere is destroyed in naturally occurring chemical reactions and in reactions involving human-produced chemicals. Tropospheric ozone can also be destroyed when ozone reacts with a variety of surfaces, such as those of soils and plants.

Balance of chemical processes. Ozone abundances in the stratosphere and troposphere are determined by the *balance* between chemical processes that produce ozone and processes that destroy ozone. The balance is determined by the amounts of reacting gases and how the rate or effectiveness of the various reactions varies with sunlight intensity, location in the atmosphere, temperature, and other factors. As atmospheric conditions change to favor ozone-producing reactions in a certain location, ozone abundances will increase. Similarly, if conditions change to favor reactions that destroy ozone, abundances will decrease. The balance of production and loss reactions combined with atmospheric air motions determines the global distribution of ozone on time scales of days to many months. Global ozone has decreased in the last decades because the amounts of reactive gases containing chlorine and bromine have increased in the stratosphere (see Q13).

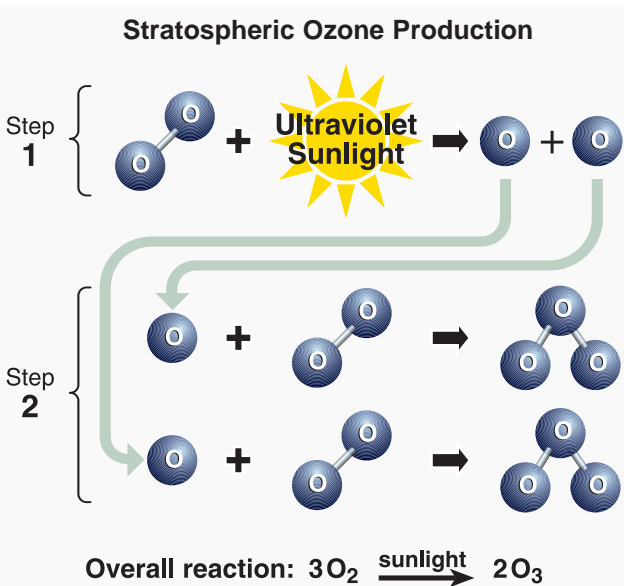


Figure Q2-1. Stratospheric ozone production. Ozone is naturally produced in the stratosphere in a two-step process. In the first step, ultraviolet sunlight breaks apart an oxygen molecule to form two separate oxygen atoms. In the second step, each atom then undergoes a binding collision with another oxygen molecule to form an ozone molecule. In the overall process, three oxygen molecules plus sunlight react to form two ozone molecules.

Q3: Why do we care about atmospheric ozone?

Ozone in the stratosphere absorbs some of the Sun’s biologically harmful ultraviolet radiation. Because of this beneficial role, stratospheric ozone is considered “good” ozone. In contrast, excess ozone at Earth’s surface that is formed from pollutants is considered “bad” ozone because it can be harmful to humans, plants, and animals. The ozone that occurs naturally near the surface and in the lower atmosphere is also beneficial because ozone helps remove pollutants from the atmosphere.

Natural ozone. In the absence of human activities on Earth’s surface, ozone would still be present near the surface and throughout the troposphere and stratosphere because ozone is a natural component of the clean atmosphere. All ozone molecules are chemically identical, with each containing three oxygen atoms. However, ozone in the stratosphere (good ozone) has very different environmental consequences for humans and other life forms than excess ozone in the troposphere near Earth’s surface (bad ozone). Natural ozone in the troposphere is also considered “good” because it initiates the chemical removal of many pollutants, such as carbon monoxide and nitrogen oxides, as well as greenhouse gases such as methane.

Good ozone. Stratospheric ozone is considered good for humans and other life forms because it absorbs ultraviolet (UV)-B radiation from the Sun (see Figure Q3-1). If not absorbed, UV-B would reach Earth’s surface in amounts that are harmful to a variety of life forms. In humans, increased exposure to UV-B increases the risk of skin cancer (see Q17), cataracts, and a suppressed immune system. UV-B exposure before adulthood and cumulative exposure are both important factors in the risk. Excessive UV-B exposure also can damage terrestrial plant life, single-cell organisms, and aquatic ecosystems. Other UV radiation, UV-A, which is not absorbed significantly by ozone, causes premature aging of the skin.

The absorption of UV-B radiation by ozone is a source of heat in the stratosphere. This helps to maintain the stratosphere as a stable region of the atmosphere, with temperatures increasing with altitude. As a result, ozone plays a key role in controlling the temperature structure of Earth’s atmosphere.

Protecting good ozone. In the mid-1970s, it was discovered that halogen source gases released in human activities could cause stratospheric ozone depletion (see Q6). Ozone depletion increases harmful UV-B amounts at Earth’s surface. Global efforts have been undertaken to protect the ozone layer through regulation of ozone-depleting gases (see Q15 and Q16).

Bad ozone. Excess ozone formed near Earth’s surface in reactions caused by the presence of human-made pollutant gases is considered bad ozone. Increased ozone amounts are harmful to humans, plants, and other living systems because ozone reacts strongly to destroy or alter many other molecules. Excessive ozone exposure reduces crop yields and forest growth. In humans, exposure to

high levels of ozone can reduce lung capacity; cause chest pains, throat irritation, and coughing; and worsen pre-existing health conditions related to the heart and lungs. In addition, increases in tropospheric ozone lead to a warming of Earth’s surface (see Q18). The negative effects of increasing tropospheric ozone contrast sharply with the positive effects of stratospheric ozone as an absorber of harmful UV-B radiation from the Sun.

Reducing bad ozone. Reducing the emission of pollutants can reduce bad ozone in the air surrounding humans, plants, and animals. Major sources of pollutants include large cities where fossil fuel consumption and industrial activities are greatest. Many programs around the globe have already been successful in reducing the emission of pollutants that cause excess ozone production near Earth’s surface.

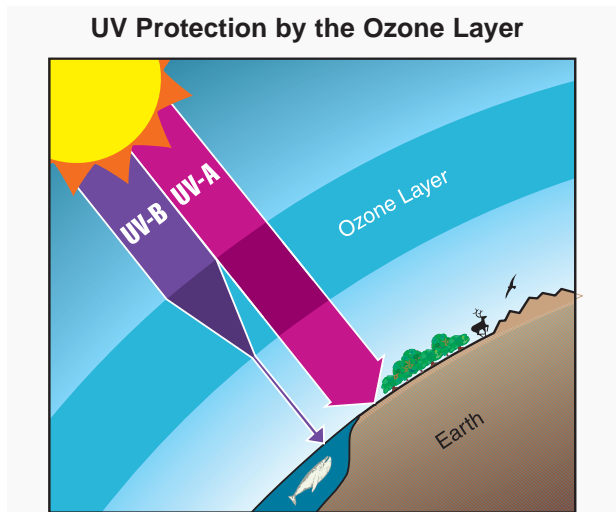


Figure Q3-1. UV-B protection by the ozone layer. The ozone layer resides in the stratosphere and surrounds the entire Earth. UV-B radiation (280- to 315-nanometer (nm) wavelength) from the Sun is partially absorbed in this layer. As a result, the amount of UV-B reaching Earth’s surface is greatly reduced. UV-A (315- to 400-nm wavelength) and other solar radiation are not strongly absorbed by the ozone layer. Human exposure to UV-B increases the risk of skin cancer, cataracts, and a suppressed immune system. UV-B exposure can also damage terrestrial plant life, single-cell organisms, and aquatic ecosystems.

Q4: Is total ozone uniform over the globe?

No, the total amount of ozone above the surface of Earth varies with location on time scales that range from daily to seasonal and longer. The variations are caused by stratospheric winds and the chemical production and destruction of ozone. Total ozone is generally lowest at the equator and highest near the poles because of the seasonal wind patterns in the stratosphere.

Total ozone. Total ozone at any location on the globe is found by measuring all the ozone in the atmosphere directly above that location. Total ozone includes that present in the stratospheric ozone layer and that present throughout the troposphere (see Figure Q1-2). The contribution from the troposphere is generally only about 10% of total ozone. Total ozone values are often reported in *Dobson units*, denoted “DU.” Typical values vary between 200 and 500 DU over the globe (see Figure Q4-1). A total ozone value of 500 DU, for example, is equivalent to a layer of pure ozone gas on Earth’s surface having a thickness of only 0.5 centimeters (0.2 inches).

Global distribution. Total ozone varies strongly with latitude over the globe, with the largest values occurring at middle and high latitudes (see Figure Q4-1). This is a result of winds that circulate air in the stratosphere, moving tropical air rich in ozone toward the poles. Since about 1980, regions of low total ozone have occurred at polar latitudes in winter and spring as a result of the chemical destruction of ozone by chlorine and bromine gases (see Q11 and Q12). The smallest values of total ozone (other than in the Antarctic in spring) occur in the tropics in all seasons, in part because the troposphere extends to a higher altitude in the tropics, and consequently, the thickness of the ozone layer is smallest there.

Natural variations. The variations of total ozone with latitude and longitude come about for two reasons. First, natural air motions mix air between regions of the stratosphere that have high ozone values and those that have low ozone values. Air motions also increase the vertical thickness of the ozone layer near the poles, which increases the value of total ozone in those regions. Tropospheric weather systems can temporarily reduce the thickness of the stratospheric ozone layer in a region, lowering total ozone at the same time. Second, variations occur as a result of changes in the balance of chemical production and loss processes as air moves to different locations over the globe. Reductions in ultraviolet radiation from the sun in its 11-year cycle, for example, reduce the production of ozone.

Scientists have a good understanding of how chemistry and air motions work together to cause the observed large-scale features in total ozone, such as those seen in Figure Q4-1. Ozone changes are carefully monitored by a large group of investigators using satellite, airborne, and

ground-based instruments. The analysis of these observations helps scientists to estimate the contribution of human activities to ozone depletion.

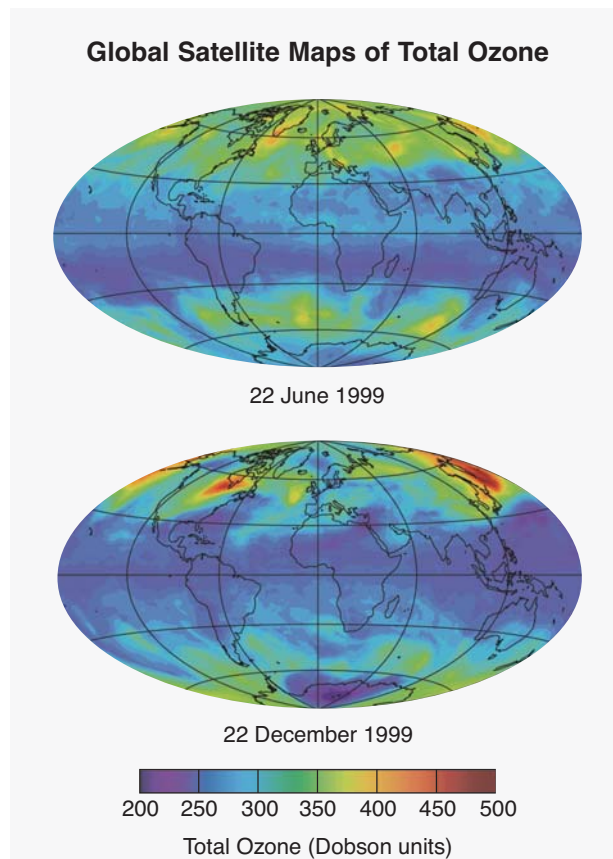


Figure Q4-1. Total ozone. A total ozone value is obtained by measuring all the ozone that resides in the atmosphere over a given location on Earth’s surface. Total ozone values shown here are reported in “Dobson units” as measured by a satellite instrument from space. Total ozone varies with latitude, longitude, and season, with the largest values at high latitudes and the lowest values in tropical regions. Total ozone at most locations varies with time on a daily to seasonal basis as ozone-rich air is moved about the globe by stratospheric winds. Low total ozone values over Antarctica in the 22 December image represent the remainder of the “ozone hole” from the 1999 Antarctic winter/spring season (see Q11).

Q5: How is ozone measured in the atmosphere?

The amount of ozone in the atmosphere is measured by instruments on the ground and carried aloft on balloons, aircraft, and satellites. Some measurements involve drawing air into an instrument that contains a system for detecting ozone. Other measurements are based on ozone’s unique absorption of light in the atmosphere. In that case, sunlight or laser light is carefully measured after passing through a portion of the atmosphere containing ozone.

The abundance of ozone in the atmosphere is measured by a variety of techniques (see Figure Q5-1). The techniques make use of ozone’s unique optical and chemical properties. There are two principal categories of measurement techniques: *local* and *remote*. Ozone measurements by these techniques have been essential in monitoring changes in the ozone layer and in developing our understanding of the processes that control ozone abundances.

Local measurements. Local measurements of atmospheric ozone abundance are those that require air to be drawn directly into an instrument. Once inside an instrument, ozone can be measured by its absorption of ultraviolet (UV) light or by the electrical current produced in an ozone chemical reaction. The latter approach is used in the construction of “ozonesondes,” which are lightweight, ozone-measuring modules suitable for launching on small balloons. The balloons ascend far enough in the atmosphere to measure ozone in the stratospheric ozone layer. Ozonesondes are launched regularly at many locations around the world. Local ozone-measuring instruments using optical or chemical detection schemes are also used routinely on board research aircraft to measure the distribution of ozone in the troposphere and lower stratosphere. High-altitude research aircraft can reach the ozone layer at most locations over the globe and can reach farthest into the layer at high latitudes in polar regions. Ozone measurements are also being made on some commercial aircraft.

Remote measurements. Remote measurements of ozone abundance are obtained by detecting the presence of ozone at large distances away from the instrument. Most remote measurements of ozone rely on its unique absorption of UV radiation. Sources of UV radiation that can be used are the Sun and lasers. For example, satellites use the absorption of UV sunlight by the atmosphere or the absorption of sunlight scattered from the surface of Earth to measure ozone over nearly the entire globe on a daily basis. A network of ground-based detectors measures ozone by the amount of the Sun’s UV light that reaches Earth’s surface. Other instruments measure ozone

using its absorption of infrared or visible radiation or its emission of microwave or infrared radiation. Total ozone amounts and the altitude distribution of ozone can be obtained with remote measurement techniques. Lasers are routinely deployed at ground sites or on board aircraft to detect ozone over a distance of many kilometers along the laser light path.

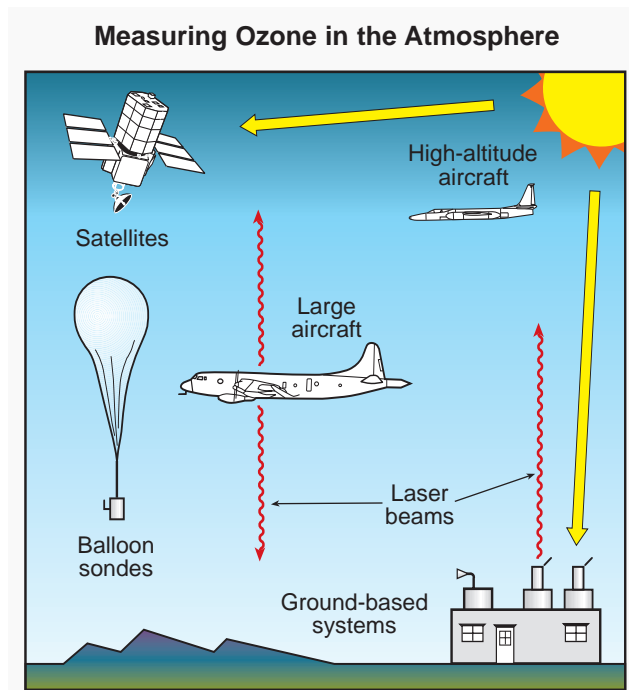


Figure Q5-1. Ozone measurements. Ozone is measured throughout the atmosphere with instruments on the ground and on board aircraft, high-altitude balloons, and satellites. Some instruments measure ozone locally in sampled air and others measure ozone remotely some distance away from the instrument. Instruments use optical techniques, with the Sun and lasers as light sources, or use chemical reactions that are unique to ozone. Measurements at many locations over the globe are made regularly to monitor total ozone amounts.

Global Ozone Dobson Network

The first instrument for routine monitoring of total ozone was developed by Gordon M. B. Dobson in the 1920s. The instrument, now called a Dobson spectrophotometer, measures the intensity of sunlight at two ultraviolet wavelengths: one that is strongly absorbed by ozone and one that is weakly absorbed. The difference in light intensity at the two wavelengths is used to provide a measurement of total ozone above the location of the instrument.

A global network of ground-based, total-ozone observing stations was established in 1957 as part of the International Geophysical Year. Today, there are about 100 sites distributed throughout the world (from South Pole, Antarctica (90°S), to Ellesmere Island, Canada (83°N)), many of which routinely measure total ozone with Dobson instruments. The accuracy of these observations is maintained by regular calibrations and intercomparisons. Data from the network have been essential for understanding the effects of chlorofluorocarbons (CFCs) and other ozone-depleting gases on the global ozone layer, starting before the launch of space-based ozone-measuring instruments and continuing to the present day. Because of their stability and accuracy, the Dobson instruments are now routinely used to help calibrate space-based observations of total ozone.

Pioneering scientists have traditionally been honored by having units of measure named after them. Accordingly, the unit of measure for total ozone is called the “Dobson unit” (see Q4).

II. THE OZONE DEPLETION PROCESS

Q6: What are the principal steps in stratospheric ozone depletion caused by human activities?

The initial step in the depletion of stratospheric ozone by human activities is the emission, at Earth's surface, of ozone-depleting gases containing chlorine and bromine. Most of these gases accumulate in the lower atmosphere because they are unreactive and do not dissolve readily in rain or snow. Eventually, these emitted source gases are transported to the stratosphere, where they are converted to more reactive gases containing chlorine and bromine. These more reactive gases then participate in reactions that destroy ozone. Finally, when air returns to the lower atmosphere, these reactive chlorine and bromine gases are removed from Earth's atmosphere by rain and snow.

Emission, accumulation, and transport. The principal steps in stratospheric ozone depletion caused by human activities are shown in Figure Q6-1. The process begins with the *emission*, at Earth's surface, of source gases containing the halogens chlorine and bromine (see Q7). The halogen source gases include manufactured chemicals released to the atmosphere by a variety of human activities. Chlorofluorocarbons (CFCs) are an important example of chlorine-containing gases. Emitted source gases *accumulate* in the lower atmosphere (troposphere) and are eventually *transported* to the stratosphere. The accumulation occurs because most source gases are unreactive in the lower atmosphere. However, small amounts of these gases dissolve or are taken up in ocean waters.

Some emissions of halogen gases come from natural sources (see Q7). These emissions also accumulate in the troposphere and are transported to the stratosphere.

Conversion, reaction, and removal. Halogen source gases do not react directly with ozone. Once in the stratosphere, halogen source gases are chemically converted to reactive halogen gases by ultraviolet radiation from the Sun (see Q8). The rate of conversion is related to the atmospheric lifetime of a gas (see Q7). Source gases with lifetimes greater than a few years may circulate between the troposphere and stratosphere multiple times before full conversion occurs.

The reactive gases formed in the eventual conversion of the halogen source gases react chemically to destroy ozone in the stratosphere (see Q9). The average depletion

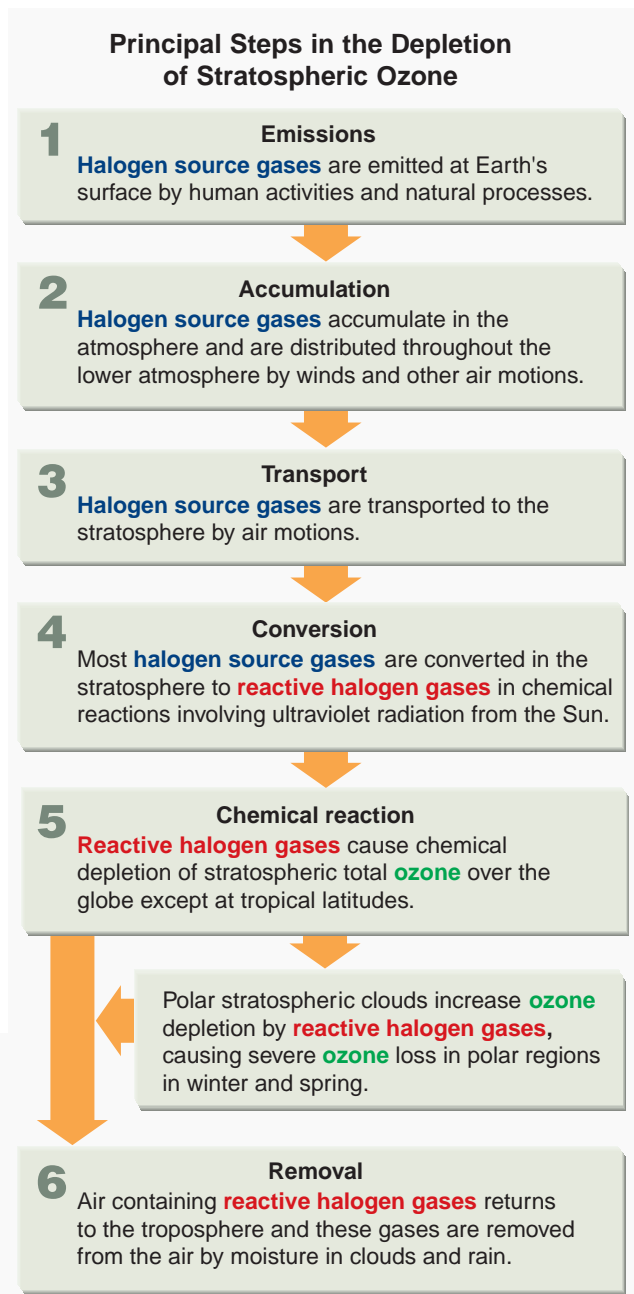


Figure Q6-1. Principal steps in stratospheric ozone depletion. The stratospheric ozone depletion process begins with the emission of halogen source gases at Earth's surface and ends when reactive halogen gases are removed by rain and snow in the troposphere and deposited on Earth's surface. In the stratosphere, the reactive halogen gases, namely chlorine monoxide (ClO) and bromine monoxide (BrO), destroy ozone.

TWENTY QUESTIONS: 2006 UPDATE

of total ozone attributed to reactive gases is smallest in the tropics and largest at high latitudes (see Q13). In polar regions, the presence of polar stratospheric clouds greatly increases the abundance of the most reactive halogen gases (see Q10). This results in substantial ozone destruction in polar regions in winter and spring (see Q11 and Q12).

After a few years, air in the stratosphere returns to the troposphere, bringing along reactive halogen gases. These gases are then removed from the atmosphere by rain and other precipitation and deposited on Earth's surface. This removal brings to an end the destruction of ozone by chlorine and bromine atoms that were first released to the atmosphere as components of halogen source gas molecules.

Tropospheric conversion. Halogen source gases with short lifetimes (see Q7) undergo significant chemical conversion in the troposphere, producing reactive halogen gases and other compounds. Source gas molecules that are not converted accumulate in the troposphere and are transported to the stratosphere. Because of removal by precipitation, only small portions of the reactive halogen gases produced in the troposphere are also transported to the stratosphere. Important examples of gases that undergo some tropospheric removal are the HCFCs, which are used as substitute gases for other halogen source gases (see Q15 and Q16), bromoform, and gases containing iodine (see Q7).

Understanding Stratospheric Ozone Depletion

Scientists learn about ozone destruction through a combination of laboratory studies, computer models, and stratospheric observations. In *laboratory studies* scientists are able to discover and evaluate individual chemical reactions that also occur in the stratosphere. Chemical reactions between two gases follow well-defined physical rules. Some of these reactions occur on the surfaces of particles formed in the stratosphere. Reactions have been studied that involve a wide variety of molecules containing chlorine, bromine, fluorine, and iodine and other atmospheric constituents such as oxygen, nitrogen, and hydrogen. These studies show that there exist several reactions involving chlorine and bromine that can directly or indirectly cause ozone destruction in the atmosphere.

With *computer models*, scientists can examine the overall effect of a large group of known reactions under the chemical and physical conditions found in the stratosphere. These models include winds, air temperatures, and the daily and seasonal changes in sunlight. With such analyses, scientists have shown that chlorine and bromine can react in catalytic cycles in which one chlorine or bromine atom can destroy many ozone molecules. Scientists use model results to compare with past observations as a test of our understanding of the atmosphere and to evaluate the importance of new reactions found in the laboratory. Computer models also enable scientists to explore the future by changing atmospheric conditions and other model parameters.

Scientists have conducted *observations* to find out which gases are present in various regions of the stratosphere and at what concentrations. They have monitored the change in these abundances over time periods spanning a daily cycle to decades. Observations have shown that halogen source gases and reactive halogen gases are present in the stratosphere at expected amounts. Ozone and chlorine monoxide (ClO), for example, have been observed extensively with a variety of instruments. Instruments on the ground and on board satellites, balloons, and aircraft detect ozone and ClO at a distance (remotely) using optical and microwave signals. High-altitude aircraft and balloon instruments detect both gases locally in the stratosphere (see Q5). For example, these observations show that ClO is present at elevated amounts in the Antarctic and Arctic stratospheres in the late winter/early spring season, when the most severe ozone depletion occurs (see Q8).

Q7: What emissions from human activities lead to ozone depletion?

Certain industrial processes and consumer products result in the emission of “halogen source gases” to the atmosphere. These gases bring chlorine and bromine to the stratosphere, which cause depletion of the ozone layer. For example, chlorofluorocarbons (CFCs), once used in almost all refrigeration and air conditioning systems, eventually reach the stratosphere, where they are broken apart to release ozone-depleting chlorine atoms. Other examples of human-produced ozone-depleting gases are the “halons,” which are used in fire extinguishers and contain ozone-depleting bromine atoms. The production and consumption of all principal halogen source gases by human activities are regulated worldwide under the Montreal Protocol.

Principal human-produced chlorine and bromine gases. Human activities cause the emission of *halogen source gases* that contain chlorine and bromine atoms. These emissions into the atmosphere ultimately lead to stratospheric ozone depletion. The source gases that contain only carbon, chlorine, and fluorine are called “chlorofluorocarbons,” usually abbreviated as CFCs. CFCs, along with carbon tetrachloride (CCl_4) and methyl chloroform (CH_3CCl_3), historically have been the most important chlorine-containing gases that are emitted by human activities and destroy stratospheric ozone (see Figure Q7-1). These and other chlorine-containing gases have been used in many applications, including refrigeration, air conditioning, foam blowing, aerosol propellants, and cleaning of metals and electronic components. These activities have typically caused the emission of halogen-containing gases to the atmosphere.

Another category of halogen source gases contains bromine. The most important of these are the “halons” and methyl bromide (CH_3Br). Halons are halogenated hydrocarbon gases originally developed to extinguish fires. Halons are widely used to protect large computers, military hardware, and commercial aircraft engines. Because of these uses, halons are often directly released into the atmosphere. Halon-1211 and halon-1301 are the most abundant halons emitted by human activities (see Figure Q7-1). Methyl bromide, used primarily as an agricultural fumigant, is also a significant source of bromine to the atmosphere.

Human emissions of the principal chlorine- and bromine-containing gases have increased substantially since the middle of the 20th century (see Q16). The result has been global ozone depletion, with the greatest losses occurring in polar regions (see Q11 to Q13).

Other human sources of chlorine and bromine. Other chlorine- and bromine-containing gases are released regularly in human activities. Common examples are the use of chlorine gases to disinfect swimming pools and wastewater, fossil fuel burning, and various industrial processes. These activities do not contribute significantly

to stratospheric amounts of chlorine and bromine because either the global source is small or the emitted gases are short-lived (very reactive or highly soluble) and, therefore, are removed from the atmosphere before they reach the stratosphere.

Natural sources of chlorine and bromine. There are a few halogen source gases present in the stratosphere that have large natural sources. These include methyl chloride (CH_3Cl) and methyl bromide (CH_3Br), both of which are emitted by oceanic and terrestrial ecosystems. Natural sources of these two gases contribute about 17% of the chlorine currently in the stratosphere and about 30% of the bromine (see Figure Q7-1). Very short-lived source gases containing bromine, such as bromoform (CHBr_3), are also released to the atmosphere primarily from the oceans. Only a small fraction of these emissions reaches the stratosphere, because these gases are rapidly removed in the lower atmosphere. The contribution of these very short-lived gases to stratospheric bromine is estimated to be about 24%, but this has a large uncertainty. The contribution to stratospheric chlorine of short-lived chlorinated gases from natural and human sources is much smaller (< 3%) and is included in the “Other gases” category in Figure Q7-1. Changes in the natural sources of chlorine and bromine since the middle of the 20th century are not the cause of observed ozone depletion.

Lifetimes and emissions. After emission, halogen source gases are either naturally removed from the atmosphere or undergo chemical conversion. The time to remove or convert about 60% of a gas is often called its atmospheric “lifetime.” Lifetimes vary from less than 1 year to 100 years for the principal chlorine- and bromine-containing gases (see Table Q7-1). Gases with the shortest lifetimes (e.g., the HCFCs, methyl bromide, methyl chloride, and the very short-lived gases) are substantially destroyed in the troposphere, and therefore only a fraction of each emitted gas contributes to ozone depletion in the stratosphere.

The amount of a halogen source gas present in the atmosphere depends on the lifetime of the gas and the

Primary Sources of Chlorine and Bromine for the Stratosphere in 2004

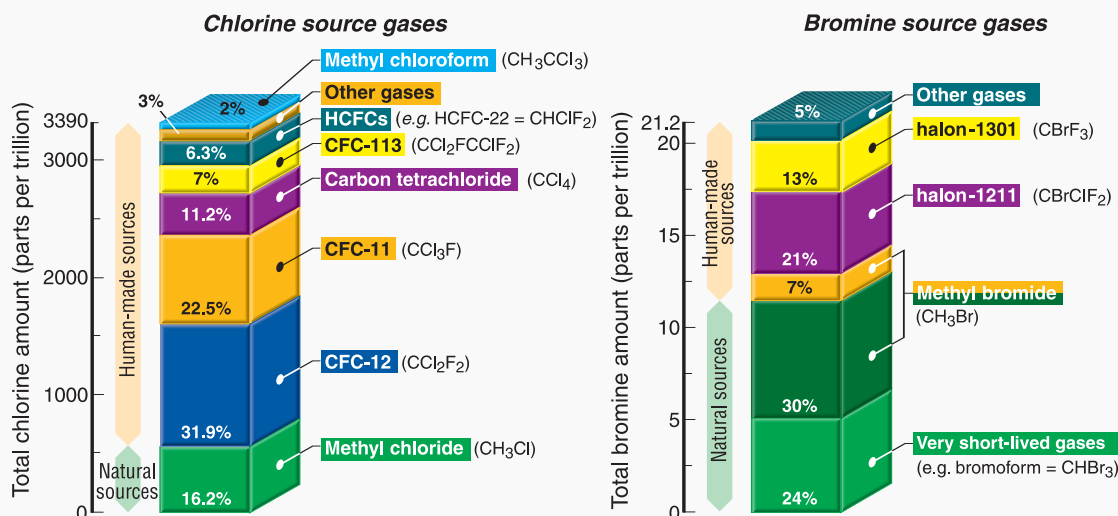


Figure Q7-1. Stratospheric source gases. A variety of gases transport chlorine and bromine into the stratosphere. These gases, called halogen source gases, are emitted from natural sources and by human activities. These partitioned columns show how the principal chlorine and bromine source gases contribute to the respective total amounts of chlorine and bromine as measured in 2004. Note the large difference in the vertical scales: total chlorine in the stratosphere is 160 times more abundant than total bromine. For chlorine, human activities account for most that reaches the stratosphere. The CFCs are the most abundant of the chlorine-containing gases released in human activities. Methyl chloride is the most important natural source of chlorine. HCFCs, which are substitute gases for CFCs and also are regulated under the Montreal Protocol, are a small but growing fraction of chlorine-containing gases. The “Other gases” category includes minor CFCs and short-lived gases. For bromine that reaches the stratosphere, halons and methyl bromide are the largest sources. Both gases are released in human activities. Methyl bromide has an additional natural source. Natural sources are a larger fraction of total bromine than of total chlorine. (The unit “parts per trillion” is used here as a measure of the relative abundance of a gas in air: 1 part per trillion indicates the presence of one molecule of a gas per trillion other air molecules.)

amount emitted to the atmosphere. Emissions vary greatly for the principal source gases, as indicated in Table Q7-1. Emissions of most gases regulated by the Montreal Protocol have decreased since 1990, and emissions from all regulated gases are expected to decrease in the coming decades (see Q16).

Ozone Depletion Potential. The halogen source gases in Figure Q7-1 are also known as “ozone-depleting substances” because they are converted in the stratosphere to reactive gases containing chlorine and bromine (see Q8). Some of these reactive gases participate in reactions that destroy ozone (see Q9). Ozone-depleting substances are compared in their effectiveness to destroy stratospheric ozone using the “Ozone Depletion Potential” (ODP), as listed in Table Q7-1 (see Q18). A gas with a larger ODP has a greater potential to destroy ozone over its lifetime in the atmosphere. The ODP is calculated on a “per mass” basis for each gas relative to CFC-11, which

has an ODP defined to be 1. Halon-1211 and halon-1301 have ODPs significantly larger than CFC-11 and most other emitted gases, because bromine is much more effective overall (about 60 times) on a per-atom basis than chlorine in chemical reactions that destroy ozone in the stratosphere. The gases with small ODP values generally have short atmospheric lifetimes or fewer chlorine and bromine atoms. The production and consumption of all principal halogen source gases by humans are regulated under the provisions of the Montreal Protocol (see Q15).

Fluorine and iodine. Fluorine and iodine are also halogen atoms. Many of the source gases in Figure Q7-1 also contain fluorine atoms in addition to chlorine or bromine. After the source gases undergo conversion in the stratosphere (see Q6), the fluorine content of these gases is left in chemical forms that do not cause ozone depletion. Iodine is a component of several gases that are naturally emitted from the oceans. Although iodine can

Table Q7-1. Atmospheric lifetimes, emissions, and Ozone Depletion Potentials of halogen source gases. ^a

Halogen Source Gas	Atmospheric Lifetime (years)	Global Emissions in 2003 ^b	Ozone Depletion Potential (ODP) ^d
Chlorine			
CFC-12	100	101-144	1
CFC-113	85	1-15	1
CFC-11	45	60-126	1
Carbon tetrachloride (CCl ₄)	26	58-131	0.73
HCFCs	1-26	312-403	0.02-0.12
Methyl chloroform (CH ₃ CCl ₃)	5	~20	0.12
Methyl chloride	1.0	1700-13600	0.02
Bromine			
Halon-1301	65	~3	16
Halon-1211	16	7-10	7.1
Methyl bromide (CH ₃ Br)	0.7	160-200	0.51
Very short-lived gases (e.g., CHBr ₃)	< 0.5	c	c

^a Includes both human activities and natural sources.

^b Emission in gigagrams per year (1 gigagram = 10⁹ grams = 1000 metric tons).

^c Estimates are uncertain for most species.

^d Values are calculated for emissions of equal mass for each gas.

participate in ozone destruction reactions, these iodine-containing source gases generally have very short lifetimes and, as a result, most are removed in the troposphere before they reach the stratosphere.

Other gases. Other gases that influence stratospheric ozone abundances also have increased in the stratosphere as a result of human activities. Important examples are methane (CH₄) and nitrous oxide (N₂O), which react in the stratosphere to form water vapor and reactive hydrogen, and nitrogen oxides, respectively. These reactive products also participate in the production and loss balance of stratospheric ozone (see Q2). The overall effect of increases in these other gases on ozone is much smaller than that caused by increases in chlorine- and bromine-containing gases from human activities (see Q18).

Heavier-Than-Air CFCs

CFCs and other halogen source gases reach the stratosphere despite the fact that they are “heavier than air.” All the principal source gases are emitted and accumulate in the lower atmosphere (troposphere). The distributions of gases in the troposphere and stratosphere are not controlled by the molecular weight of the gases because air is in continual motion in these regions as a result of winds and convection. Air motions ensure that most source gases become horizontally and vertically well mixed throughout the troposphere in a matter of months. It is this well-mixed air that enters the lower stratosphere from upward air motions in tropical regions, bringing with it source gas molecules emitted from a wide variety of locations on Earth’s surface.

Atmospheric measurements confirm that halogen source gases with long atmospheric lifetimes are well mixed in the troposphere and are present in the stratosphere (see Figure Q8-2). The amounts found in these regions are consistent with the emissions estimates reported by industries and governments. Measurements also show that gases that are “lighter than air,” such as hydrogen (H₂) and methane (CH₄), are also well mixed in the troposphere, as expected. Only at altitudes well above the troposphere and stratosphere (above 85 kilometers (53 miles)), where much less air is present, does the influence of winds and convection diminish to the point where heavy gases begin to separate from lighter gases as a result of gravity.

Q8: What are the reactive halogen gases that destroy stratospheric ozone?

Emissions from human activities and natural processes include large sources of chlorine- and bromine-containing gases that eventually reach the stratosphere. When exposed to ultraviolet radiation from the Sun, these halogen source gases are converted to more reactive gases also containing chlorine and bromine. Important examples of the reactive gases that destroy stratospheric ozone are chlorine monoxide (ClO) and bromine monoxide (BrO). These reactive gases participate in “catalytic” reaction cycles that efficiently destroy ozone. Volcanoes can emit some chlorine-containing gases, but these gases are ones that readily dissolve in rainwater and ice and are usually “washed out” of the atmosphere before they can reach the stratosphere.

Reactive gases containing the halogens chlorine and bromine lead to the chemical destruction of stratospheric ozone. Halogen-containing gases present in the stratosphere can be divided into two groups: *halogen source gases* and *reactive halogen gases*. The source gases are emitted at Earth’s surface by natural processes and by human activities (see Q7). Once in the stratosphere, the halogen source gases chemically convert at different rates to form the reactive halogen gases. The conversion occurs in the stratosphere instead of the troposphere because solar UV radiation is more intense in the stratosphere.

Reactive halogen gases. The chemical conversion of halogen source gases, which involves ultraviolet sunlight and other chemical reactions, produces a number of reactive halogen gases. These reactive gases contain all of the chlorine and bromine atoms originally present in the source gases.

The most important reactive chlorine- and bromine-containing gases that form in the stratosphere are shown

in Figure Q8-1. Away from polar regions, the most abundant are hydrogen chloride (HCl) and chlorine nitrate (ClONO₂). These two gases are considered *reservoir* gases because they do not react directly with ozone but can be converted to the most reactive forms that do chemically destroy ozone. The *most reactive* forms are chlorine monoxide (ClO) and bromine monoxide (BrO), and chlorine and bromine atoms (Cl and Br). A large fraction of available stratospheric bromine is generally in the form of BrO, whereas usually only a small fraction of stratospheric chlorine is in the form of ClO. In polar regions, the reservoirs ClONO₂ and HCl undergo a further conversion on polar stratospheric clouds to form ClO (see Q10). In that case, ClO becomes a large fraction of available reactive chlorine.

Reactive chlorine observations. Reactive chlorine gases have been observed extensively in the stratosphere with both local and remote measurement techniques. The measurements from space at middle latitudes displayed in

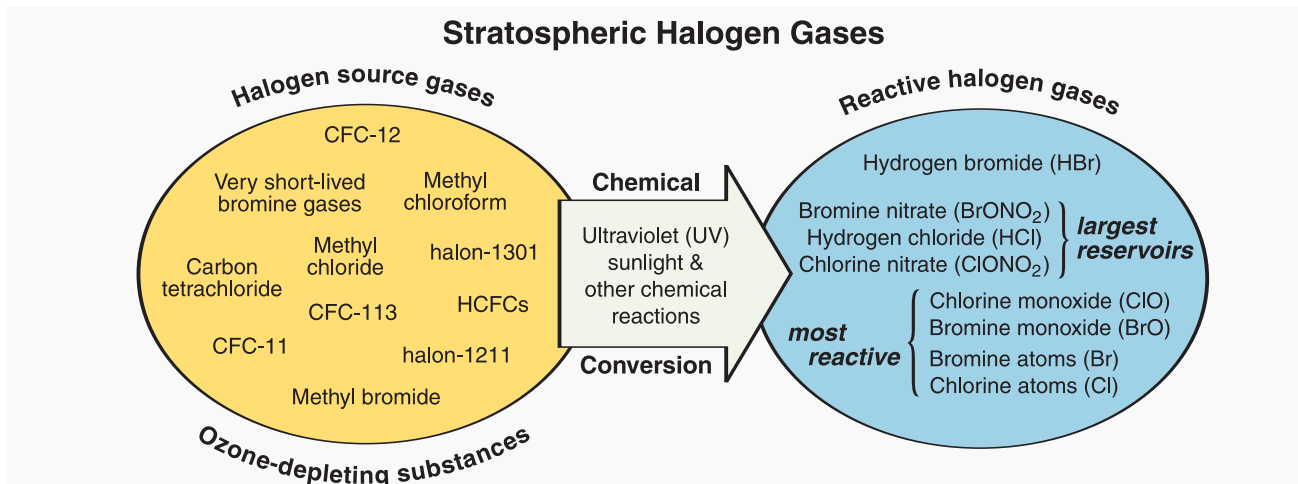


Figure Q8-1. Conversion of halogen source gases. Halogen source gases (also known as ozone-depleting substances) are chemically converted to reactive halogen gases primarily in the stratosphere. The conversion requires ultraviolet sunlight and a few other chemical reactions. The short-lived gases undergo some conversion in the troposphere. The reactive halogen gases contain all the chlorine and bromine originally present in the source gases. The reactive gases separate into reservoir gases, which do not destroy ozone, and reactive gases, which participate in ozone destruction cycles (see Q9).

Figure Q8-2 are representative of how the amounts of chlorine-containing gases change between the surface and the upper stratosphere. Available chlorine (see red line in Figure Q8-2) is the sum of chlorine contained in halogen source gases and the reactive gases HCl, ClONO₂, ClO, and other minor gases. Available chlorine is constant within a few percent from the surface to 47 kilometers (31 miles) altitude. In the troposphere, available chlorine is contained almost entirely in the source gases described in Figure Q7-1. At higher altitudes, the source gases become a smaller fraction of available chlorine as they are converted to reactive chlorine gases. At the highest altitudes, available chlorine is all in the form of reactive chlorine gases.

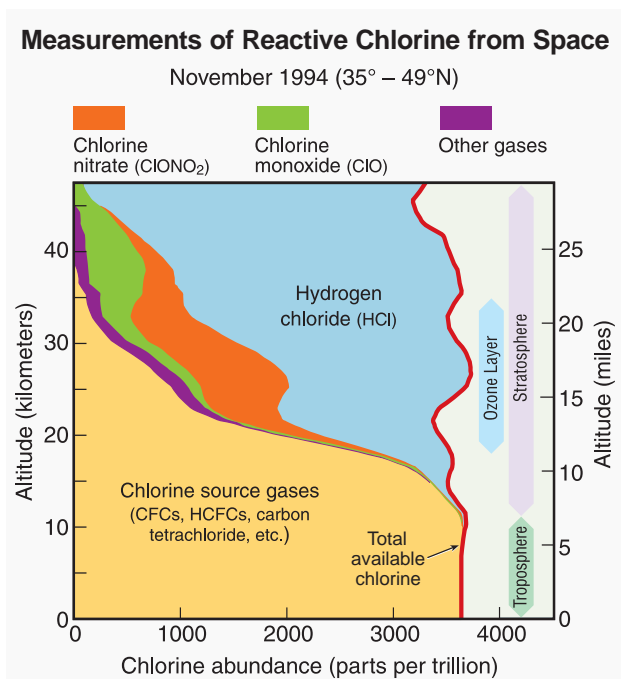


Figure Q8-2. Reactive chlorine gas observations.

The abundances of chlorine source gases and reactive chlorine gases as measured from space are displayed with altitude for a midlatitude location. In the troposphere (below about 10 kilometers), all chlorine is contained in the source gases. In the stratosphere, reactive chlorine gases increase with altitude as chlorine source gases decrease. This is a consequence of chemical reactions involving ultraviolet sunlight (see Figure Q8-1). The principal reactive gases formed are HCl, ClONO₂, and ClO. Summing the source gases with the reactive gases gives *total available chlorine*, which is nearly constant with altitude up to 47 km. In the ozone layer, HCl and ClONO₂ are the most abundant reactive chlorine gases. (The unit “parts per trillion” is defined in the caption of Figure Q7-1.)

In the altitude range of the ozone layer at midlatitudes, as shown in Figure Q8-2, the reactive chlorine gases HCl and ClONO₂ account for most of available chlorine. ClO, the most reactive gas in ozone depletion, is a small fraction of available chlorine. This small value limits the amount of ozone destruction that occurs outside of polar regions.

Reactive chlorine in polar regions. Reactive chlorine gases in polar regions in summer look similar to the altitude profiles shown in Figure Q8-2. In winter, however, the presence of polar stratospheric clouds (PSCs) causes further chemical changes (see Q10). PSCs convert HCl and ClONO₂ to ClO when temperatures are near minimum values in the winter Arctic and Antarctic stratosphere. In that case, ClO becomes the principal reactive chlorine species in sunlit regions and ozone loss becomes very rapid. An example of the late-winter ClO and ozone distributions is shown in Figure Q8-3 for the Antarctic stratosphere. These space-based measurements show that ClO abundances are high in the lower stratosphere over a region that exceeds the size of the Antarctic continent (greater than 13 million square kilometers or 5 million square miles). The peak abundance of ClO exceeds 1500 parts per trillion, which is much larger than typical midlatitude values shown in Figure Q8-2 and represents a large fraction of reactive chlorine in that altitude region. Because high ClO amounts cause rapid ozone loss (see Q9), ozone depletion is found in regions of elevated ClO (see Figure Q8-3).

Reactive bromine observations. Fewer measurements are available for reactive bromine gases in the lower stratosphere than for reactive chlorine, in part because of the lower abundance of bromine. The most widely observed bromine gas is bromine monoxide (BrO). Recent observations have shown that measured BrO abundances in the stratosphere are larger than expected from the conversion of the halons and methyl bromide to BrO, suggesting a significant contribution from the very short-lived bromine-containing gases.

Other sources. Some reactive halogen gases are also produced at Earth’s surface by natural processes and by human activities. However, because reactive halogen gases are soluble in water, almost all become trapped in the lower atmosphere by dissolving in rainwater and ice, and ultimately are returned to Earth’s surface before they can reach the stratosphere. For example, reactive chlorine is present in the atmosphere as sea salt (sodium chloride) produced by evaporation of ocean spray. Because sea salt dissolves in water, this chlorine is removed and does not reach the stratosphere in appreciable quantities. Another ground-level source is emission of chlorine gases from swimming pools, household bleach, and other uses.

Satellite Observations in the Lower Stratosphere

30 August 1996

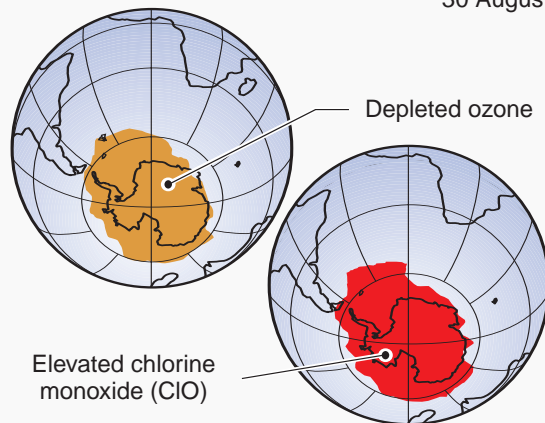


Figure Q8-3. Antarctic chlorine monoxide and ozone.

Satellite instruments monitor ozone and reactive chlorine gases in the global stratosphere. Results are shown here for Antarctic winter for a narrow altitude region within the ozone layer. In winter, chlorine monoxide (ClO) reaches high values (1500 parts per trillion) in the ozone layer, much higher than observed anywhere else in the stratosphere because ClO is produced by reactions on polar stratospheric clouds (see Q10). These high ClO values in the lower stratosphere last for 1 to 2 months, cover an area that at times exceeds that of the Antarctic continent, and efficiently destroy ozone in sunlit regions in late winter/early spring. Ozone values measured simultaneously within the ozone layer show very depleted values.

When released to the atmosphere, this chlorine is rapidly converted to forms that are soluble in water and removed. The Space Shuttle and other rocket motors release reactive chlorine gases directly in the stratosphere: in this case, the quantities are very small in comparison with other tropospheric sources.

Volcanoes. Volcanic plumes generally contain large quantities of chlorine in the form of hydrogen chloride

(HCl). Because the plumes also contain a considerable amount of water vapor, the HCl is efficiently scavenged by rainwater and ice and removed from the atmosphere. As a result, most of the HCl in the plume does not enter the stratosphere. After large recent eruptions, the increase in HCl in the stratosphere has been small compared with the total amount of chlorine in the stratosphere from other sources.

Replacing the Loss of Ozone in the Stratosphere

The idea is sometimes put forth that humans could replace the loss of global stratospheric ozone by making ozone and transporting it to the stratosphere. Ozone amounts in the stratosphere reflect a balance between continual production and destruction by mostly naturally occurring reactions (see Q2). The addition of chlorine and bromine to the stratosphere from human activities has increased ozone destruction and lowered stratospheric ozone amounts. Adding manufactured ozone to the stratosphere would upset the existing balance. As a consequence, most added ozone would be destroyed in chemical reactions within weeks to months as the balance was restored. So, it is not practical to consider replacing the loss of global stratospheric ozone because the replacement effort would need to continue indefinitely, or as long as increased chlorine and bromine amounts remained.

Other practical difficulties in replacing stratospheric ozone are the large amounts of ozone required and the delivery method. The total amount of atmospheric ozone is approximately 3,000 megatons (1 megaton = 1 billion kilograms) with most residing in the stratosphere. The replacement of the average global ozone loss of about 4% would require 120 megatons of stratospheric ozone to be distributed throughout the layer located many kilometers above Earth's surface. The energy required to produce this amount of ozone would be a significant fraction of the electrical power generated in the United States, which is now approximately 5 trillion kilowatt hours. Processing and storing requirements for ozone, which is explosive and toxic in large quantities, would increase the energy requirement. In addition, methods suitable to deliver and distribute large amounts of ozone to the stratosphere have not been demonstrated. Concerns for a global delivery system would include further significant energy use and unforeseen environmental consequences.

Q9: What are the chlorine and bromine reactions that destroy stratospheric ozone?

Reactive gases containing chlorine and bromine destroy stratospheric ozone in “catalytic” cycles made up of two or more separate reactions. As a result, a single chlorine or bromine atom can destroy many hundreds of ozone molecules before it reacts with another gas, breaking the cycle. In this way, a small amount of reactive chlorine or bromine has a large impact on the ozone layer. Certain ozone destruction reactions become most effective in polar regions because the reactive gas chlorine monoxide reaches very high levels there in the late winter/early spring season.

Stratospheric ozone is destroyed by reactions involving *reactive halogen gases*, which are produced in the chemical conversion of *halogen source gases* (see Figure Q8-1). The most reactive of these gases are chlorine monoxide (ClO), bromine monoxide (BrO), and chlorine and bromine atoms (Cl and Br). These gases participate in three principal reaction cycles that destroy ozone.

Cycle 1. Ozone destruction Cycle 1 is illustrated in Figure Q9-1. The cycle is made up of two basic reactions: $\text{ClO} + \text{O}$ and $\text{Cl} + \text{O}_3$. The net result of Cycle 1 is to convert one ozone molecule and one oxygen atom into two oxygen molecules. In each cycle, chlorine acts as a *catalyst* because ClO and Cl react and are reformed. In this way, one Cl atom participates in many cycles, destroying many ozone molecules. For typical stratospheric conditions at middle or low latitudes, a single chlorine atom can destroy hundreds of ozone molecules

before it happens to react with another gas, breaking the catalytic cycle.

Polar Cycles 2 and 3. The abundance of ClO is greatly increased in polar regions during winter as a result of reactions on the surfaces of polar stratospheric cloud (PSC) particles (see Q10). Cycles 2 and 3 (see Figure Q9-2) become the dominant reaction mechanisms for polar ozone loss because of the high abundances of ClO and the relatively low abundance of atomic oxygen (which limits the rate of ozone loss by Cycle 1). Cycle 2 begins with the self-reaction of ClO. Cycle 3, which begins with the reaction of ClO with BrO, has two reaction pathways to produce either Cl and Br or BrCl. The net result of both cycles is to destroy two ozone molecules and create three oxygen molecules. Cycles 2 and 3 account for most of the ozone loss observed in the Arctic and Antarctic stratospheres in the late winter/early spring

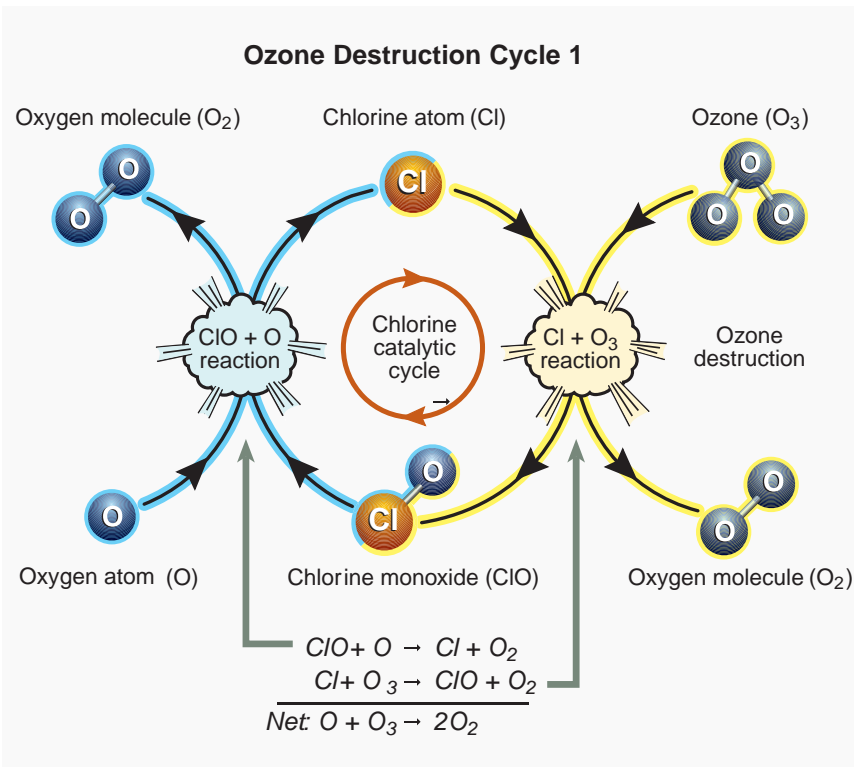


Figure Q9-1. Ozone destruction Cycle 1. The destruction of ozone in Cycle 1 involves two separate chemical reactions. The net or overall reaction is that of atomic oxygen with ozone, forming two oxygen molecules. The cycle can be considered to begin with either ClO or Cl. When starting with ClO, the first reaction is ClO with O to form Cl. Cl then reacts with (and thereby destroys) ozone and reforms ClO. The cycle then begins again with another reaction of ClO with O. Because Cl or ClO is reformed each time an ozone molecule is destroyed, chlorine is considered a catalyst for ozone destruction. Atomic oxygen (O) is formed when ultraviolet sunlight reacts with ozone and oxygen molecules. Cycle 1 is most important in the stratosphere at tropical and middle latitudes, where ultraviolet sunlight is most intense.

Ozone Destruction Cycles

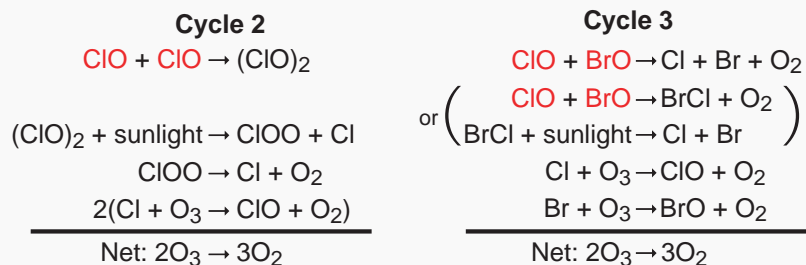


Figure Q9-2. Polar ozone destruction Cycles 2 and 3. Significant destruction of ozone occurs in polar regions because ClO abundances reach large values. In this case, the cycles initiated by the reaction of ClO with another ClO (Cycle 2) or the reaction of ClO with BrO (Cycle 3) efficiently destroy ozone. The net reaction in both cases is two ozone molecules forming three oxygen molecules. The reaction of ClO with BrO has two pathways to form the Cl and Br product gases. Ozone destruction Cycles 2 and 3 are catalytic, as illustrated for Cycle 1 in Figure Q9-1, because chlorine and bromine gases react and are reformed in each cycle. Sunlight is required to complete each cycle and to help form and maintain ClO abundances.

season (see Q11 and Q12). At high ClO abundances, the rate of ozone destruction can reach 2 to 3% per day in late winter/early spring.

Sunlight requirement. Sunlight is required to complete and maintain Cycles 1 through 3. Cycle 1 requires sunlight because atomic oxygen is formed only with ultraviolet sunlight. Cycle 1 is most important in the stratosphere at tropical and middle latitudes, where ultraviolet sunlight is most intense.

Cycles 2 and 3 require visible sunlight to complete the reaction cycles and to maintain ClO abundances. In the continuous darkness of winter in the polar stratospheres, reaction Cycles 2 and 3 cannot occur. It is only in late winter/early spring when sunlight returns to the polar regions that these cycles can occur. Therefore, the greatest destruction of ozone occurs in the partially to fully sunlit periods after midwinter in the polar stratospheres. The

visible sunlight needed in Cycles 2 and 3 is not sufficient to form ozone because this process requires ultraviolet sunlight. In the stratosphere in the late winter/early spring period, ultraviolet sunlight is weak because Sun angles are low. As a result, ozone is destroyed by Cycles 2 and 3 in the sunlit winter stratosphere but is not produced in significant amounts.

Other reactions. Global ozone abundances are controlled by many reactions that both produce and destroy ozone (see Q2). Chlorine and bromine catalytic reactions are but one group of ozone destruction reactions. Reactive hydrogen and reactive nitrogen gases, for example, are involved in other catalytic ozone-destruction cycles that also occur in the stratosphere. These reactions occur naturally in the stratosphere and their importance has not been as strongly influenced by human activities as have reactions involving halogens.

Q10: Why has an “ozone hole” appeared over Antarctica when ozone-depleting gases are present throughout the stratosphere?

Ozone-depleting gases are present throughout the stratospheric ozone layer because they are transported great distances by atmospheric air motions. The severe depletion of the Antarctic ozone layer known as the “ozone hole” occurs because of the special weather conditions that exist there and nowhere else on the globe. The very low temperatures of the Antarctic stratosphere create ice clouds called polar stratospheric clouds (PSCs). Special reactions that occur on PSCs and the relative isolation of polar stratospheric air allow chlorine and bromine reactions to produce the ozone hole in Antarctic springtime.

The severe depletion of stratospheric ozone in Antarctic winter is known as the “ozone hole” (see Q11). Severe depletion first appeared over Antarctica because atmospheric conditions there increase the effectiveness of ozone destruction by reactive halogen gases (see Q8). The formation of the Antarctic ozone hole requires abundant reactive halogen gases, temperatures low enough to form polar stratospheric clouds (PSCs), isolation of air from other stratospheric regions, and sunlight.

Distributing halogen gases. Halogen source gases emitted at Earth’s surface are present in comparable abundances throughout the stratosphere in both hemispheres

even though most of the emissions occur in the Northern Hemisphere. The abundances are comparable because most source gases have no important natural removal processes in the lower atmosphere and because winds and warm-air convection redistribute and mix air efficiently throughout the troposphere. Halogen gases (in the form of source gases and some reactive products) enter the stratosphere primarily from the tropical upper troposphere. Atmospheric air motions then transport them upward and toward the poles in both hemispheres.

Low temperatures. The severe ozone destruction represented by the ozone hole requires that low tempera-

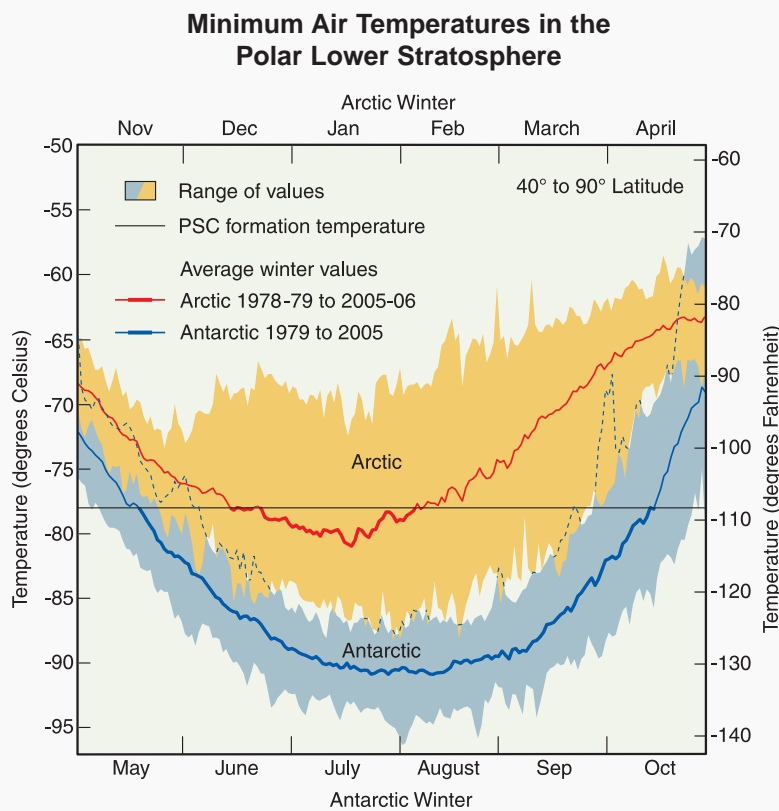


Figure Q10-1. Arctic and Antarctic temperatures. Stratospheric air temperatures in both polar regions reach minimum values in the lower stratosphere in the winter season. Average minimum values over Antarctica are as low as -90°C in July and August in a typical year. Over the Arctic, average minimum values are near -80°C in January and February. Polar stratospheric clouds (PSCs) are formed when winter minimum temperatures fall below the formation temperature (about -78°C). This occurs on average for 1 to 2 months over the Arctic and 5 to 6 months over Antarctica (see heavy red and blue lines). Reactions on PSCs cause the highly reactive chlorine gas ClO to be formed, which increases the destruction of ozone (see Q9). The range of winter minimum temperatures found in the Arctic is much greater than in the Antarctic. In some years, PSC formation temperatures are not reached in the Arctic, and significant ozone depletion does not occur. In the Antarctic, PSCs are present for many months, and severe ozone depletion now occurs in each winter season.

TWENTY QUESTIONS: 2006 UPDATE

tures be present over a range of stratospheric altitudes, over large geographical regions, and for extended time periods. Low temperatures are important because they allow polar stratospheric clouds (PSCs) to form. Reactions on the surfaces of the cloud particles initiate a remarkable increase in the most reactive halogen gases (see below and Q8). Temperatures are lowest in the stratosphere over both polar regions in winter. In the Antarctic winter, minimum temperatures are generally lower and less variable than in the Arctic winter (see Figure Q10-1). Antarctic temperatures also remain below the PSC formation temperature for much longer periods during winter. This occurs, in part, because there are significant meteorological differences between the hemispheres, resulting from the differences in the distributions of land, ocean, and mountains at middle and high latitudes. The winter temperatures are low enough for PSCs to form for nearly the entire Antarctic winter but usually only for part of every Arctic winter.

Isolated conditions. Air in the polar stratospheric regions is relatively isolated from other stratospheric regions for long periods in the winter months. The isolation comes about because of strong winds that encircle the poles, preventing substantial motion of air in or out of the polar stratospheres. The isolation is much more effective in the Antarctic than the Arctic. Once chemical changes occur in the cold air as a result of the presence of PSCs, the changes remain for many weeks to months.

Polar stratospheric clouds (PSCs). Polar stratospheric clouds cause changes in the relative abundances of reactive chlorine gases. Reactions occur on the surfaces of PSC particles that convert the reservoir forms of reactive chlorine gases, ClONO_2 and HCl , to the most reactive form, ClO (see Figure Q8-1). ClO increases from a small fraction of available reactive chlorine gases to nearly all that is available (see Q8). With increased ClO , additional catalytic cycles involving ClO and BrO become active in the chemical destruction of ozone when sunlight is available (see Q9).

PSCs form when stratospheric temperatures fall below about -78°C (-108°F) in polar regions (see Figure Q10-1). As a result, PSCs are often found over large areas of the winter polar regions and over a significant altitude range. At low polar temperatures, nitric acid (HNO_3) and water condense on preexisting sulfur-containing particles to form solid and liquid PSC particles. At even lower temperatures, ice particles also form. PSC particles grow large enough and are numerous enough that cloud-like features can be observed from the ground under certain conditions, particularly when the Sun is near the horizon (see Figure Q10-2). PSCs are often found near mountain

ranges in polar regions because the motion of air over the mountains can cause local cooling of stratospheric air.

When temperatures increase by early spring, PSCs no longer form and the production of ClO ends. Without continued ClO production, ClO amounts decrease as other chemical reactions reform ClONO_2 and HCl . As a result, the intense period of ozone depletion ends.

PSC removal. Once formed, PSC particles move downward because of gravity. The largest particles move down several kilometers or more in the stratosphere during the low-temperature winter/spring period. Because most PSCs contain nitric acid, their downward motion removes nitric acid from regions of the ozone layer. That process is called *denitrification*. With less nitric acid, the

Arctic Polar Stratospheric Clouds

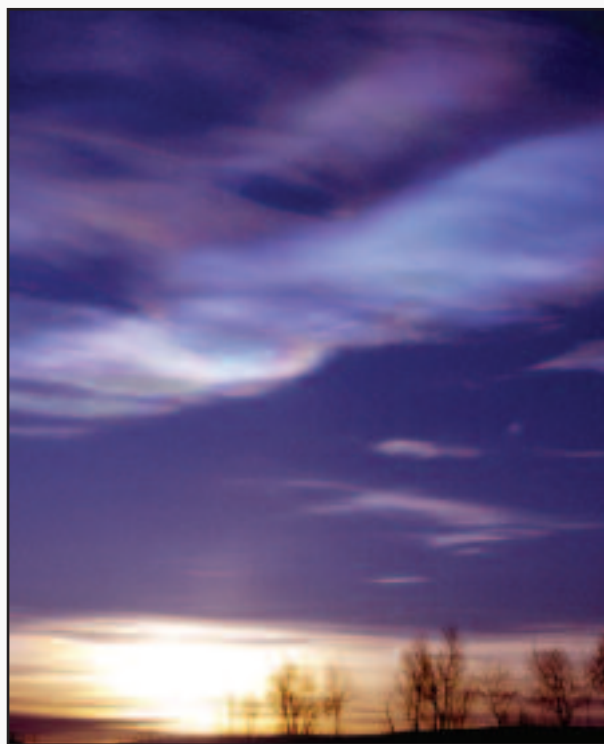


Figure Q10-2. Polar stratospheric clouds. This photograph of an Arctic polar stratospheric cloud (PSC) was taken from the ground at Kiruna, Sweden (67°N), on 27 January 2000. PSCs form during winters in the Arctic and Antarctic stratospheres. The particles grow from the condensation of water and nitric acid (HNO_3). The clouds often can be seen with the human eye when the Sun is near the horizon. Reactions on PSCs cause the highly reactive chlorine gas ClO to be formed, which is very effective in the chemical destruction of ozone (see Q9).

highly reactive chlorine gas ClO remains chemically active for a longer period, thereby increasing chemical ozone destruction. Denitrification occurs each winter in the Antarctic and in some, but not all, Arctic winters, because PSC formation temperatures are required over an extensive time period.

Discovering the role of PSCs. The formation of PSCs has been recognized for many years from ground-based observations. However, the geographical and altitude extent of PSCs in both polar regions was not known

fully until PSCs were observed by a satellite instrument in the late 1970s. The role of PSCs in converting reactive chlorine gases to ClO was not understood until after the discovery of the Antarctic ozone hole in 1985. Our understanding of the PSC role developed from laboratory studies of their surface reactivity, computer modeling studies of polar stratospheric chemistry, and sampling of PSC particles and reactive chlorine gases, such as ClO, in the polar stratospheric regions.

The Discovery of the Antarctic Ozone Hole

The first decreases in Antarctic total ozone were observed in the early 1980s over research stations located on the Antarctic continent. The measurements were made with ground-based Dobson spectrophotometers (see box in Q5). The observations showed unusually low total overhead ozone during the late winter/early spring months of September, October, and November. Total ozone was lower in these months compared with previous observations made as early as 1957. The early published reports came from the British Antarctic Survey and the Japan Meteorological Agency. The results became more widely known in the international community after three scientists from the British Antarctic Survey published them in the journal *Nature* in 1985. Soon after, satellite measurements confirmed the spring ozone depletion and further showed that in each late winter/early spring season starting in the early 1980s, the depletion extended over a large region centered near the South Pole. The term “ozone hole” came about from satellite images of total ozone that showed very low values encircling the Antarctic continent each spring (see Q11). Currently, the formation and severity of the Antarctic “ozone hole” are documented each year by a combination of satellite, ground-based, and balloon observations of ozone.

III. STRATOSPHERIC OZONE DEPLETION

Q11: How severe is the depletion of the Antarctic ozone layer?

Severe depletion of the Antarctic ozone layer was first observed in the early 1980s. Antarctic ozone depletion is seasonal, occurring primarily in late winter and early spring (August-November). Peak depletion occurs in early October when ozone is often completely destroyed over a range of altitudes, reducing overhead total ozone by as much as two-thirds at some locations. This severe depletion creates the “ozone hole” in images of Antarctic total ozone made from space. In most years the maximum area of the ozone hole far exceeds the size of the Antarctic continent.

The severe depletion of Antarctic ozone, known as the “ozone hole,” was first observed in the early 1980s. The depletion is attributable to chemical destruction by reactive halogen gases, which increased in the stratosphere in the latter half of the 20th century (see Q16). Conditions in the Antarctic winter stratosphere are highly suitable for ozone depletion because of (1) the long periods of extremely low temperatures, which promote polar stratospheric cloud (PSC) formation; (2) the abundance of reactive halogen gases, which chemically destroy ozone; and (3) the isolation of stratospheric air during the winter, which allows time for chemical destruction to occur (see Q10). The severity of Antarctic ozone depletion can be seen using satellite observations of total ozone, ozone altitude profiles, and long-term average values of polar total ozone.

Antarctic ozone hole. The most widely used images of Antarctic ozone depletion are those from space-based measurements of total ozone. Satellite images made during Antarctic winter and spring show a large region centered near the South Pole in which total ozone is highly depleted (see Figure Q11-1). This region has come to be called the “ozone hole” because of the near-circular contours of low ozone values in the images. The area of the ozone hole is defined here as the area contained within the 220-Dobson unit (DU) contour in total ozone maps (light blue color in Figure Q11-1). The maximum area has reached 25 million square kilometers (about 10 million square miles) in recent years, which is nearly twice the area of the Antarctic continent (see Figure Q11-2). Minimum values of total ozone inside the ozone hole averaged in late September have reached below 100 DU, which is well below normal springtime values of about 200 DU (see Figure Q11-2).

Altitude profiles of Antarctic ozone. Ozone within the “ozone hole” is also measured using balloonborne instruments (see Q5). Balloon measurements show changes within the ozone layer, the vertical region that contains the highest ozone abundances in the stratosphere. At geographic locations where the lowest total ozone

values occur in ozone hole images, balloon measurements show that the chemical destruction of ozone is complete over a vertical region of several kilometers. Balloon

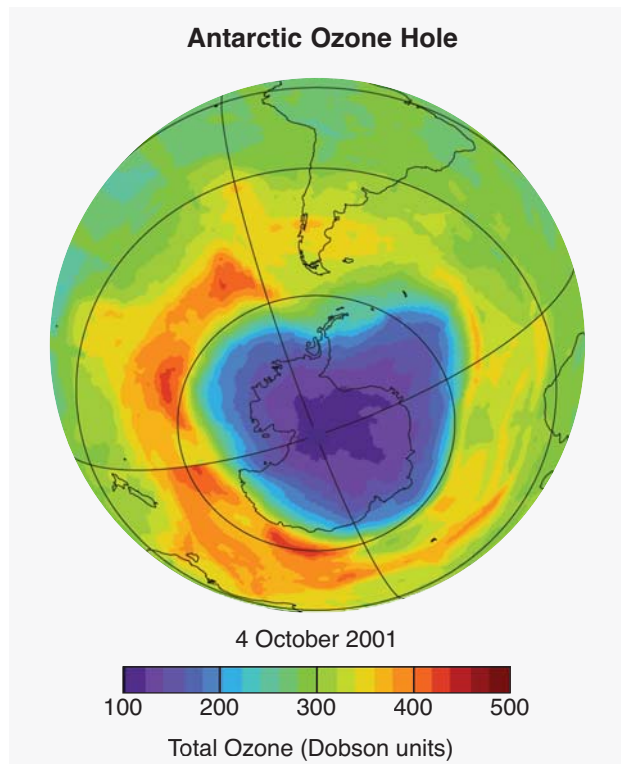


Figure Q11-1. Antarctic “ozone hole.” Total ozone values are shown for high southern latitudes as measured by a satellite instrument. The dark blue and purple regions over the Antarctic continent show the severe ozone depletion or “ozone hole” now found during every spring. Minimum values of total ozone inside the ozone hole are close to 100 Dobson units (DU) compared with normal springtime values of about 200 DU (see Q4). In late spring or early summer (November-December) the ozone hole disappears in satellite images as ozone-depleted air is displaced and mixed with ozone-rich air transported poleward from outside the ozone hole.

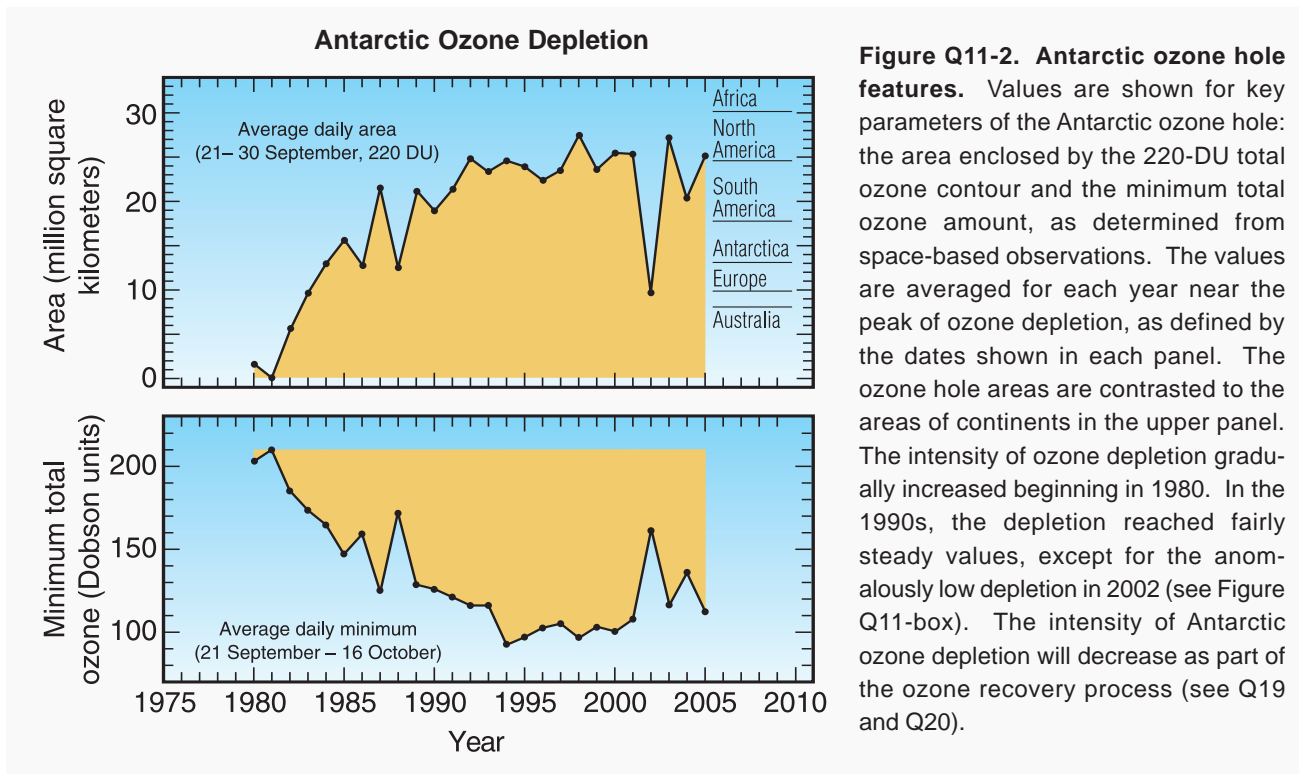


Figure Q11-2. Antarctic ozone hole features. Values are shown for key parameters of the Antarctic ozone hole: the area enclosed by the 220-DU total ozone contour and the minimum total ozone amount, as determined from space-based observations. The values are averaged for each year near the peak of ozone depletion, as defined by the dates shown in each panel. The ozone hole areas are contrasted to the areas of continents in the upper panel. The intensity of ozone depletion gradually increased beginning in 1980. In the 1990s, the depletion reached fairly steady values, except for the anomalously low depletion in 2002 (see Figure Q11-box). The intensity of Antarctic ozone depletion will decrease as part of the ozone recovery process (see Q19 and Q20).

measurements shown in Figure Q11-3 give an example of such depletion over South Pole, Antarctica, on 2 October 2001. The altitude region of total depletion (14-20 kilometers) in the profile corresponds to the region of lowest winter temperatures and highest chlorine monoxide (ClO) abundances. The average South Pole ozone profiles for the decades 1962-1971 and 1992-2001 (see Figure Q11-3) show how reactive halogen gases have dramatically altered the ozone layer. For the 1960s, the ozone layer is clearly evident in the October average profile and has a peak near 16 kilometers. For the 1990s, minimum average values in the center of the layer have fallen by 90% from the earlier values.

Long-term total ozone changes. Low winter temperatures and isolated conditions occur each year in the Antarctic stratosphere, but significant spring ozone depletion has been observed every year only since the early 1980s. In prior years, the amounts of reactive halogen gases in the stratosphere were insufficient to cause significant depletion. Satellite observations can be used to examine how ozone depletion has changed with time in both polar regions for the last three decades. Changes in ozone hole areas and minimum Antarctic ozone amounts are shown in Figure Q11-2. Depletion has increased since 1980 to become fairly stable in the 1990s and early 2000s, with the exception of 2002 (see Q11-box). Total ozone

averaged over the Antarctic region in late winter/early spring shows similar features (Figure Q12-1). Average values decreased steadily through the 1980s and 1990s, reaching minimum values that were 37% less than in pre-ozone-hole years (1970-1982). The year-to-year changes in the average values reflect variations in the meteorological conditions, which affect the extent of low polar temperatures and the transport of air into and out of the Antarctic winter stratosphere (see Figure Q11-box). However, essentially all of the ozone depletion in the Antarctic in most years is attributable to chemical loss from reactive halogen gases.

Restoring ozone in spring. The depletion of Antarctic ozone occurs primarily in the late winter/early spring season. In spring, temperatures in the lower polar stratosphere eventually warm, thereby ending PSC formation as well as the most effective chemical cycles that destroy ozone (see Q10). The transport of air between the polar stratosphere and lower latitudes also increases during this time, ending winter isolation. This allows ozone-rich air to be transported to polar regions, displacing air in which ozone has been severely depleted. This displaced air is mixed at lower latitudes with more abundant ozone-rich air. As a result, the ozone hole disappears by December and Antarctic ozone amounts remain near normal until the next winter season.

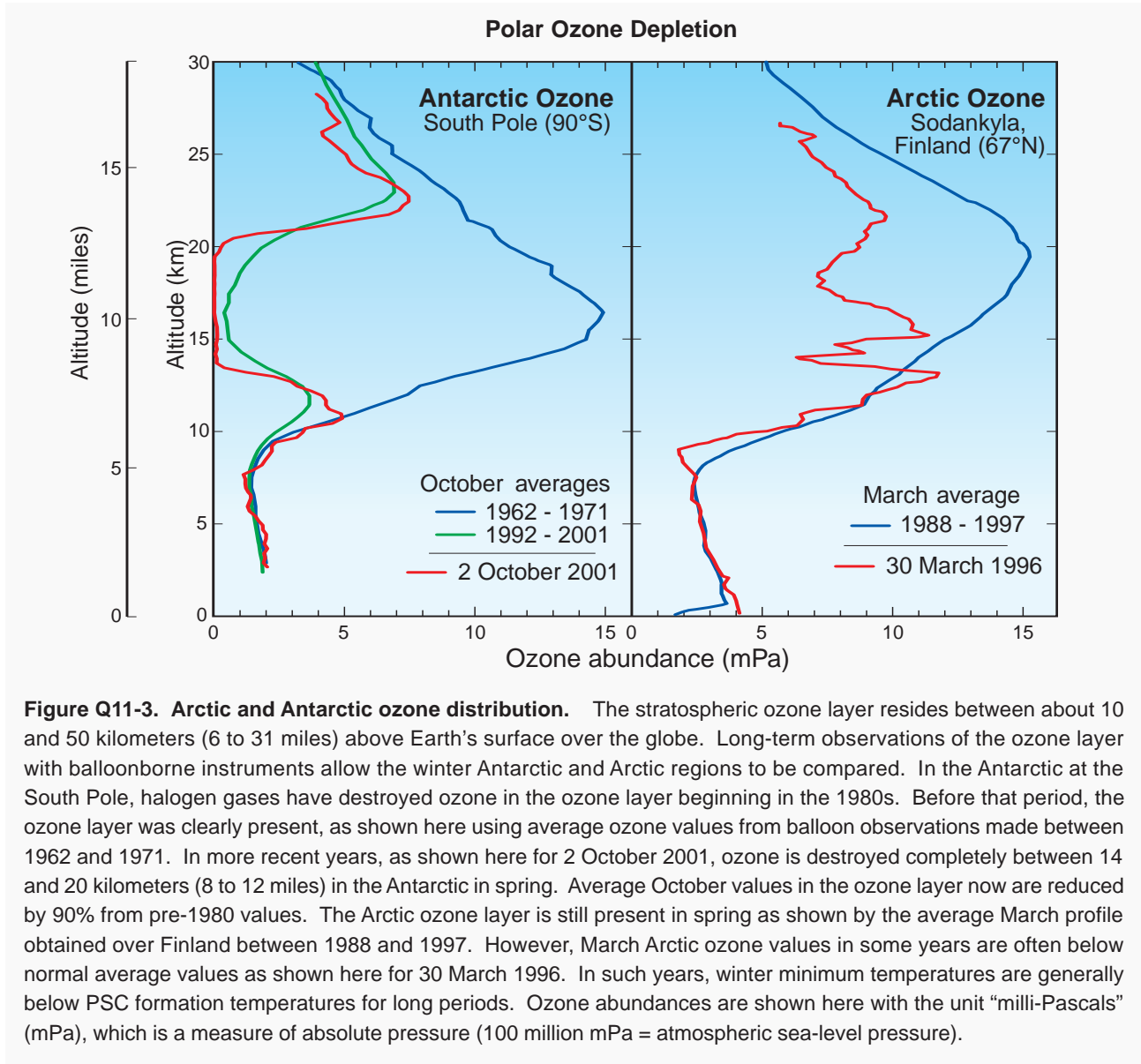


Figure Q11-3. Arctic and Antarctic ozone distribution. The stratospheric ozone layer resides between about 10 and 50 kilometers (6 to 31 miles) above Earth’s surface over the globe. Long-term observations of the ozone layer with balloonborne instruments allow the winter Antarctic and Arctic regions to be compared. In the Antarctic at the South Pole, halogen gases have destroyed ozone in the ozone layer beginning in the 1980s. Before that period, the ozone layer was clearly present, as shown here using average ozone values from balloon observations made between 1962 and 1971. In more recent years, as shown here for 2 October 2001, ozone is destroyed completely between 14 and 20 kilometers (8 to 12 miles) in the Antarctic in spring. Average October values in the ozone layer now are reduced by 90% from pre-1980 values. The Arctic ozone layer is still present in spring as shown by the average March profile obtained over Finland between 1988 and 1997. However, March Arctic ozone values in some years are often below normal average values as shown here for 30 March 1996. In such years, winter minimum temperatures are generally below PSC formation temperatures for long periods. Ozone abundances are shown here with the unit “milli-Pascals” (mPa), which is a measure of absolute pressure (100 million mPa = atmospheric sea-level pressure).

The Anomalous 2002 Antarctic Ozone Hole

The 2002 Antarctic ozone hole showed features that surprised scientists. They considered it anomalous at the time because the hole had much less area as viewed from space and much less ozone depletion as measured by minimum column ozone amounts when compared with values in several preceding years (see Figure Q11-box). The 2002 ozone hole area and minimum ozone values stand out clearly in displays of the year-to-year changes in these quantities (see Figure Q11-2). The smaller area was unexpected because the conditions required to deplete ozone, namely low temperatures and available reactive halogen gases, are not expected to have large year-to-year variations. Ozone was being depleted in August and early September 2002, but the hole *broke apart* into two separate depleted regions during the last week of September. The depletion in these two regions was significantly less than was observed inside either the 2001 or 2003 ozone holes, but still substantially greater than was observed in the early 1980s.

The anomalous behavior in 2002 occurred because of specific atmospheric air motions that sometimes occur in polar regions, not large decreases in reactive chlorine and bromine amounts in the Antarctic stratosphere. The Antarctic stratosphere was warmed by very strong, large-scale weather systems in 2002 that originated in the lower atmosphere (troposphere) at midlatitudes in late September. In late September, Antarctic temperatures are generally very low (see Q10) and ozone destruction rates are near their peak values. These tropospheric systems traveled poleward and upward into the stratosphere, upsetting the circumpolar wind flow and warming the lower stratosphere where ozone depletion was ongoing. The higher-than-normal impact of these weather disturbances during the critical time period for ozone loss reduced the total loss of ozone in 2002.

The warming in 2002 was unprecedented in Antarctic meteorological observations. Warming events are difficult to predict because of their complex formation conditions.

Large Antarctic ozone depletion returned in 2003 through 2005, in a manner similar to that observed from the mid-1990s to 2001 (see Figures Q11-box and Q11-2). The high ozone depletion found since the mid-1990s, with the exception of 2002, is expected to be typical of coming years. A significant, sustained reduction of Antarctic ozone depletion, defined as ozone recovery, requires the removal of halogen source gases from the stratosphere (see Q19 and Q20).

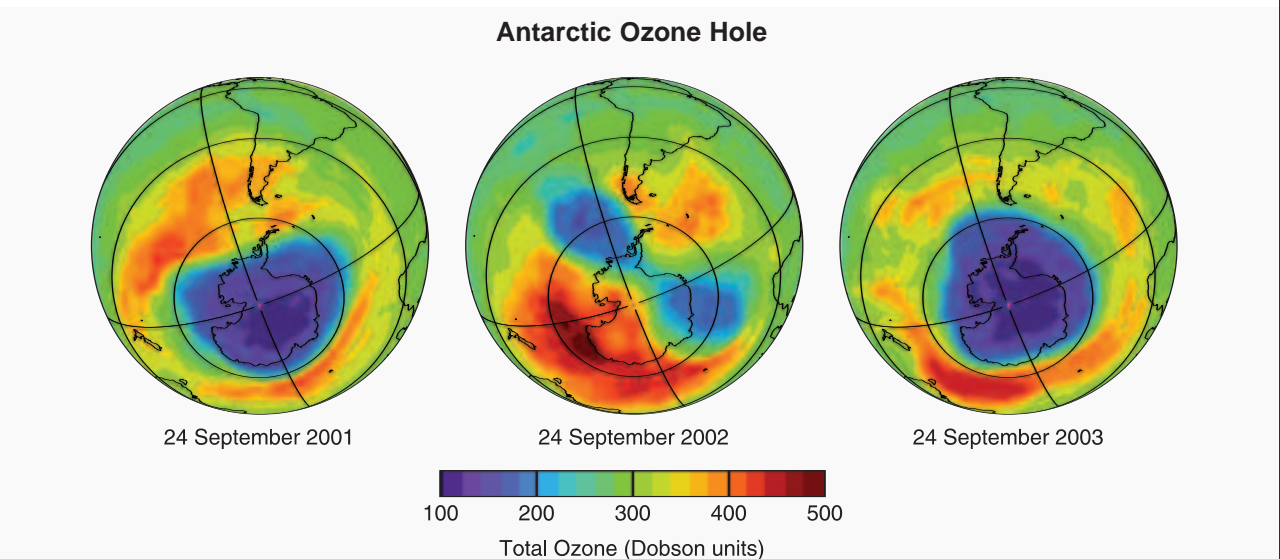


Figure Q11-Box. Anomalous 2002 ozone hole. Views from space of the Antarctic ozone hole as observed on 24 September in each of three consecutive years. The hole split and elongated in 2002, reducing the total depletion of ozone observed that year in comparison with 2001 and 2003. The anomalous depletion in 2002 is attributable to an early warming of the polar stratosphere caused by air disturbances originating in midlatitudes, rather than to large changes in the amounts of reactive chlorine and bromine in the Antarctic stratosphere.

Q12: Is there depletion of the Arctic ozone layer?

Yes, significant depletion of the Arctic ozone layer now occurs in some years in the late winter/early spring period (January-April). However, the maximum depletion is less severe than that observed in the Antarctic and is more variable from year to year. A large and recurrent “ozone hole,” as found in the Antarctic stratosphere, does not occur in the Arctic.

Significant ozone depletion in the Arctic stratosphere occurs in cold winters because of reactive halogen gases. The depletion, however, is much less than the depletion that now occurs in every Antarctic winter and spring. Although Arctic depletion does not generally create persistent “ozone hole”-like features in Arctic total ozone maps, depletion is observed in altitude profiles of ozone and in long-term average values of polar ozone.

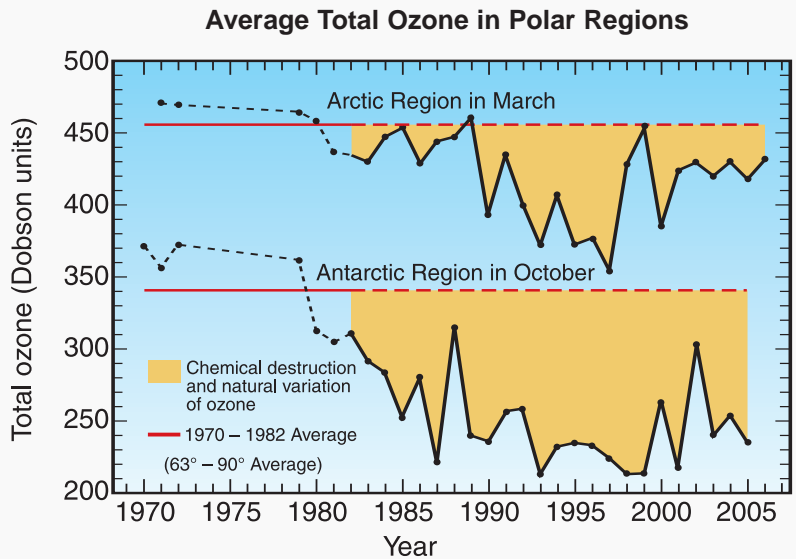
Altitude profiles of Arctic ozone. Arctic ozone is measured using a variety of instruments (see Q5), as for the Antarctic (see Q11). These measurements show changes within the ozone layer, the vertical region that contains the highest ozone abundances in the stratosphere. Figure Q11-2 shows an example of balloonborne measurements of a depleted ozone profile in the Arctic region on 30 March 1996, and contrasts the depletion with that found in the Antarctic. The 30 March spring profile shows much less depletion than the 2 October spring profile in the Antarctic. In general, some reduction in the Arctic ozone layer occurs each late

winter/early spring season. However, complete depletion each year over a broad vertical layer, as is now common in the Antarctic stratosphere, is not found in the Arctic.

Long-term total ozone changes. Satellite and ground-based observations can be used to examine the average total ozone abundances in the Arctic region for the last three decades and to contrast them with Antarctic abundances (see Figure Q12-1). Decreases from the pre-ozone-hole average values (1970-1982) were observed in the Arctic beginning in the 1980s, when similar changes were occurring in the Antarctic. The decreases have reached a maximum of about 30% but have remained smaller than those found in the Antarctic since the mid-1980s. The year-to-year changes in the Arctic and Antarctic average ozone values reflect annual variations in meteorological conditions that affect the extent of low polar temperatures and the transport of air into and out of the polar stratosphere. The effect of these variations is generally greater for the Arctic than the Antarctic.

Figure Q12-1. Average polar ozone.

Total ozone in polar regions is measured by well-calibrated satellite instruments. Shown here is a comparison of average springtime total ozone values found between 1970 and 1982 (solid and dashed red lines) with those in later years. Each point represents a monthly average in October in the Antarctic or in March in the Arctic. After 1982, significant ozone depletion is found in most years in the Arctic and all years in the Antarctic. The largest average depletions have occurred in the Antarctic since 1990. The ozone changes are the combination of chemical destruction and natural variations. Variations in meteorological conditions influence the year-to-year changes in depletion, particularly in the Arctic. Essentially all of the decrease in the Antarctic and usually most of the decrease in the Arctic each year are attributable to chemical destruction by reactive halogen gases. Average total ozone values over the Arctic are naturally larger at the beginning of each winter season because more ozone is transported poleward each season in the Northern Hemisphere than in the Southern Hemisphere.



Arctic vs. Antarctic. The Arctic winter stratosphere is generally warmer than its Antarctic counterpart (see Figure Q10-1). Higher temperatures reduce polar stratospheric cloud (PSC) formation, which slows the conversion of reactive chlorine gases to form ClO and, as a consequence, reduces the amount of ozone depletion (see Q10). Furthermore, the temperature and wind conditions are much more variable in the Arctic from winter to winter and within a winter season than in the Antarctic. Large year-to-year differences occur in Arctic minimum temperatures and the duration of PSC-forming temperatures into early spring. In a few Arctic winters, minimum temperatures are not low enough for PSCs to form. These factors combine to cause ozone depletion to be variable in the Arctic from year to year, with some years having little to no ozone depletion.

As in the Antarctic, depletion of ozone in the Arctic

is confined to the late winter/early spring season. In spring, temperatures in the lower stratosphere eventually warm, thereby ending PSC formation as well as the most effective chemical cycles that destroy ozone. The subsequent transport of ozone-rich air into the Arctic stratosphere displaces ozone-depleted air. As a result, ozone layer abundances are restored to near-normal values until the following winter.

High Arctic total ozone. A significant difference exists between the Northern and Southern Hemispheres in how ozone-rich stratospheric air is transported into the polar regions from lower latitudes during fall and winter. In the northern stratosphere, the poleward and downward transport of ozone-rich air is stronger. As a result, total ozone values in the Arctic are considerably higher than in the Antarctic at the beginning of each winter season (see Figure Q12-1).

Q13: How large is the depletion of the global ozone layer?

The ozone layer has been depleted gradually since 1980 and now is about an average of 4% lower over the globe. The average depletion exceeds the natural variability of the ozone layer. The ozone loss is very small near the equator and increases with latitude toward the poles. The larger polar depletion is primarily a result of the late winter/early spring ozone destruction that occurs there each year.

Stratospheric ozone has decreased over the globe since the 1980s. The depletion, which in the period 1997-2005 averaged about 4% (see Figure Q13-1), is larger than natural variations in ozone. The observations shown in Figure Q13-1 have been smoothed to remove regular ozone changes that are due to seasonal and solar effects (see Q14). The increase in reactive halogen gases in the stratosphere is considered to be the primary cause of the average depletion. The lowest ozone values in recent years occurred following the 1991 eruption of Mt. Pinatubo, which increased the number of sulfur-containing particles in the stratosphere. The particles remain in the stratosphere for several years, increasing the effectiveness of reactive halogen gases in destroying ozone (see Q14).

Observed ozone depletion varies significantly with latitude on the globe (see Figure Q13-1). The largest losses occur at the highest southern latitudes as a result of the severe ozone loss over Antarctica each late winter/early spring period. The next largest losses are observed in the Northern Hemisphere, caused in part by late winter/early spring losses over the Arctic. Ozone-depleted air over both polar regions is dispersed away from the poles during and after each winter/spring period. Ozone depletion also occurs directly at latitudes between the equator and polar regions but is smaller because of the presence of lower amounts of reactive halogen gases (see Q8).

Tropical regions. There has been little or no depletion of total ozone in the tropics (between about 20° latitude north and south of the equator in Figure Q13-1). In

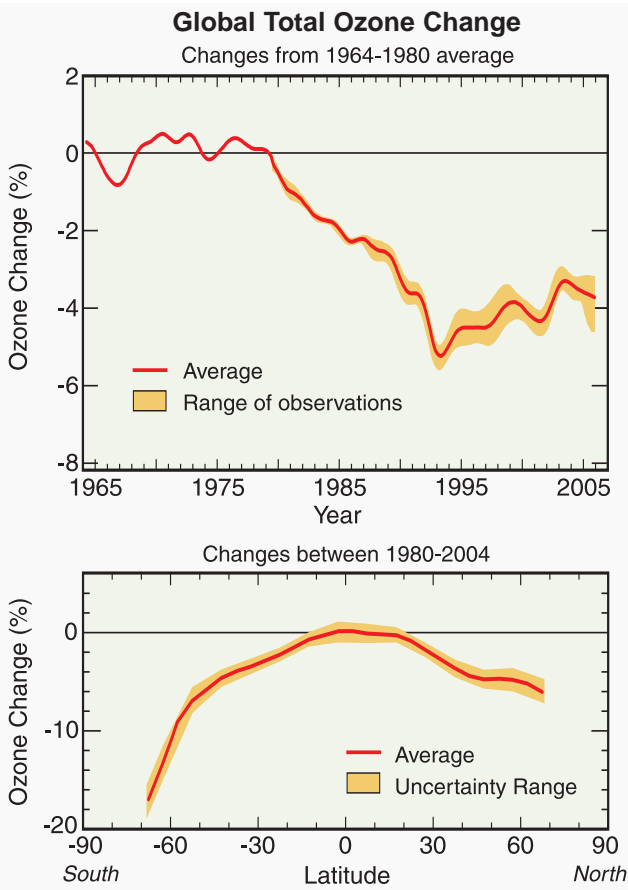


Figure Q13-1. Global total ozone changes. Satellite observations show a decrease in global total ozone values over more than two decades. The top panel compares global ozone values (annual averages) with the average from the period 1964 to 1980. Seasonal and solar effects have been removed from the data. On average, global ozone decreased each year between 1980 and the early 1990s. The decrease worsened during the few years when volcanic aerosol from the Mt. Pinatubo eruption in 1991 remained in the stratosphere. Now global ozone is about 4% below the 1964-to-1980 average. The bottom panel compares ozone changes between 1980 and 2004 for different latitudes. The largest decreases have occurred at the highest latitudes in both hemispheres because of the large winter/spring depletion in polar regions. The losses in the Southern Hemisphere are greater than those in the Northern Hemisphere because of the Antarctic ozone hole. Long-term changes in the tropics are much smaller because reactive halogen gases are less abundant in the tropical lower stratosphere.

this region of the lower stratosphere, air has only recently (less than 18 months) been transported from the lower atmosphere. As a result, the conversion of halogen source gases to reactive halogen gases is very small. Because of the low abundance of reactive gases, total ozone depletion in this region is very small. In contrast, stratospheric air in polar regions has been in the stratosphere for an average of 4 to 7 years; therefore, the abundance of reactive halogen gases is much larger.

Seasonal changes. The magnitude of global ozone

depletion also depends on the season of the year. In comparison with the 1964-1980 averages, total ozone averaged for 2002-2005 is about 3% lower in northern middle latitudes (35°N-60°N) and about 6% lower at southern middle latitudes (35°S-60°S). The seasonality of these changes is also somewhat different in the two hemispheres. In the summer/autumn periods, the decline in total ozone is about 2% in the Northern Hemisphere and 5% in the Southern Hemisphere. In winter/spring, the decline is about 5-6% in both hemispheres.

Q14: Do changes in the Sun and volcanic eruptions affect the ozone layer?

Yes, factors such as changes in solar radiation, as well as the formation of stratospheric particles after volcanic eruptions, do influence the ozone layer. However, neither factor can explain the average decreases observed in global total ozone over the last two decades. If large volcanic eruptions occur in the coming decades, ozone depletion will increase for several years after the eruption.

Changes in solar radiation and increases in stratospheric particles from volcanic eruptions both affect the abundance of stratospheric ozone, but they have not caused the long-term decreases observed in total ozone.

Solar changes. The formation of stratospheric ozone is initiated by ultraviolet (UV) radiation coming from the Sun (see Figure Q2-1). As a result, an increase in the Sun's radiation output increases the amount of ozone in Earth's atmosphere. The Sun's radiation output and sunspot number vary over the well-known 11-year solar cycle.

Observations over several solar cycles (since the 1960s) show that global total ozone levels vary by 1 to 2% between the maximum and minimum of a typical cycle. Changes in solar output at a wavelength of 10.7 cm, although much larger than changes in total solar output, are often used to show when periods of maximum and minimum total output occur (see Figure Q14-1). The Sun's output has gone through maximum values around 1969, 1980, 1991, and 2002. In 2006, the solar output was decreasing towards a minimum.

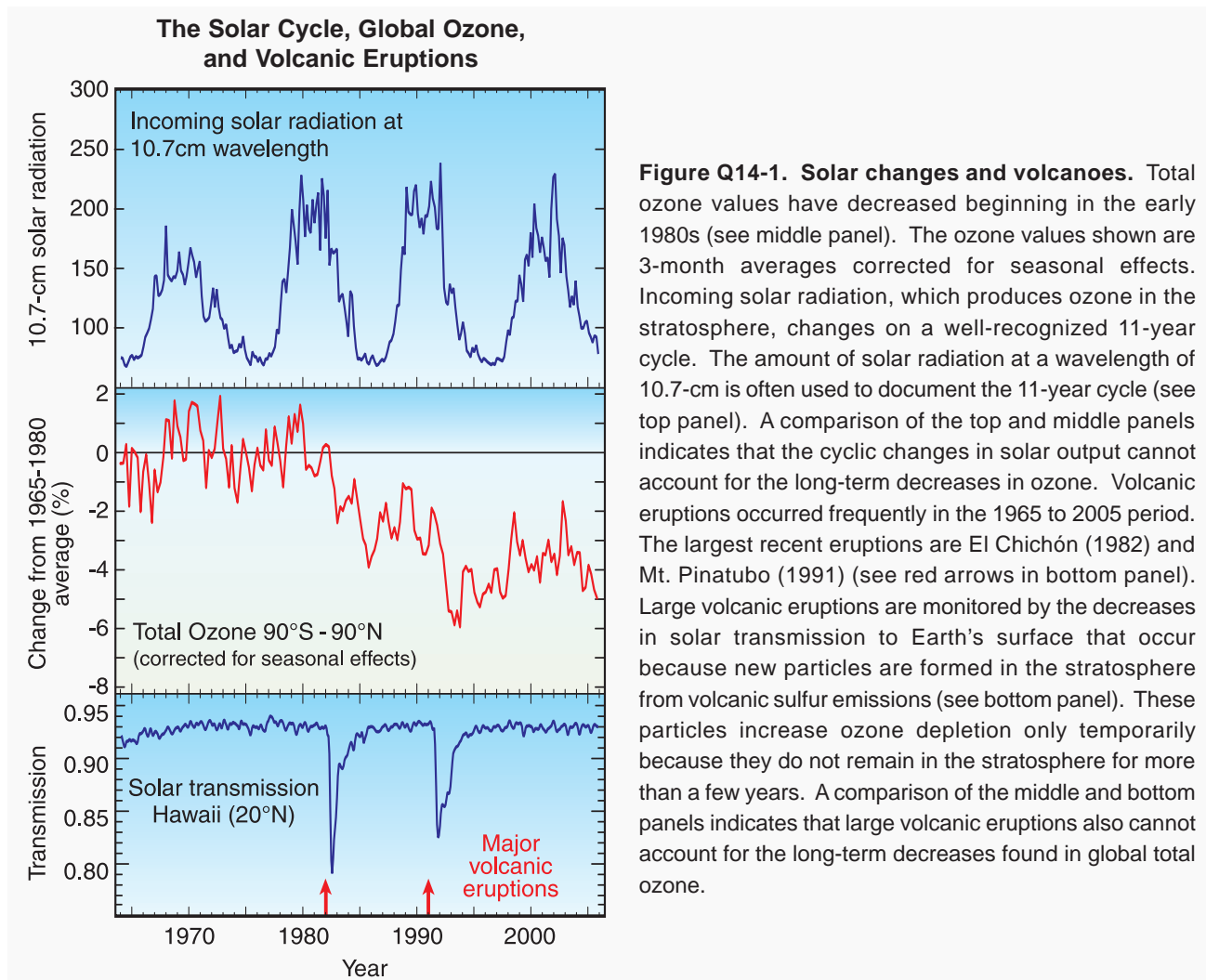


Figure Q14-1. Solar changes and volcanoes. Total ozone values have decreased beginning in the early 1980s (see middle panel). The ozone values shown are 3-month averages corrected for seasonal effects. Incoming solar radiation, which produces ozone in the stratosphere, changes on a well-recognized 11-year cycle. The amount of solar radiation at a wavelength of 10.7-cm is often used to document the 11-year cycle (see top panel). A comparison of the top and middle panels indicates that the cyclic changes in solar output cannot account for the long-term decreases in ozone. Volcanic eruptions occurred frequently in the 1965 to 2005 period. The largest recent eruptions are El Chichón (1982) and Mt. Pinatubo (1991) (see red arrows in bottom panel). Large volcanic eruptions are monitored by the decreases in solar transmission to Earth's surface that occur because new particles are formed in the stratosphere from volcanic sulfur emissions (see bottom panel). These particles increase ozone depletion only temporarily because they do not remain in the stratosphere for more than a few years. A comparison of the middle and bottom panels indicates that large volcanic eruptions also cannot account for the long-term decreases found in global total ozone.

Over the last two decades, average total ozone has decreased over the globe. Average values in recent years show about 4% depletion from pre-1980 values (see Figure Q14-1). The ozone values shown are 3-month averages corrected for seasonal effects but not for solar effects. Over the same period, changes in solar output show the expected 11-year cycle but do not show a decrease with time. For this reason, the long-term decreases in global ozone cannot result from changes in solar output alone. Most examinations of long-term ozone changes presented in this and previous international scientific assessments quantitatively account for the influence of the 11-year solar cycle.

Past volcanoes. Large volcanic eruptions inject sulfur gases directly into the stratosphere, causing new sulfate particles to be formed. The particles initially form in the stratosphere above and downwind of the volcano location and then often spread throughout the hemisphere or globally as air is transported by stratospheric winds. The presence of volcanic particles in the stratosphere is shown in observations of solar transmission through the atmosphere. When large amounts of particles are present in the stratosphere, transmission of solar radiation is significantly reduced. The large eruptions of El Chichón (1982) and Mt. Pinatubo (1991) are recent examples of events that temporarily reduced solar transmission (see Figure Q14-1).

Laboratory measurements and stratospheric observations have shown that chemical reactions on the surface of volcanically produced particles increase ozone destruction by increasing the amounts of the highly reactive chlorine gas, chlorine monoxide (ClO). The amount of ClO produced is proportional to the total abundance

of reactive chlorine in the stratosphere (see Figure Q16-1). Ozone depletion increases as a consequence of increased ClO. The most recent large eruption was that of Mt. Pinatubo, which resulted in up to a 10-fold increase in the number of particles available for surface reactions. Both El Chichón and Mt. Pinatubo increased global ozone depletion for a few years (see Figure Q14-1). After a few years, however, the effect of volcanic particles on ozone is diminished by their gradual removal from the stratosphere by natural air circulation. Because of particle removal, the two large volcanic eruptions of the last two decades cannot account for the long-term decreases observed in ozone over the same period.

Future volcanoes. Observations and atmospheric models indicate that the record-low ozone levels observed in 1992-1993 resulted from the large number of particles produced by the Mt. Pinatubo eruption, combined with the relatively large amounts of reactive halogen gases present in the stratosphere in the 1990s. If the Mt. Pinatubo eruption had occurred before 1980, changes to global ozone would have been much smaller than observed in 1992-1993 because the abundances of reactive halogen gases in the stratosphere were smaller. In the early decades of the 21st century, the abundance of halogen source gases will still be substantial in the global atmosphere (see Figure Q16-1). If large volcanic eruptions occur in these early decades, ozone depletion will increase for several years. If an eruption larger than Mt. Pinatubo occurs, ozone losses could be larger than previously observed and persist longer. Only later in the 21st century when halogen gas abundances have declined close to pre-1980 values will the effect of volcanic eruptions on ozone be lessened.

IV. CONTROLLING OZONE-DEPLETING GASES

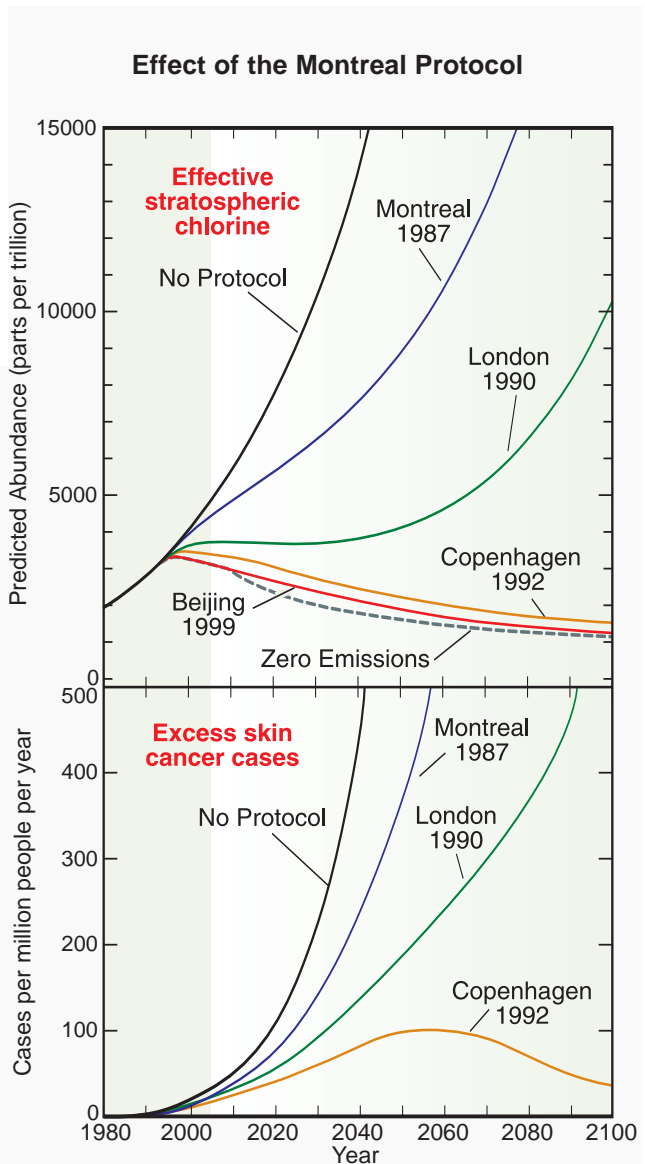
Q15: Are there regulations on the production of ozone-depleting gases?

Yes, the production of ozone-depleting gases is regulated under a 1987 international agreement known as the “Montreal Protocol on Substances that Deplete the Ozone Layer” and its subsequent Amendments and Adjustments. The Protocol, now ratified by over 190 nations, establishes legally binding controls on the national production and consumption of ozone-depleting gases. Production and consumption of all principal halogen-containing gases by developed and developing nations will be significantly phased out before the middle of the 21st century.

Montreal Protocol. In 1985, a treaty called the *Vienna Convention for the Protection of the Ozone Layer* was signed by 20 nations in Vienna. The signing nations agreed to take appropriate measures to protect the ozone layer from human activities. The Vienna Convention supported research, exchange of information, and future protocols. In response to growing concern, the *Montreal Protocol on Substances that Deplete the Ozone Layer* was signed in 1987 and, following country ratification, entered into force in 1989. The Protocol established legally binding controls for developed and developing nations on the production and consumption of halogen source gases known to cause ozone depletion. National consumption of a halogen gas is defined as the amount that production and imports of a gas exceed its export to other nations.

Amendments and Adjustments. As the scientific basis of ozone depletion became more certain after 1987 and substitutes and alternatives became available to replace the principal halogen source gases, the Montreal

Figure Q15-1. Effect of the Montreal Protocol. The purpose of the Montreal Protocol is to achieve reductions in stratospheric abundances of chlorine and bromine. The reductions follow from restrictions on the production and consumption of manufactured halogen source gases. Projections of the future abundance of *effective stratospheric chlorine* (see Q16) are shown in the top panel assuming (1) no Protocol regulations, (2) only the regulations in the original 1987 Montreal Protocol, and (3) additional regulations from the subsequent Amendments and Adjustments. The city names and years indicate where and when changes to the original 1987 Protocol provisions were agreed upon. Effective stratospheric chlorine as used here accounts for the combined effect of chlorine and bromine gases. Without the Protocol, stratospheric halogen gases are projected to increase significantly in the 21st century. The “zero emissions” line shows a hypothetical case of stratospheric abundances if all emissions were reduced to zero beginning in 2007. The lower panel shows how excess skin cancer cases (see Q17) might increase with no regulation and how they might be reduced under the Protocol provisions. (The unit “parts per trillion” is defined in the caption of Figure Q7-1.)



Protocol was strengthened with Amendments and Adjustments. These revisions put additional substances under regulation, accelerated existing control measures, and prescribed phaseout dates for the production and consumption of certain gases. The initial Protocol called for only a slowing of chlorofluorocarbon (CFC) and halon production. The 1990 London Amendments to the Protocol called for a phaseout of the production and consumption of the most damaging ozone-depleting substances in developed nations by 2000 and in developing nations by 2010. The 1992 Copenhagen Amendments accelerated the date of the phaseout to 1996 in developed nations. Further controls on ozone-depleting substances were agreed upon in later meetings in Vienna (1995), Montreal (1997), and Beijing (1999).

Montreal Protocol projections. Future stratospheric abundances of effective stratospheric chlorine (see Q16) can be calculated based on the provisions of the Montreal Protocol. The concept of *effective stratospheric chlorine* accounts for the combined effect on ozone of chlorine- and bromine-containing gases. The results are shown in Figure Q15-1 for the following cases:

- No Protocol and continued production increases of 3% per year (business-as-usual scenario).
- Continued production and consumption as allowed by the Protocol's original provisions agreed upon in Montreal in 1987.
- Restricted production and consumption as outlined in the subsequent Amendments and Adjustments as decided in London in 1990, Copenhagen in 1992, and Beijing in 1999.
- Zero emissions of ozone-depleting gases starting in 2007.

In each case, production of a gas is assumed to result in its eventual emission to the atmosphere. Without the Montreal Protocol and with continued production and use of CFCs and other ozone-depleting gases, effective stratospheric chlorine is projected to have increased tenfold by the mid-2050s compared with the 1980 value. Such high values likely would have increased global ozone depletion far beyond that currently observed. As a result, harmful UV-B radiation would have also increased substantially at Earth's surface, causing a rise in excess skin cancer cases (see Q17 and lower panel of Figure Q15-1).

The 1987 provisions of the Montreal Protocol alone would have only slowed the approach to high effective chlorine values by one or more decades in the 21st century. Not until the 1992 Copenhagen Amendments and Adjustments did the Protocol projections show a *decrease* in future effective stratospheric chlorine values. Now, with full compliance to the Montreal Protocol and its Amendments and Adjustments, use of the major human-

produced ozone-depleting gases will ultimately be phased out and effective stratospheric chlorine will slowly decay, reaching pre-1980 values in the mid-21st century (see Q16).

Zero emissions. Effective chlorine values in the coming decades will be influenced by emissions of halogen source gases produced in those decades, as well as the emission of currently existing gases that are now being used or stored in various ways. Examples of long-term storage are CFCs in refrigeration equipment and foams, and halons in fire-fighting equipment. Some continued production and consumption of ozone-depleting gases is allowed, particularly in developing nations, under the agreements. As a measure of the contribution of these continued emissions to the effective chlorine value, the "zero emissions" case is included in Figure Q15-1. In this hypothetical case, all emissions of ozone-depleting gases are set to zero beginning in 2007. The reductions in effective stratospheric chlorine below the values expected with the 1999 Beijing agreement would be relatively small.

HCFC substitute gases. The Montreal Protocol provides for the transitional use of hydrochlorofluorocarbons (HCFCs) as substitute compounds for principal halogen source gases such as CFC-12. HCFCs differ chemically from most other halogen source gases in that they contain hydrogen (H) atoms in addition to chlorine and fluorine atoms. HCFCs are used for refrigeration, for blowing foams, and as solvents, which were primary uses of CFCs. HCFCs are 88 to 98% less effective than CFC-12 in depleting stratospheric ozone because they are chemically removed primarily in the troposphere (see Q18). This removal partially protects stratospheric ozone from the halogens contained in HCFCs. In contrast, CFCs and many other halogen source gases are chemically inert in the troposphere and, hence, reach the stratosphere without being significantly removed. Because HCFCs still contribute to the chlorine abundance in the stratosphere, the Montreal Protocol requires a gradual phaseout of HCFC consumption in developed and developing nations that will be complete in 2040.

HFC substitute gases. Hydrofluorocarbons (HFCs) are also used as substitute compounds for CFCs and other halogen source gases. HFCs contain only hydrogen, fluorine, and carbon atoms. Because HFCs contain no chlorine or bromine, they do not contribute to ozone depletion (see Q18). As a consequence, the Montreal Protocol does not regulate the HFCs. However, HFCs (as well as all halogen source gases) are radiatively active gases that contribute to human-induced climate change as they accumulate in the atmosphere (see Q18). HFCs are included in the group of gases listed in the Kyoto Protocol of the United Nations Framework Convention on Climate Change (UNFCCC).

Q16: Has the Montreal Protocol been successful in reducing ozone-depleting gases in the atmosphere?

Yes, as a result of the Montreal Protocol, the total abundance of ozone-depleting gases in the atmosphere has begun to decrease in recent years. If the nations of the world continue to follow the provisions of the Montreal Protocol, the decrease will continue throughout the 21st century. Some individual gases, such as halons and hydrochlorofluorocarbons (HCFCs), are still increasing in the atmosphere but will begin to decrease in the next decades if compliance with the Protocol continues. Around midcentury, the effective abundance of ozone-depleting gases should fall to values that were present before the Antarctic “ozone hole” began to form in the early 1980s.

Effective stratospheric chlorine. The Montreal Protocol has been successful in slowing and reversing the increase of ozone-depleting gases (halogen source gases) in the atmosphere. An important measure of its success is the change in the value of *effective stratospheric chlorine*. Effective stratospheric chlorine values are a measure of the potential for ozone depletion in the stratosphere, obtained by summing over adjusted amounts of all chlorine and bromine gases. The adjustments account for the different rates of decomposition of the gases and the greater per-atom effectiveness of bromine in depleting ozone (see Q7). Although chlorine is much more abundant in the stratosphere than bromine (160 times) (see Figure Q7-1), bromine atoms are about 60 times more effective than chlorine atoms in chemically destroying ozone molecules. Increases in effective stratospheric chlorine in the past decades have caused ozone depletion. Accordingly, ozone is expected to recover in the future as effective stratospheric chlorine values decrease.

Effective stratospheric chlorine changes. In the latter half of the 20th century up until the 1990s, effective stratospheric chlorine values steadily increased (see Figure Q16-1). Values are derived from individual halogen source gas abundances obtained from measurements, historical estimates of abundance, and projections of future abundance. As a result of the Montreal Protocol regulations, the long-term increase in effective stratospheric chlorine slowed, reached a peak, and began to decrease in the 1990s. This initial decrease means that the potential for stratospheric ozone depletion has begun to lessen as a result of the Montreal Protocol. The decrease in effective chlorine is projected to continue throughout the 21st century if all nations continue to comply with the provisions of the Protocol. The decrease will continue because, as emissions become small, natural destruction processes gradually remove halogen-containing gases from the global atmosphere. Reduction of effective stratospheric chlorine amounts to 1980 values or lower will require many decades because the lifetimes of halogen

source gas molecules in the atmosphere range up to 100 years (see Figure Q16-1 and Table Q7-1).

Individual halogen source gas reductions. The reduction in the atmospheric abundance of a gas in response to regulation depends on a number of factors that include (1) how rapidly gas reserves are used and released to the atmosphere, (2) the lifetime for the removal of the gas from the atmosphere, and (3) the total amount of the gas that has already accumulated in the atmosphere.

The regulation of human-produced halogen source gases under the Montreal Protocol is considered separately for each class of one or more gases and is based on several factors. The factors include (1) the effectiveness of each class in depleting ozone in comparison with other halogen source gases, (2) the availability of suitable substitute gases for domestic and industrial use, and (3) the impact of regulation on developing nations.

Methyl chloroform and CFCs. The largest reduction in the abundance of a halogen source gas has occurred for methyl chloroform (CH_3CCl_3) (see Figure Q16-1). The implementation of the Montreal Protocol caused global production of methyl chloroform to be reduced to near zero. Atmospheric abundances subsequently dropped rapidly because methyl chloroform has a short atmospheric lifetime (about 5 years). Methyl chloroform is used mainly as a solvent and has no significant long-term storage following production. The reduction in effective chlorine in the 1990s came primarily from the reduction in methyl chloroform abundance in the atmosphere. Significant emissions reductions have also occurred for the chlorofluorocarbons CFC-11, CFC-12, and CFC-113 starting in the 1990s. As a result, the atmospheric amounts of these gases have all peaked, and CFC-11 and CFC-113 abundances have decreased slightly (see Figure Q16-1). As emissions of CFCs are reduced, their atmospheric abundances will decrease more slowly than methyl chloroform because of longer CFC atmospheric lifetimes (see Table Q7-1) and because CFCs escape very slowly to the atmosphere from their use in refrigeration

Past and Expected Future Abundances of Atmospheric Halogen Source Gases

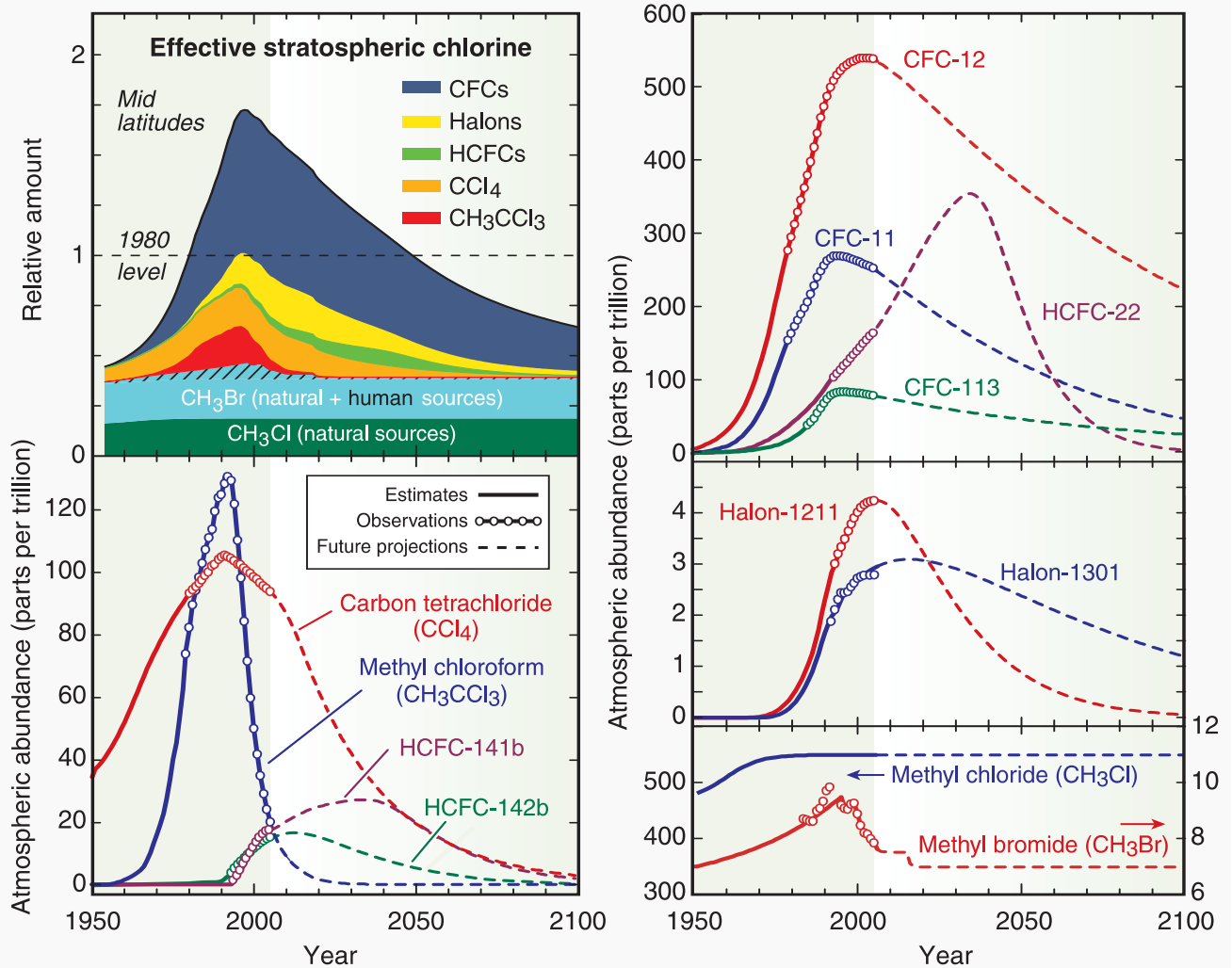


Figure Q16-1. Halogen source gas changes. The rise in effective stratospheric chlorine values in the 20th century has slowed and reversed in the last decade (top left panel). Effective stratospheric chlorine values are a measure of the potential for ozone depletion in the stratosphere, obtained by summing over adjusted amounts of all chlorine and bromine gases. Effective stratospheric chlorine levels as shown here for midlatitudes will return to 1980 values around 2050. The return to 1980 values will occur around 2065 in polar regions. In 1980, ozone was not significantly depleted by the chlorine and bromine then present in the stratosphere. A decrease in effective stratospheric chlorine abundance follows reductions in emissions of individual halogen source gases. Overall emissions and atmospheric concentrations have decreased and will continue to decrease given international compliance with the Montreal Protocol provisions (see Q15). The changes in the atmospheric abundance of individual gases at Earth’s surface shown in the panels were obtained using a combination of direct atmospheric measurements, estimates of historical abundance, and future projections of abundance. The past increases of CFCs, along with those of CCl₄ and CH₃CCl₃, have slowed significantly and most have reversed in the last decade. HCFCs, which are used as CFC substitutes, will continue to increase in the coming decades. Some halon abundances will also continue to grow in the future while current halon reserves are depleted. Smaller relative decreases are expected for CH₃Br in response to production and use restrictions because it has substantial natural sources. CH₃Cl has large natural sources and is not regulated under the Montreal Protocol. (See Figure Q7-1 for chemical names and formulas. The unit “parts per trillion” is defined in the caption of Figure Q7-1.)

TWENTY QUESTIONS: 2006 UPDATE

and foam products.

HCFC substitute gases. The Montreal Protocol allows for the use of hydrochlorofluorocarbons (HCFCs) as short-term substitutes for CFCs. As a result, the abundances of HCFC-22, HCFC-141b, and HCFC-142b continue to grow in the atmosphere (see Figure Q16-1). HCFCs pose a lesser threat to the ozone layer than CFCs because they are partially destroyed in the troposphere by chemical processes, thus reducing the overall effectiveness of their emissions in destroying stratospheric ozone. Under the Montreal Protocol, HCFC consumption will reach zero in developed nations by 2030 and in developing nations by 2040 (see Q15). Thus, the future projections in Figure Q16-1 show HCFC abundances reaching a peak in the first decades of the 21st century and steadily decreasing thereafter.

Halons. The atmospheric abundances of halon-1211 and halon-1301 account for a significant fraction of bromine from all source gases (see Figure Q7-1) and continue to grow despite the elimination of production in developed nations in 1994 (see Figure Q16-1). The growth in abundance continues because substantial reserves are held in fire-extinguishing equipment and are gradually being released, and production and consumption are still allowed in developing nations. Atmospheric

halon abundances can be expected to remain high well into the 21st century because of their long lifetimes and continued release.

Methyl chloride and methyl bromide. Both methyl chloride (CH_3Cl) and methyl bromide (CH_3Br) are distinct among principal halogen source gases because a substantial fraction of their emissions is associated with natural processes (see Q7). The average atmospheric abundance of methyl chloride, which is not regulated under the Montreal Protocol, will remain fairly constant throughout this century if natural sources remain unchanged. At century's end, methyl chloride is expected to account for a large fraction of remaining effective stratospheric chlorine because the abundances of other gases, such as the CFCs, are expected to be greatly reduced (see Figure Q16-1). The abundance of methyl bromide, which is regulated under the Protocol, has already decreased in recent years and is projected to decrease further as a result of production phaseouts in developed and developing countries. For the later decades of the century, methyl bromide abundances are shown as nearly constant in Figure Q16-1. However, these abundances are uncertain because the amounts of exempted uses of methyl bromide under the Montreal Protocol are not known for future years.

V. IMPLICATIONS OF OZONE DEPLETION

Q17: Does depletion of the ozone layer increase ground-level ultraviolet radiation?

Yes, ultraviolet radiation at Earth’s surface increases as the amount of overhead total ozone decreases, because ozone absorbs ultraviolet radiation from the Sun. Measurements by ground-based instruments and estimates made using satellite data have confirmed that surface ultraviolet radiation has increased in regions where ozone depletion is observed.

The depletion of stratospheric ozone leads to an increase in surface ultraviolet radiation. The increase occurs primarily in the ultraviolet-B (UV-B) component of the Sun’s radiation. UV-B is defined as radiation in the wavelength range of 280 to 315 nanometers. Changes in UV-B at the surface have been observed directly and can be estimated from ozone changes.

Surface UV-B radiation. The amount of ultraviolet radiation reaching Earth’s surface depends in large part on the amount of ozone in the atmosphere. Ozone molecules in the stratosphere absorb UV-B radiation, thereby significantly reducing the amount of this radiation that reaches Earth’s surface (see Q3). If total ozone amounts are reduced in the stratosphere, then the amount of UV radiation reaching Earth’s surface generally increases. This relationship between total ozone and surface UV radiation has been studied at a variety of locations with direct measurements of both ozone and UV. The actual amount of UV reaching a location depends on a large number of additional factors, including the position of the Sun in the sky, cloudiness, and air pollution. In general, surface UV at a particular location on Earth changes throughout the day and with season as the Sun’s position in the sky changes.

Long-term surface UV changes. Satellite observations of long-term global ozone changes can be used to estimate changes in global surface UV that have occurred over the past two decades. These changes are of interest because UV radiation can cause harm to humans, other life forms, and materials (see Q3). The amount of UV that produces an “erythema” or sunburning response in humans is often separately evaluated. Long-term changes in sunburning UV at a particular location have been estimated from the changes in total ozone at that location. The results show that average erythema UV has increased due to ozone reduction by up to a few percent per decade between 1979 and 1998 over a wide range of latitudes (see Figure Q17-1). The largest increases are found at high polar latitudes in both hemispheres. As expected, the increases occur where decreases in total ozone are observed to be the largest

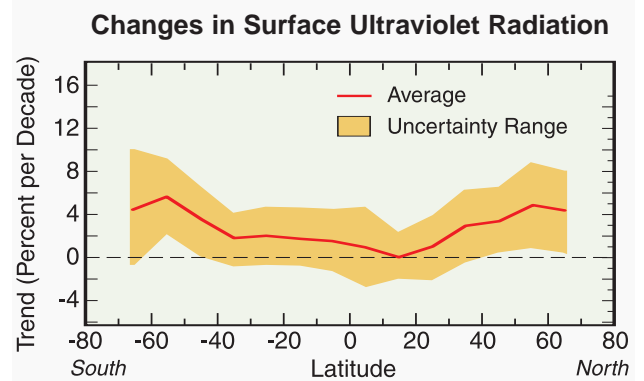


Figure Q17-1. Changes in surface UV radiation. Ultraviolet (UV) radiation at Earth’s surface has increased over much of the globe since 1979. Also known as “erythema radiation,” sunburning UV is harmful to humans and other life forms. The increases shown here for 1979-1998 are estimated from observed decreases in ozone and the relationship between ozone and surface UV established at some surface locations. The estimates are based on the assumption that all other factors that influence the amount of UV radiation reaching the Earth’s surface, such as aerosol abundances and cloudiness, are unchanged. The estimated changes in ultraviolet radiation in the tropics are the smallest because observed ozone changes are the smallest there.

(see Figure Q13-1). The smallest changes in erythema UV are in the tropics, where long-term total ozone changes are smallest.

UV Index changes. The “UV Index” is a measure of daily surface UV levels that is relevant to the effects of UV on human skin. The UV Index is used internationally to increase public awareness about the detrimental effects of UV on human health and to guide the need for protective measures. The UV Index is essentially the amount of erythema irradiance as measured on a horizontal surface. The daily maximum UV Index varies with location and season, as shown for three locations in

TWENTY QUESTIONS: 2006 UPDATE

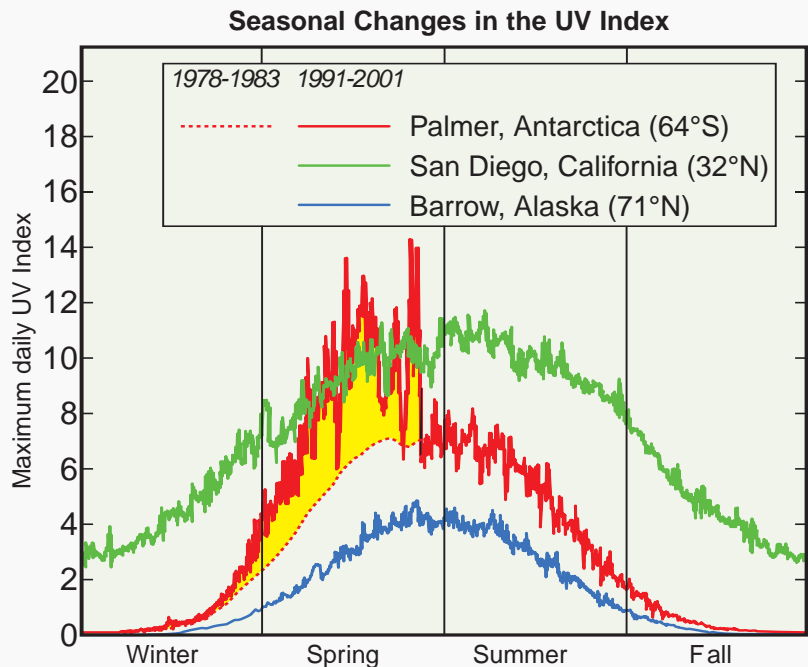
Figure Q17-2. The highest daily values generally occur at the lowest latitudes (tropics) and in summer when the midday Sun is closest to overhead. Values in San Diego, California, for example, normally are larger year round than those found in Barrow, Alaska, which is at higher latitude. At a given latitude, UV Index values increase in mountainous regions. The UV Index becomes zero in periods of continuous darkness found during winter at high-latitude locations.

An illustrative example of how polar ozone depletion increases the maximum daily UV Index is shown in Figure Q17-2. Normal UV Index values for Palmer, Antarctica, in spring were estimated from satellite measurements made during the period 1978-1983, before the appearance of the “ozone hole” over Antarctica (see red dotted line). In the last decade (1991-2001), severe and persistent ozone depletion in spring has increased the UV Index well above normal values for several months (see thick red line). Now, spring UV Index values in Palmer, Antarctica (64°S), sometimes equal or exceed even the peak summer values measured in San Diego, California (32°N).

Other causes of long-term UV changes. The surface UV values may also change as a result of other human activities or climate change. Long-term changes in cloudiness, aerosols, pollution, and snow or ice cover will cause long-term changes in surface UV. At some ground sites, measurements indicate that long-term changes in UV have resulted from changes in one or more of these factors. The impact of some of the changes can be complex. For example, an increase in cloud cover usually results in a reduction of UV radiation below the clouds, but can increase radiation above the clouds (in mountainous regions).

UV changes and skin cancer. Skin cancer cases in humans are expected to increase with the amount of UV reaching Earth’s surface. Atmospheric scientists working together with health professionals can estimate how skin cancer cases will change in the future. The estimates are based on knowing how UV increases as total ozone is depleted and how total ozone depletion changes with effective stratospheric chlorine (see Q16). Estimates of future excess skin cancer cases are shown in Figure Q15-1 using future estimates of effective stratospheric chlo-

Figure Q17-2. Changes in UV Index. The maximum daily UV Index is a measure of peak sunburning UV that occurs during the day at a particular location. UV-B, which is absorbed by ozone, is an important component of sunburning UV. The UV Index varies with latitude and season, and with the Sun’s elevation in the local sky. The highest values of the maximum daily UV Index occur in the tropics, where the midday Sun is highest throughout the year and where total ozone values are lowest. The lowest average UV Index values occur at high latitudes. As an example, the figure compares the seasonal UV Index at three locations. The UV Index is higher throughout the year in San Diego, a low-latitude location, than in Barrow, a high-latitude location. Index values are zero at high latitudes in winter when darkness is continuous. The effect of Antarctic ozone depletion is demonstrated by comparing the Palmer and San Diego data in the figure. Normal values estimated for Palmer are shown for the 1978-1983 period before the “ozone hole” occurred each season (see red dotted line). In the decade 1991-2001, Antarctic ozone depletion has increased the maximum UV Index value at Palmer throughout spring (see yellow shaded region). Values at Palmer now sometimes equal or exceed those measured in spring and even in the summer in San Diego, which is located at much lower latitude.



rine based on the 1992 and earlier Montreal Protocol provisions and assuming that other factors (besides ozone) affecting surface UV are unchanged in the future. The cases are those that would occur in a population with the UV sensitivity and age distribution such as that of the United States. The cases counted are those in *excess* of the number that occurred in 1980 before ozone depletion was observed (about 2000 per million population), with the assumption that the population's sun exposure remains unchanged. The case estimates include the fact

that skin cancer in humans occurs long after the exposure to sunburning UV. The results illustrate that, with current Protocol provisions, excess skin cancer cases are predicted to increase in the early to middle decades of the 21st century. By century's end, with the expected decreases in halogen source gas emissions, the number of excess cases is predicted to return close to 1980 values. Without the provisions of the Protocol, excess skin cancer cases would have been expected to increase substantially throughout the century.

Q18: Is depletion of the ozone layer the principal cause of climate change?

No, ozone depletion itself is not the principal cause of climate change. However, because ozone absorbs solar radiation and is a greenhouse gas, ozone changes and climate change are linked in important ways. Stratospheric ozone depletion and increases in global tropospheric ozone that have occurred in recent decades both contribute to climate change. These contributions to climate change are significant but small compared with the total contribution from all other greenhouse gases. Ozone and climate change are indirectly linked because both ozone-depleting gases and substitute gases contribute to climate change.

Radiative forcing of climate change. Human activities and natural processes have led to the accumulation in the atmosphere of several long-lived and radiatively active gases known as “greenhouse gases.” Ozone is a greenhouse gas, along with carbon dioxide (CO₂), methane (CH₄), nitrous oxide (N₂O), and halogen source gases. The accumulation of these gases in Earth’s atmosphere changes the balance between incoming solar radiation and outgoing infrared radiation. Greenhouse gases generally change the balance by absorbing outgoing radiation, leading to a warming at Earth’s surface. This change in Earth’s radiative balance is called a *radiative forcing of climate change*.

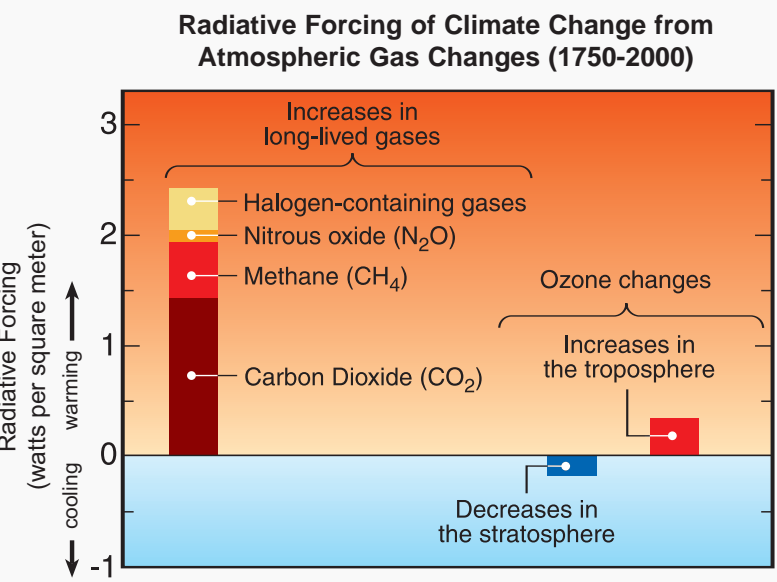
A summary of radiative forcings resulting from the increases in long-lived greenhouse gases in the industrial era is shown in Figure Q18-1. All forcings shown relate to human activities. Positive forcings generally lead to

warming and negative forcings lead to *cooling* of Earth’s surface. The accumulation of carbon dioxide represents the largest forcing term. Carbon dioxide concentrations are increasing in the atmosphere primarily as the result of burning coal, oil, and natural gas for energy and transportation; and from cement manufacturing. The atmospheric abundance of carbon dioxide is currently about 35% above what it was 250 years ago, in preindustrial times. In other international assessments, much of the observed surface warming over the last 50 years has been linked to increases in carbon dioxide and other greenhouse gas concentrations caused by human activities.

Stratospheric and tropospheric ozone. Stratospheric and tropospheric ozone both absorb infrared radiation emitted by Earth’s surface, effectively trapping heat in the atmosphere. Stratospheric ozone also significantly absorbs solar radiation. As a result, increases or decreases

Figure Q18-1. Radiative forcing of climate change from atmospheric gas changes.

Human activities since the start of the Industrial Era (around 1750) have caused increases in the abundances of several long-lived gases, changing the radiative balance of Earth’s atmosphere. These gases, known as “greenhouse gases,” result in radiative forcings, which can lead to climate change. Other international assessments have shown that the largest radiative forcings come from carbon dioxide, followed by methane, tropospheric ozone, the halogen-containing gases (see Figure Q7-1), and nitrous oxide. Ozone increases in the troposphere result from pollution associated with human activities. All these forcings are positive, which leads to a warming of Earth’s surface. In contrast, stratospheric ozone depletion represents a small negative forcing, which leads to cooling of Earth’s surface. In the coming decades, halogen gas abundances and stratospheric ozone depletion are expected to be reduced along with their associated radiative forcings. The link between these two forcing terms is an important aspect of the radiative forcing of climate change.



in stratospheric or tropospheric ozone cause radiative forcings and represent direct links of ozone to climate change. In recent decades, stratospheric ozone has decreased due to rising chlorine and bromine amounts in the atmosphere, while troposphere ozone in the industrial era has increased due to pollution from human activities (see Q3). Stratospheric ozone depletion causes a negative radiative forcing, while increases in tropospheric ozone cause a positive radiative forcing (see Figure Q18-1). The radiative forcing due to tropospheric ozone increases is currently larger than that associated with stratospheric ozone depletion. The negative forcing from ozone depletion represents an offset to the positive forcing from the halogen source gases, which cause ozone depletion.

Halogen source gases and HFCs. An important link between ozone depletion and climate change is the radiative forcing from halogen source gases and hydrofluorocarbons (HFCs). Halogen source gases are the cause of ozone depletion (see Q7) and HFCs are substitute gases (see Q15). Both groups of gases cause radiative forcing in the atmosphere, but with a wide range of effectiveness. The principal gases in each group are intercompared in Figure Q18-2 (top panel) using their “*ozone depletion potentials*” (ODPs) and “*global warming potentials*” (GWPs), which indicate the effectiveness of each gas in causing ozone depletion and climate change, respectively. The ODPs of CFC-11 and CFC-12, and the GWP of CO₂ all are assigned a value of 1.0. For ozone depletion, the halons are the most effective gases (for equal mass amounts) and HFCs cause no ozone depletion (see Q7). For climate change, all gases make a contribution, with CFC-12 and HFC-23 having the largest effect (for equal mass amounts). Montreal Protocol actions (see Q15) that have led to reductions in CFC concentrations and increases in HCFC and HFC concentrations have also reduced the total radiative forcing from these gases. It is important to note that, despite a GWP that is small in comparison to many other greenhouse gases, CO₂ is the most important greenhouse gas related to human activities because its atmospheric abundance is so much greater than the abundance of other gases.

The relative importance of total emissions of halogen source gases and HFCs to ozone depletion and climate change is illustrated for a single year (2004) of emissions in the bottom panel of Figure Q18-2. The values displayed are proportional to the product of 2004 annual global emissions and the ODP or GWP. The results in the lower panel are shown relative to CFC-11, because it is often

used as a reference gas. The comparison shows that the importance of CFC emissions in 2004 to future ozone depletion exceeds that of the halons, despite the higher halon ODP values, because CFC emissions are larger. Similarly, the contributions of CFC and HCFC-22 emissions in 2004 to climate change are currently larger than the halon or HFC contributions. These 2004 results represent only incremental contributions of these gases to either ozone depletion or climate change. The overall contribution of a gas depends on its total accumulation in the atmosphere, which in turn depends on its long-term emission history and atmospheric lifetime (see Q7 and Q16). In the case of ozone depletion, the relative contributions of the halogen source gases can be compared through their respective contributions to effective stratospheric chlorine (see Q16).

As a group, the principal halogen source gases represent a positive direct radiative forcing in the Industrial Era that is comparable to the forcing from methane, the second most important greenhouse gas. In the coming decades, the abundances of these ozone-depleting gases and their associated positive radiative forcings are expected to decrease (see Q16). Future growth in HFC emissions, while uncertain, will contribute a positive forcing that will counter the decrease from ozone-depleting gases. Finally, reductions in ozone-depleting gases will be followed by reductions in stratospheric ozone depletion and its associated *negative* radiative forcing.

Impact of climate change on ozone. Certain changes in Earth’s climate could affect the future of the ozone layer. Stratospheric ozone is influenced by changes in temperatures and winds in the stratosphere. For example, lower temperatures and stronger polar winds could both affect the extent and severity of winter polar ozone depletion. While the Earth’s surface is expected to warm in response to the net positive radiative forcing from greenhouse gas increases, the stratosphere is expected to cool. A cooler stratosphere would extend the time period over which polar stratospheric clouds (PSCs) are present in polar regions and, as a result, might increase winter ozone depletion. In the upper stratosphere at altitudes above PSC formation regions, a cooler stratosphere is expected to increase ozone amounts and, hence, hasten recovery, because lower temperatures favor ozone production over loss (see Q2). Similarly, changes in atmospheric composition that lead to a warmer climate may also alter ozone amounts (see Q20).

Evaluation of Selected Ozone-Depleting Substances and Substitute Gases

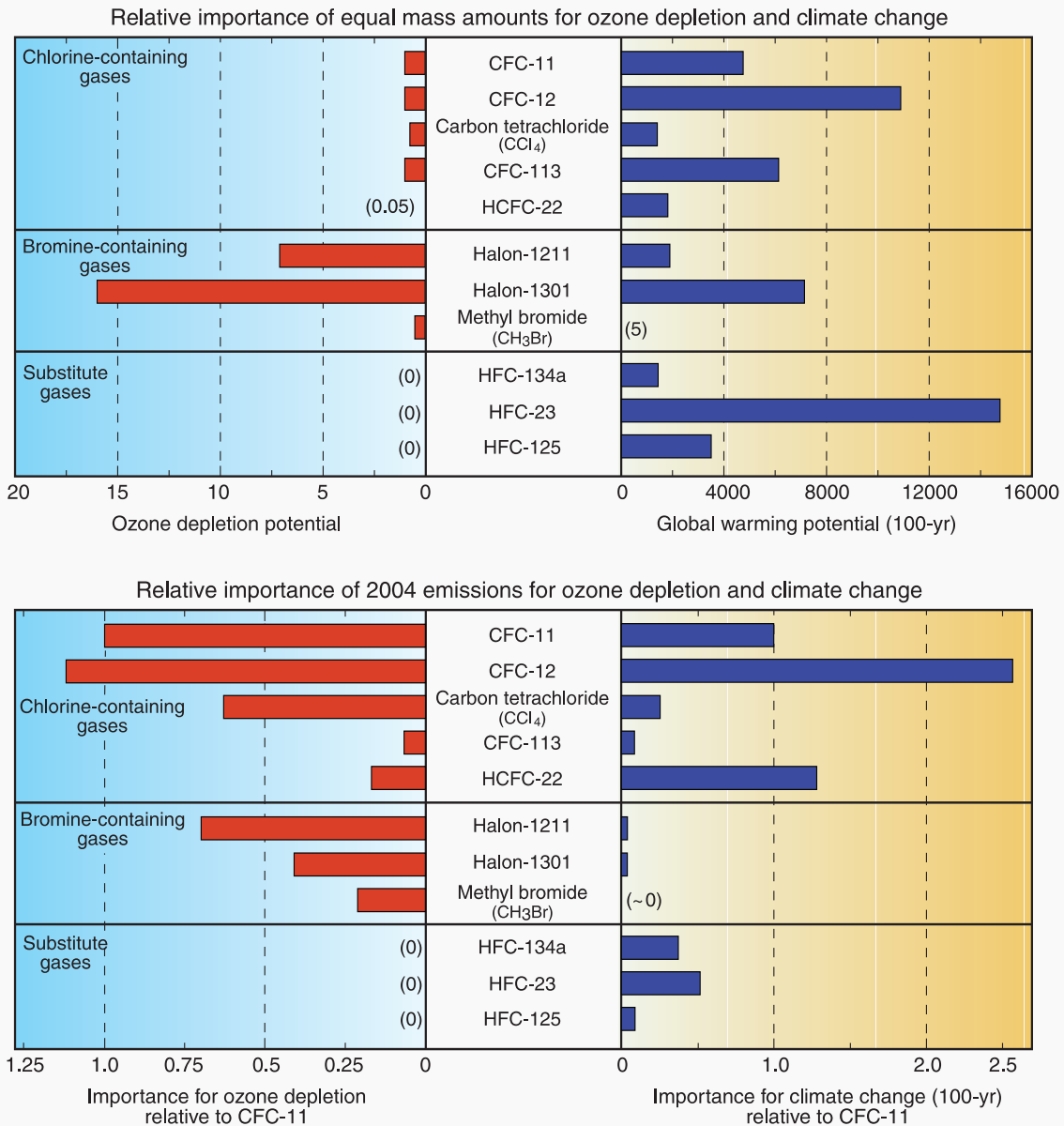


Figure Q18-2. Evaluation of ozone-depleting gases and their substitutes. Ozone-depleting gases (halogen source gases) and their substitutes can be compared via their ozone depletion potentials (ODPs) and global warming potentials (GWPs). The GWPs are evaluated for a 100-yr time interval after emission. The CFCs, halons, and HCFCs are ozone-depleting gases (see Q7) and HFCs, used as substitute or replacement gases, do not destroy ozone. The ODPs of CFC-11 and CFC-12, and the GWP of CO₂ have values of 1.0 by definition. Larger ODPs or GWPs indicate greater potential for ozone depletion or climate change, respectively. The top panel compares ODPs and GWPs for emissions of equal mass amounts of each gas. The ODPs of the halons far exceed those of the CFCs. HFCs have zero ODPs. All gases have non-zero GWPs that span a wide range of values. The bottom panel compares the contributions of the 2004 emissions of each gas, using CFC-11 as the reference gas. Each bar represents the product of a global emission value and the respective ODP or GWP factor. The comparison shows that 2004 emissions of ozone-depleting gases currently contribute more than substitute gas emissions to both ozone depletion and climate change. Future projections guided by Montreal Protocol provisions suggest that the contributions of ozone-depleting gases to climate change will decrease, while those of the substitute gases will increase.

VI. STRATOSPHERIC OZONE IN THE FUTURE

Q19: How will recovery of the ozone layer be identified?

Scientists expect to identify the recovery of the ozone layer with detailed ozone measurements in the atmosphere and with global models of ozone amounts. Increases in global ozone and reductions in the extent and severity of the Antarctic “ozone hole” will be important factors in gauging ozone recovery. Natural variations in ozone amounts will limit how soon recovery can be detected with future ozone measurements.

Recovery process. Identifying the recovery of the ozone layer from depletion associated with halogen gases will rely on comparisons of the latest ozone values with values measured in the past. Because of its importance, ozone will likely be measured continuously in the future using a variety of techniques and measurement platforms (see Q5). Atmospheric computer models will be used to predict future abundances of ozone and attribute observed changes to ozone-depleting gases and other factors.

The recovery process is schematically shown for global ozone in Figure Q19-1. Ozone has declined from pre-1980 amounts due to past increases in halogen gases in the stratosphere (see Q16). In the future, as the overall decline in these gases continues in response to Montreal Protocol provisions, global ozone is expected to recover, approaching or exceeding pre-1980 values (see Q20). Ozone recovery attributable to decreases in ozone-depleting gases can be described, in general, as a process

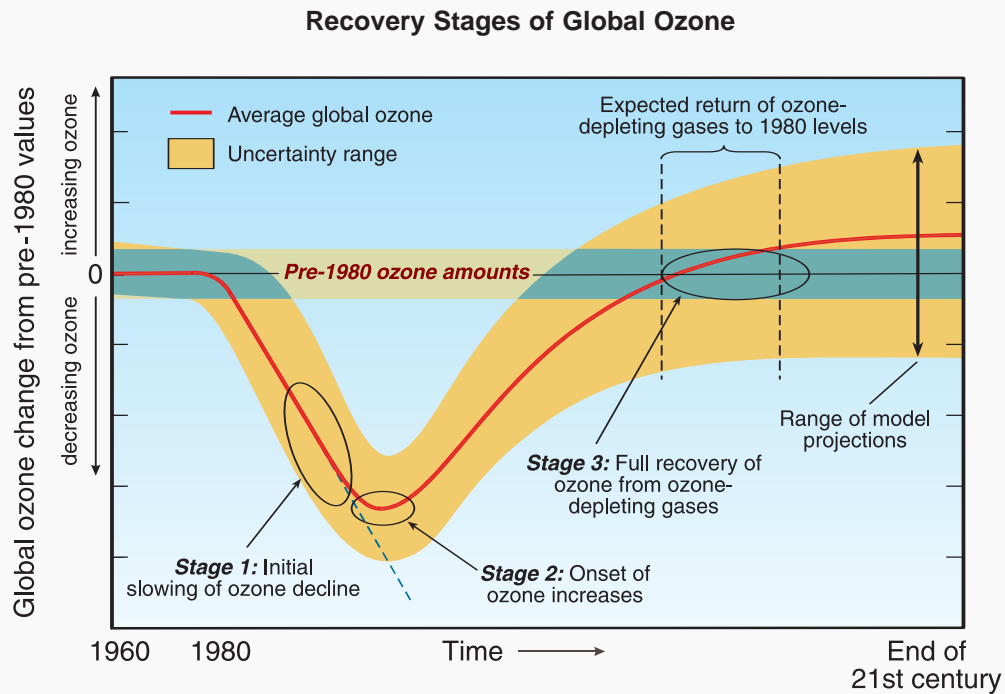


Figure Q19-1. Recovery stages of global ozone. Significant ozone depletion from the release of ozone-depleting gases in human activities first became recognized in the 1980s. The Montreal Protocol provisions are expected to further reduce and eliminate these gases in the atmosphere in the coming decades, thereby leading to the return of ozone amounts to near pre-1980 values. The timeline of the recovery process is schematically illustrated with three stages identified. The large uncertainty range illustrates natural ozone variability in the past and potential uncertainties in global model projections of future ozone amounts. When ozone reaches the full recovery stage, global ozone values may be above or below pre-1980 values, depending on other changes in the atmosphere (see Q20).

TWENTY QUESTIONS: 2006 UPDATE

involving three stages:

- (1) The **initial slowing of ozone decline**, identified as the occurrence of a statistically significant reduction in the rate of decline in ozone.
- (2) The **onset of ozone increases (turnaround)**, identified as the occurrence of statistically significant increases in ozone above previous minimum values.
- (3) The **full recovery of ozone from ozone-depleting gases**, identified as when ozone is no longer significantly affected by ozone-depleting gases from human activities.

Each recovery stage is noted in Figure Q19-1. The red line and shaded region in the figure indicate the expected average value and the uncertainty range, respectively, in global ozone amounts. The large uncertainty range illustrates natural ozone variability in the past and potential uncertainties in global model projections of future ozone amounts.

In the full recovery of global ozone, the milestone of the return of ozone to pre-1980 levels is considered important because prior to 1980 ozone was not significantly affected by human activities. As a consequence, this milestone is useful, for example, to gauge when the adverse impacts of enhanced surface ultraviolet (UV) radiation on human health and ecosystems caused by ozone-depleting

substances are likely to become negligible. The uncertainty range in model results indicates that ozone amounts may be below or above pre-1980 values when ozone has fully recovered from the effects of ozone-depleting gases from human activities (see Q20). The wide range of uncertainty for global ozone in the final stage of recovery represents, in part, the difficulty in accurately forecasting the effects of future changes in climate and atmospheric composition on the abundance of ozone (see Q20).

Natural factors. Stratospheric ozone is influenced by two important natural factors, namely, changes in the output of the Sun and volcanic eruptions (see Q14). Evaluations of ozone recovery include the effects of these natural factors. The solar effect on ozone is expected to be predictable based on the well-established 11-year cycle of solar output. The uncertainty range in Figure Q19-1 includes solar changes. Volcanic eruptions are particularly important because they enhance ozone depletion caused by reactive halogen gases, but cannot be predicted. The occurrence of a large volcanic eruption in the next decades when effective stratospheric chlorine levels are still high (see Figure Q16-1) may obscure progress in overall ozone recovery by temporarily increasing ozone depletion. The natural variation of ozone amounts also limits how easily small improvements in ozone abundances can be detected.

Q20: When is the ozone layer expected to recover?

Substantial recovery of the ozone layer is expected near the middle of the 21st century, assuming global compliance with the Montreal Protocol. Recovery will occur as chlorine- and bromine-containing gases that cause ozone depletion decrease in the coming decades under the provisions of the Protocol. However, the influence of changes in climate and other atmospheric parameters could accelerate or delay ozone recovery, and volcanic eruptions in the next decades could temporarily reduce ozone amounts for several years.

Halogen source gas reductions. Ozone depletion caused by human-produced chlorine and bromine gases is expected to gradually disappear by about the middle of the 21st century as the abundances of these gases decline in the stratosphere. The decline in *effective stratospheric chlorine* will follow the reductions in emissions that are expected to continue under the provisions of the Montreal Protocol and its Adjustments and Amendments (see Figure Q16-1). The emission reductions are based on the assumption of full compliance by the developed and developing nations of the world. The slowing of increases in atmospheric abundances and the initial decline of several halogen gases have already been observed (see Figure Q16-1). One gas, methyl chloroform, has already decreased by about 90% from its peak value. Natural chemical and transport processes limit the rate at which halogen gases are removed from the stratosphere. The

atmospheric lifetimes of the halogen source gases range up to 100 years (see Table Q7-1). Chlorofluorocarbon-12 (CFC-12), with its 100-year lifetime, will require about 200 to 300 years before it is removed (less than 5% remaining) from the atmosphere (see Figure Q16-1). At midlatitudes, effective stratospheric chlorine is not expected to reach pre-1980 values until about 2050.

Ozone projections. Computer models of the atmosphere are used to assess past changes in the global ozone distribution and to project future changes. Two important measures of ozone considered by scientists are global total ozone averaged between 60°N and 60°S latitudes, and minimum ozone values in the Antarctic “ozone hole.” Both measures show ongoing ozone depletion that began in the 1980s (see Figure Q20-1). The model projections indicate that for 60°N-60°S total ozone, the first two stages of recovery (slowing of the decline and turnaround

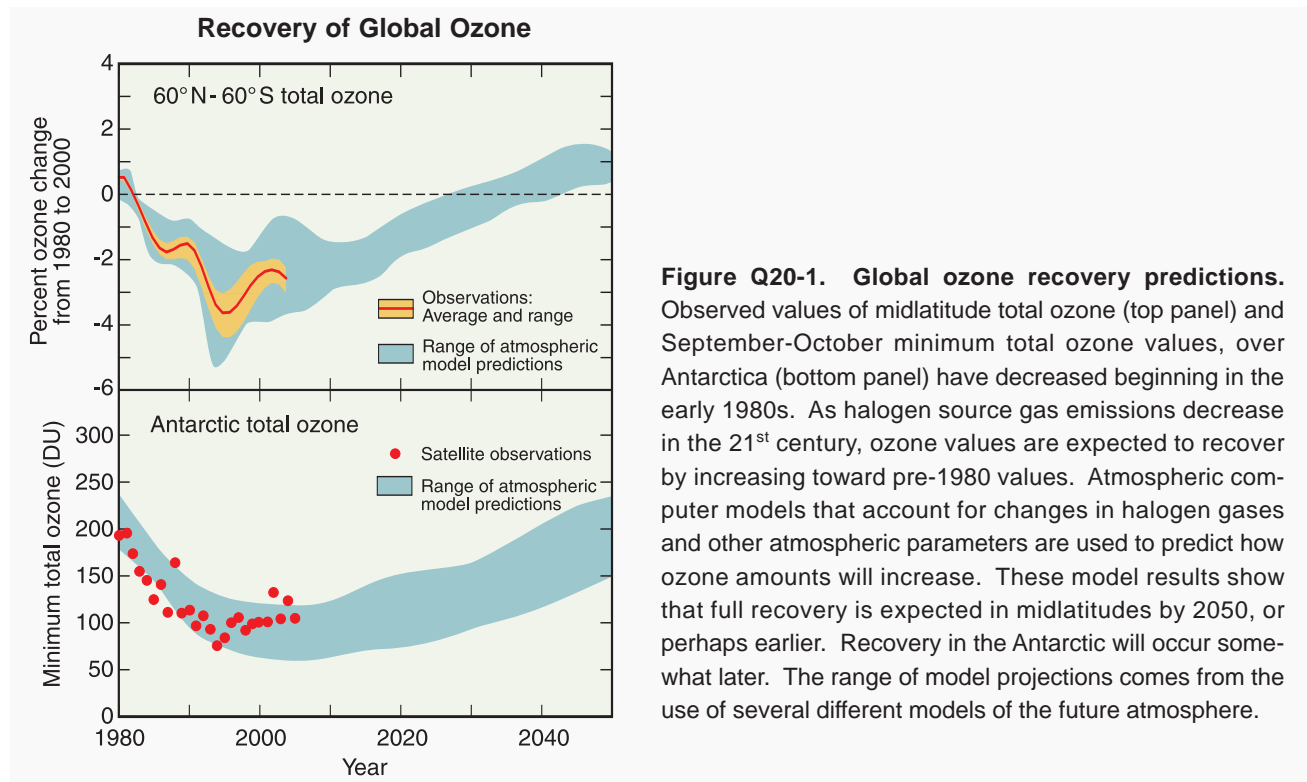


Figure Q20-1. Global ozone recovery predictions. Observed values of midlatitude total ozone (top panel) and September-October minimum total ozone values, over Antarctica (bottom panel) have decreased beginning in the early 1980s. As halogen source gas emissions decrease in the 21st century, ozone values are expected to recover by increasing toward pre-1980 values. Atmospheric computer models that account for changes in halogen gases and other atmospheric parameters are used to predict how ozone amounts will increase. These model results show that full recovery is expected in midlatitudes by 2050, or perhaps earlier. Recovery in the Antarctic will occur somewhat later. The range of model projections comes from the use of several different models of the future atmosphere.

TWENTY QUESTIONS: 2006 UPDATE

(see Q19)) will be reached before 2020. Full recovery, with ozone reaching or exceeding pre-1980 values, is expected to occur by the middle of the 21st century. The range of projections comes from several computer models of the atmosphere. Some of these models indicate that recovery of 60°N-60°S total ozone may come well before midcentury.

Models predict that Antarctic ozone depletion will also reach the first two stages of recovery by 2020, but somewhat more slowly than 60°N-60°S total ozone. Full recovery could occur by mid-century but some models show later recovery, between 2060 and 2070. Declines in effective stratospheric chlorine amounts will occur later over the Antarctic than at lower latitudes because air in the Antarctic stratosphere is older than air found at lower latitudes. As a result, reductions in halogen loading to pre-1980 values will occur 10-15 years later in the Antarctic stratosphere than in the midlatitude stratosphere.

A different atmosphere in 2050. By the middle of the 21st century, halogen amounts in the stratosphere are expected to be similar to those present in 1980 before the onset of significant ozone depletion (see Figure Q16-1). However, climate and other atmospheric factors will not be the same in 2050 as in 1980, and this could cause ozone abundances in 2050 to be somewhat different from those observed in 1980. Stratospheric ozone abundances are affected by a number of natural and human-caused factors in addition to the atmospheric abundance of halogen gases. Important examples are stratospheric temperatures and air motions, volcanic eruptions, solar activity, and changes in atmospheric composition. Separating the effects of these factors is challenging because of the complexity of atmospheric processes affecting ozone.

The ozone recovery projections in Figures Q19-1 and Q20-1 attempt to take these various factors into account.

For example, since 1980 human activities have increased the atmospheric abundance of important greenhouse gases, including carbon dioxide, methane, and nitrous oxide. Other international assessments have shown that the accumulation of these gases is linked to the warmer surface temperatures and lower stratospheric temperatures observed within recent decades. Warmer surface temperatures could change the emission rates of naturally occurring halogen source gases. Lower temperatures in the upper stratosphere (at about 40 kilometers (25 miles) altitude) accelerate ozone recovery because ozone destruction reactions proceed at a slower rate. In contrast, reduced temperatures in the polar lower stratosphere during winter might increase the occurrence of polar stratospheric clouds (PSCs) and, therefore, enhance chemical ozone destruction (see Q10). Further increases of stratospheric water vapor, such as those that have occurred over the last two decades, could also increase PSC occurrences and associated ozone destruction. Therefore, a cooler, wetter polar stratosphere could delay polar ozone recovery beyond what would be predicted for the 1980 atmosphere. Increased abundances of methane and nitrous oxide due to human activities also cause some change in the overall balance of the chemical production and destruction of global stratospheric ozone. Finally, one outcome that cannot be included precisely in models is the occurrence of one or more large volcanic eruptions in the coming decades. Large eruptions would increase stratospheric sulfate particles for several years, temporarily reducing global ozone amounts (see Q14).

As a consequence of these potential changes, the return of effective stratospheric chlorine and ozone to pre-1980 levels may not occur at the same time. In some regions of the stratosphere, ozone may remain below pre-1980 values after effective chlorine has declined to pre-1980 levels.